OS DEPÓSITOS DE JATOBÁ E ONÇA ROSA, PROVÍNCIA MINERAL DE CARAJÁS, BRASIL: DISCUSÕES GENÉTICAS SOBRE MINERALIZAÇÕES EM SISTEMAS IOCG RICOS EM NI

Yuri Tatiana Campo Rodríguez

Pós-Graduação em Geologia

Doutorado em Geologia (Geologia Economica e Prospeção), em acordo de cotutela com The University of Adelaide

Tese N°: **211**

Universidade de Brasília

The University of Adelaide

2024

Ficha catalográfica elaborada automaticamente,
com os dados fornecidos pelo(a) autor(a)

CC198od

Campo Rodriguez, Yuri Tatiana
OS DEPÓSITOS DE JATOBÁ E ONÇA ROSA, PROVÍNCIA MINERAL DE CARAJÁS, BRASIL: DISCUSÕES GENÉTICAS SOBRE MINERALIZAÇÕES EM SISTEMAS IOCG RICOS EM NI. / Yuri Tatiana Campo Rodriguez; orientador Maria Emilia Schutesky; co-orientador Nigel Cook. -- Brasília, 2024.
654 p.

Tese(Doutorado em Geologia) -- Universidade de Brasília, 2024.

1. NON-CLASSICAL PYRIBOLES IN MAGNETITE. 2. PLATINUM GROUP MINERALS ASSOCIATED WITH NICKEL-BEARING SULPHIDES . 3. TELESCOPED TRANSITION FROM TRELLIS TO SILICATE-MOTTLED MAGNETITE. 4. COUPLED LU-HF AND U-PB APATITE GEOCHRONOLOGY IN CARAJÁS DOMAIN, BRAZIL. 5. MAGNETITE AND REE-RICH CALCIC AMPHIBOLE PROVIDE EVIDENCE FOR A SKARN-IOCG SYSTEM . I. Schutesky, Maria Emilia, orient. II. Cook, Nigel , co-orient. III. Título.

MAGNETITE, SULPHIDES AND ASSOCIATED MINERAL ACCESSORIES IN NI-BEARING ORES FROM JATOBÁ AND ONÇA ROSA (JAGUAR OREFIELD), CARAJÁS DOMAIN, BRAZIL: GENETIC INSIGHTS INTO IOCG ORE FORMING SYSTEMS

Yuri Tatiana Campo Rodríguez

This thesis is submitted for the degree of Doctor of Philosophy under a jointly awarded agreement with UnB University of Brasilia

in the

School of Chemical Engineering

Faculty of Sciences, Engineering and Technology

at

The University of Adelaide

November 2024

OS DEPÓSITOS DE JATOBÁ E ONÇA ROSA, PROVÍNCIA MINERAL DE CARAJÁS, BRASIL: DISCUSÕES GENÉTICAS SOBRE MINERALIZAÇÕES EM SISTEMAS IOCG RICOS EM NI

Yuri Tatiana Campo Rodríguez

Tese submetida ao Programa de Pós-Graduação em Geologia como requisito parcial para a obtenção do título de Doutora em Geologia (Geologia Economica e Prospeção), em acordo de cotutela com The University of Adelaide

Orientadora: Prof. Dra. Maria Emilia Schutesky
Co-orientadores: Prof. Dr. Nigel J. Cook, Dra. Cristiana L. Ciobanu

Universidade de Brasília – Instituto de Geociências

Novembro 2024

O presente trabalho foi realizado com apoio da Coordenação de Aperfeiçoamento de Pessoal de Nível Superior - Brasil (CAPES) – Código de Financiamento 001, e do Conselho Nacional de Desenvolvimento Científico e Tecnológico do Brasil CNPq.

Para Cony, Yesid, Ana, Juan...

Y Cristi.

"What would life be if we had no courage to attempt anything?"

Vincent Van Gogh

TABLE OF CONTENTS

ABSTRACT **25**

RESUMO **29**

DECLARATION **33**

ACKNOWLEDGEMENTS **35**

PREFACE **39**

PREFÁCIO **43**

CHAPTER 1: INTRODUCTION **47**

1.1 Research objectives and thesis structure 53

1.2 Introdução 58

1.3 Objetivos e estrutura 63

1.2 References 67

CHAPTER 2: POLYSOMATIC INTERGROWTHS BETWEEN AMPHIBOLES AND NON-CLASSICAL PYRIBOLES IN MAGNETITE: SMALLEST-SCALE FEATURES RECORDING A PROTRACTED GEOLOGICAL HISTORY **73**

2.1 Abstract 77

2.2 Introduction 77

2.3 Analytical methods 78

2.4 Results 78

2.4.1 Nanoscale inclusions in magnetite 78

2.5 Nanoscale Characterization 81

2.5.1 Crystal structures of chain silicates 81

2.5.2 Sequences of polysomatic intergrowths 83

2.5.3 Defects 86

2.5.4 Sheet silicates 90

2.6 Discussion 92

2.6.1 Polysomatic and chain-width disorder: primary vs. replacement reactions 92

2.6.2 Chemical patterning and fluid evolution recorded by chain silicates in magnetite 94

2.6.3 Genetic implications..... 94

2.7 Summary and Implications 95

2.8 Acknowledgments and Funding 96
2.9 References 96

CHAPTER 3: PLATINUM GROUP MINERALS ASSOCIATED WITH NICKEL-BEARING SULFIDES FROM THE JATOBÁ IRON OXIDE-COPPER-GOLD DEPOSIT, CARAJÁS DOMAIN, BRAZIL 99

3.1 Abstract 103
3.2 Introduction 104
3.3 Background 105
3.3.1 Geology and geological evolution of the Carajás Domain 105
3.3.2 IOCG deposits of the Carajás Domain 107
3.3.3 Nickel and Platinum Group Element endowment in the Carajás Domain 107
3.3.4 The Jatobá deposit 108
3.4 Samples and analytical methodology 109
3.5 Results 110
3.5.1 Ore petrography and mineralogy 112
3.5.2 Accessory ore minerals 114
3.5.3 Platinum Group Minerals 115
3.5.4 Trace element concentrations in sulfides 118
3.5.5 Grain-scale trace element distributions in pyrite 122
3.6 Discussion 125
3.6.1 Origin, trace element signatures, and successive generations of Jatobá sulfides 125
3.6.2 PGM in Ni-bearing sulfides - Identifying the potential source 127
3.6.3 Which ore genesis model best explains the evidence? 128
3.7 Conclusions and implications 129
3.8 References 130

CHAPTER 4: TELESCOPED TRANSITION FROM TRELLIS TO SILICATE-MOTTLED MAGNETITE RECORDS DEEP SHEAR METAMORPHISM IN THE IOCG DEPOSIT AT JATOBÁ, CARAJÁS, BRAZIL 137

4.1 Abstract 141
4.2 Introduction 143
4.3 Geological background 144
4.3.1 Deposit geology 147
4.4 Samples and analytical methods 150

4.5 Results 151
4.5.1 Petrography 151
4.5.2 Magnetite composition and textures 157
4.6 Trace element geochemistry: concentrations and distributions 159
4.6.1 Element concentrations and trends in magnetite 159
4.6.2 Chondrite-normalized REY fractionation patterns 162
4.6.3 Trace element distributions in magnetite 164
4.6.4 Nanoscale characterization 166
4.7 Discussion 171
4.7.1 How many generations of magnetite? 171
4.7.2 Magnetite trace element signatures 172
4.7.3 Deep shear zone metamorphism - telescoped transition of trellis to silicate-mottled magnetite 174
4.8 Summary and Implications 178
4.9 Acknowledgements 181
4.10 References 180

CHAPTER 5: COUPLED LU-HF AND U-PB APATITE GEOCHRONOLOGY OF JATOBÁ OREBODY SUPPORTS ~2.5 GA METAMORPHISM IN DEEP SHEAR ZONES FROM SOUTHERN COPPER BELT, CARAJÁS DOMAIN, BRAZIL 189

5.1 Abstract 191
5.2 Introduction 192
5.3 Geological background 194
5.3.1 Main tectono-stratigraphic units and recent models of geodynamic evolution 194
5.3.2 Deposit geology 198
5.4 Methodology 201
5.5 Results 203
5.5.1 Apatite petrography 203
5.5.2 Apatite composition, grain-scale heterogeneity and cathodoluminescence response 205
5.5.3 Chondrite-normalized REY fractionation patterns 212
5.5.4 U-Pb isotope data 212
5.5.5 Lu-Hf isotope data 214
5.6 Discussion 218
5.6.1 Comparing the U-Pb and Lu-Hf age data 218
5.6.2 Interpretation of ages - primary versus overprint? 219
5.6.3 Comparison with radiometric ages for other deposits in the Carajás Province 221
5.6.4 Geochronology to support a genetic model for the Jatobá deposit 224

5.7 Conclusions 228
5.8 Acknowledgements 230
5.9 References 230

CHAPTER 6: MAGNETITE AND REE-RICH CALCIC AMPHIBOLE PROVIDE EVIDENCE FOR A SKARN-IOCG SYSTEM AT ONÇA-ROSA, JAGUAR OREFIELD, CARAJÁS MINERAL PROVINCE, BRAZIL 239

6.1 Abstract 243
6.2 Introduction 245
6.3 Geological background 247
6.3.1 Deposit geology 249
6.4 Analytical methods 251
6.5 Results 252
6.5.1 Petrography 252
6.5.2 Trace element geochemistry 256
6.5.3 Chondrite-normalized REY fractionation patterns 258
6.5.4 Nanoscale characterization of magnetite 260
6.6 Discussion 268
6.6.1 Textural and mineralogical inferences for petrogenesis and ore formation 268
6.6.2 Mineral trace element signatures - is there an IOCG connection? 270
6.6.3 From skarn to IOCG stages - what is recorded in magnetite? 271
6.6.4 Reconstructing the sequence of mineralization-a brie comparison with other deposits 272
6.7 Conclusions 275
6.8 Acknowledgements 277
6.9 References 278

CHAPTER 7: ARSENOHAUCHECORNITE, OGNITITE, PARKERITE, AND RELATED MINERALS FROM ONÇA ROSA OREBODY, CARAJÁS, BRAZIL: FINGERPRINTING PGE SIGNATURES IN HYDROTHERMAL NI ORES 287

7.1 Abstract 291
7.2 Introduction 293
7.3 Samples and analytical methodology 295
7.3.1 Samples 295
7.3.2 Analytical methodology 295
7.4 Results 297

7.4.1 Petrography and geochemistry of common sulfide assemblages 297
7.4.2 Accessory minerals: arsenohauchecornite, ognitite, and accompanying phases in sulfides - Micron-scale characterization 302
7.4.3 Compositional data 307
7.4.4 Nanoscale characterization 308
7.4.5 Reaction zones and nanoparticles 312
7.5 Discussion 317
7.5.1 Petrogenetic significance of the 'exotic' Ni-Bi-Te-Pb-Ag-S trace mineral associations 317
7.5.2 Trace element mobility during replacement reactions 318
7.5.3 Insights into the crystal-structure and chemistry of arsenohauchecornite and ognitite 319
7.5.5 Fingerprinting PGE signatures 320
7.6 Summary and implications 321
7.7 Acknowledgements and funding 324
7.8 References 324

CHAPTER 8: SUMMARY, RECOMMENDATIONS AND CONCLUDING REMARKS 331

8.1 Recomendações e Considerações Finais 333
8.2 Conclusions 336
8.3 Conclusões 340
8.4 References 346

CHAPTER 9: SUPPLEMENTARY AND ADDITIONAL MATERIAL 351

Supplementary Material A: for Chapter 2 353
Appendix A: for Chapter 2 354
Appendix B: for Chapter 2 355
Appendix C: for Chapter 2 364
Supplementary Material B: for Chapter 3 366
Appendix A: for Chapter 3 367
Supplementary Material C: for Chapter 4 378
Appendix A: for Chapter 4 379
Appendix B: for Chapter 4 388
Supplementary Material D: for Chapter 5 425

Appendix A: for Chapter 5 426
Appendix B: for Chapter 5 433
Supplementary Material E: for Chapter 6 538
Appendix A: for Chapter 6 539
Appendix B: for Chapter 6 546
Supplementary Material F: for Chapter 7 593
Appendix A: for Chapter 7 594
Appendix B: for Chapter 7 601

Additional Material G: Coupled microstructural EBSD and LA-ICP-MS trace element mapping of pyrite constrains the deformation history of breccia-hosted IOCG ore systems 619
Additional Material H: EBSD mapping of Cu-Fe-sulfides reveal microstructures enriched in critical/precious metals and resolve deformation histories 621
Additional Material I: Monazite, lanthanide-rich glasses, and other trace elements in copper smelter slags: Constraints on critical metal behaviour in Si-Fe-rich melts 624
Additional Material J: Trace element distributions among Cu-(Fe)-sulphides from the Olympic Dam Cu-U-Au-Ag deposit, South Australia 626

CHAPTER 10: REFERENCES.....630

LIST OF FIGURES AND TABLES

CHAPTER 1:

Figure 1 Geological map of Carajás Domain showing main lithologies, fault zones and the location of main deposits, including the Jatobá and Jaguar deposits 50

Figura 1. Mapa geológico do Domínio Carajás mostrando as litologias, zonas de falhas e a localização dos principais depósitos, incluindo o Jatobá e Jaguar 59

CHAPTER 2:

Figure 1 Reflected light and BSE images showing representative magnetite textures and location of FIB cuts for S/TEM sample preparation 79

Figure 2 HAADF-STEM images showing variation in size and shape of NCP-bearing amphiboles from the three foils as coarser aggregates, subrounded and euhedral, prismatic grains 80

Figure 3 Low-resolution images illustrating amphibole-NCP intergrowths from rounded, and subhedral grains, and aggregates 81

Figure 4 STEM EDS maps and overlays of densely mottled areas, aggregate 3, and aggregate 2 82

Figure 5 STEM EDS maps and overlays showing Ce-bearing magnesio-hornblende (Ce-Mhbl) and (ferro)-tschermakite (Fts) 83

Figure 6 Models and images of chain silicates each plotted on [001] zone axis 84

Figure 7 HAADF STEM images atom fill models and I_{beam} schematics for pyroxene slabs as zippers in other chain silicates for [001] zone axis 85

Figure 8 Larger (up to 100 nm long) polysomatic sequences from aggregates (A1–A3) along profiles marked on Figures 3c, 3d, and 3g 86

Figure 9 High-resolution images of amphiboles showing chain-width disorder and chemical zoning 87

Figure 10 Wider, more regular blocks triple chain slabs (up to 23) within amphibole 88

Figure 11 High-resolution images showing polysomes with the widest I_{beams} and I_{beam} schematic 89

Figure 12 Overview of chain-width disorder and defects in NCP-rich amphiboles as images and I_{beam} schematics 90

Figure 13 Details of chain-width disorder and defects in NCP-rich areas as images and I_{beam} schematics 91

Figure 14 Overview of replacement between sheet and chain silicates 93
Figure 15 Schematic showing staged evolution of magnetite 95

CHAPTER 3:

Figure 1 Geological map of the Carajás Domain showing the location of Jatobá orefield 105
Figure 2 Simplified geological map of the Jatobá-Pista-Sequeirinho-Sossego orefield map 108
Figure 3 Schematic lithological cross-section of sampled drillhole with sample locations, reflected light microphotographs, and drillcore 111
Figure 4 Reflected light images showing sulfide assemblages in the Jatobá samples 113
Figure 5 BSE images and EDS element map showing details of sulfide assemblages in Jatobá samples 114
Figure 6 BSE images showing sulfide assemblages containing PGM 116
Figure 7 BSE images and respective EDS element maps for selected elements 117
Figure 8 Fracture in pyrite containing chalcopyrite and inclusions of Pd-Pt minerals 117
Figure 9 Box-and-whisker plots comparing the concentrations of thirteen key trace elements in pyrite from three different samples, as well as in chalcopyrite and pyrrhotite 118
Figure 10 Time-resolved LA-ICP-MS depth profiles for representative pyrite grain in sample Jt10 120
Figure 11 Binary plots of LA-ICP-MS concentration data for selected elements in pyrite and associated sulfides from Jatobá 121
Figure 12 Binary plots of LA-ICP-MS concentration data for selected elements in pyrite and associated sulfides from Jatobá 122
Figure 13 Reflected light image and selected LA-ICP-MS element maps of a representative pyrite grain from sample Jt4 showing subtle oscillatory zoning 123
Figure 14 Reflected light image and selected LA-ICP-MS element maps of a representative pyrite grain from sample Jt10 124
Figure 15 Reflected light image and selected LA-ICP-MS element maps of the margin of a coarser pyrite grain in sample Jt10 125

Table 1 Compositional data (SEM-EDS) for selected PGM 110
Table 2 Summary of LA-ICP-MS trace element data for Jatobá sulfides 119

CHAPTER 4:

Figure 1 Geological map of the Carajás Domain indicating the main tectono-structural units . 145

Figure 2 Schematic stratigraphic column for the sampled interval 152
Figure 3 Automated Mineralogy maps showing constituent minerals in thin sections from the orebody 154
Figure 4 BSE images showing textural details of apatite, epidote-group minerals and scapolite associated with biotite and amphiboles, Fe-Ti-oxides, sulfides and trace mineral inclusions 156
Figure 5 BSE images showing main textures and a range of inclusions within magnetite 158
Figure 6 LA-ICP-MS trace element concentration data for magnetite presented as box-and-whiskers plots and as binary plots 161
Figure 7 Representative time-resolved downhole LA-ICP-MS depth profiles, comparison of REY concentrations in different samples and selected chondrite-normalized REY fractionation patterns for magnetite 163
Figure 8 LA-ICP-MS element maps and corresponding reflected light images of selected magnetite grains annotated to highlight internal features 165
Figure 9 Overall images of the five foils analyzed from magnetite samples 167
Figure 10 EDS STEM maps and HAADF STEM images showing nanoscale aspects of trellis (Jt4), transition to blebby (Jt6) and patchy ilmenite as inclusions in the dense silicate-mottled magnetite from sample Jt10 168
Figure 11 EDS STEM maps of allanite attached to actinolite in and titanite-ferrotschermakite as inclusions in magnetite 170
Figure 12 Schematics showing the micron- to nanoscale textural evolution of magnetite from host basalt to ore 175

CHAPTER 5:

Figure 1 Geological map of the Carajás Domain (CD) showing main lithologies and location of Jatobá and other deposits 196
Figure 2 Schematic stratigraphic column showing location of samples used in this study 204
Figure 3 Ternary plots of Cl, F, and (calculated) OH contents for basalt-hosted (Jt1 and Jt4) and ore apatite (Jt7 and Jt10) 206
Figure 4 BSE images and EPMA element maps illustrating grain-scale distribution of Cl, F, Ce, Y, and Fe 208
Figure 5 LA-ICP-MS trace element maps for selected elements in apatite from samples as labelled. Ce is used as a proxy for LREE and Y, Lu for HREE 210

Figure 6 Chondrite-normalized REY fractionation trends (T) for apatite from samples as labelled 211
Figure 7 U-Pb Tera-Wasserburg diagrams for all apatite data (SM Table S3) split by sample as labelled 213
Figure 8 Apatite LA–ICP–MS/MS Lu–Hf isochrons for each sample/category as labelled (data in SM Table S4) 217
Figure 9 BSE images and time-resolved LA-ICP-MS depth profiles showing grain-scale differences between Lu-Hf and U-Pb ages in fluorapatite 218
Figure 10 Summary of selected geochronological data for IOCG/Cu-Au-(Mo) deposits from the northern and southern parts (Copper Belts) of the Carajás Domain. Data tabulated in Table 1 222
Figure 11 Schematic showing proposed model for the Jatobá IOCG system based on the new petrochronological apatite data 226
Table 1 New apatite age data and selected published geochronological data for mineral deposits in the Carajás Domain 216

CHAPTER 6:

Figure 1 Geological map of the Carajás Domain (CD) showing the location of the Jaguar deposit and other major deposits 248
Figure 2 Schematic stratigraphic column for drillhole DH00127. Reflected and transmitted light microphotographs showing the main petrographic aspects of ores and host lithologies as described in the main text 253
Figure 3 Reflected light images showing amphibole assemblages and rock fabrics 254
Figure 4 BSE images showing ore mineral associations in the orebody and granite 255
Figure 5 LA-ICP-MS trace element concentration data for magnetite, amphibole and apatite ..257
Figure 6 Selected chondrite-normalized REY fractionation patterns for magnetite, apatite and amphibole from different association (data from Supplementary data SD Table 1e) 259
Figure 7 BSE and reflected light images of mottled magnetite 261
Figure 8 HAADF STEM images and EDS STEM maps showing representative NCP-bearing cummingtonite + TBC inclusions in magnetite 263
Figure 9 Atomic scale resolution images and STEM simulations for the most common chain silicates (as labelled) projected on [001] zone axis 265
Figure 10 High-resolution images showing straight contacts between $[100]_{Bt\text{-}Chl}$ and $[001]_{Cum}$ 266
Figure 11 Silician magnetite as defects of variable widths ($2n\ d_{111\text{-}magnetite}$) in magnetite 267

CHAPTER 7:

Figure 1 Reflected light microphotographs and back-scattered electron images showing petrographic aspects of common sulfides 298

Figure 2 BSE images, EPMA EDS SEM and LA-ICP-MS maps of pentlandite replaced by secondary phases, violarite, bravoite, Ni-Cu-sulfate, and mixtures thereof 299

Figure 3 Reflected light image and LA-ICP-MS maps of euhedral pyrite grain associated with pentlandite-sphalerite ore. As, Co and Ni show weak oscillatory zoning patterns 301

Figure 4 BSE images showing the 'exotic' Bi-Ni-Te-S-Ag-Pb associations present as accessory minerals in the pentlandite-pyrite ores 305

Figure 5 BSE images and EDS SEM maps of other grains representing the Bi-Ni-Te-S-Ag-Pb association 306

Figure 6 Low-resolution HAADF STEM images from foil #1 showing arsenohauchecornite in contact with pentlandite and inclusions of chlorite 309

Figure 7 Low-resolution HAADF STEM image of ognitite in contact with pentlandite and parkerite (foil #2) 310

Figure 8 BF and HAADF STEM images showing nanotextures of ognitite 311

Figure 9 BF and HAADF STEM images showing details of reaction areas within pentlandite and at contacts with parkerite 313

Figure 10 Images and EDS STEM maps of moncheite nanoparticles in pentlandite 315

Figure 11 Images and EDS STEM maps of various nanoparticles representing Bi-(Ag)-Te-, Ag-, Pb-tellurides, galena and native Bi 316

Table 1a Electron microprobe data for accessory ore minerals 303

Table 1b EDS STEM data for nanoparticles in pentlandite 304

LIST OF ABBREVIATIONS

A

Act -	actinolite
Ahau -	arsenohauchecornite
Alb -	albite
Aln -	allanite
Alt -	altaite
AM -	Automated Mineralogy
AMICS -	Advanced mineral identification and characterization system
Amp -	amphibole
Ap -	apatite
APD -	antiphase boundaries or domains
Apfu -	atoms per formula unit

B

BD -	Bacajá Domain
BF -	Bright-field
BIF -	Banded iron formation
Bri -	britholite
BSE -	Backscattered electron
Brav -	bravoite
Bt -	biotite
Bvk -	borovskite

C

Cal -	calcite
Cbt -	cobaltite
CD -	Carajás Domain
Ccp / Cp -	chalcopyrite
Chl -	chlorite
Cjim -	clinojimthompsonite
CL -	cathodoluminescence
CMP -	Carajás Mineral Province
CP -	Carajás Province
Cps -	counts-per-second
Cum -	cummingtonite

D

DCFI-	Drift corrected frame integration

E

ED -	Electron diffractions
EDS -	Energy dispersive spectrometry
Ep -	epidote
EPMA -	electron probe microanalyzer
Eux -	euxenite

F

Fact -	ferro-actinolite
Fap -	fluorapatite
Feb -	ferberite
FFT -	Fast Fourier transform
FIB -	Focused ion beam
Fts -	ferro-tschermakite

G

Gru -	grunerite
Gbs -	gibbsite
Ghn -	gahnite
Gn -	galena
Gus -	gustavite

H

HAADF -	High-angle annular dark-field
Hbl -	hornblende
Hc -	hercynite
Hes -	hessite
HREE -	Heavy rare earth elements
HRTEM -	High-resolution transmission electron microscopy
Hyv -	heyrovskýite

I

Ilm -	ilmenite
IOA -	Iron-oxide apatite
IOCG -	Iron oxide-copper-gold

K

Kfs -	k-feldspar
Ktu -	kotulskite

L

LA-ICP-MS -	Laser Ablation Inductively Coupled Plasma Mass Spectrometry

Lil - Lillianite
LREE - Light rare earth elements
M
Mag / Mgt - magnetite
Mch - michenerite
Mhbl - magnesio-hornblende
Mlb / Mol - molybdenite
Mlt - melonite
Mnz - monazite
Mon - moncheite
MREE - Middle rare earth elements
Mrk - merenskyite
Ms - muscovite
MSS - Monosulfide solid solutions
MSWD - Mean Square Weighted Deviation
N
NCP - Non-classical pyriboles
Nld - naldrettite
NP - nanoparticles
O
O - Ribbons of cation octahedra
Ogn - ognitite
P
PGE - Platinum group elements
Pl - plagioclase
PGM - Platinum group minerals
Ppm - parts per million
Pn - pentlandite
Prk - parkerite
P-T - Pressure-temperature
Py - pyrite
Pyh - pyrrhotite
Q
Qz - quartz
R
REY - Rare earth elements + yttrium
REE - Rare earth elements
RMD - Rio Maria Domain
Rt - rutile
S
Sbd - sudburyite
Sch - scheelite
Scp - scapolite
Seg / Sie - siegenite
SEM - Scanning electron microscope
SMS - seafloor massive sulfide
Sp - sphalerite
Spy - sperrylite
Srp - serpentine
STEM - Scanning transmission electron microscopy
T
T - SiO_4 tetrahedra
Tbi - Tellurobismuthite
TCB - talc+chlorite+biotite
TEM - Transmission electron microscopy
Thau - tellurohauchecornite
Tho - thorite
Tlc – talc
Ts - tschermakite
Tsm - tsumoite
Ttn - titanite
TTG - Trondhjemite–Tonalite–Granodiorite
Tur - tourmaline
T-W - Terra-Wasserburg
U
Urn - uraninite
V
Vio - violarite
VMS / VHMS - Volcanogenic massive sulfide
Vol - volynskite
W
WDS - Wavelength dispersive
X
XRF - X-ray fluorescence

ABSTRACT

The Carajás Domain, central-north Brazil, is host to large iron-oxide–copper–gold (IOCG) deposits. The mechanisms and timing of ore genesis are addressed in two Ni-bearing IOCG systems, Jatobá and Onça-Rosa. Jatobá is located along the Canaã dos Carajás shear zone and hosted within bimodal volcanic sequences of the Neoarchean Grão Pará Group. Onça-Rosa is a granite-hosted orebody located at contacts with mafic/ultramafic units of Serra do Puma layered Complex.

At Jatobá, spectacular polysomatic intergrowths between amphiboles and non-classical pyriboles (NCPs) are observed in magnetite cores. Nanoscale imaging of NCPs are used to model crystallization via self-patterning during amphibole growth in a close-to-equilibrium system. These observations support a multi-stage evolution for Jatobá. Ferrotschermakite indicates formation at ~7.5 kbar.

Fractures and grain boundaries in pyrite from Jatobá host platinum group minerals (PGM) associated with rare earth- and U-minerals. Differences in sulphide chemistry, and the distribution and speciation of PGM further support a two-stage genetic model. IOCG-style mineralization was superimposed onto a pre-existing assemblage, resulting in partial dissolution, replacement and remobilization textures. Platinum group elements (PGE), released from common sulphides combined with Sb-Bi-Te-bearing fluids during the retrograde stage of a syn-deformational metamorphic event. An alternative model involves leaching of Ni and PGE from komatiites within the sequence or from basement ultramafics.

Substantiation of the two-stage model comes from two texturally and geochemically distinct magnetite types: ‘trellis’ in country rocks, with a telescoped transition to ‘silicate-mottled’ in ore. Magnetite geochemistry evolves from Ti-Cr-Co-Mn (‘trellis’) to REE enrichment in the silicate-

mottled type. Ilmenite-magnetite nano-thermobarometry (728-414°C), ferrotschermakite geobarometry (6.4-7.4 kbar), and observed deformation textures suggests amphibolite facies at ~20 km, concordant with deep shear zone metamorphism. Such a scenario allows metal leaching from lithologies at the base of the Canaã dos Carajás strike-slip structure.

The age of mineralization is constrained from apatite associated with magnetite. Initial deposition of apatite in a volcanic rift sequence at 2.76–2.73 Ga is supported by a preserved 'mafic' Cl-rich signature. IOCG system initiation took place during shearing at ~2.5 Ga. The ~2.5 Ga age coincides with Cinzento Shear zone reactivation and published ages for deposits in the northern copper belt, strongly suggesting deep-rooted connections between mineralising systems across the region.

Onça-Rosa is substantially different. Magnetite textures, including inclusion-rich cores with NCPs are indicative of early formation relative to coexisting sulphides. Contrasting with previous interpretations, Onça-Rosa is considered a 'hybrid' Fe-Zn-Ni skarn system formed in two distinct stages: an early magnesian skarn during deposition of magnetite+sphalerite; and a later calcic skarn associated with pentlandite+amphibole. High REY concentrations in amphiboles and apatite and association with uraninite are concordant with IOCG-style mineralization.

Nickel-rich sulphide mineralization at Onça-Rosa comprises pentlandite, violarite/bravoite, pyrite, sphalerite and minor chalcopyrite. Microtextures are concordant with cycles of replacement via dissolution-reprecipitation reaction. Characteristic accessories are arsenohauchecornite, ognitite, parkerite, tellurides, and Pb-Bi-sulfosalts. Nanostructures in pentlandite reveal fluid pathways that host nanoparticles of moncheite, volynskite, hessite, altaite, and Bi-chalcogenides. The observed assemblages and NPs are attributed to interaction between metasomatic-hydrothermal fluids with pentlandite-rich ores at contacts between ultramafic rocks and granite-derived fluids.

RESUMO

O Neoarqueano-Proterozoico Domínio Carajás, localizado no centro-norte do Brasil, abriga uma diversidade de depósitos minerais. Entre eles, e de grande relevância econômica, estão os da classe de óxido de ferro–cobre–ouro (IOCG). A gênese e a cronologia desses depósitos são temas de intenso debate, com evidências e interpretações frequentemente conflitantes na literatura. Esta tese aborda os mecanismos e o momento da formação de minério em duas mineralizações IOCG enriquecidas em Ni. O prospecto Jatobá e o corpo de minério Onça Rosa, localizado no campo mineral de Jaguar, situam-se no cinturão cuprífero sul da Província Mineral de Carajás. Diferentes contextos geológicos envolvem os dois sistemas. Enquanto Jatobá está hospedado em sequências vulcânicas bimodais do Grupo Grão Pará, de idade Neoarqueana, localizadas ao longo de estruturas E-O pertencentes à zona de cisalhamento Canaã dos Carajás, Onça Rosa é um corpo mineral com alto teor de Ni, hospedado em granitos em contato com unidades máficas/ultramáficas do Complexo Máfico-ultramáfico Acamadado do Puma.

Este estudo aplicou várias técnicas investigativas modernas e inovadoras para caracterização mineralógica e geoquímica detalhada, em escalas nanométrica e micrométrica. Coletivamente, novas interpretações foram possibilitadas, com implicações para a exploração mineral e o aproveitamento de recursos em toda a região.

A magnetita é o principal mineral dos depósitos de Jatobá e Onça-Rosa. Em Jatobá, intercrescimentos polissomáticos entre anfibólios e piribólios não-comuns (NCPs) foram identificados como inclusões na magnetita, sugerindo uma evolução com múltiplos estágios de formação. Duas populações de anfibólios foram registradas, entre eles a ferrotschermakita, que indica formação sob pressões de até 7,5 kbar. A presença de elementos do grupo da platina (PGE), em minerais como merenskyita, sudburyita e kotulskita, reinforçãm o modelo genétio em dois estágios, no qual a mineralização de estilo IOCG foi superposta a uma assembleia preexistente,

resultando nas texturas observadas de dissolução parcial, substituição, remobilização e sobreposição.

A análise da magnetita revelou duas variedades distintas: uma magnetita do tipo ‘treliça’ (das rochas encaixantes) e uma ‘mosqueada’ por silicatos, com transições telescópicas evidenciadas por mudanças texturais e geoquímicas, incluindo enriquecimento em elementos das terras raras. Geotermometria e geobarometria indicam condições de 728 a 414 °C e pressões de 6,4–7,4 kbar, coerentes com formação sob metamorfismo de fácies anfibolito a 20 km de profundidad, possivelmente associado à zona de cisalhamento Canaã dos Carajás. Geocronologia de U-Pb e Lu-Hf em apatitas, permitiu datar o início da mineralização do tipo IOCG em ~2,5 G, com uma atividade hidrotermal tardia em ~2 Ga, sugerindo uma conexão com reativações das zonas de cisalhamento na região.

Em Onça-Rosa, a mineralização ocorre como um skarn rico em Fe-Zn-Ni formado por alterações intensas de rochas ultramáficas em contato com um granito sin-cinemático. A mineralização evoluiu de um estágio inicial de skarn magnesiano com magnetita+esfalerita para um estágio posterior de skarn cálcico associado à pentlandita+anfibólio. Uma série de teluretos e sulfossais, e minerais raros de Ni-Bi suportam uma interação entre fluidos hidrotermais e minérios ricos em pentlandita nos contatos com o complexo acamadado da Serra do Puma.

Esses achados avançam significativamente o entendimento da formação dos minérios de Ni e PGE em sistemas IOCG na província de Carajás, destacando o potencial exploratório e econômico da região.

Palavras chave: IOCG, Magnetita, Apatita, Província Mineral de Carajás, PGE, Níquel.

DECLARATION

I certify that this work contains no material which has been accepted for the award of any other degree or diploma in my name, in any university or other tertiary institution and, to the best of my knowledge and belief, contains no material previously published or written by another person, except where due reference has been made in the text. In addition, I certify that no part of this work will, in the future, be used in a submission in my name, for any other degree or diploma in any university or other tertiary institution without the prior approval of the University of Adelaide and where applicable, any partner institution responsible for the joint award of this degree.

I acknowledge that copyright of published works contained within the thesis resides with the copyright holder(s) of those works.

I give permission for the digital version of my thesis to be made available on the web, via the University's digital research repository, the Library Search and also through web search engines, unless permission has been granted by the university to restrict access for a period of time.

Signed: Date: 11/11/2024

ACKNOWLEDGEMENTS

To God.

I foremost acknowledge the major efforts and contributions of my supervisors.

Thank you, Dr. Emilia, for giving me the opportunity to be your student and for allowing me the freedom to approach the Carajás puzzle in the way I wanted. I am especially grateful for your care, trust, and patience throughout this long challenge.

Heartfelt thanks and appreciation to Dr. Nigel, who welcomed and supported me over these past few years. Your dedication and guidance have been invaluable. Thank you for the countless revisions of drafts, your constant positivity, and your unwavering belief in the successful progress of the research, which would not have been possible without all those shared coffees that motivated me until the end.

My sincerest gratitude to my dear friend Dr. Cristi. Thank you for your genuine dedication to all your students. Your passion for understanding and solving problems made this journey an incredibly rewarding experience. The constant challenges to think and learn beyond my limits pushed me to achieve many of the ambitious goals of this work. This project would not have been possible without you and your belief that one day I could accomplish it.

I extend my gratitude to Dr. Kathy Ehrig for sharing your knowledge and expertise in ore mineralogy with Nigel's team, especially with Cristi and me. Thank you for giving us the opportunity to conduct this research. Your kind and resolute support and dedication to research have been a true inspiration in my life.

I would like to acknowledge the great work of the Adelaide Microscopy staff, with special thanks to Drs. Benjamin P. Wade, Sarah E. Gilbert, Ashley Slattery, Animesh Basak, and Nobuyuki Kawashima, who have consistently supported our analytical work and contributed in many valuable ways. I sincerely appreciate your assistance, and I am truly grateful for your dedication and willingness to help.

I thank CNPq and CAPES for supporting research in Brazil and promoting it globally, and for the CAPES PrInt program, which allowed me to complement this research in Australia.

To my dear friends, Naza, Gabi and Angel, thank for your companionship and support, that helped me stay strong through the toughest moments. I'm also deeply grateful to my colleagues and friends, Sam, Lucy, Jing, Sammy and Clara for welcoming me and being part of my experience in Adelaide. Thank you, Mariam, for all your support and company during our endless 'work parties', and special thanks to Robbie. One of my greatest joys since I came to Adelaide has been getting to know you, your support means so much to me. Thank you all! for the chance to have met and shared with you over the past years.

Last, but most important, I would like to express my gratitude to my family, for all their continuous love and support despite the distance. Your faith in me has been my pillar in all the challenges and adventures I wanted to pursue. To my mother, for all your endless blessings, I wouldn't be able to walk through this life if it weren't for you.

O presente trabalho foi realizado com apoio da Coordenação de Aperfeiçoamento de Pessoal de Nível Superior - Brasil (CAPES) – Código de Financiamento 001, e do Conselho Nacional de Desenvolvimento Científico e Tecnológico do Brasil CNPq.

PREFACE

This thesis comprises a portfolio of articles and manuscripts, which have been published or are under review in international peer-reviewed journals. The journals in which these articles are published or have been submitted to are *'American Mineralogist'* (**Chapter 2**, published), *'Minerals'* (**Chapter 3**, published), *'Mineralium Deposita'* (**Chapter 4**, submitted), *'Precambrian Research'* (**Chapter 5**, submitted), *'The Canadian Journal of Mineralogy and Petrology'* (**Chapter 6**, submitted), and *'American Mineralogist'* (**Chapter 7**, submitted). All 6 chapters summarise key findings and interpretations to be read as standalone contributions. Recommendations have been made in **Chapter 8**, as a direct result of the main outcomes of this research.

The two published articles, and four submitted manuscripts, which form the basis of this thesis are:

1. Campo-Rodríguez, Y.T., Ciobanu, C.L., Slattery, A., Cook, N.J., Schutesky, M.E., Ehrig, K., King, S.A., and Yao, J. (2024) Polysomatic intergrowths between amphiboles and non-classical pyriboles in magnetite: smallest-scale features recording a protracted geological history. American Mineralogist 109 (10): 1798–1818. https://doi.org/10.2138/am-2023-9188

2. Campo-Rodriguez, Y.T., Cook, N.J., Ciobanu, C.L., Schutesky, M.E., King, S.A., Gilbert, S., and Ehrig, K. (2024) Platinum Group Minerals Associated with Nickel-Bearing Sulfides from the Jatobá Iron Oxide-Copper-Gold Deposit, Carajás Domain, Brazil. Minerals 14, 757. https://doi.org/10.3390/min14080757

3. Campo-Rodriguez, Y.T.., Ciobanu, C.L., Cook, N.J., Schutesky, M.E., Ehrig, K., Slattery, A., Gilbert, S., King, S.A. (*in review, a*) Telescoped transition from trellis to silicate mottled magnetite records deep shear zone metamorphism in the IOCG deposit at Jatobá, Carajás, Brazil. Mineralogical Magazine.

4. Campo Rodriguez, Y.T., Ciobanu, C.L., Gilbert, S., Wade, B., Cook, N.J., Schutesky, M.E., and Ehrig, K. (*in review, b*) Coupled Lu-Hf and U-Pb apatite geochronology of Jatobá orebody supports ~2.5 Ga metamorphism in deep shear zones from Southern Copper Belt, Carajás Domain, Brazil. Precambrian Research.

5. Campo Rodriguez, Y.T., Ciobanu, C.L., Cook, N.J., Schutesky, M.E., Ehrig, K., Slattery, A., Gilbert, S., and King, S.A. (*in review, c*) Magnetite and REE-rich calcic amphibole provide evidence for a skarn-IOCG system at Onça Rosa, Jaguar Orefield, Carajás Mineral Province, Brazil. The Canadian Journal of Mineralogy and Petrology.

6. Campo Rodriguez, Y.T., Ciobanu, C.L., Cook, N.J., Slattery, A., Wade, B., Gilbert, S., Schutesky, M.E., and Ehrig, K. (*in review, d*) Arsenohauchecornite, ognitite, parkerite, and related minerals from Onça Rosa orebody, Carajás, Brazil: fingerprinting PGE signatures in hydrothermal Ni ores. American Mineralogist.

Chapter 9 contains supplementary material for all chapters outlined above, as well as additional material comprising co-authored publication abstracts, that have been produced during the Ph.D. candidature.

The supplementary material is as follows:

A. Supplementary material for Chapter 2 (American Mineralogist)
B. Supplementary material for Chapter 3 (Minerals)
C. Supplementary material for Chapter 4 (Mineralogical Magazine, *in review*)
D. Supplementary material for Chapter 5 (Precambrian Research, *in review*)
E. Supplementary material for Chapter 6 (The Canadian Journal of Mineralogy and Petrology, *in review*)
F. Supplementary material for Chapter 7 (American Mineralogist, *in review*)

Abstracts of co-authored articles:

G. King, S.A., Cook, N.J., Ciobanu, C.L., Ehrig, K., Campo Rodriguez, Y.T., Basak, A., and Gilbert, S. (2024) Coupled Microstructural EBSD and LA-ICP-MS Trace Element Mapping of Pyrite Constrains the Deformation History of Breccia-Hosted IOCG Ore Systems. Minerals, 14(2), 198. https://doi.org/10.3390/min14020198

H. King, S.A., Cook, N.J., Ciobanu, C.L., Ehrig, K., Rodriguez, Y.T.C., Gilbert, S., and Basak, A. (2024) EBSD mapping of Cu-Fe-sulfides reveal microstructures enriched in critical/precious metals and resolve deformation histories. American Mineralogist. https://doi.org/10.2138/am-2024-9396

I. Gezzaz, H., Ciobanu, C., Cook, N., Ehrig, K., Slattery, A., Wade, B., Gilbert, S., and Campo Rodriguez, Y.T. (Submitted). Monazite, lanthanide-rich glasses, and other trace elements in copper smelter slags: Constraints on critical metal behaviour in Si-Fe-rich melts. Mineralogy and Petrology

J. King, S.A., Cook, N.J., Ciobanu, C.L., Ehrig, K., Gilbert, S., Wade, B., and Rodriguez, Y.T.C. (Submitted) EBSD mapping of Cu-Fe-sulfides reveal microstructures enriched in critical/precious metals and resolve deformation histories. Mineralium Deposita.

The final chapter of this thesis (**Chapter 10**) consists of a complete reference list of all publications cited within any of the manuscripts, chapters and supplementary materials submitted as a component of this thesis.

PREFÁCIO

Esta tese compreende um portfólio de artigos e manuscritos, que foram publicados ou estão em revisão em periódicos internacionais revisados por pares. Os periódicos em que esses artigos foram publicados ou submetidos são '*American Mineralogist*' (**Capítulo 2**, publicado), '*Minerals*' (**Capítulo 3**, publicado), '*Mineralogical Magazine*' (**Capítulo 4**, submetido), *'Precambrian Research*' (**Capítulo 5**, submetido), *'The Canadian Journal of Mineralogy and Petrology*' (**Capítulo 6**, submetido) e *'American Mineralogist*' (**Capítulo 7**, submetido). Todos os 6 capítulos resumem as principais descobertas e interpretações para serem lidos como contribuições independentes. Recomendações foram feitas no **Capítulo 8**, como resultado direto dos principais resultados desta pesquisa.

Os dois artigos publicados e quatro manuscritos submetidos, que formam a base desta tese são:

1. Campo-Rodríguez, Y.T., Ciobanu, C.L., Slattery, A., Cook, N.J., Schutesky, M.E., Ehrig, K., King, S.A., and Yao, J. (2024) Polysomatic intergrowths between amphiboles and non-classical pyriboles in magnetite: smallest-scale features recording a protracted geological history. American Mineralogist 109 (10): 1798–1818. https://doi.org/10.2138/am-2023-9188

2. Campo-Rodriguez, Y.T., Cook, N.J., Ciobanu, C.L., Schutesky, M.E., King, S.A., Gilbert, S., and Ehrig, K. (2024) Platinum Group Minerals Associated with Nickel-Bearing Sulfides from the Jatobá Iron Oxide-Copper-Gold Deposit, Carajás Domain, Brazil. Minerals 14, 757. https://doi.org/10.3390/min14080757

3. Campo-Rodriguez, Y.T.., Ciobanu, C.L., Cook, N.J., Schutesky, M.E., Ehrig, K., Slattery, A., Gilbert, S., King, S.A. (*submitted*) Telescoped transition from trellis to silicate mottled magnetite records deep shear zone metamorphism in the IOCG deposit at Jatobá, Carajás, Brazil. Mineralogical Magazine.

4. Campo Rodriguez, Y.T., Ciobanu, C.L., Gilbert, S., Wade, B., Cook, N.J., Schutesky, M.E., and Ehrig, K. (*submitted*) Coupled Lu-Hf and U-Pb apatite geochronology of Jatobá orebody supports ~2.5 Ga metamorphism in deep shear zones from Southern Copper Belt, Carajás Domain, Brazil. Precambrian Research.

5. Campo Rodriguez, Y.T., Ciobanu, C.L., Cook, N.J., Schutesky, M.E., Ehrig, K., Slattery, A., Gilbert, S., and King, S.A. (*submitted*) Magnetite and REE-rich calcic amphibole provide evidence for a skarn-IOCG system at Onça Rosa, Jaguar Orefield, Carajás Mineral Province, Brazil. The Canadian Journal of Mineralogy and Petrology.

6. Campo Rodriguez, Y.T., Ciobanu, C.L., Cook, N.J., Slattery, A., Wade, B., Gilbert, S., Schutesky, M.E., and Ehrig, K. (*submitted*) Arsenohauchecornite, ognitite, parkerite, and related minerals from Onça Rosa orebody, Carajás, Brazil: fingerprinting PGE signatures in hydrothermal Ni ores. American Mineralogist.

O **Capítulo 9** contém material suplementar para todos os capítulos descritos acima, bem como material adicional composto por resumos de publicações co-autoradas, que foram produzidos durante a candidatura ao doutorado.

O material suplementar é o seguinte:

A. Material suplementar do Capítulo 2 (American Mineralogist)
B. Material suplementar do Capítulo 3 (Minerals)
C. Material suplementar do Capítulo 4 (Mineralium Deposita, *in review*)
D. Material suplementar do Capítulo 5 (Precambrian Research, *in review*)
E. Material suplementar do Capítulo 6 (Canadian Journal of Mineralogy and Petrology, *in review*)
F. Material suplementar do Capítulo 7 (American Mineralogist, *in review*)

Resumos de artigos co-autorados:

G. King, S.A., Cook, N.J., Ciobanu, C.L., Ehrig, K., Campo Rodriguez, Y.T., Basak, A., and Gilbert, S. (2024) Coupled Microstructural EBSD and LA-ICP-MS Trace Element Mapping of Pyrite Constrains the Deformation History of Breccia-Hosted IOCG Ore Systems. Minerals, 14(2), 198. https://doi.org/10.3390/min14020198

H. King, S.A., Cook, N.J., Ciobanu, C.L., Ehrig, K., Rodriguez, Y.T.C., Gilbert, S., and Basak, A. (2024) EBSD mapping of Cu-Fe-sulfides reveal microstructures enriched in critical/precious metals and resolve deformation histories. American Mineralogist. https://doi.org/10.2138/am-2024-9396

I. Gezzaz, H., Ciobanu, C., Cook, N., Ehrig, K., Slattery, A., Wade, B., Gilbert, S., and Campo Rodriguez, Y.T. (Submitted). Monazite, lanthanide-rich glasses, and other trace elements in copper smelter slags: Constraints on critical metal behaviour in Si-Fe-rich melts. Mineralogy and Petrology

J. King, S.A., Cook, N.J., Ciobanu, C.L., Ehrig, K., Gilbert, S., Wade, B., and Rodriguez, Y.T.C. (Submitted) EBSD mapping of Cu-Fe-sulfides reveal microstructures enriched in critical/precious metals and resolve deformation histories. Mineralium Deposita.

O capítulo final desta tese (**Capítulo 10**) consiste em uma lista de referências completa de todas as publicações citadas em qualquer um dos manuscritos, capítulos e materiais suplementares submetidos como componente desta tese.

CHAPTER 1

INTRODUCTION

CHAPTER 1: INTRODUCTION

One of the most fascinating yet enigmatic types of ore deposits are iron-oxide copper gold (IOCG) systems. IOCG mineralization is characterized by economic concentrations of Cu, and commonly also Au, in association with abundant Fe-oxides (magnetite and/or hematite) (Barton 2014; Skirrow 2022). Many IOCG ores also feature a marked enrichment in chalcophile-siderophile elements, including uranium and rare earths. The wide range of geological-tectonic settings for IOCGs includes orogenic, post-orogenic and continental margins, with many of the world's main IOCG provinces closely related to tectonothermal events within major fault systems (Skirrow 2022). Broadly, genetic schemes for IOCGs consider magmatic-hydrothermal processes that evolve from early Na ± Ca hydrothermal alteration, followed by combinations of Fe-, Ca- and K-rich minerals that precedes or accompanies Cu-Au mineralization, and which overprints the sodic alteration (Corriveau et al. 2016; Kontonikas-Charos et al. 2017; Verdugo-Ihl et al. 2020a).

The Carajás Mineral Province (CMP) is an Archean crustal segment in the south-eastern part of the Amazonian Craton, northern Brazil (Santos et al. 2000). It is one of the largest and oldest IOCG provinces on Earth. The CMP can be divided into two tectonostratigraphic domains that are separated by regional, E-W trending shear zones: the Carajás Domain (CD) to the north; and the Rio Maria Domain (RMD) to the south (Vasquez et al. 2008; Fig. 1). The two domains are distinct with respect to metallogeny. Older Mesoarchean lode-Au deposits in the RMD are hosted in >2.9 Ga granitoid-greenstone sequences (e.g., Costa et al. 2020). In contrast, the CD is characterized by two styles of mineralization: Neoarchean IOCG deposits and Paleoproterozoic Cu-Au-(polymetallic) deposits (Grainger et al. 2008).

The CD comprises a Mesoarchean basement with greenstone belts and tonalitic-tronhjemitic high-grade gneisses and migmatites of the Xingu Complex (e.g., Tavares et al. 2018; Costa et al. 2020). Cover rocks are made up by: Neoarchean volcano-sedimentary sequences of the Itacaiúnas

Supergroup, which includes the 2.76–2.85 Ga Salobo-Pojuca Group (Machado et al. 1991), the 2.74–2.76 Ga Grão Pará Group (e.g., Martins et al. 2017); and Paleoproterozoic siliciclastic units of the Águas Claras Formation (e.g., Araújo and Nogueira 2020). IOCG deposits in the CD are distributed along two major shear zones, the NW-SE Cinzento Shear Zone to the North and the E-W Canaã dos Carajás Shear Zone to the South, thus defining the Northern and Southern Copper belts, respectively (Xavier et al. 2012). Ore mineralogy is, nevertheless, relatively consistent throughout IOCG deposits with magnetite as the main iron-oxide, and chalcopyrite and/or bornite, as the main expression of Cu-enrichment (Schutesky and de Oliveira 2020).

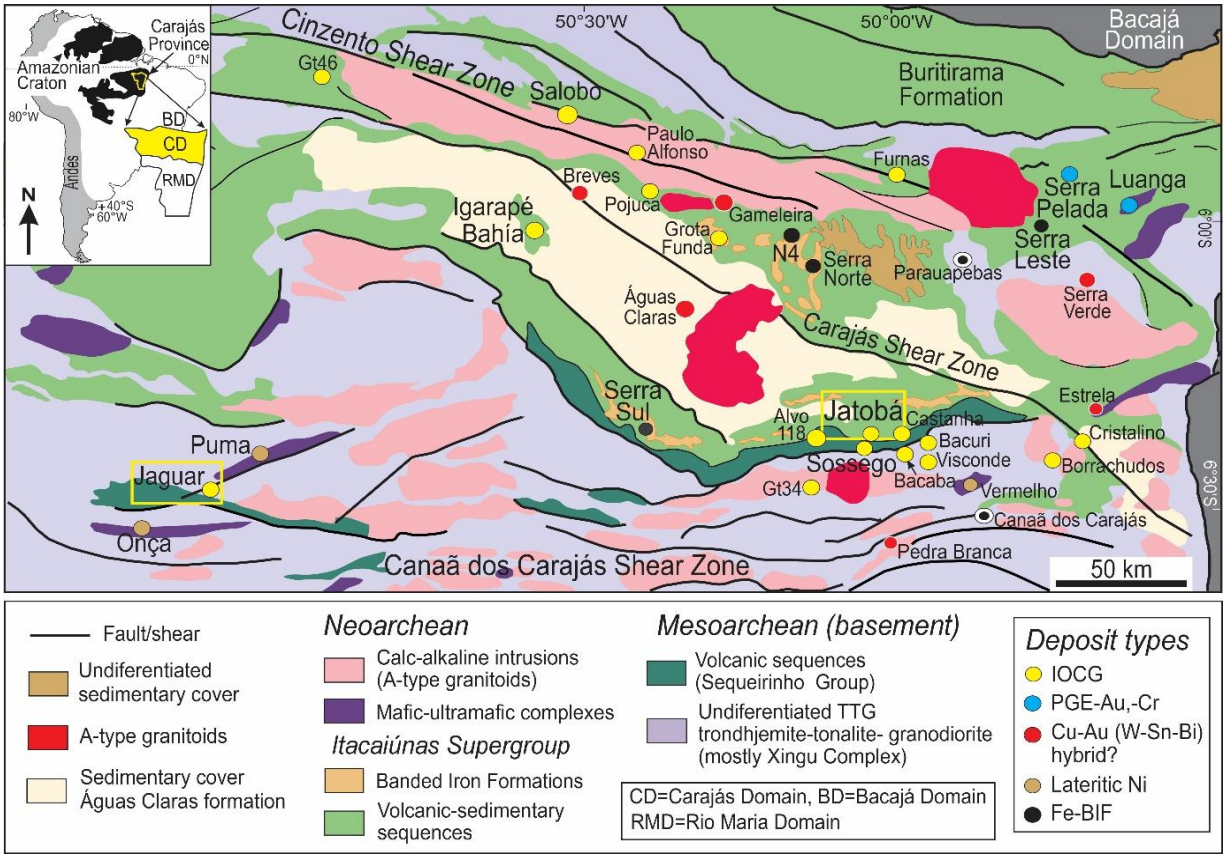

Figure 1. Geological map of the Carajás Domain showing main lithologies, fault zones and the location of main deposits, including the Jatobá and Jaguar deposits (yellow rectangles). Modified from Tavares et al. (2018). Deposit types are from Grainger et al. (2008) and Trunfull et al. (2020). The inset shows the location of the Carajás Domain within the Amazonian Craton, South America.

The location of IOCG deposits along such major strike-slip systems and multiple episodes of hydrothermal alteration and/or remobilization events (i.e. at 2.72-2.68 Ga, 2.56-2.45 Ga and 1.88 Ga; Trunfull et al. (2020) and references therein) contributes to the complexity encountered when

developing a generalised genetic model for IOCG system in the CD. Existing metallogenetic interpretations are largely based on geochronological data (e.g., Monteiro et al 2008; Moreto et al. 2015a, b; Schutesky and de Oliveira 2020; Teixeira et al 2021; Toledo et al. 2024), with scant attention often paid to the relationship between gangue- and ore minerals. Moreover, detailed characterization of Fe-oxides or apatite, both key minerals from the early hydrothermal stage of these deposits, is often absent.

Salobo, the largest IOCG deposit in the northern part of the CD is considered to have been formed at ~2.5 Ga (e.g., Melo et al. 2017), whereas geochronological study of the archetypal deposits in the southern belt, Sequeirinho and Sossego, yielded mineralization ages at ~2.7 Ga and ~2.0 Ga, respectively (Moreto et al. 2015a). In both cases, late hydrothermal activity and overprinting due to shear zone reactivation were identified but the link between mineralization stages and the main tectonic-magmatic events from the Neoarchean to Paleoproterozoic remains poorly constrained or debateable.

Further complexity in the metal endowment and evolution of the IOCG ores is shown by atypical Ni-enrichment accompanying the Fe-oxides in two of the deposits spatially related to the Canaã dos Carajás shear zone: Jaguar and Jatobá. Both have been considered to represent the deeper parts (IOA) of the IOCG system in the Carajás Domain (Veloso et al. 2020; Ferreira Filho et al. 2021; Mansur et al. 2023). The Jatobá deposit features copper-(nickel) mineralization defined by the presence of chalcopyrite and pyrrhotite and is characterized by pervasive scapolite alteration, high volumes of magnetite and apatite, and a chemical signature featuring enrichment in Cu-(Ni) and Ti-V (Veloso et al. 2020). In contrast, the Jaguar deposit is interpreted as an unusual hydrothermal Ni deposit with pyrite, pentlandite and millerite associated with magnetite-apatite rich bodies (Ferreira Filho et al. 2021; Mansur et al. 2023). Open questions raised include whether these two systems, which share some common features yet differ in others, could represent different expressions of the same deep-rooted Ni-hydrothermal system?

Magnetite is a major mineral common to all IOCG deposits in the CD and is present throughout all hydrothermal evolution stages. Diverse magnetite textures, often reflecting distinct chemical compositions, can signify multiple stages of overprinting and/or origins of ore-forming fluids, e.g., early magmatic and hydrothermal processes, multiple vein generations, fluid/rock interaction, and various stages of alteration and overprinting (e.g., Ciobanu et al. 2019; Courtney-Davies et al. 2020b; Verdugo-Ihl et al. 2021). The most typical and less common magnetite features identified in IOCG mineralization include mineral inclusions, oscillatory zoning, re-equilibration reactions, such as oxy-exsolution, coupled dissolution-reprecipitation, and/or recrystallization (e.g., Ciobanu et al. 2019; Huang and Beaudoin 2019; Courtney-Davies et al. 2020b). Various, and often contradictory magnetite textures can consequently make it difficult to attribute any specific texture to a single set of physio-chemical conditions (Courtney-Davies et al. 2020b).

Textural features and detailed characterization of iron oxides (both magnetite and hematite) from the meso- to nanoscale have led to meaningful interpretations of ore evolution and associated alteration in IOCG systems of South Australia (Verdugo-Ihl et al. 2017, 2020a, 2020b). Moreover, the presence of U and Pb in the lattice of iron oxides facilitated the development of U-Pb iron oxide geochronology as a tool to directly provide an age for mineralization Courtney-Davies et al. 2019a, 2019b, 2020a, 2020b, 2021). The inclusions preserved as nanoscale inclusions in Fe-oxides are valuable petrogenetic indicators capable of providing additional criteria to discriminate between a wide range of formation scenarios (Ciobanu et al. 2019; Verdugo-Ihl et al. 2021).

If coupled with careful textural and compositional characterisation at the micron-scale, nanoscale analysis has been used to solve petrogenetic questions of ore deposit evolution. For instance, Ciobanu et al. (2019) documented ‘silician magnetite’ from the outer shell of the Olympic Dam deposit using high angle annular dark field scanning transmission electron

microscopy (HAADF STEM). Nanoinclusions of discrete minerals, including (ferro)actinolite, diopside and epidote, represent the otherwise poorly preserved alkali-calcic alteration in the deposit.

With the exception of work by Huang (Huang and Beaudoin 2019; 2021; Huang et al. 2022), no previous published study has addressed the mineralogical and element deportment at the nanoscale in magnetite from any deposit from Carajás. Expression of nickel enrichment within the IOCG systems, despite its major economic significance, also remains poorly constrained. This thesis therefore aims to couple these two important research gaps and addresses the petrographic features of magnetite and associated minerals at the micron- to nanoscale, correlating mineral textures with trace element endowment to constrain ore genesis and evolution. One key aspect of this work was to determine the origin of the Ni-bearing IOCG ores closely associated with magnetite from the Jatobá deposit and the Onça Rosa orebody (Jaguar orefield). This research also aimed to advance understanding of the ore formation conditions and contribute to genetic models for the two IOCG systems, and thus add new insights into the Carajás Domain as a complex and enigmatic metallogenic province. Outcomes also constraint the unusual Ni-enrichment and occurrence of platinum group elements (PGE) and platinum group minerals (PGM) in deposits of the broader IOCG clan, opening a new window for exploration in less conventional geological environments.

1.1. Research objectives and structure

The research reported in this thesis aimed to address key questions regarding the ore formation and evolution of the unusual Ni-bearing IOCG-style mineralization in the Jatobá prospect and Onça Rosa orebody. The broad objective was to characterize magnetite, sulphides, gangue silicates, accessory minerals, and where present and associated with magnetite also apatite, in

these ore systems. Emphasis was placed on the integrated study of micro- to nano-scale textures with geochemical-isotopic signatures, using an innovative analytical approach that spanned the micron- and nanoscale. These techniques included conventional petrography using reflected light optical microscopy, scanning electron microscopy (SEM) in back scatter electron imaging mode, automated mineralogy mapping, cathodoluminescence imaging, compositional major element analysis via electron probe microanalysis, mineral specific trace element analysis and chemical mapping by laser ablation inductively coupled plasma mass spectrometry, and dedicated nanoscale analysis using high angle annular dark field scanning transmission electron microscopy on thinned foils extracted from the sample surface on a focussed ion beam SEM platform. For Jatobá, this characterization was complemented by apatite geochronology using both U-Pb and Lu-Hf systems.

The main body of this thesis comprises six chapters (**Chapters 2** to **7**), each of which is a stand-alone published paper or submitted manuscript designed to be read independently. All are, however, interlinked by a common theme: mineralogy, mineral/isotopic chemistry and nanoscale features to constrain the genesis and evolution of mineralization. The first two chapters (**Chapters 2** and **3**) were published during the Ph.D. candidature, whereas **Chapters 4** to **7** are under review by the respective journals at the time of thesis submission. This thesis can be divided into two parts: (i) mineral characterisation of magnetite-apatite and sulphides ores, and deposit evolution of Jatobá (**Chapters 2** to **5**), and (ii) mineralogy of magnetite-apatite-amphibole and geochemical signatures of Ni-bearing sulphides from Onça Rosa orebody (**Chapters 6** and **7**).

Chapter 2 (Campo-Rodriguez et al. 2024a) documents nanoscale inclusions hosted by magnetite from the Jatobá deposit. These include some of the most spectacular examples of polysomatic intergrowths between amphiboles and non-classical pyriboles (NCP) that have ever been reported. A formulae $nI_{beam} = T(2 + n) = C(5 + 3n) = A(1 + n)$, n = integer, is proposed to define the increase in the number of *C* and *A* cations from amphibole ($2\text{-}I_{beam}$) to n chain silicates

(nI_{beam}). Empirical crystal structure models, supported and validated by STEM simulations, were created to illustrate the 4- and 5 I_{beam} chain silicates. Two chemical populations of amphiboles hosting NCPs, Mg-(Fe)- and Ca-(Al)-amphiboles, support a multi-stage evolution for Jatobá magnetite. Among these, clinojimthompsonite and Ce-bearing Mg-hornblende are observed for the first time within magnetite. The Ce-bearing species are considered to indicate influx of IOCG-related fluids at the onset of mineralization, while the results of (ferro)tschermakite geobarometry (~7.5 kbar) reveal high-pressure shearing at the time of main ore deposition.

Chapter 3 (Campo-Rodriguez et al. 2024b) comprises a detailed mineralogical and geochemical study of the Jatobá sulphide ores that reveals not only the distribution of Ni in the ore but also the presence of PGE, with major implications for ore genesis models. Pyrite is the main Ni carrier with measurable concentrations of both palladium (Pd) and platinum (Pt) noted. For the first time, several platinum group minerals (PGM) are reported including merenskyite, naldrettite, sudburyite, kotulskite, sperrylite, and borovskite. Differences in sulphide chemistry between the magnetite-hosted ore and magnetite-stringer mineralization, further support a two-stage genetic model for Jatobá, either as IOCG-style mineralization superimposed onto a pre-existing VHMS-like assemblage, possibly during the retrograde stage of a syn-deformational metamorphic event, or alternatively, via leaching of Ni and PGE from ultramafic rocks in the basement by the IOCG-type fluids.

Chapter 4 (Campo-Rodriguez et al. *in review, a*) returns to the information in Jatobá magnetite and defines two textural and geochemical distinct types: ‘trellis’ magnetite from host lithologies and ‘silicate-mottled’ magnetite in the ore. Minor element geochemical signatures change from Ti, Cr, Co, and Mn in trellis magnetite to a pronounced enrichment of rare earths and other lithophile elements in the mottled type. The telescoped transition from trellis to silicate-mottled magnetite is recorded by textural changes of ilmenite from trellis to blebby and patchy. Syn-metamorphic deformation textures include magnetite+apatite as pods, banding and folds, as

well pressure shadows surrounding magnetite. P-T conditions were estimated from Al-in-hornblende ferrotschermakite geobarometry (6.4–7.4 kbar) from host rock, and ilmenite-magnetite nano-thermobarometry (414–728 °C and logfO_2 values -31 to -12). Together, the new data supports a two-stage genetic model concordant with deep shear zone metamorphism.

Chapter 5 (Campo-Rodriguez et al. *in review, b*) expands on several of the themes in earlier chapters with a petrochronological characterization of apatite from Jatobá deposit. In tandem with conventional U-Pb geochronology, the study employs the recently developed Lu-Hf LA-ICP-MS geochronometer (Simpson et al. 2021). Chlorine-rich signatures confirm a primary igneous origin for basalt-hosted apatite, in which REE-rich and syn-metamorphic deformed cores record a ~2.5 Ga Lu-Hf age. A second ~2 Ga age related to a late overprint is obtained from apatite grains with a partially re-equilibrated U-Pb system. The relative timing of apatite with distinct textural and geochemical signatures counter previous genetic models in which a ~2.6-2.5 tectonothermal event appeared restricted to IOCG deposits from the north of the Carajás Domain. These new results carry implications well beyond questions of ore genesis at Jatobá and Jaguar and, hint at a model in which deposits formed along the Canaã dos Carajás Shear Zone in the south may be linked to the same activation event as those located along the Cinzento Shear zone in the north.

Chapter 6 (Campo-Rodriguez et al. *in review, c*) is focused on detailed micron- to nanoscale petrography and geochemistry of magnetite and calcic-amphiboles from the granite-hosted Onça Rosa orebody in the north of the Jaguar orefield. Unlike Jatobá, magnetite from Onça Rosa is associated with sphalerite instead of apatite. Some textures are analogous to those observed in Jatobá, including brecciation, deformation and mottled inclusion-rich cores. Cummingtonite, with NCP intergrowths, is also observed, albeit both simpler and less disordered and without any spatial relationship with calcic amphiboles. Silician magnetite is documented for the first time in magnetite from the CD. Relationships between the talc-chlorite groundmass and amphibole indicate multiple stages of shear during which small-scale remobilization of sulfide occurred.

Basis on the observed features, Onça Rosa is considered to represent an atypical 'hybrid' Fe-Zn-Ni skarn system that evolved from early magnesian (magnetite+sphalerite) to late calcic (amphibole+pentlandite) consistent with the location of mineralization at the contact between the ultramafic Serra do Puma layered complex and a granite-derived hydrothermal source. Superimposed IOCG-style mineralization is recorded by the high concentrations of REY in amphibole precipitated together with accessory uraninite.

Chapter 7 (Campo-Rodriguez et al. *in review, d*) is an account of the ore mineralogy of the Ni-rich sulphide mineralization at Onça Rosa. The work describes scarce Ni-Bi-minerals not previously reported from the CD, including arsenohauchecornite, parkerite and the second-world occurrence of ognitite, and documents the presence of nanoscale platinum group minerals using HAADF STEM methods. This chapter also describes the presence of bismuth tellurides and Pb-Bi sulfosalts such as Ag-bearing lillianite and heyrovskýite, as well as the trace element chemistry of the host common sulphides. Crystal structure models and simulations of arsenohauchecornite verify the I-centered, tetragonal superstructure described previously. Compositional data confirm a solid solution between melonite and ognitite, and show the presence of measurable Pd in this mineral. Pentlandite records replacement via dissolution-reprecipitation reactions with local remobilization and reprecipitation of metals at the micro-scale. Fluid pathways within pentlandite are host to nanoscale moncheite, volynskite, hessite, altaite, tellurobismuthite and tsumoite. The observed assemblages and inferred reactions are consistent with the genetic model outlined in **Chapter 6**.

Chapter 8 provides a brief summary of the key findings and implications of the research. The chapter also highlights questions that remain open and discusses potential directions for future investigation.

Chapter 9 compiles additional material, including Supplementary Material relating to **Chapters 2** to **7**, as well as co-authored publications made during this candidature. A complete reference list for all chapters is provided in **Chapter 10**.

1.2. Introdução

Um dos tipos de depósitos de minério mais fascinantes e enigmáticos, são os depósitos de óxido de ferro–cobre–ouro (IOCG) e os sistemas afiliados ricos em magnetita tipo óxido de ferro-apatita (IOA). A mineralização é caracterizada por concentrações econômicas de Cu-Au associadas a abundantes óxidos de Fe e um enriquecimento único em elementos calcófilos-siderófilos, incluindo U e elementos de terras raras (Barton 2014; Skirrow 2022). De maneira geral, os esquemas genéticos consideram processos magmáticos-hidrotermais que evoluem a partir da alteração hidrotermal inicial de Na±Ca, seguidos por associações de minerais ricos em Fe, Ca e K, que precedem ou acompanham a mineralização de Cu-Au e que sobrepõem a alteração sódica (Corriveau et al. 2016; Kontonikas-Charos et al. 2017; Verdugo-Ihl et al. 2020a). A extraordinária ampla gama de ambientes geológico-tectônicos inclui orogênicos, pós-orogênicos e margens continentais, com muitas das principais províncias IOCG do mundo estreitamente relacionadas a eventos tectonotermais dentro de grandes sistemas de falhas (Skirrow 2022).

A Província Mineral de Carajás (PMC), é uma das maiores e mais antigas províncias IOCG do mundo, essa representa um segmento crustal Arqueano localizado na parte sudeste do Cráton Amazônico, no norte do Brasil (Santos et al. 2000). A PMC se divide em dois domínios tectonoestratigráficos separados por zonas de cisalhamento regionais com tendência E-O: o Domínio Carajás (DC) ao norte; e o Domínio Rio Maria (DRM) ao sul (Vasquez et al. 2008; Fig. 1). A metalogenia é distinta entre os dois domínios: no DRM ocorrem depósitos de Au hospedados em terrenos granito-gnáissicos e sequências tipo greenstone, de idades superiores 2,9 Ga (e.g., Costa et al. 2020). Em contraste, o DC é caracterizado por dois estilos de mineralização: depósitos IOCG neoarqueanos e depósitos polimetálicos Cu-Au paleoproterozoicos (Grainger et al. 2008).

O Domínio Carajás (DC) é composto por um embasamento Mesoarqueano composto por sequências greenstones e terrenos tonalítico-trondhjemíticos, gnaisses e migmatitos do Complexo Xingu (e.g., Tavares et al. 2018; Costa et al. 2020). O embasamento apresenta uma cobertura de: sequências vulcano-sedimentares Neoarqueanas do Supergrupo Itacaiúnas, que incluem os Grupos Salobo-Pojuca de 2,76–2,85 Ga (Machado et al. 1991) e o Grupo Grão Pará de 2,74–2,76 Ga (e.g., Martins et al. 2017); e unidades siliciclásticas Paleoproterozoicas da Formação Águas Claras (e.g., Araújo e Nogueira 2019). Os depósitos IOCG no DC estão distribuídos ao longo de duas grandes zonas de cisalhamento: a zona WN-ES Cinzento ao norte, e a zona E-O Canaã dos Carajás ao sul, que conformam os cinturões cupríferos norte e sul, respectivamente (Xavier et al. 2012). A mineralogia dos minérios é, no entanto, relativamente consistente ao longo dos depósitos IOCG, com a magnetita como principal óxido de ferro e calcopirita como principal expressão de enriquecimento em Cu (Schutesky e de Oliveira 2020).

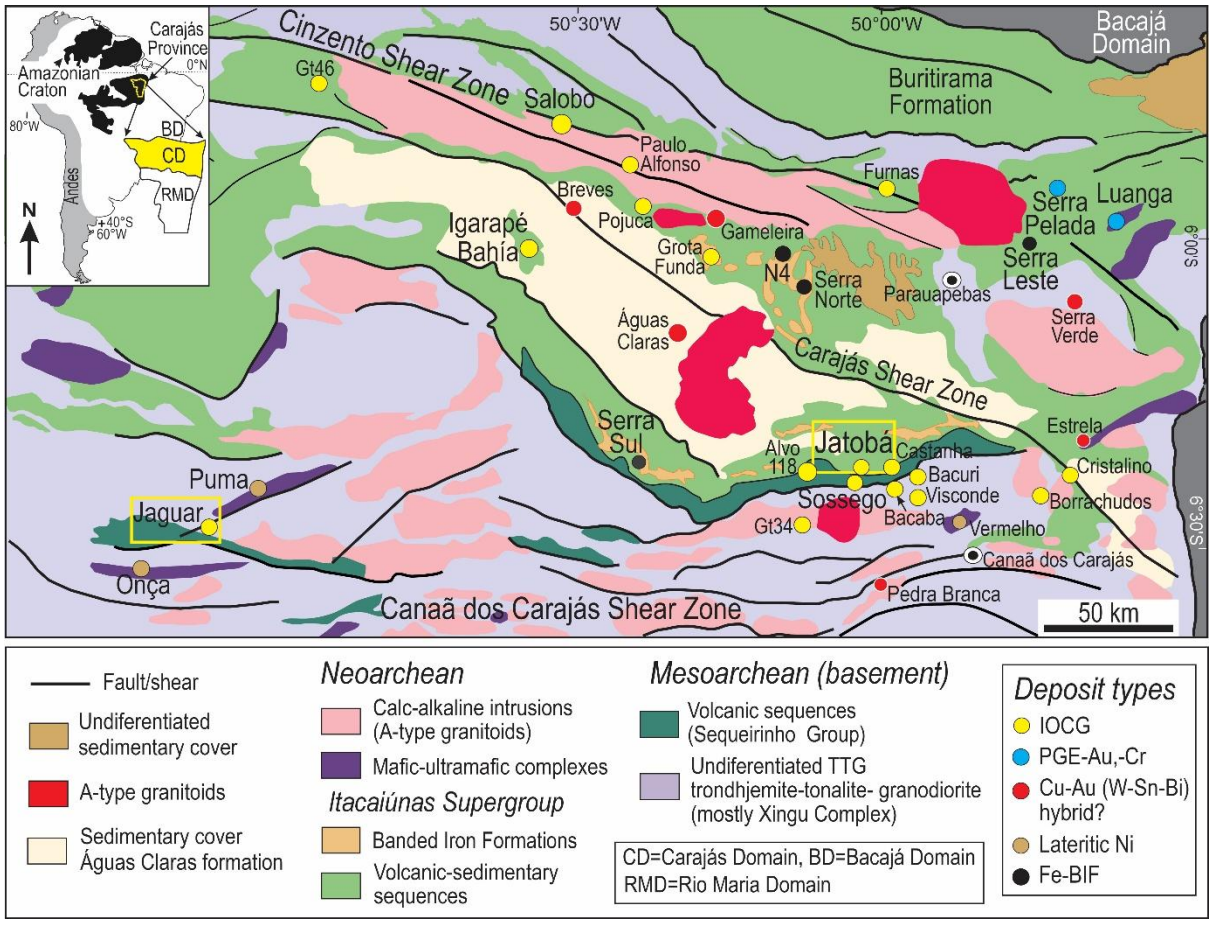

Figura 1. Mapa geológico do Domínio Carajás mostrando as litologias, zonas de falhas e a localização dos principais depósitos, incluindo o Jatobá e Jaguar (retângulos amarelos). Modificado de Tavares et al. (2018). Os tipos de depósito de Grainger et al. (2008) e Trunfull et al. (2020). O mapa incluso apresenta a localização do Domínio Carajás dentro do Cráton Amazônico, América do Sul.

A localização dos depósitos IOCG ao longo de grandes sistemas de cisalhamento e os múltiplos episódios de alteração hidrotermal e/ou eventos de remobilização (i.e., 2,72-2,68 Ga, 2,56-2,45 Ga e 1,88 Ga; Trunfull et al. (2020) e referências ali citadas) demonstram a complexidade para o estabelecimento de um modelo genético geral para o sistema IOCG do Domínio Carajás. As interpretações metalogenéticas existentes são baseadas quase que exclusivamente em dados geocronológicos (e.g., Monteiro et al. 2008; Moreto et al. 2015a, b; Schutesky e de Oliveira 2020; Teixeira et al. 2021; Toledo et al. 2024), com pouca atenção dada à relação entre minerais de ganga e desprovido de caracterizações detalhadas dos óxidos de Fe ou da apatita, minerais-chave do estágio hidrotermal inicial nesse tipo de depósitos. Por exemplo, o depósito Salobo, o maior depósito IOCG localizado na parte norte do DC, foi considerado de idade de ~2,5 Ga (e.g., Melo et al. 2017), enquanto os depósitos arquétipos do cinturão sul, Sequeirinho e Sossego, apresentaram idades de mineralização em ~2,7 Ga e ~2,0 Ga, respectivamente (Moreto et al., 2015a). Em ambas as localidades, foram identificados estágios tardios de atividade hidrotermal e sobreposição de eventos devido à reativação de zonas de cisalhamento, mas a conexão entre os estágios de mineralização e os principais eventos tectônicos-magmáticos do Neoarqueano ao Paleoproterozoico permanece pouco abordada.

Uma complexidade adicional na ocorrência dos metais e na evolução do minério IOCG é evidenciada pelo enriquecimento atípico em Ni que acompanha os óxidos de Fe em depósitos espacialmente relacionados à zona de cisalhamento Canaã dos Carajás, os depósitos Jaguar e Jatobá. Ambos foram interpretados como as partes mais profundas (IOA) do sistema IOCG no Domínio Carajás (Veloso et al. 2020; Ferreira Filho et al. 2021; Mansur et al. 2023). O depósito Jatobá, foi definido como uma mineralização de cobre-(níquel) com calcopirita-pirrotita, é caracterizado por uma alteração pervasiva de escapolita, altos teores de magnetita-(apatita) e uma assinatura química enriquecida em Cu-(Ni) e Ti-V (Veloso et al. 2020). Em contraste, o depósito Jaguar foi interpretado como um inusual depósito hidrotermal de Ni, com pirita, pentlandita e milerita associados a corpos ricos em magnetita-apatita (Ferreira Filho et al. 2021; Mansur et al.

2023). Outras considerações foram apresentadas, como a possibilidade de ambos representarem expressões semelhantes de um só sistema hidrotermal de Ni de raízes profundas.

A magnetita é tipicamente um mineral majoritário comum a todos os depósitos IOCG no Domínio Carajás e está presente em todos os estágios de evolução hidrotermal desses sistemas. A diversidade de texturas de magnetita reflete diferentes composições químicas e, portanto, pode registrar múltiplos estágios de sobreposições e/ou origens dos fluidos formadores de minério, assim como processos magmáticos e hidrotermais iniciais, múltiplas gerações de veios, interações fluido/rocha, várias fases de alteração/sobreposição e intemperismo secundário (e.g., Verdugo-Ihl et al. 2021; Courtney-Davies et al. 2020b).

As características mais típicas e menos comuns da magnetita observadas na mineralização do tipo IOCG abarcam inclusões minerais, zoneamento oscilatório, reações de reequilíbrio, como oxi-exsolução, dissolução-reprecipitação e/ou recristalização (Courtney-Davies et al. 2020b). A variedade, e frequentemente a sobreposição, das texturas da magnetita podem, portanto, dificultar a atribuição de uma textura a condições físico-químicas específicas (Courtney-Davies et al. 2020b). Essas texturas, juntamente com caracterizações detalhadas em escala meso à nanométrica, têm contribuído com interpretações significativas da evolução do minério e da alteração associada, da fonte de metais e da nova geocronologia de óxidos de ferro aplicada a sistemas IOCG, especialmente aqueles formados nas fases hidrotermais iniciais da formação de minério (Ciobanu et al. 2019; Courtney-Davies et al. 2019a, b; 2020a, b; 2021; Verdugo-Ihl et al. 2020a; b; 2021). Além disso, inclusões nanominerais em óxidos de Fe são indicadores petrogenéticos valiosos que podem fornecer critérios adicionais para discriminar entre uma ampla gama de cenários de formação.

A aplicação de análises em escala nanométrica por microscopia eletrônica de transmissão (TEM), incluindo varredura de campo escuro anular de alto ângulo (HAADF) - S/TEM, tem sido usada para resolver questões petrogenéticas sobre a evolução de depósitos de minério. Por exemplo, Ciobanu et al. (2019) documentaram a "magnetita enriquecida em silíca" na parte

externa do depósito Olympic Dam usando HAADF STEM, a magnetita com textura mosqueada e uma ampla gama de inclusões nanominerais, incluindo (ferro)actinolita, diopsídio e epídoto, minerais que caracterizam a alteração alcali-cálcica mal preservada no depósito. Assim, as inclusões de nanominerais em óxidos de Fe servem como indicadores petrogenéticos valiosos, oferecendo informações adicionais para uma ampla gama de cenários de formação. Com exceção dos trabalhos iniciais (Huang e Beaudoin 2019; 2021; Huang et al. 2022), nenhum estudo publicado anteriormente abordou a mineralogia e o comportamento de elementos em escala nanométrica na magnetita de nenhum depósito de Carajás. A ocorrência de enriquecimento em Ni nos sistemas IOCG, apesar de sua significativa importância econômica, também permanece pouco compreendida.

Esta tese tem como objetivo abordar uma importante lacuna de pesquisa relacionada às características petrográficas da magnetita e minerais accesórios associados nas escalas micrométrica a nanométrica, correlacionando texturas minerais com o comportamento de elementos menores e traço para compreender a gênese e evolução do minério. Um aspecto importante deste trabalho foi determinar a origem dos excepcionais minérios IOCG portadores de Ni, intimamente associados à magnetita no depósito Jatobá e no corpo de minério Onça Rosa (dentro do sistema mineral de Jaguar). Esta pesquisa também buscou contribuir para o entendimento das condições de formação de minério e os modelos genéticos dos sistemas IOCG. Os resultados indubitavelmente fornecem novas perspectivas sobre a complexidade indefinida do Domínio Carajás, com contribuições também sob o não usual enriquecimento em Ni e a ocorrência de minerais do grupo da platina em depósitos IOCG, abrindo uma nova perspectiva para exploração em ambientes geológicos não convencionais.

1.3. Objetivos e estrutura

A pesquisa relatada nesta tese teve como objetivo abordar questões-chave relacionadas à formação e evolução dos depósitos/corpos de minério inusuais do tipo IOCG enriquecidos com Ni, Jatobá e Onça Rosa, por meio do estudo integrado das assinaturas geoquímicas-isotópicas vinculadas a texturas de minério em escalas micro a nanométricas. O objetivo geral deste projeto foi caracterizar a magnetita e minerais acessórios associados que caracterizam os sistemas IOCG, incluindo o mineral de ganga dominante (apatita) e minerais de minério (sulfetos de Cu-Fe-Ni). A abordagem analítica compreendeu técnicas microanalíticas avançadas para caracterização em escalas micrométrica a nanométrica. Essas técnicas envolveram petrografia convencional de microscopia óptica de luz refletida e microscopia de elétrons retro espalhados (BSE), mapeamento com mineralogia automatizada (AM), catodoluminescência (CL), análise composicional via EPMA e LA-ICP-MS, geocronologia usando os sistemas isotópicos de U-Pb e Lu-Hf, e análise dedicada em escala nanométrica empregando FIB (Feixe de Íons Focado) e HAADF S/TEM.

O corpo principal desta tese é composto por seis capítulos (**Capítulos 2** a **7**), que são manuscritos independentes que podem ser lidos separadamente. Todos estão, no entanto, interligados por um tema comum: mineralogia, química mineral/isotópica e características em escala nanométrica para caracterizar a gênese e a evolução da mineralização. Os dois primeiros capítulos (**Capítulos 2** e **3**) foram publicados durante a candidatura de doutorado, enquanto os **Capítulos 4** a **7** estavam em revisão no momento da submissão da tese. Esta tese pode ser dividida em duas partes: (i) caracterização mineral do minério de magnetita-apatita e sulfetos, e evolução do depósito de Jatobá (**Capítulos 2** a **5**), e (ii) mineralogia de magnetita-apatita-anfibólio e assinaturas geoquímicas de sulfetos de Ni do corpo de minério Onça Rosa (**Capítulos 6** e **7**).

O **Capítulo 2** (Campo-Rodriguez et al. 2024a) mostra inclusões nano-escala em magnetita do depósito de Jatobá, com os mais incríveis intercrescimentos polissomáticos entre anfibólios e piribólios não-clássicos (NCP) reportados até o momento. Propõe a fórmula $nI_{beam} = T(2 + n) = C(5 + 3n) = A(1 + n)$, n = inteiro, para definir o aumento no número de cátions C e A de anfibólios ($2\text{-}I_{beam}$) para silicatos de cadeia n (nI_{beam}). Ilustra silicatos de cadeia 4- e $5\text{-}I_{beam}$ mediante modelos empíricos de estrutura cristalina validados por simulações STEM. Uma evolução multiestágio da magnetita de Jatobá é suportada por duas populações químicas de anfibólios com NCPs, Mg-(Fe)- e Ca-(Al)-anfibólios, entre os quais, clinojimthompsonita e Mg-hornblenda rica em Ce são observadas pela primeira vez como inclusões na magnetita. O anfibólio rico em Ce sugere fluidos do tipo IOCG no início da mineralização, e a formação da (ferro)tschermakita a ~7,5 kbar indica uma alta pressão associada a um cisalhamento durante a principal deposição de minério.

O **Capítulo 3** (Campo-Rodriguez et al. 2024b) compreende um estudo detalhado da mineralogia e geoquímica dos sulfetos de Jatobá, revelando mineralização de Ni e PGE com implicações para a compreensão da gênese do minério. A pirita é o principal portador de Ni, com concentrações mensuráveis de paládio (Pd) e platina (Pt). Pela primeira vez, vários minerais do grupo da platina (PGM) são reportados em Jatobá, entre eles merenskyita, naldrettita, sudburyita, kotulskita, sperrylita e borovskita. As diferenças químicas dos sulfetos hospedados em magnetita e os de tipo bandados, suportam ainda mais um modelo genético em duas fases para Jatobá: como mineralização do tipo IOCG sobreposta a uma associação pré-existente do tipo VHMS, possivelmente durante o estágio retrógrado de um evento metamórfico sin-deformacional; ou lixiviação de Ni e PGE de rochas ultramáficas no embasamento por fluidos do tipo IOCG.

O **Capítulo 4** (Campo-Rodriguez et al. *in review, a*) definiu dois tipos textural e geoquimicamente distintos para a magnetita de Jatobá: magnetita 'treliça' das rochas encaixantes e a magnetita 'manchada de silicato' do minério. As assinaturas geoquímicas mudam de Ti, Cr,

Co e Mn na magnetita treliça para um enriquecimento pronunciado de terras raras e outros elementos litófilos no tipo mosqueado. A transição telescópica da magnetita treliça para a mosqueada de silicato é registrada por mudanças texturais das inclusões de ilmenita, de treliça a "blebby" e irregular. Texturas de deformação sin-metamórfica incluem magnetita+apatita em cápsulas (pods), bandamento e dobras, bem como sombras de pressão em torno da magnetita. As condições P-T foram estimadas a partir da geobarometria Al-em-hornblenda da ferrotschermakita (6,4 – 7,4 Kbar) em rocha encaixante e nano-termometria ilmenita-magnetita (414–728 °C, log*f*O2 -12 a -31). Os dados em conjunto suportam um modelo genético de duas etapas concordante com o metamorfismo de zona de cisalhamento profundo.

O **Capítulo 5** (Campo-Rodriguez et al. *in review, b*) apresenta um contexto geológico do Domínio Carajás para a caracterização petrocronológica de apatita do depósito de Jatobá por datação LA-ICP-MS de U-Pb e Lu-Hf. As assinaturas ricas em Cl confirmam uma origem ígnea primária para a apatita hospedada em basaltos, da qual núcleos deformados e ricos em elementos das terras raras registram uma idade Lu-Hf de ~2,5 Ga. Uma segunda idade de ~2 Ga relacionada a uma superimposição tardia é obtida de grãos de apatita com um sistema U-Pb parcialmente reequilibrado. O tempo relativo da apatita com distintas assinaturas texturais e geoquímicas contradiz modelos genéticos anteriores que mostram um evento tectônico de ~2,6-2,5 Ga restrito aos depósitos IOCG do norte do Domínio Carajás. Os resultados mostram que os depósitos formados ao longo da Zona de Cisalhamento Canaã dos Carajás (ao sul) estão temporalmente relacionados ao mesmo evento de ativação de tectónica registrado em depósitos da zona de Cisalhamento Cinzento (ao norte).

O **Capítulo 6** (Campo-Rodriguez et al. *in review, c*) foca na petrografia e geoquímica detalhada em micro e nano escala da magnetita e anfibólios cálcicos do corpo de minério Onça Rosa. Ao contrário de Jatobá, a magnetita de Onça Rosa está associada a esfalerita em vez de

apatita, enquanto a ilmenita se apresenta com pentlandita, em vez da magnetita. No entanto, texturas análogas incluem brechação, deformação e núcleos de magnetita ricos em inclusões (tipo mosqueada). Também se observa cummingtonita com intercrescimentos de NCP, embora sem relação espacial com anfibólios cálcicos. A magnetita silícica é documentada pela primeira vez em depósitos do Domínio Carajás. As relações texturais entre talco-clorita e os anfibólios apontam para múltiplas etapas de cisalhamento durante as quais ocorreu uma remobilização em pequena escala de sulfetos. Onça Rosa é considerado um sistema 'híbrido' do tipo skarn Fe-Zn-Ni atípico, evoluindo da deposição inicial do Mg skarn (magnetita+esfalerita) para o skarn cálcico (anfibólio+pentlandita). A mineralização do tipo IOCG é registrada pela alta concentração de elementos de terras raras e Y em anfibólios associado com uraninita.

O **Capítulo 7** (Campo-Rodriguez et al. *in review, d*) identifica as assinaturas de PGM da mineralização sulfetada rica em Ni de Onça Rosa usando caracterização HAADF STEM. Este capítulo também descreve minerais raros de Ni-Bi nunca antes reportados no Domínio Carajás, incluindo arsenohauchecornita, parkerita e a segunda ocorrência mundial de ognitita com ~600 ppm de Pd. Também foram abordados teluretos de Bi e sulfossais de Pb-Bi, como lilianita e heyrovskýita portadora de Ag. Modelos de estrutura cristalina e simulações da arsenohauchecornita verificam a superestrutura tetragonal centrada-I descrita anteriormente. Os dados composicionais confirmam uma solução sólida entre melonita e ognitita. A pentlandita apresenta substituição por meio de reações de dissolução-reprecipitação com remobilização e reprecipitação local de metais em microescala e canais de circulação de fluidos na nanoescala hospedeiros de moncheita, volynskita, hessite, altaita, telurobismutita e tsumoita. As assembleias minerais e nanopartículas observados foram atribuídos a reações de fluidos metassomáticos-hidrotermais com minérios ricos em pentlandita nos contatos entre corpos ultramáficos (Complexo Acamadado Serra do Puma) e uma fonte hidrotermal derivada do granito.

O **Capítulo 8** resume as principais descobertas e implicações da pesquisa, destacando também questões em aberto e potenciais direções para futuras investigações.

O **Capítulo 9** compila material adicional, incluindo material suplementar associado aos Capítulos **2** a **7**, e publicações em co-autoria durante esta candidatura. Uma lista de referências completa para todos os capítulos é fornecida no **Capítulo 10**.

1.4. References

Araújo Filho, R.C., Nogueira, A.C., and Araújo, R.N. (2020) New stratigraphic proposal of a Paleoproterozoic siliciclastic succession: Implications for the evolution of the Carajás Basin, Amazonian craton, Brazil. Journal of South American Earth Sciences 102, 102665. https://doi.org/10.1016/j.jsames.2020.102665

Barton, M. (2014) Iron oxide (–Cu–Au–REE–P–Ag–U–Co) systems. Treatise on Geochemistry, 2nd edition, vol 13. Elsevier, Amsterdam, p/ 515-541. https://doi.org/10.1016/B978-0-08-095975-7.01123-2

Campo-Rodríguez, Y.T., Ciobanu, C.L., Slattery, A., Cook, N.J., Schutesky, M.E., Ehrig, K., King, S.A., and Yao, J. (2024a) Polysomatic intergrowths between amphiboles and non-classical pyriboles in magnetite: smallest-scale features recording a protracted geological history. American Mineralogist 109 (10), 1798–1818. https://doi.org/10.2138/am-2023-9188

Campo-Rodriguez, Y.T., Cook, N.J., Ciobanu, C.L., Schutesky, M.E., King, S.A., Gilbert, S., and Ehrig, K. (2024b) Platinum Group Minerals Associated with Nickel-Bearing Sulfides from the Jatobá Iron Oxide-Copper-Gold Deposit, Carajás Domain, Brazil. Minerals 14, 757. https://doi.org/10.3390/min14080757

Campo-Rodriguez, Y.T., Ciobanu, C.L., Cook, N.J., Schutesky, M.E., Ehrig, K., Slattery, A., Gilbert, S., and King, S.A. (*in review, a*) Telescoped transition from trellis to silicate mottled magnetite records deep shear zone metamorphism in the IOCG deposit at Jatobá, Carajás, Brazil. Mineralogical Magazine.

Campo Rodriguez, Y.T., Ciobanu, C.L., Gilbert, S., Wade, B., Cook, N.J., Schutesky, M.E., and Ehrig, K. (*in review, b*) Coupled Lu-Hf and U-Pb apatite geochronology of Jatobá orebody supports ~2.5 Ga metamorphism in deep shear zones from Southern Copper Belt, Carajás Domain, Brazil. Precambrian Research.

Campo Rodriguez, Y.T., Ciobanu, C.L., Cook, N.J., Schutesky, M.E., Ehrig, K., Slattery, A., Gilbert, S., and King, S.A. (*in review, c*) Magnetite and REE-rich calcic amphibole provide evidence for a skarn-IOCG system at Onça Rosa, Jaguar Orefield, Carajás Mineral Province, Brazil. Canadian Journal of Mineralogy and Petrology.

Campo Rodriguez, Y.T., Ciobanu, C.L., Cook, N.J., Slattery, A., Wade, B., Gilbert, S., Schutesky, M.E., and Ehrig, K. (*in review, d*) Arsenohauchecornite, ognitite, parkerite, and related minerals from Onça Rosa orebody, Carajás, Brazil: fingerprinting PGE signatures in hydrothermal Ni ores. American Mineralogist.

Ciobanu, C.L., Verdugo-Ihl, M.R., Slattery, A., Cook, N.J., Ehrig, K., Courtney-Davies, L., and Wade, B.P. (2019) Silician magnetite: Si–Fe-nanoprecipitates and other mineral inclusions in magnetite from the Olympic Dam Deposit, South Australia. Minerals 9, 311. https://doi.org/10.3390/min9050311

Corriveau, L., Montreuil, J.F., and Potter, E.G. (2016) Alteration facies linkages among iron oxide copper-gold, iron oxide-apatite, and affiliated deposits in the Great Bear magmatic zone, Northwest Territories, Canada. Economic Geology 111, 2045-2072. https://doi.org/10.2113/econgeo.111.8.2045

Costa, F.G., Santos, P.A., Serafim, I.C.C.O., Costa, I.S.L., and Roopnarain, S. (2020) From Mesoarchean drips to modern–style tectonics in the Carajás Province, Amazonian Craton. Journal of South American Earth Science 104, 102817. https://doi.org/10.1016/j.jsames.2020.102817

Courtney-Davies, L., Ciobanu, C.L., Verdugo-Ihl, M.R., Dmitrijeva, M., Cook, N.J., Ehrig, K., and Wade, B.P. (2019a) Hematite geochemistry and geochronology resolve genetic and temporal links among iron-oxide copper gold systems, Olympic Dam district, South Australia. Precambrian Research 335, 105480. https://doi.org/10.1016/j.precamres.2019.105480

Courtney-Davies, L., Tapster, S.R., Ciobanu, C.L., Cook, N.J., Verdugo-Ihl, M.R., Ehrig, K.J., Kennedy, A.K., Gilbert, S.E., Condon, D.J., and Wade, B.P. (2019b) A multi-technique evaluation of hydrothermal hematite U-Pb isotope systematics: Implications for ore deposit geochronology. Chemical Geology 513, 54-72. https://doi.org/10.1016/j.chemgeo.2019.03.005

Courtney-Davies, L., Ciobanu, C.L., Tapster, S.R., Cook, N.J., Ehrig, K., Crowley, J.L., Verdugo-Ihl, M.R., Wade, B.P., and Condon, D.J. (2020a) Opening the magmatic-hydrothermal window: High-precision U-Pb geochronology of the mesoproterozoic olympic dam Cu-U-Au-Ag deposit, South Australia. Economic Geology 115, 1855-1870. https://doi.org/10.5382/econgeo.4772

Courtney-Davis, L., Ciobanu, C.L., Verdugo-Ihl, M.R., Cook, N.J., Ehrig, K.J., Wade, B.P., Zhu, Z.Y., and Kamenetsky, V.S. (2020b) ~1760 Ma magnetite-bearing protoliths in the Olympic Dam deposit, South Australia: Implications for ore genesis and regional metallogeny. Ore Geology Reviews 118, 103337. https://doi.org/10.1016/j.oregeorev.2020.103337

Courtney-Davies, L., Gilbert, S.E., Ciobanu, C.L., Tapster, S.R., Richardson, M.W., Cook, N.J., Wade, B.P., Verdugo-Ihl, M.R., Ehrig, K., and Condon, D.J. (2021) A synthetic haematite reference material for LA-ICP-MS U-Pb geochronology and application to iron Oxide-Cu-Au Systems. Geostandards and Geoanalytical Research 45, 143-159. https://doi.org/10.1111/ggr.12365

Ferreira Filho, C.F., Ferraz de Oliveira, M.M., Mansur, E.T., and Rosa, W.D. (2021) The Jaguar hydrothermal nickel sulfide deposit: evidence for a nickel-rich member of IOCG-type deposits in the Carajás Mineral Province, Brazil. Journal of South American Earth Science 111, 103501. https://doi.org/10.1016/j.jsames.2021.103501

Grainger, C.J., Groves, D.I., Tallarico, F.H., and Fletcher, I.R. (2008) Metallogenesis of the Carajás mineral province, southern Amazon craton, Brazil: Varying styles of Archean through Paleoproterozoic to Neoproterozoic base-and precious-metal mineralisation. Ore Geology Reviews 33 (3-4), 451-489. https://doi.org/10.1016/j.oregeorev.2006.10.010

Huang, X.W. and Beaudoin, G. (2019) Textures and chemical compositions of magnetite from iron oxide copper-gold (IOCG) and Kiruna-type iron oxide-apatite (IOA) deposits and their implications for ore genesis and magnetite classification schemes. Economic Geology 114, 953-979. https://doi.org/10.5382/econgeo.4651

Huang, X.W., and Beaudoin, G. (2021) Nanoinclusions in zoned magnetite from the Sossego IOCG deposit, Carajás, Brazil: Implication for mineral zoning and magnetite origin discrimination. Ore Geology Reviews 139, 104453. https://doi.org/10.1016/j.oregeorev.2021.104453

Huang, X.W., Beaudoin, G., and Yang, Y. (2022) A HR-TEM study on two generations of magnetite from the Alemao IOCG deposit, Carajás, Brazil: Implication for Fe-Cu mineralization. Ore Geology Reviews 146, 104934. https://doi.org/10.1016/j.oregeorev.2022.104934

Kontonikas-Charos, A., Ciobanu, C.L., Cook, N.J., Ehrig, K., Krneta, S., and Kamenetsky, V.S. (2017) Feldspar evolution in the Roxby Downs granite, host to Fe-oxide cu-au-(U) mineralisation at Olympic dam, South Australia. Ore Geology Reviews 80, 838-859. https://doi.org/10.1016/j.oregeorev.2016.08.019

Machado, N., Lindenmayer, Z., Krogh, T.E., and Lindenmayer, D. (1991) U-Pb geochronology of Archean magmatism and basement reactivation in the Carajás area, Amazon shield, Brazil. Precambrian Research 49, 329-354. https://doi.org/10.1016/0301-9268(91)90040-H

Mansur, E.T., Dare, S.A.S., Ferreira Filho, C.F., Rodrigues Miranda, A.C., and Soares Monteiro, L.V. (2023) The distribution of trace elements in sulfides and magnetite from the Jaguar hydrothermal nickel deposit: Exploring the link with IOA and IOCG deposits within the Carajás Mineral Province, Brazil. Ore Geology Reviews 152, 105256. https://doi.org/10.1016/j.oregeorev.2022.105256

Martins, P.L.G, Toledo, C.L.B, Silva, A.M., Chemale, Jr.F., Santos J.O.S., and Assis, L.M. (2017) Neoarchean magmatism in the southeastern Amazonian Craton, Brazil: Petrography, geochemistry and tectonic significance of basalts from the Carajás Basin. Precambrian Research 302, 340-357. https://doi.org/10.1016/j.precamres.2017.10.013

Melo, G.H.C., Monteiro, L.V.S., Xavier, R.P., Moreto, C.P.N., Santiago, E.S.B., Dufrane, S.A., Aires, B., and Santos, A.F.F. (2017) Temporal evolution of the giant Salobo IOCG deposit, Carajás Province (Brazil): constraints from paragenesis of hydrothermal alteration and U-Pb geochronology. Mineralium Deposita 52, 709-732. https://doi.org/10.1007/s00126-016-0693-5

Monteiro, L.V.S., Xavier, R.P., Carvalho, E.R., Hitzman, M.W., Johnson, C.A., Souza, C.R., Filho, C.R., and Torresi, I. (2008) Spatial and temporal zoning of hydrothermal alteration and mineralization in the Sossego iron oxide–copper–gold deposit Carajás Mineral Province, Brazil: paragenesis and stable isotope constraints. Mineralium Deposita 43, 129-159. https://doi.org/10.1007/s00126-006-0121-3

Moreto, C.P.N., Monteiro, L.V.S., Xavier, R.P., Creaser, R.A., Dufrane, S.A., Tassinari, C.C.G., Sato, K., Kemp, A.I.S., and Amaral, W.S. (2015a) Neoarchean and Paleoproterozoic iron oxide-copper-gold events at the Sossego deposit, Carajás Province, Brazil, Re-Os and U-Pb geochronological evidence. Economic Geology 110, 809-835. https://doi.org/10.2113/econgeo.110.3.809

Moreto, C.P.N., Monteiro, L.V.S., Xavier, R.P., Creaser, R.A., Dufrane, S.A., Melo, G.H.C., Silva, M.A.D., Tassinari, C.C.G., and Sato, K. (2015b) Timing of multiple hydrothermal events in the iron oxide–copper gold deposits of the Southern Copper Belt, Carajás Province, Brazil. Mineralium Deposita 50, 517-546. https://doi.org/10.1007/s00126-014-0549-9

Santos J.O.S., Hartmann L.A., Gaudette H.E., Groves D.I., McNaughton N.J., and Fletcher I.R. (2000) A New Understanding of the Provinces of the Amazon Craton Based on Integration of Field Mapping and U-Pb and Sm-Nd Geochronology. Gondwana Research 3, 453-488. https://doi.org/10.1016/S1342-937X(05)70755-3

Schutesky, M.E. and de Oliveira, C.G. (2020) From the roots to the roof: an integrated model for the Neoarchean Carajás IOCG System, Brazil. Ore Geology Reviews 127, 103833. https://doi.org/10.1016/j.oregeorev.2020.103833

Skirrow, R.G. (2022) Iron oxide copper-gold (IOCG) deposits–A review (part 1): Settings, mineralogy, ore geochemistry and classification. Ore Geology Reviews 140, 104569. https://doi.org/10.1016/j.oregeorev.2021.104569

Tavares, F.M., Trouw, R.A.J, da Silva, C.M.G., Justo, A.P., and Oliveira, J.K.M. (2018) The multistage tectonic evolution of the northeastern Carajás Province, Amazonian Craton, Brazil: Revealing complex structural patterns. Journal of South American Earth Science 88, 238-252. https://doi.org/10.1016/j.jsames.2018.08.024

Teixeira, N.A., Campos, L.D., de Paula, R.R., Lacasse, C.M., Ganade, C.E., Monteiro, C.F., L.B.L., and de Oliveira, C.G. (2021) Carajás Mineral Province-Example of metallogeny of a rift above a cratonic lithospheric keel. Journal of South America Earth Sciences 108, 103091. https://doi.org/10.1016/j.jsames.2020.103091

Toledo, P.I.F., Moreto, C.P.N., Monteiro, L.V.S., Melo, G.H.C., Matos, F.M.V., Xavier, R.P., Carvalho, J.A., Filho, C.A.M., Navarro, M.S., and Lana, C.C. (2024) Breaking up the temporal link between granitic magmatism and iron oxide?copper-gold (IOCG) deposits in the Carajás Mineral Province, NW Brazil. Mineralium Deposita 59, 601-625. https://doi.org/10.1007/s00126-023-01224-5

Trunfull, E.F., Hagemann, S.G., Xavier, R.P., and Moreto, C.P.N. (2020) Critical assessment of geochronological data from the Carajás Mineral Province, Brazil: Implications for metallogeny and tectonic evolution. Ore Geology Reviews 121, 103556. https://doi.org/10.1016/j.oregeorev.2020.103556

Vasquez, L.V., Rosa-Costa, L.R., Silva, C.G., Ricci, P.F., Barbosa, J.O., Klein, E.L., Lopes, E.S., Macambira, E.B., Chaves, C.L., Carvalho, J.M., Oliveira, J.G., Anjos, G.C., and Silva, HR. (2008) Geologia e Recursos Minerais do Estado do Pará: Sistema de Informações Geográficas — SIG: texto explicativo dos mapas Geológico e Tectônico e de Recursos Minerais do Estado do Pará 1:1.000.000. CPRM, Belém, Brazil, 328 p.

Veloso, A.S.R., Monteiro, L.V.S., and Juliani, C. (2020) The link between hydrothermal nickel mineralization and an iron oxide-copper-gold (IOCG) system: Constraints based on mineral chemistry in the Jatobá deposit, Carajás Province. Ore Geology Reviews 121, 103555. https://doi.org/10.1016/j.oregeorev.2020.103555

Verdugo-Ihl, M.R., Ciobanu, C.L., Cook, N.J., Ehrig, K.J., and Courtney-Davies, L. (2020a) Defining early stages of IOCG systems: evidence from iron oxides in the outer shell of the Olympic Dam deposit, South Australia. Mineralium Deposita 55, 429-452. https://doi.org/10.1007/s00126-019-00896-2

Verdugo-Ihl, M.R., Ciobanu, C.L., Cook, N.J., Ehrig, K., Slattery, A., and Courtney-Davies, L. (2020b) Trace-element remobilisation from W–Sn–U–Pb zoned hematite: Nanoscale insights into a mineral geochronometer behaviour during interaction with fluids. Mineralogical Magazine 84, 502-516. https://doi.org/10.1180/mgm.2020.49

Verdugo-Ihl, M.R., Ciobanu, C.L., Cook, N.J., Ehrig, K.J., Slattery, A., Courtney-Davies, L., and Dmitrijeva, M. (2021) Nanomineralogy of hydrothermal magnetite from Acropolis, South Australia: Genetic implications for iron-oxide copper gold mineralization. American Mineralogist 106, 1273-1293. https://doi.org/10.2138/am-2021-7557

Xavier, R.P., Soares Monteiro, L.V., Moreto, C.P.N., Pestilho, A.L.S., Coelho de Melo, G.H., Delinardo da Silva, M.A., Aires, B., Ribeiro, C., and Freitas e Silva, F.H. (2012) The Iron Oxide Copper-Gold Systems of the Carajás Mineral Province, Brazil. In: Geology and Genesis of Major Copper Deposits and Districts of the World: A Tribute to Richard H. Sillitoe (Hedenquist, J.W., Harris, M., Camus, F., eds.). Society of Economic Geologists 16.

CHAPTER 2

POLYSOMATIC INTERGROWTHS BETWEEN AMPHIBOLES AND NON-CLASSICAL PYRIBOLES IN MAGNETITE: SMALLEST-SCALE FEATURES RECORDING A PROTRACTED GEOLOGICAL HISTORY

Yuri Tatiana Campo-Rodriguez[1,2], Cristiana L. Ciobanu[1], Ashley Slattery[3], Nigel J. Cook[1], Maria E. Schutesky[2], Kathy Ehrig[1,4], Samuel A. King[1], Jie Yao[1]

[1]*School of Chemical Engineering, The University of Adelaide, Adelaide, SA, 5005, Australia*
[2]*University of Brasilia, Institute of Geosciences, Graduate Program in Geology, Brasília DF 70910-900, Brazil*
[3]*Adelaide Microscopy, The University of Adelaide, Adelaide, SA, 5005, Australia*
[4]*BHP Olympic Dam, 10 Franklin Street, Adelaide, SA, 5000, Australia*

Article published in *American Mineralogist* (2024) 109 (10): 1798 – 1818.

Statement of Authorship

Title of Paper	Polysomatic intergrowths between amphiboles and non-classical pyriboles in magnetite: Smallest-scale features recording a protracted geological history
Publication Status	☑ Published ☐ Accepted for Publication ☐ Submitted for Publication ☐ Unpublished and Unsubmitted work written in manuscript style
Publication Details	Campo-Rodriguez, Y.T., Ciobanu, C.L., Slattery, A., Cook, N.J., Schutesky, M.E., Ehrig, K., King, S.A., and Yao, J. (2024) Polysomatic intergrowths between amphiboles and non-classical pyriboles in magnetite: smallest-scale features recording a protracted geological history. American Mineralogist. 109 (10): 1798–1818. https://doi.org/10.2138/am-2023-9188

Principal Author

Name of Principal Author (Candidate)	Yuri Tatiana Campo Rodriguez		
Contribution to the Paper	Performed analytical work, evaluation and interpretation of results and prepared the manuscript.		
Overall percentage (%)	60		
Certification:	This paper reports on original research I conducted during the period of my Higher Degree by Research candidature and is not subject to any obligations or contractual agreements with a third party that would constrain its inclusion in this thesis. I am the primary author of this paper.		
Signature	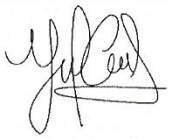	Date	06.11.2024

Co-Author Contributions

By signing the Statement of Authorship, each author certifies that:

i. the candidate's stated contribution to the publication is accurate (as detailed above);

ii. permission is granted for the candidate in include the publication in the thesis; and

iii. the sum of all co-author contributions is equal to 100% less the candidate's stated contribution.

Name of Co-Author	Cristiana L. Ciobanu		
Contribution to the Paper	Helped to define the direction of the manuscript, guides manuscript preparation and assisted with the interpretation of the results and evaluation of the manuscript. (15%)		
Signature	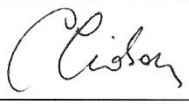	Date	06.11.2024

Name of Co-Author	Ashley Slattery		
Contribution to the Paper	Assisted with HAADF-STEM data acquisition. (6%)		
Signature		Date	06.11.2024

Name of Co-Author	Nigel J. Cook		
Contribution to the Paper	Helped with the preparation and evaluation of the manuscript. (5%)		
Signature	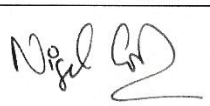	Date	06.11.2024

Name of Co-Author	Maria Emilia Schutesky		
Contribution to the Paper	Helped with the preparation and evaluation of the manuscript. (5%)		
Signature		Date	06.11.2024

Name of Co-Author	Kathy Ehrig		
Contribution to the Paper	Assisted with the evaluation of the manuscript. (5%)		
Signature	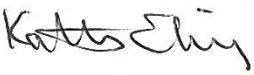	Date	06.11.2024

Name of Co-Author	Samuel Anthony King		
Contribution to the Paper	Assisted with the evaluation of the manuscript. (2%)		
Signature		Date	06.11.2024

Name of Co-Author	Jie Yao		
Contribution to the Paper	Assisted with the evaluation of the manuscript. (2%)		
Signature	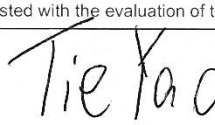	Date	06.11.2024

American Mineralogist, Volume 109, pages 1798–1818, 2024

Polysomatic intergrowths between amphiboles and non-classical pyriboles in magnetite: Smallest-scale features recording a protracted geological history

YURI TATIANA CAMPO RODRIGUEZ[1,2,*], CRISTIANA L. CIOBANU[1,†], ASHLEY SLATTERY[3], NIGEL J. COOK[1,‡], MARIA EMILIA SCHUTESKY[2], KATHY EHRIG[1,4,§], SAMUEL A. KING[1], AND JIE YAO[1,‖]

[1]School of Chemical Engineering, The University of Adelaide, Adelaide, South Australia 5005, Australia
[2]Geosciences Institute, University of Brasília, Brasília DF 70910-900, Brazil
[3]Adelaide Microscopy, The University of Adelaide, Adelaide, South Australia 5005, Australia
[4]BHP Olympic Dam, 10 Franklin Street, Adelaide, South Australia 5000, Australia

ABSTRACT

Non-classical pyriboles (NCPs) have tetrahedral silicate chains (I_{beam}) of multiplicity higher than single (pyroxene) or double (amphibole) I_{beams} and are known from amphiboles in altered mafic-ultramafic complexes. NCPs, their polysomatic sequences, and inherent chain-width disorder are petrogenetic tools for interpreting igneous and metamorphic processes. Magnetite, a refractory mineral that can trap and preserve NCPs is a major constituent of iron oxide-copper-gold (IOCG) deposits. We undertook a nanoscale study to show that NCPs and amphiboles are hosted within magnetite cores from the Jatobá Ni-bearing IOCG deposit, Carajás Mineral Province, Brazil. Monoclinic amphiboles and NCPs form polysomatic intergrowths or occur as sparse inclusions along $\{111\}_{magnetite}$. There are two chemical populations of amphiboles: Mg-Fe- and Ca-(Al)-amphiboles, the latter including Ce-bearing Mg-hornblende and (ferro)tschermakite. The occurrence contains one of the widest ranges of chain silicates ever recorded, from simple intergrowths of single to triple I_{beam} zippers, including pyroxene slabs, to longer NCP polysomes up to 15-I_{beam} chains. Clinojimthompsonite (Cjim) is observed for the first time within magnetite. Although no discrete polysomes could be defined, the NCP-amphibole intergrowths have compositions between Mg-Fe amphiboles and Cjim based on I_{beam} averages of 2.5–2.7. Relationships between increase in the number of *C* and *A* cations from amphibole (2-I_{beam}) to n chain silicates (nI_{beam}) are formulated as $nI_{beam} = T(2 + n) = C(5 + 3n) = A(1 + n)$, n = integer. Empirical models of crystal structures, validated by STEM simulation, are shown for 4- and 5-I_{beam} chain silicates. Co-crystallization of double- and triple-chain silicate structures with rhythmic intergrowths as larger blocks along *b* is often accompanied by rhythmic Ca-Fe zonation along *a*, supporting primary NCP crystallization via self-patterning during amphibole growth within magnetite in a close-to-equilibrium system. Chain-width disorder is documented from defects including planar faults, derailments, jogs, and swells.

Violations of zipper termination rules indicate primary growth rather than replacement. Amphibole-NCPs inclusions support a multi-stage evolution for Jatobá magnetite. They formed during the first cycle of magnetite overprinting within a mafic/ultramafic lithology that records syn-shearing events. Subsequent formation of calcic-amphiboles, including Ce-bearing species, indicate IOCG-related fluids at the onset of mineralization. (Ferro) tschermakite formed at ~7.5 kbar during high-pressure shearing is preserved during main ore deposition. The multi-stage amphibole-NCPs generations in magnetite revealed by our nanoscale study emphasize the interpretive value of magnetite for overprinting events in terranes with protracted geological histories. Analogous NCPs are likely to be abundant in magnetite from magmatic-hydrothermal deposits hosted by greenstone belts and altered mafic/ultramafic complexes. Likewise, discovery of Ce-rich hornblende provides new avenues to understand the early, alkali-calcic alteration stages of IOCG systems and models for REE incorporation into, and subsequent release from chain silicates.

Keywords: Non-classical pyriboles, (Ce-bearing) amphiboles, magnetite, polysomatic sequences, chain-width disorder, Jatobá Ni-IOCG deposit

INTRODUCTION

One of the most outstanding examples of crystal-structural modularity in silicates is the group of non-classical pyriboles (NCP) (Bozhilov 2013 and references therein). These minerals are structurally related to inosilicates but have tetrahedral silicate chains with multiplicity higher than single (pyroxene) or double (amphibole) chains. The NCPs are also linked to the biopyribole concept that considers smaller structural modules of pyroxene and mica to build any other chain silicate (Thompson 1978). Such building principles, bridging chain and sheet silicates, lie at the heart of polysomatism concepts used to define polysomatic series and order-disordered intergrowths between various members of those series (e.g., Veblen 1991; Hatert et al. 2023 and references therein). The most recent model (Nespolo and Bouznari 2017) unifies biopyribole and palysepiole polysomatic series using a framework of topochemical cell twinning. The

* Corresponding author E-mail: yuri.camporodriguez@adelaide.edu.au. Orcid https://orcid.org/0000-0003-0644-916X
† Orcid https://orcid.org/0000-0001-7045-919X
‡ Orcid https://orcid.org/0000-0002-7470-3935
§ Orcid https://orcid.org/0000-0002-5381-9445
‖ Orcid https://orcid.org/0009-0003-0513-1376

0003-004X/24/0010–1798$05.00/DOI: https://doi.org/10.2138/am-2023-9188

discovery of triple chain silicates, clinojimthompsonite (Cjim), and alternating double and triple chain silicates in chesterite from metamorphosed ultramafic rocks from Chester, Vermont, allowed confirmation of these building principles (Veblen and Burnham 1978a, 1978b).

Early studies of silicates using high-resolution transmission electron microscopy (HRTEM) (Buseck and Iijima 1974) have shown the feasibility of the method to underpin chain-width disorder, intergrowths, microstructures, and reaction mechanisms between pyriboles and sheet silicates (Veblen and Buseck 1979, 1980, 1981). These studies provided a systemized approach to pyriboles that defines "zippers" (slabs of a different chain width to a host pyribole) and their terminations considered to obey two theoretical rules: "Rule l: the terminating zipper must have the same number of sub-chains as the material it replaces. Rule 2: the numbers of silicate chains in the zipper and in the material that it replaces must both be even, or they must both be odd" (Veblen and Buseck 1980).

Inspired by the idea that biopyriboles play a key role in understanding petrogenetic processes spanning igneous and metamorphic environments and across a broad range of geological settings and epochs, HRTEM studies of natural and synthetic materials have addressed pyriboles and NCPs polysomatic intergrowths and their formation (e.g., Cressey et al. 1982; Akai 1982; Akai et al. 1997; Yau et al. 1986; Schumacher and Czank 1987; Droop 1994; Grobéty 1996, 1997; Najorka and Gottschalk 2003; Ams et al. 2009; Konishi et al. 2008, 2010; Ferrari and Viti 2010). An overview of experimental synthesis and compositional limits of monoclinic triple-chain silicates was provided by Jenkins et al. (2012).

Ciobanu et al. (2022) used high-angle annular dark-field (HAADF) scanning TEM (STEM) instead of conventional bright-field (BF) TEM imaging technique to show an unusual assemblage of NCPs (triple-chain silicate as zippers within ferrotschermakite) occurring as nanoinclusions hosted by magnetite from Wirrda Well (South Australia). This study provided a basis for interpreting NCP structures that allowed enhanced similitude to crystal structure models than the BF TEM imaging technique.

Magnetite is an early mineral in iron oxide copper gold (IOCG) deposits and is preserved as the dominant Fe-oxide if the system does not evolve to hydrolytic-hematite alteration. Magnetite is representative of main ore stages in deposits from some of the world's largest IOCG terranes, such as the Carajás Mineral Province, Brazil (e.g., Monteiro et al. 2008; Schutesky and de Oliveira 2020; Veloso et al. 2020; Campo-Rodríguez et al. 2022). In the giant Mesoproterozoic Olympic Cu-Au Province of South Australia, however, magnetite is restricted to deeper and outer margin of orebodies (Ciobanu et al. 2019, 2022; Verdugo-Ihl et al. 2020, 2021). Nanoscale studies of hydrothermal magnetite have shown this mineral can contain abundant inclusions of various types, including spinels, calc-silicates, etc., and that these inclusions represent valuable evidence that can help validate genetic models (Ciobanu et al. 2019, 2022; Verdugo-Ihl et al. 2021).

Magnetite from the Carajás Province has also been shown to host nanoscale inclusions (Huang and Beaudoin 2021; Huang et al. 2022). In this study, we employ HAADF STEM to characterize silicate inclusions in magnetite from the Jatobá Cu-Ni deposit in the Carajás Province. Jatobá is one of many IOCG deposits hosted along a major shear zone within mafic-ultramafic sequences (Veloso et al. 2020). Considering that a majority of reported occurrences of NCPs derive from altered mafic/ultramafic complexes (Veblen and Burnham 1978a, 1978b; Cressey et al. 1982; Schumacher and Czank 1987; Droop 1994; Grobéty 1996, 1997; Akai et al. 1997; Konishi et al. 2008, 2010; Ferrari and Viti 2010), we aim to find whether NCP is present in Jatobá magnetite. In addition, we raise the question of whether magnetite preserves silicate inclusions typical of IOCG alteration like those described by Ciobanu et al. (2019, 2022). Systematic investigation of magnetite from ore deposits opens a compelling path to better understand NCPs, their polysomatic sequences, and inherent chain-width disorder beyond the classical occurrences known from amphiboles in country rocks.

Analytical methods

Two thin polished sections of magnetite-bearing samples were studied at the nanoscale: (1) chalcopyrite-rich ore sample (Jt7) and (2) altered mafic/ultramafic rock (Jt10). The two samples are from the same drillhole (DH0032), 60 m apart. Sample characterization comprised reflected light optical and scanning electron microscopy (SEM) using a FEI Quanta 450 instrument operated in backscattered electron (BSE) mode to assess magnetite grains and select areas for nanoscale investigation. Three S/TEM (<100 nm) foils were prepared from the sections using a FEI-Helios nanoLab Dual Focused Ion Beam and SEM (FIB-SEM) as outlined by Ciobanu et al. (2011). Each foil was analyzed employing HAADF STEM imaging and energy-dispersive X-ray spectrometry (EDS)-STEM mapping using an ultrahigh-resolution, probe-corrected FEI Titan Themis S/TEM operated at 200 kV. This instrument is equipped with a X-FEG Schottky source and Super-X EDS geometry. The Super-X EDS detector provides geometrically symmetric EDS detection with an effective solid angle of 0.8 sr. Probe correction delivered sub-angstrom spatial resolution, and an inner collection angle >50 mrad was used for HAADF imaging with a Fischione detector. Velox software was used for image acquisition, including drift-corrected frame integration package (DCFI), and EDS data acquisition and processing. Various filters were used to eliminate noise. Quantification of the collected EDS spectra was performed using Thermo-Scientific Velox software (v3.10), which utilizes standard Cliff-Lorimer quantification and includes absorption correction optimized for both the Super-X detector geometry and also the effect of sample holder shadowing for the double-tilt Super-X holder used. Quantification was performed using the Brown-Powell empirical ionization cross-section model and uncertainty values reported incorporate an estimated 20% error in the k-factors. Calculation of mineral formulas was performed using a spreadsheet adapted from Ridolfi et al. (2018). Indexing of diffraction patterns was conducted with WinWulff (JCrystalSoft) and publicly available data from the American Mineralogist Crystal Structure Database (http://rruff.geo.arizona.edu/AMS/amcsd.php). Crystal structure models were generated in CrystalMaker and image simulations using STEM for xHREM software. Empirical models were derived by using "slicing and merging" modules of known structures using CrystalMaker software. All instruments are housed at Adelaide Microscopy, The University of Adelaide.

Results

Nanoscale inclusions in magnetite

In both samples, magnetite is mainly associated with sulfides (chalcopyrite and pyrite), biotite, chlorite, and quartz; apatite is an abundant component (Figs. 1a–1b). Magnetite is a relatively minor component of the ore sample where it displays a banded texture with respect to sulfides and gangue minerals. In contrast, magnetite is a major component (>75%) of the altered lithology, where it forms massive lenses. The magnetite has a subhedral morphology (Figs. 1c–1d), albeit slightly deformed and more marginally corroded by gangue and sulfides than in the ore sample. Magnetite is characterized by abundant inclusions (e.g., silicates, sulfides, and ilmenite), is partially fractured, and displays irregular domains of enhanced porosity.

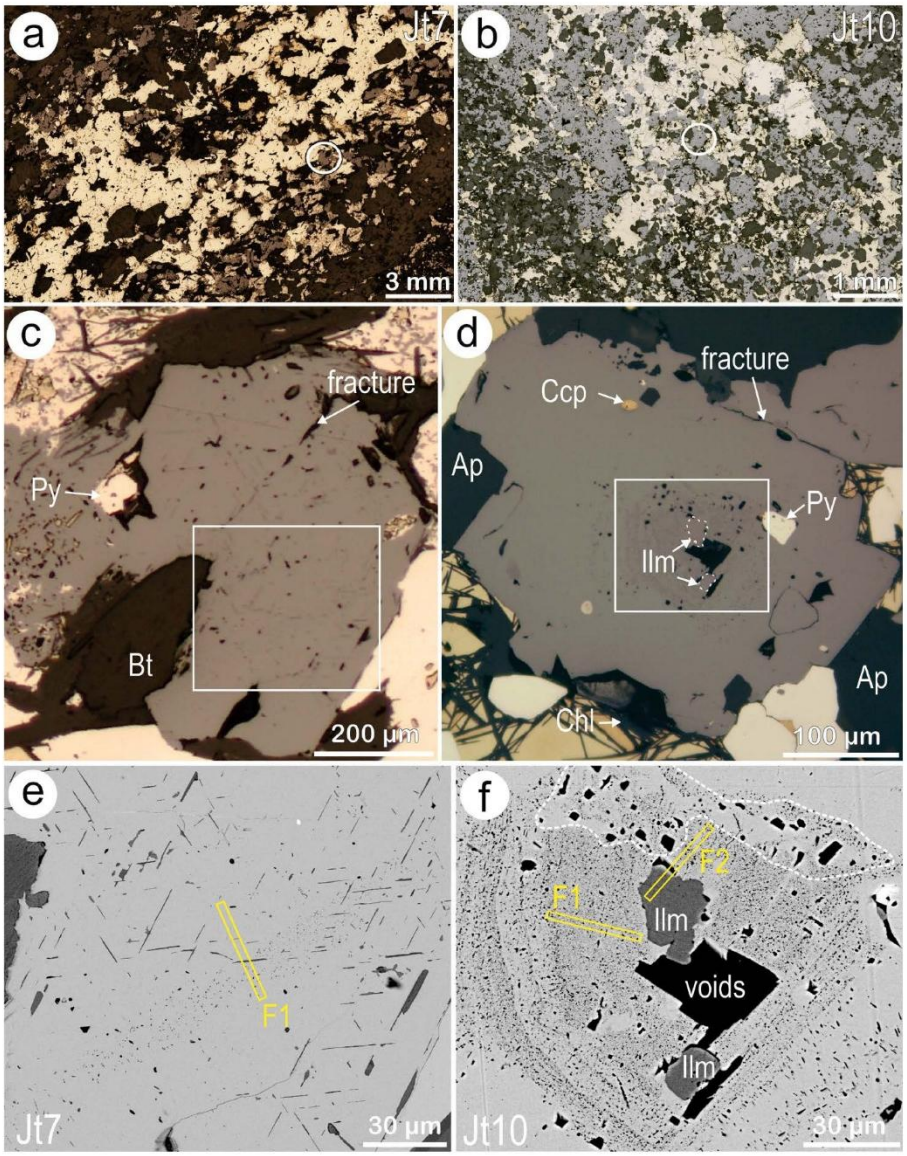

FIGURE 1. Reflected light (**a**–**d**) and BSE images (**e** and **f**) showing representative magnetite textures and location of FIB cuts (**f**) for S/TEM sample preparation. (**a** and **b**) Magnetite from the analyzed ore sample and altered mafic/ultramafic rock. Note that sulfides are predominantly chalcopyrite (Ccp) in **a** and pyrite (Py) in **b**. (**c** and **d**) Details of subhedral magnetite grains from areas circled in **a** and **b**, showing silicate, sulfide, and other inclusions as labeled. Note marginal corrosion, porosity, and fractures. (**e** and **f**) Details of areas (rectangles in **c** and **d**) selected for FIB-slicing across silicate inclusions. In **e**, acicular inclusions along $\{111\}_{magnetite}$ are crossed by bands mottled with finer inclusions. In **f**, the magnetite core displays concentric zoning and is densely mottled with inclusions. The core outline is partially irregular; coarser ilmenite (Ilm) and voids are present in the middle. Abbreviations: Ap = apatite; Bt = biotite, Chl = chlorite. (Color online.)

The distribution of silicate inclusions varies from scarce in the ore sample to abundant in the altered mafic/ultramafic rock (Figs. 1e–1f). In the ore sample, silicates form acicular <111> networks in magnetite and these are crosscut by ~10–20 µm wide bands with mottled, finer inclusions (Fig. 1e). Densely mottled cores are found in the magnetite from the mafic/ultramafic sample (Fig. 1f). In detail, a concentric pattern of inclusions is observed around relatively coarser (20–30 µm sized) grains of ilmenite. Toward the edges, the mottled area displays irregular domains with coarsening of the silicate inclusions (Fig. 1f). The three S/TEM foils for nanoscale study were prepared from slices cut by FIB placed across areas with densest inclusions (Figs. 1e–1f). One slice was cut across the boundary between magnetite and ilmenite to establish whether this is accompanied by ulvöspinel and/or other spinel phases.

The foils (Online Materials[1] Fig. A1) show that the distribution of inclusions at depth is comparable with that observed on the magnetite surface, i.e., scarce and densely mottled, respectively, for grains from the two samples. The inclusions are silicates, without any spinels present, although an inclusion-free area is observed adjacent to the ilmenite boundary. The silicate assemblage is dominated by amphiboles, with minor biotite, talc, chlorite, and trace titanite and allanite. In addition, Si-rich blebs or square-shaped inclusions are present, some of which also contain Mg and are amorphous. The foil from sample Jt7 shows amphiboles as two long (micrometer-sized) acicular grains parallel with one another and an isolated, stubby aggregate of different orientations. In contrast, foils from sample Jt10 feature clustered nanometer-scale amphibole inclusions of comparable orientation interspersed with larger clots of amphibole, each several

hundreds of nanometers in length. In the foil obtained across the ilmenite/magnetite boundary, a longer, micrometer-sized inclusion of mica/chlorite(?) crosscuts the amphiboles, but this was plucked out during FIB milling.

A selection of aggregates and amphibole grains are shown in Figure 2. The aggregates, up to 1 µm in length, show rectangular and elongate shapes attributable to different orientations relative to the plane of view (Fig. 2a). Some are associated with an amorphous Si-(Mg)-rich phase or are partially mantled by diverse talc+chlorite+biotite assemblages (TCB) and minor titanite. Subrounded grains are interspersed among the dominant population of thin, prismatic amphiboles (Figs. 2b–2c).

Common to all inclusions are lamellar intergrowths readily seen as irregular rhythms of bright and dark bands on HAADF STEM images. Such intergrowths always contain slabs displaying the crystal structure of amphibole (see below), which correspond to the brighter bands. The darker bands are composed of irregular sequences of other chain silicates, spanning a wide range of I_{beams}, from conventional pyriboles (pyroxene and amphibole) to NCPs such as clinojimthompsonite and (clino)chesterite. Intergrowth patterns vary widely from one case to another and are more pronounced in the subhedral grains (Fig. 2b), whereas the thin amphiboles display only a few such bands (Fig. 2c). Parts or grains forming the aggregates can also lack such banding. A second peculiarity is the rhythmic zoning across the grain elongation observed as bright or dark strips on the HAADF STEM images. Some grains combine domains with and without lamellar intergrowths (see below).

Compositions obtained from STEM mapping of inclusions of all types are given in Online Materials[1] Tables OM1 and OM2 and plotted on Figure 2d. The data was obtained from integrated spectra over areas without (or with only negligible) intergrowths but over the entire grains whenever they are banded. The overall composition of grains with lamellar intergrowths are also given relative to amphibole-only areas selected from the same grains. There are two main categories: calcic [actinolite, magnesio-hornblende and (ferro) tschermakite]; and Mg-(Fe)-amphiboles (cummingtonite) (Fig. 2d). We note the ratio of cations (Me) in *B* and *C* sites $^{B}Me/^{C}Me$ is close to ideal 2/5 = 0.4 for all except one calcic amphibole (0.33 for analysis #10-bottom in Online Materials[1] Table OM1). The upper Mg-(Fe) amphibole of the same inclusion also has a lower $^{B}Me/^{C}Me$ ratio (0.31 for analysis #10-top in Online Materials[1] Table OM2). Lower $^{B}Me/^{C}Me$ ratios are also obtained for Mg-(Fe)-amphiboles with the densest NCP intergrowths from the four aggregates (mean = 0.34; Online Materials[1] Table OM2). However, the mean ratio becomes 0.38 when obtaining compositions from selected areas/bands without intergrowths from the same aggregates.

(Ferro)tschermakite containing up to 14.9 wt% Al_2O_3, is identified from the largest acicular inclusions in the ore sample. (Ferro)tschermakite displays the highest *A*-site occupancy, with the average composition: $^{A}(Ca_{0.43}Na_{0.27}K_{0.13}\square_{0.17})_1{}^{B}(Mg_{0.44}Ca_{1.56})_2{}^{C}(Fe^{2+}_{1.94}Mg_{1.45}Al_{0.9}Fe^{3+}_{0.7}Ti_{0.02})_5{}^{T}(Si_{6.37}Al_{1.64})_8O_{22}(OH)_2$.

Most of the amphiboles in the aggregates that lack lamellar intergrowths correspond to actinolite, except for magnesio-hornblende in aggregate 1 from the ore sample.

Intriguingly, a single grain (Figs. 2c–2d) imaged throughout as dominantly amphibole (see below) and plotting in the field of magnesio-hornblende, contains 6.7 wt% Ce_2O_3. The calculated empirical formula for this Ce-bearing amphibole is: $^{B}(Ca_{1.66}\square_{0.34})_2{}^{C}(Mg_{2.37}Fe^{2+}_{1.11}Al_{0.64}Fe^{3+}_{0.53}Ce_{0.36})_5{}^{T}(Si_{7.16}Al_{0.84})_8O_{22}(OH)_2$.

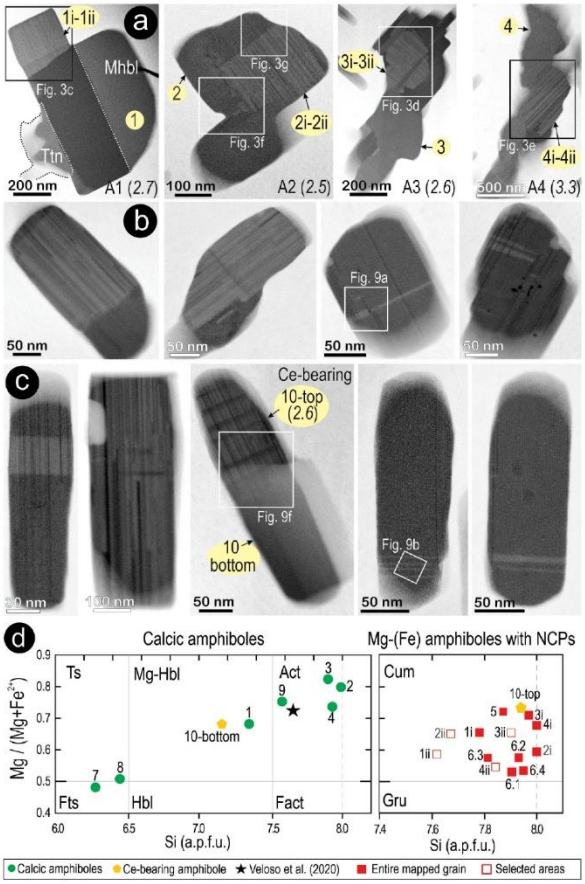

FIGURE 2. (**a**–**c**) HAADF-STEM images showing variation in size and shape of NCP-bearing amphiboles from the three foils: (**a**) coarser aggregates (A1–A4), (**b** and **c**) subrounded and euhedral, prismatic grains. Note fine-rhythmic intergrowths between NCPs (darker) and amphibole (lighter) along the length and presence of Fe-rich bands (lighter) across the width of the grains. The italicized numbers in parentheses represent the I_{beam} average for analyzed amphibole-NCP sequences. The numbers highlighted in yellow correspond to data plotted in **d**. (**d**) Amphibole classification plots (after Leake et al. 1997) showing two compositional groups, calcic- (left) and Mg-Fe-amphibole (right) using data from Online Materials[1] Tables OM1 and OM2. Numbers 1–4 correspond to aggregates in **a**; 5, 6 are analyses collated from small grains (e.g., map in Fig. 4a); 7–9 amphibole grains from various maps (e.g., Fig. 5b), and Ce-amphibole from the map in Figure 5a. The aggregates numbered 1–4 are further sub-divided into: (1) entire mapped grain, and (2) selected area (no NCPs). Abbreviations: Act = actinolite; Amp = amphibole; Cum = cummingtonite; Fact = Ferro-actinolite; Fts = Ferro-tschermakite; Gru = grunerite; Hbl = hornblende; Mg-Hbl = magnesio-hornblende; Ts = tschermakite; Ttn = titanite. (Color online.)

The effect introduced by the presence of chain width disorder on measured compositions in the two analysis #10 were assessed using the method of Bozhilov et al. (2007). Calculated $^{B}Me/^{C}Me$ ratios are 0.37 and 0.289 for #10-top and -bottom, respectively (Online Materials[1] Fig. A2). These values show 0.06 and 0.04 difference to the measured ratios implying the EDS STEM data are reliable.

For the sake of comparison, compositions obtained from the entire grains with lamellar intergrowths in the four aggregates were also plotted assuming an overall amphibole crystal chemistry (Fig. 2d). These show an increase in Mg content relative to the non-banded parts, except for one case (Aggregate 2) in which Fe-enrichment is observed. The part of the Ce-bearing amphibole featuring dense intergrowths also plots in the cummingtonite field, like the aggregates. The same grain also shows an association between a calcic (Ce-bearing) and Mg-(Fe) amphibole, like the paired composition of amphiboles in the aggregates.

The lamellar intergrowths within single grains or amphibole aggregates are shown in closer detail in Figure 3. Such intergrowths can be continuous along the length of the grain, irrespective of whether the inclusions are rounded or subhedral (Figs. 3a–3b). A relative increase in Mg within grains from aggregates correlates with NCPs as darker bands in the lamellar intergrowths (Figs. 3c–3g). Some aggregates also show changes in composition, from Ca- to Fe-rich zones across lamellae of variable rhythms (Fig. 3c). Calcium-rich strips across the intergrowths are observed in other cases (Fig. 3d). Direct contacts between actinolite and cummingtonite (and associated Mg-richer intergrowths) are depicted in aggregates 2 and 4 (Figs. 3e–3f). Highlighting the complexity between the textures and chemical changes in the inclusions are Fe-rich strips that crosscut actinolite (Fig. 3f) and the observed changes in Ca/Fe ratio along the same bands within a lamellar intergrowth (Fig. 3g).

EDS STEM maps were generated to further constrain compositional variation, intergrowths, and zonation patterns among amphiboles (Figs. 4 and 5; extended maps in Online Materials[1] Figs. A3–A4). Maps of larger areas with densely mottled inclusions show the two distinct populations of amphiboles (Ca- and Mg-rich: Fig. 4a). Tiny Ce-bearing inclusions are present, close to, or attached to amphibole grains (inset in Fig. 4a). An association between calcic (actinolite) and Mg-(Fe)-amphibole (cummingtonite), typical of the aggregates (Figs. 4b–4c) is partially replaced by TCB along straight or scalloped boundaries. The rhythms of bright bands (amphibole) in an intergrowth are mimicked by the variation in Fe concentration (Fig. 4c).

EDS STEM mapping of the binary inclusion comprising cummingtonite and Ce-bearing magnesio-hornblende shows a rhythmic zonation with respect to Ca and Fe across the banding in the cummingtonite (top of Fig. 5a), whereas Ce and Al are evenly distributed only throughout the Ce-bearing magnesio-hornblende (bottom of Fig. 5a). Ca and Mg are present across both grains, whereas Fe is enriched in cummingtonite. EDS STEM element maps of (ferro)-tschermakite and associated biotite show the amphibole is not zoned with respect to Ca, Al, or Mg, and contains measurable Na (Fig. 5b). Notably, Ti is enriched in the mica and to a lesser degree in the enclosing magnetite relative to the amphibole (Online Materials[1] Fig. A4).

NANOSCALE CHARACTERIZATION

Crystal structures of chain silicates

Interpretation of high-resolution HAADF STEM images is dependent upon fitting crystal models with simulations onto projections that are relevant for the identification of specific motifs and how those motifs adapt to structural modularity. The atoms on such images are observed as dots of variable size and intensity (I), in turn, controlled by the atomic number of each element (I~Z^2), site occupancy, and their density along the atomic columns perpendicular to the view plane.

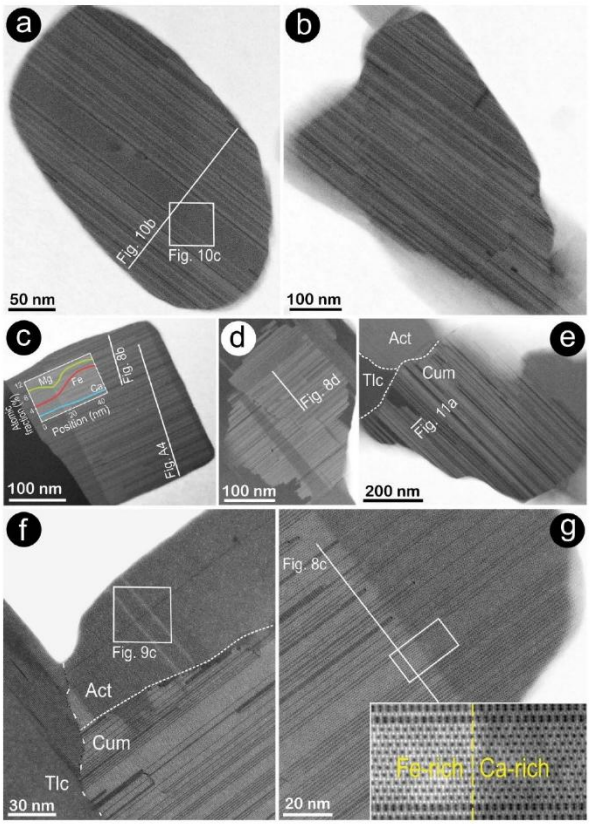

FIGURE 3. Low-resolution images illustrating amphibole-NCP intergrowths from (**a**) rounded, and (**b**) subhedral grains, and (**c**–**g**) aggregates (areas marked on Fig. 2). Crystal of clinojimthompsonite with amphibole intergrowths (lighter bands) in **a**. Note changes in chemical composition along and parallel to the intergrowths in **c** and **g** and (**d** and **f**) respectively. Profile in **c** shows the inverse variation between Mg, Ca (dark), and Fe (light) across banding. Crop in **g** shows that the same I_{beam} structures are preserved across chemical banding with respect to Fe (lighter) and Ca (darker) (see map in Fig. 4c). Boundaries between distinct phases are marked by dashed lines. Abbreviations: Act = actinolite; Cum = cummingtonite; Tlc = talc. (Color online.)

In a simplified sense, all chain silicate structures display a central ribbon of atoms representing the C cations (octahedral coordination), bordered by two B cations (dodecahedral) at the ribbon edges (Fig. 6). Pairs of Si-tetrahedra (T) flank the ribbon on both sides and their number is considered for the I_{beam} notation of each species: 2 for amphibole; 3 for clinojimthompsonite; and 2 combined with 3 for chesterite (Veblen and Burnham 1978b). The A cations are located at the edges of the central ribbon and between each pair of T cations.

Whereas the number of B cations remains unchanged, the increase in the number of C and A cations from amphibole to n chain silicates (nI_{beam}) can be expressed by the formula:

$$nI_{beam} = T(2 + n) = C(5 + 3n) = A(1 + n), \quad (1)$$

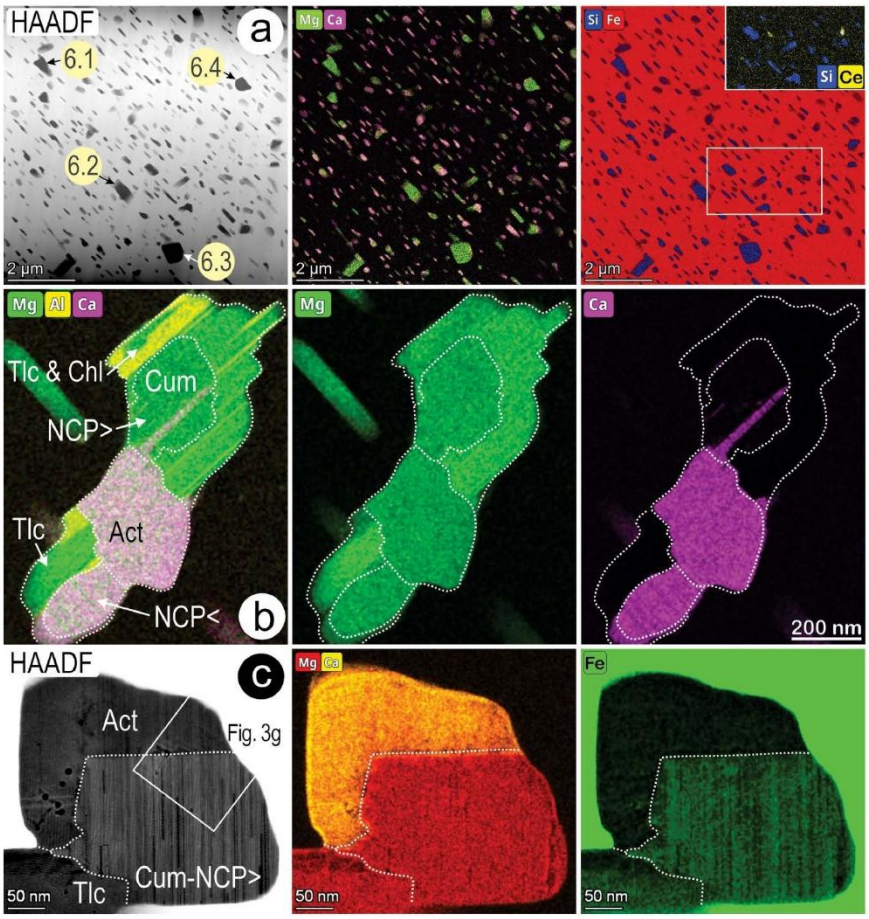

FIGURE 4. STEM EDS maps and overlays of (**a**) densely mottled areas, (**b**) aggregate 3, and (**c**) aggregate 2. Inset in **a** shows Ce-rich nanoparticles attached to amphiboles. (**b**) Aggregate comprising NCP rich (NCP>) cummingtonite (Cum) and NCP poor (NCP<) actinolite (Act). Fine-rhythmic banding with respect to Fe across the NCP-rich cummingtonite from aggregate 2. Note straight contacts (dotted line) with marginal actinolite. The numbers highlighted in yellow correspond to data plotted in Figure 2d. (Color online.)

where n is an integer. The increase in the number of *C*- and *T*-site cations controls expansion of the *b* unit-cell parameter (by ~9 Å per additional I_{beam}). The *a* and *c* parameters remain relatively constant.

The same formula is valid for polysomes of chain silicates combining two or more I_{beams}, in which the structure results from addition of elements within the component units. For example, chesterite (2- and 3-I_{beams}), the only polysome for which the crystal structure has been determined (Veblen and Burnham 1978b), is orthorhombic (space group $A2_1ma$), and thus distinct from the monoclinic space groups ($C2/m$ and $C2/c$) of the other chain silicates discussed here. The modular structures of chain silicates can be compared when projected on [001] zone axis. For consistency, polysomatic sequences of NCP and amphibole were also imaged on three additional zone axes: [$10\bar{2}$], [$10\bar{1}$], and [101] (Online Materials[1] Figs. A6–A7) by tilting along the *b* axis. Imaging of Ca-Al-amphibole (Fts) on [010] zone axis shows no disorder (Online Materials[1] Fig. A8).

The above description of crystal modularity is shown using actinolite (Evans and Yang 1998), clinojimthompsonite and chesterite (Veblen and Burnham 1978b) as illustrative structures of 2-, 3-, and (23) chain silicates, respectively (Fig. 6). STEM simulations for these structures show a good match with the atom fill models, whereby the *B* and *C* cations are recognized as bright dots of variable intensity and flanked by the *T* cations. In the cases selected here, the *B* cations are brighter than the *C* cations due to their relative atomic mass, e.g., Ca (Z = 20) compared to Mg (Z = 12) in actinolite. The *A* sites, which host Na and/or K cations but with very low occupancy in actinolite (K + Na = 0.037) and missing altogether in clinojimthompsonite and chesterite, are depicted as black, diamond-shaped motifs. Beneath the models and simulations, we show a selection of HAADF STEM images [on different zone axes] illustrating the same structures (Fig. 6) and their excellent fit with the models.

Using Equation 1 above and existing structures for actinolite and clinojimthompsonite, we have generated 4- and 5-I_{beam} models to illustrate how the appearance of the structures change systematically on HAADF STEM images as cell size increases (Fig. 6). We note that the monoclinic I_{beam} structures with even and uneven number are likely to correspond to space groups $C2/m$ and $C2/c$, respectively, or a corresponding subgroup. The

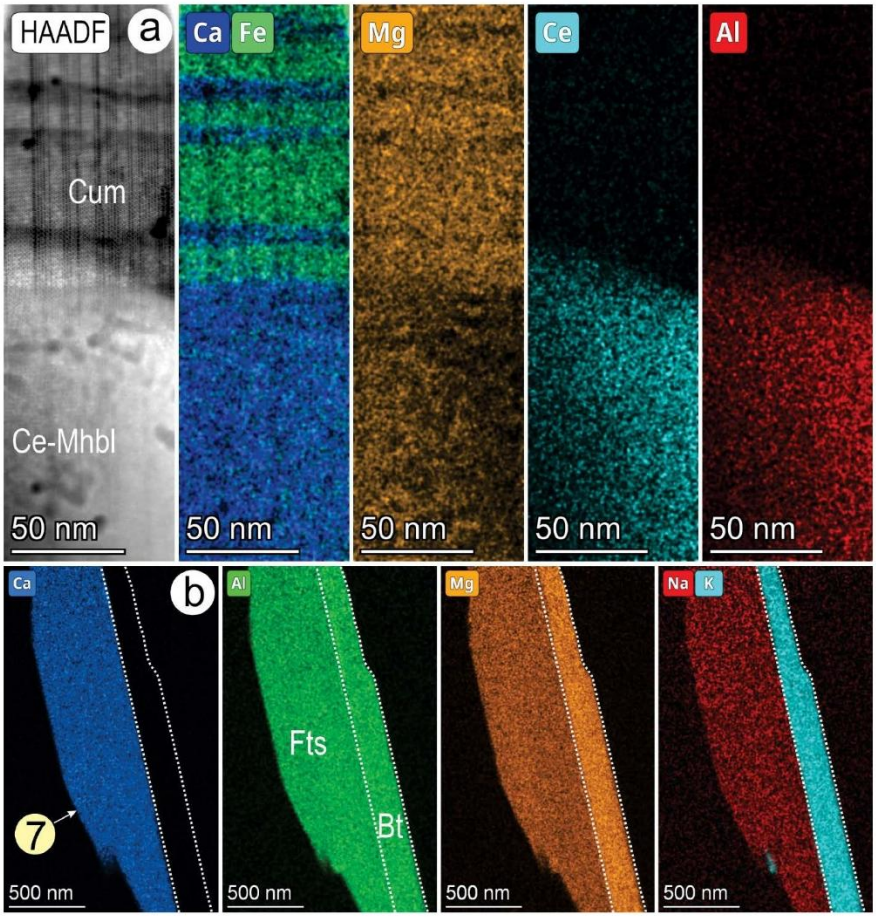

FIGURE 5. STEM EDS maps and overlays showing (**a**) Ce-bearing magnesio-hornblende (Ce-Mhbl) and (**b**) (ferro)-tschermakite (Fts). In **a**, the top part corresponds to cummingtonite (Cum) displaying Ca-Fe rhythmic zonation. Note biotite (Bt) on the side of Fts in **b**. The number highlighted in yellow corresponds to data plotted in Figure 2d. (Color online.)

STEM simulations for each structure clearly show the number of atoms along the ribbon, the *T* pairs, and the diamond-shaped black motifs.

Pyroxene, the simplest I_{beam} structure (1), is also observed but only as single slabs, or zippers, that occur within sequences of other chain silicates, mostly 2- and 3-I_{beams} (Figs. 7a–7b). Pyroxene has four cations along the central ribbon (with two *C* cations and two *B* cations at the ribbon edges) flanked by a single pair of Si-tetrahedra (*T*). There are no *A* sites (Fig. 7c). Such structure can be joined along $(010)_{planes}$ with other chain silicates by *a*/2 offset of the pyroxene central ribbon relative to that in the host silicate (Figs. 7c–7d). The structures and I_{beam} schematics illustrate the resulting zipper sequences displaying two types of alternating $(010)_{planes}$ with *a*/2 periodicity along *b*: (1) (212) and (213) and (2) (2gap2) and (2gap3). The gap links adjacent *B* cations in the host structures and stands for a narrower interval than their *A* site(s) (Figs. 7c–7d).

A sequence with abundant pyroxene zippers within amphibole (Fig. 7e) illustrates the additional in such intergrowths. Notable in this example is the presence of 5-I_{beam} zippers forming polysomatic intergrowths with 1-, 2-, and 3-I_{beam} slabs.

Sequences of polysomatic intergrowths

Assessment of polysomatic intergrowths over longer length intervals, from 60 to ~250 nm from three aggregates in Figures 2, 3, 8, and Online Materials[1] Figure A5 shows these have I_{beam} averages ($\bar{I}_{beam}$) around 2.5–2.6. These were calculated using the formula:

$$\bar{I}_{beam} = \Sigma n I_{beam}(i)/N I_{beam} \quad (2)$$

where n = number of each I_{beam} of index (i), and N = total number of I_{beams} in the sequence. This implies that the composition of such grains lies between that of Mg-Fe amphiboles and clinojimthompsonite, as confirmed by their locations on Figure 2d. Most of these sequences show polysomes with combinations between 3-I_{beam} and other NCPs (4- to 6-I_{beams}) within host amphibole.

The longest sequence, 247 nm (Online Materials[1] Fig. A5), is from aggregate 1 and shows rhythms between amphibole and polysomes dominated by the 3-I_{beam}. Shorter sequences from the same aggregate show I_{beams} that average to comparable dimensions as in the longer profile (Figs. 8a–8b). There are, however, differences between parts of the grain that are Ca- or Mg-rich

($\bar{I}_{beam}$ size 2.22 and 2.63, respectively; Fig. 8a). The Fe-rich profile shows a greater number of higher order NCPs (Fig. 8b), concordant with the increased in $\bar{I}_{beam}$ size. The polysomes are always highly irregular and can change sequence across the Ca-rich/Fe-rich boundary where zipper terminations within the polysomes are common (Figs. 8a and 8c). Comparable features are illustrated in Figures 8c and 8d from ~100 nm long profiles obtained from two other aggregates that also display compositional boundaries. In the Fe-rich part of aggregate 2, one side is dominated by a greater abundance of 3-I_{beam} structures, whereas the other shows NCP zippers terminated either below or at the boundary to the Ca-rich part (Fig. 8c). In contrast, the 3-I_{beams} traverse the composition boundary.

Profile 4 from aggregate 3 displays simpler polysomes with sequence changes and defects rather than terminations across the Ca-rich/Fe-rich boundary (Fig. 8d). A range of such sequence

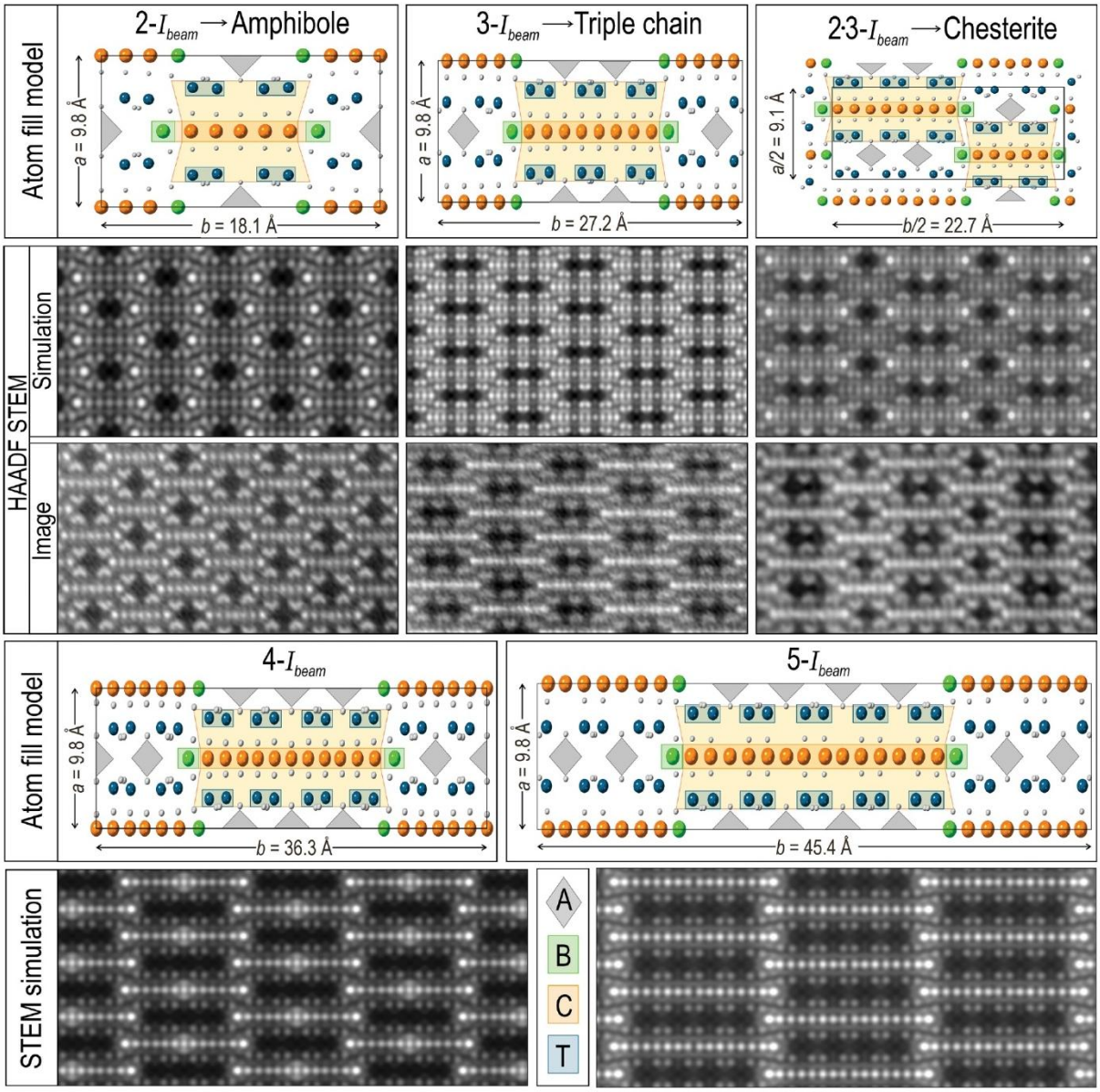

FIGURE 6. Models and images of chain silicates as labeled, each plotted on [001] zone axis. The structures used for the three models at the top are: actinolite for amphibole (Evans and Yang 1998), clinojimthompsonite for triple-chain silicate, and chesterite for the alternating double and triple chain silicate (Veblen and Burnham 1978b). Empirical models for the 4- and 5-I_{beam} structures (bottom) are shown and compared with STEM simulations; these can be compared with images in Figure 11d. I-beam outlines as overlays on atom-fill models. Note increase in the I_{beam} number is associated with increase in the length of *b* (by ~9 Å). Legend for cation positions is according to the general amphibole formula of Hawthorne et al. (2012): $AB_2C_5T_8O_{22}W_2$, where *A* = vacancy (□), Na, K, Ca, Pb, Li; *B* = Na, Ca, Mn^{2+}, Fe^{2+}, Mg, Li; *C* = Mg, Fe^{2+}, Mn^{2+}, Al, Fe^{3+}, Mn^{3+}, Ti^{4+}, Li; *T* = Si, Al, Ti^{4+}, Be; and *W* = (OH), F, Cl, O^{2-}. See text for further explanations. (Color online.)

changes and zipper terminations are shown in Figures 8e–8f.

The most abundant population of inclusions is represented by amphibole with zippers comprising various pyriboles or NCPs (Fig. 9). Such zippers mostly extend along the entire length of the grain but can also display terminations and defects related to Fe-rich compositional bands (Fig. 9a). Otherwise, thin rhythms of Fe banding (<5 nm wide) are observed within regular amphibole sequences (Figs. 9b–9c). The Fe-banding can cross over triple-chain or pyroxene zippers in amphibole (Figs. 9c–9d). We note the presence of (1233) polysome as one of the more complex zippers within amphibole (Fig. 9d). Epitaxial relationships between $[11\bar{2}]_{magnetite}$ and $[001]_{amphibole}$ are shown in Figure 9e.

The Ce-bearing amphibole (Fig. 9f) shows a highly ordered 2-I_{beam} sequence with some disorder toward the margins represented by intergrowth of single pyroxene or triple 3-I_{beam} structures (Fig. 9g). Fast Fourier transform (FFT) patterns (insets in Figs. 9c and 9f) indicate these amphiboles have monoclinic symmetry. The other part of the Ce-bearing amphibole shows more complex polysomes that include 4- and 5-I_{beam} NCPs (Fig. 10h).

Several polysomatic sequences display wider, rhythmic intergrowths between amphibole and the triple chain silicate (Figs. 10a–10b). Blocks of 10 or 11 rows of 2-I_{beam} are interspersed with blocks of up to 8 rows of 3-I_{beam} in sequences dominated by amphibole, which nonetheless show domains of chain disorder (Fig. 10a). A switch to sequences dominated by triple chains is noted in the grain from Figure 3a, in which a block of 19 rows of 3-I_{beam} structure is flanked by finer rhythms of both 2- and 3-I_{beam} intergrowths (Fig. 10b). This block becomes wider (up to 23 rows of 3-I_{beam}) and shows NCP zippers as single rows of 5-I_{beam} structures (Fig. 10c). The FFT pattern indicate a monoclinic structure corresponding to clinojimthompsonite. There is also a very good match between the HAADF STEM image and the clinojimthompsonite simulation (Fig. 10d). In detail, combinations of (523) or (235) mark the end of the wider block in the center of this clinojimthompsonite grain (Figs. 10e–10f).

NCP-bearing polysomes (e.g., aggregate 4 shown in Fig. 3e) are highly disordered and display I_{beams} in the range of 4 to 7 within hosts of triple and double-I_{beam} structures (Fig. 11a). We note, however, the presence of repeats such as (737) or (5656), the latter being terminated on one side by a (354) I_{beam} sequence. Higher I_{beam} structures, 11 and 12, form single zippers with changes in size along $(010)_{planes}$ (Figs. 11b–11c). For example, the 11-I_{beam} becomes a (335) sequence, and the 12-I_{beam} becomes a (93) sequence. In addition, we note the presence of 5- and 6-I_{beams} zippers associated with rows of 3-I_{beams} in the same locations as such wide NCPs. None of these NCP-bearing polysomes form regular repeats. Details of the NCPs identified are shown in Figure 11d, spanning the entire range from 4- to 7-, and 9-, 11-, and 12-I_{beam} structures. The 8- and 10-I_{beam} structures are not observed within the longer polysomes.

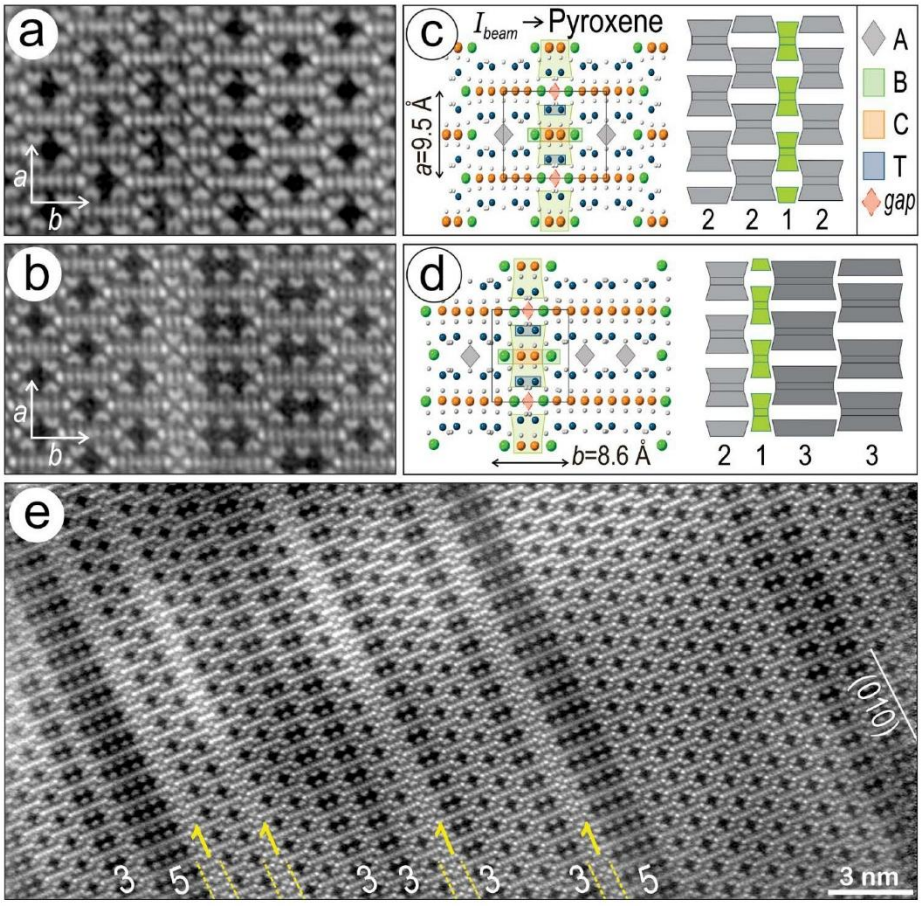

FIGURE 7. HAADF STEM images (**a**, **b**, **e**), atom fill models and I-beam schematics (**c** and **d**) for pyroxene slabs as zippers in other chain silicates for [001] zone axis. Diopside structure used for pyroxene model (Thompson and Downs 2008). A single slab of pyroxene, parallel with (010), is shown within amphibole in **a** and between amphibole and triple chain silicate in **b**. (**c** and **d**) Overlays on crystal models show the I_{beam} for pyroxene. The joint between 1-I_{beam} with 2- and 3-I_{beam} structures is realized by *a*/2 offset of the pyroxene central ribbon relative to that in the host silicate. Adjacent ribbons in the host silicates are separated by gaps (red diamonds) smaller than the *A* site (gray diamond) which is not present in pyroxene. The I_{beam} schematics show the resulting polysomes, numbers underneath: (212) and (213), respectively. (**e**) Polysomatic sequence in amphibole showing four pyroxene slabs across an interval of ~20 nm, two of which are placed at contacts with 5-I_{beams}. (Color online.)

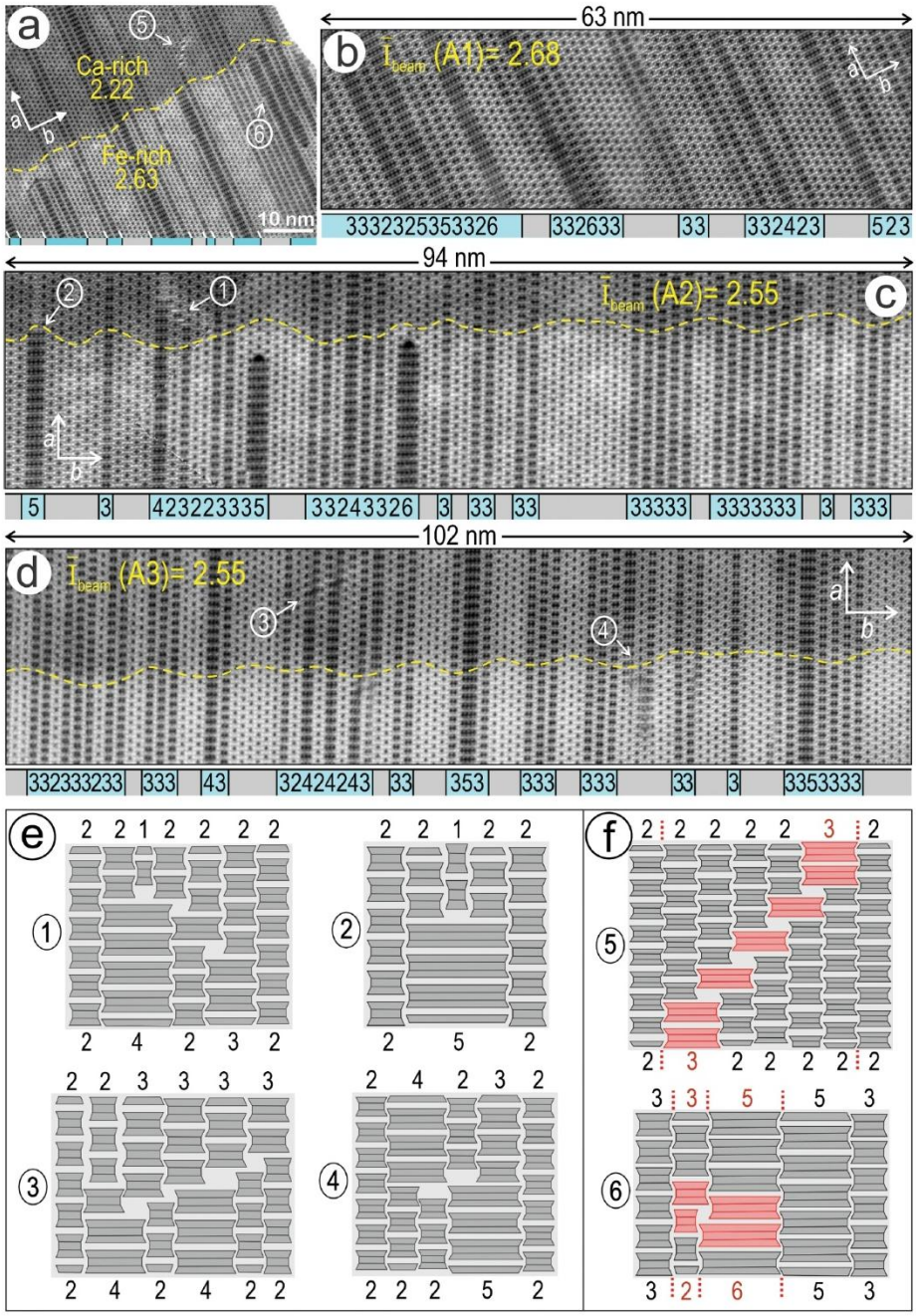

FIGURE 8. (**a**–**d**) Larger (up to 100 nm long) polysomatic sequences from aggregates (A1–A3) along profiles marked on Figures 3c, 3d, and 3g. The NCPs sequences within amphibole are marked by numbers in the blue boxes. Note compositional boundaries (dashed lines) in **a**, **c**, and **d**. The average $\bar{I}_{beam}$ for these sequences is in the range 2.22–2.68. (**e** and **f**) I_{beam} schematics showing zipper terminations for areas as labeled by circled numbers. Coherent terminations are shown in **e**. The red I_{beams} in **f** show derailment for case 5 and a zipper modification breaking termination rule 1. (Color online.)

Defects

A wide range of defects are present throughout the studied chain silicates (Figs. 12 and 13). Larger fields of amphibole with more regular zipper sequences comprising double or triple rows of 3-I_{beam} structures display chain derailment, sequence changes, or loops with simple or hairpin geometry and terminations (Fig. 12a). A glossary of defect structures is provided in the online materials. These chain modifications are abundant in areas where single NCPs are included within 3-I_{beam} zipper sequences. Planar defects are represented by sets of normal and inverse faults that can run over tens of nanometers and which link different zipper sequences (Figs. 12a–12b). Simple derail-

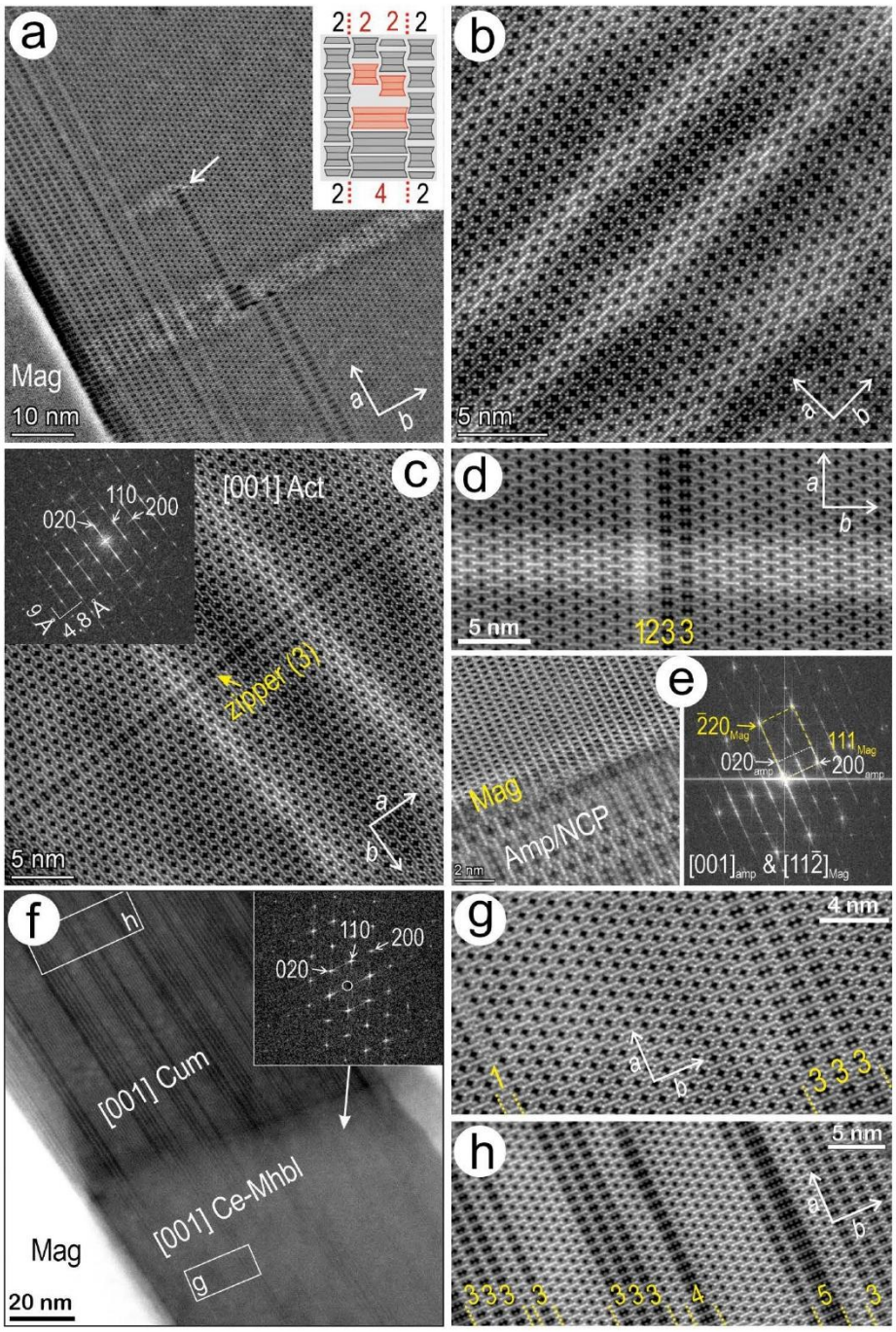

FIGURE 9. High-resolution images of amphiboles showing chain-width disorder and chemical zoning. (**a**) Single and double zippers of 4-I_{beam} with modifications across a Fe-rich chemical band in the middle of the image. The grain displays pyroxene zippers and a more regular sequence of triple-chain silicate toward the boundary to magnetite. Inset shows the zipper termination (arrowed) breaking rule 2. (**b**) Narrow (<5 nm wide) Fe-rich bands (brighter) along the *b* axis in a regular sequence of amphibole. (**c** and **d**) Fe-rich bands crossing single and triple zippers without changes in the structure. Inset in **c** shows fast Fourier transform (FFT) pattern on [001] actinolite (grain mapped in Fig. 4c) obtained from the whole image. Note presence of ($\bar{1}$10) reflections indicative of monoclinic symmetry. (**e**) Epitaxial contact between $[001]_{amphibole}$ and $[112]_{magnetite}$ typical for the zipper-bearing amphiboles. FFT pattern shows $(100)^{*}_{Amph}//(111)^{*}_{Mag}$. (**f**) Boundary between NCP-rich cummingtonite (top) and Ce-bearing magnesio-hornblende (bottom) (grain mapped in Fig. 5a). FFT pattern in inset obtained from the bottom part shows this is a monoclinic amphibole. (**g** and **h**) High-resolution images from areas marked on **f** showing the sequences in the two amphiboles. Note rare pyroxene and triple chain zippers in **g** and denser NCPs in **h**. (Color online.)

ments are relatively rare; more commonly, they are associated with "jogs," shorter defects assisting chain dislocation and, in some cases, sequence inversion (Fig. 12c). Short displacements are produced by conjugate, oblique sets of defects, crossing over up to as many as 10 to 12 chains (Fig. 12d). In detail, these are low-angle defects with step-displacements along their trajectories.

Formation of 8- and 10-I_{beam} structures is observed in sequences involving NCP zippers with chain defects (Figs. 12e–12f). Three ribbons of 8-I_{beam} silicate occur along the derailment of a quadruple zipper (Fig. 12e). A 10-I_{beam} structure (Fig. 12f) is observed along an unusually wide NCP zipper with multiple width changes, from 15-I_{beam} structure to evolving polysome sequences: (627) → (62.11) → (62.10) (Fig. 12d). Schematics in Figures 12g and 12h show details of the 8- and 10-I_{beam} structures.

En-echelon defects are also noted across some NCP zipper sequences (Fig. 13a). An unusual coherent zipper change is the

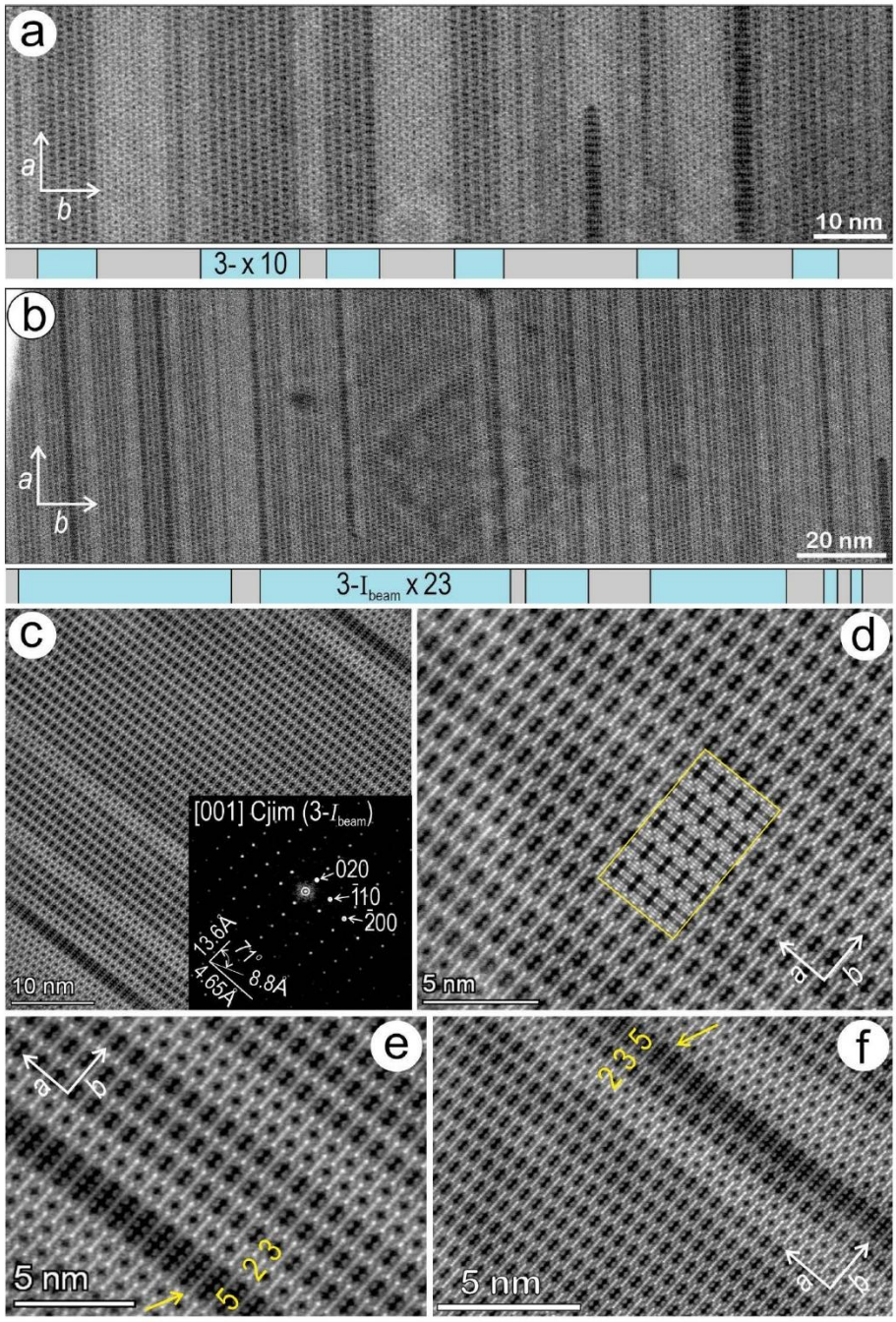

FIGURE 10. (**a** and **b**) Wider, more regular blocks triple chain slabs (up to 23; in blue) within amphibole (gray ribbon underneath). Sequence in **b** represent a full transect of clinojimthompsonite (Cjim) (grain in Fig. 3a) shown as high-resolution images in **c**–**f**. FFT pattern as inset to **c** is from the whole image. (**d**) Regular sequence (>17 slabs) of Cjim. STEM simulation shown as overlay. (**e** and **f**) Polysomatic disorder as (523) and (235) sequences on the edges of sequence in **c**. (Color online.)

sequence switch from (226) to (523) polysomes taking place along the *b* axis without any displacement. On the other side of the zipper sequence displaying the en-echelon defects, we note that a change from (326) to (22223) polysomes is assisted by an asymmetric "bow" defect.

Other, less common defects are those linking multiple NCP zippers (Fig. 13b). Such defects assist local changes in sequence and/or terminations. Details of the oblique defects and jogs are shown in Figs. 13c–13d). The jogs show *b*/2 displacements of the chain silicate, e.g., the switch between 4- and 3-I_{beam} chains shown in Figure 13d. We note changes in the HAADF signal intensity along the ribbon accompanying such jogs.

A further type of defect that is associated with distortion in the host silicate involves "swells" between adjacent NCPs and/or pyriboles (Figs. 13e–13f). Such swells result in *a*/2 disruption of the chains across the defects. The swell can be either a

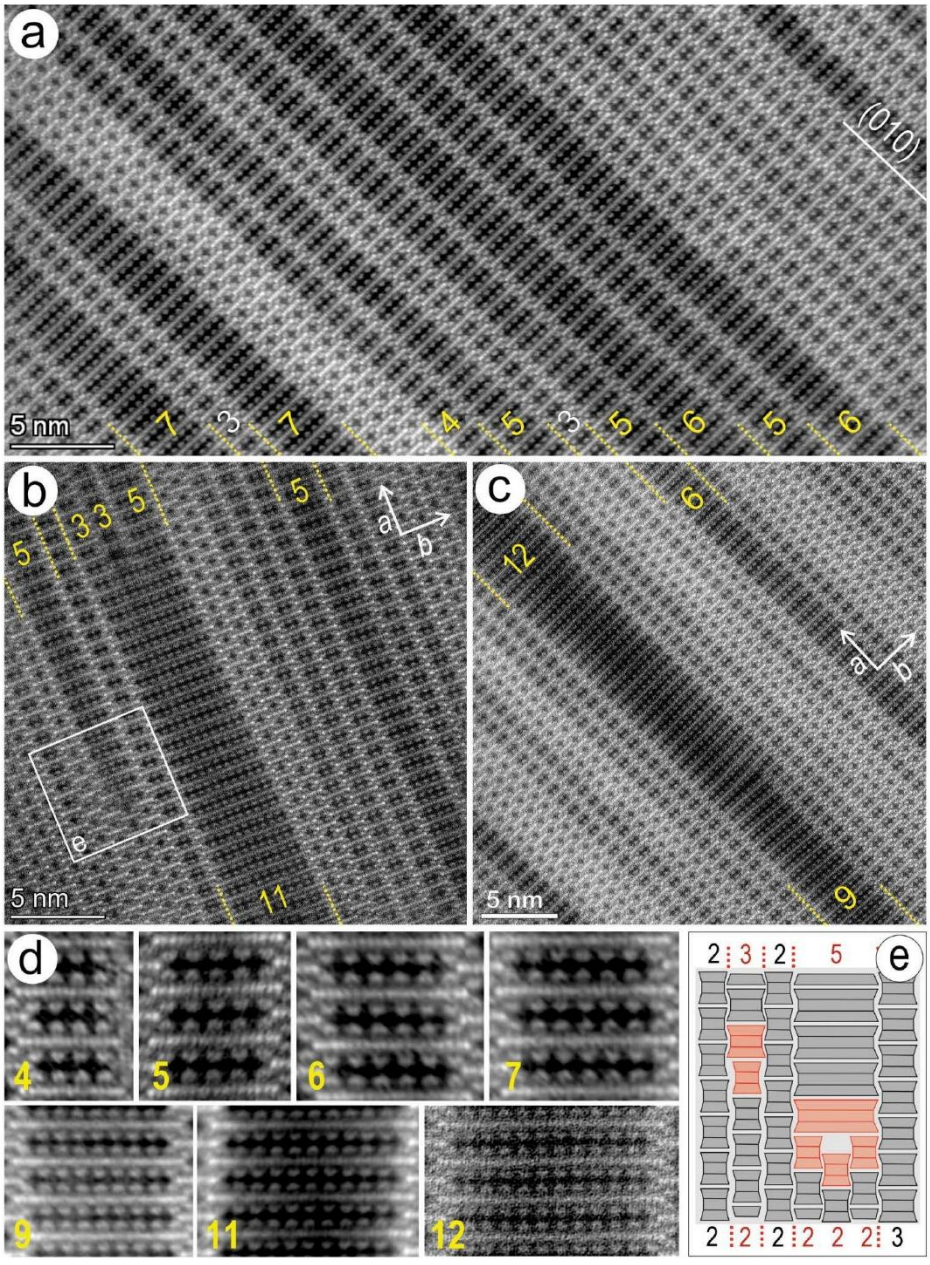

FIGURE 11. High-resolution images showing polysomes with the widest I_{beams} and I_{beam} schematic. (**a**) Sequences comprising (737) and (45355656) polysomes in amphibole and triple-chain silicate. (**b** and **c**) Sequences with 11- and 12-I_{beam} structures with changes along *a* direction. (**d**) Details of NCPs with I_{beams} in the ranges 4–7 and 9, 11, and 12. Note the numbers of diamond-shaped motifs (A sites) and the dots along the cation ribbon (B+C sites) in agreement with formula (1). (**e**) Termination of 3- and 5-I_{beam} zippers breaking rule 1. (Color online.)

single or double step, e.g., across sequences with changes from 12- to (93)-I_{beam} or from (532) to (46)-I_{beam}. The two types of swells are shown schematically in Figures 13g–13h.

Both coherent and incoherent terminations are observed for short NCP zippers (Figs. 13i–13j). Coherent, arcuate terminations of multiple zippers are also noted, such as the (32423) sequence shown in Figure 13k. The I_{beam} schematic of the switch between I_{beam} zippers is shown in Figure 13l.

Sheet silicates

High-resolution imaging of the aggregates displaying marginal replacement, such as those shown in Figures 4b–4c, confirms the presence of sheet silicates represented by talc, biotite, and chlorite in direct contact with chain silicates (Fig. 14). Integrated EDS spectra for the three species are shown in Online Materials[1] Figure A9. The replacement boundary can display a ragged outline with $talc_{[100]}$ (also identified from the FFT pattern in the

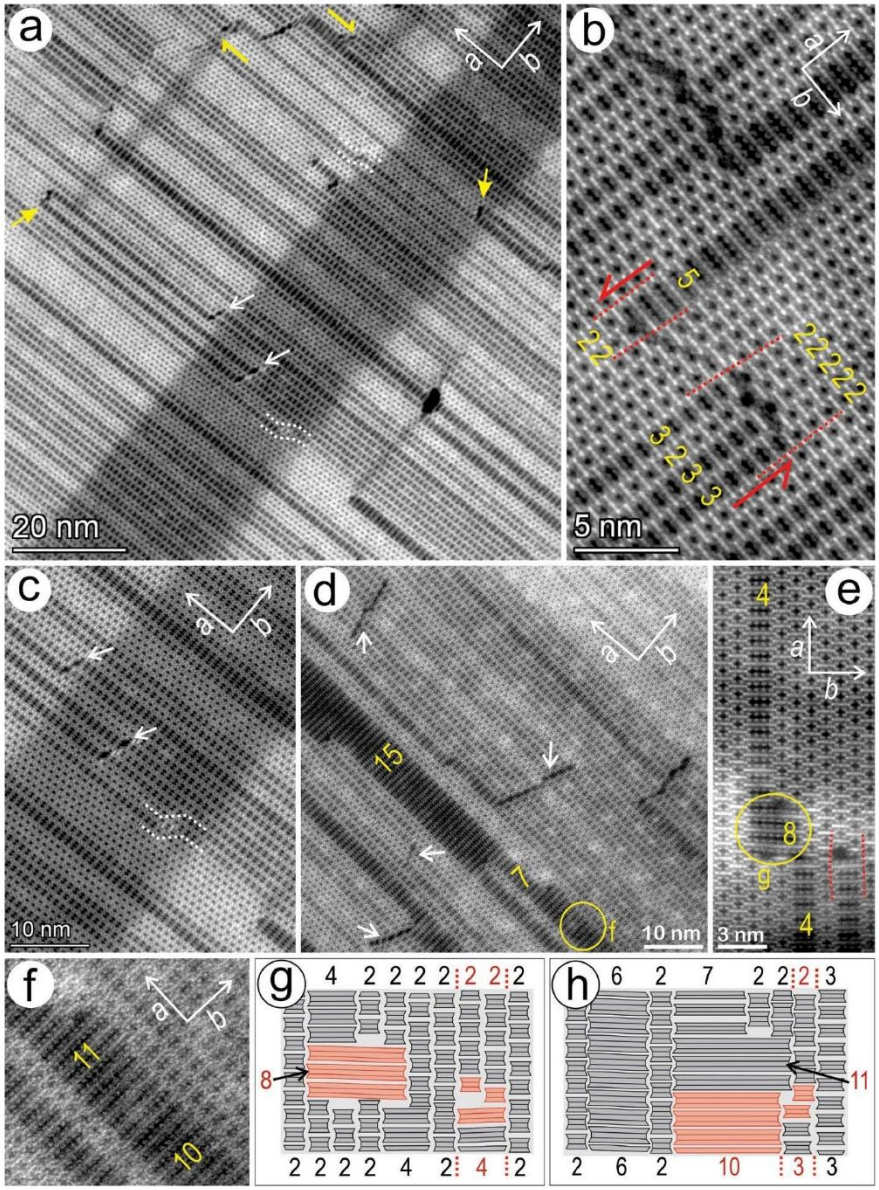

FIGURE 12. Overview of chain-width disorder and defects in NCP-rich amphiboles as images and I_{beam} schematics. (**a**) Field showing a wide range of defects as chain derailment (dotted line), jogs (white arrows), and hairpin structures (yellow arrows). Normal fault with displacement movement marked in red. (**b**) Inverse fault (movement marked in red) transforming zippers sequences (as numbered) in amphibole with violation of both termination rules. (**c**) Detail from **a** showing jog defect zipper transformation. (**d**) Oblique defects (arrowed) in the vicinity of 15-I_{beam} zipper with multiple width changes along *a*. (**e**) Occurrence of the 8-I_{beam} zipper along a 4-I_{beam} derailment in amphibole. (**f**) Detail from **d** showing formation of the 10-I_{beam} structure. (**g** and **h**) Neighborhood of 8- and 10-I_{beams} structures showing changes in sequences breaking zipper termination rules. (Color online.)

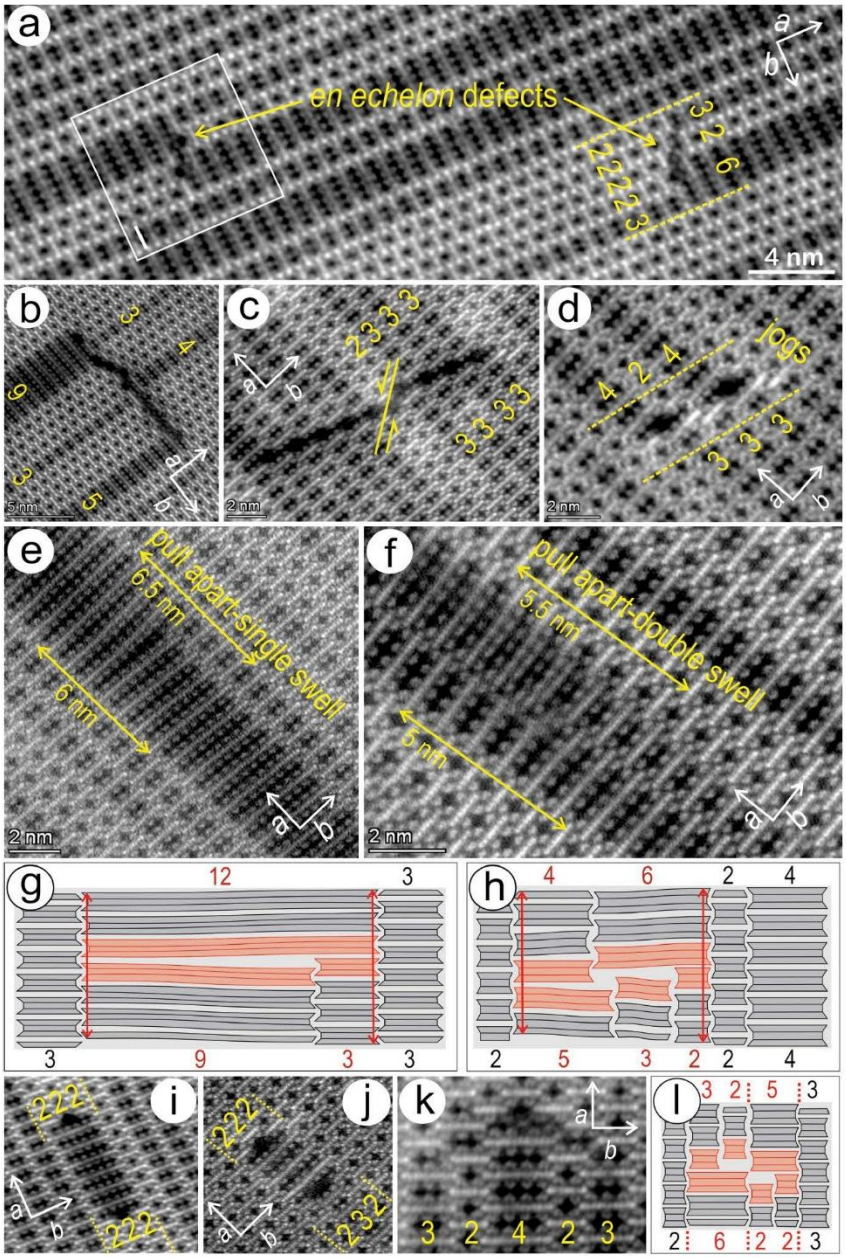

FIGURE 13. Details of chain-width disorder and defects in NCP-rich areas as images and I_{beam} schematics. (**a**) En-echelon defects bridging 6-I_{beam} zippers via the (233535) polysome. (**b**) Coherent zipper termination linking multiple NCP zippers. (**c**) Oblique defects marking a shear plane (arrowed) cutting across triple-and double-chain sequences with changes breaking termination rule 1. (**d**) Detail of jogs showing displacement along *b* assisting changes between 3- and 4-I_{beam} structures (note violation of rule 1). (**e** and **f**) Wide NCP zippers with single and double pull-apart swells shown as schematics in **g** and **h**. Note violation of termination rule 2 in both cases. (**i** and **j**) Short, double terminations zipper with coherent and incoherent ends. (**k**) Arcuate defect assisting coherent zipper termination. (**l**) Schematic showing area from rectangle in **a** showing a switch between 6- and 5-I_{beams} breaking both termination rules. (Color online.)

figure inset) forming inliers along the *a* axis of the amphibole$_{[001]}$ (Fig. 14a). The direct contact is marked by voids(?) occurring as black motifs along common <010> directions. Displacement of 7-I_{beam} zippers within the amphibole is noted along jog-type defects. Straight contacts along <010> directions are also common between sheet and chain silicates (Fig. 14b). Changes from talc to mica sequences are observed on one of the stepwise <110> margins, exposing coherence between cation ribbons in the two types of silicates along <010> directions. The FFT pattern obtained from the area confirms the crystallographic alignment

between them (inset in Fig. 14b).

NCP polysomes evolving from (253322623) to (15.13) sequences show a transition to the talc structure marked by slight corrugation of the sheet silicate (Fig. 14c). Swell-type defects are present in the talc. Replacement of amphibole by talc along two directions, <100> and <010>, also shows a straight outline, albeit with stepwise geometry on one side (Fig. 14d). Defects in the talc sequence are marked by a patch of chlorite. Straight contacts along <010> directions between mica (biotite) and amphibole (actinolite) are also coherent (Fig. 14e).

Sequences of talc and chlorite are also observed (Fig. 14f). The FFT pattern of chlorite is distinct from both talc and mica on the [100] zone axis (Fig. 14f inset). Swelling defects and transition between talc and other sheet silicates are very common (Fig. 14g).

The changes in the HAADF STEM images between the three sheet silicates are highlighted by atom-fill models (Figs. 14h–14j). Although the FFT patterns for talc and mica are undistinguishable on [100] zone axes (Figs. 14a and 14e), the HAADF STEM image shows a "dot" between the *T* sites (Fig. 14e), representing the K atoms in the mica structure (Fig. 14h). On the other hand, the sandwich-type structure of chlorite$_{[100]}$ displaying cation ribbons flanked by alternating *T* sites and OH modules (Fig. 14i) is also visible on the HAADF STEM images (Figs. 14d and 14f). Talc has the simplest structure (Fig. 14j). This is reproduced by STEM simulations (overlay in Fig. 14f) with relatively good fit to the images.

DISCUSSION

Polysomatic and chain-width disorder: primary vs. replacement reactions

We attribute the observed features to co-crystallization of double- and triple-chain silicate structures since the majority of the polysomatic sequences we observe are constrained within comparable $\bar{I}_{beam}$ ranges between 2 and 3-I_{beams}, despite their wide variation across or along a single grain (Figs. 3a, 3b, and 8). Although some grains record wider intergrowths of 2- and 3-I_{beam} structures, neither the larger blocks nor the finer scale intergrowths form regular repeats (Fig. 10). Therefore, polysomatic disorder is the main feature of the chain silicate packages described here. Nonetheless, the presence of rhythmic intergrowths, either as blocks (Figs. 10a–10b), or short 3-I_{beam} sequences within amphibole (Fig. 9f), indicates that the crystallization process is self-organized at a scale of hundreds-of-nanometers intervals rather than randomly.

Primary co-crystallization is also inferred from the fact that the NCPs, either as single or more complex zippers, form along the entire length of the crystal. However, changes in the sequences along the crystal, and in particular, terminations of wider zippers, are indicative of polysomatic reactions between different I_{beam} sequences (Figs. 3g, 8, and 9f). This is especially true in the aggregates enveloped by sheet silicates in which the widest NCP sequences are recorded (Figs. 2a, 11, and 14).

Additionally, disorder is defined by the fact that polysome ranges across any given profile are always combinations of wider structures (up to 13 discrete I_{beams} each) with shorter (down to single I_{beam} structures) sequences (Fig. 8). Although all the polysome sequences do not show repeats of sufficiently long range to enable definition of specific species, we note the presence of the 5-I_{beam} as a polytype of the (23)-I_{beam}, albeit as single zippers or as a component of multiple zippers (Figs. 10e–10f).

The presence of wider chain silicates as metastable phases during the replacement of amphibole by talc (Veblen and Buseck 1980) is a viable interpretation for the widest NCP polysomes reported here as "fronts" protruding from the sheet silicates (Figs. 14a and 14c). However, the observed formation of isolated NCPs across longer sequences of double and/or triple-chain silicates is attributable to kinetic instabilities developed during primary growth that result in coherent zipper terminations within the host structure (Figs. 8 and 10). Some of the widest chain sequences documented by us (Fig. 11) can be linked to kinetic models involving increasing and decreasing chain width during the primary formation of the triple-chain silicate (Grobéty 1997). Such schemes invoke "species" mobility by side-stepping glide mechanisms along the *b* direction (e.g., triple chain zipper displaying a four-step derailment in amphibole; Fig. 8f).

The chain-width disorder is also widely represented in the studied material and can be discussed in terms of the two rules of coherent zipper termination (Veblen and Buseck 1980). Although the polysome sequences obey these rules (Fig. 8e), breaches are common, particularly in areas with defects associated with wider I_{beam} structures.

Violation of rule 1 (sub chain number N_i) is found when displacive planar faults or short jogs transform sequences with non-matching N number on the two sides of the defects, e.g., N_1 = 11(2333) → N_2 = 12(3333) (Fig. 13c), or N_1 = 10(424) → N_2 = 9(333) (Fig. 13d). Moreover, violation of rule 1 is also encountered along zippers that change in width without planar defects as we show in Figures 12e–12h for the occurrence of 8- and 10-I_{beams}. For example, the 8-I_{beam} is placed both between sequences with N_1 = 8(422) and N_2 = 6(222), or with N_2 = 10(2224), depending on how the length of the sequence is selected (Fig. 12g). Terminations of a single 6-I_{beam} zipper leads to sequences such as N_1 = 6(222) and N_2 = 7(232) (Fig. 13j), also infringing on rule 1.

Examples of single zippers doubling [12-I_{beam} → (93), or double zippers changing into triple zippers (46) → (532) (Figs. 13e–13f)] break rule 2, since the zipper numbers are not both either even or uneven. Notably, these changes are not associated with zipper terminations or planar defects.

Even more common are examples in which both rules are violated. For example, the en-echelon zippers shown in Figure 13a feature a 6-I_{beam} on one side changing into a (32) sequence, and a 5-I_{beam} becoming a (22) sequence, both with non-conserved N (Fig. 13l). In contrast, the other side of the same en-echelon structure displays conservative changes from N_1 = 11(32222) to N_2 = 11(326). A further example that breaks both rules occurs along the inverse fault illustrated in Figure 12b. This shows a single 5-I_{beam} changing to a double (22) zipper and a quadruple zipper of N_1 = 11(3233) changing to a quintuple zipper of N_2 = 10(22222). We note that the terminations of the 5-I_{beam} zippers are those that most commonly break the conservation rules (Figs. 8f, 11b, and 11e).

The occurrence of planar faults and other defects during replacement reactions among pyriboles is concentrated in regions of chain-width disorder with a violation of the two termination

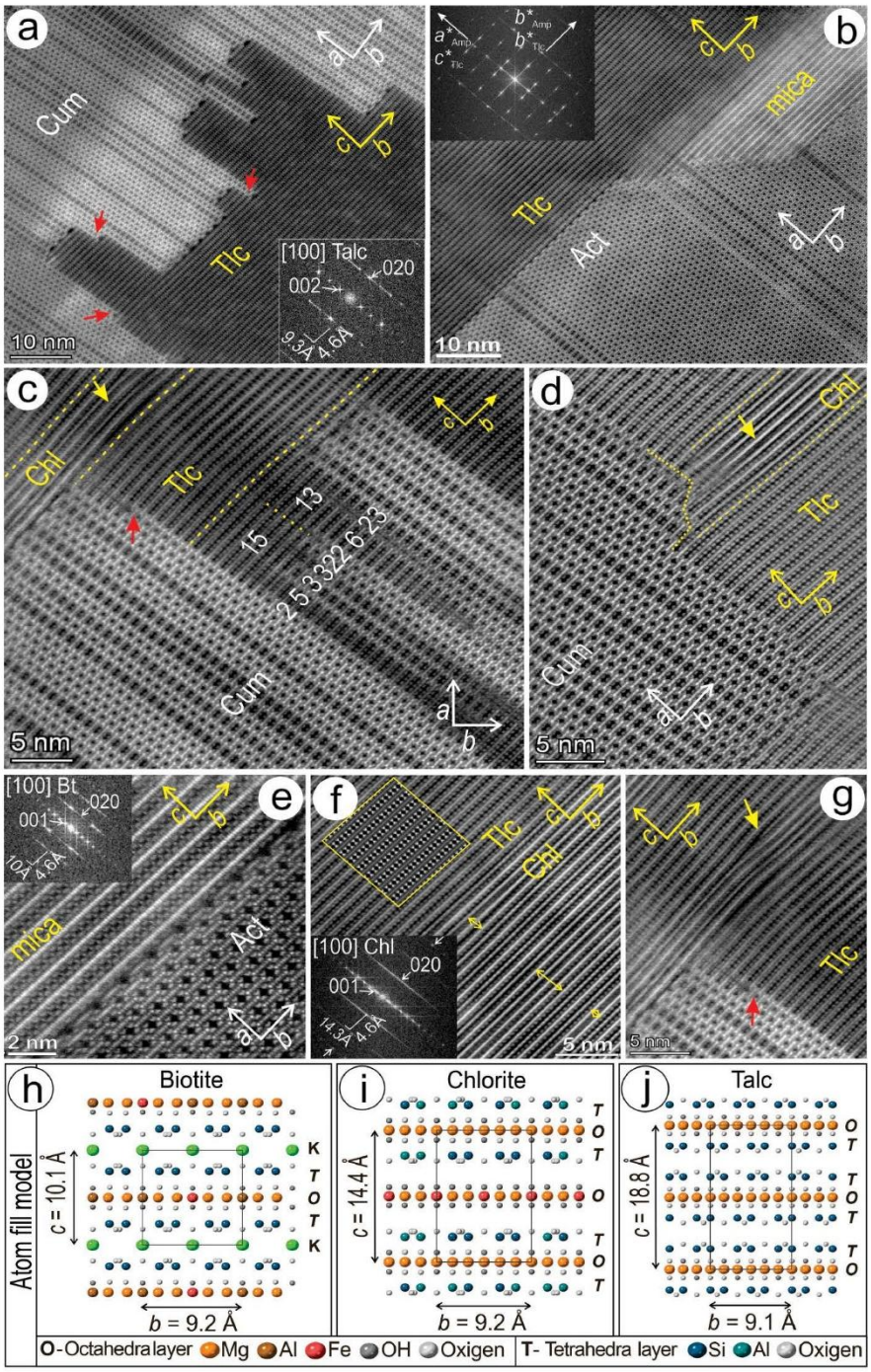

FIGURE 14. Overview of replacement between sheet and chain silicates. (**a**) Contact between $[100]_{Tlc}$ and $[001]_{Cum}$. Note the ragged contact outline with ledges (arrowed) and voids (dark areas). FFT pattern for talc (Tlc) as inset. (**b**) Stepwise contact between actinolite (Act) and sheet silicates comprising talc and a package of mica. FFT pattern (inset) shows coherent orientation between the two silicates which share b* axes. (**c**) Replacement front between talc and cummingtonite (Cum) along two directions with straight contact (c_{Tlc} parallel to a_{Cum}). Wide NCP zippers show increase of I_{beam} numbers toward the contact to talc. Swell defects (arrowed) produced by intercalation of chlorite (Chl). (**d**) Edge of cummingtonite showing replacement by talc with straight and stepwise (dotted line) contacts. Note a chlorite package (dashed line) and disorder (arrowed) in talc. (**e**) Contact between mica (FFT pattern indexed as biotite, Bt) and actinolite. (**f**) Chlorite (FFT pattern as inset) displaying stacking disorder intervals (marked) at the contact to talc (STEM simulation as overlay). (**g**) Swell defects (arrowed) in sheet silicates with mix packages (Tlc and Chl). (**h**–**j**) Models showing typical *T-O-T* packages (*T*, *O* = tetrahedral, octahedral layer) for the three sheet silicates. The packages are sandwiched with either K or *O* layers in biotite and chlorite. Note match between models and images above. (Color online.)

rules (Veblen and Buseck 1980). However, primary growth was also invoked either for the formation of isolated wider chains in amphibole (Cressey et al. 1982), or for the simultaneous growth of NCPs with rule violation (Konishi et al. 2010). The NCPs discussed here are outstanding examples of chain-width disorder with defects disobeying the terminations rules. Among these defects, jogs, swells, oblique/low-angle, and en-echelon faults are indicative of strain-induced deformation during growth. Violation of the two rules and, especially, the lack of planar displacive faults accompanying chain-width disorder in pyriboles intergrown with anthophyllite was interpreted as associated with metamorphic deformation of host lithologies by Konishi et al. (2010) in their study of Archean ultramafic rocks from Greenland.

The relationships between chain and sheet silicates indicate coherent grain replacement (Fig. 14), as discussed by Veblen and Buseck (1980). This is represented by grain boundaries in which the transition from (010) to (100) takes place via (210) interfaces (Figs. 14b and 14d). Nevertheless, the (210) interface also shows stepwise displacement where the sheet silicate changes from one species to another (talc to mica or chlorite). We also note the presence of either single or double ledges between amphibole and talc along the (100) interface (Figs. 14a and 14g). Features along this interface, which we interpret as channels, are clearly visible on HAADF STEM images (Figs. 14a, 14b, and 14e).

Chemical patterning and fluid evolution recorded by chain silicates in magnetite

The two groups, calcic and Mg-(Fe) amphiboles (Fig. 2d), indicate distinct generations of inclusion growth in magnetite. Among these, the presence of Al-rich and Ce-bearing calcic amphibole is indicative of variable physical-chemical conditions (high pressure for ferrotschermakite) or REE-enriched fluid sources. Moreover, the concentration of NCPs in Mg-Fe- rather than calcic amphiboles in the altered mafic/ultramafic rock hints at the better preservation of a geochemical signature inherited from the host lithology in the former. This correlates with the preferred affiliation of NCPs with altered and/or metamorphosed mafic-ultramafic complexes noted in the literature (e.g., Veblen and Burnham 1978a, 1978b; Cressey et al. 1982; Schumacher and Czank 1987; Droop 1994; Grobéty 1996, 1997; Akai et al. 1997; Konishi et al. 2008, 2010; Ferrari and Viti 2010). Several occurrences of triple-chain silicate in amphiboles from lithologies hosting magmatic-hydrothermal ore deposits, e.g., the Atakani skarn, Japan (Akai 1982), Wirrda Well IOCG deposit, South Australia (Ciobanu et al. 2022) and metamorphosed nickel ores from the Norseman-Wiluna belt, Western Australia (Akai et al. 1997) are still related to the presence of mafic/ultramafic rocks.

A notable exception is the unusual occurrence of "wide chain Ca-pyriboles" precipitated under a geothermal gradient within sediment-hosted cavities from the Salton Sea Geothermal Field, California (Yau et al. 1986). In this case, primary growth at greenschist facies conditions (~300 °C; 1 to 1.5 km) is considered based on the NCP-pyribole associations and their micro- to nanoscale textures. Likewise, calcic-rich analogs of clinojimthompsonite are reported from Oeyama ophiolite, Japan (Konishi et al. 1993), that compare with the NCPs-rich, calcic amphiboles reported here (Fig. 2d). The Fe-rich NCP varieties reported from the Norseman-Wiluna belt by Akai et al. (1997) are also represented in the NCPs intergrowths reported here (Fig. 4c).

An outstanding, novel feature of the Jatobá amphibole inclusions is the rhythmic Ca-Fe zonation, with bands ranging in width from tens or hundreds of nanometers (Figs. 3g and 5a) down to just a few nanometers (Fig. 9b), along the *a* direction. This type of zonation reinforces the idea of self-patterning via oscillatory chemical gradients in a closed, close-to-equilibrium system, i.e., a decoupling of inclusion growth from the enclosing magnetite. However, the silicate chain sequence remains unchanged throughout the zoning along *a* (e.g., Figs. 8a–8d), contrasting with the self-patterning along *b* that can be attributed to the formation of rhythmic polysome sequences (Figs. 10a–10b). Hence, we suggest significant differences in growth kinetics during inclusion crystallization (faster along *a* compared to *b*). Taken together, these chemical-structural characteristics strengthen the idea of primary NCP crystallization during amphibole formation in magnetite.

In contrast to the above, the observed transition from NCP-rich cummingtonite to Ce-bearing magnesio-hornblende along the *a* direction in a single inclusion (Figs. 5a and 9f) implies changes in the fluid signature from a mafic- to felsic-affiliation if we consider, for example, the REE enrichment in sodic amphiboles formed during the magmatic-hydrothermal evolution of peralkaline granitoids (Bernard et al. 2020). The Ce-concentration reported here (~6.7 wt% Ce_2O_3) is however orders of magnitude higher than the tens to hundreds of ppm ΣREE measured in Na-amphiboles from six alkaline igneous complexes (Bernard et al. 2020). Such extreme REE concentrations can be attributed to the onset of the Jatobá magmatic-hydrothermal system with REE-rich fluids percolating through existing lithologies. Abundant Ce-bearing nanoparticles (Fig. 4a) are formed in magnetite adjacent to the orebody. Crystallization of thinner, Ce-bearing calcic amphibole inclusions is predominant and partially replaces pre-existing NCP-rich amphibole. Higher influx of percolating fluids is also recorded by the replacement of larger NCP-bearing aggregates by sheet silicates, dominantly talc (Fig. 14a). Moreover, these fluids are K- and Al-bearing as indicated by formation of mica and/or chlorite (Figs. 14b and 14d–14f). An increase in Al at this stage is also supported by the composition of Ce-bearing magnesio-hornblende from the same sample.

The highest Al contents are measured in Fts inclusions from the ore sample (Fig. 5b). Using Al^{tot} values of 2.47 and 2.59 apfu for the two Fts grains (Online Materials[1] Table OM1; Fig. 2d) and the formula $P(kbar) = 0.5 + 0.331(8) \times Al^{tot} + 0.995(4) \times (Al^{tot})^2$ for the revised Al-in-hornblende geobarometer (Mutch et al. 2016), we obtain pressures of 7.4 and 8.04 kbar. Such high-pressure might be attributed to shearing along faults prior to or during ore deposition. At this stage, magnetite has recrystallized resulting in most of the amphibole inclusions being lost (Fig. 1c). Some NCP-rich aggregates are nonetheless preserved, likely inherited from pre-ore stages. These display no marginal replacement by sheet silicates (Fig. 3c; Online Materials[1] Fig. A1).

Genetic implications

The evolution of magnetite, host to the amphibole-NCPs inclusions, is shown schematically in Figure 15. The earliest stage of magnetite formation is recorded by the NCP-amphibole

inclusions preserved within mottled cores with irregular shapes. The morphology of the Mg-Fe-amphiboles (coarser aggregates, rounded shapes), the lack of coherence between the NCPs and host magnetite, and the abundance of NCPs, indicates formation during regional metamorphism of host lithologies and prior to the main sulfide deposition (Fig. 15a). Syn-metamorphic deformation is recorded by widespread chain-width disorder in NCPs. The second generation of inclusions, defined by their occurrence in thinner, euhedral amphiboles and the presence of zipper NCPs only marks an overprint of the core magnetite (Fig. 15b). At this stage, epitaxial growth of inclusions indicates magnetite recrystallization which is also associated with a marked chemical change from Mg-Fe- to calcic, REE-bearing amphibole (actinolite; Ce-bearing Mg-hornblende). Such minerals, together with their REE-enriched signature are typical of deposition from magma-derived hydrothermal fluids during the onset of IOCG systems (Corriveau et al. 2016; Ciobanu et al. 2019; Courtney-Davies et al. 2020; Verdugo-Ihl et al. 2020).

The Jatobá orebodies are hosted along shear zones (Veloso et al. 2020) which act as channels focusing fluid flow resulting in obliteration of the mottled cores within magnetite (Fig. 15c).

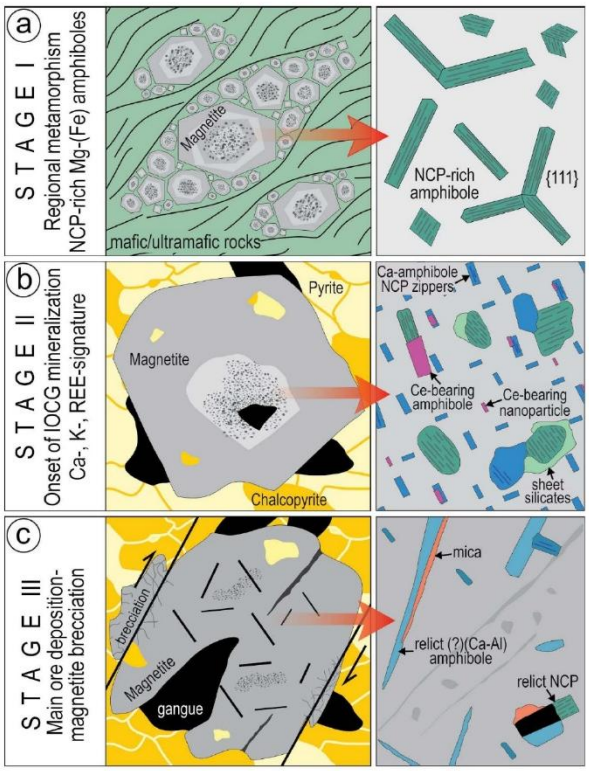

FIGURE 15. Schematic showing staged evolution of magnetite as labeled. (**a**) Metamorphic segregation results in lenses of magnetite with cores clustered by Mg-(Fe)-amphiboles with NCPs. (**b**) Recrystallized magnetite preserves cores mottled by new-formed Ca-(Ce)-amphiboles. NCPs-rich-amphiboles are preserved as rounded grains and aggregates with marginal replacement by sheet silicates. (**c**) Shearing and brecciation of magnetite during ore stage preserves high-pressure calcic-Al-amphiboles and NCP-aggregates. NCP-aggregates preserved from the first stage. (Color online.)

High-pressure (~7.5 kbar) ferrotschemakite typifies a generation of calcic amphiboles, which coexists with biotite+titanite, but may be inherited from an earlier stage. Despite reworking, magnetite still preserves NCP-rich Mg-Fe-amphiboles from the earliest stage.

Although few amphiboles were observed in the studied mafic/ultramafic sample, the amphibole species described in magnetite have been recorded among the many varieties reported from host diabase and ore-associated magnetite at Jatobá (Veloso et al. 2020). The paragenetic scheme developed by Veloso et al. (2020) differs, however, from our interpretation in that they considered the multiple generations of calcic and Mg-Fe amphiboles to have formed through the deposit evolution, from pre- to ore-stages.

This is the second reported occurrence of a NCPs-amphibole association in magnetite from an IOCG system. However, in contrast to that documented from Wirrda Well, South Australia (Ciobanu et al. 2022), the Jatobá magnetite does not show silician defects. This difference may be attributed to the longer history of magnetite overprinting at Jatobá causing obliteration of such features. The discovery of NCPs in amphiboles represents a strong link between magnetite from the Neoarchean Carajás Province (Brazil) and the Mesoproterozoic Olympic Province, South Australia, the two largest IOCG terranes on Earth.

SUMMARY AND IMPLICATIONS

Results of this work are summarized as follows:

(1) Jatobá magnetite hosts monoclinic amphiboles and NCPs within mottled cores or as sparse inclusions along {111} directions. The NCPs and amphiboles form polysomatic intergrowths along the *b* axis documented using HAADF STEM imaging on [001] zone axis. This is the first occurrence of clinojimthompsonite within magnetite and our observations represent one of the widest ranges of chain silicates yet recorded, up to 15-I_{beam} chains. Single to triple rows of I_{beam} zippers, including pyroxene slabs, in amphibole are the simplest intergrowths.

(2) EDS STEM mapping shows two chemical populations: Mg-Fe- and Ca-(Al)-amphiboles, dominantly cummingtonite, and actinolite; the first category being richer in NCPs. The calcic amphiboles include Ce-rich (up to 6.7 wt% Ce_2O_3) varieties of Mg-hornblende and (ferro)tschermakite, with the compositions $^{B}(Ca_{1.66}\square_{0.34})_2{}^{C}(Mg_{2.37}Fe^{2+}_{1.11}Al_{0.64}Fe^{3+}_{0.53}Ce_{0.36})_5{}^{T}(Si_{7.16}Al_{0.84})_8O_{22}(OH)_2$, and $^{A}(Ca_{0.43}Na_{0.27}K_{0.13}\square_{0.17})_1{}^{B}(Mg_{0.44}Ca_{1.56})_2{}^{C}(Fe^{2+}_{1.94}Mg_{1.45}Al_{0.9}Fe^{3+}_{0.7}Ti_{0.02})_5{}^{T}(Si_{6.37}Al_{1.64})_8O_{22}(OH)_2$, respectively.

(3) Based on HAADF STEM imaging, we formulate a relationship between the increase in the number of *C* and *A* cations from amphibole (2-I_{beam}) to n chain silicates (nI_{beam}) as: $nI_{beam} = T(2 + n) = C(5 + 3n) = A(1 + n)$, n = integer. The increase in the number of *C* and *T* cations controls the expansion of the *b* unit-cell parameter (by ~9 Å per additional I_{beam}). The *a* and *c* parameters remain relatively constant. Using this formula, we produced empirical models of crystal structures for 4- and 5-I_{beam} chain silicates. These models were validated by STEM simulation.

(4) Although no discrete polysomes could be defined, the NCP-amphibole intergrowths have I_{beam} averages ($\bar{I}_{beam}$) around 2.5–2.7 (composition between Mg-Fe amphiboles and clinojimthompsonite).

(5) Co-crystallization of double- and triple-chain silicate structures in many cases with rhythmic intergrowths as larger

blocks along *b* is often accompanied by rhythmic Ca-Fe zonation along *a*. Such chemical-structural characteristics strengthen the idea of primary NCP crystallization via self-patterning during amphibole growth in magnetite in a close-to-equilibrium system.

(6) Chain-width disorder is documented from a wide range of defects, e.g., planar faults, derailments, jogs, swells, assisting changes of the intergrowth sequences. Many violations of zipper termination rules indicate primary growth rather than replacement. The latter is represented by sheet silicates, dominantly talc, but also biotite and chlorite, which replace coarser NCP-amphibole aggregates.

(7) The multi-stage evolution of Jatobá magnetite is constrained from the amphibole-NCPs inclusions. The NCPs formed in abundance during the first cycle of magnetite overprinting (Mg-rich NCPs, talc present) within an [older] mafic/ultramafic lithology recording syn-shearing events (oblique defects, jogs, etc.). This was followed by formation of NCP-zippers in calcic-amphiboles and the formation of some Ce-bearing species, indicating fluid influx with IOCG signature at the onset of the mineralizing system. High-pressure Fts (~7.5 kbar) and NCPs formed in magnetite during shearing events and are preserved. NCPs have been preserved throughout the history of magnetite overprinting.

This study shows the suitability of HAADF STEM imaging for depicting crystal structure modularity in pyriboles and NCPs since the images are readily interpretable in accordance with crystal structure models. The generic formula suggested here for chain silicates expansion toward longer I_{beam} numbers predicts new structures that need to be assessed in terms of their thermodynamic stability. Discovery of Ce-rich amphibole offers an opportunity for research that can lead to models of REE incorporation into, and subsequent release from chain silicates.

The multi-stage amphibole-NCPs generations depicted here reinforce the idea that magnetite is a key mineral for tracking overprinting events in terranes with protracted geological histories. The study emphasizes the need for characterization down to the nanoscale when dealing with trace element concentrations and their distributions within a host mineral, in this case magnetite. All too commonly, genetic models and trace element substitution mechanisms are proposed based solely on empirical measurement of trace element concentrations without recognizing whether those elements are in solid solution or occur as nanoscale inclusions.

The occurrence of NCPs in magnetite from magmatic-hydrothermal deposits is likely to be widespread and is readily predictable in those deposits hosted by greenstone belts and other altered mafic/ultramafic complexes. Metamorphism and associated deformation, often obliterated in altered lithologies, can be tracked through careful observation of the range of microtextures and/or defects in magnetite-hosted NCPs. On the other hand, the presence of key minerals (actinolite, biotite) and associated chemical signatures (K, Ca, REE) within magnetite provides clues to the early alkali-calcic alteration stages in IOCG systems.

Acknowledgments and Funding

We extend thanks to Animesh Basak for technical support with FIB analyses and Max Verdugo-Ihl for his assistance with EDS analyses. Y.T.C.R and M.E.S acknowledges continuous support from the Brazilian Research Council (CNPq – Project 409015/2021-0) and the Coordenação de Aperfeiçoamento de Pessoal de Nível Superior, Brasil (CAPES), Finance Code 001. Analytical expenses were supported by a grant from the Institute of Sustainability, Energy and Resources, The University of Adelaide. N.J.C. and K.E. acknowledge funding through Australian Research Council Linkage grant LP200100156 (Critical Minerals from Complex Ores). We acknowledge constructive comments from two anonymous reviewers and thank Associate Editor Bradley De Gregorio for his handling of the manuscript.

References Cited

Ahn, J.H., Cho, M., Jenkins, D.M., and Buseck, P.R. (1991) Structural defects in synthetic tremolite amphiboles. American Mineralogist, 76 , 1811–1823.

Akai, J. (1982) Polymerization process of biopyriboles in metasomatism at the Akatani ore deposit, Japan. Contributions to Mineralogy and Petrology, 80, 117–131, https://doi.org/10.1007/BF00374889.

Akai, J., Chiba, A., Konishi, H., Komatsu, M., and Matsubara, S. (1997) New occurrences of non-classical pyriboles formed during ocean-floor and regional metamorphism: Estimated *PT* conditions of formation. European Journal of Mineralogy, 9, 1237–1256, https://doi.org/10.1127/ejm/9/6/1237.

Ams, B.E., Jenkins, D.M., Boerio-Goates, J., Morcos, M.R., Navrotsky, A., and Bozhilov, K.N. (2009) Thermochemistry of a synthetic Na-Mg-rich triple-chain silicate: Determination of thermodynamic variables. American Mineralogist, 94, 1242–1254, https://doi.org/10.2138/am.2009.2980.

Bernard, C., Estrade, G., Salvi, S., Béziat, D., and Smith, M. (2020) Alkali pyroxenes and amphiboles: A window on rare earth elements and other high field strength elements behavior through the magmatic-hydrothermal transition of peralkaline granitic systems. Contributions to Mineralogy and Petrology, 175, 81, https://doi.org/10.1007/s00410-020-01723-y.

Bozhilov, K.N. (2013) Structures and microstructures of non-classical pyriboles. EMU Notes in Mineralogy, 14, 109–152.

Bozhilov, K.N., Brownstein, D., and Jenkins, D.M. (2007) Biopyribole evolution during tremolite synthesis from dolomite and quartz in CO_2-H_2O fluid. American Mineralogist, 92, 898–908, https://doi.org/10.2138/am.2007.2376.

Buseck, P.R. and Iijima, S. (1974) High resolution electron microscopy of silicates. American Mineralogist, 59, 1–21.

Campo-Rodríguez, Y.T., Schutesky, M.E., de Oliveira, C.G., and Whitehouse, M.J. (2022) Unveiling the polyphasic evolution of the Neoarchean IOCG Salobo deposit, Carajás Mineral Province, Brazil: Insights from magnetite trace elements and sulfur isotopes. Ore Geology Reviews, 140, 104572, https://doi.org/10.1016/j.oregeorev.2021.104572.

Ciobanu, C.L., Cook, N.J., Utsunomiya, S., Pring, A., and Green, L. (2011) Focused ion beam-transmission electron microscopy applications in ore mineralogy: Bridging micro- and nanoscale observations. Ore Geology Reviews, 42, 6–31, https://doi.org/10.1016/j.oregeorev.2011.06.012.

Ciobanu, C.L., Verdugo-Ihl, M.R., Slattery, A., Cook, N.J., Ehrig, K., Courtney-Davies, L., and Wade, B.P. (2019) Silician magnetite: Si–Fe-nanoprecipitates and other mineral inclusions in magnetite from the Olympic Dam Deposit, South Australia. Minerals, 9, 311, https://doi.org/10.3390/min9050311.

Ciobanu, C.L., Verdugo-Ihl, M.R., Cook, N.J., Ehrig, K., Slattery, A., and Courtney-Davies, L. (2022) Ferro-tschermakite with polysomatic chain-width disorder identified in silician magnetite from Wirrda Well, South Australia: A HAADF STEM study. American Mineralogist, 107, 765–777, https://doi.org/10.2138/am-2022-7975.

Corriveau, L., Montreuil, J.F., and Potter, E.G. (2016) Alteration facies linkages among iron oxide copper-gold, iron oxide-apatite, and affiliated deposits in the Great Bear magmatic zone, Northwest Territories, Canada. Economic Geology and the Bulletin of the Society of Economic Geologists, 111, 2045–2072, https://doi.org/10.2113/econgeo.111.8.2045.

Courtney-Davies, L., Ciobanu, C.L., Verdugo-Ihl, M.R., Cook, N.J., Ehrig, K.J., Wade, B.P., Zhu, Z.Y., and Kamenetsky, V.S. (2020) ~1760 Ma magnetite-bearing protoliths in the Olympic Dam deposit, South Australia: Implications for ore genesis and regional metallogeny. Ore Geology Reviews, 118, 103337, https://doi.org/10.1016/j.oregeorev.2020.103337.

Cressey, B.A., Whittaker, E.J.W., and Hutchison, J.L. (1982) Morphology and alteration of asbestiform grunerite and anthophyllite. Mineralogical Magazine, 46, 77–87, https://doi.org/10.1180/minmag.1982.046.338.13.

Droop, G.T.R. (1994) Triple-chain pyriboles in Lewisian ultramafic rocks. Mineralogical Magazine, 58, 1–20, https://doi.org/10.1180/minmag.1994.058.390.01.

Evans, B.W. and Yang, H. (1998) Fe-Mg order-disorder in tremolite-actinolite-ferro-actinolite at ambient and high temperature. American Mineralogist, 83, 458–475, https://doi.org/10.2138/am-1998-5-606.

Ferrari, M. and Viti, C. (2010) Retrograde hydration sequence in disordered Mg amphiboles: A TEM investigation. American Mineralogist, 95, 81–91, https://doi.org/10.2138/am.2010.3254.

Grobéty, B.H. (1996) New short-range biopyribole polysomes from the Lepontine Alps, Switzerland. American Mineralogist, 81, 404–417, https://doi.org/10.2138/am-1996-3-415.

——— (1997) The replacement of anthophyllite by jimthompsonite: A model for hydration reactions in biopyriboles. Contributions to Mineralogy and Petrology, 127, 237–247, https://doi.org/10.1007/s004100050277.

Hatert, F., Mills, S.J., Pasero, M., Miyawaki, R., and Bosi, F. (2023) CNMNC guidelines for the nomenclature of polymorphs and polysomes. Mineralogical Magazine, 87, 225–232, https://doi.org/10.1180/mgm.2023.13.

Hawthorne, F.C., Oberti, R., Harlow, G.E., Maresch, W.V., Martin, R.F., Schumacher,

J.C., and Welch, M.D. (2012) Nomenclature of the amphibole supergroup. American Mineralogist, 97, 2031–2048, https://doi.org/10.2138/am.2012.4276.
Huang, X.W. and Beaudoin, G. (2021) Nanoinclusions in zoned magnetite from the Sossego IOCG deposit, Carajás, Brazil: Implication for mineral zoning and magnetite origin discrimination. Ore Geology Reviews, 139, 104453, https://doi.org/10.1016/j.oregeorev.2021.104453.
Huang, X.W., Beaudoin, G., and Yang, Y. (2022) A HR-TEM study on two generations of magnetite from the Alemao IOCG deposit, Carajás, Brazil: Implication for Fe-Cu mineralization. Ore Geology Reviews, 146, 104934, https://doi.org/10.1016/j.oregeorev.2022.104934.
Jenkins, D.M., Gilleaudeau, G.J., Kawa, C., Dibiase, J.M., and Fokin, M. (2012) Compositional limits and analogs of monoclinic triple-chain silicates. Contributions to Mineralogy and Petrology, 164, 229–244, https://doi.org/10.1007/s00410-012-0735-7.
Konishi, H., Akai, J., and Kurokawa, K. (1993) Calcic analog of clinojimthompsonite from the Oeyama Ophiolite, Southwest Japan. Chishitsugaku Zasshi, 99, 679–682, https://doi.org/10.5575/geosoc.99.679.
Konishi, H., Buseck, P.R., Xu, H., and Li, X. (2008) Proto-polymorphs of jimthompsonite and chesterite in contact-metamorphosed serpentinites from Japan. American Mineralogist, 93, 351–359, https://doi.org/10.2138/am.2008.2637.
Konishi, H., Xu, H., and Dymek, R.F. (2010) High-resolution TEM study of jimthompsonite, chesterite, and chain-width disorder in Archean ultramafic rocks from Isua, West Greenland. American Mineralogist, 95, 73–80, https://doi.org/10.2138/am.2010.3212.
Leake, B.E., Woolley, A.R., Arps, C.E.S., Birch, W.D., Gilbert, M.C., Grice, J.D., Hawthorne, F.C., Kato, A., Kisch, H.J., Krivovichev, V.G., and others. (1997) Nomenclature of amphiboles: Report of the subcommittee on amphiboles of the international mineralogical association, commission on new minerals and mineral names. Canadian Mineralogist, 35, 219–246.
Monteiro, L.V.S., Xavier, R.P., Hitzman, M.W., Juliani, C., de Souza Filho, C.R., and Carvalho, E. (2008) Mineral chemistry of ore and hydrothermal alteration at the Sossego iron oxide-copper-gold deposit, Carajás Mineral Province, Brazil. Ore Geology Reviews, 34, 317–336, https://doi.org/10.1016/j.oregeorev.2008.01.003.
Mutch, E.J.F., Blundy, J.D., Tattitch, B.C., Cooper, F.J., and Brooker, R.A. (2016) An experimental study of amphibole stability in low-pressure granitic magmas and a revised Al-in-hornblende geobarometer. Contributions to Mineralogy and Petrology, 171, 85, https://doi.org/10.1007/s00410-016-1298-9.
Najorka, J. and Gottschalk, M. (2003) Crystal chemistry of tremolite-tschermakite solid solutions. Physics and Chemistry of Minerals, 30, 108–124, https://doi.org/10.1007/s00269-002-0291-1.
Nespolo, M. and Bouznari, K. (2017) Modularity of crystal structures: A unifying model for the biopyribole-palysepiole series. European Journal of Mineralogy, 29, 369–383, https://doi.org/10.1127/ejm/2017/0029-2632.
Ridolfi, F., Zanetti, A., Renzulli, A., Perugini, D., Holtz, F., and Oberti, R. (2018) AMFORM, a new mass-based model for the calculation of the unit formula of amphiboles from electron microprobe analyses. American Mineralogist, 103, 1112–1125, https://doi.org/10.2138/am-2018-6385.
Schumacher, J.C. and Czank, M. (1987) Mineralogy of triple- and double-chain pyriboles from Orijärvi, southwest Finland. American Mineralogist, 72, 345–352.
Schutesky, M.E. and de Oliveira, C.G. (2020) From the roots to the roof: An integrated model for the Neoarchean Carajás IOCG System, Brazil. Ore Geology Reviews, 127, 103833, https://doi.org/10.1016/j.oregeorev.2020.103833.
Thompson, J.B. Jr. (1978) Biopyriboles and polysomatic series. American Mineralogist, 63, 239–249.
Thompson, R.M. and Downs, R.T. (2008) The crystal structure of diopside at pressure to 10 GPa. American Mineralogist, 93, 177–186, https://doi.org/10.2138/am.2008.2684.
Veblen, D.R. (1991) Polysomatism and polysomatic series: A review and applications. American Mineralogist, 76, 801–826.
Veblen, D.R. and Burnham, C.W. (1978a) New biopyriboles from Chester, Vermont: I. Descriptive mineralogy. American Mineralogist, 63, 1000–1009.
——— (1978b) New biopyriboles from Chester, Vermont: II. The crystal chemistry of jimthompsonite, clinojimthompsonite, and chesterite, and the amphibole-mica reaction. American Mineralogist, 63, 1053–1073.
Veblen, D.R. and Buseck, P.R. (1979) Chain-width order and disorder in biopyriboles. American Mineralogist, 64, 687–700.
——— (1980) Microstructures and reaction mechanisms in biopyriboles. American Mineralogist, 65, 599–623.
——— (1981) Hydrous pyriboles and sheet silicates in pyroxenes and uralites: Intergrowth microstructures and reaction mechanism. American Mineralogist, 66, 1107–1134.
Veloso, A.S.R., Monteiro, L.V.S., and Juliani, C. (2020) The link between hydrothermal nickel mineralization and an iron oxide-copper-gold (IOCG) system: Constraints based on mineral chemistry in the Jatobá deposit, Carajás Province. Ore Geology Reviews, 121, 103555, https://doi.org/10.1016/j.oregeorev.2020.103555.
Verdugo-Ihl, M.R., Ciobanu, C.L., Cook, N.J., Ehrig, K., and Courtney-Davies, L. (2020) Defining early stages of IOCG systems: Evidence from iron oxides in the outer shell of the Olympic Dam deposit, South Australia. Mineralium Deposita, 55, 429–452, https://doi.org/10.1007/s00126-019-00896-2.
Verdugo-Ihl, M.R., Ciobanu, C.L., Cook, N.J., Ehrig, K.J., Slattery, A., Courtney-Davies, L., and Dmitrijeva, M. (2021) Nanomineralogy of hydrothermal magnetite from Acropolis, South Australia: Genetic implications for iron-oxide copper gold mineralization. American Mineralogist, 106, 1273–1293, https://doi.org/10.2138/am-2021-7557.
Yau, Y.C., Peacor, D.R., and Essene, E.J. (1986) Occurrence of wide-chain Ca-pyriboles as primary crystals in the Salton Sea Geothermal Field, California, USA. Contributions to Mineralogy and Petrology, 94, 127–134, https://doi.org/10.1007/BF00371233.

MANUSCRIPT RECEIVED SEPTEMBER 12, 2023
MANUSCRIPT ACCEPTED JANUARY 26, 2024
ACCEPTED MANUSCRIPT ONLINE FEBRUARY 21, 2024
MANUSCRIPT HANDLED BY BRADLEY T. DE GREGORIO

Endnote:

[1]Deposit item AM-24-109188. Online Materials are free to all readers. Go online, via the table of contents or article view, and find the tab or link for supplemental materials.

CHAPTER 3

PLATINUM GROUP MINERALS ASSOCIATED WITH NICKEL-BEARING SULPHIDES FROM THE JATOBÁ IRON OXIDE-COPPER-GOLD DEPOSIT, CARAJÁS DOMAIN, BRAZIL

Yuri Tatiana Campo-Rodriguez[1,2], Nigel J. Cook[1], Cristiana L. Ciobanu[1], Maria E. Schutesky[2], Samuel A. King[1], Sarah Gilbert[3], Kathy Ehrig[1,4]

[1]*School of Chemical Engineering, The University of Adelaide, Adelaide, SA, 5005, Australia*

[2]*University of Brasilia, Institute of Geosciences, Graduate Program in Geology, Brasília DF 70910-900, Brazil*

[3]*Adelaide Microscopy, The University of Adelaide, Adelaide, SA, 5005, Australia*

[4]*BHP Olympic Dam, 10 Franklin Street, Adelaide, SA, 5000, Australia*

Article published in *Minerals* (2024) 14 (8): 757.

Statement of Authorship

Title of Paper	Platinum Group Minerals Associated with Nickel-Bearing Sulfides from the Jatobá Iron Oxide-Copper-Gold Deposit, Carajás Domain, Brazil
Publication Status	☑ Published ☐ Accepted for Publication ☐ Submitted for Publication ☐ Unpublished and Unsubmitted work written in manuscript style
Publication Details	Campo-Rodriguez, Y.T., Cook, N.J., Ciobanu, C.L., Schutesky, M.E., King, S.A., Gilbert, S., and Ehrig, K. (2024) Platinum Group Minerals Associated with Nickel-Bearing Sulfides from the Jatobá Iron Oxide-Copper-Gold Deposit, Carajás Domain, Brazil. Minerals, 14, 757. https://doi.org/10.3390/min14080757

Principal Author

Name of Principal Author (Candidate)	Yuri Tatiana Campo Rodriguez		
Contribution to the Paper	Performed analytical work, evaluation and interpretation of results and prepared the manuscript.		
Overall percentage (%)	60		
Certification:	This paper reports on original research I conducted during the period of my Higher Degree by Research candidature and is not subject to any obligations or contractual agreements with a third party that would constrain its inclusion in this thesis. I am the primary author of this paper.		
Signature		Date	06.11.2024

Co-Author Contributions

By signing the Statement of Authorship, each author certifies that:

i. the candidate's stated contribution to the publication is accurate (as detailed above);

ii. permission is granted for the candidate in include the publication in the thesis; and

iii. the sum of all co-author contributions is equal to 100% less the candidate's stated contribution.

Name of Co-Author	Nigel J. Cook		
Contribution to the Paper	Helped to define the direction of the manuscript, guides manuscript preparation and assisted with the interpretation of the results and evaluation of the manuscript. (15%)		
Signature	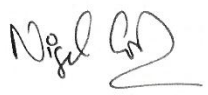	Date	06.11.2024

Name of Co-Author	Cristiana L. Ciobanu		
Contribution to the Paper	Helped with the preparation and evaluation of the manuscript. (11%)		
Signature	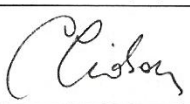	Date	06.11.2024

Name of Co-Author	Maria Emilia Schutesky		
Contribution to the Paper	Helped with the preparation and evaluation of the manuscript. (8%)		
Signature		Date	06.11.2024

Name of Co-Author	Samuel Anthony King		
Contribution to the Paper	Assisted with the evaluation of the compositional data and the manuscript. (2%)		
Signature		Date	06.11.2024

Name of Co-Author	Sarah Gilbert		
Contribution to the Paper	Helped in the operation of analytical equipment and data interpretation. (2%)		
Signature		Date	06.11.2024

Name of Co-Author	Kathy Ehrig		
Contribution to the Paper	Assisted with the evaluation of the manuscript. (2%)		
Signature		Date	06.11.2024

minerals

MDPI

Article

Platinum Group Minerals Associated with Nickel-Bearing Sulfides from the Jatobá Iron Oxide-Copper-Gold Deposit, Carajás Domain, Brazil

Yuri Tatiana Campo Rodriguez [1,2,*], Nigel J. Cook [1], Cristiana L. Ciobanu [1], Maria Emilia Schutesky [2], Samuel A. King [1], Sarah Gilbert [3] and Kathy Ehrig [1,4]

[1] School of Chemical Engineering, The University of Adelaide, Adelaide, SA 5005, Australia; nigel.cook@adelaide.edu.au (N.J.C.); cristiana.ciobanu@adelaide.edu.au (C.L.C.); samuel.king@adelaide.edu.au (S.A.K.); kathy.ehrig@bhp.com (K.E.)
[2] Geosciences Institute, University of Brasília, Brasília 70910-900, DF, Brazil; maria_emilia@unb.br
[3] Adelaide Microscopy, The University of Adelaide, Adelaide, SA 5005, Australia; sarah.gilbert@adelaide.edu.au
[4] BHP Olympic Dam, 10 Franklin Street, Adelaide, SA 5000, Australia
* Correspondence: yuri.camporodriguez@adelaide.edu.au

Abstract: An enrichment in nickel (Ni) or platinum group elements (PGE) is seldom observed in ores of the iron oxide–copper–gold (IOCG) type. This phenomenon is, however, known from a few deposits and prospects in the Carajás Mineral Province, Brazil. The Ni-PGE enrichment is explained, in part, by the spatial association of the IOCG-type ores with altered mafic-ultramafic lithologies, as well as by reworking and remobilization of pre-existing Ni and PGE during multiple mineralization and tectonothermal events across the Archean-Proterozoic. One such example of this mineralization is the Jatobá deposit in the southern copper belt of the Carajás Domain. This is the first detailed study of the Ni and PGE mineralization at Jatobá, with implications for understanding ore genesis. Petrographic and compositional study of sulfides shows that pyrite is the main Ni carrier, followed by pyrrhotite and exsolved pentlandite. Measurable concentrations of palladium (Pd) and platinum (Pt), albeit never more than a few ppm, are noted in pyrite. More importantly, however, the trace mineral signature of the Jatobá deposit features several platinum group minerals (PGM), including merenskyite, naldrettite, sudburyite, kotulskite, sperrylite, and borovskite. These PGM occur as sub-10 µm-sized grains that are largely restricted to fractures and grain boundaries in pyrite. All Pd minerals reported contain mobile elements such as Te, Bi, and Sb and are associated with rare earth- and U-minerals. This conspicuous mineralogy, differences in sulfide chemistry between the magnetite-hosted ore and stringer mineralization without magnetite, and microstructural control point to a genetic model for the sulfide mineralization at Jatobá and its relative enrichment in Ni and PGE. Observations support two alternative scenarios for ore genesis. In the first, an initial precipitation of disseminated or semi-massive Ni-PGE-bearing sulfides took place within the mafic rock pile, possibly in a VHMS-like setting. Later partial dissolution and remobilization of this pre-existing mineralization by mineralizing fluids of IOCG-type, possibly during the retrograde stage of a syn-deformational metamorphic event, led to their re-concentration within magnetite along structural conduits. The superposition of IOCG-style mineralization onto a pre-existing assemblage resulted in the observed replacement and overprinting in which PGE combined with components of the IOCG fluids like Sb, Bi, and Te. An alternative model involves leaching, by the IOCG-type fluids, of Ni and PGE from komatiites within the sequence or from ultramafic rocks in the basement. The discovery of PGM in Jatobá emphasizes the potential for additional discoveries of Ni-PGE-enriched ores elsewhere in the Carajás Domain and in analogous settings elsewhere.

Keywords: Carajás Mineral Province; Jatobá; IOCG systems; sulfide minerals; nickel; platinum group minerals

check for updates

Citation: Campo Rodriguez, Y.T.; Cook, N.J.; Ciobanu, C.L.; Schutesky, M.E.; King, S.A.; Gilbert, S.; Ehrig, K. Platinum Group Minerals Associated with Nickel-Bearing Sulfides from the Jatobá Iron Oxide-Copper-Gold Deposit, Carajás Domain, Brazil. *Minerals* **2024**, *14*, 757. https://doi.org/10.3390/min14080757

Academic Editor: Olivier Blein

Received: 26 June 2024
Revised: 22 July 2024
Accepted: 23 July 2024
Published: 26 July 2024

Copyright: © 2024 by the authors. Licensee MDPI, Basel, Switzerland. This article is an open access article distributed under the terms and conditions of the Creative Commons Attribution (CC BY) license (https://creativecommons.org/licenses/by/4.0/).

Minerals **2024**, *14*, 757

1. Introduction

Iron oxide-copper-gold (IOCG) deposits encompass a variety of mineralization styles and geological settings unified by a dominance of iron oxides (e.g., [1,2]). Research in the 30 or so years since the term 'IOCG deposit' was first used [3] has significantly advanced understanding of their origin, even if some aspects of their genesis remain ill constrained, while others continue to be controversial. Although implicitly concentrating copper and gold, along with subordinate silver, and in rare cases, also uranium, some IOCG systems have attracted attention in recent years due to the recognized relative enrichment of valuable critical elements such as Co and rare earth elements (REE) [2]. In contrast, IOCG deposits are not generally noted for an enrichment in nickel (Ni) or platinum group elements (PGE), yet recent discoveries have led to IOCGs, among other deposit types, to be touted as potential future sources of Ni and other valuable metals, e.g., [4].

The Neoarchean Carajás Mineral Province (CMP; Figure 1) is located in the southeastern portion of the Amazonian Craton, Brazil. In addition to several other genetic types of mineralization, IOCGs are a prominent style of mineralization within the Carajás Domain. These deposits occur within varied host lithologies that have geological ages spanning the Neoarchean and Paleoproterozoic [5–10]. The Carajás Domain of the CMP is one of the world's largest IOCG provinces [11]. Giant copper reserves occur in deposits such as including, Sossego-Sequeirinho [12–14], Salobo [15–17], Igarapé Bahia [18,19], and many others.

Although a relative enrichment of Ni in the IOCG deposits is atypical and not fully understood, some Carajás ore systems represent attractive exploration targets due to the presence of this high-value metal. Among the deposits classified as IOCGs that display an enrichment of Ni is Jatobá, a medium-sized deposit within an IOCG orefield that includes Sossego-Sequeirinho. Lithologies present in the Jatobá deposit include a series of mafic-ultramafic sequences, metabasaltic units, altered volcanoclastic breccias, and minor felsic volcanic units. The Jatobá deposit lies immediately north of a major fault and thrust zone between Mesoarchean mafic and ultramafic rocks and the Grão Para Group of the Itacaiúnas Supergroup, comprising Neoarchean bimodal volcanic sequences. Jatobá displays a spatial association yet arguably ambiguous genetic relationship with altered mafic-ultramafic lithologies [20].

Other Ni-enriched systems in the Carajás Domain are affiliated to the IOCG class, or to what is proposed as a "continuum between IOCGs and hydrothermal Ni deposits", the latter being a rather rare, enigmatic, and only recently identified class of unconventional ores [21]. Nickel-enriched systems in the Carajás Domain include the Ni-dominant Jaguar deposit [22–24], the GT-34 prospect [25], Cristalino [26], and Castanha [27]. In the cited publications, the anomalous enrichment in Ni has typically been explained, admittedly in often rather vague terms, by invoking the contribution of deep, high-temperature fluids of (ortho)magmatic origin or an affinity to the deeper zones of an IOCG system. The relative abundance of Ni-laterites associated with Neoarchean mafic-ultramafic complexes clearly indicates that Ni is widespread within supracrustal rocks of the Carajás Domain. We also note the report of spinifex-textured komatiites in the Selva greenstone belt, close to Jatobá [28]. This wealth of nickel in the Carajás Domain opens up not only the possibility of early mineralization stages within IOCG genesis but also the leaching, remobilization, and recycling of Ni, PGE, and to some extent, also Co and Cr, from pre-existing mineralization during a later IOCG-type event. The potential for new discoveries in the region has catalyzed new work aiming at identifying structural controls and relationships between the deposits and deep architecture, e.g., [29].

Although the nickel endowment of the Jatobá deposit has been noted previously [20], the present contribution sets out to establish a detailed understanding of ore mineralogy and how it has evolved over geological time. We focus on both the major and minor ore components of the ores, as well as on trace elements hosted by common sulfides. Importantly, this contribution describes the presence of Pd and Pt within common sulfides and as discrete platinum group minerals (PGM). The distinct geochemical-mineralogical signature of the sulfide assemblages from Jatobá is evaluated in the context of geological

setting, host rocks, and geological history. This represents the first report of PGM from an IOCG system in the Carajás Domain, even though "Pd-rich melonite" is reported (without composition provided) from Sossego [12]. Mansur et al. [24] provided evidence for traces of PGE from the base metal sulfides in the Jaguar deposit. Although mostly below minimum limits of detection in most cases (~0.1 ppm), concentrations up to 1 ppm were noted in pentlandite. They also noted low but still measurable concentrations of Ru, Rh, Ir, and Os in pyrite.

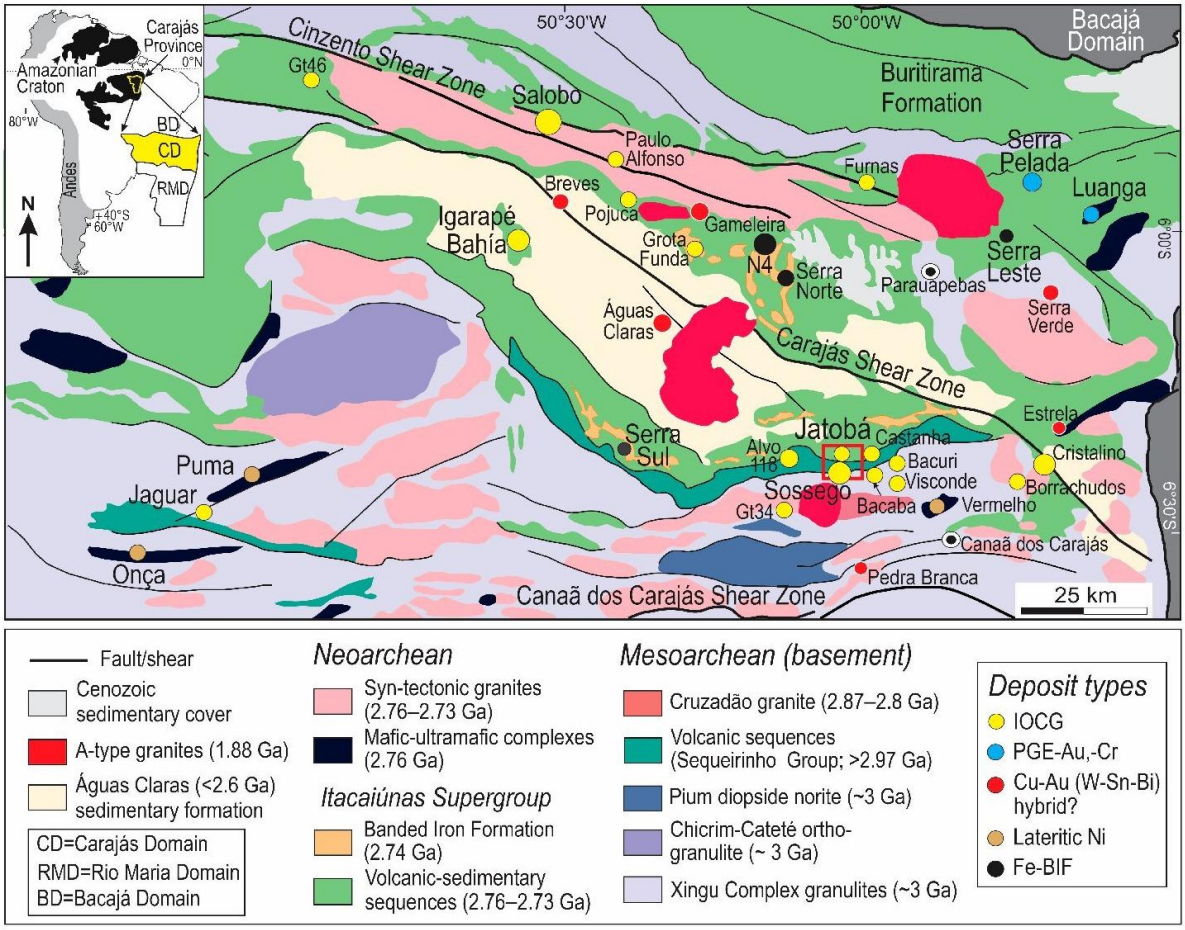

Figure 1. Geological map of the Carajás Domain showing the location of Jatobá orefield (red rectangle). Modified from Vasquez et al. [30] and Tavares et al. [7]. Named deposits referred to in the text are indicated. Deposit types are from Grainger et al. [5] and Trunfull et al. [9]. Circles indicate the relative sizes of the deposits. The inset shows the location of the Carajás Domain within the Amazonian Craton, South America.

2. Background

2.1. Geology and Geological Evolution of the Carajás Domain

The Carajás Mineral Province in the Amazonian Craton of Brazil (e.g., [30]) is one of the largest metallogenic belts on Earth. It comprises two major tectonostratigraphic domains: the Carajás Domain in the north, which hosts Neoarchean IOCG deposits and Paleoproterozoic Cu-Au mineralization, and the Rio Maria Domain (RMD) to the south with its Mesoarchean lode-Au deposits (e.g., [31]). Several other styles of mineralization

Minerals 2024, 14, 757

are recorded, spanning ages from 2.6 Ga to 1.6 Ga [9]. The Carajás Mineral Province is bound to the north by the Bacajá Domain (BD on the inset to Figure 1).

In brief, the Carajás Domain (equivalent to the Itacaiúnas Belt of Araújo et al. [32] is composed of a Mesoarchean basement made up of orthogranulites, gneisses and migmatites, granites, and the 3–2.9 Ga greenstone belts of the Sequeirinho Group (Figure 1; [7,33]). These oldest rocks experienced overprinting multiple times during the Archean and Paleoproterozoic. The basement is covered by Neoarchean (2.76–2.73 Ga) volcano-sedimentary sequences of the Itacaiúnas Supergroup (e.g., [31,34]). Lithologies within the Itacaiúnas Supergroup [33,35] include basaltic lithologies of the Grão Para Group, which host the Jatobá deposit.

Neoarchean igneous activity is represented by mafic-ultramafic complexes (e.g., [33]), syntectonic and A-type granites [7,36,37]. Other important igneous events include the peralkaline to meta-aluminous intrusions of Old Salobo (2573 ± 3 Ma [16,33]). Less voluminous Itacaiúnas granites (2560 ± 37 Ma; [33] are identified within the Cinzento shear zone [16]. Further anorogenic A-type granites were emplaced at 1.88–1.86 Ma during the Transamazonian orogeny (e.g., [38,39]).

Paleoproterozoic sedimentary rocks define the Águas Claras Formation and unconformably overlie the abovementioned lithostratigraphic units. These are sandstones and siltstones deposited in fluvial to shallow marine environments and outcrop mainly in the central part of the Carajás District [40].

Several publications (e.g., [7,9,31,34]) cover the geodynamic evolution of the Carajás Domain and the implications this has for metallogeny. There is little consensus about the timing of the IOCG systems in the literature or whether or not these systems are associated with magma-derived fluids (magmatic-hydrothermal IOCG type *sensu stricto*). Several recent publications consider there were at least two events in which IOCG deposits formed [9,10,31]. By far the most innovative and somewhat non-conventional geodynamic model for the Carajás Domain is that of Costa et al. [31] who attribute the deposition of the early Itacaiúnas Supergroup during the Mesoarchean (2.87–2.83 Ga), at least for some districts, such as Rio Novo. This is followed by BIF deposition (in the Salobo-Pojuca Formation) during a ~70 Ma-long (2.83–2.76 Ga) magmatic quiescence. The first IOCG event is placed during Neoarchean deformation associated with a transtensional or transpressional strike-slip regime at 2.76–2.73 Ga, after the deposition of the Itacaiúnas Supergroup. We note that this same time interval is generally attributed to the Itacaiúnas Supergroup (Figure 1). Based on the ages of crosscutting dykes and an alkaline granite in the case of Salobo, the second IOCG event, at <2.6 Ga, occurred in an extensional rifting to passive margin geotectonic setting [9].

Trunfull et al. [9] also considered two IOCG events occurring within transpressional or transtensional regimes, both being post-Itacaiúnas Supergroup deposition (rifting at 2.76 Ga). In this model, several scenarios are discussed. These involve either basin inversion (commencing at 2.74 Ga) followed by more basin inversion or rifting (2.72–2.68 Ga), which is also the interval of the first IOCG event. We note that this time interval follows the deposition of the Itacaiúnas Supergroup. A yet more recent interval (2.6–2.45 Ga) is provided for an IOCG event in the Northern Copper Belt, during episodic reactivation of the "Cinzeto Shear Zone and metamorphism". In either case, coeval volcanism or emplacement of (syn-tectonic) granitoids is inferred to occur contemporaneously with the IOCG events.

The younger 2.55 Ga age of IOCG deposits in the Northern Copper Belt is reiterated in a study of boron isotopes [41]. This study considers the formation of seafloor hydrothermal systems with hydrothermal vents during the 2.76–2.73 Ga interval prior to the leaching of older seafloor exhalative rocks by "magmatic-hydrothermal fluids to form the IOCG deposits of the Carajás Province".

Minerals **2024**, *14*, 757

2.2. IOCG Deposits of the Carajás Domain

The Carajás Domain hosts IOCG deposits (Figure 1), characterized by multiple Archean-Paleoproterozoic episodes of mineralization within two major regional structures, the Canaã dos Carajás and Cinzento shear zones [9]. A generic model for Neoarchean IOCG systems is provided by Schutesky and Oliviera [8]. This model considers the significance of crustal shear zones to drive upward fluid flow of 'magmatic-hydrothermal fluids', with this latter term used explicitly to highlight the high temperature of the fluids derived from inferred, deep-seated intrusions, as well as the magmatic isotopic signatures recorded in all IOCG deposits studied so far in the Carajás Province. IOCG mineralization is attributed to 2.76–2.73 Ga, i.e., coeval with bimodal magmatism in the Itacaiúnas Supergroup. The large compilation of geochronological data provided by Trunfull et al. [9] places IOCG genesis at 2.72–2.68 Ga, after deposition of the Itacaiúnas Supergroup at ~2.76 Ga in a rift formed during an extensional regime. Recently, the proposed temporal link between granitic magmatism and IOCG deposits in the Carajás Domain has been questioned [10]. The latter authors argue for a slightly younger age of IOCG genesis and contend that hydrothermal activity took place after granite emplacement (2.72–2.68 Ga and again at 2.59–2.53 Ga).

IOCG systems in the Carajás Domain commonly display Na-, Na-Mg/Ca alteration with scapolite-grunerite-hastingsite, followed by Ca-Fe assemblages (actinolite-magnetite-apatite) and K-Fe (biotite and K-feldspar). The late alteration stage is propylitic (chlorite-epidote), accompanied by hydrolytic (veinlet) alteration and carbonatization [8,11].

Magnetite is the dominant iron oxide, and chalcopyrite ($CuFeS_2$) is the main expression of copper enrichment ([8] and references therein). The deposits have variable enrichment in Ni, Co, Pb, and Zn [5]. Tin is also reported in the form of cassiterite from the Sequeirinho/Sossego mines [12,14]. Ore mineralogy is, however, relatively consistent across the province, irrespective of their local settings and host rocks.

A later IOCG event is proposed to have occurred at 1.88 Ga and is widely attributed to the waning stages of the Transamazonian Orogeny [42]. There is, however, uncertainty about whether this is a distinct event or simply a Cu-Au overprint or remobilization superimposed onto a pre-existing IOCG deposit.

2.3. Nickel and Platinum Group Element Endowment in the Carajás Domain

A detailed treatment of the diverse and complex metallogeny and timeframe of the Carajás Mineral Province [5,9] is beyond the scope of the present contribution. Of importance here, however, is that the northern Carajás Domain hosts many other deposits alongside the IOCG deposits [11,43], of which Sossego and Salobo are perhaps among the best known. Among the other deposit styles are the giant Serra Norte iron ores and several deposits related to mafic-ultramafic complexes of ~2.76–2.72 Ga age, including the Luanga and Lago Grande Complexes [33,44]. These mafic-ultramafic complexes constitute a major magmatic event that intrudes Mesoarchean units and is coeval with the extensive basaltic volcanism of the Grão Pará Group [33,34].

There are three main types of mineralization associated with these layered complexes. Firstly, the world-class laterite nickel–cobalt deposits such as Serra da Onça-Puma, Vermelho, and Jacaré-Jacarezinho are associated with major structures along the Southern Copper Belt, such as the Canaã dos Carajás shear zone and McCandless fault system [8,28]. Secondly, there are the sulfide-rich PGE-Cr and PGE-Au deposits such as Luanga and Lago Grande [38,45–47]. Various PGM, including kotulskite, palarstanide, sperrylite, paolovite, arsenopalladinite, and hollingworthite, are documented from Luanga and Lago Grande [44,47]. A third type of mineralization is represented by Serra Pelada, an enigmatic, exceptionally high-grade Au-Pd-Pt deposit [48], in which multiple rare PGMs have been identified [49,50]. The deposit formed at 1.88–1.86 Ga [5] and, although not fully understood, is widely assumed to have been formed by leaching and remobilization of metals from ultramafic complexes [44]. The contribution of metals from mafic-ultramafic

complexes has also been invoked to explain the relatively high Ni-Co contents noted in Cu-Au deposits [11].

A distinct group of Cu-Au deposits with different mineralization styles yet conspicuously lacking iron oxides are observed associated with a Paleoproterozoic (ca. 1.9–1.8 Ga) anorogenic an alkaline to sub-alkaline plutonic event (e.g., Serra dos Carajás, Young Salobo, Pojuca, and Cigano [14,33], and references therein). These deposits are sulfide-quartz-rich with a variable content of F, B, and Li [5,51]. Pollard et al. [51] suggested that these Paleoproterozoic Cu-Au deposits represent the expression of thermal remobilization or the reactivation of older structures and associated mineralization.

2.4. The Jatobá Deposit

Jatobá is one of a cluster of four ore deposits in the southern copper belt of the Carajás Domain (Figure 2A). Each of the four deposits (Pista, Sequeirinho, Sossego, and Jatobá) lies along the E-W-striking structures of the Canaã dos Carajás shear zone system. Fabrics in ores and host rocks are characterized by widespread mylonitic foliation attributable to this structural control. Jatobá is, however, unique in being the only one hosted by rocks of the Neoarchean Grão Para Group. Age constraints on mineralization were provided by Moreto et al. [37] for Sequeirinho (2712 Ma, U-Pb monazite) and Pista (2710–2685 Ma, Re-Os molybdenite) orebodies. Sossego provided a younger U-Pb monazite age of 1904–1879 Ma, but it is hosted within an older (2740 Ma) granite [37].

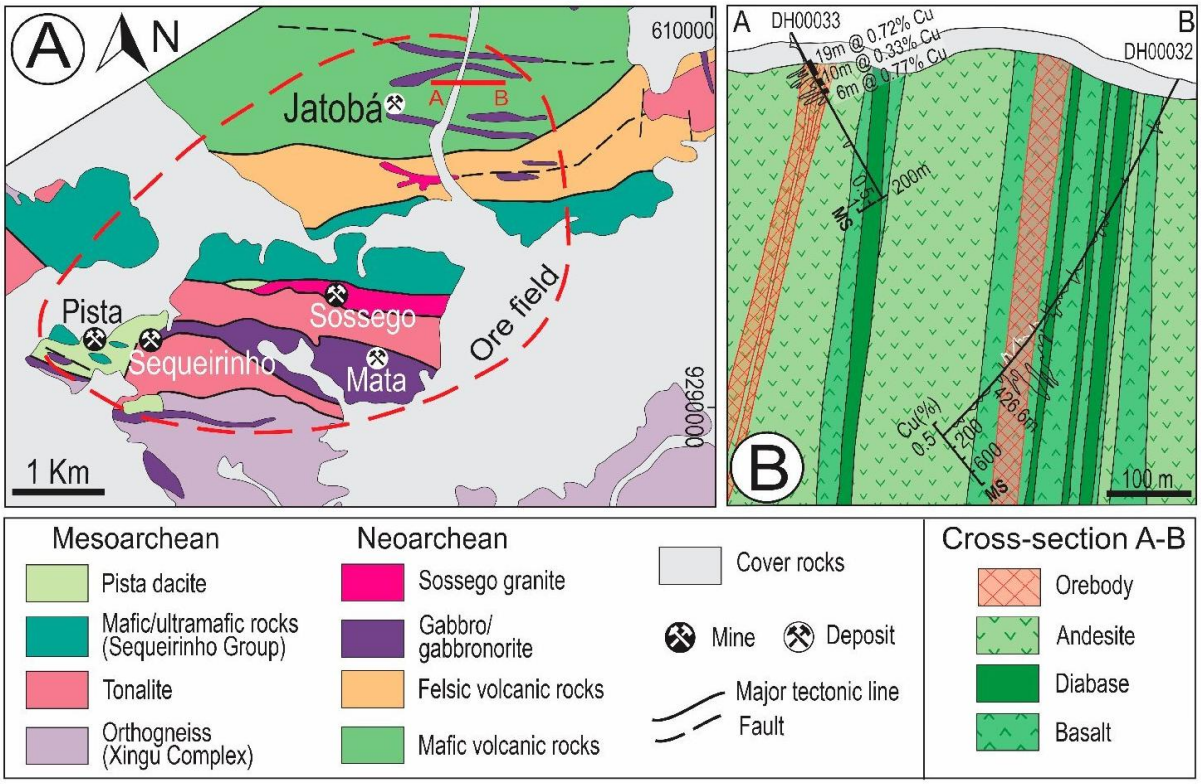

Figure 2. (**A**) Simplified geological map of the Jatobá-Pista-Sequeirinho-Sossego orefield map (modified after Veloso et al. [20]. (**B**) E-W cross-section A-B as marked on (a) indicating sampled drillhole DH00032, host lithologies Cu grades, and magnetic susceptibility (MS).

Exploration of the Jatobá deposit has been sporadic and is presently dormant. Except for Veloso et al. [20], who considered magnetite formation "at the transition from magmatic

Minerals **2024**, *14*, 757

to deep magmatic-hydrothermal systems, including the IOA deposits, especially on the onset of the early nickel-enriched mineralization stage", little information is available in the public domain. Prior publications, including Veloso et al. [20], cite the resource and grade of the Pista-Sequeirinho-Sossego orefield as 355 Mt @ 1.5% Cu and 0.28 g/t Au, drawing on data originally provided in a conference abstract by Lancaster et al. [52]. We are unaware of any published resource data for nickel or PGE in the Jatobá deposit, nor of any publicly available information on the distribution of Ni or PGE at the deposit scale, apart from the statement that Ni contents are higher in massive magnetite-sulfide ore [20]. Veloso [53] provides some "lithochemical data for ore samples" that includes 1270–3930 ppm Ni, 670–2320 ppm Co, 81–372 ppb Pd, and 2–17 ppb Pt.

A major E-W fault separates rhyolites and dacites from the main body of dominantly mafic lithologies that host Jatobá (amygdaloidal basalts and andesites but considered rhyodacites by Veloso et al. [20]. In a previous study of eight drillholes from Jatobá that intersect a 250 m-wide orezone [20,53], the deposit is said to be hosted by "Itacaiúnas rhyodacites and felsic volcaniclastic breccias in the footwall zone, and amygdaloidal basalts associated with mafic tuffs in the hanging wall". Veloso et al. [20] go on to describe a protolith defined by an assemblage of andesine + actinolite onto which eleven pre-, syn-, and late-tectonic alteration stages are superimposed. Proximal (scapolite-hastingsite) and distal (albite-scapolite-quartz-magnetite-biotite) zones are identified.

Sulfide orebodies occur as relatively narrow zones that are spatially associated with magnetite-apatite mineralization and form sub-vertical lenses located close to diabase dikes and contact zones within the mafic lithologies (Figure 2B). Copper and Ni minerals are concentrated within pyrite-pyrrhotite ores that occur as disseminations within magnetite and as veins oriented parallel to the biotite-chlorite mylonitic foliation [20]. The presence of ferrotschermakite, Mg-amphiboles, and non-classical pyriboles (NCPs) preserved as nanoscale inclusions within magnetite enabled Campo-Rodriguez et al. [54] to arrive at the realization that the magnetite had undergone metamorphism at amphibolite facies conditions, consistent with deep burial.

3. Samples and Analytical Methodology

Our set of ten representative samples from the Jatobá deposit derived from a drillhole (Figure 2B; DH0032) that intersects magnetite-rich parts of the deposit and covers dominantly mafic lithologies. Twelve polished thin sections were examined using a reflected light microscope and subsequently using an FEI Quanta 450 field emission scanning electron microscope (SEM) (FEI Company, Hillsboro, OR, USA) in backscatter electron (BSE) mode. The SEM is housed at Adelaide Microscopy, The University of Adelaide, and is equipped with a silicon-drift energy-dispersive X-ray spectrometer. Energy-dispersive X-ray spectrometry (EDS) is utilized for mineral identification. SEM examination allowed for detailed assessment of microstructural features, grain size, morphology, relationships between main minerals, and identification of fine-grained accessory phases.

LA-ICP-MS trace element spot analysis and mapping was undertaken using a RESOlution-SE 193 nm Excimer laser (Applied Spectra, Inc., West Sacramento, CA, USA) coupled to an Agilent 8900x quadrupole ICP mass spectrometer (Agilent Technologies, Inc., Santa Clara, CA, USA) in the same laboratory. Background measurement was 30 s, followed by the acquisition of a signal during ablation of 50 or 60 s. The following thirty-six isotopes were measured, with corresponding dwell times (in ms) provided in brackets: ^{27}Al (5) ^{34}S (5), ^{49}Ti (5), ^{55}Mn (10), ^{57}Fe (5), ^{59}Co (10), ^{60}Ni (10), ^{65}Cu (10), ^{66}Zn (10), ^{75}As (10), ^{77}Se (20), ^{88}Sr (10), ^{90}Zr (5), ^{95}Mo (20), ^{105}Pd (30), ^{106}Pd (30), ^{107}Ag (20), ^{111}Cd (10), ^{113}In (10), ^{115}In (10), ^{118}Sn (10), ^{121}Sb (10), ^{125}Te (20), ^{182}W (10), ^{193}Ir (30), ^{195}Pt (30), ^{197}Au (30), ^{204}Pb (10), ^{205}Tl (10), ^{206}Pb (10), ^{207}Pb (10), ^{208}Pb (10), ^{209}Bi (10), ^{232}Th (10), and ^{238}U (10). Longer dwell times were employed for isotopes of greatest interest. For all analyses, reference materials STD-GL3 [55], NiS-3 [56], and GSD-1G (USGS) were analyzed before, during, and after pyrite ablation. The laser spot diameter was a consistent 50 µm diameter at a pulse repetition rate of 5 Hz and fluence of 3 J/cm^2. Iron was used as an internal calibration

standard for pyrite and pyrrhotite, whereas Cu was used for chalcopyrite. Stoichiometric compositions were assumed in all cases.

Typical minimum detection limits (mdl, in ppm) for isotopes measured quantitatively are as follows: ^{55}Mn (0.05), ^{57}Fe (2), ^{59}Co (0.03), ^{60}Ni (0.03), ^{65}Cu (0.05), ^{66}Zn (0.12), ^{75}As (0.3), ^{77}Se (0.7), ^{95}Mo (0.03), ^{105}Pd (0.0002), ^{106}Pd (0.0002), ^{107}Ag (0.0006), ^{111}Cd (0.001), ^{113}In (0.003), ^{115}In (0.003), ^{118}Sn (0.06), ^{121}Sb (0.03), ^{125}Te (0.06), ^{182}W (<0.0001), ^{195}Pt (0.0005), ^{197}Au (0.0003), ^{204}Pb (0.006), ^{206}Pb (0.001), ^{207}Pb (0.001), ^{208}Pb (0.001), ^{209}Bi (0.003), and ^{238}U (<0.0001). No quantitative data are presented for Al, S, Ti, Mn, Cu, Zn, Sr, and Zr, as isotopes of these elements were measured only to identify the presence of inclusions. Tungsten, Ir, Tl, and Th were consistently at or below their respective mdl values in all analyses and are also not tabulated. Rhodium, Ru, and Os are not present in available reference materials and were therefore not quantified. Based on measurement of Pt, Pd and Ir, however, they are very likely to be extremely low and probably <mdl.

LADR software version 1.1.07 (Norris Scientific Pty Ltd., Kingston, Hobart, TAS, Australia) was utilized for data processing. Total Pb concentration data provided in Table 1 were calculated as the sum of ^{204}Pb, ^{206}Pb, ^{207}Pb, and ^{208}Pb. The areas selected for analysis were carefully chosen to avoid inclusions and the time-resolved depth profiles for each ablation spot were carefully examined for evidence of sub-surface inclusions or other artefacts that could bias results and interpretation. Where obvious inclusions were noted, the integrated interval was modified to avoid them. Data indicative of abundant inclusions or obvious mineral mixtures were rejected.

Table 1. Compositional data (SEM-EDS) for selected PGM.

	1	2	3	4	5
	Bi-Bearing Merenskyite (Jt4)	**Merenskyite (Jt9)**	**Ni-Bi-Bearing Merenskyite (Jt9)**	**Merenskyite (Jt8)**	**Naldrettite (Jt10)**
	Mean (n = 4, single grain)	Mean (n = 3, single grain)	Mean (n = 4, single grain)		
Pd	27.8 ± 1.53	29.9 ± 0.60	22.3 ± 0.29	26.9	67.0
Bi	16.4 ± 0.76	2.1 ± 0.2	15.8 ± 1.11		
Te	53.4 ± 2.10	67.9 ± 0.40	54.5 ± 2.50	73.1	
Pt			3.4 ± 0.10		
Ni		2.4 ± 0.07	1.8 ± 0.26		
Sb					33.0
Total	97.6 ± 3.03	100.1 ± 0.06	97.7 ± 1.67	100.0	100.0

Calculated formulae: 1. $Pd_{1.03}(Te_{1.66}Bi_{0.31})_{1.97}$, 2. $(Pd_{1.00}Ni_{0.09})_{1.09}(Te_{1.89}Bi_{0.02})_{1.91}$, 3. $(Pd_{0.83}Ni_{0.12}Pt_{0.07})_{1.02}(Te_{1.69}Bi_{0.30})_{1.98}$, 4. $Pd_{0.92}Te_{2.08}$, 5. $Pd_{2.10}Sb_{0.90}$.

For element imaging, the laser was rastered across the sample, forming a rectangular grid across the area of interest with a beam size of 10 µm. Rasters were then compiled and processed into trace element intensity maps using 'Iolite' software [57], version Iolite 3, with extension Igor Pro 6.37 used for the generation of laser maps. Mapped intensities are scaled independently for each element to enhance different features; unless stated otherwise, the scale used is logarithmic (10^n). Similar values between ^{105}Pd and ^{106}Pd were checked to avoid any interference from inclusions of chalcopyrite for ^{105}Pd and sphalerite for ^{106}Pd. ^{57}Fe was selected as the internal standard, assuming ideal stoichiometry for the sulfides.

4. Results

The studied samples cover a ~450 m-long interval and represent different assemblages within mafic lithologies (Figure 3A). The orebody intersected by this drillcore is a magnetite-rich interval, ca. 50 m in length, with grades of ~0.5% Cu situated in the lower part of the drillhole (samples Jt7–Jt10).

Minerals **2024**, *14*, 757

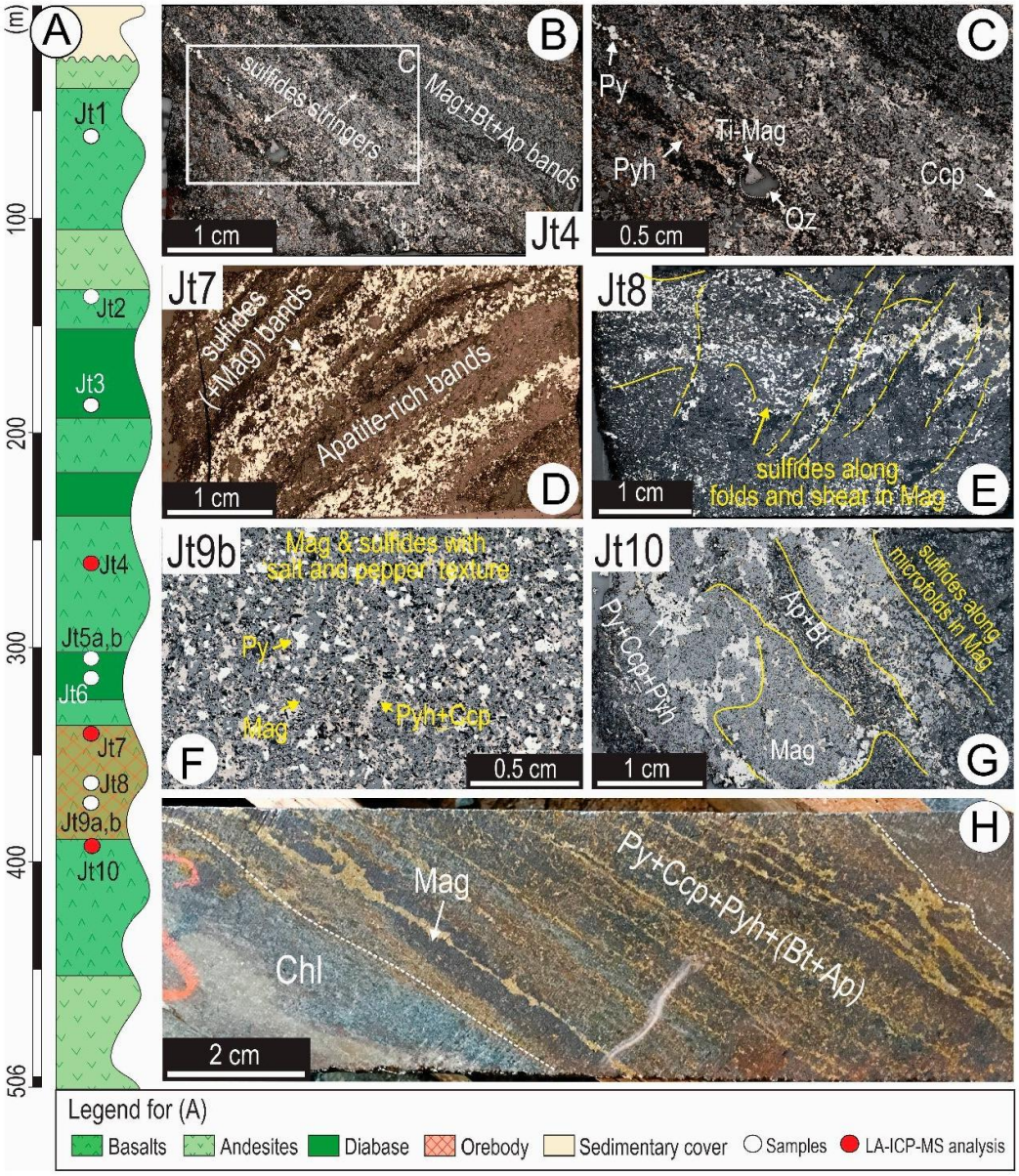

Figure 3. Schematic lithological cross-section of sampled drillhole with sample locations (**A**), reflected light microphotographs (**B**–**G**), and drillcore photograph (**H**). (**B**–**H**) show styles of sulfide mineralization and rock fabrics as labeled and described in the main text. Abbreviations: Ap—apatite; Bt—biotite; Ccp—chalcopyrite; Chl—chlorite; Mag—magnetite; Py—pyrite; Pyh—pyrrhotite; Qz—quartz. Image in (**H**) is from lower part of the drillhole.

Outside the magnetite-dominant orebody, notably in sample Jt4, the sulfides occur as disseminations, stringers, and bands following the rock fabrics (Figure 3B). Sulfide stringers are present within bands intercalated with magnetite + apatite + biotite within metabasalts. There is no close relationship between the sulfides, dominantly pyrrhotite and pyrite, and magnetite (Figure 3C).

In contrast, samples from the orebody display an intimate association with magnetite. Centimeter-sized bands of sulfides + magnetite are intercalated with apatite-rich bands (Figure 3D). The sulfides follow the folding and microshearing of magnetite (Figure 3E). A characteristic 'salt-and-pepper' texture comprising fine-grained sulfides and magnetite is found in pockets of massive ore (Figure 3F). At the lower contact of the orebody with host rocks, sulfides are concentrated as coarser (mm-sized) pods following microfolding within host magnetite (Figure 3G).

Throughout the drillhole, the most prominent fabric displayed by sulfides is that of fine-stringers and bands that follow a mylonitic foliation across magnetite-rich intervals alternating with gangue minerals (Figure 3H).

4.1. Ore Petrography and Mineralogy

The sulfide assemblage across the roughly 50 m-thick interval of magnetite-bearing rocks at Jatobá is composed of pyrite and pyrrhotite, with subordinate amounts of chalcopyrite and minor pentlandite (Figure 4). The proportions of minerals vary significantly, with the sulfides + magnetite assemblage making up to ~60% of the rock. Pyrrhotite and chalcopyrite are dominant in pockets of massive ore (e.g., sample Jt9b) where they are intergrown with or interstitial to magnetite (Figure 4A). We note the abundance of pentlandite [$(Fe,Ni)_9S_8$] as short 'flames' throughout pyrrhotite, indicative of exsolution from monosulfide $(Fe,Ni)_{1-x}S$ solid solution. Pyrrhotite is also present as tiny inclusions within magnetite. Other ore minerals are abundant magnetite (locally 30–50% of the rock) and minor ilmenite. The boundaries between sulfides and magnetite are sealed by apatite and clusters of fibrous silicates (mainly biotite, chlorite, and actinolite). Details of pentlandite forming relatively coarser segregations (10–50 μm-sized grains) in pyrrhotite are illustrated in Figure 4B,C. Otherwise, pyrrhotite appears homogeneous, excluding minor fracturing, polishing pits, and incipient alteration to oxides.

Pyrrhotite commonly co-exists with pyrite, although it is only present in minor amounts in samples with banding or stringer fabrics where an enrichment in pyrite relative to other minerals is observed. In most cases, no apparent zoning is observed in pyrite under reflected light. Some pyrite grains have a mottled appearance due to dense, fine inclusions of different types (Figure 4D). The boundaries between sub-grains within aggregates of finer (20–50 μm) pyrite grains outside the orebody are infilled by chalcopyrite (Figure 4E). The mutual 120° triple junctions between the pyrites in such cases represent foam textures, indicative of equilibrium recrystallization or slow cooling and annealing. Scarce sphalerite is noted along trails in pyrite.

Disseminated pyrite in the orebody has variable grain size (50–600 μm) and is often fractured. The grain margins are typically irregular, which is indicative of replacement by assemblages of gangue minerals (e.g., biotite-apatite; Figure 3F). Nonetheless, idiomorphic grain margins are also present, and these likely indicate overgrowths rather than preservation of euhedral habit (Figure 3F, inset). Pockets of pyrite, chalcopyrite, and in some cases, pyrrhotite occur interstitial to magnetite aggregates (Figure 4G,H). Sulfide formation within cavities in magnetite is suggested by the inward growth of pyrite from the magnetite boundary to the center of the pocket, which is infilled by chalcopyrite (Figure 4H). Intimate relationships between chalcopyrite and pyrite (Figure 4I) are observed along the folds and shears in magnetite (Figure 3D). It is not, however, unambiguously clear whether chalcopyrite replaces pyrite or whether the latter forms new crystals growing within dilational jogs. Chalcopyrite can form pockets without other sulfides and, in such cases, is crosscut by sets of thin (<30 μm) needles of silicates (associations of actinolite, biotite, and chlorite) (Figure 4J).

Minerals **2024**, *14*, 757

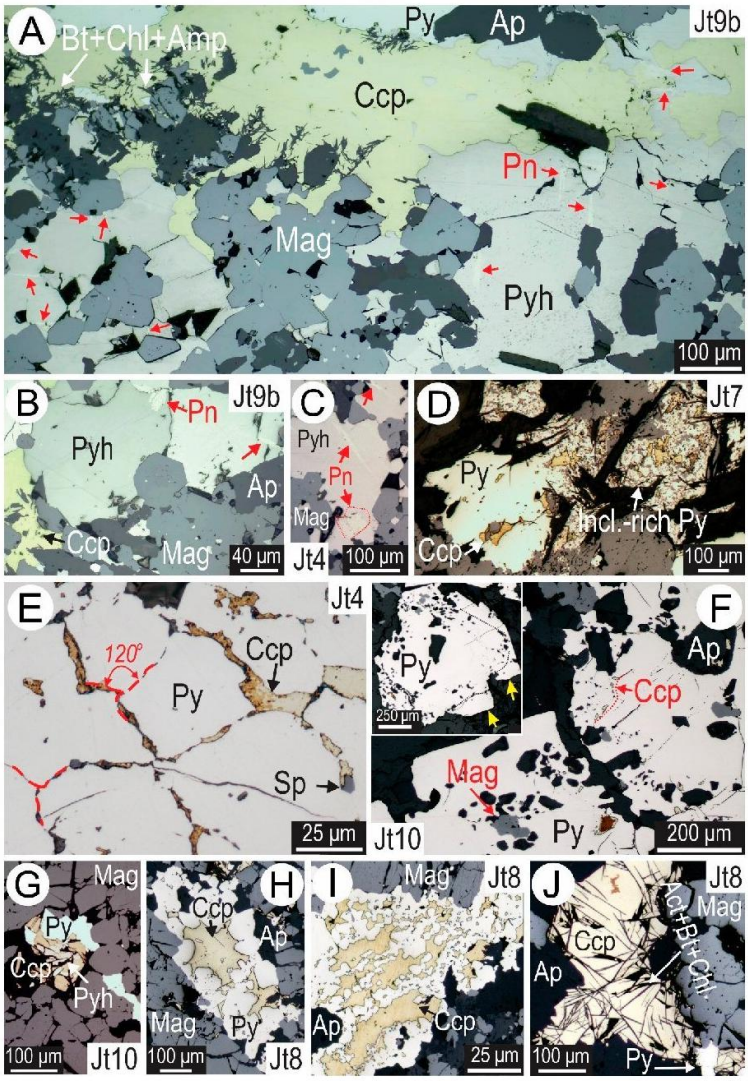

Figure 4. Reflected light images showing sulfide assemblages in the Jatobá samples as labeled. (**A**) Core sample exhibiting banded sulfide mineralization, comprising pyrite (Py), pyrrhotite (Pyh), chalcopyrite (Ccp), and flame-like exsolutions of pentlandite (Pn, red arrows) within a gangue assemblage of magnetite (Mag), biotite (Bt), chlorite (Chl), amphibole (Amp), and apatite (Ap). (**B**,**C**) Pentlandite forming 10–50 µm-sized segregations (grains) in pyrrhotite. (**D**) Pyrite-chalcopyrite assemblage in which the pyrite has a mottled appearance due to dense, fine inclusions of different types. (**E**) Characteristic foam-textured pyrite with 120° triple junctions. Chalcopyrite infills some fractures; minor sphalerite (Sp) is noted along pyrite sub-grain boundaries. (**F**) Pyrite grain margins are irregular and often cuspate, suggestive of replacement. Preserved idiomorphic grain margins (**F** inset) may indicate overgrowths. (**G**) Pyrite interstitial within magnetite associated with pyrrhotite and chalcopyrite. (**H**) Pyrite containing irregular and variably sized inclusions of fluorapatite, magnetite, and chalcopyrite close to the grain margin. Note the curvilinear margins of pyrite against chalcopyrite. (**I**) Extensive replacement of pyrite by chalcopyrite in contact with chlorite, magnetite, and fluorapatite. (**J**) Chalcopyrite overprinted by acicular actinolite (Act).

Minerals **2024**, *14*, 757

4.2. Accessory Ore Minerals

A range of Co-, As-, Ni-, and PGE minerals are found throughout the sulfide assemblages (Figure 5). In sulfide-poor samples such as those from the upper part of the sampled interval (sample Jt1), the margins between pyrite and chalcopyrite are marked by small grains of a Co-As-bearing mineral, likely cobaltite (CoAsS; Figure 5A).

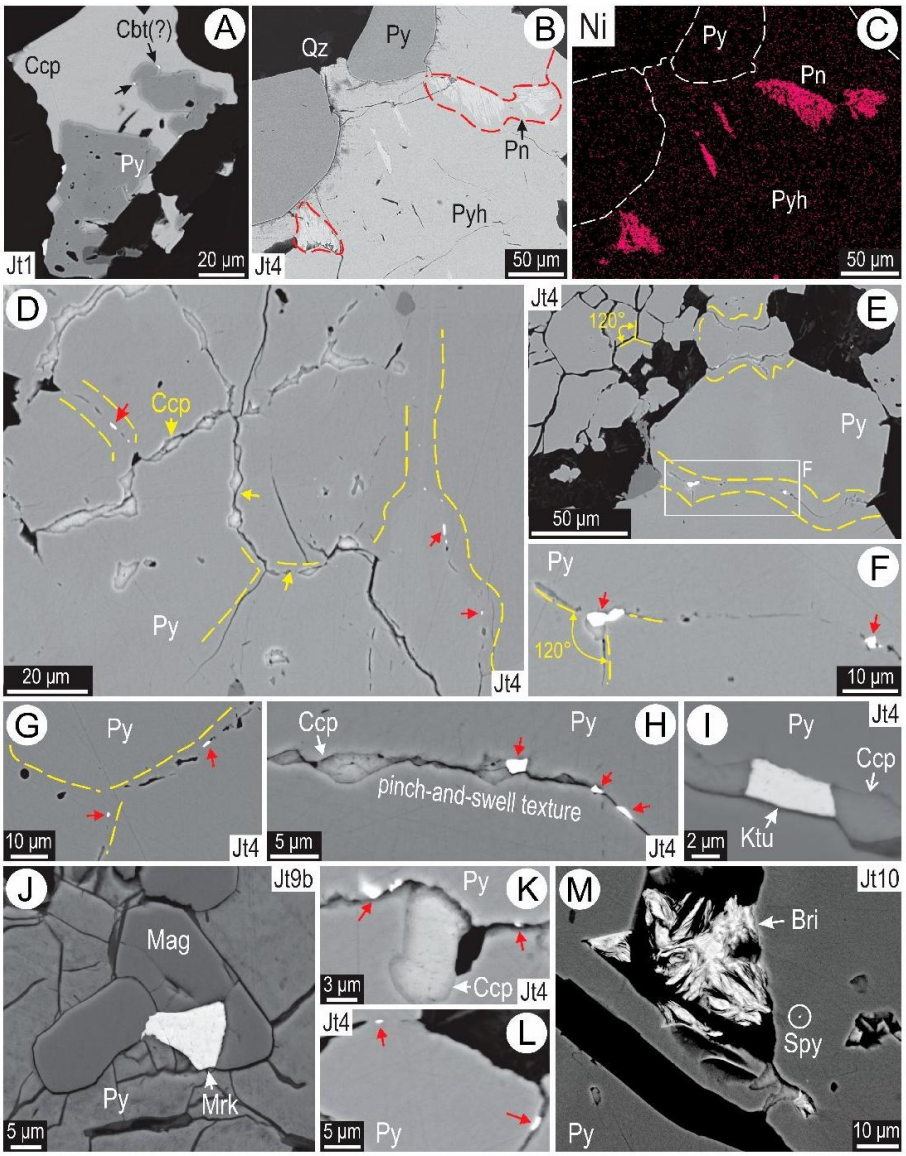

Figure 5. BSE images (except C, EDS element map) showing details of sulfide assemblages in Jatobá samples as labeled. (**A**) Fine cobaltite (Cbt, black arrows) at boundary between pyrite and chalcopyrite. (**B**) Rounded (milled) pyrite enclosed by pyrrhotite. Note the relative abundance of pentlandite lamellae close to grain and sub-grain boundaries. (**C**) EDS element map showing distribution of Ni in area imaged in B, highlighting the pentlandite lamellae. (**D**) Characteristic foam-textured pyrite with remobilized chalcopyrite located along pinch-and-swell fractures (yellow arrows), which also host tiny PGM inclusions (red arrows). (**E**–**G**) Pyrite displaying indentation with curvilinear boundaries and 120° triple-junctions and PGM inclusions (red arrows). (**H**,**I**) Nucleation and coarsening of chalcopyrite

Minerals **2024**, *14*, 757

chalcopyrite and PGM occur along pinch-and-swell textures in foam-textured pyrite are typical of the stringer sulfides in sample Jt4. (**J**) Coarser inclusions of PGM at grain boundaries between magnetite and pyrite in ore zone sample. (**K**,**L**) PGM inclusions associated with gangue biotite, apatite, and quartz along the trails or close to grain boundaries and large pores in pyrite. (**M**) Pore-filled aggregate of britholite-(Ce) within pyrite. Circle highlights sub-micron-sized PGM inclusions adjacent to the pore. Abbreviations: Bri—britholite-(Ce); Cbt—cobaltite; Ccp—chalcopyrite; Ktu—kotulskite; Mag—magnetite; Mrk—merenskyite; Py—pyrite; Pyh—pyrrhotite; Spy—sperrylite.

In stringer sulfides outside the magnetite-rich orebody represented by sample Jt4, the heterogeneous distribution of pentlandite, with coarser segregations towards grain and sub-grain boundaries in pyrrhotite, suggests remobilization of this mineral (Figure 5B,C). The rounded morphology of the pyrite along margins adjacent to pyrrhotite suggests an episode of grain milling of refractory pyrite followed by remobilization of more ductile pyrrhotite. Pentlandite lamellae are most abundant close to grain and sub-grain boundaries in the pyrrhotite. Sulfide textures featuring abundant but small PGM inclusions in foam-textured pyrite are typical of the stringer mineralization (Figure 5D–I).

Remobilization of chalcopyrite, the most ductile among sulfide minerals, along pinch-and-swell fractures in pyrite is not only common but is accompanied by the nucleation of tiny PGE-bearing minerals (Figure 5D). In closer detail, the pyrite grains show indentation with curvilinear boundaries and 120° triple-junctions, many of which are marked by the presence of tiny grains of platinum-group minerals (PGM) (Figure 5E–G). Nucleation and coarsening of chalcopyrite and PGM occur along the pinch-and-swell textures (Figure 5H,I).

In contrast, sulfides from the orebody include somewhat larger inclusions of PGM (up to 20 μm), some of which are located interlocked at grain boundaries between magnetite and pyrite (Figure 5J). Moreover, these PGM inclusions are associated with gangue minerals (e.g., biotite, apatite, quartz) along the trails or close to grain boundaries, as well as in large pores in pyrite from the orebody samples (Figure 5K–M). Britholite-(Ce), $(Ce,Ca)_5(SiO_4)_3OH$, and uraninite are conspicuous components of assemblages formed within such pores. Aggregates of britholite-(Ce) are seen infilling some of the larger pore spaces (Figure 5M). We also note the presence of sub-micron-sized PGM inclusions adjacent to the pore.

Other trace minerals identified in the Jatobá ores include an eclectic range of oxides, sulfides, and rare earth element (REE) phosphates. Titanite is present as sporadic, micron-sized inclusions in magnetite, whereas ferberite and scheelite occur typically as inclusions in ilmenite, either as isolated inclusions or as dense swarms of sub-micron-sized nanograins in the center of the ilmenite. Molybdenite is also found in relatively coarse (tens of microns) yet scarce inclusions in magnetite. Allanite, huttonite or thorite (ThO_2), euxenite-(Y) $[(Y,Ca,Ce,U,Th)(Nb,Ta,Ti)_2O_6]$, and uraninite ($UO_2$) up to 60 μm in size and with inclusions of galena are common and are typically included in magnetite.

4.3. Platinum Group Minerals

Although typically small (0.5 to 10 μm across), the suite of PGM forming inclusions within or otherwise associated with Jatobá pyrite were characterized in terms of their composition and association with one another (Figures 6–8; Table 1).

The PGM phases tentatively identified comprise species from three distinct groups: (i) Pd-Te-Bi compounds, merenskyite [(Pd,Pt,Ni)(Te,Bi)], kotulskite, $[Pd(Te,Bi)_{2-x}]$, and michenerite (PdBiTe)]; (ii) compounds of Pd with Sb, borovskite (Pd_3SbTe_4), naldrettite (Pd_2Sb), and sudburyite (PdSb); and (iii) Pt-As compounds, notably sperrylite ($PtAs_2$). Despite their small size, empirical formulae could be calculated for merenskyite, by far the most common PGM with variable Ni and Bi contents, and for naldrettite (Table 1).

Merenskyite occurs as single-phase thin slivers (Figure 6A–C), blebby grains (Figure 6D), or as binary inclusions together with kotulskite (Figure 6E). Other relatively large (5 μm-sized) inclusions occurring as single phases are kotulskite, sudburyite, and naldrettite (Figures 6F,G and 7B,C). Micron-sized native gold (97.9% Au) is also observed within pyrite from the orebody, as is native bismuth. (Figure 6H,I).

Minerals **2024**, *14*, 757

Analysis and EDS mapping of a grain of merenskyite located at the boundary between pyrite and magnetite (Figure 7A) yields the empirical formula $(Pd_{0.83}Ni_{0.12}Pt_{0.07})_{1.02}(Te_{1.69}Bi_{0.29})_{1.98}$ (analysis 3 in Table 1), consistent with the tendency of this mineral to incorporate significant concentrations of Pt and Ni substituting for Pd and of Bi substituting for Te. The brighter patch within the grain gives ~PdBiTe (michenerite?) (Figure 7A). Sperrylite and borovskite were identified from some of the smallest inclusions, for which EDS spectra are shown in Figure 8.

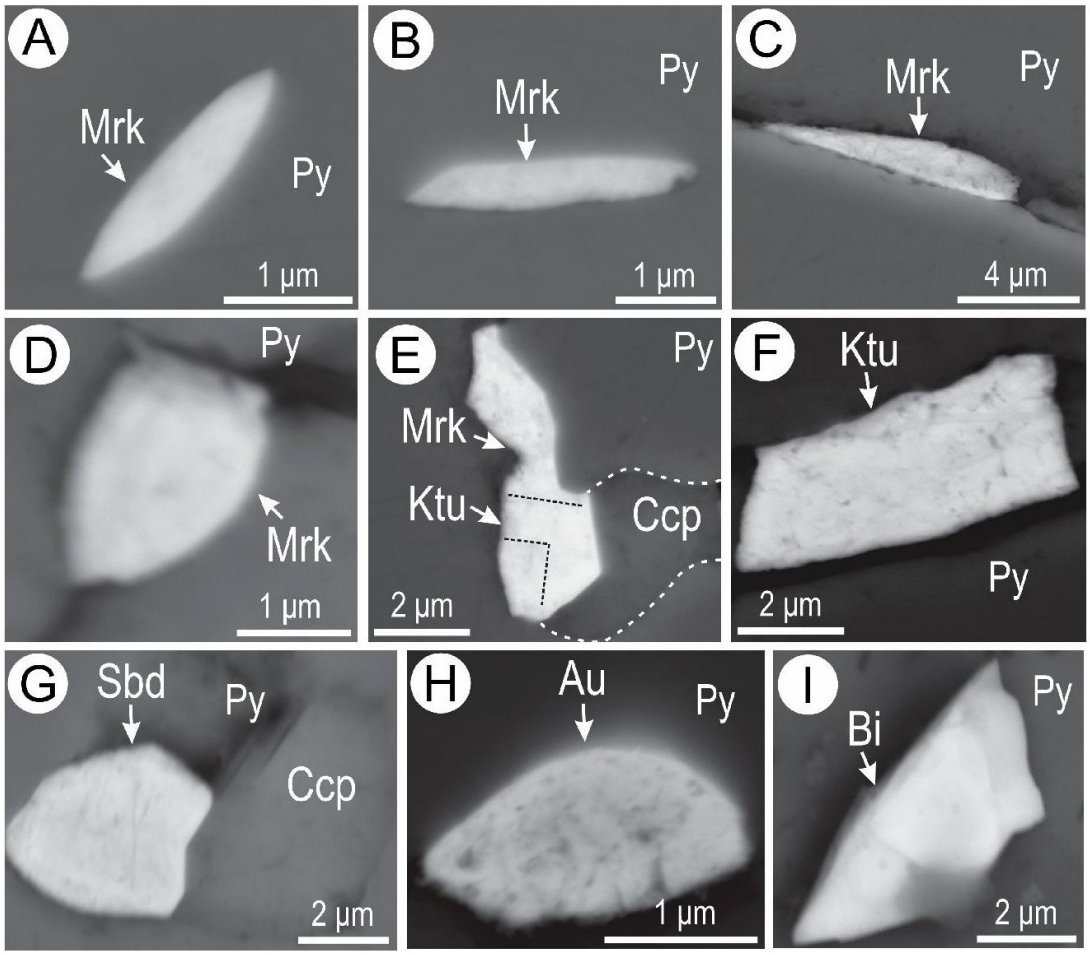

Figure 6. BSE images showing sulfide assemblages containing PGM. (**A**–**C**) Lozenge-shaped inclusions of merenskyite (Mrk) within pyrite (Py). (**D**) Merenskyite located at a triple junction within pyrite aggregate. (**E**) Two-phase inclusion of merenskyite and kotulskite (Ktu) within pyrite. (**F**) Grain of kotulskite within a fracture in pyrite. (**G**) Rounded bleb of sudburyite (Sbd) with chalcopyrite (Ccp) along a microfracture in pyrite. (**H**) Sub-rounded bleb of native gold (Au) within pyrite. (**I**) inclusion of native bismuth (Bi).

Minerals **2024**, *14*, 757

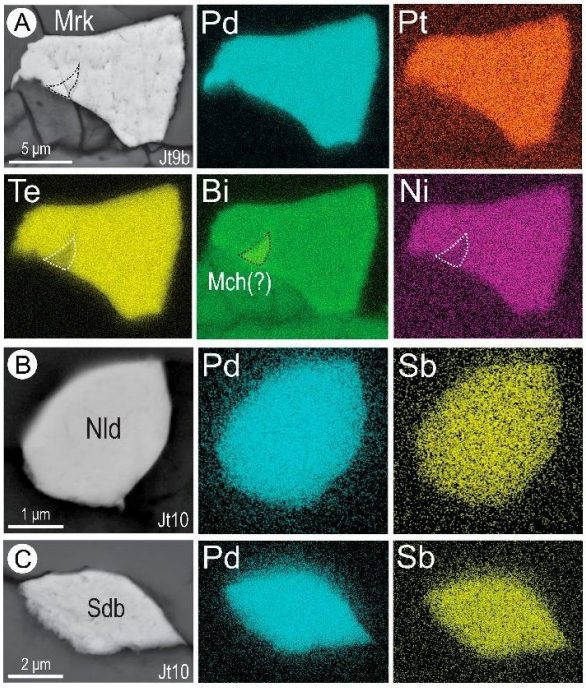

Figure 7. BSE images and respective EDS element maps for selected elements in (**A**) relatively coarse grain of merenskyite (Mrk) at pyrite-magnetite boundary, with brighter patch corresponding to michenerite (Mch), (**B**) naldrettite (Nld) within pyrite, and (**C**) sudburyite (Sdb) within pyrite.

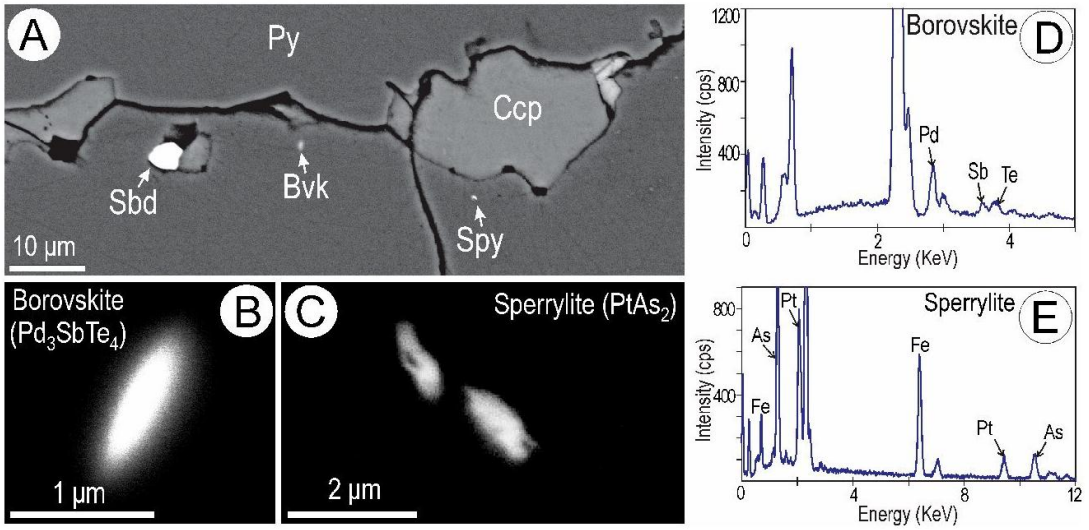

Figure 8. (**A**) Fracture in pyrite (Py) containing chalcopyrite (Ccp) and inclusions of Pd-Pt minerals including borovskite (Bvk), sudburyite (Sdb), and sperrylite (Spy). (**B**,**C**) High-magnification images of borovskite and sperrylite, respectively. (**D**,**E**) EDS spectra supporting identification of sub-micron-sized inclusions shown in B and C.

Minerals **2024**, *14*, 757

4.4. Trace Element Concentrations in Sulfides

Trace element concentrations in Jatobá pyrite are summarized in Table 2 and shown on box-and-whisker plots in Figure 9. The full dataset is provided in Supplementary Materials Table S1. Concentration ranges are relatively wide for Ni (~10 to ~1000 ppm) and As (<1 to ~1000 ppm). Cobalt also shows concentration ranges across four orders of magnitude (<10 to >20,000 ppm). Selenium concentrations are typically a couple of hundred ppm. These elements all give smooth signals on time-resolved LA-ICP-MS depth profiles (Figure 10). Other trace elements such as Cu, Bi, Sb, and Te yield irregular signals and are thus considered largely inclusion bound.

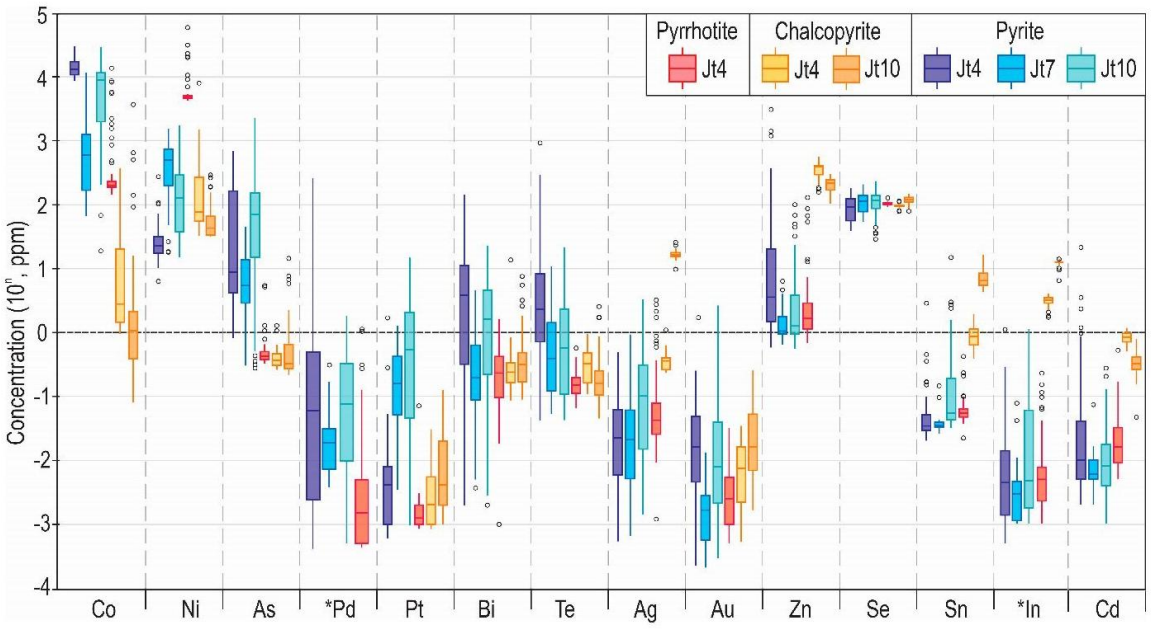

Figure 9. Box-and-whisker plots comparing the concentrations of thirteen key trace elements in pyrite from three different samples, as well as in chalcopyrite (in two samples) and pyrrhotite. *Pd refers to mean Pd calculated based on ^{105}Pd and ^{106}Pd, and *In refers to the calculated mean for concentration of ^{113}In and ^{115}In.

There is a variability in the concentration ranges of Co, Ni, and As across pyrite in different samples. Although part of this variability is due to grain-scale compositional zoning, we draw attention to differences in the measured concentrations of Pd (mean 7.4 ppm in sample Jt4 but <1 ppm in samples Jt7 and Jt10) and Pt (mean 1.7 ppm in Jt10, and <1 ppm in Jt7 and Jt4). We note that the highest Pd is measured in pyrite from sample Jt4, whereas the highest Pt is from sample Jt10. Neither Pd nor Pt correlates with Cu, Zn, or other elements and thus are interpreted as genuine and not an artefact of mass interference from argides.

Table 2. Summary of LA-ICP-MS trace element data for Jatobá sulfides (in ppm).

Pyrite Jt 4	**Co**	**Ni**	**Cu**	**As**	**Zn**	**Bi**	**Te**	**Au**	**Ag**	**Se**	**Cd**	***In**	**Sb**	**Sn**	**ΣPb**	**^{105}Pd**	**^{106}Pd**	***Pd**	**Pt**
Mean (n = 56)	14,532	33	2002	99	136	12	31	0.060	0.054	97	0.585	0.043	0.336	0.108	5.1	8.7	6.1	7.4	0.043
S.D.	4823	38	8203	167	473	24	131	0.230	0.091	40	2.9	0.155	0.570	0.378	6.9	43	26	35	0.228
Median	13,104	23	6.0	8.8	3.6	3.9	2.3	0.008	0.023	97	0.010	0.004	0.102	0.034	1.9	0.033	0.027	0.033	0.004
Maximum	29,711	273	57,218	697	3080	144	923	1.7	0.497	187	21.1	1.1	2.8	2.8	32	311	181	246	1.7
Minimum	8666	6.3	0.225	0.828	0.582	<0.002	<0.042	0.001	<0.001	40	0.002	0.001	0.004	0.02	0.008	0.001	0.001	0.000	<0.001
Pyrite Jt 7																			
Mean (n = 29)	2441	546	78	11	1.7	0.613	1.2	0.002	0.082	116	0.009	0.007	0.397	0.041	3.0	0.046	0.041	0.044	0.294
S.D.	3799	419	90	13	1.4	0.972	2.1	0.003	0.188	40	0.013	0.016	0.476	0.023	3.9	0.077	0.064	0.070	0.329
Median	599	500	292	5.4	1.1	0.195	0.395	0.001	0.021	116	0.006	0.003	0.149	0.035	1.3	0.016	0.015	0.018	0.161
Maximum	11,669	1533	0.9	45	6.4	4.6	11	0.013	0.937	211	0.073	0.078	1.6	0.144	12	0.362	0.266	0.314	1.3
Minimum	67	18	1450	<0.305	0.645	0.004	<0.054	0.001	<0.001	55	0.002	0.001	0.012	0.026	0.010	0.001	0.001	0.000	0.004
Pyrite Jt 10																			
Mean (n = 99)	8012	229	1371	181	6.0	3.5	1.8	0.051	0.351	116	0.021	0.092	0.575	0.381	6.6	0.247	0.223	0.235	1.7
S.D.	5766	291	3413	400	14	4.7	2.9	0.266	0.620	40	0.041	0.205	0.662	1.5	10	0.358	0.348	0.350	2.8
Median	8912	128	7.9	71	1.3	1.6	0.580	0.006	0.101	119	0.008	0.005	0.285	0.054	2.8	0.081	0.077	0.076	0.489
Maximum	28,916	1721	19,113	2302	100	23	22	2.6	3.3	238	0.272	1.1	2.8	15	51	1.8	1.8	1.8	15
Minimum	19	15	0.156	<0.278	0.563	<0.002	<0.043	0.001	<0.001	30	0.001	0.001	0.010	0.031	0.010	0.001	0.001	0.001	<0.001
Pyrrhotite Jt4	**Co**	**Ni**	**Cu**	**As**	**Zn**	**Bi**	**Te**	**Au**	**Ag**	**Se**	**Cd**	***In**	**Sb**	**Sn**	**ΣPb**	**^{105}Pd**	**^{106}Pd**	***Pd**	
Mean (n = 61)	981	12,023	961	0.620	7.9	0.315	0.177	0.004	0.254	106	0.033	0.017	0.033	0.067	6.4	0.059	0.045	0.052	
S.D.	2403	23,152	5996	0.885	22	0.333	0.098	0.006	0.634	6.2	0.069	0.039	0.043	0.056	11	0.238	0.166	0.200	
Median	201	4899	2.1	0.426	1.7	0.232	0.151	0.001	0.043	106	0.016	0.005	0.021	0.054	3.2	0.001	0.001	0.001	
Maximum	13,582	11,5245	45,434	5.4	129	1.6	0.571	0.032	3.2	131	0.520	0.228	0.288	0.415	68	1.5	0.968	1.1	
Minimum	143	20	0.433	0.328	0.680	<0.001	<0.065	0.001	<0.001	95	0.005	0.001	<0.005	0.022	0.037	0.001	0.001	0.000	
Chalcopyrite Jt 4	**Co**	**Ni**	**Cu**	**As**	**Zn**	**Bi**	**Te**	**Au**	**Ag**	**Se**	**Cd**	***In**	**Sb**	**Sn**	**ΣPb**				**Pt**
Mean (n = 23)	28	538		0.447	348	0.861	0.365	0.011	0.380	100	0.826	3.0	0.061	0.932	11				0.005
S.D.	77	1643		0.251	102	2.8	0.231	0.010	0.183	7.2	0.175	0.609	0.052	0.408	10				0.008
Median	2.8	77		0.368	390	0.240	0.326	0.006	0.361	99	0.840	3.2	0.035	0.856	6.9				0.002
Maximum	372	7943		1.3	557	14	0.950	0.035	1.1	113	1.2	4.0	0.233	1.9	40				0.031
Minimum	0.956	32		<0.262	157	0.087	0.108	<0.001	0.237	86	0.504	1.7	0.018	0.381	1.6				<0.001
Chalcopyrite Jt 10																			
Mean (n = 45)	114	68		1.2	206	0.755	0.330	0.044	17	121	0.337	12	0.084	7.3	15				0.015
S.D.	558	60		2.6	52	1.4	0.496	0.063	2.6	17	0.135	1.3	0.091	2.9	11				0.026
Median	1.1	43		0.325	218	0.316	0.162	0.013	16	123	0.320	12	0.045	6.4	13				0.003
Maximum	3686	291		14	306	7.6	2.5	0.258	26	151	0.788	15	0.383	16	48				0.125
Minimum	0.081	32		<0.219	104	0.090	<0.046	0.001	10	86	0.047	6.4	<0.011	4.2	1.6				<0.001

Note: ^{105}Pd and ^{106}Pd refer to calculated total Pd concentration calculated based on measurement of ^{105}Pd and ^{106}Pd isotope signals, respectively. Mean concentration reported as *Pd. *In refers to the calculated mean for concentration of ^{113}In and ^{115}In. Measurements of Mo, W, and U are consistently below minimum limits of detection.

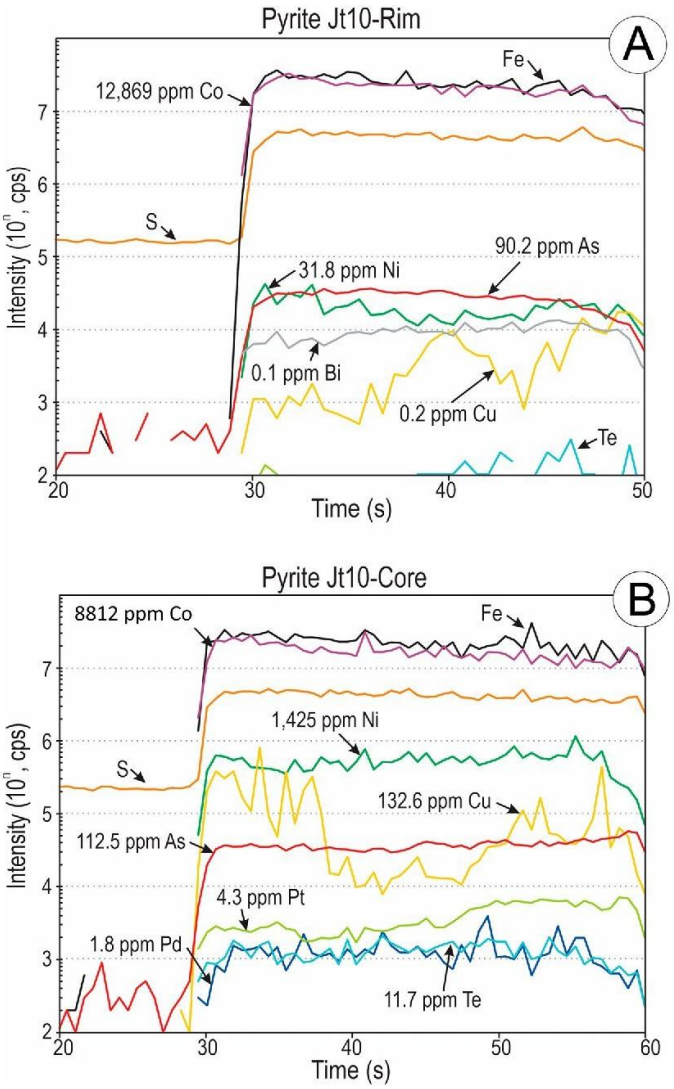

Figure 10. Time-resolved LA-ICP-MS depth profiles for representative pyrite grain in sample Jt10 (rim: (**A**); core: (**B**)). Note the generally flat signals, including for ppm-level Pt and Pd (on (**B**)), but ragged signals for inclusion-hosted elements such as Cu (on (**B**)).

The other main sulfides are also carriers of several trace elements (Table 2). Pyrrhotite contains the highest concentrations of Ni (mean 12,023 ppm, but in part attributable to flames of pentlandite or other impurities), hundreds of ppm Co and Cu (mean 981 and 961 ppm, respectively), and 106 ppm Se. Other elements that are measurable in trace concentrations include Pd (mean 0.059 ppm). Chalcopyrite also concentrates Ni and Co (means 538 and 28 ppm in sample Jt4, and 68 and 114 ppm, respectively, in sample Jt10) as well as Se (100 ppm in sample Jt4 and 121 ppm in sample Jt10). Chalcopyrite also contains the highest Zn (348 and 206 ppm in samples Jt4 and Jt10, respectively) as well as measurable concentrations of In (6.1 ppm in sample Jt4 and 17 ppm in sample Jt10). Sample Jt10 contains greater concentrations of both Ag (17 ppm) and Sn (7.3 ppm) than sample Jt4.

A series of binary plots for trace elements in the Jatobá sulfides are shown in Figures 11 and 12. A plot of Co vs. Ni is shown for all sulfides in the sample outside the orebody (sample

Minerals **2024**, *14*, 757

Jt4) on Figure 11A and in the two samples from the orebody (samples Jt7 and Jt10) in Figure 11B). In sample Jt4, a strong positive correlation (r = 0.86) is seen between Co and Ni in chalcopyrite and pyrrhotite, whereas pyrite forms a separate cluster, rich in Co but poorer in Ni. Pyrite from the orebody shows different clusters for the two samples, partially overlapping with each other, whereas chalcopyrite from sample Jt10 is distinct, with the lowest Co concentrations. Plots of As vs. Co/Ni for pyrite show distinct trends for the stringer and orebody sulfides. A weak negative correlation (r = −0.27) is seen for sample Jt4 (Figure 11C), whereas a reasonably strong positive correlation (r = 0.66) exists in the orebody samples (Jt7 and Jt10; Figure 11D). A strong positive correlation (r = 0.88) is observed between In and Zn across all sulfides in the three samples (Figure 11E). The lower concentration is in pyrrhotite from sample Jt4, and the highest is from chalcopyrite. A plot for In vs. Sn in chalcopyrite shows the strongest positive correlation (r = 0.95), whereby concentrations are lower in sample Jt4 relative to Jt10 (Figure 11F).

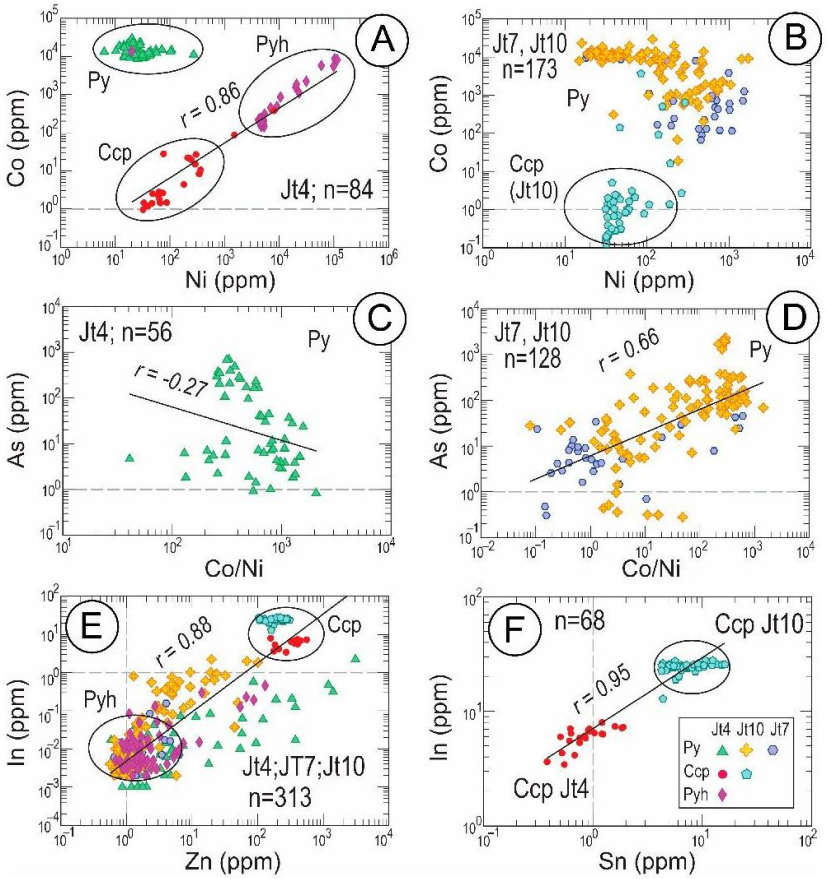

Figure 11. Binary plots of LA-ICP-MS concentration data for selected elements in pyrite and associated sulfides from Jatobá. (**A**,**B**) Ni vs. Co in samples Jt4 (stringer sulfides) and Jt7/Jt10 (ore), respectively. (**C**,**D**) Co/Ni vs. As in sample Jt4 (stringer sulfides) and Jt7/Jt10 (ore), respectively. (**E**) Zn vs. In in various sulfides. (**F**) Sn vs. In in various sulfides.

Minerals **2024**, *14*, 757

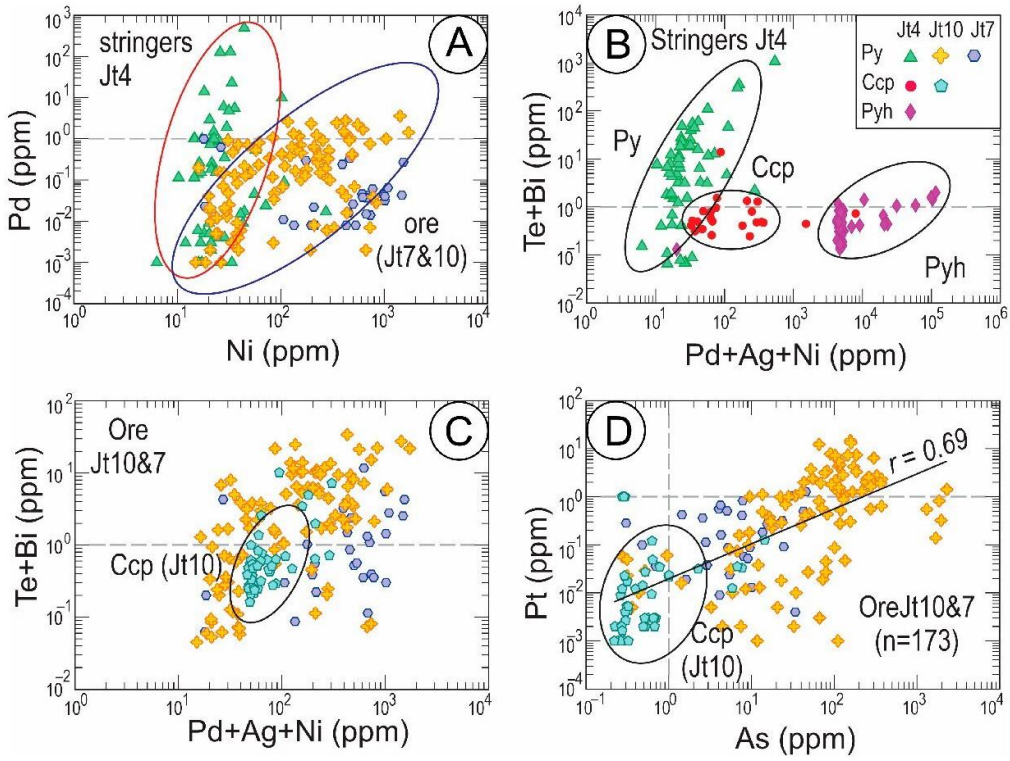

Figure 12. Binary plots of LA-ICP-MS concentration data for selected elements in pyrite and associated sulfides from Jatobá. (**A**) Pd vs. Ni in pyrite (**B**) Pd + Ag + Ni vs. Te + Bi in sulfides from sample Jt4. (**C**) Pd + Ag + Ni vs. Te + Bi in pyrite from the orezone (**D**) As vs. Pt in pyrite. See text for further discussion.

Plots of Pd vs. Ni in pyrite (Figure 12A) also show distinct trends for the stringer sulfides (sample Jt4) relative to orebody samples (Jt7 and Jt10). Combining the data for the three sulfides in sample Jt4 on a plot of (Te + Bi) vs. (Pd + Ag + Ni) (Figure 12B), we show that only pyrite has a positive correlation. This agrees with the presence of merenskyite as the dominant PGM included in pyrite. The same plot for ore samples (Jt7 and Jt10; Figure 12C) shows an undifferentiated cluster (chalcopyrite, also overlapping with pyrite). This is concordant with the wider speciation of PGM in the ore samples. A positive correlation (r = 0.69) is, however, obtained for sulfides in the ore samples if Pt is plotted against As (Figure 12D), agreeing with the presence of sperrylite in these samples.

4.5. Grain-Scale Trace Element Distributions in Pyrite

Compositional zoning is highlighted in three LA-ICP-MS element maps of pyrite (Figures 13–15). Subtle oscillatory zoning with respect to Co and As is observed in a pyrite grain from outside the orebody (sample Jt4; Figure 13). We note that Co is higher at the grain margin, whereas As is concentrated in the core. This is concordant with the plot in Figure 11C. Fractures in pyrite are highlighted by enhanced concentrations of Ni, suggesting this element is leached from the sulfide during brecciation. A homogenous distribution of Se is observed, whereas Pd shows features that somewhat match those shown by Ni. Small, high-concentration spots on the element map for Pd may be attributed to PGM inclusions that nucleated along such fractures.

Minerals **2024**, *14*, 757

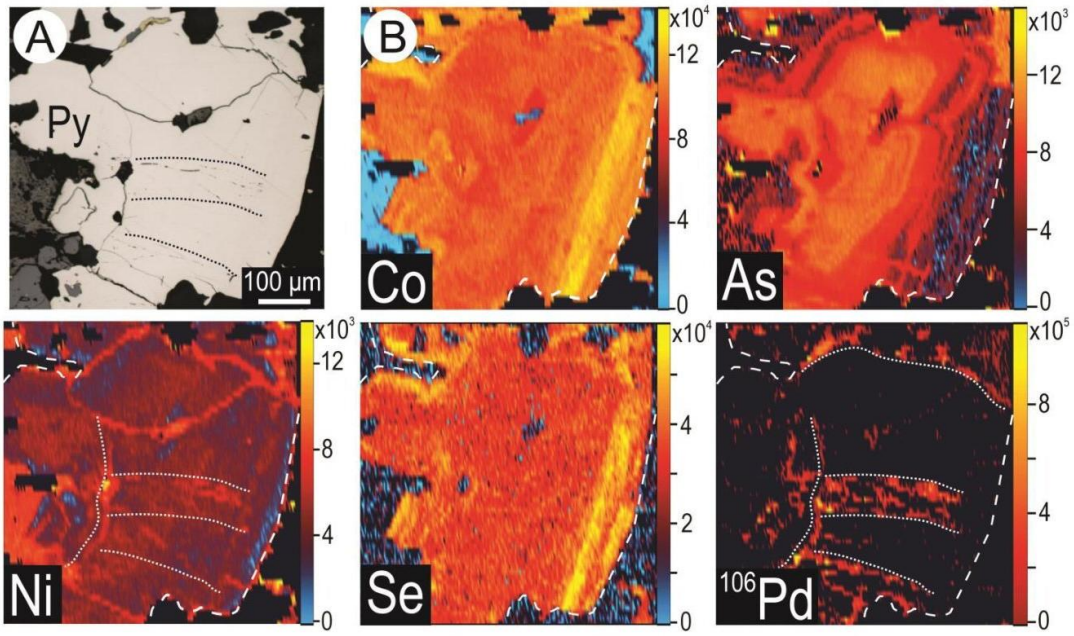

Figure 13. Reflected light image (**A**) and selected LA-ICP-MS element maps (**B**) of a representative pyrite grain from sample Jt4 showing subtle oscillatory zoning with respect to Co and As, in which Co is higher at the grain margin and As is relatively concentrated in the grain core. Open and healed microfractures in pyrite are highlighted on the maps for Ni and, to some degree, also by Pd. The Se map suggests a homogenous distribution across the grain. Small yellow spots of high concentration on the Pd map are attributed to fracture-bound inclusions of PGM. Scales in counts per second.

Element maps of a pyrite grain in orezone sample Jt10 (Figure 14) feature distinct patterns. Annealing of pyrite aggregates is supported by the Co-, Pt-, As-enriched, and Ni-depleted cores of individual sub-grains. We note that, despite the low absolute concentrations of Pt, the Pt element map shows a perfect correlation with the Co-rich grain cores. Cobalt also shows oscillatory zoning highlighting individual grains that form a fused aggregate. Subtle, slightly patchy zoning is depicted by the distribution of Se. Palladium reflects grain boundaries in the annealed aggregate whereas Cu (inclusion of chalcopyrite in the middle of the aggregate) correlates with higher concentrations of Ag, Sn, and to some extent also Bi. The latter is also redistributed along grain boundaries. We note that the map for U also highlights grain boundaries, consistent with our observations of uraninite.

In contrast, fractures and submicron trails of inclusions are shown on the element maps obtained from the margin of a coarser, mm-sized pyrite grain in sample Jt10 (Figure 15). A subtle oscillatory zoning with respect to Co, Se, and Pt is depicted on the respective maps, whereas As is relatively homogenous across the mapped area except for a small domain of high concentration. Sets of parallel fractures are highlighted by the relative enrichment of Ni, Pd, Ag, and Sb, fully consistent with our observations of micron-sized phases in which Pd is combined with these elements. Other inclusions, comprising U-, Se-, and Mn-bearing minerals, are also picked out in the pyrite.

Minerals **2024**, *14*, 757

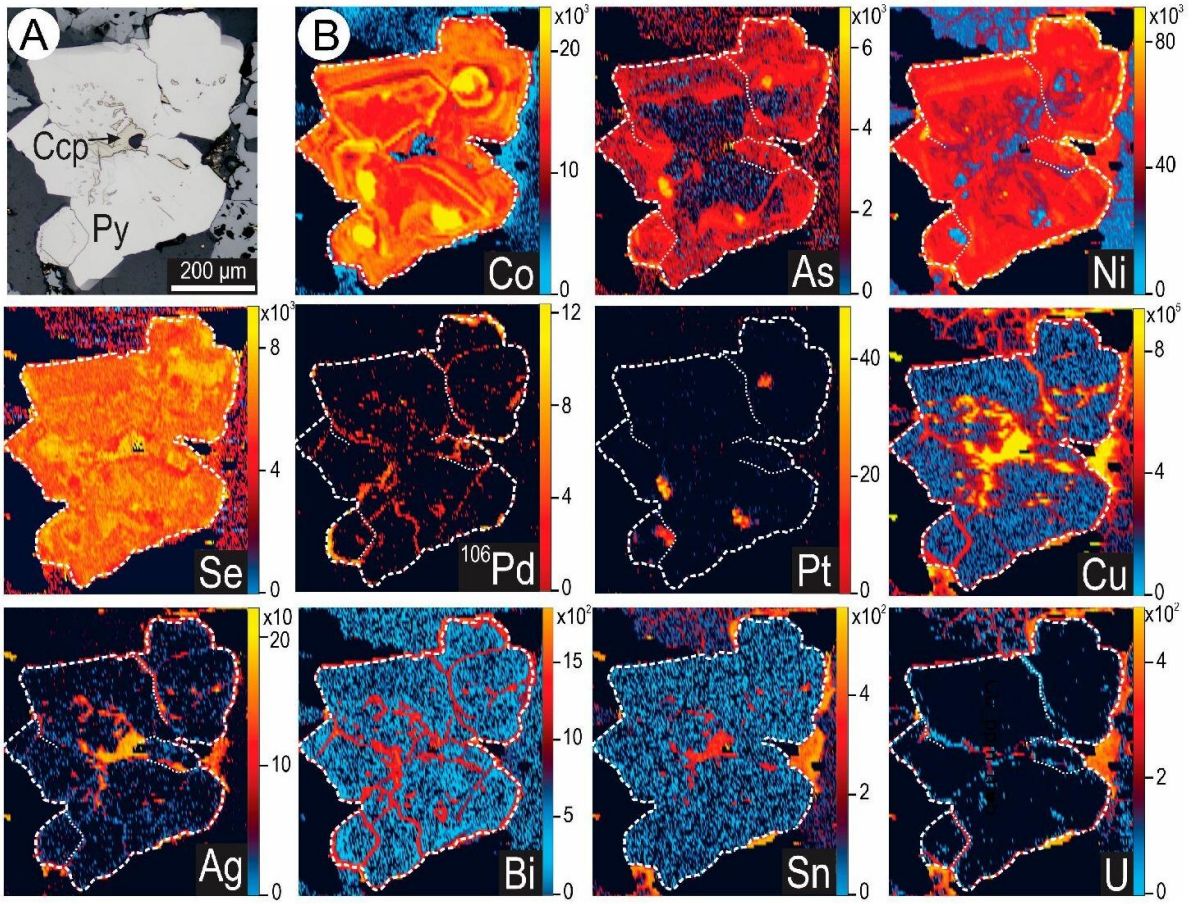

Figure 14. Reflected light image (**A**) and selected LA-ICP-MS element maps (**B**) of a representative pyrite grain from sample Jt10. Maps for Co, Pt, As, and Ni indicate annealing of a multi-grain pyrite aggregates in which individual grain cores can be picked out, notably on the Co map. Pt distributions correlate strongly with those of Co. Pd distributions and reflect grain boundaries in the annealed aggregate. Cu distributions correspond to inclusions of chalcopyrite, which are also picked out on the Ag, Sn, and Bi maps. Maps for Ag, Bi, and U also highlight the sub-grain boundaries. Scales in counts per second. Py—pyrite; Ccp—chalcopyrite.

Minerals **2024**, *14*, 757

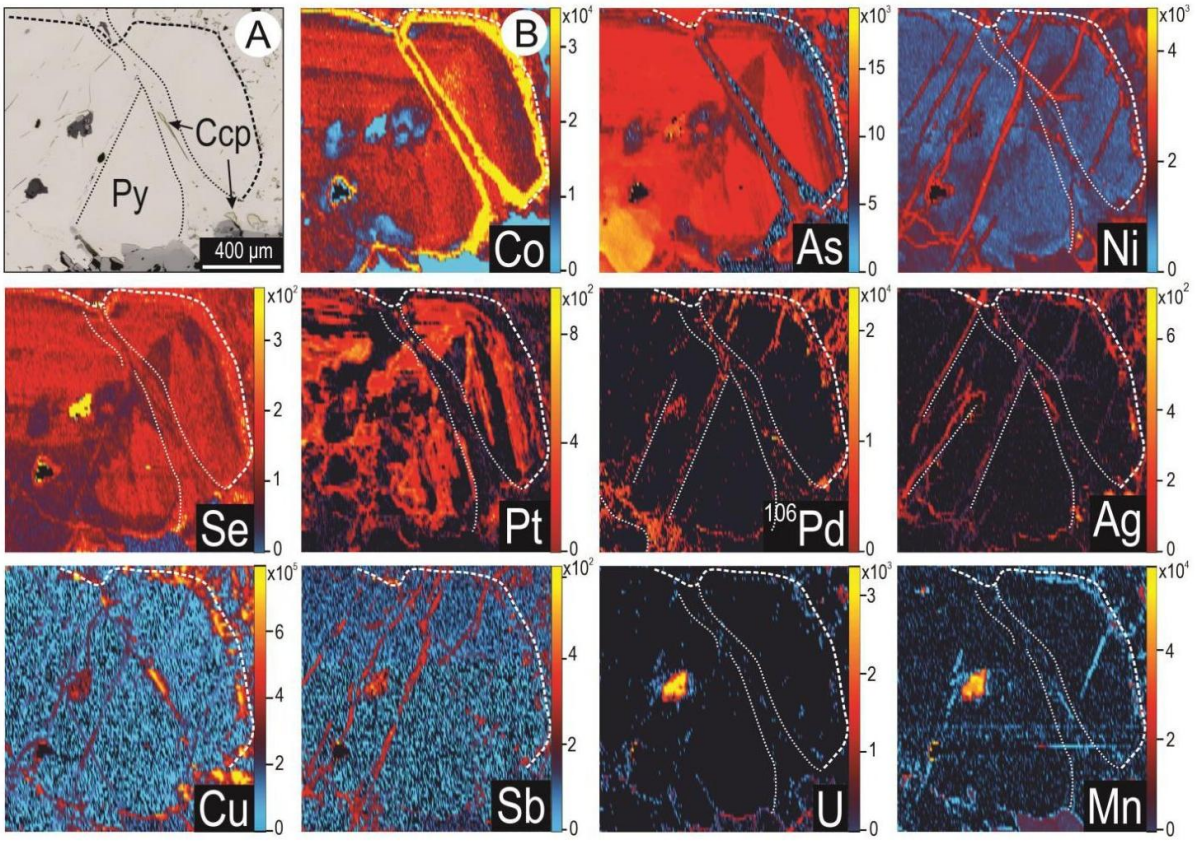

Figure 15. Reflected light image (**A**) and selected LA-ICP-MS element maps (**B**) of the margin of a coarser pyrite grain in sample Jt10. The maps define subtle oscillatory zoning (Co, Se, and Pt) fractures and submicron trails of inclusions and sets of parallel fractures highlighted by the relative enrichment of Ni, Pd, Ag, and Sb. Py—pyrite; Ccp—chalcopyrite.

5. Discussion

5.1. Origin, Trace Element Signatures, and Successive Generations of Jatobá Sulfides

The orebody studied from Jatobá is associated with magnetite + apatite rich assemblages that are interpreted to be of IOCG affiliation. The Ni-bearing character of the sulfide assemblages was recognized by Veloso et al. [20], who considered 'Ni-pyrrhotite and Ni-pyrite' to be the main phases and that they represented the first stage of mineralization that introduced Ni into the system. Veloso et al. [20] explained the formation of Ni-mineralization in the context of a deep, evolving IOCG system at the transition between an initial magmatic stage and a subsequent stage termed 'magmatic-hydrothermal' to infer the high temperature of early fluids. In this model, magnetite-apatite associations formed first in an IOA deposit-like scenario, enabling hot, Cl-rich, saline fluids to leach Ni from mafic-ultramafic rocks. According to Veloso et al. [20], such fluids would transport and discharge episodically, resulting in a concentration of the Ni-bearing sulfide ores in the deeper part of the Jatobá ore zones.

The present study shows that sulfides also occur outside of the magnetite-rich orebody and form stringer zones throughout the mafic host rocks, which are similarly metamorphosed, deformed, and hydrothermally altered (Figure 3). Although the mineral associations within and outside the orebody are essentially similar (pyrrhotite + chalcopyrite + pyrite, in addition to dominant magnetite), the relative proportions of these components vary considerably, with the orebody featuring a greater volume of pyrite than other sulfides.

Minerals **2024**, *14*, 757

Pyrrhotite is also a key mineral. It contains pentlandite with only negligible Co content and is closely associated with chalcopyrite (Figure 4) both within and outside the orebody. Apart from pentlandite, pyrrhotite contains the most Ni (Figure 9). By virtue of its greater relative abundance, at least in our samples, pyrite is likely the major Ni carrier in the deposit, followed by pyrrhotite.

Apart from being a Ni carrier, pyrite is also markedly enriched in Co, much more so than the co-existing pyrrhotite (Figure 9). Textures between pyrite and pyrrhotite point to a syn-deformational metamorphic event in which pyrite has been abraded (rounded), whereas pyrrhotite behavior was largely, although not necessarily entirely, ductile, and pentlandite underwent reincorporation into pyrrhotite and subsequent re-exsolution concentrated along the grain contacts with pyrite (Figure 5B). Pyrite displays the widest range of sizes and overprint textures (Figures 4 and 13–15). Among the key features of the pyrite are the foam textures and pinch-and-swell grain boundaries in the stringer sulfides outside the orebody that can be attributed to syn-deformational metamorphism and annealing (Figures 4E, 5D and 14).

Although Veloso et al. [20] acknowledged the importance of tectonic control on ore formation at Jatobá, direct evidence for deep burial metamorphism at amphibolite facies only came from the later identification of high-pressure ferrotschermakite inclusions in magnetite [54] and as discrete grains in the rock matrix. The origin and timing of initial sulfide formation are thus debatable, at least relative to that of the IOCG system, since the seafloor rift setting proposed [7,31] may have provided for a prior accumulation of sulfides (e.g., volcanic-hosted massive sulfide; VHMS), prior to any IOCG overprint.

The geochemical signatures in pyrite defined by As, Ni, and Co concentrations (Figure 11A–D) coupled with LA-ICP-MS element maps (Figures 13–15) lead us to infer there are at least two distinct generations of pyrite growth both outside and within the orebody. The first, characteristically observed as (partially resorbed?) grain cores and thus the earliest, is defined by high Co concentrations at variable but generally low Ni concentrations. The second generation of pyrite is clearly later and has wide-ranging concentrations of As, Ni, and Co and, on some maps at least, shows a patchy oscillatory zoning, albeit disrupted or obliterated altogether, as exemplified by the complex overprinting textures illustrated in Figures 4F, 13–15. The distinct geochemical trends displayed on the plots of As vs. Co/Ni in pyrite recorded by pyrite outside and within the orebody, ~100 m apart (Figure 11C,D), may also be evidence for a multistage origin. The observed assemblage is thus considered the product of the metamorphism and deformational reworking of an early sulfide assemblage and a superimposed fluid event that introduced additional metals and further modified the assemblage. Although partially overlapping, the two events were not necessarily spatially coupled, and their temporal relationships remain ill-constrained.

Pyrite contains measurable concentrations of both Pd and Pt, even if Pd is an order of magnitude higher (mean 7.4 ppm) in pyrite from outside the orebody (Figure 12). The flat LA-ICP-MS depth profiles suggest that PGE are dissolved in the sulfide, yet the positive correlation between Pd and Ni, Te, Bi (and Sb, Ag), and Pt with As may suggest nanoscale inclusions of Pd-Bi-Te and Pt-As phases as much as solid solution, even if no nanoinclusions could be identified on the time-resolved downhole profiles.

A remarkable and hitherto unrecognized PGM signature is seen in Jatobá pyrite (Figure 5D–M, Figures 6–8), largely restricted to fractures and pressure shadows in pyrite. The more diverse range of mineral species and greater size of individual PGM in orebody pyrite contrasts with a dominance of abundant yet smaller grains of merenskyite in pyrite from outside the orebody. In the latter case, ductile migration of chalcopyrite along pinch and swell textures is accompanied by PGM nucleation, suggesting formation in the waning stages of deformation from PGE released from the annealed pyrite (Figure 5D–I). In contrast, sustained fluid infiltration would result in PGM coarsening and deposition of abundant gangue minerals (e.g., biotite, apatite, quartz) like those observed along the PGM-trails or close to grain boundaries in orebody pyrite (Figure 5J–M). Any PGE that was contained in solid solution within the sulfide minerals was likely expelled and remobilized during metamorphism and shearing.

Minerals **2024**, *14*, 757

The relative differences in terms of Pd and Pt concentrations in pyrite and the size of the discrete PGM within and outside the orezone are likely explained by the more intense overprinting of the latter during tectonic activation of the shear zone hosting the orebody.

The better preservation of deformation textures in pyrite outside the orebody is attributable to the dry conditions operating during prograde metamorphism. The fluids associated with retrograde metamorphism were largely focused along crustal shear zones, generating IOCG-style mineralization, associated alteration, and more extensive reworking of ore textures. Under such conditions, an input of metals and sulfur from deeper basement can be hypothesized to account for the potassic-Fe metasomatism defining the onset of IOCG mineralization. This is consistent with the available isotopic evidence (e.g., [58]), indicating multiple but largely mantle- and magmatic-derived sulfur and the involvement of highly saline, hot, and deep-seated metalliferous fluids. The characteristic accessory mineral signature of IOCG deposits, notably the relative abundance of REE, U-, and W-bearing minerals (apatite, allanite, uraninite, huttonite or thorite, ferberite, and scheelite) is especially pronounced throughout the magnetite-rich orebody.

5.2. PGM in Ni-Bearing Sulfides—Identifying the Potential Source

A positive correlation exists between the PGE content of present-day seafloor massive sulfide (SMS) and PGE enrichment in their ancient VMS analogues. For example, active seafloor deposits of the PACMANUS hydrothermal field, eastern Manus basin, Papua New Guinea, contain 356 ppb Pd [59], remarkably similar to VMS ores from the Iberian Pyrite Belt (203–350 ppb ΣPGE; [60]. These PGE concentrations are within the range reported for Jatobá [53]. Such a SMS-like scenario might be invoked for the initial deposition of Ni- and PGE-bearing sulfides at Jatobá, considering the volcanic sequence hosting the deposit. The stringer sulfides outside the magnetite-rich intervals preserve the initial conditions better than the ores since they have been less affected by fluid infiltration along shear zones. We cannot, however, fully rule out a potential source of a different genetic type, provided that PGE are increasingly identified in 'non-traditional' deposits, including porphyry copper deposits (e.g., [61]).

Whatever the primary source of PGE, was the fluid that transported the PGE directly derived from magma, or alternatively, a product of seafloor hydrothermal alteration via convective cells leaching PGE from the host volcanics? Studies have shown that Cu-rich sulfides, like those at Jatobá, likely relate to a magmatic source, whereas Zn-rich SMS correspond to the second hypothesis (e.g., [59]). On the other hand, the PGE geochemistry of the volcanic rocks is considered to control the chalcophile element fertility of VMS mineralization, as was, for example, shown in the study of the Jaguar and Bentley VMS-style Cu–Zn deposits in Western Australia [62]. VHMS have long been suspected and indeed invoked by Melo et al. [41], but they have never been unambiguously confirmed in the Carajás Domain. They would certainly be expected in the Neoarchean Itacaiúnas Supergroup or in the older Rio Novo Group, as suggested by Costa et al. [31], perhaps also considering the presence of iron formations in the same sequences.

PGE have been used to test the hypothesis that the time of sulfide saturation, relative to volatile saturation, also controls the fertility of porphyry Cu and porphyry Cu–Au deposits [63], and references therein. Indeed, the enrichment of PGE in porphyry Cu-Au deposits is well documented in a variety of metallogenic belts (e.g., [64], and references therein). A relative enrichment in PGE is considered to occur during the high-T potassic alteration stage of porphyry deposit formation [64]. Although a comparable scenario could have been involved at Jatobá, no prospective magmatic source for a derived IOCG fluid, such as granite, has been identified. Porphyry-type mineralization has not been observed in the Carajás Domain, but this discourse serves to illustrate that PGE are not restricted to ore systems associated with mafic-ultramafic rocks as popularly yet falsely believed.

Minerals **2024**, *14*, 757

5.3. Which Ore Genesis Model Best Explains the Evidence?

Data in the present contribution show that Jatobá is not only a Ni-bearing sulfide deposit of probable IOCG-type hosted within a sequence dominated by mafic rocks, but also that it stands out from other Ni-bearing IOCG deposits in the Carajás Domain in terms of a relative enrichment of Pd and Pt, expressed as both measurable PGE in sulfides and as discrete PGM. Two alternative genetic models for the deposit are supported, at least in part, by observations of ore mineralogy, textures, and geochemical signatures of the main minerals and are compounded by the local geological and structural setting.

The favored model envisages two distinct stages of mineralization. Pre-existing stringer sulfides of as-yet poorly constrained origin within a mafic rock pile contain both Ni and PGE and are superposed by a strongly focused flow of metal-bearing fluids along crustal shears, resulting in IOCG-style mineralization with evidence of replacement and overprinting. The presence of Ni and PGE from pre-existing mineralization, combined with elements more typical of IOCG deposits, including REE and U, led to the observed assemblage, notably the diverse suite of platinum group minerals illustrated in Figures 5–8. Noting the abundance of Sb, Te, Se, and Bi in Ni-PGE deposits like Norilsk [65] as much as in IOCG deposits, these elements could be derived from either the pre-existing Ni-PGE source or from the IOCG fluids.

An alternative model considers IOCG-type fluids that have dissolved and remobilized Ni and PGE from pre-existing mineralization within the mafic sequence hosting the ores, from basement rocks at depth, or even from the host rocks themselves, and re-concentrated them along structural conduits. Potential sources would include komatiites and ultramafic rocks in the basement. Both are well documented in the region. Mesoarchean komatiites would be a major source for Ni (and subordinate PGE). We note descriptions of spinifex textures in proximity to Jatobá [28]. Unfortunately, due to extensive soil and forest cover in the area and the play of tectonics, it is impossible to ascertain with any certainty whether these komatiites belong to the Mesoarchean greenstone sequences, or to the Neoarchean Itacaiúnas Supergroup. If the former could be confirmed, it would also explain the evidence for pre-IOCG amphibolite facies metamorphism in the magnetite-sulfide assemblages reported by Campo-Rodriguez et al. [54]. Such a model would also be concordant with the occurrence of several other Ni-rich IOCG deposits nearby and their apparent concentration in the southern copper belt (Jaguar, GT-34, Cristalino, and Castanha), close to the Rio Maria TTG-greenstone domain.

Although the mobility of both Pt and Pd has been well documented in experimental studies (e.g., [66–68]) and many Ni-PGE ores display overprinting, either in the waning stages of formation or during later metamorphic-deformation events (e.g., [69]), there are relatively few antecedents for large-scale remobilization and re-concentration of PGE and related metals. Wang et al. [70] describe the redistribution and re-concentration of ore-forming metals in the Huangshandong deposit, China, while a second example comes from another part of Brazil [71], in which parts of the komatiite-hosted Fortaleza de Minas deposit are remobilized and subsequently redeposited as discordant veins. Hydrothermal nickel deposits (e.g., [21,72]) also appear proximal relative to the source and are often relatively small in scale).

Except for the Pt-arsenide sperrylite, the speciation of all PGM observed in the present study is conspicuous because Pd is combined only with highly mobile elements such as Te, Bi, and Sb, all of which are typically present in IOCG fluids. They are strongly associated with REE- and U-bearing minerals typical of IOCG mineralization, such as britholite and uraninite.

Metamorphism in the Carajás Domain has traditionally been considered as a single event at ~2.82 Ga that was restricted to the basement. Rocks of the Itacaíúnas Supergroup are not considered to display evidence of regional metamorphism. Nevertheless, a study by Fernandes et al. [73] of an area in western Carajás describes a ca. 2.7 Ga dynamic metamorphic event as having "reached amphibolite-facies conditions and overprinted previous metamorphic textures" in basement rocks. The same authors also describe "chalcopyrite-

rich amphibole and amphibole schist concordant with metamorphic foliation". These are considered amphibolites, representing the metamorphosed expression of mafic protoliths belonging to a volcano-sedimentary succession in the Sao Felix Group of the Itacaíúnas Supergroup. Other authors (e.g., [8]) favored a later "dynamic metamorphism", implying only very low temperatures and essentially inducing only mechanical changes, to account for the mylonitic fabrics observed in alteration assemblages in IOCG deposits of the Carajás Domain. The high-pressure conditions (ca. 6.4–7.4 kbar) estimated from the composition of ferrochermakite in magnetite [54]) represent a hitherto unrecognized "smoking gun" that cannot be easily ignored. Both they and the syn-deformational textures displayed by pyrite are, however, entirely compatible with amphibolite facies metamorphism. Formation of the ore textures and the relationships between minerals illustrated in the present contribution can only be attributed to deformation at conditions of burial, with applied heat and pressure approximating to amphibolite facies, clearly more than the near-surface brittle deformation episode invoked for "dynamic metamorphism" by other authors.

Both models remain conjectural without additional supporting evidence or geochronological constraints, and each has advantages and drawbacks, possibly indicating a more complex sequence of events that incorporates elements of both models. Evidence is needed to constrain the timing of copper precipitation, the nature and age of any pre-existing mineralization, or the relative timing of the IOCG overprinting event(s). Do they, for example, represent stages within a (semi)-continuous evolution (e.g., prograde and retrograde cycles within a single metamorphic event)? We cannot discount a hybrid model involving both dissolution-remobilization-reprecipitation from depth and in-situ replacement.

6. Conclusions and Implications

Jatobá is recognized as a structurally controlled IOCG deposit based on the main commodities, the abundance of iron oxides, and the observed styles of alteration. It is conspicuous in terms of the contained nickel and the remarkable co-enrichment of Pd and Pt. Observations of ore mineralogy, textures, and the geochemical signatures of the main minerals, compounded by the local geological and structural setting, allow a tentative genetic model to be proposed. Although speculative and not yet tied to specific geological events or validated by geochronological evidence, one scenario for Jatobá considers that both Ni and PGE were contained within pre-existing sulfides, possibly resulting from precipitation in a VHMS-like setting within a mafic rock pile, onto which the IOCG-style mineralization was superposed. The IOCG overprint is recorded by replacement and local-scale remobilization, in which PGE are largely though not completely, released from sulfides and combine with components of the IOCG fluids like Sb, Bi, and Te to form the range of PGM observed, notably tellurides and antimonides, as well as their association with REE- and U-bearing minerals typical of IOCG systems. An alternative model also involves fluids of hydrothermal or crustal origin but assumes a single influx of fluid instead of overprinting and partially replacing existing mineralization. In this case, the fluid dissolved and remobilized Ni and PGE from pre-existing mineralization located within (e.g., from komatiites) within the mafic sequence or from the basement (ultramafic rocks) and re-concentrated them within a pre-existing oxide assemblage, possibly during the retrograde stage of regional metamorphism at amphibolite facies.

LA-ICP-MS analysis of pyrite from Jatobá revealed concentrations of Pd and Pt well above the minimum limits of detection, with clear, flat signals indicative of incorporation within the crystal lattice. We were also able to identify an enrichment of both Pd and Pt within healed fractures in Jatobá pyrite on element maps. Most importantly, in terms of recognizing the PGE-enriched character of the Jatobá deposit, is the identification of more than half a dozen distinct PGMs. Although PGE mineralization is documented from the Carajás Domain in deposits such as Luanga associated with mafic-ultramafic intrusions [47] and enigmatic deposits like Serra Pelada [49], our new data thus represent the first description of discrete PGM and sulfide-hosted PGM within mineralization from a deposit considered an IOCG-type deposit. Further study of representative samples is

recommended to evaluate the deposit-scale distribution of PGM at Jatobá, the average grade of PGM and Ni, and the degree to which these grades correlate with Cu. If the PGE enrichment can be confirmed across the deposit, future work might also aim to adequately understand the geometallurgical implications of PGE enrichment in Jatobá ores.

The discovery of PGE at Jatobá emphasizes the potential for additional discoveries in structurally and lithologically comparable sulfide ore systems in which Ni enrichment is recognized. The PGM identified are small, largely restricted to filled fractures in pyrite, and thus will only be identified by analysis for PGE, high-magnification imaging, and using LA-ICP-MS to drill down with a large spot size and high Hz to look for elevated PGE counts. Specimens would also need to be carefully prepared and polished to avoid plucking out of phases from grain boundaries. Further examples of analogous mineralization outside the Carajás district that combine the characteristics of magmatic Ni-PGE and IOCG-style mineralization may be rare but are certainly not impossible, extending the diversity of deposit types that may be vital sources of PGE supply in the future.

Supplementary Materials: The following supporting information can be downloaded at: https://www.mdpi.com/article/10.3390/min14080757/s1, Table S1. (LA-ICP-MS trace element data for sulfide minerals (complete dataset, element concentrations in ppm).

Author Contributions: Y.T.C.R.: conceptualization, experimental, validation, writing—original draft. N.J.C.: conceptualization, writing—original draft, supervision. C.L.C.: writing—original draft, supervision. M.E.S.: conceptualization, supervision. S.A.K. and S.G.: experimental. K.E.: validation, guidance and discussion. All authors have read and agreed to the published version of the manuscript.

Funding: Y.T.C.R. and M.E.S. acknowledges continuous support from the Brazilian Research Council (CNPq—Project 409015/2021-0) and the Coordenação de Aperfeiçoamento de Pessoal de Nível Superior—Brasil (CAPES)—Finance Code 001. Analytical expenses were supported by a grant from the Institute of Sustainability, Energy and Resources, The University of Adelaide. N.J.C. and K.E. acknowledge funding through Australian Research Council Linkage grant LP200100156 (Critical Minerals from Complex Ores).

Data Availability Statement: Data will be made available on request.

Acknowledgments: We acknowledge the constructive comments from two anonymous reviewers that helped us improve expression and clarity.

Conflicts of Interest: The authors declare that they have no known competing financial interests relevant to the reported research.

References

1. Barton, M. Iron oxide (-Cu-Au-REE-P-Ag-U-Co) systems. In *Treatise on Geochemistry*, 2nd ed.; Elsevier: Amsterdam, The Netherlands, 2014; Volume 13, pp. 515–541.
2. Skirrow, R.G. Iron oxide copper-gold (IOCG) deposits-a review (part 1): Settings, mineralogy, ore geochemistry and classification. *Ore Geol. Rev.* **2022**, *140*, 104569. [CrossRef]
3. Hitzman, M.W.; Oreskes, N.; Einaudi, M.T. Geological characteristics and tectonic setting of Proterozoic iron oxide (Cu-U-Au-REE) deposits. *Precambr. Res.* **2002**, *58*, 241–287. [CrossRef]
4. Bidgood, A.; Hitzman, M. New models to aid the discovery of critical raw material deposits for the Green Stone Age. In *The Green Stone Age: Exploration and Exploitation of Minerals for Green Technologies*; Smelror, M., Hanghøj, K., Schiellerup, H., Eds.; Geological Society, London, Special Publications: London, UK, 2022; Volume 526, pp. 183–191. [CrossRef]
5. Grainger, C.J.; Groves, D.I.; Tallarico, F.H.B.; Fletcher, I.R. Metallogenesis of the Carajás mineral province, southern Amazon Craton, Brazil: Varying styles of Archean through Paleoproterozoic to Neoproterozoic base- and precious-metal mineralisation. *Ore Geol. Rev.* **2008**, *33*, 451–489. [CrossRef]
6. Monteiro, L.V.S.; Xavier, R.P.; de Souza Filho, C.R.; Moreto, C. Metalogênese da Província Carajás. In *Metalogênese das Províncias Tectônicas Brasileiras*; da Glória da Silva, M., da Costa Neto, M.B., Jost, H., Kuyumjian, R.M., Eds.; CPRM Serviço Geológico do Brasil: Belo Horizonte, Brazil, 2014; pp. 43–92.
7. Tavares, F.M.; Trouw, R.A.J.; Silva, C.M.G.; Justo, A.P.; Oliveira, J.K.M. The multistage tectonic evolution of the northeastern Carajás Province, Amazonian Craton, Brazil: Revealing complex structural patterns. *J. S. Am. Earth Sci.* **2018**, *88*, 238–252. [CrossRef]

8. Schutesky, M.E.; de Oliveira, C.G. From the roots to the roof: An integrated model for the Neoarchean Carajás IOCG System, Brazil. *Ore Geol. Rev.* **2020**, *127*, 103833. [CrossRef]
9. Trunfull, E.F.; Hagemann, S.G.; Xavier, R.P.; Moreto, C.P.N. Critical assessment of geochronological data from the Carajás Mineral Province, Brazil: Implications for metallogeny and tectonic evolution. *Ore Geol. Rev.* **2020**, *121*, 103556. [CrossRef]
10. Toledo, P.I.F.; Moreto, C.P.N.; Monteiro, L.V.S.; Melo, G.H.C.; Matos, F.M.V.; Xavier, R.P.; Carvalho, J.A.; Filho, C.A.M.; Navarro, M.S.; Lana, C.C. Breaking up the temporal link between granitic magmatism and iron oxide-copper-gold (IOCG) deposits in the Carajás Mineral Province, NW Brazil. *Miner. Depos.* **2024**, *59*, 601–625. [CrossRef]
11. Xavier, R.P.; Soares Monteiro, L.V.; Moreto, C.P.N.; Pestilho, A.L.S.; Coelho de Melo, G.H.; Delinardo da Silva, M.A.; Aires, B.; Ribeiro, C.; Freitas e Silva, F.H. The Iron Oxide Copper-Gold Systems of the Carajás Mineral Province, Brazil. In *Geology and Genesis of Major Copper Deposits and Districts of the World: A Tribute to Richard H. Sillitoe*; Hedenquist, J.W., Harris, M., Camus, F., Eds.; Society of Economic Geologists: Littleton, CO, USA, 2012; Volume 16, 22p.
12. Monteiro, L.V.S.; Xavier, R.P.; Carvalho, E.R.; Hitzman, M.W.; Johnson, C.A.; Souza, C.R.; Filho, C.R.; Torresi, I. Spatial and temporal zoning of hydrothermal alteration and mineralization in the Sossego iron oxide-copper-gold deposit Carajás Mineral Province, Brazil: Paragenesis and stable isotope constraints. *Miner. Depos.* **2008**, *43*, 129–159. [CrossRef]
13. Monteiro, L.V.; Xavier, R.P.; Hitzman, M.W.; Juliani, C.; de Souza Filho, C.R.; Carvalho, E.D. Mineral chemistry of ore and hydrothermal alteration at the Sossego iron oxide-copper-gold deposit, Carajás Mineral Province, Brazil. *Ore Geol. Rev.* **2008**, *34*, 317–336. [CrossRef]
14. Moreto, C.P.N.; Monteiro, L.V.S.; Xavier, R.P.; Creaser, R.A.; Dufrane, S.A.; Tassinari, C.C.G.; Sato, K.; Kemp, A.I.S.; Amaral, W.S. Neoarchean and Paleoproterozoic iron oxide-copper-gold events at the Sossego deposit, Carajás Province, Brazil, Re-Os and U-Pb geochronological evidence. *Econ. Geol.* **2015**, *110*, 809–835. [CrossRef]
15. Tassinari, C.C.G.; Mellito, M.K.; Babinski, M. Age and origin of the Cu (Au-Mo-Ag) Salobo 3A ore deposit, Carajás Mineral Province, Amazonian Craton, northern Brazil. *Episodes* **2003**, *26*, 2–9. [CrossRef]
16. Melo, G.H.C.; Monteiro, L.V.S.; Xavier, R.P.; Moreto, C.P.N.; Santiago, E.S.B.; Dufrane, S.A.; Aires, B.; Santos, A.F.F. Temporal evolution of the giant Salobo IOCG deposit, Carajás Province (Brazil): Constraints from paragenesis of hydrothermal alteration and U-Pb geochronology. *Miner. Depos.* **2017**, *52*, 709–732. [CrossRef]
17. Campo-Rodríguez, Y.T.; Schutesky, M.E.; de Oliveira, C.G.; Whitehouse, M.J. Unveiling the polyphasic evolution of the Neoarchean IOCG Salobo deposit, Carajás Mineral Province, Brazil: Insights from magnetite trace elements and sulfur isotopes. *Ore Geol. Rev.* **2021**, *140*, 104572. [CrossRef]
18. Tallarico, F.H.B.; Figueiredo, B.R.; Groves, D.I.; Kositcin, N.; McNaughton, N.J.; Fletcher, I.R.; Rego, J.L. Geology and SHRIMP U-Pb geochronology of the Igarape Bahia Deposit, Carajás copper-gold belt, Brazil, an Archean (2.57 Ga) example of iron-oxide Cu-Au-(U-REE) mineralization. *Econ. Geol.* **2005**, *100*, 7–28. [CrossRef]
19. de Melo, G.H.C.; Monteiro, L.V.S.; Xavier, R.P.; Moreto, C.P.N.; Santiago, E. Tracing Fluid Sources for the Salobo and Igarape Bahia Deposits: Implications for the Genesis of the Iron Oxide Copper-Gold Deposits in the Carajás Province, Brazil. *Econ. Geol.* **2019**, *114*, 697–718. [CrossRef]
20. Veloso, A.S.R.; Monteiro, L.V.S.; Juliani, C. The link between hydrothermal nickel mineralization and an iron oxide-copper-gold (IOCG) system: Constraints based on mineral chemistry in the Jatobá deposit, Carajás Province. *Ore Geol. Rev.* **2020**, *121*, 103555. [CrossRef]
21. González-Álvarez, I.; Pirajno, F.; Kerrich, R. Hydrothermal nickel deposits: Secular variation and diversity. *Ore Geol. Rev.* **2013**, *52*, 1–3. [CrossRef]
22. Oliveira, M.M.F. Caracterização e Metalogênese do Depósito de Ni do Jaguar, Província Mineral de Carajás. Master's Thesis, Universidade de Brasília, Brasília, Brazil, 2017; 115p.
23. Ferreira Filho, C.F.; Ferraz de Oliveira, M.M.; Mansur, E.T.; Rosa, W.D. The Jaguar hydrothermal nickel sulfide deposit: Evidence for a nickel-rich member of IOCG-type deposits in the Carajás Mineral Province, Brazil. *J. S. Am. Earth Sci.* **2021**, *111*, 103501. [CrossRef]
24. Mansur, E.T.; Dare, S.A.S.; Ferreira Filho, C.F.; Rodrigues Miranda, A.C.; Soares Monteiro, L.V. The distribution of trace elements in sulfides and magnetite from the Jaguar hydrothermal nickel deposit: Exploring the link with IOA and IOCG deposits within the Carajás Mineral Province, Brazil. *Ore Geol. Rev.* **2023**, *152*, 105256. [CrossRef]
25. Garcia, V.B.; Schutesky, M.E.; Oliveira, C.G.; Whitehouse, M.J.; Huhn, S.R.B.; Augustin, C.T. The Neoarchean GT-34 Ni deposit, Carajás mineral Province, Brazil: An atypical IOCG-related Ni sulfide mineralization. *Ore Geol. Rev.* **2020**, *127*, 103773. [CrossRef]
26. Craveiro, G.S.; Xavier, R.P.; Villas, R.N.N. The Cristalino IOCG deposit: An example of multi-stage events of hydrothermal alteration and copper mineralization. *Braz. J. Geol.* **2019**, *49*, e20180015. [CrossRef]
27. Pestilho, A.L.S.; Monteiro, L.V.S.; de Melo, G.H.C.; Moreto, C.P.N.; Juliani, C.; Fallick, A.E.; Xavier, R.P. Stable isotopes and fluid inclusion constraints on the fluid evolution in the Bacaba and Castanha iron oxide-copper-gold deposits, Carajás Mineral Province, Brazil. *Ore Geol. Rev.* **2020**, *126*, 103738. [CrossRef]
28. Siepierski, L.; Ferreira Filho, C.F. Spinifex-textured komatiites in the south border of the Carajás ridge, Selva Greenstone belt, Carajás Province, Brazil. *J. S. Am. Earth Sci.* **2016**, *66*, 41–55. [CrossRef]
29. Dutra, L.F.; Louro, V.H.A.; Monteiro, L.V.S. The southern IOCG and hydrothermal nickel mineralization trend of the Carajás Mineral Province: Airborne geophysical and remote sensing evidences for structural controls and hydrothermal signature. *J. Appl. Geophys.* **2023**, *213*, 105016. [CrossRef]

30. Vasquez, L.V.; Rosa-Costa, L.R.; Silva, C.G.; Ricci, P.F.; Barbosa, J.O.; Klein, E.L.; Lopes, E.S.; Macambira, E.B.; Chaves, C.L.; Carvalho, J.M.; et al. *Geologia e Recursos Minerais do Estado do Pará: Sistema de Informações Geográficas-SIG: Texto explicativo dos mapas Geológico e Tectônico e de Recursos Minerais do Estado do Pará 1:1.000.000*; CPRM: Belém, Brazil, 2008; 328p.
31. da Costa, F.G.; Araújo dos Santos, P.; de Oliveira Serafim, I.C.C.; Costa, I.S.L.; Roopnarain, S. From Mesoarchean drips to modern-style tectonics in the Carajás Province, Amazonian Craton. *J. S. Am. Earth Sci.* **2020**, *104*, 102817. [CrossRef]
32. Araújo, O.D.; Maia, R.G.N.; João, X.J.; Costa, J.B.S. A megaestruturação arqueana da folha Serra dos Carajás. In *Congresso Latino-Americano de Geologia*; SBG: Belém, Brazil, 1988; Volume 7, pp. 324–338.
33. Machado, N.; Lindenmayer, Z.; Krogh, T.E.; Lindenmayer, D. U-Pb geochronology of Archean magmatism and basement reactivation in the Carajás area, Amazon shield, Brazil. *Precambr. Res.* **1991**, *49*, 329–354. [CrossRef]
34. Martins, P.L.G.; Toledo, C.L.B.; Silva, A.M.; Chemale, F., Jr.; Santos, J.O.S.; Assis, L.M. Neoarchean magmatism in the southeastern Amazonian Craton, Brazil: Petrography, geochemistry and tectonic significance of basalts from the Carajás Basin. *Precambr. Res.* **2017**, *302*, 340–357. [CrossRef]
35. DOCEGEO. Revisão litoestratigráfica da província mineral de Carajás. In *Litoestratigrafia e Principais Depósitos Minerais, Proceedings of the Anexo do 35. Congresso Brasileiro de Geologia, Belém, Brazil, 1988*; SBG, Anexo aos anais: Belém, Brazil, 1988; Volume 35, pp. 11–54.
36. Feio, G.R.L.; Dall'Agnol, R.; Dantas, E.L.; Macambira, M.J.B.; Santos, J.O.S.; Althoff, F.J.; Soares, J.E.B. Archean granitoid magmatism in the Canaã dos Carajás area: Implications for crustal evolution of the Carajás province, Amazonian Craton, Brazil. *Precambr. Res.* **2013**, *227*, 157–185. [CrossRef]
37. Moreto, C.P.N.; Monteiro, L.V.S.; Xavier, R.P.; Creaser, R.A.; Dufrane, S.A.; Melo, G.H.C.; Silva, M.A.D.; Tassinari, C.C.G.; Sato, K. Timing of multiple hydrothermal events in the iron oxide-copper gold deposits of the Southern Copper Belt, Carajás Province, Brazil. *Miner. Depos.* **2015**, *50*, 517–546. [CrossRef]
38. Teixeira, M.F.B.; Dall'Agnol, R.; Santos, J.O.S.; de Oliveira, D.C.; Lamarão, C.N.; McNaughton, N.J. Crystallization ages of Paleoproterozoic A-type granites of Carajás province, Amazon craton: Constraints from U-Pb geochronology of zircon and titanite. *J. S. Am. Earth Sci.* **2018**, *88*, 312–331. [CrossRef]
39. Teixeira, W.; Hamilton, M.A.; Girardi, V.A.V.; Faleiros, F.M. U-Pb baddeleyite ages of key dyke swarms in the Amazonian Craton (Carajás/Rio Maria and Rio Apa areas): Tectonic implications for events at 1880, 1110 Ma, 535 Ma and 200 Ma. *Precambr. Res.* **2019**, *329*, 138–155. [CrossRef]
40. Araújo Filho, R.C.; Nogueira, A.C.R.; Araújo, R.N. New stratigraphic proposal of a Paleoproterozoic siliciclastic succession: Implications for the evolution of the Carajás Basin, Amazonian Craton, Brazil. *J. S. Am. Earth Sci.* **2020**, *102*, 102665. [CrossRef]
41. de Melo, G.H.C.; Monteiro, L.V.S.; Hunger, R.B.; Toledo, P.I.F.; Xavier, R.P.; Zhao, X.F.; Su, Z.K.; Moreto, C.P.N.; Pereira de Jesus, S.d.S.G. Magmatic-hydrothermal fluids leaching older seafloor exhalative rocks to form the IOCG deposits of the Carajás Province, Brazil: Evidence from boron isotopes. *Precambr. Res.* **2021**, *365*, 106412. [CrossRef]
42. Almeida, F.F.M.; Hasui, Y.; Brito Neves, B.B.; Fuck, R.A. Brazilian structural provinces: An introduction. *Earth Sci. Rev.* **1981**, *17*, 1–29. [CrossRef]
43. Xavier, R.P.; Moreto, C.; de Melo, G.H.C.; Toledo, P.; Hunger, R.; Delinardo, M.; Faustinoni, J.; Lopes, A.; Monteiro, L.V.S.; Previato, M.; et al. Geology and Metallogeny of Neoarchean and Paleoproterozoic Copper Systems of the Carajás Domain, Amazonian Craton, Brazil. In Proceedings of the Mineral Resources to Discover-14th SGA Biennial Meeting, Quebec, QC, Canada, 20–23 August 2017; pp. 899–902.
44. Teixeira, A.S.; Ferreira Filho, C.F.; Della Giustina Schutesky, M.E.; Araújo, S.M.; da Silva, H.H.A.B. Geology, petrology and geochronology of the Lago Grande layered complex: Evidence for a PGE-mineralized magmatic suite in the Carajás Mineral Province, Brazil. *J. S. Am. Earth Sci.* **2015**, *64*, 116–138. [CrossRef]
45. Diella, V.; Ferrario, A.; Girardi, V.A.V. PGE and PGM in the Luanga mafic-ultramafic intrusion in Serra dos Carajás (Pará State, Brazil). *Ore Geol. Rev.* **1995**, *9*, 445–453. [CrossRef]
46. Mansur, E.T.; Ferreira Filho, C.F. Magmatic structure and geochemistry of the Luanga Mafic-Ultramafic Complex: Further constraints for the PGE-mineralized magmatism in Carajás, Brazil. *Lithos* **2016**, *266–267*, 28–43. [CrossRef]
47. Mansur, E.T.; Ferreira Filho, C.F.; Oliveira, D.P.L. The Luanga deposit, Carajás Mineral Province, Brazil: Different styles of PGE mineralization hosted in a medium-size layered intrusion. *Ore Geol. Rev.* **2020**, *118*, 103340. [CrossRef]
48. Moroni, M.; Girardi, V.A.; Ferrario, A. The Serra Pelada Au-PGE deposit, Serra dos Carajás (Pará State, Brazil): Geological and geochemical indications for a composite mineralising process. *Miner. Depos.* **2001**, *36*, 768–785. [CrossRef]
49. Cabral, A.R.; Lehmann, B.; Kwitko, R.; Costa, C.H.C. The Serra Pelada Au-Pd-Pt deposit, Carajás mineral province, northern Brazil: Reconnaissance mineralogy and chemistry of very high grade palladian gold mineralization. *Econ. Geol.* **2002**, *97*, 1127–1138. [CrossRef]
50. Cabral, A.R.; Lehmann, B.; Burgess, R. Late Cretaceous bonanza-style metal enrichment in the Serra Pelada Au-Pd-Pt deposit Pará Brazil. *Econ. Geol.* **2011**, *106*, 119–125. [CrossRef]
51. Pollard, P.J.; Taylor, R.G.; Peters, L.; Matos, F.; Freitas, C.; Saboia, L.; Huhn, S. 40Ar-39Ar dating of Archean iron oxide Cu-Au and Paleoproterozoic granite-related Cu-Au deposits in the Carajás Mineral Province, Brazil: Implications for genetic models. *Miner. Depos.* **2018**, *54*, 329–346. [CrossRef]

52. Lancaster, J.O.; Fanton, J.; Almeida, A.J.; Leveille, R.A.; Vieira, S. Discovery and geology of the Sossego copper-gold deposit, Carajás District, Pará State, Brazil. In Proceedings of the 31st International Geological Congress, Rio de Janeiro, Brazil, 6–17 August 2000.
53. Veloso, A.S.R. Evolução Metalogenetica do Deposito de Cu-(Zn) Jatobá, Provincia Mineral de Carajás. Ph.D. Thesis, University of São Paolo, São Paulo, Brazil, 2017; 197p.
54. Campo-Rodriguez, Y.T.; Ciobanu, C.L.; Slattery, A.; Cook, N.J.; Schutesky, M.E.; Ehrig, K.; King, S.A.; Yao, J. Polysomatic intergrowths between amphiboles and non-classical pyriboles in magnetite: Smallest-scale features recording a protracted geological history. *Am. Mineral.* 2024, *in press*. [CrossRef]
55. Belousov, I.; Danyushevsky, L.; Goemann, K.; Gilbert, S.; Olin, P.; Thompson, J.; Lounejeva, E.; Garbe-Schönberg, D. STDGL3, a reference material for analysis of sulfide minerals by Laser Ablation ICP-MS: An assessment of matrix effects and the impact of laser wavelengths and pulse widths. *Geostand. Geoanal. Res.* **2023**, *47*, 493–508. [CrossRef]
56. Gilbert, S.; Danyushevsky, L.; Robinson, P.; Wohlgemuth-Ueberwasser, C.; Pearson, N.; Savard, D.; Norman, M.; Hanley, J. A comparative study of five reference materials and the Lombard meteorite for the determination of the platinum-group elements and gold by LA-ICP-MS. *Geostand. Geoanalytical Res.* **2013**, *37*, 51–64. [CrossRef]
57. Paton, C.; Hellstrom, J.; Paul, B.; Woodhead, J.; Hergt, J. Iolite: Freeware for the visualisation and processing of mass spectrometric data. *J. Anal. At. Spectrom.* **2011**, *26*, 2508–2518. [CrossRef]
58. Santiago, E.S.B.; Xavier, R.P.; Hagemann, S.G.; Monteiro, L.V.S.; Cliff, J. Multiple sulfur isotopes constraints on origin and evolution of the Neoarchean and Paleoproterozoic Cu-Au systems from the Carajás Domain, Amazonian Craton, Brazil. *Ore Geol. Rev.* **2021**, *129*, 103872. [CrossRef]
59. Pašava, J.; Vymazalová, A.; Petersen, S.; Herzig, P. PGE distribution in massive sulfides from the PACMANUS hydrothermal field, eastern Manus basin, Papua New Guinea: Implications for PGE enrichment in some ancient volcanogenic massive sulfide deposits. *Miner. Depos.* **2004**, *39*, 784–792. [CrossRef]
60. Pašava, J.; Vymazalová, A.; Tornos, F. PGE distribution in massive sulfide deposits of the Iberian Pyrite Belt. *Miner. Depos.* **2007**, *42*, 309–314. [CrossRef]
61. McFall, K.; McDonald, I.; Wilkinson, J.J. Chapter 15: Assessing the role of tectono-magmatic setting in the precious metal (Au, Ag, PGE) and critical metal (Te, Se, Bi) endowment of porphyry Cu deposits. In *Tectonomagmatic Influences on Metallogeny and Hydrothermal Ore Deposits: A Tribute to Jeremy P. Richards (Volume II)*; Society of Economic Geologists: Littleton, CO, USA, 2021; Volume 2, pp. 277–295. [CrossRef]
62. Park, J.-W.; Campbell, I. Platinum-group element geochemistry of the volcanic rocks associated with the Jaguar and Bentley Cu-Zn volcanogenic massive sulfide (VMS) deposits, Western Australia: Implications for the role of chalcophile element fertility on VMS mineralization. *Miner. Depos.* **2021**, *56*, 583–600. [CrossRef]
63. Lowczak, J.N.; Campbell, I.H.; Cocker, H.; Park, J.W.; Cooke, D.R. Platinum-group element geochemistry of the Forest reef Volcanics, southeastern Australia: Implications for porphyry au-cu mineralisation. *Geochim. Cosmochim. Acta* **2018**, *220*, 385–406. [CrossRef]
64. Crespo, J.; Reich, M.; Barra, F.; Verdugo, J.J.; Martínez, C. Critical Metal Particles in Copper Sulfides from the Supergiant Río Blanco Porphyry Cu-Mo Deposit, Chile. *Minerals* **2018**, *8*, 519. [CrossRef]
65. Duran, C.J.; Barnes, S.J.; Pleše, P.; Prašek, M.K.; Zientek, M.L.; Pagé, P. Fractional crystallization-induced variations in sulfides from the Noril'sk-Talnakh mining district (polar Siberia, Russia). *Ore Geol Rev.* **2017**, *90*, 326–351. [CrossRef]
66. Barnes, S.J.; Liu, W. Pt and Pd mobility in hydrothermal fluids: Evidence from komatiites and from thermodynamic modelling. *Ore Geol. Rev.* **2012**, *44*, 49–58. [CrossRef]
67. Sullivan, N.A.; Zajacz, Z.; Brenan, J.M.; Tsay, A. The solubility of platinum in magmatic brines: Insights into the mobility of PGE in ore-forming environments. *Geochim. Cosmochim. Acta* **2022**, *316*, 253–272. [CrossRef]
68. Sullivan, N.A.; Zajacz, Z.; Brenan, J.M.; Hinde, J.C.; Tsay, A.; Yin, Y. The solubility of gold and palladium in magmatic brines: Implications for PGE enrichment in mafic-ultramafic and porphyry environments. *Geochim. Cosmochim. Acta* **2022**, *316*, 230–252. [CrossRef]
69. Mukwakwami, J.; Lafrance, B.; Lesher, C.M.; Tinkham, D.K.; Rayner, N.M.; Ames, D.E. Deformation, metamorphism, and mobilization of Ni-Cu-PGE sulfide ores at Garson Mine, Sudbury. *Miner. Depos.* **2014**, *49*, 175–198. [CrossRef]
70. Wang, S.M.; Wu, C.Z.; Muhtar, M.N.; Lei, R.X.; Brzozowski, M.J. Mobilization of ore-forming metals during post-magmatic hydrothermal overprinting of the Huangshandong Ni-Cu sulfide deposit, Eastern Tianshan, NW China. *Ore Geol. Rev.* **2021**, *137*, 104315. [CrossRef]
71. Almeida, C.M.; Olivo, G.R.; Carvalho, S.G. The Ni-Cu-PGE sulfide ores of the komatiite-hosted Fortaleza de Minas deposit, Brazil: Evidence of hydrothermal remobilization. *Can. Mineral.* **2007**, *45*, 751–773. [CrossRef]

72. Keays, R.R.; Jowitt, S.M. The Avebury Ni deposit, Tasmania: A case study of an unconventional nickel deposit. *Ore Geol. Rev.* **2013**, *52*, 4–17. [CrossRef]
73. Fernandes, C.M.D.; Galarza, M.A.; Teixeira de Gouvêa, R.C.; Tavares de Souza, H.P. Geochemical, geochronological, and isotopic constraints for the Archean metamorphic rocks of the westernmost part of the Carajás Mineral Province, Amazonian Craton, Brazil. *J. S. Am. Earth Sci.* **2021**, *110*, 103340. [CrossRef]

Disclaimer/Publisher's Note: The statements, opinions and data contained in all publications are solely those of the individual author(s) and contributor(s) and not of MDPI and/or the editor(s). MDPI and/or the editor(s) disclaim responsibility for any injury to people or property resulting from any ideas, methods, instructions or products referred to in the content.

CHAPTER 4

TELESCOPED TRANSITION FROM TRELLIS TO SILICATE-MOTTLED MAGNETITE RECORDS DEEP SHEAR METAMORPHISM IN THE IOCG DEPOSIT AT JATOBÁ, CARAJÁS, BRAZIL

Yuri Tatiana Campo-Rodriguez[1,2], Cristiana L. Ciobanu[1], Nigel J. Cook[1], Maria E. Schutesky[2], Kathy Ehrig[1,3], Ashley Slattery[4], Sarah Gilbert[4], Samuel A. King[1]

[1]*School of Chemical Engineering, The University of Adelaide, Adelaide, SA, 5005, Australia*

[2]*University of Brasilia, Institute of Geosciences, Graduate Program in Geology, Brasília DF 70910-900, Brazil*

[3]*BHP Olympic Dam, 10 Franklin Street, Adelaide, SA, 5000, Australia*

[4]*Adelaide Microscopy, The University of Adelaide, Adelaide, SA, 5005, Australia*

Article submitted to *Mineralogical Magazine,*
November 27th (2024) MIDE-D-24-00282.

Statement of Authorship

Title of Paper	Telescoped transition from trellis to silicate-mottled magnetite records deep shear metamorphism in the IOCG deposit at Jatobá, Carajás, Brazil
Publication Status	☐ Published ☐ Accepted for Publication ☑ Submitted for Publication ☐ Unpublished and Unsubmitted work written in manuscript style
Publication Details	Campo-Rodriguez, Y.T., Ciobanu, C.L., Cook, N.J., Schutesky, M.E., Ehrig, K., Slattery, A., Gilbert, S., King, S.A. Telescoped transition from trellis to silicate-mottled magnetite records deep shear metamorphism in the IOCG deposit at Jatobá, Carajás, Brazil. Submitted to *Mineralium Deposita*

Principal Author

Name of Principal Author (Candidate)	Yuri Tatiana Campo Rodriguez		
Contribution to the Paper	Performed analytical work, evaluation and interpretation of results and prepared the manuscript.		
Overall percentage (%)	60		
Certification:	This paper reports on original research I conducted during the period of my Higher Degree by Research candidature and is not subject to any obligations or contractual agreements with a third party that would constrain its inclusion in this thesis. I am the primary author of this paper.		
Signature		Date	06.11.2024

Co-Author Contributions

By signing the Statement of Authorship, each author certifies that:

i. the candidate's stated contribution to the publication is accurate (as detailed above);

ii. permission is granted for the candidate in include the publication in the thesis; and

iii. the sum of all co-author contributions is equal to 100% less the candidate's stated contribution.

Name of Co-Author	Cristiana L. Ciobanu		
Contribution to the Paper	Helped to define the direction of the manuscript, guides manuscript preparation and assisted with the interpretation of the results and evaluation of the manuscript. (20%)		
Signature		Date	06.11.2024

Name of Co-Author	Nigel J. Cook		
Contribution to the Paper	Helped with the preparation and evaluation of the manuscript. (8%)		
Signature	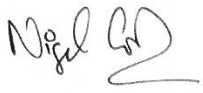	Date	06.11.2024

Name of Co-Author	Maria Emilia Schutesky		
Contribution to the Paper	Helped with the preparation and evaluation of the manuscript. (5%)		
Signature	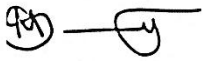	Date	06.11.2024

Name of Co-Author	Kathy Ehrig		
Contribution to the Paper	Assisted with the evaluation of the manuscript. (2%)		
Signature		Date	06.11.2024

Name of Co-Author	Ashley Slattery		
Contribution to the Paper	Assisted with HAADF-STEM data acquisition. (2%)		
Signature		Date	06.11.2024

Name of Co-Author	Sarah Gilbert		
Contribution to the Paper	Helped in the operation of analytical equipment and data interpretation. (2%)		
Signature		Date	06.11.2024

Name of Co-Author	Samuel Anthony King		
Contribution to the Paper	Assisted with the evaluation of the manuscript. (1%)		
Signature		Date	06.11.2024

Telescoped transition from trellis to silicate-mottled magnetite records deep shear metamorphism in the IOCG deposit at Jatobá, Carajás, Brazil

Yuri Tatiana Campo Rodriguez[1,2,*], Cristiana L. Ciobanu[1], Nigel J. Cook[1], Maria Emilia Schutesky[2], Kathy Ehrig[1,3], Ashley Slattery[4], Sarah Gilbert[4], Samuel A. King[1]

[1]*School of Chemical Engineering, The University of Adelaide, Adelaide S.A. 5005, Australia*

[2]*University of Brasilia, Institute of Geosciences, Graduate Program in Geology, Brasília DF 70910-900, Brazil*

[3]*BHP Olympic Dam, 10 Franklin Street, Adelaide S.A. 5000, Australia*

[4]*Adelaide Microscopy, The University of Adelaide, Adelaide S.A. 5005, Australia*

** Corresponding author.*

Abstract

Jatobá is a magnetite-hosted Cu-Ni deposit in the Carajás Domain, Brazil. The deposit is located along E-W structures belonging to the Canaã dos Carajás shear zone and hosted within the Neoarchean Grão Pará Group. Micron to nanoscale investigation of magnetite from mafic host lithologies and Cu-Ni-mineralization facilitate constraints on ore genesis. Two texturally and geochemically distinct types of magnetite are defined: 'trellis' (country rocks) and 'silicate-mottled' (ore). An overlap between the two types is recognized as ilmenite changes from lamellar trellis to blebby and patchy textures, in the silicate-mottled magnetite. The blebby type comprises

Al-hydroxides (gibbsite) and talc, replacing hercynite and Mg-amphibole, respectively. The mottled magnetite contains Mg-(Fe)- and Ce-bearing calcic amphiboles, both associated with nonclassical pyriboles (NCP). Geochemical signatures change from Ti-Cr-Co-Mn in trellis magnetite to a pronounced REE enrichment in the mottled type. Nanoinclusions of allanite occur as epitactic intergrowths with actinolite within magnetite. Amphiboles in the host rocks mirror those found in magnetite, with ferrotschermakite present in both cases.

Ilmenite-magnetite nano-thermobarometry yields a range of temperature and logfO_2 values temperature (from 728°C at logfO2=-12 to 414°C at logfO2=-31) for reequilibration between magnetite and ilmenite from initial trellis to the trellis+blebby and to patchy ilmenite in the densely mottled magnetite. Ferrotschermakite geobarometry enables an estimate of 6.4-7.4 kbar, compatible with amphibolite facies metamorphism at ~20 km depth. Syn-metamorphic deformation textures include magnetite+apatite as pods, banding and folds, as well as sigmoidal scapolite and pressure shadows surrounding magnetite. Collectively, the data support a genetic model implying deep shear zone metamorphism at the base of the Canaã dos Carajás strike-slip structure. This area is a reservoir for metal sources as fluids can tap into granitoids and ultramafic lithologies in the basement. The telescoped transition from trellis to silicatemottled magnetite records fluid fluxes of variable overprinting effects during protracted fluid-rock interaction.

Keywords: Magnetite, nanoscale characterization, trace elements, IOCG deposits, Jatobá, Carajás Domain.

Introduction

Magnetite, (Fe_3O_4), is typical of the early potassic alteration stages of evolution in iron-oxide copper-gold (IOCG) deposits (e.g., Barton 2014 and references therein). Several genetic models, in which fluids are derived from diverse sources (magmatic, surficial/basinal, metamorphic, and combinations thereof) have been proposed (e.g., Barton 2014). A subclass of the IOCG deposit clan, containing magnetite and apatite, so-called iron oxide apatite (IOA) deposits, was proposed as a Cu-poor member, Kiruna-type deposit (Williams et al. 2005).

Magnetite is a member of the spinel group (e.g., Biagioni and Pasero 2014) and forms over a wide range of temperatures spanning almost all geological environments. Magnetite is also a refractory mineral that displays an extensive range of textures, mineral inclusions and geochemical trends. When studied across different scales of observation, magnetite represents a powerful tool to recognize igneous versus hydrothermal signatures and thus provide insights for interpretation of deposit evolution in space and time. In Precambrian terranes with protracted geological histories, distinguishing between protolith- and IOCG-derived signatures of magnetite is of paramount importance.

Recent studies of magnetite from IOCG deposits worldwide have shown that correct interpretation of geochemical trends is a far from trivial task since the range of trace and minor elements present at measurable concentrations is varied and may reflect transition from a magmatic to a hydrothermal regime (e.g., Knipping et al. 2015). The presence of sub-micron scale inclusions in magnetite can lead to misinterpretation of geochemical trends, necessitating detailed nanoscale characterization (e.g., Ciobanu et al. 2019, 2022; Huang and Beaudoin 2021; Verdugo-Ihl et al. 2021; Huang et al. 2022; Campo-Rodriguez et al. 2024a).

Magnetite is the dominant Fe-oxide throughout the Neoarchean IOCG deposits from the Carajás Province, Brazil (Schutesky and Oliveira 2020). The Carajás Province comprises Archean greenstone-granite terranes formed during multiple tectonothermal events (Fig. 1a) and

hosts many IOCG deposits with complex magmatic-hydrothermal evolution. In this context, magnetite is one of the key pathfinders for decrypting mineralizing history. For example, polysomatic intergrowths between amphibole and non-classical pyriboles (NCPs) in magnetite from the Jatobá IOCG deposit, SE Carajás Province, were interpreted as evidence for a prolonged geological history from a mafic-ultramafic protolith to superimposed alkali-calcic, REE-bearing alteration (Campo-Rodriguez et al. 2024a). Several other studies have emphasized the importance of microtextural and geochemical signatures in magnetite from IOCG deposits in the Carajás Province (e.g., Huang and Beaudoin 2019; 2021; Huang et al. 2022; Mansur et al. 2023; Campo-Rodriguez et al. 2022; in review).

In this contribution we link micron- to nanoscale observations to constrain textural and geochemical changes recorded by magnetite from mafic/ultramafic host rocks to sulfide mineralization. We aim to decipher the protracted history of the fluid-rock interaction that defines the IOCG system in a shear zone setting at Jatobá. The results have implications for understanding the role and utility of magnetite in other IOCG systems from the Carajás Province or elsewhere.

Geological background

The Carajás Province (CP) is part of the Amazonian Craton and comprises two tectonostratigraphic domains: the Carajás Domain (CD) to the north; and the Rio Maria Domain (RMD) to the south, collectively making up the Carajás Mineral Province (CMP; Vasquez et al. 2008; Fig. 1a). Distinct metallogenic trends are recognized in each domain, whereby the RMD comprises Mesoarchean lode-Au deposits, Neoarchean IOCG deposits and Paleoproterozoic Cu-Au ores are the main expression of mineralization in the CD (e.g., Costa et al. 2020). Further detail on the geochronology, metallogeny and tectonic evolution of the CMP is given by Trunfull et al. (2020).

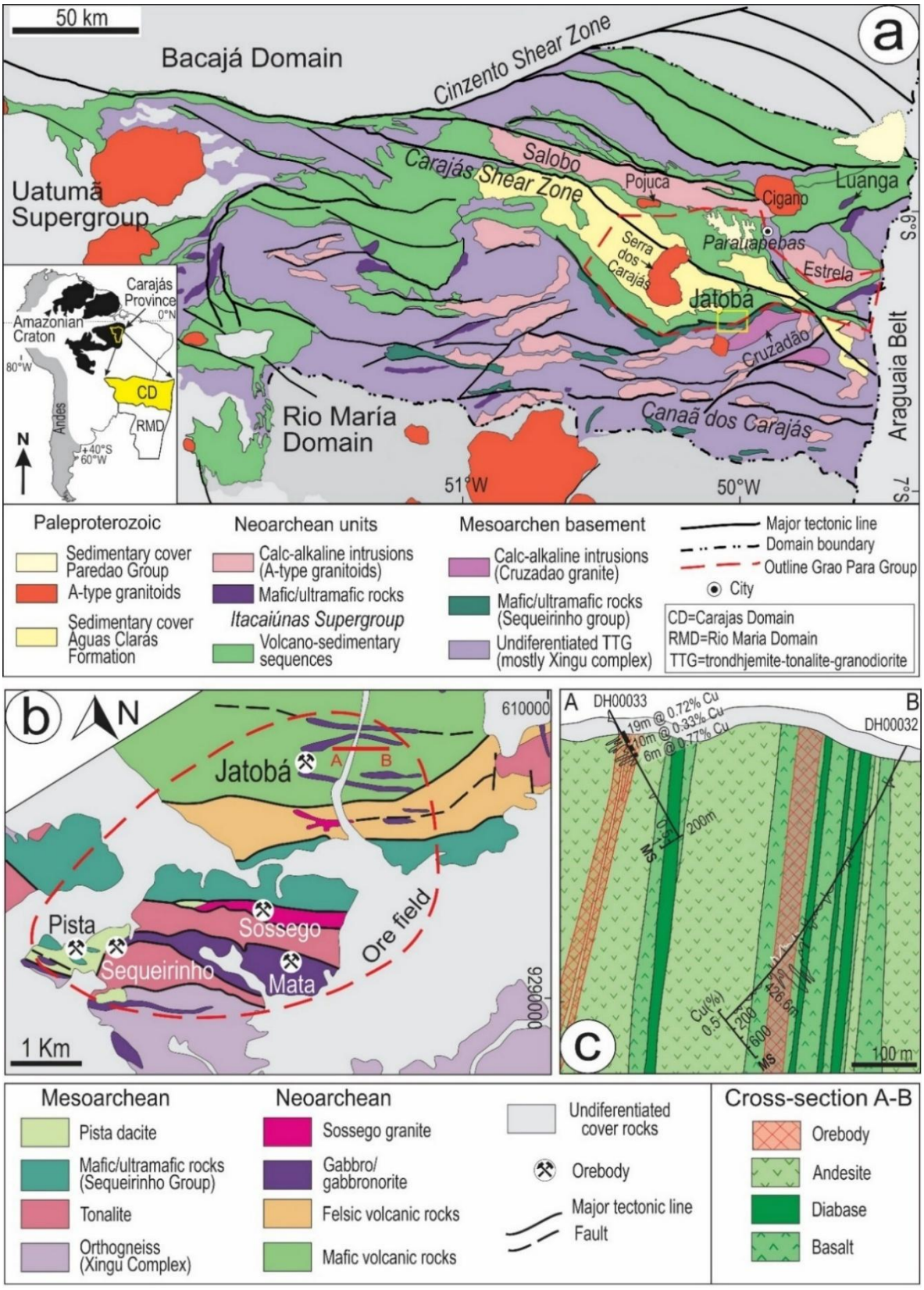

Figure 1. (a) Geological map of the Carajás Domain indicating the main tectono-structural units (modified from Tavares et al. 2018). Location of the Carajás Domain within the Amazonian Craton shown in inset. (b) Simplified geological map of the Jatobá-Sossego-Sequeirinho-Pista orefield (modified after Veloso et al. (2020). (c) Geological cross-section A-B depicting drillhole DH00032 intersecting copper mineralization. MS–magnetic susceptibility.

The Mesoarchean basement of the CD has a Neoarchean volcano-sedimentary cover and Paleoproterozoic sedimentary cover (Fig. 1a; e.g., Tavares et al. 2018; Costa et al. 2020). The basement comprises TTG (Trondhjemite–Tonalite–Granodiorite) rocks (mainly gneisses, migmatites and granulite from the 3−2.83 Ga Xingu Complex) and greenstone belts of the Sequeirinho Group (3−2.9 Ga); these units are intruded by calc-alkaline granitoids such as the Cruzadão Granite (ca. 2.87 Ga) (Tavares et al. 2018 and references therein). The Neoarchean cover is made up by volcano-sedimentary sequences of the Itacaiúnas Supergroup (2.76 and 2.73 Ga; DOCEGEO 1988), for which many divisions are described but with the stratigraphic correlation between them, at present, only poorly resolved.

One of the major divisions in the Itacaiúnas Supergroup is the Grão Pará Group, host to the Jatobá deposit. The Parauapebas Fm. of the Grão Pará Group is constrained by U-Pb zircon dating of rhyodacites/rhyodacite (ID-TIMS; 2759±2 Ma; Machado et al. 1991) and basaltic rocks (SHRIMP; 2745±5 Ma; Martins et al. 2017).

Both an intra-plate rift model (e.g., Olszewski et al. 1989; Tavares et al. 2018, and references therein) and a subduction-related setting (Costa et al. 2020, and references therein) are proposed for deposition of the Itacaiúnas Supergroup. Although Martins et al. (2017) show petrological evidence to support a back-arc continental basin, the authors conclude that a rift setting is more plausible, suggesting slab breakoff and subsequent asthenosphere upwelling.

Completing Neoarchean igneous activity in the CD are bimodal intrusions comprising: (i) mafic-ultramafic rocks of the Luanga Complex (2763±6 Ma; Machado et al. 1991) and its equivalents; and (ii) syn-tectonic/A-type granites of the Estrela Granite and equivalents (Tavares et al. 2018).

The Carajás Domain has a linear E-W-trending belt-like morphology (also called the Itacaiúnas Belt; Araújo et al. 1988), thus contrasting with the dome–and–keel structure of the RMD (Costa et al. 2020). The prominent Cinzento Shear Zone, a strike-slip system in the north of the CD, which branches into the Carajás Shear Zone (Fig. 1a), outlines a central sigmoid

domain, defined by formations of the Carajás Basin. The Canaã dos Carajás Shear Zone is the main tectonic structure in the south of the CD and links with the Carajás Shear Zone. IOCG mineralization is distributed across two belts, northern and southern (Xavier et al. 2012), with most deposits clustering along the major tectonic structures.

The succession of multiple deformation regimes throughout extensional-compressional cycles from the Archean to Neoproterozoic-Cambrian is heavily debated in the Brazilian literature (e.g., Tavares et al. 2018). Nevertheless, most authors agree that the Itacaiúnas Belt inherits Mesoarchean structural patterns and was overprinted during the 2.14 to 1.94 Ga Transamazonian Orogeny, and again by brittle reactivation at 1.88 Ga associated with emplacement of the Uatumã Supergroup (Antonio et al. 2021).

Deposit geology

Jatobá is one of four IOCG deposits within a 10 km^2 orefield along the southern Copper Belt (Fig. 1b). All four deposits are located along E-W structures belonging to the Canaã dos Carajás shear zone system, but only Jatobá is hosted within the Neoarchean Grão Pará Group. Pista (historical mine), Sossego and Sequeirinho (355 Mt @ 1.1% Cu, 0.29 g/t Au) are open pits along an E-W alignment, each with distinctive morphology and structure. Jatobá, located 3 km north of Sossego Mine comprises 30+ orebodies containing Cu-Ni mineralization. No resource estimate is available for the Jatobá deposit, which remains under evaluation (Veloso 2017). Copper-Au ore zones of the Sequeirinho-Pista system are located at the contact between Neoarchean gabbronorite and Mesoarchean granitoids/felsic metavolcanics. Mineralization has been dated between 2712 Ma (U-Pb monazite; Sequeirinho) and 2710–2685 Ma (Re-Os molybdenite; Pista) (Moreto et al. 2015). The Sossego orebody, dated at 1904–1879 Ma (U-Pb monazite) is hosted within older (2740 Ma) granites (Moreto et al. 2015).

The Jatobá deposit lies north of a major fault/thrust zone between Mesoarchean mafic/ultramafic rocks and Neoarchean bimodal volcanic sequences of the Grão Pará Group (Fig. 1b). At this location, a 1–2 km-thick interval of felsic volcanics (rhyolite and dacites) is separated from the main body of dominantly mafic lithologies hosting the Jatobá deposit by a major E-W fault. Several gabbroic lenses occur throughout the volcanic rocks following lineaments oriented similarly to the faults (Fig. 1b). Other subdivisions in the mafic sequence include diabase and tuffs. The contacts between lithologies are sub-vertical and the orebodies occur as narrow zones up to ~20 m-thick roughly parallel to such contacts (Fig. 1c).

Orebodies can be located within the basalt/diabase sequence (0.5% Cu) (samples studied here) and/or within andesites (0.33–0.775% Cu), but in both cases Cu grades correlate with the presence of magnetite as proven by high magnetic susceptibility, which is highest in the basalt-hosted mineralization (Fig. 1c). Nanoscale characterization of magnetite from the basalt-hosted orebody (samples from drillhole DH00032, the same as studied here; Fig. 1c) shows various degrees of brecciation and mottling with respect to chain-silicate inclusions (Campo-Rodriguez et al. 2024a). The authors show these inclusions comprise Mg-(Fe)- and (Ce)-calcic amphiboles, both displaying complex polysomatic intergrowths with non-classical pyriboles (NCP). The formation of Mg-(Fe)-amphiboles+NCPs is attributed to ocean floor metamorphism whereas calcic amphiboles are ascribed to the onset of the IOCG system. Ferrotschermakite (no NCPs) is also identified among the calcic amphibole inclusions in magnetite. High-pressure conditions at ~7.5 kbar are suggested for magnetite formed during main ore deposition based on ferrotschermakite geobarometry.

Secondly, the discovery of platinum group minerals (PGM) associated with Ni-bearing sulfides in basalt-hosted orebody at Jatobá is linked to either an initial VHMS-mineralization in the host basalts or to IOCG-type fluids that leached Ni+PGE from komatiites within the sequence/ultramafic rocks in the basement (Campo-Rodriguez et al. 2024b). Deformation during metamorphism is inferred based on annealing textures in pyrite and other microtextural fabrics.

Previous work on a suite of samples covering eight drillholes (Veloso 2017; Veloso et al. 2020) used mineral chemistry to address the link between "hydrothermal nickel mineralization and IOCG systems in the Carajás Province". Veloso et al. (2020) describe the deposit as hosted by "Itacaiúnas rhyodacites and felsic volcaniclastic breccias in the footwall zone, and amygdaloidal basalts associated with mafic tuffs in the hanging wall". It is however unclear where the felsic lithologies referred to as metarhyodacites occur since the cross-section through a ~250 m-wide ore zone is not located.

Veloso et al. (2020) interpret no less than eleven hydrothermal alteration stages overprinting host lithologies, a protolith defined by an assemblage of andesine+actinolite and accessory Ti-rich magnetite. These stages are considered in a generic zonal IOCG footprint (e.g., Barton 2014) but with index mineralogy following the scheme introduced for the Great Bear zone, Canada (e.g., Corriveau et al. 2016). The proposed stages are split into pre-tectonic and syn- to late-tectonic, with a range of ductile to brittle structures spanning all stages. The resultant model shows a lateral zonation centered on the mineralized zone with potassic alteration (biotite). Two spatially distinct parts are identified: (i) upper epidotite-chlorite + Cu-mineralization and (ii) lower (actinolite) + Cu-Ni mineralization. Veloso et al. (2020) define two lateral zones of sodic alteration: proximal (scapolite + hastingsite) and distal (albite + scapolite + quartz + magnetite + biotite). We note that magnetite occurs throughout, except in the proximal scapolite + hastingsite zone. Seven amphibole species are recognized: actinolite, hornblende, hastingsite, ferrotschermakite, cannilloite and pargasite from the calcic group; and cummingtonite from the Fe-Mg amphibole group. These amphiboles are claimed to form starting with actinolite in the precursor rock and continuing through the hydrothermal stages. Other minerals such as chlorapatite are products of both the pre-tectonic and mineralization stages. Potassic feldspar appears in the pre-tectonic and late tectonic stages, whereas chlorite is produced by late, retrograde alteration concentrated in the upper part of the mineralized zone. Altogether, the mineralization style evolved from replacement fronts, e.g., amphiboles show replacement as core-

rim zonation, generation I by generation II or biotite, etc., controlled by the mylonitic foliation, to hydraulic breccia zones.

Samples and analytical methods

The sampled interval from drillhole DH00032 (10 samples across ~400 m) comprises micro-folded, fine-grained metabasalts intercalated with diabase units (Fig. 1c). Common fabrics range from foliated, thinly banded to massive, whereby banding is chiefly expressed by the relative abundances of sulfides (e.g., Jt4, Jt7) and magnetite±apatite (ESM Fig. S1). Salt-and-pepper textures occurs in the orebody in samples with dense disseminations of sulfides within altered mafic rocks (e.g., Jt9b). Deformation associated with micro-folding is accompanied by formation of coarser (cm-sized) lenses of quartz (e.g., Jt9a). Twelve polished thin sections (ESM Fig. S2) were prepared from the ten core samples. Selection is based on textures relevant for magnetite and associated alteration. Sample characterization included reflected light optical and scanning electron microscopy (SEM) using a FEI Quanta 450 instrument operated in back-scattered electron (BSE) mode. Microbeam scanning X-ray fluorescence maps were obtained using a Bruker Tornado desktop scanner at National Institute of Criminalistics, Brasilia, Brazil. Automated Mineralogy (AM) mapping on a Hitachi SU3800 SEM instrument was undertaken to provide the concentrations of component phases in two representative thin sections.

Mineral chemistry of amphibole and magnetite was obtained using a JEOL JXA-8230 SuperProbe electron probe microanalyzer (EPMA) equipped with 5-spectrometer crystals and located in the Crti Laboratory, Federal University of Goiás, Brazil. Analytical details are given in Electronic Supplementary Material. Quantitative measurement of trace element concentrations in magnetite was determined using a RESOlution-SE 193 nm Excimer laser coupled to an Agilent 8900x quadrupole ICP-MS. Full details of analysis, reference materials, and data reduction

procedures are given in Electronic Supplementary Material. LA-ICP-MS trace element mapping was conducted on three representative magnetite grains.

Magnetite was studied at the nanoscale using five S/TEM (<100 nm) foils prepared on a FEI-Helios nanoLab Dual Focused Ion Beam-SEM platform. High angle annular dark field (HAADF) scanning transmission electron microscopy (STEM) imaging and energy-dispersive X-ray spectrometry (EDS)-STEM mapping were carried out using an ultra-high resolution, probe-corrected, FEI Titan Themis S/TEM operated at 200 kV. Diffraction patterns indexing was conducted with WinWulff© (JCrystalSoft) and publicly available data from the American Mineralogist Crystal Structure Database (http://rruff.geo.arizona.edu/AMS/amcsd.php). Crystal structure models were produced in CrystalMaker® and image simulations using STEM for xHREM™ software. Unless otherwise stated above, analysis was undertaken at Adelaide Microscopy, The University of Adelaide, Australia.

Results

Petrography

The lithologies and distribution of magnetite and its association with apatite and sulfides throughout the drillhole are shown in Figure 2. A schematic stratigraphic column (Fig. 2a) shows the dominant lithologies are green rocks (metabasalt and -diabase) intercalated with one another and hosting a ~50 m-thick orebody towards the lower part of the drillhole. Copper-(Ni)-Fe-sulfide mineralization occurs as disseminations, larger clots, bands and/or veinlets with highest concentration within the orebody (Campo-Rodriguez et al. 2024b).

The lithologies are intensely folded (ESM Fig. S2) and display mm-scale banded (Fig. 2b) or foliated to mylonitic fabrics (Fig. 2c). The banding comprises rhythms of magnetite, apatite, and mica (mainly biotite) (Fig. 2b). Apatite in the same sample is coarse-grained, fractured, and clustered with inclusions of quartz and allanite.

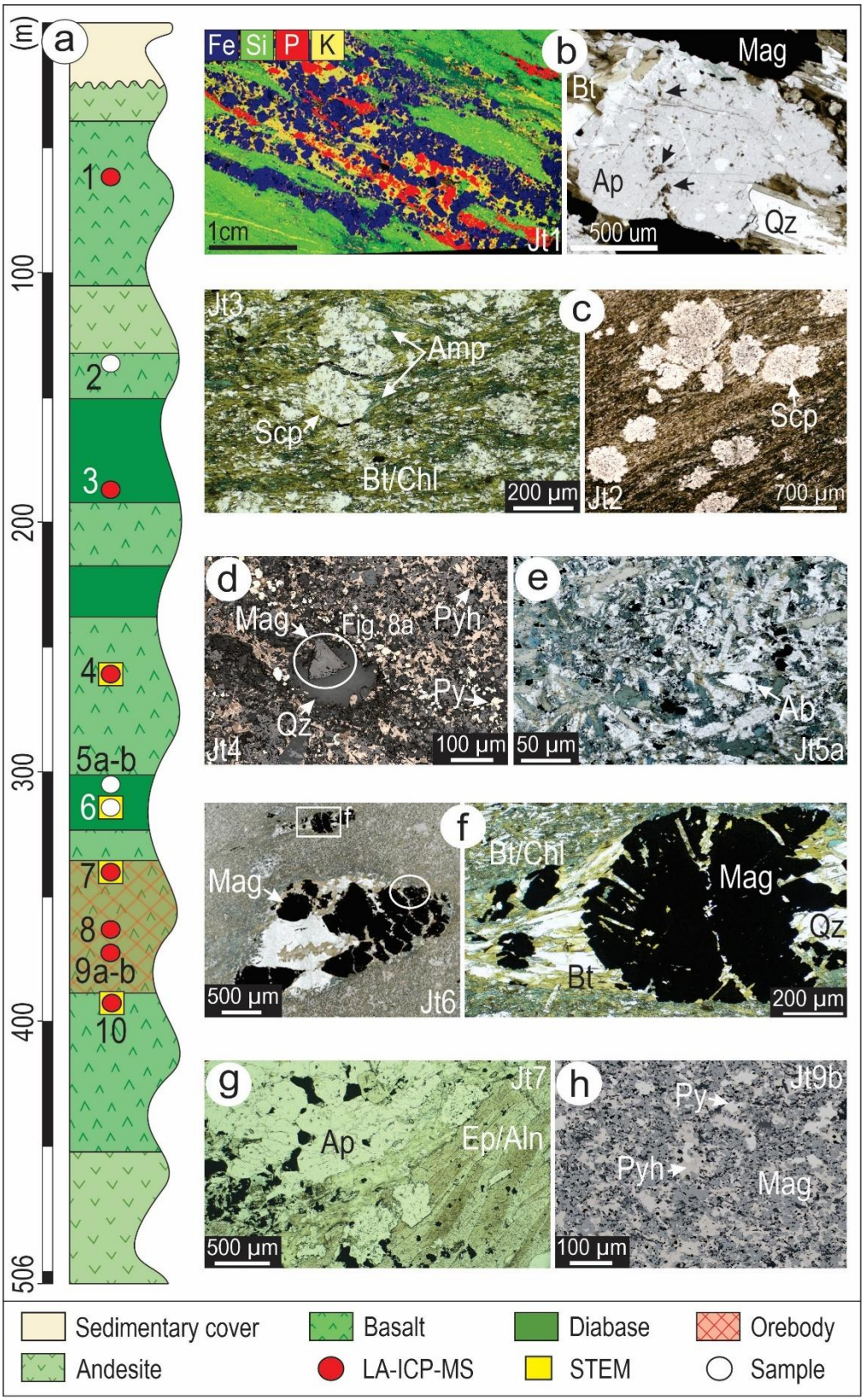

Figure 2. (a) Schematic stratigraphic column for the sampled interval. (b) XRF map and (c-h) transmitted (c-g) and reflected light (h) microphotographs showing key petrographic aspects of ores and host lithologies. White circles in (d) and (f) show location of FIB cuts for trellis magnetite. Abbreviations: Ab–albite; Aln–allanite; Amp–amphibole; Ap–apatite: Bt–biotite; Chl–chlorite; Ep–epidote; Mag–magnetite; Pl–plagioclase; Py–pyrite; Pyh–pyrrhotite; Qz–quartz; Scp–scapolite.

Magnetite, ubiquitous throughout all lithologies, decreases in abundance within the scapolite-bearing intervals that are common in the upper part of the drillhole. Sigmoidal scapolite, dominantly marialite, is embedded within a foliated matrix of biotite+amphibole-chlorite (Fig. 2c). Coarse-grained (mm-sized) magnetite which is embayed within quartz is observed in metabasalt that otherwise displays fine-grained disseminations of magnetite and sulfides (Fig. 2d).

Domains of plagioclase laths occur within the groundmass of mafic rocks, albeit altered to albite (Fig. 2e). Some textures, notably 'pinch-and-swell' and pressure shadows (biotite+quartz) are indicative of syn-metamorphic deformation. Pressure shadows are widely observed around some of the coarsest magnetite grains (Fig. 2f). Larger aggregates of epidote±allanite occur together with apatite in samples close to the upper boundary of the orebody (Fig. 2g). Fine intergrowths of magnetite and sulfide patches that contain abundant pyrrhotite are typical of massive ore samples (Figs. 2h; ESM Fig. S2).

To understand the changes in mineralogy, and implicitly the context for the contained magnetite, automated mineralogy mapping was performed on thin sections, representative of lower and upper contacts with the orebody (Fig. 3). At the lower contact of the orebody (Jt10), magnetite is the main component (51.5 wt%), followed by apatite (16 wt%) and sulfides (19.6 wt% pyrite + chalcopyrite), quartz (6.4 wt%) and minor amphibole (3.4 wt%). Chlorite, ilmenite and epidote/allanite occur only as traces (Fig. 3a). The area surrounding the magnetite in sample Jt10 analyzed at the nanoscale was mapped at higher resolution (Fig. 3b). This shows a local increase in sulfide content (45.7 wt%), with a predominance of chalcopyrite over pyrite. Ilmenite and allanite are present in comparable proportions (0.7 and 0.8 wt%), but the former is finer grained (Fig. 3b, c). Higher-resolution mapping of the area surrounding magnetite in sample Jt7 analyzed at the nanoscale shows that this is closely associated with increased proportions of pyrite (52.3 wt%) and chalcopyrite (4 wt%) (Fig. 3d).

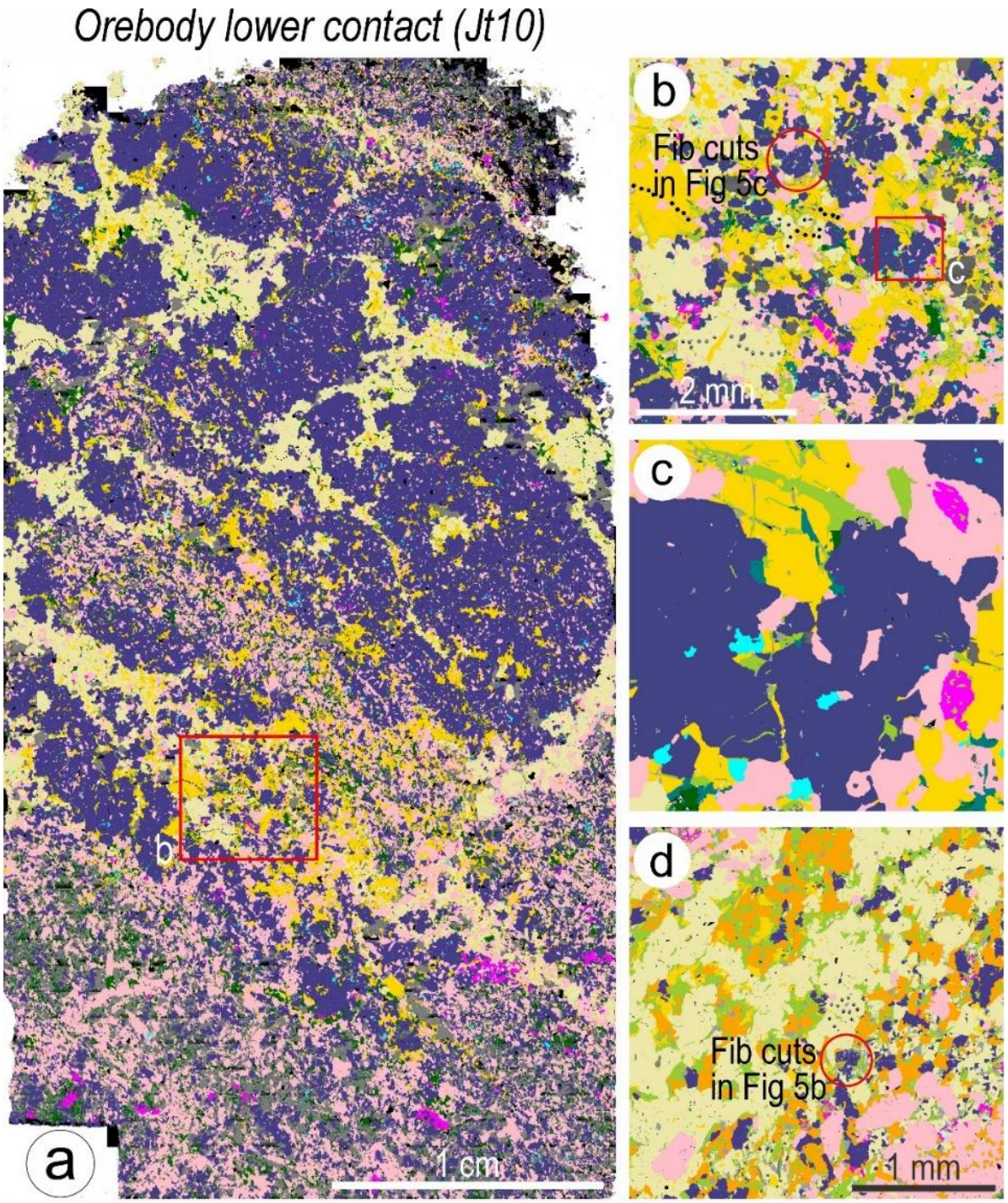

Wt%	Mag	Ap	Py	Ccp	Qz	Amp	Chl	Bt	Ilm	Ep/Aln
a	51.5	16	12.7	6.9	16.4	3.4	1.2	-	0.6	0.5
b	27.6	14	21.7	24	2.7	2.2	4.7	-	0.7	0.8
d	10	9.2	52.3	4	-	0.1	10.9	12.8	-	0.7

Figure 3. Automated Mineralogy maps showing constituent minerals in thin sections from the orebody as labelled. Mineral proportions (wt% basis) are given in associated tables. Abbreviations: Aln–allanite; Amp–amphibole; Ap–apatite; Bt–biotite; Ccp–chalcopyrite; Chl–chlorite; Ep–epidote; Ilm–ilmenite; Mag–magnetite; Py–pyrite; Qz–quartz.

Textural and mineralogical aspects of alteration species, apatite, epidote group minerals, and scapolite, from the upper part of the studied interval (Jt1-2) are illustrated in Figure 4a-f. Coarser crystals of apatite show patchy zoning with the brighter areas on BSE images corresponding to elevated REE content, as well as trails of allanite inclusions (Fig. 4a). Epidote group minerals are abundant and display a marked marginal enrichment in REE, corresponding to allanite in some cases (Fig. 4b-d). In the same sample, epidote can form either large radial aggregates (Fig. 4b) or clusters of small grains within biotite at the contact with scapolite (Fig. 4c). Allanite forms well-developed haloes around the epidote at the contact to biotite (Fig. 4d). In contrast, acicular aggregates of allanite form at the center of epidote aggregates in the scapolite-rich intervals (Fig. 4e). Scapolite aggregates with inclusion-rich cores and clear margins, like those shown in Fig. 2c, are marginally intergrown with actinolite and/or hornblende (Fig. 4f).

Elongated patches of ilmenite, each several hundred microns in length, display a pseudopoikilitic texture (biotite and quartz) and coexist with magnetite (Fig. 4g) from the same apatite-rich sample (Jt1) at the upper part of the studied interval (see Fig. 2b). Trellis ilmenite lamellae and apatite veinlets are observed in the adjacent magnetite. In contrast, smaller bodies of ilmenite (tens of μm) occur in the lower part of the sequence at the contact with the orebody (Jt10; Fig. 4h, i). Magnetite displays mottled silicate inclusions (see below). Ilmenite also contains dusty inclusions of W-minerals (ferberite or scheelite) throughout the sampled interval. Blebby inclusions of pyrrhotite, in turn hosting pentlandite are observed (Fig. 4j). Clastic deformation of ilmenite along the contact to magnetite is accompanied by formation of epidote/allanite (Fig. 4h, k).

Although minor, amphiboles (Fig. 4l) are also preserved throughout the lithologies and correspond to two main compositional groups: calcic- and Mg/Fe-amphiboles (ESM Table S1a; Fig. 4m). Aside from hornblende and actinolite, the calcic amphiboles also include Al-rich-species, notably ferrotschermakite. Actinolite is dominant in the mineralized samples, e.g., Jt10 at the contact to the orebody.

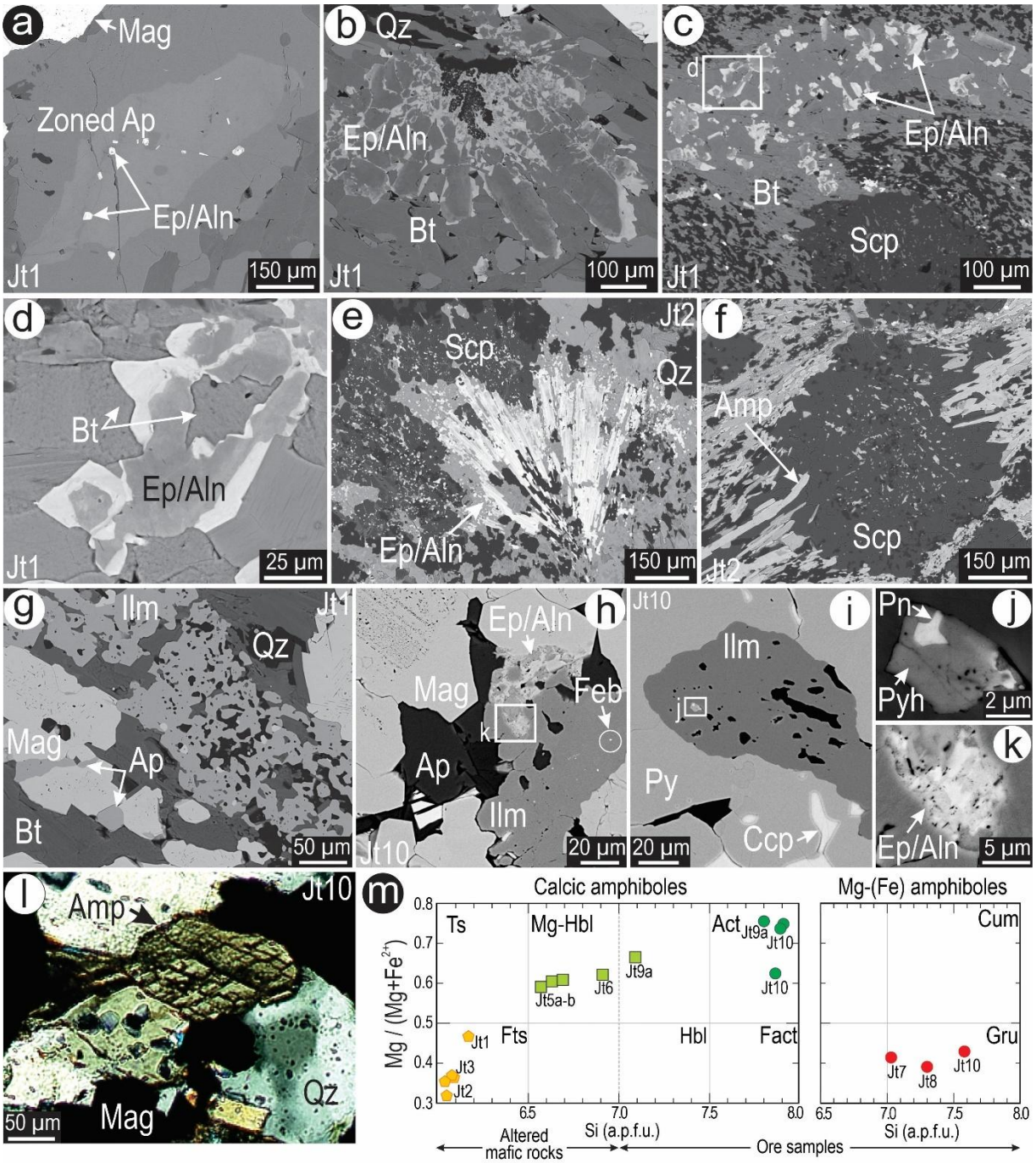

Figure 4. BSE images showing textural details of (a-f) apatite (Ap), epidote- group minerals (Ep) and scapolite (Scp) associated with biotite (Bt) and amphiboles (Amp), (g-k) Fe-Ti-oxides, sulfides and trace mineral inclusions. (l) Crossed-polars transmitted light image showing a basal section of an amphibole preserved within quartz (Qz). (m) Plots of amphibole composition (classification after Leake et al. 1997) from different samples as labelled. Data from ESM Table 1a (Electronic Supplementary Material). Other abbreviations: Act–actinolite; Aln–allanite; Ccp–chalcopyrite; Cum–cummingtonite; Fact–ferroactinolite; Feb–ferberite; Fts–ferrotschermakite; Gru–grunerite; Hbl–hornblende; Ilm–ilmenite; Mag–magnetite; Pn–pentlandite; Py–pyrite; Pyh–pyrrhotite; Ts–tschermakite.

Magnetite composition and textures

Microprobe analysis of magnetite from across the sampled interval (ESM Table S1b) shows varying amounts of minor elements (in wt%), e.g., 0.01-0.04 SiO_2, 0.01-0.04 CaO, 0.004-0.02 MgO, 0.03-0.07 TiO_2, 0.007-0.01 NiO, 0.03-0.1 Cr_2O_3, and 0.03-0.09 Al_2O_3, but relatively constant and high concentrations of V_2O_3 (0.24-0.39 wt%). Such compositions only partially reflect magnetite chemistry as they are characterized by various textures directly related to the presence of (sub)micron-sized inclusions of various types, particularly ilmenite and silicates (Fig. 5a-f).

Two main textural types of magnetite are defined: (i) trellis - comprising lamellar networks of ilmenite with preferential orientation in magnetite, e.g., <111> (Fig. 5a); and (ii) mottled – displaying silicate inclusions of variable density (Fig. 5b, c). Trellis magnetite displays contrasting sizes of lamellar networks (Jt4; Fig. 5a) and typifies magnetite within lithologies outside the orebody (metabasalt/diabase). The mottled magnetite is common at the contact with the orebody and shows inclusions, mostly silicates (Campo-Rodriguez et al. 2024a), resembling the ilmenite-trellis in addition to blebby morphologies (upper orebody contact; Jt7; Fig. 5b). An exceptional case of dense mottling is observed in wedges/sectors of preserved magnetite cores (Jt10; Fig. 5c). In such cases, the inclusions also display a concentric distribution away from the wedge apex. Micron-sized patches of ilmenite are also present, either within the mottled areas (Fig. 4c) or along the trellis-free margins of magnetite (Jt1; Fig. 5d).

An outstanding case of magnetite from sample Jt6 (Fig. 5e, f) shows transitional textures combining trellis and mottled. Overlap between the two inclusion types shows that the blebby morphology comprises binary inclusions of ilmenite and Al-bearing phases (see below) attached to ilmenite lamellae (Fig. 5e). These types of textures have been sampled using *in-situ* FIB-SEM slicing (transects marked in red on Fig. 5a-c, e) for nanoscale study.

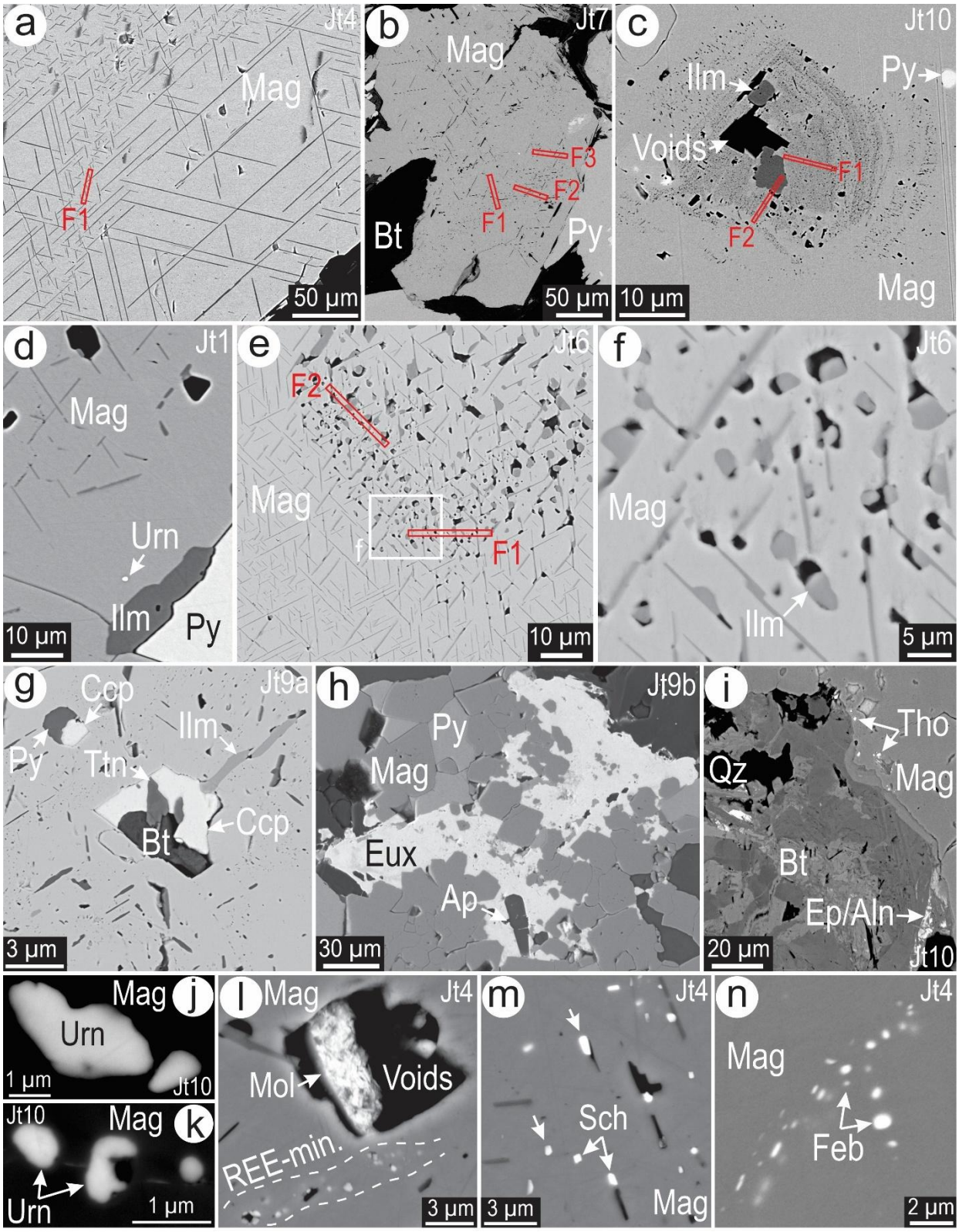

Figure 5. BSE images showing main textures and a range of inclusions within magnetite (Mag). (a) Typical trellis textures as <111> ilmenite (Ilm) lamellae. Rare (b) and dense (c) mottled textures with silicates in magnetite. (d-e) Transition from trellis to blebby-mottled textures. Five of the eight foils extracted from locations as marked are presented here (see Figure 9). Other abbreviations: Aln–allanite; Bt–biotite; Ccp–chalcopyrite; Ep–epidote; Eux–euxenite; Feb–ferberite; Mol–molybdenite; Py–pyrite; Tho–thorianite; Ttn–titanite; Urn–uraninite; Sch–scheelite.

Titanite ($CaTiSiO_5$), associated with sulfides and biotite, can spatially co-exist with ilmenite veinlets in silicate-mottled magnetite from the orebody (Jt10; Fig. 5g). An eclectic range of different inclusion species, defining a REE-Th-Mo-W-U geochemical association, is spread throughout magnetite from the sampled interval (Fig. 5h-n). In ore samples, unusually coarse grains of euxenite occur interstitial to magnetite and aggregates of pyrite. Fine particles of thorianite cluster around the contacts between epidote and allanite, and blebby uraninite is noted as inclusions within some mottled magnetite grains (Fig. 5h-k). Trails of REE-mineral fine particles, scheelite and ferberite are common in magnetite from the altered metabasalts outside the orebody (Fig. 5l-n). Large (micron-size) pores host inclusions of molybdenite (Fig. 5l).

Trace element geochemistry: concentrations and distributions

Element concentrations and trends in magnetite

Trace element concentration data (ESM Table S3a,b) reflect the different textural types of magnetite. We divide the dataset into 'trellis' magnetite (samples Jt1, Jt3 and Jt4), and 'mottled' magnetite, which is in turn sub-divided into 'rare mottled' (Jt7) and 'dense mottled' (Jt8, Jt9b) The two sub-divisions are based on the density of silicate inclusions in magnetite which increases from the upper to the lower contact of the orebody.

Four broad groups of analyzed elements and their measured concentrations are shown on a boxplot sub-divided into the three textural categories (Fig. 6a; ESM Table S3c).

Except for Ti and V, the concentrations of all lithophile elements are typically in the hundreds to thousands of parts-per-million (ppm) range. Among these, Si and Mg are lower in trellis magnetite, whereas there is no statistical difference in the concentrations of Al and Ca across the different textural categories. Titanium concentrations are highest in trellis magnetite (mean 7,100 ppm), where they also show the widest concentration range. The lowest contents are noted in dense mottled magnetite (mean 3,017 ppm). In contrast, V is relatively constant across the dataset

(means of 1,682, 1,633, and 2,167 ppm in trellis, dense and rare mottled magnetite, respectively). Niobium is never more than a few ppm, albeit with relatively wide concentrations ranges. Chromium concentrations are higher in trellis magnetite (mean 170 ppm) than in mottled magnetite (mean ~30 ppm). Nickel concentrations are relatively constant across the dataset (mean concentrations of 87, 80, and 60 ppm for trellis, dense and rare mottled magnetite, respectively). Cobalt concentrations are markedly lower than Ni, although slightly higher in trellis magnetite (mean 19 ppm) against 6-4 ppm in mottled magnetite. Manganese is highest in trellis magnetite (mean 342 ppm) and slightly lower in mottled magnetite (means of 101-230 ppm). Zinc concentrations are some tens of ppm across the dataset.

The mean total (REE+Y) concentrations, hereafter termed ΣREY are 9, 19 and 62 ppm in trellis, rare mottled, and dense mottled categories of magnetite, respectively. There are subtle differences in the relative concentrations of light and middle REE (La-Tb) relative to heavy REE (Dy-Lu, including Y) in that densely mottled magnetite from the ore samples not only contains more ΣREY but also a greater proportion of HREE. The U-Pb-W-Sn-Mo group of elements, hereafter referred to as 'granitophile', are present in only low concentrations (means <1 ppm) across all magnetite categories.

The variation in trace element concentrations is illustrated on a series of binary plots (Fig. 6b). No correlation is seen between Ni and Cr throughout the dataset, although we note that Cr has a far greater variability in the trellis magnetite (highest values in Jt4) than nickel. This contrasts with the mottled varieties in which the range of Ni concentration does not correlate with Cr (<100 ppm). The variation in Ti relative to the relatively constant V concentration shows the highest Ti in the lamellar trellis magnetite (e.g., Jt3) and lowest concentrations in the rare mottled (Jt7), even though some higher concentration values attributable to blebby ilmenite inclusions are noted. Pairs of transition elements that show very good correlations with one another include Nb-Ti (r'=0.95) and Mn-Ti (r'=8) if we exclude data for the rare-mottled magnetite sample (Jt7).

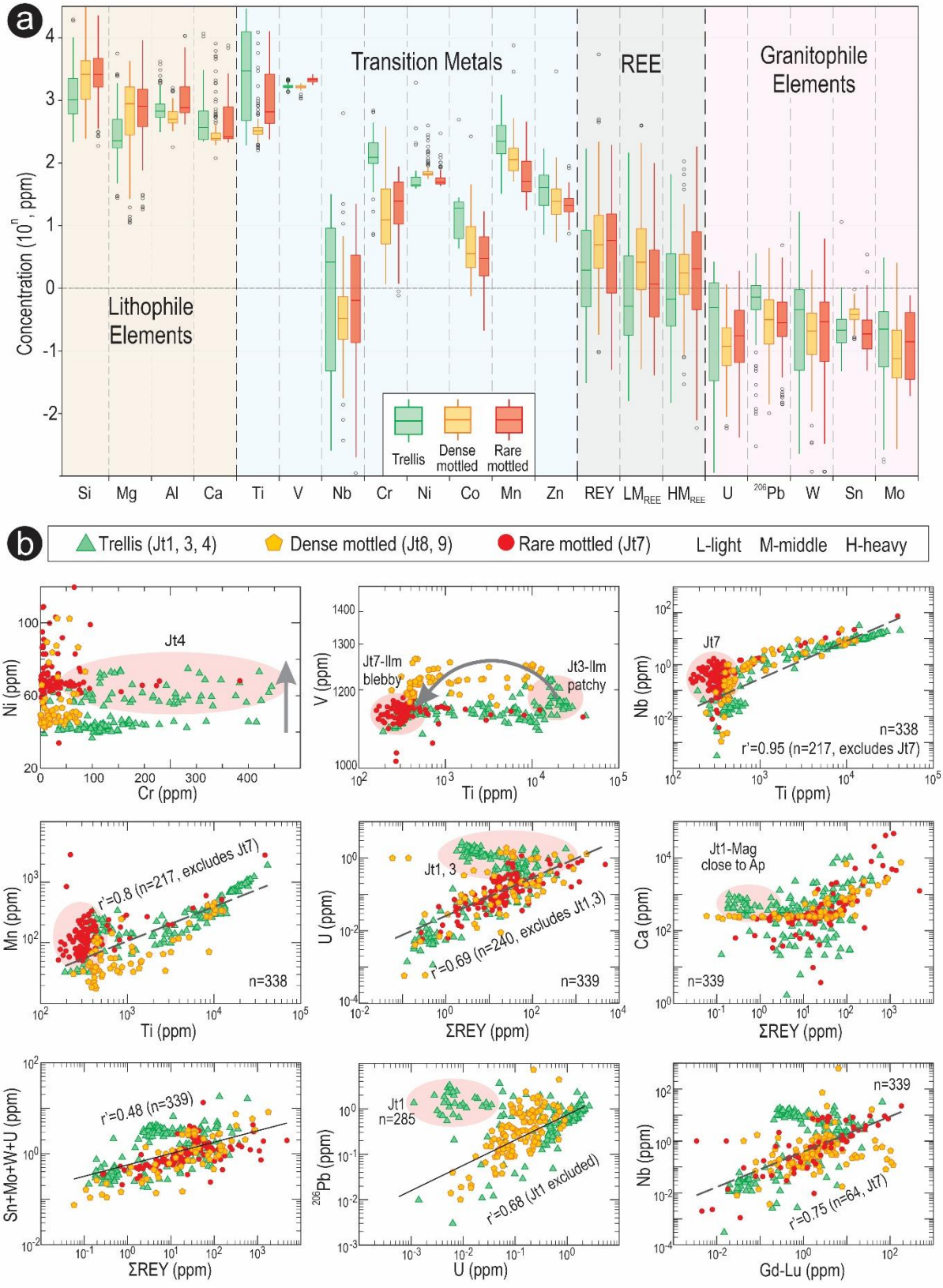

Figure 6. LA-ICP-MS trace element concentration data for magnetite presented as (a) box-and-whiskers plots showing ranges for groups of elements, and (b) as binary plots for selected element/group pairs sub-divided by sample and textural type. Solid lines within the box on (a) represent median values. Abbreviations: Ap–apatite; Mag–magnetite.

There is also a relatively good correlation between U and ΣREY (r'=0.69) across the dataset, excluding trellis magnetite in Jt1 and Jt3). The plot of Ca vs. ΣREY depicts data clusters representing low ΣREY magnetite adjacent to high ΣREY, correlating to trellis sample Jt1. Otherwise, the plot shows higher concentrations of ΣREY, but with noisy distribution, so little evidence for Ca as a proxy for the presence of apatite inclusions. The correlation between ΣREY and granitophile elements is relatively low across the dataset (r'=0.48). A better correlation is obtained for U versus ^{206}Pb (r'=0.68), if we exclude magnetite close to apatite in sample Jt1. Notable is the good correlation (r'=0.75) between Nb and middle to HREE (Gd-Lu) across the dataset, excluding rare mottled (Jt7).

Time-resolved downhole LA-ICP-MS profiles show relatively smooth signals for V, Ni, and Cr, whereas Ti, Al, and Mg can be either smooth or ragged with smaller or large amplitude variation (Fig. 7a). This indicates the presence of sub-micron sized mineral inclusions containing Ti, Al, and Mg within the analyzed magnetite. In contrast, V, Ni and Cr appear to be incorporated within the magnetite structure (solid solution). Cerium (as a proxy for LREE) either displays small-amplitude variation (e.g., Jt8, Jt9b) or high-amplitude irregularities typical of a mineral containing micron-size inclusions of REE-minerals (e.g., Jt4, Jt7). Yttrium and Dy, as proxies for HREE, mostly display smooth signals but occasionally also show high-amplitude irregularities (e.g., Jt4, Jt7). Interestingly, Nb, which generally correlates with signals for HREE, may also show decoupling (e.g., sample Jt4). A Nb-HREE correlation implies the presence of (sub)-micron-size inclusions of REY-minerals, some of which are Nb-bearing (e.g., euxenite).

Chondrite-normalized REY fractionation patterns

After eliminating data attributable to obvious REE-mineral inclusions (ESM Table S2d), chondrite-normalized REY fractionation patterns display a spectrum of trends that reflect the different categories of magnetite (Fig. 7b).

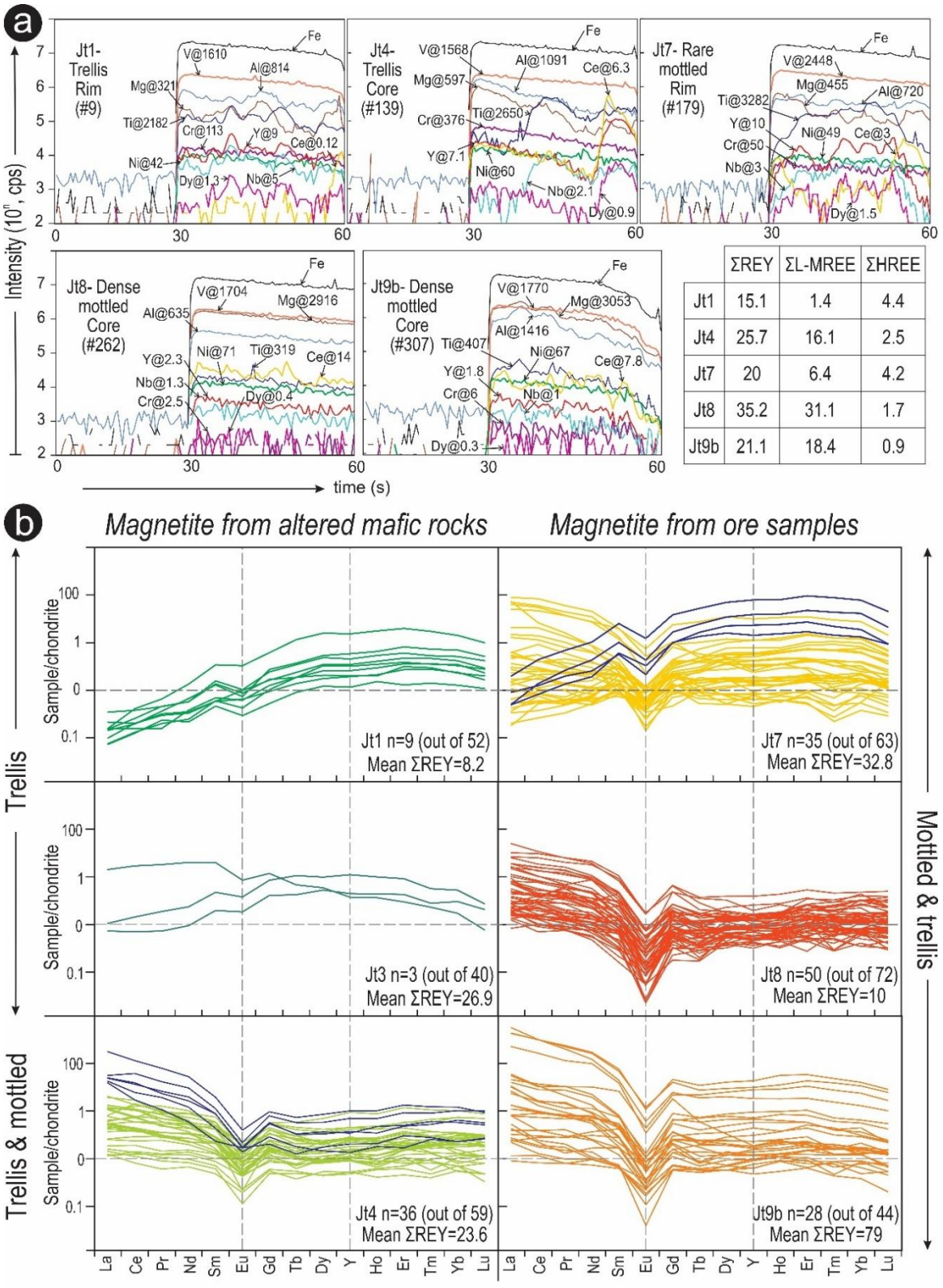

	ΣREY	ΣL-MREE	ΣHREE
Jt1	15.1	1.4	4.4
Jt4	25.7	16.1	2.5
Jt7	20	6.4	4.2
Jt8	35.2	31.1	1.7
Jt9b	21.1	18.4	0.9

Figure 7. (a) Representative time-resolved downhole LA-ICP-MS depth profiles illustrating features as labelled and discussed in text. Trace element concentration data in ppm. Table compares REY concentrations in different samples broken down as LREE+MREE and HREE. (b) Selected chondrite-normalized REY fractionation patterns for magnetite in different samples as labelled (data from ESM Table 2d. Note difference between the fractionation patterns for magnetite from altered mafic rocks and ore samples. Chondrite values from McDonough and Sun (1995).

Although the noisiest, a selection of trellis magnetite from sample Jt1 displays upwards-sloping chondrite-normalized fractionation patterns. A flatter REY fractionation pattern is seen in a subgroup of analyses from sample Jt3. Sample Jt4, representing trellis and mottled magnetite, displays trends featuring modest enrichment in LREE. Ore samples in which mottled magnetite is dominant are typified by REY trends with slightly LREE-enriched to flat patterns (Jt7, Jt8, Jt9b). A sub-group of REY trends in sample Jt7 show a tendency towards patterns more characteristic of trellis magnetite as in sample Jt1. All REY patterns show negative Eu anomalies, although this anomaly is less pronounced in trellis magnetite.

Trace element distributions in magnetite

LA-ICP-MS element maps of magnetite grains representing each of the three categories are shown in Fig. 8 (extended map sets are given as ESM Figs. S3, S4). One of the largest trellis magnetite (Fig. 2d) shows the core enriched in Ti, Mn, Nb and U when compared to the grain margin (Fig. 8a). We note that ilmenite lamellae cannot be picked out on the Ti map as they are narrower than the map resolution. Chromium appears relatively depleted within parts of the magnetite margin that are porous, whereas V is homogenous throughout the grain.

Rare-mottled magnetite (Fig. 8b) with homogenous concentrations of Fe, Al and Mg show a porous part of the grain that is depleted in Ti, V, Cr, and Ni (local remobilization?). However, preferential partitioning of Ti, V, Cr and Ni in mica and sulfides surrounding magnetite is suggested by enrichment of these elements.

The mottled core of the inclusion-rich magnetite, from which amphibole and NCPs were described by Campo-Rodriguez et al. (2024a), is picked out on the element maps by higher concentration of Si, Mg, Al and to some extent, Ce (Fig. 8c). Titanium shows ilmenite inclusions whereas V is homogenously distributed throughout the grain.

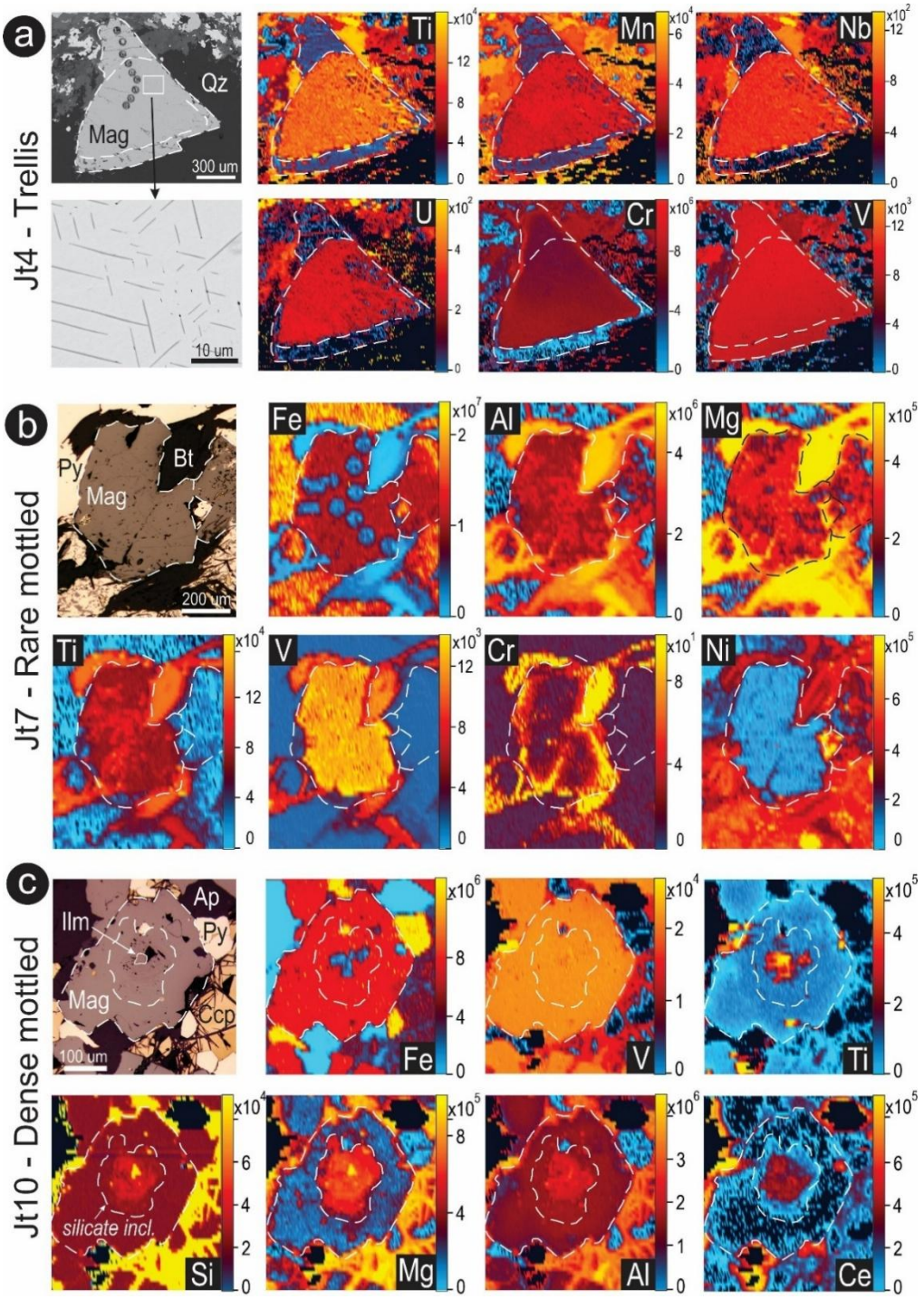

Figure 8. LA-ICP-MS element maps and corresponding reflected light images of selected magnetite (Mag) grains annotated to highlight internal features. (a) Trellis magnetite (Jt4; Fig. 2d) shows core enriched in Ti, Mn, Nb and U, whereas V is homogenously distributed. Cr is depleted in porous parts of the grain margin. BSE image shows ilmenite (Ilm) lamellae are too small (1-2 µm-thick) for map resolution. (b) Rare-mottled magnetite (Jt7) with homogenous concentrations of Fe, Al and Mg and a porous part being depleted in Ti, V, Cr, and Ni. Note preferential enrichment of Ti, V, Cr and Ni in mica and sulfides surrounding magnetite. (c) Dense mottled magnetite (Jt10) with amphibole-NCPs rich core depicted by higher concentration of Si, Mg, Al and to some extent, and Ce. Titanium shows ilmenite inclusions whereas V is homogenously distributed throughout the grain. Scales on all maps in counts-per-second (cps). Other abbreviations: Ap–apatite; Bt–biotite; Ccp–chalcopyrite; Py–pyrite; Qz–quartz.

Nanoscale characterization

Complementing the nanoscale study of Campo-Rodriguez et al. (2024a), which focused on inclusions of amphiboles and associated NCPs in mottled magnetite, here we target other types of mineral inclusions using additional S/TEM foils (Fig. 9). EDS spectra for such inclusions are shown in ESM Figure S5.

Relationships between magnetite and ilmenite across the transition from trellis to mottled types were assessed from three samples, Jt4, Jt6 and Jt10. Ilmenite occurs as oriented lamellae (widely spaced and each up to several hundred nm in width) along <111> directions in magnetite and as patchy bodies, several microns in width, in mottled magnetite (Figs. 9a, d, e, g; 10a-c). The Mn content in ilmenite decreases with changes in the morphology and association. It is highest in the best-preserved trellis lamellae (Jt4) and lowest in blebby (Jt6) to patchy ilmenite (Jt10).

Nano-thermobarometry for ilmenite-magnetite pairs was employed using the calculation template of Lepage (2003, and references therein) to estimate the temperature (T)–fO_2 formation conditions (Fig. 10d, ESM Table S3). The wide range of temperature (728 to 414 °C) and logfO_2 (-12 to -31) corresponds to re-equilibration between magnetite and ilmenite from initial trellis to the trellis+blebby and to densely mottled magnetite.

The highest temperatures, 728-500 °C, were obtained from pairs in which ilmenite lamellae have tiny crystals of gahnite, $ZnAl_2O_4$, attached to their edges (Jt4; Figs. 9b; 10a, e, f). This corresponds to trellis magnetite as shown in Figure 5a. Some ilmenite lamellae also feature segments that are filled by a Mg-bearing silicate identified from HR STEM imaging (Figs. 9b, c; 10f) and EDS spectra as talc. Estimated temperatures plot at the lowest end of the range (~500 °C) suggesting that the talc is an alteration product of a pre-existing, higher-temperature Mg-amphibole.

Temperatures in the range from 482 to 556 °C are obtained for magnetite-ilmenite pairs where blebs or acicular inclusions of an Al-hydroxide are attached to ilmenite lamellae (Jt6;

Fig. 10g). This phase represents the darker tips of blebby ilmenite inclusions in magnetite with textural transition from trellis to mottled (see Figure 5e, f). Temperatures obtained from one such blebby ilmenite inclusion also in sample Jt6 (Fig. 10h) are within the lowest part of the estimated interval (~484 °C).

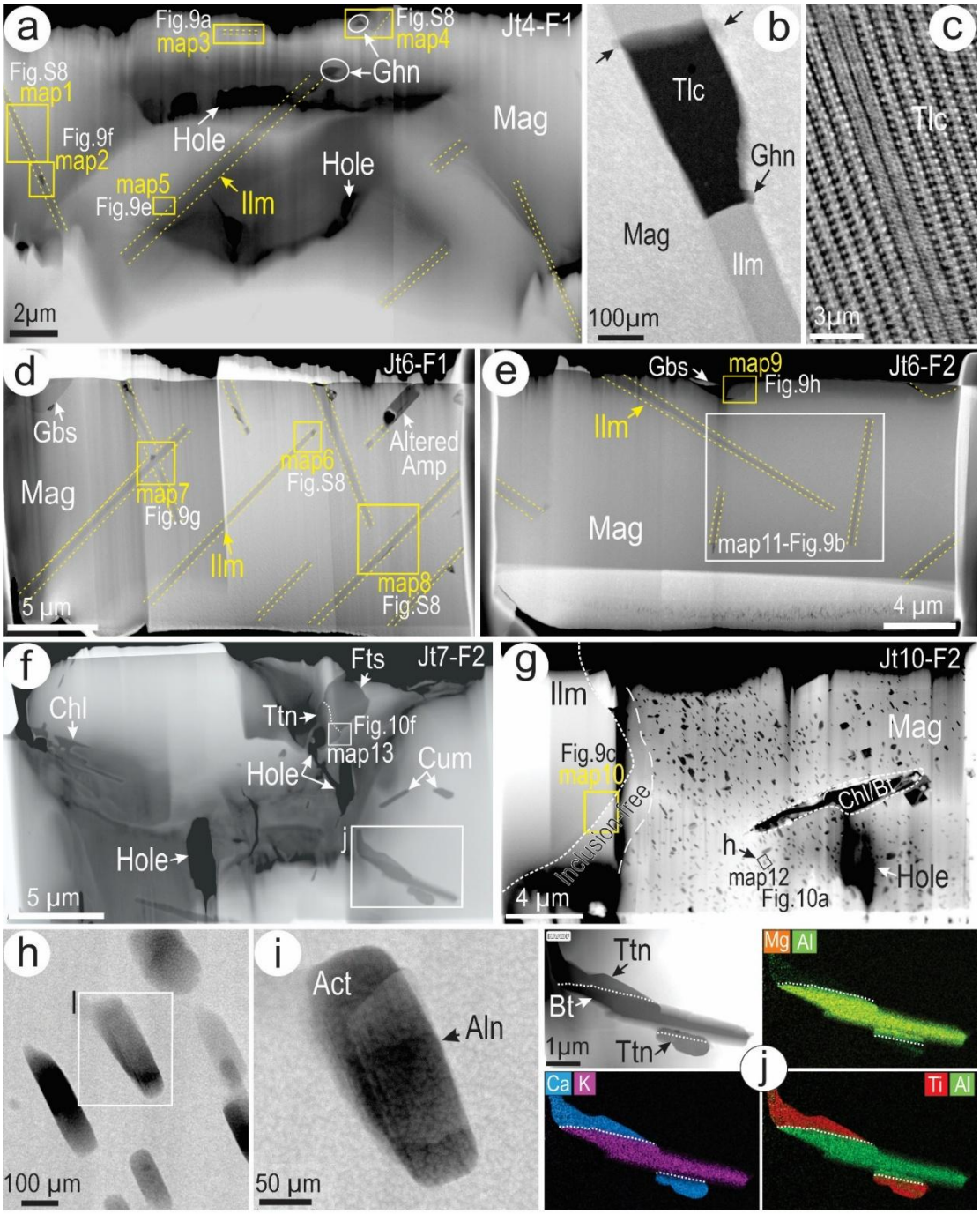

Figure 9. Overall images of the five foils analyzed from magnetite (Mag) samples as labelled. Details of talc (Tlc) along ilmenite (Ilm) lamellae in (b, c) and the field of actinolite (Act) with attached allanite (Aln) in (h, i). EDS STEM maps for titanite (Ttn) associated with biotite (Bt) in (j). Abbreviations: Bt–biotite; Chl–chlorite; Cum–cummingtonite; Gbs–gibbsite; Ghn–gahnite; Fts–ferrotschermakite.

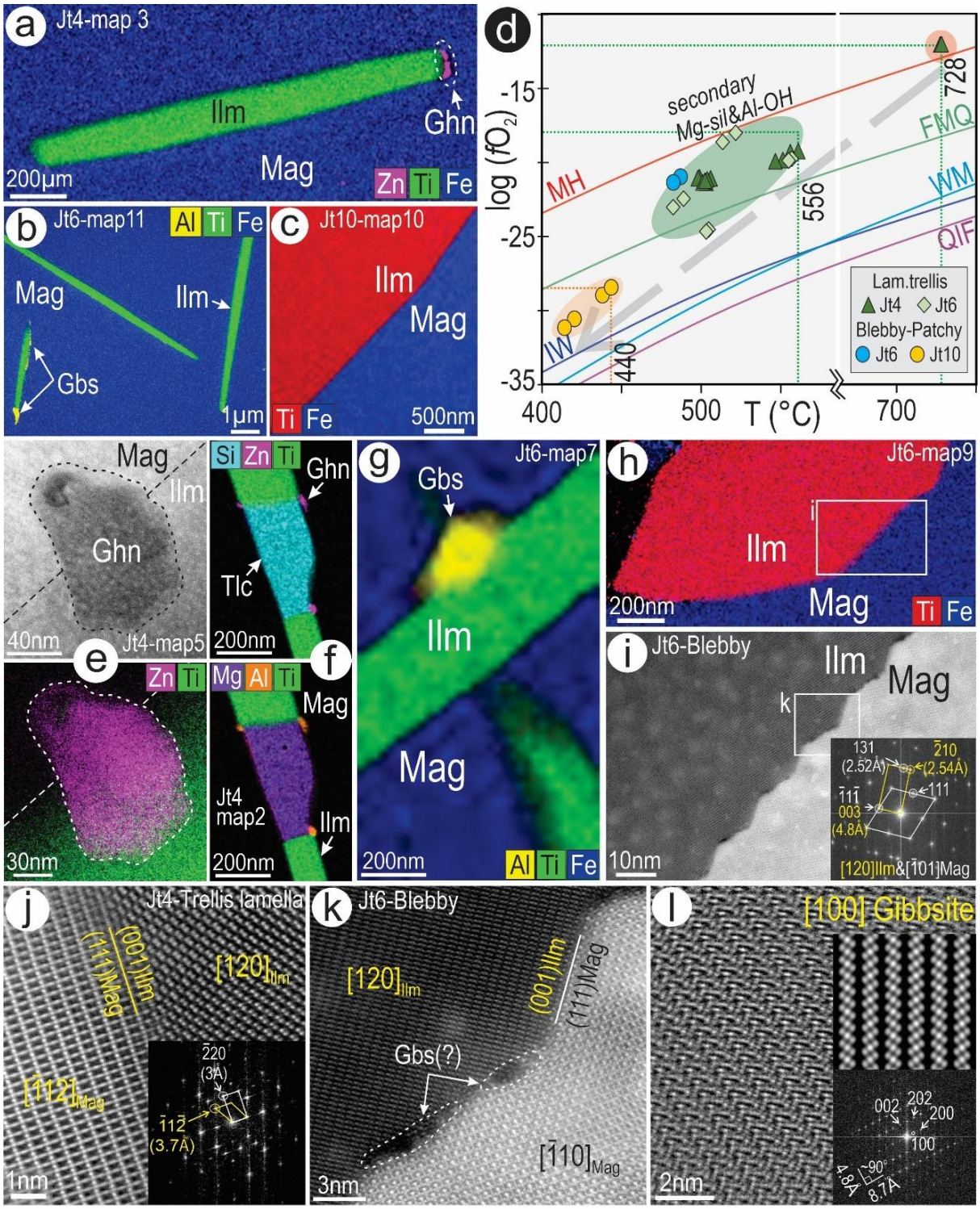

Figure 10. EDS STEM maps (a-c, e-h) and HAADF STEM images (i-l) showing nanoscale aspects of trellis (Jt4), transition to blebby (Jt6) and patchy ilmenite (Ilm) as inclusions in the dense silicate-mottled magnetite (Mag) from sample Jt10. STEM simulation for gibbsite as overlap in (l). FFT patterns for the full images as insets in (i,j,l). (d) logfO_2-T plot showing results of nano-thermobarometry for ilmenite-magnetite pairs. Data from ESM Table 3. Mineral buffers plotted: MH–magnetite-hematite; FMQ–fayalite-magnetite-quartz; WM–wüstite-magnetite; QIF–quartz-iron-fayalite. Other abbreviations: Ghn–gahnite; Gbs–gibbsite; Tlc–Talc.

The lowest temperatures (414 to 443 °C) were obtained from pairs of patchy ilmenite-magnetite (Jt10, Fig. 10c) in the dense mottled magnetite (see Figure 5c).

In closer detail, blebby ilmenite and magnetite features a stepwise mutual boundary (Fig. 10i). Nonetheless, the two oxides display epitactic relationships with one another in which $(111)_{magnetite}$ and $(001)_{ilmenite}$ planes are parallel. The fast Fourier transform (FFT) pattern shows their coherent intergrowth between $[\bar{1}01]_{magnetite}$ and $[120]_{ilmenite}$ where the distance of ~4.8 Å corresponds to the same distance along the lattice vectors $(\bar{1}1\bar{1})$* and (003)* in magnetite and ilmenite, respectively (inset in Figure 10i). Likewise, epitactic relationships between $[11\bar{2}]_{magnetite}$ and $[110]_{ilmenite}$ are observed between trellis ilmenite and host magnetite (Fig. 10j and FFT in inset). In this case, straight mutual boundaries are typical with parallel alignment between (111) and (001) planes in magnetite and ilmenite, respectively.

Nanometer-scale inclusions of Al-hydroxide species occur along the stepwise boundary between blebby ilmenite and magnetite (Fig. 10k). The Al-hydroxide phase from a larger area at the end of one ilmenite lamella (Fig. 10l) was identified as gibbsite, $Al(OH)_3$, from high resolution imaging and FFT pattern. STEM simulation of $[100]_{gibbsite}$ matches the image for this species, albeit imperfectly.

Aside from amphiboles and ilmenite, the most abundant inclusions in magnetite, we also observe allanite and titanite within mottled magnetite (Figs. 9h-j and 11 foils Jt7-F2 and Jt10-F2,). Allanite, $(CaCe)(AlAlFe^{2+})O[Si_2O_7][SiO_4](OH)$, is associated with actinolite within a field also containing other Ca- and Mg-amphiboles (Fig. 9h, i) within the dense mottled magnetite (JT10). EDS STEM element maps (Fig. 11a) show intragranular banding with respect to Ca which is likely attributable to the actinolite (see also Campo-Rodriguez et al. 2024a) and a clear Al and Ce distribution reproducing allanite grain morphology. The identity of this species was obtained from high-resolution HAADF STEM imaging of the grain and its marginal contacts with the amphibole (Fig. 11b, c). The upper and lower contacts on Figure 11b are characterized by straight and scalloped boundaries between allanite and actinolite tilted on the same zone axes, i.e. $[\bar{1}\bar{1}1]$

and [001], respectively. Coherent relationships are documented for both types of contacts from the parallel alignment between $(\bar{1}10)^*_{allanite}$ and $(100)^*_{actinolite}$ lattice vectors (with spacings at ~4.7 Å) on the FFT pattern (Fig 11b inset) representing both images in Figure 11b. The straight contact is between $(011)_{allanite}$ and $(\bar{1}10)_{actinolite}$ and a second set of planes $(1\bar{1}0)_{allanite}$ and $(110)_{actinolite}$ in the scalloped boundary. The image of allanite shows densely packed arrays of Ce atoms as brighter arrays that are reproduced by STEM simulations matching the crystal structure model (Fig. 11c).

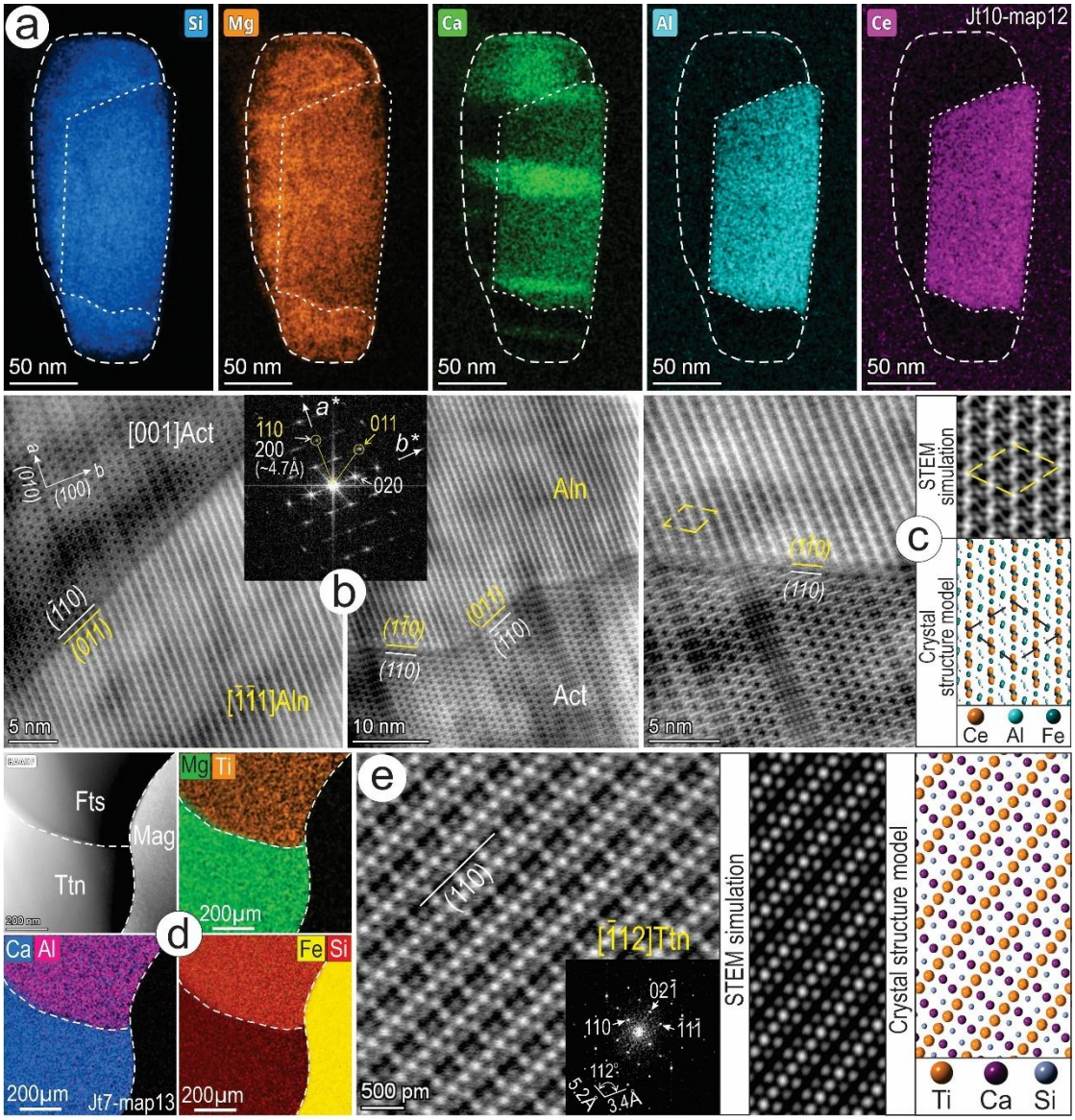

Figure 11. EDS STEM maps of allanite (Aln) attached to actinolite (Act) in (a) and titanite (Ttn)-ferrotschermakite (Fts) in (d) as inclusions in magnetite (Mag). HAADF STEM images of boundaries between allanite and actinolite in (b, c) and of titanite in (e). FFT patterns representing the images as insets in (b, e).

Titanite, identified from the foil exposing the rare-mottled magnetite (Jt7-F2; Figs. 9j; 11d, e), occurs as inclusions associated with ferrotschermakite (Figs. 9f; 11d) and along laths of biotite (Fig. 9j), but no ilmenite is observed. High-resolution imaging combined with STEM simulation and crystal structure model on [$\bar{1}$12] zone axis of titanite confirm its identity (Fig. 11e).

Discussion

How many generations of magnetite?

Characteristics observable down to the nanoscale (textures, inclusions, and geochemical trends; Figs. 2; 3; 5-9) indicate at least two distinct generations of magnetite: (i) trellis type - of mafic igneous affiliation; and (ii) mottled type. The transition from trellis to mottled magnetite is marked by a change in ilmenite inclusions from trellis to blebby, the appearance of patchy ilmenite textures during episodes of brecciation, and a pronounced mottling with silicates (Fig5 a-f). Although overprinting can also be invoked for the trellis-type magnetite during subsequent events (textural and chemical re-equilibration, inclusion formation; Figs. 5; 9) preservation of trellis magnetite throughout the entire sequence, albeit with variable abundance, supports the hypothesis that this generation is an inherited accessory mineral from the host lithologies.

Trellis magnetite records a range of temperatures and fO_2 conditions attributable to re-equilibration during temperature decrease from 720 to 400 °C and increasingly reduced conditions ($\log fO_2$ = -12 to -30) from under the magnetite-hematite to above iron-wüstite stability curves (Fig. 9d; ESM Table S3). Importantly, such evolution corresponds to the formation conditions of magnetite as this evolves from trellis to mottled types (Fig. 5a-f). The occurrence of secondary phases including Mg-silicates and gibbsite (Fig. 9) records an intermediate stage of the same cooling event (~550-480 °C) during which ilmenite is also redistributed as blebs followed by patchy inclusions at still lower temperature (440-420 °C) rather than as lamellae throughout magnetite.

The silicate inclusions typical of the mottled magnetite vary in speciation and abundance with early associations of NCPs and Mg-Fe-amphiboles attributed to metamorphism of an initial mafic-ultramafic sequence followed by calcic-amphiboles formed during the IOCG system at Jatobá (Campo-Rodriguez et al. 2024a). Most outstanding of all, however, is the discovery of allanite growing epitaxially with actinolite within host magnetite (Fig. 11a-c). We interpret the allanite as having formed from Ce-bearing amphibole described from dense mottled magnetite (Campo-Rodriguez et al. 2024a) via the diffusion/percolation of waning-stage fluids. Disappearance of ilmenite and formation of titanite (Fig. 11d, e) is associated with an increase in the abundance of mica and chlorite inclusions (Fig. 9i) within the rare-mottled magnetite.

Magnetite trace element signatures

Trellis magnetite is not exclusive to mafic/ultramafic host rocks since comparable textures are reported from igneous magnetite in granitoids and hydrothermal magnetite from IOCG systems hosted by sequences of felsic magmatic rocks (e.g., Ciobanu et al. 2019; Hu et al. 2020; Verdugo-Ihl et al. 2021; Zeng et al. 2022). IOCG magnetite can contain as much as 3 wt% TiO_2; Verdugo-Ihl et al. 2021), comparable with the highest Ti (~30,000 ppm) reported here from Jatobá magnetite. A mafic/ultramafic origin for the Jatobá magnetite is however supported by the conspicuous Cr-enriched signature of Ti-rich trellis magnetite (Fig. 6). The modest, relatively steady Ni concentrations of ~40-70 ppm in magnetite is explained by the presence of Ni-bearing sulfides (Campo-Rodriguez et al. 2024b) and preferential partitioning of these elements, as well as V and Ti, into sulfides and mica adjacent to magnetite (Fig. 8b, c).

Contrasting with trellis magnetite, mottled magnetite is relatively enriched in lithophile elements, even if these are, in part, due to presence of amphibole inclusions. Importantly, the same inclusions and associated allanite also account, to some extent, for the prominent REY

signature (Fig. 6a). Nonetheless, magnetite can also structurally incorporate up to several hundred ppm ΣREY, as shown by a micron- to atomic-scale study of Fe-oxides (Cook et al. 2022).

Discrimination between the two generations of magnetite is further facilitated by their distinct chondrite-normalized REY fractionation patterns (Fig. 7). The upwards-sloping HREE segment seen in trellis magnetite contrasts with the markedly LREE-enriched signature of the mottled magnetite, the latter likely mirroring fractionation trends of the contained nanoinclusions of allanite.

Enrichment of REY in magnetite from mean <10 ppm ΣREY to ~100 ppm accompanying the transition from trellis to rare- and dense mottled textures (Fig. 7) indicates additional metal source(s) that also account for enrichment in spatially co-existing Cu-(Ni, PGE) mineralization (Campo-Rodriguez et al. 2024b). Comparable REY-bearing geochemical signatures are reported in magnetite from IOCG deposits, notably at Olympic Dam and adjacent deposits (Courtney-Davies et al. 2019; Cook et al. 2022) and IOA deposits along the northern Chilean iron belt such as Los Colorados (Knipping et al. 2015), albeit with variable concentrations. We thus consider that the REY-enriched signatures displayed by Jatobá magnetite represent a fingerprint of IOCG-related fluids.

Reinforcing the idea that REE are an intrinsic signature of IOCG mineralization in the CMP are the Fe-ores from the Salobo Cu-Au-Mo deposit in the Northern Copper Belt. Whole rock analyses of iron formations (of banded iron formation-BIF origin; Justo et al. 2020) and mineralized lenses from the Salobo deposit given by Lindenmayer and Teixeira (1999) show ΣREE values of up to 2,200 ppm, mean 938 ppm). REE-enrichment is attributed to potassic alteration.

The characteristic IOCG-like signature of magnetite from Jatobá is emphasized by the presence of ‘granitophile elements’ and the marked correlation between granitophile and REY enrichment (mottled magnetite; Fig. 6), a feature identified in IOCG deposits of the Olympic Cu-Au Province, South Australia (Courtney-Davies et al. 2019; Verdugo-Ihl et al. 2020).

Other studies of trace element signatures in magnetite from Carajás deposits (Huang and Beaudoin 2019; Mansur et al. 2023) used lithophile elements (Al, Ca, Mg, Si) and transition metals (V, Cr, Ti, Ni, Mn) to distinguish individual "generations" of magnetite, as well as diagrams considered to be helpful for discriminating magmatic from hydrothermal origin and/or evolution. In the present study, we show why such diagrams are not reliable, at least if applied to at Jatobá, because of the effect that ilmenite and amphibole nanoinclusions have on lithophile element distributions at the grain-scale. We contend that a decoupling among transition metals occurs during evolution from trellis to mottled magnetite, e.g., core-rim preferential distribution of Cr, Nb, and Mn, but not V (Fig. 8).

Deep shear zone metamorphism – telescoped transition of trellis to silicate-mottled magnetite

The schematic in Figure 12 illustrates magnetite transformations both in terms of grain textures and contained nanoscale inclusions. This shows a telescoped transition between trellis and silicate-mottled magnetite as the temperature gradually decreases from 730 to 400 °C (estimated from magnetite-ilmenite pairs; Fig. 10d), during which the ilmenite changes from trellis to blebby and patchy textures (Fig. 12a-c). Silicate-mottled magnetite coexists with the patchy ilmenite textures but becomes dominant in ore-hosted magnetite (Fig. 12c, d). Amphiboles in the silicate-mottled magnetite mirror those in the country rocks (Fig. 4m), and, in both cases, ferrotschermakite records pressures of ~7 kbar (6.4-7.4 kbar). Such P-T conditions are compatible with amphibolite facies metamorphism at a depth of ~20 km.

Initial titanomagnetite is affected by fracturing and crosscutting sets of trellis lamellae (Fig. 12a). Blebby ilmenite textures occur in fragmented magnetite, resulting from deformed grains now filling swell textures in the country rock (Fig. 12b). Primary hercynite in the igneous

magnetite is replaced by Al-hydroxides (gibbsite) whereas ilmenite is partially replaced by Mg-amphiboles (later altered to talc).

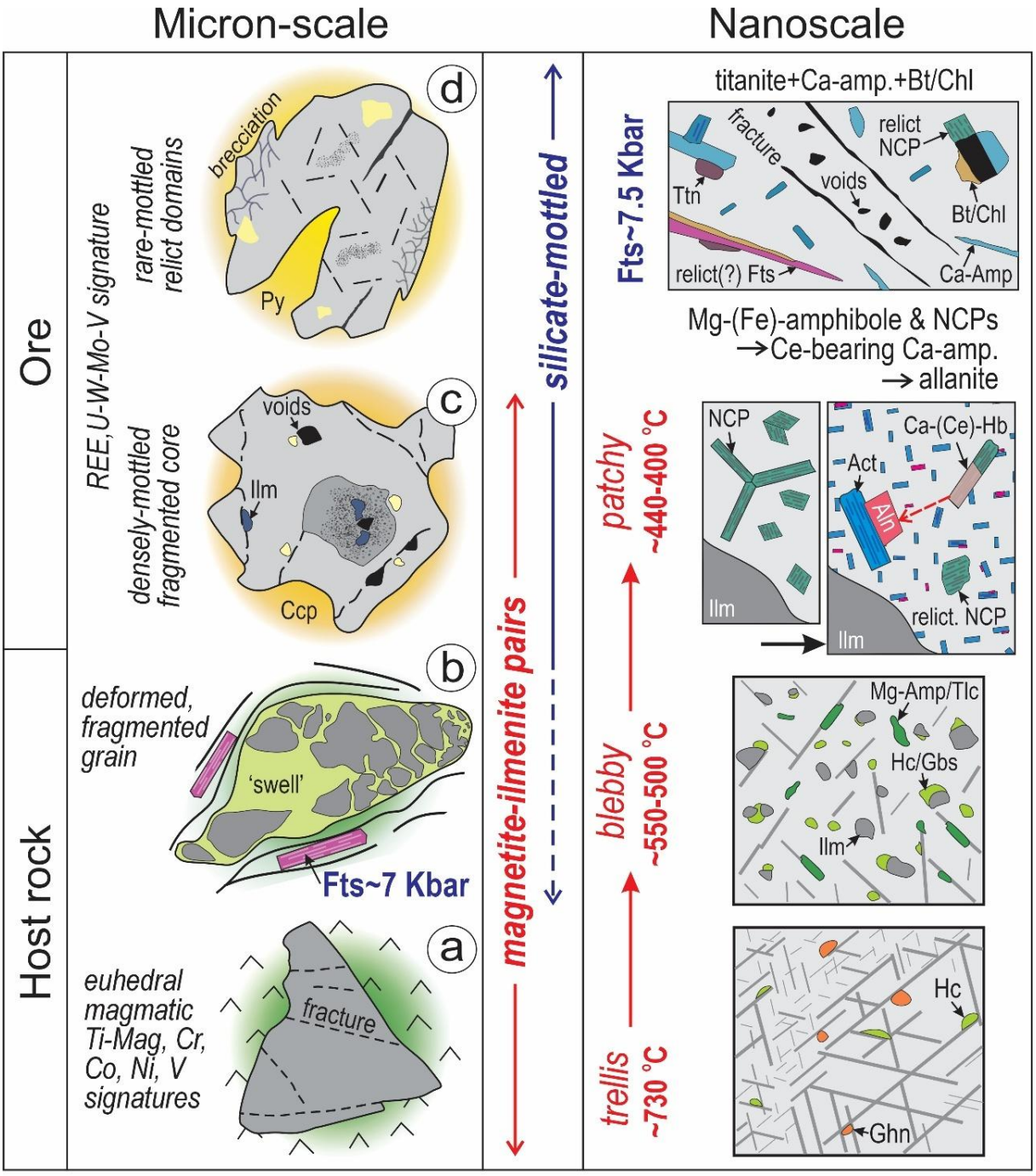

Figure 12. Schematics showing the micron- to nanoscale textural evolution of magnetite from host basalt to ore. See text for additional explanation. The dashed lines indicate fractures. Abbreviations: Act–actinolite; Aln–allanite; Amp–amphibole; Bt–biotite; Ccp–chalcopyrite; Chl–chlorite; Fts–ferrotschermakite; Gbs–gibbsite; Ghn–gahnite; Hb–hornblende; Hc–Hercynite; Ilm–ilmenite; NCP– non-classical pyribole; Py–pyrite; Tlc–talc; Ttn-titanite.

The mottled magnetite is typical of the ore interval, whereby fragmented cores preserve densely mottled domains surrounded by overgrowths (Fig. 12c). In this case, an evolution from Mg-(Fe)-amphibole and NCPs to Ce-bearing calcic amphibole and local formation of allanite (Fig. 11a-c) is recorded throughout the mottled areas. This magnetite preserves patchy ilmenite throughout cores and overgrowths, and contains abundant sulfide (pyrite, chalcopyrite) inclusions.

Rare-mottled magnetite displays sets of fractures with gangue minerals infill, sulfide inclusions, brecciated margins and high porosity (Fig. 12d). In this case, relict NCPs, sparse calcic amphibole associated with mica and titanite (the sole Ti-phase present) and micron-scale fractures with numerous voids are typical (Figs. 9f, 11d-e). These changes suggest replacement of the densely mottled magnetite via dissolution-reprecipitation reactions, during an increase in the fluid flux.

Magnetite trace element signatures change from Ti-Cr-Ni to REE-U+W+Mo following transition from trellis to mottled textures. The same geochemical trend is emphasized by nucleation of micron-scale inclusions of REE-minerals, uraninite, molybdenite, and scheelite/ferberite throughout Fe-(Ti)-oxides (Fig. 5h-n).

Metamorphism is supported by the range of fabrics and textures in magnetite and the country rocks indicative of deformation during a tectonothermal event subsequent to deposition of volcanic sequences in an active rift. Whereas the initial titanomagnetite represents a magmatic accessory in the host lithologies, magnetite is accumulated in pods, folds and bands instead of preserved as single grains (Figs. ESM 1, 2). Such textures could result from metamorphic segregation (Robin 1979) in otherwise non-banded lithologies. The banding could also be an inherited depositional fabric resulting from Fe-rich, thin BIF-like horizons intercalated within the volcanic sequences. For example, BIFs interlayered with mica schists and chalcopyrite-rich amphibole and amphibole schist concordant with metamorphic foliation are considered as amphibolites representing the metamorphosed expression of mafic protoliths belonging to a

volcano-sedimentary succession (Fernandes et al. 2021). However, the close association between magnetite and apatite, which increases in abundance towards the orebody (16 wt% of rock volume), rules out a BIF connection.

Deformation associated with metamorphism is also suggested by the sigmoidal morphology of scapolite, pressure shadows surrounding magnetite porphyroblasts, pinch-and swell structures (Fig. 2), and the grain-scale fabrics exhibited by pyrite (Campo-Rodriguez et al. 2024b). Unlike Veloso et al. (2020), who considered the scapolite to be an expression of sodic alteration associated with the IOCG system, we suggest that scapolite may instead relate to ocean floor alteration of basaltic sequences (Hekinian 1982) prior to metamorphism at higher P-T conditions. Arguments favoring such a hypothesis include scapolite textures (overgrowth on sigmoidal shaped grains), its occurrence as thin intervals rather than distinct zones, and in particular, the association with epidote group minerals and albite (Figs. 2e; 4c, e). Syn-metamorphic deformation is also supported by the widespread chain-width disorder observed in NCPs from mottled magnetite and the annealing textures in pyrite (Campo-Rodriguez et al. 2024a, b).

Amphibolite facies metamorphism at an estimated depth of 20 km based on multiple lines of evidence can take place in strike-slip deep shear zones via mechanisms of ‘shear heating by friction’ (Leloup and Kienast, 1993). Jatobá is placed within the Canaã dos Carajás shear zone, one of the three main strike slip systems identified in the CD (e.g., Pinheiro and Holdworth 1997). Recent geodynamic models (Costa et al. 2020; Trunfull et al. 2020) have postulated activation of strike slip systems accompanied by deformation or metamorphism post rifting. As documented by thermomechanical modelling and field examples, the ascent of hot fluids/magmas along shear zones enhances temperature in shallower parts while leading to strain localization in the deeper parts of the strike slip faults (Leloup et al. 1999).

We therefore suggest that the transition from trellis to silicate-mottled magnetite records deep shear metamorphism in the Canaã dos Carajás system with telescoping of multiple fluid fluxes. We explain the textural-geochemical differences between magnetite (and other minerals) present

in both host rocks and orezones by the variable overprinting effects during protracted fluid-rock interaction. The IOCG system is enhanced in areas of highest fluid flux and can be fingerprinted by a marked enrichment in REE and granitophile elements.

Summary and Implications

The major findings of this study are as follows:

Jatobá magnetite from mafic host lithologies and an orebody (massive magnetite with Cu-Ni-mineralization) show two distinct textures defined by the type of mineral inclusions: (i) trellis ilmenite and (ii) silicate-mottled, respectively. Trace element signatures for the two types of magnetite show distinct trends with higher Ti, Cr, Co, and Mn in trellis magnetite, and a pronounced enrichment of REY and lithophile elements in the mottled type. Other elements, notably V, attain comparable concentrations (thousands of ppm) in both types. Trace elements from the so-called 'granitophile group' (U-Pb-W-Sn-Mo) are present in low, yet measurable quantities with abundant U-, W-, Mo-bearing inclusions observed in magnetite.

Magnetite records transitional textures from trellis to silicate-mottled with overlap between the two types, while ilmenite changes from lamellar to blebby and patchy textures. In the blebby subtype, Al-hydroxides (gibbsite) and talc (formed on behalf of pre-existing Mg-amphibole) are documented.

Nanoscale ilmenite-magnetite thermobarometry yields a range of temperature (414–728 °C) and logfO_2 values (-31 to -12) for re-equilibration between magnetite and ilmenite from initial trellis to the blebby and to patchy in densely mottled magnetite. Allanite and titanite are documented from associations with calcic amphiboles within mottled magnetite. Formation of allanite from Ce-bearing calcic amphibole is recognized from epitaxial intergrowths between the two species at the nanoscale.

Pressure estimates at 6.4-7.4 kbar from ferrotschermakite in the country rocks correlate with those recorded by the same amphibole species contained within magnetite. Such P-T conditions are compatible with amphibolite facies metamorphism at a depth of ~20 km. Syn-metamorphic deformation is documented from a range of textures such as segregation of magnetite+apatite within pods, folds and bands, as well as sigmoidal scapolite and pressure shadows surrounding magnetite.

These multiple lines of mineralogical-geochemical evidence support a genetic model involving deep shear zone metamorphism in the root of the Canaã dos Carajás strike-slip structure. The transition from trellis to silicate-mottled magnetite records telescoping of fluid fluxes, with variable overprinting effects during protracted fluid-rock interaction, instead of hydrothermal system zonation as invoked by previous models. Further constraints on the new model could come from geochronological data for minerals typical of IOCG system evolution such as apatite, which is ubiquitous throughout the Jatobá system. The new model may have broad applicability to other IOCG systems hosted within shear zones from the Carajás Domain.

Acknowledgements

We extend thanks to the staff of Adelaide Microscopy, particularly Animesh Basak and Nobuyuki Kawashima for their continuous support with analytical work. We thank Sergio Huhn for his assistance with geological data.

Funding

Y.T.C.R and M.E.S acknowledge the Brazilian Research Council (CNPq – Project 409015/2021-0) and the Coordenação de Aperfeiçoamento de Pessoal de Nível Superior - Brasil (CAPES) - Finance Code 001. The Institute of Sustainability, Energy and Resources, The University of

Adelaide, supported analytical work. N.J.C. and K.E. acknowledge Australian Research Council Linkage grant LP200100156 (Critical Minerals from Complex Ores).

Supplementary Materials

ESM A: Analytical Methods and Additional figures

ESM B: Additional tables, EPMA and LA-ICP-MS results

References

Antonio, P.Y.J., D'Agrella-Filho, M.S., Nédélec, A., Poujol, M., Sanchez, C., Dantas, E.L., Dall'Agnol, R., Teixeira, M.F.B., Proietti, A., MartínezDopico C.I., Oliveira, D.C., Silva, F.F., Marangoanha, B., and Trindade, R.I.F. (2021) New constraints for paleogeographic reconstructions at ca. 1.88 Ga from geochronology and paleomagnetism of the Carajás dyke swarm (eastern Amazonia). Precambrian Research 353, 106039. https://doi.org/10.1016/j.precamres.2020.106039

Araújo, O.D., Maia, R.G.N., João, X.J., and Costa, J.B.S. (1988) A megaestruturação arqueana da folha Serra dos Carajás. In Congresso Latino-Americano de Geologia SBG-NO Belém vol. 7, p. 324-338.

Barton, M. (2014) Iron oxide (–Cu–Au–REE–P–Ag–U–Co) systems. Treatise on Geochemistry, 2nd edition, vol 13. Elsevier, Amsterdam 515-541. https://doi.org/10.1016/B978-0-08-095975-7.01123-2

Biagoni, C., and Pasero, M. (2014) The systematics of the spinel-type minerals: An overview. American Mineralogist 99, 1254–1264. https://doi.org/10.2138/am.2014.4816

Campo-Rodríguez, Y.T., Schutesky, M.E., de Oliveira, C.G., and Whitehouse, M.J. (2022) Unveiling the polyphasic evolution of the Neoarchean IOCG Salobo deposit, Carajás Mineral Province, Brazil: Insights from magnetite trace elements and sulfur isotopes. Ore Geology Reviews 140, 104572. https://doi.org/10.1016/j.oregeorev.2021.104572

Campo-Rodríguez, Y.T., Ciobanu, C.L., Slattery, A., Cook, N.J., Schutesky, M.E., Ehrig, K., King, S.A., and Yao, J. (2024a) Polysomatic intergrowths between amphiboles and non-classical pyriboles in magnetite: smallest-scale features recording a protracted geological history. American Mineralogist 109 (10), 1798–1818. https://doi.org/10.2138/am-2023-9188

Campo-Rodriguez, Y.T., Cook, N.J., Ciobanu, C.L., Schutesky, M.E., King, S.A., Gilbert, S., and Ehrig, K. (2024b) Platinum Group Minerals Associated with Nickel-Bearing Sulfides from the Jatobá Iron Oxide-Copper-Gold Deposit, Carajás Domain, Brazil. Minerals 14, 757. https://doi.org/10.3390/min14080757

Campo Rodriguez, Y.T., Ciobanu, C.L., Cook, N.J., Schutesky, M.E., Ehrig, K., Slattery, A., Gilbert, S., and King, S.A. (*in review, c*) Magnetite and REE-rich calcic amphibole provide evidence for a skarn-IOCG system at Onça Rosa, Jaguar Orefield, Carajás Mineral Province, Brazil. The Canadian Journal of Mineralogy and Petrology.

Ciobanu, C.L., Verdugo-Ihl, M.R., Slattery, A., Cook, N.J., Ehrig, K., Courtney-Davies, L., and Wade, B.P. (2019) Silician magnetite: Si–Fe-nanoprecipitates and other mineral inclusions in magnetite from the Olympic Dam Deposit, South Australia. Minerals 9, 311. https://doi.org/10.3390/min9050311

Ciobanu, C.L., Verdugo-Ihl, M.R., Cook, N.J., Ehrig, K., Slattery, A., and Courtney-Davis, L. (2022) Ferro-tschermakite with polysomatic chain-width disorder identified in silician magnetite from Wirrda Well, South Australia: A HAADF STEM study. American Mineralogist 107, 765-777. https://doi.org/10.2138/am-2022-7975

Cook, N.J., Ciobanu, C.L., Ehrig, K., Slattery, A.D., and Gilbert, S.E. (2022) Micron- to atomic-scale investigation of rare earth elements in iron oxides. Frontiers in Earth Science 10, 967189. https://doi.org/10.3389/feart.2022.967189

Corriveau, L., Montreuil, J.F., and Potter, E.G. (2016) Alteration facies linkages among iron oxide copper-gold, iron oxide-apatite, and affiliated deposits in the Great Bear magmatic zone, Northwest Territories, Canada. Economic Geology 111, 2045-2072. https://doi.org/10.2113/econgeo.111.8.2045

Costa, F.G., Santos, P.A., Serafim, I.C.C.O., Costa, I.S.L., and Roopnarain, S. (2020) From Mesoarchean drips to modern–style tectonics in the Carajás Province, Amazonian Craton. Journal of South American Earth Science 104, 102817. https://doi.org/10.1016/j.jsames.2020.102817

Courtney-Davies, L., Ciobanu, C.L., Verdugo-Ihl, M.R., Dmitrijeva, M., Cook, N.J., Ehrig, K., and Wade, B.P. (2019) Hematite geochemistry and geochronology resolve genetic and temporal links among iron-oxide copper gold systems, Olympic Dam district, South Australia. Precambrian Researchs 335, 105480. https://doi.org/10.1016/j.precamres.2019.105480

DOCEGEO (1988) Revisão litoestratigráfica da Província Mineral de Carajás-Litoestratigrafia e principais depósitos minerais, 35th Congresso Brasileiro de Geologia: Brazil p. 11-54.

Fernandes, C.M.D., Galarza, M.A., Teixeira de Gouvêa, R.C., and Tavares de Souza, H.P. (2021) Geochemical, geochronological, and isotopic constraints for the Archean metamorphic rocks of the westernmost part of the Carajás Mineral Province, Amazonian Craton, Brazil. Journal of South America Earth Sciences 110, 103340. https://doi.org/10.1016/j.jsames.2021.103340

Hekinian, R. (1982) Chapter 9 Ocean floor metamorphism. Elsevier Oceanography Series. Elsevier 33:265-290.

Hu, H., Li, J.W., Harlov, D.E., Lentz, D.R., McFarlane, C.R.M., and Yang, Y.H. (2020) A genetic link between iron oxide-apatite and iron skarn mineralization in the Jinniu volcanic basin, Daye district,

eastern China: Evidence from magnetite geochemistry and multi-mineral U-Pb geochronology. GSA Bulletin 132 (5-6), 899–917. https://doi.org/10.1130/B35180.1

Huang, X.W., and Beaudoin, G. (2019) Textures and chemical compositions of magnetite from iron oxide copper-gold (IOCG) and Kiruna-type iron oxide-apatite (IOA) Deposits and their implications for ore genesis and magnetite classification schemes. Economic Geology 114, 953–979. https://doi.org/10.5382/econgeo.4651

Huang, X.W., and Beaudoin, G. (2021) Nanoinclusions in zoned magnetite from the Sossego IOCG deposit, Carajás, Brazil: Implication for mineral zoning and magnetite origin discrimination. Ore Geology Reviews 139, 104453. https://doi.org/10.1016/j.oregeorev.2021.104453

Huang, X.W., Beaudoin, G., and Yang, Y. (2022) A HR-TEM study on two generations of magnetite from the Alemao IOCG deposit, Carajás, Brazil: Implication for Fe-Cu mineralization. Ore Geology Reviews 146, 104934. https://doi.org/10.1016/j.oregeorev.2022.104934

Justo, A.P., Dantas, E.L., Bau, M., Freitas-Silva, F.H., Santos, R.V., and Schorscher, J.H.D. (2020) Paleobasinal to band-scale REE + Y distribution in iron formations from Carajás, Amazon Craton, Brazil. Ore Geology Reviews 127, 103750. https://doi.org/10.1016/j.oregeorev.2020.103750

Knipping, J.L., Bilenker, L.D., Simon, A.C., Reich, M., Barra, F., Deditius, A.P., Wälle, M., Heinrich, C.A., Holtz, F., and Munizaga, R. (2015) Trace elements in magnetite from massive iron oxide-apatite deposits indicate a combined formation by igneous and magmatic-hydrothermal processes. Geochimica et Cosmochimica Acta 171, 15-38. https://doi.org/10.1016/j.gca.2015.08.010

Leake, B.E., Woolley, A.R., ARPS, C.E.S., Birch, W.D., Gilbert, M.C., Grice, J.D., Hawthorne, F.C., Kato, A., Kisch, H.J., Krivovichev, V.G., and others. (1997) Nomenclature of amphiboles: report of the subcommittee on amphiboles of the international mineralogical association, commission on new minerals and mineral names. The Canadian Mineralogist 35, 219-246. https://doi.org/10.1180/minmag.1997.061.405.13

Leloup, P.H., and Kienast, J.R. (1993) High-temperature metamorphism in a major strike-slip shear zone: the Ailao Shan—Red River, People's Republic of China. Earth and Planetary Science Letters 118(1-4), 213-234. https://doi.org/10.1016/0012-821X(93)90169-A

Leloup, P.H., Ricard, Y., Battaglia, J., and Lacassin, R. (1999) Shear heating in continental strike-slip shear zones: model and field examples. Geophysical Journal International 136(1), 19-40. https://doi.org/10.1046/j.1365-246X.1999.00683.x

Lepage, L.D. (2003) ILMAT: an Excel worksheet for ilmenite–magnetite geothermometry and geobarometry. Computers & Geosciences 29, 673-678. https://doi.org/10.1016/S0098-3004(03)00042-6

Lindenmayer, Z.G., and Teixeira, J.B.G. (1999) Ore genesis at the Salobo copper deposit, Serra dos Carajás. Base Metal Deposits of Brazil. Belo Horizonte, MME/CPRM/DNPM p. 33-43.

Machado, N., Lindenmayer, T.E, Krogh, T.E., and Lindenmayer, D. (1991) U-Pb geochronology of Archean magmatism and basement reactivation in the Carajás area, Amazon shield, Brazil. Precambrian Research 49, 329-354. https://doi.org/10.1016/0301-9268(91)90040-H

Mansur, E.T., Dare, S.A.S., Ferreira Filho, C.F., Miranda, A.C.R, and Monteiro, L.V.S. (2023) The distribution of trace elements in sulfides and magnetite from the Jaguar hydrothermal nickel deposit: Exploring the link with IOA and IOCG deposits within the Carajás Mineral Province, Brazil. Ore Geology Reviews 152, 105256. https://doi.org/10.1016/j.oregeorev.2022.105256

Martins, P.L.G, Toledo, C.L.B, Silva, A.M., Chemale, Jr.F., Santos J.O.S., and Assis, L.M. (2017) Neoarchean magmatism in the southeastern Amazonian Craton, Brazil: Petrography, geochemistry and tectonic significance of basalts from the Carajás Basin. Precambrian Research 302, 340-357. https://doi.org/10.1016/j.precamres.2017.10.013

McDonough, W.F. and Sun, S.S. (1995) The composition of the Earth. Chemical Geology 120, 223–253. https://doi.org/10.1016/0009-2541(94)00140-4

Moreto, C.P.N., Monteiro, L.V.S., Xavier, R.P., Creaser, R.A., Dufrane, S.A., Melo, G.H.C., Silva, M.A.D., Tassinari, C.C.G., and Sato, K. (2015b) Timing of multiple hydrothermal events in the iron oxide–copper gold deposits of the Southern Copper Belt, Carajás Province, Brazil. Mineralium Deposita 50, 517-546. https://doi.org/10.1007/s00126-014-0549-9

Olszewski, W.J., Wirth, K.R., Gibbs, A.K., and Gaudette, H.E. (1989) The age, origin, and tectonics of the Grão Pará Group and associated rocks, Serra dos Carajás Brazil: Archean continental volcanism and rifting. Precambrian Research 42, 229-254. https://doi.org/10.1016/0301-9268(89)90013-2

Pinheiro, R.V., and Holdsworth, R.E. (1997) Reactivation of Archaean strike-slip fault systems, Amazon region, Brazil. Journal of the Geological Society 154(1), 99-103. https://doi.org/10.1144/gsjgs.154.1.0099

Robin, P-Y.F. (1979) Theory of metamorphic segregation and related processes. Geochemical and Cosmochemical Acta 43, 1587-1600. https://doi.org/10.1016/0016-7037(79)90179-0

Schutesky, M.E., and de Oliveira, C.G. (2020) From the roots to the roof: An integrated model for the Neoarchean Carajás IOCG System, Brazil. Ore Geology Reviews 127, 103833. https://doi.org/10.1016/j.oregeorev.2020.103833

Tavares, F.M., Trouw, R.A.J, da Silva, C.M.G., Justo, A.P., and Oliveira, J.K.M. (2018) The multistage tectonic evolution of the northeastern Carajás Province, Amazonian Craton, Brazil: Revealing complex structural patterns. Journal of South American Earth Science 88, 238-252. https://doi.org/10.1016/j.jsames.2018.08.024

Trunfull, E.F., Hagemann, S.G., Xavier, R.P., and Moreto, C.P.N. (2020) Critical assessment of geochronological data from the Carajás Mineral Province, Brazil: Implications for metallogeny and

tectonic evolution. Ore Geology Reviews 121, 103556. https://doi.org/10.1016/j.oregeorev.2020.103556

Vasquez, L.V., Rosa-Costa, L.R., Silva, C.G., Ricci, P.F., Barbosa, J.O., Klein, E.L., Lopes, E.S., Macambira, E.B., Chaves, C.L., Carvalho, J.M., Oliveira, J.G., Anjos, G.C., and Silva, HR. (2008) Geologia e Recursos Minerais do Estado do Pará: Sistema de Informações Geográficas — SIG: texto explicativo dos mapas Geológico e Tectônico e de Recursos Minerais do Estado do Pará 1:1.000.000. CPRM, Belém, Brazil, 328 p.

Veloso, A.S.R. (2017) Evolução Metalogenetica do Deposito de Cu-(Zn) Jatobá, Provincia Mineral de Carajás. Unpublished PhD thesis, University of São Paolo, Brazil, 197 pp. https://doi.org/10.11606/T.44.2017.tde-21012019-150709

Veloso, A.S.R., Monteiro, L.V.S., and Juliani, C. (2020) The link between hydrothermal nickel mineralization and an iron oxide-copper-gold (IOCG) system: Constraints based on mineral chemistry in the Jatobá deposit, Carajás Province.

Verdugo-Ihl, M.R., Ciobanu, C.L., Cook, N.J., Ehrig, K., and Courtney-Davis, L. (2020) Defining early stages of IOCG systems: evidence from iron oxides in the outer shell of the Olympic Dam deposit, South Australia. Mineralium Deposita 55, 429-452. https://doi.org/10.1007/s00126-019-00896-2

Verdugo-Ihl, M.R., Ciobanu, C.L., Cook, N.J., Ehrig, K.J., Slattery, A., Courtney-Davies, L., and Dmitrijeva, M. (2021) Nanomineralogy of hydrothermal magnetite from Acropolis, South Australia: Genetic implications for iron-oxide copper gold mineralization. American Mineralogist 106, 1273-1293. https://doi.org/10.2138/am-2021-7557

Williams, P.J., Barton, M.D., Johnson, D.A., Fontbote, L., De Haller, A., Mark, G., Oliver, N.H.S., and Marshik, R. (2005) Iron Oxide Copper-Gold Deposits: Geology, Space-Time Distribution, and Possible Modes of Origin. Economic Geology, 100th Anniversary Volume 371–405. https://doi.org/10.5382/AV100.13

Xavier, R.P., Soares Monteiro, L.V., Moreto, C.P.N., Pestilho, A.L.S., Coelho de Melo, G.H., Delinardo da Silva, M.A., Aires, B., Ribeiro, C., and Freitas e Silva, F.H. (2012) The Iron Oxide Copper-Gold Systems of the Carajás Mineral Province, Brazil. In: Geology and Genesis of Major Copper Deposits and Districts of the World: A Tribute to Richard H. Sillitoe (Hedenquist, J.W., Harris, M., Camus, F., eds.). Society of Economic Geologists 16, 22 pp. https://doi.org/10.5382/SP.16.17

Zeng, L.P., Zhao, X.F., Spandler, C., Hu, H., Hu, B., Li, J.W., and Hu, Y. (2022) Origin of high-Ti magnetite in magmatic-hydrothermal systems: evidence from iron oxide-apatite (IOA) deposits of eastern China. Economic Geology 117, 923-942. https://doi.org/10.5382/econgeo.4901

CHAPTER 5

COUPLED LU-HF AND U-PB APATITE GEOCHRONOLOGY OF JATOBÁ OREBODY SUPPORTS ~2.5 GA METAMORPHISM IN DEEP SHEAR ZONES FROM SOUTHERN COPPER BELT, CARAJÁS DOMAIN, BRAZIL

Yuri Tatiana Campo-Rodriguez[1,2], Cristiana L. Ciobanu[1], Sarah Gilbert[3], Benjamin Wade[3], Nigel J. Cook[1], Maria E. Schutesky[2], Kathy Ehrig[1,4]

[1]*School of Chemical Engineering, The University of Adelaide, Adelaide, SA, 5005, Australia*

[2]*University of Brasilia, Institute of Geosciences, Graduate Program in Geology, Brasília DF 70910-900, Brazil*

[3]*Adelaide Microscopy, The University of Adelaide, Adelaide, SA, 5005, Australia*

[4]*BHP Olympic Dam, 10 Franklin Street, Adelaide, SA, 5000, Australia*

Article submitted to *Precambrian Research,* November 11th (2024) PRECAM-D-24-00505.

Statement of Authorship

Title of Paper	Coupled Lu-Hf and U-Pb apatite geochronology of Jatobá orebody supports ~2.5 Ga metamorphism in deep shear zones from Southern Copper Belt, Carajás Domain, Brazil
Publication Status	☐ Published ☐ Accepted for Publication ☑ Submitted for Publication ☐ Unpublished and Unsubmitted work written in manuscript style
Publication Details	Campo-Rodriguez, Y.T., Ciobanu, C.L., Gilbert, S., Wade, B., Cook, N.J., Schutesky, M.E., and Ehrig, K. Coupled Lu-Hf and U-Pb apatite geochronology of Jatobá orebody supports ~2.5 Ga metamorphism in deep shear zones from Southern Copper Belt, Carajás Domain, Brazil. Submitted to *Precambrian Research*.

Principal Author

Name of Principal Author (Candidate)	Yuri Tatiana Campo Rodriguez		
Contribution to the Paper	Performed analytical work, evaluation and interpretation of results and prepared the manuscript.		
Overall percentage (%)	60		
Certification:	This paper reports on original research I conducted during the period of my Higher Degree by Research candidature and is not subject to any obligations or contractual agreements with a third party that would constrain its inclusion in this thesis. I am the primary author of this paper.		
Signature	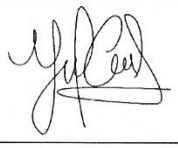	Date	06.11.2024

Co-Author Contributions

By signing the Statement of Authorship, each author certifies that:

i. the candidate's stated contribution to the publication is accurate (as detailed above);

ii. permission is granted for the candidate in include the publication in the thesis; and

iii. the sum of all co-author contributions is equal to 100% less the candidate's stated contribution.

Name of Co-Author	Cristiana L. Ciobanu		
Contribution to the Paper	Helped to define the direction of the manuscript, guides manuscript preparation and assisted with the interpretation of the results and evaluation of the manuscript. (13%)		
Signature		Date	06.11.2024

Name of Co-Author	Sarah Gilbert		
Contribution to the Paper	Helped in the operation of analytical equipment and data interpretation. (8%)		
Signature		Date	06.11.2024

Name of Co-Author	Benjamin Wade		
Contribution to the Paper	Helped in the operation of analytical equipment and data interpretation. (8%)		
Signature	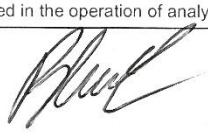	Date	06.11.2024

Name of Co-Author	Nigel J. Cook		
Contribution to the Paper	Helped with the preparation and evaluation of the manuscript. (6%)		
Signature		Date	06.11.2024

Name of Co-Author	Maria Emilia Schutesky		
Contribution to the Paper	Helped with the preparation and evaluation of the manuscript. (3%)		
Signature		Date	06.11.2024

Name of Co-Author	Kathy Ehrig		
Contribution to the Paper	Assisted with the evaluation of the manuscript. (2%)		
Signature		Date	06.11.2024

Coupled Lu-Hf and U-Pb apatite geochronology of Jatobá orebody supports ~2.5 Ga metamorphism in deep shear zones from Southern Copper Belt, Carajás Domain, Brazil

Yuri Tatiana Campo-Rodriguez[1,2*], Cristiana L. Ciobanu[1], Sarah Gilbert[3], Benjamin Wade[3], Nigel J. Cook[1], Maria Emilia Schutesky[2], Kathy Ehrig[1,4]

[1]*School of Chemical Engineering, The University of Adelaide, Adelaide, SA, 5005, Australia*

[2]*University of Brasilia, Institute of Geosciences, Graduate Program in Geology, Brasília DF 70910-900, Brazil*

[3]*Adelaide Microscopy, The University of Adelaide, Adelaide, SA, 5005, Australia*

[4]*BHP Olympic Dam, 10 Franklin Street, Adelaide, SA, 5000, Australia*

** Corresponding author.*

Abstract

A multi-technique geochronological study of apatite (U-Pb, Lu-Hf) in host basalts and mineralization from the Jatobá orebody, Southern Copper Belt, Carajás Domain, Brazil, constrains the age and setting of mineralization. Supported by cathodoluminescence imaging, electron probe microanalysis and LA-ICP-MS trace element data, the new ages point to initiation of an iron-oxide-copper-gold system at 2.5 Ga during a deformation event linked to amphibolite facies metamorphism in deep (up to 20 km) shear zones. The ~2.5 Ga Lu-Hf age is obtained from deformed, REE-rich cores of basalt-hosted apatite and is contemporaneous with metamorphism of a volcanic sequence deposited in a rift active during 2.76–2.73 Ga. Some apatite grains retain a mafic, Cl-rich signature, testifying to a primary igneous origin. The Lu-Hf ages stretching from 2527 to 2384 Ma are obtained from apatite displaying textural diversity and geochemical heterogeneity, consistent with a prolonged event featuring dissolution-reprecipitation in response

to fluid release during the retrograde cycle. Although the U-Pb system displays dominantly open behaviour, a younger ~2 Ga U-Pb age is obtained from apatite grains in which the U-Pb system has partially re-equilibrated. This age corresponds to post-uplift mylonitization of the host sequences. Although novel, a ~2.5 Ga age for mineralization in a deposit from the southern Copper Belt coincides with Cinzento Shear zone reactivation in the northern copper belt, and the ages of deposits there. Fluid flow along shears leached metals from the basement, later deposited as sulphides intimately associated with the reworked apatite. We propose deep-rooted connections between mineralizing systems across the region.

Keywords: Lu-Hf; U-Pb, apatite geochronology; Carajás Domain; Jatobá orebody.

Introduction

Apatite has a special place among the mineral tools available to petrologists and geochemists to understand and interpret the origin of rocks and mineral deposits. Apatite group minerals, $Ca_5(PO_4)_3(F,Cl,OH)$, are abundant in a wide variety of rock types and ores, are relatively refractory during metamorphism and alteration, and can incorporate a diverse range of trace elements, including rare earth elements and Y (REY). In studies of magmatic-hydrothermal ore deposits, the relative proportions of F, Cl, and OH, and the concentrations of trace elements substituting for Ca, and their relative variations, can inform on fluid parameters and the conditions of ore deposition (Harlov, 2015). Chondrite-normalized REY fractionation patterns in apatite are routinely used to detect changes in fluid parameters such as pH, temperature, salinity, redox conditions and fluid composition.

Apatite is an important component of many iron-oxide copper gold (IOCG) systems, especially the apatite-magnetite assemblages that define the early stage of IOCG deposit evolution, and in the related class of iron-oxide apatite (IOA)-type deposits. Their compositions and textures have thus contributed significantly to constraining IOCG genesis across different terranes (e.g., Belousova et al., 2001; Harlov et al., 2002; Ismail et al., 2014; Krneta et al., 2017a, b). Critical insights into IOCG deposit evolution have

been established by combining trace element analysis and cathodoluminescence (CL) imaging to reveal internal structures, overgrowths and alteration (e.g., Mercer et al., 2020; Steadman et al., 2022).

Apatite commonly contains low but measurable concentrations of uranium and retains lead produced from uranium decay within its structure, making it a valued U-Pb geochronometer (Chew et al., 2011; Kirkland et al., 2018; Chew and Spikings, 2021). The relatively low closure temperature of apatite, low levels of U, and the high common lead in some apatite are nevertheless disadvantages rendering U-Pb apatite dating unreliable in some instances where there is open system behaviour. The recent development of *in-situ* Lu-Hf apatite geochronology (Glorie et al., 2022, 2024; Simpson et al., 2022; Brown et al., 2024), to be used either independently or in tandem with U-Pb apatite geochronology, offers improved age constraints in complex terranes on account of the significantly higher closure temperature of the Lu-Hf system.

Apatite, associated with magnetite, is a ubiquitous component of Neoarchean IOCG deposits from the Carajás Domain (CD), Brazil (e.g., Xavier et al., 2012). Despite this, there have only been few attempts until now to date this apatite, either by U-Pb or Sm-Nd methods (Hernandez-Tasco et al., 2023; Smith 2023). In the CD, IOCG deposits occur within two distinct copper belts situated along the main regional shear zones, the Cinzento Shear Zone in the North and the Canaã dos Carajás Shear Zone in the South (Xavier et al., 2012). Open questions remain about the link between mineralization stages and the main tectonic-magmatic events with deposit ages spanning the Neoarchean and Paleoproterozoic (e.g., Grainger et al., 2008; Toledo et al., 2024).

The current consensus is that the ~2.6-2.5 Ga event is restricted to deposits from the northern belt and relates to reactivation of the Cinzento Shear zone, locally reaching amphibolite facies metamorphism (e.g., Melo et al., 2017). Recent U-Pb dating of allanite from deposits in the southern belt (Smith, 2023) counter this paradigm. Whereas the Salobo deposit in the north is considered representative of the ~2.5 Ga event, the Sequeirinho and Sossego deposits in the south display mineralization ages of ~2.7 Ga and ~2.0 Ga, respectively (e.g., Melo et al., 2017; Moreto et al., 2015a).

The present study aims at petrochronological characterization of apatite from the IOCG deposit at Jatobá in the Southern Copper belt. We use both U-Pb and Lu-Hf LA-ICP-MS dating methods to constrain

the relative timing of apatite with distinct textural and geochemical signatures within the context of host lithology and mineralization and compare to other deposits within the region.

Geological background

Main tectono-stratigraphic units and recent models of geodynamic evolution

The Carajás Province (CP) is part of the Amazonian Craton (Fig. 1A inset) and displays a marked transition from drip-tectonics in the Mesoarchean to modern–style tectonics in the Neoarchean (Costa et al., 2020). There are two tectonostratigraphic domains: the Carajás Domain (CD) to the north; and the Rio Maria Domain (RMD) to the south, collectively making up the Carajás Mineral Province (CMP; Vasquez et al., 2008; Fig. 1A). CMP metallogeny is distinct across the two domains, encompassing Neoarchean IOCG deposits and Paleoproterozoic Cu-Au mineralization in the CD, and Mesoarchean lode-Au deposits in the RMD (e.g., Costa et al., 2020).

The CD has a Mesoarchean basement (Fig. 1A) that comprises: (i) TTG (Trondhjemite–Tonalite–Granodiorite) units, mainly gneisses, migmatites and granulite from the 3−2.83 Ga Xingu Complex; (ii) greenstone belts of the Sequeirinho Group (3−2.9 Ga); and (iii) calc-alkaline intrusions of the Cruzadão Granite (ca. 2.87 Ga) (e.g., Tavares et al., 2018; Costa et al., 2020). The basement has a Neoarchean cover made up by: (i) volcano-sedimentary sequences of the Itacaiúnas Supergroup; and (ii) Paleoproterozoic sedimentary cover of the Águas Claras Fm. The Itacaiúnas Supergroup comprises many divisions, among which the Grão Pará Group hosts the Jatobá deposit, with an age generally considered between 2.76 and 2.73 Ga (e.g., Martins et al., 2017, and references therein). An older age, <2.87 Ga (in the Salobo–Pojuca, Aquiri and/or Rio Novo metavolcanic–sedimentary sequences or groups) has, however, been proposed for the opening of the Carajás Basin (Costa et al., 2020 and references therein).

The setting in which deposition of the Itacaiúnas Supergroup took place is disputed. Both an intra-plate rift model (e.g., Olszewski et al., 1989; Tavares et al., 2018, and references therein)

and a subduction-related setting (Costa et al., 2020, and references therein) are proposed. Martins et al., (2017) show petrological evidence for a back-arc continental basin, but conclude that a rift setting is more plausible, going on to suggest slab breakoff and subsequent asthenosphere upwelling. Formation of the volcanic sedimentary sequences in the Parauapebas Fm. of the Grão Pará Group is constrained by U-Pb zircon of rhyodacites/rhyodacite (ID-TIMS; 2759±2; Machado et al., 1991) and basaltic rocks (SHRIMP; 2745±5 Ma; Martins et al., 2017).

Lastly, completing the Neoarchean igneous activity in the CD are bimodal intrusions comprising: (i) mafic-ultramafic rocks of the Luanga Complex (2763±6 Ma; Machado et al., 1991) and its equivalents; and (ii) syn-tectonic/A-type granites of the Estrela Granite and equivalents (Tavares et al., 2018).

In contrast to the dome–and–keel structure of the RMD, the CD has a linear E-W-trending belt-like morphology (Costa et al., 2020), also named the Itacaiúnas Belt (Araújo et al., 1988). In closer detail, a central sigmoid domain, defined by formations of the Carajás Basin, is outlined by the prominent Cinzento strike-slip system to the north, which branches with the major Carajás Shear Zone (Fig. 1A). Although much debated in terms of the succession of multiple deformation regimes throughout extensional-compressional cycles from the Archean to Neoproterozoic-Cambrian (Tavares et al., 2018), the Itacaiúnas Belt inherits Mesoarchean structural patterns and is overprinted during the Transamazonian Orogeny, and again by brittle reactivation at 1.88 Ga associated with emplacement of the Uatumã Supergroup (Antonio et al., 2021).

Among the recent geodynamic models considering the timing of IOCG systems relative to Neoarchean magmatism in the CD, Costa et al. (2020) is the most provocative. In this model, a link between regional metamorphism in the lower crust and initiation of the Carajás Basin within an intracontinental or passive margin (?) setting at an earlier stage (2.87−2.83 Ga), is considered a distinct event during basin evolution. This is followed by a period of magmatic quiescence for ~70 Ma during which sedimentation of early sequences of banded iron formations (BIFs) took place in the Carajás Domain (Salobo-Pojuca Group?). Magmatism, comprising syntectonic

granitoids and volcanism (Grão Pará Group, 2.76−2.73 Ga) is generated during the first period of Neoarchean deformation along transtension/transpression strike slip systems.

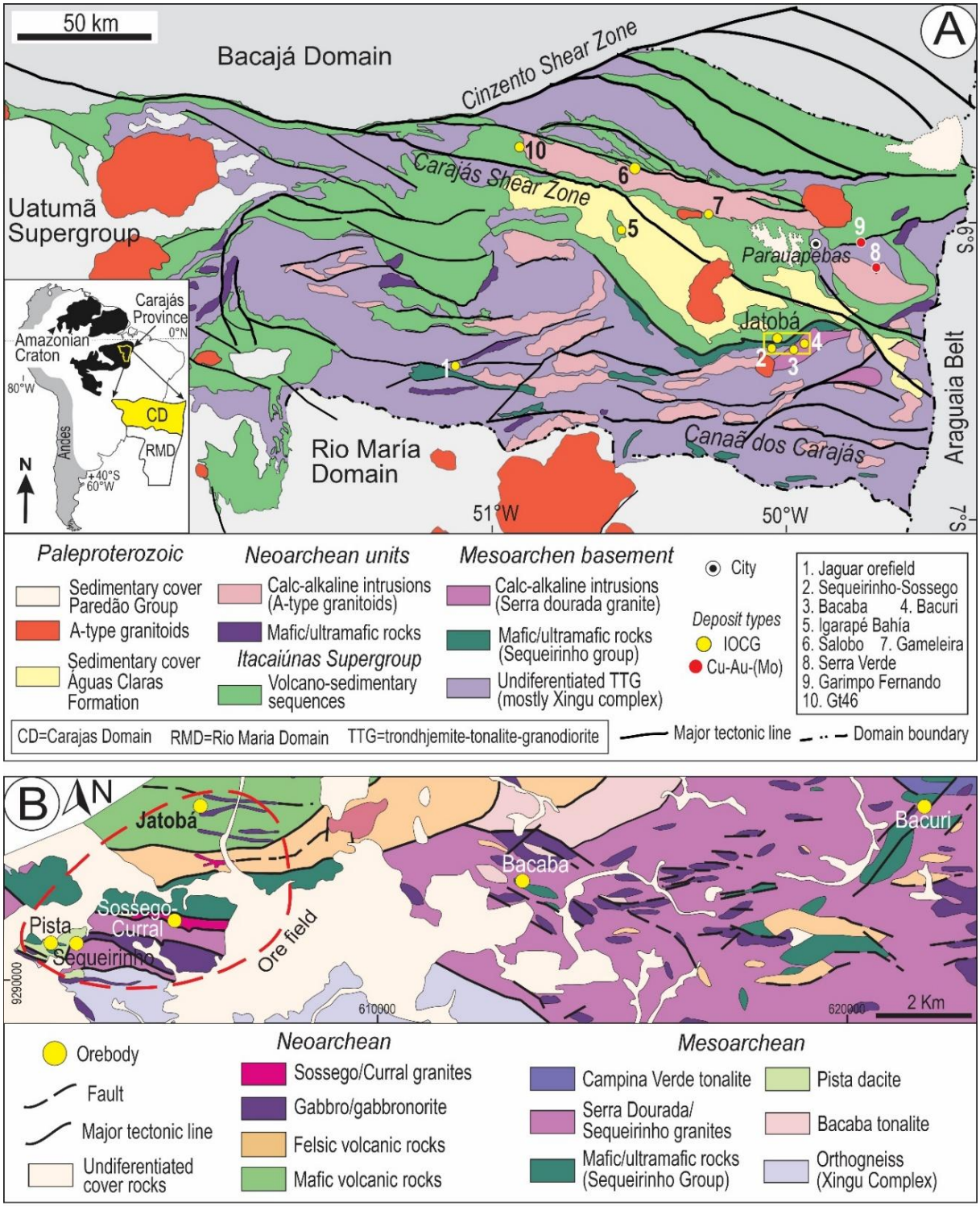

Figure 1. (A) Geological map of the Carajás Domain (CD) showing main lithologies and location of Jatobá and other deposits discussed in the text (modified from Tavares et al., 2018 and Trunfull et al., 2020). Inset shows location of the CD within the Amazonian Craton, South America. (B) Simplified geological map of part of the Southern Copper Belt (yellow rectangle in A) (modified from Moreto et al., 2015 and Veloso et al., 2020). Dashed line shows the cluster of deposits within the Jatobá orefield.

Based on compilation of geochronological data, Costa et al. (2020) linked the first IOCG event to this tectono-magmatic stage. A third stage of volcanic activity and emplacement of associated granitoids at 2.6−2.55 Ga (e.g., Old Salobo granite; Melo et al., 2017), as well as another suite of IOCG systems, occurred within the passive rift margin during an extensional regime after 2.6 Ga. In the Bacajá Domain, to the north of CD, Rhyacian and Transamazonian ages from 2.3 to 2.05 Ga represent a sequence of arc collages (Macambira et al., 2009; Klein et al., 2012). Anorogenic A-type granites are intruded between 1880 and 1860 Ma (e.g., Teixeira et al., 2018); for example, the Serra dos Carajás Granite in the center of the Carajás Basin (Fig. 1A) dated to the Transamazonian orogeny (1880±2 Ma; Machado et al., 1991).

An alternative geodynamic model (Trunfull et al., 2020) considers commencement of rifting at 2.76 Ga following the major Mesoarchean (2.87-2.83 Ga) collision between RMD and CD. A first stage of IOCG mineralization is suggested at ca. 40-80 Ma after rift initiation, during either (i) an Archean basin inversion with sinistral transpression (2.74−2.68 Ga) or (ii) continued rift extension but with dextral transtension at 2.72−2.68 Ga. The 2.6−2.45 Ga episodic reactivation of the Cinzento Shear Zone, along which the Old Salobo granite sits, could be associated with either of these two scenarios. A second IOCG event at 1.88 Ga is attributed to the waning stages of the Transamazonian Orogeny, albeit with uncertainty whether this is perhaps just a Cu-Au overprint or remobilization from a pre-existing IOCG deposit.

An integrated model, termed the ‘Neoarchean Carajás IOCG system’ is presented as a ‘roots to roof’ generic mineralization system sourced from magma-derived fluids driven along crustal shear zones (Schutesky and Oliviera, 2020). The authors discuss mineralogical-petrological data, alteration footprints and available dating for some nineteen deposits that are collectively considered as the expression of a crustal continuum from deeper, ductile, to shallower, brittle domains. Schutesky and Oliviera (2020) suggest the timing of IOCG mineralization to be between 2.76 and 2.73 Ga, coeval with the bimodal magmatism in the Itacaiúnas Supergroup. In contrast, a slightly younger interval (2.72–2.68 Ga) is reported by Trunfull et al. (2020) based on a

compilation of geochronological data. The temporal link between granitic magmatism and IOCG deposits in the CD is questioned by Toledo et al. (2024) based on new LA-ICP-MS U-Pb zircon ages from granitoids along the Cinzento Shear Zone. The overlap of these ages with published geochronological data for granites (2.76–2.73 Ga) and IOCG events at 2.72–2.68 Ga and 2.59–2.53 Ga is interpreted as a hydrothermal overprint of igneous zircon.

Deposit geology

Jatobá is part of the southern Copper Belt and is located along E-W and NE-SW-trending structures belonging to the Canaã dos Carajás shear zone (Fig. 1B). The geological map suggests a clustering of deposits within a single IOCG orefield, roughly 5 x 5 km in size, in which Jatobá is the northernmost in the cluster. However, unlike the other deposits in this orefield, Jatobá is hosted within the Neoarchean Grão Pará Group. Pista (historical mine), Sossego and Sequeirinho (355 Mt @ 1.1% Cu, 0.29 g/t Au) are open pits located along an E-W alignment, each with distinctive morphology and structure. Jatobá, located 3 km north of Sossego Mine comprises 30+ orebodies containing Cu-Ni mineralization. No resource estimate is available for the Jatobá deposit, which remains under evaluation (Veloso, 2020). Copper-Au ore zones of the Sequeirinho-Pista system are located at the contact between Neoarchean gabbronorite and Mesoarchean granitoids/felsic metavolcanics whereas the Sossego-Curral orebodies are hosted within two Neoarchean (2740 Ma) granites (Moreto et al., 2015a).

The Jatobá deposit lies north of a major fault/thrust zone between Mesoarchean mafic/ultramafic rocks and Neoarchean bimodal volcanic sequences of the Grão Pará Group (Fig. 1B). At this location, a 1–2 km-thick interval of felsic volcanics (rhyolite and dacites) is separated from the main body of dominantly mafic lithologies hosting the Jatobá deposit by a major E-W fault. Several gabbroic lenses occur throughout the volcanic rocks following lineaments oriented

similarly to the faults. Orebodies are located within the basalt/diabase sequence (samples studied here) and/or within andesites.

Previous work (Veloso et al., 2020) used mineral chemistry to address the link between "hydrothermal nickel mineralization and IOCG systems in the Carajás Province". The authors interpret eleven hydrothermal alteration stages overprinting host lithologies, a protolith defined by an assemblage of andesine+actinolite and accessory Ti-rich magnetite. The proposed stages are split into pre-tectonic and syn- to late-tectonic, with a range of ductile to brittle structures spanning all stages. The resultant model shows a lateral zonation centered on the mineralized zone with potassic alteration (biotite). Two spatially distinct parts are identified: (i) upper epidotite-chlorite + Cu-mineralization and (ii) lower (actinolite) + Cu-Ni mineralization. Veloso et al. (2020) define two lateral zones of sodic alteration: proximal (scapolite + hastingsite) and distal (albite + scapolite + quartz + magnetite + biotite). We note that magnetite occurs throughout, except in the proximal zone. Six calcic amphiboles (actinolite, hornblende, hastingsite, ferrotschermakite, cannilloite and pargasite) are recognized, along with cummingtonite from the Fe-Mg amphibole group. These amphiboles are claimed to form starting with actinolite in the precursor rock and continuing through the hydrothermal stages. Other minerals such as chlorapatite are products of both the pre-tectonic and mineralization stages. Potassic feldspar appears in the pre-tectonic and late tectonic stages, whereas chlorite is produced by late, retrograde alteration concentrated in the upper part of the mineralized zone. Altogether, the mineralization style evolved from replacement fronts, e.g., amphiboles show replacement as core-rim zonation, generation I by generation II or biotite, etc., controlled by the mylonitic foliation, to hydraulic breccia zones. The conclusion reached by Veloso et al. (2020) is that Jatobá represents the deep parts of an IOCG system formed from "channeling of overpressured superheated deep-seated fluids of probable magmatic origin". Veloso's model, specifying zonation of key minerals, is challenged by new data showing that magnetite and sulfides cannot

be directly related to an overall 'magmatic origin' (Campo-Rodriguez et al., 2024a, b; *in review a*).

Firstly, two texturally and geochemically distinct types of magnetite 'trellis' and 'silicate mottled' are defined based on micron- to nanoscale characterization of a basalt-hosted orebody at Jatobá (Campo-Rodriguez et al., 2024a; *in review a*). Trellis magnetite is clearly of igneous origin and contains lamellae of ilmenite and greater concentrations of Ti, Cr, Co, and Mn. The transition to silicate mottled magnetite is marked by a change in ilmenite inclusions from trellis to blebby, the appearance of patchy textures, evidence for episodes of brecciation, and a pronounced mottling with silicates. This type is rich in chain-silicate inclusions and features a pronounced enrichment of rare earths and other lithophile elements (Campo-Rodriguez et al., *in review a*). Ilmenite-magnetite nano-thermobarometry yields a range of temperature (414–728 °C) and logfO_2 values (-12 to -31) for re-equilibration between magnetite and ilmenite from initial trellis to the trellis+blebby and to patchy ilmenite in the densely mottled magnetite.

The chain-silicate inclusions are complex and comprise Mg-(Fe)- and (Ce)-calcic amphiboles, both displaying polysomatic intergrowths with non-classical pyriboles (NCP) (Campo-Rodriguez et al., 2024a). The formation of Mg-(Fe)-amphiboles+NCPs is attributed to ocean floor metamorphism whereas the calcic amphiboles are considered to mark the onset of the IOCG system. Based on the presence of ferrotschermakite (no NCPs) high-pressure conditions are suggested for magnetite formed during main ore deposition. Importantly, amphibole speciation in the host rocks mirrors that found as inclusions in magnetite (Campo-Rodriguez et al., *in review a*). Ferrotschermakite geobarometry facilitates a pressure estimate of 6.4-7.4 kbar for both host lithologies and magnetite.

Secondly, the recent discovery of platinum group minerals (PGM) associated with Ni-bearing sulfides at Jatobá is linked to either an initial VHMS-mineralization in the host basalts or to IOCG-type fluids that leached Ni+PGE from komatiites within the sequence/ultramafic rocks in the basement (Campo-Rodriguez et al., 2024b). Deformation during metamorphism is evidenced

by pressure shadows around magnetite, sigmoid-shaped scapolite (related to spilitization intervals), widespread chain-width disorder in NCPs, and annealing textures in pyrite (Campo-Rodriguez et al., 2024a, b; *in review a*).

Methodology

Four representative polished thin sections from drillhole 00032, all containing abundant apatite, were selected for study based on the presence of relevant textures. Initial sample characterization involved reflected light microscopy and scanning electron microscope (SEM) imaging using a FEI Quanta 450 instrument operated in back-scattered electron (BSE) mode. Automated Mineralogy (AM) mapping on a Hitachi SU3800 SEM instrument was undertaken to provide the concentrations of component phases in one representative thin section from the upper limit of the orebody. All analyses were conducted with instrumentation housed at Adelaide Microscopy, the University of Adelaide.

Cathodoluminescence (CL) imaging of apatite grains was performed on a Hitachi SU7000 SEM with attached Delmic SPARC Spectral CL detector. Beam settings were 20 kV and ~20 nA. Due to intense long-lived emission in the red part of the spectrum, to avoid long dwell times needed for removal of "streaking" of images, PMT images of apatite grains were collected using the 450/50nm filter, then falsely coloured in Odemis Viewer.

Compositional data and X-Ray element mapping were obtained using a Cameca SX-Five electron probe microanalyzer (EPMA). Instrument specifications and the full list of elements analyzed along with primary and interference standards, typical minimum limits of detection, and further details of matrix correction procedures, are presented in Supplemental Materials.

Analysis of apatite U-Pb isotopes and trace elements was conducted simultaneously using a RESOlution-SE 193 nm Excimer laser-ablation system (Applied Spectra, USA) coupled to an Agilent 8900x quadrupole ICP-MS/MS (Agilent Technologies, USA), following Glorie et al

(2019). Apatite was analysed using a spot size of 30µm, repetition rate of 5Hz, and fluence of ~3.5 Jcm^{-2}. Each spot consisted of 30s of background analysis followed by 30s of acquisition, with standard bracketing every 30-40 unknowns. The U-Pb data were corrected for instrument drift, mass bias and fractionation using the primary reference Madagascar MAD apatite (474.25±0.41 Ma (Thomson et al., 2012). The $^{207}Pb/^{206}Pb$ ratios and trace element concentrations were calibrated against NIST610 (Jochum et al., 2011). Both the 401 apatite (530.3±3.5 Ma (Thompson et al., 2016) compared to 522±6 Ma $^{206}Pb/^{238}U$ weighted average, this study), and McClure apatite (523.1±1.47 Ma (Schoene and Bowring, 2006) compared to 514±7 Ma lower intercept age, this study), were used as secondary reference materials. LADR software (Norris and Danyushevsky, 2018) was used for data reduction for both U-Pb and trace element data. The U-Pb data requires a ^{207}Pb correction applied to both the primary Madagascar reference material and the 401 secondary standard apatite. This was done using the common Pb removal function in LADR which utilizes the Stacey and Kramers (1975) Pb evolution curve. Trace element data was processed using ^{43}Ca as the internal standard element.

LA-ICP-MS trace element mapping was conducted on five representative apatite grains across the area of interest with a beam size of 10 µm. Mapped intensities are scaled independently for each element to enhance different features. ^{43}Ca was selected as the internal standard, assuming ideal stoichiometry for apatite.

For Lu-Hf analysis, apatite crystals were selected that were sufficiently large to allow placement of a second ablation spot close to previous U-Pb craters. Analysis utilized a RESOlution LR 193 nm excimer laser-ablation system, coupled to an Agilent 8900 ICP-MS/MS, following protocols and analytical conditions described by Simpson et al. (2021). Apatite grains were ablated using laser diameters of 67-100 µm depending on their size with a repetition rate of 10 Hz and a fluence of 3.5 J/cm^2. The laser-based Lu–Hf method depends on reacting Hf with NH_3 reaction gas promoting the formation of $Hf(NH)(NH_2)(NH_3)_3$ in the reaction cell of the mass spectrometer. This allows isobaric interferences between ^{176}Hf and ^{176}Lu to be avoided by

analysing the high-order reaction products of ^{176}Hf and ^{178}Hf, respectively. Assuming natural abundances, ^{175}Lu and ^{178}Hf were monitored as proxies for ^{176}Lu and ^{177}Hf, respectively. For detailed descriptions of the method, the reader is referred to Simpson et al. (2021). Isotope ratios were calculated with a sample-standard approach in LADR (Norris and Danyushevsky, 2018). First, the $^{176}Lu/^{176}Hf$ and $^{177}Hf/^{176}Hf$ ratios were normalized to NIST 610 to correct for instrument drift and mass bias, and then corrected for matrix-induced fractionation (cf. Roberts et al., 2017) using the in-house apatite reference material Bamble (1097 ± 5 Ma, Glorie et al., 2024). The secondary reference materials, Harts Range (HR; corrected Lu–Hf age: 342 ± 2.8 Ma) and Wallaroo Range (corrected Lu–Hf age: 1557 ± 23 Ma), were checked for accuracy having good agreement with previously published data (344 ± 2 Ma and 1545 ± 26 Ma, respectively; Glorie et al., 2024; Simpson et al., 2021). Calculated LA-ICP-MS dates for all reference materials and both corrected and non-corrected ratios for samples can be found in Supplementary Data Table S4.

Results

Apatite petrography

Apatite is present in variable amounts and associations throughout the studied interval. Our sample selection comprises two examples from the host metabasalt and two examples from the magnetite-rich orebody, representative of the upper and lower limits thereof (Fig. 2A). Apatite is associated with magnetite and follows the rock foliation in most cases (Fig. 2B-F). Markedly, however, some of the coarsest grains of apatite occur along crosscutting fabrics/shears (in sample Jt4; Fig 2C). This contrasts with sub-rounded apatite grains embedded within sulphides generally oriented along the main rock fabric in the same sample. The greatest proportion of apatite (25.4 wt%), is recorded at the upper contact of the orebody (sample Jt7; Fig. 2D).

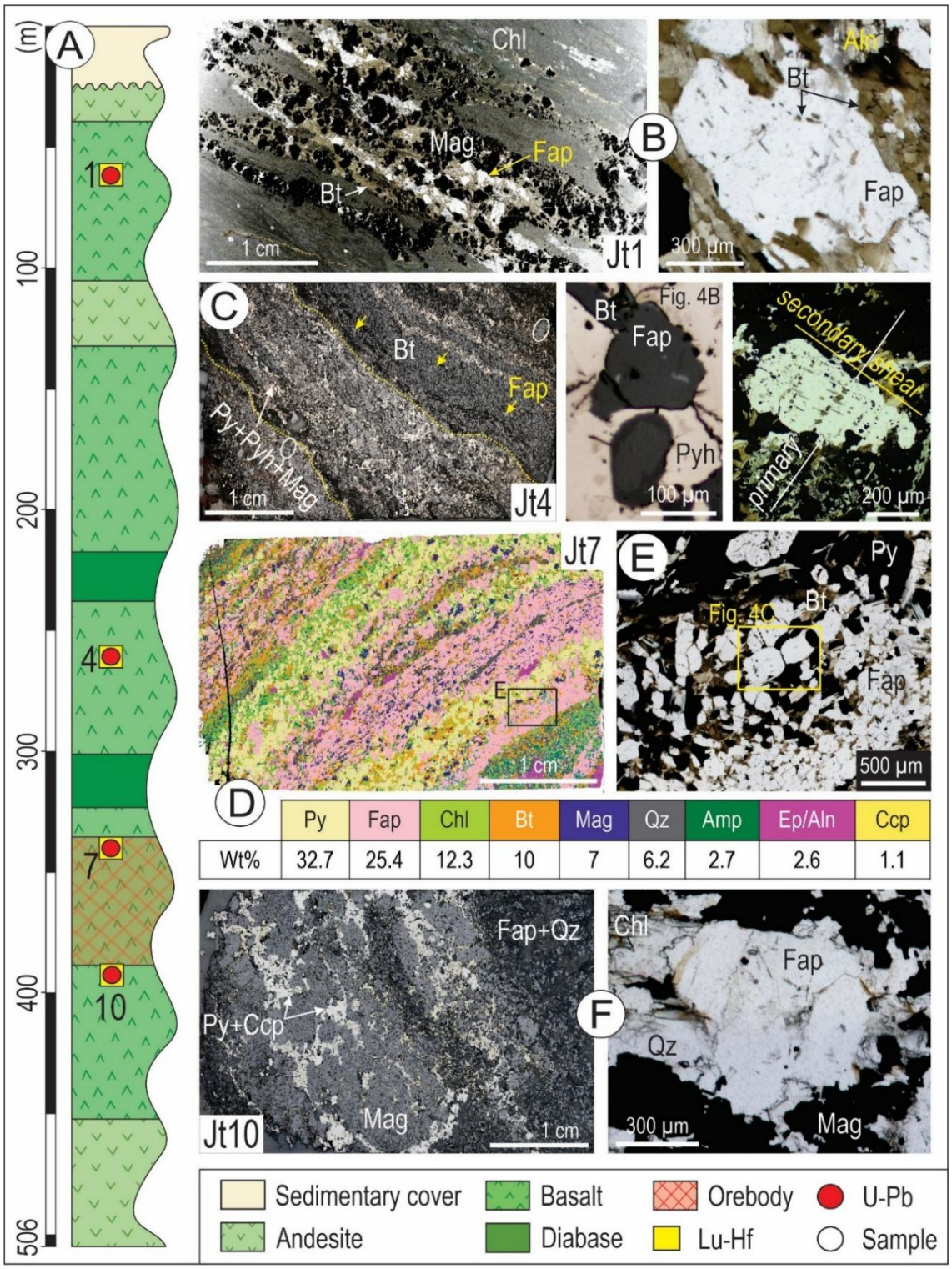

Figure 2. (A) Schematic stratigraphic column showing location of samples used in this study. (B-F) Petrographic aspects of host lithologies and fluorapatite (Fap) grains. Maps of thin sections (left of each figure) are in transmitted light (B) or reflected light (C and F). Detailed images of fluorapatite are all transmitted light microphotographs except for the central image in C, which is a reflected light microphotograph. (D) Automated mineralogy map showing constituent minerals in a thin section from the upper limit of the orebody. Mineral proportions (wt% basis) are given in the table underneath. Other abbreviations: Aln=allanite; Amp=amphibole; Bt=biotite; Ccp=chalcopyrite; Chl=chlorite; Ep=epidote; Mag=magnetite; Py=pyrite; Pyh=pyrrhotite; Qz=quartz.

In this case, apatite forms cm-sized bands, alternating with sulphides + biotite/chlorite + amphibole. Magnetite and epidote group minerals are scattered throughout the apatite bands. The apatite bands consist of tightly packed finer grains (up to ~150 μm) and margins with larger, randomly oriented, mostly (sub)euhedral grains (up to ~1000 μm) (Fig. 2E). In the other cases, apatite displays marginal corrosion and cataclasis, with the latter more advanced in sample Jt10 from the lower contact of the orebody (Fig. 2F).

Apatite composition, grain-scale heterogeneity and cathodoluminescence response

Data from EPMA reveal restricted compositional ranges with few minor elements present at concentrations significantly above minimum limits of detection. Trace impurities include Si, Mg, Fe, Ce and Y, which are elaborated on in greater detail below from corresponding LA-ICP-MS data. The SO_2 contents are below detection limits in almost all spot analyses. Calculated formulae fit to expected stoichiometry: Σ(F+Cl) ranges from 0.777 (Jt1) to 0.897 (Jt4), inferring 0.1-0.2 a.p.f.u. OH content. Supplementary Table S1A reports statistical data for each sample and selected line profiles across illustrated grains, while the complete dataset is given in Supplementary Table S1B. Most data plots along the Cl-OH tie-line on a ternary F-Cl-OH plot, close to the F-rich corner (Fig. 3A). The Cl-component is however richer in the sample furthest away from the orebody (Jt1), whereas the data for the other three samples overlap with one another (Fig. 3A). Fluorapatite from these samples shows up to 0.2 a.p.f.u. calculated OH, whereas the Cl-rich sample spans a range between 0.2 and a.p.f.u. 0.3 OH (Fig. 3B).

Cathodoluminescence (CL) imaging of fluorapatite shows patchiness with variable signal intensity in different parts of most grains (Fig. 3C-H). Commonly, however, zoning expressed as a (bright) core and (dark) rim is observed in most grains (Fig. 3C), although the Cl signal is disrupted by cataclastic deformation (Fig. 3E, F, H). A sub-population of grains appears relatively

opaque, irrespective of the host matrix, e.g., pyrrhotite or a mixture of biotite/chlorite (Fig. 3D, G).

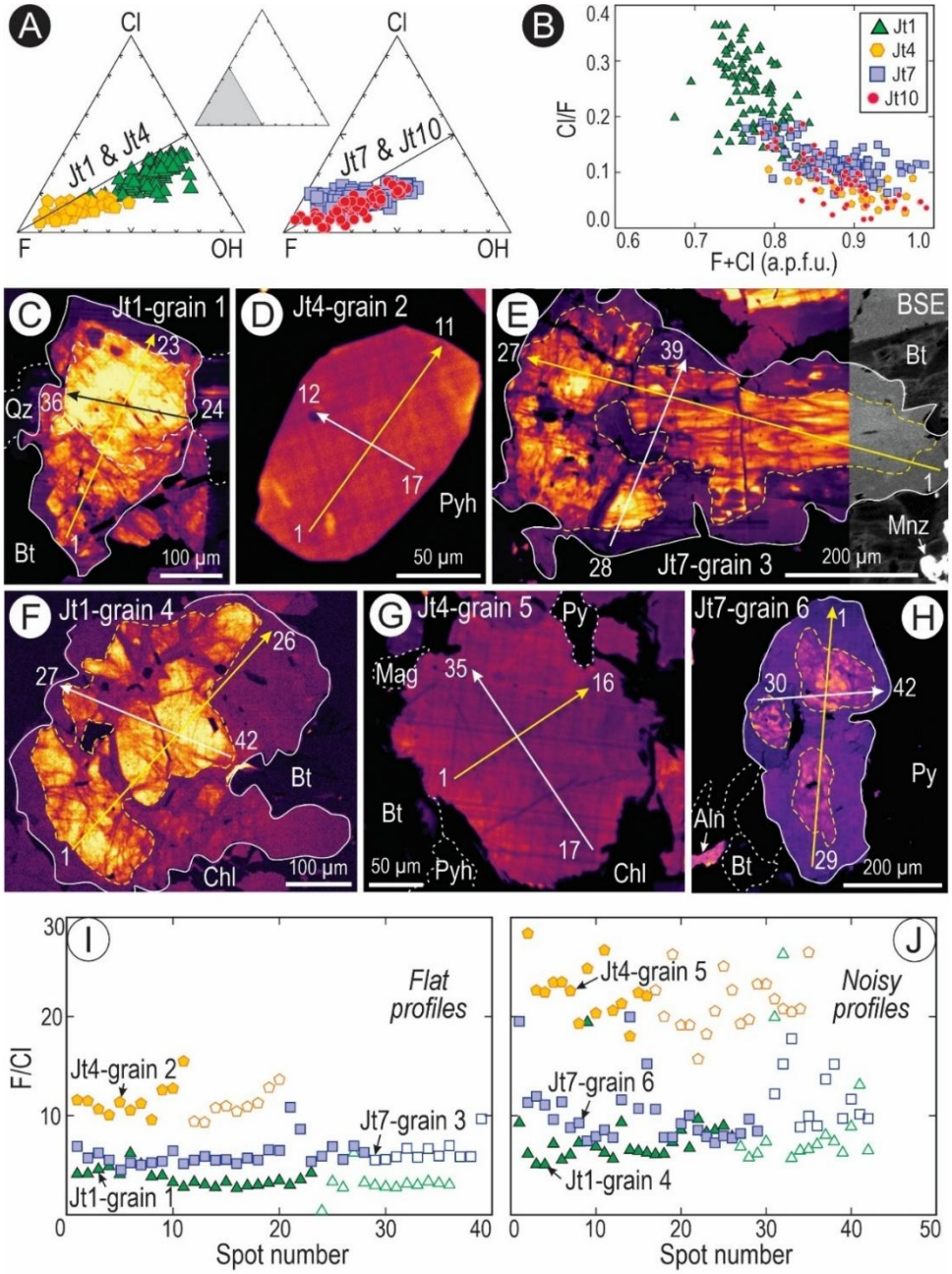

Figure 3. (A) Ternary plots of Cl, F, and (calculated) OH contents for basalt-hosted (Jt1 and Jt4) and ore apatite (Jt7 and Jt10). (B) Plots of (F+Cl) *vs.* Cl/F for apatite from the four samples. a.p.f.u.= atoms per formula unit. (C-H) CL images of apatite grains representing different textures (see text for additional explanation). (I, J) Plots of F/Cl obtained from EPMA spots taken along line profiles as marked by arrowed lines on (C-H). These show either flat (I) or noisy distributions (J). Note lack of direct correlation between the textures and the halogen ratios. The highest variability is from the F-richest grain #5 in Jt4, which displays a homogenous CL pattern. The grain with lowest F with flat profiles (Jt1 grain #1) displays strong CL heterogeneity. Spot numbers on X axes correspond to those marked at the ends of each profile on (C-H). Abbreviations: Aln=allanite; Bt=biotite; Chl=chlorite; Mag=magnetite; Mnz=monazite; Py=pyrite; Pyh=pyrrhotite; Qz=quartz.

Compositional profiles along and across fluorapatite grains with clear zonation on CL images show the relative proportions of halogens (F/Cl) can be both constant or erratic (Fig. 3I, J). The highest F/Cl ratios are recorded in opaque grains from sample Jt4 (Fig. 3D, G), whereas the lowest F/Cl values are noted in grains with complex CL responses (Jt1 and Jt7; Fig. 3C, E, F, H). Based on CL imaging and complementary EPMA data on the same grains, we conclude there is no direct correlation between F/Cl and CL signal intensity, other than the noise induced by fractures and other deformation features (e.g., Fig. 3H, J).

The grain-scale distribution of F and Cl, as well as the most abundant minor components (Ce and Y) is addressed by EPMA mapping of fluorapatite with variable textures from both host basalt and ore (Fig. 4A-D). Many grains from host basalt show overgrowths surrounding a deformed core that is relatively rich in Cl, Ce, and Y, but slightly depleted in F relative to the rim (Fig. 4A). Rounded grains embedded in sulphides show a patchy distribution of all these elements (Fig. 4B).

Core-to-rim compositional zoning expressed by the same elements is seen in fluorapatite from the ore samples (Fig. 4C). An unusual 'fibrous' texture is shown on the Cl and Ce maps, this feature is best explained by trails of sub-micron-sized grains of monazite. Xenomorphic fluorapatite displays Cl-rich, F-depleted domains (Fig. 4D). There is a weak correlation between Y and Cl within such patterns. These textures are indicative of (re)crystallization following syn-deformational dissolution.

Cathodoluminescence images for the textures described above show the bright areas correlate with high Ce and Cl for those grains with well-defined core-to-rim zoning (Fig. 4E). Bright domains on the CL images correlate with relative enrichment in Y, both in fluorapatite embedded in pyrrhotite and in recrystallized fluorapatite (Fig. 4F).

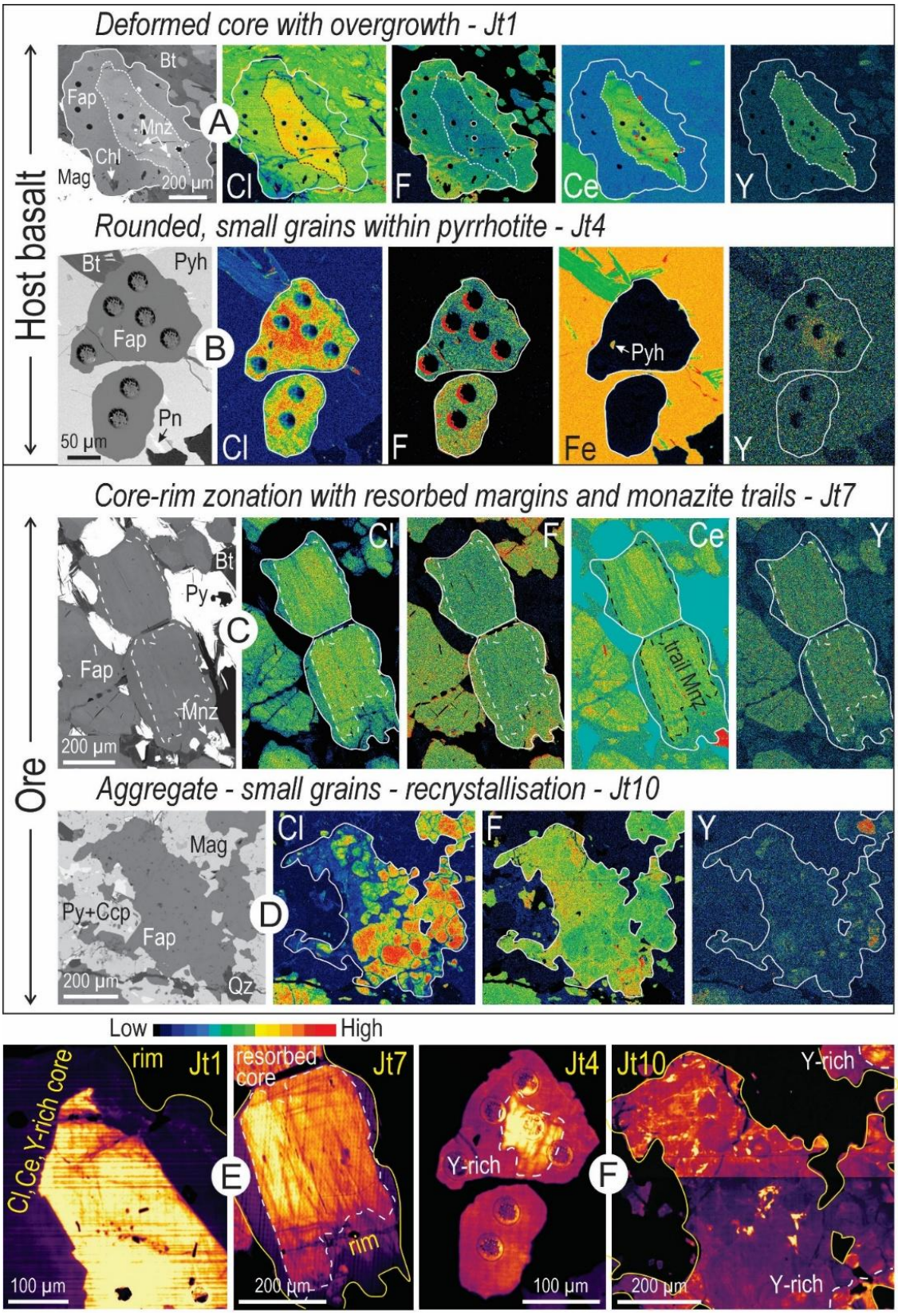

Figure 4. (A-D) BSE images (left) and EPMA element maps illustrating grain-scale distribution of Cl, F, Ce, Y, and Fe (B only). Element interference between Ce and Fe (from Fe-bearing minerals) affects Ce display. (E, F) CL images of the same apatite grains shown in (A-D). Abbreviations: Bt=biotite; Chl=chlorite; Ccp=chalcopyrite; Fap=fluorapatite; Mag=magnetite; Mnz=monazite; Pn=pentlandite; Py=pyrite; Pyh=pyrrhotite; Qz=quartz.

Supplementary Table S2 lists all LA-ICP-MS trace element data for fluorapatite in the four samples (n=572), including each individual REE and Y, as well as ΣREY, LREE (La+Ce+Pr+Nd), MREE (Sm+Eu+Gd+Tb+Dy) and HREE (Y+Ho+Er+Tm+Yb+Lu). ΣREY concentrations can reach thousands of ppm. The greatest enrichment is noted in samples Jt1 and Jt7 (mean ΣREY 3820 and 5120 ppm, respectively), whereas concentrations are more modest in apatite from samples Jt10 and Jt4 (mean ΣREY 2490 and 1990 ppm, respectively).

The relative enrichment in ΣHREE (Y-Lu) is notable, especially in sample Jt7 (mean 1700 ppm) and Jt1 (mean 1140 ppm), and actually higher than ΣLREE (La-Nd) in both Jt4 and Jt10 (570 and 490 ppm, respectively). In samples Jt1 and Jt7, ΣLREE (means 2160 and 2810 ppm, respectively) is slightly higher than ΣHREE. ΣMREE is typically some hundreds ppm in all samples, in the range from 230 ppm (sample Jt4) to 610 ppm (sample Jt7).

We also note typical concentrations of 200-300 ppm Sr, 300-400 ppm Mn, and at most a few tens of As in fluorapatite across all samples. All spot analyses contain measurable U and ^{206}Pb (each a few tens of ppm) as well as Th (<10 ppm to >100 ppm). Other elements, notably Si, Al, and Fe, are best interpreted as resulting from sub-surface inclusions of silicate minerals.

LA-ICP-MS element maps show the grain-scale distributions of REE and other trace elements in fluorapatite. All mapped examples show a consistent core-to-rim zoning (Fig. 5; SM Figure S1, S2). Grain cores are consistently enriched in REY, U, ^{206}Pb and Th, albeit with domains of relative LREE enrichment (Ce) that are conspicuously smaller than those of HREE (Y, Lu). The presence of included monazite and allanite is associated with LREE depletion within the grain (Fig. 5A, C). Notably, Sr is seen to be relatively enriched in F-richer domains within the rims (Fig. 5A, D and Fig. 4A, SM Figure S1, S2).

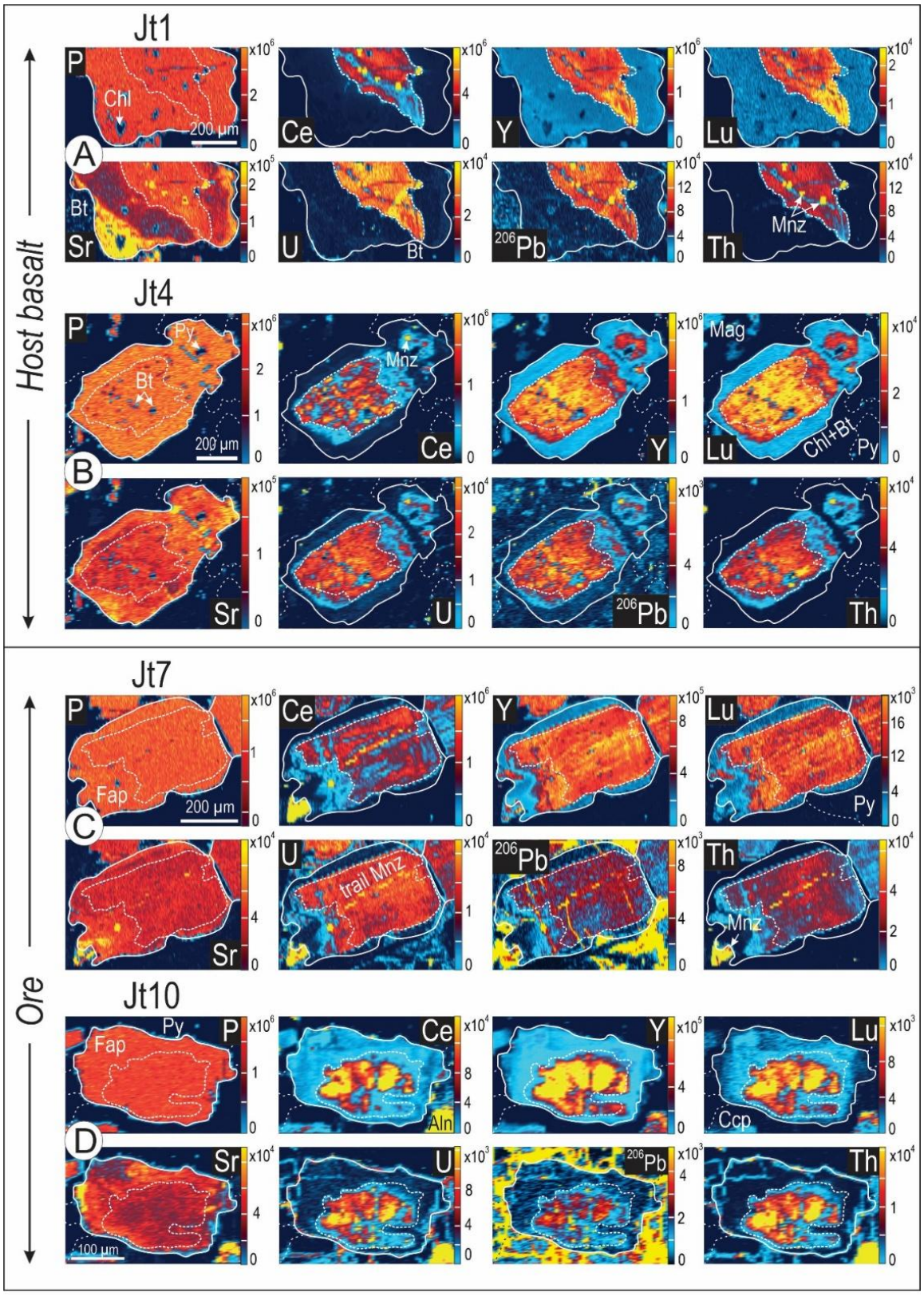

Figure 5. LA-ICP-MS trace element maps for selected elements in apatite from samples as labelled. Ce is used as a proxy for LREE and Y, Lu for HREE. Note the pronounced core-to-rim zonation expressed by REY, U, Pb, and Th distributions in all cases, albeit patchy in some grains (e.g., in ore apatite, D). Scales in counts-per-second. Abbreviations: Aln=allanite; Bt=biotite; Chl=chlorite; Ccp=chalcopyrite; Fap=fluorapatite; Mag=magnetite; Mnz=monazite; Py=pyrite.

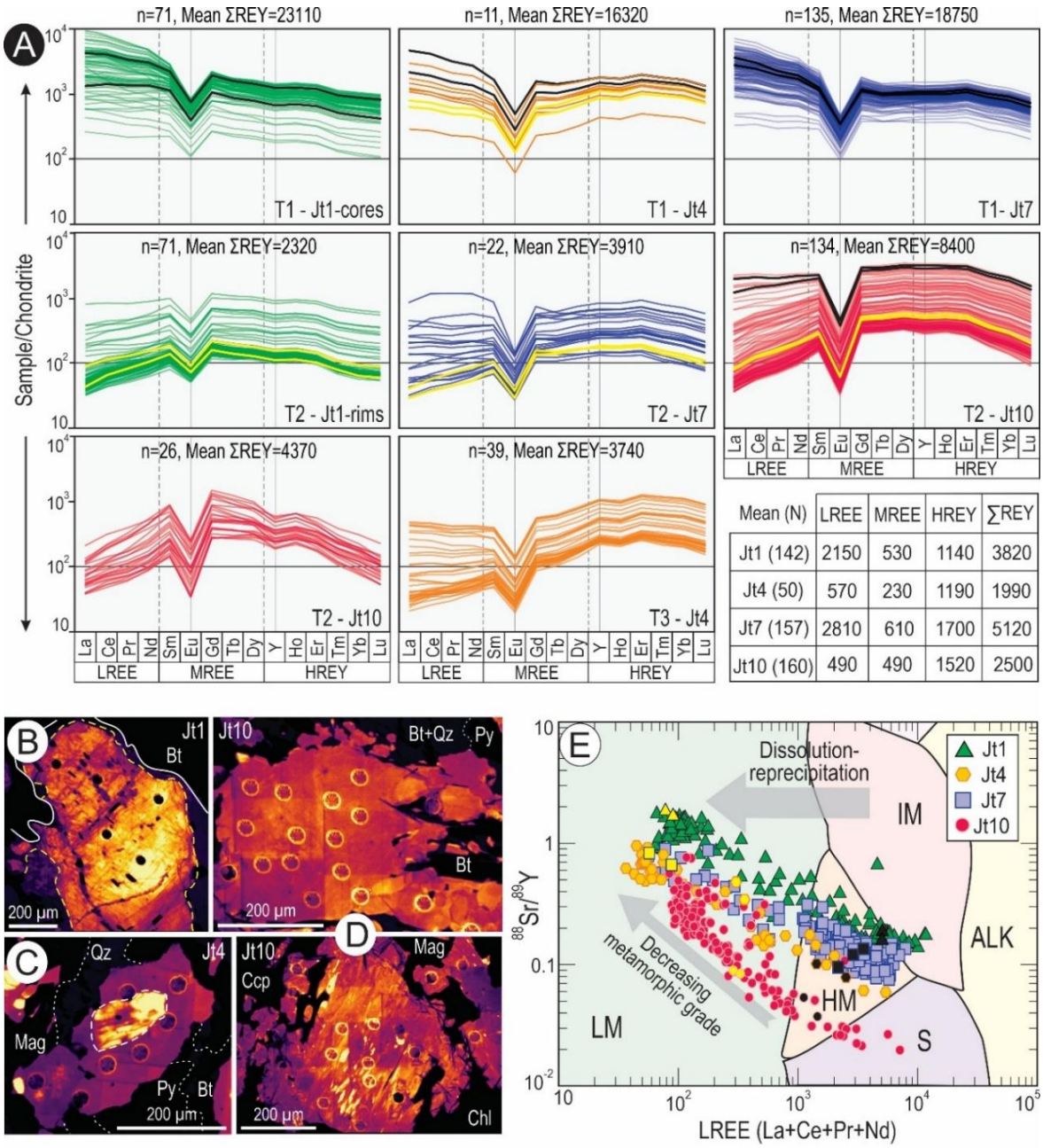

Figure 6. (A) Chondrite-normalized REY fractionation trends (T) for apatite from samples as labelled. N=all spot analyses; n=spot analyses representing specific trend types. Trends are defined as T1=LREE-enriched, T2=flat to MREE-enriched, and T3=HREE-enriched. (B-D) CL images of apatite grains representing different textures and trends: (B) T1-core and T2-rim in grains from JT1; (C), T1 and T3 in sample JT4; (D) T2 in sample JT10 with no obvious core-to-rim zonation. (E) Plot of LREE vs. Sr/Y with lithological discrimination fields from O'Sullivan et al. (2020) plotting data from SM Table S2. Field abbreviations: IM = mafic igneous rocks (and mafic I-type, granitoids); HM = high-grade metamorphic (partial-melts/leucosomes); LM = low-and medium-grade metamorphic and metasomatic; S = S-type granitoids (high aluminium saturation index "felsic" I-types); ALK = alkali-rich igneous rocks. The legend adopted in (E) corresponds to the colour code used for the fractionation diagrams in (A). Apatite data that plots in the HM and LM fields, and indicated by as black and yellow symbols, respectively, can have differing fractionation trends. HM apatite: T1 (Jt1, Jt4, Jt7) and T2 (Jt10), and LM apatite: T1 (Jt4) and T2 (Jt1, Jt7 and Jt10). Other abbreviations: Bt=biotite; Chl=chlorite; Ccp=chalcopyrite; Fap=fluorapatite; Mag=magnetite; Mnz= monazite; Py=pyrite; Qz=Quartz.

Chondrite-normalized REY fractionation patterns

Chondrite normalized REY fractionation patterns (Fig. 6A) fall into three distinct groups: (1) LREE-rich, (2) flat to MREE-rich, and (3) LREE-depleted and HREE-rich. Irrespective of grouping, all patterns display a pronounced negative Eu anomaly.

Trends (1) and (2) are the most common and are present in three of the four samples, albeit in different combinations. Trend (1) is noted in in J1, Jt4, and Jt7, and Trend (2) in Jt1, Jt7, and Jt10. Trend (3) appears unique to sample Jt4. Sample Jt10 (ore) lacks both Trends (1) and (3) but displays a transition from a flat to a pronounced MREE-rich trend for Trend (2). Trend (1) and (2) are typical of core and rims, respectively, which is particularly well expressed in grains from samples Jt1 (Fig. 6B) and Jt7. A combination of trends (1) and (3) is recorded in grains from sample Jt4 (Fig. 6C). In sample Jt10, trend (2) is obtained from grains without obvious core-to-rim zoning (Fig. 6D).

On a plot of Sr/Y vs. LREE (Fig. 6E), we note that each sample forms a continuous downwards-sloping cluster with roughly comparable slope, although slightly steeper for sample Jt10. The datasets for the four samples straddle the fields of high- and low-metamorphism/metasomatism (HM and LM, respectively), as defined by O'Sullivan et al. (2020). Points plotting within the two fields may represent apatite with a single fractionation trend (e.g., Trend (1) in sample Jt4). In contrast, points from samples Jt1 and Jt7 plotting within the HM and LM fields represent fractionation Trends (1) and (2), respectively.

U-Pb isotope data

Apatite U-Pb data are presented on Terra-Wasserburg (T-W) concordia plots (Figure 7). The different colours of ellipses on the figure represent differing La/Yb ratios. These ratios cover a wide range in sample Jt1, but are mostly towards the lower end of this range in the other samples, albeit with occasional individual spots with elevated La/Yb (Fig. 7A-D).

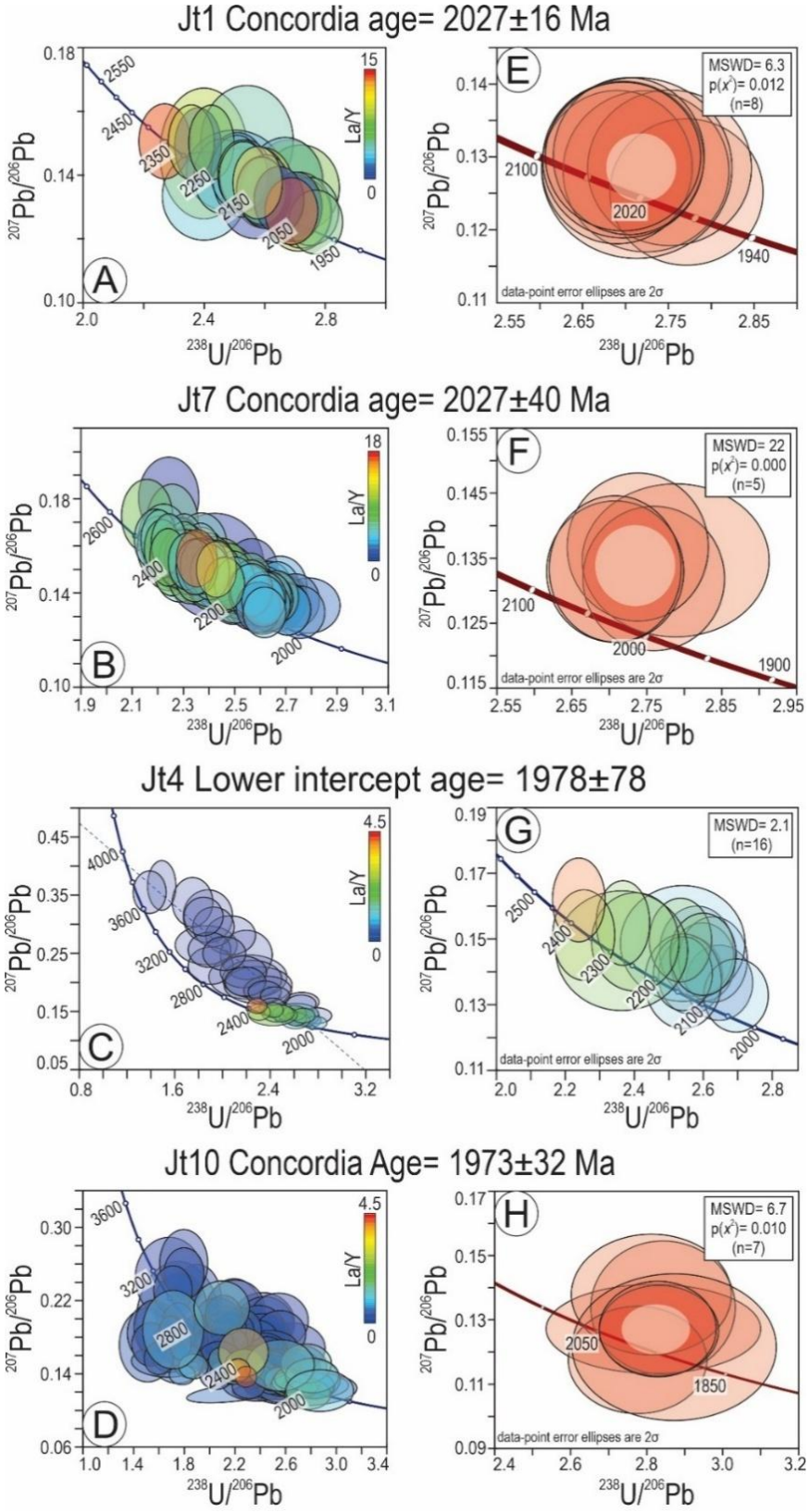

Figure 7. (A-D) U-Pb Tera-Wasserburg diagrams for all apatite data (SM Table S3) split by sample as labelled. Intercept date uncertainties are internal (analytical) followed by fully propagated systematic uncertainties. All samples are un-anchored isochrons, sample Jt4 represents a lower intercept age on concordia. (E-H) Data points selected for age calculation as labelled. MSWD= mean squared weighted deviation and P(x^2)=Chi-squared probability for a single data population. La/Y is plotted on a log scale.

Correlation between La/Yb ratios with their position on the T-W concordia varies, younger ages typically correspond to higher La/Yb in samples JT4 and 10, whereas the opposite is true in sample Jt4 (Fig. 7B-D). In sample Jt1 La/Yb ratios are spread along the entire age interval for this sample (Fig. 7A).

Based on the correspondence between $^{238}U/^{206}Pb$ and $^{207}Pb/^{206}Pb$ (Table 1 and SM Table S3A), we selected a cluster of points for calculation of ages (Fig. 7E-H). The ages for samples Jt1, Jt7, and Jt10 were determined by selecting the youngest concordant population and calculating concordia ages based on this choice. The ages obtained are 2027±16, 2027±40 and 1972±32 Ma for Jt1, Jt7, and Jt10, respectively. In contrast, ages for sample Jt4 showed a spread of data that allowed a discordia line to be fitted through the data and calculation of a lower intercept age at 1978±78 Ma. Importantly, the spread of ellipses along concordia are seen to represent a partial resetting event. Therefore, the samples with calculated ages via concordia ages are interpreted to represent 'maximum' ages for the resetting event, whereas the age estimated for Jt4 by the lower intercept method may record a more accurate age for the resetting. Altogether, the ages overlap within uncertainty.

Lu-Hf isotope data

Inverse Lu-Hf isochrones for apatite in each sample are shown in Figure 8A-E. The data is summarized in Table 1 and given in full in SM Table S4. Unfilled ellipses either have very low Lu contents or variable common Hf and/or inclusions of other minerals. The data for sample Jt1 is split into two distinct groups; Jt1-c (grain cores); and Jt1-r (grain rims), which correspond to mean Σ(La+Ce+Nd+Sm) of 6000 ppm and 430 ppm, respectively. The Lu-Hf apatite age of Jt1-c is 2527±17 Ma, slightly older (by ~40 Ma) than the ages obtained for apatite in samples Jt7 (2489±12 Ma) or Jt10 (2483±18 Ma). The Jt7 and Jt10 ages overlap within uncertainty (Fig. 8A-

C). The isotopic dispersion for the Lu-Hf dataset is smaller than for the U-Pb data (range MSWD = 2.3–4.4).

The data for Jt1-r gives a younger age (2438±59 Ma) and displays a low isotopic dispersion (MSWD = 2.6; Fig. 8D). This age overlaps within uncertainty with Jt7 and Jt10, but not with that of Jt1-c. The youngest age, from sample Jt4 (2384±19 Ma, MSWD = 6; Fig. 8E), overlaps at 2σ error with the age for the Jt1-r subgroup.

The data used for calculation of Lu-Hf ages (coloured ellipses) is plotted on the apatite trace element discrimination diagram (Fig. 8F). The data for the Jt1-c and Jt1-r sub-groups plot in distinct fields, suggesting a transition from high metamorphism/partial melt (HT) to low metamorphism/ metasomatism (LM) protoliths during the interval 2527±17 to 2438±59 Ma. A subgroup of points typifying older apatite cores in sample Jt1 plot within the igneous mafic (IM) field, coincident with an interpretation in the trace element signature of JI1-c apatite is, at least partially, inherited from host basalts, or the magmatic source for these rocks.

In contrast, the younger, ~2.48 Ga age representing grains of ore apatite in samples Jt7 and Jt10 (2489±12 and 2483±18 Ma) is associated with trace element signatures falling within either the HM (Jt7) or LM (Jt10) fields, albeit with a scatter of points from each sample across both domains (Fig. 8F). In this case, the data represent the ‘bulk’ of the apatite grains in which no well-defined core-to-rim textures are preserved (e.g., Fig. 4E, F).

The youngest apatite (sample Jt4, 2384±19 Ma) is characterized by trace element signatures that plot across the same HM and LM fields. For these samples, data points were obtained either from larger grains that crosscut the rock foliation (Fig. 2C) or from smaller grains without any zonation on CL images (Fig. 3D, G).

Table 1. New apatite age data and selected published geochronological data for mineral deposits in the Carajás Domain

Deposit	Mineral	Technique	Method	Sample	Age (Ma)	2σ	MSDW (n)
Jatobá	Apatite	LA-ICP-MS	Lu-Hf	Jt1 - outside ore - cores	2527	17	2.3 (30)
Jatobá	Apatite	LA-ICP-MS	Lu-Hf	Jt7 - upper ore limit	2489	12	6.0 (50)
Jatobá	Apatite	LA-ICP-MS	Lu-Hf	Jt10 - lower ore limit	2483	18	3.5 (26)
Jatobá	Apatite	LA-ICP-MS	Lu-Hf	Jt1 - outside ore - rims	2438	59	2.6 (12)
Jatobá	Apatite	LA-ICP-MS	Lu-Hf	Jt4 - outside ore	2384	19	4.4 (25)
Jatobá	Apatite	LA-ICP-MS	U-Pb	Jt1 - outside ore	2027	16	6.3 (8)
Jatobá	Apatite	LA-ICP-MS	U-Pb	Jt7 - upper ore limit	2027	40	2.1 (6)
Jatobá	Apatite	LA-ICP-MS	U-Pb	Jt4 - outside ore	1978	78	22 (30) lower intercept
Jatobá	Apatite	LA-ICP-MS	U-Pb	Jt10 - lower ore limit	1973	32	6.7 (7)

No.*	Deposit/Orebody	Mineral	Technique	Method	Sample	Age (Ma)	2σ	Reference
1	Jaguar Sul	Apatite	LA-ICP-MS	U-Pb	Alteration-mineralization in porphyritic subvolcanic rock	2187	83	Hernández-Tasco et al (2023)
1	Jaguar Sul	Apatite	LA-ICP-MS	U-Pb	In quartz and chlorite halos	1896	62	Hernández-Tasco et al (2023)
1	Jaguar Sul	Apatite	LA-ICP-MS	U-Pb	In quartz and chlorite halos	1882	44	Hernández-Tasco et al (2023)
1	Onça Preta	Apatite	LA-ICP-MS	U-Pb	Associated with magnetite, talc, cumingtonite and pyrite	1840	36	Hernández-Tasco et al (2023)
2	Sequeirinho	Monazite	LA-ICP-MS	U-Pb	As inclusion in apatite	2712	4.7	Moreto et al (2015a)
3	Sequeirinho	Allanite	SHRIMP	U-Pb	In clasts of apatite-actinolite-magnetite in chalcopyrite mat	2691	23	Smith (2023)
3	Sequeirinho	Allanite	SHRIMP	U-Pb	In clasts of apatite-actinolite-magnetite in chalcopyrite mat	2468	69	Smith (2023)
3	Sequeirinho	Apatite	LA-ICP-MS	Sm-Nd	Apatite from chalcopyrite veins	2090	54	Smith (2023)
2	Pista	Molybdenite	TIMS	Re-Os	Silicified volanic rock - ore	2710	11	Moreto et al (2015a)
2	Pista	Molybdenite	TIMS	Re-Os	Na-altered volcanic rock - ore	2685	11	Moreto et al (2015a)
3	Sossego	Apatite	LA-ICP-MS	Sm-Nd	Apatite from chalcopyrite veins	2150	170	Smith (2023)
3	Sossego	Apatite	LA-ICP-MS	Sm-Nd	Apatite from chalcopyrite veins	2059	98	Smith (2023)
2	Sossego	Monazite	SHRIMP	U-Pb	Chalcopyrite fragments from the ore breccia	1904	5.2	Moreto et al (2015a)
2	Sossego	Monazite	SHRIMP	U-Pb	Chalcopyrite fragments from the ore breccia	1879	4.1	Moreto et al (2015a)
2	Curral	Monazite	SHRIMP	U-Pb	In apatite and chalcopyrite fragments from the ore breccia	1890	8.5	Moreto et al (2015a)
4	Bacaba	Monazite	LA-ICP-MS	U-Pb	In altered and silicified albite, Serra dourada granite	2720	15	Moreto et al (2015b)
4	Bacaba	Monazite	LA-ICP-MS	U-Pb	As inclusions in apatite in bacaba tonalite	2681	20	Moreto et al (2015b)
3	Bacaba	Allanite	SHRIMP	Sm-Nd	In clasts of apatite-actinolite-magnetite in chalcopyrite mat	2551	140	Smith (2023)
4	Bacaba	Monazite	LA-ICP-MS	U-Pb	As inclusions in apatite in bacaba tonalite	2060	9.6	Moreto et al (2015b)
4	Bacuri	Molybdenite	TIMS	Re-Os	Molybdenite with chalcopyrite vein cutting granite	2758	11	Moreto et al (2015b)
4	Bacuri	Monazite	LA-ICP-MS	U-Pb	As inclusion in altered chlorite	2703	6.2	Moreto et al (2015b)
5	Igarapé Bahía	Molybdenite	Triton MS	Re-Os	Molybdenite in massive magnetite and chalcopyrite	2627	11	Perelló et al (2023)
6	Igarapé Bahía	Monazite	SHRIMP	U-Pb	Magnetite breccias	2575	12	Tallarico et al (2005)
7	Igarapé Bahía	Monazite	SHRIMP	U-Pb	Low grade ore associated with chalcopyrite and magnetite	2559	34	de Melo et al (2019)
8	Salobo	Molybdenite	ID-NTIMS	Re-Os	Molybdenite vein with bornite+magnetite	2576	8	Réquia et al (2003)
8	Salobo	Molybdenite	ID-NTIMS	Re-Os	Molybdenite vein with bornite+magnetite	2562	8	Réquia et al (2003)
9	Salobo	Monzazite	LA-ICP-MS	U-Pb	Almandine-grunerite-biotite-magnetite rich rocks	2452	12	de Melo et al (2017)
10	Gameleira	Molybdenite	ID-NTIMS	Re-Os	Minerlization associated with biotite alteration	2614	14	Marschik et al (2005)
10	Serra Verde	Molybdenite	ID-NTIMS	Re-Os	Mineralised vein with chalchopyrite	2609	13	Marschik et al (2005)
10	Garimpo Fernando	Molybdenite	ID-NTIMS	Re-Os	Massive ore lense of chalcopyrite	2602	13	Marschik et al (2005)
10	Garimpo Fernando	Molybdenite	ID-NTIMS	Re-Os	Associated with mineralization (unlocated- weathering pro	2592	13	Marschik et al (2005)
11	GT46	Molybdenite	ID-NTIMS	Re-Os	Amphibolite	2711	9	Silva et al (2005)
11	GT46	Monazite	LA-ICP-MS	U-Pb	Gray granitoid (Mineralization II)	2612	1.5	Silva et al (2005)
11	GT46	Molybdenite	ID-NTIMS	Re-Os	Granite (Mineralization II)	2600	8	Silva et al (2005)
11	GT46	Molybdenite	ID-NTIMS	Re-Os	Pegmatitic granite	2557	8	Silva et al (2005)
11	GT46	Molybdenite	ID-NTIMS	Re-Os	Pegmatitic granite	2554	8	Silva et al (2005)
12	GT46	Molybdenite	LA-ICP-MS	Re-Os	Pegmatitic granite (Later hydrothermal veins)	2503	51	Toledo et al (2019)
12	GT46	Molybdenite	LA-ICP-MS	Re-Os	Intensely chloritized rock (Later hydrothermal veins)	2449	44	Toledo et al (2019)

*numbering refers to Figure 10

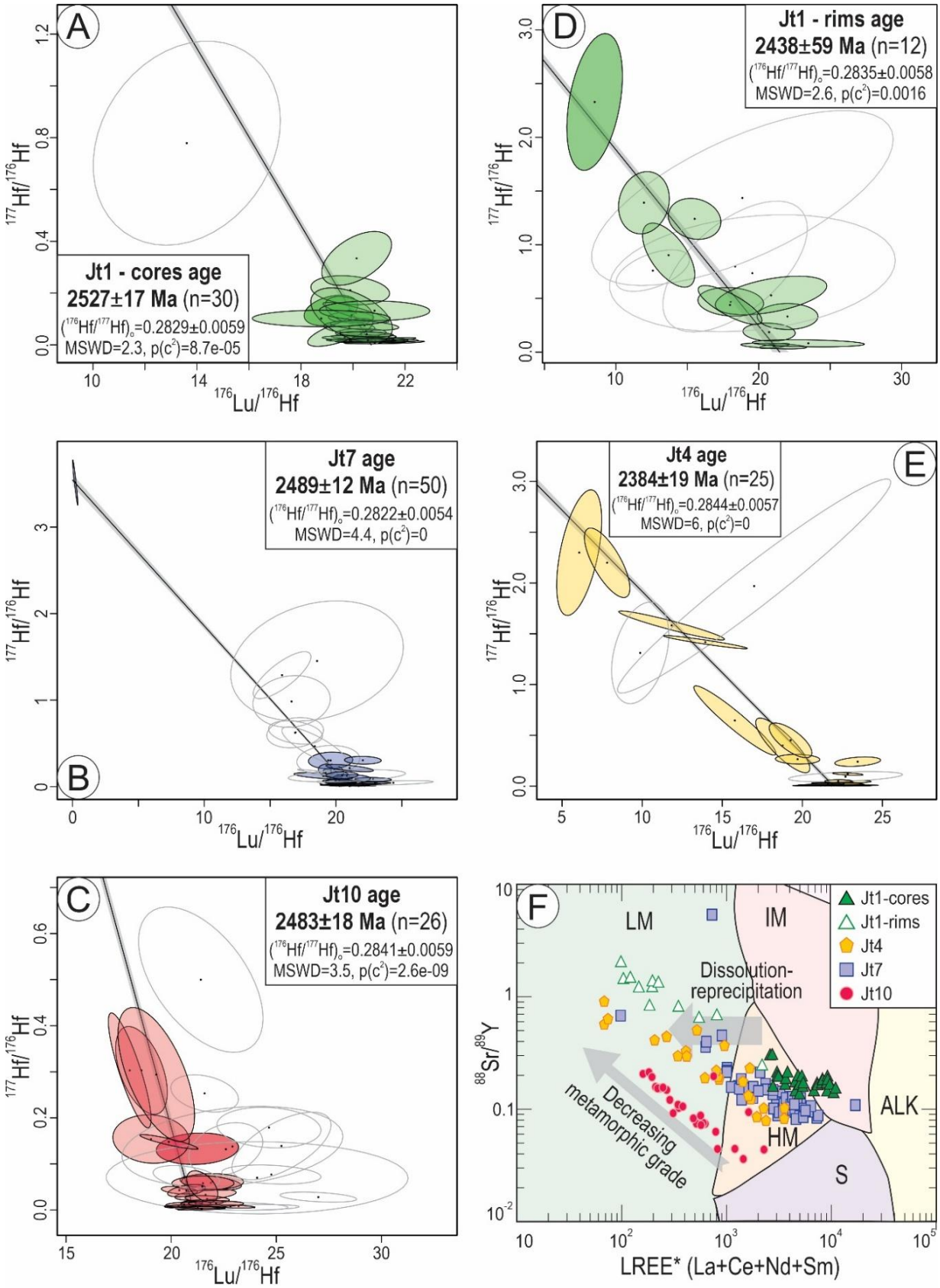

Figure 8. (A-E) Apatite LA–ICP–MS/MS Lu–Hf isochrons for each sample/category as labelled (data in SM Table S4). Unfilled uncertainty ellipses (2σ) represent those excluded from the age calculations. (F) Plot of LREE(La+Ce+Nd+Sm) vs. Sr/Y with lithological discrimination fields from O'Sullivan et al. (2020) for apatite dated by Lu-Hf. Field abbreviations as in Figure 6E.

Discussion

Comparing the U-Pb and Lu-Hf age data

The fluorapatite grains studied here display a wide size range (from tens of μm up to as large as 1 mm) and varied textures (Figs. 2-5, 6B-D), which generally show no correlation with distinct age groups. An exception to this is the Lu-Hf dating of core-to-rim zonation in apatite grains from sample Jt1 (2527±17 Ma core age, 2438±59 Ma rim age; Fig. 8A, D).

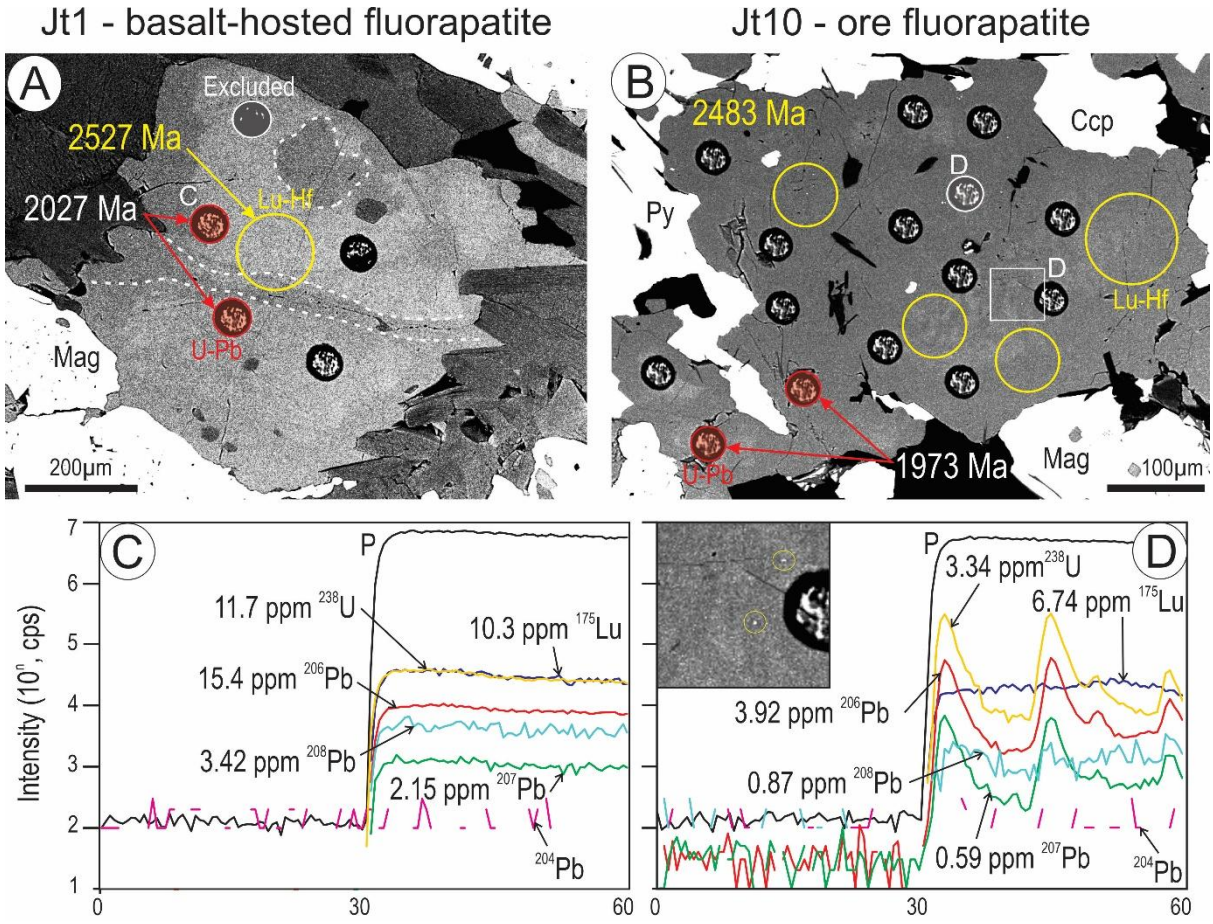

Figure 9. BSE images (A, B) and time-resolved LA-ICP-MS depth profiles (C, D) showing grain-scale differences between Lu-Hf and U-Pb ages in fluorapatite. (A, C) Grain representative of REY-rich cores (dated by Lu-Hf method) and domains of U-Pb re-equilibration. The dashed line indicates fractures and areas of low REY (darker). Note that U and Pb isotopes signals are relatively smooth despite spot analyses being close to a fracture. (B, D) Grain illustrating open U-Pb system behaviour in areas with sub-micron-scale U-, Pb-bearing inclusions (inset in D). Ragged signals for U and Pb isotopes infer the presence of the inclusions. A couple of LA-ICP-MS spots show U-Pb re-equilibration. Abbreviations: Ccp=chalcopyrite; cps=counts-per-second; Mag=magnetite; Py=pyrite.

A combination of older Lu-Hf ages and younger U-Pb ages recorded in the apatite grains is not an uncommon phenomenon and is readily explained by the very different closure temperatures of the two isotope systems: 660–730 °C for Lu-Hf (e.g., Glorie et al., 2022) compared with 375–550 °C for U-Pb (e.g., Schone and Bowring 2007; Chew et al., 2011).

Interpretation of ages - primary versus overprint?

To explain the major age differences between the two geochronometers in a single apatite grain (Fig. 9), we need to assess the ages in the context of the wide variation in intragrain textures and geochemical signatures (Figs. 3-6). The lack of any oscillatory zoning exposed on the CL, EPMA or LA-ICP-MS maps rules out a genuine or preserved igneous origin for Jatobá fluorapatite. The patchy character of many fluorapatite grains can be associated with fracture-induced brecciation. Analogous textures are reported from apatite in other breccia-hosted IOCG deposits, e.g., Ernest Henry, Cloncurry District, Australia (Steadman et al., 2022). The peculiar 'fibrous' patterns we observe in Jatobá apatite (Figs. 3E, 4C, E), closely match the 'tiger-striped' CL-patterns in apatite from amphibolite to granulite gneisses (Main Mylonites, Northern Pyrenees; Odlum and Stockli, 2020). These authors interpreted the patterns in terms of dynamically recrystallized apatite, recording LREE-enriched fractionation trends and younger U-Pb ages. The tiger-striped Jatobá apatite, however, records different REE trends (T1-T3 on Fig. 6).

The Lu-Hf age of fluorapatite in sample Jt1 (~2527 Ma) cannot be reconciled with the age of host Itacaiúnas basalts (~ 2.75-2.76 Ga; e.g., Machado et al., 1991; Martins et al., 2017), even though a subgroup of fluorapatite plots within the igneous mafic field on Fig. 8F, pointing to the possibility of preserved magmatic apatite at Jatobá. Indeed, a mafic igneous signature is inferred from the relatively high-Cl content in fluorapatite from this sample (Fig. 3A, B) by comparison with overviews of halogens in magmatic apatite (Webster and Piccoli, 2015).

This apatite subgroup with a Lu-Hf age of ~2527 Ma plots in the HM field on the same figure and is thus correlated with formation during metamorphism at the high P-T conditions (~700 °C and ~7.5–6.8 kbar) evidenced in Campo Rodriguez et al. (2024; in review). Such an interpretation is reinforced by the deformation-induced textures we have illustrated (e.g., Fig. 4A). If this interpretation is correct, then the age of apatite inheriting an igneous mafic signature represents metamorphic recrystallization, likely via thermally activated volume diffusion, as has been suggested for apatite in metamorphosed granites and mafic rocks from South Australia (Glorie et al., 2024; Brown et al., 2024). Following on from this, the younger Lu-Hf ages of overgrowths (~2438 Ma) can be assigned to formation via dissolution-reprecipitation at lower metamorphic and/or metasomatic conditions ('LM' field on Fig. 8F).

The notable spread across the HM to LM fields shown by the 2489–2483 Ma fluorapatite associated with ore (Fig. 8B, C. F) suggests that dissolution-reprecipitation and dynamic recrystallization processes, evidenced by the patchy and fibrous/tiger-striped textures, controlled apatite (re)crystallization during a prograde-to-retrograde metamorphic cycle, constrained here as having a duration of some tens of Ma.

The Lu-Hf age of 2384 Ma from fluorapatite in sample Jt4 (Fig. 8E, F) could be viewed as a later episode of apatite growth via comparable processes (grains crosscutting foliation; Fig. 2C). The veracity of this age, ca 140 Ma younger than the metamorphic event postulated above, should however, be viewed as debatable given that it appears unique to this sample. The age might, perhaps best be considered as a minimum age for the same event rather than a distinct episode.

The younger U-Pb ages (2027-1973 Ma) obtained in this study are attributable to a distinct event during which the U-Pb isotopic system has re-equilibrated. Apatite associated with mylonitization in the Pyrenees (the tiger textures mentioned above) has shown that deformation and Pb* loss (isotopically reset) are coeval with one another and thus the U-Pb ages directly represent the timing of ductile deformation (Odlum et al., 2022).

Comparison with radiometric ages for other deposits in the Carajás Province

In Figure 10 we present our new geochronological data for Jatobá alongside a compilation of ages for mineralization obtained utilizing a range of different mineral geochronometers, including those that are considered highly robust and accurate notably the Re-Os molybdenite geochronology (Stein et al., 2002). We included all ages obtained from apatite, to compare with our results, as well as monazite and allanite ages well constrained relative to ore. A comprehensive review of all geochronological data is presented in Trunfull et al. (2020).

The two age intervals we have obtained for fluorapatite: Lu-Hf 2527-2384 Ma and U-Pb 2027-1973 Ma, are both younger than the estimated age of host lithologies in the Itacaiúnas Supergroup (2760-2730 Ma; Fig. 10).

For purposes of comparison, our compilation includes several deposits within the same cluster as Jatobá (Fig. 1A). The oldest ages are reported from the Bacuri and Bacaba deposits, ~15 km southeast from Jatobá, hosted within Mesoarchean granite intruded by Neoarchean mafic/ultramafic rocks (Moreto et al., 2015b). At Bacuri, the oldest Re-Os molybdenite age (2758 Ma) is obtained from deformed chalcopyrite veinlets crosscutting granite and is considered to pre-date a main ore stage, which is dated at 2703 Ma (U-Pb monazite). At Bacaba, U-Pb monazite ages of 2720-2681 Ma are considered as distinct mineralising episodes (Moreto et al., 2015b). Closer still to Jatobá, the Sequeirinho and Pista deposits at the contact between Neoarchean gabbronorite and Mesoarchean granite (Fig. 1B), show similar old ages as Bacuri and Bacaba (2712-2685 Ma; Moreto et al., 2015b; Smith, 2023).

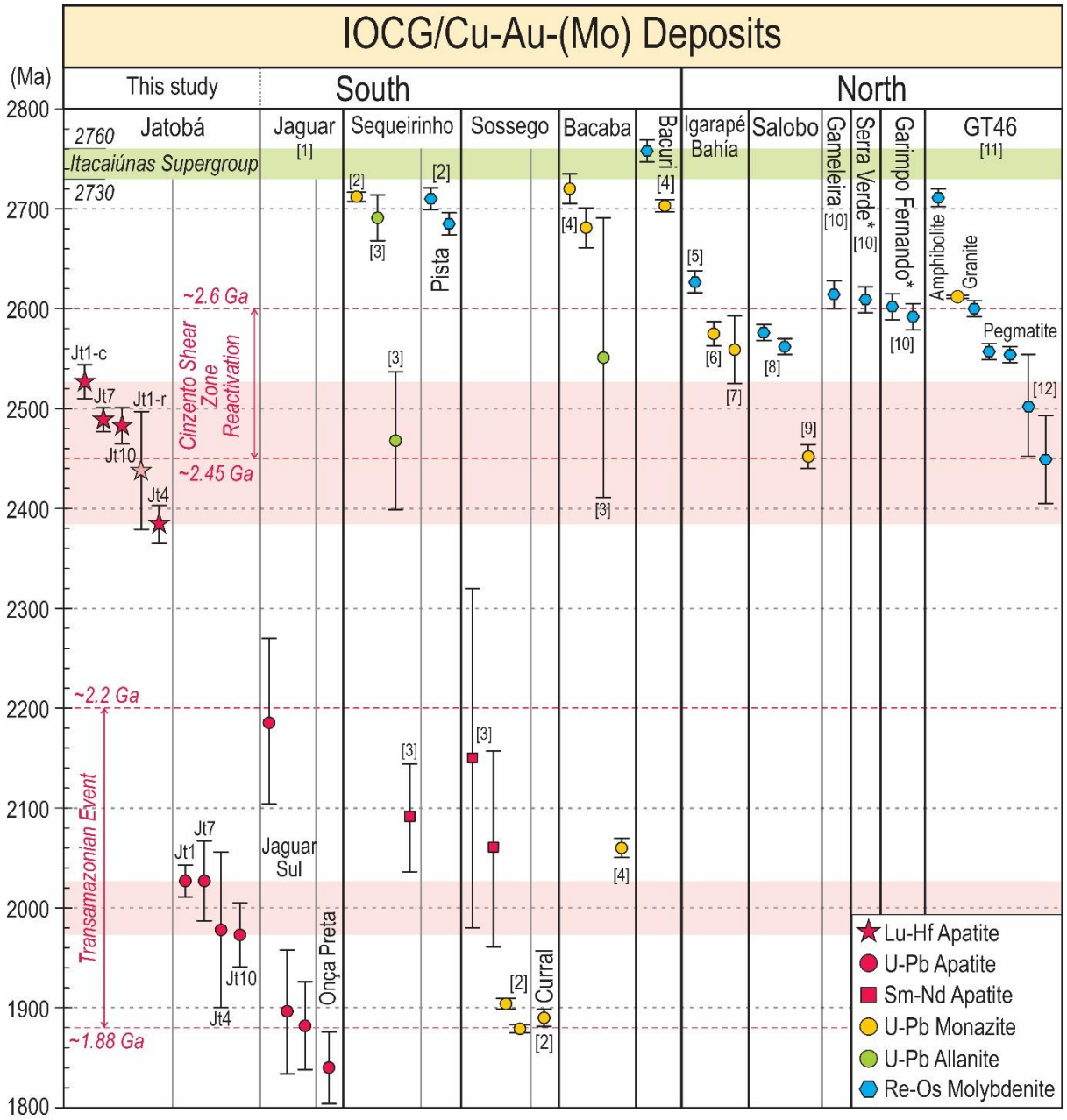

Figure 10. Summary of selected geochronological data for IOCG/Cu-Au-(Mo) deposits from the northern and southern parts (Copper Belts) of the Carajás Domain. Data tabulated in Table 1. See text for additional comments. [1] Hernández-Tasco et al. (2023), [2] Moreto et al. (2015a), [3] Smith (2023), [4] Moreto et al. (2015b), [5] Perelló et al. (2023), [6] Tallarico et al. (2005), [7] de Melo et al. (2019), [8] Réquia et al. (2003), [9] de Melo et al. (2017), [10] Marschik et al. (2005), [11] Silva et al. (2005), [12] Toledo et al. (2019).

Although a couple of younger U-Pb allanite ages (2468 and 2551 Ma) are reported for Sequeirinho and Bacaba (Smith, 2023), surprisingly perhaps, the best correlation with the ~2.5 Ga age at Jatobá is seen at a number of deposits in the north of the Carajás Domain (e.g., Salobo

and GT46; Fig. 10). Re-Os molybdenite ages for the Salobo deposit lie within the interval 2576-2562 Ma (Requia et al., 2003). U-Pb monazite ages for the same deposit give a slightly younger 2452 Ma age (Melo et al., 2017), which was considered an overprint produced by hydrothermal activity. Ages for the Igarape Bahia/Alemao orefield are comparable to those from Salobo: an older Re-Os molybdenite age (2627 Ma; Perelló et al., 2023) and younger U-Pb monazite ages of 2575 Ma (Tallarico et al., 2005) and 2559 Ma (Melo et al., 2019). The latter authors interpret these monazite ages to represent the timing of IOCG mineralization, which overprinted an older copper mineralization of syngenetic-exhalative type. In contrast, Perelló et al. (2023) consider the younger monazite ages in terms of "resetting due to regional fluid and thermal activity". Further emphasizing the importance of a widespread metallogenetic event at ~2.6 Ga, younger than Itacaiúnas Supergroup, are Re-Os molybdenite ages in the interval 2614-2592 Ma obtained from the IOCG deposit at Gamelaria, Cu-Au-(Mo) veins at Serra Verde, as well as from the nearby Garimpo Fernando gold prospect (Marschik et al., 2005).

Most complex of all is the cluster of ages obtained for the GT46 deposit. Three distinct stages of mineralization, spanning ~156 Ma, are inferred from Re-Os molybdenite ages of amphibolite, granite and pegmatite: (1) 2711 Ma; (2) 2600; and (3) 2557-2554 Ma (Silva et al., 2005). This interval was expanded further by subsequent additional Re-Os molybdenite geochronology (Toledo et al., 2019), which yielded ages of 2503-2449 Ma interpreted as "a recurrence of younger hydrothermal events".

The amphibolite-hosted mineralization in GT46, Jatobá, and the deposits in the northern belt discussed above all cluster around the interval ~2.68-2.5 Ga. Teixeira et al. (2021) attributed a geodynamic event described as a "metasome stage" with crustal extension and deep (60-100 km) mantle flash melting, to this same time span. However, this interval partially overlaps with a period between 2.6-2.45 Ga in which episodic reactivation of the Cinzento Shear Zone is attributed to a compressional regime, at least in the tectonic reconstruction of Trunfull et al. (2020). Whichever way, formation of two of the largest IOCG deposits in the Carajás Domain,

Salobo (1,112 Mt @ 0.69% Cu and 0.43 g/t Au; Vale 2012 report) and Igarape Bahia (219 Mt @ 1.4% Cu and 0.86 g/t Au; Tallarico et al., 2005) fall squarely within the 2.6-2.5 Ga timespan (Fig. 10).

The ~2.0 Ga U-Pb apatite age for Jatobá is comparable with Paleoproterozoic ages obtained by various geochronometers from all deposits in the south of the Carajás Domain, except for Bacuri (Fig. 10). The widest age range, 2.187-1.84 Ga, is for Jaguar Sul and Onça Preta, which are dated by U-Pb apatite methods (Hernandez-Tasco et al., 2023). Moreto et al. (2015a) consider the age of the Sossego-Curral deposits to be well constrained from U-Pb monazite ages of 1.9-1.89 Ga, although more recent Sm-Nd apatite dating shows an older age at 2.15-2.06 Ga (Smith, 2023). The two age groups are obtained from accessory minerals associated with chalcopyrite either in breccia fragments or as veins, respectively. Smith (2023) explains the age difference by considering monazite formation via dissolution-reprecipitation from earlier apatite (paragenetically associated with magnetite and actinolite).

The range of Paleoproterozic ages are broadly attributable to the 2.2-1.9 Ga 'Transamazonian' orogeny (Teixeira et al., 2018). The tectonic reconstruction of Tavares et al. (2018) interprets the 2.2-1.85 Ga interval as a series of subduction, collisional and extension events, culminating with emplacement of large A-type granites (the 1.9-1.85 Ga Uatuma magmatism).

Even though the selection of ages plotted in Figure 10 for the northern deposits might suggest these are unaffected by events in this interval, there are a scatter of ages, Ar-Ar amphibole (1.86 Ga) and Sm-Nd whole rock (1.75 Ga) for GT46 and Pb-Pb magnetite (2.11 Ga) for Salobo, that lie within the same Paleoproterozoic interval (Trunfull et al., 2020).

Geochronology to support a genetic model for the Jatobá deposit

The cartoon in Figure 11 illustrates a modified genetic model for Jatobá based on the new apatite petrochronology. Volcanic sequences displaying spilitization (albite + epidote + carbonate + chlorite) and minor massive sulfides (Cu-Ni-PGE) on or immediately below the seafloor (Campo-

Rodriguez et al. 2024b; *in review a*) formed in an active rift environment at 2.76-2.73 Ga (Fig. 11A). Igneous apatite of mafic affiliation associated with high-T, trellis magnetite (700 °C) would have featured a Cl-rich signature, and oscillatory zoning patterns.

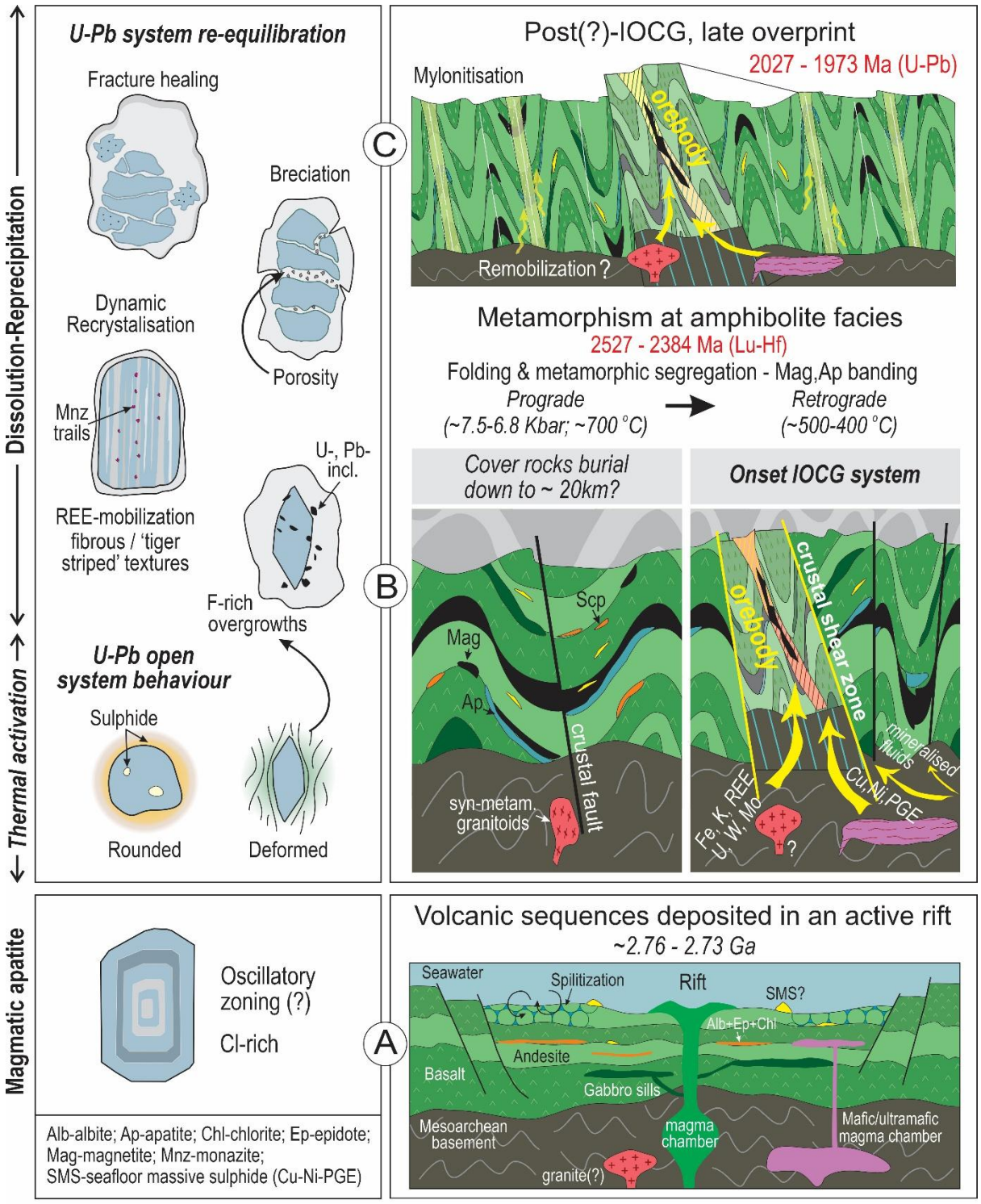

Figure 11. Schematic showing proposed model for the Jatobá IOCG system based on the new petrochronological apatite data. Textural grain changes in apatite are indicated on the left, and the main stages of geological setting evolution are shown on the right.

The shift from extensional to compressional tectonics is a plausible scenario for IOCG formation in the Carajás Domain, even though the timing of this remains the topic of lively debate (Costa et al., 2020; Trunfull et al., 2020). For example, the Igarape Cinzento/GT46 deposit is synchronous with development of Cinzento Shear Zone at ca. 2.71 Ga (Toledo et al., 2019) whereas textures and early hydrothermal alteration at Bacuri located along the Canaã Shear Zone (Melo et al., 2014) support formation of IOCG deposits during basin inversion. Trunfull et al. (2020) put forward two alternative scenarios for tectonic evolution of Carajás Domain, both converging to episodic reactivation of Cinzento Shear Zone and metamorphism at 2.60-2.45 Ga.

If we assume the latter interpretation is also applicable to the southern Canaã Shear Zone at Jatobá, we can associate the ubiquitous banding and irregular magnetite+apatite pods in lithologies described from Jatobá (Fig. 11B) to folding and metamorphic segregation (Campo-Rodriguez et al., 2024a; in review). Pressure-temperature (P-T) conditions are estimated at 7.4-6.4 kbar, ~700-400 °C from magnetite-ilmenite geothermobarometry and Al-in-amphibole geobarometer applied to ferrochermakite in host basalt and magnetite (Campo-Rodriguez et al., 2024a; in review) compatible with amphibolite facies metamorphism at a depth of ~20 km.

To attain such depth, rapid burial during an interval of ~ 100-200 Ma is required if we assume conservative rates of subsidence (1-2 cm/yr). Considering the end of rifting at 2.73 Ga, we can estimate an age interval of 2.63−2.53 Ga for a metamorphic event. The Lu-Hf apatite age of 2527 Ma matches this well and would represent the apatite grain cores and sulfide-hosted rounded grains and thus attributable to deformation. The same deformation is recorded by scapolite and magnetite (Campo-Rodriguez et al., in review). Shear heating by friction is an important phenomenon in collisional belts and can explain the often very high-grade metamorphic conditions encountered in strike-slip deep shear zones (e.g., Leloup and Kienast, 1993). Thermomechanical modelling and multiple examples studied in the field show that the ascent of magma and/or hot fluids along shear zones would enhance temperature in shallower parts of the

system and lead to strain localization in the deeper parts of the strike-slip faults (Leloup et al., 1999).

Although the dated apatite can be traced back to a mafic affiliation (Cl-rich grains in JT1), we contend the 2.5 Ga age reflects metamorphic recrystallization of apatite via thermally activated volume diffusion. If this interpretation is correct, the younger Lu-Hf ages (2438-2384 Ma), would represent the prograde to retrograde metamorphic cycle, in which later-stage fluids can account for overgrowths, brecciation, and dissolution-reprecipitation of apatite. Dynamic recrystallization, in some cases accompanied by REE-mobilization (dusty monazite marking fibrous texture; Fig. 4C), is recorded by the ore apatite in particular.

At this stage, we assume that fluids released during down-temperature retrograde metamorphism are focused along the dominant shear structures resulting in REY-enriched apatite and sulfide deposition. Although the onset of the IOCG system could have been during the rift stage, e.g., with metals sourced from granite-derived hydrothermal fluids, evidence for such a scenario is yet to be found. Instead, we suggest that the substantial increase in apatite (up 25 wt.; Fig. 2D) and the significant REE-enrichment at this stage is likely related to the ~2.5 Ga metamorphism. Involvement of a metamorphic fluid has been invoked to account for sodic-calcic alteration in the Cloncurry district, Queensland, Australia (Duncan et al., 2011).

The Salobo deposit is an example of shear-zone hosted mineralization. The affiliation of mineralization with host lithologies, metamorphism and emplacement of late granites are discussed in relation with recurrent activation of the Cinzento Shear Zone (e.g., Lindemayer and Teixeira, 1999; Requia et al., 2003; Melo et al 2017; Campo-Rodriguez et al., 2022). The deposit is hosted by the Igarape Gelado Gneiss, contains lithologies that were metamorphosed at pyroxene-hornfels facies (fayalite-ferrosilite-hastingite-almandine), and is considered to have formed at a depth of ~7 km (Lindenmayer and Teixeira, 1999). The main stage of mineralization at Salobo is considered coeval with emplacement of the 2.6-2.5 Ga Old Salobo Granite followed by deformation and ore redistribution (Requia et al., 2003: Melo et al., 2017). Based on

petrography, trace elements in magnetite and sulphur isotopes, Campo-Rodriguez et al. (2022) contend that subsequent deformation during low-grade dynamic metamorphism of an older pre-existing (~2.7 Ga) mineralization is related to reactivation of the Cinzento Shear Zone at ca. 2.5 Ga rather than emplacement of coeval granitic intrusions.

Healing of porosity and re-equilibration of the U-Pb system in Jatobá apatite at ~2.0 Ga (Fig. 11C) is associated with a strong mylonitization and intense chloritization making up to ~12 wt% of the rock mass (Fig. 2D). Fluid circulation along pre-existing structures at various scales can be anticipated to contribute to metal concentrations via remobilization and reconcentration. Whether more metals had been introduced into the ore system at this stage is yet to be constrained.

Conclusions

Fluorapatite from both the host basalts and mineralization in the Jatobá orebody records dominantly open behaviour of the U-Pb system due to syn-metamorphic deformation and brecciation. In contrast, the ~2.5 Ga Lu-Hf age obtained from the deformed, REY-rich cores of basalt-hosted apatite correlates with peak metamorphism in the deeper parts of the Canaã dos Carajás Shear Zone. A mafic Cl-rich geochemical signature is retained in some apatite grains, but the age is ~200-260 Ma younger than the host basaltic rocks. A range of Lu-Hf ages spanning ~150 Ma (2527-2384 Ma) is obtained from grains affected by dissolution-reprecipitation processes resulting in variable textures including REY-poor, F-rich overgrowths, development of porosity, and grain-scale brecciation during which inclusions of U- and Pb-bearing minerals are formed.

An unusual fibrous/tiger-striped texture is interpreted as a product of dynamic recrystallization by analogy with metasomatism in ultra-mylonitic sequences from shear zones reported elsewhere. Remobilization of REE is evidenced by nucleation of monazite grains along trails following the fibrous texture. A younger ~2 Ga U-Pb age is obtained from apatite grains in

which the U-Pb system is re-equilibrated within small-scale domains displaying fracture healing and porosity obliteration within grains that otherwise retain evidence of brecciation. Local textural and chemical adjustments are highlighted by the high variability in chondrite-normalized REY fractionation trends.

These multiple lines of evidence support a new model for the Jatobá orebody. Distinct from previous models, we propose that the IOCG system at Jatobá was initiated at 2.5 Ga within deeper portions (~20 km) of Canaã dos Carajás shear structures that affect a volcanic sequence deposited within an active rift at 2.76-2.73 Ga. High temperatures, up to 700 °C did not affect the Lu-Hf isotopic system but pressures of 7.5-6.8 kbar in the shear structures could account for observed effects including thermally activation volume diffusion during peak metamorphism. Release of fluids during the retrograde metamorphic cycle assisted dissolution-reprecipitation reaction via metasomatism or fracture-assisted brecciation in apatite. Fluids channelled along the shear zone structures tapped into metal sources from the basement and deposited sulphides that are intimately associated with reworked apatite. A last event is recorded during strong post-uplift mylonitization of the sequences at ~2 Ga.

Ages of ~2.5 Ga for mineralization in the southern Copper Belt of the Carajás Domain is equivalent to not only the timing of Cinzento Shear zone reactivation in the northern belt but also to the amphibolite facies metamorphism recognized in the northern belt and documented here for the first time in the southern belt. The younger ~2 Ga age correlates with that indicated for the Sossego-Curral deposit drawing attention to possible deep-rooted connections among the hydrothermal system(s) feeding the Jatobá IOCG orefield.

The Carajás Domain is undoubtedly more complex in terms of its evolution and sequence of events than some other globally important ore provinces. Systematic studies, ideally incorporating the use of complementary techniques on well-characterized samples, are urgently needed to correlate evidence across the region. Apatite, an abundant component of ore systems and host rocks across the CD can play an important role in future studies. The present study has

emphasized the interpretative 'power' of apatite to accurately date geological events, especially when multi-technique geochronological study is accompanied by supporting petrographic and geochemical data.

Acknowledgements

Nobuyuki Kawashima (Adelaide Microscopy) is thanked for his assistance with AM operation. Y.T.C.R and M.E.S acknowledges continuous support from the Brazilian Research Council (CNPq – Project 409015/2021-0) and the Coordenação de Aperfeiçoamento de Pessoal de Nível Superior - Brasil (CAPES) - Finance Code 001. Analytical expenses were supported by the Institute of Sustainability, Energy and Resources, The University of Adelaide. N.J.C. and K.E. acknowledge funding through Australian Research Council Linkage grant LP200100156 (Critical Minerals from Complex Ores).

Supplementary Material

Appendix A: Analytical methods, additional figures, summary of EPMA results and mineral formula calculations, and summary statistics of trace element data from Fe-oxides by LA-ICP-MS. Summary of EPMA data for apatite (by sample and selected line profiles)

Appendix B:

Supplementary Table 1B. Complete data set of EPMA data for apatite

Supplementary Table 2. LA-ICP-MS trace element data for fluorapatite (complete dataset, element concentrations in ppm, calculated from measurement of given isotope, except for the 4 Pb isotopes)

Supplementary Table 3A. Summary of U-Pb data for selected apatite

Supplementary Table 3B. Summary of U-Pb data for in-house reference materials

Supplementary Table 4. Summary of Lu-Hf data and trace elements for selected apatite and in-house reference materials

References

Antonio, P.Y.J., D'Agrella-Filho, M.S., Nedelec, A., Poujol, M., Sanchez, C., Dantas, E. L., Dall'Agnol, R., Teixeira, M.F.B., Proietti, A., Martínez Dopico, C.I., Oliveira, D.C., Silva, F.F., Marangoanha, B., and Trindade, R.I.F.D. (2021). New constraints for paleogeographic reconstructions at ca. 1.88 Ga

from geochronology and paleomagnetism of the Carajás dyke swarm (eastern Amazonia). Precambrian Research 353, 106039. https://doi.org/10.1016/j.precamres.2020.106039

Araújo, O.D., Maia, R.G.N., João, X.J., and Costa, J.B.S. (1988). A megaestruturação arqueana da folha Serra dos Carajás. In Congresso Latino-Americano de Geologia SBG-NO Belém. vol. 7, p. 324-338.

Belousova, E.A., Walters, S., Griffin, W.L., O'Reilly, S.Y. (2001) Trace-element signatures of apatites in granitoids from the Mt Isa Inlier, northwestern Queensland. Australian Journal of Earth Sciences 48(4), 603-619. https://doi.org/10.1046/j.1440-0952.2001.00879.x

Brown, D.A., Reid, A., Jagodzinski, E.A., Williams, M., Simpson, A., Pawley, M., Kirkland, C.L., Wade, C., Leeuwen, A.T.V.V., Glorie, S. (2024) Testing in-situ apatite Lu–Hf dating in polymetamorphic mafic rocks: a case study from Palaeoproterozoic southern Australia. Contributions to mineralogy and petrology 179(5), 46. https://doi.org/10.1007/s00410-024-02117-0

Campo-Rodríguez, Y.T., Schutesky, M.E., de Oliveira, C.G., Whitehouse, M.J. (2022) Unveiling the polyphasic evolution of the Neoarchean IOCG Salobo deposit, Carajás Mineral Province, Brazil: Insights from magnetite trace elements and sulfur isotopes. Ore Geology Reviews 140, 104572. https://doi.org/10.1016/j.oregeorev.2021.104572

Campo-Rodriguez, Y.T.C., Ciobanu, C.L., Slattery, A., Cook, N.J., Schutesky, M.E., Ehrig, K., King, S.A., Yao, J. (2024a) Polysomatic intergrowths between amphiboles and non-classical pyriboles in magnetite: smallest-scale features recording a protracted geological history. American Mineralogist 109 (10), 1798–1818. https://doi.org/10.2138/am-2023-9188

Campo Rodriguez, Y.T., Cook, N.J., Ciobanu, C.L., Schutesky, M.E., King, S.A., Gilbert, S., Ehrig, K. (2024b) Platinum Group Minerals Associated with Nickel-Bearing Sulfides from the Jatobá Iron Oxide-Copper-Gold Deposit, Carajás Domain, Brazil. Minerals 14(8), 757. https://doi.org/10.3390/min14080757

Campo-Rodriguez, Y.T., Ciobanu, C.L., Cook, N.J., Schutesky, M.E., Ehrig, K., Slattery, A., Gilbert, S., King, S.A., in review. Telescoped transition from trellis to silicate mottled magnetite records deep shear zone metamorphism in the IOCG deposit at Jatobá, Carajás, Brazil. Mineralium deposita

Chew, D.M., Sylvester, P.J., Tubrett, M.N. (2011) U–Pb and Th–Pb dating of apatite by LA-ICPMS. Chemical Geology 280(1-2), 200-216. https://doi.org/10.1016/j.chemgeo.2010.11.010

Chew, D.M., and Spikings, R.A. (2021) Apatite U-Pb thermochronology: A review. Minerals 11(10), 1095. https://doi.org/10.3390/min11101095

Costa, F.G., Santos, P.A., Serafim, I.C.C.O., Costa, I.S.L., Roopnarain, S. (2020) From Mesoarchean drips to modern–style tectonics in the Carajás Province, Amazonian Craton. Journal of South America Earth Sciences 104, 102817. https://doi.org/10.1016/j.jsames.2020.102817

Duncan, R.J., Stein, H.J., Evans, K.A., Hitzman, M.W., Nelson, E.P., Kirwin, D.J. (2011) A new geochronological framework for mineralization and alteration in the Selwyn-Mount Dore corridor, Eastern fold belt, Mount Isa inlier, Australia: Genetic implications for iron oxide copper-gold deposits. Economic Geology 106(2), 169-192. https://doi.org/10.2113/econgeo.106.2.169

Glorie, S., Jepson, G., Konopelko, D., Mirkamalov, R., Meeuws, F., Gilbert, S., Gillespie, J., Collins, A.S., Xiao, W., Dewaele, S., de Grave, J. (2019) Thermochronological and geochemical footprints of post-orogenic fluid alteration recorded in apatite: Implications for mineralisation in the Uzbek Tian Shan. Gondwana Research 71, 1-15. https://doi.org/10.1016/j.gr.2019.01.011

Glorie, S., Gillespie, J., Simpson, A., Gilbert, S., Khudoley, A., Priyatkina, N., Hand, M., Kirkland, C.L. (2022) Detrital apatite Lu–Hf and U–Pb geochronology applied to the southwestern Siberian margin. Terra Nova 34(3), 201-209. https://doi.org/10.1111/ter.12580

Glorie, S., Hand, M., Mulder, J., Simpson, A., Emo, R.B., Kamber, B., Fernie, N., Nixon, A., Gilbert, S. (2024) Robust laser ablation Lu–Hf dating of apatite: an empirical evaluation. Journal of the Geological Society London 537(1), 165-184. https://doi.org/10.1144/SP537-2022-205

Grainger, C.J., Groves, D.I., Tallarico, F.H., Fletcher, I.R. (2008) Metallogenesis of the Carajás mineral province, southern Amazon craton, Brazil: Varying styles of Archean through Paleoproterozoic to Neoproterozoic base-and precious-metal mineralisation. Ore Geology Reviews 33(3-4), 451-489. https://doi.org/10.1016/j.oregeorev.2006.10.010

Harlov, D.E., Andersson, U.B., Förster, H.J., Nyström, J.O., Dulski, P., Broman, C. (2002) Apatite–monazite relations in the Kiirunavaara magnetite–apatite ore, northern Sweden. Chemical Geology 191(1-3), 47-72. https://doi.org/10.1016/S0009-2541(02)00148-1

Harlov, D.E. (2015) Apatite: A fingerprint for metasomatic processes. Elements 11(3), 171-176. https://doi.org/10.2113/gselements.11.3.171

Hernandez-Tasco, L., Monteiro, L.V.S., Ribeiro, B.V., Dutra, L.F., Ferreira Filho, C.F., Mansur, E.T., Montresor, G. (2023) In situ high-resolution U-Pb geochronology of apatite: understanding the alteration-mineralization timing of the Jaguar hydrothermal nickel deposit, Carajás Mineral Province. Simpósio da Pós Graduação, Universidade de São Paulo. (accessed 05 September 2024). https://repositorio.usp.br/directbitstream/d5ca9a19-7683-427c-80b6-64775ed7c03c/3152535.pdf

Ismail, R., Ciobanu, C.L., Cook, N.J., Teale, G.S., Giles, D., Mumm, A.S., Wade, B. (2014) Rare earths and other trace elements in minerals from skarn assemblages, Hillside iron oxide–copper–gold deposit, Yorke Peninsula, South Australia. Lithos, 184, 456-477. https://doi.org/10.1016/j.lithos.2013.07.023

Jochum, K.P., Weis, U., Stoll, B., Kuzmin, D., Yang, Q., Raczek, I., Jacob, D.E., Stracke, A., Birbaum, K., Frick, D.A., Günther, D., Enzweiler, J. (2011) Determination of reference values for NIST SRM 610–617 glasses following ISO guidelines. Geostandards and Geoanalytical Research 35(4), 397-429. https://doi.org/10.1111/j.1751-908X.2011.00120.x

Kirkland, C.L., Yakymchuk, C., Szilas, K., Evans, N., Hollis, J., McDonald, B., Gardiner, N.J. (2018) Apatite: a U-Pb thermochronometer or geochronometer?. Lithos. 318, 143-157. https://doi.org/10.1016/j.lithos.2018.08.007

Klein, E.L., Rodrigues, J.B., Lopes, E.C., Soledade, G.L. (2012) Diversity of Rhyacian granitoids in the basement of the Neoproterozoic-Early Cambrian Gurupi Belt, northern Brazil: Geochemistry, U–Pb

zircon geochronology, and Nd isotope constraints on the Paleoproterozoic magmatic and crustal evolution. Precambrian Research 220, 192-216. https://doi.org/10.1016/j.precamres.2012.08.007

Krneta, S., Cook, N.J., Ciobanu, C.L., Ehrig, K., Kontonikas-Charos, A. (2017a) The Wirrda Well and Acropolis prospects, Gawler Craton, South Australia: Insights into evolving fluid conditions through apatite chemistry. Journal of Geochemical exploration 181, 276-291. https://doi.org/10.1016/j.gexplo.2017.08.004

Krneta, S., Ciobanu, C.L., Cook, N.J., Ehrig, K., Kontonikas-Charos, A. (2017b) Rare earth element behaviour in apatite from the Olympic Dam Cu–U–Au–Ag deposit, South Australia. Minerals 7(8), 135. https://doi.org/10.3390/min7080135

Leloup, P.H., and Kienast, J.R. (1993) High-temperature metamorphism in a major strike-slip shear zone: the Ailao Shan—Red River, People's Republic of China. Earth and Planetary Science Letters 118(1-4), 213-234. https://doi.org/10.1016/0012-821X(93)90169-A

Leloup, P.H., Ricard, Y., Battaglia, J., Lacassin, R. (1999) Shear heating in continental strike-slip shear zones: model and field examples. Geophysical Journal International 136(1), 19-40. https://doi.org/10.1046/j.1365-246X.1999.00683.x

Lindenmayer, Z.G., and Teixeira, J.B.G. (1999) Ore genesis at the Salobo copper deposit, Serra dos Carajás. Base Metal Deposits of Brazil. Belo Horizonte, MME/CPRM/DNPM. p. 33-43.

Macambira, M.J.B., Vasquez, M.L., da Silva, D.C.C., Galarza, M.A., de Mesquita Barros, C.E., de Freitas Camelo, J. (2009) Crustal growth of the central-eastern Paleoproterozoic domain, SW Amazonian craton: Juvenile accretion vs. reworking. Journal of South America Earth Sciences 27(4), 235-246. https://doi.org/10.1016/j.jsames.2009.02.001

Machado, N., Lindenmayer, Z., Krogh, T.E., Lindenmayer, D. (1991) U-Pb geochronology of Archean magmatism and basement reactivation in the Carajás area, Amazon shield, Brazil. Precambrian Research 49(3-4), 329-354. https://doi.org/10.1016/0301-9268(91)90040-H

Marschik, R., Mathur, R., Ruiz, J., Leveille, R.A., de Almeida, A.J. (2005) Late Archean Cu-Au-Mo mineralization at Gameleira and Serra Verde, Carajás Mineral Province, Brazil: constraints from Re-Os molybdenite ages. Mineralium deposita 39, 983-991. https://doi.org/10.1007/s00126-004-0450-z

Martins, P.L.G., Toledo, C.L.B., Silva, A.M., Chemale Jr,F., Santos, J.O.S., Assis, L.M. (2017) Neoarchean magmatism in the southeastern Amazonian Craton, Brazil: Petrography, geochemistry and tectonic significance of basalts from the Carajás Basin. Precambrian Research 302, 340-357. http://dx.doi.org/10.1016/j.precamres.2017.10.013

Melo, G.H.C., Monteiro, L.V.S., Moreto, C., Xavier, R.P., Silva, M.A.D.D. (2014) Paragenesis and evolution of the hydrothermal Bacuri iron oxide-copper-gold deposit, Carajás Province (PA). Brazilian Journal of Geology 44(1), 73-90. 10.5327/Z2317-4889201400010007

Melo, G.H., Monteiro, L.V.S., Xavier, R.P., Moreto, C.P., Santiago, E.S.B., Dufrane, S.A., Aires, B., Santos, A.F.F. (2017) Temporal evolution of the giant Salobo IOCG deposit, Carajás Province (Brazil): constraints from paragenesis of hydrothermal alteration and U-Pb geochronology. Mineralium deposita 52, 709-732. https://doi.org/10.1007/s00126-016-0693-5

Melo, G.H., Monteiro, L.V., Xavier, R.P., Moreto, C.P., Arquaz, R.M., Silva, M.A.D. (2019) Evolution of the Igarapé Bahia Cu-Au deposit, Carajás province (Brazil): early syngenetic chalcopyrite overprinted by IOCG mineralization. Ore Geology Reviews 111, 102993. https://doi.org/10.1016/j.oregeorev.2019.102993

Mercer, C.N., Watts, K.E., Gross, J. (2020) Apatite trace element geochemistry and cathodoluminescent textures—A comparison between regional magmatism and the Pea Ridge IOAREE and Boss IOCG deposits, southeastern Missouri iron metallogenic province, USA. Ore Geology Reviews 116, 103129. https://doi.org/10.1016/j.oregeorev.2019.103129

Moreto, C.P.N., Monteiro, L.V.S., Xavier, R.P., Creaser, R.A., DuFrane, S.A., Tassinari, C.C.G., Sato, K., Kemp, A.I.S., Amaral, W.S. (2015a) Neoarchean and Paleoproterozoic iron oxide-copper-gold events at the Sossego deposit, Carajás Province, Brazil: Re-Os and U-Pb geochronological evidence. Economic Geology 110(3), 809-835. https://doi.org/10.2113/econgeo.110.3.809

Moreto, C.P.N., Monteiro, L.V.S., Xavier, R.P., Creaser, R.A., Dufrane, S.A., Melo, G.H.C., Silva, M.A.D., Tassinari, C.C.G., Sato, K. (2015b) Timing of multiple hydrothermal events in the iron oxide–copper gold deposits of the Southern Copper Belt, Carajás Province, Brazil. Miner Deposita. 50, 517-546. https://doi.org/10.1007/s00126-014-0549-9

Norris, A., and Danyushevsky, L. (2018) Towards estimating the complete uncertainty budget of quantified results measured by LA-ICP-MS. Goldschmidt: Boston, MA, USA.

Odlum, M.L., and Stockli, D.F. (2020) Geochronologic constraints on deformation and metasomatism along an exhumed mylonitic shear zone using apatite U-Pb, geochemistry, and microtextural analysis. Earth and Planetary Science Letters 538, 116177. https://doi.org/10.1016/j.epsl.2020.116177

Odlum, M.L., Levy, D.A., Stockli, D.F., Stockli, L.D., DesOrmeau, J.W. (2022) Deformation and metasomatism recorded by single-grain apatite petrochronology. Geology 50(6), 697-703. https://doi.org/10.1130/G49809.1

Olszewski, W.J., Wirth, K.R., Gibbs, A.K., Gaudette, H.E. (1989) The age, origin, and tectonics of the Grão Pará Group and associated rocks, Serra dos Carajás Brazil: Archean continental volcanism and rifting. Precambrian Research 42, 229-254. https://doi.org/10.1016/0301-9268(89)90013-2

O'Sullivan, G., Chew, D., Kenny, G., Henrichs, I., Mulligan, D. (2020) The trace element composition of apatite and its application to detrital provenance studies. Journal of South America Earth Sciences 201, 103044. https://doi.org/10.1016/j.earscirev.2019.103044

Perelló, J., Zulliger, G., García, A., Creaser, R.A. (2023) Revisiting the IOCG geology and age of Alemão in the Igarapé Bahia camp, Carajás province, Brazil. Journal of South America Earth Sciences 124, 104273. https://doi.org/10.1016/j.jsames.2023.104273

Requia, K., Stein, H., Fontboté, L., Chiaradia, M. (2003) Re–Os and Pb–Pb geochronology of the Archean Salobo iron oxide copper–gold deposit, Carajás mineral province, northern Brazil. Mineralium deposita 38, 727-738. https://doi.org/10.1007/s00126-003-0364-1

Roberts, N.M., Rasbury, E.T., Parrish, R.R., Smith, C.J., Horstwood, M.S., Condon, D.J. (2017) A calcite reference material for LA-ICP-MS U-Pb geochronology. Geochemistry, Geophysics, Geosystems 18(7), 2807-2814. https://doi.org/10.1002/2016GC006784

Schoene, B., and Bowring, S.A. (2006) U–Pb systematics of the McClure Mountain syenite: thermochronological constraints on the age of the 40Ar/39Ar standard MMhb. Contributions to mineralogy and petrology 151(5), 615-630. https://doi.org/10.1007/s00410-006-0077-4

Schoene, B., and Bowring, S.A. (2007) Determining accurate temperature–time paths from U–Pb thermochronology: An example from the Kaapvaal craton, southern Africa. Geochemical and Cosmochemical Acta 71(1), 165-185. https://doi.org/10.1016/j.gca.2006.08.029

Schutesky, M.E., and Oliveira, C.G. (2020) From the roots to the roof: An integrated model for the Neoarchean Carajás IOCG System, Brazil. Ore Geology Reviews 127, 103833. https://doi.org/10.1016/j.oregeorev.2020.103833

Silva, M.G., Teixeira, J.B.G., Pimentel, M.M., Vasconcelos, P.M., Arielco, A., Rocha, W.J.S.F. (2005) Geologia e mineralizações de Fe-Cu-Au do alvo GT 46 (Igarapé Cinzento) Carajás. Caracterização em depósitos minerais em distritos mineiros da Amazônia. Eds., Marini, O.J., Queiroz, E.T., Ramos, B.W. Brasília, Brazil: DNPM-CT/Mineral-ADIMB; República das Letras. 94-151. (accessed 30 September 2024). https://www.adimb.com.br/site/publicacoes_amazonia/indice/Cap_III.pdf

Simpson, A., Gilbert, S., Tamblyn, R., Hand, M., Spandler, C., Gillespie, J., Nixon, A., Glorie, S. (2021) In-situ Lu Hf geochronology of garnet, apatite and xenotime by LA ICP MS/MS. Chemical Geology 577, 120299. https://doi.org/10.1016/j.chemgeo.2021.120299

Simpson, A., Glorie, S., Hand, M., Spandler, C., Gilbert, S., Cave, B. (2022) In-situ Lu–Hf geochronology of calcite. Geochronology Discussions 2022, 1-18. https://doi.org/10.5194/gchron-4-353-2022

Smith, E. (2023) The age and source of Cu-Au deposits in the Carajás Mineral Province, Brazil. Doctoral Thesis, The University of Western Australia. https://doi.org/10.26182/wbsa-rj59

Stacey, J.S., and Kramers, J.D. (1975) Approximation of terrestrial lead isotope evolution by a two-stage model. Earth and Planetary Science Letters 26(2), 207-221. https://doi.org/10.1016/0012-821X(75)90088-6

Steadman, J.A., Goemann, K., Thompson, J.M., MacRae, C.M., Belousov, I., Hohl, M. (2022) Hyperspectral cathodoluminescence, trace element, and U-Pb geochronological characterization of apatite from the Ernest Henry iron oxide copper-gold (IOCG) deposit, Cloncurry district, Queensland. Frontiers in Earth Sciences 10, 926114. https://doi.org/10.3389/feart.2022.926114

Stein, H.J., Markey, R.J., Morgan, J.W., Hannah, J.L., Scherstén, A. (2001) The remarkable Re–Os chronometer in molybdenite: how and why it works. Terra Nova 13(6), 479-486. https://doi.org/10.1046/j.1365-3121.2001.00395.x

Tallarico, F.H.B., Figueiredo, B.R., Groves, D.I., Kositcin, N., McNaughton, N.J., Fletcher, I.R., Rego, J.L. (2005) Geology and SHRIMP U-Pb geochronology of the Igarapé Bahia deposit, Carajás copper-gold belt, Brazil: An Archean (2.57 Ga) example of iron-oxide Cu-Au-(U-REE) mineralization. Economic Geology 100(1), 7-28. https://doi.org/10.2113/100.1.0007

Tavares, F.M., Trouw, R.A.J., da Silva, C.M.G., Justo, A.P., Oliveira, J.K.M. (2018) The multistage tectonic evolution of the northeastern Carajás Province, Amazonian Craton, Brazil: Revealing complex structural patterns. Journal of South America Earth Sciences 88, 238-252. https://doi.org/10.1016/j.jsames.2018.08.024

Teixeira, W., Tassinari, C.C.G., Cordani, U.G., Kawashita, K. (1989) A review of the geochronology of the Amazonian Craton: tectonic implications. Precambrian Research 42(3-4), 213-227. https://doi.org/10.1016/0301-9268(89)90012-0

Teixeira, M.F.B., Dall'Agnol, R., Santos, J.O.S., de Oliveira, D.C., Lamarão, C.N., McNaughton, N.J. (2018) Crystallization ages of Paleoproterozoic A-type granites of Carajás province, Amazon craton: Constraints from U-Pb geochronology of zircon and titanite. Journal of South America Earth Sciences 88, 312-331. https://doi.org/10.1016/j.jsames.2018.08.020

Teixeira, N.A., Campos, L.D., de Paula, R.R., Lacasse, C.M., Ganade, C.E., Monteiro, C.F., L.B.L., de Oliveira, C. G. (2021) Carajás Mineral Province-Example of metallogeny of a rift above a cratonic lithospheric keel. Journal of South America Earth Sciences 108, 103091. https://doi.org/10.1016/j.jsames.2020.103091

Thomson, S.N., Gehrels, G.E., Ruiz, J., Buchwaldt, R. (2012) Routine low-damage apatite U-Pb dating using laser ablation–multicollector–ICPMS. Geochemistry, Geophysics, Geosystems 13(2). https://doi.org/10.1029/2011GC003928

Thompson, J., Meffre, S., Maas, R., Kamenetsky, V., Kamenetsky, M., Goemann, K., Ehrigc, K., Danyushevsky, L. (2016) Matrix effects in Pb/U measurements during LA-ICP-MS analysis of the mineral apatite. Journal of Analytical Atomic Spectrometry 31(6), 1206-1215. https://doi.org/10.1039/C6JA00048G

Toledo, P.I.F., Moreto, C.P.N., Xavier, R.P., Gao, J., Matos, J.H.S.N., de Melo, G.H.C. (2019) Multistage evolution of the Neoarchean (ca. 2.7 Ga) Igarapé cinzento (GT-46) iron oxide copper-gold deposit, Cinzento shear zone, Carajás Province, Brazil. Economic Geology 114(1), 1-34. https://doi.org/10.5382/econgeo.2019.4617

Toledo, P.I.F., Moreto, C.P.N., Monteiro, L.V.S., Melo, G.H.C., Matos, F.M.V., Xavier, R.P., Carvalho, J.A., Filho, C.A.M., Navarro, M.S., Lana, C.C. (2024) Breaking up the temporal link between granitic magmatism and iron oxide-copper–gold (IOCG) deposits in the Carajás Mineral Province, NW Brazil. Mineralium deposita 59, 601-625. https://doi.org/10.1007/s00126-023-01224-5

Trunfull, E.F., Hagemann, S.G., Xavier, R.P., Moreto, C.P.N. (2020) Critical assessment of geochronological data from the Carajás Mineral Province, Brazil: Implications for metallogeny and tectonic evolution. Ore Geology Reviews 121, 103556. https://doi.org/10.1016/j.oregeorev.2020.103556

Vale, (2012) Vale obtains operation license for Salobo. (http://saladeimprensa.vale.com /en/release/interna.asp?id= 22000)

Vasquez, L.V., Rosa-Costa, L.R., Silva, C.G., Ricci, P.F., Barbosa, J.O., Klein, E.L., Lopes, E.S., Macambira, E.B., Chaves, C.L., Carvalho, J.M., Oliveira, J.G., Anjos, G.C., Silva, H.R. (2008)

Geologia e Recursos Minerais do Estado do Pará: Sistema de Informações Geográficas — SIG: texto explicativo dos mapas Geológico e Tectônico e de Recursos Minerais do Estado do Pará 1:1.000.000. CPRM, Belém, Brazil, 328 p

Veloso, A.S.R. (2017) Evolução Metalogenetica do Deposito de Cu-(Zn) Jatobá, Provincia Mineral de Carajás. Unpublished PhD thesis, University of São Paolo, Brazil, 197 pp. https://doi.org/10.11606/T.44.2017.tde-21012019-150709

Veloso, A.S.R., Monteiro, L.V.S., Juliani, C. (2020) The link between hydrothermal nickel mineralization and an iron oxide-copper–gold (IOCG) system: Constraints based on mineral chemistry in the Jatobá deposit, Carajás Province. Ore Geology Reviews 121, 103555. https://doi.org/10.1016/j.oregeorev.2020.103555

Webster, J.D., and Piccoli, P.M. (2015) Magmatic apatite: A powerful, yet deceptive, mineral. Elements 11(3), 177-182. https://doi.org/10.2113/gselements.11.3.177

Xavier, R.P., Monteiro, L.V.S., Moreto, C.P.N., Pestilho, A.L.S., de Melo, G.H.C., da Silva, M.A.D., Aires, B., Ribeiro, C., e Silva, F.H.F. (2012) The iron oxide copper-gold systems of the Carajás mineral province, Brazil. In: Hedenquist JW, Harris M, Camus F (eds), Geology and Genesis of Major Copper Deposits and Districts of the World: A Tribute to Richard H. Sillitoe Spec. Pub Econ Geol 16

CHAPTER 6

MAGNETITE AND REE-RICH CALCIC AMPHIBOLE PROVIDE EVIDENCE FOR A SKARN-IOCG SYSTEM AT ONÇA-ROSA, JAGUAR OREFIELD, CARAJÁS MINERAL PROVINCE, BRAZIL

Yuri Tatiana Campo-Rodriguez[1,2], Cristiana L. Ciobanu[1], Nigel J. Cook[1], Maria E. Schutesky[2], Kathy Ehrig[1,3], Ashley Slattery[4], Sarah Gilbert[4], Samuel A. King[1]

[1]*School of Chemical Engineering, The University of Adelaide, Adelaide, SA, 5005, Australia*

[2]*University of Brasilia, Institute of Geosciences, Graduate Program in Geology, Brasília DF 70910-900, Brazil*

[3]*BHP Olympic Dam, 10 Franklin Street, Adelaide, SA, 5000, Australia*

[4]*Adelaide Microscopy, The University of Adelaide, Adelaide, SA, 5005, Australia*

Article submitted to *Canadian Journal of Mineralogy and Petrology,* September 20th (2024) CJMP-D-24-00032.

Statement of Authorship

Title of Paper	Magnetite and REE-rich calcic amphibole provide evidence for a Skarn-IOCG system at Onça-Rosa, Jaguar Orefield, Carajás Mineral Province, Brazil
Publication Status	☐ Published ☐ Accepted for Publication ☑ Submitted for Publication ☐ Unpublished and Unsubmitted work written in manuscript style
Publication Details	Campo-Rodriguez, Y.T., Ciobanu, C.L., Cook, N.J., Schutesky, M.E., Ehrig, K., Slattery, A., Gilbert, S., and King, S. Magnetite and REE-rich calcic amphibole provide evidence for a Skarn-IOCG system at Onça-Rosa, Jaguar Orefield, Carajás Mineral Province, Brazil. Submitted to *The Canadian Journal of Mineralogy and Petrology*.

Principal Author

Name of Principal Author (Candidate)	Yuri Tatiana Campo Rodriguez		
Contribution to the Paper	Performed analytical work, evaluation and interpretation of results and prepared the manuscript.		
Overall percentage (%)	60		
Certification:	This paper reports on original research I conducted during the period of my Higher Degree by Research candidature and is not subject to any obligations or contractual agreements with a third party that would constrain its inclusion in this thesis. I am the primary author of this paper.		
Signature	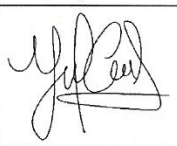	Date	06.11.2024

Co-Author Contributions

By signing the Statement of Authorship, each author certifies that:

i. the candidate's stated contribution to the publication is accurate (as detailed above);

ii. permission is granted for the candidate in include the publication in the thesis; and

iii. the sum of all co-author contributions is equal to 100% less the candidate's stated contribution.

Name of Co-Author	Cristiana L. Ciobanu		
Contribution to the Paper	Helped to define the direction of the manuscript, guides manuscript preparation and assisted with the interpretation of the results and evaluation of the manuscript. (20%)		
Signature		Date	06.11.2024

Name of Co-Author	Nigel J. Cook		
Contribution to the Paper	Helped with the preparation and evaluation of the manuscript. (5%)		
Signature	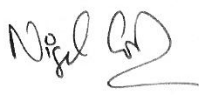	Date	06.11.2024

Name of Co-Author	Maria Emilia Schutesky		
Contribution to the Paper	Helped with the preparation and evaluation of the manuscript. (5%)		
Signature		Date	06.11.2024

Name of Co-Author	Kathy Ehrig		
Contribution to the Paper	Assisted with the evaluation of the manuscript. (3%)		
Signature		Date	06.11.2024

Name of Co-Author	Ashley Slattery		
Contribution to the Paper	Assisted with HAADF-STEM data acquisition. (3%)		
Signature		Date	06.11.2024

Name of Co-Author	Sarah Gilbert		
Contribution to the Paper	Helped in the operation of analytical equipment and data interpretation. (3%)		
Signature		Date	06.11.2024

Name of Co-Author	Samuel Anthony King		
Contribution to the Paper	Assisted with the evaluation of the manuscript. (1%)		
Signature		Date	06.11.2024

Magnetite and REE-rich calcic amphibole provide evidence for a Skarn-IOCG system at Onça-Rosa, Jaguar Orefield, Carajás Mineral Province, Brazil

Yuri Tatiana Campo-Rodriguez[1,2*], Cristiana L. Ciobanu[1], Nigel J. Cook[1], Maria E. Schutesky[2], Kathy Ehrig[1,3], Ashley Slattery[4], Sarah Gilbert[4], Samuel A. King[1]

[1]*School of Chemical Engineering, The University of Adelaide, Adelaide, SA, 5005, Australia*

[2]*University of Brasilia, Institute of Geosciences, Graduate Program in Geology, Brasília DF 70910-900, Brazil*

[3]*BHP Olympic Dam, 10 Franklin Street, Adelaide, SA, 5000, Australia*

[4]*Adelaide Microscopy, The University of Adelaide, Adelaide, SA, 5005, Australia*

[*]*Corresponding author*

Abstract

Detailed nano- to micron-scale petrography and trace element analysis of refractory minerals provides crucial information on the progression of geological processes involved in ore formation. Onça-Rosa is a Ni-rich, granite-hosted orebody located at contacts with mafic/ultramafic units of Serra do Puma layered Complex in the Jaguar orefield, Carajás Mineral Province, Brazil. Pentlandite is the main Ni mineral whereas sphalerite is a ubiquitous albeit minor component. Magnetite, the main ore mineral, displays brecciation, deformation, and mottled inclusion-rich cores indicative of early formation relative to coexisting sulfides and calcic amphibole. Dense mottled magnetite preserves inclusions of cummingtonite with coherent intergrowths of non-classical pyriboles (3 to 5 I-beam chains). No calcic amphiboles are present.

Talc, chlorite and mica are also abundant, associated with amphiboles or along fractures. Lizardite and chrysotile are identified within disordered sequences of the sheet silicates. Widespread silician magnetite defects are identified within less-mottled domains. Fracturing of magnetite is accompanied by nanoscale recrystallization and precipitation of pentlandite and chalcopyrite fine particles. Amphiboles and apatite are conspicuous by their elevated REY content (up to ~100 and ~1700 ppm, respectively). Magnetite also contains REY (~13 ppm). Ferrous phlogopite+tourmaline alteration defines contacts with granite whereas talc+chlorite alteration is observed in the magnetite-rich orebody. Calcic amphiboles (actinolite and Mg-hornblende) are superposed onto this association. Relationships between the talc-chlorite groundmass and amphibole indicate multiple stages of shear during which small-scale remobilization of sulfide occurred. Conspicuous ilmenite-pentlandite associations are observed along such structures. Onça-Rosa is interpreted as an atypical Fe-Zn-Ni skarn system formed by intense alteration of an ultramafic protolith belonging to the Serra do Puma layered complex at its contact with a younger syn-kinematic granite. Two distinct skarn stages are recorded: an early magnesian skarn during deposition of magnetite+sphalerite; and a later calcic skarn associated with pentlandite deposition. High REY concentrations in amphibole from calcic skarn, and an association with accessory uraninite are concordant with IOCG-style mineralization. Regional-scale fault-and-shear systems played a major role in control of mineralization. We conclude that Onça-Rosa is a hybrid type of mineralization that also shares characteristics with other unusual, Ni rich deposits worldwide.

Keywords: Carajás Mineral Province, Onça-Rosa, Jaguar, magnetite, amphiboles, nanoscale, skarn-IOCG system.

Introduction

Magnetite, (Fe_3O_4), is a characteristic mineral in the early stages of iron-oxide copper-gold (IOCG) deposits (e.g. Barton 2014 and references therein). Genetic models for IOCG deposits invoke different metal sources ranging from magmatic through surficial to metamorphic, as well as broad alteration footprints. A widely recognized sub-class of the IOCG deposit clan, containing essential magnetite and apatite but typically containing little copper or gold, are the so-called iron oxide apatite (IOA) deposits (Williams *et al.* 2005). In some IOA deposits, the role of amphibole has been also acknowledged (e.g. Deditius *et al.* 2018). Deposit evolution can be traced from the preserved REE+Y mineral signatures, particularly in IOCG systems that have a skarn setting (e.g. the Hillside deposit in South Australia; Ismail *et al.* 2014).

Magnetite is the most common member of the spinel mineral group (e.g. Biagioni & Pasero 2014). It forms and is stable at a wide range of temperatures spanning geological environments as diverse as supergene to abyssal. Magnetite is shown to be sufficiently refractory that it readily preserves compositions, textures, and mineral inclusions over geological time, collectively representing a valuable tool for interpretation of ore genesis (e.g. Ciobanu *et al.* 2019). Particularly if characterization encompasses both the micron- and nanoscale, magnetite can be used to distinguish igneous from hydrothermal origin and deposit evolution in time and space. This capacity has found particular value for distinguishing between protolith- and IOCG-derived signatures in Archean and Precambrian terranes with lengthy geological histories and multiple superimposed events (Ciobanu *et al.* 2022, Campo-Rodriguez *et al.* 2024a).

Several studies have shown that accurate interpretation of magnetite geochemistry can be challenging in that the range of measurable trace and minor elements present and their concentrations often vary considerably and may indicate a dynamic transition from a magmatic to a hydrothermal regime (e.g. Knipping *et al.* 2015). Sub-micron scale inclusions within magnetite can aid interpretation and elucidate ore genesis but detailed nanoscale characterization

is often needed to corroborate observations at the micron-scale (Ciobanu *et al.* 2019, 2022, Huang & Beaudoin 2021, Verdugo-Ihl *et al.* 2021, Huang *et al.* 2022, Campo-Rodriguez *et al.* 2024a).

Neoarchean IOCG deposits from the Carajás Province of Brazil contain magnetite as the dominant Fe-oxide (Schutesky & Oliveira 2020). The Carajás Province comprises Archean greenstone-granite terranes formed during multiple tectonothermal events (Fig. 1a) and is host to several dozen deposits considered as IOCGs yet all characterized by a complex magmatic-hydrothermal evolution. In this context, magnetite represents a key pathfinder for understanding ore formation. One example is the presence of polysomatic intergrowths between amphiboles and non-classical pyriboles (NCPs) in magnetite from the Jatobá IOCG deposit in the southeast of the Carajás Province (Campo-Rodriguez *et al.* 2024a). These nanoscale features were interpreted as critical evidence for a prolonged geological history in which a mafic-ultramafic protolith was subject to superimposed alkali-calcic, REE-bearing alteration and associated Cu mineralization.

This contribution addresses magnetite from the Onça-Rosa orebody in the Jaguar orefield, ~200 km to the west of Jatobá, with which it shares several features, even if the host rocks are distinct and the mineralization is possibly younger (Hernandez-Tasco *et al.* 2023). A few studies have addressed the Jaguar deposit in terms of ore petrology and the distribution of trace elements in sulfides and magnetite (de Oliviera 2017, Ferreira Filho *et al.* 2021, Mansur *et al.* 2023). These studies explored the link between Jaguar and other IOA and IOCG deposits within the Carajás Mineral Province, concluding that this is a 'hydrothermal Ni deposit', and thus a 'Ni-rich member of IOCG'-type deposit. No emphasis was, however, placed on the differences among the individual orebodies at Jaguar, which have different host lithologies and range widely in the amounts of magnetite, as a means to understand the broader IOCG system.

Onça-Rosa is the subject of our study because this orebody is magnetite-rich and is associated with mafic/ultramafic rocks (Serra do Puma layered complex), thus representing a critical term of reference when compared with magnetite from volcanic hosted orebodies such as those at Jatobá. Of particular interest are the nanoscale characteristics of magnetite which could preserve

clues to the genetic evolution of the ores. We employ a micron- to nanoscale study of magnetite in the context of host lithology/alteration to further constrain the mineralogical and geochemical signatures relevant for IOCG systems.

Geological background

The Carajás Mineral Province (Fig. 1a) in the Amazonian Craton of Brazil (e.g. Vasquez *et al.* 2008) and comprises two major tectonostratigraphic domains: the Carajás Domain in the north, which hosts Neoarchean IOCG deposits and Paleoproterozoic Cu-Au mineralization, and the Rio Maria Domain (RMD) to the south with its Mesoarchean lode-Au deposits (e.g. Costa *et al.* 2020). Among other deposit types within the Carajás Domain are a number of PGE-Au/-Cr, lateritic Ni and Fe-BIF deposits with ages spanning ages from 2.6 Ga to 1.6 Ga (see compilation in Trunfull *et al.* 2020).

The Carajás Domain is composed of a Mesoarchean basement made up of orthogranulites, gneisses, migmatites, granites, and the 3-2.9 Ga greenstone belts of the Sequeirinho Group (Fig. 1a; Machado *et al.* 1991, Tavares *et al.* 2018). The basement is covered by Neoarchean (2.76 - 2.73 Ga) volcano-sedimentary sequences of the Itacaiúnas Supergroup (e.g. Martins *et al.* 2017, Costa *et al.* 2020) and has experienced several overprinting events from Archean to Paleoproterozoic.

Neoarchean igneous activity is represented by mafic-ultramafic complexes (e.g. Machado *et al.* 1991), syntectonic and A-type granites (Feio *et al.* 2013, Moreto *et al.* 2015, Tavares *et al.* 2017). The Carajás Domain comprises major mafic-ultramafic layered complexes, which are among the largest in the Amazonian Craton. Examples include northeastern layered complexes (Luanga and Lago Grande), which are associated with PGE mineralization (e.g. Teixeira *et al.* 2015, Mansur & Ferreira Filho 2016) and layered complexes in the southwest, Serra do Puma and Serra da Onça, which are associated with world-class lateritic Ni-mineralization (e.g. Rosa 2014, Machado *et al.* 2023).

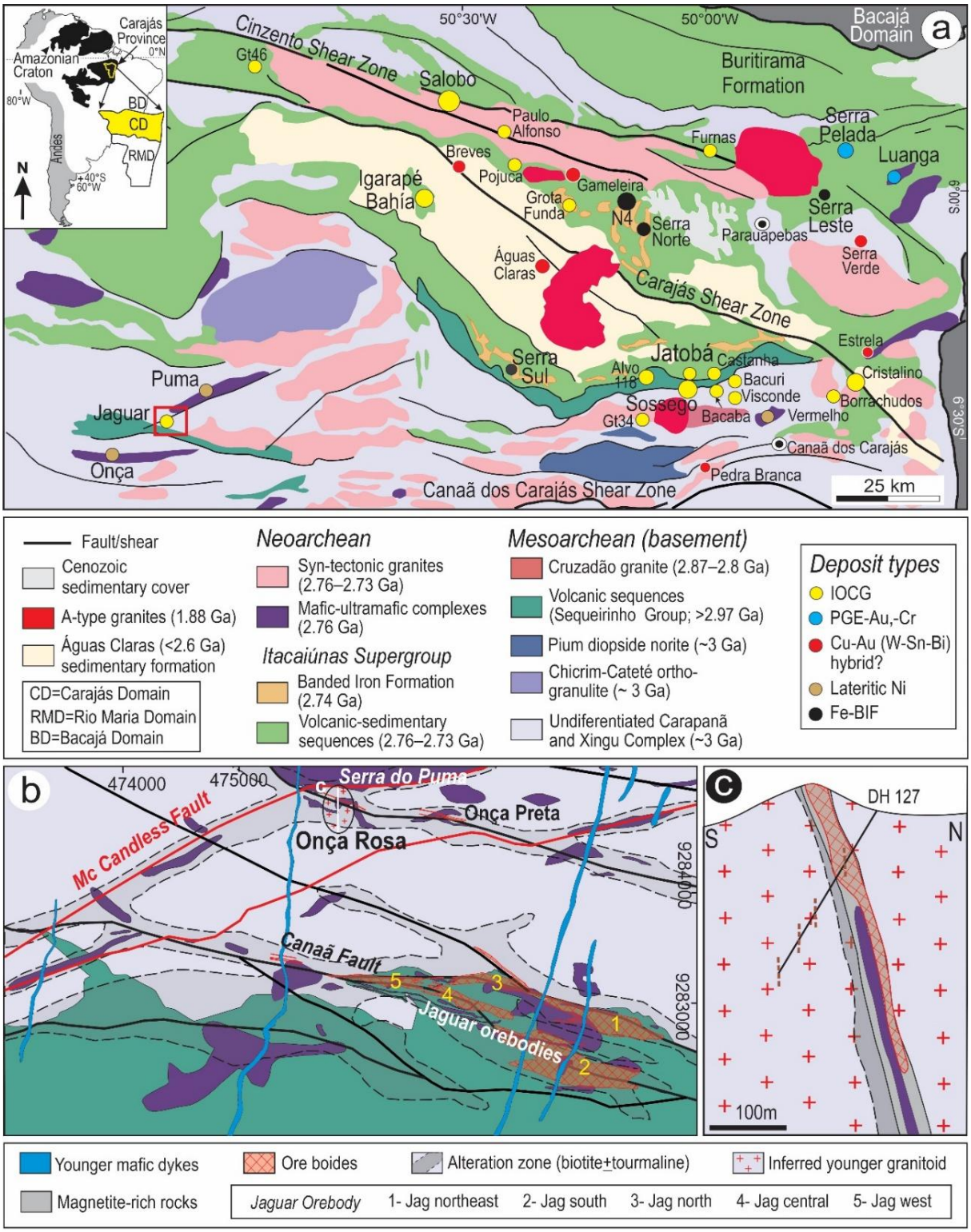

Figure 1. (a) Geological map of the Carajás Domain (CD) showing the location of the Jaguar deposit (red rectangle) and other major deposits. Modified from Vasquez *et al.* (2008) and Tavares *et al.* (2018). Inset shows location of the CD within the Amazonian Craton, South America. The deposit types and respective names are from Grainger *et al.* (2008) and Trunfull *et al.* (2020). Circles represent the relative sizes of the deposits. (b) Simplified geological map of the Jaguar orefield map depicting main host rocks modified from Centaurus Metals 2024. (c) S-N cross-section as marked on (b) showing the sampled drillhole DH00127.

Other igneous events include the peralkaline to meta-aluminous intrusions of Old Salobo (2573±3 Ma; Machado *et al.* 1991, Melo *et al.* 2017) and the Itacaiúnas granites (2560±37 Ma; Machado *et al.* 1991) identified within the Cinzento shear zone (Melo *et al.* 2017). Younger anorogenic A-type granites were emplaced at 1.88-1.86 Ma during the Transamazonian orogeny (e.g. Teixeira *et al.* 2018). Paleoproterozoic sedimentary rocks of the Águas Claras Formation unconformably overlie the abovementioned lithostratigraphic units. These are sandstones and siltstones deposited in fluvial to shallow marine environments and outcrop mainly in the central part of the Carajás District (Araújo Filho *et al.* 2020).

Deposit geology

The Jaguar deposit (Fig. 1b) occurs within an intricate domain of mafic-ultramafic layered intrusions of the Serra do Puma and Serra da Onça complexes, which host Ni-laterite deposits along the intersection of the Canaã dos Carajás fault system with the NE-SW-striking McCandless fault (Mansur *et al.* 2023). The host rocks in the northern part of the deposit are predominantly granitic with local granodioritic-tonalitic orthogneisses of the Carapanã and Xingu Complex, whereas in the southern part, the deposit is mainly hosted by porphyritic felsic sub-volcanic rocks (Mansur *et al.* 2023, Ferreira Filho *et al.* 2021). Sub-vertical orebodies of massive nickel sulfides and associated hydrothermal alteration are structurally controlled by regional brittle-ductile mylonitic shear zones (Ferreira Filho *et al.* 2021). In detail, the massive mineralization, mainly Ni- and Zn-bearing sulfides, is accompanied by disseminations and veins parallel to mylonitic foliation. Sulfide mineralization is related to crystallization of magnetite-apatite and later vein/alteration stage with carbonates (Ferreira Filho *et al.* 2021).

The Jaguar orefield (Fig. 1b) has a total ore reserve of 109.2 Mt @ 0.87% Ni (Centaurus Metals 2024) and is located southwest of the word-class Puma-Onça lateritic nickel deposit in the southwest of the Carajás Domain (Fig. 1a). The Jaguar deposit comprises several orebodies located along two major fault systems, McCandless and Canaã, which have NE-SW and NW-SE

strikes, respectively. The largest orebodies (Jaguar group, North, Northeast, Central and West), lie in the southern part of the orefield and are hosted in Mesoarchean volcano sedimentary sequences and BIF horizons of the Serra Arqueada Fm. These orebodies are the major focus of exploration and are located along a direction following the strike of the Canaã Fault system. Onça-Rosa and Onça-Preta are smaller orebodies with a tabular morphology to the north of the Jaguar cluster and lie along the direction of the McCandless fault (Centaurus Metals 2024). Host rocks are granitoids/gneisses from the Carapanã Complex (part of the ~3 Ga basement), at the contact with mafic-ultramafic units (Centaurus Metals 2023). Alteration comprising amphibole and/or biotite/chlorite rocks is recognized along the faults (Fig. 1b, c). The Onça-Rosa orebody, the target of the present study, has a reserve of 1.9 Mt @ 0.98 Ni and 0.08 Cu.

Prior work on ores from Jaguar is limited to one thesis and two published papers (de Oliviera 2017, Ferreira Filho *et al.* 2021, Mansur *et al.* 2023). Oliviera (2017) recognized the hydrothermal and IOCG-like character of the mineralization, the marked alteration and strong structural control. Ferreira Filho *et al.* (2021) described the geology and petrography of the deposit and undertook whole-rock analysis. Importantly for the present work, they were the first to recognize an enrichment in rare earths and trace elements like Pb, Bi, and Te, as well as a conspicuous lack of measurable platinum-group elements (PGE). Ferreira Filho *et al.* (2021) concluded that Jaguar was an example of iron-oxide-apatite (IOA) mineralization. Based on their study of the compositions of magnetite, pyrite, and chalcopyrite in ore and host rock, Mansur *et al.* (2023) concluded that the deposit has features commensurate with a hydrothermal genesis comparable with other IOCG deposits in the region and where Ni was sourced from Neoarchean mafic–ultramafic layered intrusions. On this basis, Jaguar was therefore regarded as a particularly Ni-rich member of the IOCG clan, even if Mansur *et al.* (2023) acknowledge that the discriminant diagrams they employ are by no means unequivocal with respect to a hydrothermal rather than magmatic origin.

Analytical Methods

Fifteen polished thin sections (Supplementary data (SD) Figs. S1-S3) were prepared from eleven drillcore samples. Preliminary sample characterization involved reflected light optical and scanning electron microscopy (SEM) using a FEI Quanta 450 instrument operated in back-scattered electron (BSE) mode. Microbeam scanning X-ray fluorescence maps were obtained using a Bruker Tornado desktop scanner (National Institute of Criminalistics, Brasilia, Brazil). Quantitative analysis of amphiboles was undertaken using a JEOL JXA-8230 SuperProbe electron probe microanalyzer (EPMA) located in the Crti Laboratory, Federal University of Goiás, Brazil. Trace element LA-ICP-MS spot analysis of magnetite was conducted using a RESOlution-SE 193 nm Excimer laser coupled to an Agilent 8900x quadrupole ICP-MS. Two thinned S/TEM (<100 nm) foils were prepared from the sections using a FEI-Helios nanoLab Dual Focused Ion Beam and SEM (FIB-SEM) as outlined by Ciobanu *et al.* (2011). Each foil was analyzed with HAADF STEM equipped with a X-FEG Schottky source and Super-X EDS geometry. Imaging and energy-dispersive X-ray spectrometry (EDS)-STEM mapping using an ultra-high resolution, probe-corrected, FEI Titan Themis S/TEM operated at 200 kV. Unless otherwise indicated, all instrumentation is housed at Adelaide Microscopy, the University of Adelaide. Full details of methodologies, settings and standards are given as Supplementary data.

Calculation of mineral formulae was performed using a spreadsheet adapted from Ridolfi *et al.* (2018). Indexing of diffraction patterns was conducted with WinWulff© (JCrystalSoft) and publicly available data from the American Mineralogist Crystal Structure Database (http://rruff.geo.arizona. edu/AMS/amcsd.php). Crystal structure models were generated in CrystalMaker® and image simulations using STEM for xHREM™ software.

Results

Petrography

The studied sample are shown on the schematic stratigraphic column in Figure 2a and in greater detail in SD Figures S1-S3. Mineralization (the orebody), represented by a ~30 m-long interval along drillhole 127, is hosted within magnetite-bearing lithologies comprising chlorite+talc+amphibole in variable proportions. This is hosted, in turn, within a granitoid with a contact to the orebody marked by biotite+tourmaline alteration. Intervals still richer in magnetite, a few meters in width, are present throughout both the orebody and granite.

At the upper part of the sampled interval, magnetite is associated with sphalerite and pentlandite (+violarite), with pyrite in variable abundance (Fig. 2b, c). Amphibole is a main gangue component and apatite is also relatively abundant. Fabrics in which pentlandite and amphibole are located along shears crosscutting brecciated and deformed magnetite are typical of mineralization in the lower part of the orebody (Fig. 2d). A weak banding in magnetite is highlighted by pyrite ribbons whereas sphalerite occurs interstitial to the magnetite (SD Fig. S2). The banding is further marked by bands of talc+chlorite intercalated within the magnetite-rich matrix (Fig. 2e; SD Fig. S1). Amphiboles are abundant throughout both magnetite and talc+chlorite domains. Sulfides (pentlandite, pyrite, minor sphalerite) occur as disseminations throughout the magnetite-rich bands but also form stringers parallel with rock foliation and crosscut coarser grains of amphibole. Apatite is also present as bands throughout the gangue, and to a lesser extent within magnetite. Of particular interest is the presence of abundant ilmenite as thin needles along the foliation and following the sulfide stringers. The lower part of the orebody comprises the same association of sulfides (pentlandite+sphalerite) and magnetite with amphibole as the main gangue mineral (Fig. 2f, g). Violarite is abundant following brittle brecciation of pentlandite (Fig. 2f). Sphalerite displays ‘chalcopyrite disease’ but with variable textures, inclusions, thin veinlets and larger bodies of chalcopyrite along boundaries between sphalerite

and amphibole (Fig. 2g). Magnetite grains display inclusion-rich cores and clean, inclusion-free margins.

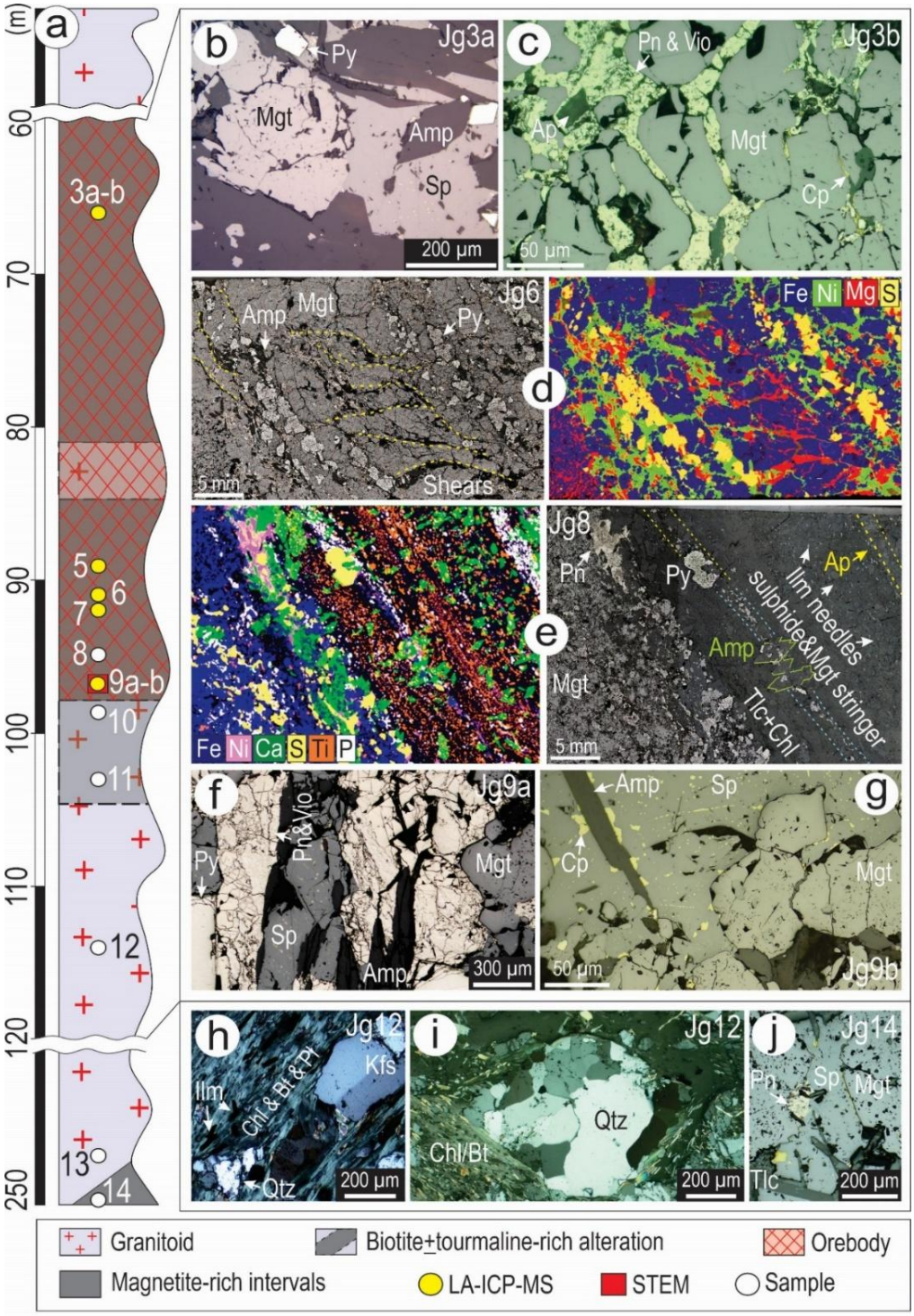

Figure 2. (a) Schematic stratigraphic column for drillhole DH00127. Reflected (b-g, j) and transmitted light (h-i) microphotographs showing the main petrographic aspects of ores and host lithologies as described in the main text. The right panel in (d) and left panel in (e) are XRF maps of the identical areas as the reflected light images. Amp–amphibole; Ap–apatite; Bt–biotite; Cp–chalcopyrite; Chl–chlorite; Ilm–ilmenite; Kfs–k-feldspar; Mgt–magnetite; Pl–plagioclase; Pn–pentlandite; Py–pyrite; Qtz–quartz; Sp–sphalerite; Vio–violarite.

The granitoid is typified by phenocrysts of orthoclase and ocular aggregates of quartz within a fine-grained matrix of chlorite+biotite+plagioclase with a fluidal texture (Fig. 2h, i). Magnetite-sulfide intervals, albeit with talc and carbonate gangue, occur throughout the granitoid and are illustrated from the lowermost part of the drillhole in Fig. 2j.

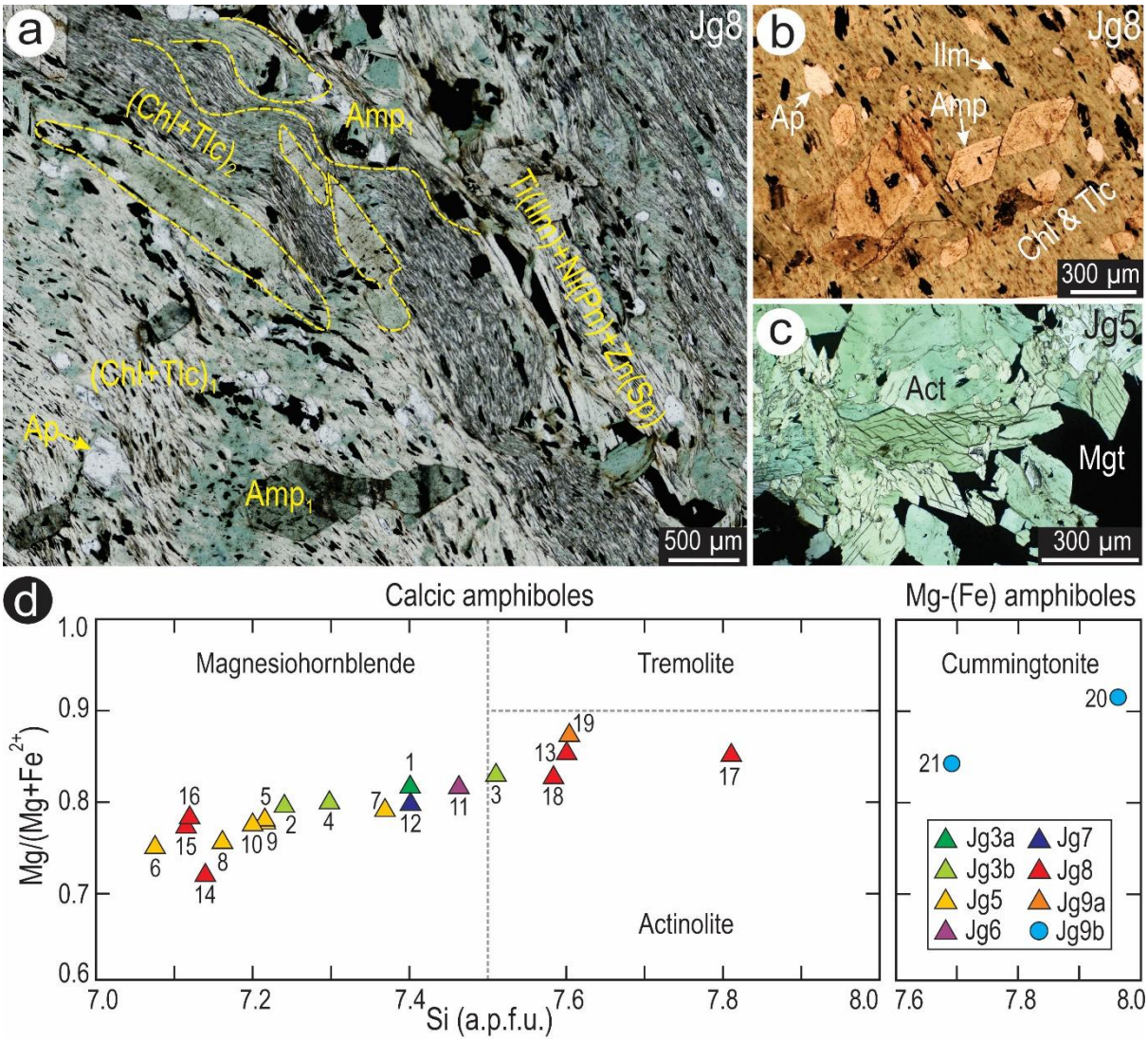

Figure 3. (a-c) Reflected light images showing amphibole assemblages and rock fabrics. (d) Compositional plots for amphibole classification (after Leake *et al.* 1997) from different samples as labelled. Data from SD Table 1a (Supplementary Data). Amp–amphibole; Ap–apatite; Chl–chlorite; Ilm–ilmenite; Mgt–magnetite; Pn–pentlandite; Sp–sphalerite.

The talc+chlorite matrix shows coarser- and finer-grained domains with microfolding around amphibole phenocrysts parallel to foliation but crosscut by coarser, euhedral amphibole (Fig. 3a). Small grains of apatite are also embedded in the matrix, whereas abundant ilmenite needles

highlight the fluidal fabric and crosscut amphibole phenocrysts (Fig. 3b). This is, however, not the case in amphibole from the mineralized intervals (Fig. 3c). Irrespective of the environment, these amphiboles are calcic, and plot in the magnesiohornblede and actinolite fields (Fig. 3d; SD Table S1a).

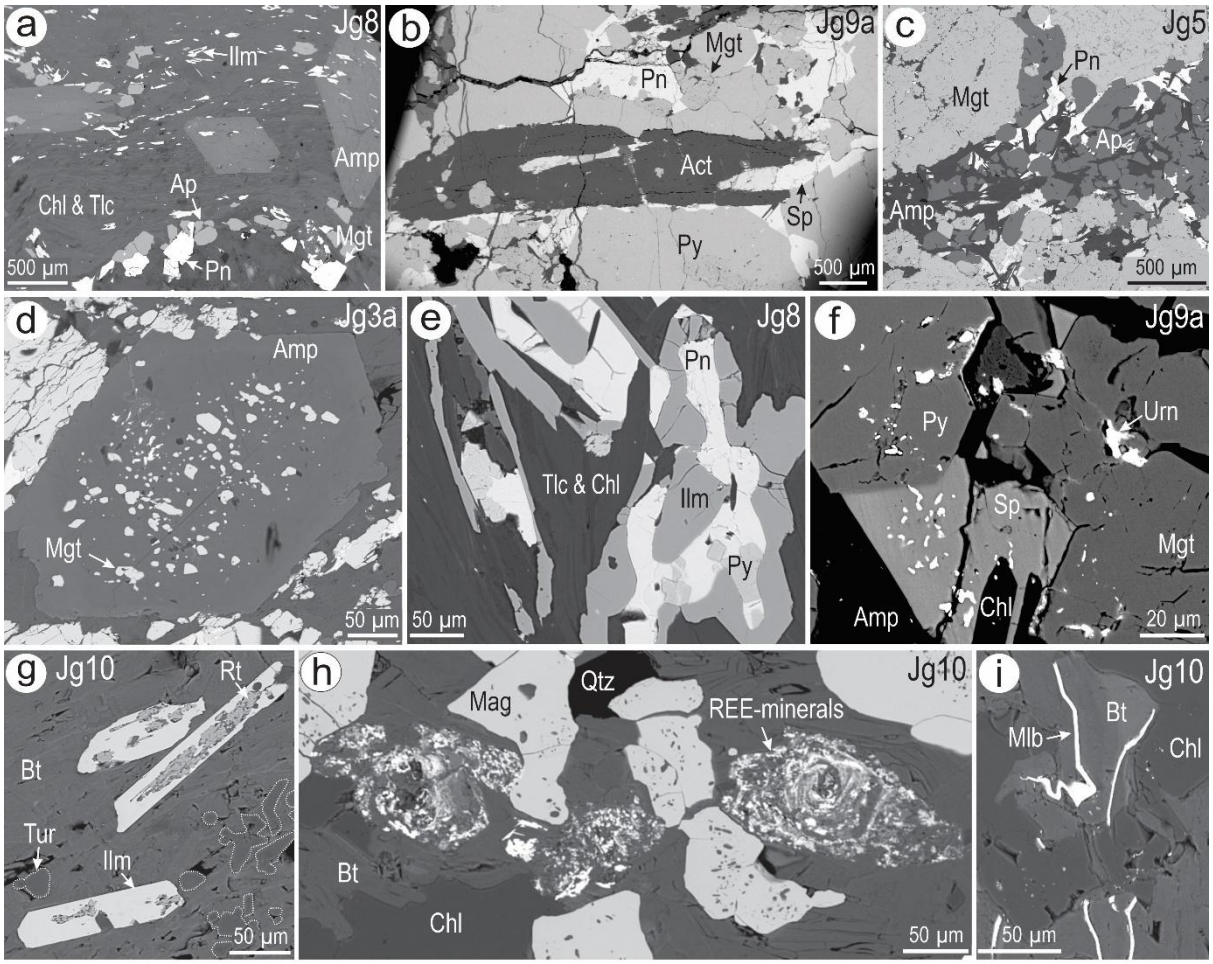

Figure 4. BSE images showing ore mineral associations in the orebody (a-f) and granite (g-i). (a) Amphibole (Amp) from bands of talc (Tlc)-chlorite (Chl) that are crosscut by stringers. Note the presence of ilmenite (Ilm), apatite (Ap) and pentlandite (Pn). (b) Late actinolite (Act) crosscutting boundaries between magnetite (Mgt) and sulfides. Minor replacement of actinolite by sulfides is also noted. (c) Cluster of apatite within brecciated amphibole enclosed by magnetite. (d) Field of magnetite inclusions within amphibole. (e) Detail of ilmenite from stringers in (a) showing a close association with pentlandite. (f) Cluster of uraninite (Urn) crosscutting mutual boundaries between magnetite, sphalerite (Sp) and pyrite (Py). (g) Accessory igneous ilmenite from granite showing inner replacement by rutile (Rt). Tourmaline (Tur) is abundant in this case. (h) Field of 'ghost' REE minerals and inclusion-rich magnetite in altered granite. Note quartz (Qtz) grains between magnetite grains. (i) Filaments of molybdenite (Mlb) within granite. Note infill of biotite (Bt) – chlorite boundaries.

In closer detail, the stringers crosscutting amphibole contain apatite, magnetite, and pentlandite, alongside ilmenite (Fig. 4a). Elongate laths of amphibole crosscut sulfides (Fig. 4b). Inclusions of sulfides, apatite and magnetite are, however, also present in variable proportions within the amphibole (Fig. 4b-d). Ilmenite located along the stringers (Fig. 2e) shows unusual symplectitic intergrowths with pentlandite and minor pyrite (Fig. 4e). Clusters of fine uraninite crystals are observed across boundaries between magnetite and sphalerite (Fig. 4f).

Oriented laths of ilmenite are also abundant in the granitoid (Fig. 4g). In this case, internal alteration of ilmenite to rutile is common. The granitoids also contain ghost-like rare earth minerals (monazite and/or bastnäsite?) and abundant filaments of molybdenite (Fig. 4h, i). Magnetite is abundant and contains clustered inclusions of gangue minerals (Fig. 4h).

Trace element geochemistry

Trace element concentrations in minerals characteristic of the IOCG signature (magnetite, amphibole, and apatite) are listed in SD Tables 1b, c.

Box-and-whisker plots of the trace element data (Fig. 5a) are grouped into four categories: lithophile elements, transition metals, Σ(REE+Y) (hereafter REY), and a group encompassing U, ^{206}Pb, W, Sn, and Mo, which we term 'granitophile elements'. The cores of magnetite grains contain greater concentrations of most lithophile elements and transition metals compared to the inclusion-free rims. Concentrations of Ni, Co, and Mo are however roughly comparable. Among the transition metals, Ni reaches the greatest concentration in magnetite and amphibole with only limited least variation (means of 1974 $\pm$ 1259 and 2288 $\pm$ 3019 ppm in core and rim magnetite and 1742 $\pm$ 641 ppm in amphibole). Titanium concentrations are also broadly comparable, with means of 355 $\pm$ 122 and 253 $\pm$ 56 ppm in core and rim magnetite and 505 $\pm$ 393 ppm in amphibole. In contrast, V is higher in magnetite (means 507 $\pm$ 138 and 610 $\pm$ 211 ppm in core and rim) than in amphibole (mean 66 $\pm$ 23 ppm).

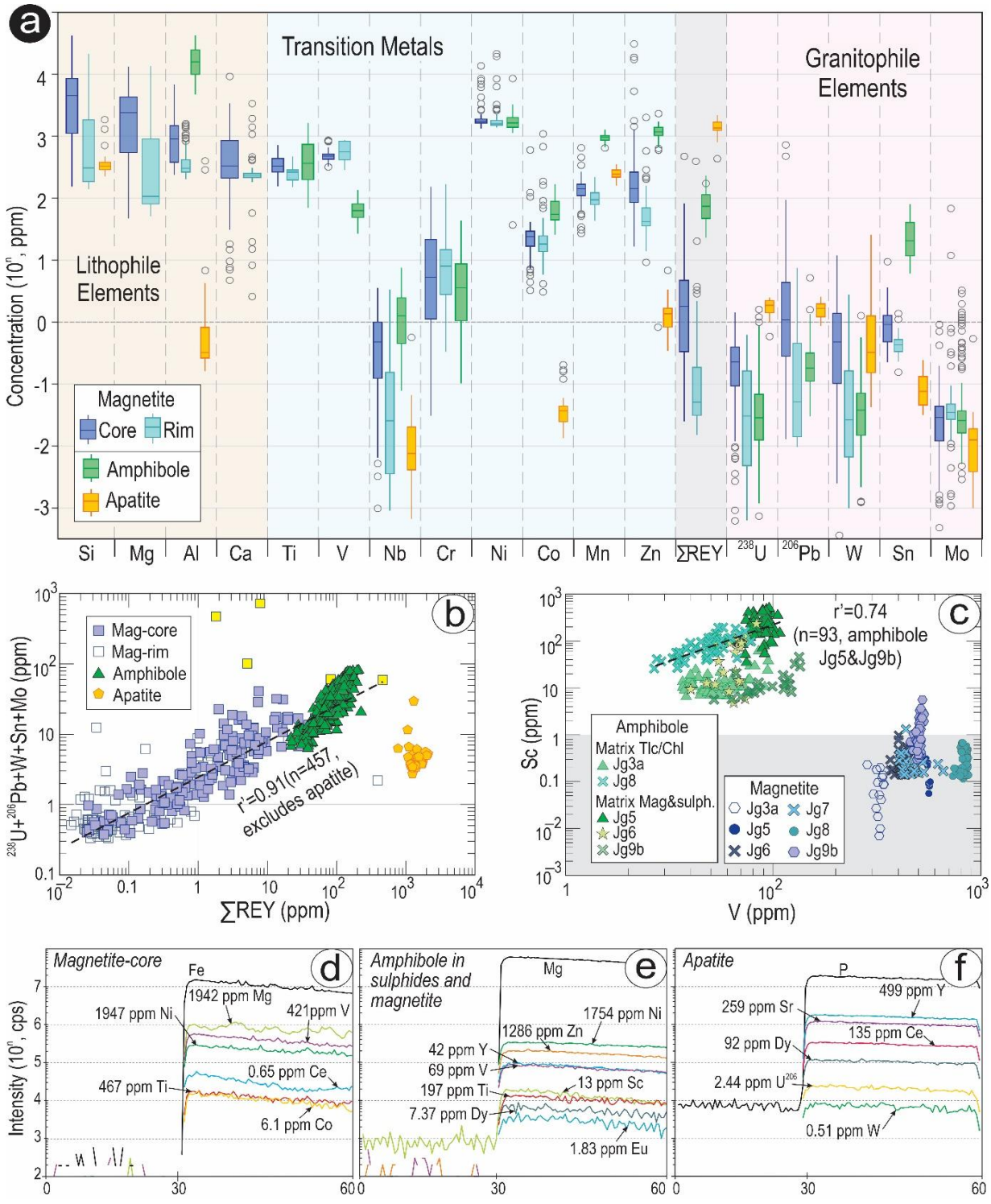

Figure 5. LA-ICP-MS trace element concentration data for magnetite, amphibole and apatite. (a) Box-and-whiskers plots showing ranges for groups of elements as labelled. (b) Binary plot showing strong correlation between ΣREY and granitophile elements across magnetite and amphibole. (c) Correlation between Sc and V inn amphibole from different context as labelled. No correlation is observed for magnetite, which is enriched in V but depleted in Sc relative to the amphibole. (d-f) Time-resolved depth profiles for representative spot analyses of magnetite, amphibole and apatite as labelled. Trace element concentration data in ppm. Solid lines within the box on (a) represent median values.

Chromium is only a trace component (18 ppm in core and rim magnetite and 6 ppm in amphibole. Cobalt is slightly higher in amphibole (mean 63 ± 25 ppm) relative to magnetite (27 and 45 ppm in core and rim, respectively). Zinc concentrations are far higher in amphibole (mean 1208 ± 251 ppm) than in magnetite (608 and 94 ppm for core and rim).All minerals contain measurable ΣREY, albeit with differences. Apatite is the preferred host (mean 1428 ± 314ppm), followed by amphibole (mean 84 ± 44 ppm) and magnetite (5 ppm in both core and rim).

Concentrations of granitophile elements are generally low (<1 ppm) but measurable. Relatively greater concentrations of U and Pb are measured in apatite (~2 ppm), and magnetite cores (11 ppm for ^{206}Pb). Tin is highest in amphibole (mean 28 ± 20 ppm).

Binary plots confirm a strong correlation (r'=0.91) between ΣREY and granitophile elements in both magnetite and amphibole, whereas apatite forms a tight cluster on this plot (Fig. 5b). A plot of Sc vs. V discriminates amphiboles within distinct matrices (talc/chlorite or magnetite/sulfides (Fig. 5c). A good correlation (r'=0.74) is seen for amphiboles in a magnetite/sulfide matrix, in which the mean Sc concentrations in amphibole lie between 56 ppm (sample Jg6) and 214 ppm (sample Jg5). In contrast, no correlation is seen in amphibole from the talc/chlorite matrix, in which Sc concentrations are much lower (mean ~15 ppm, samples Jg3a and 8).

Many LA-ICP-MS spot analyses of magnetite, amphibole and apatite feature time-resolved downhole depth profiles with smooth signals for elements of interest indicating these occur within the lattice rather than as micron-scale inclusions (Fig. 5d-f).

Chondrite-normalized REY fractionation patterns

After eliminating data attributable to obvious REE-mineral inclusions (SD Table S1e), chondrite-normalized REY fractionation patterns for magnetite, apatite and amphibole display a spectrum of trends that reflect differences within the population (Fig. 6).

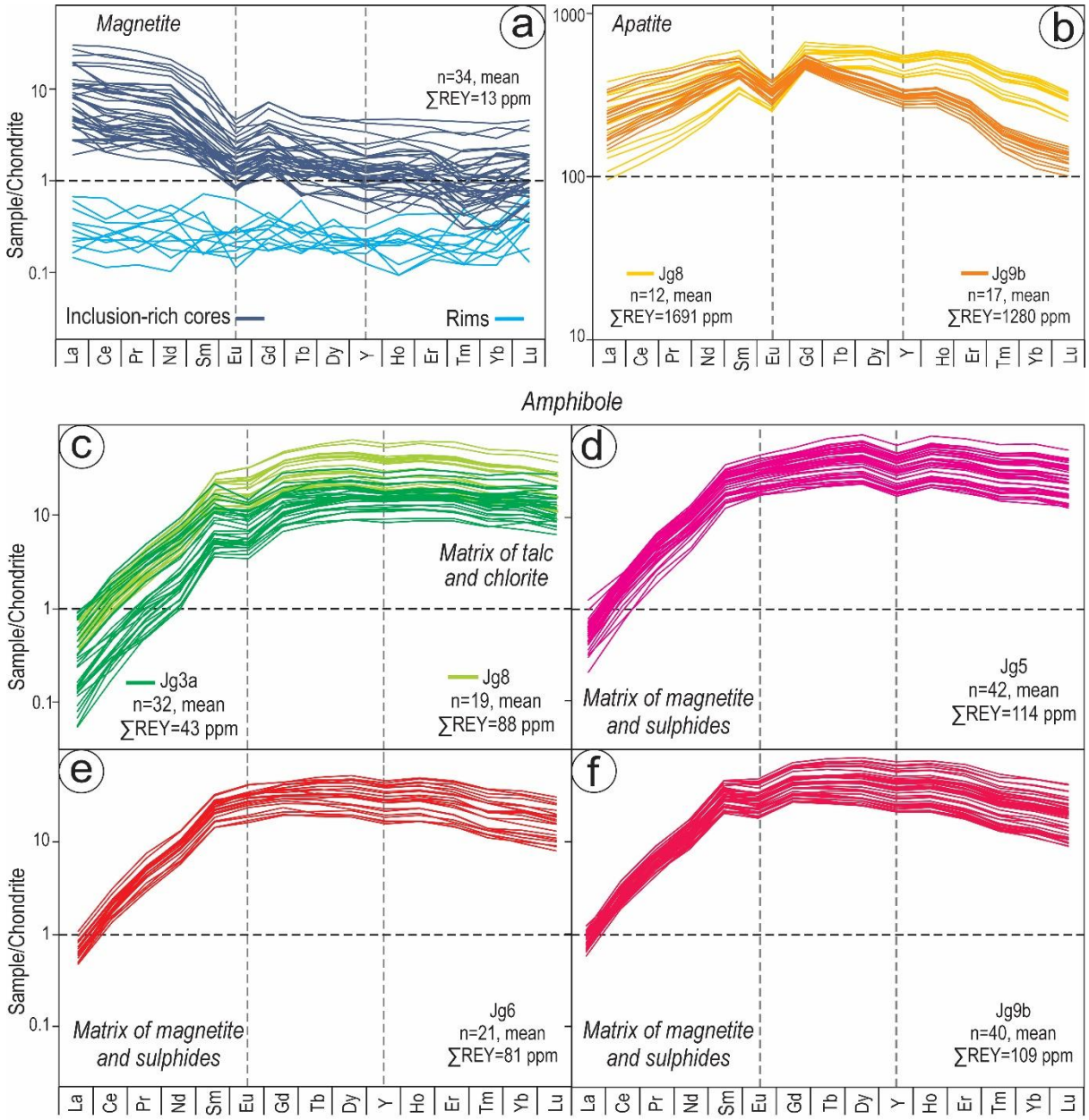

Figure 6. Selected chondrite-normalized REY fractionation patterns for magnetite (a), apatite (b) and amphibole (c-f) from different association as labelled (data from Supplementary data SD Table 1e. Chondrite values from McDonough & Sun (1995).

Magnetite cores display a consistent pattern in which the LREE segment is downwards sloping, with a negative Eu anomaly (Fig. 6a). In contrast, rim magnetite is characterized by flat and generally noisy trends due to very low absolute values. Apatite from distinct matrices (talc+chlorite or magnetite+sulfides) shows comparable concave trends with mild enrichment in MREE, as well as a well pronounced negative Eu anomaly (Fig. 6b). The concavity of the HREE segment is, however, less pronounced for apatite hosted by talc+chlorite.

REY fractionation trends for amphiboles in different samples and/or host associations display comparable trends with a steep increase from LREE to MREE, followed by a relative flat HREE segment (Fig. 6c-f). There are nevertheless, some differences in terms of Eu and Y anomalies (Fig. 6c-f). Amphibole in a matrix of talc+chlorite displays common patterns in all studied samples with a marked negative Eu anomaly (Fig. 6c). In contrast, amphibole hosted in a matrix of magnetite+sulfide shows variation in terms of Eu and Y anomalies, from a negative Y anomaly in sample Jg5, no Eu or Y anomalies in sample Jg6, to a negative Eu anomaly in sample Jg9b (Fig. 6d-f).

Nanoscale characterization of magnetite

Magnetite features silicate-mottled domains of variable density and complexity (Fig. 7a-c). In addition to the fine-grained silicates that dominate the mottled areas, relatively coarser (μm-sized) inclusions of talc, chlorite and/or biotite (hereafter 'TBC') occur, in variable proportions, along preferential directions in magnetite and also infill microfractures (Fig. 7a). Some of these domains display curvilinear boundaries against apparently clean, inclusion-free magnetite (Fig. 7b). A characteristic texture in which the inclusions have a fan-like distribution is seen in some mottled domains (Fig. 7c).

One grain of magnetite, from the ore sample at the granite contact (sample Jg9b) and associated with sphalerite and pentlandite, was selected for nanoscale study (Fig. 7d). Various shades of grey are indicated on the BSE images, along with sub-μm-scale inclusions of Pb-(Bi) minerals and uraninite, LA-ICPMS spot analysis of magnetite shows up to 4 ppm U (Fig. 7e). Two locations within the grain, with variable inclusion density, were selected for FIB cuts to obtain S/TEM foils (Fig. 7f, g). The less mottled area within the magnetite also contains some inclusions of Pb-Bi-bearing phases adjacent to a larger patch of TBC.

Images of the two foils show that the mottling observed on the surface of the polished block surface continues at depth (Fig. 7h, i). In addition, relatively coarser (µm-sized) TBC inclusions are noted, more abundant in the foil obtained from the less-mottled magnetite.

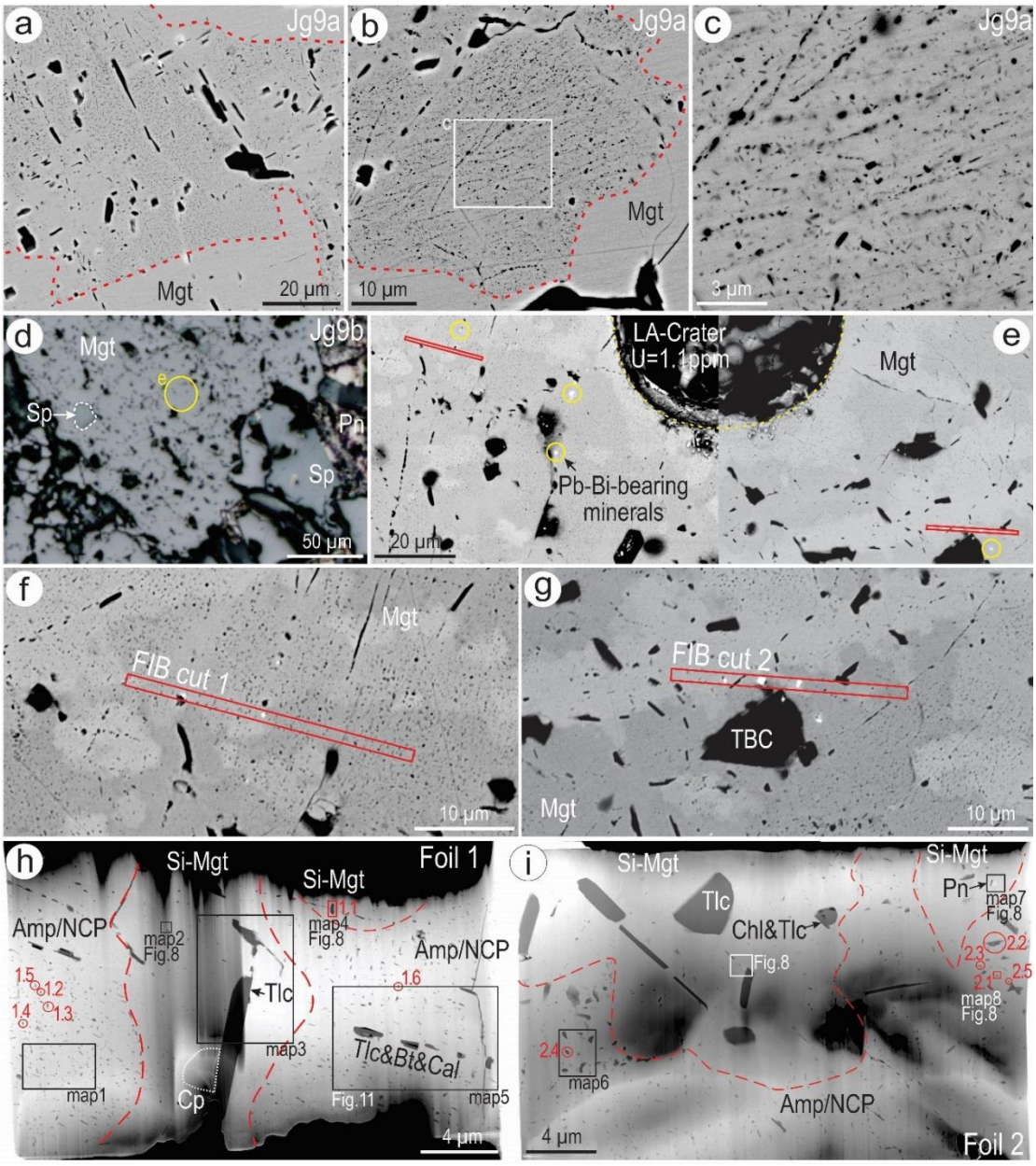

Figure 7. (a-c, e-g) BSE and (d) reflected light images of mottled magnetite (Mgt). (a) Magnetite displaying inclusion- and pore-rich and -poor domains separated by dashed lines. (b, c) Details of inclusions rich domains showing fan-like distribution. Location of (c) marked by rectangle in (b). (d-g) Location of the two FIB cuts from which S/TEM foils were prepared. Note the differences in inclusion density for each of the two foils, i.e., denser in (f) and less dense in (g). (h, i). HAADF STEM images of the two foils extracted from locations in (f, g). dashed lines separate domains of different inclusion types as labelled. Abbreviations: Amp–amphibole; Bt–biotite; Cal–calcite; Chl–chlorite; Cp–chalcopyrite; NCP–non-classical pyriboles; Pn–pentlandite; Si-Mgt–silician magnetite defects; TBC–talc+biotite+chlorite; Tlc–talc.

In both foils, we observe that the nanoscale inclusions of silicates within the mottled domains are typically amphiboles, each up to several hundred nm in length (Fig. 8a-c). Element maps of wider fields also show that the dominant inclusion types in the mottled magnetite domains comprise amphibole+NCP assemblages (SD Fig. S4). Amphibole compositions obtained from EDS STEM maps (SD Table 1a) plot in the field of cummingtonite (Fig. 3d).

Cummingtonite is typified by a chemical zoning with respect to the relative proportions of Ca and (Mg, Fe) (Fig. 8a). Higher Ca defines rhythmic bands up to tens of nm in width and distinct domains within the same amphibole grain. This Ca-banding is typical of all studied grains (Fig. 8b, c). A second characteristic feature is the presence of lattice disorder, which is defined by coherent intergrowths between cummingtonite and non-classical pyriboles (NCPs) of variable chain width and abundance along *a*.

The NCPs in amphiboles from the most densely mottled domains are more frequent and also more varied in size and arrangement. In contrast, the NCPs are mostly either single slabs or up to three slabs wide across the entire grain width (such features are termed 'zippers') in less densely mottled domains. Some of the widest NCPs, up to 9-I_{beams} in width, are recognized at direct contacts between cummingtonite and talc (Fig. 8b). Mixtures of TBC are more common in grains from the less mottled magnetite and can also form distinct lamellae within the talc (Fig. 8c).

A further feature of the magnetite from Jaguar is the presence of silician magnetite defects along <111>* directions. These occur within fields throughout the cleaner domains between amphibole inclusions (Fig. 7h, i). Some fields display an association between such defects, all of which are oriented along $<111>^*_{magnetite}$ and the relatively coarser inclusions (up to 50 nm) (Fig. 8d). Mapping of such fields show the presence of Mg, Al and K in addition to Si (Fig. 8e; SD Fig. 5). A profile across some of the narrowest inclusions shows concentrations of these elements, with a dominance of Si relative to minor Mg, K and Al (Fig. 8f).

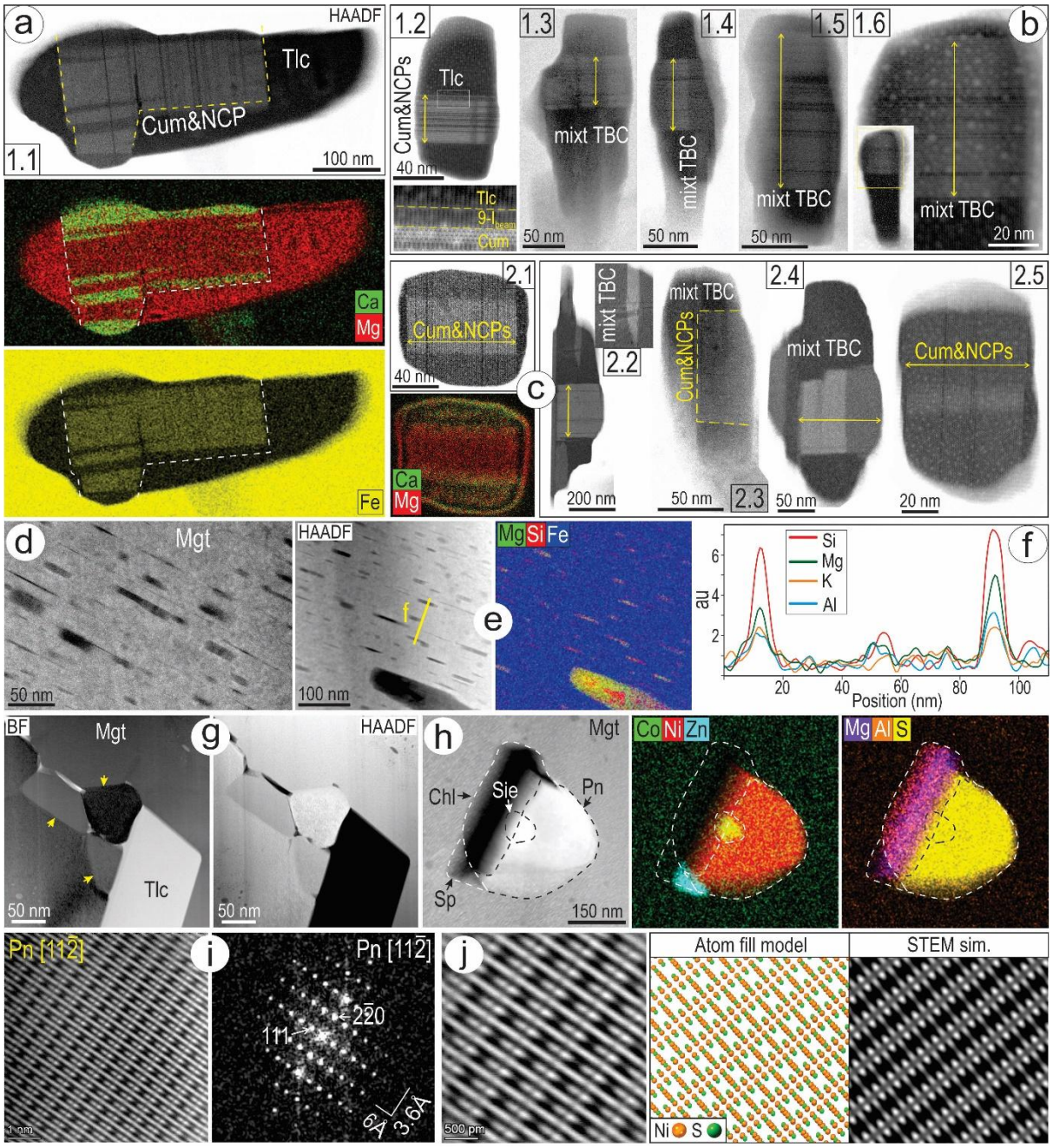

Figure 8. (a-c) HAADF STEM images and EDS STEM maps showing representative NCP-bearing cummingtonite (Cum) + TBC inclusions in magnetite (Mgt). Length of Cum marked by yellow arrows. Note the presence of Ca-rich rhythmic bands (darker) across all the grains. One of the longest chain silicates, 9-I_{beam}, marks the boundary between Cum and talc (Tlc) inset for grain 1.2. (d) Field of Si-magnetite defects attached to Si-Mg-inclusions from lens dense mottled domains in magnetite. (e) EDS STEM map of Si-Mg-bearing inclusions in magnetite. (f) Profile, located on (e), showing the presence of Al and K besides Si and Mg within such inclusions. (g) BF and HAADF STEM images showing recrystallized magnetite along a fracture at the contact with talc (Tlc). (h) EDS STEM maps of pentlandite (Pn) associated with chlorite (Chl). Note nanoparticles of sphalerite (Sp) and siegenite (Sie). (i) HAADF STEM image and corresponding fast Fourier transform (FFT) pattern of pentlandite in (h) on zone axis as labelled. (j) Image crop from (i) showing the match with crystal model and STEM simulation for pentlandite.

The magnetite exposed in each foil is a single grain, with an identical orientation across each foil) but fine-grained aggregates of magnetite (up to 200 nm width) are also identified along fractures (Fig. 8g). Relatively coarser talc also occurs along such fractures (SD Fig. 5). Sulfides (chalcopyrite, Fig. 7h; and pentlandite, Fig. 7i) are also identified along fractures. Pentlandite is associated with fine particles of sphalerite and siegenite. A lamella of chlorite is attached to the pentlandite, which could be assessed by high-resolution imaging (Fig. 8i). The crystal model and STEM simulation show a good match with the HAADF STEM image.

The identities of chain silicates, amphiboles and NCPs are recognized from high-resolution HAADF STEM images and STEM simulations on [001] zone axis, adopting previously introduced models (Ciobanu *et al.* 2022; Campo-Rodriguez *et al.* 2024a). These were used for cummingtonite and higher-order chain silicate structures, i.e., 3- to 5-I_{beams} as shown in Figure 9a.

Cummingtonite and talc display a coherent crystallographic orientation with a_{Cum} parallel to c_{Tlc} (Fig. 9b). Disorder in cummingtonite is defined by the presence of NCPs of variable chain width, ranging from 3- to 17-I_{beams} along b_{Cum}. In the less mottled magnetite, the NCPs occur as single zippers, albeit of variable I-beam width (Fig. 9c). In contrast, in the denser mottled magnetite, intergrowths between different chain silicates, ranging from 3- to 6-I-beams in width, are present as disordered sequences within the amphibole (Fig. 9d). Such complex sequences of NCP intergrowths within cummingtonite are common and can also be defined as polysomes: e.g. (3325), (636), and (334253) (Fig. 9e).

Figure 9. (a) Atomic scale resolution images and STEM simulations for the most common chain silicates (as labelled) projected on [001] zone axis. Note that the sequence representing 3-, 4- and 5-I_{beams} is in the interval marked by dashed lines. Scales bars: 1nm. (b) Coherent contact between cummingtonite (Cum) and talc (Tlc). Note dark bands corresponding to Ca-rich zones. (c-e) Intergrowths between cummingtonite and NCPs zippers ranging from rare in (c) to dense in (d, e). Numbers correspond to I-beam notation. A longer polysomatic sequence comprising variable chain silicates, up to 6I_{beam}, is marked for (e).

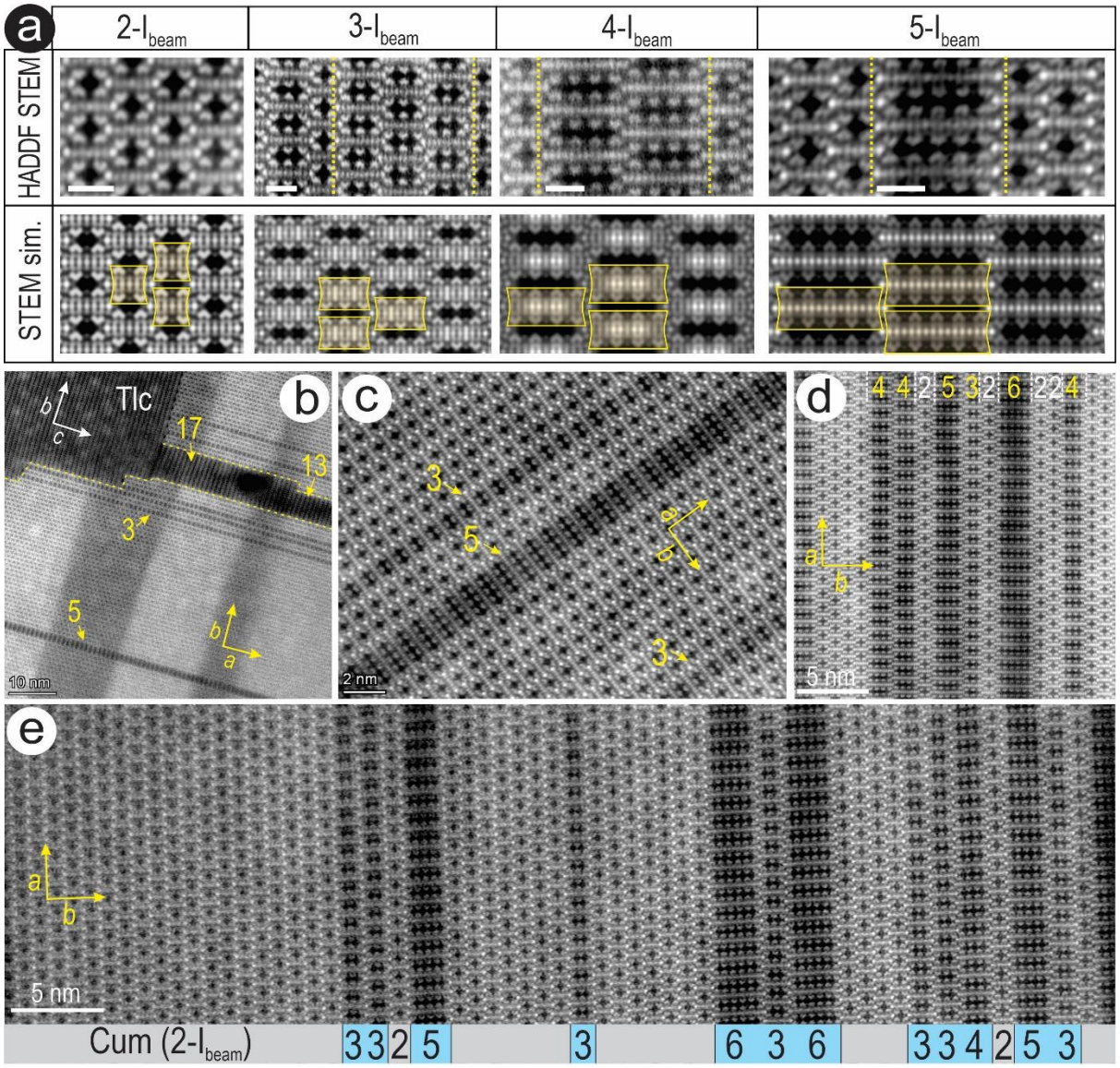

Other sheet silicates, such as biotite and chlorite, are also identified along the margins of cummingtonite in the less mottled magnetite (Fig. 10a, b). Stacking disorder in a ~30 nm-wide chlorite sequence between cummingtonite and biotite is depicted along the *c* axis on both the image and the fast Fourier transform FFT pattern (Fig. 10b). The most complex sequences of sheet silicates, ~100 nm in width, display intergrowths of talc, chlorite and serpentine group minerals (Fig. 10c). In closer detail, we observe (*T*-*O*-*T*)-*O*-(*T*-*O*-*T*) arrangements, where *T*= SiO_4 tetrahedra and *O*=ribbons of cation octahedra, in a slab typical of polytypes of the two-layer chlorite group (Fig. 10d). Comparison with STEM simulations tentatively indicates the IIb-4 triclinic variety described by Lister & Bailey (1967) (Fig. 10e). This is distinct from the other two

sheet silicates, which comprise (T-O-T) slabs, i.e., K-(T-O-T)-K in biotite, and (T-O-T)-(T-O-T) in talc. Both are associated with amphibole inclusions in magnetite from Jaguar.

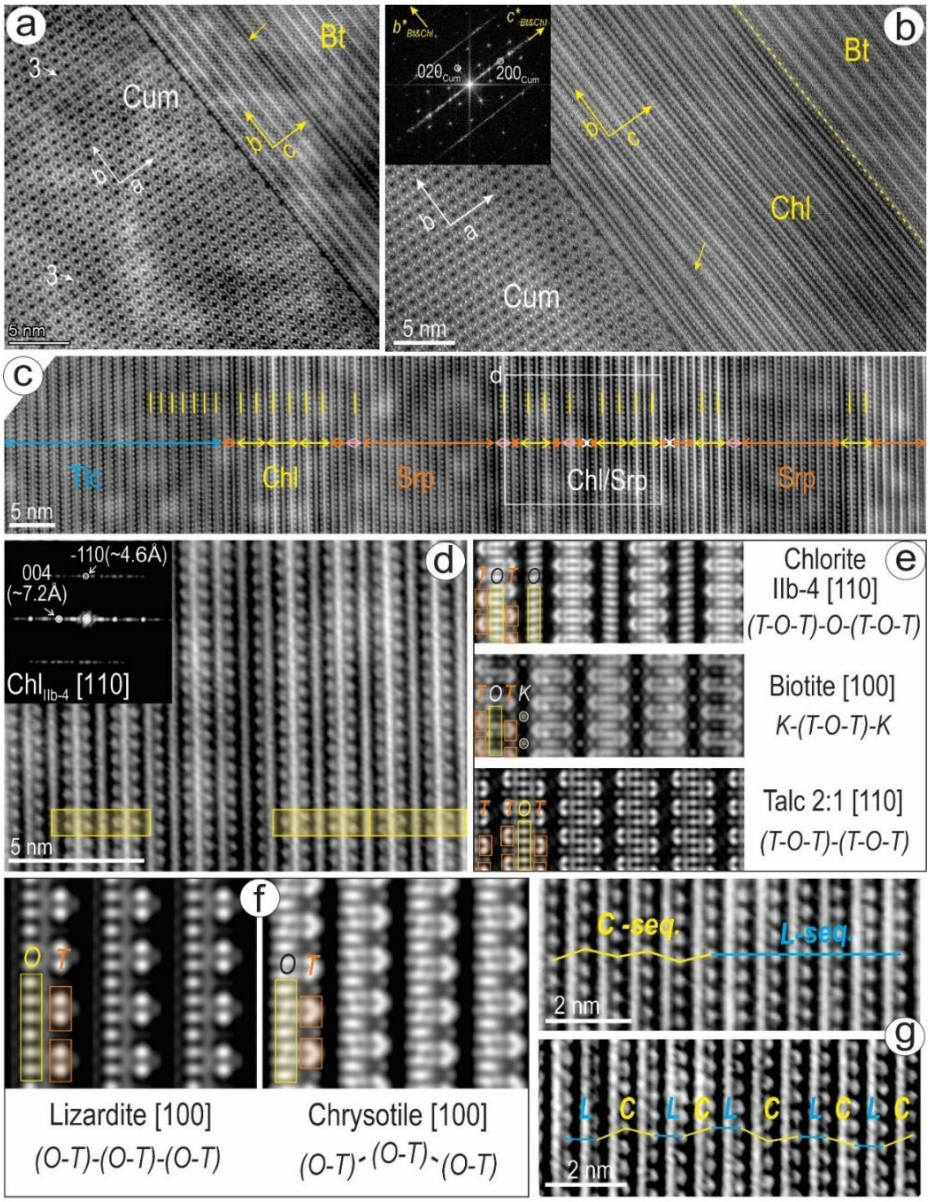

Figure 10. (a-b) High-resolution images showing straight contacts between $[100]_{Bt\text{-}Chl}$ and $[001]_{Cum}$. Note the stacking disorder in biotite (Bt) from (a) and defects in chlorite (Chl) from (b) marked by yellow arrows. Inset in (b) is the FFT pattern corresponding to the image and showing coherent orientation between the two silicates. (c) Longer interval (~100 nm) of sheet silicates comprising sequences of talc (Tlc), chlorite and serpentine (Srp) as labelled. Yellow bars indicate the repeats along c axis corresponding to different species. (d) Crop from (c) marked by rectangle showing the layer stacks for $chlorite_{IIb\text{-}4}$ (yellow overlays) on [110] zone axis. Inset shows the corresponding FFT pattern. Note disorder along c^*. (e, f) STEM simulations of sheet silicates on zone axes as labelled and accompanying schematics for the representative layer stacks within each of them. *T*, *O* = tetrahedral, octahedral layer; K=potassium intralayer in biotite. The O and T modules are also marked as overlays on the STEM simulations. (g) Crop images from (c) showing details of serpentine group minerals displaying stacking disorder. This is marked by lines linking pairs of *T* modules across a single *O* (octahedral) ribbon. Interpretation along the lines as slabs of chrysotile (C, yellow) and lizardite (L, blue) was made using the models shown in (f).

In contrast, lizardite and chrysotile are two species from the serpentine group that are typified by simpler (O-T)-(O-T) slabs albeit with different array configurations (Fig. 10f). Both species are recognized within disordered sequences displaying alternating sequences or single layers of lizardite and chrysotile (Fig. 10g).

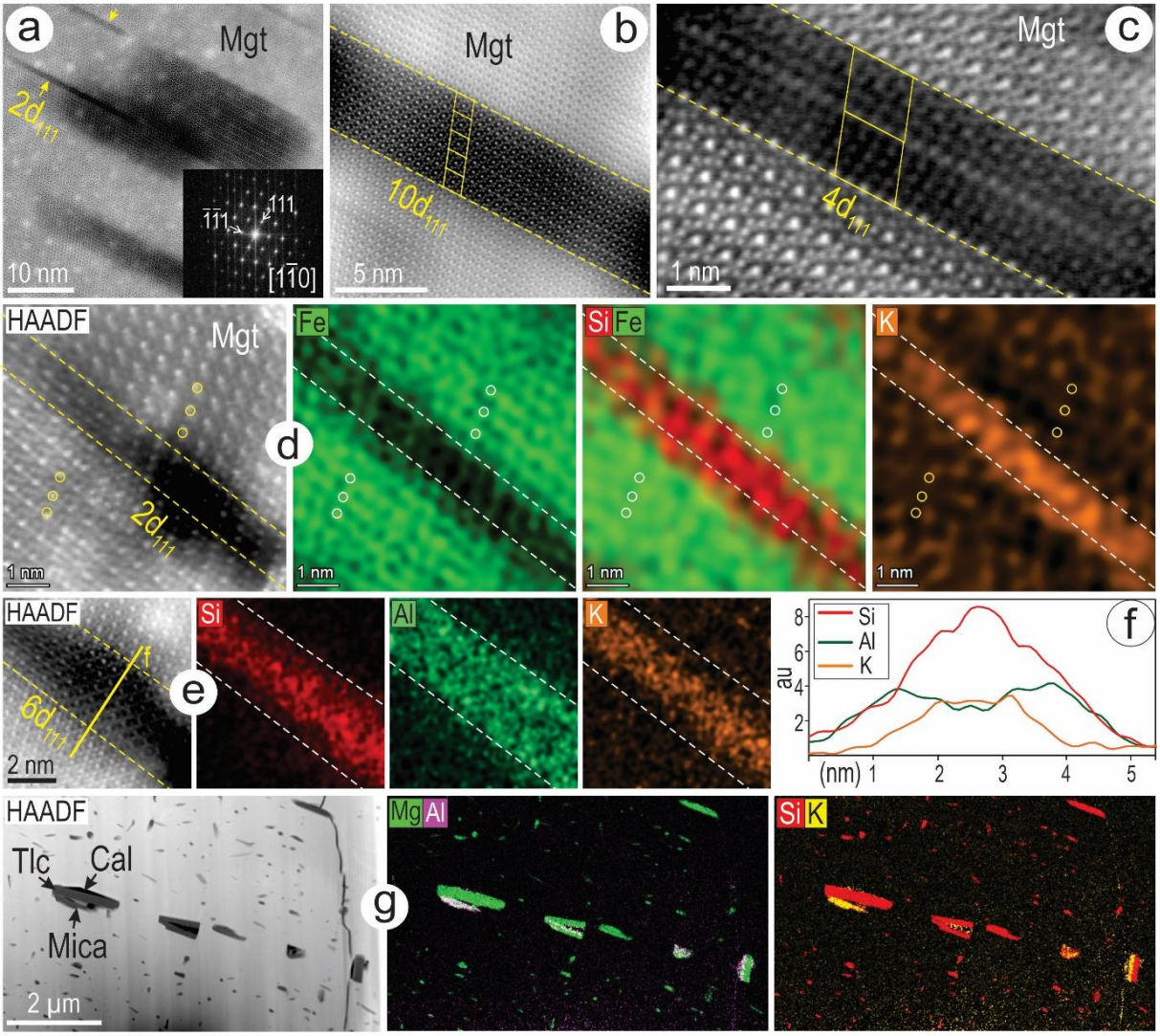

Figure 11. (a-c) Silician magnetite (Si-Mgt) as defects of variable widths (2n $d_{111\text{-magnetite}}$ as labelled) in magnetite. FFT pattern in (a) shows magnetite (Mgt) on [1-10] zone axis. Note the typical STEM image for magnetite on this zone axis remains the same across the defect in (b) but shows some changes in (c). The defects (outlined by dashed lines) are visible in both cases by darker HAADF contrast on the images. (d) Narrow Si-Mgt strip in magnetite and atomic resolution maps showing that Si is accompanied by K along the defect. Note the Fe map depicts the columns of 2 $Fe^{octahedral}$ sites that appear as brighter dots on the image (see Xu *et al.* 2014 and Ciobanu *et al.* 2019 for additional explanations). (e) Image and element maps of one of the wider Si-Mgt strip in magnetite showing presence of Al in addition to Si and K. (f) profile marked in (e) shows the relative distribution of these elements with K in the inner part and Al on the margins of the Si-rich strip. (g) Image and element maps of a string of sheet inclusions interpreted to form from the Si-Mgt defects. Note presence of mica, talc (Tlc) and minor calcite (Cal).

Silician magnetite defined by 2n x d_{111} occurs as needles associated with darker, platelet-shaped inclusions (Fig. 11a). The widest defect has n=5 and preserves the typical appearance of magnetite on the [1$\bar{1}$0] zone axis, albeit within a darker strip (Fig. 11b). The Si-substituted magnetite along <111> directions was defined using STEM imaging and density functional theory calculations, as a discrete maghemite-related structure of composition γ-$Fe_{1.5}SiO_4$ (Xu *et al.* 2014). The observed darkening relates to incorporation of Si^{4+} cations that replace Fe^{3+} in tetrahedral (*T*) sites whereas vacancies are introduced in octahedral (*M*) sites.

Some of the Si-magnetite defects show changes in the structure, but these are difficult to assess given their small size (Fig. 11c). Nonetheless, additional elements are mapped along such modified Si-magnetite defects, e.g. K through the inner part of one of the narrowest 2 d_{111} defect (Fig. 11d). Aluminum can also be present together with K as observed in wider defects (Fig. 11e). In such cases, Al is placed on the edges of the defect, whereas K is located in the center (Fig. 11f).

A correlation between Si-magnetite defects and formation of discrete sheet silicate associations comprising talc and mica is documented from EDS STEM mapping (Fig. 11g). Mapping also shows that talc infills wider (up to 1 µm-wide) fractures within magnetite (SD Fig. S5).

Discussion

Textural and mineralogical inferences for petrogenesis and ore formation

The position of the Onça-Rosa orebody at the top of a mafic/ultramafic unit (marginal to the Puma layered complex?) suggests that the observed mineralization, restricted to talc-magnetite-bearing rocks, is related to metasomatism of a mafic/ultramafic protolith in the contact aureola of a granite. The lack of ilmenite and spinels within the magnetite rules out the likelihood that it originated as an accessory component of the igneous rock. Ilmenite of inferred igneous origin can only be considered for that observed in the host granite (Fig. 4i). The abundant magnetite in the Onça-Rosa orebody is therefore assumed to be the product of early-stage (hydrothermal) metasomatism. The presence of widespread talc alteration within the lithologies indicates that the

(pyroxene/olivine-bearing) protolith had an ultramafic rather than mafic affiliation. This hypothesis is further supported by the identification of serpentine group minerals as inclusions within magnetite (Fig. 10g).

Remarkably, the presence of pentlandite as the dominant Ni-sulfide mimics the assemblages reported from so-called 'hydrothermal Ni deposits' such as Avebury, Tasmania (Keays & Jowitt 2013). The lack of pyrrhotite may indicate that this was extensively replaced by Co-Ni-bearing pyrite (Fig. 2f). Prolonged formation of sphalerite can be inferred from its co-existence with deformed magnetite and both pentlandite and Co-Ni-bearing pyrite that were precipitated later (Figs. 2b, f). This differs from the associations in the Avebury deposit where sphalerite is restricted to sulfide ores (Keays & Jowitt 2013).

We interpret the formation of magnetite, typified by rounded, deformed grains, as having taken place prior to a main shearing event that controls pentlandite deposition (Fig. 2d). Formation of calcic amphiboles (actinolite, hornblende) along the same shears together with pentlandite indicates an episode of calcic metasomatism (Fig. 2f). Comparable assemblages involving late amphiboles are recognized in skarn assemblages at Avebury and clearly overprint sulfides (Keays & Jowitt 2013). In the Jaguar deposit, formation of apatite can be connected to distinct stages of alteration, i.e., as bands within talc-chlorite and as clustered grains within amphibole from magnetite-sulfide ore (Figs. 4a, c).

The latest stage of mineralization is marked by stringer zones hosting often eclectic ore mineral assemblages (sulfides, magnetite, ilmenite, monazite, molybdenite, etc.) that crosscut amphiboles. In this case, the unusual association of ilmenite with pentlandite (Fig. 4e) indicates likely remobilization of Ni and Ti, elements that are often, although erroneously, considered to be relatively immobile. Clustered inclusions of uraninite flood across magnetite-sulfide boundaries marking the infill of pores produced during and/or post ore brecciation (Fig. 4f).

The coexistence of ferrous-phlogopite (de Oliveira 2017) and tourmaline (a high-volatile mineral) can be considered as an index association for endoskarn formation within the granite,

outside the orebody. This also explains why the endoskarnised granite contains magnetite-sphalerite+pentlandite associations comparable to those seen in the orebody (Fig. 2f). The presence of molybdenite and abundant ilmenite is suggestive of an A-type granite (Ishihara & Murakami 2006; Ludington & Plumlee 2009).

Mineral trace element signatures - is there an IOCG connection?

Generally, in any IOCG deposit, magnetite and amphibole+apatite would be part of the same stage of alteration. In the Onça-Rosa orebody, however, only the inclusion-free rims of magnetite can reliably be constrained to such a stage. Meaningful, readily interpretable trends among trace elements are, however, influenced by scavenging effects whenever minerals precipitate simultaneously. Additionally, crystal structure strongly controls partitioning of trace elements, e.g. V into magnetite and Sn into amphibole, irrespective of growth stage (Fig. 5a). The high Sc recognized in amphibole shows an affiliation with mafic-ultramafic rocks, which are presumably leached by the granite-derived fluid (Wang *et al.* 2021).

High REY concentrations in the fluids at this stage are reflected in the compositions of both apatite and amphibole (Fig. 6). Such a geochemical signature is readily attributable to IOCG systems. Magnetite contains the least ΣREY among the major minerals yet is most abundant and thus likely accounts for a majority of the REY endowment in the mineralizing system. The marked contrast between the chondrite-normalized REY fractionation trends in magnetite cores and amphibole (Fig. 6) is evidence for formation of the two minerals from the same hydrothermal fluid source, which evolved from initial enrichment in LREE to late dominance of HREE. Changes in redox conditions are inferred from the presence or absence of any Eu anomaly in amphibole from different associations and/or locations in the orebody (Fig. 6c-f). Comparable REY fractionation trends and concentrations are reported for skarn amphibole from the Haobugao Zn-Fe-Sn deposit, Great Xing'an Range, NE China (Liu *et al.* 2024).

The common, MREE-enriched fractionation trends displayed by apatite, with their pronounced negative Eu anomalies, are indicative of comparable physical-chemical conditions, irrespective of local association (Fig. 6b). Comparable fractionation trends are typical of early hematite-sericite mineralization stages in IOCG deposits from the Olympic Cu-Au Province based on both empirical data and numerical simulation (Krneta *et al.* 2017, 2018). Formation conditions correspond to the field of pyrite+chalcopyrite stability at 300 °C, mildly acid conditions (pH ~4.5), and with numerical simulation inferring hematite-stable oxidizing conditions (logfO_2~-31) (Krneta *et al.* 2018). Comparable trends are reported for apatite from the Boss IOCG-(Co) deposit, Missouri, USA, in association with early magnetite-rich ore (Mercer *et al.* 2020), supporting the hypothesis that apatite fractionation trends are heavily dependent upon pH and less upon any variation in fO_2 (Krneta *et al.* 2018). Therefore, we consider that the distinctive MREE-enriched trend likely represents hydrothermal rather than igneous accessory apatite at Onça-Rosa. However, variation in the REY-patterns, e.g., differences in the slopes of the Gd-Lu segment, are controlled by local conditions and particularly by formation of other REE-bearing phases, e.g. spatially co-existing HREE-enriched amphibole (Fig. 4c).

From skarn to IOCG stages - what is recorded in magnetite?

The correlation between micron-scale textures (mottling, brecciation, shear-induced deformation; Figs. 2d, 7) and nanoscale characteristics (inclusion types, defects, recrystallization; Figs. 7h-i, 8g) in magnetite indicates a protracted history of fluid-mineral interaction.

Formation of NCP intergrowths associated with Mg-rich amphiboles, a phenomenon usually related to metamorphic alteration of mafic-ultramafic complexes (Akai *et al.* 1998), can instead be attributed to an early skarn stage at Onça-Rosa that predates Ni-sulfide mineralization and is followed by deposition of calcic amphibole. Such Mg-to-Ca zonation is common in skarn systems and is also typified by different ore minerals (e.g. Einaudi *et al.* 1981; Meinert 1997).

It remains unclear why all amphibole+NCP inclusions feature margins that comprise assemblages of talc±serpentine. We can nevertheless speculate that these Mg-rich sheet silicates and their textures are the result of prograde replacement of pre-existing forsterite or other Mg-rich minerals known as inclusions in skarn magnetite (Xu *et al.* 2021). The transition from calcic to magnesian skarn is subtly marked by zonation patterns in cummingtonite inclusions (Fig. 8a, b).

Fluid infiltration during ore deposition is marked by recrystallization of magnetite and nucleation of sulfides (pentlandite, chalcopyrite) as fine particles along fractures (Figs. 7h, 8h). The complex chemistry of such fluid-mineral reactions is indicated by presence of siegenite and sphalerite as NPs that cluster the coarser sulfides (Fig. 8h).

The final stage of metasomatism is recorded within domains of Si-bearing defects in magnetite that promoted infiltration of K- and Al-bearing fluids (Fig. 11). This is a fingerprint of an incipient potassic alteration event during the inferred IOCG stage at Onça-Rosa.

Reconstructing the sequence of mineralization - a brief comparison with other deposits

The contact zones between granitoids and mafic/ultramafic complexes and/or dikes marginal to the Serra do Puma layered complex offer a fertile geological environment for initiation of metasomatic processes that subsequently lead to the formation of ores of skarn type or similar. The surrounding granitoid at Onça-Rosa is considered a tonalite or granodiorite that belongs to the Carapanã Complex, part of the Mesoarchean basement (Centaurus Metals 2023). Compositional data given by de Oliveira (2017) plots within the granodiorite-tonalite fields on a AQP diagram whereas the petrological evidence presented here (e.g. the presence of ilmenite and molybdenite) suggests this unit could belong to one of the younger, Neoarchean (?) syn-kinematic suites of A-type granitoids known from the Carajás Domain (e.g. Barros *et al.* 2009). Moreover, new Rb-Sr data for biotite-chlorite intervals within the Onça-Rosa granite (Centaurus Metals

2023) indicate much younger ages (2044±49 and 1986±12 Ma), which are interpreted as cooling ages and/or resetting due to fluid input and fracturing along the fault systems. Overall, the Jaguar orebodies are interpreted as structurally related and controlled by shearing along the two main fault systems. There is also the possibility of a distinct younger mineralization event at ~1.85 Ga, coeval with Uatumã A-type-granite emplacement (Antonio *et al.* 2021).

The data presented here for the Onça-Rosa orebody suggests that the Ni-rich mineralization relates to a skarn-IOCG system that was initiated by infiltration of granite-derived fluids along its contact with a mafic-ultramafic protolith. Irrespective of the present ambiguities, such a causative granite intrusion could also be hypothesized at depth. The dolerite dike beneath the Onça-Rosa, clearly a protolith for skarn associations, may connect, below 400 m, to a larger igneous body affiliated with the Serra do Puma layered complex. Although Onça-Rosa is located in proximity to a gabbroic component of the complex, ultramafic rocks (peridotite, pyroxenite) are present as lenses throughout the gabbroic units (Rosa 2014, Machado *et al.* 2023).

Magnesium skarn is associated with magnetite+sphalerite mineralization in the protolith and ferrous-phlogopite (endoskarn) in the granite. Calcic skarn (calcic amphibole) is associated with Ni-rich sulfides (pentlandite and pyrite) and is structurally controlled by shears. Brecciation and overprinting illustrate multi-stage shearing of all assemblages. The high REY content of calcic minerals, amphibole and apatite, supports a hybrid skarn-IOCG type mineralization system resembling that considered for some deposits in other IOCG terranes, notably at Hillside, South Australia (Ismail *et al.* 2014).

Onça-Rosa is mineralogically distinct from the two larger orebodies, Jaguar South and Jaguar Central, which lie to the south of Onça-Rosa and are hosted in metavolcanic rocks. Besides the different host lithologies, the conspicuous presence of pentlandite, the absence of both pyrrhotite and millerite, and the lack of association between a mica (ferrous-phlogopite at Onça-Rosa) and the amphibole are most significant mineralogical features of Onça-Rosa. The pentlandite-rich ore at Onça-Rosa also differs from the Ni-bearing sulfide ores at Jatobá where the pentlandite is

confined to exsolutions from pyrrhotite (Campo-Rodriguez *et al.* 2024b). Such an association is also present in the southern Jaguar orebodies (Ferraz 2017, Mansur *et al.* 2023). Although Mansur et al. (2023) report measurable Pd (<2 ppm) in pentlandite from the southern Jaguar orebodies, these authors consider the apparent absence of Ir-group PGE (Ru, Rh, Ir, and Os) in pyrite as an argument for a hydrothermal rather than magmatic origin. A hydrothermal origin for Jaguar, and to some extent for other Ni-rich deposits in the southern IOCG belt of the Carajás Domain, has been suggested previously (e.g. Ferraz 2017, Ferreira-Filho *et al.* 2021), assuming relatively high-temperature conditions inferred from magnetite trace element signatures (Mansur *et al.* 2023).

Even though high temperature is undoubtedly an important factor, the crucial role played by pH is demonstrated by thermodynamic modelling of the system Ni-Fe-S-Na-Cl (Staude *et al.* 2023). Their results indicate that a hydrothermal fluid can efficiently transport Ni not only at high temperatures but also at mildly acidic conditions (rocks rich in serpentine/talc). Nickel remains soluble as long the fluid is unaffected by interaction with carbonate-rich rocks causing an increase in pH (to slightly alkaline conditions), which would then trigger precipitation of Ni-bearing phases. Observations of pentlandite veins containing biotite in altered granitoids from Kambalda, Western Australia, was interpreted as the result of Ni-transport from serpentinites and deposition in the granite by either wall-rock neutralization or cooling (Staude *et al.* 2023). We favor an analogous interpretation in which the presence of mica-rich intervals at contacts between the Onça-Rosa orebody and host granite suggest comparable discharge of Ni from fluids. However, the mild acidic conditions suggested by the REY partitioning trends in apatite during shearing (Figs. 4c, 6b) may also indicate that cooling rather than the buffering by mica was the precipitation mechanism at Onça-Rosa. At such conditions and in the absence of arsenide minerals, gold is soluble in the fluid and will not precipitate (Staude *et al.* 2023).

An additional factor leading to metal discharge could have been pressure variation during fault activation.

Whereas the location of Onça-Rosa along the McCandless fault system provides a conduit for fluid transport of Ni, the origin of these fluids relative to the Serra do Puma Layered Complex requires more detailed understanding of orefield geology than known at the present time.

The mottled magnetite described here from Onça-Rosa closely resembles the same textural type observed in the Jatobá deposit (Campo-Rodriguez *et al.* 2024a) in that it also contains intergrowths between amphibole and NCPs. The Onça-Rosa magnetite stands out, however, by a lack of calcic amphibole inclusions. It also contains an abundance of silician defects that were not observed from Jatobá. Magnetite from IOCG deposits in South Australia (Olympic Dam and Wirrda Well; Ciobanu *et al.* 2019, 2022, Cook *et al.* 2022) is typified by the presence of silician defects like those shown here. Amphibole inclusions are also present in the two Australian deposits and are reported from IOCGs elsewhere (Colorados, Chile; Deditius *et al.* 2018), including other Carajás deposits (Sossego, Alemão; Huang & Beaudoin 2021, Huang *et al.* 2022). In contrast, the presence of NCPs associated with amphibole inclusions is only known from Wirrda Well, where the magnetite forms at the contact between granite and mafic rocks (Ciobanu *et al.* 2022). Secondly, in both Jatobá and Wirrda Well, high-pressure Al-calcic amphibole, ferrotschermakite is also present. This is not the case in the Onça-Rosa magnetite despite the fact that such magnetite is clearly fractured and deformed.

Conclusions

Onça-Rosa is a tabular orebody hosted by a granite and preserves mafic/ultramafic enclaves at depth. Mica (ferrous-phlogopite)+tourmaline alteration is present at the contact to and within the granite, whereas talc+chlorite defines alteration of host lithology in the magnetite-rich orebody. This association is superimposed by calcic amphiboles (actinolite and Mg-hornblende). Apatite is minor and less abundant than in the southern Jaguar orebodies. Pentlandite is the main Ni-sulfide and sphalerite is ubiquitous but relatively minor.

Magnetite displays a range of textures (brecciation, deformation, mottled inclusion cores) indicating its early formation relative to the spatially coexisting sulfides and amphibole. The latter minerals occur along shears overprinting the magnetite.

Relationships between the talc-chlorite groundmass and amphibole indicate multiple stages of shearing during which small-scale remobilization of sulfide and oxide occurs as stringers. An unusual association of ilmenite and pentlandite is observed along such structures. Ore brecciation and development of porosity assists formation of uraninite, one of the trace minerals accompanying the marked enrichment in REE.

Consistent high concentrations of REY are measured in amphibole (up to ~100 ppm) and apatite (up to ~1700 ppm). Measurable amounts of REY are also noted in magnetite (~13 ppm). The chondrite-normalized REY patterns display characteristic trends in which HREE-, MREE- and LREE are fractionated between amphibole, apatite and magnetite.

Other trace element signatures indicate that magnetite is richest in V (507 ppm) and has contents of Ni and Ti (1974 and 355 ppm) that are comparable with those in amphibole (1742 and 505 ppm). High Sc values are recorded in the amphibole (up to 497 ppm).

Dense mottled magnetite preserves Mg-amphibole (cummingtonite) with coherent intergrowths of non-classical pyriboles, commonly combining sequences of between 3 and 5-I_{beam} chains. Although these inclusions are marked by Ca-bearing oscillatory patterns, no calcic amphiboles are present. Sheet silicates (talc, chlorite, mica) are also abundant, either associated with amphiboles or along fractures (talc). Serpentine group minerals (lizardite and chrysotile) were identified within disordered sequences of such silicates. Fracturing of magnetite is accompanied by nanoscale recrystallization and formation of sulfides (pentlandite, chalcopyrite) as fine particles.

Widespread silician magnetite defects are identified as 2n x $d_{111\text{-}magnetite}$ within less-mottled domains. Such defects are K- and Al-bearing and lead to formation of a new generation of phyllosilicates, including mica.

We interpret formation of the Onça-Rosa orebody in the context of a Fe-Zn-Ni skarn system formed by in-situ alteration of an ultramafic protolith at its contact with granite. We infer the protolith belongs to the Serra do Puma layered complex. The granite may be part of a syn-kinematic, A-type suite (ilmenite- and molybdenite-bearing) that is younger than the layered complex, although this hypothesis is yet to be tested. Two skarn stages are depicted: (i) magnesian (talc, cummingtonite in magnetite) during magnetite+sphalerite deposition; and (ii) calcic (actinolite, Mg-hornblende) during pentlandite deposition. The magnesian stage is also manifested by formation of ferrous phlogopite within host granite. The high-REY content in the amphibole typical of the calcic skarn stage is attributable to an IOCG-style of mineralization in conjecture with regional metallogenetic interpretations. Onça-Rosa, like most if not all IOCG-style deposits throughout the Carajás Mineral Province, is controlled by regional scale fault-and-shear systems. Overall, the Onça-Rosa orebody is a hybrid type of mineralization that shares characteristics with other unusual, Ni rich deposits worldwide, including the skarn-hosted Ni-sulfide ores from Avebury, Tasmania (Keays & Jowitt 2013).

Acknowledgements

We thank Grant (Rocky) Osborne for his assistance with geological data and Animesh Basak for technical support with FIB analyses. Y.T.C.R and M.E.S acknowledges continuous support from the Brazilian Research Council (CNPq – Project 409015/2021-0). This study was financed in part by the Coordenação de Aperfeiçoamento de Pessoal de Nível Superior - Brasil (CAPES) - Finance Code 001. Analytical expenses were supported by the Institute of Sustainability, Energy and Resources, The University of Adelaide. N.J.C. and K.E. acknowledge funding through Australian Research Council Linkage grant LP200100156 (Critical Minerals from Complex Ores).

Supplementary Material

Appendix A: Analytical methods and additional figures.

Appendix B:

SD Table 1a. Compositions of amphiboles from EPMA and STEM EDS maps data.

SD Table 1b. LA-ICP-MS trace element data for magnetite.

SD Table 1c. LA-ICP-MS trace element data for amphibole and apatite.

SD Table 1d. LA-ICP-MS data for magnetite, amphibole and apatite used for box-and-whisker plots.

SD Table 1e. LA-ICP-MS data selected for REE plots.

References

Akai, J., Chiba, A., Konishi, H., Komatsu, M., and Matsubara, S. (1997) New occurrences of non-classical pyriboles formed during ocean-floor and regional metamorphism: estimated PT conditions of formation. European Journal of Mineralogy 9, 1237-1255. https://doi.org/10.1127/ejm/9/6/1237

Antonio, P.Y.J., D'Agrella-Filho, M.S., Nédélec, A., Poujol, M., Sanchez, C., Dantas, E.L., Dall'Agnol, R., Teixeira, M.F.B., Proietti, A., MartínezDopico C.I., Oliveira, D.C., Silva, F.F., Marangoanha, B., and Trindade, R.I.F. (2021) New constraints for paleogeographic reconstructions at ca. 1.88 Ga from geochronology and paleomagnetism of the Carajás dyke swarm (eastern Amazonia). Precambrian Research 353, 106039. https://doi.org/10.1016/j.precamres.2020.106039

Araújo Filho, R.C., Nogueira, A.C., and Araújo, R.N. (2020) New stratigraphic proposal of a Paleoproterozoic siliciclastic succession: Implications for the evolution of the Carajás Basin, Amazonian craton, Brazil. Journal of South American Earth Sciences 102, 102665. https://doi.org/10.1016/j.jsames.2020.102665

Bailey, S.W. (1988) Chlorites: structures and crystal chemistry. In S.W. Bailey Ed., Hydrous Phyllosilicates (exclusive of micas), 19, 347.403. Reviews in Mineralogy and Geochemistry Mineralogical Society of America, Chantilly, Virginia.

Barros, C.E.M., Sardinha, A.S., Barbosa, J.D.P.O., Macambira, M.J.B., Barbey, P., and Boullier, A.M. (2009) Structure, petrology, geochemistry and zircon U/Pb and Pb/Pb geochronology of the synkinematic Archean (2.7 Ga) A-type granites from the Carajás Metallogenic Province, northern Brazil. The Canadian Mineralogist 47(6), 1423-1440. https://doi.org/10.3749/canmin.47.6.1423

Barton, M. (2014) Iron oxide (–Cu–Au–REE–P–Ag–U–Co) systems. Treatise on Geochemistry, 2nd edition, vol 13. Elsevier, Amsterdam 515-541. https://doi.org/10.1016/B978-0-08-095975-7.01123-2

Biagoni, C., and Pasero, M. (2014) The systematics of the spinel-type minerals: An overview. American Mineralogist 99, 1254–1264. https://doi.org/10.2138/am.2014.4816

Campo-Rodríguez, Y.T., Ciobanu, C.L., Slattery, A., Cook, N.J., Schutesky, M.E., Ehrig, K., King, S.A., and Yao, J. (2024a) Polysomatic intergrowths between amphiboles and non-classical pyriboles in magnetite: smallest-scale features recording a protracted geological history. American Mineralogist 109 (10): 1798–1818. https://doi.org/10.2138/am-2023-9188

Campo-Rodriguez, Y.T., Cook, N.J., Ciobanu, C.L., Schutesky, M.E., King, S.A., Gilbert, S., and Ehrig, K. (2024b) Platinum Group Minerals Associated with Nickel-Bearing Sulfides from the Jatobá Iron Oxide-Copper-Gold Deposit, Carajás Domain, Brazil. Minerals 14, 757. https://doi.org/10.3390/min14080757

Centaurus Metals. (2023) Jaguar Nickel Deposit, Carajás – the world's largest and oldest (?) hydrothermal nickel sulfide deposit. Presentation, MEGWA Monthly Meeting, 15th March 2023, Perth, W.A., Australian Institute of Geoscientists. https://www.youtube.com/watch?v=duO6_7Lj2vM (accessed 4 September 2024).

Centaurus Metals. (2024) Jaguar Nickel Sulphide Project. https://www.centaurus.com.au/site/projects/jaguar-nickel-sulphide-project (accessed 05 September 2024).

Ciobanu, C.L., Cook, N.J., Utsunomiya, S., Pring, A., and Green, L. (2011) Focussed ion beam–transmission electron microscopy applications in ore mineralogy: Bridging micro- and nanoscale observations: Ore Geology Reviews 42, 6–31. https://doi.org/10.1016/j.oregeorev.2011.06.012

Ciobanu, C.L., Verdugo-Ihl, M.R., Slattery, A., Cook, N.J., Ehrig, K., Courtney-Davies, L., and Wade, B.P. (2019) Silician magnetite: Si–Fe-nanoprecipitates and other mineral inclusions in magnetite from the Olympic Dam Deposit, South Australia. Minerals 9, 311. https://doi.org/10.3390/min9050311

Ciobanu, C.L., Verdugo-Ihl, M.R., Cook, N.J., Ehrig, K., Slattery, A., and Courtney-Davis, L. (2022) Ferro-tschermakite with polysomatic chain-width disorder identified in silician magnetite from Wirrda Well, South Australia: A HAADF STEM study. American Mineralogist 107, 765-777. https://doi.org/10.2138/am-2022-7975

Cook, N.J., Ciobanu, C.L., Ehrig, K., Slattery, A.D., and Gilbert, S.E. (2022) Micron- to atomic-scale investigation of rare earth elements in iron oxides. Frontiers in Earth Science 10, 967189. https://doi.org/10.3389/feart.2022.967189

Costa, F.G., Santos, P.A., Serafim, I.C.C.O., Costa, I.S.L., and Roopnarain, S. (2020) From Mesoarchean drips to modern–style tectonics in the Carajás Province, Amazonian Craton. Journal of South American Earth Science 104, 102817. https://doi.org/10.1016/j.jsames.2020.102817

Deditius, A.P., Reich, M., Simon, A.C., Suvorova, A., Knipping, J., Roberts, M.P., Rubanov, S., Dodd, A., and Saunders, M. (2018) Nanogeochemistry of hydrothermal magnetite. Contributions to Mineralogy and Petrology 173, 46. https://doi.org/10.1007/s00410-018-1474-1

De Oliveira, M.M.F. (2017) Caracterização e Metalogênese do depósito de Ni do Jaguar, Província Mineral de Carajás. Unpublished Master thesis, University of Brasília Brazil, 133 pp.

Einaudi, L.D., Meinert, L.D., and Newberry, R.J. (1981) Skarn deposits. Economic Geology Seventy-Fifth Anniversary Volume. Society of Economic Geologists p. 317–391.

Feio, G.R.L., Dall'Agnol, R., Dantas, E.L., Macambira, M.J.B., Santos, J.O.S., Althoff, F.J., and Soares, J.E.B. (2013) Archean granitoid magmatism in the Canaã dos Carajás area: implications for crustal evolution of the Carajás province, Amazonian craton, Brazil. Precambrian Research 227, 157-185. https://doi.org/10.1016/j.precamres.2012.04.00

Ferreira-Filho, C.F., de Oliveira, M.M.F., Mansur, E.T., and Rosa, W.D. (2021) The Jaguar hydrothermal nickel sulphide deposit: evidence for a nickel-rich member of IOCG-type deposits in the Carajás Mineral Province, Brazil. Journal of South American Earth Science 111, 103501. https://doi.org/10.1016/j.jsames.2021.103501

Grainger, C.J., Groves, D.I., Tallarico, F.H., and Fletcher, I.R. (2008) Metallogenesis of the Carajás mineral province, southern Amazon craton, Brazil: Varying styles of Archean through Paleoproterozoic to Neoproterozoic base-and precious-metal mineralisation. Ore Geology Reviews 33 (3-4), 451-489. https://doi.org/10.1016/j.oregeorev.2006.10.010

Gait, R.I., and Harris, D.C. (1980) Arsenohauchecornite and tellurohauchecornite: new minerals in the hauchecornite group. Mineralogical Magazine 43, 877-888. https://doi.org/10.1180/minmag.1980.043.331.09

Hernandez-Tasco, L., Monteiro, L.V.S., Ribeiro, B.V., Dutra, L.F., Ferreira Filho, C.F., Mansur, E.T., and Montresor, G. (2023) In situ high-resolution U-Pb geochronology of apatite: understanding the alteration-mineralization timing of the Jaguar hydrothermal nickel deposit, Carajás Mineral Province. Simpósio da Pós-Graduação, Universidade de São Paulo. (accessed 05 September 2024). https://repositorio.usp.br/directbitstream/d5ca9a19-7683-427c-80b6-64775ed7c03c/3152535.pdf

Huang, X.W., and Beaudoin, G. (2021) Nanoinclusions in zoned magnetite from the Sossego IOCG deposit, Carajás, Brazil: Implication for mineral zoning and magnetite origin discrimination. Ore Geology Reviews 139, 104453. https://doi.org/10.1016/j.oregeorev.2021.104453

Huang, X.W., Beaudoin, G., and Yang, Y. (2022) A HR-TEM study on two generations of magnetite from the Alemao IOCG deposit, Carajás, Brazil: Implication for Fe-Cu mineralization. Ore Geology Reviews 146, 104934. https://doi.org/10.1016/j.oregeorev.2022.104934

Ishihara, S., and Murakami, H. (2006) Fractionated ilmenite-series granites in Southwest Japan: Source magma for REE-Sn-W mineralizations. Resource Geology 56 (3), 245-256. https://doi.org/10.1111/j.1751-3928.2006.tb00282.x

Ismail, R., Ciobanu, C.L., Cook, N.J., Teale, G.S., Giles, D., Mumm, A.S., and Wade, B. (2014) Rare earths and other trace elements in minerals from skarn assemblages, Hillside iron oxide–copper–gold deposit, Yorke Peninsula, South Australia. Lithos 184, 456-477. https://doi.org/10.1016/j.lithos.2013.07.023

Keays, R.R., and Jowitt, S.M. (2013) The Avebury Ni deposit, Tasmania: A case study of an unconventional nickel deposit. Ore Geology Reviews 52, 4-17. https://doi.org/10.1016/j.oregeorev.2012.07.001

Knipping, J.L., Bilenker, L.D., Simon, A.C., Reich, M., Barra, F., Deditius, A.P., Wälle, M., Heinrich, C.A., Holtz, F., and Munizaga, R. (2015) Trace elements in magnetite from massive iron oxide-apatite deposits indicate a combined formation by igneous and magmatic-hydrothermal processes. Geochimica et Cosmochimica Acta 171, 15-38. https://doi.org/10.1016/j.gca.2015.08.010

Krneta, S., Ciobanu, C.L., Cook, N.J., Ehrig, K., and Kontonikas-Charos, A. (2017b) Rare earth element behaviour in apatite from the Olympic Dam Cu–U–Au–Ag deposit, South Australia. Minerals 7 (8), 135. https://doi.org/10.3390/min7080135

Krneta, S., Ciobanu, C.L., Cook, N.J., and Ehrig, K.J. (2018) Numerical modeling of REE fractionation patterns in fluorapatite from the Olympic Dam deposit (South Australia). Minerals 8 (8), 342. https://doi.org/10.3390/min8080342

Leake, B.E., Woolley, A.R., ARPS, C.E.S., Birch, W.D., Gilbert, M.C., Grice, J.D., Hawthorne, F.C., Kato, A., Kisch, H.J., Krivovichev, V.G., and others. (1997) Nomenclature of amphiboles: report of the subcommittee on amphiboles of the international mineralogical association, commission on new minerals and mineral names. The Canadian Mineralogist 35, 219-246. https://doi.org/10.1180/minmag.1997.061.405.13

Lister, J.S., and Bailey, S.W. (1967) Chlorite polytypism: IV. Regular two-layer structures. American Mineralogist 52 (11-12), 1614-1631.

Liu, L., Zhou, T., Jiang, S.Y., Zhang, D., and White, N.C. (2024) Amphibole geochemistry in the Haobugao skarn Zn-Fe-Sn deposit in the southern Great Xing'an Range: Implications for the ore-forming process. Ore Geology Reviews 170, 106122. https://doi.org/10.1016/j.oregeorev.2024.106122

Ludington, S., and Plumlee, G.S. (2009) Climax-type porphyry molybdenum deposits (p. 16). US Department of the Interior, Geological Survey.

Machado, N., Lindenmayer, Z, Krogh, T.E., and Lindenmayer, D. (1991) U-Pb geochronology of Archean magmatism and basement reactivation in the Carajás area, Amazon shield, Brazil. Precambrian Research 49, 329-354. https://doi.org/10.1016/0301-9268(91)90040-H

Machado, A.L., Garnier, J., Ratié, G., Guimaraes, E., Monvoisin, G., Cloquet, C., and Quantin, C. (2023) Nickel mass balance and isotopic records in a serpentinic weathering profile: Implications on the continental Ni budget. Chemical Geology 634, 121586. https://doi.org/10.1016/j.chemgeo.2023.121586

McDonough, W.F. and Sun, S.S. (1995) The composition of the Earth. Chemical Geology 120, 223–253. https://doi.org/10.1016/0009-2541(94)00140-4

Mansur, E.T., and Ferreira Filho, C.F. (2016) Magmatic structure and geochemistry of the Luanga Mafic–Ultramafic Complex: Further constraints for the PGE-mineralized magmatism in Carajás, Brazil. Lithos 266, 28-43. https://doi.org/10.1016/j.lithos.2016.09.036

Mansur, E.T., Dare, S.A.S., Ferreira Filho, C.F., Miranda, A.C.R, and Monteiro, L.V.S. (2023) The distribution of trace elements in sulfides and magnetite from the Jaguar hydrothermal nickel deposit: Exploring the link with IOA and IOCG deposits within the Carajás Mineral Province, Brazil. Ore Geology Reviews 152, 105256. https://doi.org/10.1016/j.oregeorev.2022.105256

Martins, P.L.G, Toledo, C.L.B, Silva, A.M., Chemale, Jr.F., Santos J.O.S., and Assis, L.M. (2017) Neoarchean magmatism in the southeastern Amazonian Craton, Brazil: Petrography, geochemistry and tectonic significance of basalts from the Carajás Basin. Precambrian Research 302, 340-357. https://doi.org/10.1016/j.precamres.2017.10.013

Meinert, L.D. (1997) Application of skarn deposit zonation models to mineral exploration. Exploration and Mining Geology 6, 185-208.

Melo, G.H.C., Monteiro, L.V.S., Xavier, R.P., Moreto, C.P.N., Santiago, E.S.B., Dufrane, S.A., Aires, B., and Santos, A.F.F. (2017) Temporal evolution of the giant Salobo IOCG deposit, Carajás Province (Brazil): constraints from paragenesis of hydrothermal alteration and U-Pb geochronology. Mineralium Deposita 52, 709-732. https://doi.org/10.1007/s00126-016-0693-5

Mercer, C.N., Watts, K.E., and Gross, J. (2020) Apatite trace element geochemistry and cathodoluminescent textures—A comparison between regional magmatism and the Pea Ridge IOAREE and Boss IOCG deposits, southeastern Missouri iron metallogenic province, USA. Ore Geology Reviews 116, 103129. https://doi.org/10.1016/j.oregeorev.2019.103129

Moreto, C.P.N., Monteiro, L.V.S., Xavier, R.P., Creaser, R.A., Dufrane, S.A., Melo, G.H.C., Silva, M.A.D., Tassinari, C.C.G., and Sato, K. (2015b) Timing of multiple hydrothermal events in the iron oxide–copper gold deposits of the Southern Copper Belt, Carajás Province, Brazil. Mineralium Deposita 50, 517-546. https://doi.org/10.1007/s00126-014-0549-9

Ridolfi, F., Zanetti, A., Renzulli, A., Perugini, D., Holtz, F., and Oberti, R. (2018) AMFORM, a new mass-based model for the calculation of the unit formula of amphiboles from electron microprobe analyses. American Mineralogist 103, 1112-1125. https://doi.org/10.2138/am-2018-6385

Rosa, W.D. (2014) Complexos acamadados da serra da onça e serra do puma: geologia e petrologia de duas intrusões máfico-ultramáficas com sequencia de cristalização distinta na província arqueana de carajás, brasil. Unpublished Master thesis, University of Brasília, Brazil, 87 pp. (in Portuguese)

Schutesky, M.E., and de Oliveira, C.G. (2020) From the roots to the roof: An integrated model for the Neoarchean Carajás IOCG System, Brazil. Ore Geology Reviews 127, 103833. https://doi.org/10.1016/j.oregeorev.2020.103833

Staude, S., Scharrer, M., Markl, G., Simon, I., Pfaff, K., Monecke, T., and Blanc, P. (2023) Hydrothermal Pentlandite (Ni,Fe)9S8 from Kambalda, Western Australia: Occurrences, Formation Conditions, and Association with Orogenic Gold. The Canadian Journal of Mineralogy and Petrology 61 (2), 239-271. https://doi.org/10.3749/2200032

Tavares, F.M., Trouw, R.A.J, da Silva, C.M.G., Justo, A.P., and Oliveira, J.K.M. (2018) The multistage tectonic evolution of the northeastern Carajás Province, Amazonian Craton, Brazil: Revealing complex structural patterns. Journal of South American Earth Science 88, 238-252. https://doi.org/10.1016/j.jsames.2018.08.024

Teixeira, A.S., Ferreira Filho, C.F., Della Giustina, M.E.S., Araújo, S.M., and da Silva, H.H.A.B. (2015) Geology, petrology and geochronology of the Lago Grande layered complex: evidence for a PGE-mineralized magmatic suite in the Carajás Mineral Province, Brazil. Journal of South American Earth Sciences 64, 116-138. https://doi.org/10.1016/j.jsames.2015.09.006

Teixeira, M.F.B, Dall'Agnol, R., Santos, J.O.S, de Oliveira, DC, Lamarão CN, and McNaughton, N.J. (2018) Crystallization ages of Paleoproterozoic A-type granites of Carajás province, Amazon craton: Constraints from U-Pb geochronology of zircon and titanite. Journal of South American Earth Science 88, 312-331. https://doi.org/10.1016/j.jsames.2018.08.020

Trunfull, E.F., Hagemann, S.G., Xavier, R.P., and Moreto, C.P.N. (2020) Critical assessment of geochronological data from the Carajás Mineral Province, Brazil: Implications for metallogeny and tectonic evolution. Ore Geology Reviews 121, 103556. https://doi.org/10.1016/j.oregeorev.2020.103556

Vasquez, L.V., Rosa-Costa, L.R., Silva, C.G., Ricci, P.F., Barbosa, J.O., Klein, E.L., Lopes, E.S., Macambira, E.B., Chaves, C.L., Carvalho, J.M., Oliveira, J.G., Anjos, G.C., and Silva, HR. (2008) Geologia e Recursos Minerais do Estado do Pará: Sistema de Informações Geográficas — SIG: texto explicativo dos mapas Geológico e Tectônico e de Recursos Minerais do Estado do Pará 1:1.000.000. CPRM, Belém, Brazil, 328 p.

Verdugo-Ihl, M.R., Ciobanu, C.L., Cook, N.J., Ehrig, K.J., Slattery, A., Courtney-Davies, L., and Dmitrijeva, M. (2021) Nanomineralogy of hydrothermal magnetite from Acropolis, South Australia: Genetic implications for iron-oxide copper gold mineralization. American Mineralogist 106, 1273-1293. https://doi.org/10.2138/am-2021-7557

Wang, Z., Li, M.Y.H., Liu, Z.R.R., and Zhou, M.F. (2021) Scandium: Ore deposits, the pivotal role of magmatic enrichment and future exploration. Ore Geology Reviews 128, 103906. https://doi.org/10.1016/j.oregeorev.2020.103906

Williams, P.J., Barton, M.D., Johnson, D.A., Fontbote, L., De Haller, A., Mark, G., Oliver, N.H.S., and Marshik, R. (2005) Iron Oxide Copper-Gold Deposits: Geology, Space-Time Distribution, and Possible Modes of Origin. Economic Geology, 100th Anniversary Volume 371–405. https://doi.org/10.5382/AV100.13

Xu, H.F., Shen, Z.Z., and Konishi, H. (2014) Si-magnetite nano-precipitates in silician magnetite from banded iron formation: Z-contrast imaging and ab initio study. American Mineralogist 99, 2196–2202. https://doi.org/10.2138/am-2014-4964

Xu, J., Cook, N.J., Ciobanu, C.L., Li, X., Kontonikas-Charos, A., Gilbert, S., and Lv, Y. (2021) Indium distribution in sphalerite from sulfide–oxide–silicate skarn assemblages: a case study of the Dulong Zn–Sn–In deposit, Southwest China. Mineralium Deposita 56, 307–324. https://doi.org/10.1007/s00126-020-00972-y

CHAPTER 7

ARSENOHAUCHECORNITE, OGNITITE, PARKERITE, AND RELATED MINERALS FROM ONÇA ROSA OREBODY, CARAJÁS, BRAZIL: FINGERPRINTING PGE SIGNATURES IN HYDROTHERMAL NI ORES

Yuri Tatiana Campo-Rodriguez[1,2], Cristiana L. Ciobanu[1], Nigel J. Cook[1], Ashley Slattery[3], Benjamin Wade[3], Sarah Gilbert[3], Maria E. Schutesky[2], Kathy Ehrig[1,4]

[1]*School of Chemical Engineering, The University of Adelaide, Adelaide, SA, 5005, Australia*

[2]*University of Brasilia, Institute of Geosciences, Graduate Program in Geology, Brasília DF 70910-900, Brazil*

[3]*Adelaide Microscopy, The University of Adelaide, Adelaide, SA, 5005, Australia*

[4]*BHP Olympic Dam, 10 Franklin Street, Adelaide, SA, 5000, Australia*

Article submitted to *American Mineralogist,*
October 10th (2024) AM-9647.

Statement of Authorship

Title of Paper	Arsenohauchecornite, ognitite, parkerite, and related minerals from Onça Rosa orebody, Carajás, Brazil: fingerprinting PGE signatures in hydrothermal Ni ores
Publication Status	☐ Published ☐ Accepted for Publication ☑ Submitted for Publication ☐ Unpublished and Unsubmitted work written in manuscript style
Publication Details	Campo-Rodriguez, Y.T., Ciobanu, C.L., Gilbert, S., Wade, B., Cook, N.J., Schutesky, M.E., and Ehrig, K. Arsenohauchecornite, ognitite, parkerite, and related minerals from Onça Rosa orebody, Carajás, Brazil: fingerprinting PGE signatures in hydrothermal Ni ores. Submitted to *American Mineralogist*.

Principal Author

Name of Principal Author (Candidate)	Yuri Tatiana Campo Rodriguez		
Contribution to the Paper	Performed analytical work, evaluation and interpretation of results and prepared the manuscript.		
Overall percentage (%)	60		
Certification:	This paper reports on original research I conducted during the period of my Higher Degree by Research candidature and is not subject to any obligations or contractual agreements with a third party that would constrain its inclusion in this thesis. I am the primary author of this paper.		
Signature	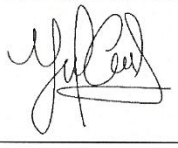	Date	06.11.2024

Co-Author Contributions

By signing the Statement of Authorship, each author certifies that:

i. the candidate's stated contribution to the publication is accurate (as detailed above);

ii. permission is granted for the candidate in include the publication in the thesis; and

iii. the sum of all co-author contributions is equal to 100% less the candidate's stated contribution.

Name of Co-Author	Cristiana L. Ciobanu		
Contribution to the Paper	Helped to define the direction of the manuscript, guides manuscript preparation and assisted with the interpretation of the results and evaluation of the manuscript. (20%)		
Signature		Date	06.11.2024

Name of Co-Author	Nigel J. Cook		
Contribution to the Paper	Helped with the preparation and evaluation of the manuscript. (10%)		
Signature		Date	06.11.2024

Name of Co-Author	Ashley Slattery		
Contribution to the Paper	Assisted with HAADF-STEM data acquisition. (2%)		
Signature		Date	06.11.2024

Name of Co-Author	Benjamin Wade		
Contribution to the Paper	Helped in the operation of analytical equipment and data interpretation. (2%)		
Signature		Date	06.11.2024

Name of Co-Author	Sarah Gilbert		
Contribution to the Paper	Helped in the operation of analytical equipment and data interpretation. (2%)		
Signature		Date	06.11.2024

Name of Co-Author	Maria Emilia Schutesky		
Contribution to the Paper	Helped with the preparation and evaluation of the manuscript. (2%)		
Signature	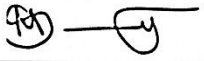	Date	06.11.2024

Name of Co-Author	Kathy Ehrig		
Contribution to the Paper	Assisted with the evaluation of the manuscript. (2%)		
Signature		Date	06.11.2024

Arsenohauchecornite, ognitite, parkerite, and related minerals from Onça Rosa orebody, Carajás, Brazil: fingerprinting PGE signatures in hydrothermal Ni ores

Yuri Tatiana Campo-Rodriguez[1,2*], Cristiana L. Ciobanu[1], Nigel J. Cook[1], Ashley Slattery[3], Benjamin Wade[3], Sarah Gilbert[3], Maria Emilia Schutesky[2], Kathy Ehrig[1,4]

[1]*School of Chemical Engineering, The University of Adelaide, Adelaide, SA, 5005, Australia*

[2]*University of Brasilia, Institute of Geosciences, Graduate Program in Geology, Brasília DF 70910-900, Brazil*

[3]*Adelaide Microscopy, The University of Adelaide, Adelaide, SA, 5005, Australia*

[4]*BHP Olympic Dam, 10 Franklin Street, Adelaide, SA, 5000, Australia.*

[*]*Corresponding author*

Abstract

Nickel-rich sulfide mineralization from the Onça Rosa orebody, Jaguar, Carajás, Brazil, comprises pentlandite, violarite/bravoite, pyrite, sphalerite and minor chalcopyrite. Microtextures preserved in pentlandite are concordant with cycles of replacement via dissolution-reprecipitation reaction. Grain-scale element mapping reveals evidence for remobilization and reprecipitation of metals as inclusions and/or at grain boundaries. Assemblages of rare accessory Ni-Bi-minerals, including arsenohauchecornite $[(Ni_{16.5}Fe_{1.28}Co_{0.39}Zn_{0.17}Cu_{0.01})_{18.35}(Bi_{2.9}As_{0.77}Sb_{0.08}Te_{0.08})_{3.8}(S_{15.85}Se_{0.01})_{15.9}]$, ognitite $[(Ni_{1.02}Fe_{0.01}Pd_{0.004})_{1.04}(Bi_{0.58}Pb_{0.002}As_{0.001})_{0.585}(Te_{1.36}S_{0.02}Se_{0.001})_{1.38}]$, and parkerite

[$(Ni_{2.85}Fe_{0.045}Ag_{0.007}Pd_{0.001})_{2.9}(Bi_{2.024}Pb_{0.005})_{2.03}(S_{2.02}Te_{0.038}Se_{0.008})_{2.07}$] are relatively abundant in the sulfide mineralization. The new occurrence of ognitite, which also contains up to 0.68 wt. % Pd, is a second world occurrence of the mineral. The accessory mineral assemblage also contains Bi-tellurides of the tetradymite group and Pb-Bi-sulfosalts from the lillianite homologous series (Ag-bearing lillianite and heyrovskýite). High angle annular dark field scanning transmission electron microscope imaging, crystal structure models and simulations of arsenohauchecornite confirm the I-centered, tetragonal superstructure described previously. Ognitite is observed to share the trigonal symmetry and space group of melonite. Mixed Bi-Te sites confirm extensive solid solution between melonite and ognitite, concordant with compositional data. Variation of Bi relative to Te is noted at the nanoscale and can be attributed to rhythmic variation of chemical gradients during crystal growth. Nanoscale aggregates of parkerite found at boundaries between ognitite and pentlandite are associated with abundant defects and/or misorientation fabrics in pentlandite. Nanostructures in pentlandite reveal fluid pathways and host nanoparticles of moncheite, volynskite, hessite, altaite, tellurobismuthite and tsumoite. The arsenohauchecornite-ognitite-parkerite assemblages and associated PGE-, and Bi-Ag-Pb-Te-bearing nanoparticles in pentlandite are attributed to interaction of metasomatic-hydrothermal fluids with pentlandite-rich ores at the contacts between the ultramafic Serra do Puma layered complex and a granite-derived hydrothermal source. The presence of Pd in ognitite and at ppm levels in pentlandite, and observation of nanoparticle moncheite at Onça Rosa further extends the potential for PGE in hydrothermal Ni-sulfide ores associated with IOCG systems in the southern Carajás Domain, a finding with implications for exploration in the region and analogous terranes elsewhere. The study emphasizes the critical importance of nanoscale observation for adequate characterization of PGE mineralization.

***Keywords**:* Arsenohauchecornite, ognitite, parkerite, moncheite nanoparticles, PGE-signatures, pentlandite, Carajás

Introduction

"Hydrothermal Ni-mineralization" is a term used for a subgroup of Ni-rich deposits found in an eclectic range of geological settings and with a poorly defined origin (Gonzalez-Alvarez et al. 2013). The Jaguar deposit, located in the southwest part of the Carajás Domain, Brazil, is among the ore systems affiliated with hydrothermal Ni deposits, as well as with iron oxide copper gold (IOCG) systems (Ferreira et al. 2021; Mansur et al. 2023). Pentlandite-rich ores define the Onça Rosa orebody in the north of the Jaguar orefield, an ore system interpreted as an IOCG-skarn system based on studies of magnetite and REE-rich amphibole (Campo Rodriguez et al. in review). These authors conclude that the skarn formed at the contact between ultramafic rocks belonging to the Serra do Puma layered complex and a younger syn-kinematic granite.

In this contribution, we use micron- and nanoscale analysis to characterize mineralogically and geochemically the sulfide assemblages from Onça Rosa. We report the presence of an unusual assemblage comprising arsenohauchecornite (a member of the hauchecornite group; Gait and Harris 1980), ognitite, parkerite, Bi-tellurides of the tetradymite group, and Pb-Bi sulfosalts (lillianite homologous series) occurring as accessory minerals within the main sulfide ores.

Hauchecornite group minerals are seldom encountered in Nature, possibly of the restricted number of occurrences in which Ni and Group V metalloids (As, Sb, Bi) are sufficiently concentrated by natural igneous or hydrothermal processes to crystallize together as discrete minerals. There are six named minerals in the group: arsenohauchecornite ($Ni_{18}Bi_3AsS_{16}$), arsenotučekite ($Ni_{18}Sb_3AsS_{16}$), bismutohauchecornite ($Ni_9Bi_2S_8$), hauchecornite (Ni_9BiSbS_8), hrabákite (Ni_9PbSbS_8), tellurohauchecornite [$Ni_9Bi(Te,Bi)S_8$], and tučekite ($Ni_9Sb_2S_8$). Hauchecornite was first reported as a new species in 1893 (Scheibe 1893). The type locality of bismutohauchecornite (originally approved as hauchecornite, but later revised; Just 1980) is the Oktyabr'skoe deposit, Noril'sk, Russia (Kovalenker et al. 1978). Gait and Harris (1980) introduced arsenohauchecornite and tellurohauchecornite, both new species from Ni-Cu mines in

the Sudbury area of Ontario, Canada. Tučekite was first described from the Kanowna Goldfield, Kalgoorlie, Western Australia (Just and Feather 1978). Arsenotučekite and hrabákite are the most recent additions to the group. Arsenotučekite was first identified from the Tsangli chromite mine, Greece (Zaccarini et al. 2020), while hrabákite is identified from the Příbram uranium mine, Czech Republic (Sejkora et al. 2021). All group members crystallize in the tetragonal system, but the As-bearing varieties are considered as superstructures of the basic hauchecornite cell (Grice and Ferguson 1989). These authors also suggest that compositional variation (Te, Sb) can lead to occurrence of distinct arsenohauchecornite polytypes.

Ognitite, NiBiTe, is the sole named mineral species containing essential Ni, Bi, and Te (Barkov et al. 2019). Ognitite is structurally related to melonite, $NiTe_2$. Prior to the present work, ognitite was known only from the type locality (Ognit Ultramafic Complex, Russia). Ognitite is isostructural with melonite ($NiTe_2$), raising the possibility of partial or complete solid solution of a trigonal $P\bar{3}m1$ structure along the $NiTe_2$-NiBiTe join, as well as solid solutions with other members of the melonite group, notably those containing platinum group elements, such as merenskyite ($PdTe_2$) and moncheite [$Pt(Te,Bi)_2$]. There is a complete solid solution series between melonite and merenskyite series and all members of the melonite group may host PGE (e.g. Garuti and Rinaldi 1986). Type ognitite, for example, has the empirical composition $(Ni_{1.11}Cu_{0.008}Fe_{0.005}Pd_{0.005})_{\Sigma 1.13}Bi_{0.90}Te_{0.97}$ (Barkov et al. 2019).

Parkerite, $Ni_3(Bi,Pb)_2S_2$, is also a relatively rare species (e.g., Petruk et al. 1969; Fleet 1973; Ponomarenko et al. 1987) and apart from bismutohauchecornite, with which it may co-exist (e.g., Koroteev et al. 2017), it is the only other named mineral containing essential Ni, Bi, and S only. Lead is often present but not essential.

We employ high angle annular dark field scanning transmission electron microscopy (HAADF STEM) imaging and EDS analysis, electron diffraction and STEM simulations to assess these rare minerals, the presence of nanostructures and discrete nanoparticles (NPs), and their relationships with co-exiting sulfides. We provide evidence for a PGE signature in terms of minor

Pd content in ognitite and moncheite NPs contained in pentlandite. Our objectives are to provide new constraints on the origin of these unusual mineral assemblages and their potential for fingerprinting PGE signatures in ores. Their occurrence in Onça Rosa sulfide mineralization enables new constraints to be placed on the formation of these ores.

Samples and analytical methodology

Samples

We investigated ore mineral assemblages in six thin polished sections prepared from four samples collected from a representative drillcore (no. 127) intersecting the Onça Rosa (1.9 Mt @ 0.98% Ni, 0.08% Cu; Centaurus Metals 2024), a relatively small orebody the northern part of the Jaguar deposit.

Analytical methodology

Sample characterization comprised reflected light optical and scanning electron microscopy (SEM) using a FEI Quanta 450 instrument. The SEM platform was used for backscattered electron (BSE) mode imaging, spot analysis and grain-scale mapping using routine energy-dispersive X-ray spectrometry (EDS) procedures.

Element maps for pentlandite were obtained using a JEOL JXA-8230 SuperProbe electron probe microanalyzer (EPMA) hosted at the Crti Laboratory (Regional Center for Technological Development and Innovation - Federal University of Goiás, Brazil). Quantitative compositions of minerals were determined using a Cameca SX-Five electron probe microanalyzer. Both instruments are equipped with five tunable wavelength-dispersive spectrometers. The instruments run PeakSite v6.2 software for microscope operation, and Probe for EPMA software (distributed by Probe Software Inc.) for all data acquisition and processing. Analysis was performed at operating conditions of 15 kV / 20 nA and 20 kV/20 nA for mapping and quantitative analysis,

respectively, and with a focused beam due to the required spatial resolution. The full list of elements analyzed along with primary and interference standards, typical minimum limits of detection, and further details of matrix correction procedures, are presented in Supplemental Materials.

Trace element LA-ICP-MS spot analysis of sulfides and element mapping was conducted using a RESOlution-SE 193 nm Excimer laser coupled to an Agilent 8900x quadrupole ICP-MS. Details of measurement parameters, operating conditions, analyzed isotopes, dwell times, reference materials, calibration routines, and typical minimum limits of detection are given in Supplemental Materials.

Preparation of thinned (<100 nm) foils from the polished blocks for TEM investigation was performed using a FEI-Helios nanoLab Dual Focused Ion Beam and Scanning Electron Microscope (FIB-SEM) in the same laboratory, following procedures outlined by Ciobanu et al. (2011). Each foil was analyzed employing HAADF and bright field (BF) STEM imaging and EDS-STEM mapping/spot analysis using an ultrahigh-resolution, probe-corrected FEI Titan Themis S/TEM operated at 200 kV and equipped with a double-tilt holder. This instrument has a X-FEG Schottky source and a Super-X EDS detector providing geometrically symmetric EDS detection with an effective solid angle of 0.8 sr. Probe correction delivered sub-angstrom spatial resolution, and an inner collection angle >50 mrad was used for HAADF imaging with a Fischione detector. Thermo-Scientific Velox software (v3.10) was used for image acquisition, including drift-corrected frame integration package and EDS data acquisition and processing. Various filters were used to eliminate noise. Velox software utilizes standard Cliff-Lorimer quantification and includes absorption correction optimized for both the Super-X detector geometry and the effect of sample holder shadowing for the double-tilt Super-X holder used. We used the Brown-Powell empirical ionization cross-section model and uncertainty values reported incorporate an estimated 20% error in the k-factors. Indexing of diffraction patterns was conducted with WinWulff (JCrystalSoft v.1.6) and publicly available data from the American

Mineralogist Crystal Structure Database (http://rruff.geo.arizona.edu/AMS/amcsd.php). Crystal structure models were generated in CrystalMaker (v.10.8.2) and image simulations using STEM for xHREM software (v5.3.2.0).

All instruments, except the JEOL JXA-8230 SuperProbe, are hosted at Adelaide Microscopy, The University of Adelaide.

Results

Petrography and geochemistry of common sulfide assemblages

Pentlandite, the main Ni-sulfide in the studied samples, is fractured and replaced by secondary Ni-bearing sulfides (violarite and bravoite, a Ni-Co-bearing variety of pyrite; Fig. 1a). Pyrite associated with ore displays euhedral morphology against sphalerite yet caries-like boundaries when seen in contact with magnetite (Fig. 1b, c). Sphalerite (3-5 at% Fe) is the dominant μm-sized inclusion species in pyrite. Sub-euhedral pyrite clustered by silicate inclusions is found within host alteration assemblages (chlorite+talc±amphibole) (Fig. 1d).

Tile-like pyrite and pentlandite arranged in a jig-saw pattern are part of the locally brecciated margins of pentlandite (Fig. 1e), with aggregates of violarite growing perpendicular to the pentlandite tiles (Fig. 1f). Such violarite alteration can propagate throughout an entire tile and create nodule-like bodies of bravoite (Fig. 1g). At higher magnification, the pentlandite replacement/breakdown textures are shown to be more complex, featuring a variety of lamellar and symplectitic intergrowths between different Ni-(Co)-bearing sulfides and minor chalcopyrite (Fig. 1h-j).

Altogether, these intergrowths define pseudomorphic grains of bravoite formed along the edges of brecciated pentlandite (Fig. 2a, b). Grain-scale element maps show that fine-lamellar intergrowths of violarite and bravoite (like those in Fig. 1h) appear as a mesh with domains having higher-Ni concentration (violarite+relict pentlandite) and other domains with relatively greater

Fe and S (bravoite) (Fig. 2a). Skeletal inclusions of pentlandite and chalcopyrite are mapped throughout the bravoite pseudomorphs (Fig. 2b) representing fine scale symplectites (Fig. 1i, j). In places, such pseudomorphs are further altered to secondary Ni-(Co)-sulfates, whereas still retaining relict pentlandite (Fig. 2c).

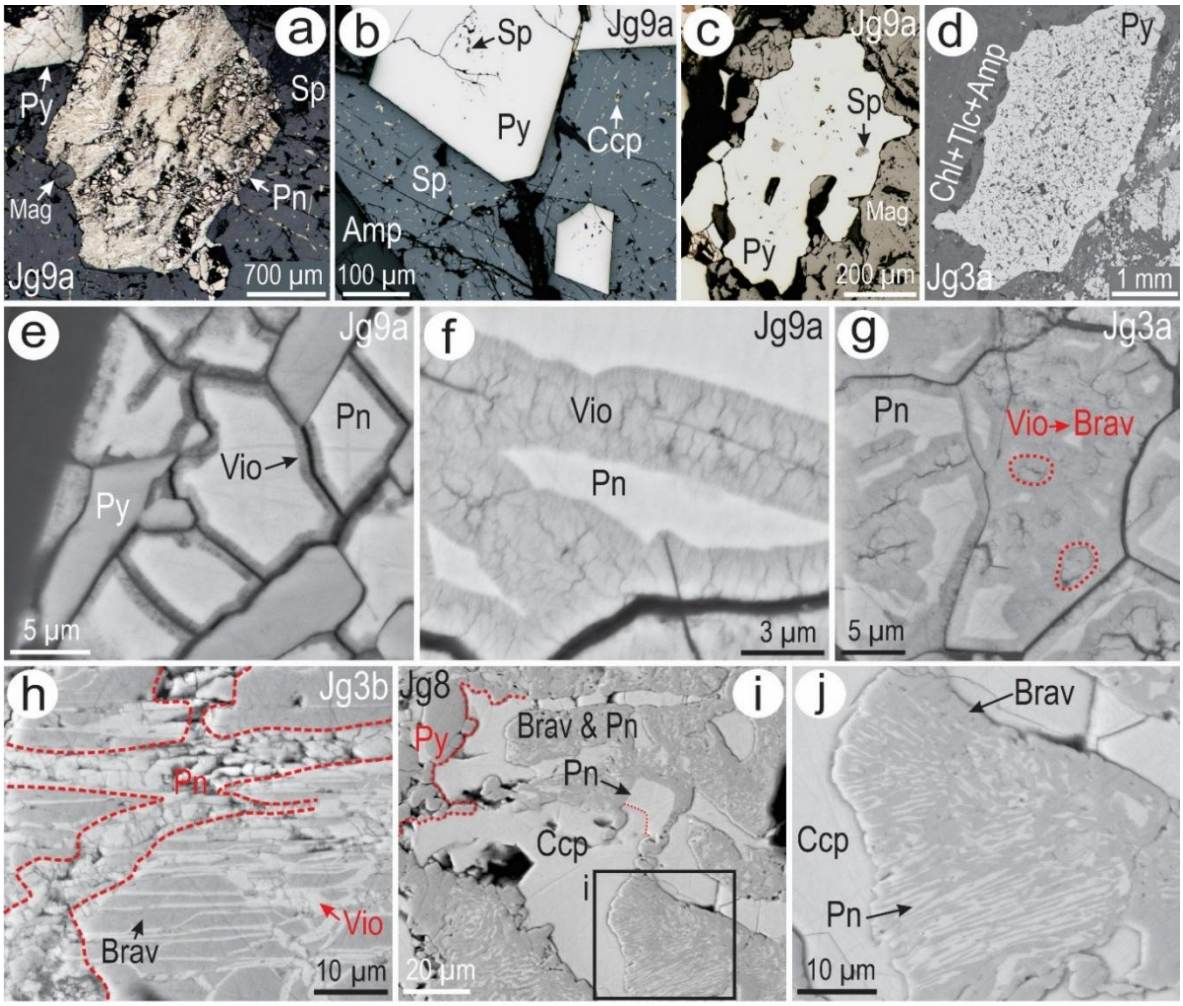

Figure 1. Reflected light microphotographs (a-d) and back-scattered electron images (BSE) (e-j) showing petrographic aspects of common sulfides. (a) Pentlandite (Pn) displaying shear-induced brecciation. (b) Euhedral pyrite (Py) associated with sphalerite (Sp). Note chalcopyrite inclusions (Ccp) in sphalerite ('chalcopyrite disease'). Pyrite contains fracture-associated inclusions of sphalerite. (c) Subhedral pyrite with corrosion boundaries within magnetite (Mag). (d) Silicate/gangue-rich inclusions in pyrite from alteration assemblages comprising chlorite (Chl)+talc (Tlc)+ amphibole (Amp). (e-j) Replacement of pentlandite by secondary minerals. (e) Tiling texture of pentlandite with violarite (Vio) forming along grain boundaries and/or fractures. Note that pyrite is part of the tiling texture. (f) Detail from (e) showing typical short lamellae of violarite growing perpendicular to the margin/fracture. (g) Advanced replacement of pentlandite by masses of violarite+bravoite (Brav). Circles show relict violarite surrounded by bravoite. (h) Fine-scale lamellar symplectites between violarite and bravoite in pentlandite. (i, j) Myrmekite-like symplectite intergrowths between pentlandite and bravoite (+violarite) replacing pentlandite. Note presence of chalcopyrite within such areas.

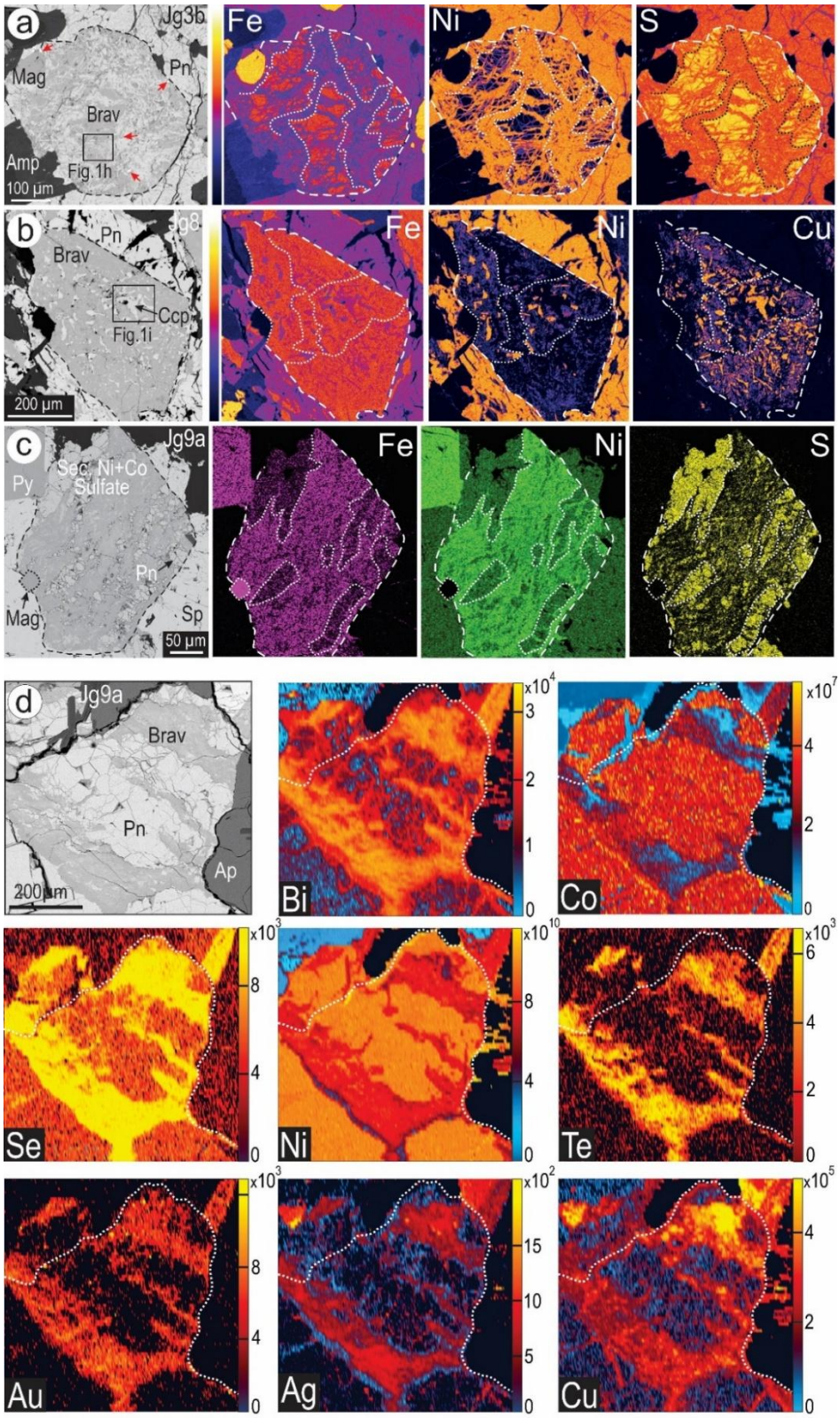

Figure 2. BSE images, EPMA (a, b) EDS SEM (c) and LA-ICP-MS (d) maps of pentlandite replaced by secondary phases, violarite (Vio), bravoite (Brav), Ni-Cu-sulfate, and mixtures thereof. (a, b) Element maps obtained for full grains from with textural details as shown in Figure 1h-j. Sub-micron inclusions of Bi (Te)-bearing minerals are marked by arrows in (a). In (d) note enrichment in Bi, Te, Se, Au, Ag, and Cu in bravoite relative to pentlandite. Scales are in 10^n counts per seconds (cps). Other abbreviations: Ap–apatite; Ccp–chalcopyrite; Mag–magnetite; Sp–sphalerite.

LA-ICP-MS element maps of pentlandite and its alteration phases (considered as bravoite with characteristic lower Ni content than parent pentlandite) show trace element patterns with preferential enrichment in Bi, Te, Ag, Au, and Cu in bravoite, and Co and Se in pentlandite (Fig. 2d).

Element maps of euhedral pyrite show distribution of As>Co>Ni being affected by the presence of sub-micron-scale inclusions containing Ni, Se, Te, Bi, Ag and partially, also Mo (Fig. 3a). Enrichment in these elements is observed within the domain hosting such inclusions and is associated with relative depletion of As in Co. Other maps (SM Fig. S1) show comparable effects of inclusions on main trace elements (As, Co, Ni) distribution in euhedral pyrite.

The concentration of trace elements in common sulfides is tabulated in SM Table S1a. Data for the selected elements plotted in the box-and-whiskers plot (Fig. 3b) is given as SM Table S1b.

Analyses of (sub)euhedral ore-associated pyrite (samples Jg5 and 9a) are separated from those of pyrite clustered by silicate/gangue inclusions in sample Jg3a. Despite such differences in morphology and inclusions, both types contain elevated Co with comparable mean concentrations (6535 and 5644 ppm, respectively. Nickel is higher in the (sub)euhedral pyrite (mean 5310 ppm) relative to sample Jg3a (mean 2004 ppm). Mean arsenic concentrations are an order of magnitude lower than Co or Ni (444 ppm in pyrite from sample Jg3a and 681 ppm in (sub)euhedral pyrite. Concentrations of Co approaching 1 wt% are observed in pentlandite (6751 ppm) and violarite/bravoite (8603 ppm). Sphalerite shows modest Co and Ni contents (means 372 and 75 ppm, respectively). Copper measured in sphalerite (4173 ppm) and violarite/bravoite (9414 ppm) is due to sub-µm-sized inclusions of chalcopyrite.

Figure 3. (a) Reflected light image and LA-ICP-MS maps of euhedral pyrite (Py) grain associated with pentlandite-sphalerite (Sp) ore. As, Co and Ni show weak oscillatory zoning patterns. A trail of inclusions is marked by spots of high-concentrations of Co, Ni, Bi and Ag as well as a halo of enrichment in these elements (less for As and Co) as well as Se and Mo. (b) Box-and-whiskers plot of trace elements in sulfides as labelled. Arrows show relative enrichment of Cu, Bi, Te, Ag and Au for pentlandite and violarite/bravoite and between the two types of pyrite. Data from SM Table 1b. (c) Plot of (Ag+Au) *vs.*

(Bi+Te) showing a strong correlation (r'=0.85) between these elements for pyrite, pentlandite and violarite/bravoite. Sphalerite and chalcopyrite show variation in Bi+Te but at the same Ag+Au content. Legend as in (d). (d) Plot of (Bi+Te+Ag+Au+Se) *vs.* (Co+As) showing distinct clusters for each sulfide.

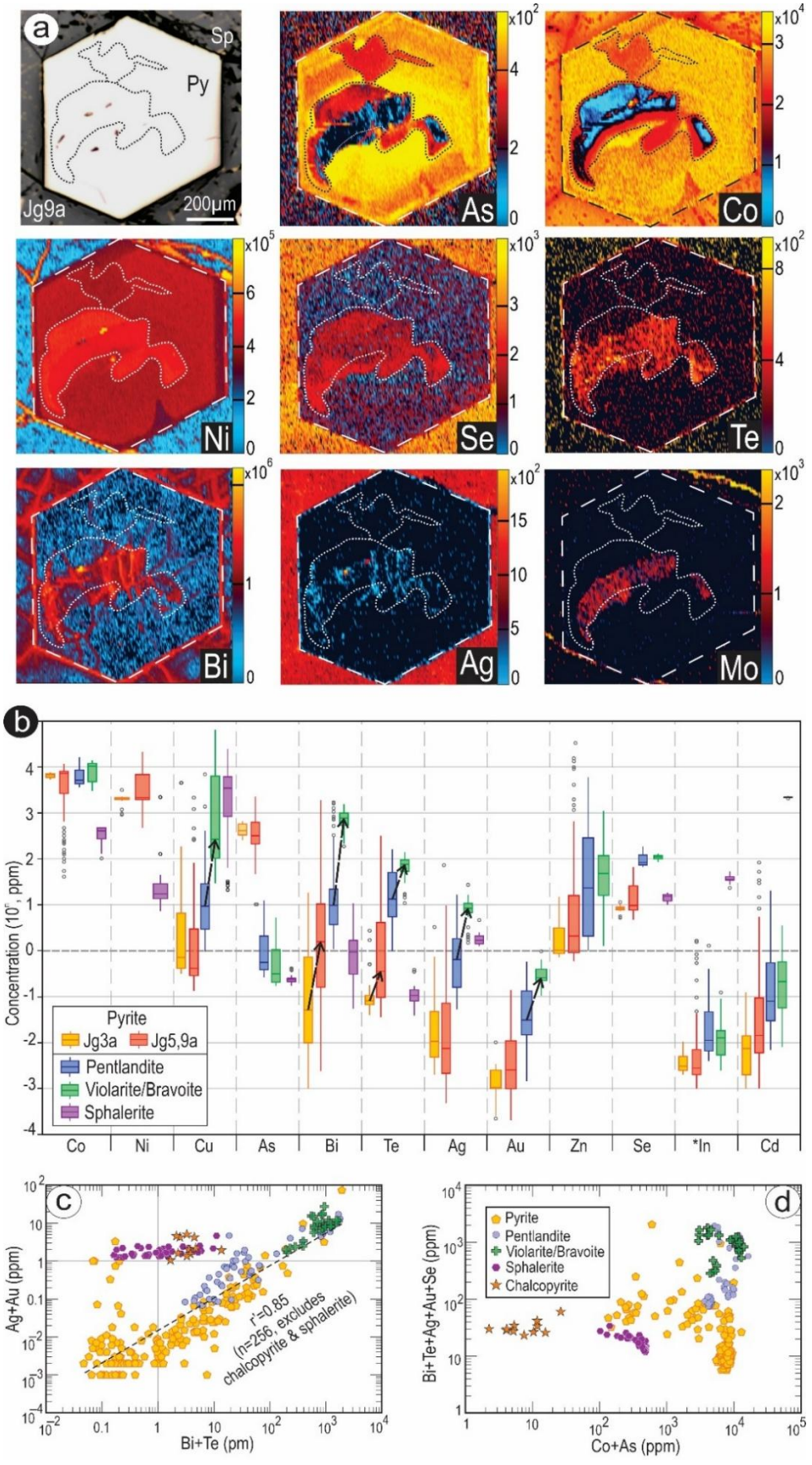

Pentlandite and its alteration products (violarite/bravoite) feature the highest concentrations of chalcophile and chalcogen elements, but with all elements higher in the alteration products. For example, 199 ppm Bi in pentlandite and 770 ppm in violarite/bravoite. The same trend is seen for Te (32 and 73 ppm, respectively), Ag (2 and 9 ppm, respectively), and Se (99 and 107 ppm, respectively). Sphalerite contains measurable concentrations of In and Cd (means 37 and 2190 ppm, respectively).

Binary plots for sulfides show a good correlation (r'=0.85) between (Au+Ag) and (Bi+Te) for pyrite, pentlandite and violarite/bravoite (Fig. 3c). Sphalerite and chalcopyrite form a separate cluster on the same plot without any correlation. Distinct clusters for each of the five analyzed sulfides are seen (Fig. 3d), on which (Co+As) is plotted against (Bi+Te+Se+Ag+Au).

Accessory minerals: arsenohauchecornite, ognitite, and accompanying phases in sulfides

Micron-scale characterization

An abundance of Ni-Bi-Pb-Te-S phases occur as trace mineral inclusions throughout the sulfide samples (Figs. 4, 5; Table 1a). These belong to several distinct mineral groups: Ni-(Bi)-sulfides and tellurides (arsenohauchecornite, parkerite, ognitite); Bi-chalcogenides from the tetradymite group; and Pb-Bi-sulfosalts from the lillianite homologous series.

The Ni-(Bi)-sulfides/tellurides occur as small blebs or filaments along grain boundaries in pyrite (Fig. 4a, b). Rare parkerite, ideally $Ni_3(Bi,Pb)_2S_2$, is observed along microfractures in pyrite (Fig. 4c). Coarser grains of arsenohauchecornite, ideally $Ni_{18}Bi_3AsS_{16}$, occur between jigsaw boundaries of pentlandite and other minerals, including magnetite and amphibole (Fig. 4d-f). We note amphibole grains crosscutting boundaries between pentlandite and arsenohauchecornite. Sphalerite is present as small inclusions within or along the margins of arsenohauchecornite (Fig. 4d).

Table 1a Electron microprobe data for accessory ore minerals

Arsenohauchecornit					**Ognitite-Melonite**					**Parkerite**			**Heyrovskyite**			**Lillianite**			**Tellurobismuthite**		
Wt.%	**Mean n=29**	**S.D.**	**Max**	**Min**	**Wt.%**	**Mean n=14**	**S.D.**	**Max**	**Min**	**Wt.%**	**Mean n=4**	**S.D.**	**Wt.%**	**Mean n=5**	**S.D.**	**Wt.%**	**Mean n=5**	**S.D.**	**Wt.%**	**Mean n=7**	**S.D.**
Ni	42.99	0.87	44.05	40.27	Ni	16.92	0.42	17.77	15.88	Ni	25.49	0.38	Cu	-	-	Cu	0.11	0.01	Cu	0.09	0.08
Co	1.01	0.20	1.39	0.80	Co	-	-	-	-	Co	-	-	Ag	1.90	0.23	Ag	2.22	0.07	Ag	0.27	0.36
Cu	0.02	0.03	0.10	0.00	Pd	0.13	0.18	0.68	0.03	Pd	0.01	0.01	Cd	0.00	0.01	Cd	0.01	0.01	Cd	-	
Fe	3.19	0.44	3.95	2.37	Pb	0.04	0.09	0.33	0.00	Pb	0.16	0.30	Pb	57.69	0.30	Pb	42.43	0.33	Pb	0.49	0.38
Zn	0.50	1.25	4.73	0.00	Sb	0.00	0.01	0.04	0.00	As	-	-	Bi	25.18	0.28	Bi	40.02	0.34	Bi	-	2.72
Bi	26.81	0.37	27.46	26.01	As	0.02	0.02	0.06	0.00	Sb	-	-	As	-	-	As	-	-	As	0.03	0.03
Pb	0.04	0.04	0.18	0.00	Bi	34.30	2.32	39.89	31.66	Bi	64.45	1.34	Sb	-	-	Sb	-	-	Sb	-	-
As	2.58	0.27	3.01	2.03	Cu	0.00	0.01	0.02	0.00	Ag	0.11	0.23	S	15.06	0.11	S	16.11	0.06	S	1.92	2.95
S	22.59	0.21	23.17	22.29	Ag	0.01	0.01	0.04	0.00	Fe	0.38	0.17	Se	0.01	0.01	Se	0.01	0.02	Se	0.10	0.10
Sb	0.44	0.23	0.91	0.10	Fe	0.28	0.29	1.25	0.10	S	9.89	0.27	Te	0.00	0.00	Te	-	-	Te	42.99	5.03
Se	0.02	0.02	0.05	0.00	S	0.15	0.41	1.56	0.00	Se	0.09	0.12	**Total**	**99.8**	**0.31**	**Total**	**100.9**	**0.60**	**Total**	**100.7**	**0.84**
Te	0.48	0.35	1.36	0.00	Se	0.03	0.03	0.12	0.00	Te	0.73	0.79									
Total	**100.7**	**0.79**	**101.9**	**99.4**	Te	48.93	1.90	51.40	44.65	**Total**	**101.3**	**0.97**									
					Total	**100.8**	**0.58**	**101.8**	**99.5**												

Calculated formulae

	38 a.p.f.u.					3 a.p.f.u.					7 a.p.f.u.			17 a.p.f.u.			11 a.p.f.u.			5 a.p.f.u.	
Ni	16.47	0.35	16.82	15.21	Ni	1.021	0.025	1.049	0.952	Ni	2.850	0.046	Cu	-	-	Cu	0.020	0.002	Cu	0.011	0.010
Fe	1.28	0.17	1.574	0.945	Fe	0.013	0.013	0.056	0.005	Fe	0.045	0.019	Ag	0.337	0.039	Ag	0.246	0.009	Ag	0.020	0.026
Co	0.385	0.079	0.537	0.307	Co	-	-	-	-	Co	-	-	Cd	0.001	0.001	Cd	0.001	0.001	Cd	-	-
Cu	0.006	0.010	0.036	0.000	Pd	0.008	0.011	0.040	0.001	Pd	0.001	0.000	Pb	5.339	0.057	Pb	2.445	0.011	Pb	0.019	0.014
Zn	0.172	0.427	1.604	0.000	Cu	0.000	0.000	0.000	0.000	Cu	0.000	0.000	Bi	2.310	0.017	Bi	2.286	0.012	Bi	1.974	0.112
Total	**18.32**	**0.10**	**18.48**	**18.13**	Ag	0.000	0.000	0.001	0.000	Ag	0.007	0.014	As	-	-	As	-	-	As	0.003	0.003
Sb	0.082	0.043	0.169	0.018	**Total A**	**1.041**	**0.015**	**1.072**	**1.010**	**Total**	**2.903**	**0.037**	Sb	-	-	Sb	-	-	Sb	-	-
Bi	2.88	0.04	2.96	2.77	Bi	0.582	0.048	0.698	0.517	Bi	2.024	0.029	**Total**	**7.987**	**0.023**	**Total**	**4.997**	**0.009**	**Total**	**2.026**	**0.132**
As	0.775	0.082	0.900	0.612	Pb	0.002	0.003	0.011	0.000	Pb	0.005	0.010	S	9.010	0.022	S	6.001	0.011	S	0.400	0.603
Pb	0.005	0.005	0.020	0.000	Sb	0.000	0.001	0.002	0.000	Sb	-	-	Se	0.003	0.003	Se	0.002	0.002	Se	0.009	0.009
Te	0.084	0.061	0.240	0.000	As	0.001	0.001	0.002	0.000	As	-	-	Te	0.000	0.000	Te	-	-	Te	2.564	0.487
Total	**3.83**	**0.05**	**3.93**	**3.69**	**Total B**	**0.584**	**0.050**	**0.705**	**0.518**	**Total**	**2.029**	**0.024**	**Total**	**9.01**	**0.02**	**Total**	**6.003**	**0.009**	**Total**	**2.974**	**0.132**
S	15.85	0.10	16.02	15.64	S	0.016	0.043	0.164	0.000	S	2.023	0.042									
Se	0.006	0.005	0.015	0.000	Se	0.001	0.001	0.005	0.000	Se	0.008	0.010	eV dif (%)	-0.43	0.57	eV dif (%)	0.08	0.37			
Total	**15.85**	**0.10**	**16.02**	**15.64**	Te	1.358	0.047	1.428	1.279	Te	0.038	0.041									
					Total C	**1.375**	**0.047**	**1.452**	**1.286**	**Total**	**2.068**	**0.018**									
					Total B+C	**1.959**	**0.015**	**1.990**	**1.928**												

Table 1b. EDS STEM data for nanoparticles in pentlandite. Numbers correspond to NP labels in Figures 10 and 11.

	Moncheite							**Vol.**	**Hes**	**Alt**	**Tsumoite**			**Tbi**
At. fract	1	2	3	4a	4b	5	**At. fract**	6	7a	7b	8	10	11	9
Pt	36.9	32.9	39.4	40.9	39.9	34.2	Ag	19.0	62.7					
Bi	20.2	22.3	18.2	16.0	18.8	25.3	Bi	44.4			58.0	61.7	69.5	52.6
Te	42.9	44.8	42.5	43.2	41.4	40.5	Pb			63.5	42.0	38.3	39.5	47.5
							Te		37.3	36.5				
Calculated formulae														
	3 apfu							4 apfu	3 apfu	2 apfu				5 apfu
Pt	0.91	0.81	0.97	1.01	0.99	0.86	Bi	1.26			0.92	0.99	1.04	2.02
Bi	0.47	0.51	0.42	0.37	0.44	0.59	Ag	1.04	2.00					
Te	1.62	1.68	1.61	1.63	1.57	1.55	Pb			1.03				
Bi+Te	**2.09**	**2.19**	**2.03**	**1.99**	**2.01**	**2.14**	Te	1.70	1.00	0.97	1.08	1.01	0.96	2.98

Total elements =100.0; Alt=altaite; Hes=hessite; Tbi=tellurobismuthite; Vol=volynskite

Phases with compositions along the melonite-ognitite join ($NiTe_2$-NiBiTe), can also form coarser grains, up to >100 μm across, associated with inclusions of altaite (PbTe), hessite (Ag_2Te) and pentlandite (Fig. 4g, h). Notably, parkerite is present as a lamella along the margin of ognitite.

Phases from the tetradymite group (tellurobismuthite, Bi_2Te_3, and subordinate tetradymite, Bi_2Te_2S) and Pb-Bi sulfosalts of the lillianite homologous series are mostly restricted to samples from lower contact between orebody and granite (Fig. 4i-o). The tetradymite lamellae are associated with sphalerite along boundaries between magnetite and pyrite (Fig. 4i). Coarser tetradymite and tellurobismuthite (several tens of μm-wide) occur within pyrite or along the margins of pyrite and chalcopyrite, in which the Bi-chalcogenides characteristically contain inclusions of pentlandite (Fig. 4j, k).

Lillianite homologues occur as inclusions (10-30 μm-wide) associated with chalcopyrite and sphalerite in pyrite (Fig. 4l-o). We note the presence of heyrovskýite (ideally $Pb_6Bi_2S_9$), and Ag-bearing lillianite (ideally $Pb_3Bi_2S_6$) and could confirm their identities by electron microprobe analysis (Table 1). Both species contain 1-2 wt.% Ag.

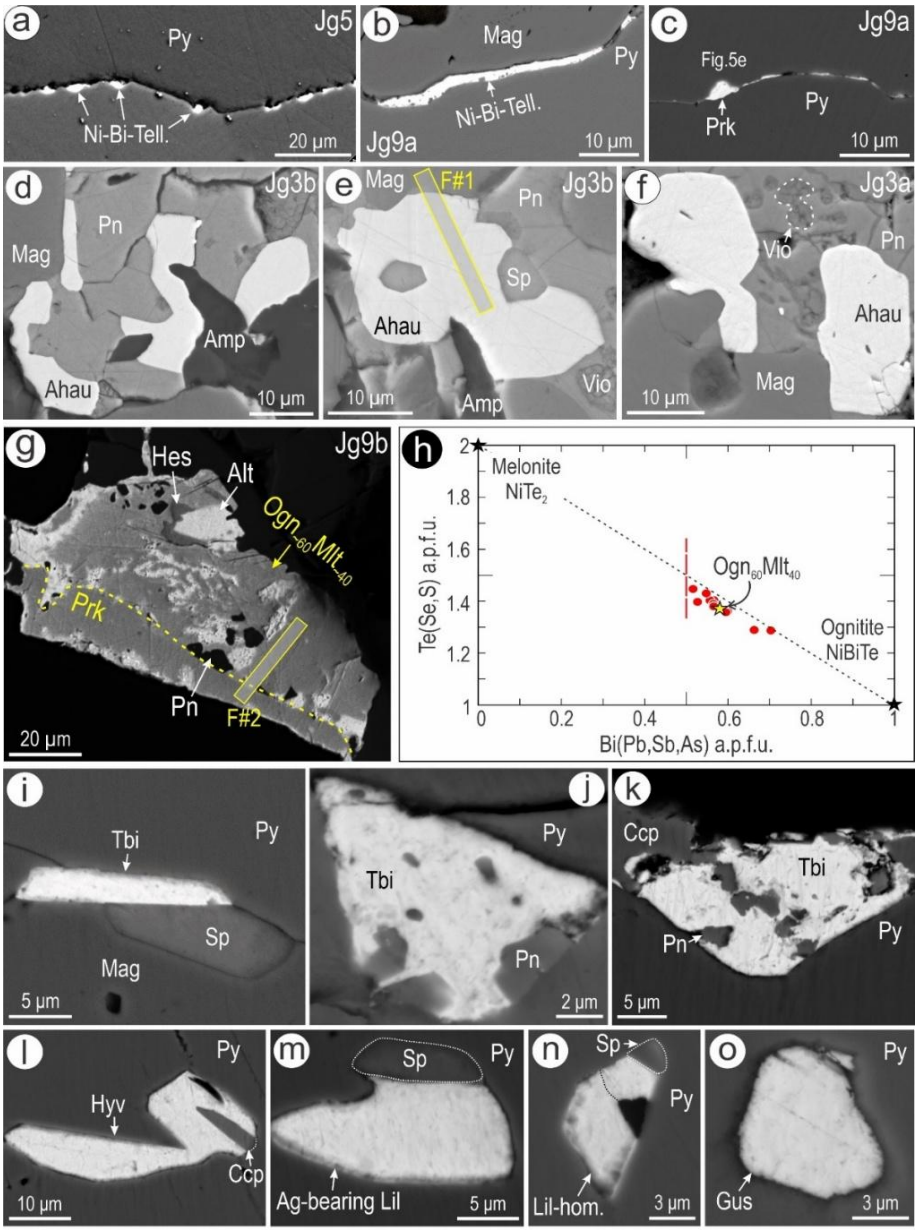

Figure 4. BSE images, all except (h), showing the 'exotic' Bi-Ni-Te-S-Ag-Pb associations present as accessory minerals in the pentlandite (Pn)-pyrite (Py) ores. (a-c) Ni-Bi-tellurides and parkerite (Prk) forming blebs or filaments along grain boundaries or fractures. (d-f) Arsenohauchecornite (Ahau) grains in pentlandite. Note the Ni-Bi-As-sulfide occurs along grain boundaries between pentlandite and magnetite (Mag) and amphibole (Amp). In (d), S-shaped appearance of Ahau in correlates with shear-induced tiling in pentlandite prior to formation of amphibole (observed as protruding grain in Ahau). Note incipient alteration of pentlandite to violarite (Vio) in (f). (g) Large grain of Ni-Bi-telluride with marginal parkerite. Note breakdown symplectites with pentlandite, altaite (Alt) and hessite (Hes). (h) Plot of Te(Se,S) *vs.* Bi(Pb,Sb,As) from EPMA data for Bi-Ni-telluride in (g) showing this is an intermediate member in the proposed melonite (Mlt) - ognitite (Ogn) solid solution with composition in the ognitite field. (i-k) Tellurobismuthite (Tbi) grains in pyrite or at boundaries between pyrite and magnetite in (i). Note presence of pentlandite within tellurobismuthite or sphalerite (Sp) and chalcopyrite (Ccp) as small bodies along the margins. (l-o) Lillianite (Lil) homologues as labeled in pyrite. Note small grains of sphalerite and chalcopyrite along the margins of Pb-Bi-sulfosalts. Other abbreviations: Gus–gustavite; Hyv–heyrovskýite. Location of FIB cuts from which the two S/TEM foils were prepared is marked by yellow rectangles in (e and g).

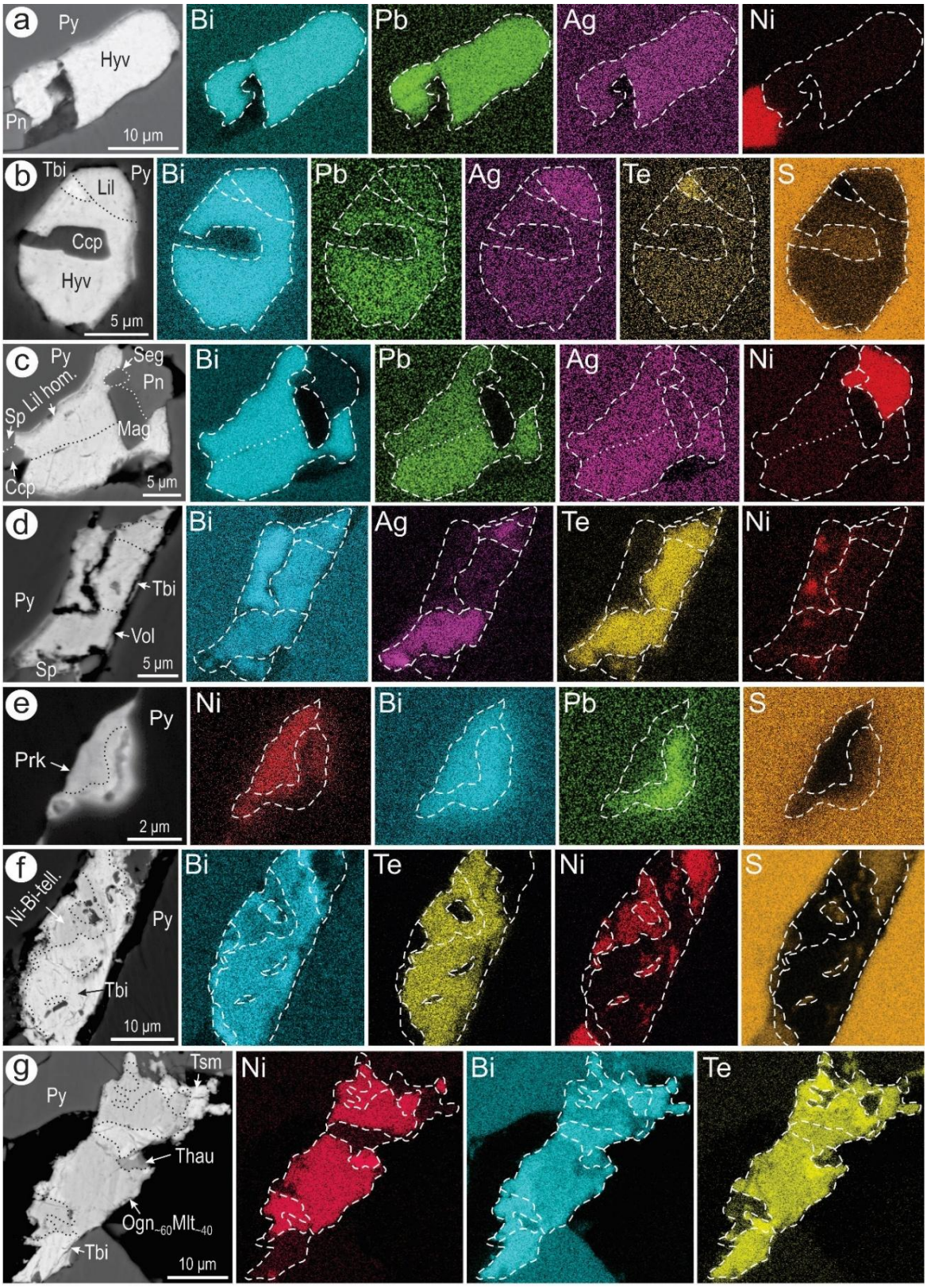

Figure 5. BSE images and EDS SEM maps of other grains representing the Bi-Ni-Te-S-Ag-Pb association. (a-c) lillianite homologues (a-c); (d) tellurobismuthite (Tbi) and volynskite (Vol); (e) parkerite (Prk); (f) Ni-Bi-telluride and tellurobismuthite and (g) ognitite (Ogn). Note association between the sulphosalts and tellurides of various types. Parkerite shows zoning with respect to Pb. Other abbreviations: Ccp–chalcopyrite; Hyv–heyrovskýite; Lil–lillianite; Mag–magnetite; Pn–pentlandite; Py–pyrite; Seg–siegenite; Sp–sphalerite; Thau–tellurohauchecornite; Tsm–tsumoite.

EDS SEM maps of lillianite homologues show both single (compositionally homogenous) species and intimate associations between lillianite and heyrovskýite (Fig. 5a, b). In the latter case, inclusions of tellurobsimuthite are also present. Compositional zoning with respect to Ag (and Pb) across lillianite homologues is noted, as are small grains of siegenite within the assemblage (Fig. 5c). Notably, pentlandite is also present along the margins of lillianite homologues (Fig. 5a, c). Rare volynskite ($AgBiTe_{2;}$) is also noted in association with tellurobismuthite, sphalerite and an altered Ni-bearing phase (Fig. 5d).

Smaller grains of parkerite appear compositionally heterogeneous, albeit with variable Pb content (Fig. 5e). Patchy intergrowths between Bi-chalcogenides, Ni-(Bi)-sulfides/tellurides and arseno- and tellurohauchecornite are observed in the coarser multiphase inclusions (Fig. 5f, g).

Compositional data

Electron microprobe data for arsenohauchecornite indicate close to ideal stoichiometry, with little variation between analyzed grains. The mineral contains ~3 wt% Fe and ~1 wt% Co in the Ni-site, and traces of Sb and Te for Bi. Relatively coarser grains of parkerite are similarly stoichiometric, without low Pb content and measurable albeit trace Pd (0.01-0.02 wt%).

The empirical formulae for arsenohauchecornite and parkerite are: $(Ni_{16.5}Fe_{1.28}Co_{0.39}Zn_{0.17}Cu_{0.01})_{18.35}(Bi_{2.9}As_{0.77}Sb_{0.08}Te_{0.08})_{3.8}(S_{15.85}Se_{0.01})_{15.9}$ and $(Ni_{2.85}Fe_{0.045}Ag_{0.007}Pd_{0.001})_{2.9}(Bi_{2.024}Pb_{0.005})_{2.03}(S_{2.02}Te_{0.038}Se_{0.008})_{2.07}$, respectively.

The $Ni(Te,Bi)_2$ phase yields the mean composition $(Ni_{1.02}Fe_{0.01}Pd_{0.004})_{1.04}(Bi_{0.58}Pb_{0.002}As_{0.001})_{0.585}(Te_{1.36}S_{0.02}Se_{0.001})_{1.38}$. We believe this to be a trigonal melonite group phase located along the melonite-orgnitite join but with (1-Bi/Te)=0.6 placing it in the ognitite field (Fig. 4h). The phase also contains measurable Pd (mean 0.13 wt%, with up to 0.68 wt% (0.022 a.p.f.u.) in individual analyses). Hauchecornite group minerals, parkerite, and Ni-Bi-Te phases are rare. Ognitite is only known from a single occurrence, the type locality (Ognit ultramafic complex,

Russia), where the average composition is $(Ni_{1.11}Cu_{0.008}Fe_{0.005}Pd_{0.005})_{1.13}Bi_{0.90}Te_{0.97}$ (Barkov et al. 2019).

Heyrovskýite and lillianite have empirical formulae as: $(Pb_{5.5}Ag_{0.35}Bi_{0.35})_{6.2}Bi_2S_{9.2}$ and $(Pb_{2.5}Ag_{0.3}Bi_{0.3})_{3.1}Bi_2S_{6.2}$, whereas tellurobismuthite (measured from coarser grains) is very close to stoichiometry.

Nanoscale characterization

Arsenohauchechornite studied from foil #1 (location on Fig. 3e) is in contact with pentlandite (Fig. 6a). The latter is also present as fine particles within the arsenohauchechornite that have the same orientation as the larger grains. The orientation between arsenohauchechornite and pentlandite is slightly offset (Fig. 6b). Chlorite is the only other species present and occurs as a thin sliver embedded within arsenohauchechornite (Fig. 6c). Identification of arsenohauchechornite and pentlandite was done by tilting the specimen on several zone axes (Fig. 6d-i).

High-resolution imaging of arsenohauchechornite shows HAADF signals corelate mainly with the Bi atom columns as depicted by crystal models and STEM simulations (Fig. 6d-f; SM Fig. S2). Electron diffractions (ED) and fast Fourier transform (FFT) patterns (insets in Fig. 6d-f) were indexed using the structure of Grice and Ferguson (1989). High-resolution imaging of pentlandite shows an excellent match with the STEM simulations (Fig. 6g-i). Comparison with crystal structure models shows that Ni and S can both be picked up by the intensity of HAADF signal (SM Fig. 3). Imaging on [010] zone axis of chlorite (from the sliver in Fig. 6c) shows a good match with the two-layer polytype of Lister and Bailey (1967) (Fig. 6j, k).

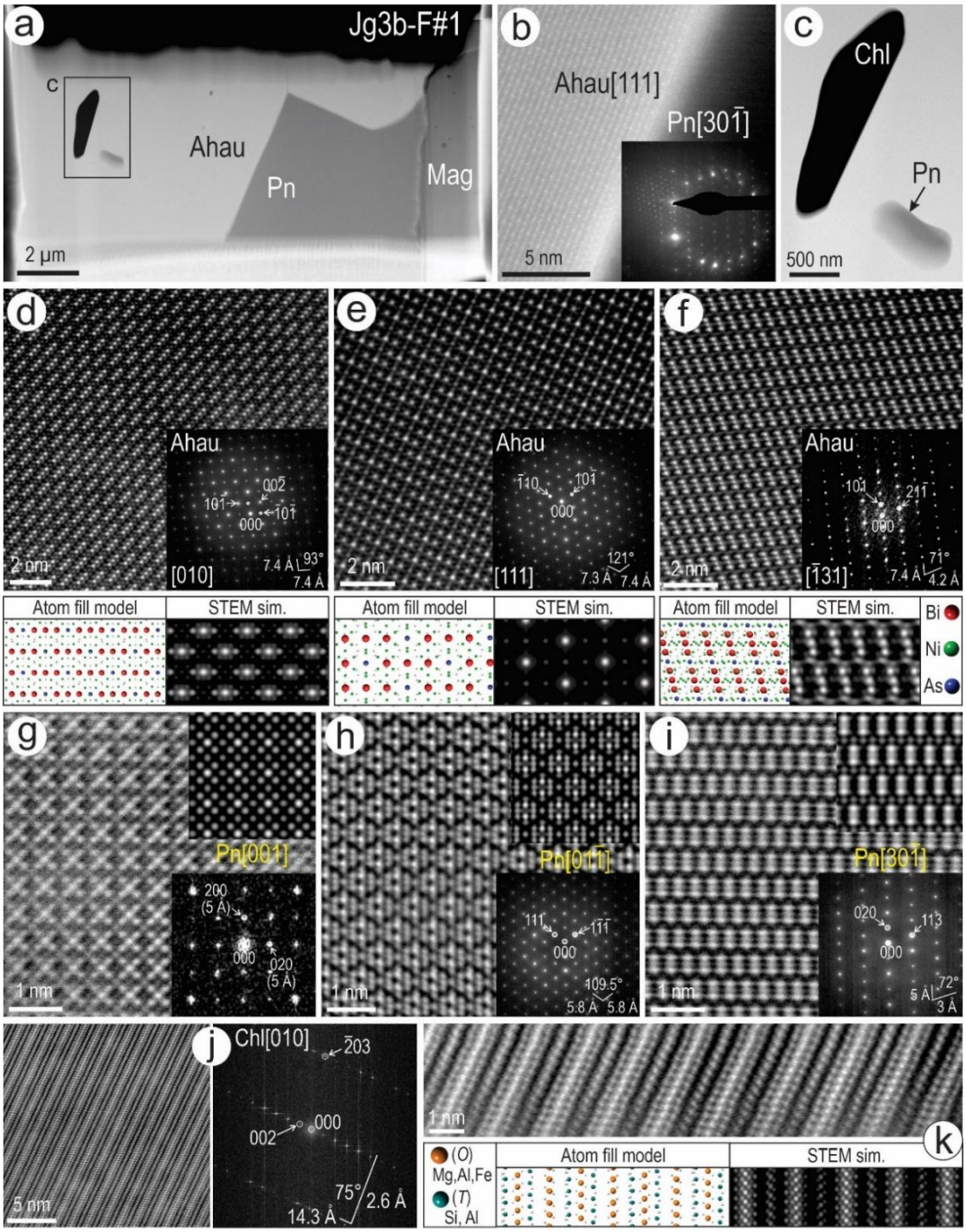

Figure 6. (a-c) Low-resolution HAADF STEM images from foil #1 showing arsenohauchecornite (Ahau) in contact with pentlandite (Pn) and inclusions of chlorite (Chl). Electron diffraction (ED) in (b) shows the slight offset between Ahau and Pn on zone axes as labelled. (d-f) High-resolution HAADF STEM images and corresponding ED and fast Fourier transform (FFT) pattern in (f) of arsenohauchecornite on zone axes as labelled. Underneath are crystal models and STEM simulations for the same orientation. (g-i) High resolution HAADF STEM images and corresponding FFT (in g) and ED patterns of pentlandite on zone axes as labelled. STEM simulations as insets on top right side of each image. See more details in SM Figures Sx. (j) HAADF STEM image and FFT pattern on zone axis as labelled for chlorite from (c). (k) Strip of stacking sequence cropped from (j) with crystal model and STEM simulations showing the distribution of octahedral cation layers (*O*) flanked by the tetrahedral modules (*T*). Note the typical "*T-O-T/O/T-O-T*" sequence of layering.

Ognitite studied from foil #2 cut across its boundary with parkerite (location on Fig. 3g) also shows an association with pentlandite (Fig. 7a). EDS STEM maps from several areas indicate that parkerite is present as fine aggregates between ognitite and pentlandite (Fig. 7b-d). Unlike the straight contact between pentlandite and parkerite at the margin of the foil, areas comprising parkerite aggregates are embayed within pentlandite with irregular and/or scalloped margins. Trace minerals identified within such areas include fine particles of hessite, altaite, and galena, as well as a larger body of a Bi-telluride. A whole range of nanoparticles are also found close to the parkerite-pentlandite boundaries (see below).

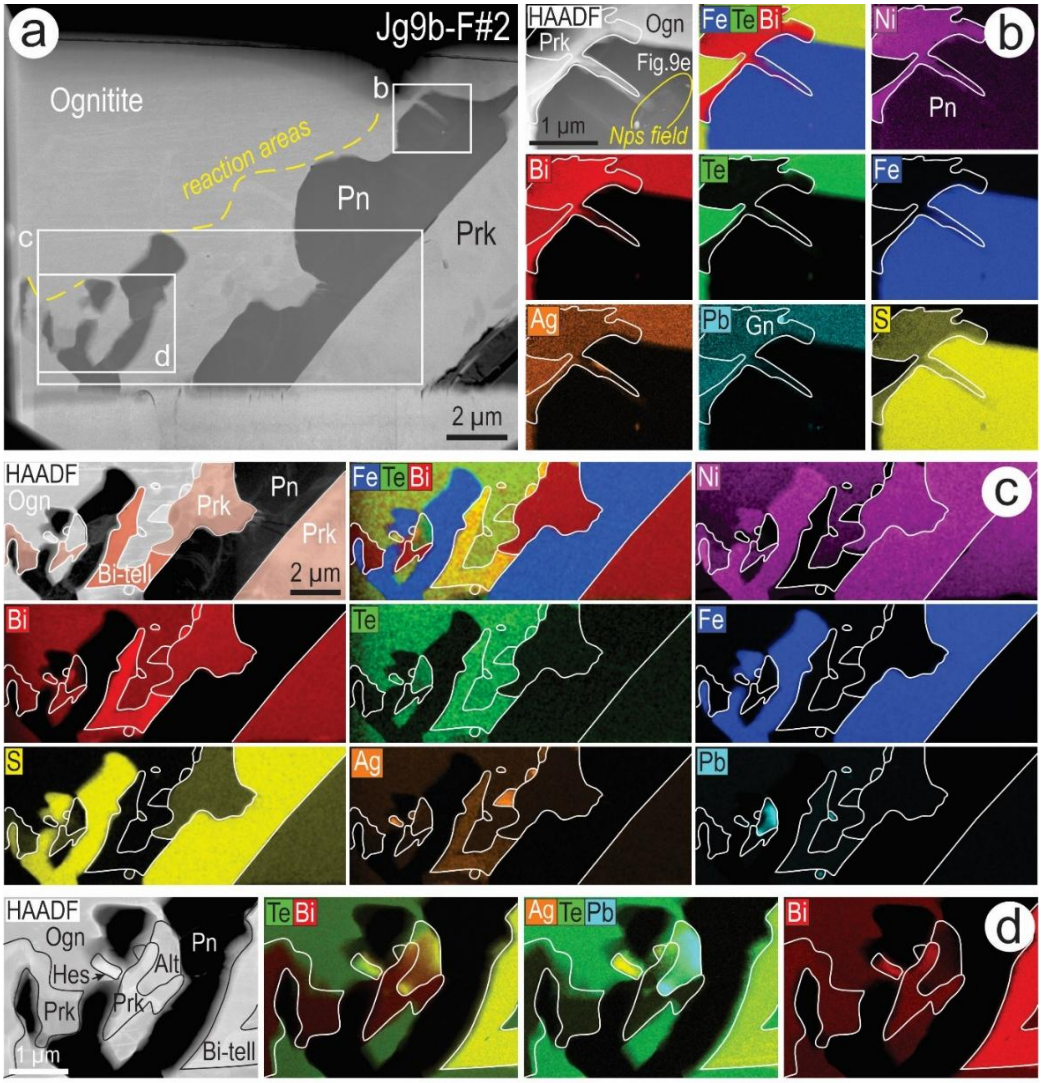

Figure 7. Low-resolution HAADF STEM image of ognitite (Ogn) in contact with pentlandite (Pn) and parkerite (Prk) (foil #2). (b-d) Images and EDS STEM maps of areas as marked in (a) showing formation of nanoscale aggregates of parkerite associated with nanoparticles (NP) as reaction zones along the contacts between ognitite and pentlandite. See text for more explanations. Other abbreviations: Alt–altaite; Bi-tell–bismuth telluride; Gn–galena; Hes–hessite.

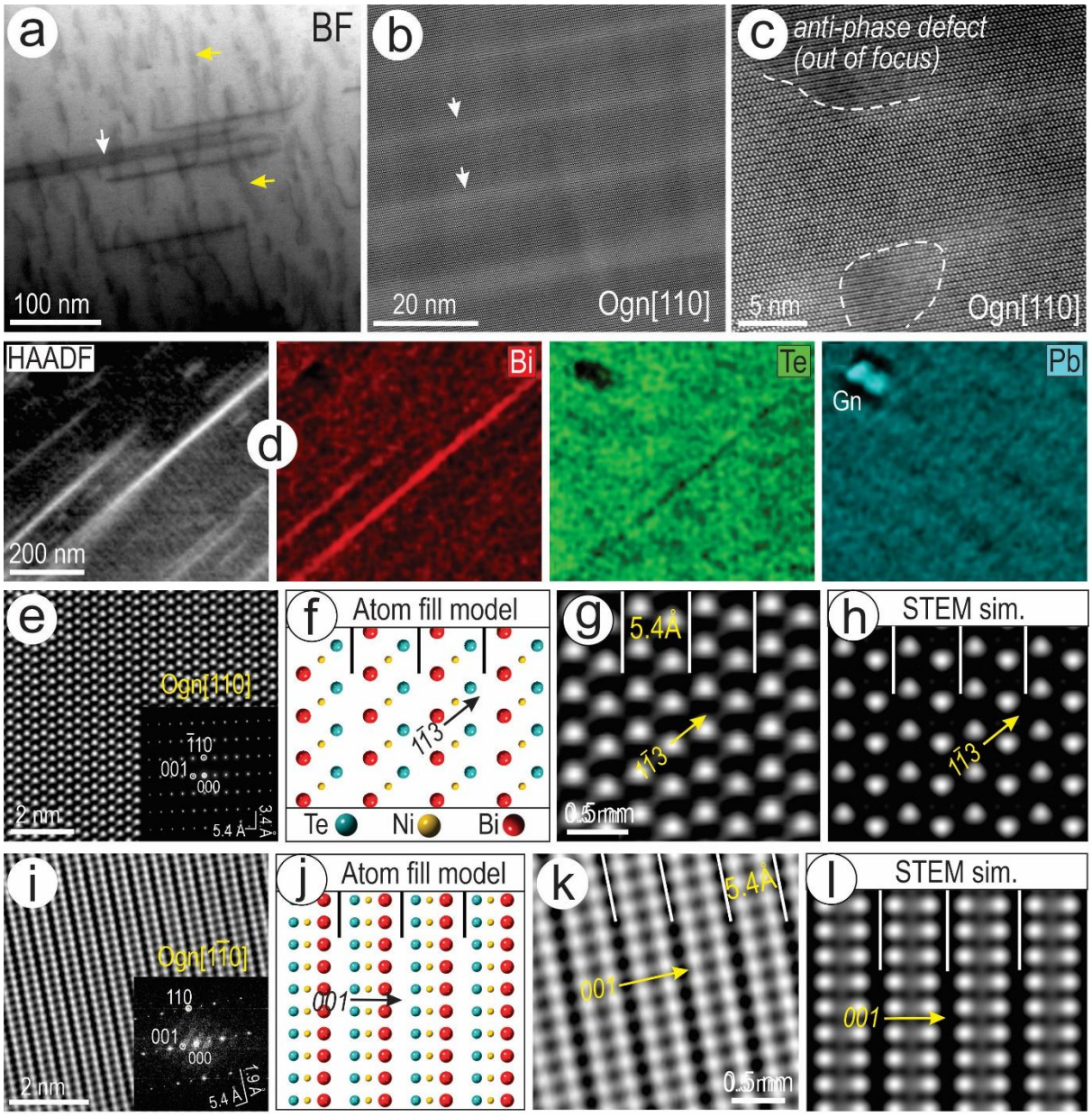

Figure 8. (a) BF and (b, c) HAADF STEM images showing nanotextures of ognitite. (a) Bi-richer lamellae crosscutting worm-like defects (white and yellow arrows) attributed to antiphase boundaries in ognitite. (b) Rhythmic banding of Bi-rich bands in ognitite. (c) Detail of antiphase boundary defect. (d) Image and EDS STEM maps of Bi-rich, Te-poor bands in ognitite. Note presence of a fine particle of galena (Gn). (e-l) Atomic-scale image and corresponding electron diffraction for ognitite on [110] in (e) and [1-10] in (i) zone axes. In (f, j), Crystal structure models using ideal ognitite structure of Barkov et al. (2019). Black lines mark the ~5.4 Å periodicity of the layer stacking. (g, k) Image (crops from (e, i)) and STEM simulations in (h, l) using Bi/Te mixed sites showing good fit for the layer stacks.

Ognitite displays two crosscutting patterns, one as well-defined strips of variable density, and a second typified by short, worm-like defects, both especially visible on BF STEM images (Fig. 8a). HAADF STEM imaging on [110] zone axis relevant for the layered telluride structure shows

high contrast lamellae which can be rhythmically distributed across lengths of ~100 nm (Fig. 8b). The worm-like features also show HAADF STEM contrast and variable focus across the defect boundary (Fig. 8c), indicative of antiphase boundaries or domains (APD). The APD is a planar crystallographic defect in which the atoms within a region of a crystal are configured in the opposite order to those in the perfect lattice system (e.g., Courtney 2000). The high-contrast strips are mapped as Bi-rich, Te-poor bands (Fig. 8d). Occasional inclusions of galena are present.

High-resolution imaging on [110] zone axis shows pairs of bright dots (atoms) defining a length of ~5.4 Å (corresponding to the *c* axis) with a slight jog between them (Fig. 8e). The crystal structure of ideal ognitite (Barkov et al. 2019) shows however, that each 5.4 Å lamella comprises arrays of Bi-Ni-Te atoms (Fig. 8f). Considering the significant difference in Z number for Bi, Ni, and Te (Z=83, 28 and 52, respectively) and the fact that the $I \sim Z^2$ on HAADF STEM images, a notable difference between Bi and Te would be expected, if these are well separated sites, whereas Ni may not appear at all. As expected, the Ni atoms are not resolved on the HAADF STEM images, but the lack of intensity contrast between the two dots corresponding to the heavier Bi and Te atoms (Fig. 8g) implies their presence within mixed Bi-Te sites. This is concordant with the compositional data indicating an intermediate member of the ognitite-melonite series (Fig. 4h). Using a mixed occupancy approach for both Bi and Te sites, we produced STEM simulations (Fig. 8h) which show an excellent match with the analytical data. We also checked a second zone axis, $[1\bar{1}0]$, relevant for such a layered structure and obtained the same match between the simulation and data (Fig. 8i-l).

Reaction zones and nanoparticles

The areas with parkerite aggregates between pentlandite and ognitite are considered as ‘reaction zones’ since they show intragrain fabrics, subtle compositional changes and fields of an eclectic range of nanoparticles (NPs) in pentlandite (Fig. 9).

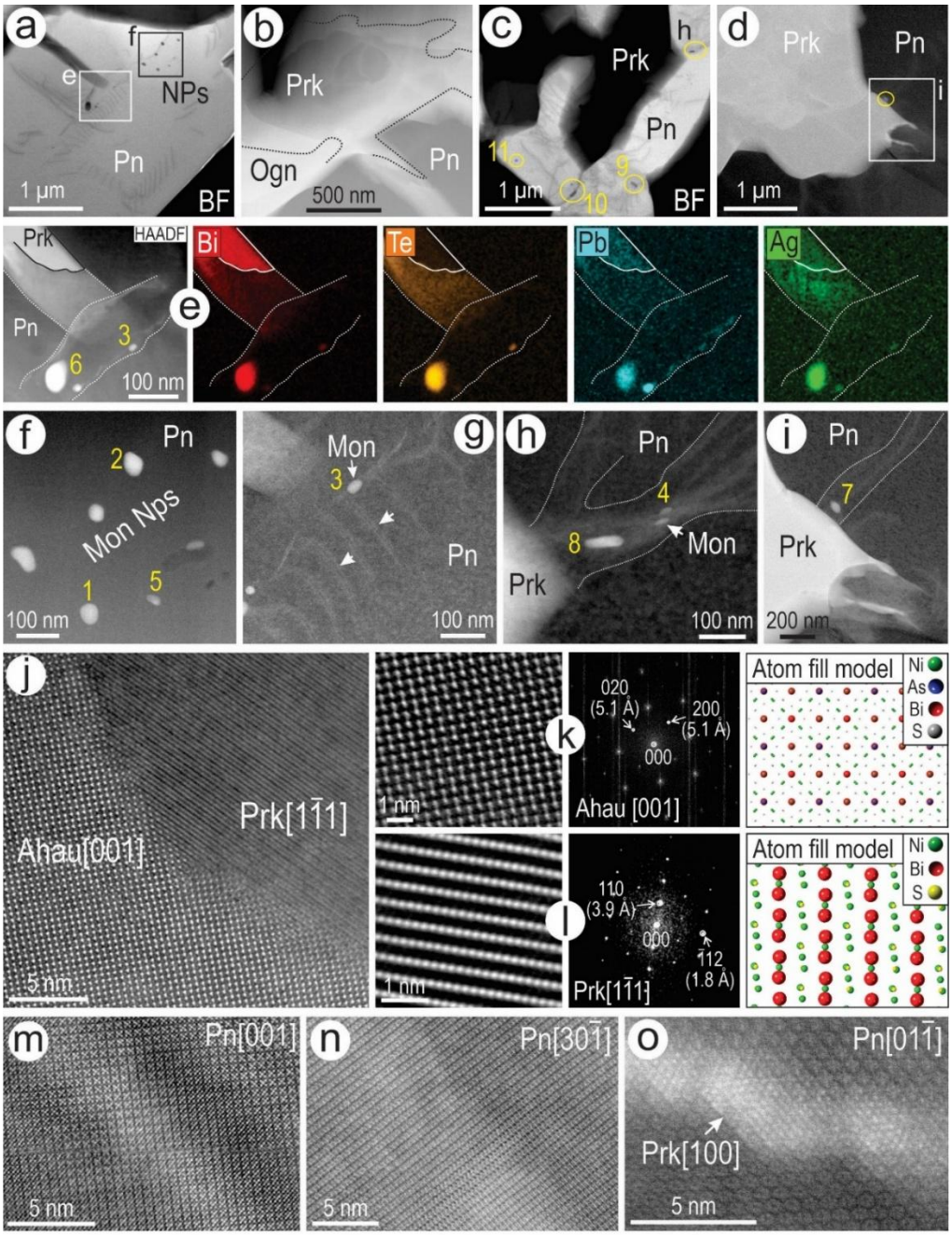

Figure 9. (a, c) BF and (b, d) HAADF STEM images showing details of reaction areas within pentlandite (Pn) and at contacts with parkerite (Prk). (e) Image and EDS STEM maps of parkerite protruding into pentlandite. Dotted lines highlight a domain and defects in pentlandite showing faint chemical changes (Bi, Te, Pb and Ag). Note nanoparticles (NPs) embedded along such nanostructures. (f) Cluster of moncheite (Mon) NPs in pentlandite. (g) Lamellar set of misorientation defects (arrowed) host to NPs in pentlandite. (h) Nanoparticle hosted by a splay of defects (dotted line) in pentlandite in contact with parkerite. (j) Fine-scale protrusions of parkerite in pentlandite. Note NP along defects (dotted line). (j) High-resolution image showing arsenohauchecornite (Ahau) in contact with parkerite from the nanoscale aggregate in (b). (k-l) Images corresponding FFT patterns and crystal models for the two phases in (j). (m-n) High-resolution images showing misorientation in pentlandite across defects as those shown in (g). The same defect is shown tilted on two zone axes as labelled. (o) Atomic scale image of one of the finest (few nm wide) parkerite protrusions in pentlandite (from area shown in (i)). Numbers correspond to NPs shown in figures 10 and 11.

One of the densest NP fields is found at the edge of a protrusion of parkerite within pentlandite (Fig. 9a). Pentlandite is marked by a series of defects, some forming sets of short lamellae, others occurring as filaments (Fig. 9a). This protrusion relates to the nanosized aggregate of parkerite within ognitite at the top of the foil (Figs. 7b, 9b). Single nanoparticles are located at pentlandite grain boundaries with anastomosed defects indicative of brecciation (Fig. 9c). Replacement of pentlandite by parkerite along thin inliers is also documented (Fig. 9d). The thicker protrusion of parkerite at the top of the foil shows enrichment in Te, Pb and Ag at the grain boundary with pentlandite (Fig. 9e). A larger NP (volynskite $AgBiTe_2$, see below) occurs along a string with smaller NPs (galena and moncheite $Pt(BiTe)_2$; see below) within pentlandite. A cluster of moncheite NPs is present within the same area (Fig. 9f). Some NPs are directly located along the defects in pentlandite (Fig. 9g-i).

High-resolution imaging reveals small grains of arsenohauchecornite (Fig. 9j) in the parkerite aggregate at the top of the foil (Fig. 9b). Identification of $[001]_{\text{arsenohauchecornite}}$ and $[1\bar{1}1]_{\text{parkerite}}$ from imaging, FFT patterns, and crystal models are shown in Figure 9k and l.

High-resolution imaging of defects in pentlandite on different zone axes, [001] and $[30\bar{1}]$ shows slight variation in HAADF signal intensity but no apparent lattice distortion (Fig. 9m, n). Imaging of the thin (<5 nm-wide) bright sliver protruding into $[01\bar{1}]_{\text{pentlandite}}$ from area in Figure 9i shows an incipient rearrangement of bright dots into $[100]_{\text{parkerite}}$ (Fig. 9o; SM Fig. S3).

Nanoparticles of moncheite (Fig. 10) were identified by EDS STEM mapping and quantification (Table 1b), as well as from high-resolution imaging. The majority of moncheite NPs are single phase (Fig. 10a, b). Generally, the NPs have a rounded, blebby appearance (Fig. 10a-c) but lensed-shaped NPs (Fig. 10d) were also observed at brecciated contacts between pentlandite grains (location in Fig. 9h). A two-phase NP comprising moncheite and galena (Fig. 10e) was identified in the field illustrated in Figure 9f. A single layer of moncheite is observed "protruding" into galena (Fig. 10f). A high-resolution image, FFT pattern and crystal model of moncheite on [100] zone axis are shown in Figure 10g.

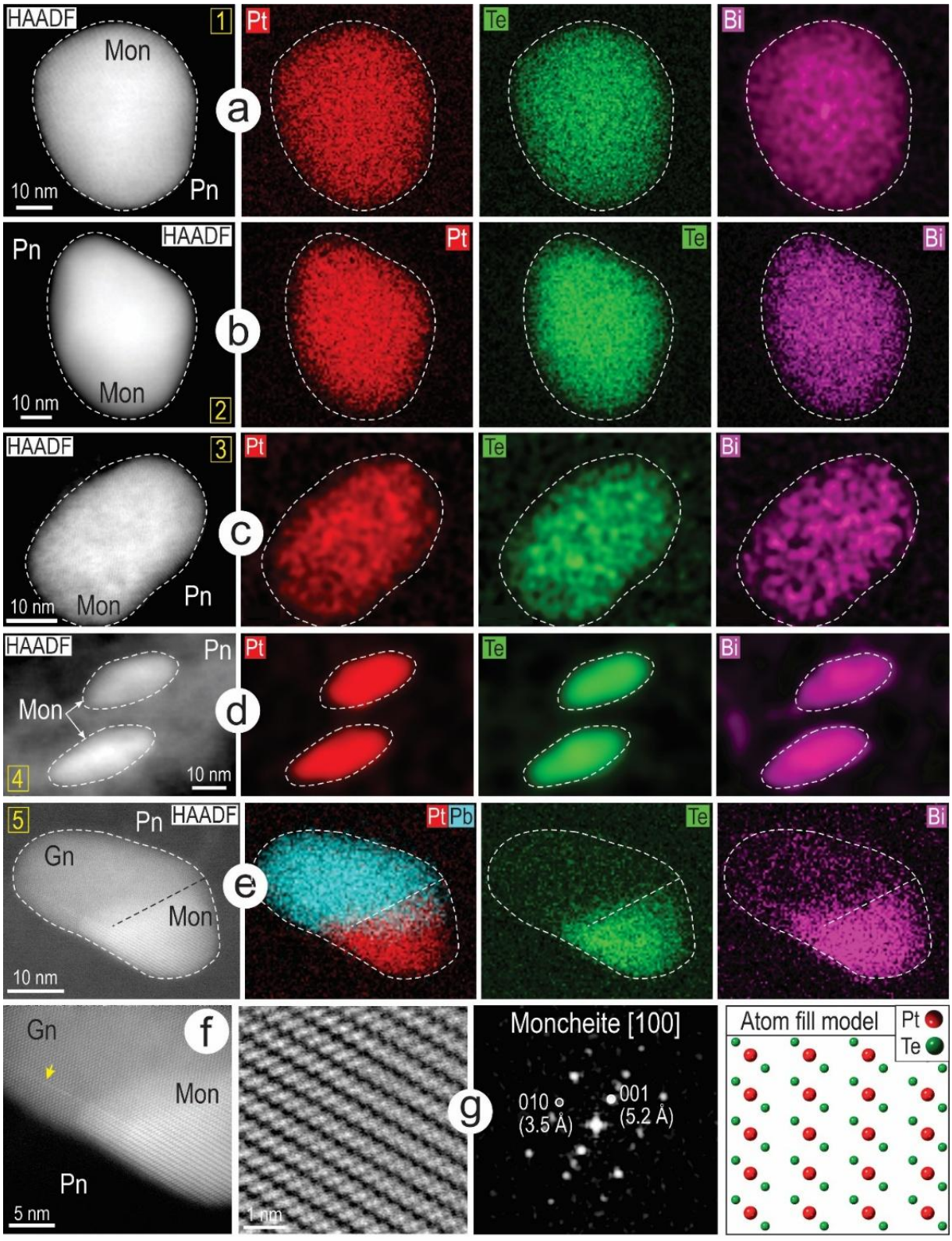

Figure 10. (a-e) Images and EDS STEM maps of moncheite (Mon) nanoparticles (NP) in pentlandite (Pn). Note all, except (e) are single phase. (e) Two-phase NP containing moncheite and galena (Gn). (f) Detail of NP in (e) showing the coherent boundary between the two phases with moncheite protruding into galena (arrowed). (g) Atomic scale images, corresponding FFT pattern and crystal model of moncheite (cif file for Bi-free moncheite, $PtTe_2$, from Wyckoff 1963) on [100] zone axis. Layer stacks are marked by lines on the image and model.

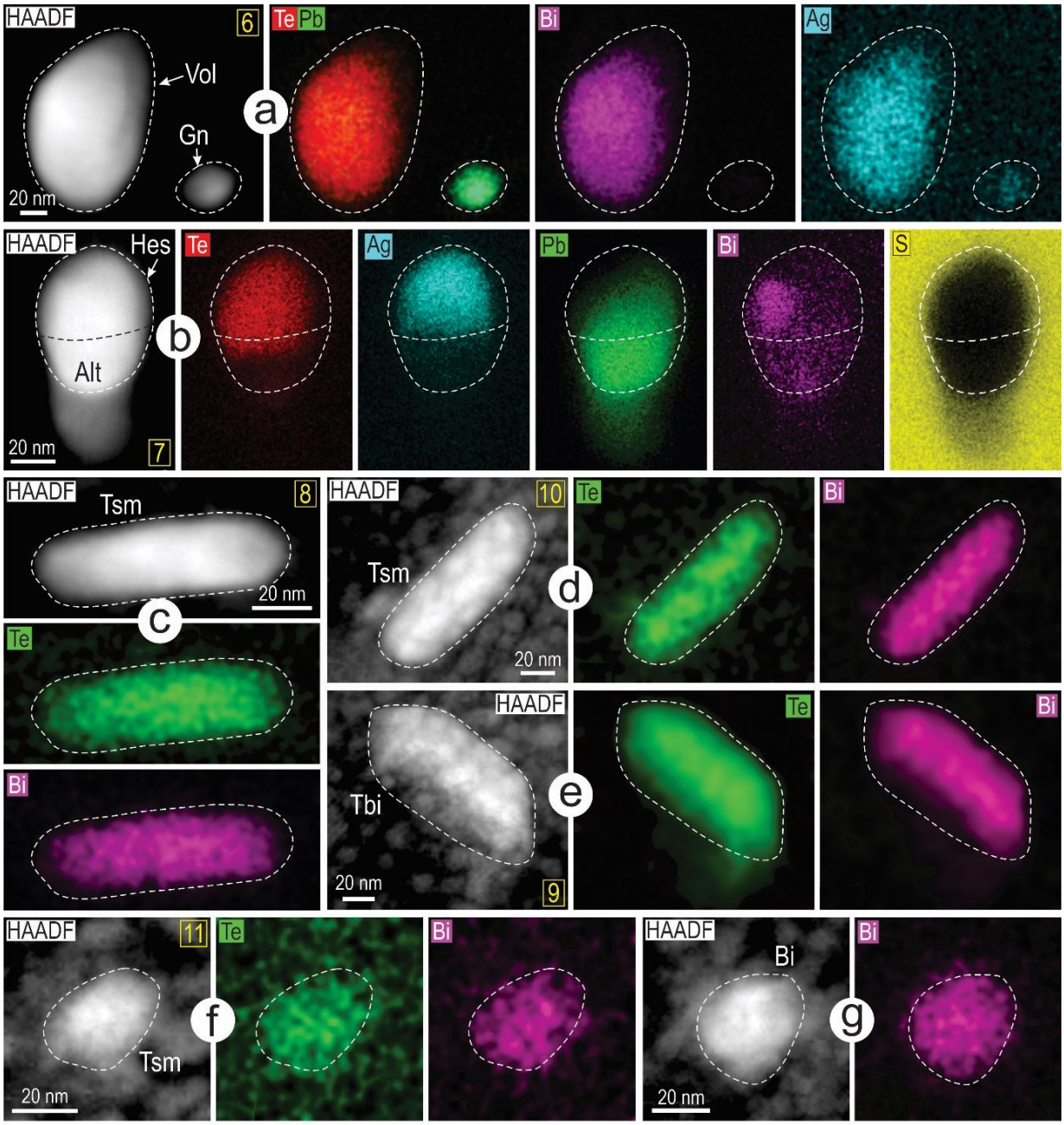

Figure 11. Images and EDS STEM maps of various nanoparticles representing Bi-(Ag)-Te-, Ag-, Pb-tellurides, galena (Gn) and native Bi (in g). (a) Large volynskite (Vol) NP next to galena (from area in Fig. 9a, e). (b) Binary NP composed of altaite (Alt) and hessite (Hes). Note a cluster of Bi attached to hessite. (c-f) Nanoparticles of Bi-tellurides corresponding to tellurobismuthite (Tbi) and tsumoite (Tsm).

A smaller population of NPs corresponds to an eclectic range of Bi-, Ag-, and Pb-tellurides (Fig. 11; Table 1b). A relatively large, single phase volynskite NP adjacent to a small galena NP (Fig. 11a) was mapped from area in Figure 9e. A binary hessite-altaite NP (Fig. 11b) located in the area from Figure 9i, also shows a Bi-rich cluster. Bismuth tellurides (tellurobismuthite and

tsumoite) generally have well-defined lamellar morphology and are mostly present at grain boundaries in pentlandite (Fig. 11c-f). Native bismuth (Fig. 11g) is noted adjacent to Bi-telluride NPs.

Discussion

Petrogenetic significance of the 'exotic' Ni-Bi-Te-Pb-Ag-S trace mineral associations

Onça Rosa is interpreted by Campo-Rodriguez et al. (in review) as an atypical Fe-Zn-Ni skarn system formed by intense alteration of an ultramafic protolith belonging to the Serra do Puma layered complex at its contact with a younger syn-kinematic granite. The hydrothermal origin of the Jaguar Ni-rich ores was discussed previously (Ferreira et al. 2021; Mansur et al. 2023) but the distinct character of pentlandite-rich ores from Onça Rosa was recognized by Campo-Rodriguez et al. (in review) who attributed its origin to the calcic skarn stage.

Discovery of the 'exotic' Ni-Bi-Te-Pb-Ag-S mineral association and, specifically, the presence of arsenohauchecornite, parkerite, and ognitite, is significant as it places the genetic relationship of the Onça Rosa ore with the Puma ultramafic layered complex beyond doubt. We note that such rare Ni-Bi-sulfides and -tellurides are hitherto almost exclusively reported from Ni-Cu-PGE ores formed in ultramafic (layered) complexes such as the Oktyabr'skoe deposit, Noril'sk (Kovalenker et al. 1978), the Ognit Ultramafic Complex, Irkutskaya Siberian Craton (Barkov et al. 2019), both in Russia, from Ni-Cu mines at Sudbury, Ontario, Canada (e.g. Gait and Harris 1980), and from chromitites in ophiolitic complexes in the Russian Urals (Koroteev et al. 2017).

Onça Rosa represents the second documented occurrence of ognitite worldwide and remarkably, shows Pd concentrations up to four times higher (maximum ~ 0.68 wt. %) than those reported from the type locality (0.16 wt%; Barkov et al. 2019). The presence of Pd in these

minerals at Onça Rosa is reinforced by measurements above minimum detection limits in a scatter of parkerite analyses (up to 0.02 wt. % Pd).

Trace element mobility during replacement reactions

Formation of the rare Ni-Bi-(Ag)-(Pb)-Te-S-phases in sulfide ores from Onça Rosa is intimately associated with replacement of pentlandite by violarite/bravoite and fluid-assisted cataclasis of pyrite (Fig. 1). The microtextural complexity observed in pentlandite ores (rounding, tiling, symplectites) indicates cycles of replacement via dissolution-reprecipitation reactions during which metals were locally remobilized and re-precipitated as inclusions in the host sulfides and/or at their grain boundaries (Figs. 2, 3a). These overprinting events are illustrated by the distinctive chalcophile (Cu-Ag-Te-Se-Bi-(Au)-Co-As) trace element signatures depicted in all common sulfides except sphalerite and chalcopyrite (Fig. 3b, d). Remarkable also is the strong correlation between (Ag+Au) and (Bi+Te) in pyrite, pentlandite and violarite/bravoite (Fig. 3c).

Formation of the Ni-Bi-Te-S minerals is controlled by fluids percolating grain boundaries of pentlandite or between pentlandite and magnetite, and/or pyrite (Figs. 4, 5). We contend that such grains nucleate from Ni, Te, Bi (and Pd) that was remobilized from pentlandite during its replacement by violarite/bravoite (Figs. 1, 2). Pentlandite is widely recognized as a good host for Pd but not Pt, a finding confirmed by dry experiments in the systems Pd-Fe-S and Pt-Fe-S (Makovicky et al. 1988). The ubiquitous presence of tiny grains of other sulfides, (sphalerite, chalcopyrite) within the Ni-Bi-Te-Pb-Ag-S mineral assemblages trapped at grain boundaries reinforces the idea that such Ni-Bi-Te-S minerals are produced by fluid-mineral reactions, rather than being formed during an early ore stage (pentlandite precipitation). Further fluid- or diffusion assisted reworking is evident from the observed decomposition of ognitite into symplectites of altaite and parkerite, a stage also marked by an influx of Pb and also Ag (noting the presence of

hessite; Fig. 4g). Formation of amphibole at this stage (calcic skarn) is indicated by its direct grain contacts with arsenohauchecornite.

Whether the Bi and Te within these assemblages is sourced entirely from trace elements released from pentlandite is, however, debatable. The notable abundance of Bi-chalcogenides and Pb-Bi-(Ag)-sulfosalts (Fig. 3i-o) within pyrite towards the lower contact of the orebody with the granite suggests additional metal sources from granite-derived hydrothermal fluids. The intimate association between tellurides and sulfosalts of various types, and with tiny grains of common sulfides, indicates these are formed at the same time, likely with participation of fluids of granitic affiliation. Pyrite and violarite also record percolation of such Bi, Te, Ag-(Au)-bearing fluids through pores and/or microfractures (Figs. 2a, 3a; SM S1).

The key role of parkerite in accommodating replacement reactions between ognitite and pentlandite is tracked down to the nanoscale (Figs. 7, 9). Fluid pathways can be attributed to defects and/or misorientation fabrics in pentlandite, some of which are also marked by subtle chemical changes (Fig. 9e). Importantly, such nanostructures host a broad range of nanoparticles (Figs. 10, 11).

Insights into the crystal-structure and chemistry of arsenohauchecornite and ognitite

Arsenohauchecornite features two Me^{3+} elements, Bi and As, that have a greater difference between their covalent radii (1.46 and 1.19 Å, respectively) (Grice and Ferguson 1989) than the covalent radii of Sb (1.38 Å) and Te (1.35 Å), metalloids present in the other species from the hauchecornite group (Gait and Harris 1980). On the other hand, ordering of As and Bi into two different Ni-coordinated body-centered cubes (a consequence of the As-Ni bonds being much shorter than the Bi-Ni bonds) leads to formation of an I-type tetragonal (space group *I*4/*mmm*) superstructure of the basic hauchecornite cell (Grice and Ferguson 1989). The authors discuss the

possibility of polytypes within the group, particularly if Te or Sb are present, as is the case of Onça Rosa specimen.

Imaging and crystal structure simulations on a set of relevant zone axes (Figs. 6b-f; SM S2) shows however, the analyzed specimen has the typical I-centered superstructure of arsenohauchecornite. The presence of relict pentlandite, as fine particles and larger bodies of pentlandite with the same crystallographic orientation (Fig. 6a) further support the formation of arsenohauchecornite as the result of replacement reactions.

High-resolution imaging and STEM modelling (Fig. 8) confirms that ognitite has the same trigonal $P\bar{3}m1$ structure as melonite. Ognitite also has mixed Bi-Te sites, thus confirming the solid solution inferred from the compositional data (Fig. 4h). The specimen from Onça Rosa, represents the first documented example of an intermediate member ($Ogn_{60}Mlt_{40}$) of the ognitite-melonite solid-solution series. Moreover, the Bi vs. Te compositional field (Fig. 4h) is depicted at the nanoscale and can be attributed to rhythmic variation of chemical gradients during crystal growth.

Fingerprinting PGE signatures

Besides the presence of Pd as a trace component of ognitite, the discovery of moncheite, a Pt-Bi-telluride occurring among the NPs observed in pentlandite (Fig. 10) further emphasizes the distinct PGE signature of the Onça Rosa ores. Although most NPs are single-phase, the presence of two-or three-phase inclusions (moncheite-galena, hessite-altaite-bismuth), implies that Pt is linked to the exotic Bi-Ag-Pb-Te trace mineral association revealed at the micron-scale (Figs. 4, 5).

Two distinct stages are invoked to explain the PGE signatures in the ores as revealed by the ognitite-pentlandite assemblage. Firstly, release of Pd from pentlandite (~0.4 ppm; SM Table S1a) during dissolution-reprecipitation reactions leads to formation of ognitite. A second stage, recorded by the breakdown of ognitite forming nanoscale aggregates of parkerite along the

margins with pentlandite (Fig. 7), involves percolation of a Bi-rich, S-bearing fluid. The lack of Pd-bearing NPs indicates this element is likely retained within the telluride structure and is not released. If we assume that Pt is present in the percolating fluids at this stage, this will precipitate as moncheite NPs rather than being incorporated within the host sulfides. The Bi-bearing moncheite, as well as its association with galena in a two-phase NP (Fig. 10e, f), is further evidence for precipitation of this PGM from such a fluid. Transport of Pt as bisulfide complexes in acidic-neutral solutions under reduced and moderate oxidation conditions was modelled for temperatures as low as 300 °C (Barnes and Liu 2012). Such conditions were suggested for the formation of hydrothermal pentlandite at Onça Rosa (Campo-Rodriguez et al. in review).

According to experimental studies, if Pt is hosted in monosulfide solid solutions (MSS) as discrete Pt-nanocrystals, including $PtTe_2$ (Bi-free moncheite), these will be crystallographically aligned within the host MSS (Helmy et al. 2023). This is not the case for the moncheite NPs within pentlandite, even though subsolidus replacement of galena by moncheite is epitaxial (Fig. 10f).

Merenskyite, the Pd-bearing mineral isotructural with moncheite was documented as a prominent species in a varied PGM association from the Jatobá deposit, ~150 km east from Jaguar (Campo-Rodriguez et al. 2024b). In Jatobá, however, the PGMs are hosted by Ni-bearing pyrite rather than pentlandite.

Summary and Implications

The Ni-rich sulfide ore from Onça Rosa comprises pentlandite, violarite/bravoite, pyrite, sphalerite and minor chalcopyrite. Pentlandite, the main primary Ni-sulfide, shows microtextural complexity such as grain rounding, tiling, and symplectites with violarite/bravoite, all indicating cycles of replacement via dissolution-reprecipitation reactions. Remobilization and reprecipitation of metals as inclusions and/or at grain boundaries is revealed by grain-scale element mapping. Chalcophile elements and chalcogens (Bi-Ag-Te-Se) define a trace element

signature in both pentlandite and pyrite. Pentlandite also contains measurable Pd (up to 1.3 ppm). Pyrite is a minor Ni-carrier and also displays a weak oscillatory zoning with respect to Co and As.

Arsenohauchecornite (ideally $Ni_{18}Bi_3AsS_{16}$), ognitite (NiBiTe), and parkerite ($Ni_3Bi_2S_2$) are relatively abundant accessories in the sulfide mineralization. Respective empirical formulae are:

$(Ni_{16.5}Fe_{1.28}Co_{0.39}Zn_{0.17}Cu_{0.01})_{18.35}(Bi_{2.9}As_{0.77}Sb_{0.08}Te_{0.08})_{3.8}(S_{15.85}Se_{0.01})_{15.9}$;

$(Ni_{1.02}Fe_{0.01}Pd_{0.004})_{1.04}(Bi_{0.58}Pb_{0.002}As_{0.001})_{0.585}(Te_{1.36}S_{0.02}Se_{0.001})_{1.38}$, and

$(Ni_{2.85}Fe_{0.045}Ag_{0.007}Pd_{0.001})_{2.9}(Bi_{2.024}Pb_{0.005})_{2.03}(S_{2.02}Te_{0.038}Se_{0.008})_{2.07}$.

The ognitite reported here represents the second world occurrence and contains up to 0.68 wt. % Pd, four times higher than from the type locality.

In addition to the rare Ni-Bi minerals, Bi-tellurides of the tetradymite group (mainly tellurobismuthite and tsumoite) and Pb-Bi-sulfosalts from the lillianite homologous series (Ag-bearing lillianite and heyrovskýite) are part of the exotic trace mineralogy at Onça Rosa.

High-resolution HAADF STEM imaging, crystal structure models and STEM simulations of arsenohauchecornite show the Onça Rosa specimen has an I-centered, tetragonal (space group *I*4/*mmm*) superstructure as described previously, even though it contains Te and Sb. Ognitite shares its trigonal symmetry and space group ($P\bar{3}m1$) with melonite. The Bi-Te mixed sites characterized by atomic-scale imaging and simulations confirm extensive solid solution between melonite and ognitite, concordant with compositional data. The specimen from Onça Rosa is the first documented example of an intermediate member ($Ogn_{60}Mlt_{40}$) in this solid solution series. Variation of Bi relative to Te is also depicted at the nanoscale and can be attributed to rhythmic variation of chemical gradients during crystal growth.

Nanoscale aggregates of parkerite found at boundaries between ognitite and pentlandite are associated with abundant defects and/or misorientation fabrics in pentlandite, some of which are also marked by subtle chemical changes (Ag, Te). Such nanostructures, attributable to fluid pathways, host a broad range of nanoparticles: Bi-bearing moncheite, volynskite, hessite, altaite,

tellurobismuthite and tsumoite. Among these, moncheite, a platinum group mineral, together with the Pd content in ognitite, highlights PGE enrichment in the sulfide ores from Onça Rosa.

Formation of the scarce association of arsenohauchecornite, ognitite, and parkerite is attributable to fluids interacting with pentlandite-rich ores at the contacts between an ultramafic protolith (Serra do Puma layered complex) and a granite-derived hydrothermal source. The latter is emphasized by the presence of abundant Bi-tellurides and -sulfosalts. Moreover, the reaction zones in pentlandite are attributable to further brecciation and fluid percolation (misorientation nanostructures) leading to formation of PGE-, and Bi-Ag-Pb-Te-bearing nanoparticles.

Although ognitite, arsenohauchecornite, and parkerite are generally considered as accessory minerals formed in ultramafic rocks, we contend a metasomatic-hydrothermal origin for the Onça Rosa occurrence considering the range of micron- to nanoscale textures, geochemical signatures and associated NPs. If so, this type of associations represents a valuable fingerprint for the fluid-mineral reactions between existing ores (pentlandite, pyrite) and granite-sourced fluids.

The Onça Rosa orebody and the Jatobá deposit (Campo-Rodriguez et al. 2024) represent two occurrences of PGMs in hydrothermal Ni-sulfide ores associated with IOCG systems in the Carajás Domain. PGM associations are reported previously but only from ultramafic layered complexes, Luanga, Lago Grande and Serra Pelada (Diella et al. 1995; Cabral et al. 2011; Teixeira et al. 2015; Mansur and Ferreira Filho 2016; Mansur et al. 2020), all of which are located in the northeast part of the Carajás Domain. We suggest that PGE enrichment in hydrothermal Ni ores is more common than previously recognized and can lead to formation of PGM minerals during overprinting events. This observation carries implications for exploration in the southern areas of the Carajás Domain and may indeed lead to new discoveries here and in analogous terranes elsewhere.

As shown here and in several previous studies (e.g., Wirth et al. 2013; Junge et al. 2015; Helmy et al. 2023), *in situ* FIB-S/TEM analysis is a pre-requisite for assessing the presence of nanoparticulate PGM. Such characterization is crucial for unveiling the physical status of any

PGE present and is particularly pertinent for ores where the PGE content is relatively low. Detailed knowledge of the mineralogical distribution of PGE is critical for successful recovery.

Acknowledgements and funding

Animesh Basak is acknowledged for technical support with FIB analyses. Y.T.C.R and M.E.S acknowledges continuous support from the Brazilian Research Council (CNPq – Project 409015/2021-0) and the Coordenação de Aperfeiçoamento de Pessoal de Nível Superior - Brasil (CAPES) - Finance Code 001. Analytical expenses were supported by the Institute of Sustainability, Energy and Resources, The University of Adelaide. N.J.C. and K.E. acknowledge funding through Australian Research Council Linkage grant LP200100156 (Critical Minerals from Complex Ores).

Supplementary Material

Appendix A: LA-ICP-MS trace element data for sulfide minerals..

Appendix B:

ESM Table 1a. LA-ICP-MS trace element data for sulfide minerals.

ESM Table 1b. LA-ICP-MS data for sulphides used for box-and-whisker plots.

References

Barkov, A.Y., Bindi, L., Tamura, N., Shvedov, G.I., Winkler, B., Stan, C.V., Morgenroth, W., Martin, R.F., Zaccarini, F., and Stanley, C.J. (2019) Ognitite, NiBiTe, a new mineral species, and Co-rich maucherite from the Ognit ultramafic complex, Eastern Sayans, Russia. Mineralogical Magazine 83, 695-703. https://doi.org/10.1180/mgm.2019.31

Barnes, S.J., and Liu, W. (2012) Pt and Pd mobility in hydrothermal fluids: Evidence from komatiites and from thermodynamic modelling. Ore Geology Reviews 44, 49–58. https://doi.org/10.1016/j.oregeorev.2011.08.004

Cabral, A.R., Lehmann, B., and Burgess, R. (2011) Late Cretaceous bonanza-style metal enrichment in the Serra Pelada Au-Pd-Pt deposit Pará Brazil. Economic Geology 106, 119-125. https://doi.org/10.2113/econgeo.106.1.119

Campo-Rodriguez, Y.T., Cook, N.J., Ciobanu, C.L., Schutesky, M.E., King, S.A., Gilbert, S., and Ehrig, K. (2024b) Platinum Group Minerals Associated with Nickel-Bearing Sulfides from the Jatobá Iron Oxide-Copper-Gold Deposit, Carajás Domain, Brazil. Minerals 14, 757. https://doi.org/10.3390/min14080757

Campo Rodriguez, Y.T., Ciobanu, C.L., Cook, N.J., Schutesky, M.E., Ehrig, K., Slattery, A., Gilbert, S., and King, S.A. (*in review c*) Magnetite and REE-rich calcic amphibole provide evidence for a skarn-IOCG system at Onça Rosa, Jaguar Orefield, Carajás Mineral Province, Brazil. The Canadian Journal of Mineralogy and Petrology.

Centaurus Metals. (2024) Jaguar Nickel Sulphide Project. https://www.centaurus.com.au/site/projects/jaguar-nickel-sulphide-project (accessed 05 September 2024).

Ciobanu, C.L., Cook, N.J., Utsunomiya, S., Pring, A., and Green, L. (2011) Focussed ion beam–transmission electron microscopy applications in ore mineralogy: Bridging micro- and nanoscale observations: Ore Geology Reviews 42, 6–31. https://doi.org/10.1016/j.oregeorev.2011.06.012

Courtney, T. (2000). Mechanical Properties of Materials. McGraw Hill. pp. 203–205.

Diella, V., Ferrario, A., and Girardi, V.A.V. (1995) PGE and PGM in the Luanga mafic-ultramafic intrusion in Serra dos Carajás (Pará State, Brazil). Ore Geology Reviews 9, 445-453. https://doi.org/10.1016/0169-1368(95)00002-J

Ferreira-Filho, C.F., de Oliveira, M.M.F., Mansur, E.T., and Rosa, W.D. (2021) The Jaguar hydrothermal nickel sulphide deposit: evidence for a nickel-rich member of IOCG-type deposits in the Carajás Mineral Province, Brazil. Journal of South American Earth Science 111, 103501. https://doi.org/10.1016/j.jsames.2021.103501

Fleet, M.E. (1973) The crystal structure of parkerite (Ni3Bi2S2) American Mineralogist 58, 435-439.

Gait, R.I., and Harris, D.C. (1980) Arsenohauchecornite and tellurohauchecornite: new minerals in the hauchecornite group. Mineralogical Magazine 43, 877-888. https://doi.org/10.1180/minmag.1980.043.331.09

Garuti, G., and Rinaldi, R. (1986) Mineralogy of melonite-group and other tellurides from the Ivrea–Verbano basic complex, western Italian Alps. Economic Geology 81, 1213–1217. https://doi.org/10.2113/gsecongeo.81.5.1213

Grice, J.D., and Ferguson, R.B. (1989) The crystal structure of arsenohauchecornite, The Canadian Mineralogist 27, 137-142.

González-Álvarez, I., Pirajno, F., and Kerrich, R. (2013) Hydrothermal nickel deposits: Secular variation and diversity. Ore Geology Reviews 52, 1-3. https://doi.org/10.1016/j.oregeorev.2012.11.006

Helmy, H.M., Botcharnikov, R., Ballhaus, C., Wirth, R., Schreiber, A., and Buhre, S. (2023) How Pt and Pd are hosted in magmatic sulfides, substitutions and/or inclusions? Contributions to Mineralogy and Petrology 178, 41. https://doi.org/10.1007/s00410-023-02018-8

Junge, M., Wirth, R., Oberthür, T., Melcher, F., and Schreiber, A. (2015) Mineralogical siting of platinum-group elements in pentlandite from the Bushveld Complex, South Africa. Mineralium Deposita 50, 41–54. https://doi.org/10.1007/s00126-014-0561-0

Just, J., and Feather, C.E. (1978) Tucekite, a new antimony analogue of hauchecornite. Mineralogical Magazine 42, 278. https://doi.org/10.1180/minmag.1978.042.322.18

Just, J. (1980) Bismutohauchecornite—new name: hauchecornite redefined. Mineralogical Magazine 43, 873–876. https://doi.org/10.1180/minmag.1980.043.331.08

Koroteev, V.A., Popov, M.P., Erokhin, Y.V., and Khiller, V.V. (2017) Parkerite and bismutohauchecornite in chromitites of the Urals: Example of the Uralian Emerald Mines. Doklady Earth Sciences 473, 438-440. https://doi.org/10.1134/S1028334X17040109

Kovalenker, V.A., Evstigneeva, T.L., Begizov, V.D., Vyal'sov, L.N., Smirnov, A.V., Krakovetskii, Y.K., and Balbin, V.S. (1978) Hauchecornite from copper-nickel ores of the Oktyabr'skoe deposit. Trudy Min. muzeya Akad. Nauk SSSR 26, 201–205 (in Russian).

Lister, J.S., and Bailey, S.W. (1967) Chlorite polytypism: IV. Regular two-layer structures. American Mineralogist 52 (11-12), 1614-1631.

Makovicky, M., Makovicky, E., and Rose-Hansen, J. (1988) Experimental evidence on the formation and mineralogy of platinum and palladium ore deposits. In Mineral deposits within the European Community (pp. 303-317). Berlin, Heidelberg: Springer Berlin Heidelberg https://doi.org/10.1007/978-3-642-51858-4_17

Mansur, E.T., and Ferreira Filho, C.F. (2016) Magmatic structure and geochemistry of the Luanga Mafic–Ultramafic Complex: Further constraints for the PGE-mineralized magmatism in Carajás, Brazil. Lithos 266, 28-43. https://doi.org/10.1016/j.lithos.2016.09.036

Mansur E.T., Ferreira Filho C.F., and Oliveira D.P.L. (2020) The Luanga deposit, Carajás Mineral Province, Brazil: Different styles of PGE mineralization hosted in a medium-size layered intrusion. Ore Geology Reviews 118, 103340. https://doi.org/10.1016/j.oregeorev.2020.103340

Mansur, E.T., Dare, S.A.S., Ferreira Filho, C.F., Miranda, A.C.R, and Monteiro, L.V.S. (2023) The distribution of trace elements in sulfides and magnetite from the Jaguar hydrothermal nickel deposit: Exploring the link with IOA and IOCG deposits within the Carajás Mineral Province, Brazil. Ore Geology Reviews 152, 105256. https://doi.org/10.1016/j.oregeorev.2022.105256

Petruk, W., Harris, D.C., and Stewart, J.M. (1969) Langisite, a new mineral, and the rare minerals cobalt pentlandite, siegenite, parkerite, and bravoite from the Langis mine, Cobalt-Gowganda area, Ontario, Canada. The Canadian Mineralogist 9, 597-616.

Scheibe, R. (1893) Ueber hauchecornit, ein nickelwismuthsulfid von der Grube Friedrich. Jahrbuch der Königlich Preussischen Geologischen Landesanstalt und Bergakademie zu Berlin für das Jahr 1891: 12: 91-125.

Sejkora, J., Škácha, P., Plášil, J., Dolníček, Z., and Ulmanová, J. (2021) Hrabákite, Ni9PbSbS8, a new member of the hauchecornite group from Příbram, Czech Republic. Mineralogical Magazine 85, 189-196. https://doi.org/10.1180/mgm.2021.1

Teixeira, A.S., Ferreira Filho, C.F., Della Giustina, M.E.S., Araújo, S.M., and da Silva, H.H.A.B. (2015) Geology, petrology and geochronology of the Lago Grande layered complex: evidence for a PGE-mineralized magmatic suite in the Carajás Mineral Province, Brazil. Journal of South American Earth Sciences 64, 116-138. https://doi.org/10.1016/j.jsames.2015.09.006

Wirth, R., Reid, D., and Schreiber, A. (2013) Nanometer-sized platinum-group minerals (PGM) in base metal sulfides: New evidence for an orthomagmatic origin of the Merensky Reef PGE ore deposit, Bushveld Complex, South Africa. The Canadian Mineralogist 51(1), 143-155. https://doi.org/10.3749/canmin.51.1.143

Wyckoff, R.W.G. (1963) Crystal structures 1. Interscience Publishers, New York, New York, 1, 239-444.

Zaccarini, F., Bindi, L., Tsikouras, B., Grammatikopoulos, T., Stanley, C.J., and Garuti, G. (2020) Arsenotucekite, Ni18Sb3AsS16, a new mineral from the Tsangli chromite mine, Othrys ophiolite, Greece. Mineralogy and Petrology 114, 435–442. https://doi.org/10.1007/s00710-020-00712-0

CHAPTER 8

SUMMARY, RECOMMENDATIONS AND CONCLUDING REMARKS

CHAPTER 8: SUMMARY, RECOMMENDATIONS AND CONCLUDING REMARKS

The research contained within this thesis represents a contribution to understanding one of the most complex metallogenic provinces on planet Earth, the Neoarchean Carajás Domain of central-north Brazil. Results, both for the Jatobá deposit (**Chapters 2** to **5**) and the Onça Rosa orebody at Jaguar (**Chapters 6** and **7**), have constrained the mechanisms and timing of ore genesis and carry implications for the exploitation of the deposits. The six chapters in this thesis also demonstrate the value of utilizing novel and innovative investigative techniques and how using, in parallel, different methodologies on the same well-chosen and well-characterized sample material can significantly advance interpretation. Examples include nanoscale imaging and analysis of nanoscale inclusions in common minerals (**Chapters 2**, **4**, and **6**), the ultra-detailed characterization of rare trace minerals (**Chapters 3** and **7**), and not least, in-tandem U-Pb and Lu-Hf apatite geochronology on samples well studied chemically and texturally (**Chapter 5**).

Although conclusions are given in each chapter and therefore need not be repeated here, several highlights deserve to be stated. These include the spectacular polysomatic intergrowths between chain silicates enclosed in magnetite from Jatobá, which provide evidence for previously unrecognized metamorphism (**Chapter 2**), and the successful application of Lu-Hf apatite geochronology to give a robust 2.5 Ga age for that event (**Chapter 5**). In turn, these findings allowed a modified geological model to be put forward that acknowledges the significant role played by deep shear zones at Jatobá and, intriguingly, points to links between the northern and southern copper belts. Likewise, detailed mineralogical study revealed how cycles of remobilization and replacement contribute to enrichment in rare earths and unusual Ni-Bi-Te-S-minerals (**Chapters 3** and **7**), and perhaps most importantly, led to recognition of platinum group

elements in both ore systems, a finding of lasting value for mineral exploration. The diversity of geological settings and ore mineral assemblages in the Carajás IOCG deposits certainly pose challenges for validation of ore genesis models, but also provides an exemplar natural laboratory to address the impact of local geological environment and metal scavenging from host rocks on IOCG-type mineralization.

Even though of critical importance as a source of copper to meet fast growing demand, iron-oxide copper gold (IOCG) deposits remain an eclectic group of ore systems formed at vastly different ages and in a range of geological settings. They are, however, readily recognizable as a distinct group by the dominance of iron oxides – even if the origin of the iron may differ fundamentally in individual settings. The number of truly global-scale studies of IOCG systems remains relatively limited (Hitzmann et al. 2002; Williams et al. 2005; Groves et al. 2010; Barton 2014; Skirrow 2022), even though the literature is replete with detailed and often highly descriptive studies of individual IOCG systems across all continents. Many of these studies are limited to specific regions - in many cases, to areas without any mining activity at present or likely in the foreseeable future due to low grade or other adverse factors (e.g., Corriveau et al. 2016). Research on the Carajás Domain is thus vital, not only because it is one of the world's largest IOCG provinces, but also because it is the site of active mining and active mineral exploration, providing improved exposure to geology.

There is substantial need for further work. This might focus on systematic mineralogical studies of magnetite from selected deposits across the Carajás Domain to address the presence of chain-silicate inclusions like those shown in **Chapters 2** and **6** that enabled assembly of evidence supporting a protracted geological history. Further work might also further consolidate the timing of Cu-Ni-PGE mineralization in these and other deposits through the acquisition of additional geochronological data, and expanded knowledge of Ni-PGE mineralogy. The research results reported in this thesis and the time spent poring over inconsistencies in the literature over the past

three years emphasize the importance of detailed mineral characterization of all samples and the need for a systematic and rigorous approach to all laboratory analysis and interpretation of results.

During the course of this thesis, much thought was given to how a better generic understanding of IOCG deposits might be achieved by a rigorous comparison between the Carajás Domain and the Olympic Cu-Au Province, South Australia (e.g., Reid 2019), the world's largest concentration of IOCG deposits. The two provinces broadly share main lithologies and characteristic geochemical signatures yet the Carajás Province spans wider age ranges of igneous and hydrothermal activity, sedimentation and metamorphism. This study has identified some common features, e.g., preservation of amphibole inclusions in magnetite (c.f. **Chapter 2** and Verdugo-Ihl et al. 2021). Other approaches that have been remarkably successful in South Australia (e.g., U-Pb iron-oxide geochronology; Courtney-Davies et al. 2019) proved elusive when attempted on Carajás samples. One pivotal question that should be part of any future attempt to compare the two largest Precambrian IOCG provinces on Earth is what determines the extraordinary REE-U endowment in the Olympic Cu-Au Province and, in contrast, Ni-PGE in the Carajás Domain? Answers can underpin strategies for exploration, sustainable mining and by-product extraction.

8.1. Recomendações e Considerações Finais

A pesquisa contida nesta tese representa uma contribuição para o entendimento de uma das províncias metalogenéticas mais complexas do planeta, o Domínio Neoarqueano de Carajás, no centro-norte do Brasil. Os resultados obtidos, tanto para o depósito de Jatobá (**Capítulos 2-4**) quanto para o corpo de minério de Onça Rosa em Jaguar (**Capítulos 5** e **6**), apresentaram os mecanismos e o momento de gênese do minério com implicações para a exploração dos depósitos. Os seis capítulos desta tese também demonstram o valor da utilização de técnicas de investigação

modernas e inovadoras e seu uso, em paralelo, com diferentes metodologias no mesmo material de minério e amostras bem escolhidas e caracterizadas pode avançar significativamente nas interpretações genéticas. Exemplos incluem imagens e análises em nanoescala de nano inclusões em minerais comuns (**Capítulos 2, 4** e **6**), a caracterização ultradetalhada de minerais traço raros (**Capítulos 3** e **7**) e, não menos importante, a geocronologia U-Pb e Lu-Hf apatita em conjunto em amostras bem estudadas química e texturalmente (**Capítulo 5**).

Embora conclusões sejam apresentadas em cada capítulo e, portanto, não precisam ser repetidas aqui, vários destaques merecem ser mencionados. Estes incluem os intercrescimentos polissomáticos entre silicatos de cadeia inclusos na magnetita de Jatobá, que fornecem evidências para um metamorfismo não reconhecido anteriormente (**Capítulo 2**), e a aplicação bem-sucedida da geocronologia Lu-Hf apatita para fornecer uma idade robusta de 2,5 Ga para esse evento (**Capítulo 5**). Por sua vez, essas descobertas permitiram que um modelo geológico diferente fosse proposto, reconhecendo o papel significativo desempenhado pelas zonas de cisalhamento profundas em Jatobá e, intrigantemente, apontando para ligações entre os cinturões de cobre do norte e do sul do Domínio Carajás. Da mesma forma, estudos mineralógicos detalhados revelaram como ciclos de remobilização e substituição contribuem para o enriquecimento em terras raras e minerais raros de Ni-Bi-Te-S (**Capítulos 3** e **7**), e talvez mais importante, levaram ao reconhecimento de elementos do grupo da platina em ambos os sistemas de minério, uma descoberta de valor duradouro para a exploração mineral. A diversidade de ambientes geológicos e assembleias mineralógicas de minério nos depósitos de IOCG de Carajás certamente representa desafios para a validação de modelos de gênese de minério, mas também fornece um laboratório natural exemplar para abordar o impacto do ambiente geológico local e da captura de metais de rochas hospedeiras na mineralização do tipo IOCG.

Apesar da importância crítica como fonte de cobre para atender à demanda em rápido crescimento, os depósitos de óxido de ferro cobre-ouro (IOCG) permanecem como um grupo eclético de sistemas de minério formados em idades muito diferentes e em uma ampla variedade

de ambientes geológicos. No entanto, eles são facilmente reconhecíveis como um grupo distinto pela dominância dos óxidos de ferro - mesmo que a origem do ferro possa diferir fundamentalmente em configurações individuais. O número de estudos verdadeiramente globais de sistemas IOCG permanece relativamente limitado (Hitzmann et al. 2002; Williams et al. 2005; Groves et al. 2010; Barton 2014; Skirrow 2002), embora a literatura seja rica de estudos detalhados e muitas vezes altamente descritivos de sistemas IOCG individuais em todos os continentes. Muitos desses estudos são limitados a regiões específicas - em muitos casos, a áreas sem qualquer atividade mineira no presente ou provavelmente no futuro previsível devido ao baixa grau económico ou outros fatores adversos (e.g., Corriveau et al. 2016). A pesquisa no Domínio de Carajás é, portanto, vital, não apenas porque é uma das maiores províncias de IOCG do mundo, mas também porque é um local de mineração e exploração mineral ativa, proporcionando uma melhor exposição à geologia.

Há uma necessidade substancial de trabalho adicional. Isso pode se concentrar em estudos mineralógicos sistemáticos de magnetita de depósitos selecionados em todo o Domínio de Carajás para abordar a presença de inclusões de silicatos de cadeias, como as mostradas nos **Capítulos 2** e **6**, que permitiram a montagem de evidências que sustentam uma história geológica prolongada. Trabalhos futuros também podem consolidar ainda mais o tempo da mineralização Cu-Ni-PGE nesses e em outros depósitos por meio da aquisição de dados geocronológicos adicionais e do conhecimento expandido da mineralogia Ni-PGE. Os resultados da pesquisa relatados nesta tese e a análise de inconsistências na literatura nos últimos três anos enfatizam a importância da caracterização mineralógica detalhada de todas as amostras e a necessidade de uma abordagem sistemática e rigorosa para todas as análises de laboratório e interpretação de resultados.

Durante o curso desta tese, muita atenção foi dada a como uma melhor compreensão genérica dos depósitos de IOCG poderia ser alcançada por meio de uma comparação rigorosa entre o Domínio de Carajás e a Província de Cobre-Ouro Olympic Dam, na Austrália do Sul (e.g., Reid 2019), a maior concentração mundial de depósitos de IOCG. As duas províncias compartilham

amplamente litologias e assinaturas geoquímicas características, mas a Província de Carajás abrange faixas de idades mais amplas de atividade ígnea e hidrotermal, sedimentação e metamorfismo. Este estudo identificou algumas características comuns, como a preservação de inclusões de anfibólios em magnetita (cf. **Capítulo 2** e Verdugo-Ihl et al. 2021). Outras abordagens que foram notavelmente bem-sucedidas na Austrália do Sul (por exemplo, a geocronologia U-Pb de óxido de ferro; Courtney-Davies et al. 2019) provaram ser evasivas quando tentadas em amostras de Carajás. Uma questão fundamental que deve fazer parte de qualquer tentativa futura de comparar as duas maiores províncias de IOCG pré-cambrianas da Terra é o que determina o extraordinário enriquecimento de REE-U na Província de Cobre-Ouro Olympic Dam, em contraste, com Ni-PGE no Domínio de Carajás? As respostas podem fundamentar estratégias de exploração, mineração sustentável e extração de subprodutos.

8.2. Conclusions

The Neoarchean Carajás Domain of central-north Brazil is one of the most complex metallogenic provinces on planet Earth, and host to a diverse suite of mineral deposits. Among these, and of prime economic significance, are the large iron oxide-copper-gold (IOCG) deposits. The genesis and chronology of these deposits is intensely debated in the literature, especially regarding the source of the iron and geodynamic environment of mineralization, as well as the relative roles of magmatic and hydrothermal processes.

IOCG ores are, however, readily recognizable as a distinct group by the relative dominance of iron oxide minerals, with economic concentrations of Cu-(Fe)-sulphides, and commonly Au (e.g., Barton 2014; Skirrow 2022). Many IOCG ores also feature a marked enrichment in chalcophile-siderophile elements, including uranium and rare earth elements (REE). Broadly, genetic schemes for IOCG ore systems evolve from early Na ± Ca hydrothermal alteration,

followed by combinations of Fe-, Ca- and K-rich minerals that precede or accompany mineralization (e.g., Corriveau et al. 2016; Kontonikas-Charos et al. 2017; Verdugo-Ihl et al. 2020a).

The protracted history of the Carajás Domain begins in the Mesoarchean (3 to ~2.83 Ga) recorded in basement lithologies, which includes greenstone belts and tonalitic-tronhjemitic high-grade gneisses and migmatites of the Xingu Complex (e.g., Tavares et al. 2018; Costa et al. 2020). Following this, Neoarchean volcano-sedimentary sequences (2.76–2.73 Ga; e.g., Machado et al. 1991, Martins et al. 2017) form the Itacaiúnas Supergroup. This supergroup comprises many divisions, among which lithologies of the Grão Para Group host the Jatobá deposit. Completing the Neoarchean igneous activity in the Carajás Domain are bimodal intrusions comprising: (i) mafic-ultramafic rocks of the Serra do Puma and Luanga Complexes (2763±6 Ma; e.g., Machado et al. 1991) and its equivalents; and (ii) syn-tectonic/A-type granites of the Estrela Granite and equivalents (Tavares et al. 2018). Lastly finalising the geological history are Paleoproterozoic siliciclastic units of the Águas Claras Formation (e.g., Araújo and Nogueira 2020) and anorogenic ~1.8 Ga A-type granites (e.g., Teixeira et al. 2018, 2019) related to the Transamazonian event y (e.g., 1880±2 Ma; Machado et al. 1991).

The Carajás Domain has a linear E-W-trending belt-like morphology (e.g., Costa et al. 2020) with a central sigmoidal domain outlined by two major shear zones, the Cinzento strike-slip system to the north, and the Canaã dos Carajás to the south. IOCG deposits are distributed along both these shear zones, clustering and defining the Northern and Southern Copper belts, respectively (Xavier et al. 2012). Ore mineralogy is, nevertheless, relatively consistent throughout all IOCG deposits with magnetite as the main Fe-oxide always closely associated with apatite. Chalcopyrite and/or bornite are the main expression of Cu-enrichment (Schutesky and de Oliveira 2020).

The current ore genesis model involves an initial stage of IOCG mineralisation ca. 40-80 Ma after deposition of the Itacaiúnas Supergroup at ca. 2.76 Ga (Trunfull et al. 2020) with episodic reactivation of the Cinzento Shear Zone ~ 2.5 Ga. A second IOCG event at 1.88 Ga is attributed to the waning stages of the Transamazonian Orogeny, albeit with uncertainty whether this is perhaps just a Cu-Au overprint/remobilisation from a pre-existing IOCG deposit. In an alternative 'roots to roof' model, encompassing deeper, ductile, and shallower, brittle domains, IOCG mineralization is considered to be sourced from magma-derived fluids driven along crustal shear zones (Schutesky and Oliviera 2020). The timing of IOCG mineralization is considered to be between 2.76 and 2.73 Ga, coeval with bimodal magmatism in the Itacaiúnas Supergroup. Recently, Toledo et al. (2024) questioned the temporal link between granitic magmatism and IOCG deposits in the Carajás Domain.

The new geological model advocating a multi-stage evolution for Ni-rich IOCG ores at Jatobá acknowledges the significant role played by deep shear zones. This model is supported by a range of observations and, intriguingly, links the northern and southern copper belts, thus significantly advancing our understanding of this world-class metallogenic province as a whole (Campo-Rodriguez et al., Mineral Mag - *in review*, Precambr Res - *in review*).

Measurable concentrations of palladium (Pd) and platinum (Pt) in pyrite from Jatobá and the recognition of several discrete platinum group minerals (PGM) restricted to fractures and grain boundaries support initial mineralization of disseminated or semi-massive Ni-PGE-bearing sulphides, possibly in a VHMS-like setting during deposition of the Itacaiúnas Supergroup (Campo-Rodriguez et al., 2024a, 2024b). At the same time, the formation of magnetite and apatite as accessory minerals is supported by the preservation of trellis magnetite with nano-thermobarometry data (728 °C), and the 'mafic' Cl-rich signature retained by apatite (Campo-Rodriguez et al., Mineral Mag - *in review*, Precambr Res - *in review*). Trellis magnetite is also reported from the Salobo IOGC deposit in the northern copper belt of the Carajás Domain

(Campo-Rodriguez et al. 2022). However, emphasising the critical importance of local geological setting, such magnetite is not found in other deposits, such as Onca Rosa, Jaguar orefield (Campo-Rodriguez et al., Can. J. Mineral. Petrol, in review). This small orebody is not hosted by volcanic sequences of the Itacaiúnas Supergroup but occurs at ultramafic/granitic contacts providing a fertile environment for development of skarn.

A PGE signature is also documented in the context of a Fe-Zn-Ni skarn system at Onça Rosa, which was formed by intense alteration of an ultramafic protolith belonging to the Serra do Puma layered complex at its contact with a younger syn-kinematic granite (Campo-Rodriguez et al., Can. J. Mineral. Petrol - *in review*). The PGE signature is associated with Bi-tellurides and sulphosalts indicative of granite-derived hydrothermal fluids interacting with Ni-PGE-phases (Campo-Rodriguez et al., Amer Min - *in review*).

Magnetite is a mineral widely respected as a valuable source of evidence for overprinting events in terranes with protracted geological histories, given the proven ability to preserve inherited geochemical and textural signatures. Remarkably, a common feature of world-class IOCG deposits (e.g., Olympic Cu-Au Province, Ciobanu et al. 2022) is the preservation of amphibole inclusions in magnetite with intergrowths of non-classical pyriboles (NCP). At Jatobá, magnetite cores are host to some of the most spectacular polysomatic intergrowths between amphiboles and NCP ever reported, featuring chain-width disorder indicative of syn-metamorphic deformation (Campo-Rodriguez et al. 2024a). Simpler and less disordered NCPs are observed at Onça Rosa (Campo-Rodriguez et al., Can. J. Mineral. Petrol - *in review*). In both deposits, IOCG-style mineralization is superimposed onto a pre-existing Ni-bearing sulphide assemblage, mainly pyrrhotite in Jatobá and pentlandite in Onça Rosa (Campo-Rodriguez et al., Amer Min - *in review*).

The onset of the IOCG system at Jatobá is marked by silicate (amphibole) formation resulting in partial dissolution, replacement, remobilization, and overprinting textures. Critically, the

presence of ferrotschermakite is indicative of formation under pressures of ~7.5 kbar during shearing and probably coincidental with main ore deposition at temperatures of 728 – 414 °C (ilmenite-magnetite nano-thermobarometry; Campo-Rodriguez et al. 2024a). A distinct pre-mineralization geochemical signature (Ti, Cr, Co, and Mn) in the cores of magnetite grains transitions to a marked enrichment in REE and other lithophile elements during a deep amphibolite facies shear event. Lu-Hf apatite geochronology yields an age of ~2.5 Ga for this event (Campo-Rodriguez et al., Mineral Mag - *in review*, Precambr Res - *in review*). Intriguingly, this coincides with the reported U-Pb monazite age for the Salobo deposit in the northern copper belt (Melo et al. 2017). At this stage, amphiboles, apatite and even magnetite are conspicuous by their REY contents. PGE were likely released from common sulphides during the retrograde stage of a syn-metamorphic deformational event, subsequently combining with components of the IOCG fluids, like Sb, Bi, and Te to form a distinct suite of accessory ore minerals (Campo-Rodriguez et al. 2024b, Amer Min - *in review*).

Collectively, a number of new interpretations using traditional and new techniques facilitate a geological model for the Carajás Domain in which regional-scale fault-and-shear systems played a major role in the control of mineralization. However, local geological setting is responsible for the mineralogical expression of a deposit.

8.3. Conclusões

O Domínio Neoarqueano de Carajás, localizado no centro-norte do Brasil, é uma das províncias metalogenéticas mais complexas do planeta, abrigando uma ampla variedade de depósitos minerais. Entre eles, e de significativa importância econômica, destacam-se os grandes depósitos de óxido de ferro-cobre-ouro (IOCG). A gênese e a cronologia desses depósitos são intensamente

debatidas na literatura, especialmente respeito à origem do ferro, ao ambiente geodinâmico da mineralização e a influência relativa dos processos magmáticos e hidrotermais.

No entanto, os minérios IOCG são reconhecíveis como um grupo distinto devido à predominância relativa de minerais de óxido de ferro, com concentrações econômicas de sulfetos de Cu-(Fe) e, frequentemente, de Au (por exemplo, Barton 2014; Skirrow 2022). Muitos minérios do tipo IOCG também apresentam um notável enriquecimento em elementos calcófilos-siderófilos, incluindo urânio e elementos das terras raras (ETR). De forma geral, os esquemas genéticos para sistemas de minério IOCG evoluem a partir de uma alteração hidrotermal inicial de Na ± Ca, seguida por combinações de minerais ricos em Fe, Ca e K que precedem ou acompanham a mineralização (por exemplo, Corriveau et al. 2016; Kontonikas-Charos et al. 2017; Verdugo-Ihl et al. 2020a).

A longa história geológica do Domínio Carajás começa no Mesoarqueano (3 a ~2,83 Ga), registrada em litologias do embasamento, que incluem cinturões de greenstone e gnaisses tonalíticos-trondhjemíticos de alto grau, além de migmatitos do Complexo Xingu (por exemplo, Tavares et al. 2018; Costa et al. 2020). Posteriormente, as sequências vulcano-sedimentares Neoarqueanas (2,76–2,73 Ga; por exemplo, Machado et al. 1991, Martins et al. 2017) formam o Supergrupo Itacaiúnas, composto por várias divisões, dentre as quais as litologias do Grupo Grão Pará hospedam o depósito de Jatobá.

Completando a atividade ígnea do Neoarqueano no Domínio Carajás, encontram-se as intrusões bimodais: (i) rochas máfico-ultramáficas dos Complexos Serra do Puma e Luanga (2763±6 Ma; por exemplo, Machado et al. 1991) e seus equivalentes; e (ii) granitos sin-tectônicos/de tipo A, como o Granito Estrela e seus equivalentes (Tavares et al. 2018). Por fim, encerrando a história, encontram-se as unidades siliciclásticas paleoproterozoicas da Formação Águas Claras (Araújo et al. 2020) e os granitos anorogênicos de tipo A (~1,8 Ga; por exemplo, Teixeira et al. 2018, 2019) relacionados ao evento Transamazônico (por exemplo, 1880±2 Ma; Machado et al. 1991).

O Domínio Carajás possui uma morfologia linear em forma de cinturão com orientação E-O (por exemplo, Costa et al. 2020), apresentando um domínio sigmoidal central delimitado por duas zonas de cisalhamento principais: o sistema transcorrente Cinzento ao norte e o Canaã dos Carajás ao sul. Os depósitos IOCG estão distribuídos ao longo dessas zonas de cisalhamento, formando agrupamentos que definem os cinturões de cobre do Norte e do Sul (Xavier et al. 2012). A mineralogia do minério é, no entanto, relativamente consistente em todos os depósitos IOCG, com a magnetita como o principal óxido de ferro, sempre estreitamente associada à apatita. Calcopirita e/ou bornita são as principais expressões do enriquecimento em Cu (Schutesky e de Oliveira 2020).

O modelo atual de gênese dos minérios envolve um estágio inicial de mineralização IOCG por volta de 40-80 Ma após a deposição do Supergrupo Itacaiúnas, em aproximadamente 2,76 Ga (Trunfull et al. 2020), com reativação episódica da Zona de Cisalhamento Cinzento em ~2,5 Ga. Um segundo evento IOCG em 1,88 Ga é atribuído aos estágios finais da Orogênese Transamazônica, embora haja incerteza se isso representa apenas uma sobreposição/remobilização de Cu-Au a partir de um depósito IOCG pré-existente. Em um modelo alternativo desde as "raízes ao topo", abrangendo domínios mais profundos, dúcteis, e mais rasos, frágeis, a mineralização IOCG é considerada derivada de fluidos magmáticos direcionados ao longo das zonas de cisalhamento crustal (Schutesky e Oliveira 2020). O momento da mineralização IOCG é considerado entre 2,76 e 2,73 Ga, coincidente com o magmatismo bimodal no Supergrupo Itacaiúnas. Recentemente, Toledo et al. (2024) questionaram a relação temporal entre o magmatismo granítico e os depósitos IOCG no Domínio Carajás.

O novo modelo geológico que defende uma evolução em múltiplos estágios para os minérios IOCG ricos em Ni em Jatobá reconhece o papel significativo desempenhado por zonas de cisalhamento profundas. Esse modelo é respaldado por uma série de observações e, de forma intrigante, conecta os cinturões de cobre do norte e do sul, avançando significativamente nossa

compreensão sobre essa província metalogênica de classe mundial como um todo (Campo-Rodriguez et al., Mineral Mag - em revisão, Precambr Res - em revisão).

Concentrações mensuráveis de paládio (Pd) e platina (Pt) em pirita de Jatobá e o reconhecimento de vários minerais discretos do grupo da platina (PGM) restritos a fraturas e limites de grãos suportam uma mineralização inicial de sulfetos disseminados ou semi-maciços contendo Ni-PGE, possivelmente em um ambiente do tipo VHMS durante a deposição do Supergrupo Itacaiúnas (Campo-Rodriguez et al., 2024a, 2024b). Simultaneamente, a formação de magnetita e apatita como minerais acessórios é sustentada pela preservação de magnetita em treliça com dados de nano-termobarometria (728 °C) e pela assinatura "máfica" rica em Cl retida pela apatita (Campo-Rodriguez et al., Mineral Mag - em revisão, Precambr Res - em revisão). A magnetita em treliça também é descrita no depósito IOCG Salobo, no cinturão de cobre do norte do Domínio Carajás (Campo-Rodriguez et al., 2022). No entanto, enfatizando a importância crítica do ambiente geológico local, tal magnetita não é encontrada em outros depósitos, como Onça Rosa, no campo mineral de Jaguar (Campo-Rodriguez et al., Can. J. Mineral. Petrol, em revisão). Esse pequeno corpo de minério não está hospedado em sequências vulcânicas do Supergrupo Itacaiúnas, mas ocorre em contatos ultramáficos/graníticos, proporcionando um ambiente fértil para o desenvolvimento de uma mineralização do tipo skarn.

Assinaturas de PGE também são documentadas no contexto do sistema skarn de Fe-Zn-Ni em Onça Rosa, formado por intensa alteração de um protólito ultramáfico pertencente ao Complexo Estratificado Serra do Puma, em seu contato com um granito sincinemático mais jovem (Campo-Rodriguez et al., Can. J. Mineral. Petrol - em revisão). A assinatura de PGE está associada a Bi-teluretos e sulfossais, indicativos de fluidos hidrotermais derivados de granitos interagindo com fases de Ni-PGE (Campo-Rodriguez et al., Amer Min - em revisão).

A magnetita é amplamente reconhecida como uma fonte valiosa de evidências para eventos de sobreposição em terrenos com histórias geológicas prolongadas, dada sua comprovada capacidade de preservar assinaturas geoquímicas e texturais herdadas. Notavelmente, uma

característica comum de depósitos IOCG de classe mundial (por exemplo, Província Cu-Au Olímpica, Ciobanu et al. 2022) é a preservação de inclusões de anfibólio em magnetita com intercrescimentos de piribólios não clássicos (NCP). Em Jatobá, os núcleos de magnetita hospedam alguns dos mais espetaculares intercrescimentos polisomáticos entre anfibólios e NCP já relatados, apresentando desordem na largura das cadeias quem indicam uma deformação sin-metamórfica (Campo-Rodriguez et al., 2024a). NCPs mais simples e menos desordenados são observados em Onça Rosa (Campo-Rodriguez et al., Can. J. Mineral. Petrol - em revisão). Em ambos os depósitos, a mineralização no estilo IOCG está sobreposta a uma assembleia pré-existente de sulfetos contendo Ni, principalmente pirrotita em Jatobá e pentlandita em Onça Rosa (Campo-Rodriguez et al., Amer Min - em revisão).

O início do sistema IOCG em Jatobá é marcado pela formação de silicatos (anfibólios), resultando em dissolução parcial, substituição, remobilização e texturas de sobreposição. De maneira crucial, a presença de ferrotschermakita indica formação sob pressões de aproximadamente 7,5 kbar durante cisalhamento, provavelmente coincidente com a principal deposição de minério em temperaturas entre 728 e 414 °C (nanotermobarometria em ilmenita-magnetita; Campo-Rodriguez et al., 2024a). Uma assinatura geoquímica pré-mineralização distinta (Ti, Cr, Co e Mn) nos núcleos dos grãos de magnetita transita para um enriquecimento marcante em ETR e outros elementos litófilos durante um evento de cisalhamento em fácies anfibolito profundo. A geocronologia Lu-Hf em apatita fornece uma idade de ~2,5 Ga para este evento (Campo-Rodriguez et al., Mineral Mag - em revisão, Precambr Res - em revisão). Curiosamente, coincide com a idade U-Pb em monazita relatada para o depósito Salobo no cinturão de cobre norte (Melo et al., 2017).

Nesse estágio, anfibólios, apatita e até magnetita se destacam por seus conteúdos de ETR. Os PGE foram provavelmente liberados de sulfetos comuns durante a fase retrógrada de um evento deformacional sinmetamórfico, combinando-se posteriormente com componentes dos fluidos

IOCG, como Sb, Bi e Te, para formar um conjunto distinto de minerais acessórios de minério (Campo-Rodriguez et al., 2024b, Amer Min - em revisão).

Coletivamente, várias novas interpretações utilizando técnicas tradicionais e inovadoras facilitam um modelo geológico para o Domínio Carajás, no qual sistemas regionais de falhas e zonas de cisalhamento desempenharam um papel central no controle da mineralização. No entanto, o contexto geológico local é responsável pela expressão mineralógica de cada depósito.

8.4. References

Araújo Filho, R.C., Nogueira, A.C., and Araújo, R.N. (2020) New stratigraphic proposal of a Paleoproterozoic siliciclastic succession: Implications for the evolution of the Carajás Basin, Amazonian craton, Brazil. Journal of South American Earth Sciences 102, 102665. https://doi.org/10.1016/j.jsames.2020.102665

Barton, M. (2014) Iron oxide (–Cu–Au–REE–P–Ag–U–Co) systems. Treatise on Geochemistry, 2nd ed, vol 13. Elsevier, Amsterdam, p. 515-541. https://doi.org/10.1016/B978-0-08-095975-7.01123-2

Campo-Rodríguez, Y.T., Schutesky, M.E., de Oliveira, C.G., and Whitehouse, M.J. (2022) Unveiling the polyphasic evolution of the Neoarchean IOCG Salobo deposit, Carajás Mineral Province, Brazil: Insights from magnetite trace elements and sulfur isotopes. Ore Geology Reviews 140, 104572. https://doi.org/10.1016/j.oregeorev.2021.104572

Campo-Rodríguez, Y.T., Ciobanu, C.L., Slattery, A., Cook, N.J., Schutesky, M.E., Ehrig, K., King, S.A., and Yao, J. (2024a) Polysomatic intergrowths between amphiboles and non-classical pyriboles in magnetite: smallest-scale features recording a protracted geological history. American Mineralogist 109 (10), 1798–1818. https://doi.org/10.2138/am-2023-9188

Campo-Rodriguez, Y.T., Cook, N.J., Ciobanu, C.L., Schutesky, M.E., King, S.A., Gilbert, S., and Ehrig, K. (2024b) Platinum Group Minerals Associated with Nickel-Bearing Sulfides from the Jatobá Iron Oxide-Copper-Gold Deposit, Carajás Domain, Brazil. Minerals 14, 757. https://doi.org/10.3390/min14080757

Campo-Rodriguez, Y.T., Ciobanu, C.L., Cook, N.J., Schutesky, M.E., Ehrig, K., Slattery, A., Gilbert, S., and King, S.A. (*in review, a*) Telescoped transition from trellis to silicate mottled magnetite records deep shear zone metamorphism in the IOCG deposit at Jatobá, Carajás, Brazil. Mineralogical Magazine.

Campo Rodriguez, Y.T., Ciobanu, C.L., Gilbert, S., Wade, B., Cook, N.J., Schutesky, M.E., and Ehrig, K. (*in review, b*) Coupled Lu-Hf and U-Pb apatite geochronology of Jatobá orebody supports ~2.5 Ga metamorphism in deep shear zones from Southern Copper Belt, Carajás Domain, Brazil. Precambrian Research.

Campo Rodriguez, Y.T., Ciobanu, C.L., Cook, N.J., Schutesky, M.E., Ehrig, K., Slattery, A., Gilbert, S., and King, S.A. (*in review, c*) Magnetite and REE-rich calcic amphibole provide evidence for a skarn-IOCG system at Onça Rosa, Jaguar Orefield, Carajás Mineral Province, Brazil. The Canadian Journal of Mineralogy and Petrology.

Campo Rodriguez, Y.T., Ciobanu, C.L., Cook, N.J., Slattery, A., Wade, B., Gilbert, S., Schutesky, M.E., and Ehrig, K. (*in review, d*) Arsenohauchecornite, ognitite, parkerite, and related minerals from Onça

Rosa orebody, Carajás, Brazil: fingerprinting PGE signatures in hydrothermal Ni ores. American Mineralogist.

Ciobanu, C.L., Verdugo-Ihl, M.R., Cook, N.J., Ehrig, K., Slattery, A., and Courtney-Davis, L. (2022) Ferro-tschermakite with polysomatic chain-width disorder identified in silician magnetite from Wirrda Well, South Australia: A HAADF STEM study. American Mineralogist 107, 765-777. https://doi.org/10.2138/am-2022-7975

Corriveau, L., Montreuil, J-F., and Potter, E.G. (2016) Alteration facies linkages among iron oxide copper-gold, iron oxide-apatite, and affiliated deposits in the Great Bear Magmatic Zone, Northwest Territories, Canada. Economic Geology 111, 2045-2072. https://doi.org/10.2113/econgeo.111.8.2045

Courtney-Davies, L., Tapster, S.R., Ciobanu, C.L., Cook, N.J., Verdugo-Ihl, M.R., Ehrig, K.J., Kennedy, A.K., Gilbert, S.E., Condon, D.J., and Wade, B.P. (2019a) A multi-technique evaluation of hydrothermal hematite U-Pb isotope systematics: Implications for ore deposit geochronology. Chemical Geology 513, 54-72. https://doi.org/10.1016/j.chemgeo.2019.03.005

Costa, F.G., Santos, P.A., Serafim, I.C.C.O., Costa, I.S.L., and Roopnarain, S. (2020) From Mesoarchean drips to modern–style tectonics in the Carajás Province, Amazonian Craton. Journal of South American Earth Science 104, 102817. https://doi.org/10.1016/j.jsames.2020.102817

Groves, D.I., Bierlein, F.P., Meinert, L.D., and Hitzman, M.W. (2010) Iron Oxide Copper-Gold (IOCG) deposits through earth history: implications for origin, lithospheric setting, and distinction from other epigenetic iron oxide deposits: Economic Geology 105, p. 641–654. https://doi.org/10.2113/gsecongeo.105.3.641

Hitzman, M.W., Oreskes, N., and Einaudi, M.T. (2002). Geological characteristics and tectonic setting of Proterozoic iron oxide (Cu-U-Au-REE) deposits. Precambrian Research 58, 241-287. https://doi.org/10.1016/0301-9268(92)90121-4

Kontonikas-Charos, A., Ciobanu, C.L., Cook, N.J., Ehrig, K., Krneta, S., and Kamenetsky, V.S. (2017) Feldspar evolution in the Roxby Downs granite, host to Fe-oxide cu-au-(U) mineralisation at Olympic dam, South Australia. Ore Geology Reviews 80, 838-859. https://doi.org/10.1016/j.oregeorev.2016.08.019

Machado, N., Lindenmayer, Z, Krogh, T.E., and Lindenmayer, D. (1991) U-Pb geochronology of Archean magmatism and basement reactivation in the Carajás area, Amazon shield, Brazil. Precambrian Research 49, 329-354. https://doi.org/10.1016/0301-9268(91)90040-H

Martins, P.L.G, Toledo, C.L.B, Silva, A.M., Chemale, Jr.F., Santos J.O.S., and Assis, L.M. (2017) Neoarchean magmatism in the southeastern Amazonian Craton, Brazil: Petrography, geochemistry and tectonic significance of basalts from the Carajás Basin. Precambrian Research 302, 340-357. https://doi.org/10.1016/j.precamres.2017.10.013

Melo, G.H.C., Monteiro, L.V.S., Xavier, R.P., Moreto, C.P.N., Santiago, E.S.B., Dufrane, S.A., Aires, B., and Santos, A.F.F. (2017) Temporal evolution of the giant Salobo IOCG deposit, Carajás Province

(Brazil): constraints from paragenesis of hydrothermal alteration and U-Pb geochronology. Mineralium Deposita 52, 709-732. https://doi.org/10.1007/s00126-016-0693-5

Williams, P.J., Barton, M.D., Johnson, D.A., Fontbote, L., De Haller, A., Mark, G., Oliver, N.H.S., and Marshik, R. (2005) Iron Oxide Copper-Gold Deposits: Geology, Space-Time Distribution, and Possible Modes of Origin. Econ Geol 100th Anniv Vol, p. 371–405. https://doi.org/10.5382/AV100.13

Reid, A. (2019) The Olympic Cu-Au Province, Gawler Craton: a review of the lithospheric architecture, geodynamic setting, alteration systems, cover successions and prospectivity. Minerals 9, 371. https://doi.org/10.3390/min9060371

Schutesky, M.E., and de Oliveira, C.G. (2020) From the roots to the roof: An integrated model for the Neoarchean Carajás IOCG System, Brazil. Ore Geology Reviews 127, 103833. https://doi.org/10.1016/j.oregeorev.2020.103833

Skirrow, R.G. (2022) Iron oxide copper-gold (IOCG) deposits–A review (part 1): Settings, mineralogy, ore geochemistry and classification. Ore Geology Reviews 140, 104569. https://doi.org/10.1016/j.oregeorev.2021.104569

Tavares, F.M., Trouw, R.A.J, da Silva, C.M.G., Justo, A.P., and Oliveira, J.K.M. (2018) The multistage tectonic evolution of the northeastern Carajás Province, Amazonian Craton, Brazil: Revealing complex structural patterns. Journal of South American Earth Science 88, 238-252. https://doi.org/10.1016/j.jsames.2018.08.024

Teixeira, M.F.B, Dall'Agnol, R., Santos, J.O.S, de Oliveira, DC, Lamarão CN, and McNaughton, N.J. (2018) Crystallization ages of Paleoproterozoic A-type granites of Carajás province, Amazon craton: Constraints from U-Pb geochronology of zircon and titanite. Journal of South American Earth Science 88, 312-331. https://doi.org/10.1016/j.jsames.2018.08.020

Toledo, P.I.F., Moreto, C.P.N., Monteiro, L.V.S., Melo, G.H.C., Matos, F.M.V., Xavier, R.P., Carvalho, J.A., Filho, C.A.M., Navarro, M.S., and Lana, C.C. (2024) Breaking up the temporal link between granitic magmatism and iron oxide?copper-gold (IOCG) deposits in the Carajás Mineral Province, NW Brazil. Mineralium deposita 59, 601-625. https://doi.org/10.1007/s00126-023-01224-5

Trunfull, E.F., Hagemann, S.G., Xavier, R.P., and Moreto, C.P.N. (2020) Critical assessment of geochronological data from the Carajás Mineral Province, Brazil: Implications for metallogeny and tectonic evolution. Ore Geology Reviews 121, 103556. https://doi.org/10.1016/j.oregeorev.2020.103556

Verdugo-Ihl, M.R., Ciobanu, C.L., Cook, N.J., Ehrig, K., and Courtney-Davis, L. (2020a) Defining early stages of IOCG systems: evidence from iron oxides in the outer shell of the Olympic Dam deposit, South Australia. Mineralium Deposita 55, 429-452. https://doi.org/10.1007/s00126-019-00896-2

Xavier, R.P., Soares Monteiro, L.V., Moreto, C.P.N., Pestilho, A.L.S., Coelho de Melo, G.H., Delinardo da Silva, M.A., Aires, B., Ribeiro, C., and Freitas e Silva, F.H. (2012) The Iron Oxide Copper-Gold Systems of the Carajás Mineral Province, Brazil. In: Geology and Genesis of Major Copper Deposits

and Districts of the World: A Tribute to Richard H. Sillitoe (Hedenquist, J.W., Harris, M., Camus, F., eds.). Society of Economic Geologists 16.

CHAPTER 9

SUPPLEMENTARY AND ADDITIONAL MATERIAL

SUPPLEMENTARY MATERIAL A

FOR CHAPTER 2 – POLYSOMATIC INTERGROWTHS BETWEEN AMPHIBOLES AND NON-CLASSICAL PYRIBOLES IN MAGNETITE: SMALLEST-SCALE FEATURES RECORDING A PROTRACTED GEOLOGICAL HISTORY

APPENDIX A: GLOSSARY

APPENDIX B: ADDITIONAL FIGURES

APPENDIX C: TABLES AND EDS STEM RESULTS

APPENDIX A FOR CHAPTER 2

American Mineralogist: October 2024 Online Materials AM-24-109188
Campo Rodriguez et al.: Non-classical pyriboles in magnetite

GLOSSARY for terminology used in the "Defects" section

Bow defect: arcuate or shaped like a bow zipper termination. This can be either symmetrical or asymmetrical.

Chain derailment: a shift of a zipper sequence along the *b* direction.

***En-echelon* defects:** these describe an arrangement where a set of short linear features overlap or are staggered in a line that runs obliquely to the strike of the individual features.

Fault: planar fracture or discontinuity across the chain structures or at zipper terminations. Those faults that show displacement (relative movement of chain sequences one to another) are commonly along (210) cleavage planes in the amphibole/pyriboles, i.e., displacement along n/4<010>directions when projected on [001] zone axis. Depending upon the sense of movement of the chain sequences relative to the fault trajectory, normal and inverse faults can be defined by analogy with geological terminology. In a **normal fault**, the chain sequence above the planar fault has moved downward relative to the chain sequence below. This type of faulting occurs in response to extension. A **reverse fault** is the opposite, the upper chain sequence, above the fault plane, moves up and over the lower chain sequence. This type of faulting is common in areas of compression.

Hairpin structures: a zipper showing a U-shaped structure within a given chain silicate.

Jogs: short or limited changes in direction marked by direct contact between the two arrays of 'A' cavities at a zipper termination or along a derailment. The double A cavities, either empty or not fully occupied, create spaces or channels for further fluid-mineral reactions. Also used in association with the geological term 'dilational jogs' that occur as space filling in the bend of a fault that undergoes sudden movements.

Oblique defects: defects marked by an array of 'A' cavities at a low angle (oblique) to the chain sequence in the pyribole-amphibole matrix. These differ from a fault in that, although it shifts some chains, it does not show a displacement of a well-defined chain sequence.

Pull-apart swells defects: bends or steps in a chain sequence that shows extension on one side of a zipper relative to the other side.

APPENDIX B FOR CHAPTER 2

American Mineralogist: October 2024 Online Materials AM-24-109188
Campo Rodriguez et al.: Non-classical pyriboles in magnetite

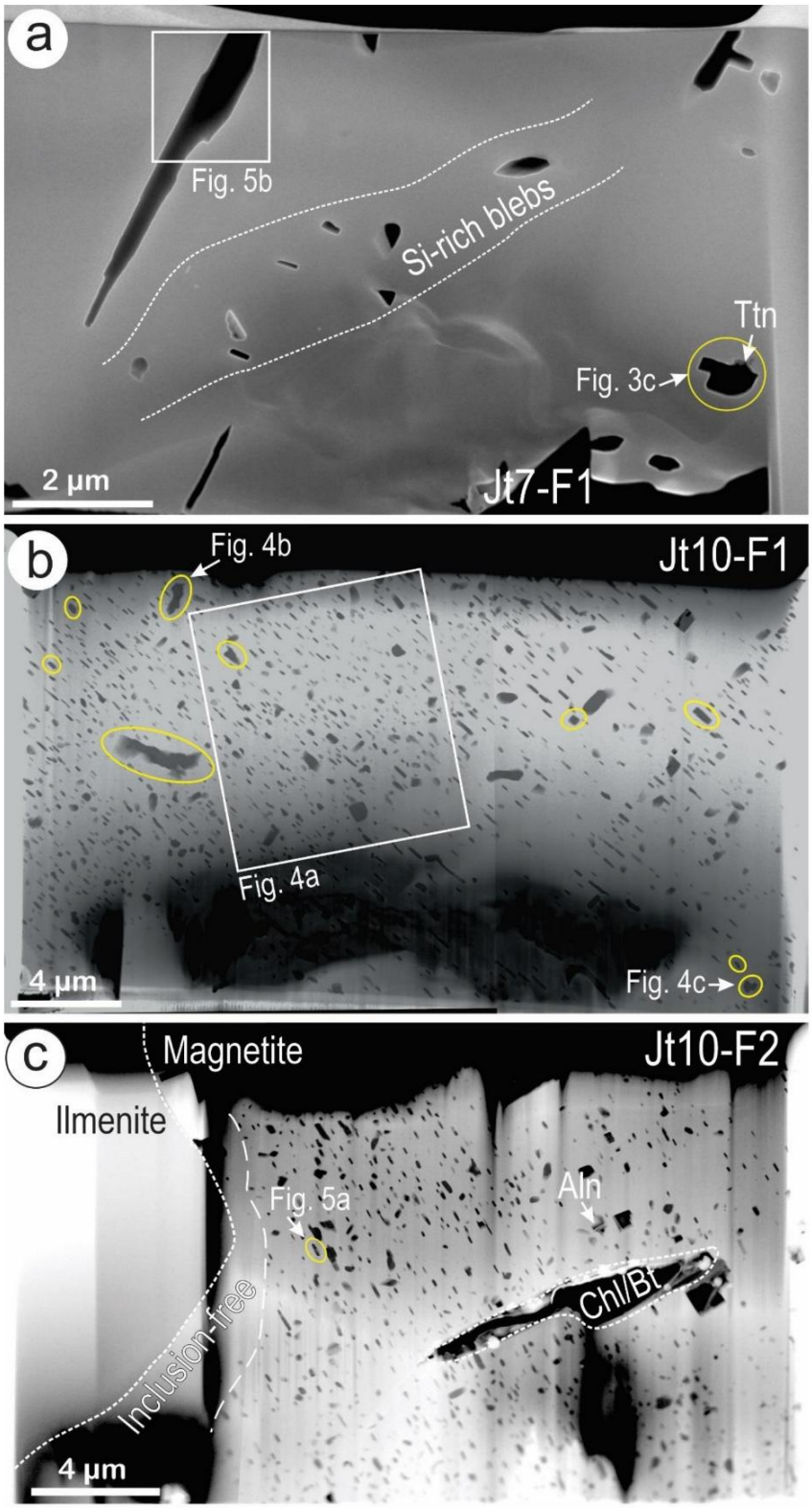

Figure A1. Overview of the three studied TEM foils, as labelled and relationship to figures in the main paper. See main text for further explanations. Aln–allanite, Bt–biotite, Chl–chlorite, Ttn–titanite.

American Mineralogist: October 2024 Online Materials AM-24-109188
Campo Rodriguez et al.: Non-classical pyriboles in magnetite

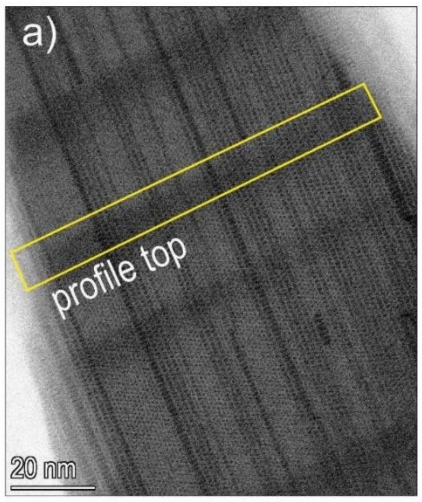

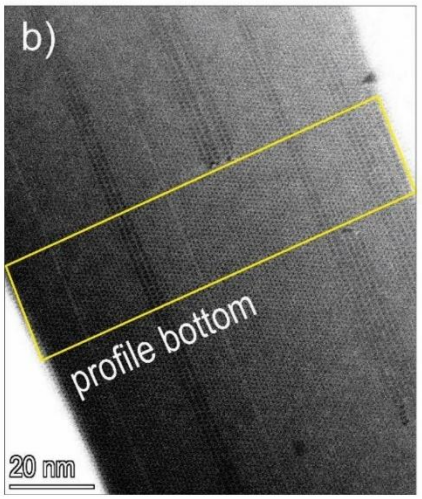

$A'(i)$= sum of I_{beam} structures of index i, where i=1, 2,...n) counted across a profile through a crystal:

$A'(i)$= $n_i.i$ / Σ ($n_i.i$); n_i = number of I_{beam} structures (eq. 1; Ahn et al. 1991)

$$\frac{Ca}{Mg} = \frac{2}{\sum_{1}^{i_{max}} A'(i)(3i-1)}$$ (eq. 2; Bozhilov et al. 2007)

$$\frac{^{B}Me}{^{C}Me} = \frac{2}{\sum_{1}^{i_{max}} A'(i)(3i-1)}$$ (eq. 2a)

Top

i	$n(i)$	$A(i)$
1	2	0.0092
2	93	0.8532
3	10	0.1376

$\sum_{1}^{i_{max}} A'(i)(3i-1)$ = 5.3853

Bottom

i	$n(i)$	$A(i)$
2	40	0.4960
3	31	0.3631
4	3	0.0556

$\sum_{1}^{i_{max}} A'(i)(3i-1)$ = 6.8973

analyses 10 (Tables 1 and 2)

Top		Bottom	
Si	7.94	Si	7.16
Al	0.06	Al	0.84
T	**8.0**	**T**	**8.0**
Ce	0.01	Al	0.64
Fe^{3+}	0.99	Ce	0.36
Fe^{2+}	1.35	Fe^{3+}	0.53
Mn	0.03	Fe^{2+}	1.11
Mg	2.62	Mg	2.36
C	**5.0**	**C**	**5.0**
Mg	1.16	Mg	0.01
Ca	0.37	Ca	1.66
B	**1.53**	**B**	**1.67**

calculated $^{B}Me/^{C}Me$ (using eq. 2a)
profile top: 0.37 **profile bottom: 0.289**

measured $^{B}Me/^{C}Me$ (EDS STEM data)
profile top: 0.31 **profile bottom: 0.33**

Figure A2. Assessment of the effect introduced by the presence of chain width disorder in amphiboles of composition given as analyses #10-top and -bottom (Tables 1 and 2 Online Materials). The number of I_{beam} structures $n(i)$ was counted across the profiles in (a) and (b). Calculation of $A'(i)$ values was performed using equation (1) from Ahn et al. (1991). The presence of I_{beam} units with chain multiplicity i different from i=2 corresponding to the host amphibole affects the ratio between cations (Me) in B and C sites from ideal 2/5=0.4. Bozhilov et al. (2007) observed that $^{B}Me/^{C}Me$ ratio is smaller in synthetically produced crystals of tremolite. Knowing that B and C cations are Ca and Mg in tremolite, the authors accordingly introduced equation (2) to calculate the Ca/Mg ratios from stack sequences of calculated $A'(i)$ values. These values were compared with EDS analysis obtained from analytical electron microscopy data showing a good match. As the amphiboles analysed here comprise other cations in both B and C sites, we use equation (2a) instead. We assess the two amphiboles which have $^{B}Me/^{C}Me$ measured ratios smaller than 0.4 (0.31 and 0.33 for profile a and b respectively) and show the calculated values using eq. (2a) as 0.37 and 0.289 giving differences of 0.06 and 0.04. This shows the EDS STEM data is reliable.

Ahn, J.H., Cho, M., Jenkins, D.M., Buseck, P.R. (1991) Structural defects in synthetic tremolite amphiboles. American Mineralogist 76, 1811–1823.

Bozhilov, K.N., Brownstein, D., and Jenkins, D.M. (2007) Biopyribole evolution during tremolite synthesis from dolomite and quartz in CO_2-H_2O fluid. American Mineralogist 92, 898–908.

American Mineralogist: October 2024 Online Materials AM-24-109188
Campo Rodriguez et al.: Non-classical pyriboles in magnetite

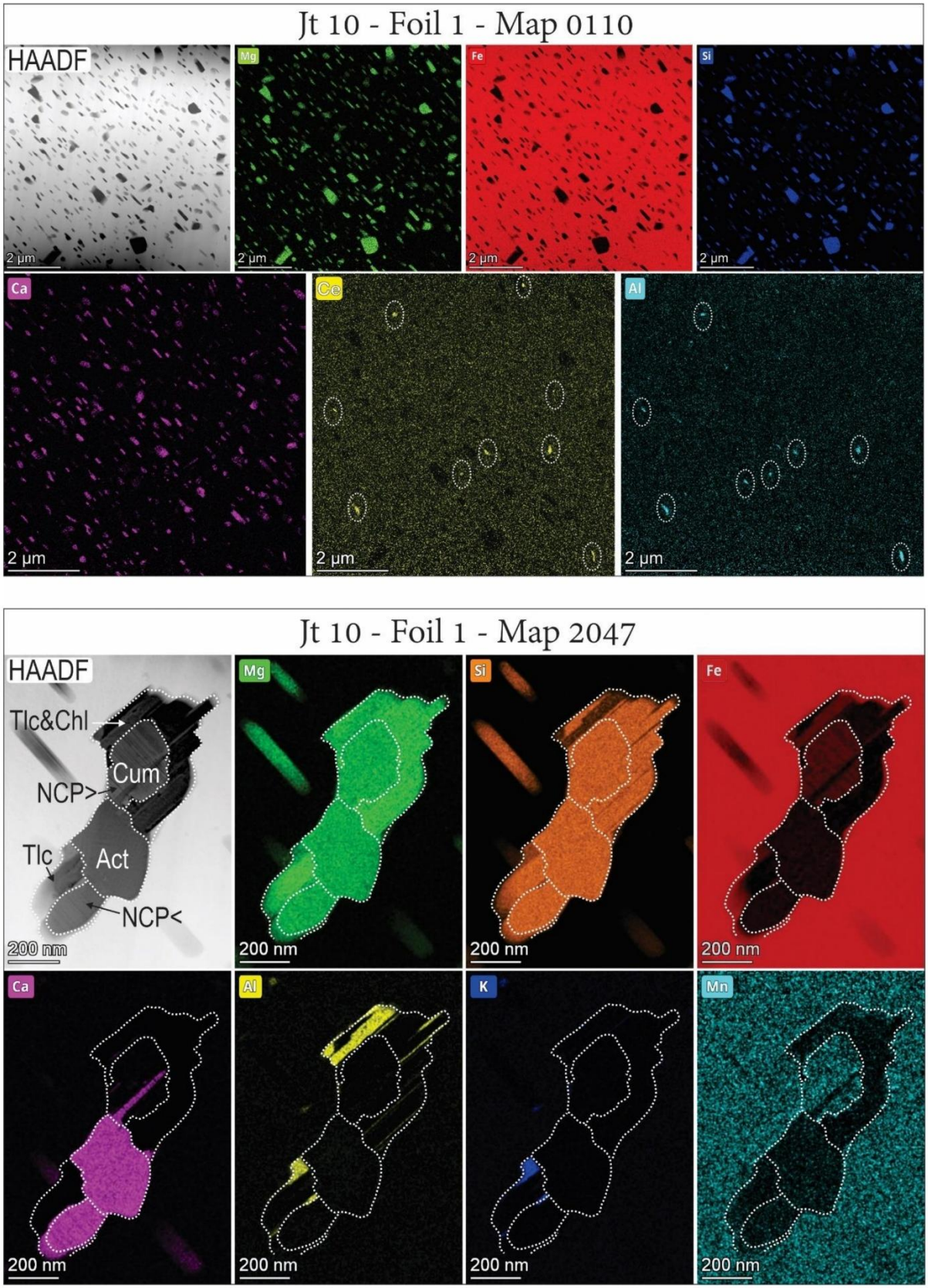

Figure A3. EDS STEM illustrating compositional variation, intergrowths, and zonation patterns among amphiboles, as labelled. See main text for further explanations. Act–actnolite, Chl–chlorite, Cum–cummingtonite, Tlc–talc.

American Mineralogist: October 2024 Online Materials AM-24-109188
Campo Rodriguez et al.: Non-classical pyriboles in magnetite

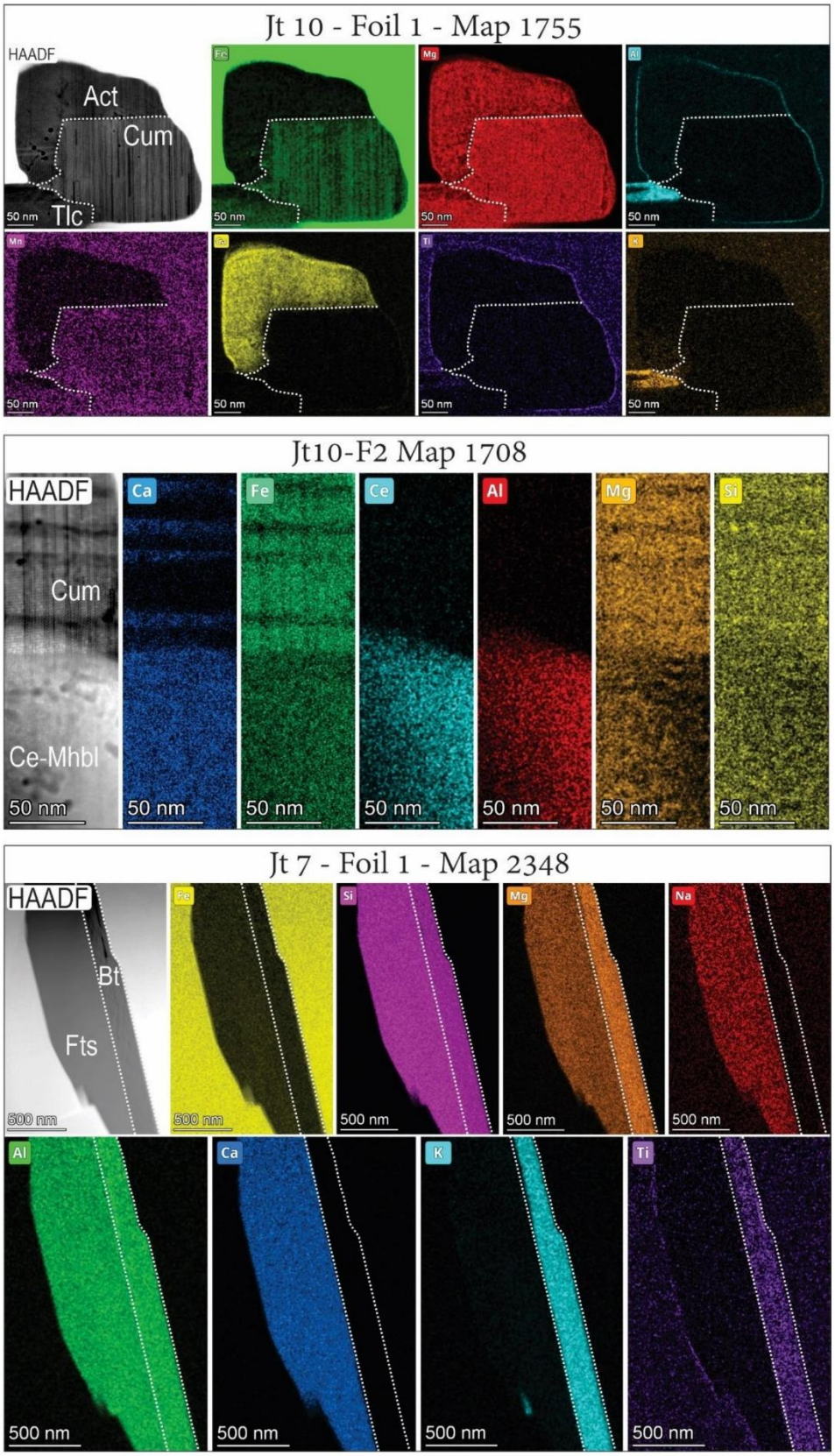

Figure A4. EDS STEM illustrating compositional variation, intergrowths, and zonation patterns among amphiboles, as labelled. See main text for further explanations. Act–actinolite, Bt–biotite, Ce-Mhbl–Ce-bearing magnesian hornblende, Chl–chlorite, Cum–cummingtonite, Fts–ferrotschermakite.

American Mineralogist: October 2024 Online Materials AM-24-109188
Campo Rodriguez et al.: Non-classical pyriboles in magnetite

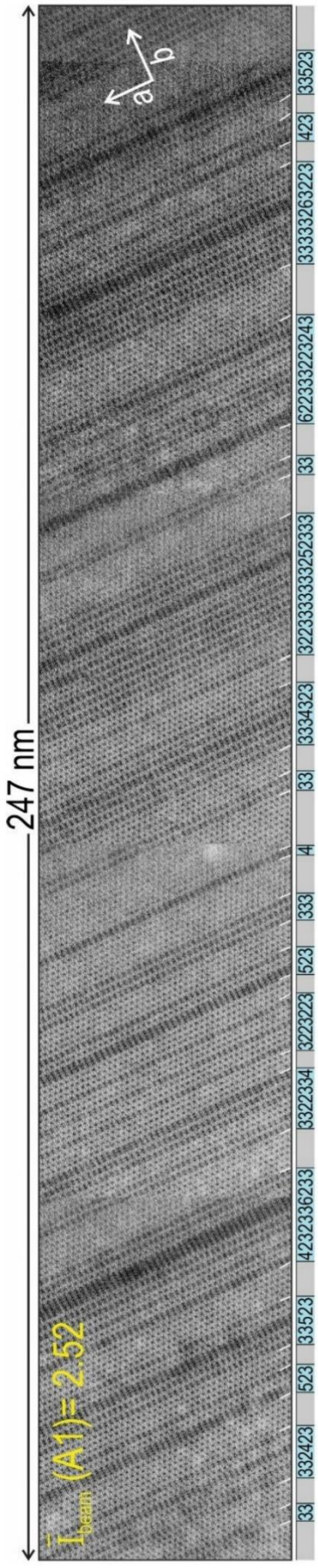

Figure A5. Assessment of polysomatic intergrowths over a longer length interval of ~250 nm. See main text for further explanations.

American Mineralogist: October 2024 Online Materials AM-24-109188
Campo Rodriguez et al.: Non-classical pyriboles in magnetite

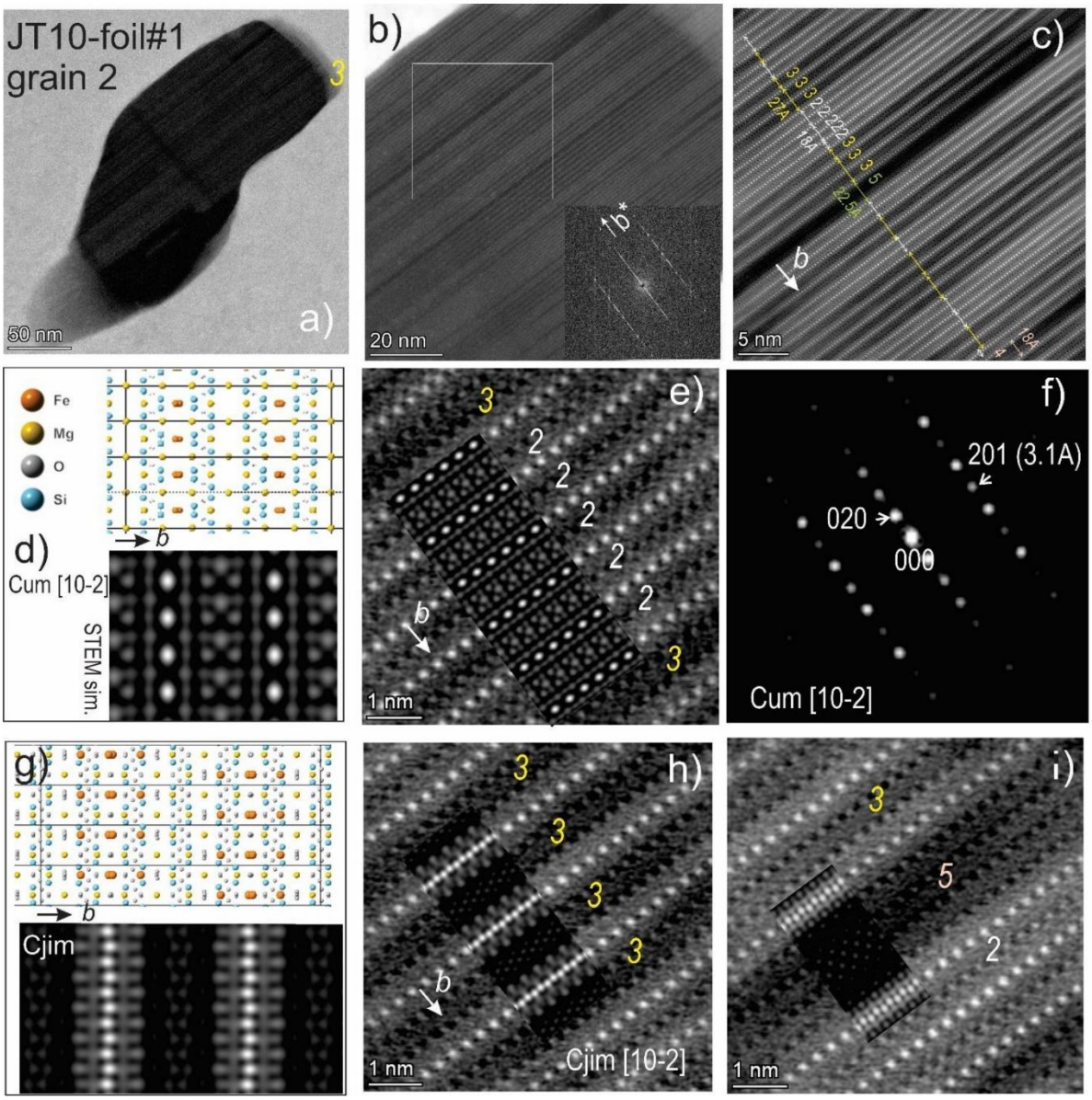

Figure A6. HAADF STEM images (a-c; e, h, i), crystal structure models and simulations (d, g) and fast Fourier transform (FFT) pattern (f) for cummingtonite (Cum) and clinojimthompsonite (Cjim) tilted on [10-2] zone axis. FFT pattern for the image in (b) shown as inset. Image in (c) marked by white rectangle in (b). STEM simulations of I_{beams} 2, 3 and 5 as overlays on (e, h and i). The width of I_{beam} structures along the *b* axis is marked on (c). Note the STEM simulation match with the crystal structures and images for NCPs corresponding to I_{beams} as considered.

American Mineralogist: October 2024 Online Materials AM-24-109188
Campo Rodriguez et al.: Non-classical pyriboles in magnetite

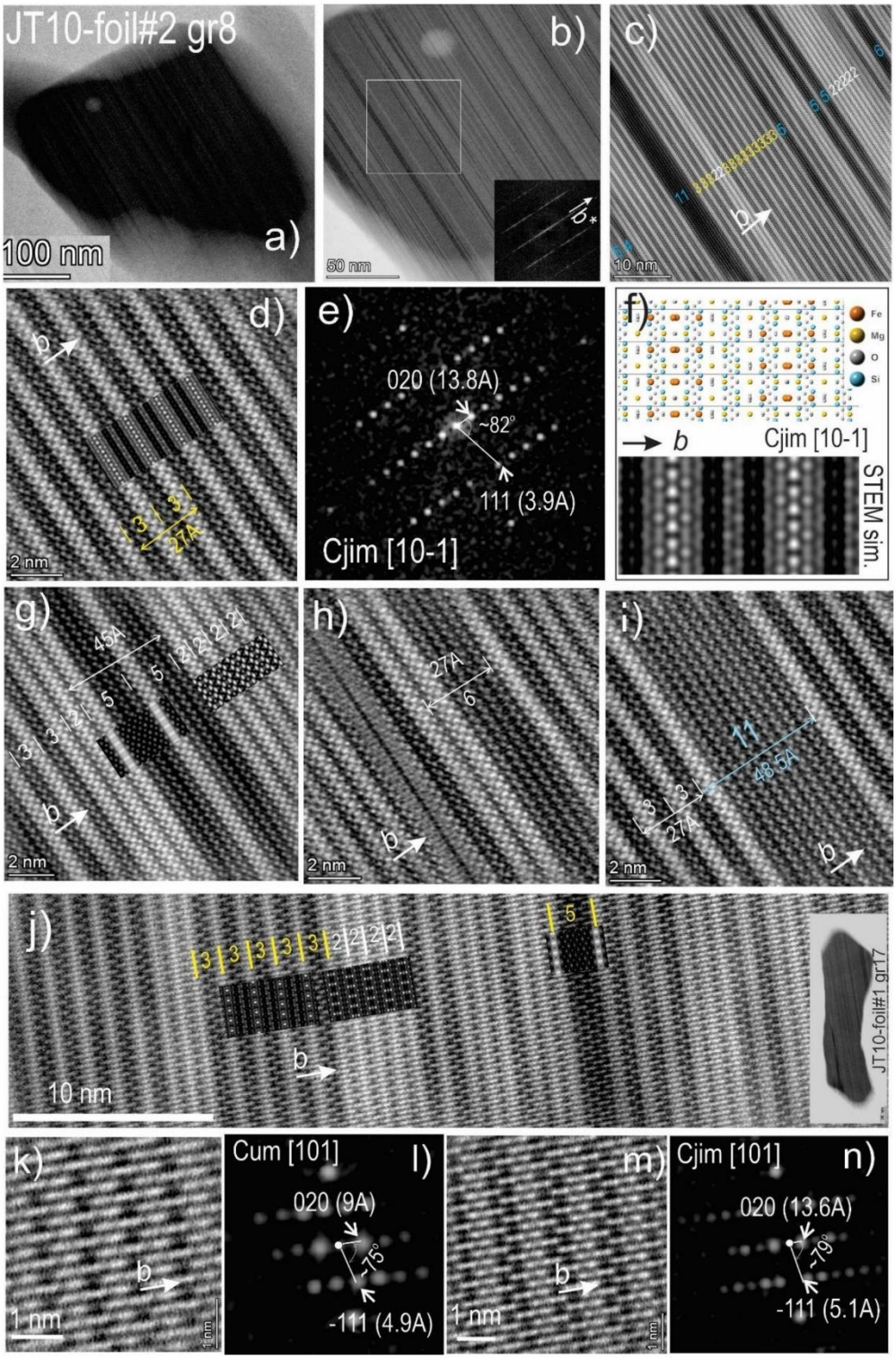

Figure A7. HAADF STEM images (a-d; g-i) crystal structure model and simulation (f) and fast Fourier transform (FFT) pattern (e) for clinojimthompsonite (Cjim) tilted on [10-1] zone axis. FFT pattern for the image in (b) shown as inset. Image in (c) marked by white rectangle in (b). Other I_{beams}, i=2, 4, 5, 6 and 11, encountered along the transect in (c) are also shown on crops in (g-i). STEM simulations for 2 I_{beam} (cummingtonite) and $5I_{beam}$ are shown as overlays on image in (g). (j) Profile showing a sequence of dominantly 2- and 3-I_{beams} and tilted on [101] zone axis. Also note the presence of a single 5-I_{beam} along the profile. STEM simulations as overlays. (k-n) Crops of ordered Cum and Cjim sequences and corresponding FFT patterns as labelled.

American Mineralogist: October 2024 Online Materials AM-24-109188
Campo Rodriguez et al.: Non-classical pyriboles in magnetite

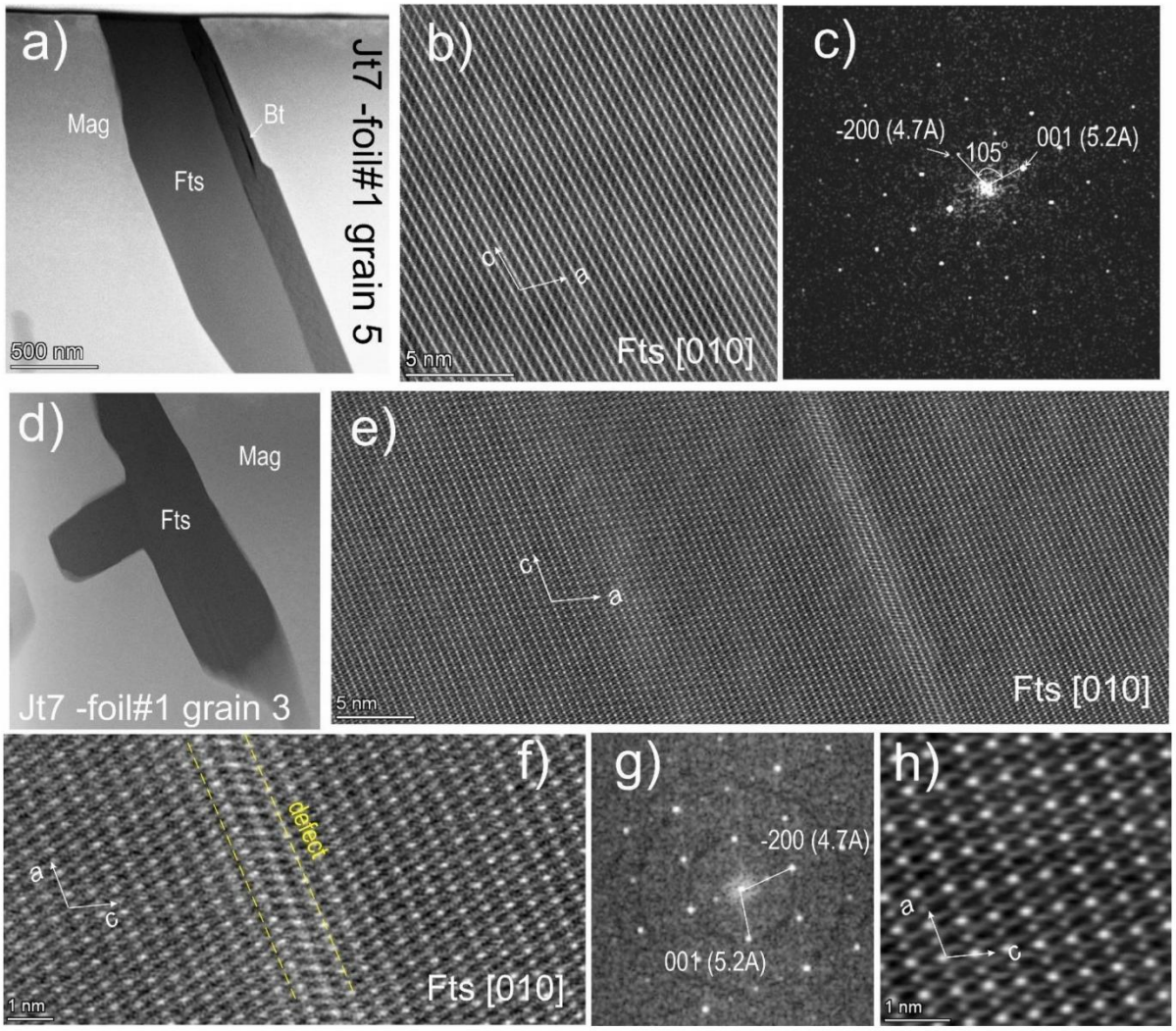

Figure A8. HAADF STEM images (a-c; d-f; h) and fast Fourier transform (FFT) patterns (c, g) for ferrotschermakite (Fts) grains tilted on [010] zone axis. The images show these grains are free of chain width disorder. Narrow dislocations occurring as defects (in f) are also marked by changes in the intensity of the HAADF signal in (e). Bt–biotite; Mag–magnetite.

American Mineralogist: October 2024 Online Materials AM-24-109188
Campo Rodriguez et al.: Non-classical pyriboles in magnetite

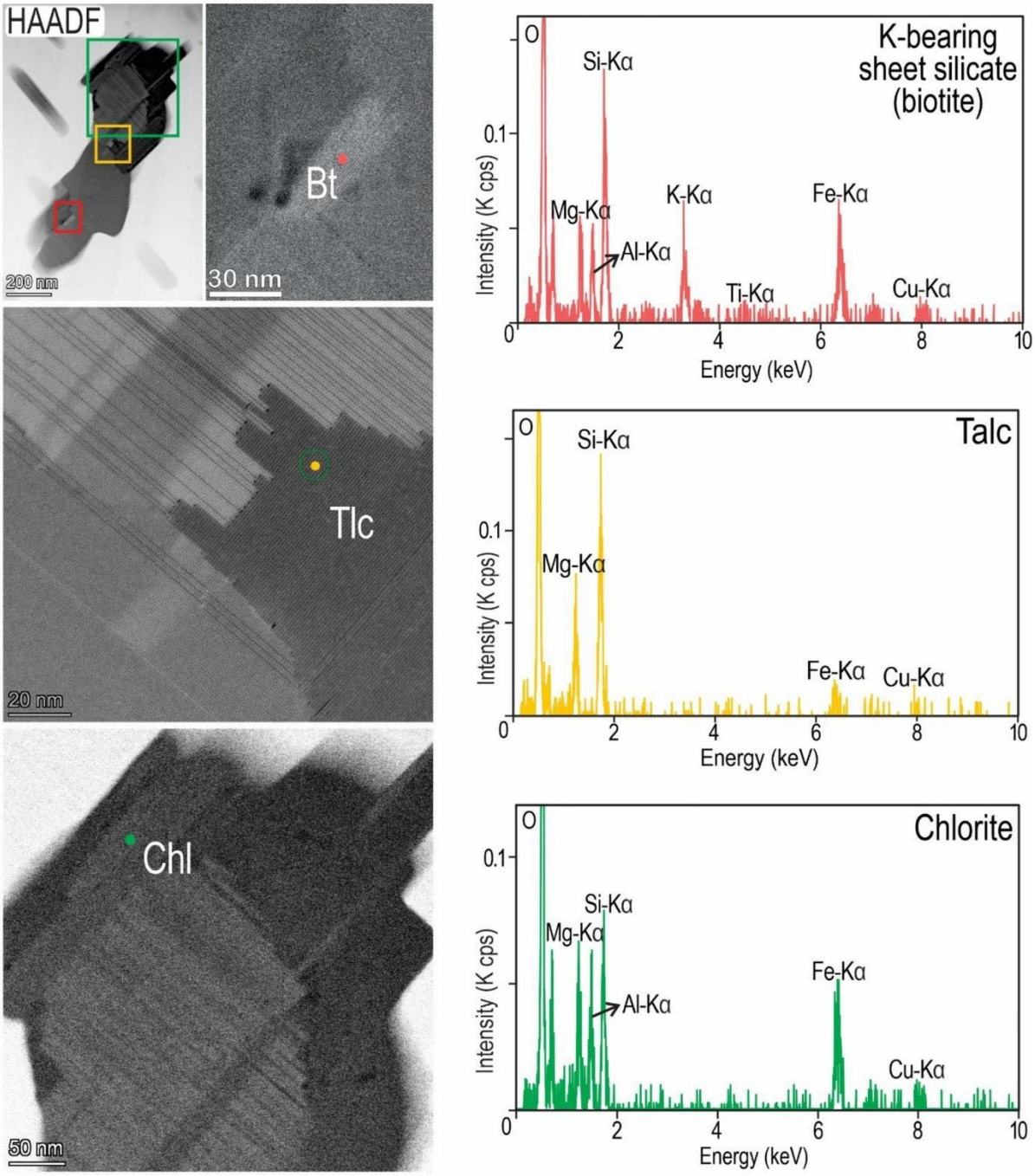

Figure A9. Images and integrated EDS spectra for biotite (Bt), talc (Tlc) and chlorite (Chl). See main text for further explanation.

APPENDIX C FOR CHAPTER 2

OM Table 1. Composition of calcic amphiboles

American Mineralogist: October 2024 Online Materials AM-24-109188 (use tabs to navigate to other tables)
Campo Rodriguez et al.: Non-classical pyriboles in magnetite
Online Materials Table 1. Compositions of calcic amphiboles from this study (EDS STEM data) and literature (EPMA) as labelled

	Actinolite (very little chain disorder if any)												Magnesiohornb.		Ferrotschermakite	
									Veloso et al. (2020)				Ce-bearing			
	aggregate number			grain	mean				mean				aggreg. 1	grain	grain number	
wt%	(2)	(3)	(4)	(9)	**n=4**	STDEV	MIN	MAX	**n=10**	STDEV	MIN	MAX	(1)	10-bottom	(7)	(8)
SiO_2	57.94	57.30	56.48	54.01	**56.43**	1.72	54.01	57.94	**52.96**	1.25	50.28	54.02	51.11	49.11	42.58	41.54
TiO_2	0	0	0	0	**0**	0	0	0	**0.16**	0.08	0	0.28	0	0	0	0.28
Al_2O_3	0.54	0.88	0.34	2.49	**1.06**	0.98	0.34	2.49	**2.80**	1.07	1.93	4.77	2.83	8.64	14.90	13.52
Fe_2O_3	2.14	3.49	0.31	3.82	**2.44**	1.60	0.31	3.82	**0**	0	0	0	1.47	4.79	4.41	7.77
FeO	8.44	7.04	11.12	10.24	**9.21**	1.82	7.04	11.12	**12.28**	0.89	11.39	13.89	14.08	9.09	15.46	15.12
MnO	0	0	0.14	0.13	**0.07**	0.08	0	0.14	**0.09**	0.01	0.07	0.11	0	0	0	0
MgO	18.68	18.40	17.49	17.44	**18.00**	0.63	17.44	18.68	**16.01**	0.81	14.59	16.78	16.85	10.90	8.03	8.73
CaO	11.75	12.50	13.45	11.57	**12.32**	0.86	11.57	13.45	**12.07**	0.45	10.91	12.59	13.16	10.63	12.41	12.19
Na_2O	0	0	0	0	0	0	0	0	**0.24**	0.09	0.16	0.42	0	0	1.24	0.62
K_2O	0	0	0	0	0	0	0	0	**0.25**	0.33	0	1.09	0	0	0.88	0.48
Ce_2O_3	0	0	0	0	0	0	0	0	**0**	0	0	0	0	6.69	0	0
Total	99.48	99.62	99.31	99.70	**99.53**	0.17	99.31	99.70	**97.42**	0.61	96.45	98.60	99.50	99.86	99.90	100.3
	Formula calculation (apfu cation basis)															
	15	15	15	15									15	15	15	16
^{T}Si	7.99	7.90	7.93	7.58	**7.85**	0.18	7.58	7.99	**7.65**	0.13	7.41	7.76	7.35	7.16	6.28	6.45
^{T}Al	0.01	0.10	0.06	0.41	**0.14**	0.18	0.01	0.41	**0.19**	0.20	0.00	0.59	0.48	0.84	1.72	1.55
T total	8.00	8.00	7.99	8.00	**8.00**	0.01	7.99	8.00	**8.00**	0	8.00	8.00	7.83	8.00	8.00	8.00
^{C}Al	0.08	0.04	0	0	**0.03**	0.04	0	0.08	**0.13**	0.06	0.07	0.24	0	0.64	0.87	0.92
^{C}Ti	0	0	0	0	**0**	0	0	0	**0.02**	0.01	0.00	0.03	0	0	0	0.03
^{C}Ce	0	0	0	0	**0**	0	0	0	**0**	0	0	0	0	0.36	0	0
$^{C}Fe^{3+}$	0.22	0.36	0.03	0.40	**0.26**	0.17	0.03	0.40	**0.13**	0.04	0.08	0.23	0.16	0.53	0.49	0.91
$^{C}Fe^{2+}$	0.97	0.81	1.31	1.20	**1.07**	0.22	0.81	1.31	**1.27**	0.08	1	1.40	1.69	1.11	1.91	1.96
^{C}Mn	0	0	0.02	0.02	**0.01**	0.01	0.00	0.02	**0.01**	0	0.01	0.01	0	0.00	0.00	0
^{C}Mg	3.72	3.78	3.66	3.38	**3.64**	0.18	3.38	3.78	**3.45**	0.15	3.15	3.59	3.15	2.36	1.73	1.18
C total	5.00	5.00	5.01	5.00	**5.00**	0.01	5.00	5.01	**5.00**	0	5.00	5.00	5.00	5.00	5.00	5.00
^{B}Mg	0.12	0	0	0.27	**0.10**	0.13	0.00	0.27	**0.02**	0	0	0	0.47	0.01	0.04	0.84
^{B}Ca	1.74	1.85	2.00	1.73	**1.83**	0.13	1.73	2.00	**1.87**	0.06	1.72	1.97	1.53	1.66	1.96	1.16
B total	1.85	1.85	2.00	2.00	**1.93**	0.09	1.85	2.00	**2.00**	0	2.00	2.00	2.00	1.67	2.00	2.00
^{A}Ca	0	0	0.03	0.01	**0.01**	0.01	0	0.03	**0.04**	0.01	0.02	0.06	0.50	0	0	0.87
^{A}Na	0	0	0	0	**0.00**	0	0	0	**0.04**	0.01	0.02	0.06	0	0	0.354	0.19
^{A}K	0	0	0	0	**0.00**	0	0	0	**0.05**	0.06	0.01	0.21	0	0	0.17	0.10
A total	0	0	0.03	0.01	**0.01**	0.01	0	0.03	**0**	0	0	0	0.50	0	0.52	1.15
SUM cations	14.85	14.85	15.03	15.01	**14.93**	0.10	14.83	15.04	**15.07**	0.10	15.01	15.40	15.33	14.67	15.52	16.15
B/C	0.37	0.37	0.40	0.40	**0.38**				**0.40**				0.40	0.33	0.40	0.40

Notes: Analyses 1-4 correspond to aggregates in Fig. 2a; 5- 6 were obtained from small grains as marked in Fig. 4a. Analyses 7-9 from various maps e.g. map Fig. 4a. Number 10 relates to the Ce-bearing amphibole. Top and bottom refer to their position on Fig. 5a.
All values were noramlized on a volatile free basis. Measurement error within +20%

OM Table 2. Composition of Mg-(Fe)-amphiboles

American Mineralogist: October 2024 Online Materials AM-24-109188 (use tabs to navigate to other tables)
Campo Rodriguez et al.: Non-classical pyriboles in magnetite
Online Materials Table 2. Compositions of Mg-(Fe)-amphiboles from this study (EDS STEM)

	Cummingtonite									Cummingtonite								Cummingtonite								
	aggregate number				gr. num	mean				selected areas from aggregate				mean				grain	grain number				mean			
	(1i)	(2i)	(3i)	(4i)	(5)	n=5	STDEV	MIN	MAX	(1ii)	(2ii)	(3ii)	(4ii)	n=4	STDEV	MIN	MAX	10-Top	(6.2)	(6.4)	(6.1)	(6.3)	n=4	STDEV	MIN	MAX
SiO_2	54.79	56.57	57.38	57.20	56.49	**56.49**	1.02	54.79	57.38	52.07	53.75	56.20	54.01	**54.01**	1.70	52.07	56.20	57.38	55.20	54.65	54.29	54.07	**54.55**	0.49	54.07	55.20
TiO_2	0	0	0	0	0	**0**	0	0	0	0	0	0	0	**0**	0	0	0	0	0	0	0	0	**0.00**	0	0	0
Al_2O_3	0.49	0.00	0.16	0.0	1.13	**0.36**	0.48	0.00	1.13	0.25	0.24	0.63	0.72	**0.46**	0.25	0.24	0.72	0.39	0.81	0.25	0.19	0.73	**0.49**	0.32	0.19	0.81
Fe_2O_3	3.38	2.60	6.42	3.73	2.65	**3.75**	1.57	2.60	6.42	7.53	5.78	7.17	1.87	**5.59**	2.59	1.87	7.53	9.53	0.08	0.23	1.30	0.08	**0.42**	0.59	0.08	1.30
FeO	18.88	20.00	14.32	17.30	14.08	**16.92**	2.66	14.08	20.00	21.46	18.90	17.00	24.95	**20.58**	3.44	17.00	24.95	11.66	23.50	25.69	25.75	24.09	**24.76**	1.14	23.50	25.75
MnO	0.62	0.61	0.59	0.61	0.23	**0.53**	0.17	0.23	0.62	0.74	0.61	0.48	0.53	**0.59**	0.11	0.48	0.74	0.22	0.81	0.87	0.89	0.83	**0.85**	0.04	0.81	0.89
MgO	20.07	19.44	19.57	20.41	20.11	**19.92**	0.40	19.44	20.41	17.36	19.87	18.20	17.01	**18.11**	1.27	17.01	19.87	18.35	18.21	16.84	16.47	18.89	**17.60**	1.14	16.47	18.89
CaO	1.41	0.32	1.47	0.40	4.86	**1.69**	1.85	0.32	4.86	0.68	0.75	0.32	0.42	**0.54**	0.21	0.32	0.75	2.52	0.70	0.79	0.55	0.64	**0.67**	0.10	0.55	0.79
Na_2O	0	0	0	0	0	**0**	0	0	0	0	0	0	0	**0**	0	0	0	0	0	0	0	0	**0**	0	0	0
K_2O	0	0	0	0	0	**0**	0	0	0	0	0	0	0	**0**	0	0	0	0	0	0	0	0	**0**	0	0	0
Ce_2O_3	0	0	0	0	0	**0**	0	0	0	0	0	0	0	**0**	0	0	0	0.18	0	0	0	0	**0**	0	0	0
Total	99.64	99.54	99.91	99.65	99.55	**99.66**	0.15	99.54	99.91	100.09	99.90	100.00	99.50	**99.87**	0.26	99.50	100.09	100.23	99.31	99.33	99.44	99.32	**99.35**	0.06	99.31	99.44
	Formula calculation (apfu cation basis)																									
	15	15	15	15	15	**15**				15	15	15	15	**15**				15	15	15	15	15	**15**			
^{T}Si	7.78	8.00	7.97	8.00	7.87	**7.92**	0.10	7.78	8.00	7.62	7.67	7.90	7.84	**7.76**	0.13	7.62	7.9	7.94	7.93	7.95	7.91	7.81	**7.90**	0.06	7.81	7.95
^{T}Al	0.08	0.00	0.03	0.00	0.13	**0.05**	0.06	0.00	0.13	0.04	0.04	0.10	0.12	**0.08**	0.04	0.04	0.122	0.06	0.07	0.04	0.03	0.13	**0.07**	0.04	0.03	0.13
T total	7.86	8.00	8.00	8.00	8.00	**7.97**	0.06	7.86	8.00	7.66	7.71	8.00	7.96	**7.84**	0.17	7.66	8.00	8.00	8.00	7.99	7.94	7.94	**7.97**	0.03	7.94	8.00
^{C}Al	0	0	0	0	0.05	**0.01**	0.02	0.00	0.05	0	0	0	0	**0**	0	0	0	0	0.06	0	0	0	**0.02**	0.03	0	0.06
^{C}Ti	0	0	0	0	0	**0**	0	0.00	0	0	0	0	0	**0**	0	0	0	0	0	0	0	0	**0**	0	0	0
^{C}Ce	0	0	0	0	0	**0**	0	0.00	0	0	0	0	0	**0**	0	0	0	0.01	0	0	0	0	**0**	0	0	0
$^{C}Fe^{3+}$	0.36	0.28	0.67	0.39	0.28	**0.40**	0.16	0.28	0.67	0.82	0.62	0.76	0.21	**0.60**	0.28	0.21	0.82	0.99	0.01	0.03	0.14	0.01	**0.05**	0.06	0.01	0.14
$^{C}Fe^{2+}$	2.24	2.37	1.66	2.02	1.64	**1.99**	0.33	1.64	2.37	2.61	2.26	2.00	3.03	**2.47**	0.45	2.00	3.03	1.35	2.82	3.12	3.14	2.91	**3.00**	0.16	2.82	3.14
^{C}Mn	0.07	0.07	0.07	0.07	0.03	**0.06**	0.02	0.03	0.07	0.09	0.07	0.06	0.07	**0.07**	0.01	0.06	0.09	0.03	0.10	0.11	0.11	0.10	**0.10**	0.01	0.10	0.11
^{C}Mg	2.32	2.29	2.60	2.51	3.00	**2.54**	0.29	2.29	3.00	1.48	2.05	2.19	1.70	**1.85**	0.32	1.48	2.19	2.62	2.01	1.74	1.61	1.98	**1.83**	0.19	1.61	2.01
C total	5.00	5.00	5.00	5.00	5.00	**5.00**	0.00	5.00	5.00	5.00	5.00	5.00	5.00	**5.00**	0.00	5.00	5.00	5.00	5.00	5.00	5.00	5.00	**5.00**	0.00	5.00	5.00
^{B}Mg	1.93	1.18	1.46	1.74	1.17	**1.50**	0.34	1.17	1.93	2.00	2.00	1.63	1.98	**1.90**	0.18	1.63	2.00	1.16	1.89	1.91	2.00	1.97	**1.94**	0.05	1.89	2.00
^{B}Ca	0.08	0	0.22	0.06	0.73	**0.23**	0.29	0.05	0.73	0	0	0.05	0.02	**0.02**	0.02	0	0.05	0.37	0.11	0.09	0	0.03	**0.06**	0.05	0	0.11
B total	2.00	1.23	1.68	1.80	1.90	**1.72**	0.30	1.23	2.00	2.00	2.00	1.67	2.00	**1.92**	0.16	1.67	2.00	1.53	2.00	2.00	2.00	2.00	**2.00**	0.00	2.00	2.00
^{A}Ca	0.14	0	0	0	0	**0.03**	0.06	0	0.14	0.11	0.11	0.00	0.07	**0.07**	0.05	0.00	0.11	0	0	0	0.09	0.06	**0.05**	0.04	0	0.09
$*^{A}Mg$	0	0	0	0	0	**0.0**	0	0	0	0.28	0.18	0	0	**0.11**	0.14	0	0.28	0	0	0	0	0	**0**	0	0	0
A total	0.14	0	0	0	0	**0.03**	0.06	0	0.14	0.39	0.29	0	0.07	**0.19**	0.18	0	0.39	0	0	0.03	0	0	**0.05**	0.04	0	0.09
SUM cations	15.00	14.23	14.67	14.80	14.90	**14.72**	0.30	14.23	15.00	15.05	15.00	14.68	15.03	**14.94**	0.18	14.68	15.05	14.53	15.00	15.02	15.03	15.00	**15.01**	0.02	15.00	15.03
Mg/(Mg+Fe^{2+})	0.655	0.594	0.709	0.678	0.718	**0.670**				0.571	0.642	0.656	0.549	**0.603**				0.737	0.580	0.539	0.535	0.576	**0.557**			
B/C	0.4	0.25	0.34	0.36	0.38	**0.34**				0.4	0.4	0.33	0.4	**0.38**				0.31	0.4	0.4	0.4	0.4	**0.4**			

Notes: Analyses 1i-4i correspond to aggregates in Fig. 2a; 5, 6 were obtained from small grains as marked in Fig. 4a. Analyse 7 is marked in Fig. 4c. Other analyses were obtained from additional foils.
Number 10 relates to the Ce-bearing amphibole. Top and bottom refer to their position on Fig. 5a. All values were noramlized on a volatile-free basis.
* Excess for banded areas. Measurement error within +20%

SUPPLEMENTARY MATERIAL B

FOR CHAPTER 3 – PLATINUM GROUP MINERALS ASSOCIATED WITH NICKEL-BEARING SULPHIDES FROM THE JATOBÁ IRON OXIDE-COPPER-GOLD DEPOSIT, CARAJÁS DOMAIN, BRAZIL

APPENDIX A: ADDITIONAL TABLES AND LA-ICP-MS RESULTS

APPENDIX A FOR CHAPTER 3

SM Table S1. LA-ICP-MS trace element data for sulfide minerals

Supplementary Materials Table S1. LA-ICP-MS trace element data for sulfide minerals (complete dataset, element concentrations in ppm, calculated from measurement of given isotope, except for the 4 Pb isotopes)
Note: data reported here are raw data; typical minimum detection limits are given in the main text

#	Pyrite	^{34}S	^{57}Fe	^{65}Cu	^{49}Ti	^{55}Mn	^{59}Co	^{60}Ni	^{66}Zn	^{75}As	^{77}Se	^{88}Sr	^{90}Zr	^{95}Mo	^{105}Pd	^{106}Pd	^{107}Ag	^{111}Cd	^{113}In
1	Jt 4 - Py 1 - 01	578079	407347	1.1	3.0	1.1	14395	18	1.5	1.0	150	0.035	0.007	0.024	0.004	0.001	0.012	0.004	0.001
2	Jt 4 - Py 1 - 02	566751	406588	0.985	3.4	0.114	26491	21	2.0	28	111	0.024	0.002	0.017	0.002	0.000	0.001	0.014	0.001
3	Jt 4 - Py 1 - 03	575118	414223	0.391	2.6	0.089	10549	15	1.2	30	60	0.015	0.002	0.023	0.000	0.000	0.006	0.003	0.001
4	Jt 4 - Py 1 - 04	573401	407572	0.706	2.7	0.064	18869	12	0.862	24	117	0.058	0.024	0.028	0.001	0.002	0.002	0.003	0.001
5	Jt 4 - Py 1 - 05	576201	411127	1.5	4.4	1.0	12492	20	3.8	7.2	126	0.030	0.023	0.026	0.004	0.001	0.035	0.003	0.001
6	Jt 4 - Py 1 - 06	566594	416222	0.330	2.8	0.392	17053	16	2.0	7.6	99	1.8	0.000	0.023	0.000	0.001	0.006	0.004	0.001
7	Jt 4 - Py 1 - 07	579489	407309	0.896	3.0	0.275	13096	24	7.3	0.916	69	0.046	0.008	0.025	0.001	0.003	0.005	0.014	0.012
8	Jt 4 - Py 1 - 08	584393	396911	705	3.3	5.4	17746	22	5.2	9.8	132	0.039	0.026	0.025	0.756	0.729	0.119	0.025	0.009
9	Jt 4 - Py 1 - 09	579719	390346	2.1	2.4	0.167	29711	20	1.1	5.2	187	0.012	0.000	0.023	0.006	0.003	0.016	0.003	0.009
10	Jt 4 - Py 1 - 10	562851	426142	1.4	37	1.4	10856	17	1.5	41	51	0.015	0.037	0.021	0.001	0.000	0.001	0.003	0.009
11	Jt 4 - Py 1 - 11	561650	423083	676	2.8	1.0	14340	108	5.5	1.8	116	0.025	0.004	0.025	0.048	0.040	0.039	0.027	0.005
12	Jt 4 - Py 2 - 01	574150	412583	0.668	2.9	0.186	13111	6.3	1.2	0.828	144	0.040	0.009	0.028	0.000	0.001	0.004	0.008	0.005
13	Jt 4 - Py 2 - 02	546053	434725	0.777	1.6	0.097	19065	14	1.1	3.8	133	0.011	0.003	0.030	0.000	0.000	0.001	0.007	0.005
14	Jt 4 - Py 2 - 03	558962	430369	1.0	2.5	0.208	10107	27	4.7	485	42	0.039	0.003	0.027	0.000	0.001	0.006	0.007	0.002
15	Jt 4 - Py 2 - 04	559617	430637	0.552	2.7	0.124	8975	27	1.4	697	41	0.017	0.013	0.025	0.003	0.001	0.005	0.010	0.040
16	Jt 4 - Py 2 - 05	569559	419036	0.647	3.5	0.188	10644	34	1.3	680	40	0.012	0.011	0.023	0.001	0.000	0.001	0.010	0.002
17	Jt 4 - Py 2 - 06	546075	444220	0.813	3.6	0.185	9596	15	2.1	40	47	0.042	0.006	0.024	0.000	0.000	0.008	0.010	0.002
18	Jt 4 - Py 3 - 01	569377	416846	0.295	7.4	2.5	13621	44	1.2	5.7	89	0.021	0.002	0.025	0.011	0.006	0.016	0.006	0.009
19	Jt 4 - Py 3 - 02	563822	423534	0.233	2.1	0.061	12508	22	0.582	1.4	96	0.003	0.000	0.028	0.135	0.125	0.037	0.006	0.016
20	Jt 4 - Py 3 - 03	553640	435830	1.2	17	57	10266	43	25	5.4	106	0.052	0.040	0.021	0.005	0.004	0.013	0.006	0.005
21	Jt 4 - Py 3 - 04	562500	415286	0.322	2.1	0.055	22024	17	0.743	1.9	166	0.003	0.000	0.031	0.000	0.000	0.002	0.005	0.004
22	Jt 4 - Py 3 - 05	540835	392506	57218	3.1	0.641	9165	18	86	1.9	105	0.122	0.028	0.028	8.1	5.9	0.101	0.159	0.328
23	Jt 4 - Py 3 - 06	568735	408115	333	3.0	0.726	22539	28	11	7.0	155	0.021	0.011	0.026	3.0	2.9	0.192	0.022	0.059
24	Jt 4 - Py 3 - 07	540070	432938	10269	15	90	13235	102	3080	6.2	96	0.115	1.4	0.023	5.5	4.3	0.425	21	1.6
25	Jt 4 - Py 3 - 08	550763	434151	232	3.9	0.485	14588	56	54	2.2	146	0.014	0.020	0.016	0.018	0.028	0.028	0.172	0.003
26	Jt 4 - Py 3 - 09	557467	430964	0.679	2.3	0.062	11156	273	1.0	4.7	127	0.076	0.002	0.024	0.010	0.007	0.035	0.005	0.006
27	Jt 4 - Py 3 - 10	534837	449781	1.2	47	141	14978	72	57	7.0	63	0.872	0.019	0.042	0.007	0.016	0.028	0.046	0.005
28	Jt 4 - Py 3 - 11	545466	427467	4816	3.1	0.319	21692	22	373	2.9	146	0.030	0.010	0.025	0.165	0.027	0.497	1.2	0.030
29	Jt 4 - Py 4 - 01	544283	425712	17395	2.5	1.0	12355	57	58	4.3	109	0.056	0.000	0.024	0.422	0.118	0.070	0.368	0.003
30	Jt 4 - Py 4 - 02	573571	411600	586	2.8	0.349	13757	10	332	2.1	127	0.013	0.000	0.021	0.048	0.068	0.054	0.853	0.196
31	Jt 4 - Py 4 - 03	540211	441797	773	7.0	3.2	17028	16	2.6	3.8	139	1.3	0.028	0.024	0.088	0.050	0.076	0.027	0.018
32	Jt 4 - Py 4 - 04	556879	426536	424	3.0	0.185	15992	16	2.1	4.0	127	0.046	0.000	0.026	0.143	0.119	0.049	0.009	0.015
33	Jt 4 - Py 4 - 05	563848	420639	29	2.5	0.153	15342	17	1.5	4.3	111	0.028	0.006	0.024	0.069	0.085	0.028	0.023	0.001
34	Jt 4 - Py 4 - 06	569386	412533	10.0	2.8	0.458	17890	17	1.8	7.9	149	0.062	0.011	0.022	0.002	0.001	0.007	0.016	0.001
35	Jt 4 - Py 5 - 01	567349	420249	1043	56	9.8	9710	36	1191	203	56	1.2	42	10	2.9	2.7	0.105	2.3	0.405
36	Jt 4 - Py 5 - 02	563330	427517	11	2.6	0.058	8666	26	3.3	393	47	0.050	0.000	0.026	0.544	0.319	0.013	0.014	0.007
37	Jt 4 - Py 5 - 03	571608	415099	11	41	3.3	12580	21	374	165	64	0.748	0.000	0.025	1.4	1.5	0.018	0.955	0.007
38	Jt 4 - Py 5 - 04	561141	429299	140	17	2.6	8828	34	5.0	371	43	0.573	0.002	0.023	12	11	0.051	0.022	0.007
39	Jt 4 - Py 5 - 05	561403	424483	1254	2.8	2.8	11350	44	19	293	71	0.359	0.028	0.027	311	181	0.149	0.100	0.044
40	Jt 4 - Py 5 - 06	552454	434022	312	148	4.6	12658	30	5.2	262	72	0.091	0.010	0.024	0.990	0.930	0.079	0.019	0.002
41	Jt 4 - Py 5 - 07	554828	433954	134	3.0	1.5	8877	33	1405	348	46	1.5	0.004	0.022	69	61	0.122	3.5	0.272
42	Jt 4 - Py 5 - 08	562859	423729	45	7.9	1.8	12853	26	3.3	95	71	0.620	0.002	0.025	65	62	0.131	0.039	0.002
43	Jt 4 - Py 6 - 01	558379	430563	0.225	2.9	0.060	10693	26	2.0	286	47	0.003	0.000	0.026	0.000	0.001	0.001	0.002	0.002
44	Jt 4 - Py 6 - 02	568178	419628	7.5	4.6	10	11902	21	1.3	164	59	15	0.037	0.027	0.080	0.102	0.010	0.002	0.006
45	Jt 4 - Py 6 - 03	537257	429052	734	14258	314	18077	24	120	44	82	0.031	0.005	0.029	0.083	0.072	0.091	0.382	0.005
46	Jt 4 - Py 6 - 04	561464	414673	99	2.8	2.7	23547	29	3.9	12	139	0.113	0.010	0.022	0.186	0.161	0.060	0.030	0.004
47	Jt 4 - Py 6 - 05	551469	438933	4.5	4.3	6.8	9333	31	4.9	107	56	0.085	0.178	0.028	0.450	0.513	0.033	0.002	0.005
48	Jt 4 - Py 6 - 06	569411	419462	126	2.6	2.4	10564	31	94	207	46	0.297	0.019	0.022	2.5	2.4	0.057	0.241	0.005
49	Jt 4 - Py 6 - 07	572911	413526	66	7.1	22	13312	16	6.7	7.6	120	0.177	0.004	0.027	0.002	0.004	0.028	0.002	0.025
50	Jt 4 - Py 6 - 08	567441	396931	14649	2.6	2.1	20589	22	190	2.9	141	0.036	0.007	0.027	0.694	0.250	0.094	0.967	0.016
51	Jt 4 - Py 7 - 01	573583	413346	1.2	582	25	12140	21	4.0	226	56	0.099	0.002	0.017	0.293	0.438	0.003	0.007	0.005
52	Jt 4 - Py 7 - 02	577096	405213	3.0	466	15	17055	15	1.8	37	90	0.465	0.004	0.020	0.066	0.049	0.003	0.005	0.005
53	Jt 4 - Py 7 - 03	563020	423499	1.6	558	46	12706	41	18	11	78	0.021	0.000	0.035	0.006	0.009	0.017	0.007	0.002
54	Jt 4 - Py 7 - 04	566431	422495	0.339	2.6	0.087	10834	23	0.806	171	43	0.005	0.000	0.025	0.000	0.000	0.007	0.005	0.002
55	Jt 4 - Py 7 - 05	574924	402285	10	3.7	0.152	22617	21	3.3	12	122	0.030	0.000	0.020	0.001	0.002	0.016	0.010	0.002
56	Jt 4 - Py 7 - 06	554804	425326	2.4	3.8	0.142	19671	29	1.6	6.3	154	0.010	0.002	0.026	0.002	0.002	0.001	0.002	0.002
57	Jt 7 - Py 1 - 01	532730	461829	0.455	461	10	3827	993	1.9	5.2	129	0.022	0.000	0.033	0.011	0.032	0.020	0.003	0.002
58	Jt 7 - Py 1 - 02	551863	439679	0.391	2.5	0.051	7939	393	0.905	15	99	0.005	0.000	0.031	0.106	0.134	0.076	0.002	0.008
59	Jt 7 - Py 1 - 03	559980	437004	0.298	2.0	0.056	1255	1533	0.680	5.4	211	0.005	0.004	0.030	0.151	0.122	0.061	0.002	0.002
60	Jt 7 - Py 1 - 04	539394	452020	1.7	308	16	7968	175	3.5	29	80	0.035	0.003	0.030	0.173	0.124	0.105	0.002	0.002
61	Jt 7 - Py 1 - 05	567799	422520	1.8	2.5	0.119	9515	18	0.992	25	119	0.006	0.002	0.031	0.000	0.000	0.005	0.002	0.002

#	Pyrite	^{34}S	^{57}Fe	^{65}Cu	^{49}Ti	^{55}Mn	^{59}Co	^{60}Ni	^{66}Zn	^{75}As	^{77}Se	^{88}Sr	^{90}Zr	^{95}Mo	^{105}Pd	^{106}Pd	^{107}Ag	^{111}Cd	^{113}In
62	Jt 7 - Py 1 - 06	561179	427452	0.163	1.8	0.103	11240	18	0.759	45	60	0.006	0.000	0.022	0.010	0.013	0.001	0.006	0.015
63	Jt 7 - Py 1 - 07	568236	419911	9.8	2.9	0.248	11669	26	0.645	42	76	0.034	0.281	0.025	0.362	0.266	0.055	0.012	0.006
64	Jt 7 - Py 1 - 08	543529	447537	1.6	90	11	8679	48	3.8	7.8	77	0.083	0.157	0.025	0.066	0.072	0.060	0.005	0.014
65	Jt 7 - Py 2 - 01	543283	455080	14	4.0	52	735	705	4.0	5.1	102	0.174	0.003	0.030	0.016	0.026	0.937	0.016	0.080
66	Jt 7 - Py 2 - 02	545182	453922	0.854	3.6	1.6	225	500	1.1	10	152	0.029	0.000	0.032	0.013	0.013	0.026	0.005	0.003
67	Jt 7 - Py 2 - 03	552598	445852	0.294	2.5	0.702	410	1016	0.957	8.1	110	0.005	0.000	0.026	0.013	0.019	0.064	0.005	0.006
68	Jt 7 - Py 2 - 04	568043	431437	0.070	2.4	0.052	168	134	0.867	34	180	0.003	0.000	0.026	0.005	0.003	0.003	0.005	0.003
69	Jt 7 - Py 2 - 05	555537	442579	355	2.3	1.6	798	612	1.8	4.0	107	0.005	0.000	0.029	0.030	0.016	0.130	0.013	0.003
70	Jt 7 - Py 2 - 06	556741	442027	0.304	3.2	0.053	481	677	0.963	1.6	68	0.007	0.002	0.025	0.016	0.021	0.002	0.016	0.006
71	Jt 7 - Py 2 - 07	567267	430922	31	11	16	599	1014	6.4	7.7	116	0.007	0.000	0.024	0.025	0.015	0.007	0.006	0.006
72	Jt 7 - Py 2 - 08	559702	439794	3.3	4.1	2.1	158	197	0.953	9.0	127	0.089	0.210	0.149	0.001	0.007	0.037	0.006	0.003
73	Jt 7 - Py 2 - 09	547960	450437	620	2.1	0.053	705	209	4.6	1.4	55	0.010	0.004	0.024	0.016	0.006	0.478	0.073	0.003
74	Jt 7 - Py 2 - 10	549827	448800	1.4	2.9	0.052	1112	106	1.0	0.696	148	0.003	0.000	0.021	0.006	0.004	0.005	0.006	0.003
75	Jt 7 - Py 2 - 11	559821	438877	0.653	2.6	0.075	433	735	1.1	9.6	118	0.020	0.002	0.025	0.005	0.008	0.021	0.016	0.002
76	Jt 7 - Py 3 - 01	550794	448175	0.410	2.2	0.056	270	670	1.0	4.3	82	0.003	0.000	0.029	0.004	0.011	0.001	0.010	0.002
77	Jt 7 - Py 3 - 02	546297	451981	6.1	2.7	0.530	978	620	1.4	4.2	88	0.065	0.002	0.030	0.022	0.016	0.018	0.004	0.002
78	Jt 7 - Py 3 - 03	566007	433469	0.903	2.8	0.098	242	214	1.4	2.8	59	0.005	0.007	0.027	0.003	0.005	0.011	0.006	0.008
79	Jt 7 - Py 3 - 04	555731	442843	0.808	2.8	2.6	115	1085	1.7	24	191	0.009	0.000	0.028	0.031	0.035	0.010	0.005	0.008
80	Jt 7 - Py 3 - 05	545350	453909	35	2.4	0.055	89	466	1.1	2.6	141	0.007	0.000	0.028	0.147	0.188	0.031	0.004	0.002
81	Jt 7 - Py 3 - 06	572920	424585	1450	2.3	0.052	121	773	2.3	0.305	145	0.022	0.000	0.030	0.058	0.003	0.155	0.006	0.048
82	Jt 7 - Py 3 - 07	567497	431806	0.409	3.0	0.045	130	429	0.878	2.9	128	0.004	0.000	0.025	0.004	0.004	0.004	0.016	0.002
83	Jt 7 - Py 3 - 08	546208	452995	0.630	2.8	0.083	131	530	0.960	4.1	126	0.006	0.000	0.026	0.004	0.003	0.006	0.006	0.002
84	Jt 7 - Py 3 - 09	544391	453276	0.392	2.9	0.047	716	1483	0.874	14	113	0.004	0.008	0.029	0.023	0.021	0.001	0.006	0.002
85	Jt 7 - Py 3 - 10	550672	448557	78	2.9	0.185	67	454	1.2	0.478	154	0.039	0.005	0.028	0.011	0.005	0.060	0.006	0.019
86	Jt 10 - Py 1 - 01	531228	456924	6911	8.3	49	4159	425	19	55	158	0.098	0.025	0.025	1.4	1.4	1.4	0.039	0.536
87	Jt 10 - Py 1 - 02	549223	428019	16278	2.5	0.822	5921	155	100	131	142	0.009	0.000	0.028	0.477	0.237	2.4	0.272	0.894
88	Jt 10 - Py 1 - 03	554852	438438	5406	3.5	19	704	348	4.9	34	169	0.045	0.012	0.028	1.3	1.2	1.2	0.006	0.362
89	Jt 10 - Py 1 - 04	544116	453048	164	2.2	1.1	1795	621	1.2	14	177	0.032	0.000	0.029	0.801	0.887	0.139	0.011	0.003
90	Jt 10 - Py 1 - 05	550566	446418	118	1.9	3.9	2602	157	1.7	17	102	3.4	0.005	0.029	0.035	0.065	0.131	0.008	0.003
91	Jt 10 - Py 1 - 06	546466	442887	5116	2.1	0.116	5122	150	16	103	112	0.063	0.000	0.024	0.761	0.405	1.2	0.035	0.270
92	Jt 10 - Py 1 - 07	553837	441143	762	2.6	6.2	3911	138	5.0	26	150	4.4	0.000	0.032	0.103	0.062	0.312	0.018	0.003
93	Jt 10 - Py 2 - 01	551259	444307	240	2.4	1.9	3611	436	1.7	14	122	0.006	0.000	0.028	0.012	0.004	0.060	0.007	0.039
94	Jt 10 - Py 2 - 02	557860	427442	37	2.9	0.083	14205	25	0.763	324	100	0.002	0.000	0.023	0.004	0.001	0.013	0.002	0.003
95	Jt 10 - Py 2 - 03	563590	423445	0.331	2.5	0.052	12715	21	0.880	135	90	0.001	0.002	0.048	0.001	0.001	0.014	0.010	0.006
96	Jt 10 - Py 2 - 04	560171	428169	16	2.0	0.050	11424	24	0.769	128	62	0.002	0.000	0.022	0.005	0.000	0.037	0.005	0.002
97	Jt 10 - Py 2 - 05	561977	426670	0.590	2.8	0.046	10981	31	0.650	298	36	0.004	0.000	0.019	0.034	0.015	0.004	0.004	0.002
98	Jt 10 - Py 2 - 06	567997	420117	1.9	3.1	0.058	9936	34	0.742	1855	49	0.006	0.002	0.022	0.229	0.247	0.009	0.004	0.002
99	Jt 10 - Py 2 - 07	567908	420539	12	4.2	19	9157	1721	3.0	373	224	0.435	0.002	0.025	0.677	0.748	0.292	0.004	0.067
100	Jt 10 - Py 2 - 08	565888	422347	0.343	2.1	0.168	11550	20	1.0	118	72	0.003	0.002	0.019	0.020	0.020	0.008	0.004	0.006
101	Jt 10 - Py 2 - 09	548142	441165	133	3.1	4.1	8812	1425	50	113	89	0.155	0.006	0.020	1.8	1.8	0.322	0.127	0.052
102	Jt 10 - Py 2 - 10	560787	426940	5.9	2.2	0.306	11907	51	44	156	95	0.051	0.000	0.019	0.068	0.084	0.059	0.118	0.002
103	Jt 10 - Py 2 - 11	562481	421495	5490	2.8	0.711	10099	223	32	43	119	0.026	0.004	0.020	0.210	0.107	1.0	0.086	0.393
104	Jt 10 - Py 2 - 12	559849	436368	487	2.2	0.059	2262	835	2.0	18	153	0.004	0.000	0.023	0.016	0.012	0.180	0.006	0.021
105	Jt 10 - Py 3 - 01	558087	432669	71	2.6	0.486	8912	62	1.5	66	119	0.047	0.004	0.073	0.362	0.447	0.164	0.009	0.025
106	Jt 10 - Py 3 - 02	575603	399319	4850	1.8	0.283	19720	214	5.6	82	151	0.116	0.002	1.4	0.294	0.277	1.7	0.043	0.160
107	Jt 10 - Py 3 - 03	552449	432971	3.1	4.1	0.296	13739	490	0.839	185	132	0.180	0.000	0.027	0.213	0.185	0.399	0.006	0.002
108	Jt 10 - Py 3 - 04	559604	427834	1.2	2.2	0.066	12267	19	0.677	157	100	0.006	0.023	0.029	0.000	0.001	0.053	0.001	0.007
109	Jt 10 - Py 3 - 05	559955	424542	0.412	232	8.9	15036	21	1.1	90	105	0.025	0.000	0.026	0.004	0.006	0.008	0.008	0.002
110	Jt 10 - Py 3 - 06	556216	430485	0.837	2.4	0.053	12974	21	0.634	167	131	0.003	0.000	0.044	0.010	0.008	0.233	0.001	0.002
111	Jt 10 - Py 3 - 07	563511	422296	1.0	2.6	0.054	13863	58	1.0	117	140	0.014	0.000	0.021	0.270	0.262	0.062	0.008	0.002
112	Jt 10 - Py 3 - 08	572671	414797	1.3	3.1	0.223	12211	87	0.804	101	124	0.021	0.000	0.023	0.022	0.026	0.045	0.001	0.003
113	Jt 10 - Py 3 - 09	578848	413044	0.287	3.1	0.092	7924	15	0.627	92	71	0.006	0.005	0.029	0.000	0.001	0.009	0.018	0.003
114	Jt 10 - Py 3 - 10	556957	429766	1.0	3.4	0.116	13109	28	0.649	77	53	0.017	0.000	0.029	0.031	0.040	0.005	0.001	0.016
115	Jt 10 - Py 3 - 11	558863	409574	2231	3.2	0.076	28916	117	5.0	66	158	0.021	0.000	2.4	1.1	1.5	1.5	0.008	0.118
116	Jt 10 - Py 3 - 12	554701	436285	2631	2.2	0.392	5852	292	4.9	40	157	0.110	0.008	0.030	0.320	0.198	1.2	0.010	0.094
117	Jt 10 - Py 4 - 01	558038	439156	825	2.2	0.079	1393	432	1.5	12	127	0.005	0.006	0.028	0.658	0.585	0.881	0.001	0.008
118	Jt 10 - Py 4 - 02	561847	436364	1.2	2.2	0.388	1276	391	1.0	9.5	101	0.017	0.000	0.025	0.042	0.012	0.088	0.001	0.005
119	Jt 10 - Py 4 - 03	546723	452006	216	2.8	0.061	497	429	3.0	13	107	0.012	0.000	0.027	0.024	0.016	0.151	0.011	0.081
120	Jt 10 - Py 4 - 04	556811	431841	0.320	2.8	0.057	11096	26	0.563	114	104	0.006	0.000	0.035	0.000	0.001	0.002	0.001	0.003
121	Jt 10 - Py 4 - 05	540729	445104	9817	2.4	0.235	3889	255	23	9.5	143	0.026	0.000	0.033	0.583	0.329	1.8	0.043	0.403
122	Jt 10 - Py 4 - 06	554872	434555	1.7	2.9	0.345	10211	211	1.0	0.278	145	0.023	0.003	0.029	0.000	0.008	0.006	0.001	0.003
123	Jt 10 - Py 4 - 07	552575	437084	1.6	1.8	0.064	10128	41	0.827	52	102	0.022	0.003	0.134	0.004	0.002	0.255	0.001	0.009
124	Jt 10 - Py 4 - 08	568963	417361	1.7	3.2	0.112	13483	30	0.875	23	132	0.010	0.006	0.032	0.005	0.008	0.009	0.005	0.009
125	Jt 10 - Py 4 - 09	541262	452293	4964	3.3	0.592	1067	228	22	6.7	140	0.041	0.005	0.025	0.166	0.100	1.1	0.028	0.312

#	Pyrite	^{34}S	^{57}Fe	^{65}Cu	^{49}Ti	^{55}Mn	^{59}Co	^{60}Ni	^{66}Zn	^{75}As	^{77}Se	^{88}Sr	^{90}Zr	^{95}Mo	^{105}Pd	^{106}Pd	^{107}Ag	^{111}Cd	^{113}In
126	Jt 10 - Py 5 - 01	515417	483581	17	2.7	0.417	561	279	1.7	8.5	132	0.030	0.005	0.036	0.003	0.003	0.063	0.015	0.011
127	Jt 10 - Py 5 - 02	556053	441085	5.1	2.7	1.1	2063	666	1.6	0.359	123	0.033	0.043	0.051	0.000	0.002	0.002	0.008	0.004
128	Jt 10 - Py 5 - 03	534068	463811	1.4	2.7	0.260	1264	731	0.902	0.435	120	0.036	0.043	0.035	0.005	0.002	0.003	0.007	0.004
129	Jt 10 - Py 5 - 04	534799	462654	2.0	2.9	0.289	1910	516	0.826	7.4	105	0.031	0.022	0.034	0.033	0.036	0.002	0.004	0.004
130	Jt 10 - Py 5 - 05	569616	429026	2.5	3.4	0.453	1034	194	1.2	4.5	119	0.025	0.004	0.033	0.000	0.002	0.006	0.004	0.004
131	Jt 10 - Py 5 - 06	553779	445024	4.8	3.6	0.544	817	282	1.2	3.3	80	0.082	0.014	0.041	0.051	0.060	0.003	0.016	0.004
132	Jt 10 - Py 5 - 07	563144	434100	1673	3.0	0.536	623	288	9.5	0.515	152	0.052	0.034	0.050	0.189	0.140	0.289	0.063	0.049
133	Jt 10 - Py 5 - 08	558952	429440	2440	3.0	1.6	8859	124	9.4	7.1	149	0.497	0.057	0.040	0.240	0.148	0.569	0.100	0.220
134	Jt 10 - Py 5 - 09	525984	472761	33	2.6	0.461	882	178	1.4	5.9	143	0.046	0.031	0.034	0.093	0.089	0.128	0.004	0.031
135	Jt 10 - Py 5 - 10	568118	419327	61	3.1	0.699	12204	39	1.2	172	64	0.046	0.127	0.037	0.277	0.449	0.144	0.011	0.004
136	Jt 10 - Py 6 edge - 01	552758	437397	3.9	3.3	0.374	9612	85	1.3	50	88	0.115	0.044	0.066	0.002	0.001	0.010	0.014	0.004
137	Jt 10 - Py 6 edge - 02	563495	410696	5688	3.2	0.738	19654	61	6.3	216	164	0.129	0.011	0.032	0.184	0.050	0.986	0.016	0.313
138	Jt 10 - Py 6 edge - 03	551822	434899	55	2.8	2.6	12929	38	5.7	130	112	0.109	0.014	0.026	0.067	0.017	0.090	0.003	0.002
139	Jt 10 - Py 6 cent - 01	553449	435516	2.6	2.1	0.436	10610	21	1.3	301	89	0.043	0.018	0.022	0.014	0.006	0.014	0.003	0.802
140	Jt 10 - Py 6 cent - 02	562081	427125	4.0	3.0	0.228	10355	26	0.953	327	63	0.088	0.003	0.036	0.063	0.090	0.013	0.003	0.002
141	Jt 10 - Py 6 cent - 03	555599	432016	1.1	2.7	0.311	10579	48	0.998	1688	45	0.079	0.045	0.033	0.355	0.357	0.027	0.008	0.002
142	Jt 10 - Py 6 cent - 04	554284	432328	0.448	2.8	0.062	10997	38	0.746	2302	45	0.010	0.002	0.022	0.005	0.005	0.001	0.003	0.008
143	Jt 10 - Py 6 cent - 05	549667	437613	1.2	2.2	0.154	10676	38	1.2	1964	37	0.030	0.002	0.032	0.001	0.004	0.002	0.003	0.002
144	Jt 10 - Py 6 cent - 06	539617	451805	0.582	2.9	0.118	7204	28	0.951	1310	30	0.042	0.005	0.028	0.069	0.079	0.006	0.012	0.002
145	Jt 10 - Py 6 cent - 07	556305	433565	6.4	2.8	1.2	9925	31	2.8	83	67	0.221	0.019	0.033	0.453	0.458	0.133	0.008	0.002
146	Jt 10 - Py 6 edge - 04	554618	434889	1.9	2.3	0.267	10241	30	1.2	112	92	0.029	0.003	0.105	0.012	0.006	0.444	0.007	0.002
147	Jt 10 - Py 6 edge - 05	575635	410298	3.4	3.0	0.364	13640	102	1.6	159	133	0.088	0.006	0.029	0.224	0.203	0.137	0.008	0.002
148	Jt 10 - Py 6 edge - 06	535860	450188	1.3	2.7	0.235	13635	24	1.1	146	130	0.064	0.005	0.034	0.010	0.003	0.008	0.006	0.002
149	Jt 10 - Py 6 edge - 07	556587	419283	712	2.5	0.216	23172	16	3.8	69	152	0.020	0.008	0.026	0.115	0.082	0.167	0.006	0.038
150	Jt 10 - Py 6 edge - 08	566748	422497	318	4.0	1.2	10174	83	4.2	44	113	0.052	0.014	0.072	0.082	0.036	0.272	0.048	0.003
151	Jt 10 - Py 7 - 01	552651	446918	0.224	2.4	0.053	309	39	0.835	5.6	75	0.006	0.000	0.030	0.002	0.000	0.025	0.011	0.003
152	Jt 10 - Py 7 - 02	556709	433629	2.7	5.4	0.181	9144	39	1.5	375	92	0.051	0.016	0.031	0.000	0.004	0.011	0.010	0.003
153	Jt 10 - Py 7 - 03	535577	461628	1561	2.3	0.387	1005	104	3.9	5.4	109	0.059	0.011	0.032	0.063	0.006	0.312	0.032	0.209
154	Jt 10 - Py 7 - 04	569352	412650	15554	7.8	23	1411	729	68	40	106	0.194	1.4	0.144	0.538	0.224	3.1	0.203	0.986
155	Jt 10 - Py 7 - 05	542088	446850	2264	2.5	1.4	8320	84	15	249	82	0.048	0.003	0.028	0.545	0.522	0.776	0.051	0.090
156	Jt 10 - Py 7 - 06	555727	426129	8813	3.0	1.2	8783	133	9.4	244	106	0.100	0.006	0.028	0.747	0.581	0.848	0.120	0.541
157	Jt 10 - Py 7 - 07	538801	459377	37	2.1	0.629	1119	329	3.2	80	238	0.038	0.006	0.031	0.002	0.005	0.179	0.023	0.003
158	Jt 10 - Py 8 - 01	563092	433886	3.2	2.5	0.259	2089	783	1.2	12	127	0.029	0.008	0.025	0.019	0.019	0.031	0.010	0.003
159	Jt 10 - Py 8 - 02	554906	437479	101	2.8	0.235	6635	474	1.4	186	161	0.026	0.000	0.031	0.478	0.560	0.093	0.002	0.018
160	Jt 10 - Py 8 - 03	534679	444581	19113	2.2	0.620	835	555	20	9.3	143	0.136	0.000	0.064	1.3	0.960	3.3	0.057	1.2
161	Jt 10 - Py 8 - 04	544585	454523	21	2.8	0.125	537	173	1.2	1.4	150	0.020	0.011	1.4	0.074	0.056	0.058	0.002	0.002
162	Jt 10 - Py 8 - 05	562312	433297	3026	3.1	0.052	879	299	2.9	0.952	174	0.008	0.000	0.024	0.078	0.022	0.600	0.002	0.188
163	Jt 10 - Py 8 - 06	558707	431601	1076	3.1	0.054	7965	460	7.4	0.312	163	0.004	0.003	0.025	0.539	0.369	0.239	0.049	0.073
164	Jt 10 - Py 8 - 07	556749	439762	1.4	4.8	0.199	3016	272	0.919	0.314	192	0.005	0.003	0.019	0.083	0.106	0.016	0.004	0.002
165	Jt 10 - Py 8 - 08	541603	444140	5063	1.7	0.176	8809	209	4.8	17	133	0.011	0.048	0.027	0.367	0.275	0.936	0.025	0.212
166	Jt 10 - Py 8 - 09	554886	434922	12	3.5	0.414	9722	78	1.5	263	98	0.025	0.028	0.026	0.169	0.175	0.055	0.022	0.009
167	Jt 10 - Py 8 - 10	559979	428410	9.0	2.7	0.753	11310	34	1.2	120	133	0.011	0.005	0.031	0.002	0.002	0.017	0.019	0.006
168	Jt 10 - Py 8 - 11	547298	441763	2.5	66	3.1	10357	36	0.849	365	107	0.010	0.008	0.021	0.059	0.076	0.020	0.003	0.006
169	Jt 10 - Py 8 - 12	559146	429118	904	2.7	0.504	10245	159	2.8	276	126	0.068	0.016	0.051	0.267	0.189	0.588	0.008	0.079
170	Jt 10 - Py 9 edge - 01	544517	447315	2.0	3.7	0.191	7857	143	1.1	35	119	0.019	0.007	0.021	0.253	0.297	0.030	0.003	0.023
171	Jt 10 - Py 9 edge - 02	576533	410427	0.156	2.8	0.055	12869	32	0.760	73	63	0.002	0.000	0.036	0.013	0.012	0.002	0.010	0.003
172	Jt 10 - Py 9 edge - 03	552957	428188	0.458	2.3	0.060	18612	29	0.800	115	94	0.004	0.000	0.028	0.015	0.006	0.020	0.003	0.003
173	Jt 10 - Py 9 cent - 01	516063	466288	1.3	3059	193	14141	46	2.4	48	57	17	0.128	0.031	0.081	0.048	0.105	0.010	0.284
174	Jt 10 - Py 9 cent - 02	545176	443993	7.9	4.8	0.348	10622	45	0.758	79	62	0.102	0.016	0.026	0.102	0.116	0.037	0.004	0.002
175	Jt 10 - Py 9 cent - 03	552517	435695	20	2.3	0.219	11494	86	1.0	103	67	0.043	0.009	0.037	0.016	0.017	0.101	0.004	0.002
176	Jt 10 - Py 9 cent - 04	538480	446970	9.7	2.2	0.356	14020	128	1.2	275	91	0.058	0.003	0.032	0.306	0.329	0.125	0.004	0.003
177	Jt 10 - Py 9 cent - 05	536993	455243	1.0	2.2	0.068	7416	109	0.758	67	151	0.025	0.009	0.033	0.130	0.088	0.127	0.008	0.002
178	Jt 10 - Py 9 cent - 06	556349	430750	3.1	2.8	0.219	12443	222	0.994	111	97	0.054	0.009	0.076	0.609	0.626	0.146	0.022	0.002
179	Jt 10 - Py 9 cent - 07	537780	456881	2.6	4266	167	205	490	2.0	33	151	0.043	0.007	0.021	0.183	0.241	0.121	0.012	0.003
180	Jt 10 - Py 9 cent - 08	565427	434053	3.9	5.5	2.9	68	236	1.2	22	163	0.043	0.003	0.023	0.168	0.218	0.077	0.021	0.003
181	Jt 10 - Py 9 edge - 04	534142	465420	5.2	4.6	0.465	19	240	1.3	28	134	0.024	0.039	0.028	0.074	0.077	0.083	0.002	0.003
182	Jt 10 - Py 9 edge - 05	546874	449856	167	2.8	0.267	1867	1044	0.978	23	144	0.097	0.010	0.026	0.498	0.506	0.377	0.002	0.003
183	Jt 10 - Py 9 edge - 06	555353	443402	2.9	3.1	0.226	653	408	0.965	21	145	0.040	0.006	0.088	0.780	0.737	0.092	0.010	0.003
184	Jt 10 - Py 9 edge - 07	569486	423618	124	2.9	3.7	6362	197	2.3	71	121	0.033	0.018	0.057	1.3	1.1	0.116	0.002	0.003

#	Pyrrhotite	^{34}S	^{57}Fe	^{65}Cu	^{49}Ti	^{55}Mn	^{59}Co	^{60}Ni	^{66}Zn	^{75}As	^{77}Se	^{88}Sr	^{90}Zr	^{95}Mo	^{105}Pd	^{106}Pd	^{107}Ag	^{111}Cd	^{113}In
1	Jt 4 - Pyh 1 - 01	419922	574682	1.2	1.8	0.340	201	5077	1.7	0.506	112	0.010	0.000	0.041	0.005	0.000	0.011	0.020	0.012
2	Jt 4 - Pyh 1 - 02	425934	568893	1.1	3.3	3.0	180	4875	2.9	1.1	102	0.380	0.015	0.042	0.006	0.004	0.053	0.014	0.052
3	Jt 4 - Pyh 1 - 03	430734	564001	1.9	2.8	0.420	186	4968	1.5	0.467	102	0.024	0.023	0.037	0.001	0.000	0.014	0.009	0.010
4	Jt 4 - Pyh 1 - 04	436608	558311	0.781	2.8	0.207	198	4773	1.1	0.438	105	0.075	0.009	0.041	0.002	0.000	0.029	0.085	0.009
5	Jt 4 - Pyh 1 - 05	428641	566088	1.6	3.1	1.4	187	4957	2.2	0.502	113	0.051	0.090	0.043	0.003	0.003	0.043	0.009	0.010
6	Jt 4 - Pyh 1 - 06	413756	552059	103	103	236	2219	31308	87	0.655	108	0.103	0.006	0.085	0.051	0.057	0.879	0.010	0.136
7	Jt 4 - Pyh 1 - 07	416167	578580	1.2	2.2	0.709	176	4953	0.823	0.474	108	0.012	0.000	0.049	0.001	0.036	0.022	0.016	0.004
8	Jt 4 - Pyh 1 - 08	413192	581425	1.3	2.7	0.439	201	5066	1.6	0.386	108	0.032	0.016	0.053	0.001	0.000	0.018	0.015	0.004
9	Jt 4 - Pyh 1 - 09	427459	562836	2.1	2.0	0.806	483	9112	1.7	0.400	95	0.036	0.011	0.049	0.006	0.000	0.205	0.008	0.004
10	Jt 4 - Pyh 1 - 10	421822	573054	2.2	2.9	1.2	195	4813	3.2	0.440	106	0.090	0.042	0.070	0.001	0.000	0.054	0.041	0.004
11	Jt 4 - Pyh 1 - 11	408614	478809	11	24	144	8650	103490	54	5.4	116	3.1	0.105	0.213	0.312	0.313	1.7	0.033	0.038
12	Jt 4 - Pyh 1 - 12	424668	570005	1.7	4.0	8.2	195	5003	4.1	0.511	108	0.018	0.000	0.064	0.001	0.000	0.039	0.011	0.004
13	Jt 4 - Pyh 1 - 13	425030	569502	1.3	1.6	1.6	201	5153	1.0	0.532	108	0.022	0.041	0.049	0.001	0.003	0.011	0.011	0.004
14	Jt 4 - Pyh 2 - 01	414802	580336	2.3	3.3	1.2	202	4542	1.9	0.460	104	1.5	0.008	0.050	0.002	0.000	0.031	0.009	0.003
15	Jt 4 - Pyh 2 - 02	412044	576400	5.0	2.9	0.784	859	10568	2.2	0.439	100	0.041	0.012	0.042	0.002	0.009	0.369	0.013	0.012
16	Jt 4 - Pyh 2 - 03	414564	580488	1.1	2.6	1.4	200	4636	1.1	0.378	104	0.028	2.6	0.048	0.001	0.000	0.042	0.014	0.009
17	Jt 4 - Pyh 2 - 04	416653	578422	1.6	2.5	0.117	230	4587	1.1	0.371	102	0.012	0.000	0.048	0.023	0.000	0.019	0.013	0.082
18	Jt 4 - Pyh 2 - 05	421166	574001	1.6	2.7	0.323	214	4502	0.921	0.355	103	0.042	0.004	0.042	0.002	0.001	0.046	0.031	0.009
19	Jt 4 - Pyh 2 - 06	403623	591605	1.7	1.4	0.648	219	4442	1.1	0.405	103	0.133	0.000	0.044	0.001	0.001	0.020	0.034	0.025
20	Jt 4 - Pyh 2 - 07	413173	581969	1.4	2.4	0.251	231	4520	1.3	0.328	100	0.017	0.012	0.056	0.001	0.001	0.018	0.018	0.011
21	Jt 4 - Pyh 2 - 08	411549	580920	3.9	2.9	0.368	450	6960	2.1	0.347	108	0.035	0.013	0.041	0.025	0.029	0.212	0.050	0.004
22	Jt 4 - Pyh 2 - 09	412965	582242	2.7	1.7	0.148	235	4439	1.0	0.340	96	0.025	0.008	0.048	0.001	0.001	0.057	0.018	0.013
23	Jt 4 - Pyh 2 - 10	429231	566228	2.1	1.1	0.127	222	4210	1.0	0.359	98	0.008	0.000	0.048	0.001	0.000	0.106	0.071	0.003
24	Jt 4 - Pyh 2 - 11	417226	576799	159	6.8	6.3	306	5389	2.7	0.437	100	0.030	0.016	0.048	0.014	0.017	0.079	0.019	0.076
25	Jt 4 - Pyh 2 - 12	408918	569404	12	2.0	0.138	1546	20005	1.2	0.450	104	0.101	0.000	0.038	0.136	0.112	0.592	0.050	0.004
26	Jt 4 - Pyh 2 - 13	421095	573312	19	2.7	11	143	5297	4.4	0.385	99	0.118	0.004	0.056	0.004	0.001	0.078	0.018	0.027
27	Jt 4 - Pyh 2 - 14	417031	558560	104	2.2	0.111	1103	23096	1.2	0.358	95	0.010	0.004	0.045	0.274	0.272	0.677	0.017	0.017
28	Jt 4 - Pyh 2 - 15	392140	491020	12204	3.0	0.502	5501	98997	14	0.351	100	0.063	0.021	0.041	1.1	0.968	3.2	0.168	0.153
29	Jt 4 - Pyh 2 - 16	411001	584012	5.7	5.0	0.552	220	4643	1.4	0.368	103	0.030	0.057	0.038	0.006	0.002	0.050	0.054	0.011
30	Jt 4 - Pyh 2 - 17	415847	579580	2.4	1.8	0.182	204	4254	1.1	0.348	103	0.013	0.004	0.047	0.002	0.008	0.044	0.007	0.011
31	Jt 4 - Pyh 3 - 01	416983	577631	3.6	4.1	1.6	198	5055	5.5	0.788	113	0.120	0.081	0.181	0.001	0.000	0.051	0.033	0.003
32	Jt 4 - Pyh 3 - 02	409627	585221	1.6	2.2	0.446	186	4847	2.4	0.507	110	0.053	0.006	0.082	0.001	0.000	0.034	0.017	0.003
33	Jt 4 - Pyh 3 - 03	421488	573301	2.5	2.9	0.800	180	4916	2.9	0.418	106	0.081	0.045	0.058	0.007	0.000	0.027	0.010	0.003
34	Jt 4 - Pyh 3 - 04	412732	581946	1.0	3.0	1.4	178	5016	1.5	0.480	108	0.052	0.000	0.045	0.001	0.000	0.076	0.010	0.003
35	Jt 4 - Pyh 3 - 05	432823	561828	1.6	2.6	0.486	193	5034	1.6	0.462	113	0.033	0.006	0.054	0.001	0.003	0.039	0.007	0.003
36	Jt 4 - Pyh 3 - 06	425401	569240	2.0	1.5	0.364	212	5025	1.5	0.411	114	0.054	0.031	0.114	0.001	0.000	0.026	0.043	0.003
37	Jt 4 - Pyh 3 - 07	411520	583038	1.7	1.6	0.125	206	5121	0.879	0.451	109	0.006	0.000	0.045	0.001	0.000	0.024	0.007	0.003
38	Jt 4 - Pyh 4 - 01	409558	585035	443	2.0	0.390	187	4663	1.7	0.446	99	0.022	0.000	0.051	0.007	0.000	0.085	0.020	0.021
39	Jt 4 - Pyh 4 - 02	414032	580738	1.9	1.1	0.167	219	4899	1.4	0.568	106	0.023	0.000	0.047	0.001	0.003	0.041	0.007	0.006
40	Jt 4 - Pyh 4 - 03	416546	578308	2.4	2.4	0.380	222	4807	1.7	0.486	108	0.024	0.019	0.055	0.001	0.002	0.041	0.022	0.006
41	Jt 4 - Pyh 4 - 04	412298	582327	1.6	2.6	0.198	226	5027	1.5	0.543	114	0.021	0.013	0.059	0.003	0.003	0.058	0.005	0.006
42	Jt 4 - Pyh 4 - 05	405977	529214	6.0	6.4	11	5748	58900	6.2	0.518	105	0.333	0.239	0.082	0.017	0.014	2.1	0.062	0.005
43	Jt 4 - Pyh 4 - 06	415799	578771	4.4	2.8	0.781	206	5087	5.2	0.454	113	0.137	0.144	0.205	0.001	0.000	0.081	0.023	0.005
44	Jt 4 - Pyh 4 - 07	429088	565567	2.0	2.2	0.870	222	5005	2.3	0.391	110	0.065	0.020	0.070	0.001	0.003	0.033	0.005	0.010
45	Jt 4 - Pyh 5 - 01	430695	564277	3.5	2.9	3.8	148	4748	6.4	0.415	112	0.154	0.185	0.105	0.002	0.001	0.021	0.073	0.009
46	Jt 4 - Pyh 5 - 02	422607	572360	9.2	7.8	5.0	154	4743	7.3	0.560	102	0.243	0.170	0.471	0.001	0.000	0.035	0.052	0.010
47	Jt 4 - Pyh 5 - 03	391033	439789	45434	3.0	1.0	8215	115245	129	0.406	103	0.172	0.022	0.039	1.5	0.802	2.7	0.520	0.210
48	Jt 4 - Pyh 5 - 04	433780	560711	24	19	7.6	168	5156	13	1.3	110	0.962	0.218	0.289	0.017	0.022	0.053	0.023	0.014
49	Jt 4 - Pyh 5 - 05	427067	567995	2.1	2.7	0.138	150	4673	0.976	0.347	107	0.025	0.020	0.044	0.000	0.002	0.047	0.005	0.013
50	Jt 4 - Pyh 5 - 06	423196	571929	2.0	2.3	0.169	151	4611	0.857	0.385	107	0.013	0.000	0.039	0.000	0.001	0.023	0.026	0.013
51	Jt 4 - Pyh 5 - 07	429642	565396	3.0	1.5	0.122	153	4691	0.680	0.380	111	0.004	0.000	0.031	0.001	0.001	0.026	0.006	0.005
52	Jt 4 - Pyh 5 - 08	422748	572342	3.2	2.7	1.7	162	4635	2.6	0.358	98	0.138	0.008	0.047	0.000	0.001	0.021	0.010	0.005
53	Jt 4 - Pyh 5 - 09	563360	422897	0.433	2.5	0.057	13582	20	0.912	5.2	131	0.003	0.000	0.026	0.000	0.000	0.001	0.006	0.003
54	Jt 4 - Pyh 5 - 10	424885	570165	1.5	1.7	0.091	179	4657	0.791	0.414	105	0.011	0.004	0.046	0.000	0.001	0.038	0.005	0.005
55	Jt 4 - Pyh 5 - 11	432812	562028	2.1	2.4	0.265	198	4823	2.3	0.335	117	0.020	0.004	0.041	0.002	0.001	0.045	0.011	0.012
56	Jt 4 - Pyh 5 - 12	424052	569915	1.1	1010	17	195	4702	2.1	0.344	105	0.014	0.015	0.044	0.002	0.001	0.009	0.032	0.017
57	Jt 4 - Pyh 6 - 01	422042	573184	1.4	3.5	0.420	200	4456	2.0	0.396	110	0.045	0.031	0.062	0.000	0.000	0.037	0.009	0.002
58	Jt 4 - Pyh 6 - 02	418098	577069	3.4	2.2	0.234	206	4503	1.6	0.409	110	0.024	0.000	0.037	0.000	0.000	0.046	0.025	0.048
59	Jt 4 - Pyh 6 - 03	424957	570469	2.8	1.2	0.141	190	4267	1.2	0.397	111	0.016	0.000	0.038	0.000	0.000	0.044	0.008	0.002
60	Jt 4 - Pyh 6 - 04	414283	580712	3.6	2.6	0.274	196	4690	1.9	0.426	110	0.086	0.004	0.041	0.002	0.000	0.025	0.007	0.002
61	Jt 4 - Pyh 6 - 05	399050	578012	4.6	35	171	1832	20723	67	0.553	100	0.063	0.000	0.048	0.036	0.047	0.742	0.009	0.087

#	Chalcopyrite	^{34}S	^{57}Fe	^{65}Cu	^{49}Ti	^{55}Mn	^{59}Co	^{60}Ni	^{66}Zn	^{75}As	^{77}Se	^{88}Sr	^{90}Zr	^{95}Mo	^{105}Pd	^{106}Pd	^{107}Ag	^{111}Cd	^{113}In
1	Jt 4 - Ccp 1 - 01	384299	275956	338829	3.1	1.7	8.3	344	449	0.275	96	0.156	0.047	0.080	5.2	0.034	0.392	0.932	3.2
2	Jt 4 - Ccp 1 - 02	382239	283303	333611	4.0	2.2	11	365	348	0.298	94	0.076	0.090	0.056	5.5	0.000	0.361	0.756	3.0
3	Jt 4 - Ccp 1 - 03	387126	274277	329791	8.8	2.0	372	7943	357	0.287	99	0.321	0.584	0.038	5.7	0.432	1.1	0.665	3.0
4	Jt 4 - Ccp 1 - 04	374814	281372	343120	2.5	0.494	4.4	181	398	0.273	98	0.051	0.075	0.035	5.7	0.013	0.355	0.891	2.6
5	Jt 4 - Ccp 1 - 05	382085	270761	346530	3.0	0.311	1.5	88	412	0.262	98	0.083	0.010	0.026	5.2	0.006	0.275	0.701	3.2
6	Jt 4 - Ccp 2 - 01	381247	281904	336362	9.1	1.4	1.4	47	321	0.391	98	0.314	0.388	0.041	5.6	0.006	0.258	0.611	3.1
7	Jt 4 - Ccp 2 - 02	369064	275416	354983	2.5	0.482	0.956	32	395	0.326	97	0.071	0.036	0.050	5.8	0.002	0.265	0.569	2.9
8	Jt 4 - Ccp 2 - 03	382817	276600	340016	6.0	0.584	1.2	40	411	0.388	97	0.127	0.022	0.141	5.8	0.010	0.375	0.840	2.8
9	Jt 4 - Ccp 2 - 04	379622	273737	346123	3.1	0.623	1.2	37	364	0.339	99	0.082	19	0.033	5.7	0.021	0.423	0.718	2.5
10	Jt 4 - Ccp 2 - 05	362991	283906	352546	2.7	0.859	1.4	33	406	0.355	100	0.341	0.062	0.048	5.7	0.001	0.411	1.2	2.7
11	Jt 4 - Ccp 2 - 06	370528	276922	351946	17	2.3	2.5	48	405	0.442	111	0.163	0.058	0.173	5.7	0.001	0.636	1.0	2.4
12	Jt 4 - Ccp 2 - 07	379153	286449	333568	74	11	2.6	75	557	0.493	93	3.0	7.2	0.053	5.6	0.024	0.387	0.906	3.4
13	Jt 4 - Ccp 2 - 08	371557	281711	346152	4.4	3.2	1.8	65	407	0.533	88	1.9	0.058	0.056	5.6	0.001	0.472	1.0	3.1
14	Jt 4 - Ccp 2 - 09	386025	299911	313161	32	26	27	301	386	1.1	102	3.6	20	0.138	5.3	0.019	0.395	0.591	3.5
15	Jt 4 - Ccp 2 - 10	384249	276826	338339	9.2	11	2.8	63	390	0.416	90	7.3	0.360	0.057	5.5	0.001	0.280	1.1	2.6
16	Jt 4 - Ccp 2 - 11	370758	283713	344909	13	15	2.2	62	397	0.518	100	7.2	0.785	0.039	5.4	0.002	0.464	0.961	3.1
17	Jt 4 - Ccp 2 - 12	368732	273829	356869	1.7	0.500	1.4	67	403	0.315	86	0.258	2.1	0.049	5.5	0.024	0.256	0.959	3.3
18	Jt 4 - Ccp 3 - 01	342883	366782	289715	48	25	22	212	175	0.368	102	0.195	0.141	0.056	4.8	0.001	0.305	0.758	1.8
19	Jt 4 - Ccp 3 - 02	373324	293884	332098	3.0	100	19	248	183	1.3	102	19	0.194	0.037	5.7	0.001	0.248	0.839	2.3
20	Jt 4 - Ccp 3 - 03	381695	272962	344841	13	33	28	77	192	0.307	113	0.149	0.062	0.029	5.4	0.001	0.364	0.950	1.8
21	Jt 4 - Ccp 3 - 04	375509	372660	249660	22	249	87	1513	157	0.371	109	0.097	0.085	0.041	4.2	0.020	0.251	0.504	3.7
22	Jt 4 - Ccp 3 - 05	383061	277696	338598	40	18	21	232	210	0.327	110	0.071	0.034	0.038	5.8	0.012	0.245	0.701	1.7
23	Jt 4 - Ccp 3 - 06	390468	279048	329768	3.8	2.4	15	291	271	0.647	110	0.456	0.099	0.048	5.4	0.000	0.237	0.869	1.4
24	Jt 10 - Ccp 1 - 01	386617	273491	339434	2.8	61	2.1	70	170	0.315	106	0.135	0.019	0.078	5.9	0.026	17	0.224	11
25	Jt 10 - Ccp 1 - 02	379352	278489	341725	23	55	3.1	66	165	0.262	102	0.164	0.028	0.184	6.0	0.018	16	0.229	11
26	Jt 10 - Ccp 1 - 03	381958	290195	327215	3.4	108	92	138	107	1.0	117	0.224	0.006	0.042	5.3	0.032	19	0.376	10
27	Jt 10 - Ccp 1 - 04	379540	274940	345100	2.0	10.0	5.0	38	222	0.273	104	0.025	0.007	0.034	5.8	0.016	16	0.269	11
28	Jt 10 - Ccp 1 - 05	384444	272067	343076	2.6	1.9	0.895	58	164	0.309	122	0.104	0.004	0.037	6.0	0.009	19	0.272	11
29	Jt 10 - Ccp 1 - 06	383379	273600	342539	4.5	80	1.4	106	128	0.323	107	0.167	0.018	0.033	6.0	0.040	19	0.309	11
30	Jt 10 - Ccp 1 - 07	376632	276729	346219	2.7	15	1.0	58	201	0.293	91	0.096	0.031	0.062	5.9	0.015	19	0.415	12
31	Jt 10 - Ccp 2 - 01	383181	269640	346772	3.1	1.2	0.386	33	221	0.259	106	0.040	0.167	0.084	5.8	0.002	17	0.353	11
32	Jt 10 - Ccp 2 - 02	378388	278446	342704	1.3	0.195	0.098	32	268	0.269	110	0.015	0.004	0.028	5.9	0.012	17	0.414	10
33	Jt 10 - Ccp 2 - 03	365317	284880	349348	1.2	0.284	0.174	32	257	0.298	119	0.021	0.017	0.026	6.0	0.017	17	0.503	12
34	Jt 10 - Ccp 2 - 04	377891	287718	333955	2.0	16	0.310	48	198	0.324	111	11	0.024	1.7	6.1	0.039	16	0.558	11
35	Jt 10 - Ccp 2 - 05	384334	274138	341070	2.2	0.471	0.281	41	231	0.290	122	0.164	0.029	0.074	5.9	0.002	18	0.455	11
36	Jt 10 - Ccp 2 - 06	384537	265505	349525	1.4	0.158	0.081	34	222	0.263	126	0.016	0.017	0.026	5.8	0.012	16	0.379	11
37	Jt 10 - Ccp 2 - 07	384579	268106	346855	1.8	0.308	0.207	34	253	0.242	131	0.021	0.004	0.032	5.8	0.000	16	0.474	11
38	Jt 10 - Ccp 2 - 08	376191	270926	352486	1.9	1.7	0.145	32	169	0.265	122	0.020	0.004	0.027	5.9	0.023	19	0.312	11
39	Jt 10 - Ccp 2 - 09	375725	292109	331363	9.4	300	1.4	189	104	0.301	127	3.5	0.088	0.538	5.6	0.086	21	0.271	12
40	Jt 10 - Ccp 2 - 10	376267	276495	346851	2.0	0.567	0.125	32	221	0.219	89	0.042	0.011	0.051	5.8	0.008	16	0.313	11
41	Jt 10 - Ccp 2 - 11	387112	275258	337199	2.0	0.568	0.228	34	267	0.224	86	0.031	0.015	0.062	6.0	0.011	16	0.322	11
42	Jt 10 - Ccp 2 - 12	387432	273102	339054	2.6	0.339	0.196	32	245	0.269	91	0.022	0.007	0.040	5.9	0.028	15	0.224	11
43	Jt 10 - Ccp 3 - 01	474910	342270	178695	2.0	0.368	3686	84	161	14	116	0.315	0.000	0.038	3.2	0.161	9.8	0.260	6.0
44	Jt 10 - Ccp 3 - 02	379028	272248	348105	2.1	0.315	140	47	245	0.396	131	0.263	0.000	0.065	5.8	0.035	16	0.345	9.4
45	Jt 10 - Ccp 3 - 03	428428	300901	269625	2.9	0.463	505	155	178	2.3	126	0.881	0.005	0.130	4.4	0.084	26	0.299	8.3
46	Jt 10 - Ccp 3 - 04	380701	281457	337371	2.2	1.6	1.0	60	217	5.9	116	13	0.018	0.108	5.7	0.002	14	0.243	11
47	Jt 10 - Ccp 3 - 05	382872	281276	335322	5.5	3.5	2.1	72	223	7.7	131	20	0.196	0.447	6.0	0.039	16	0.416	11
48	Jt 10 - Ccp 3 - 06	385233	286377	327587	6.1	231	16	192	116	0.484	147	0.981	0.044	0.336	6.2	0.029	18	0.280	11
49	Jt 10 - Ccp 3 - 07	387047	268343	344191	2.2	0.409	0.321	37	205	0.274	126	0.242	0.018	0.046	5.8	0.004	15	0.320	10
50	Jt 10 - Ccp 3 - 08	437193	306661	254826	4.3	2.5	647	291	148	6.7	146	7.9	0.019	0.069	5.2	0.471	13	0.264	9.1
51	Jt 10 - Ccp 3 - 09	389646	269385	340583	1.4	4.6	0.633	33	176	0.297	121	0.072	0.035	0.078	5.7	0.023	14	0.332	11
52	Jt 10 - Ccp 3 - 10	376085	284151	339343	1.9	3.6	0.710	45	199	0.325	123	0.194	0.076	0.304	6.0	0.013	14	0.330	10
53	Jt 10 - Ccp 3 - 11	379903	277052	342510	4.0	72	0.775	92	190	0.274	115	0.302	0.037	0.700	5.8	0.025	16	0.237	11
54	Jt 10 - Ccp 3 - 12	384706	288429	326457	3.7	18	0.840	55	132	0.288	131	1.1	0.035	0.230	6.0	0.015	18	0.406	9.5
55	Jt 10 - Ccp 3 - 13	387159	273201	339105	2.2	0.921	0.443	46	283	1.0	125	6.6	0.015	0.103	5.7	0.025	16	0.383	12
56	Jt 10 - Ccp 4 - 01	417898	270544	311046	9.0	5.0	1.6	61	236	0.520	138	0.852	0.178	0.605	6.3	0.034	19	0.047	12
57	Jt 10 - Ccp 4 - 02	377755	282952	338801	8.6	3.0	1.4	33	306	0.492	98	0.305	0.168	0.175	5.7	0.001	16	0.428	11
58	Jt 10 - Ccp 4 - 03	427262	267334	304933	2.5	1.9	0.670	40	255	0.566	130	0.170	0.301	0.218	6.2	0.002	14	0.376	12
59	Jt 10 - Ccp 4 - 04	382182	278260	339159	10	6.7	2.0	33	159	0.699	124	0.833	0.422	0.915	6.4	0.019	18	0.195	11
60	Jt 10 - Ccp 4 - 05	375183	277328	346998	2.9	11	1.2	36	246	0.639	133	0.293	0.083	0.700	6.1	0.003	17	0.679	11
61	Jt 10 - Ccp 4 - 06	424760	256275	318475	9.5	8.9	2.3	43	218	0.779	149	0.415	0.297	0.526	6.3	0.072	16	0.155	12
62	Jt 10 - Ccp 4 - 07	392200	269330	337942	9.8	8.8	1.9	47	285	0.670	127	0.369	0.187	0.891	6.2	0.001	16	0.152	12
63	Jt 10 - Ccp 4 - 08	373155	300866	325499	4.9	5.2	1.4	36	244	0.654	139	0.205	0.316	0.562	5.5	0.024	15	0.256	11
64	Jt 10 - Ccp 4 - 09	398030	273186	328321	8.2	6.7	2.4	41	196	0.621	147	0.367	0.489	0.475	6.6	0.050	17	0.270	13

65	Jt 10 - Ccp 4 - 10	389683	268775	341063	6.2	3.8	1.6	39	237	0.676	147	0.305	0.554	0.664	6.1	0.021	15	0.788	12
66	Jt 10 - Ccp 4 - 11	386222	256341	356971	4.7	3.3	1.0	32	270	0.519	112	0.155	0.021	0.311	5.5	0.016	15	0.170	11
67	Jt 10 - Ccp 4 - 12	384383	278115	337060	3.6	4.6	1.1	40	222	0.512	128	0.156	0.104	0.132	7.1	0.001	15	0.331	15
68	Jt 10 - Ccp 4 - 13	370707	276158	352306	9.4	190	2.7	264	106	0.629	151	2.6	0.064	0.433	5.9	0.107	23	0.527	12

SM Table S1. (Continued)

#	Pyrite	^{115}In	^{118}Sn	^{121}Sb	^{125}Te	^{178}Hf	^{181}Ta	^{182}W	^{193}Ir	^{195}Pt	^{197}Au	^{205}Tl	^{209}Bi	^{232}Th	^{238}U	^{204}Pb	^{206}Pb	^{207}Pb	^{208}Pb
1	Jt 4 - Py 1 - 01	0.000	0.027	0.109	0.574	0.000	0.000	0.006	0.000	0.001	####	0.025	0.929	0.002	0.079	0.005	0.684	0.156	0.357
2	Jt 4 - Py 1 - 02	0.000	0.024	0.013	3.2	0.000	0.001	0.006	0.001	0.004	####	0.003	0.066	0.005	0.001	0.005	0.014	0.009	0.024
3	Jt 4 - Py 1 - 03	0.000	0.028	0.013	0.064	0.000	0.000	0.005	0.000	0.001	####	0.002	0.002	0.000	0.000	0.006	0.003	0.003	0.003
4	Jt 4 - Py 1 - 04	0.000	0.033	0.010	0.291	0.000	0.000	0.002	0.000	0.004	####	0.002	0.113	0.000	0.000	0.005	0.010	0.008	0.017
5	Jt 4 - Py 1 - 05	0.001	0.035	0.348	1.7	0.002	0.000	0.008	0.000	0.007	####	0.021	2.6	0.002	0.089	0.041	6.1	1.6	3.4
6	Jt 4 - Py 1 - 06	0.000	0.025	0.019	0.731	0.000	0.000	0.002	0.000	0.001	####	0.002	1.00	0.000	0.011	0.006	0.134	0.070	0.195
7	Jt 4 - Py 1 - 07	0.000	0.020	0.010	0.125	0.000	0.000	0.011	0.000	0.001	####	0.006	0.286	0.005	0.002	0.004	0.068	0.021	0.043
8	Jt 4 - Py 1 - 08	0.016	0.052	0.974	19	0.002	0.001	0.003	0.000	0.018	####	0.053	29	0.001	0.048	0.075	9.4	2.9	5.9
9	Jt 4 - Py 1 - 09	0.000	0.031	0.015	3.0	0.000	0.000	0.004	0.000	0.003	####	0.003	1.9	0.001	0.000	0.004	0.122	0.071	0.160
10	Jt 4 - Py 1 - 10	0.000	0.031	0.016	0.095	0.004	0.004	0.024	0.000	0.000	####	0.003	0.333	0.003	0.003	0.005	0.051	0.025	0.075
11	Jt 4 - Py 1 - 11	0.003	0.034	0.126	1.5	0.000	0.000	0.009	0.000	0.004	####	0.022	3.1	0.002	0.005	0.044	5.6	1.8	3.6
12	Jt 4 - Py 2 - 01	0.000	0.025	0.009	0.149	0.000	0.000	0.010	0.000	0.001	####	0.007	0.003	0.002	0.000	0.005	0.002	0.002	0.011
13	Jt 4 - Py 2 - 02	0.001	0.029	0.010	1.8	0.000	0.000	0.012	0.000	0.002	####	0.005	0.003	0.001	0.000	0.005	0.004	0.002	0.005
14	Jt 4 - Py 2 - 03	0.000	0.034	0.011	0.062	0.000	0.000	0.016	0.005	0.000	####	0.003	0.005	0.001	0.002	0.006	0.003	0.003	0.007
15	Jt 4 - Py 2 - 04	0.000	0.027	0.016	0.066	0.000	0.000	0.013	0.001	0.001	####	0.004	0.004	0.002	0.000	0.006	0.002	0.004	0.007
16	Jt 4 - Py 2 - 05	0.000	0.029	0.017	0.086	0.000	0.000	0.006	0.003	0.001	####	0.003	0.003	0.000	0.000	0.005	0.002	0.005	0.004
17	Jt 4 - Py 2 - 06	0.001	0.033	0.016	0.104	0.000	0.001	0.020	0.000	0.001	####	0.002	0.004	0.001	0.000	0.005	0.005	0.002	0.008
18	Jt 4 - Py 3 - 01	0.001	0.031	0.057	0.911	0.000	0.002	0.000	0.000	0.002	####	0.004	2.4	0.000	0.016	0.010	0.538	0.306	0.656
19	Jt 4 - Py 3 - 02	0.001	0.031	0.308	4.3	0.000	0.000	0.000	0.000	0.001	####	0.003	7.5	0.000	0.000	0.009	0.985	0.372	0.783
20	Jt 4 - Py 3 - 03	0.007	0.033	0.102	1.2	0.008	0.001	0.003	0.000	0.004	####	0.009	5.2	0.000	0.020	0.006	1.7	0.399	0.817
21	Jt 4 - Py 3 - 04	0.000	0.027	0.004	0.680	0.000	0.000	0.000	0.000	0.001	####	0.003	0.003	0.000	0.000	0.005	0.001	0.000	0.002
22	Jt 4 - Py 3 - 05	0.240	0.097	1.9	21	0.000	0.000	0.036	0.000	0.281	####	0.042	19	0.002	0.005	0.044	11	2.8	5.7
23	Jt 4 - Py 3 - 06	0.009	0.056	1.6	22	0.000	0.000	0.001	0.000	0.023	####	0.011	33	0.000	0.010	0.064	8.2	2.6	5.2
24	Jt 4 - Py 3 - 07	0.596	2.8	2.8	17	0.056	0.002	0.012	0.000	0.049	1.7	0.278	29	0.004	0.293	0.058	12	3.0	6.1
25	Jt 4 - Py 3 - 08	0.007	0.045	0.059	0.779	0.000	0.000	0.000	0.000	0.001	####	0.002	2.3	0.000	0.005	0.005	0.260	0.157	0.334
26	Jt 4 - Py 3 - 09	0.001	0.025	0.086	0.640	0.000	0.000	0.001	0.000	0.001	####	0.018	1.6	0.000	0.036	0.007	0.919	0.212	0.500
27	Jt 4 - Py 3 - 10	0.020	0.087	0.058	2.6	0.012	0.012	0.028	0.000	0.002	####	0.018	10	0.002	0.168	0.008	1.2	0.301	0.591
28	Jt 4 - Py 3 - 11	0.092	0.349	0.093	2.4	0.000	0.000	0.022	0.000	0.000	####	0.002	4.1	0.000	0.000	0.026	0.978	0.604	1.3
29	Jt 4 - Py 4 - 01	0.059	0.087	0.482	3.1	0.000	0.000	0.000	0.000	0.017	####	0.065	8.6	0.000	0.052	0.018	5.2	1.3	2.7
30	Jt 4 - Py 4 - 02	0.013	0.028	0.145	2.8	0.000	0.000	0.000	0.000	0.026	####	0.003	4.8	0.000	0.004	0.012	1.5	0.421	0.874
31	Jt 4 - Py 4 - 03	0.024	0.077	0.140	2.5	0.000	0.000	0.038	0.000	0.005	####	0.014	5.5	3.5	2.2	0.008	2.4	0.603	1.1
32	Jt 4 - Py 4 - 04	0.009	0.028	0.415	4.5	0.000	0.000	0.001	0.000	0.003	####	0.002	7.9	0.069	0.043	0.011	1.4	0.433	0.919
33	Jt 4 - Py 4 - 05	0.000	0.024	0.102	2.1	0.000	0.000	0.012	0.000	0.004	####	0.002	2.2	0.003	0.005	0.010	0.204	0.092	0.179
34	Jt 4 - Py 4 - 06	0.000	0.024	0.016	0.984	0.000	0.000	0.015	0.000	0.006	####	0.002	0.922	0.003	0.000	0.005	0.080	0.058	0.115
35	Jt 4 - Py 5 - 01	0.067	0.048	0.589	27	1.4	0.008	0.033	0.000	0.005	####	0.012	33	0.010	0.795	0.121	9.5	3.5	7.6
36	Jt 4 - Py 5 - 02	0.001	0.040	0.012	2.1	0.000	0.000	0.000	0.000	0.007	####	0.002	1.0	0.000	0.002	0.005	0.712	0.249	0.547
37	Jt 4 - Py 5 - 03	0.010	0.044	0.215	14	0.000	0.006	0.010	0.000	0.006	####	0.006	14	0.000	0.002	0.034	1.4	0.858	1.9
38	Jt 4 - Py 5 - 04	0.003	0.033	0.516	60	0.000	0.000	0.004	0.000	0.054	####	0.007	50	0.000	0.007	0.086	3.4	2.1	4.4
39	Jt 4 - Py 5 - 05	0.037	0.070	2.0	923	0.000	0.001	0.000	0.000	1.7	####	0.003	144	0.001	0.018	0.033	2.9	1.2	2.4
40	Jt 4 - Py 5 - 06	0.005	0.051	0.254	13	0.000	0.007	0.020	0.000	0.001	####	0.007	12	0.001	0.152	0.052	2.7	1.3	2.8
41	Jt 4 - Py 5 - 07	0.040	0.037	1.0	289	0.000	0.000	0.178	0.000	0.048	####	0.012	66	0.001	0.004	0.057	3.9	1.6	3.3
42	Jt 4 - Py 5 - 08	0.005	0.040	1.1	227	0.000	0.001	0.000	0.000	0.023	####	0.005	72	0.000	0.004	0.061	2.9	1.6	3.5
43	Jt 4 - Py 6 - 01	0.000	0.040	0.018	0.042	0.000	0.000	0.000	0.000	0.001	####	0.002	0.026	0.000	0.000	0.005	0.002	0.001	0.002
44	Jt 4 - Py 6 - 02	0.000	0.037	0.026	2.2	0.000	0.003	0.130	0.001	0.009	####	0.003	5.8	0.001	0.025	0.006	0.716	0.254	0.520
45	Jt 4 - Py 6 - 03	0.054	0.447	0.630	11	0.002	0.841	0.212	0.000	0.006	####	0.018	13	0.003	0.038	0.037	6.8	1.8	3.8
46	Jt 4 - Py 6 - 04	0.010	0.049	0.248	9.3	0.000	0.001	0.003	0.000	0.001	####	0.035	8.9	0.008	0.213	0.031	5.1	1.4	3.0
47	Jt 4 - Py 6 - 05	0.004	0.035	0.654	8.1	0.002	0.001	0.001	0.000	0.008	####	0.161	11	0.003	0.113	0.083	18	4.4	9.0
48	Jt 4 - Py 6 - 06	0.009	0.032	0.501	17	0.002	0.000	0.001	0.000	0.001	####	0.005	28	0.000	0.006	0.055	2.4	1.4	2.9
49	Jt 4 - Py 6 - 07	0.047	0.052	0.017	1.4	0.000	0.000	0.000	0.000	0.005	####	0.006	3.6	0.000	0.019	0.006	0.324	0.087	0.139
50	Jt 4 - Py 6 - 08	0.181	0.167	0.262	7.5	0.002	0.000	0.003	0.000	0.028	####	0.006	11	0.000	0.000	0.028	5.2	1.4	3.0
51	Jt 4 - Py 7 - 01	0.001	0.031	0.121	4.7	0.000	0.077	0.252	0.000	0.008	####	0.002	5.6	0.001	0.014	0.033	1.3	0.895	1.9
52	Jt 4 - Py 7 - 02	0.000	0.164	0.111	2.5	0.000	0.060	0.477	0.000	0.006	####	0.002	4.3	0.001	0.122	0.008	0.400	0.233	0.453
53	Jt 4 - Py 7 - 03	0.002	0.150	0.266	2.6	0.000	0.043	0.013	0.000	0.031	####	0.071	13	0.006	0.474	0.018	2.6	0.603	1.3
54	Jt 4 - Py 7 - 04	0.000	0.035	0.020	0.048	0.000	0.000	0.000	0.002	0.004	####	0.004	0.030	0.000	0.000	0.005	0.001	0.000	0.004

#	Pyrite	^{115}In	^{118}Sn	^{121}Sb	^{125}Te	^{178}Hf	^{181}Ta	^{182}W	^{193}Ir	^{195}Pt	^{197}Au	^{205}Tl	^{209}Bi	^{232}Th	^{238}U	^{204}Pb	^{206}Pb	^{207}Pb	^{208}Pb
55	Jt 4 - Py 7 - 05	0.001	0.031	0.016	1.2	0.000	0.000	0.015	0.000	0.001	####	0.002	0.067	0.001	0.000	0.004	0.012	0.011	0.024
56	Jt 4 - Py 7 - 06	0.000	0.031	0.035	0.801	0.000	0.000	0.003	0.000	0.005	####	0.002	0.738	0.000	0.008	0.005	0.149	0.045	0.097
57	Jt 7 - Py 1 - 01	0.003	0.041	1.6	0.940	0.000	0.029	0.056	0.000	0.087	####	0.001	4.6	0.002	0.001	0.058	2.2	1.4	3.2
58	Jt 7 - Py 1 - 02	0.000	0.042	0.617	2.2	0.000	0.000	0.000	0.000	0.273	####	0.001	1.0	0.000	0.000	0.014	0.908	0.486	1.1
59	Jt 7 - Py 1 - 03	0.000	0.030	1.0	2.7	0.000	0.000	0.000	0.000	0.024	####	0.002	1.5	0.000	0.000	0.018	1.1	0.653	1.5
60	Jt 7 - Py 1 - 04	0.005	0.032	0.114	0.543	0.002	0.028	0.056	0.000	1.1	####	0.008	0.483	0.001	0.201	0.006	0.810	0.225	0.518
61	Jt 7 - Py 1 - 05	0.000	0.034	0.020	0.054	0.000	0.000	0.002	0.000	0.091	####	0.001	0.009	0.000	0.001	0.006	0.006	0.005	0.010
62	Jt 7 - Py 1 - 06	0.000	0.038	0.019	0.059	0.000	0.000	0.000	0.000	1.3	####	0.002	0.142	0.000	0.000	0.006	0.013	0.012	0.026
63	Jt 7 - Py 1 - 07	0.000	0.026	1.1	2.4	0.013	0.002	0.021	0.000	0.499	####	0.009	1.9	0.393	9.8	0.035	6.0	1.4	2.4
64	Jt 7 - Py 1 - 08	0.003	0.095	1.5	1.0	0.016	0.004	0.045	0.000	0.827	####	0.037	2.4	0.017	0.164	0.085	3.5	1.9	4.2
65	Jt 7 - Py 2 - 01	0.076	0.144	0.712	0.518	0.005	0.006	0.000	0.000	0.508	####	0.869	0.571	0.003	0.538	0.057	5.9	1.8	4.1
66	Jt 7 - Py 2 - 02	0.000	0.034	0.033	0.109	0.000	0.000	0.000	0.000	0.013	####	0.004	0.412	0.000	0.021	0.005	0.167	0.073	0.161
67	Jt 7 - Py 2 - 03	0.000	0.035	0.257	0.121	0.000	0.000	0.001	0.000	0.057	####	0.003	0.181	0.000	0.000	0.012	0.431	0.261	0.558
68	Jt 7 - Py 2 - 04	0.000	0.033	0.017	0.076	0.000	0.000	0.000	0.000	0.004	####	0.004	0.011	0.000	0.000	0.007	0.014	0.006	0.014
69	Jt 7 - Py 2 - 05	0.014	0.034	0.101	0.116	0.000	0.000	0.000	0.000	0.560	####	0.006	0.239	0.000	0.020	0.006	0.551	0.232	0.510
70	Jt 7 - Py 2 - 06	0.000	0.038	0.018	0.110	0.000	0.000	0.000	0.000	0.019	####	0.002	0.004	0.000	0.000	0.004	0.002	0.001	0.002
71	Jt 7 - Py 2 - 07	0.000	0.036	0.888	0.375	0.000	0.000	0.000	0.000	0.410	####	0.002	1.1	0.000	0.001	0.080	2.8	1.8	3.9
72	Jt 7 - Py 2 - 08	0.000	0.040	0.241	0.194	0.004	0.000	0.004	0.000	0.052	####	0.004	0.195	0.021	0.010	0.008	0.452	0.287	0.622
73	Jt 7 - Py 2 - 09	0.013	0.033	0.866	0.178	0.000	0.000	0.001	0.000	0.423	####	0.312	0.382	0.000	0.001	0.024	1.3	0.629	1.3
74	Jt 7 - Py 2 - 10	0.000	0.034	0.082	0.123	0.000	0.000	0.000	0.000	0.036	####	0.003	0.177	0.000	0.000	0.010	0.319	0.199	0.416
75	Jt 7 - Py 2 - 11	0.000	0.036	0.149	0.267	0.000	0.000	0.000	0.000	0.088	####	0.015	0.129	0.000	0.001	0.006	0.170	0.091	0.197
76	Jt 7 - Py 3 - 01	0.000	0.039	0.012	1.3	0.000	0.000	0.002	0.000	0.161	####	0.002	0.005	0.000	0.000	0.004	0.012	0.004	0.010
77	Jt 7 - Py 3 - 02	0.000	0.038	0.863	11	0.000	0.000	0.011	0.000	0.671	####	0.474	0.815	0.000	0.012	0.036	3.0	1.1	2.3
78	Jt 7 - Py 3 - 03	0.001	0.030	0.029	0.155	0.000	0.000	0.002	0.000	0.113	####	0.002	0.068	0.000	0.000	0.006	0.100	0.061	0.118
79	Jt 7 - Py 3 - 04	0.000	0.035	0.211	2.7	0.000	0.000	0.000	0.000	0.316	####	0.052	0.090	0.000	0.006	0.005	0.265	0.134	0.315
80	Jt 7 - Py 3 - 05	0.001	0.043	0.305	1.8	0.000	0.000	0.000	0.000	0.362	####	0.002	0.635	0.000	0.000	0.016	0.609	0.402	0.829
81	Jt 7 - Py 3 - 06	0.036	0.035	0.057	0.266	0.000	0.000	0.002	0.000	0.282	####	0.260	0.089	0.000	0.000	0.006	0.236	0.115	0.248
82	Jt 7 - Py 3 - 07	0.000	0.041	0.019	1.4	0.000	0.000	0.000	0.000	0.038	####	0.003	0.064	0.001	0.000	0.005	0.087	0.055	0.116
83	Jt 7 - Py 3 - 08	0.000	0.035	0.021	0.395	0.000	0.000	0.002	0.000	0.009	####	0.004	0.170	0.000	0.000	0.005	0.089	0.054	0.133
84	Jt 7 - Py 3 - 09	0.000	0.032	0.016	2.5	0.000	0.000	0.000	0.000	0.181	####	0.003	0.065	0.000	0.000	0.007	0.089	0.058	0.123
85	Jt 7 - Py 3 - 10	0.003	0.032	0.635	0.540	0.000	0.000	0.002	0.000	0.100	####	0.018	0.324	0.000	0.000	0.098	4.2	2.3	5.1
86	Jt 10 - Py 1 - 01	0.484	1.5	1.9	11	0.002	0.005	0.000	0.000	2.4	####	0.176	23	0.109	1.5	0.033	10	2.4	6.5
87	Jt 10 - Py 1 - 02	0.956	2.7	0.557	3.3	0.000	0.001	0.000	0.000	1.1	####	0.002	11	0.001	0.005	0.028	2.1	0.987	1.9
88	Jt 10 - Py 1 - 03	0.399	0.375	1.5	3.8	0.004	0.003	0.000	0.000	1.1	####	0.062	5.6	0.059	0.536	0.013	4.4	0.891	2.1
89	Jt 10 - Py 1 - 04	0.008	0.031	0.735	2.6	0.000	0.001	0.000	0.000	1.1	####	0.015	4.6	0.000	0.003	0.171	23	7.7	20
90	Jt 10 - Py 1 - 05	0.007	0.066	0.094	3.4	0.000	0.000	0.058	0.000	0.377	####	0.006	1.9	0.063	0.360	0.010	1.9	0.361	0.803
91	Jt 10 - Py 1 - 06	0.335	0.482	0.747	3.1	0.000	0.000	0.000	0.000	2.2	####	0.014	7.2	0.010	0.053	0.012	5.8	1.3	3.5
92	Jt 10 - Py 1 - 07	0.077	0.254	0.285	2.9	0.002	0.000	0.042	0.000	0.688	####	0.009	3.6	0.115	0.684	0.011	3.0	0.604	1.5
93	Jt 10 - Py 2 - 01	0.026	0.104	0.134	3.3	0.000	0.001	0.000	0.000	0.489	####	0.003	0.884	0.000	0.004	0.006	0.157	0.095	0.198
94	Jt 10 - Py 2 - 02	0.000	0.046	0.017	0.126	0.000	0.000	0.000	0.000	2.4	####	0.002	0.076	0.000	0.000	0.007	0.085	0.019	0.054
95	Jt 10 - Py 2 - 03	0.000	0.038	0.010	0.082	0.000	0.000	0.000	0.000	0.047	####	0.001	0.003	0.000	0.000	0.005	0.001	0.005	0.002
96	Jt 10 - Py 2 - 04	0.001	0.034	0.016	0.070	0.000	0.000	0.000	0.000	2.8	####	0.003	0.172	0.000	0.000	0.005	0.326	0.069	0.227
97	Jt 10 - Py 2 - 05	0.000	0.038	0.024	0.204	0.000	0.000	0.000	0.000	1.9	####	0.003	0.450	0.000	0.000	0.006	0.010	0.005	0.011
98	Jt 10 - Py 2 - 06	0.001	0.035	0.182	0.950	0.000	0.000	0.000	0.000	0.822	####	0.007	4.1	0.000	0.000	0.012	0.369	0.244	0.515
99	Jt 10 - Py 2 - 07	0.067	0.341	1.9	5.3	0.000	0.004	0.001	0.000	0.639	####	0.034	17	0.003	0.168	0.052	6.3	2.1	5.9
100	Jt 10 - Py 2 - 08	0.001	0.041	0.067	0.102	0.000	0.000	0.000	0.000	0.277	####	0.002	0.233	0.000	0.000	0.006	0.174	0.064	0.134
101	Jt 10 - Py 2 - 09	0.111	0.073	1.7	12	0.000	0.000	0.001	0.000	4.3	####	0.013	16	0.004	0.022	0.086	15	4.2	11
102	Jt 10 - Py 2 - 10	0.035	0.033	0.944	0.852	0.000	0.000	0.001	0.000	0.304	####	0.018	3.0	0.021	0.556	0.015	2.3	0.803	1.7
103	Jt 10 - Py 2 - 11	0.438	1.2	0.782	1.8	0.002	0.001	0.000	0.000	2.0	####	0.005	4.2	0.000	0.004	0.032	1.0	0.646	1.6
104	Jt 10 - Py 2 - 12	0.018	0.169	0.048	22	0.000	0.000	0.000	0.000	0.226	####	0.004	0.596	0.000	0.000	0.006	0.170	0.078	0.167
105	Jt 10 - Py 3 - 01	0.006	0.054	0.514	1.7	0.000	0.000	0.005	0.000	0.806	####	0.058	2.1	0.006	0.004	0.012	1.5	0.470	1.5
106	Jt 10 - Py 3 - 02	0.235	0.260	0.790	2.5	0.000	0.000	0.000	0.000	3.4	####	0.016	8.5	0.000	0.000	0.059	17	3.9	13
107	Jt 10 - Py 3 - 03	0.001	0.051	1.6	1.2	0.000	0.000	0.006	0.000	7.4	####	0.287	2.3	0.000	0.001	0.018	5.9	1.4	5.2
108	Jt 10 - Py 3 - 04	0.002	0.062	0.148	0.053	0.000	0.000	0.000	0.000	15	####	0.048	0.006	0.000	0.001	0.005	0.014	0.002	0.004
109	Jt 10 - Py 3 - 05	0.000	0.060	0.035	0.058	0.000	0.034	0.098	0.000	7.8	####	0.005	0.886	0.000	0.001	0.005	0.131	0.066	0.171
110	Jt 10 - Py 3 - 06	0.001	0.058	0.556	0.050	0.000	0.000	0.000	0.000	1.3	####	0.018	0.003	0.000	0.000	0.005	0.286	0.065	0.248
111	Jt 10 - Py 3 - 07	0.001	0.052	1.9	0.266	0.000	0.000	0.000	0.000	4.6	####	0.003	2.0	0.000	0.000	0.014	1.1	0.444	1.1
112	Jt 10 - Py 3 - 08	0.001	0.059	0.036	0.570	0.000	0.000	0.002	0.000	0.087	####	0.017	0.908	0.000	0.000	0.006	1.3	0.293	1.2
113	Jt 10 - Py 3 - 09	0.001	0.056	0.025	0.043	0.000	0.000	0.000	0.000	1.8	####	0.003	0.002	0.000	0.000	0.007	0.002	0.001	0.006
114	Jt 10 - Py 3 - 10	0.001	0.054	0.384	0.105	0.000	0.000	0.000	0.000	3.2	####	0.003	0.604	0.000	0.004	0.010	0.355	0.201	0.455
115	Jt 10 - Py 3 - 11	0.137	0.532	1.1	5.2	0.000	0.000	0.000	0.000	12	####	0.007	8.6	0.000	0.001	0.029	17	3.9	14

#	Pyrite	^{115}In	^{118}Sn	^{121}Sb	^{125}Te	^{178}Hf	^{181}Ta	^{182}W	^{193}Ir	^{195}Pt	^{197}Au	^{205}Tl	^{209}Bi	^{232}Th	^{238}U	^{204}Pb	^{206}Pb	^{207}Pb	^{208}Pb
116	Jt 10 - Py 3 - 12	0.185	0.239	0.640	4.8	0.000	0.000	0.000	0.000	1.2	####	0.095	8.7	0.022	0.111	0.021	9.8	2.0	5.1
117	Jt 10 - Py 4 - 01	0.002	0.205	0.791	1.4	0.000	0.000	0.000	0.000	0.001	2.6	0.001	5.1	0.000	0.000	0.007	1.3	0.448	1.0
118	Jt 10 - Py 4 - 02	0.001	0.058	0.178	0.872	0.000	0.000	0.000	0.000	0.000	####	0.006	1.4	0.000	0.000	0.007	1.9	0.362	1.6
119	Jt 10 - Py 4 - 03	0.025	0.131	0.275	0.387	0.000	0.000	0.000	0.000	0.013	####	0.003	1.4	0.000	0.000	0.006	0.751	0.257	0.781
120	Jt 10 - Py 4 - 04	0.001	0.058	0.028	0.060	0.000	0.000	0.000	0.000	5.7	####	0.004	0.002	0.000	0.000	0.006	0.001	0.002	0.001
121	Jt 10 - Py 4 - 05	0.532	2.4	1.5	1.7	0.000	0.000	0.000	0.000	0.180	####	0.002	10	0.002	0.002	0.089	3.1	1.9	4.7
122	Jt 10 - Py 4 - 06	0.001	0.047	0.029	0.083	0.000	0.000	0.004	0.000	0.056	####	0.002	0.030	0.001	0.003	0.006	0.022	0.011	0.035
123	Jt 10 - Py 4 - 07	0.001	0.053	0.085	0.384	0.000	0.000	0.000	0.000	3.7	####	0.010	0.347	0.000	0.000	0.006	5.3	0.996	2.7
124	Jt 10 - Py 4 - 08	0.001	0.054	0.030	0.128	0.000	0.000	0.002	0.000	0.290	####	0.003	0.177	0.000	0.001	0.007	0.050	0.016	0.050
125	Jt 10 - Py 4 - 09	0.326	0.724	0.477	0.825	0.000	0.001	0.004	0.000	0.074	####	0.004	4.4	0.003	0.030	0.025	1.5	0.697	1.7
126	Jt 10 - Py 5 - 01	0.002	0.052	0.031	0.155	0.000	0.001	0.018	0.000	0.012	####	0.002	0.094	0.004	0.008	0.008	0.039	0.023	0.062
127	Jt 10 - Py 5 - 02	0.002	0.054	0.029	0.048	0.000	0.000	0.006	0.000	0.005	####	0.002	0.026	0.005	0.011	0.009	0.019	0.007	0.029
128	Jt 10 - Py 5 - 03	0.000	0.048	0.030	0.078	0.000	0.002	0.008	0.000	0.010	####	0.002	0.003	0.000	0.002	0.007	0.011	0.008	0.023
129	Jt 10 - Py 5 - 04	0.000	0.055	0.091	1.8	0.000	0.000	0.000	0.000	0.002	####	0.001	0.503	0.000	0.001	0.008	0.024	0.015	0.034
130	Jt 10 - Py 5 - 05	0.000	0.051	0.025	0.443	0.000	0.000	0.009	0.000	0.002	####	0.004	0.012	0.004	0.015	0.009	0.012	0.007	0.013
131	Jt 10 - Py 5 - 06	0.001	0.050	0.109	4.4	0.000	0.003	0.003	0.000	0.005	####	0.005	0.065	0.001	0.016	0.006	0.143	0.048	0.125
132	Jt 10 - Py 5 - 07	0.109	0.314	0.685	0.301	0.000	0.000	0.008	0.000	0.029	####	0.001	1.7	0.005	0.005	0.007	0.770	0.385	0.819
133	Jt 10 - Py 5 - 08	0.202	0.565	0.774	2.3	0.000	0.001	0.003	0.000	0.158	####	0.003	7.3	0.002	0.025	0.014	1.4	0.567	1.2
134	Jt 10 - Py 5 - 09	0.015	0.062	0.594	1.7	0.000	0.001	0.008	0.000	0.010	####	0.003	4.6	0.001	0.047	0.008	0.387	0.194	0.417
135	Jt 10 - Py 5 - 10	0.002	0.047	0.316	1.6	0.000	0.001	0.017	0.000	4.2	####	0.007	2.3	0.009	0.005	0.006	0.303	0.091	0.310
136	Jt 10 - Py 6 edge - 01	0.000	0.048	0.056	0.580	0.000	0.000	0.002	0.000	0.440	####	0.003	0.288	0.001	0.013	0.007	0.023	0.014	0.032
137	Jt 10 - Py 6 edge - 02	0.262	0.242	0.193	0.521	0.000	0.001	0.000	0.000	1.3	####	0.003	2.5	0.003	0.011	0.010	4.0	0.930	2.8
138	Jt 10 - Py 6 edge - 03	0.000	0.040	0.250	0.099	0.000	0.000	0.009	0.000	0.888	####	0.005	0.129	0.032	0.700	0.008	0.430	0.126	0.275
139	Jt 10 - Py 6 cent - 01	0.000	0.046	0.026	0.074	0.000	0.001	0.002	0.000	6.4	####	0.003	0.020	0.006	0.015	0.005	0.094	0.058	0.112
140	Jt 10 - Py 6 cent - 02	0.001	0.050	1.3	0.305	0.000	0.001	0.002	0.000	2.8	####	0.004	6.5	0.003	0.011	0.033	1.1	0.651	1.3
141	Jt 10 - Py 6 cent - 03	0.005	0.179	1.1	0.094	0.000	0.000	0.004	0.000	0.138	####	0.002	1.6	0.002	0.009	0.143	5.5	3.4	7.1
142	Jt 10 - Py 6 cent - 04	0.000	0.040	0.035	0.055	0.000	0.000	0.000	0.000	1.4	####	0.004	0.055	0.000	0.000	0.006	0.094	0.030	0.077
143	Jt 10 - Py 6 cent - 05	0.001	0.040	0.029	0.057	0.000	0.001	0.002	0.000	0.323	####	0.002	0.015	0.002	0.007	0.005	0.024	0.010	0.024
144	Jt 10 - Py 6 cent - 06	0.001	0.043	0.075	0.071	0.002	0.000	0.000	0.000	0.550	####	0.002	0.209	0.001	0.010	0.006	0.396	0.232	0.480
145	Jt 10 - Py 6 cent - 07	0.001	0.064	0.691	1.3	0.003	0.000	0.000	0.000	0.437	####	0.015	6.7	0.006	0.040	0.008	1.0	0.386	0.945
146	Jt 10 - Py 6 edge - 04	0.002	0.042	0.209	0.539	0.000	0.000	0.004	0.000	1.3	####	0.012	1.1	0.000	0.008	0.007	5.2	0.963	2.6
147	Jt 10 - Py 6 edge - 05	0.001	0.043	1.5	0.408	0.000	0.000	0.000	0.000	13	####	0.041	0.653	0.001	0.010	0.014	4.1	1.0	3.6
148	Jt 10 - Py 6 edge - 06	0.000	0.046	0.737	0.101	0.000	0.001	0.000	0.000	7.4	####	0.004	1.5	0.001	0.005	0.010	0.390	0.247	0.558
149	Jt 10 - Py 6 edge - 07	0.057	0.114	0.220	0.589	0.000	0.000	0.005	0.000	1.9	####	0.003	0.706	0.001	0.005	0.007	0.028	0.015	0.041
150	Jt 10 - Py 6 edge - 08	0.045	0.090	0.185	0.466	0.000	0.000	0.002	0.000	0.408	####	0.008	1.2	0.003	0.021	0.015	5.3	1.2	4.3
151	Jt 10 - Py 7 - 01	0.000	0.041	0.019	0.043	0.000	0.000	0.002	0.000	0.031	####	0.005	0.015	0.000	0.000	0.006	0.010	0.003	0.007
152	Jt 10 - Py 7 - 02	0.000	0.043	0.024	0.053	0.000	0.000	0.002	0.000	2.3	####	0.003	0.017	0.002	0.013	0.007	0.009	0.005	0.014
153	Jt 10 - Py 7 - 03	0.156	0.546	0.116	0.131	0.000	0.000	0.000	0.000	0.080	####	0.002	0.921	0.004	0.014	0.006	0.258	0.141	0.288
154	Jt 10 - Py 7 - 04	1.0	2.9	0.974	2.8	0.049	0.007	0.012	0.000	0.255	####	0.099	12	0.044	2.9	0.063	18	3.9	9.3
155	Jt 10 - Py 7 - 05	0.197	0.209	0.540	6.0	0.000	0.000	0.004	0.000	2.4	####	0.004	16	0.001	0.018	0.024	9.4	2.2	7.2
156	Jt 10 - Py 7 - 06	0.485	1.6	0.991	6.9	0.000	0.000	0.013	0.000	2.0	####	0.004	18	0.002	0.107	0.047	9.8	2.7	8.2
157	Jt 10 - Py 7 - 07	0.008	0.048	0.054	0.513	0.000	0.000	0.000	0.000	0.045	####	0.007	2.1	0.028	1.4	0.007	6.7	1.0	2.2
158	Jt 10 - Py 8 - 01	0.000	0.041	0.076	1.2	0.000	0.000	0.002	0.000	0.038	####	0.003	0.954	0.006	0.022	0.006	0.483	0.138	0.433
159	Jt 10 - Py 8 - 02	0.006	0.044	0.498	1.1	0.000	0.002	0.000	0.000	3.3	####	0.005	2.7	0.001	0.007	0.200	20	6.9	19
160	Jt 10 - Py 8 - 03	1.1	0.692	2.0	4.8	0.000	0.000	0.000	0.000	0.101	####	0.037	17	0.003	0.134	0.051	18	4.1	12
161	Jt 10 - Py 8 - 04	0.008	0.046	0.483	0.315	0.000	0.000	0.000	0.000	0.016	####	0.017	1.2	0.000	0.021	0.007	0.799	0.318	0.829
162	Jt 10 - Py 8 - 05	0.134	0.256	0.065	0.325	0.000	0.000	0.000	0.000	0.060	####	0.004	1.4	0.000	0.005	0.007	1.6	0.409	1.1
163	Jt 10 - Py 8 - 06	0.044	0.197	1.0	2.8	0.000	0.000	0.000	0.000	0.050	####	0.002	6.6	0.000	0.000	0.065	1.9	1.1	3.1
164	Jt 10 - Py 8 - 07	0.000	0.036	0.106	0.111	0.000	0.001	0.011	0.000	0.023	####	0.009	0.095	0.000	0.000	0.005	0.115	0.054	0.131
165	Jt 10 - Py 8 - 08	0.293	0.161	0.682	2.4	0.000	0.000	0.002	0.000	0.301	####	0.005	7.8	0.001	0.018	0.014	3.1	0.785	2.2
166	Jt 10 - Py 8 - 09	0.004	0.039	0.266	0.971	0.000	0.000	0.002	0.000	2.6	####	0.005	2.3	0.004	0.136	0.031	3.6	1.3	3.5
167	Jt 10 - Py 8 - 10	0.001	0.048	0.019	0.098	0.000	0.000	0.004	0.000	0.525	####	0.005	0.021	0.001	0.007	0.006	0.015	0.008	0.022
168	Jt 10 - Py 8 - 11	0.000	0.035	0.160	0.079	0.000	0.013	0.038	0.000	1.9	####	0.003	0.506	0.002	0.003	0.006	0.089	0.028	0.066
169	Jt 10 - Py 8 - 12	0.043	0.046	0.254	3.3	0.000	0.001	0.007	0.000	1.7	####	0.025	7.1	0.004	0.128	0.010	4.0	0.857	2.6
170	Jt 10 - Py 9 edge - 01	0.000	0.043	0.688	1.2	0.000	0.000	0.000	0.000	0.010	####	0.004	2.4	0.000	0.001	0.006	0.965	0.399	1.0
171	Jt 10 - Py 9 edge - 02	0.000	0.040	0.019	0.059	0.000	0.000	0.000	0.000	0.019	####	0.002	0.068	0.000	0.000	0.007	0.003	0.004	0.003
172	Jt 10 - Py 9 edge - 03	0.000	0.038	0.049	0.181	0.000	0.000	0.000	0.000	1.5	####	0.002	0.178	0.000	0.000	0.006	0.149	0.062	0.167
173	Jt 10 - Py 9 cent - 01	0.272	15	0.114	0.141	0.011	0.397	0.584	0.000	0.027	####	0.006	3.0	46	6.9	0.006	6.4	1.0	5.2
174	Jt 10 - Py 9 cent - 02	0.008	0.131	0.392	0.628	0.003	0.000	0.081	0.000	0.027	####	0.006	1.6	0.157	0.126	0.007	2.7	0.625	2.4
175	Jt 10 - Py 9 cent - 03	0.003	0.035	0.329	0.105	0.000	0.000	0.004	0.000	7.3	####	0.012	0.445	0.030	0.008	0.007	2.9	0.728	2.6
176	Jt 10 - Py 9 cent - 04	0.000	0.039	1.8	2.0	0.000	0.001	0.002	0.000	0.554	####	0.020	9.6	0.019	0.012	0.016	3.3	1.0	3.1

#	Pyrite	^{115}In	^{118}Sn	^{121}Sb	^{125}Te	^{178}Hf	^{181}Ta	^{182}W	^{193}Ir	^{195}Pt	^{197}Au	^{205}Tl	^{209}Bi	^{232}Th	^{238}U	^{204}Pb	^{206}Pb	^{207}Pb	^{208}Pb
177	Jt 10 - Py 9 cent - 05	0.001	0.037	0.286	3.0	0.000	0.000	0.006	0.000	0.003	####	0.003	2.1	0.010	0.008	0.051	4.4	1.6	4.4
178	Jt 10 - Py 9 cent - 06	0.001	0.038	2.8	1.6	0.000	0.000	0.000	0.000	0.001	####	0.006	8.7	0.006	0.004	0.032	3.5	1.3	3.6
179	Jt 10 - Py 9 cent - 07	0.001	0.222	2.6	4.0	0.003	1.2	0.208	0.000	0.002	####	0.055	4.3	0.028	0.029	0.038	3.9	1.7	4.4
180	Jt 10 - Py 9 cent - 08	0.002	0.042	1.8	4.6	0.000	0.001	0.006	0.000	0.000	####	0.013	5.0	0.003	0.005	0.021	2.3	0.887	2.6
181	Jt 10 - Py 9 edge - 04	0.002	0.040	0.519	0.498	0.003	0.005	0.008	0.000	0.000	####	0.021	1.2	0.004	0.008	0.007	0.930	0.361	0.943
182	Jt 10 - Py 9 edge - 05	0.001	0.041	1.1	2.0	0.000	0.001	0.002	0.000	0.018	####	0.233	3.9	0.003	0.022	0.019	6.1	1.5	5.4
183	Jt 10 - Py 9 edge - 06	0.000	0.045	2.3	0.559	0.000	0.000	0.000	0.000	0.005	####	0.095	3.1	0.000	0.006	0.021	1.7	0.619	1.7
184	Jt 10 - Py 9 edge - 07	0.014	0.061	1.7	2.1	0.000	0.001	0.008	0.000	0.574	####	0.006	4.1	0.003	0.024	0.014	1.4	0.532	1.3

#	Pyrrhotite	^{115}In	^{118}Sn	^{121}Sb	^{125}Te	^{178}Hf	^{181}Ta	^{182}W	^{193}Ir	^{195}Pt	^{197}Au	^{205}Tl	^{209}Bi	^{232}Th	^{238}U	^{204}Pb	^{206}Pb	^{207}Pb	^{208}Pb
1	Jt 4 - Pyh 1 - 01	0.000	0.052	0.019	0.152	0.000	0.000	0.006	0.000	0.000	####	0.016	0.032	0.001	0.001	0.009	0.253	0.076	0.156
2	Jt 4 - Pyh 1 - 02	0.000	0.053	0.028	0.078	0.009	0.001	0.132	0.000	0.000	####	0.026	0.339	0.002	0.218	0.011	2.5	0.547	1.3
3	Jt 4 - Pyh 1 - 03	0.000	0.060	0.028	0.094	0.000	0.000	0.012	0.003	0.000	####	0.006	0.098	0.002	0.008	0.008	0.547	0.138	0.328
4	Jt 4 - Pyh 1 - 04	0.000	0.051	0.018	0.086	0.000	0.000	0.013	0.000	0.000	####	0.004	0.070	0.000	0.000	0.008	0.557	0.158	0.305
5	Jt 4 - Pyh 1 - 05	0.001	0.047	0.026	0.191	0.000	0.000	0.004	0.000	0.000	####	0.003	0.247	0.002	0.008	0.011	2.7	0.651	1.4
6	Jt 4 - Pyh 1 - 06	0.056	0.231	0.161	0.411	0.000	0.004	0.014	0.000	0.002	####	0.630	0.648	0.001	0.196	0.051	10	2.4	5.0
7	Jt 4 - Pyh 1 - 07	0.000	0.040	0.029	0.284	0.000	0.000	0.004	0.000	0.000	####	0.007	0.435	0.000	0.023	0.030	5.9	1.6	3.2
8	Jt 4 - Pyh 1 - 08	0.000	0.055	0.016	0.237	0.000	0.000	0.000	0.000	0.002	####	0.004	0.101	0.012	0.002	0.017	0.646	0.156	0.351
9	Jt 4 - Pyh 1 - 09	0.001	0.055	0.015	0.148	0.000	0.000	0.012	0.000	0.000	####	0.007	0.269	0.005	0.007	0.025	3.9	0.991	2.3
10	Jt 4 - Pyh 1 - 10	0.018	0.057	0.025	0.155	0.000	0.000	0.032	0.000	0.000	####	0.008	0.024	0.006	0.010	0.010	0.077	0.032	0.080
11	Jt 4 - Pyh 1 - 11	0.086	0.415	0.288	0.571	0.005	0.008	1.5	0.000	0.002	####	3.9	0.854	0.024	2.5	0.139	40	9.2	19
12	Jt 4 - Pyh 1 - 12	0.000	0.053	0.027	0.089	0.000	0.000	0.000	0.001	0.002	####	0.027	0.232	0.000	0.004	0.009	0.911	0.229	0.483
13	Jt 4 - Pyh 1 - 13	0.001	0.047	0.017	0.113	0.000	0.000	0.000	0.000	0.001	####	0.007	0.045	0.001	0.020	0.012	0.519	0.139	0.257
14	Jt 4 - Pyh 2 - 01	0.001	0.044	0.028	0.140	0.004	0.000	0.027	0.000	0.001	####	0.016	0.170	0.004	0.055	0.009	1.9	0.488	0.966
15	Jt 4 - Pyh 2 - 02	0.001	0.043	0.041	0.223	0.000	0.000	0.008	0.000	0.001	####	0.119	1.2	0.002	0.031	0.044	9.1	2.3	4.7
16	Jt 4 - Pyh 2 - 03	0.002	0.049	0.016	0.151	0.063	0.001	0.000	0.000	0.002	####	0.091	0.136	0.031	0.135	0.011	0.653	0.179	0.363
17	Jt 4 - Pyh 2 - 04	0.001	0.039	0.017	0.129	0.000	0.000	0.005	0.000	0.002	####	0.002	0.078	0.000	0.001	0.008	0.365	0.100	0.170
18	Jt 4 - Pyh 2 - 05	0.001	0.045	0.017	0.306	0.000	0.000	0.025	0.000	0.002	####	0.035	0.538	0.001	0.002	0.025	4.8	1.2	2.5
19	Jt 4 - Pyh 2 - 06	0.000	0.045	0.022	0.112	0.000	0.000	0.000	0.000	0.003	####	0.021	0.098	0.001	0.075	0.008	0.503	0.134	0.292
20	Jt 4 - Pyh 2 - 07	0.000	0.051	0.005	0.105	0.000	0.000	0.013	0.000	0.001	####	0.003	0.264	0.002	0.005	0.009	0.731	0.214	0.412
21	Jt 4 - Pyh 2 - 08	0.001	0.058	0.006	0.130	0.000	0.000	0.013	0.000	0.001	####	0.104	0.260	0.006	0.018	0.007	1.3	0.338	0.705
22	Jt 4 - Pyh 2 - 09	0.002	0.051	0.013	0.226	0.000	0.000	0.032	0.000	0.001	####	0.002	0.931	0.001	0.002	0.053	9.1	2.4	4.8
23	Jt 4 - Pyh 2 - 10	0.000	0.045	0.014	0.183	0.000	0.000	0.011	0.000	0.001	####	0.005	0.309	0.000	0.000	0.025	3.3	0.861	1.9
24	Jt 4 - Pyh 2 - 11	0.057	0.053	0.014	0.079	0.000	0.000	0.025	0.000	0.001	####	0.296	0.240	0.003	0.026	0.008	2.6	0.602	1.3
25	Jt 4 - Pyh 2 - 12	0.000	0.053	0.007	0.195	0.000	0.000	0.000	0.000	0.003	####	0.005	0.466	0.002	0.005	0.026	3.7	0.953	2.0
26	Jt 4 - Pyh 2 - 13	0.015	0.100	0.026	0.369	0.000	0.000	0.049	0.001	0.002	####	0.985	0.477	0.020	0.259	0.027	8.4	2.0	4.2
27	Jt 4 - Pyh 2 - 14	0.001	0.037	0.017	0.228	0.000	0.000	0.008	0.000	0.002	####	0.060	0.213	0.001	0.001	0.016	2.8	0.689	1.3
28	Jt 4 - Pyh 2 - 15	0.148	0.047	0.036	0.260	0.000	0.002	0.023	0.000	0.002	####	0.035	1.3	0.005	0.004	0.034	7.7	2.1	4.3
29	Jt 4 - Pyh 2 - 16	0.002	0.039	0.011	0.164	0.003	0.000	0.005	0.000	0.003	####	0.005	0.499	0.012	0.003	0.019	4.6	1.2	2.5
30	Jt 4 - Pyh 2 - 17	0.001	0.047	0.021	0.116	0.000	0.000	0.005	0.001	0.000	####	0.004	0.422	0.000	0.000	0.009	2.8	0.752	1.5
31	Jt 4 - Pyh 3 - 01	0.005	0.057	0.044	0.168	0.060	0.000	0.072	0.000	0.001	####	0.209	0.156	0.021	0.023	0.012	2.2	0.565	1.2
32	Jt 4 - Pyh 3 - 02	0.000	0.050	0.021	0.192	0.000	0.000	0.004	0.000	0.001	####	0.009	0.137	0.002	0.000	0.010	0.820	0.195	0.478
33	Jt 4 - Pyh 3 - 03	0.000	0.056	0.018	0.188	0.000	0.000	0.012	0.000	0.002	####	0.007	0.069	0.007	0.006	0.009	0.512	0.144	0.289
34	Jt 4 - Pyh 3 - 04	0.000	0.076	0.055	0.157	0.006	0.000	0.004	0.000	0.002	####	0.177	0.708	0.000	0.034	0.020	6.7	1.7	3.7
35	Jt 4 - Pyh 3 - 05	0.005	0.057	0.021	0.120	0.000	0.000	0.009	0.000	0.002	####	0.009	0.241	0.002	0.000	0.011	1.8	0.463	0.956
36	Jt 4 - Pyh 3 - 06	0.000	0.069	0.017	0.071	0.000	0.000	0.008	0.000	0.002	####	0.005	0.192	0.005	0.000	0.012	0.776	0.239	0.470
37	Jt 4 - Pyh 3 - 07	0.000	0.063	0.031	0.102	0.000	0.000	0.000	0.001	0.001	####	0.005	0.088	0.000	0.000	0.013	0.388	0.098	0.220
38	Jt 4 - Pyh 4 - 01	0.000	0.066	0.017	0.085	0.000	0.000	0.031	0.000	0.001	####	0.006	0.758	0.000	0.001	0.021	5.5	1.4	3.1
39	Jt 4 - Pyh 4 - 02	0.000	0.056	0.018	0.251	0.000	0.003	0.012	0.001	0.002	####	0.007	0.037	0.001	0.001	0.009	0.102	0.028	0.060
40	Jt 4 - Pyh 4 - 03	0.000	0.070	0.029	0.184	0.000	0.000	0.008	0.001	0.001	####	0.005	0.286	0.000	0.000	0.011	0.884	0.269	0.507
41	Jt 4 - Pyh 4 - 04	0.000	0.064	0.026	0.236	0.000	0.000	0.009	0.000	0.001	####	0.006	0.126	0.004	0.000	0.008	0.701	0.200	0.388
42	Jt 4 - Pyh 4 - 05	0.004	0.098	0.171	0.409	0.015	0.000	0.038	0.000	0.002	####	2.8	0.676	0.008	0.612	0.061	11	2.5	5.1
43	Jt 4 - Pyh 4 - 06	0.001	0.064	0.043	0.098	0.000	0.004	0.014	0.001	0.071	####	0.711	0.374	0.004	0.057	0.024	4.6	1.2	2.6
44	Jt 4 - Pyh 4 - 07	0.000	0.057	0.024	0.130	0.000	0.000	0.023	0.000	0.002	####	0.009	0.135	0.001	0.003	0.010	0.626	0.158	0.349
45	Jt 4 - Pyh 5 - 01	0.000	0.070	0.027	0.091	0.003	0.000	0.013	0.000	0.001	####	0.196	0.053	0.018	0.426	0.010	1.3	0.330	0.671
46	Jt 4 - Pyh 5 - 02	0.004	0.071	0.045	0.197	0.006	0.000	0.159	0.000	0.001	####	0.346	0.107	0.023	0.038	0.011	1.4	0.415	0.843
47	Jt 4 - Pyh 5 - 03	0.246	0.097	0.074	0.356	0.013	0.000	0.013	0.000	0.001	####	0.091	1.6	0.003	0.078	0.106	24	6.0	13
48	Jt 4 - Pyh 5 - 04	0.001	0.065	0.038	0.347	0.000	0.003	0.302	0.000	0.001	####	0.131	0.335	0.047	0.529	0.018	4.2	1.1	2.3
49	Jt 4 - Pyh 5 - 05	0.000	0.057	0.023	0.066	0.003	0.000	0.011	0.000	0.001	####	0.006	0.069	0.000	0.000	0.012	0.585	0.159	0.293

#	Pyrrhotite	^{115}In	^{118}Sn	^{121}Sb	^{125}Te	^{178}Hf	^{181}Ta	^{182}W	^{193}Ir	^{195}Pt	^{197}Au	^{205}Tl	^{209}Bi	^{232}Th	^{238}U	^{204}Pb	^{206}Pb	^{207}Pb	^{208}Pb
50	Jt 4 - Pyh 5 - 06	0.001	0.055	0.027	0.082	0.000	0.000	0.013	0.000	0.001	####	0.006	0.137	0.001	0.000	0.008	0.826	0.218	0.454
51	Jt 4 - Pyh 5 - 07	0.000	0.056	0.032	0.075	0.000	0.000	0.003	0.000	0.001	####	0.003	0.139	0.001	0.001	0.009	0.719	0.190	0.419
52	Jt 4 - Pyh 5 - 08	0.000	0.054	0.015	0.141	0.000	0.000	0.032	0.000	0.001	####	0.026	0.148	0.002	0.110	0.009	1.9	0.523	1.0
53	Jt 4 - Pyh 5 - 09	0.000	0.022	0.015	0.130	0.000	0.000	0.001	0.000	0.002	####	0.002	0.001	0.000	0.000	0.005	0.020	0.004	0.007
54	Jt 4 - Pyh 5 - 10	0.000	0.040	0.021	0.087	0.000	0.000	0.000	0.000	0.002	####	0.004	0.274	0.002	0.002	0.013	2.9	0.723	1.5
55	Jt 4 - Pyh 5 - 11	0.001	0.047	0.031	0.190	0.000	0.000	0.008	0.000	0.002	####	0.012	0.564	0.001	0.001	0.038	7.6	2.0	4.1
56	Jt 4 - Pyh 5 - 12	0.001	0.050	0.019	0.137	0.007	0.053	0.059	0.000	0.001	####	0.007	0.050	0.000	0.017	0.009	0.287	0.071	0.134
57	Jt 4 - Pyh 6 - 01	0.000	0.049	0.025	0.132	0.003	0.000	0.013	0.000	0.001	####	0.033	0.066	0.001	0.010	0.009	0.431	0.125	0.231
58	Jt 4 - Pyh 6 - 02	0.000	0.051	0.020	0.137	0.000	0.000	0.011	0.000	0.003	####	0.084	0.356	0.000	0.008	0.015	3.4	0.906	1.9
59	Jt 4 - Pyh 6 - 03	0.000	0.057	0.015	0.183	0.000	0.000	0.015	0.000	0.001	####	0.002	0.019	0.002	0.002	0.008	0.077	0.026	0.055
60	Jt 4 - Pyh 6 - 04	0.000	0.049	0.018	0.141	0.000	0.000	0.095	0.000	0.001	####	0.073	0.028	0.001	0.015	0.010	0.083	0.031	0.072
61	Jt 4 - Pyh 6 - 05	0.142	0.207	0.016	0.195	0.000	0.000	0.010	0.000	0.001	####	0.557	0.238	0.001	0.061	0.014	2.2	0.553	1.2

#	Chalcopyrite	^{115}In	^{118}Sn	^{121}Sb	^{125}Te	^{178}Hf	^{181}Ta	^{182}W	^{193}Ir	^{195}Pt	^{197}Au	^{205}Tl	^{209}Bi	^{232}Th	^{238}U	^{204}Pb	^{206}Pb	^{207}Pb	^{208}Pb
1	Jt 4 - Ccp 1 - 01	3.7	0.908	0.022	0.286	0.000	0.000	0.012	0.000	0.002	####	0.177	0.204	0.005	0.170	0.030	3.9	1.0	2.0
2	Jt 4 - Ccp 1 - 02	3.4	0.631	0.060	0.161	0.000	0.001	0.036	0.000	0.002	####	0.345	0.311	0.009	0.071	0.037	9.7	2.2	4.5
3	Jt 4 - Ccp 1 - 03	3.8	0.965	0.045	0.517	0.006	0.001	0.033	0.000	0.001	####	0.689	0.211	0.016	0.122	0.037	8.6	2.0	4.4
4	Jt 4 - Ccp 1 - 04	3.4	0.504	0.024	0.166	0.000	0.001	0.028	0.000	0.001	####	0.008	0.245	0.005	0.005	0.008	2.9	0.700	1.5
5	Jt 4 - Ccp 1 - 05	3.5	0.926	0.018	0.260	0.000	0.001	0.063	0.000	0.001	####	0.003	14	0.005	0.001	0.007	1.3	0.295	0.684
6	Jt 4 - Ccp 2 - 01	3.3	1.0	0.071	0.108	0.000	0.002	0.060	0.000	0.001	####	0.027	0.240	0.012	0.010	0.008	1.0	0.280	0.600
7	Jt 4 - Ccp 2 - 02	3.5	1.2	0.035	0.326	0.000	0.000	0.012	0.000	0.001	####	0.004	0.087	0.010	0.005	0.008	0.900	0.222	0.509
8	Jt 4 - Ccp 2 - 03	3.3	0.841	0.021	0.333	0.007	0.000	0.031	0.000	0.002	####	0.024	0.165	0.004	0.000	0.011	2.2	0.601	1.3
9	Jt 4 - Ccp 2 - 04	3.3	0.759	0.035	0.142	0.620	0.000	0.016	0.000	0.002	####	0.007	0.173	0.017	0.248	0.015	3.9	0.858	1.8
10	Jt 4 - Ccp 2 - 05	3.2	0.856	0.021	0.214	0.000	0.000	0.043	0.001	0.006	####	0.009	0.304	0.007	0.028	0.020	2.6	0.647	1.6
11	Jt 4 - Ccp 2 - 06	3.1	0.610	0.023	0.370	0.000	0.004	0.016	0.001	0.004	####	0.164	0.449	0.036	0.016	0.053	6.7	1.8	4.0
12	Jt 4 - Ccp 2 - 07	3.9	1.9	0.031	0.797	0.093	0.003	0.255	0.001	0.001	####	0.093	0.165	0.477	1.7	0.014	2.2	0.642	1.1
13	Jt 4 - Ccp 2 - 08	3.9	0.927	0.021	0.129	0.000	0.000	0.024	0.001	0.001	####	0.052	0.130	0.021	0.050	0.012	1.6	0.416	0.853
14	Jt 4 - Ccp 2 - 09	3.6	0.621	0.085	0.950	0.751	0.017	0.291	0.001	0.010	####	0.098	0.349	0.180	0.417	0.034	9.7	2.3	4.8
15	Jt 4 - Ccp 2 - 10	3.7	1.2	0.032	0.472	0.015	0.010	0.053	0.001	0.001	####	0.076	0.103	0.202	0.046	0.011	2.4	0.619	1.4
16	Jt 4 - Ccp 2 - 11	4.1	1.8	0.042	0.497	0.110	0.003	0.085	0.001	0.031	####	0.165	0.298	1.2	3.1	0.019	6.2	1.6	2.6
17	Jt 4 - Ccp 2 - 12	4.1	1.6	0.034	0.412	0.074	0.000	0.000	0.001	0.025	####	0.094	0.091	0.001	0.086	0.010	1.4	0.349	0.721
18	Jt 4 - Ccp 3 - 01	1.8	0.381	0.233	0.590	0.018	0.012	0.055	0.001	0.007	####	1.2	0.753	0.007	0.288	0.074	17	4.0	8.5
19	Jt 4 - Ccp 3 - 02	3.0	0.754	0.134	0.420	0.014	0.000	0.076	0.001	0.016	####	0.730	0.386	0.001	0.224	0.026	6.7	1.6	3.3
20	Jt 4 - Ccp 3 - 03	2.6	0.522	0.072	0.716	0.012	0.004	0.002	0.000	0.003	####	0.561	0.838	0.003	0.033	0.091	23	5.6	12
21	Jt 4 - Ccp 3 - 04	4.3	1.2	0.134	0.123	0.027	0.008	0.018	0.000	0.003	####	1.2	0.322	0.002	0.266	0.057	14	3.3	7.1
22	Jt 4 - Ccp 3 - 05	2.4	0.683	0.088	0.147	0.010	0.002	0.010	0.000	0.000	####	0.769	0.100	0.000	0.029	0.020	4.8	1.2	2.5
23	Jt 4 - Ccp 3 - 06	2.1	0.548	0.116	0.249	0.033	0.000	0.181	0.000	0.002	####	0.394	0.233	0.012	0.095	0.040	9.0	2.3	4.4
24	Jt 10 - Ccp 1 - 01	14	5.7	0.035	0.156	0.000	0.001	0.004	0.000	0.017	####	0.048	0.137	0.055	0.766	0.009	4.0	0.678	1.7
25	Jt 10 - Ccp 1 - 02	14	5.4	0.047	0.106	0.000	0.000	0.007	0.000	0.009	####	0.069	0.171	0.079	0.814	0.007	3.8	0.664	1.7
26	Jt 10 - Ccp 1 - 03	13	4.8	0.159	0.872	0.000	0.008	0.000	0.000	0.021	####	0.197	2.6	0.065	0.802	0.018	15	2.4	5.5
27	Jt 10 - Ccp 1 - 04	13	6.1	0.020	0.069	0.000	0.002	0.002	0.000	0.000	####	0.015	0.144	0.022	0.196	0.006	2.0	0.396	1.0
28	Jt 10 - Ccp 1 - 05	14	5.1	0.028	0.197	0.000	0.003	0.003	0.000	0.005	####	0.061	0.389	0.221	0.693	0.014	16	2.6	5.7
29	Jt 10 - Ccp 1 - 06	14	4.3	0.053	0.106	0.000	0.001	0.000	0.000	0.004	####	0.170	0.362	0.133	1.8	0.007	9.4	1.4	3.5
30	Jt 10 - Ccp 1 - 07	14	4.4	0.033	0.109	0.000	0.000	0.007	0.000	0.023	####	0.032	0.316	0.088	0.773	0.006	7.3	1.4	3.6
31	Jt 10 - Ccp 2 - 01	14	6.4	0.021	0.086	0.007	0.000	0.000	0.000	0.002	####	0.011	0.121	0.010	0.088	0.007	1.7	0.355	0.940
32	Jt 10 - Ccp 2 - 02	14	5.4	0.013	0.104	0.000	0.000	0.000	0.000	0.002	####	0.021	0.434	0.001	0.017	0.007	8.5	1.4	3.3
33	Jt 10 - Ccp 2 - 03	14	5.0	0.021	0.096	0.000	0.000	0.000	0.000	0.004	####	0.010	0.310	0.001	0.038	0.007	5.3	0.981	2.5
34	Jt 10 - Ccp 2 - 04	14	5.2	0.042	0.228	0.000	0.001	0.055	0.000	0.005	####	0.022	0.541	0.008	0.710	0.009	6.3	1.2	2.8
35	Jt 10 - Ccp 2 - 05	14	5.0	0.099	0.148	0.000	0.000	0.006	0.000	0.001	####	0.155	0.688	0.003	0.049	0.018	14	2.4	5.4
36	Jt 10 - Ccp 2 - 06	14	5.7	0.031	0.127	0.004	0.000	0.006	0.000	0.001	####	0.019	0.488	0.001	0.003	0.007	7.8	1.5	3.5
37	Jt 10 - Ccp 2 - 07	13	6.6	0.082	0.062	0.000	0.000	0.005	0.000	0.001	####	0.004	0.176	0.006	0.011	0.009	2.7	0.515	1.5
38	Jt 10 - Ccp 2 - 08	14	4.3	0.070	0.097	0.000	0.000	0.005	0.000	0.001	####	0.441	0.903	0.004	0.043	0.008	22	3.4	7.7
39	Jt 10 - Ccp 2 - 09	15	5.6	0.166	0.138	0.000	0.009	0.009	0.000	0.003	####	0.453	0.505	0.523	2.2	0.017	15	2.3	5.1
40	Jt 10 - Ccp 2 - 10	14	6.0	0.019	0.088	0.000	0.000	0.008	0.000	0.001	####	0.004	0.187	0.002	0.015	0.007	3.3	0.626	1.8
41	Jt 10 - Ccp 2 - 11	13	7.3	0.021	0.090	0.000	0.000	0.005	0.000	0.002	####	0.002	0.176	0.004	0.022	0.007	2.5	0.499	1.6
42	Jt 10 - Ccp 2 - 12	14	7.2	0.011	0.087	0.000	0.001	0.000	0.000	0.002	####	0.003	0.164	0.003	0.026	0.008	2.0	0.446	1.3
43	Jt 10 - Ccp 3 - 01	6.9	4.4	0.339	2.5	0.000	0.000	0.000	0.000	0.125	####	0.009	7.6	0.001	0.060	0.022	15	3.2	8.8
44	Jt 10 - Ccp 3 - 02	13	8.6	0.081	0.779	0.000	0.000	0.003	0.000	0.012	####	0.040	1.8	0.002	0.086	0.017	6.5	1.2	3.5
45	Jt 10 - Ccp 3 - 03	11	5.7	0.216	1.7	0.000	0.000	0.014	0.000	0.031	####	0.040	3.2	0.022	0.945	0.034	16	3.0	7.7

#	Chalcopyrite	^{115}In	^{118}Sn	^{121}Sb	^{125}Te	^{178}Hf	^{181}Ta	^{182}W	^{193}Ir	^{195}Pt	^{197}Au	^{205}Tl	^{209}Bi	^{232}Th	^{238}U	^{204}Pb	^{206}Pb	^{207}Pb	^{208}Pb
46	Jt 10 - Ccp 3 - 04	13	8.1	0.055	0.274	0.000	0.000	0.007	0.000	0.012	####	0.052	0.186	0.354	0.971	0.016	9.8	1.9	4.3
47	Jt 10 - Ccp 3 - 05	14	7.3	0.075	0.304	0.004	0.000	0.082	0.000	0.033	####	0.061	0.331	1.2	2.0	0.021	15	2.6	6.2
48	Jt 10 - Ccp 3 - 06	14	6.4	0.185	0.780	0.000	0.000	0.003	0.000	0.014	####	0.389	1.2	0.676	3.1	0.028	31	5.2	12
49	Jt 10 - Ccp 3 - 07	13	6.4	0.028	0.138	0.000	0.000	0.000	0.000	0.002	####	0.052	0.231	0.004	0.006	0.007	8.3	1.4	3.4
50	Jt 10 - Ccp 3 - 08	11	6.1	0.340	1.7	0.004	0.005	0.008	0.000	0.035	####	0.065	5.5	0.007	0.186	0.010	16	3.0	7.4
51	Jt 10 - Ccp 3 - 09	13	6.7	0.056	0.172	0.000	0.000	0.000	0.000	0.000	####	0.018	0.309	0.022	0.034	0.017	8.2	1.4	3.2
52	Jt 10 - Ccp 3 - 10	13	4.6	0.034	0.059	0.000	0.000	0.000	0.000	0.001	####	0.040	0.189	0.019	0.046	0.016	9.8	1.9	3.9
53	Jt 10 - Ccp 3 - 11	14	5.8	0.150	0.383	0.000	0.004	0.006	0.000	0.012	####	0.092	0.318	0.104	0.922	0.020	13	2.2	5.6
54	Jt 10 - Ccp 3 - 12	13	4.2	0.055	0.210	0.000	0.001	0.003	0.000	0.000	####	0.299	0.414	0.098	0.493	0.015	20	3.2	7.1
55	Jt 10 - Ccp 3 - 13	13	5.5	0.045	0.225	0.000	0.000	0.000	0.000	0.023	####	0.188	0.378	0.035	0.586	0.025	21	3.7	8.1
56	Jt 10 - Ccp 4 - 01	13	8.0	0.080	0.253	0.000	0.004	0.010	0.000	0.002	####	0.080	0.258	0.029	3.2	0.017	11	2.0	4.2
57	Jt 10 - Ccp 4 - 02	13	9.4	0.015	0.046	0.000	0.000	0.107	0.000	0.002	####	0.002	0.116	0.030	0.113	0.013	0.805	0.218	0.549
58	Jt 10 - Ccp 4 - 03	13	10	0.040	0.166	0.015	0.000	0.045	0.000	0.003	####	0.005	0.112	0.034	0.139	0.012	1.1	0.255	0.658
59	Jt 10 - Ccp 4 - 04	14	7.2	0.030	0.226	0.000	0.000	0.021	0.000	0.003	####	0.054	0.317	0.085	0.447	0.020	14	2.8	4.9
60	Jt 10 - Ccp 4 - 05	15	8.4	0.039	0.244	0.000	0.000	0.041	0.000	0.049	####	0.053	0.233	0.021	0.146	0.021	12	2.2	4.5
61	Jt 10 - Ccp 4 - 06	14	9.1	0.228	0.210	0.000	0.006	0.059	0.000	0.035	####	0.058	1.2	0.061	0.223	0.022	9.7	1.9	4.3
62	Jt 10 - Ccp 4 - 07	14	14	0.123	0.161	0.000	0.007	0.015	0.000	0.003	####	0.010	0.156	0.024	0.136	0.016	2.2	0.413	1.3
63	Jt 10 - Ccp 4 - 08	15	15	0.043	0.181	0.000	0.000	0.032	0.000	0.003	####	0.006	0.154	0.004	0.126	0.019	2.2	0.238	0.536
64	Jt 10 - Ccp 4 - 09	15	11	0.015	0.162	0.371	0.000	0.033	0.000	0.009	####	0.029	0.351	0.034	0.323	0.022	11	1.7	4.0
65	Jt 10 - Ccp 4 - 10	14	12	0.024	0.139	0.019	0.006	0.014	0.000	0.002	####	0.009	0.110	0.036	0.098	0.015	1.2	0.274	0.679
66	Jt 10 - Ccp 4 - 11	14	10	0.084	0.298	0.000	0.000	0.015	0.000	0.027	####	0.028	0.090	0.024	0.090	0.014	1.2	0.261	0.738
67	Jt 10 - Ccp 4 - 12	13	12	0.043	0.129	0.000	0.000	0.015	0.000	0.003	####	0.031	0.109	0.024	0.137	0.018	1.5	0.286	0.782
68	Jt 10 - Ccp 4 - 13	14	16	0.383	0.378	0.000	0.031	0.001	0.000	0.120	####	0.135	0.342	0.087	9.7	0.033	25	4.1	9.3

SUPPLEMENTARY MATERIAL C

FOR CHAPTER 4 – TELESCOPED TRANSITION FROM TRELLIS TO SILICATE-MOTTLED MAGNETITE RECORDS DEEP SHEAR METAMORPHISM IN THE IOCG DEPOSIT AT JATOBÁ, CARAJÁS, BRAZIL

APPENDIX A: ANALYTICAL METHODS AND ADDITIONAL FIGURES

APPENDIX B: ADDITIONAL TABLES, EPMA AND LA-ICP-MS RESULTS

APPENDIX A FOR CHAPTER 4

Supplemental Materials – Analytical Methods

Identification and quantification of mineral species by AMICS

The advanced mineral identification and characterization system (AMICS) is combined with a Bruker Nano GmbH XFlash 660 instrument and housed at the National Institute of Criminalistics, Civil Police D.F., Brasilia, Brazil. The two thin-sections, Jt7 and Jt10, were mapped frame by frame using a SEM Hitachi High-Tech Co SU3800 equipped with tungsten filament running at 15 kV in high-vacuum mode. The working distance was kept at 10 mm, 100x magnification and a frame size of 1270 µm x 950 µm. AMICS utilizes image analysis of BSE images in which contrast represents the average atomic weight of the mineral phases to detect individual mineral grains and perform energy dispersive X-ray spectroscopy (EDS) spot analyses on each grain detected. Results are compared to a library of mineral spectra and each grain returned a match was labelled as that mineral.

Microprobe analysis of amphibole and magnetite

Quantitative mineral chemistry data for amphibole and magnetite was obtained using a JEOL JXA-8230 SuperProbe electron probe microanalyzer (EPMA) equipped with 5-spectrometer crystals LDE1, LDE2, ATP, PET/L-H and LIF-L/H. The instrument is located in the Crti Laboratory (Regional Center for Technological Development and Innovation, Federal University of Goiás, Brazil. Wavelength-dispersive (WDS) analysis was performed at an accelerating voltage of 15 kV, sample current of 20 nA, and electron beam diameter of 2-5 µm. Count times varied from 20 to 60 seconds per element. Both synthetic and natural oxides and silicate standards were used. Raw X-ray intensities for all elements were corrected using standard ZAF techniques with the JEOL software. Data reduction was performed using 'Probe for EPMA' software (e.g. Donovan et al. 2016).

Laser ablation ICP-MS trace element analysis

Trace element LA-ICP-MS spot analysis of magnetite was conducted using a RESOlution-SE 193 nm Excimer laser coupled to an Agilent 8900x quadrupole ICP-MS housed at Adelaide Microscopy, The University of Adelaide. Analyses comprised 30 s of background measurement

followed by acquisition of signal during ablation (60-70s). Laser spot diameter varied between 43 and 51 µm, depending on grain size, and operated at a pulse repetition rate of 5 Hz and fluence of 3.5J/cm^2. Forty nine isotopes were measured either in spot- or mapping mode: ^{24}Mg, ^{27}Al, ^{29}Si, ^{31}P, ^{43}Ca, ^{45}Sc, ^{49}Ti, ^{51}V, ^{53}Cr, ^{55}Mn, ^{57}Fe, ^{59}Co, ^{60}Ni, ^{65}Cu, ^{66}Zn, ^{69}Ga, ^{75}As, ^{88}Sr, ^{89}Y, ^{90}Zr, ^{93}Nb, ^{95}Mo, ^{118}Sn, ^{121}Sb, ^{137}Ba, ^{139}La, ^{140}Ce, ^{141}Pr, ^{146}Nd, ^{147}Sm, ^{153}Eu, ^{157}Gd, ^{159}Tb, ^{163}Dy, ^{165}Ho, ^{166}Er, ^{169}Tm, ^{172}Yb, ^{175}Lu, ^{178}Hf, ^{181}Ta, ^{182}W, ^{195}Pt, ^{204}Pb, ^{206}Pb, ^{207}Pb, ^{208}Pb, ^{232}Th, and ^{238}U. External reference materials NIST-612 and GSD were analyzed before, during, and after magnetite ablation for trace element quantification and instrument drift correction. ^{57}Fe was used as the internal standard element, assuming a stoichiometric magnetite composition.

Contributions from inclusions were minimised by carefully screening each depth profile, avoiding their interference from the integrated intervals, or otherwise rejecting the analysis. Ablation spots with a consistent presence of inclusions homogeneously distributed includes their contribution in the integrated signal. Reported Pb contents correspond to total Pb concentrations calculated from the individual measured abundances of ^{206}Pb, ^{207}Pb and ^{208}Pb. LA-ICP-MS trace element mapping, scaled in counts-per-second (cps) was conducted on three magnetite grains that were also subjected to nanoscale investigation. Sets of parallel, adjacent lines were ablated across rectangular grids with a laser spot size between 10 and 16 µm, depending on grain size. Compilation of the parallel line rasters were processed using 'Iolite' (Paton et al. 2011) to generated 2-D images displaying the combined background-subtracted intensities. Obtained mapped intensities were scaled individually for each element to enhance main features. Both logarithmic (10^n) and/or linear scales are used as labelled.

Nanoscale imaging and electron diffraction

Four thin polished sections of magnetite-bearing samples with representative and well distinguished features were studied at the nanoscale: magnetite with ilmenite exsolution lamellae (Jt4 and Jt6), and mottled (Jt7 and Jt10). Five S/TEM (<100 nm) foils were prepared on a FEI-Helios nanoLab Dual Focused Ion Beam - SEM platform. Each foil was studied employing HAADF STEM imaging and energy-dispersive X-ray spectrometry (EDS)-STEM mapping using an ultra-high resolution, probe-corrected, FEI Titan Themis S/TEM operated at 200 kV. The instrument is equipped with an X-FEG Schottky source and Super-X EDS geometry. Geometrically symmetric EDS detection with an effective solid angle of 0.8 sr were provided by the Super-X EDS detector. For HAADF imaging, the Fischione probe-corrected detector delivered sub-Ångstrom spatial resolution and an inner collection angle >50 mrad was used. Velox software was employed for image acquisition, including drift-corrected frame integration

package (DCFI), and EDS data acquisition and processing. To eliminate noise and/or enhance the images various filters (Radial Wiener, High-pass, Average and Gaussian blur) were applied.

References

Donovan, J.J., Singer, J.W., and Armstrong, J.T. (2016) A new EPMA method for fast trace element analysis in simple matrices. American Mineralogist 101(8), 1839-1853. https://doi.org/10.2138/am-2016-5628

Paton, C., Hellstrom, J., Paul, B., Woodhead, J., and Hergt, J. (2011) Iolite: Freeware for the visualisation and processing of mass spectrometric data. Journal of Analytical Atomic Spectrometr 26, 2508-2518. https://doi.org/10.1039/C1JA10172B

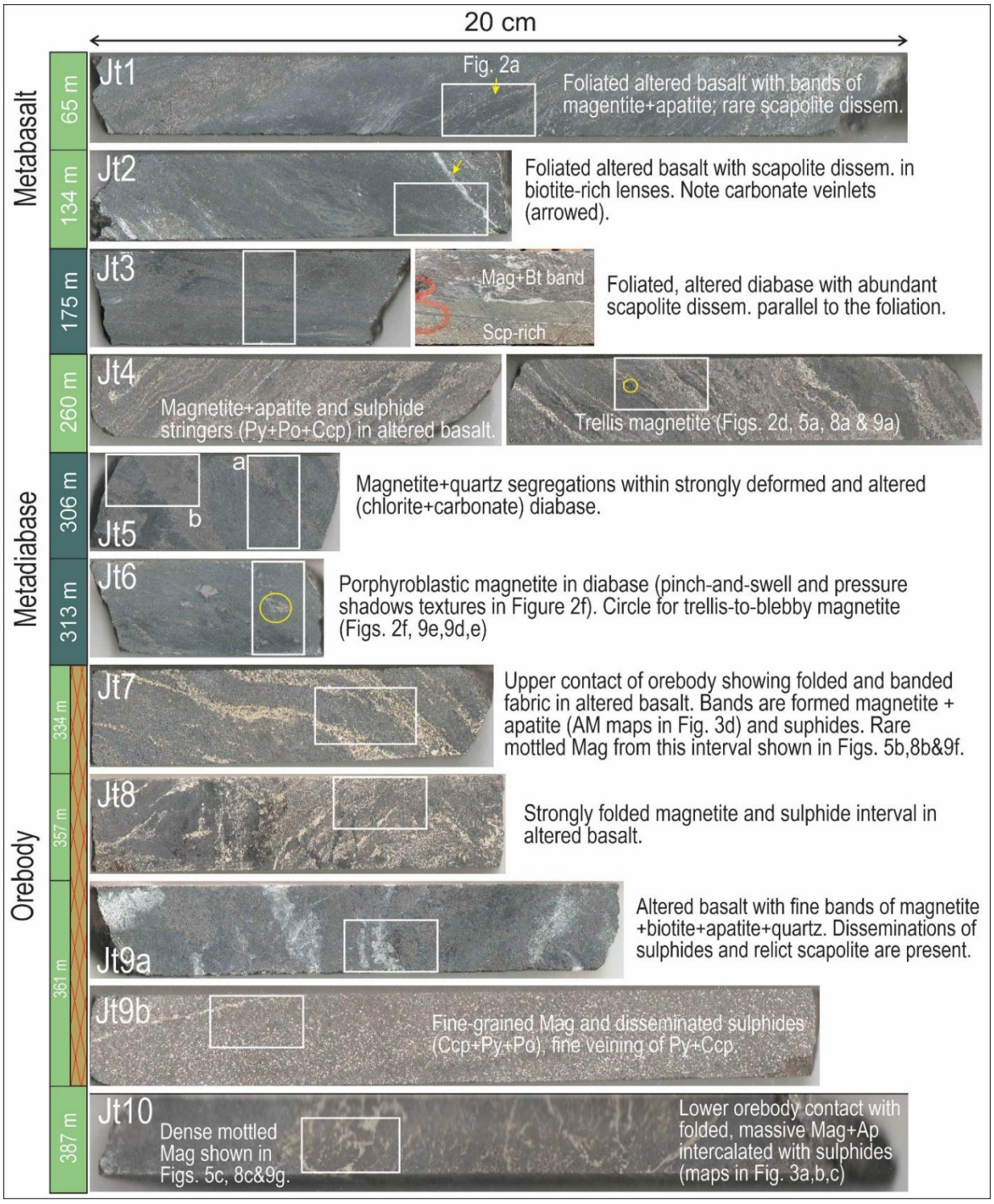

ESM Figure 1. Photographs of the drill-cores (from the drillhole DH00032) showing the fabrics of the country rocks and the orebody. The locations of the thins sections are indicated by white rectangles. Abbreviations: Ap-apatite, Bt-biotite, Ccp-chalcopyrite, Mag-magnetite, Py-pyrite, Pyh-pyrrhotite, Qz-quartz, Scp-scapolite.

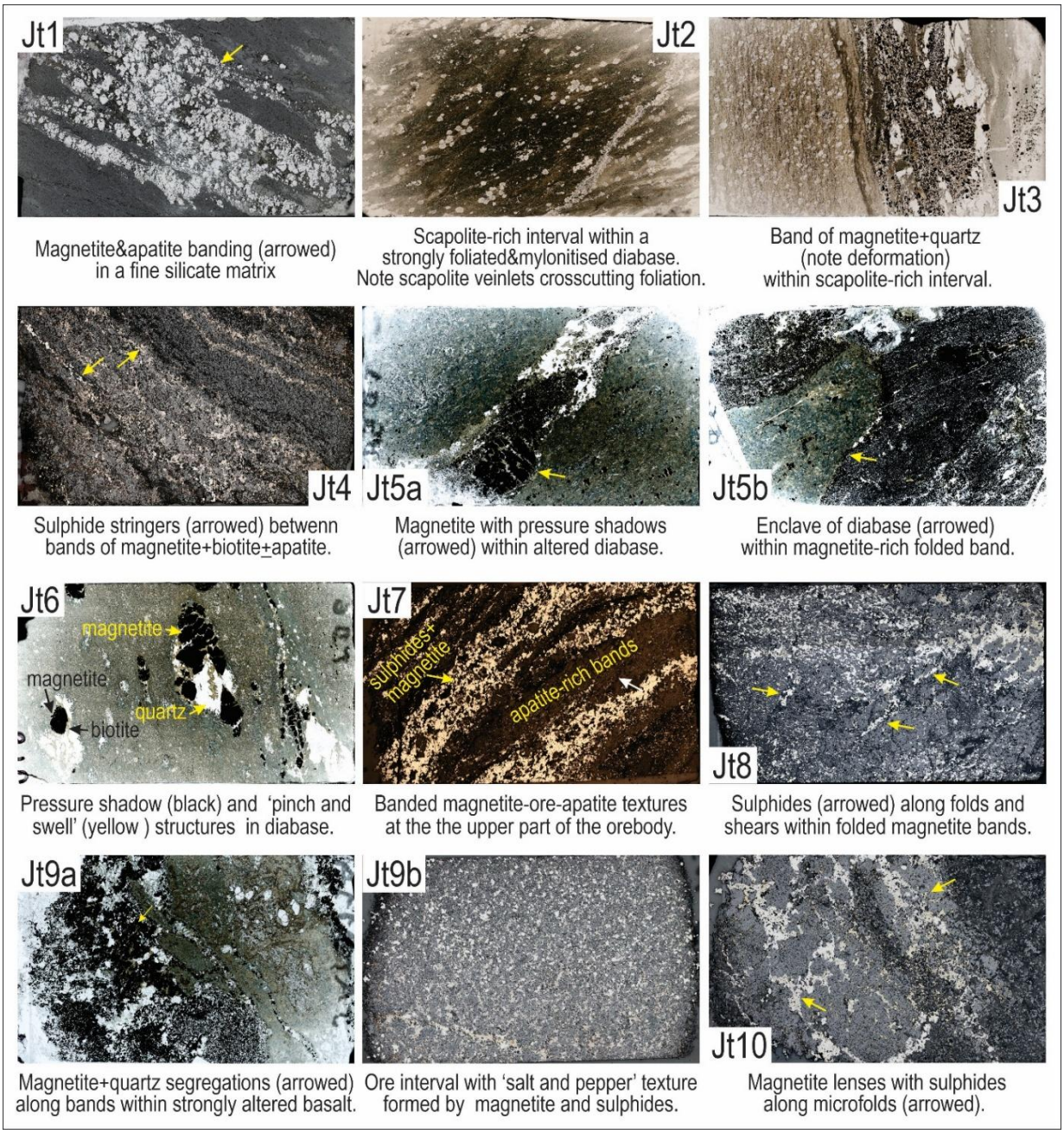

ESM Figure 2. Optical and reflected light scans of thin sections from the drillhole (DH00032), showing petrographic aspects of magnetite, sulphide and country rocks. Note the different ore textures across the samples. Details of the mineralogy are shown in figure 2.

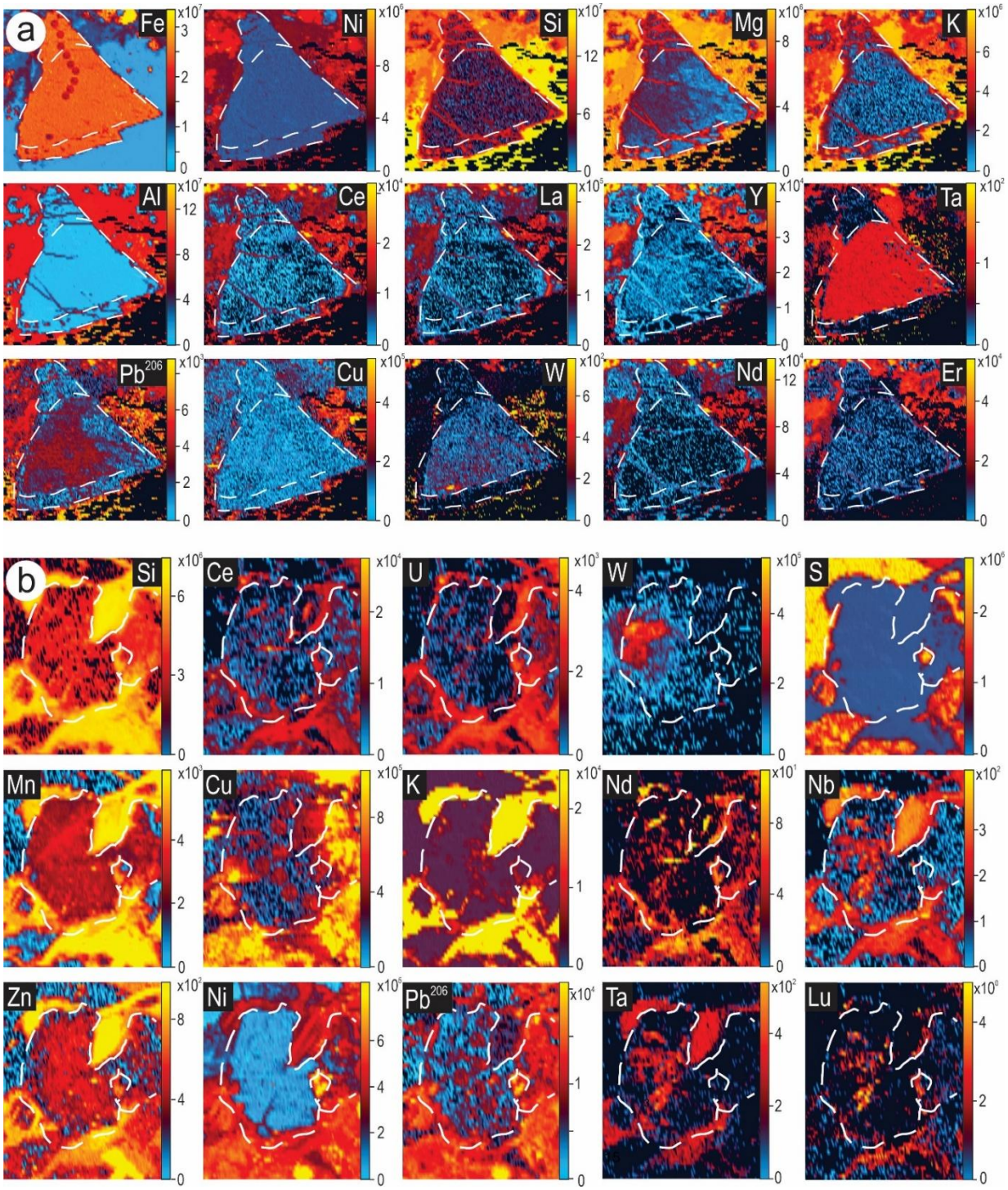

ESM Figure 3. Extended LA-ICP-MS elemental maps of selected magnetite grains. (a) trellis magnetite from sample (Jt4, Figure 8a) and (b) rare-mottled magnetite from sample (Jt7, Figure 8b). See main text for further explanations. Intensities in counts-per-second (cps), logarithmically-scaled (10^n).

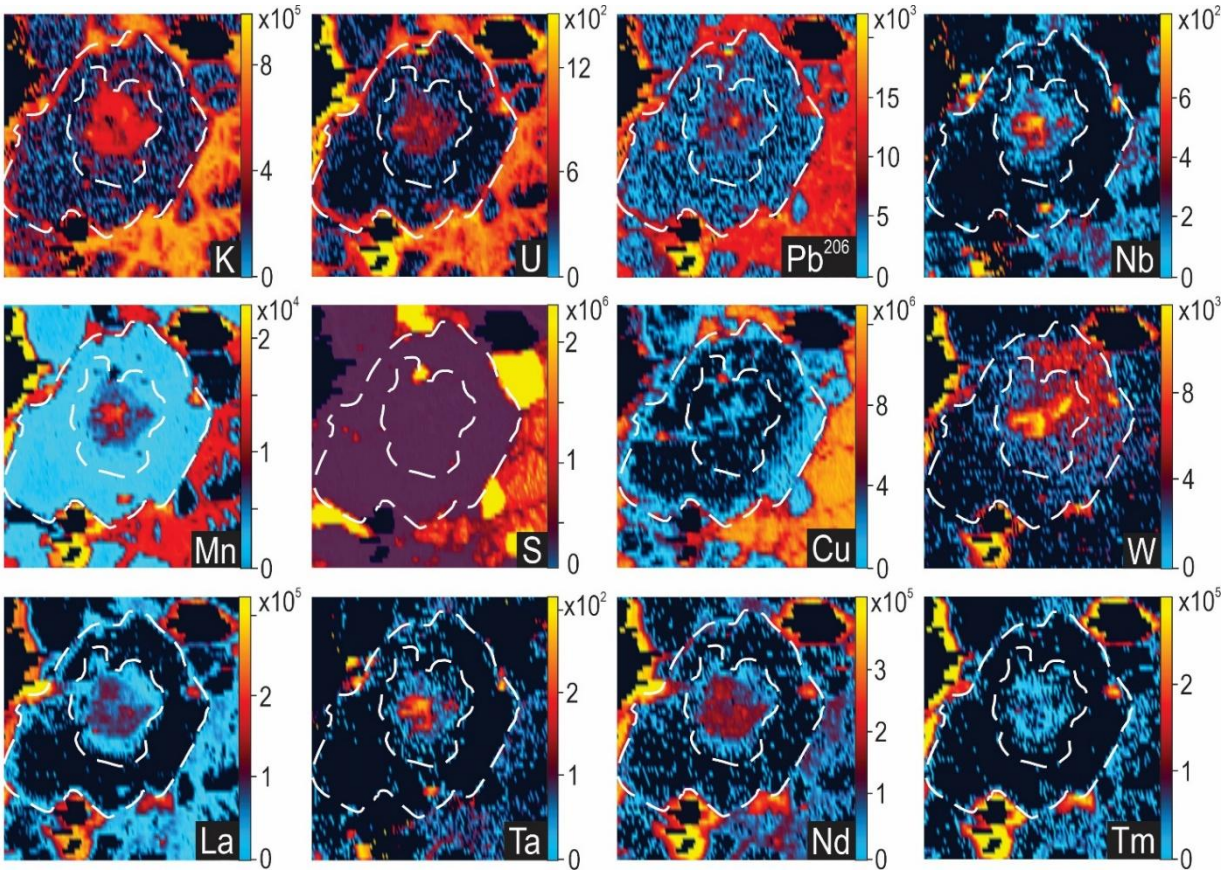

ESM Figure 4. Extended LA-ICP-MS elemental maps of selected magnetite grain with dense mottled texture from sample (Jt10, Figure 8c). See main text for further explanations. Intensities in counts-per-second (cps), logarithmically-scaled (10^n).

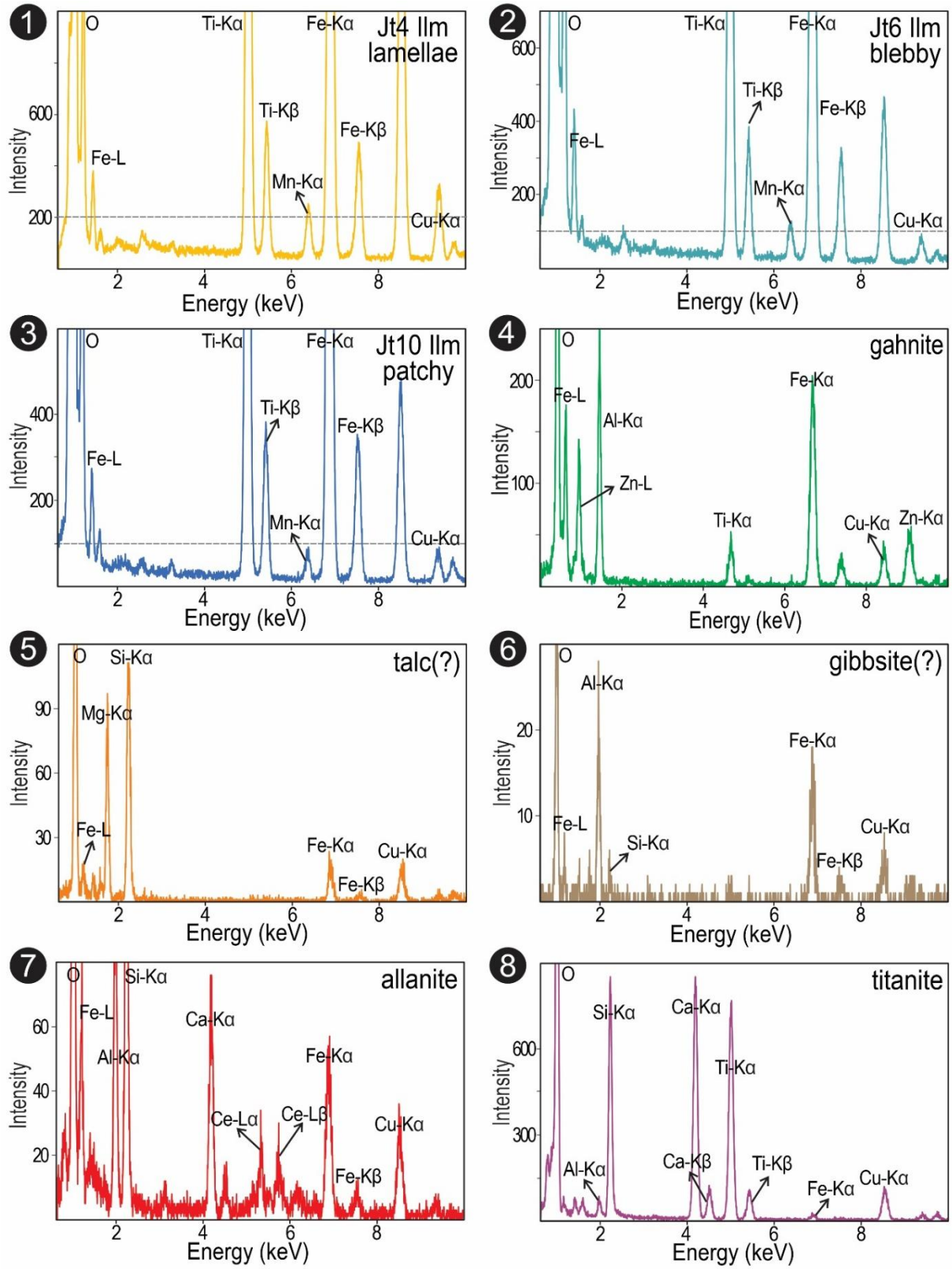

ESM Figure 5. Integrated EDS spectra for ilmenite (Ilm), gahnite, talc, gibbsite, allanite and titanite. Note difference in Mn intensity for the ilmenite types. See main text for further explanations.

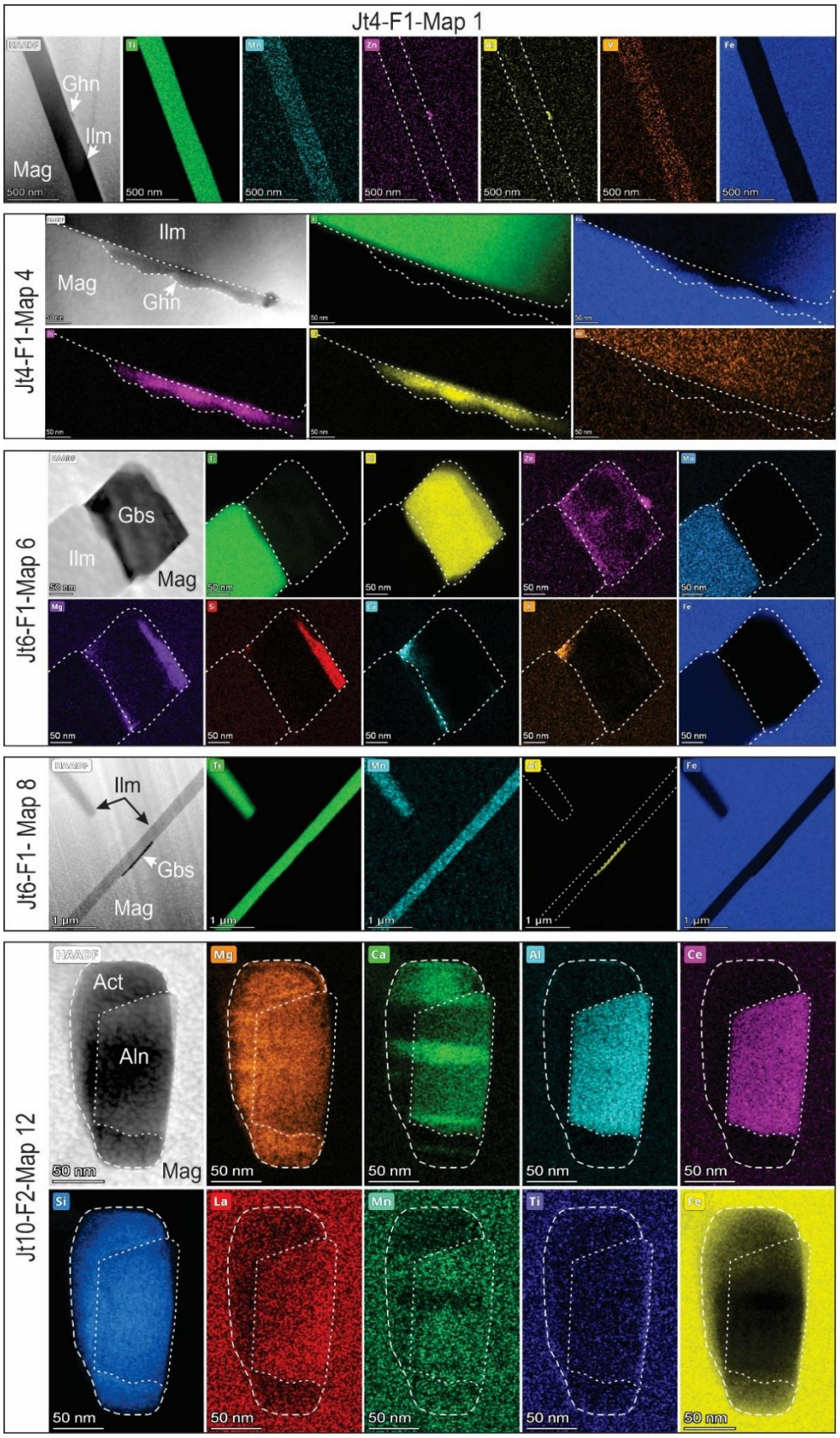

ESM Figure 6. EDS STEM maps illustrating compositional variation, intergrowths, and zonation patterns among gahnite, magnetite and ilmenite; allanite and actinote, as labelled. See main text for further explanations. Jt10-F2-Map12 is shown in Figure 11. Act–actnolite, Aln-Allanite, Gbs-Gibbsite, Ghn-gahnite, Ilm-ilmenite, Mag-magnetite.

APPENDIX B FOR CHAPTER 4

ESM Table 1a. Compositions of amphiboles from EPMA data as labelled.

ESM Table 1b. Quantitative compositional data for magnetite as determined by EPMA.

ESM Table 2a. LA-ICP-MS trace element data for magnetite.

ESM Table 2b. Summary of LA-ICP-MS trace element data for magnetite in each sample.

ESM Table 2c. LA-ICP-MS data for magnetite divided by textural type and used for box-and-whiskers plots.

ESM Table 2d. LA-ICP-MS data used for REE plots.

ESM Table 3. Nano-thermooxybarometric estimations based on magnetite and ilmenite pairs from STEM-EDX data.

ESM Table 1a. Compositions of amphiboles from EPMA data as labelled

Sample	**Jt1**	**Jt2**		**Jt3**		**Jt5a**		**Jt5b**	**Jt6**	**Jt9a**	**Jt10**					**Jt7**	**Jt8**	**Jt10**
(Wt%)	Ferrotschermakite					Magnesiohornblende					Actinolite					Grunerite		
SiO_2	40.66	38.22	39.03	39.17	39.20	45.18	43.81	44.92	47.76	49.23	55.86	56.60	54.68	56.50	55.23	45.66	47.63	50.66
TiO_2	0.27	0.06	0.28	0.24	0.24	0.18	0.25	0.22	0.19	0.16	0.03	0.02	0.03	0.02	0.09	0.01	0.02	0.01
Al_2O_3	12.53	13.78	13.78	13.55	12.89	10.00	10.94	10.47	8.87	7.01	1.36	0.48	0.85	0.54	0.06	4.44	4.30	4.80
FeO	24.67	25.67	25.50	25.79	25.63	19.04	19.14	19.41	17.17	16.09	11.52	11.20	16.24	11.69	11.08	34.97	34.22	29.35
MnO	0.16	0.12	0.11	0.12	0.13	0.19	0.18	0.18	0.18	0.35	0.28	0.13	0.16	0.09	0.10	0.11	0.20	0.33
MgO	6.50	4.94	5.83	5.13	5.94	10.36	9.21	9.72	11.82	13.10	17.16	17.42	14.25	17.72	17.74	12.11	10.52	12.27
CaO	11.99	11.84	11.96	11.95	11.84	11.12	11.60	11.71	11.64	11.76	12.83	12.99	12.17	12.64	13.11	0.04	0.01	0.02
Na_2O	1.09	1.33	1.25	1.08	1.18	1.14	1.28	1.22	1.20	0.91	0.13	0.08	0.29	0.13	0.01	0.02	0.20	0.07
K_2O	0.16	0.23	0.11	0.19	0.26	0.66	0.81	0.85	0.21	0.15	0.06	0.01	0.04	0.02	0.03	0.46	0.65	0.92
F	-	-	0.04	0.02	-	0.03	0.00	0.06	-	0.05	0.03	0.05	0.09	0.01	0.32	-	-	-
Cl	1.82	2.63	2.31	2.31	2.46	0.97	1.16	1.11	0.40	0.17	0.02	0.04	0.02	0.03	0.00	0.24	0.20	0.08
NiO	-	-	0.01	0.11	-	-	0.05	0.07	0.03	-	0.05	0.00	0.01	0.13	-	0.59	0.07	0.07
ZnO	0.04	0.09	-	-	0.04	-	0.03	0.06	0.05	0.00	0.02	0.09	0.03	-	-	-	0.06	-
Total	99.9	98.9	100.2	99.6	99.8	98.9	98.5	100.0	99.5	99.0	99.3	99.1	98.9	99.5	97.8	98.64	98.08	98.57
wt%																		
SiO_2	40.16	38.28	38.55	38.90	38.88	44.61	43.27	44.36	47.16	48.62	55.16	55.90	54.00	55.79	54.54	45.09	47.04	50.03
TiO_2	0.27	0.06	0.28	0.24	0.24	0.18	0.25	0.22	0.19	0.16	0.03	0.02	0.03	0.02	0.09	0.01	0.02	0.01
Al_2O_3	12.53	13.80	13.61	13.46	12.79	10.00	10.94	10.47	8.87	7.01	1.36	0.48	0.85	0.54	0.06	4.44	4.30	4.80
Fe_2O_3	12.69	11.52	13.54	12.12	13.46	7.95	8.64	8.94	4.84	4.86	1.58	0.98	1.24	0.41	0.58	4.92	5.35	0.23
FeO	13.24	15.35	13.00	14.70	13.31	11.88	11.36	11.37	12.82	11.72	10.09	10.33	15.12	11.31	10.56	30.54	29.40	29.14
MnO	0.16	0.12	0.10	0.12	0.13	0.19	0.18	0.18	0.18	0.35	0.28	0.13	0.16	0.09	0.10	0.11	0.20	0.33
MgO	6.50	4.95	5.76	5.10	5.89	10.36	9.21	9.72	11.82	13.10	17.16	17.42	14.24	17.71	17.74	12.11	10.52	12.27
CaO	11.99	11.86	11.82	11.87	11.75	11.12	11.60	11.71	11.64	11.76	12.83	12.99	12.17	12.64	13.11	0.04	0.01	0.02
Na_2O	1.09	1.33	1.23	1.07	1.17	1.14	1.28	1.22	1.20	0.91	0.13	0.08	0.29	0.13	0.01	0.02	0.20	0.07
K_2O	0.16	0.23	0.11	0.18	0.25	0.66	0.81	0.85	0.21	0.15	0.06	0.01	0.04	0.02	0.03	0.46	0.65	0.92
NiO	0.00	0.09	0.01	0.11	0.04	0.00	0.05	0.07	0.03	0.00	0.05	0.00	0.01	0.13	0.00	0.59	0.07	0.07
ZnO	0.04	0.00	0.00	0.00	0.00	0.00	0.03	0.06	0.05	0.00	0.02	0.09	0.03	0.00	0.00	0.00	0.06	0.00
F	0.00	0.00	0.04	0.02	0.00	0.03	0.00	0.06	0.00	0.05	0.03	0.05	0.09	0.01	0.32	0.00	0.00	0.00
Cl	1.82	2.64	2.28	2.29	2.44	0.97	1.16	1.11	0.40	0.17	0.02	0.04	0.02	0.03	0.00	0.24	0.20	0.08
H_2O	1.46	1.08	1.12	1.13	1.12	1.71	1.65	1.67	1.92	1.96	2.09	2.08	2.01	2.11	1.92	1.85	1.86	1.96
Total	100.7	100.2	100.3	100.2	100.3	99.1	98.8	100.3	99.4	98.9	98.8	98.5	98.3	98.8	97.1	98.6	98.0	98.0
TotH	102.1	101.3	101.4	101.3	101.5	100.8	100.4	102.0	101.3	100.8	100.9	100.6	100.3	100.9	99.1	100.4	99.9	99.9

ESM Table 1b. Quantitative compositional data for magnetite as determined by EPMA

	n=10 Jt1 - Trellis				n=7 Jt4 - Trellis				n=3 Jt7 - Rare mottled				n=7 Jt8 - Dense mottled				n=2 Jt9b - Dense mottled				n=12 Jt10 - Dense mottled			
Sample	**Mean**	**SD**	**Min**	**Max**	**Mean**	**SD**	**Min**	**Max**	**Mean**	**SD**	**Min**	**Max**	**Mean**	**SD**	**Min**	**Max**	**Mean**	**SD**	**Min**	**Max**	**Mean**	**SD**	**Min**	**Max**
SiO_2	0.044	0.013	0.026	0.069	0.027	0.019	0.005	0.052	0.014	0.006	0.009	0.020	0.025	0.027	0.000	0.073	0.029	0.021	0.029	0.029	0.030	0.023	0.000	0.061
TiO_2	0.070	0.036	0.019	0.136	0.056	0.037	0.012	0.096	0.052	0.012	0.041	0.065	0.026	0.008	0.012	0.034	0.053	0.002	0.052	0.054	0.057	0.031	0.022	0.092
Al_2O_3	0.046	0.028	0.000	0.089	0.037	0.015	0.017	0.060	0.088	0.008	0.080	0.094	0.072	0.039	0.030	0.145	0.038	0.008	0.032	0.044	0.034	0.024	0.000	0.066
Cr_2O_3	0.046	0.017	0.015	0.063	0.096	0.039	0.054	0.151	0.059	0.016	0.045	0.077	0.034	0.009	0.018	0.044	0.035	0.006	0.030	0.039	0.060	0.010	0.044	0.078
V_2O_3	0.239	0.032	0.192	0.283	0.275	0.026	0.238	0.314	0.315	0.037	0.274	0.345	0.268	0.049	0.189	0.338	0.247	0.006	0.243	0.251	0.390	0.026	0.356	0.444
Fe_2O_3	68.7	0.309	68.2	69.2	68.3	0.544	67.4	69.1	68.9	0.541	68.5	69.5	68.6	0.767	67.4	69.4	67.1	3.42	64.7	69.5	67.1	3.88	58.6	69.3
FeO	31.3	0.168	31.0	31.5	31.2	0.310	30.8	31.7	31.3	0.179	31.1	31.5	31.4	0.379	31.0	32.0	32.1	0.893	31.5	32.8	32.0	1.06	31.2	34.3
MnO	0.017	0.015	0.000	0.044	0.012	0.008	0.000	0.020	0.015	0.013	0.000	0.026	0.015	0.016	0.000	0.047	0.011	0.002	0.009	0.012	0.022	0.028	0.000	0.090
MgO	0.004	0.007	0.000	0.023	0.009	0.024	0.000	0.063	0.000	0.000	0.000	0.000	0.011	0.016	0.000	0.045	0.020	0.014	0.020	0.020	0.011	0.012	0.000	0.043
CaO	0.007	0.009	0.000	0.025	0.013	0.013	0.000	0.030	0.028	0.030	0.010	0.063	0.025	0.031	0.000	0.086	0.037	0.003	0.035	0.039	0.014	0.012	0.000	0.036
NiO	0.014	0.018	0.000	0.055	0.013	0.018	0.000	0.050	0.009	0.013	0.000	0.024	0.007	0.009	0.000	0.021	0.000	0.000	0.000	0.000	0.011	0.021	0.000	0.071
Total	**100.4**	**0.483**	**99.7**	**101.1**	**100.1**	**0.667**	**99.2**	**101.2**	**100.7**	**0.699**	**100.3**	**101.5**	**100.5**	**0.566**	**99.8**	**101.4**	**99.7**	**2.572**	**97.9**	**101.5**	**99.7**	**2.871**	**93.4**	**101.4**
IONS																								
Si	0.015	0.007	0.008	0.030	0.008	0.006	0.002	0.016	0.004	0.002	0.003	0.006	0.008	0.008	0.000	0.022	0.009	0.006	0.009	0.009	0.009	0.007	0.000	0.019
Ti	0.017	0.008	0.004	0.031	0.013	0.009	0.003	0.022	0.012	0.003	0.009	0.015	0.006	0.002	0.003	0.008	0.012	0.000	0.012	0.012	0.013	0.007	0.005	0.021
Al	0.017	0.010	0.000	0.033	0.014	0.006	0.006	0.022	0.032	0.003	0.028	0.034	0.026	0.014	0.011	0.052	0.014	0.003	0.012	0.016	0.012	0.009	0.000	0.024
Cr	0.010	0.004	0.004	0.015	0.023	0.009	0.013	0.036	0.014	0.004	0.011	0.019	0.008	0.002	0.004	0.011	0.008	0.002	0.007	0.009	0.014	0.003	0.006	0.019
V	0.060	0.009	0.047	0.070	0.068	0.006	0.059	0.077	0.077	0.010	0.067	0.085	0.066	0.012	0.047	0.083	0.060	0.002	0.059	0.061	0.093	0.009	0.070	0.108
Fe(iii)	15.8	0.019	15.8	15.9	15.8	0.115	15.6	15.9	15.8	0.014	15.8	15.9	15.8	0.220	15.4	15.9	15.3	0.871	14.6	15.9	15.5	0.762	13.5	15.9
Fe(ii)	8.0	0.013	8.0	8.0	8.0	0.052	8.0	8.1	8.0	0.013	8.0	8.0	8.0	0.060	8.0	8.1	8.1	0.176	8.0	8.2	8.1	0.147	8.0	8.4
Mn	0.004	0.004	0.000	0.011	0.003	0.002	0.000	0.005	0.004	0.003	0.000	0.007	0.004	0.004	0.000	0.012	0.003	0.001	0.002	0.003	0.004	0.005	0.000	0.015
Mg	0.002	0.003	0.000	0.011	0.004	0.011	0.000	0.029	0.000	0.000	0.000	0.000	0.005	0.008	0.000	0.021	0.009	0.006	0.009	0.009	0.004	0.006	0.000	0.020
Ca	0.002	0.003	0.000	0.008	0.004	0.004	0.000	0.010	0.009	0.010	0.003	0.020	0.008	0.010	0.000	0.028	0.012	0.001	0.011	0.013	0.004	0.004	0.000	0.012
Ni	0.004	0.005	0.000	0.014	0.003	0.005	0.000	0.012	0.002	0.003	0.000	0.006	0.002	0.002	0.000	0.005	0.000	0.000	0.000	0.000	0.003	0.005	0.000	0.017
TOTAL	**24.0**	**0.00**	**24.0**	**24.0**	**24.0**	**0.09**	**23.8**	**24.0**	**24.0**	**0.00**	**24.0**	**24.0**	**23.9**	**0.15**	**23.6**	**24.0**	**23.5**	**0.71**	**23.0**	**24.0**	**23.7**	**0.62**	**22.1**	**24.0**

ESM Table 2a. LA-ICP-MS trace element data for magnetite (complete dataset, concentrations in ppm)
**Note:* In red analyses shown in Figure 7a.

#	Sample	Mg	Al	Si	P	Ca	Sc	Ti	V	Cr	Mn	Co	Ni	Cu	Zn	Ga	As	Sr	Zr	Nb	Mo	Sn	Sb	Ba
1	Jt1Mt1rim 01	197	623	673	16	237	0.144	487	1639	229	115	22.7	44	0.96	42.4	19.2	0.21	3.84	0.134	0.029	0.265	0.06	0.094	14.73
2	Jt1Mt1rim 02	213	716	798	16	821	0.052	548	1690	257	253	24.0	46	2.81	99.0	21.5	0.45	16.84	0.034	0.023	0.120	0.11	0.225	58.03
3	Jt1Mt1rim 03	176	639	809	16	652	0.121	385	1658	183	187	23.2	45	1.83	78.0	20.6	0.96	10.64	0.082	0.044	0.359	0.13	0.175	33.40
4	Jt1Mt1rim 04	330	995	2990	16	3081	0.123	2820	1633	203	180	22.7	44	1.28	64.7	21.1	0.80	8.46	0.325	5.876	0.789	0.50	0.234	30.92
5	Jt1Mt1core 01	174	665	654	16	688	0.139	474	1621	196	240	24.3	44	2.23	110.2	23.7	0.53	16.61	0.044	0.018	0.101	0.12	0.090	50.03
6	Jt1Mt1core 02	184	723	637	16	496	0.211	527	1634	169	191	25.4	46	2.86	90.9	24.0	0.55	10.53	0.192	0.027	0.367	0.12	0.085	29.01
7	Jt1Mt1core 03	206	704	748	16	581	0.105	577	1665	167	206	25.5	44	1.71	79.2	23.3	0.47	12.43	0.033	0.015	0.245	0.13	0.079	43.47
8	Jt1Mt1core 04	239	706	692	16	335	0.003	559	1637	141	167	24.6	45	1.98	70.2	22.5	0.53	9.16	0.065	0.033	0.173	0.14	0.131	29.45
9	Jt1Mt1rim 05	321	814	2001	16	2392	0.294	2182	1610	113	224	23.2	42	1.65	87.3	19.4	0.84	13.29	0.274	4.6	0.213	0.42	0.191	47.22
10	Jt1Mt1rim 06	338	641	1230	16	458	0.145	543	1350	150	72	20.2	41	1.08	17.6	10.4	0.50	1.05	0.091	0.633	0.249	0.05	0.064	7.78
11	Jt1Mt2rim 07	174	526	471	16	593	0.070	610	1597	128	177	21.9	40	0.75	77.2	18.3	0.67	8.89	0.048	0.369	0.066	0.09	0.164	31.80
12	Jt1Mt2rim 08	198	687	554	16	783	0.167	533	1688	124	221	23.3	42	2.41	88.7	22.5	0.46	14.84	0.061	0.028	0.228	0.06	0.143	46.15
13	Jt1Mt2rim 09	157	662	424	16	517	0.117	628	1684	168	185	23.3	44	2.05	68.8	22.6	0.08	11.44	0.033	0.025	0.263	0.06	0.089	37.04
14	Jt1Mt2rim 10	255	717	1057	16	626	0.005	802	1528	130	134	20.6	42	0.90	56.0	18.1	0.83	6.24	0.132	1.5	0.140	0.12	0.123	21.44
15	Jt1Mt2rim 11	382	770	999	16	784	0.033	514	1608	105	241	21.4	42	1.63	99.4	18.6	0.92	14.87	0.052	0.038	0.276	0.13	0.198	50.79
16	Jt1Mt2rim 12	566	911	1836	16	936	0.215	1160	1696	170	139	21.8	44	0.45	38.6	16.7	0.65	5.34	0.115	1.6	0.150	0.18	0.089	18.98
17	Jt1Mt2core 05	196	698	587	16	450	0.149	598	1734	158	170	23.5	45	2.15	52.2	20.9	0.51	7.65	0.246	0.036	0.231	0.10	0.096	26.95
18	Jt1Mt2core 06	208	708	670	16	272	0.066	675	1687	172	161	23.6	45	1.27	50.5	21.2	0.19	8.27	0.092	0.031	0.304	0.08	0.047	31.34
19	Jt1Mt3rim 13	259	654	7632	16	585	0.054	779	1604	130	87	23.8	41	0.35	27.0	17.9	0.29	3.14	0.059	1.1	0.010	0.17	0.032	12.80
20	Jt1Mt3rim 14	1791	1945	4097	16	862	0.216	784	1606	131	114	25.3	41	1.40	39.0	18.7	0.59	3.11	0.161	1.4	0.355	0.14	0.169	23.36
21	Jt1Mt3rim 15	185	522	868	16	458	0.144	464	1642	114	87	24.2	41	0.31	32.0	19.1	0.54	2.52	0.018	0.555	0.025	0.10	0.092	13.74
22	Jt1Mt3rim 16	624	806	2055	16	1487	0.214	1100	1632	88	142	24.9	42	0.64	57.5	20.0	0.82	6.37	0.082	2.2	0.029	0.22	0.172	26.52
24	Jt1Mt4rim 17	129	469	653	16	237	0.151	324	1529	7	54	21.9	39	0.49	9.1	12.8	0.25	0.21	0.069	0.003	0.022	0.08	0.007	0.28
25	Jt1Mt4rim 18	542	1023	1400	16	275	0.061	444	1600	81	112	24.2	42	0.59	42.6	19.6	0.36	3.63	0.028	0.060	0.026	0.06	0.056	22.54
26	Jt1Mt4rim 19	177	619	617	16	814	0.075	358	1589	56	222	24.5	42	1.97	93.5	21.6	0.57	15.4	0.074	0.013	0.005	0.16	0.156	49.40
27	Jt1Mt4rim 20	418	783	1993	16	1887	0.296	5110	1664	103	355	24.8	41	1.31	100.2	19.6	0.88	12.7	0.177	5.30	0.356	0.52	0.172	42.00
28	Jt1Mt4rim 21	184	609	446	16	493	0.255	11755	1617	88	579	25.5	42	1.26	79.4	21.9	0.55	11.8	0.059	6.43	0.295	0.18	0.099	45.85
29	Jt1Mt4core 08	182	548	622	16	237	0.355	16655	1601	74	693	25.8	41	1.58	45.2	21.4	0.50	4.7	0.095	9.43	0.535	0.19	0.117	21.79
30	Jt1Mt4core 09	178	716	1434	16	2068	0.229	4610	1612	56	313	24.9	43	2.07	94.7	23.1	0.79	13.7	0.203	5.01	0.052	0.63	0.206	58.14
31	Jt1Mt4core 10	106	532	258	16	237	0.398	19392	1595	51	696	26.0	41	0.31	15.9	20.8	0.34	0.60	0.057	11.3	0.464	0.12	0.081	2.94
33	Jt1Mt5rim 23	222	562	807	16	538	0.017	533	1719	72	155	23.9	41	1.26	66.6	20.3	0.58	8.1	0.055	0.507	0.012	0.08	0.086	32.51
34	Jt1Mt5rim 24	226	477	799	16	679	0.134	391	1668	113	158	23.0	40	1.13	86.4	16.7	0.57	9.2	0.091	0.218	0.163	0.23	0.128	32.04
35	Jt1Mt5core 11	209	571	803	16	1294	0.270	771	1680	72	340	24.4	41	2.89	153.7	21.1	1.41	23.2	0.114	0.255	0.171	0.29	0.278	69.64
36	Jt1Mt6rim 25	317	752	1286	16	988	0.157	973	1746	119	143	25.0	42	1.16	51.5	21.2	0.60	6.5	0.123	1.47	0.290	0.22	0.078	27.56
37	Jt1Mt6rim 26	738	1172	1739	16	566	0.002	394	1761	115	171	25.7	43	3.89	64.5	23.0	0.25	8.4	1.976	0.028	0.259	0.29	0.074	40.64
38	Jt1Mt6rim 27	192	790	518	16	545	0.093	384	1743	108	197	24.8	42	2.19	68.8	21.9	0.15	12.9	0.040	0.026	0.180	0.12	0.038	40.39
39	Jt1Mt6rim 28	245	843	502	16	693	0.092	384	1753	115	223	25.0	43	2.49	76.9	22.7	0.25	14.6	0.033	0.011	0.358	0.17	0.095	59.28
40	Jt1Mt6rim 29	193	798	511	16	477	0.147	412	1765	115	189	25.3	43	2.36	73.7	21.3	0.25	9.6	0.033	0.013	0.151	0.17	0.064	47.43
41	Jt1Mt6rim 30	192	818	503	16	402	0.110	419	1765	131	167	24.9	43	1.66	59.1	20.7	0.27	8.5	0.041	0.011	0.168	0.12	0.038	32.03
42	Jt1Mt6rim 31	664	1358	1101	16	250	0.073	485	1781	132	121	24.4	43	1.82	51.5	20.0	0.29	5.1	0.016	0.031	0.133	0.12	0.069	21.22
43	Jt1Mt6rim 32	178	591	544	16	358	0.094	410	1608	60	166	23.9	42	1.06	70.6	18.6	0.63	9.4	0.018	0.033	0.069	0.14	0.120	35.71
44	Jt1Mt6rim 33	488	928	1039	16	407	0.125	596	1641	127	151	24.2	43	1.83	51.9	20.1	0.34	7.1	0.035	0.142	0.236	0.07	0.059	28.83

#	Sample	Mg	Al	Si	P	Ca	Sc	Ti	V	Cr	Mn	Co	Ni	Cu	Zn	Ga	As	Sr	Zr	Nb	Mo	Sn	Sb	Ba
45	Jt1Mt6rim 34	194	757	549	16	677	0.129	442	1676	123	251	24.1	43	2.69	83.0	21.6	0.28	14.2	0.027	0.020	0.304	0.10	0.080	64.23
46	Jt1Mt6rim 35	187	808	509	16	365	0.003	394	1702	123	156	24.7	43	1.68	52.4	21.5	0.18	7.7	0.032	0.011	0.124	0.17	0.038	28.60
47	Jt1Mt6rim 36	174	829	550	16	402	0.011	379	1727	120	165	24.9	43	1.45	61.0	22.1	0.56	9.0	1.433	0.015	0.214	0.07	0.039	30.68
48	Jt1Mt6rim 37	207	856	588	16	416	0.089	380	1730	121	169	25.6	43	1.84	61.9	21.9	0.38	9.6	0.020	0.017	0.340	0.12	0.057	35.03
49	Jt1Mt6rim 38	833	1340	1657	16	481	0.152	2502	1751	120	277	26.5	44	2.50	66.5	23.2	0.27	9.7	0.020	0.691	0.110	0.13	0.088	31.22
50	Jt1Mt6core 12	202	763	447	16	756	0.088	396	1762	121	334	26.6	45	2.86	123.3	24.5	0.32	14.8	0.069	0.022	0.056	0.15	0.055	159.99
51	Jt1Mt6core 13	250	922	649	16	969	0.048	381	1796	119	302	24.5	44	3.96	117.2	21.0	0.23	22.0	0.089	0.011	0.546	0.19	0.060	78.00
52	Jt1Mt6core 14	306	962	939	16	488	0.140	452	1830	115	161	24.6	44	3.69	61.4	21.2	0.27	8.7	0.156	0.022	0.531	0.24	0.060	32.58
53	Jt1Mt6core 15	194	885	470	16	433	0.133	433	1818	119	169	25.1	44	1.68	58.4	21.6	0.29	8.0	0.023	0.013	0.293	0.18	0.019	34.14
54	Jt1Mt6core 16	206	876	427	16	358	0.117	444	1778	125	145	25.1	43	1.42	55.2	22.5	0.30	7.3	0.024	0.012	0.185	0.13	0.027	25.51
55	Jt3Mt2 rim 01	248	646	1050	16	529	0.218	15684	1715	90	740	19.9	43	2.23	37.9	19.8	1.65	2.2	0.738	9.994	0.380	0.200	0.194	11.29
56	Jt3Mt2 rim 02	319	994	2407	16	2011	0.207	22659	1712	85	960	16.6	44	1.67	93.3	16.5	0.896	1.1	0.104	14.13	0.802	0.260	0.228	2.74
57	Jt3Mt2 rim 03	1848	3058	7307	19	10439	0.299	10579	1790	100	400	16.5	57	6.97	54.3	16.1	1.93	3.2	6.867	6.587	0.662	0.533	0.396	8.63
58	Jt3Mt2 rim 04	3658	5077	13706	37	10048	0.476	24797	1800	1670	849	17.8	64	4.86	60.4	20.3	1.67	2.9	1.012	14.37	0.783	0.868	0.300	5.95
59	Jt3Mt2 rim 05	187	629	780	20	558	0.229	15347	1739	86	719	22.2	44	1.68	71.3	20.2	1.19	1.5	0.220	8.789	1.156	0.215	0.100	13.17
60	Jt3Mt2 rim 06	118	563	747	20	358	0.217	418	1762	156	124	20.7	47	3.01	37.9	20.4	1.56	2.1	0.188	0.093	0.654	0.191	0.268	18.35
61	Jt3Mt2 core 01	425	903	2418	19	2302	0.247	25163	1736	319	1000	18.9	46	2.45	59.8	18.8	1.65	1.2	0.357	15.82	0.424	0.274	0.150	4.40
62	Jt3Mt2 core 02	172	637	529	17	373	0.225	22609	1740	400	956	20.9	46	2.77	148.2	21.1	1.04	0.161	0.119	14.61	0.330	0.260	0.094	0.677
63	Jt3Mt2 core 03	164	655	703	18	333	0.225	25372	1744	415	1082	22.8	45	1.15	139.2	20.3	0.772	0.198	0.057	15.87	0.335	0.227	0.108	0.797
64	Jt3Mt2 core 04	192	642	802	17	331	0.249	29038	1721	158	1240	23.2	44	1.35	128.7	20.5	0.774	0.231	0.176	18.60	0.577	0.242	0.097	0.660
65	Jt3Mt3 01	1827	2554	5328	26	2074	0.248	15031	2211	59	677	17.0	48	3.44	28.1	10.5	1.45	1.9	2.477	8.860	0.513	0.113	0.286	11.38
66	Jt3Mt3 02	417	781	1013	23	317	0.264	17158	2177	91	774	17.3	49	2.92	25.8	11.2	0.690	0.765	0.439	10.57	0.614	0.106	0.104	4.60
67	Jt3Mt3 03	104	420	520	19	279	0.203	15476	2143	102	705	16.5	40	0.846	17.6	11.0	0.700	0.679	0.049	9.044	0.513	0.082	0.086	3.31
68	Jt3Mt3 04	121	475	406	18	306	0.199	15956	2149	83	723	16.5	42	1.45	29.5	10.3	0.733	0.249	0.127	10.04	0.582	0.129	0.088	1.70
69	Jt3Mt3 05	501	1058	2761	17	2099	0.190	16404	2182	107	687	15.8	42	1.20	18.9	9.8	1.07	1.4	0.704	10.39	0.380	0.329	0.089	7.09
70	Jt3Mt4 01	5938	7617	12182	19	1375	0.461	5937	1872	131	344	23.3	58	1.35	24.7	14.4	0.986	0.970	0.131	3.65	0.051	0.100	0.130	4.41
71	Jt3Mt4 02	368	704	1028	17	761	0.172	18567	1848	56	832	18.8	44	1.30	24.9	12.4	1.42	1.8	0.069	11.59	0.176	0.138	0.083	13.0
72	Jt3Mt4 03	230	481	903	16	368	0.179	20783	1824	38	894	19.3	43	0.474	27.9	13.0	1.00	0.348	0.206	13.38	0.242	0.085	0.084	1.74
73	Jt3Mt4 04	210	519	669	16	292	0.194	24332	1772	40	1045	19.9	41	0.764	35.8	14.9	0.972	0.145	0.053	15.70	0.424	0.112	0.112	0.767
74	Jt3Mt4 05	163	464	436	16	284	0.202	23077	1796	42	968	19.9	41	0.443	63.5	15.2	1.21	0.154	0.083	15.19	0.310	0.071	0.079	0.625
75	Jt3Mt4 06	142	475	585	18	267	0.219	24747	1804	35	1049	20.3	41	0.789	56.8	17.6	0.633	1.2	0.110	16.72	0.061	0.189	0.079	0.581
76	Jt3Mt5 01	1412	2462	5829	18	1948	0.838	7258	1931	148	346	20.6	41	0.518	14.4	18.1	0.825	0.929	0.337	4.87	0.676	0.458	0.165	11.7
77	Jt3Mt5 02	157	482	403	16	275	0.162	17466	1854	120	726	20.1	40	0.393	22.3	20.0	0.782	0.541	0.168	10.10	0.451	0.140	0.074	3.6
78	Jt3Mt5 03	197	530	1273	18	287	0.193	16204	1776	177	700	21.8	43	1.12	24.1	20.7	1.12	0.460	6.930	9.55	1.280	0.150	0.144	3.5
79	Jt3Mt5 04	249	623	770	17	313	0.197	20033	1744	105	888	21.6	45	1.03	38.6	20.1	1.48	2.1	0.046	12.77	0.320	0.105	0.255	18.0
80	Jt3Mt5 05	167	501	578	20	355	0.220	20948	1806	75	905	20.3	41	1.19	21.3	18.9	1.33	0.298	1.217	13.11	0.295	0.163	0.137	2.4
81	Jt3Mt5 06	303	733	1266	21	471	0.234	16449	1881	77	743	18.6	44	2.46	25.4	17.6	0.986	1.4	0.876	10.20	0.549	0.142	0.124	8.2
82	Jt3Mt5 07	1025	989	2643	22	401	0.468	18937	1883	114	896	26.3	41	3.54	44.6	19.0	1.42	2.0	0.183	11.70	3.084	0.433	0.346	16.5
83	Jt3Mt6 01	691	1232	2833	19	878	0.205	8380	2079	96	391	16.6	42	1.81	17.7	14.5	0.907	1.5	0.119	6.21	0.317	0.302	0.119	15.8
84	Jt3Mt6 02	208	538	605	18	305	0.231	19317	2045	114	845	17.7	40	3.21	25.4	17.5	1.47	1.9	0.251	12.15	0.429	0.121	0.269	17.3
85	Jt3Mt6 03	149	460	691	17	326	0.214	20761	2028	109	878	19.5	40	1.57	35.1	19.3	0.831	0.227	0.103	13.77	0.717	0.322	0.082	0.852
86	Jt3Mt6 04	382	791	1949	19	639	0.218	15876	2039	137	698	19.0	40	1.71	33.4	18.4	1.06	1.5	0.154	9.80	0.376	0.362	0.155	11.5
87	Jt3Mt6 05	1095	1770	5419	20	1157	0.235	8576	2053	172	416	15.6	46	3.83	25.0	13.4	1.49	1.8	0.258	5.16	0.681	0.182	0.226	10.3
88	Jt3Mt7 rim 01	992	2079	5173	21	2387	1.041	1934	1674	282	127	16.2	42	2.94	18.5	13.5	1.05	1.4	1.033	2.68	0.421	1.029	0.124	9.2
89	Jt3Mt7 rim 02	582	1087	1283	21	300	0.272	12351	1700	113	599	19.8	41	3.27	35.5	18.9	1.62	1.8	0.097	7.90	0.786	0.177	0.219	14.3

#	Sample	Mg	Al	Si	P	Ca	Sc	Ti	V	Cr	Mn	Co	Ni	Cu	Zn	Ga	As	Sr	Zr	Nb	Mo	Sn	Sb	Ba
90	Jt3Mt7 rim 03	1299	2434	10300	31	7007	0.340	11212	1734	135	302	13.8	49	5.40	23.6	17.5	1.94	3.0	1.190	6.87	1.156	0.203	0.498	2.5
91	Jt3Mt7 rim 04	177	556	945	23	862	0.262	24061	1721	115	1091	15.4	42	2.89	32.1	17.8	0.877	0.493	0.147	15.9	0.969	0.174	0.317	2.8
92	Jt3Mt7 core 01	108	538	1020	21	390	0.257	26291	1695	103	1120	16.4	43	2.40	34.3	19.1	0.797	0.410	0.188	16.9	0.986	0.168	0.257	1.1
93	Jt3Mt7 core 02	156	496	657	18	347	0.244	24095	1715	97	1013	18.7	42	2.00	40.7	20.5	0.981	0.145	0.192	15.6	0.800	0.252	0.101	0.604
94	Jt3Mt7 core 03	107	493	882	21	365	0.216	22877	1678	97	953	18.4	42	2.13	38.9	21.2	0.767	0.255	0.113	15.0	0.860	0.376	0.113	0.592
95	Jt4Mt1rim 01	292	659	1044	16	237	0.365	368	1556	196	33	5.09	62	0.616	21.6	12.7	0.229	0.029	0.011	0.071	0.045	0.217	0.020	2.81
96	Jt4Mt1rim 02	344	739	1398	16	237	0.347	368	1612	114	32	5.51	67	0.418	12.8	15.4	0.219	0.170	0.067	0.128	0.083	0.237	0.040	1.77
97	Jt4Mt1rim 03	789	1407	3463	16	237	1.16	338	1643	115	55	6.06	70	0.221	35.6	16.9	0.306	0.304	0.030	0.192	0.225	0.214	0.016	1.48
98	Jt4Mt1rim 04	124	561	418	16	237	1.02	12524	1645	115	376	9.52	72	0.240	43.5	23.8	0.269	0.011	0.035	10.33	0.555	0.333	0.011	0.093
99	Jt4Mt1rim 05	99	587	540	16	237	1.07	13225	1652	123	402	10.39	71	0.116	54.8	26.4	0.249	0.012	0.031	11.69	0.352	0.354	0.043	0.001
100	Jt4Mt1rim 06	73	592	598	16	237	1.03	13075	1640	136	355	8.33	73	0.253	51.3	26.8	0.365	0.014	0.056	12.37	0.475	0.318	0.037	0.003
101	Jt4Mt1rim 07	746	1576	2695	16	237	1.45	12424	1632	143	324	5.75	72	0.826	47.9	18.8	0.200	0.090	0.038	11.47	0.390	0.385	0.025	0.499
102	Jt4Mt1core 01	91	625	567	16	237	0.983	13301	1625	154	373	9.05	74	0.116	55.9	25.2	0.100	0.019	0.035	12.04	0.492	0.368	0.035	0.035
103	Jt4Mt1core 02	155	615	569	16	237	0.932	12347	1583	154	440	13.03	73	0.227	54.9	25.7	0.266	0.014	0.049	11.57	0.451	0.419	0.032	0.005
104	Jt4Mt2 01	1387	498	4418	42	544	1.05	2959	1604	100	160	6.29	61	0.486	28.3	15.8	1.49	0.619	1.75	2.30	0.484	0.392	0.255	2.31
105	Jt4Mt2 02	1386	420	4399	56	466	0.827	3073	1615	100	152	5.37	58	0.249	12.9	14.5	1.06	0.353	2.50	2.59	0.111	0.182	0.192	1.41
106	Jt4Mt3 03	874	687	4021	470	1164	0.888	2779	1610	216	210	6.17	59	1.04	61.6	16.7	1.90	2.11	0.77	2.42	0.477	0.755	0.164	8.10
107	Jt4Mt3 04	614	1033	2676	21	318	0.636	365	1624	173	45	4.67	56	0.586	8.3	12.1	0.231	0.189	0.062	0.513	0.043	0.272	0.004	2.28
108	Jt4Mt4 05	1182	526	4013	337	844	1.30	11536	1631	177	387	6.94	66	7.25	63.7	15.7	1.53	1.06	0.036	9.08	0.054	0.420	0.292	4.89
109	Jt4Mt4 06	2639	649	10191	31	237	1.91	8407	1624	86	338	6.23	62	0.726	33.7	19.0	2.37	0.904	1.43	7.80	0.209	0.348	0.351	2.38
110	Jt4Mt4 07	1904	596	7519	29	237	0.983	5888	1677	87	280	7.01	59	0.355	40.2	22.4	0.970	0.385	0.488	5.05	0.196	0.318	0.177	1.81
111	Jt4Mt5 08	409	956	2268	90	673	0.457	1126	1934	347	65	4.93	69	4.49	16.3	13.4	0.333	0.481	0.154	1.33	0.434	0.285	0.080	1.29
112	Jt4Mt5 09	601	1248	2567	34	237	0.668	3231	1763	273	124	5.27	57	2.71	16.7	14.5	0.416	0.147	0.071	2.58	0.040	0.211	0.064	5.50
113	Jt4Mt5 10	163	542	926	16	237	0.530	2660	1757	306	99	4.61	57	2.36	7.5	12.0	0.205	0.076	0.018	1.93	0.002	0.169	0.067	0.41
114	Jt4Mt5 11	404	874	1964	16	237	0.531	6150	1699	332	175	4.34	54	0.944	8.5	12.6	0.272	0.102	0.050	4.84	0.022	0.156	0.021	0.62
115	Jt4Mt5 12	1219	2098	4408	11	237	0.908	6439	1711	283	184	5.09	60	0.541	10.4	14.2	0.709	0.154	0.009	5.34	0.002	0.342	0.090	15.76
116	Jt4Mt5 13	365	797	2025	16	237	0.567	2086	1664	284	91	6.16	75	19.76	11.1	13.3	0.170	0.108	0.060	1.66	0.055	0.294	0.005	1.41
117	Jt4Mt5 14	1287	2058	4721	40	237	0.993	2735	1720	329	138	5.50	59	3.22	42.5	14.7	0.701	6.309	0.181	2.37	0.234	0.286	0.090	18.76
118	Jt4Mt5 15	89	536	1330	59	237	1.119	6988	1664	242	248	6.07	66	1.28	40.5	21.1	0.632	0.128	0.069	5.85	0.064	0.328	0.142	1.34
119	Jt4Mt5 16	681	1336	3316	90	237	0.515	2366	1764	317	94	5.72	69	5.41	13.0	12.4	0.740	0.436	1.64	2.28	0.443	0.278	0.144	8.04
120	Jt4Mt5 17	541	1144	2811	40	237	0.571	3152	1686	260	99	5.12	59	3.41	11.2	13.2	0.146	0.297	0.156	2.63	0.132	0.284	0.017	4.47
121	Jt4Mt5 18	2464	688	6730	970	2599	1.57	3504	1605	260	193	5.91	61	2.30	28.3	13.8	2.04	1.65	0.231	3.94	0.218	0.332	0.326	2.39
122	Jt4Mt5 19	178	671	762	678	1716	0.240	797	1648	421	56	7.78	73	0.904	24.8	20.1	0.500	0.888	0.023	0.54	0.029	0.334	0.030	2.34
123	Jt4Mt6rim 08	396	664	1497	177	790	0.317	1120	1664	425	71	4.63	57	0.148	18.1	11.1	0.341	1.76	0.004	0.73	0.005	0.254	0.039	4.30
124	Jt4Mt6rim 09	207	456	1332	16	237	0.797	9772	1572	79	360	6.71	56	0.074	28.7	20.4	0.232	0.089	0.019	7.81	0.121	0.345	0.051	0.20
125	Jt4Mt6rim 10	477	490	2246	16	237	0.835	9242	1555	26	320	6.03	62	0.049	27.1	18.2	0.612	0.152	0.014	8.27	0.144	0.327	0.103	0.37
126	Jt4Mt6rim 11	260	780	19617	16	237	0.443	316	1619	413	35	28.17	358	4.54	12.8	15.8	0.247	0.044	11.31	0.04	0.005	0.251	0.019	1.97
127	Jt4Mt6rim 12	98	519	624	72	237	0.642	6807	1620	309	280	6.47	60	0.577	47.3	19.4	0.389	0.506	0.071	4.77	0.031	0.367	0.092	0.820
128	Jt4Mt6rim 13	61	502	1355	358	656	0.268	269	1625	306	34	5.17	72	0.465	9.2	12.7	0.333	0.442	0.049	0.02	0.003	0.191	0.013	0.15
129	Jt4Mt6rim 14	954	872	2046	22	521	0.718	5899	1621	138	356	7.30	61	1.22	171.1	21.8	1.934	2.43	0.705	4.48	0.253	0.397	0.193	24.69
130	Jt4Mt6rim 15	420	802	1900	221	715	0.439	4253	1587	439	143	4.94	62	0.431	20.9	12.9	0.410	0.772	0.092	3.23	0.111	0.226	0.061	3.36
131	Jt4Mt6rim 16	828	590	2221	52	237	0.852	7017	1531	94	279	5.89	61	0.459	72.0	15.7	0.700	4.01	0.013	5.13	0.009	0.318	0.068	8.37
132	Jt4Mt6rim 17	266	556	1136	175	378	0.531	7291	1536	162	263	5.36	58	0.099	50.5	14.2	0.678	1.05	0.309	5.72	0.090	0.348	0.072	5.18
133	Jt4Mt6core 03	401	688	1578	16	237	0.705	10059	1496	122	293	4.82	54	0.135	50.4	11.6	0.655	0.558	0.005	8.03	0.055	0.291	0.082	5.51
134	Jt4Mt6core 04	358	521	1366	16	237	0.691	7895	1569	217	250	5.27	60	0.326	24.7	13.6	0.665	2.24	0.013	6.61	0.088	0.281	0.072	4.16

#	Sample	Mg	Al	Si	P	Ca	Sc	Ti	V	Cr	Mn	Co	Ni	Cu	Zn	Ga	As	Sr	Zr	Nb	Mo	Sn	Sb	Ba
135	Jt4Mt6core 05	588	1078	2133	535	735	0.668	8282	1520	383	208	4.61	67	0.222	8.7	11.5	0.441	0.458	0.014	6.44	0.000	0.273	0.017	1.50
136	Jt4Mt6core 06	144	517	1022	16	237	0.509	3523	1567	257	142	5.19	55	0.151	16.4	14.8	0.403	0.406	0.009	2.47	0.007	0.243	0.022	0.93
137	Jt4Mt6core 07	2569	4163	8550	16	237	0.924	1257	1590	445	75	5.34	65	7.89	16.8	15.3	0.302	0.269	0.343	0.96	0.003	0.289	0.009	105.45
138	Jt4Mt6core 08	201	530	1395	879	2303	0.526	5341	1486	228	197	5.16	57	0.942	13.5	14.3	0.435	1.91	0.011	3.96	0.021	0.302	0.043	0.81
139	Jt4Mt6core 09	597	1091	3353	38	237	0.641	2650	1568	376	113	4.75	60	0.505	11.9	12.3	0.451	0.419	0.037	2.05	0.003	0.247	0.019	1.20
140	Jt4Mt7rim 18	104	447	5442	16	237	0.291	263	1419	396	32	4.69	56	0.084	7.2	12.8	0.326	0.041	0.002	0.027	0.003	0.199	0.004	0.38
141	Jt4Mt7rim 19	488	978	2177	16	237	0.263	284	1442	265	33	5.23	56	0.047	8.8	14.8	0.257	0.048	0.032	0.110	0.004	0.218	0.011	4.08
142	Jt4Mt7rim 20	29	457	216	16	237	0.188	315	1474	64	44	7.89	57	0.267	13.6	20.2	0.314	0.009	0.003	0.004	0.003	0.172	0.010	0.033
143	Jt4Mt7rim 21	47	354	293	16	237	0.090	263	1451	393	36	13.03	194	0.209	8.9	15.4	0.170	0.005	0.001	0.012	0.004	0.153	0.011	0.000
144	Jt4Mt7core 10	55	521	477	16	237	0.303	320	1486	54	52	10.79	64	0.367	23.1	24.5	0.163	0.007	0.003	0.003	0.008	0.217	0.006	0.026
145	Jt4Mt7core 11	30	490	342	16	237	0.245	318	1484	7	54	10.33	58	0.031	31.2	25.1	0.107	0.002	0.005	0.000	0.003	0.205	0.010	0.009
146	Jt4Mt8rim 22	153	505	3465	16	237	0.201	191	1382	652	33	492.83	4955	3.05	9.8	13.9	0.186	0.059	1.30	0.097	0.003	0.178	0.063	1.27
147	Jt4Mt8rim 23	121	484	1007	16	220	0.425	9481	1510	249	261	5.41	56	0.521	13.3	19.6	0.474	0.395	0.021	7.61	0.100	0.419	0.058	1.39
148	Jt4Mt8rim 24	88	334	3535	17	237	0.186	222	1433	649	33	5.32	58	0.370	10.5	13.9	0.222	0.046	0.757	0.04	0.003	0.150	0.018	1.24
149	Jt4Mt8rim 25	28	313	363	128	237	0.546	11962	1398	690	297	24.94	208	2.12	11.0	16.5	0.392	0.181	0.022	9.15	0.009	0.351	0.144	0.475
150	Jt4Mt8rim 26	194	522	528	16	305	0.726	11095	1435	64	504	8.39	56	0.895	101.7	24.1	0.920	0.756	0.166	8.64	0.170	0.340	0.116	4.44
151	Jt4Mt8rim 27	277	620	733	16	237	0.576	11171	1495	177	366	6.61	58	0.390	62.9	22.1	0.883	1.37	0.028	8.86	0.218	0.318	0.009	3.04
152	Jt4Mt8rim 28	5603	1859	18643	16	11682	13.4	13928	1535	16.8	302	10.95	66	1.09	41.4	25.2	0.746	2.36	0.670	31.70	2.143	11.41	0.09	3.95
153	Jt4Mt8rim 29	2438	3760	8547	16	286	1.4	4826	1505	37.9	160	5.48	59	1.02	14.1	18.2	0.325	0.754	0.088	4.43	0.039	0.502	0.030	31.77
154	Jt7Mt1 01	478	764	2113	16	813	0.328	814	2415	17.7	32	2.28	49	0.203	23.5	17.7	0.857	1.570	0.081	1.282	0.179	0.373	0.071	5.633
155	Jt7Mt1 02	1600	2082	4155	16	366	0.338	867	2270	16.3	40	2.56	78	0.226	18.5	22.0	0.719	1.757	0.043	1.261	0.179	0.263	0.076	14.735
156	Jt7Mt1 03	821	1295	3720	16	1773	0.385	1786	2189	12.9	64	9.55	52	0.207	27.1	25.5	1.199	0.806	0.964	4.084	0.050	0.944	0.080	7.278
157	Jt7Mt1 04	271	555	844	16	230	0.164	430	2142	34.7	75	11.84	49	0.198	31.3	25.7	0.643	0.414	0.004	0.057	0.607	0.116	0.064	1.229
158	Jt7Mt1 05	76	518	643	16	234	0.144	389	2132	20.4	68	11.54	49	0.220	26.2	25.6	0.573	0.018	0.002	0.043	0.413	0.062	0.073	0.010
159	Jt7Mt1 06	928	1314	2036	16	252	0.169	487	2123	27.6	61	9.80	49	0.238	19.4	25.1	0.954	0.417	0.002	0.173	0.180	0.091	0.141	9.534
160	Jt7Mt1 07	358	683	1313	16	244	0.164	412	2107	39.5	33	3.18	58	0.247	21.5	19.6	0.853	0.320	0.015	0.089	0.248	0.130	0.069	0.905
161	Jt7Mt1 08	675	806	1746	16	263	0.167	469	2115	49.7	35	3.14	47	0.222	16.9	17.6	0.940	0.785	0.011	0.562	0.049	0.159	0.084	4.469
162	Jt7Mt 2 01	3580	3859	9294	16	248	0.587	762	2160	56.2	35	0.63	102	2.5	12.3	11.0	0.919	0.248	0.012	0.842	0.033	0.238	0.194	14.1
163	Jt7Mt 2 02	2611	2998	5984	16	240	0.305	702	2222	9.1	43	2.10	58	0.235	25.5	23.4	1.149	1.981	0.009	0.662	0.024	0.114	0.474	31.8
164	Jt7Mt 2 03	2300	2586	5947	16	241	0.405	638	2244	23.1	38	2.37	50	0.254	17.6	22.6	0.608	0.779	0.021	0.617	0.025	0.193	0.067	25.4
165	Jt7Mt 2 04	601	964	2234	32	1046	0.155	1372	2161	2.7	38	2.24	44	0.510	29.1	27.4	0.727	1.838	0.114	3.893	0.111	0.904	0.072	4.982
166	Jt7Mt 2 05	2881	3554	9838	16	2196	0.658	2743	2202	23.2	35	1.54	84	0.466	13.3	19.4	1.097	1.025	0.266	9.102	0.055	1.124	0.524	26.3
167	Jt7Mt 2 06	1357	668	3873	16	236	0.354	492	2094	2.4	67	2.05	47	0.206	24.4	20.2	1.136	0.518	0.038	0.549	0.325	0.157	0.131	1.254
168	Jt7Mt 2 07	799	502	2582	16	253	0.161	392	2130	9.6	39	0.55	43	0.225	12.5	11.4	0.674	1.521	0.440	0.232	0.527	0.080	0.112	3.307
169	Jt7Mt 3 01	2742	3370	6715	16	261	0.252	506	2133	86.2	28	0.53	73	1.1	12.8	13.1	0.723	0.162	0.010	0.231	0.110	0.145	0.319	26.849
170	Jt7Mt 3 02	336	663	961	16	258	0.188	310	2249	75.1	34	1.05	50	0.473	20.5	18.5	0.524	0.830	0.010	0.086	0.036	0.116	0.073	3.332
171	Jt7Mt 3 03	5155	1631	18419	16	810	0.596	851	2252	72.7	247	2.80	87	1.2	24.8	10.9	0.896	0.244	0.112	1.533	0.036	0.317	0.177	5.983
172	Jt7Mt 3 04	1149	1991	8542	16	7518	0.604	8743	2244	2.7	71	2.26	66	0.462	20.9	21.9	1.000	1.162	1.0	22.3	0.381	3.458	0.286	9.631
173	Jt7Mt 3 05	826	698	2374	37	259	0.163	2592	2195	4.2	65	1.50	56	0.768	16.8	15.6	0.767	0.357	0.035	1.630	0.612	0.275	0.160	0.813
174	Jt7Mt 3 06	316	563	1149	16	214	0.202	5160	2221	2.3	212	2.75	49	0.440	33.0	22.7	0.698	0.157	0.017	2.141	0.550	0.120	0.067	0.255
175	Jt7Mt 3 07	787	1072	2143	16	241	0.204	517	2222	62.2	30	1.88	51	0.321	17.3	17.1	0.802	0.196	0.018	0.284	0.345	0.179	0.068	7.753
176	Jt7Mt 3 08	1368	973	4030	16	654	0.714	495	2211	69.9	51	3.07	61	1.1	15.1	14.3	0.537	0.547	0.053	0.589	0.048	0.158	0.119	3.282
177	Jt7Mt 3 09	340	709	1832	16	1237	0.251	1431	2177	13.1	48	4.68	46	0.825	28.4	21.8	0.554	2.710	0.067	2.599	0.214	0.493	0.087	6.361
178	Jt7Mt 3 10	1647	1764	4610	16	783	0.159	1096	2134	68.5	45	7.53	51	6.783	28.2	23.7	0.604	0.656	0.228	1.607	0.102	0.381	0.082	16.562
179	Jt7Mt 4 rim 01	455	720	2091	16	815	0.161	3182	2448	50.1	70	0.77	49	0.882	17.0	13.4	0.559	2.906	0.150	2.867	0.101	0.351	0.076	7.550

#	Sample	Mg	Al	Si	P	Ca	Sc	Ti	V	Cr	Mn	Co	Ni	Cu	Zn	Ga	As	Sr	Zr	Nb	Mo	Sn	Sb	Ba
180	Jt7Mt 4 rim 02	750	637	4814	16	245	0.165	12764	2406	8.4	335	3.64	44	0.305	22.8	21.6	0.545	1.387	0.035	8.277	0.570	0.248	0.062	5.236
181	Jt7Mt 4 rim 03	1342	1214	4051	16	685	0.299	8852	2425	18.1	268	7.63	46	0.248	21.4	25.5	0.646	0.273	0.067	6.284	0.179	0.311	0.097	6.723
182	Jt7Mt 4 rim 04	18	488	315	16	255	0.174	239	1992	67.3	31	3.21	47	0.679	14.2	19.1	0.494	0.048	0.011	0.014	0.175	0.077	0.065	0.121
183	Jt7Mt 4 rim 05	503	840	3012	16	1533	0.382	8188	2190	15.4	273	6.35	44	0.256	24.7	23.9	0.577	0.363	0.166	8.125	0.112	0.909	0.073	0.987
184	Jt7Mt 4 rim 06	626	997	2253	16	780	0.570	12193	2334	6.9	343	8.68	43	0.257	22.3	24.8	0.741	0.379	0.063	8.869	0.298	0.267	0.074	0.731
185	Jt7Mt 4 rim 07	1324	1093	5079	16	1193	0.286	10056	2437	7.1	307	8.63	53	0.472	24.9	25.7	0.863	0.753	0.232	9.330	0.614	0.822	0.115	5.908
186	Jt7Mt 4 core 01	779	707	2486	15	545	0.177	10345	2482	3.8	351	9.08	47	0.340	82.7	22.7	0.723	4.5	0.032	7.358	0.583	0.231	0.137	9.912
187	Jt7Mt 4 core 02	1380	649	3975	16	237	0.164	10083	2503	0.893	459	12.26	49	0.275	28.3	26.2	0.548	0.610	0.329	7.255	0.315	0.331	0.170	1.158
188	Jt7Mt 4 core 03	1911	662	4670	16	266	0.202	8442	2482	1.2	417	12.30	50	0.225	33.0	27.0	0.796	0.455	0.181	6.427	0.486	0.266	0.158	0.435
189	Jt7Mt 5 01	340	663	3707	16	276	0.210	722	2406	14.8	56	7.94	49	1.3	24.2	24.1	0.647	0.552	0.073	1.090	0.325	0.220	0.073	3.114
190	Jt7Mt 5 02	623	705	2424	16	1241	0.432	1128	2552	21.0	86	14.32	51	1.2	33.3	25.9	0.550	0.942	0.147	3.532	0.568	0.443	0.078	3.876
191	Jt7Mt 5 03	531	938	1857	69	420	0.385	477	2627	41.9	106	17.06	53	7.9	35.2	25.4	0.678	0.440	0.149	0.097	0.773	0.144	0.084	1.127
192	Jt7Mt 5 04	1218	629	3332	14	335	0.444	446	2629	30.5	122	15.59	53	0.999	32.3	25.8	0.706	0.328	0.062	0.131	0.611	0.262	0.078	3.087
193	Jt7Mt 5 05	1050	598	2704	16	236	0.383	418	2544	23.0	106	12.09	52	1.5	30.6	26.1	0.819	0.815	0.069	0.167	0.754	0.198	0.108	11.137
194	Jt7Mt 5 06	780	707	2347	17	566	0.390	643	2388	26.2	56	5.35	49	1.2	26.2	21.0	1.096	0.676	0.051	0.826	0.396	0.326	0.082	1.887
195	Jt7Mt 5 07	1953	1987	6474	45	270	1.157	665	2137	56.3	144	1.59	57	3.8	49.1	17.5	1.921	1.4	0.066	0.897	0.407	0.312	0.256	69.846
196	Jt7Mt 5 08	3731	3033	7678	38	541	0.399	397	1887	26.9	41	1.45	121	4.8	36.2	10.2	0.683	4.4	0.084	0.493	0.418	0.208	0.265	23.398
197	Jt7Mt 5 09	1164	660	2530	16	543	0.167	449	2098	51.2	97	1.48	50	1.2	89.5	20.4	1.179	6.0	0.012	0.271	0.090	0.107	0.083	19.922
198	Jt7Mt 5 10	8758	10645	22755	35	329	1.05	3904	1744	87.9	118	1.10	297	6.5	18.4	11.2	0.760	0.475	0.107	7.975	0.535	0.249	0.205	62.396
199	Jt7Mt 6 01	1475	1960	3586	16	247	0.153	450	2152	45.7	37	6.32	44	2.0	17.7	20.7	0.587	0.022	0.005	0.207	0.019	0.064	0.055	21.208
200	Jt7Mt 6 02	284	628	820	16	253	0.152	1165	2112	70.8	71	2.95	45	0.246	24.1	20.0	0.583	1.9	0.010	0.576	0.029	0.172	0.066	5.537
201	Jt7Mt 6 03	471	806	2862	16	2713	0.207	5163	2042	48.0	124	3.47	46	0.241	20.5	21.4	1.296	1.1	0.246	7.178	0.060	1.823	0.147	4.417
202	Jt7Mt 6 04	1020	623	2742	16	213	0.228	9602	2035	17.9	405	4.01	47	0.260	27.6	25.3	0.663	0.250	0.029	5.696	0.506	0.220	0.148	0.575
203	Jt7Mt 6 05	2173	1789	5938	16	2296	1.34	3369	1879	44.5	110	2.69	134	0.863	15.6	19.6	0.738	0.586	0.105	2.795	0.327	0.699	0.404	4.168
204	Jt7Mt 7 01	3848	4578	8149	16	249	0.176	387	1797	32.7	42	1.68	103	0.606	14.4	13.9	0.889	0.058	0.015	0.153	0.029	0.131	0.082	9.629
205	Jt7Mt 7 02	181	509	561	16	230	0.162	357	1924	39.8	42	4.56	46	0.225	19.7	23.9	0.656	0.108	0.002	0.001	0.026	0.072	0.092	0.369
206	Jt7Mt 7 03	123	622	733	16	226	0.150	357	1947	12.7	23	1.11	90	0.224	16.8	18.8	0.701	0.049	0.007	0.030	0.027	0.066	0.080	0.051
207	Jt7Mt 7 04	30	500	273	16	231	0.142	371	1915	0.8	47	5.93	45	0.247	19.4	24.8	0.541	0.004	0.002	0.002	0.030	0.132	0.077	0.018
208	Jt7Mt 7 05	846	1276	2258	16	249	0.145	417	1915	30.1	34	3.01	45	0.235	17.4	19.4	0.750	0.206	0.001	0.092	0.044	0.108	0.077	12.713
209	Jt7Mt 8 01	27	469	353	16	244	0.152	415	1962	18.0	23	1.23	44	0.249	7.5	12.1	0.566	0.017	0.001	0.001	0.025	0.096	0.064	0.048
210	Jt7Mt 8 02	31	526	309	16	252	0.170	436	1950	7.4	41	4.68	46	0.233	15.2	24.3	0.571	0.004	0.009	0.001	0.025	0.049	0.064	0.004
211	Jt7Mt 8 03	436	760	1220	16	245	0.178	431	1940	33.5	40	5.98	70	0.379	20.9	24.7	0.556	0.078	0.007	0.047	0.029	0.101	0.070	2.915
212	Jt7Mt 8 04	390	688	1115	16	234	0.174	435	1896	61.6	18	0.58	48	0.232	10.9	10.6	0.447	0.055	0.007	0.044	0.030	0.087	0.062	2.064
213	Jt7Mt 8 05	1091	782	2612	17	229	0.182	423	1966	56.7	20	0.48	48	0.259	12.2	13.1	0.722	0.182	0.007	0.094	0.026	0.048	0.069	3.753
214	Jt7Mt 8 06	5518	7002	13814	16	294	0.210	1171	1943	64.0	33	0.93	61	0.300	15.5	18.6	0.555	0.114	0.001	0.621	0.064	0.056	0.095	78.919
216	Jt7Mt 8 08	19	491	187	16	212	0.141	418	1945	11.0	27	2.23	46	0.232	15.9	17.4	0.517	0.013	0.002	0.002	0.021	0.087	0.062	0.058
217	Jt7Mt 8 09	20	414	265	678	1089	0.146	388	2035	7.4	18	0.21	45	0.927	8.5	11.5	0.470	0.726	0.022	0.010	0.040	0.084	0.062	0.242
218	Jt8Mt 1 01	169	518	445	16	226	0.382	324	1562	36.6	62	1.49	65	0.867	23.7	25.3	0.541	0.218	0.002	0.069	0.048	0.409	0.068	0.529
219	Jt8Mt 1 02	567	581	1953	16	235	0.446	287	1541	14.1	81	1.46	73	0.288	24.0	25.1	0.501	1.220	0.025	0.134	0.046	0.407	0.088	4.776
220	Jt8Mt 1 03	232	466	1050	16	198	0.376	321	1496	22.0	68	1.41	65	1.28	23.4	24.4	0.558	0.536	0.009	0.146	0.051	0.477	0.077	1.258
221	Jt8Mt 1 04	1651	488	4078	23	537	0.451	303	1547	29.3	135	2.61	103	0.461	57.2	25.8	1.028	4.184	0.017	0.376	0.079	0.464	0.217	16.146
222	Jt8Mt 1 05	434	434	2705	16	233	0.217	195	1608	46.4	73	0.74	258	0.528	23.7	23.5	0.790	1.903	0.025	0.339	0.094	0.296	0.186	8.363
223	Jt8Mt 2 01	699	495	1889	16	234	0.486	343	1524	6.2	109	2.20	66	0.234	38.1	27.1	0.971	0.842	0.014	0.177	0.016	0.387	0.069	1.986
224	Jt8Mt 2 02	584	521	1580	16	243	0.350	300	1637	19.4	108	1.71	66	0.256	32.1	25.1	0.611	3.383	0.009	0.231	0.056	0.440	0.134	10.482
225	Jt8Mt 2 03	1520	1033	18629	65	251	0.808	199	1495	27.1	848	0.98	397	1.11	16.3	26.8	0.791	0.912	0.030	0.711	0.380	0.673	0.233	4.663

#	Sample	Mg	Al	Si	P	Ca	Sc	Ti	V	Cr	Mn	Co	Ni	Cu	Zn	Ga	As	Sr	Zr	Nb	Mo	Sn	Sb	Ba
226	Jt8Mt 2 04	381	658	1384	16	234	0.584	365	1584	21.9	73	1.83	76	8.64	36.4	24.5	0.603	0.334	0.004	0.196	0.040	0.364	0.071	5.008
227	Jt8Mt 2 05	12	365	543	16	235	0.363	327	1540	1.5	59	1.46	59	0.224	8.4	23.2	0.520	0.001	0.001	0.001	0.033	0.334	0.065	0.025
228	Jt8Mt 2 06	1834	769	34207	16	232	1.99	220	1420	42.3	2858	3.53	92	1.551	22.8	24.0	0.549	1.068	0.024	0.252	0.340	0.501	0.195	3.563
229	Jt8Mt 3 01	2091	632	6247	16	256	0.690	297	1533	24.1	237	2.18	70	0.224	28.1	24.5	0.543	1.599	0.014	0.470	0.045	0.342	0.230	4.561
230	Jt8Mt 3 02	1845	541	4383	191	560	0.950	283	1493	12.1	210	2.78	67	0.236	64.3	27.0	1.046	2.630	0.022	0.980	0.077	0.473	0.208	10.038
231	Jt8Mt 3 03	1278	617	3253	16	249	0.313	832	1481	8.3	182	2.34	67	1.04	86.1	26.8	0.633	6.776	0.012	1.038	0.279	0.348	0.147	27.305
232	Jt8Mt 3 04	1054	486	2650	16	240	0.492	300	1470	22.1	115	2.58	66	0.245	24.1	23.4	0.614	0.390	0.005	0.311	0.220	0.425	0.085	0.908
233	Jt8Mt 3 05	1151	472	2856	16	223	0.649	318	1584	77.2	131	2.51	73	7.38	42.7	23.9	0.628	0.492	0.017	0.327	0.119	0.317	0.123	1.177
234	Jt8Mt 4 01	1065	503	2591	16	229	0.642	330	1535	39.7	170	2.99	67	0.226	64.0	25.9	0.587	4.119	0.015	0.323	0.127	0.400	0.151	16.276
235	Jt8Mt 4 02	1349	481	3994	16	221	0.608	317	1611	2.8	167	3.81	66	0.216	45.8	27.4	0.536	0.036	0.012	0.248	0.467	0.370	0.166	0.010
237	Jt8Mt 4 04	407	467	1126	16	224	0.494	512	1651	27.2	94	1.66	65	0.211	32.5	24.9	0.530	0.542	0.001	0.461	0.127	0.309	0.068	1.254
238	Jt8Mt 5 01	539	364	1718	16	296	0.380	250	1818	58.5	80	2.63	151	0.496	11.3	21.9	0.729	0.605	0.008	0.397	0.057	0.379	0.242	3.673
239	Jt8Mt 5 02	1029	1001	7544	16	282	0.511	172	1731	82.2	103	6.42	229	0.992	11.5	23.9	0.619	0.320	0.031	0.417	2.552	0.269	0.159	2.316
240	Jt8Mt 5 03	1405	643	3281	16	245	0.443	436	1693	18.8	155	3.51	68	0.241	69.0	26.6	0.566	1.947	0.007	0.693	0.152	0.500	0.190	6.779
241	Jt8Mt 5 04	550	1218	4264	117	1246	0.616	429	1843	83.1	81	1.55	67	0.584	14.8	24.0	2.491	3.857	0.014	0.420	0.177	0.616	0.069	4.893
242	Jt8Mt 5 05	941	649	2238	36	302	0.425	299	1725	49.7	150	1.74	67	0.234	58.8	24.9	0.578	8.038	0.055	0.769	0.103	0.366	0.203	22.359
243	Jt8Mt 5 06	712	497	1868	16	237	0.329	1069	1695	66.7	118	1.57	66	0.226	21.5	24.7	0.515	0.603	0.007	1.485	0.057	0.479	0.092	2.085
244	Jt8Mt 5 07	1633	504	3962	22	222	0.545	335	1679	47.3	166	1.92	66	0.218	32.6	25.3	0.546	0.386	0.012	0.642	0.039	0.498	0.157	0.308
245	Jt8Mt 5 08	1211	444	3507	24	222	0.516	283	1700	8.6	145	3.84	69	0.223	51.7	28.1	0.894	0.711	0.014	0.364	0.158	0.388	0.137	2.767
246	Jt8Mt 5 09	2211	585	5551	16	1372	2.36	325	1704	31.4	108	2.53	64	0.229	23.7	23.6	0.910	2.302	0.022	0.131	0.032	0.498	0.065	2.125
248	Jt8Mt 6 01	88	418	442	16	226	0.271	293	1766	7.9	63	2.14	61	0.221	18.2	24.0	0.466	0.392	0.002	1.709	0.055	0.425	0.077	0.437
249	Jt8Mt 6 02	536	407	2300	16	246	0.173	265	1676	96.0	80	1.56	99	2.319	23.6	23.8	0.520	1.26	0.010	0.216	0.334	0.224	0.222	4.725
250	Jt8Mt 6 03	1879	935	6109	16	244	0.608	249	1479	28.8	156	185.88	760	36.47	160.1	22.9	2.658	2.69	0.025	0.757	0.114	0.343	0.477	15.149
251	Jt8Mt 6 04	1798	496	4241	16	269	0.742	586	1681	9.6	193	2.50	67	0.262	37.4	25.2	0.881	1.32	0.015	1.478	0.045	0.410	0.225	1.696
252	Jt8Mt 6 05	1085	736	4093	16	194	0.985	5704	1655	30.1	373	2.07	67	3.272	69.6	24.7	0.713	4.02	0.037	10.732	0.141	0.960	0.275	9.838
253	Jt8Mt 6 06	561	556	1693	13	206	0.475	342	1604	35.4	95	2.71	68	0.459	37.6	25.2	0.717	1.15	0.007	0.310	0.098	0.299	0.092	2.530
254	Jt8Mt 6 07	69	479	677	16	222	0.265	314	1534	54.8	64	2.45	65	0.233	31.3	24.8	0.492	0.371	0.001	0.071	0.045	0.372	0.065	1.030
255	Jt8Mt 6 08	338	504	2035	16	243	0.354	418	1585	40.0	124	4.49	68	0.251	64.1	28.1	0.580	3.148	0.001	0.346	0.036	0.450	0.069	5.411
256	Jt8Mt 6 09	189	483	2065	16	237	0.206	259	1561	62.4	125	6.49	67	4.226	18.5	25.6	1.156	0.088	0.010	1.326	0.037	0.392	0.071	2.192
257	Jt8Mt 6 10	507	456	4155	16	224	0.349	359	1568	223.3	297	1.96	66	0.610	12.3	24.6	0.736	0.171	0.008	0.346	0.061	0.348	0.080	0.887
258	Jt8Mt 7 01	1846	518	4223	16	233	0.671	299	1583	38.7	190	3.52	67	0.212	39.4	25.9	1.257	0.746	0.015	0.834	0.027	0.427	0.223	1.862
259	Jt8Mt 7 02	3942	982	7581	16	234	0.899	608	1622	14.2	240	4.51	71	0.261	66.9	26.6	0.754	2.2	0.033	1.471	0.027	0.458	0.283	7.523
260	Jt8Mt 7 03	2506	652	7129	16	232	0.914	272	1643	10.4	230	3.21	83	0.270	36.2	26.5	1.140	1.3	0.032	1.235	0.251	0.465	0.242	5.192
261	Jt8Mt 7 04	2322	589	6067	16	258	0.961	976	1705	7.2	287	6.04	72	0.280	82.6	28.6	1.301	2.3	0.039	1.793	0.273	0.534	0.221	3.433
262	Jt8Mt 7 05	2916	635	6716	22	583	1.258	319	1704	2.4	275	4.51	71	0.384	72.2	28.0	1.140	0.589	0.089	1.290	0.465	0.533	0.305	1.425
263	Jt8Mt 7 06	2477	1080	5852	16	212	1.09	12271	1675	12.4	519	2.43	76	0.380	27.1	25.3	0.966	1.0	1.856	22.107	0.092	0.817	0.256	3.192
264	Jt8Mt 7 07	2566	683	5793	28	319	0.990	344	1704	5.1	217	3.64	69	0.283	67.3	28.2	1.012	0.647	0.039	1.016	0.483	0.510	0.320	0.948
265	Jt8Mt 7 08	2359	691	5707	16	473	0.978	357	1717	9.4	282	2.83	68	0.474	122	28.0	1.595	3.3	0.040	0.998	1.980	0.463	0.406	10.952
266	Jt8Mt 7 09	2521	699	5565	22	253	1.019	897	1726	17.8	260	4.61	100	41.5	95.4	26.8	0.967	4.1	0.026	1.653	0.037	0.554	0.366	10.742
267	Jt8Mt 7 10	2531	893	5406	22	309	0.871	1692	1684	25.5	270	3.65	65	3.51	2900	27.1	1.161	2.7	0.037	3.601	0.034	0.626	0.424	7.556
268	Jt8Mt 8 01	130	447	1284	16	259	0.226	272	1144	14.2	52	1.65	66	0.245	8.2	23.2	0.511	0.165	0.013	0.293	0.052	0.451	0.074	0.780
269	Jt8Mt 8 02	148	427	1376	16	251	0.257	711	1248	34.8	76	2.10	61	0.244	20.4	23.4	0.470	1.269	0.018	1.037	0.051	0.384	0.102	3.236
270	Jt8Mt 8 03	1821	1588	9933	16	249	0.512	219	1577	18.8	117	1.55	183	2.47	12.7	26.4	0.605	0.894	0.099	0.790	0.127	0.489	0.088	2.798
271	Jt8Mt 8 04	1193	807	6468	16	253	0.485	236	1694	6.2	103	2.01	109	1.97	13.7	24.4	0.528	0.285	0.538	0.436	0.199	0.470	0.131	1.020
272	Jt8Mt 8 05	2129	863	8598	16	276	0.682	378	1677	6.4	176	1.67	91	2.86	13.5	24.8	0.523	0.984	0.029	1.272	0.927	0.579	0.279	2.720

#	Sample	Mg	Al	Si	P	Ca	Sc	Ti	V	Cr	Mn	Co	Ni	Cu	Zn	Ga	As	Sr	Zr	Nb	Mo	Sn	Sb	Ba
273	Jt8Mt 8 06	68	432	522	16	280	0.218	268	1063	2.1	58	2.25	63	0.237	10.6	23.7	0.429	0.253	0.001	0.143	0.025	0.399	0.070	0.931
274	Jt8Mt 8 07	1026	529	3388	16	298	0.406	308	1498	34.4	116	1.95	72	2.31	22.2	24.8	0.429	1.501	0.005	0.592	0.042	0.383	0.188	3.774
275	Jt8Mt 8 08	886	453	2268	16	251	0.528	304	1490	49.1	107	2.23	67	0.233	18.4	24.4	0.466	0.884	0.012	0.249	0.030	0.428	0.145	1.998
276	Jt8Mt 9 01	761	411	2943	32	246	0.375	239	1583	57.8	107	1.87	68	0.491	26.4	23.0	0.650	4.3	0.016	0.558	0.039	0.385	0.127	20.329
277	Jt8Mt 9 02	751	722	4975	19	253	0.257	189	1519	65.2	94	1.44	120	1.18	18.3	24.0	0.822	1.5	0.047	0.306	0.044	0.332	0.112	7.818
279	Jt8Mt 9 04	759	372	2125	578	1038	0.368	2951	1530	74.9	198	1.62	75	0.531	24.1	22.9	0.522	2.1	0.010	5.313	0.027	0.468	0.168	5.557
280	Jt8Mt 9 05	1303	399	3253	16	279	0.361	255	1755	61.7	163	14.82	65	0.629	19.1	22.7	0.677	1.1	0.021	0.099	0.224	0.193	0.091	3.135
283	Jt8Mt 9 08	11	394	246	16	215	0.217	303	1594	94.5	51	2.35	64	0.341	9.3	22.9	0.453	0.080	0.005	0.135	0.056	0.337	0.069	0.271
284	Jt8Mt 9 09	308	358	2657	16	268	0.181	160	1668	74.2	52	1.33	146	5.580	7.8	22.2	0.624	0.572	0.013	0.275	0.074	0.189	0.081	2.457
285	Jt8Mt 9 10	292	362	865	21	230	0.221	299	1661	74.7	56	1.84	66	0.240	10.3	23.1	0.517	0.715	0.012	0.275	0.029	0.355	0.082	2.185
286	Jt8Mt 9 11	72	428	415	16	211	0.413	422	1580	77.9	65	3.27	62	0.926	32.7	24.3	0.563	0.019	0.001	0.156	0.064	0.321	0.082	0.087
287	Jt8Mt 9 12	152	466	574	16	236	0.439	365	1603	75.2	76	3.45	63	0.252	25.1	25.4	0.559	0.122	0.001	0.118	0.034	0.421	0.087	0.459
289	Jt8Mt 9 14	390	487	1213	16	265	0.730	333	1678	155.3	72	2.59	62	0.269	20.0	24.7	0.585	0.654	0.005	0.146	0.028	0.419	0.110	3.491
290	Jt8Mt 9 15	1236	582	3106	16	270	0.526	631	1611	12.9	159	2.59	65	1.030	48.9	25.4	0.473	1.279	0.010	0.752	0.041	0.519	0.114	3.262
291	Jt8Mt 9 16	1270	785	2857	16	254	0.491	3335	1604	17.8	201	2.45	62	0.261	38.3	23.8	0.540	2.678	0.011	6.791	0.146	0.483	0.109	8.572
292	Jt8Mt 9 17	1021	414	2562	16	260	0.363	285	1716	34.6	116	2.49	61	0.275	25.5	24.3	0.529	1.623	0.002	0.493	0.132	0.393	0.116	4.972
293	Jt8Mt 9 18	1193	448	3321	16	263	0.227	276	1729	33.7	137	19.35	83	6.632	76.4	24.6	1.294	0.508	0.028	0.477	0.034	0.524	0.118	1.198
294	Jt8Mt 9 19	893	467	3143	16	374	0.331	811	1708	23.6	111	1.63	63	2.738	21.8	23.9	0.764	2.329	0.019	1.061	0.380	0.354	0.121	9.663
295	Jt8Mt 9 20	38	364	421	16	254	0.176	322	1593	38.6	58	2.10	64	0.228	8.7	23.8	0.794	0.130	0.017	0.143	0.049	0.390	0.067	0.505
296	Jt9bMt1rim 01	313	799	1051	16	237	0.131	322	1715	4.39	75	9.96	64	5.34	18.2	32.4	0.007	0.378	0.759	0.122	0.560	0.210	0.055	2.68
297	Jt9bMt1rim 02	88	448	600	395	955	0.084	322	1717	5.64	67	8.85	59	0.682	13.5	31.8	0.315	0.412	0.921	0.219	0.108	0.203	0.037	0.617
299	Jt9bMt1rim 04	1326	1371	2871	16	237	0.021	500	1713	4.65	116	12.78	109	4.24	28.8	33.4	0.141	0.144	0.040	0.483	0.232	0.365	0.084	10.59
300	Jt9bMt1rim 05	4299	852	8318	16	613	0.176	388	1712	3.88	336	29.08	138	50.79	123.2	34.3	0.541	0.573	0.818	0.660	0.530	0.507	0.346	3.63
301	Jt9bMt1core 01	2954	650	6228	16	231	0.101	380	1697	3.41	231	11.13	63	0.719	34.2	34.6	0.370	1.339	0.164	0.575	0.077	0.318	0.236	4.84
302	Jt9bMt1core 02	3488	517	7317	16	363	0.157	329	1744	3.46	217	14.24	87	4.45	50.2	33.5	0.451	0.837	0.048	0.590	0.162	0.300	0.231	1.78
303	Jt9bMt2 01	20	337	323	16	237	0.026	276	1720	6.39	62	8.54	56	0.977	7.5	31.1	0.288	0.099	0.034	0.042	0.180	0.200	0.062	0.40
304	Jt9bMt2 02	1012	1457	2565	150	428	0.082	285	1711	6.87	88	9.42	63	0.841	13.1	37.6	0.268	0.379	0.120	0.106	0.247	0.433	0.039	0.55
305	Jt9bMt2 03	11	390	245	16	237	0.019	281	1789	4.57	75	8.79	57	0.126	7.8	31.4	0.128	0.022	0.075	0.008	0.110	0.223	0.005	0.09
306	Jt9bMt3 04	85	439	421	16	237	0.070	317	1731	5.74	79	9.75	60	0.520	15.7	32.9	0.111	0.409	0.085	0.110	0.222	0.360	0.053	1.45
307	Jt9bMt3 05	3053	1416	6440	16	266	0.167	406	1770	5.91	192	11.77	67	5.04	38.3	38.8	0.391	1.871	0.152	0.933	0.228	0.635	0.426	16.08
308	Jt9bMt3 06	760	436	1857	16	237	0.125	290	1729	4.62	87	9.68	64	1.88	11.8	32.1	0.190	0.222	0.038	0.255	0.108	0.204	0.105	0.73
309	Jt9bMt4 07	27	441	632	21	237	0.018	327	1744	5.55	72	10.86	87	0.586	10.2	31.3	0.218	0.115	0.424	0.051	0.317	0.152	0.024	0.14
310	Jt9bMt4 08	1377	902	3429	65	543	0.166	315	1632	5.12	124	45.91	282	47.12	64.4	35.0	0.244	2.833	0.134	0.293	0.067	0.326	0.221	9.57
311	Jt9bMt4 09	2084	462	4624	20	246	0.165	284	1705	4.06	147	15.73	95	91.23	34.3	32.4	0.352	0.575	0.306	0.404	0.535	0.322	0.197	1.68
312	Jt9bMt4 10	99	540	981	95	234	0.045	344	1677	4.13	89	9.85	64	1.28	24.6	33.5	0.135	0.221	0.100	0.096	0.096	0.276	0.035	1.33
313	Jt9bMt5 11	2774	835	5906	912	2909	0.196	432	1899	5.40	189	11.56	68	7.06	37.3	33.2	0.694	3.498	0.077	1.048	0.027	0.475	0.340	5.1
314	Jt9bMt5 12	2981	686	6889	16	2098	0.498	390	1788	4.71	162	10.68	61	3.83	38.4	33.2	0.431	0.906	0.244	0.346	0.096	0.446	0.134	4.56
315	Jt9bMt6 13	13	416	258	21	237	0.177	335	1625	5.23	78	9.66	61	1.14	11.9	33.6	0.268	0.056	0.103	0.004	0.006	0.288	0.017	0.05
316	Jt9bMt6 14	314	463	920	1840	4567	0.014	348	1581	384	100	10.38	68	0.820	21.3	34.3	0.374	2.869	0.127	0.152	0.418	0.363	0.061	1.09
317	Jt9bMt6 15	291	524	1023	1832	4935	0.095	335	1590	229	95	9.82	68	0.964	16.8	33.0	0.379	2.349	0.024	0.081	0.026	0.218	0.074	0.48
318	Jt9bMt6 16	1276	585	3055	2406	6160	0.150	340	1585	5.37	110	12.71	83	9.69	30.3	33.1	0.125	3.040	0.037	0.596	0.008	0.316	0.208	4.71
319	Jt9bMt7 17	110	406	370	16	237	0.033	293	1695	5.30	71	9.90	88	1.52	11.7	32.3	0.135	0.138	0.050	0.104	0.103	0.271	0.066	0.38
320	Jt9bMt7 18	203	459	965	2306	5160	0.161	214	1635	5.10	58	7.91	55	0.892	8.5	30.8	0.226	2.036	0.021	0.284	0.011	0.179	0.269	0.68
321	Jt9bMt7 19	3083	1014	8875	16	237	0.155	365	1644	2.13	165	10.56	68	1.30	41.2	36.3	0.187	1.755	0.069	0.621	0.235	0.502	0.272	8.31
322	Jt9bMt8 20	1649	601	3434	16	231	0.118	366	1720	1.76	109	10.55	66	3.13	18.6	33.6	0.211	0.503	0.046	0.319	0.453	0.344	0.071	2.62

#	Sample	Mg	Al	Si	P	Ca	Sc	Ti	V	Cr	Mn	Co	Ni	Cu	Zn	Ga	As	Sr	Zr	Nb	Mo	Sn	Sb	Ba
323	Jt9bMt8 21	2947	752	5756	22	237	0.025	413	1718	1.43	224	12.58	71	1.43	62.7	35.4	0.946	0.710	0.181	0.546	0.843	0.407	0.280	4.11
324	Jt9bMt8 22	2074	784	4059	16	237	0.085	381	1756	1.16	170	12.63	69	0.381	48.0	35.2	0.454	1.401	0.027	0.265	0.231	0.352	0.143	4.35
325	Jt9bMt8 23	1353	903	8792	261	654	0.148	345	1726	1.32	136	9.69	63	0.850	35.6	35.3	0.180	1.278	0.044	0.228	0.061	0.351	0.085	4.77
326	Jt9bMt8 24	1123	671	3106	62	119	0.046	328	1705	3.71	100	9.01	65	1.15	23.9	33.0	0.295	0.387	0.018	0.418	0.043	0.277	0.059	2.95
327	Jt9bMt9 25	14	424	349	25	237	0.052	324	1866	5.53	73	8.71	62	0.214	10.1	31.3	0.012	0.047	0.046	0.014	0.019	0.164	0.032	0.19
328	Jt9bMt9 26	1418	737	2935	19	269	0.023	357	1771	4.82	152	10.19	68	7.56	61.3	33.6	0.563	2.599	0.115	0.334	0.252	0.323	0.101	9.68
329	Jt9bMt9 27	73	324	585	28	237	0.030	254	1765	6.48	65	8.27	61	0.626	12.7	31.7	0.161	0.951	0.027	0.184	0.137	0.167	0.084	1.95
330	Jt9bMt10 28	1154	493	3108	16	331	0.014	347	1700	3.67	120	11.03	69	9.09	30.2	32.2	0.432	1.889	0.207	0.181	0.035	0.618	0.053	2.87
331	Jt9bMt10 29	302	415	1778	689	1899	0.124	271	1761	4.93	74	9.42	65	8.73	20.9	29.7	0.036	0.933	0.058	0.295	0.010	0.348	0.008	1.97
332	Jt9bMt10 30	30	373	395	37	262	0.058	317	1729	5.10	69	8.58	59	0.257	5.8	30.9	0.198	0.527	0.016	0.067	0.015	0.188	0.058	0.98
333	Jt9bMt10 31	62	363	415	160	436	0.029	314	1754	5.32	67	8.26	55	0.306	5.4	30.2	0.063	0.266	0.017	0.017	0.016	0.155	0.026	0.16
334	Jt9bMt11 32	256	388	1465	16	237	0.153	182	1603	7.82	62	11.89	157	6.02	16.1	32.8	0.031	0.539	0.110	0.231	0.153	0.579	0.034	0.81
335	Jt9bMt11 33	185	417	502	16	237	0.029	311	1616	5.35	67	8.52	63	0.810	7.1	32.0	0.100	0.079	0.013	0.054	0.003	0.206	0.012	0.58
336	Jt9Mt12 34	644	490	1574	640	1859	0.103	326	1626	3.72	115	10.48	69	8.29	26.5	32.3	0.080	0.783	0.011	0.256	0.013	0.296	0.125	1.48
337	Jt9bMt12 35	391	430	977	213	722	0.083	330	1585	4.06	96	9.21	61	0.351	13.4	32.4	0.264	0.505	0.035	0.125	0.040	0.181	0.102	0.71
338	Jt9bMt13 36	176	571	671	28	237	0.043	350	1616	5.06	77	9.34	63	0.372	14.0	33.6	0.004	0.106	0.035	0.061	0.021	0.328	0.029	1.65
339	Jt9bMt13 37	883	445	2088	16	237	0.032	309	1641	4.61	115	9.28	63	1.09	21.8	32.6	0.091	0.366	0.037	0.317	0.020	0.224	0.193	1.59
340	Jt9bMt14 38	355	493	1143	16	237	0.052	337	1597	5.86	101	11.33	72	3.46	26.5	32.9	0.168	0.428	0.107	0.146	0.214	0.331	0.083	1.92

ESM Table 2a. (Continued)

#	Sample	La	Ce	Pr	Nd	Sm	Eu	Gd	Tb	Dy	Y	Ho	Er	Tm	Yb	Lu	Hf	Ta	W	^{204}Pb	^{206}Pb	^{207}Pb	^{208}Pb	Th	^{238}U
1	Jt1Mt1rim 01	0.017	0.051	0.007	0.021	0.000	0.001	0.005	0.000	0.007	0.033	0.000	0.000	0.000	0.000	0.000	0.006	0.004	0.100	0.020	0.543	0.613	1.252	0.009	0.005
2	Jt1Mt1rim 02	0.009	0.029	0.004	0.008	0.000	0.002	0.004	0.000	0.003	0.018	0.001	0.006	0.000	0.000	0.000	0.000	0.001	0.029	0.197	2.936	3.059	6.983	0.002	0.005
3	Jt1Mt1rim 03	0.013	0.022	0.002	0.001	0.004	0.001	0.013	0.000	0.008	0.028	0.001	0.014	0.000	0.003	0.001	0.002	0.008	1.644	0.140	2.198	2.293	5.150	0.005	0.006
4	Jt1Mt1rim 04	0.038	0.252	0.061	0.620	0.508	0.184	1.231	0.419	3.914	24.09	0.971	3.190	0.433	2.296	0.245	0.032	1.052	1.899	0.055	1.107	0.987	2.225	0.025	0.327
5	Jt1Mt1core 01	0.016	0.037	0.003	0.015	0.004	0.003	0.001	0.000	0.002	0.022	0.000	0.004	0.000	0.005	0.001	0.000	0.001	0.032	0.196	2.853	2.971	6.812	0.018	0.006
6	Jt1Mt1core 02	0.027	0.096	0.010	0.040	0.015	0.000	0.006	0.001	0.004	0.021	0.000	0.000	0.000	0.005	0.001	0.004	0.001	0.042	0.130	2.296	2.427	5.643	0.012	0.005
7	Jt1Mt1core 03	0.010	0.045	0.001	0.003	0.000	0.002	0.001	0.001	0.000	0.025	0.002	0.002	0.000	0.000	0.000	0.000	0.003	0.038	0.114	1.834	1.941	4.331	0.024	0.004
8	Jt1Mt1core 04	0.018	0.060	0.001	0.019	0.000	0.000	0.001	0.006	0.008	0.028	0.000	0.006	0.000	0.000	0.000	0.000	0.002	0.030	0.117	1.669	1.842	4.513	0.010	0.019
9	Jt1Mt1rim 05	0.034	0.121	0.034	0.307	0.192	0.041	0.545	0.134	1.324	9.22	0.360	1.304	0.183	1.126	0.127	0.024	1.142	0.928	0.160	2.040	2.077	4.736	0.009	0.163
10	Jt1Mt1rim 06	0.017	0.077	0.022	0.099	0.069	0.016	0.105	0.033	0.301	1.82	0.084	0.208	0.035	0.206	0.027	0.005	0.230	2.261	0.014	0.180	0.183	0.407	0.005	0.061
11	Jt1Mt2rim 07	0.010	0.046	0.008	0.032	0.023	0.012	0.041	0.016	0.147	1.22	0.052	0.166	0.029	0.136	0.015	0.002	0.144	1.202	0.087	1.143	1.310	2.825	0.001	0.023
12	Jt1Mt2rim 08	0.031	0.041	0.001	0.016	0.000	0.002	0.008	0.000	0.003	0.017	0.000	0.004	0.001	0.000	0.001	0.000	0.004	0.025	0.157	2.439	2.632	5.933	0.007	0.007
13	Jt1Mt2rim 09	0.011	0.026	0.002	0.008	0.010	0.004	0.001	0.002	0.000	0.027	0.001	0.011	0.000	0.003	0.000	0.002	0.001	0.010	0.115	1.983	2.162	4.770	0.006	0.007
14	Jt1Mt2rim 10	0.014	0.085	0.012	0.144	0.045	0.032	0.151	0.057	0.490	2.98	0.118	0.344	0.057	0.271	0.040	0.008	0.458	0.905	0.060	1.114	1.161	2.612	0.005	0.058
15	Jt1Mt2rim 11	0.071	0.152	0.014	0.105	0.016	0.008	0.048	0.003	0.034	0.093	0.004	0.019	0.002	0.003	0.001	0.000	0.002	0.262	0.183	2.374	2.550	5.765	0.001	0.058
16	Jt1Mt2rim 12	0.038	0.097	0.015	0.175	0.103	0.035	0.252	0.068	0.509	3.20	0.111	0.503	0.074	0.370	0.049	0.012	0.501	0.471	0.043	0.668	0.682	1.457	0.000	0.085
17	Jt1Mt2core 05	0.039	0.100	0.009	0.023	0.009	0.002	0.008	0.000	0.011	0.055	0.001	0.008	0.000	0.000	0.000	0.016	0.005	0.076	0.073	1.084	1.241	2.573	0.014	0.005
18	Jt1Mt2core 06	0.010	0.039	0.001	0.014	0.004	0.001	0.003	0.000	0.000	0.025	0.002	0.000	0.000	0.000	0.001	0.002	0.006	0.005	0.076	1.151	1.255	2.909	0.012	0.010
19	Jt1Mt3rim 13	0.018	0.081	0.019	0.113	0.089	0.024	0.206	0.067	0.808	5.05	0.193	0.619	0.088	0.559	0.057	0.025	0.334	0.301	0.041	0.434	0.323	0.824	0.002	0.050
20	Jt1Mt3rim 14	0.316	0.801	0.118	0.513	0.200	0.070	0.412	0.089	0.772	4.12	0.164	0.486	0.075	0.499	0.056	0.005	0.345	0.789	0.006	0.318	0.293	0.622	0.004	0.218
21	Jt1Mt3rim 15	0.010	0.020	0.006	0.054	0.034	0.008	0.033	0.015	0.158	1.10	0.043	0.189	0.019	0.153	0.025	0.004	0.132	0.252	0.012	0.239	0.280	0.519	0.002	0.029

#	Sample	La	Ce	Pr	Nd	Sm	Eu	Gd	Tb	Dy	Y	Ho	Er	Tm	Yb	Lu	Hf	Ta	W	^{204}Pb	^{206}Pb	^{207}Pb	^{208}Pb	Th	^{238}U
22	Jt1Mt3rim 16	0.051	0.124	0.028	0.152	0.087	0.056	0.325	0.086	0.857	5.45	0.223	0.758	0.117	0.672	0.072	0.011	0.521	0.773	0.043	0.773	0.746	1.695	0.006	0.168
24	Jt1Mt4rim 17	0.032	0.083	0.011	0.073	0.051	0.006	0.069	0.001	0.028	0.076	0.005	0.006	0.000	0.007	0.000	0.004	0.000	0.003	0.006	0.029	0.014	0.040	0.005	0.140
25	Jt1Mt4rim 18	0.027	0.019	0.005	0.066	0.005	0.004	0.005	0.000	0.000	0.018	0.000	0.002	0.000	0.007	0.001	0.000	0.008	0.107	0.031	0.642	0.666	1.606	0.003	0.008
26	Jt1Mt4rim 19	0.009	0.021	0.003	0.011	0.000	0.001	0.002	0.000	0.008	0.014	0.002	0.002	0.000	0.002	0.000	0.001	0.002	0.047	0.160	2.363	2.489	5.626	0.005	0.006
27	Jt1Mt4rim 20	0.082	0.234	0.042	0.264	0.203	0.049	0.337	0.067	0.633	4.05	0.163	0.576	0.091	0.529	0.068	0.027	0.912	0.620	0.106	1.889	1.851	3.973	0.011	0.477
28	Jt1Mt4rim 21	0.037	0.053	0.006	0.044	0.008	0.002	0.001	0.002	0.023	0.110	0.008	0.022	0.005	0.032	0.006	0.003	0.561	0.043	0.103	2.286	1.672	3.468	0.006	1.560
29	Jt1Mt4core 08	0.040	0.099	0.011	0.052	0.018	0.001	0.012	0.001	0.036	0.135	0.006	0.029	0.006	0.036	0.005	0.006	0.903	0.108	0.050	1.934	1.053	1.948	0.008	2.169
30	Jt1Mt4core 09	0.036	0.157	0.043	0.262	0.233	0.058	0.485	0.125	1.195	7.16	0.296	0.966	0.133	0.824	0.103	0.037	0.712	0.818	0.119	1.970	1.963	4.411	0.021	0.303
31	Jt1Mt4core 10	0.048	0.092	0.006	0.015	0.008	0.002	0.020	0.003	0.037	0.144	0.007	0.028	0.007	0.038	0.010	0.002	0.862	0.127	0.003	1.150	0.258	0.235	0.015	2.643
33	Jt1Mt5rim 23	0.041	0.089	0.027	0.126	0.046	0.024	0.036	0.020	0.157	1.11	0.041	0.113	0.025	0.168	0.014	0.009	0.152	0.247	0.062	1.069	1.109	2.476	0.004	0.030
34	Jt1Mt5rim 24	0.264	0.690	0.080	0.365	0.049	0.010	0.079	0.010	0.108	0.594	0.033	0.103	0.012	0.105	0.010	0.002	0.045	0.165	0.073	1.354	1.447	3.351	0.025	0.028
35	Jt1Mt5core 11	0.072	0.158	0.040	0.113	0.009	0.006	0.061	0.004	0.025	0.162	0.018	0.026	0.001	0.030	0.003	0.005	0.021	0.048	0.258	3.644	3.981	9.112	0.016	0.050
36	Jt1Mt6rim 25	0.024	0.124	0.030	0.162	0.087	0.036	0.188	0.050	0.434	3.0	0.117	0.435	0.069	0.384	0.041	0.013	0.356	0.465	0.051	0.722	0.779	1.767	0.005	0.061
37	Jt1Mt6rim 26	0.096	0.231	0.030	0.144	0.025	0.001	0.036	0.004	0.029	0.124	0.006	0.018	0.001	0.012	0.000	0.057	0.004	0.029	0.052	0.742	0.737	1.600	0.015	0.060
38	Jt1Mt6rim 27	0.005	0.015	0.002	0.004	0.000	0.000	0.001	0.000	0.006	0.015	0.002	0.006	0.000	0.002	0.000	0.003	0.002	0.007	0.124	1.979	2.081	4.699	0.003	0.003
39	Jt1Mt6rim 28	0.006	0.031	0.005	0.007	0.005	0.002	0.002	0.001	0.006	0.016	0.000	0.002	0.000	0.001	0.000	0.002	0.002	0.030	0.118	1.763	1.869	4.328	0.001	0.017
40	Jt1Mt6rim 29	0.004	0.011	0.000	0.000	0.000	0.001	0.010	0.000	0.001	0.011	0.000	0.005	0.000	0.002	0.000	0.000	0.001	0.005	0.050	0.907	0.960	2.085	0.000	0.003
41	Jt1Mt6rim 30	0.007	0.022	0.004	0.004	0.002	0.000	0.005	0.000	0.003	0.009	0.000	0.000	0.000	0.002	0.000	0.000	0.000	0.004	0.051	0.742	0.796	1.771	0.002	0.004
42	Jt1Mt6rim 31	0.007	0.028	0.001	0.014	0.007	0.000	0.003	0.000	0.014	0.030	0.000	0.003	0.000	0.002	0.000	0.002	0.003	0.011	0.039	0.700	0.741	1.640	0.002	0.004
43	Jt1Mt6rim 32	0.007	0.020	0.000	0.002	0.008	0.002	0.008	0.000	0.001	0.035	0.001	0.007	0.001	0.002	0.000	0.001	0.003	0.090	0.072	1.311	1.404	3.077	0.002	0.007
44	Jt1Mt6rim 33	0.646	1.536	0.210	0.700	0.100	0.003	0.042	0.010	0.079	0.335	0.015	0.040	0.005	0.046	0.003	0.000	0.035	0.156	0.030	0.668	0.690	1.537	0.004	0.052
45	Jt1Mt6rim 34	0.014	0.007	0.004	0.010	0.000	0.000	0.002	0.001	0.002	0.010	0.001	0.003	0.000	0.000	0.000	0.001	0.001	0.012	0.086	1.373	1.473	3.263	0.000	0.005
46	Jt1Mt6rim 35	0.016	0.045	0.006	0.016	0.005	0.004	0.007	0.001	0.030	0.015	0.001	0.002	0.002	0.005	0.000	0.000	0.003	0.006	0.070	1.043	1.118	2.537	0.001	0.012
47	Jt1Mt6rim 36	0.009	0.025	0.000	0.016	0.003	0.003	0.001	0.001	0.001	0.013	0.000	0.001	0.002	0.004	0.008	0.022	0.002	0.027	0.079	1.286	1.357	3.104	0.001	0.010
48	Jt1Mt6rim 37	0.014	0.020	0.004	0.003	0.009	0.000	0.006	0.000	0.001	0.030	0.002	0.007	0.000	0.006	0.002	0.000	0.000	0.021	0.087	1.352	1.424	3.333	0.006	0.001
49	Jt1Mt6rim 38	0.077	0.226	0.027	0.138	0.051	0.007	0.047	0.006	0.029	0.127	0.004	0.019	0.001	0.005	0.001	0.000	0.043	0.027	0.121	1.847	1.984	4.363	0.002	0.092
50	Jt1Mt6core 12	0.037	0.090	0.010	0.018	0.016	0.003	0.026	0.000	0.008	0.020	0.004	0.005	0.002	0.000	0.000	0.000	0.001	0.036	0.072	1.358	1.438	3.171	0.003	0.004
51	Jt1Mt6core 13	0.012	0.032	0.002	0.007	0.003	0.001	0.001	0.001	0.004	0.009	0.000	0.000	0.001	0.002	0.001	0.004	0.000	0.003	0.226	3.303	3.585	7.886	0.004	0.006
52	Jt1Mt6core 14	0.024	0.071	0.006	0.027	0.013	0.003	0.013	0.002	0.009	0.041	0.002	0.008	0.000	0.003	0.001	0.005	0.002	0.023	0.082	1.216	1.308	2.808	0.003	0.035
53	Jt1Mt6core 15	0.010	0.027	0.002	0.018	0.000	0.002	0.002	0.001	0.001	0.013	0.000	0.000	0.000	0.001	0.001	0.000	0.001	0.012	0.048	0.751	0.806	1.820	0.001	0.006
54	Jt1Mt6core 16	0.042	0.083	0.010	0.034	0.000	0.002	0.005	0.001	0.005	0.032	0.001	0.001	0.001	0.002	0.001	0.005	0.001	0.005	0.082	1.146	1.221	2.878	0.014	0.009
55	Jt3Mt2 rim 01	0.085	0.195	0.029	0.063	0.089	0.017	0.097	0.017	0.192	1.126	0.048	0.115	0.012	0.041	0.008	0.015	0.768	0.839	0.032	0.872	0.316	0.508	0.020	1.458
56	Jt3Mt2 rim 02	1.345	2.726	0.426	1.887	0.332	0.057	0.297	0.040	0.144	0.665	0.013	0.061	0.005	0.087	0.005	0.006	0.938	0.982	0.037	0.903	0.239	0.369	0.015	1.577
57	Jt3Mt2 rim 03	3.428	10.550	1.703	9.307	2.995	0.485	2.380	0.249	1.476	5.97	0.204	0.485	0.059	0.282	0.019	0.267	0.426	2.266	0.044	0.755	0.385	0.808	0.020	1.542
58	Jt3Mt2 rim 04	2.543	8.022	1.202	5.844	1.463	0.310	1.198	0.120	0.515	2.72	0.100	0.136	0.009	0.097	0.022	0.032	1.058	1.739	0.064	1.476	0.404	0.869	0.050	1.830
59	Jt3Mt2 rim 05	0.205	0.587	0.041	0.422	0.040	0.008	0.049	0.012	0.040	0.296	0.010	0.022	0.000	0.006	0.001	0.000	0.679	0.280	0.039	0.742	0.205	0.180	0.022	1.226
60	Jt3Mt2 rim 06	0.113	0.141	0.012	0.068	0.034	0.010	0.010	0.001	0.005	0.076	0.006	0.017	0.001	0.012	0.003	0.019	0.003	0.496	0.045	0.206	0.171	0.418	0.008	0.007
61	Jt3Mt2 core 01	0.100	0.259	0.021	0.123	0.044	0.027	0.055	0.008	0.042	0.401	0.014	0.066	0.002	0.029	0.008	0.009	1.152	0.699	0.042	0.975	0.224	0.208	0.016	2.107
62	Jt3Mt2 core 02	0.048	0.136	0.016	0.031	0.059	0.001	0.010	0.004	0.017	0.204	0.013	0.035	0.000	0.031	0.004	0.000	1.046	0.401	0.043	0.986	0.196	0.081	0.009	2.063
63	Jt3Mt2 core 03	0.046	0.201	0.014	0.029	0.064	0.001	0.011	0.009	0.045	0.154	0.002	0.020	0.001	0.007	0.001	0.000	1.133	0.270	0.035	0.800	0.143	0.100	0.016	1.623
64	Jt3Mt2 core 04	0.078	0.262	0.015	0.091	0.041	0.001	0.001	0.012	0.036	0.173	0.016	0.009	0.003	0.033	0.004	0.005	1.410	0.254	0.038	0.940	0.189	0.170	0.003	2.198
65	Jt3Mt3 01	0.669	2.188	0.300	1.117	0.406	0.087	0.216	0.046	0.217	0.815	0.023	0.088	0.005	0.059	0.005	0.023	0.830	1.548	0.044	0.673	0.198	0.309	0.026	1.070
66	Jt3Mt3 02	0.442	1.211	0.211	0.762	0.134	0.061	0.110	0.015	0.121	0.384	0.016	0.017	0.008	0.044	0.006	0.020	0.969	1.040	0.041	0.659	0.164	0.170	0.016	1.202
67	Jt3Mt3 03	0.120	0.123	0.030	0.184	0.049	0.001	0.017	0.004	0.025	0.179	0.011	0.031	0.002	0.034	0.000	0.022	0.764	0.364	0.030	0.482	0.104	0.089	0.004	0.781
68	Jt3Mt3 04	0.046	0.147	0.017	0.034	0.041	0.002	0.007	0.000	0.021	0.201	0.005	0.016	0.001	0.028	0.000	0.011	0.737	0.490	0.035	0.596	0.106	0.174	0.013	1.094

#	Sample	La	Ce	Pr	Nd	Sm	Eu	Gd	Tb	Dy	Y	Ho	Er	Tm	Yb	Lu	Hf	Ta	W	^{204}Pb	^{206}Pb	^{207}Pb	^{208}Pb	Th	^{238}U
69	Jt3Mt3 05	0.402	0.976	0.213	0.970	0.313	0.035	0.328	0.027	0.209	1.186	0.039	0.094	0.014	0.112	0.006	0.008	0.753	1.633	0.030	0.640	0.164	0.189	0.179	1.023
70	Jt3Mt4 01	0.499	1.702	0.266	1.119	0.423	0.113	0.562	0.042	0.311	1.88	0.055	0.199	0.027	0.059	0.016	0.000	0.298	0.906	0.035	0.277	0.053	0.124	0.002	0.434
71	Jt3Mt4 02	0.117	0.224	0.025	0.061	0.034	0.018	0.082	0.004	0.052	0.283	0.008	0.053	0.006	0.023	0.002	0.004	0.826	1.653	0.036	0.817	0.175	0.149	0.029	1.340
72	Jt3Mt4 03	0.051	0.061	0.012	0.037	0.032	0.003	0.019	0.010	0.036	0.264	0.010	0.050	0.003	0.040	0.003	0.009	0.977	1.175	0.033	0.700	0.123	0.155	0.012	1.290
73	Jt3Mt4 04	0.051	0.123	0.006	0.040	0.040	0.001	0.018	0.008	0.046	0.306	0.014	0.049	0.006	0.035	0.003	0.000	1.093	1.121	0.030	0.780	0.132	0.082	0.016	1.754
74	Jt3Mt4 05	0.082	0.160	0.018	0.084	0.041	0.001	0.037	0.004	0.053	0.223	0.014	0.024	0.003	0.062	0.010	0.003	1.116	1.812	0.030	0.870	0.165	0.106	0.029	1.943
75	Jt3Mt4 06	0.064	0.140	0.013	0.017	0.045	0.001	0.035	0.004	0.065	0.289	0.009	0.041	0.004	0.033	0.002	0.000	1.134	1.841	0.030	1.005	0.167	0.045	0.018	2.184
76	Jt3Mt5 01	0.175	0.441	0.069	0.440	0.295	0.105	0.823	0.154	1.320	7.11	0.244	0.694	0.071	0.495	0.052	0.004	0.442	1.583	0.033	0.486	0.191	0.253	0.029	0.879
77	Jt3Mt5 02	0.051	0.072	0.005	0.056	0.031	0.002	0.019	0.005	0.022	0.148	0.010	0.017	0.003	0.024	0.002	0.013	0.744	1.251	0.029	0.481	0.115	0.080	0.010	1.067
78	Jt3Mt5 03	0.105	0.243	0.022	0.191	0.043	0.007	0.069	0.003	0.048	0.351	0.008	0.066	0.009	0.075	0.019	0.392	0.627	1.218	0.034	0.655	0.145	0.171	0.029	1.086
79	Jt3Mt5 04	0.382	0.768	0.103	0.463	0.078	0.019	0.121	0.009	0.045	0.209	0.010	0.016	0.005	0.009	0.004	0.003	0.736	2.173	0.031	0.872	0.234	0.178	0.029	1.279
80	Jt3Mt5 05	0.072	0.108	0.007	0.046	0.025	0.007	0.027	0.002	0.036	0.266	0.015	0.034	0.006	0.066	0.005	0.072	0.867	1.877	0.034	0.925	0.275	0.164	0.031	1.437
81	Jt3Mt5 06	0.333	0.887	0.123	0.600	0.156	0.045	0.125	0.014	0.067	0.331	0.014	0.023	0.007	0.033	0.001	0.017	0.712	1.653	0.034	0.730	0.182	0.244	0.016	1.210
82	Jt3Mt5 07	0.052	0.143	0.016	0.090	0.039	0.017	0.062	0.021	0.118	0.746	0.027	0.116	0.006	0.103	0.010	0.024	0.875	1.944	0.037	0.886	0.274	0.388	0.026	1.153
83	Jt3Mt6 01	0.073	0.189	0.039	0.103	0.053	0.025	0.224	0.051	0.296	1.925	0.066	0.196	0.024	0.101	0.014	0.000	0.507	1.169	0.031	0.420	0.239	0.396	0.008	0.697
84	Jt3Mt6 02	0.094	0.268	0.019	0.079	0.039	0.010	0.039	0.009	0.041	0.258	0.011	0.028	0.005	0.055	0.004	0.012	0.922	1.536	0.033	1.092	0.311	0.296	0.008	1.522
85	Jt3Mt6 03	0.072	0.172	0.021	0.079	0.058	0.005	0.020	0.003	0.048	0.181	0.002	0.015	0.006	0.026	0.002	0.007	0.900	1.188	0.034	0.922	0.167	0.105	0.019	1.683
86	Jt3Mt6 04	0.190	0.483	0.048	0.250	0.055	0.015	0.159	0.017	0.110	0.666	0.025	0.081	0.007	0.045	0.008	0.008	0.764	1.887	0.038	0.709	0.196	0.273	0.010	0.925
87	Jt3Mt6 05	1.026	2.616	0.320	1.630	0.581	0.097	0.357	0.060	0.277	1.534	0.055	0.144	0.010	0.088	0.010	0.009	0.447	1.274	0.037	0.422	0.169	0.326	0.025	0.491
88	Jt3Mt7 rim 01	0.255	0.896	0.177	1.094	0.713	0.215	1.713	0.387	2.462	17.66	0.557	1.485	0.144	0.858	0.068	0.049	0.345	0.956	0.037	0.442	0.183	0.289	0.016	0.421
89	Jt3Mt7 rim 02	0.126	0.181	0.012	0.062	0.064	0.010	0.039	0.004	0.058	0.202	0.016	0.031	0.003	0.013	0.003	0.005	0.626	0.807	0.039	0.787	0.280	0.294	0.018	0.956
90	Jt3Mt7 rim 03	2.145	7.164	1.079	4.902	1.434	0.456	1.201	0.095	0.600	2.01	0.040	0.093	0.002	0.062	0.012	0.028	0.467	1.645	0.061	1.178	0.323	0.639	0.021	0.658
91	Jt3Mt7 rim 04	0.191	0.562	0.060	0.190	0.085	0.022	0.085	0.006	0.024	0.263	0.011	0.033	0.001	0.027	0.007	0.010	1.164	1.080	0.039	1.537	0.374	0.305	0.027	1.833
92	Jt3Mt7 core 01	0.247	0.609	0.082	0.359	0.054	0.024	0.040	0.009	0.088	0.252	0.012	0.036	0.005	0.019	0.004	0.005	1.237	0.885	0.039	0.986	0.187	0.261	0.014	1.739
93	Jt3Mt7 core 02	0.088	0.254	0.016	0.102	0.053	0.002	0.029	0.004	0.034	0.201	0.011	0.017	0.000	0.019	0.010	0.010	1.116	0.794	0.042	0.903	0.160	0.109	0.019	2.018
94	Jt3Mt7 core 03	0.085	0.184	0.019	0.077	0.065	0.008	0.030	0.006	0.023	0.192	0.014	0.050	0.007	0.013	0.004	0.005	0.967	0.855	0.039	0.959	0.174	0.105	0.023	1.984
95	Jt4Mt1rim 01	0.011	0.037	0.005	0.004	0.002	0.002	0.010	0.002	0.018	0.161	0.006	0.027	0.003	0.028	0.005	0.001	0.009	0.012	0.006	0.020	0.003	0.025	0.002	0.031
96	Jt4Mt1rim 02	0.375	0.823	0.099	0.442	0.105	0.013	0.118	0.019	0.108	0.748	0.032	0.099	0.012	0.113	0.008	0.000	0.006	0.165	0.004	0.095	0.074	0.187	0.014	0.089
97	Jt4Mt1rim 03	0.269	0.859	0.116	0.627	0.147	0.073	0.208	0.028	0.199	1.413	0.041	0.168	0.022	0.110	0.020	0.001	0.006	0.050	0.005	0.213	0.132	0.267	0.003	0.280
98	Jt4Mt1rim 04	0.002	0.014	0.002	0.016	0.002	0.000	0.007	0.002	0.029	0.198	0.011	0.055	0.012	0.098	0.016	0.004	1.309	0.142	0.003	0.574	0.082	0.014	0.003	1.404
99	Jt4Mt1rim 05	0.004	0.011	0.002	0.007	0.002	0.000	0.004	0.001	0.031	0.246	0.012	0.052	0.013	0.132	0.022	0.007	1.338	0.143	0.009	0.640	0.076	0.013	0.003	1.541
100	Jt4Mt1rim 06	0.004	0.020	0.002	0.007	0.005	0.000	0.001	0.002	0.040	0.268	0.014	0.076	0.015	0.148	0.020	0.005	1.288	0.398	0.008	0.628	0.095	0.049	0.006	1.651
101	Jt4Mt1rim 07	1.294	2.689	0.327	1.490	0.321	0.048	0.461	0.051	0.422	3.50	0.113	0.306	0.050	0.332	0.043	0.001	1.096	0.460	0.006	0.603	0.089	0.025	0.006	1.598
102	Jt4Mt1core 01	0.012	0.041	0.003	0.033	0.005	0.001	0.012	0.004	0.034	0.313	0.013	0.077	0.010	0.124	0.028	0.002	1.186	0.429	0.010	0.618	0.076	0.011	0.001	1.549
103	Jt4Mt1core 02	0.009	0.035	0.005	0.036	0.000	0.001	0.015	0.006	0.045	0.340	0.015	0.094	0.015	0.202	0.027	0.004	1.098	0.487	0.010	0.748	0.117	0.006	0.002	1.839
104	Jt4Mt2 01	2.734	6.699	0.776	2.521	0.422	0.045	0.398	0.039	0.272	1.49	0.130	0.343	0.054	0.405	0.065	0.066	0.265	0.654	0.003	0.453	0.193	0.361	0.724	0.424
105	Jt4Mt2 02	4.792	8.301	0.942	2.881	0.352	0.012	0.386	0.041	0.223	1.63	0.064	0.243	0.047	0.419	0.074	0.068	0.290	0.713	0.000	0.298	0.088	0.198	0.605	0.580
106	Jt4Mt3 03	11.463	22.265	2.407	8.999	1.299	0.092	1.074	0.119	0.892	5.38	0.258	0.799	0.150	0.922	0.125	0.023	0.239	0.929	0.025	0.920	0.521	1.145	0.315	0.604
107	Jt4Mt3 04	0.613	1.769	0.273	1.003	0.322	0.044	0.407	0.059	0.331	2.37	0.083	0.345	0.034	0.203	0.028	0.005	0.041	0.040	0.009	0.132	0.063	0.075	0.011	0.658
108	Jt4Mt4 05	1.053	2.719	0.272	1.066	0.215	0.024	0.314	0.052	0.567	3.81	0.141	0.512	0.091	0.563	0.077	0.007	1.022	1.201	0.014	0.718	0.239	0.408	0.268	0.946
109	Jt4Mt4 06	1.915	8.705	0.887	4.066	1.108	0.100	1.072	0.162	1.008	7.03	0.264	0.894	0.167	1.165	0.171	0.103	0.889	2.107	0.001	1.200	0.393	0.653	0.819	1.712
110	Jt4Mt4 07	3.077	6.740	0.773	2.819	0.415	0.029	0.336	0.037	0.214	1.45	0.042	0.249	0.046	0.326	0.047	0.034	0.594	0.924	0.014	0.725	0.229	0.329	0.795	1.020
111	Jt4Mt5 08	1.519	4.397	1.031	2.404	0.618	0.058	0.810	0.086	0.479	4.45	0.125	0.469	0.075	0.434	0.068	0.005	0.139	0.507	0.023	0.156	0.086	0.177	0.189	0.407
112	Jt4Mt5 09	3.124	6.732	0.552	2.043	0.412	0.051	0.324	0.038	0.229	2.09	0.082	0.313	0.044	0.515	0.070	0.002	0.279	0.765	0.012	0.207	0.063	0.120	0.385	0.413
113	Jt4Mt5 10	7.110	9.341	0.759	2.009	0.217	0.234	0.113	0.021	0.114	1.19	0.046	0.205	0.029	0.195	0.024	0.000	0.188	0.381	0.003	0.284	0.039	0.077	0.261	0.509

#	Sample	La	Ce	Pr	Nd	Sm	Eu	Gd	Tb	Dy	Y	Ho	Er	Tm	Yb	Lu	Hf	Ta	W	^{204}Pb	^{206}Pb	^{207}Pb	^{208}Pb	Th	^{238}U
114	Jt4Mt5 11	0.280	0.760	0.113	0.554	0.129	0.024	0.186	0.026	0.224	1.44	0.046	0.194	0.032	0.143	0.019	0.000	0.489	0.482	0.004	0.236	0.044	0.052	0.011	0.560
115	Jt4Mt5 12	0.199	0.661	0.055	0.521	0.091	0.010	0.105	0.020	0.169	1.43	0.034	0.180	0.047	0.279	0.045	0.007	0.555	0.782	0.006	0.196	0.076	0.100	0.028	0.516
116	Jt4Mt5 13	2.493	7.638	1.172	4.623	0.729	0.122	0.883	0.107	0.537	2.19	0.089	0.250	0.033	0.128	0.025	0.011	0.157	0.142	0.010	0.195	0.036	0.082	0.174	0.510
117	Jt4Mt5 14	1.425	4.722	0.441	1.975	0.703	0.110	0.646	0.095	0.587	4.26	0.149	0.593	0.075	0.547	0.073	0.012	0.273	2.107	0.056	1.110	0.942	2.212	0.414	0.763
118	Jt4Mt5 15	4.532	10.274	0.853	3.316	0.843	0.068	0.788	0.105	0.850	6.39	0.232	0.928	0.144	1.183	0.171	0.000	0.647	2.255	0.008	0.546	0.098	0.200	0.535	1.319
119	Jt4Mt5 16	11.692	23.929	2.161	7.419	1.289	0.097	1.123	0.116	0.805	5.80	0.189	0.767	0.130	1.024	0.138	0.026	0.190	16.742	0.004	0.468	0.237	0.557	1.105	0.606
120	Jt4Mt5 17	2.734	6.531	0.639	2.566	0.424	0.056	0.489	0.064	0.429	3.79	0.120	0.426	0.051	0.370	0.048	0.005	0.307	0.492	0.009	0.284	0.084	0.168	0.193	0.651
121	Jt4Mt5 18	13.167	37.431	3.817	13.871	1.658	0.122	1.569	0.205	1.416	10.95	0.381	1.466	0.225	1.635	0.248	0.009	0.392	2.228	0.008	0.551	0.177	0.874	4.168	0.954
122	Jt4Mt5 19	2.625	4.711	0.645	2.637	0.704	0.083	1.124	0.209	1.705	14.63	0.478	1.872	0.263	1.629	0.212	0.000	0.044	0.199	0.004	0.163	0.039	0.076	0.268	0.355
123	Jt4Mt6rim 08	9.151	10.447	0.984	2.684	0.340	0.095	0.401	0.045	0.430	3.17	0.113	0.482	0.069	0.365	0.066	0.003	0.065	0.255	0.031	0.646	0.515	1.166	0.113	0.315
124	Jt4Mt6rim 09	0.293	0.454	0.059	0.180	0.021	0.001	0.008	0.004	0.045	0.357	0.019	0.077	0.022	0.181	0.025	0.004	0.976	0.830	0.008	0.621	0.171	0.074	0.106	1.410
125	Jt4Mt6rim 10	0.766	1.505	0.142	0.490	0.038	0.006	0.052	0.007	0.079	0.534	0.011	0.078	0.030	0.183	0.033	0.000	0.948	0.849	0.013	0.531	0.087	0.044	0.192	1.324
126	Jt4Mt6rim 11	0.438	1.165	0.134	0.690	0.186	0.025	0.352	0.037	0.237	2.03	0.053	0.236	0.044	0.369	0.069	0.308	0.004	0.010	0.017	0.491	0.073	0.176	0.008	0.459
127	Jt4Mt6rim 12	9.957	14.983	1.780	5.491	0.640	0.078	0.567	0.064	0.357	2.11	0.098	0.269	0.063	0.367	0.064	0.012	0.553	0.869	0.007	0.568	0.245	0.363	0.581	0.628
128	Jt4Mt6rim 13	0.869	2.359	0.324	1.563	0.426	0.071	0.681	0.073	0.510	3.99	0.133	0.303	0.058	0.204	0.038	0.000	0.001	0.017	0.004	0.048	0.005	0.012	0.001	0.534
129	Jt4Mt6rim 14	2.009	3.033	0.341	1.017	0.185	0.008	0.083	0.006	0.058	0.51	0.018	0.059	0.014	0.151	0.022	0.036	0.532	1.745	0.003	0.704	0.349	0.604	0.321	0.556
130	Jt4Mt6rim 15	1.123	2.264	0.328	1.553	0.377	0.037	0.473	0.075	0.498	4.27	0.151	0.548	0.074	0.402	0.055	0.002	0.357	0.441	0.004	0.364	0.165	0.292	0.039	0.492
131	Jt4Mt6rim 16	2.506	4.408	0.466	1.675	0.237	0.025	0.169	0.028	0.276	2.02	0.065	0.266	0.047	0.310	0.054	0.002	0.635	0.895	0.039	0.979	0.741	1.525	0.111	0.583
132	Jt4Mt6rim 17	1.818	3.605	0.485	2.363	0.364	0.028	0.281	0.044	0.321	2.43	0.093	0.375	0.063	0.483	0.065	0.026	0.701	0.821	0.012	0.685	0.297	0.456	0.072	0.854
133	Jt4Mt6core 03	0.293	0.496	0.056	0.306	0.071	0.011	0.110	0.013	0.131	0.818	0.034	0.113	0.024	0.190	0.028	0.000	0.947	1.302	0.003	0.648	0.186	0.232	0.036	1.080
134	Jt4Mt6core 04	0.372	0.650	0.074	0.291	0.061	0.001	0.043	0.003	0.065	0.434	0.027	0.075	0.019	0.186	0.020	0.002	0.714	1.098	0.039	1.104	0.597	1.036	0.076	1.220
135	Jt4Mt6core 05	0.989	2.394	0.284	1.223	0.307	0.032	0.297	0.044	0.369	2.83	0.102	0.286	0.049	0.247	0.027	0.000	0.658	0.288	0.014	0.124	0.084	0.062	0.035	0.329
136	Jt4Mt6core 06	0.337	0.681	0.083	0.376	0.091	0.006	0.095	0.018	0.110	0.817	0.022	0.072	0.010	0.089	0.012	0.000	0.310	0.248	0.011	0.257	0.064	0.116	0.042	0.434
137	Jt4Mt6core 07	0.594	1.443	0.224	0.896	0.193	0.041	0.249	0.022	0.235	1.77	0.050	0.128	0.020	0.114	0.012	0.009	0.087	0.102	0.002	0.163	0.065	0.122	0.004	0.289
138	Jt4Mt6core 08	41.429	69.610	7.310	23.863	2.874	0.221	1.910	0.263	2.082	15.77	0.556	2.125	0.305	1.930	0.228	0.000	0.492	0.455	0.000	0.466	0.109	0.104	0.335	0.857
139	Jt4Mt6core 09	2.798	6.257	0.815	4.018	0.869	0.073	1.077	0.145	0.900	7.071	0.229	0.700	0.093	0.535	0.067	0.002	0.231	0.303	0.002	0.243	0.114	0.180	0.031	0.529
140	Jt4Mt7rim 18	0.414	0.648	0.066	0.225	0.045	0.011	0.033	0.006	0.045	0.278	0.004	0.041	0.006	0.011	0.003	0.005	0.008	0.047	0.006	0.011	0.004	0.010	0.018	0.023
141	Jt4Mt7rim 19	1.216	2.598	0.292	1.019	0.307	0.033	0.272	0.037	0.224	1.738	0.050	0.144	0.023	0.086	0.012	0.002	0.006	0.076	0.017	0.052	0.004	0.023	0.019	0.154
142	Jt4Mt7rim 20	0.034	0.123	0.011	0.071	0.029	0.002	0.024	0.005	0.030	0.136	0.003	0.020	0.001	0.018	0.002	0.000	0.001	0.002	0.000	0.003	0.001	0.002	0.002	0.006
143	Jt4Mt7rim 21	0.082	0.194	0.025	0.195	0.070	0.001	0.055	0.007	0.032	0.158	0.005	0.013	0.003	0.013	0.003	0.000	0.000	0.001	0.011	0.058	0.009	0.036	0.002	0.022
144	Jt4Mt7core 10	0.153	0.455	0.057	0.295	0.352	0.005	0.097	0.012	0.061	0.489	0.014	0.020	0.004	0.023	0.004	0.000	0.001	0.005	0.003	0.012	0.004	0.006	0.000	0.038
145	Jt4Mt7core 11	0.003	0.003	0.000	0.006	0.003	0.000	0.001	0.000	0.004	0.007	0.001	0.000	0.000	0.000	0.000	0.000	0.006	0.005	0.015	0.010	0.011	0.004	0.001	0.001
146	Jt4Mt8rim 22	1.272	3.623	0.535	2.430	0.601	0.043	0.659	0.091	0.540	4.45	0.125	0.352	0.041	0.285	0.045	0.036	0.008	0.079	0.017	1.066	0.225	0.529	0.003	0.439
147	Jt4Mt8rim 23	0.525	0.950	0.126	0.361	0.067	0.005	0.036	0.009	0.024	0.313	0.016	0.082	0.014	0.118	0.026	0.003	0.937	0.475	0.011	0.714	0.154	0.148	0.052	1.400
148	Jt4Mt8rim 24	0.178	0.207	0.023	0.044	0.021	0.001	0.003	0.001	0.017	0.195	0.006	0.027	0.006	0.030	0.007	0.033	0.016	0.038	0.005	0.058	0.024	0.019	0.020	0.061
149	Jt4Mt8rim 25	0.076	0.168	0.017	0.065	0.012	0.006	0.037	0.016	0.134	1.064	0.043	0.150	0.028	0.210	0.024	0.000	0.922	0.780	0.004	0.401	0.163	0.331	0.059	0.474
150	Jt4Mt8rim 26	0.851	0.878	0.086	0.254	0.058	0.014	0.049	0.004	0.044	0.308	0.015	0.095	0.014	0.113	0.022	0.004	1.052	0.799	0.003	0.644	0.186	0.213	0.025	1.055
151	Jt4Mt8rim 27	0.784	0.584	0.066	0.187	0.054	0.012	0.022	0.007	0.055	0.411	0.012	0.101	0.014	0.152	0.028	0.002	1.057	1.109	0.004	0.902	0.400	0.545	0.036	1.120
152	Jt4Mt8rim 28	4.745	10.023	1.433	6.104	2.090	0.819	2.301	0.505	4.873	37.91	1.520	6.441	1.280	10.029	1.042	0.140	4.974	0.822	0.002	1.126	0.390	0.646	0.092	1.781
153	Jt4Mt8rim 29	1.200	2.475	0.254	1.230	0.305	0.028	0.228	0.035	0.205	1.41	0.037	0.166	0.014	0.168	0.027	0.014	0.533	0.227	0.020	0.543	0.216	0.413	0.016	0.890
154	Jt7Mt1 01	0.148	0.576	0.094	0.369	0.189	0.026	0.433	0.092	0.846	5.30	0.188	0.643	0.096	0.632	0.064	0.014	0.601	0.456	0.025	0.210	0.211	0.406	0.037	0.067
155	Jt7Mt1 02	0.122	0.358	0.052	0.220	0.120	0.029	0.300	0.091	0.662	4.84	0.183	0.622	0.096	0.439	0.049	0.002	0.573	0.295	0.027	0.388	0.353	0.730	0.018	0.186
156	Jt7Mt1 03	0.115	0.492	0.122	0.858	0.875	0.179	1.924	0.581	5.408	35.71	1.293	4.248	0.536	2.963	0.229	0.077	2.736	0.839	0.027	0.310	0.186	0.361	0.027	0.209
157	Jt7Mt1 04	0.022	0.058	0.007	0.077	0.059	0.006	0.089	0.011	0.100	0.330	0.016	0.045	0.001	0.012	0.003	0.000	0.014	0.320	0.025	0.233	0.220	0.487	0.012	0.026
158	Jt7Mt1 05	0.002	0.002	0.002	0.007	0.031	0.001	0.005	0.001	0.008	0.080	0.005	0.008	0.001	0.006	0.001	0.000	0.006	0.024	0.029	0.015	0.012	0.035	0.002	0.008

#	Sample	La	Ce	Pr	Nd	Sm	Eu	Gd	Tb	Dy	Y	Ho	Er	Tm	Yb	Lu	Hf	Ta	W	^{204}Pb	^{206}Pb	^{207}Pb	^{208}Pb	Th	^{238}U
159	Jt7Mt1 06	0.006	0.012	0.003	0.012	0.030	0.001	0.010	0.000	0.014	0.071	0.002	0.006	0.002	0.013	0.003	0.000	0.021	0.069	0.032	0.169	0.156	0.404	0.003	0.028
160	Jt7Mt1 07	0.130	0.295	0.040	0.177	0.065	0.009	0.048	0.013	0.115	0.849	0.030	0.103	0.010	0.036	0.003	0.002	0.022	0.121	0.032	0.184	0.103	0.227	0.001	0.321
161	Jt7Mt1 08	0.020	0.060	0.012	0.019	0.037	0.010	0.069	0.013	0.130	1.16	0.059	0.231	0.037	0.137	0.012	0.000	0.284	0.289	0.029	0.268	0.281	0.625	0.006	0.030
162	Jt7Mt 2 01	2.978	6.863	0.718	2.768	0.531	0.034	0.387	0.058	0.443	2.76	0.102	0.317	0.050	0.251	0.034	0.002	0.224	0.107	0.030	0.389	0.145	0.258	0.013	0.214
163	Jt7Mt 2 02	0.081	0.135	0.017	0.099	0.037	0.002	0.025	0.007	0.029	0.313	0.014	0.035	0.005	0.029	0.006	0.000	0.046	0.161	0.030	1.426	0.842	1.809	0.002	0.071
164	Jt7Mt 2 03	0.029	0.070	0.008	0.082	0.038	0.013	0.118	0.026	0.174	1.155	0.051	0.127	0.019	0.114	0.009	0.000	0.097	0.716	0.029	0.280	0.245	0.470	0.004	0.159
165	Jt7Mt 2 04	14.7	33.2	3.4	12.1	1.7	0.230	1.803	0.356	2.874	16.94	0.673	2.403	0.308	1.881	0.160	0.012	1.389	6.201	0.026	0.590	0.457	0.882	0.030	0.251
166	Jt7Mt 2 05	11.7	28.1	3.4	12.3	2.832	0.409	4.616	0.964	8.446	48.18	1.823	5.481	0.733	4.344	0.350	0.015	3.744	3.624	0.027	0.754	0.223	0.454	0.052	1.063
167	Jt7Mt 2 06	0.335	0.630	0.089	0.253	0.136	0.021	0.221	0.064	0.399	2.875	0.095	0.294	0.042	0.336	0.026	0.005	0.128	0.792	0.027	0.188	0.139	0.286	0.067	0.067
168	Jt7Mt 2 07	0.273	0.625	0.060	0.193	0.032	0.002	0.038	0.004	0.060	0.446	0.016	0.060	0.011	0.123	0.009	0.079	0.041	0.282	0.026	0.480	0.403	0.800	0.068	0.110
169	Jt7Mt 3 01	0.067	0.144	0.017	0.097	0.030	0.007	0.032	0.006	0.065	0.247	0.006	0.064	0.006	0.047	0.004	0.000	0.014	0.082	0.029	0.210	0.067	0.174	0.007	0.110
170	Jt7Mt 3 02	0.052	0.160	0.053	0.174	0.024	0.001	0.068	0.008	0.057	0.318	0.017	0.069	0.006	0.060	0.007	0.000	0.034	0.137	0.030	0.262	0.242	0.491	0.006	0.012
171	Jt7Mt 3 03	0.098	0.332	0.057	0.424	0.202	0.038	0.474	0.107	1.2	7.7	0.327	1.115	0.166	0.952	0.099	0.022	0.698	0.323	0.026	0.282	0.095	0.188	0.007	0.179
172	Jt7Mt 3 04	0.461	2.633	0.625	4.6	3.6	0.674	7.5	1.8	16.9	121.4	4.3	15.0	2.1	12.3	1.1	0.162	6.8	3.1	0.028	0.887	0.266	0.353	0.098	1.303
173	Jt7Mt 3 05	20.7	50.1	5.5	20.3	2.9	0.283	2.0	0.171	0.884	3.637	0.157	0.466	0.051	0.358	0.028	0.015	0.424	0.271	0.026	0.335	0.126	0.203	0.017	0.335
174	Jt7Mt 3 06	0.056	0.145	0.007	0.062	0.041	0.001	0.024	0.002	0.014	0.156	0.005	0.025	0.004	0.036	0.006	0.000	0.335	0.398	0.025	0.271	0.098	0.123	0.019	0.332
175	Jt7Mt 3 07	0.101	0.268	0.033	0.205	0.052	0.006	0.124	0.028	0.204	1.63	0.052	0.259	0.028	0.159	0.016	0.002	0.120	0.168	0.024	0.111	0.059	0.110	0.024	0.026
176	Jt7Mt 3 08	0.632	1.243	0.125	0.515	0.123	0.019	0.091	0.034	0.269	2.05	0.067	0.254	0.038	0.243	0.027	0.000	0.154	0.309	0.026	0.187	0.100	0.232	0.155	0.178
177	Jt7Mt 3 09	0.152	0.511	0.065	0.541	0.329	0.054	0.619	0.170	1.840	11.92	0.418	1.589	0.256	1.546	0.135	0.025	1.197	0.299	0.030	0.694	0.738	1.523	0.044	0.120
178	Jt7Mt 3 10	0.125	0.326	0.048	0.348	0.238	0.048	0.549	0.142	1.368	8.70	0.326	1.119	0.173	1.003	0.087	0.010	0.787	0.356	0.029	0.171	0.100	0.159	0.008	0.094
179	Jt7Mt 4 rim 01	1.196	2.497	0.266	1.073	0.434	0.062	0.684	0.166	1.455	9.43	0.334	1.168	0.173	0.982	0.085	0.013	0.743	0.512	0.027	0.601	0.530	1.119	0.069	0.244
180	Jt7Mt 4 rim 02	0.047	0.157	0.030	0.233	0.155	0.032	0.235	0.057	0.399	2.54	0.085	0.267	0.043	0.328	0.031	0.000	1.049	1.2	0.028	0.889	0.294	0.389	0.016	1.051
181	Jt7Mt 4 rim 03	0.078	0.223	0.044	0.332	0.301	0.033	0.567	0.137	0.936	6.25	0.239	0.712	0.104	0.598	0.058	0.008	0.996	1.0	0.029	0.500	0.106	0.085	0.011	0.934
182	Jt7Mt 4 rim 04	0.022	0.043	0.005	0.020	0.026	0.001	0.005	0.001	0.003	0.005	0.000	0.000	0.001	0.003	0.002	0.002	0.001	0.003	0.026	0.020	0.011	0.038	0.005	0.004
183	Jt7Mt 4 rim 05	0.042	0.311	0.057	0.308	0.299	0.062	0.817	0.145	1.331	8.59	0.345	1.156	0.173	1.179	0.130	0.020	1.661	0.652	0.025	0.645	0.153	0.058	0.029	1.008
184	Jt7Mt 4 rim 06	0.085	0.450	0.044	0.299	0.106	0.029	0.226	0.051	0.366	2.38	0.082	0.274	0.045	0.274	0.028	0.010	1.004	0.568	0.028	0.881	0.165	0.099	0.023	1.455
185	Jt7Mt 4 rim 07	0.212	0.749	0.180	1.137	0.822	0.117	1.961	0.476	3.833	21.94	0.828	2.656	0.351	2.075	0.224	0.038	1.964	1.5	0.029	0.891	0.236	0.349	0.032	1.246
186	Jt7Mt 4 core 01	0.352	1.3	0.203	0.976	0.294	0.028	0.428	0.050	0.421	2.105	0.069	0.233	0.033	0.256	0.026	0.010	0.872	1.1	0.035	1.449	0.799	1.486	0.051	1.261
187	Jt7Mt 4 core 02	0.698	1.6	0.222	0.983	0.226	0.008	0.185	0.023	0.152	0.984	0.040	0.106	0.011	0.121	0.011	0.022	0.832	0.571	0.027	1.202	0.314	0.280	0.096	1.418
188	Jt7Mt 4 core 03	1.265	2.4	0.343	1.338	0.137	0.015	0.164	0.032	0.188	1.3	0.043	0.157	0.017	0.214	0.036	0.002	0.784	0.417	0.030	1.066	0.237	0.126	0.189	1.441
189	Jt7Mt 5 01	1.460	2.4	0.411	1.683	0.404	0.059	0.388	0.082	0.907	4.9	0.189	0.691	0.079	0.505	0.038	0.008	0.326	0.130	0.032	0.166	0.110	0.244	0.070	0.078
190	Jt7Mt 5 02	0.395	1.0	0.119	0.483	0.148	0.048	0.409	0.095	1.106	9.2	0.375	1.383	0.225	1.286	0.124	0.022	1.044	0.311	0.033	0.351	0.268	0.599	0.062	0.171
191	Jt7Mt 5 03	1.1	3.3	0.291	0.978	0.231	0.013	0.215	0.018	0.123	0.699	0.034	0.085	0.005	0.059	0.007	0.003	0.006	0.263	0.031	0.218	0.121	0.205	0.079	0.059
192	Jt7Mt 5 04	3.4	8.4	0.925	2.895	0.472	0.031	0.441	0.032	0.200	1.001	0.033	0.080	0.007	0.088	0.035	0.000	0.010	0.196	0.028	0.194	0.040	0.103	0.145	0.192
193	Jt7Mt 5 05	4.8	12.2	1.216	3.876	0.650	0.048	0.367	0.044	0.181	0.802	0.032	0.116	0.009	0.138	0.014	0.000	0.011	0.327	0.031	0.422	0.407	0.767	0.064	0.115
194	Jt7Mt 5 06	1.4	5.5	0.541	1.776	0.306	0.029	0.248	0.036	0.297	1.908	0.069	0.276	0.037	0.346	0.036	0.005	0.294	0.259	0.027	0.264	0.182	0.397	0.106	0.090
195	Jt7Mt 5 07	16.9	15.7	1.457	3.826	0.350	0.025	0.269	0.026	0.205	1.238	0.048	0.142	0.029	0.244	0.043	0.006	0.170	1.181	0.029	0.454	0.369	0.813	0.301	0.229
196	Jt7Mt 5 08	16.3	35.7	4.0	15.7	1.9	0.126	1.567	0.202	1.198	3.953	0.194	0.431	0.026	0.172	0.019	0.010	0.048	1.157	0.157	3.097	2.792	6.202	0.124	1.020
197	Jt7Mt 5 09	2.3	2.5	0.288	0.681	0.060	0.021	0.083	0.006	0.079	0.330	0.006	0.048	0.007	0.077	0.010	0.000	0.013	0.930	0.315	4.860	5.258	11.863	0.054	0.052
198	Jt7Mt 5 10	0.840	1.8	0.203	0.840	0.172	0.021	0.351	0.057	0.416	1.415	0.072	0.250	0.023	0.138	0.017	0.016	0.358	0.593	0.038	0.600	0.228	0.529	0.933	1.896
199	Jt7Mt 6 01	0.001	0.002	0.003	0.024	0.025	0.001	0.014	0.001	0.025	0.313	0.012	0.033	0.004	0.027	0.001	0.000	0.027	0.039	0.026	0.018	0.016	0.041	0.000	0.015
200	Jt7Mt 6 02	0.007	0.016	0.005	0.025	0.039	0.001	0.045	0.015	0.133	0.939	0.032	0.129	0.018	0.114	0.013	0.005	0.079	0.171	0.027	0.251	0.204	0.480	0.002	0.093
201	Jt7Mt 6 03	0.117	0.825	0.238	1.937	1.467	0.235	3.251	0.867	8.311	60.04	2.130	7.460	1.063	6.500	0.509	0.055	2.731	0.938	0.030	0.430	0.182	0.316	0.020	0.506
202	Jt7Mt 6 04	0.296	1.087	0.118	0.491	0.191	0.022	0.164	0.042	0.373	2.217	0.092	0.338	0.046	0.249	0.035	0.003	0.770	0.960	0.025	0.784	0.169	0.122	0.152	1.104
203	Jt7Mt 6 05	0.206	0.672	0.130	0.712	0.499	0.065	0.845	0.258	2.426	17.31	0.608	2.248	0.307	1.989	0.167	0.034	0.549	0.452	0.027	0.877	0.248	0.529	0.032	0.438

#	Sample	La	Ce	Pr	Nd	Sm	Eu	Gd	Tb	Dy	Y	Ho	Er	Tm	Yb	Lu	Hf	Ta	W	^{204}Pb	^{206}Pb	^{207}Pb	^{208}Pb	Th	^{238}U
204	Jt7Mt 7 01	0.294	0.867	0.082	0.516	0.139	0.007	0.138	0.010	0.091	0.488	0.028	0.068	0.008	0.025	0.002	0.003	0.009	0.048	0.031	0.406	0.085	0.221	0.030	0.409
205	Jt7Mt 7 02	0.025	0.047	0.006	0.022	0.010	0.001	0.001	0.000	0.006	0.014	0.003	0.004	0.000	0.006	0.000	0.000	0.000	0.011	0.030	0.022	0.036	0.069	0.005	0.001
206	Jt7Mt 7 03	0.177	0.472	0.054	0.266	0.074	0.006	0.043	0.012	0.044	0.223	0.012	0.038	0.003	0.030	0.003	0.000	0.001	0.042	0.026	0.391	0.084	0.253	0.011	0.454
207	Jt7Mt 7 04	0.001	0.001	0.004	0.017	0.081	0.001	0.001	0.004	0.001	0.001	0.000	0.000	0.000	0.000	0.000	0.000	0.001	0.001	0.026	0.014	0.015	0.019	0.000	0.001
208	Jt7Mt 7 05	0.007	0.019	0.005	0.011	0.043	0.001	0.001	0.000	0.012	0.015	0.001	0.002	0.001	0.010	0.001	0.000	0.013	0.040	0.025	0.060	0.059	0.095	0.000	0.028
209	Jt7Mt 8 01	0.013	0.021	0.007	0.016	0.021	0.001	0.001	0.001	0.001	0.013	0.000	0.002	0.000	0.000	0.000	0.000	0.000	0.001	0.025	0.014	0.011	0.032	0.000	0.005
210	Jt7Mt 8 02	0.001	0.001	0.002	0.014	0.025	0.001	0.001	0.000	0.001	0.001	0.000	0.000	0.000	0.000	0.001	0.000	0.000	0.001	0.029	0.019	0.012	0.049	0.000	0.000
211	Jt7Mt 8 03	0.076	0.240	0.037	0.123	0.046	0.001	0.015	0.002	0.036	0.118	0.002	0.004	0.000	0.006	0.000	0.000	0.016	0.030	0.026	0.148	0.048	0.148	0.005	0.096
212	Jt7Mt 8 04	0.049	0.055	0.012	0.014	0.016	0.001	0.001	0.001	0.011	0.037	0.003	0.013	0.002	0.009	0.001	0.000	0.004	0.021	0.025	0.038	0.024	0.052	0.002	0.007
213	Jt7Mt 8 05	0.103	0.182	0.015	0.082	0.016	0.001	0.009	0.001	0.020	0.158	0.006	0.038	0.009	0.048	0.007	0.000	0.013	0.126	0.026	0.077	0.029	0.071	0.015	0.078
214	Jt7Mt 8 06	0.075	0.101	0.019	0.145	0.025	0.003	0.010	0.004	0.031	0.117	0.001	0.020	0.000	0.042	0.003	0.005	0.039	0.048	0.033	0.025	0.015	0.054	0.005	0.062
216	Jt7Mt 8 08	0.001	0.001	0.003	0.018	0.017	0.001	0.001	0.000	0.001	0.007	0.000	0.000	0.000	0.000	0.000	0.000	0.000	0.001	0.029	0.015	0.011	0.019	0.000	0.000
217	Jt7Mt 8 09	0.248	0.499	0.058	0.264	0.152	0.010	0.137	0.032	0.125	1.191	0.030	0.139	0.012	0.084	0.008	0.000	0.001	0.015	0.032	0.089	0.052	0.074	0.004	0.009
218	Jt8Mt 1 01	0.019	0.028	0.002	0.017	0.036	0.001	0.004	0.001	0.009	0.039	0.005	0.013	0.001	0.006	0.000	0.000	0.008	0.028	0.027	0.119	0.064	0.135	0.003	0.046
219	Jt8Mt 1 02	0.135	0.316	0.028	0.082	0.028	0.001	0.021	0.005	0.031	0.304	0.014	0.062	0.009	0.024	0.005	0.000	0.018	0.087	0.029	0.271	0.177	0.425	0.070	0.059
220	Jt8Mt 1 03	0.066	0.232	0.026	0.104	0.032	0.004	0.042	0.002	0.070	0.362	0.016	0.028	0.006	0.067	0.006	0.000	0.021	0.090	0.027	0.282	0.149	0.341	0.032	0.060
221	Jt8Mt 1 04	1.8	2.520	0.347	1.008	0.113	0.011	0.144	0.020	0.194	1.374	0.038	0.139	0.028	0.169	0.030	0.002	0.028	0.446	0.038	1.095	0.921	2.011	0.278	0.091
222	Jt8Mt 1 05	0.415	0.531	0.075	0.307	0.086	0.005	0.075	0.018	0.196	1.037	0.036	0.132	0.012	0.161	0.024	0.000	0.029	0.183	0.028	1.751	0.654	1.387	0.038	0.302
223	Jt8Mt 2 01	0.457	1.197	0.113	0.438	0.092	0.001	0.041	0.009	0.071	0.646	0.026	0.062	0.014	0.112	0.012	0.000	0.008	0.175	0.024	0.196	0.147	0.369	0.155	0.036
224	Jt8Mt 2 02	0.354	0.706	0.068	0.311	0.041	0.008	0.056	0.013	0.132	0.684	0.034	0.097	0.013	0.099	0.012	0.000	0.024	0.333	0.034	0.800	0.605	1.357	0.094	0.107
225	Jt8Mt 2 03	0.322	0.820	0.116	0.456	0.165	0.014	0.316	0.047	0.428	2.266	0.084	0.386	0.036	0.250	0.038	0.003	0.036	0.165	0.028	1.213	0.396	0.872	0.053	0.550
226	Jt8Mt 2 04	0.067	0.104	0.012	0.072	0.020	0.002	0.004	0.004	0.023	0.173	0.006	0.027	0.003	0.032	0.004	0.002	0.017	0.085	0.026	0.115	0.065	0.182	0.031	0.088
227	Jt8Mt 2 05	0.004	0.008	0.002	0.024	0.013	0.001	0.009	0.001	0.006	0.015	0.002	0.002	0.001	0.007	0.000	0.000	0.001	0.001	0.029	0.014	0.011	0.018	0.000	0.006
228	Jt8Mt 2 06	0.144	0.385	0.043	0.186	0.081	0.003	0.103	0.015	0.240	1.436	0.050	0.150	0.040	0.285	0.053	0.006	0.032	0.123	0.028	1.358	0.487	1.253	0.019	0.269
229	Jt8Mt 3 01	2.0	2.067	0.280	0.894	0.173	0.015	0.162	0.017	0.205	1.294	0.047	0.193	0.034	0.188	0.021	0.003	0.061	0.432	0.031	0.319	0.267	0.575	0.219	0.128
230	Jt8Mt 3 02	10.8	19.008	2.118	7.995	1.111	0.084	1.194	0.121	0.873	5.599	0.216	0.773	0.103	0.695	0.111	0.003	0.089	0.474	0.026	0.707	0.454	1.011	0.366	0.231
231	Jt8Mt 3 03	0.952	2.237	0.328	1.205	0.178	0.007	0.079	0.008	0.086	0.450	0.022	0.039	0.014	0.100	0.009	0.000	0.110	0.342	0.048	1.000	0.970	2.027	0.109	0.090
232	Jt8Mt 3 04	0.407	1.459	0.145	0.621	0.084	0.003	0.106	0.006	0.117	0.731	0.023	0.085	0.017	0.117	0.018	0.000	0.041	0.192	0.030	0.119	0.047	0.107	0.110	0.048
233	Jt8Mt 3 05	1.608	2.351	0.308	0.921	0.110	0.004	0.099	0.025	0.121	0.818	0.034	0.135	0.016	0.113	0.017	0.000	0.042	0.242	0.030	0.218	0.171	0.368	0.583	0.040
234	Jt8Mt 4 01	0.667	1.545	0.128	0.528	0.135	0.005	0.093	0.011	0.117	0.693	0.024	0.100	0.023	0.092	0.017	0.000	0.033	0.214	0.030	0.428	0.266	0.668	0.304	0.056
235	Jt8Mt 4 02	0.141	0.701	0.062	0.311	0.031	0.005	0.027	0.006	0.053	0.432	0.012	0.048	0.009	0.118	0.015	0.003	0.035	0.122	0.031	0.036	0.014	0.032	0.061	0.042
237	Jt8Mt 4 04	0.201	0.364	0.031	0.231	0.019	0.004	0.064	0.004	0.055	0.386	0.014	0.062	0.012	0.065	0.006	0.000	0.035	0.165	0.027	0.184	0.139	0.272	0.037	0.066
238	Jt8Mt 5 01	0.289	0.496	0.064	0.239	0.028	0.005	0.068	0.009	0.089	0.800	0.035	0.156	0.007	0.099	0.015	0.000	0.043	0.237	0.031	1.712	0.464	1.099	0.075	0.219
239	Jt8Mt 5 02	0.330	0.845	0.103	0.630	0.136	0.016	0.253	0.036	0.317	2.22	0.082	0.262	0.025	0.187	0.034	0.000	0.036	0.200	0.029	4.385	1.054	2.481	0.110	0.697
240	Jt8Mt 5 03	0.418	1.230	0.146	0.522	0.131	0.008	0.120	0.024	0.097	1.19	0.047	0.146	0.022	0.160	0.017	0.000	0.063	0.457	0.025	0.437	0.403	0.842	0.155	0.076
241	Jt8Mt 5 04	976	2152	232	833	104	4.2	53	3.9	12.1	27.19	1.4	2.6	0.290	1.751	0.198	0.000	0.048	0.509	0.025	1.118	0.387	2.540	20.4	0.666
242	Jt8Mt 5 05	0.612	2.208	0.477	1.232	0.606	0.025	0.476	0.054	0.511	3.64	0.136	0.523	0.066	0.635	0.054	0.003	0.057	1.190	0.058	1.101	0.912	2.072	0.257	0.126
243	Jt8Mt 5 06	1.0	2.144	0.517	2.011	0.217	0.029	0.321	0.017	0.253	1.18	0.043	0.179	0.028	0.180	0.022	0.000	0.133	0.402	0.025	0.332	0.188	0.388	0.180	0.157
244	Jt8Mt 5 07	0.776	1.587	0.236	0.909	0.322	0.018	0.216	0.024	0.176	1.37	0.047	0.212	0.031	0.211	0.026	0.000	0.081	0.477	0.025	0.151	0.079	0.209	0.198	0.088
245	Jt8Mt 5 08	0.412	1.645	0.314	1.488	0.158	0.012	0.234	0.030	0.165	1.31	0.050	0.186	0.028	0.166	0.030	0.002	0.032	0.163	0.026	0.202	0.147	0.319	0.117	0.050
246	Jt8Mt 5 09	0.612	1.851	0.227	0.654	0.101	0.007	0.168	0.019	0.166	1.23	0.047	0.193	0.020	0.201	0.022	0.021	0.025	0.109	0.027	0.142	0.069	0.216	0.150	0.058
248	Jt8Mt 6 01	0.036	0.062	0.007	0.032	0.010	0.001	0.001	0.000	0.009	0.068	0.001	0.000	0.001	0.006	0.001	0.000	0.102	0.039	0.029	0.040	0.020	0.064	0.013	0.006
249	Jt8Mt 6 02	0.349	0.714	0.105	0.351	0.095	0.005	0.107	0.011	0.130	0.631	0.036	0.082	0.007	0.086	0.011	0.000	0.018	0.119	0.027	1.520	0.576	1.281	0.120	0.120
250	Jt8Mt 6 03	2.4	4.650	0.526	1.859	0.197	0.015	0.217	0.039	0.251	1.77	0.067	0.215	0.037	0.229	0.029	0.003	0.067	0.501	0.045	7.239	2.211	5.130	0.327	0.226
251	Jt8Mt 6 04	1.5	2.306	0.314	1.145	0.136	0.007	0.144	0.024	0.169	1.23	0.038	0.157	0.029	0.176	0.025	0.003	0.170	0.539	0.024	0.254	0.155	0.396	0.252	0.095

#	Sample	La	Ce	Pr	Nd	Sm	Eu	Gd	Tb	Dy	Y	Ho	Er	Tm	Yb	Lu	Hf	Ta	W	^{204}Pb	^{206}Pb	^{207}Pb	^{208}Pb	Th	^{238}U
252	Jt8Mt 6 05	0.575	0.897	0.100	0.459	0.059	0.003	0.132	0.011	0.146	0.829	0.032	0.106	0.016	0.117	0.012	0.000	1.311	1.370	0.032	1.880	0.977	2.054	0.116	0.273
253	Jt8Mt 6 06	2.2	4.421	0.568	1.907	0.221	0.003	0.229	0.028	0.142	0.668	0.026	0.107	0.016	0.073	0.009	0.000	0.049	0.175	0.029	0.846	0.315	0.752	0.089	0.090
254	Jt8Mt 6 07	0.026	0.033	0.011	0.017	0.021	0.001	0.005	0.003	0.019	0.107	0.011	0.019	0.004	0.007	0.000	0.000	0.017	0.026	0.032	0.148	0.083	0.206	0.002	0.034
255	Jt8Mt 6 08	0.158	0.297	0.041	0.190	0.032	0.001	0.030	0.008	0.067	0.430	0.018	0.047	0.012	0.086	0.010	0.000	0.036	0.302	0.032	0.397	0.423	0.851	0.016	0.069
256	Jt8Mt 6 09	0.027	0.053	0.015	0.027	0.009	0.001	0.021	0.004	0.025	0.170	0.002	0.017	0.002	0.017	0.002	0.000	0.104	0.056	0.026	1.234	0.328	0.707	0.009	0.083
257	Jt8Mt 6 10	0.504	0.730	0.091	0.274	0.042	0.001	0.060	0.006	0.129	0.793	0.031	0.124	0.018	0.105	0.014	0.000	0.041	0.191	0.026	0.783	0.224	0.528	0.061	0.119
258	Jt8Mt 7 01	1.7	3.122	0.364	1.296	0.162	0.008	0.185	0.034	0.307	2.21	0.082	0.295	0.042	0.253	0.035	0.000	0.105	0.716	0.028	0.556	0.412	0.989	0.364	0.150
259	Jt8Mt 7 02	1.7	4.250	0.481	1.989	0.378	0.014	0.292	0.033	0.344	1.99	0.071	0.367	0.042	0.397	0.042	0.003	0.200	0.749	0.027	0.544	0.354	0.741	0.222	0.374
260	Jt8Mt 7 03	3.4	7.609	0.938	3.697	0.596	0.039	0.485	0.051	0.316	2.18	0.086	0.312	0.055	0.461	0.074	0.005	0.179	0.303	0.027	0.388	0.156	0.297	0.385	0.245
261	Jt8Mt 7 04	4.1	8.916	1.137	4.042	0.645	0.041	0.479	0.056	0.290	1.67	0.059	0.251	0.035	0.479	0.065	0.003	0.243	0.314	0.031	0.361	0.217	0.500	0.562	0.231
262	Jt8Mt 7 05	5.7	14.004	1.716	7.461	1.237	0.089	0.882	0.067	0.415	2.32	0.086	0.497	0.074	0.584	0.087	0.005	0.196	0.231	0.027	0.241	0.080	0.211	0.798	0.240
263	Jt8Mt 7 06	4.1	7.362	1.020	3.567	0.363	0.027	0.409	0.044	0.347	1.83	0.083	0.298	0.046	0.371	0.071	0.157	2.989	0.610	0.029	0.656	0.197	0.509	0.547	0.380
264	Jt8Mt 7 07	6.9	17.185	2.133	8.797	1.418	0.084	1.164	0.093	0.387	2.14	0.072	0.373	0.051	0.484	0.054	0.000	0.156	0.107	0.025	0.202	0.092	0.223	0.794	0.226
265	Jt8Mt 7 08	4.1	8.664	1.178	3.740	0.447	0.037	0.333	0.052	0.283	1.80	0.071	0.268	0.055	0.370	0.051	0.008	0.128	0.590	0.028	0.824	0.691	1.591	0.541	0.190
266	Jt8Mt 7 09	5.4	10.328	1.351	4.418	0.619	0.026	0.353	0.032	0.275	2.34	0.090	0.385	0.067	0.466	0.084	0.003	0.191	0.730	0.029	0.752	0.690	1.576	0.781	0.190
267	Jt8Mt 7 10	3.2	5.697	0.680	2.370	0.273	0.018	0.142	0.040	0.285	1.99	0.077	0.311	0.058	0.465	0.052	0.000	0.448	1.041	0.029	0.736	0.671	1.431	0.688	0.146
268	Jt8Mt 8 01	0.019	0.024	0.006	0.030	0.025	0.004	0.008	0.005	0.026	0.126	0.006	0.017	0.001	0.003	0.001	0.000	0.010	0.003	0.027	0.066	0.023	0.043	0.003	0.027
269	Jt8Mt 8 02	0.178	0.554	0.065	0.196	0.021	0.003	0.032	0.006	0.094	0.511	0.021	0.065	0.006	0.059	0.007	0.000	0.122	0.212	0.026	0.151	0.089	0.221	0.087	0.028
270	Jt8Mt 8 03	0.464	1.084	0.125	0.565	0.196	0.020	0.217	0.036	0.268	1.72	0.050	0.146	0.019	0.118	0.027	0.000	0.052	0.062	0.026	1.181	0.364	0.849	0.047	0.354
271	Jt8Mt 8 04	0.351	0.816	0.110	0.462	0.097	0.007	0.111	0.022	0.149	0.985	0.028	0.120	0.013	0.120	0.020	0.051	0.041	0.134	0.028	0.541	0.160	0.332	0.060	0.231
272	Jt8Mt 8 05	1.1	2.368	0.298	1.258	0.221	0.010	0.233	0.027	0.304	1.82	0.070	0.227	0.030	0.249	0.040	0.000	0.123	0.413	0.028	0.652	0.219	0.473	0.190	0.342
273	Jt8Mt 8 06	0.009	0.020	0.002	0.015	0.027	0.001	0.013	0.005	0.034	0.151	0.001	0.017	0.003	0.007	0.001	0.000	0.002	0.033	0.025	0.030	0.023	0.047	0.004	0.013
274	Jt8Mt 8 07	0.368	0.846	0.100	0.398	0.083	0.001	0.082	0.017	0.116	0.730	0.027	0.076	0.009	0.098	0.007	0.000	0.064	0.263	0.028	0.315	0.190	0.443	0.186	0.114
275	Jt8Mt 8 08	0.509	1.283	0.121	0.460	0.053	0.001	0.056	0.010	0.080	0.570	0.017	0.076	0.011	0.050	0.010	0.005	0.027	0.150	0.027	0.128	0.082	0.236	0.312	0.049
276	Jt8Mt 9 01	3.525	5.787	0.582	3.610	0.519	0.026	0.366	0.030	0.178	1.18	0.049	0.206	0.026	0.148	0.028	0.000	0.060	0.372	0.025	0.849	0.486	1.031	0.175	0.248
277	Jt8Mt 9 02	0.389	0.571	0.077	0.308	0.064	0.006	0.129	0.014	0.174	1.09	0.034	0.134	0.026	0.153	0.018	0.012	0.036	0.141	0.027	0.953	0.280	0.723	0.076	0.291
279	Jt8Mt 9 04	1.548	2.879	0.401	1.468	0.332	0.021	0.867	0.115	0.727	2.79	0.130	0.295	0.045	0.326	0.025	0.000	0.687	0.556	0.030	0.942	0.492	1.061	0.219	0.215
280	Jt8Mt 9 05	0.006	0.026	0.008	0.017	0.027	0.003	0.051	0.009	0.062	0.298	0.023	0.072	0.012	0.020	0.003	0.000	0.011	0.037	0.032	0.354	0.112	0.282	0.007	0.054
283	Jt8Mt 9 08	0.006	0.012	0.002	0.012	0.026	0.003	0.005	0.000	0.012	0.102	0.004	0.024	0.003	0.024	0.002	0.000	0.020	0.033	0.023	0.087	0.031	0.041	0.001	0.072
284	Jt8Mt 9 09	0.265	0.388	0.063	0.224	0.038	0.003	0.114	0.012	0.122	0.726	0.029	0.079	0.020	0.087	0.011	0.000	0.018	0.102	0.026	0.862	0.236	0.565	0.041	0.270
285	Jt8Mt 9 10	0.251	0.346	0.054	0.128	0.025	0.001	0.042	0.007	0.068	0.469	0.018	0.060	0.009	0.061	0.010	0.000	0.032	0.159	0.026	0.505	0.234	0.444	0.051	0.148
286	Jt8Mt 9 11	0.030	0.087	0.013	0.030	0.012	0.001	0.021	0.000	0.003	0.045	0.001	0.002	0.001	0.003	0.004	0.000	0.025	0.040	0.027	0.021	0.015	0.044	0.023	0.014
287	Jt8Mt 9 12	0.121	0.213	0.035	0.060	0.021	0.001	0.005	0.000	0.022	0.165	0.006	0.025	0.005	0.025	0.003	0.000	0.020	0.054	0.033	0.108	0.043	0.107	0.034	0.057
289	Jt8Mt 9 14	0.287	0.885	0.148	0.644	0.133	0.003	0.096	0.012	0.092	0.606	0.016	0.071	0.012	0.050	0.007	0.000	0.021	0.051	0.024	0.136	0.109	0.224	0.041	0.072
290	Jt8Mt 9 15	0.581	1.548	0.161	0.617	0.102	0.004	0.144	0.018	0.214	1.22	0.049	0.141	0.018	0.230	0.032	0.000	0.072	0.483	0.025	0.362	0.334	0.716	0.243	0.095
291	Jt8Mt 9 16	0.362	0.766	0.087	0.356	0.044	0.004	0.094	0.013	0.172	1.16	0.041	0.154	0.023	0.167	0.025	0.003	0.829	0.530	0.030	0.667	0.519	0.995	0.070	0.134
292	Jt8Mt 9 17	0.833	1.7	0.172	0.732	0.117	0.013	0.115	0.026	0.185	1.34	0.064	0.175	0.034	0.144	0.028	0.000	0.054	0.386	0.029	0.377	0.262	0.586	0.199	0.089
293	Jt8Mt 9 18	0.526	2.2	0.202	0.669	0.111	0.001	0.132	0.011	0.115	0.711	0.024	0.079	0.012	0.101	0.014	0.003	0.049	0.245	0.028	0.161	0.131	0.315	0.511	0.072
294	Jt8Mt 9 19	0.430	0.856	0.111	0.320	0.101	0.013	0.111	0.011	0.135	0.978	0.028	0.164	0.014	0.117	0.016	0.000	0.102	0.332	0.042	0.501	0.220	0.538	0.152	0.192
295	Jt8Mt 9 20	0.015	0.046	0.006	0.036	0.043	0.001	0.021	0.001	0.031	0.113	0.002	0.007	0.001	0.037	0.002	0.000	0.027	0.003	0.030	0.089	0.031	0.085	0.001	0.017
296	Jt9bMt1rim 01	1.1	2.4	0.281	1.123	0.200	0.023	0.263	0.030	0.159	1.3	0.037	0.097	0.007	0.068	0.006	0.014	0.011	0.088	0.009	0.317	0.298	0.704	0.062	0.109
297	Jt9bMt1rim 02	1.8	4.4	0.621	3.176	0.769	0.036	1.1	0.141	1.2	8.9	0.308	0.898	0.099	0.696	0.052	0.019	0.073	0.223	0.005	0.124	0.036	0.097	0.175	0.215
299	Jt9bMt1rim 04	0.058	0.137	0.007	0.051	0.017	0.001	0.028	0.007	0.039	0.120	0.006	0.012	0.003	0.007	0.001	0.000	0.233	0.319	0.002	0.087	0.067	0.183	0.018	0.041
300	Jt9bMt1rim 05	9.2	16.9	2.5	8.7	1.102	0.037	0.716	0.073	0.455	2.52	0.107	0.333	0.048	0.256	0.029	0.003	0.502	0.505	0.005	0.119	0.063	0.338	1.798	0.188
301	Jt9bMt1core 01	7.7	9.4	1.4	4.0	0.421	0.020	0.308	0.028	0.285	1.75	0.069	0.230	0.039	0.252	0.031	0.009	0.415	0.673	0.002	0.296	0.201	0.525	0.878	0.118

#	Sample	La	Ce	Pr	Nd	Sm	Eu	Gd	Tb	Dy	Y	Ho	Er	Tm	Yb	Lu	Hf	Ta	W	^{204}Pb	^{206}Pb	^{207}Pb	^{208}Pb	Th	^{238}U
302	Jt9bMt1core 02	12.7	19.4	3.0	10.0	1.2	0.059	0.695	0.082	0.489	2.73	0.119	0.333	0.048	0.264	0.030	0.009	0.372	0.767	0.007	0.221	0.116	0.438	1.483	0.126
303	Jt9bMt2 01	0.044	0.106	0.013	0.060	0.036	0.004	0.042	0.007	0.080	0.203	0.013	0.032	0.004	0.035	0.002	0.003	0.012	0.089	0.013	0.049	0.024	0.056	0.008	0.039
304	Jt9bMt2 02	0.208	0.490	0.072	0.424	0.097	0.019	0.215	0.025	0.225	1.46	0.058	0.137	0.021	0.141	0.016	0.000	0.033	0.031	0.002	0.171	0.037	0.054	0.017	0.280
305	Jt9bMt2 03	0.010	0.044	0.002	0.007	0.005	0.000	0.004	0.000	0.003	0.013	0.000	0.000	0.000	0.007	0.001	0.000	0.002	0.006	0.006	0.010	0.004	0.017	0.003	0.009
306	Jt9bMt3 04	0.078	0.170	0.016	0.083	0.021	0.000	0.025	0.009	0.036	0.288	0.010	0.048	0.005	0.026	0.008	0.005	0.103	0.056	0.007	0.092	0.041	0.081	0.037	0.098
307	Jt9bMt3 05	6.020	7.783	0.847	2.895	0.408	0.031	0.385	0.030	0.334	1.80	0.059	0.230	0.030	0.203	0.032	0.000	0.602	1.067	0.010	0.925	0.578	1.233	0.808	0.309
308	Jt9bMt3 06	0.624	1.140	0.156	0.436	0.101	0.006	0.112	0.018	0.139	0.970	0.047	0.101	0.021	0.102	0.011	0.000	0.077	0.203	0.006	0.097	0.056	0.111	0.171	0.076
309	Jt9bMt4 07	0.264	0.694	0.072	0.327	0.089	0.009	0.137	0.020	0.136	1.16	0.049	0.123	0.019	0.076	0.013	0.014	0.003	0.060	0.006	0.188	0.083	0.103	0.019	0.239
310	Jt9bMt4 08	13.6	20.2	1.9	5.9	0.616	0.048	0.490	0.087	0.582	3.53	0.136	0.448	0.038	0.333	0.033	0.000	0.137	0.505	0.004	0.516	0.279	0.727	0.999	0.298
311	Jt9bMt4 09	7.4	9.8	1.3	4.1	0.692	0.029	0.476	0.061	0.281	2.41	0.089	0.311	0.039	0.239	0.032	0.003	0.244	0.471	0.018	0.522	0.446	0.964	1.320	0.198
312	Jt9bMt4 10	0.189	0.365	0.041	0.167	0.069	0.004	0.037	0.009	0.070	0.68	0.011	0.068	0.006	0.086	0.013	0.000	0.058	0.114	0.003	0.087	0.050	0.096	0.013	0.086
313	Jt9bMt5 11	130	190	18	54	6.4	0.332	4.8	0.665	4.8	28.09	0.973	2.9	0.377	2.036	0.243	0.000	0.594	1.966	0.001	0.592	0.250	0.962	4.366	0.580
314	Jt9bMt5 12	1.831	2.324	0.367	1.127	0.241	0.013	0.478	0.081	0.570	3.54	0.128	0.268	0.045	0.191	0.037	0.003	0.126	0.381	0.002	0.325	0.206	0.386	0.295	0.036
315	Jt9bMt6 13	0.036	0.143	0.003	0.036	0.005	0.000	0.016	0.004	0.006	0.119	0.001	0.007	0.000	0.014	0.001	0.002	0.000	0.018	0.016	0.018	0.009	0.014	0.003	0.014
316	Jt9bMt6 14	100.5	188.0	21.6	76.3	11.0	0.589	9.0	1.2	9.7	66.21	3.0	9.1	1.2	6.3	0.689	0.003	0.081	0.272	0.000	0.427	0.131	0.311	1.926	0.843
317	Jt9bMt6 15	98	190	20	73	9.8	0.653	7.8	0.967	7.157	48.22	1.907	6.748	0.949	5.296	0.593	0.000	0.041	0.171	0.005	0.366	0.067	0.214	1.415	0.743
318	Jt9bMt6 16	11	22	3	14	3.8	0.240	4.3	0.767	5.985	42.93	1.558	5.180	0.671	3.732	0.402	0.000	0.204	0.317	0.007	0.616	0.357	0.598	0.760	0.583
319	Jt9bMt7 17	0.415	0.474	0.082	0.317	0.051	0.001	0.074	0.005	0.088	0.47	0.018	0.055	0.004	0.051	0.005	0.000	0.041	0.113	0.010	0.091	0.055	0.105	0.047	0.083
320	Jt9bMt7 18	0.547	1.7	0.260	1.639	0.609	0.034	1.3	0.206	1.595	10.40	0.338	0.904	0.097	0.569	0.059	0.000	0.037	0.057	0.006	0.103	0.034	0.041	0.036	0.198
321	Jt9bMt7 19	3.074	5.5	0.701	2.460	0.253	0.016	0.261	0.049	0.312	2.11	0.082	0.279	0.038	0.271	0.036	0.003	0.297	0.836	0.011	0.656	0.408	0.940	1.229	0.217
322	Jt9bMt8 20	0.517	1.1	0.142	0.473	0.110	0.004	0.116	0.008	0.123	0.667	0.021	0.056	0.011	0.081	0.006	0.005	0.165	0.262	0.013	0.180	0.119	0.302	0.170	0.053
323	Jt9bMt8 21	2.5	5.7	0.687	2.745	0.304	0.047	0.410	0.039	0.292	1.87	0.067	0.236	0.041	0.219	0.029	0.000	0.467	0.636	0.015	0.333	0.271	0.643	0.307	0.140
324	Jt9bMt8 22	0.912	2.3	0.273	1.091	0.173	0.013	0.142	0.022	0.166	1.39	0.059	0.165	0.016	0.122	0.020	0.003	0.208	0.319	0.001	0.158	0.094	0.273	0.276	0.059
325	Jt9bMt8 23	3.1	5.9	0.713	3.348	0.784	0.057	1.2	0.251	1.872	11.0	0.455	1.3	0.147	0.880	0.101	0.003	0.148	0.288	0.002	0.320	0.207	0.408	0.247	0.199
326	Jt9bMt8 24	52.3	98.1	10.4	44.2	5.6	0.190	3.5	0.208	0.791	2.87	0.128	0.307	0.030	0.194	0.016	0.000	0.203	0.233	0.011	0.211	0.097	0.237	0.271	0.684
327	Jt9bMt9 25	0.024	0.044	0.003	0.018	0.001	0.001	0.001	0.000	0.001	0.044	0.003	0.002	0.005	0.035	0.000	0.000	0.002	0.016	0.013	0.019	0.008	0.028	0.003	0.009
328	Jt9bMt9 26	0.992	1.252	0.116	0.428	0.052	0.004	0.110	0.018	0.078	0.757	0.029	0.092	0.013	0.063	0.008	0.008	0.121	0.362	0.019	0.820	0.654	1.408	0.186	0.123
329	Jt9bMt9 27	0.197	0.358	0.046	0.165	0.079	0.009	0.079	0.023	0.140	1.00	0.045	0.087	0.013	0.070	0.011	0.005	0.032	0.072	0.010	0.188	0.112	0.209	0.032	0.158
330	Jt9bMt10 28	1.062	1.818	0.207	0.763	0.088	0.004	0.087	0.010	0.132	0.983	0.041	0.108	0.016	0.092	0.010	0.005	0.074	0.332	0.002	0.252	0.162	0.423	0.266	0.065
331	Jt9bMt10 29	0.987	1.317	0.118	0.745	0.246	0.034	0.298	0.069	0.458	2.81	0.115	0.359	0.040	0.261	0.032	0.000	0.058	0.125	0.014	0.237	0.188	0.301	0.188	0.277
332	Jt9bMt10 30	0.570	1.055	0.136	0.617	0.093	0.012	0.261	0.031	0.175	1.48	0.067	0.192	0.029	0.190	0.017	0.000	0.010	0.088	0.010	0.056	0.012	0.061	0.072	0.058
333	Jt9bMt10 31	1.885	5.340	0.757	3.491	0.637	0.061	0.696	0.072	0.683	4.74	0.197	0.796	0.107	0.486	0.055	0.000	0.001	0.011	0.021	0.038	0.010	0.016	0.085	0.056
334	Jt9bMt11 32	0.507	0.764	0.089	0.441	0.095	0.010	0.115	0.021	0.139	0.725	0.029	0.099	0.011	0.060	0.005	0.013	0.051	0.099	0.001	0.338	0.165	0.342	0.081	0.302
335	Jt9bMt11 33	0.035	0.065	0.006	0.011	0.012	0.001	0.005	0.001	0.020	0.105	0.007	0.031	0.002	0.015	0.002	0.000	0.032	0.029	0.001	0.088	0.047	0.037	0.009	0.046
336	Jt9Mt12 34	5.405	9.430	1.040	5.053	1.055	0.070	1.723	0.257	2.079	14.57	0.525	1.624	0.174	1.015	0.130	0.000	0.132	0.213	0.001	0.559	0.190	0.360	0.346	0.899
337	Jt9bMt12 35	0.747	1.793	0.252	1.378	0.400	0.018	0.579	0.118	0.856	6.74	0.202	0.682	0.077	0.452	0.053	0.003	0.056	0.139	0.002	0.300	0.114	0.139	0.183	0.330
338	Jt9bMt13 36	0.053	0.191	0.018	0.133	0.032	0.002	0.053	0.005	0.055	0.349	0.017	0.016	0.005	0.037	0.005	0.002	0.036	0.022	0.008	0.038	0.015	0.037	0.003	0.042
339	Jt9bMt13 37	1.213	1.447	0.184	0.481	0.106	0.002	0.110	0.018	0.170	0.960	0.047	0.146	0.011	0.134	0.013	0.000	0.142	0.364	0.015	0.244	0.103	0.233	0.369	0.174
340	Jt9bMt14 38	0.356	0.841	0.072	0.282	0.052	0.001	0.045	0.007	0.046	0.342	0.018	0.043	0.004	0.032	0.004	0.003	0.060	0.193	0.002	0.129	0.085	0.235	0.128	0.059

ESM Table 2b. Summary of LA-ICP-MS trace element data for magnetite in each sample (concentrations in ppm)
**Note:* G.M. Geometric mean

Jt1	Mg	Al	Si	P	Ca	Sc	Ti	V	Cr	Mn	Co	Ni	Cu	Zn	Ga	As	Sr	Zr	Nb	Mo	Sn	Sb	Ba
Mean (n=52)	277	722	619	16	536	0.131	1770	1670	127	224	24	43	1.7	63	21	0.487	10	0.084	0.843	0.223	0.166	0.102	36
S.D.	165	249	318	0.000	260	0.089	3793	85	48	137	1.4	1.6	0.9	28	2.5	0.256	4.7	0.070	1.8	0.160	0.118	0.061	17
G.M.	246	710	599	16	497	0.088	707	1668	121	202	24	43	1.5	58	20	0.424	8.4	0.062	0.094	0.152	0.140	0.084	33
Median	206	716	602	16	495	0.124	521	1666	121	178	24	43	1.7	63	21	0.485	9.0	0.060	0.031	0.214	0.130	0.089	32
Maximum	833	995	999	16	988	0.398	19392	1830	257	696	27	46	4.0	110	25	1.4	22	0.325	9.4	0.789	0.627	0.278	78
Minimum	106	469	258	16	237	0.002	379	1350	51	112	20	39	0.306	9.1	10	0.081	1.1	0.016	0.011	0.005	0.047	0.007	7.8
Jt3																							
Mean (n=40)	272	627	894	20	409	0.279	19541	1857	166	680	19	44	2.2	36	17	1.1	1.2	0.519	11	0.530	0.250	0.172	8.4
S.D.	206	314	601	4.0	235	0.171	8600	163	259	352	2.6	5.1	1.5	19	3.4	0.362	0.928	1.1	4.3	0.283	0.196	0.101	6.0
G.M.	227	606	797	19	384	0.253	18985	1850	116	614	19	44	1.9	32	17	1.1	0.862	0.222	11	0.452	0.204	0.149	6.4
Median	194	559	758	19	347	0.225	19317	1798	106	725	19	43	1.8	32	18	1.0	1.1	0.179	12	0.513	0.190	0.127	8.2
Maximum	992	1087	2833	37	878	1.0	29038	2211	1670	968	26	64	7.0	93	21	1.9	3.2	6.9	19	1.2	1.0	0.498	18
Minimum	104	420	403	16	267	0.162	10579	1674	35	124	14	40	0.443	14	10	0.633	0.145	0.046	2.7	0.051	0.071	0.074	1.1
Jt4																							
Mean (n=59)	487	691	2493	26	313	0.687	5833	1589	256	213	6.8	62	1.0	27	17	0.540	0.449	0.171	4.7	0.135	0.297	0.073	1.7
S.D.	503	405	2128	20	182	0.385	4517	102	160	138	3.4	17	1.4	19	4.5	0.475	0.871	0.332	3.8	0.165	0.106	0.081	1.8
G.M.	289	634	1737	22	286	0.586	3654	1586	215	169	6.4	62	0.495	22	16	0.410	0.148	0.044	1.7	0.039	0.282	0.041	0.528
Median	351	590	1995	16	237	0.641	5341	1605	245	197	5.8	60	0.475	21	15	0.377	0.181	0.037	4.2	0.055	0.290	0.043	1.3
Maximum	2639	2098	8550	90	844	1.9	13928	1934	690	504	25	75	7.2	72	27	2.4	6.3	1.7	12	0.555	0.755	0.351	8.1
Minimum	28	313	216	11	220	0.090	263	1382	54	32	4.3	54	0.031	7.2	11	0.100	0.002	0.001	0.000	0.000	0.150	0.004	0.000
Jt7																							
Mean (n=63)	1278	1108	3302	19	347	0.281	2194	2172	37	97	4.2	53	0.841	24	20	0.754	0.459	0.083	1.9	0.240	0.269	0.124	5.7
S.D.	1101	893	2532	9.0	216	0.183	3335	210	26	108	3.5	18	1.4	14	5.1	0.250	0.435	0.144	2.7	0.227	0.293	0.097	6.8
G.M.	689	903	2329	18	312	0.243	842	2162	28	62	2.8	52	0.463	21	19	0.722	0.239	0.026	0.332	0.129	0.188	0.103	1.8
Median	928	709	2530	16	252	0.202	477	2152	33	45	3.0	49	0.300	21	21	0.701	0.363	0.033	0.555	0.175	0.179	0.082	3.3
Maximum	5155	3859	9838	69	815	1.1	12764	2629	88	459	12	90	7.9	90	27	1.9	2.0	0.964	9.3	0.773	1.8	0.524	32
Minimum	18	414	187	14	212	0.141	310	1744	2.4	18	0.209	43	0.198	7.5	10	0.447	0.004	0.001	0.001	0.019	0.048	0.055	0.004
Jt8																							
Mean (n=72)	1248	551	3696	18	265	0.542	359	1601	41	149	2.6	71	0.722	35	25	0.763	1.1	0.026	0.610	0.154	0.431	0.157	4.1
S.D.	874	200	2325	7.6	91	0.340	193	130	27	93	1.3	28	1.1	23	1.6	0.398	0.934	0.064	0.587	0.265	0.121	0.095	4.2
G.M.	956	532	3110	18	258	0.468	331	1595	33	129	2.4	70	0.434	29	25	0.700	0.637	0.011	0.391	0.084	0.415	0.135	2.6
Median	1085	496	3253	16	246	0.475	308	1606	35	124	2.3	67	0.273	26	25	0.613	0.842	0.014	0.397	0.057	0.414	0.125	3.2
Maximum	3942	1080	9933	65	583	2.4	976	1843	96	519	6.5	183	8.6	95	29	2.7	3.9	0.538	3.6	2.0	1.0	0.477	27
Minimum	38	358	421	13	194	0.173	160	1063	7.2	51	0.742	59	0.211	8.2	22	0.429	0.001	0.001	0.001	0.016	0.189	0.065	0.025

Jt9b																							
Mean (n=44)	1429	541	3100	57	317	0.097	331	1700	4.6	116	11	69	1.3	24	33	0.256	0.602	0.139	0.244	0.147	0.317	0.118	1.6
S.D.	1186	223	2677	140	199	0.084	54	73	1.7	71	3.6	21	1.3	16	1.8	0.193	0.578	0.208	0.192	0.174	0.124	0.105	1.4
G.M.	763	519	2015	25	287	0.069	327	1699	4.3	104	10	68	0.887	20	33	0.171	0.371	0.072	0.154	0.070	0.295	0.076	1.0
Median	1276	477	2480	16	237	0.083	329	1713	4.9	95	10	64	0.850	20	33	0.215	0.420	0.063	0.224	0.096	0.317	0.079	1.3
Maximum	4299	903	8875	912	955	0.498	500	1899	7.8	336	29	138	5.3	64	39	0.946	2.6	0.921	0.660	0.843	0.635	0.426	4.8
Minimum	11	324	245	16	119	0.014	182	1581	1.2	58	7.9	55	0.126	5.4	30	0.004	0.022	0.011	0.004	0.003	0.152	0.005	0.053

ESM Table 2b. (Continued)

Jt1	**La**	**Ce**	**Pr**	**Nd**	**Sm**	**Eu**	**Gd**	**Tb**	**Dy**	**Y**	**Ho**	**Er**	**Tm**	**Yb**	**Lu**	**Hf**	**Ta**	**W**	**^{204}Pb**	**^{206}Pb**	**^{207}Pb**	**^{208}Pb**	**Th**	**^{238}U**
Mean (n=52)	0.049	0.102	0.019	0.100	0.046	0.014	0.072	0.025	0.143	0.486	0.059	0.116	0.029	0.103	0.019	0.007	0.147	0.238	0.088	1.4	1.4	3.1	0.007	0.176
S.D.	0.101	0.145	0.035	0.154	0.087	0.029	0.130	0.065	0.281	1.2	0.152	0.222	0.070	0.196	0.042	0.011	0.258	0.406	0.058	0.774	0.825	1.9	0.007	0.507
G.M.	0.024	0.060	0.007	0.032	0.009	0.003	0.014	0.002	0.015	0.057	0.003	0.012	0.002	0.008	0.002	0.002	0.010	0.060	0.065	1.1	1.1	2.4	0.004	0.025
Median	0.021	0.060	0.007	0.029	0.009	0.003	0.010	0.001	0.010	0.029	0.002	0.008	0.001	0.005	0.001	0.003	0.004	0.042	0.075	1.2	1.3	2.9	0.005	0.018
Maximum	0.646	0.801	0.210	0.700	0.508	0.184	0.545	0.419	1.3	5.4	1.0	1.0	0.433	0.824	0.245	0.057	0.912	1.9	0.258	3.3	3.6	7.9	0.025	2.6
Minimum	0.004	0.007	0.000	0.000	0.000	0.000	0.001	0.000	0.000	0.009	0.000	0.000	0.000	0.000	0.000	0.000	0.000	0.003	0.003	0.029	0.014	0.040	0.000	0.001
Jt3																								
Mean (n=40)	0.166	0.319	0.106	0.221	0.163	0.058	0.117	0.037	0.148	0.306	0.044	0.120	0.012	0.082	0.009	0.028	0.799	1.2	0.037	0.789	0.205	0.254	0.022	1.3
S.D.	0.152	0.266	0.206	0.265	0.267	0.114	0.167	0.075	0.254	0.207	0.097	0.256	0.026	0.152	0.013	0.073	0.305	0.556	0.007	0.277	0.079	0.186	0.027	0.538
G.M.	0.121	0.241	0.039	0.119	0.082	0.013	0.052	0.012	0.071	0.267	0.018	0.052	0.005	0.042	0.005	0.006	0.671	1.0	0.037	0.736	0.191	0.204	0.017	1.1
Median	0.100	0.198	0.023	0.090	0.055	0.016	0.045	0.009	0.050	0.260	0.014	0.045	0.005	0.037	0.005	0.009	0.826	1.2	0.037	0.794	0.185	0.185	0.018	1.3
Maximum	0.669	1.0	1.2	1.1	1.5	0.485	0.823	0.387	1.5	0.815	0.557	1.5	0.144	0.858	0.068	0.392	1.2	2.2	0.064	1.5	0.404	0.869	0.179	2.2
Minimum	0.046	0.061	0.005	0.017	0.025	0.001	0.001	0.000	0.005	0.076	0.002	0.009	0.000	0.006	0.000	0.000	0.003	0.254	0.029	0.206	0.053	0.045	0.002	0.007
Jt4																								
Mean (n=59)	1.2	2.5	0.323	1.1	0.271	0.055	0.290	0.057	0.271	1.8	0.092	0.253	0.053	0.286	0.052	0.018	0.467	0.546	0.010	0.450	0.157	0.271	0.165	0.726
S.D.	1.4	2.7	0.331	1.2	0.266	0.113	0.305	0.082	0.262	1.8	0.113	0.235	0.063	0.270	0.056	0.046	0.423	0.565	0.010	0.325	0.159	0.332	0.247	0.513
G.M.	0.407	0.839	0.114	0.428	0.109	0.016	0.112	0.023	0.149	1.0	0.044	0.146	0.028	0.168	0.029	0.003	0.146	0.228	0.006	0.273	0.082	0.112	0.036	0.440
Median	0.766	1.1	0.224	0.627	0.204	0.028	0.197	0.035	0.214	1.4	0.048	0.180	0.032	0.195	0.028	0.004	0.334	0.441	0.008	0.467	0.092	0.158	0.037	0.580
Maximum	7.1	9.3	1.2	4.6	1.1	0.819	1.1	0.505	1.0	7.0	0.556	0.928	0.305	1.2	0.248	0.308	1.3	2.3	0.056	1.2	0.741	1.5	1.1	1.8
Minimum	0.002	0.003	0.000	0.004	0.000	0.000	0.001	0.000	0.004	0.007	0.001	0.000	0.000	0.000	0.000	0.000	0.000	0.001	0.000	0.003	0.001	0.002	0.000	0.001
Jt7																								
Mean (n=63)	0.366	0.862	0.127	0.466	0.202	0.052	0.259	0.096	0.412	3.0	0.167	0.397	0.090	0.327	0.050	0.012	0.311	0.331	0.035	0.390	0.192	0.331	0.055	0.313
S.D.	0.666	1.6	0.184	0.622	0.256	0.109	0.444	0.186	1.1	7.9	0.339	1.0	0.183	0.856	0.089	0.025	0.458	0.324	0.039	0.354	0.184	0.339	0.125	0.428
G.M.	0.085	0.180	0.043	0.171	0.102	0.011	0.070	0.019	0.080	0.458	0.032	0.074	0.015	0.066	0.013	0.002	0.051	0.137	0.030	0.220	0.116	0.203	0.015	0.089
Median	0.103	0.295	0.053	0.233	0.122	0.019	0.131	0.030	0.125	0.802	0.043	0.116	0.019	0.114	0.015	0.002	0.064	0.271	0.028	0.271	0.153	0.232	0.019	0.112
Maximum	3.4	8.4	0.925	2.9	1.5	0.674	3.3	1.0	8.3	60	2.1	7.5	1.1	6.5	0.509	0.162	2.7	1.2	0.315	1.4	0.842	1.8	0.933	1.5
Minimum	0.001	0.001	0.002	0.007	0.010	0.001	0.001	0.000	0.001	0.001	0.000	0.000	0.000	0.000	0.000	0.000	0.000	0.001	0.024	0.014	0.011	0.019	0.000	0.000

Jt8																								
Mean (n=72)	1.1	1.7	0.285	0.873	0.145	0.012	0.158	0.022	0.176	1.1	0.042	0.156	0.027	0.171	0.026	0.004	0.088	0.266	0.029	0.627	0.323	0.732	0.186	0.155
S.D.	1.5	2.1	0.411	1.1	0.160	0.018	0.175	0.024	0.159	0.944	0.037	0.141	0.037	0.161	0.031	0.019	0.135	0.219	0.006	0.915	0.344	0.796	0.206	0.141
G.M.	0.355	0.683	0.102	0.360	0.083	0.005	0.080	0.012	0.111	0.702	0.026	0.090	0.015	0.098	0.014	0.001	0.047	0.162	0.029	0.348	0.191	0.432	0.078	0.103
Median	0.415	0.885	0.114	0.460	0.096	0.005	0.107	0.014	0.135	0.829	0.034	0.132	0.018	0.117	0.017	0.000	0.042	0.196	0.028	0.382	0.219	0.500	0.110	0.101
Maximum	6.9	8.9	2.1	4.4	0.645	0.089	0.882	0.121	0.873	5.6	0.216	0.773	0.290	0.695	0.198	0.157	0.829	1.0	0.058	7.2	2.2	5.1	0.798	0.697
Minimum	0.004	0.008	0.002	0.012	0.009	0.001	0.001	0.000	0.003	0.015	0.001	0.000	0.001	0.003	0.000	0.000	0.001	0.001	0.023	0.014	0.011	0.018	0.000	0.006
Jt9b																								
Mean (n=44)	0.714	1.5	0.203	0.690	0.216	0.062	0.248	0.106	0.239	1.3	0.115	0.219	0.078	0.187	0.066	0.003	0.143	0.240	0.007	0.262	0.149	0.294	0.306	0.215
S.D.	0.780	1.6	0.220	0.766	0.232	0.139	0.251	0.204	0.227	1.1	0.177	0.236	0.177	0.195	0.145	0.005	0.161	0.215	0.006	0.221	0.151	0.270	0.432	0.227
G.M.	0.297	0.668	0.080	0.287	0.094	0.013	0.116	0.029	0.124	0.716	0.044	0.101	0.021	0.106	0.016	0.001	0.060	0.142	0.005	0.172	0.085	0.174	0.094	0.126
Median	0.461	0.841	0.117	0.428	0.097	0.015	0.127	0.028	0.149	1.0	0.058	0.130	0.021	0.122	0.017	0.002	0.075	0.198	0.006	0.199	0.100	0.234	0.171	0.133
Maximum	3.1	5.9	0.757	3.3	0.784	0.653	1.1	1.0	0.856	3.5	1.0	0.904	0.949	0.880	0.689	0.019	0.602	0.836	0.021	0.925	0.654	1.0	1.9	0.899
Minimum	0.010	0.044	0.002	0.007	0.001	0.000	0.001	0.000	0.001	0.013	0.000	0.000	0.000	0.007	0.000	0.000	0.000	0.006	0.000	0.010	0.004	0.014	0.003	0.009

ESM Table 2c. LA-ICP-MS data for magnetite divided by textural type and used for box-and-whiskers plots (concentrations in ppm)

	Lithophile elements				Transition metals								REY			Granitophile				
Sample	Si	Mg	Al	Ca	Ti	V	Nb	Cr	Ni	Co	Mn	Zn	ΣREY	ΣLMREE	ΣHREY	U	^{206}Pb	W	Sn	Mo
1. Trellis	673	197	623	237	487	1639	0.029	229	44	23	115	42	0.144	0.103	0.008	0.005	0.543	0.100	0.063	0.265
1. Trellis	798	213	716	821	548	1690	0.023	257	46	24	253	99	0.084	0.056	0.010	0.005	2.94	0.029	0.108	0.120
1. Trellis	809	176	639	652	385	1658	0.044	183	45	23	187	78	0.111	0.056	0.027	0.006	2.20	1.64	0.125	0.359
1. Trellis	2990	330	995	3081	2820	1633	5.88	203	44	23	180	65	38	3.31	11.1	0.327	1.11	1.90	0.504	0.789
1. Trellis	654	174	665	688	474	1621	0.018	196	44	24	240	110	0.114	0.079	0.012	0.006	2.85	0.032	0.117	0.101
1. Trellis	637	184	723	496	527	1634	0.027	169	46	25	191	91	0.228	0.196	0.011	0.005	2.30	0.042	0.122	0.367
1. Trellis	748	206	704	581	577	1665	0.015	167	44	25	206	79	0.095	0.065	0.005	0.004	1.83	0.038	0.129	0.245
1. Trellis	692	239	706	335	559	1637	0.033	141	45	25	167	70	0.150	0.106	0.016	0.019	1.67	0.030	0.138	0.173
1. Trellis	2001	321	814	2392	2182	1610	4.57	113	42	23	224	87	15.0	1.41	4.42	0.163	2.04	0.928	0.423	0.213
1. Trellis	1230	338	641	458	543	1350	0.633	150	41	20	72	17.6	3.12	0.439	0.861	0.061	0.180	2.26	0.047	0.249
1. Trellis	471	174	526	593	610	1597	0.369	128	40	22	177	77	1.95	0.189	0.544	0.023	1.14	1.20	0.088	0.066
1. Trellis	554	198	687	783	533	1688	0.028	124	42	23	221	89	0.125	0.099	0.009	0.007	2.44	0.025	0.062	0.228
1. Trellis	424	157	662	517	628	1684	0.025	168	44	23	185	69	0.106	0.063	0.015	0.007	1.98	0.010	0.060	0.263
1. Trellis	1057	255	717	626	802	1528	1.51	130	42	21	134	56	4.84	0.539	1.32	0.058	1.11	0.905	0.121	0.140
1. Trellis	999	382	770	784	514	1608	0.038	105	42	21	241	99	0.574	0.416	0.064	0.058	2.37	0.262	0.127	0.276
1. Trellis	1836	566	911	936	1160	1696	1.63	170	44	22	139	39	5.60	0.782	1.62	0.085	0.668	0.471	0.184	0.150
1. Trellis	587	196	698	450	598	1734	0.036	158	45	23	170	52	0.266	0.191	0.020	0.005	1.08	0.076	0.100	0.231
1. Trellis	670	208	708	272	675	1687	0.031	172	45	24	161	51	0.101	0.072	0.003	0.010	1.15	0.005	0.078	0.304
1. Trellis	7632	259	654	585	779	1604	1.06	130	41	24	87	27	7.99	0.617	2.32	0.050	0.434	0.301	0.171	0.010
1. Trellis	4097	1791	1945	862	784	1606	1.39	131	41	25	114	39	8.69	2.52	2.05	0.218	0.318	0.789	0.135	0.355
1. Trellis	868	185	522	458	464	1642	0.555	114	41	24	87	32	1.87	0.180	0.587	0.029	0.239	0.252	0.101	0.025
1. Trellis	2055	624	806	1487	1100	1632	2.15	88	42	25	142	58	9.05	0.907	2.70	0.168	0.773	0.773	0.220	0.029
1. Trellis	653	129	469	237	324	1529	0.003	7.40	39	22	54	9.07	0.446	0.324	0.045	0.140	0.029	0.003	0.080	0.022
1. Trellis	1400	542	1023	275	444	1600	0.060	81	42	24	112	43	0.159	0.130	0.010	0.008	0.642	0.107	0.062	0.026
1. Trellis	617	177	619	814	358	1589	0.013	56	42	24	222	94	0.075	0.047	0.014	0.006	2.36	0.047	0.160	0.005
1. Trellis	1993	418	783	1887	5110	1664	5.30	103	41	25	355	100	7.39	1.28	2.06	0.477	1.89	0.620	0.517	0.356
1. Trellis	446	184	609	493	11755	1617	6.43	88	42	25	579	79	0.358	0.152	0.096	1.56	2.29	0.043	0.178	0.295
1. Trellis	622	182	548	237	16655	1601	9.43	74	41	26	693	45	0.489	0.235	0.119	2.17	1.93	0.108	0.193	0.535
1. Trellis	1434	178	716	2068	4610	1612	5.01	56	43	25	313	95	12.1	1.40	3.52	0.303	1.97	0.818	0.627	0.052
1. Trellis	258	106	532	237	19392	1595	11.3	51	41	26	696	15.9	0.465	0.194	0.127	2.64	1.15	0.127	0.115	0.464
1. Trellis	807	222	562	538	533	1719	0.507	72	41	24	155	67	2.04	0.409	0.519	0.030	1.07	0.247	0.077	0.012
1. Trellis	799	226	477	679	391	1668	0.218	113	40	23	158	86	2.51	1.55	0.370	0.028	1.35	0.165	0.230	0.163
1. Trellis	803	209	571	1294	771	1680	0.255	72	41	24	340	154	0.726	0.463	0.102	0.050	3.64	0.048	0.287	0.171
1. Trellis	1286	317	752	988	973	1746	1.47	119	42	25	143	51	5.23	0.701	1.48	0.061	0.722	0.465	0.215	0.290
1. Trellis	1739	738	1172	566	394	1761	0.028	115	43	26	171	64	0.758	0.567	0.067	0.060	0.742	0.029	0.286	0.259
1. Trellis	518	192	790	545	384	1743	0.026	108	42	25	197	69	0.058	0.027	0.015	0.003	1.98	0.007	0.115	0.180
1. Trellis	502	245	843	693	384	1753	0.011	115	43	25	223	77	0.084	0.058	0.010	0.017	1.76	0.030	0.174	0.358

	Lithophile elements				Transition metals								REY			Granitophile				
Sample	Si	Mg	Al	Ca	Ti	V	Nb	Cr	Ni	Co	Mn	Zn	ΣREY	ΣLMREE	ΣHREY	U	^{206}Pb	W	Sn	Mo
1. Trellis	511	193	798	477	412	1765	0.013	115	43	25	189	74	0.045	0.027	0.008	0.003	0.907	0.005	0.175	0.151
1. Trellis	503	192	818	402	419	1765	0.011	131	43	25	167	59	0.060	0.045	0.005	0.004	0.742	0.004	0.121	0.168
1. Trellis	1101	664	1358	250	485	1781	0.031	132	43	24	121	51	0.110	0.060	0.020	0.004	0.700	0.011	0.116	0.133
1. Trellis	544	178	591	358	410	1608	0.033	60	42	24	166	71	0.095	0.047	0.013	0.007	1.31	0.090	0.135	0.069
1. Trellis	1039	488	928	407	596	1641	0.142	127	43	24	151	52	3.77	3.25	0.188	0.052	0.668	0.156	0.073	0.236
1. Trellis	549	194	757	677	442	1676	0.020	123	43	24	251	83	0.055	0.038	0.007	0.005	1.37	0.012	0.099	0.304
1. Trellis	509	187	808	365	394	1702	0.011	123	43	25	156	52	0.156	0.101	0.041	0.012	1.04	0.006	0.166	0.124
1. Trellis	550	174	829	402	379	1727	0.015	120	43	25	165	61	0.085	0.057	0.015	0.010	1.29	0.027	0.070	0.214
1. Trellis	588	207	856	416	380	1730	0.017	121	43	26	169	62	0.104	0.056	0.018	0.001	1.35	0.021	0.120	0.340
1. Trellis	1657	833	1340	481	2502	1751	0.691	120	44	26	277	66	0.766	0.580	0.059	0.092	1.85	0.027	0.132	0.110
1. Trellis	447	202	763	756	396	1762	0.022	121	45	27	334	123	0.239	0.200	0.019	0.004	1.36	0.036	0.151	0.056
1. Trellis	649	250	922	969	381	1796	0.011	119	44	25	302	117	0.075	0.058	0.009	0.006	3.30	0.003	0.190	0.546
1. Trellis	939	306	962	488	452	1830	0.022	115	44	25	161	61	0.223	0.159	0.024	0.035	1.22	0.023	0.238	0.531
1. Trellis	470	194	885	433	433	1818	0.013	119	44	25	169	58	0.078	0.062	0.004	0.006	0.751	0.012	0.182	0.293
1. Trellis	427	206	876	358	444	1778	0.012	125	43	25	145	55	0.218	0.176	0.011	0.009	1.15	0.005	0.134	0.185
1. Trellis	1050	248	646	529	15684	1715	9.99	90	43	19.9	740	38	2.13	0.591	0.414	1.46	0.872	0.839	0.200	0.380
1. Trellis	2407	319	994	2011	22659	1712	14.1	85	44	16.6	960	93	8.09	7.11	0.314	1.58	0.903	0.982	0.260	0.802
1. Trellis	7307	1848	3058	10439	10579	1790	6.59	100	57	16.5	400	54	40	31	2.52	1.54	0.755	2.27	0.533	0.662
1. Trellis	13706	3658	5077	10048	24797	1800	14.4	1670	64	17.8	849	60	24	21	0.878	1.83	1.48	1.74	0.868	0.783
1. Trellis	780	187	629	558	15347	1739	8.79	86	44	22	719	71	1.74	1.36	0.078	1.23	0.742	0.280	0.215	1.16
1. Trellis	747	118	563	358	418	1762	0.093	156	47	21	124	38	0.510	0.389	0.044	0.007	0.206	0.496	0.191	0.654
1. Trellis	2418	425	903	2302	25163	1736	15.8	319	46	18.9	1000	60	1.20	0.636	0.162	2.11	0.975	0.699	0.274	0.424
1. Trellis	529	172	637	373	22609	1740	14.6	400	46	21	956	148	0.609	0.304	0.100	2.06	0.986	0.401	0.260	0.330
1. Trellis	703	164	655	333	25372	1744	15.9	415	45	23	1082	139	0.605	0.375	0.076	1.62	0.800	0.270	0.227	0.335
1. Trellis	802	192	642	331	29038	1721	18.6	158	44	23	1240	129	0.775	0.500	0.102	2.20	0.940	0.254	0.242	0.577
1. Trellis	5328	1827	2554	2074	15031	2211	8.86	59	48	17.0	677	28	6.24	5.03	0.397	1.07	0.673	1.55	0.113	0.513
1. Trellis	1013	417	781	317	17158	2177	10.6	91	49	17.3	774	26	3.54	2.95	0.212	1.20	0.659	1.04	0.106	0.614
1. Trellis	520	104	420	279	15476	2143	9.04	102	40	16.5	705	17.6	0.812	0.528	0.105	0.781	0.482	0.364	0.082	0.513
1. Trellis	406	121	475	306	15956	2149	10.0	83	42	16.5	723	29	0.568	0.294	0.073	1.09	0.596	0.490	0.129	0.582
1. Trellis	2761	501	1058	2099	16404	2182	10.4	107	42	15.8	687	18.9	4.92	3.26	0.475	1.02	0.640	1.63	0.329	0.380
1. Trellis	12182	5938	7617	1375	5937	1872	3.65	131	58	23	344	25	7.27	4.73	0.666	0.434	0.277	0.906	0.100	0.051
1. Trellis	1028	368	704	761	18567	1848	11.6	56	44	18.8	832	25	0.993	0.565	0.144	1.34	0.817	1.65	0.138	0.176
1. Trellis	903	230	481	368	20783	1824	13.4	38	43	19.3	894	28	0.631	0.225	0.142	1.29	0.700	1.18	0.085	0.242
1. Trellis	669	210	519	292	24332	1772	15.7	40	41	19.9	1045	36	0.747	0.287	0.154	1.75	0.780	1.12	0.112	0.424
1. Trellis	436	163	464	284	23077	1796	15.2	42	41	19.9	968	64	0.819	0.429	0.167	1.94	0.870	1.81	0.071	0.310
1. Trellis	585	142	475	267	24747	1804	16.7	35	41	20	1049	57	0.762	0.320	0.152	2.18	1.01	1.84	0.189	0.061
1. Trellis	5829	1412	2462	1948	7258	1931	4.87	148	41	21	346	14.4	12.5	2.50	2.88	0.879	0.486	1.58	0.458	0.676
1. Trellis	403	157	482	275	17466	1854	10.1	120	40	20	726	22	0.468	0.241	0.079	1.07	0.481	1.25	0.140	0.451
1. Trellis	1273	197	530	287	16204	1776	9.55	177	43	22	700	24	1.26	0.682	0.225	1.09	0.655	1.22	0.150	1.28

	Lithophile elements				Transition metals								REY			Granitophile				
Sample	Si	Mg	Al	Ca	Ti	V	Nb	Cr	Ni	Co	Mn	Zn	ΣREY	ΣLMREE	ΣHREY	U	^{206}Pb	W	Sn	Mo
1. Trellis	770	249	623	313	20033	1744	12.8	105	45	22	888	39	2.24	1.94	0.089	1.28	0.872	2.17	0.105	0.320
1. Trellis	578	167	501	355	20948	1806	13.1	75	41	20	905	21	0.721	0.293	0.162	1.44	0.925	1.88	0.163	0.295
1. Trellis	1266	303	733	471	16449	1881	10.2	77	44	18.6	743	25	2.76	2.28	0.145	1.21	0.730	1.65	0.142	0.549
1. Trellis	2643	1025	989	401	18937	1883	11.7	114	41	26	896	45	1.57	0.440	0.380	1.15	0.886	1.94	0.433	3.08
1. Trellis	2833	691	1232	878	8380	2079	6.21	96	42	16.6	391	17.7	3.38	0.758	0.696	0.697	0.420	1.17	0.302	0.317
1. Trellis	605	208	538	305	19317	2045	12.1	114	40	17.7	845	25	0.960	0.557	0.146	1.52	1.09	1.54	0.121	0.429
1. Trellis	691	149	460	326	20761	2028	13.8	109	40	19.5	878	35	0.709	0.430	0.099	1.68	0.922	1.19	0.322	0.717
1. Trellis	1949	382	791	639	15876	2039	9.80	137	40	19.0	698	33	2.16	1.22	0.277	0.925	0.709	1.89	0.362	0.376
1. Trellis	5419	1095	1770	1157	8576	2053	5.16	172	46	15.6	416	25	8.80	6.69	0.584	0.491	0.422	1.27	0.182	0.681
1. Trellis	5173	992	2079	2387	1934	1674	2.68	282	42	16.2	127	18.5	29	5.45	5.57	0.421	0.442	0.956	1.03	0.421
1. Trellis	1283	582	1087	300	12351	1700	7.90	113	41	19.8	599	35	0.825	0.500	0.123	0.956	0.787	0.807	0.177	0.786
1. Trellis	10300	1299	2434	7007	11212	1734	6.87	135	49	13.8	302	24	21	18.5	0.810	0.658	1.18	1.64	0.203	1.16
1. Trellis	945	177	556	862	24061	1721	15.9	115	42	15.4	1091	32	1.57	1.20	0.103	1.83	1.54	1.08	0.174	0.969
1. Trellis	1020	108	538	390	26291	1695	16.9	103	43	16.4	1120	34	1.84	1.42	0.165	1.74	0.986	0.885	0.168	0.986
1. Trellis	657	156	496	347	24095	1715	15.6	97	42	18.7	1013	41	0.841	0.548	0.091	2.02	0.903	0.794	0.252	0.800
1. Trellis	882	107	493	365	22877	1678	15.0	97	42	18.4	953	39	0.776	0.473	0.111	1.98	0.959	0.855	0.376	0.860
1. Trellis	1044	292	659	237	368	1556	0.071	196	62	5.09	33	22	0.321	0.074	0.087	0.031	0.020	0.012	0.217	0.045
1. Trellis	1398	344	739	237	368	1612	0.128	114	67	5.51	32	12.8	3.12	2.00	0.371	0.089	0.095	0.165	0.237	0.083
1. Trellis	3463	789	1407	237	338	1643	0.192	115	70	6.06	55	36	4.30	2.33	0.560	0.280	0.213	0.050	0.214	0.225
1. Trellis	418	124	561	237	12524	1645	10.3	115	72	9.52	376	43	0.463	0.045	0.220	1.40	0.574	0.142	0.333	0.555
1. Trellis	540	99	587	237	13225	1652	11.7	123	71	10.4	402	55	0.539	0.031	0.261	1.54	0.640	0.143	0.354	0.352
1. Trellis	598	73	592	237	13075	1640	12.4	136	73	8.33	355	51	0.622	0.041	0.313	1.65	0.628	0.398	0.318	0.475
1. Trellis	2695	746	1576	237	12424	1632	11.5	143	72	5.75	324	48	11.4	6.68	1.27	1.60	0.603	0.460	0.385	0.390
1. Trellis	567	91	625	237	13301	1625	12.0	154	74	9.05	373	56	0.710	0.110	0.286	1.55	0.618	0.429	0.368	0.492
1. Trellis	569	155	615	237	12347	1583	11.6	154	73	13.0	440	55	0.845	0.108	0.397	1.84	0.748	0.487	0.419	0.451
1. Trellis	4418	1387	498	544	2959	1604	2.30	100	61	6.29	160	28	16.4	13.6	1.27	0.424	0.453	0.654	0.392	0.484
1. Trellis	4399	1386	420	466	3073	1615	2.59	100	58	5.37	152	12.9	20	17.7	1.07	0.580	0.298	0.713	0.182	0.111
1. Trellis	4021	874	687	1164	2779	1610	2.42	216	59	6.17	210	62	56	48	3.15	0.604	0.920	0.929	0.755	0.477
1. Trellis	2676	614	1033	318	365	1624	0.513	173	56	4.67	45	8.25	7.88	4.49	1.02	0.658	0.132	0.040	0.272	0.043
1. Trellis	4013	1182	526	844	11536	1631	9.08	177	66	6.94	387	64	11.5	5.71	1.95	0.946	0.718	1.20	0.420	0.054
1. Trellis	10191	2639	649	237	8407	1624	7.80	86	62	6.23	338	34	29	18.0	3.67	1.71	1.20	2.11	0.348	0.209
1. Trellis	7519	1904	596	237	5888	1677	5.05	87	59	7.01	280	40	16.6	14.2	0.925	1.02	0.725	0.924	0.318	0.196
1. Trellis	2268	409	956	673	1126	1934	1.33	347	69	4.93	65	16.3	17.0	10.9	1.65	0.407	0.156	0.507	0.285	0.434
1. Trellis	2567	601	1248	237	3231	1763	2.58	273	57	5.27	124	16.7	16.6	13.3	1.25	0.413	0.207	0.765	0.211	0.040
1. Trellis	926	163	542	237	2660	1757	1.93	306	57	4.61	99	7.51	22	19.8	0.612	0.509	0.284	0.381	0.169	0.002
1. Trellis	1964	404	874	237	6150	1699	4.84	332	54	4.34	175	8.54	4.17	2.07	0.658	0.560	0.236	0.482	0.156	0.022
1. Trellis	4408	1219	2098	237	6439	1711	5.34	283	60	5.09	184	10.4	3.85	1.66	0.755	0.516	0.196	0.782	0.342	0.002
1. Trellis	2025	365	797	237	2086	1664	1.66	284	75	6.16	91	11.1	21	17.8	1.06	0.510	0.195	0.142	0.294	0.055
1. Trellis	4721	1287	2058	237	2735	1720	2.37	329	59	5.50	138	43	16.4	10.1	2.02	0.763	1.11	2.11	0.286	0.234

	Lithophile elements				Transition metals								REY			Granitophile				
Sample	Si	Mg	Al	Ca	Ti	V	Nb	Cr	Ni	Co	Mn	Zn	ΣREY	ΣLMREE	ΣHREY	U	^{206}Pb	W	Sn	Mo
1. Trellis	1330	89	536	237	6988	1664	5.85	242	66	6.07	248	40	31	21	3.51	1.32	0.546	2.25	0.328	0.064
1. Trellis	3316	681	1336	237	2366	1764	2.28	317	69	5.72	94	13.0	57	48	3.05	0.606	0.468	16.7	0.278	0.443
1. Trellis	2811	541	1144	237	3152	1686	2.63	260	59	5.12	99	11.2	18.7	13.5	1.44	0.651	0.284	0.492	0.284	0.132
1. Trellis	6730	2464	688	2599	3504	1605	3.94	260	61	5.91	193	28	88	72	5.37	0.954	0.551	2.23	0.332	0.218
1. Trellis	762	178	671	1716	797	1648	0.536	421	73	7.78	56	25	34	12.7	6.16	0.355	0.163	0.199	0.334	0.029
1. Trellis	1497	396	664	790	1120	1664	0.730	425	57	4.63	71	18.1	29	24	1.52	0.315	0.646	0.255	0.254	0.005
1. Trellis	1332	207	456	237	9772	1572	7.81	79	56	6.71	360	29	1.75	1.02	0.369	1.41	0.621	0.830	0.345	0.121
1. Trellis	2246	477	490	237	9242	1555	8.27	26	62	6.03	320	27	3.95	3.00	0.414	1.32	0.531	0.849	0.327	0.144
1. Trellis	19617	260	780	237	316	1619	0.039	413	358	28	35	12.8	6.06	3.03	1.01	0.459	0.491	0.010	0.251	0.005
1. Trellis	624	98	519	237	6807	1620	4.77	309	60	6.47	280	47	37	34	1.22	0.628	0.568	0.869	0.367	0.031
1. Trellis	1355	61	502	656	269	1625	0.019	306	72	5.17	34	9.21	11.6	6.37	1.25	0.534	0.048	0.017	0.191	0.003
1. Trellis	2046	954	872	521	5899	1621	4.48	138	61	7.30	356	171	7.51	6.68	0.323	0.556	0.704	1.75	0.397	0.253
1. Trellis	1900	420	802	715	4253	1587	3.23	439	62	4.94	143	21	12.2	6.23	1.73	0.492	0.364	0.441	0.226	0.111
1. Trellis	2221	828	590	237	7017	1531	5.13	94	61	5.89	279	72	12.5	9.51	1.02	0.583	0.979	0.895	0.318	0.009
1. Trellis	1136	266	556	378	7291	1536	5.72	162	58	5.36	263	51	12.8	8.99	1.40	0.854	0.685	0.821	0.348	0.090
1. Trellis	1578	401	688	237	10059	1496	8.03	122	54	4.82	293	50	2.69	1.36	0.520	1.08	0.648	1.30	0.291	0.055
1. Trellis	1366	358	521	237	7895	1569	6.61	217	60	5.27	250	25	2.32	1.49	0.391	1.22	1.10	1.10	0.281	0.088
1. Trellis	2133	588	1078	735	8282	1520	6.44	383	67	4.61	208	8.68	9.48	5.57	1.08	0.329	0.124	0.288	0.273	0.000
1. Trellis	1022	144	517	237	3523	1567	2.47	257	55	5.19	142	16.4	2.82	1.69	0.316	0.434	0.257	0.248	0.243	0.007
1. Trellis	8550	2569	4163	237	1257	1590	0.961	445	65	5.34	75	16.8	5.99	3.66	0.559	0.289	0.163	0.102	0.289	0.003
1. Trellis	1395	201	530	2303	5341	1486	3.96	228	57	5.16	197	13.5	170	147	7.23	0.857	0.466	0.455	0.302	0.021
1. Trellis	3353	597	1091	237	2650	1568	2.05	376	60	4.75	113	11.9	26	16.1	2.52	0.529	0.243	0.303	0.247	0.003
1. Trellis	5442	104	447	237	263	1419	0.027	396	56	4.69	32	7.16	1.84	1.45	0.109	0.023	0.011	0.047	0.199	0.003
1. Trellis	2177	488	978	237	284	1442	0.110	265	56	5.23	33	8.77	8.05	5.77	0.538	0.154	0.052	0.076	0.218	0.004
1. Trellis	216	29	457	237	315	1474	0.004	64	57	7.89	44	13.6	0.509	0.297	0.075	0.006	0.003	0.002	0.172	0.003
1. Trellis	293	47	354	237	263	1451	0.012	393	194	13.0	36	8.86	0.854	0.627	0.069	0.022	0.058	0.001	0.153	0.004
1. Trellis	477	55	521	237	320	1486	0.003	54	64	10.8	52	23	2.04	1.42	0.125	0.038	0.012	0.005	0.217	0.008
1. Trellis	342	30	490	237	318	1484	0.000	7.06	58	10.3	54	31	0.031	0.017	0.006	0.001	0.010	0.005	0.205	0.003
1. Trellis	3465	153	505	237	191	1382	0.097	652	4955	493	33	9.79	15.1	9.25	1.39	0.439	1.07	0.079	0.178	0.003
1. Trellis	1007	121	484	220	9481	1510	7.61	249	56	5.41	261	13.3	2.67	2.08	0.280	1.40	0.714	0.475	0.419	0.100
1. Trellis	3535	88	334	237	222	1433	0.044	649	58	5.32	33	10.5	0.765	0.479	0.092	0.061	0.058	0.038	0.150	0.003
1. Trellis	363	28	313	237	11962	1398	9.15	690	208	25	297	11.0	2.05	0.398	0.589	0.474	0.401	0.780	0.351	0.009
1. Trellis	528	194	522	305	11095	1435	8.64	64	56	8.39	504	102	2.80	2.19	0.303	1.05	0.644	0.799	0.340	0.170
1. Trellis	733	277	620	237	11171	1495	8.86	177	58	6.61	366	63	2.49	1.72	0.362	1.12	0.902	1.11	0.318	0.218
1. Trellis	18643	5603	1859	11682	13928	1535	32	16.8	66	10.9	302	41	91	28	25	1.78	1.13	0.822	11.4	2.14
1. Trellis	8547	2438	3760	286	4826	1505	4.43	38	59	5.48	160	14.1	7.78	5.75	0.617	0.890	0.543	0.227	0.502	0.039
Mean (n=151)	2246	545	928	848	7290	1688	5.18	179	87	19.4	348	47	8.86	5.74	1.02	0.694	0.879	0.754	0.313	0.309
S.D.	3046	834	869	1598	8042	281	5.69	173	396	39	307	33	19.1	15.1	2.46	0.680	0.682	1.45	0.913	0.381
G.M.	1316	306	770	492	2727	1681	0.961	136	53	14.0	234	36	1.89	0.944	0.233	0.208	0.585	0.239	0.208	0.126
Median	1039	239	687	378	3152	1665	2.68	124	45	18.9	223	40	2.04	0.701	0.303	0.509	0.725	0.465	0.211	0.225
Maximum	19617	5938	7617	11682	29038	2211	32	1670	4955	493	1240	171	170	147	25	2.64	3.64	16.7	11.4	3.08
Minimum	216	28	313	220	191	1350	0.000	7.06	39	4.34	32	7.16	0.031	0.017	0.003	0.001	0.003	0.001	0.047	0.000

	Lithophile elements				Transition metals								REY			Granitophile				
Sample	Si	Mg	Al	Ca	Ti	V	Nb	Cr	Ni	Co	Mn	Zn	ΣREY	ΣLMREE	ΣHREY	U	^{206}Pb	W	Sn	Mo
2. Dense mottled	445	169	518	226	324	1562	0.069	37	65	1.49	62	24	0.181	0.108	0.034	0.046	0.119	0.028	0.409	0.048
2. Dense mottled	1953	567	581	235	287	1541	0.134	14.1	73	1.46	81	24	1.06	0.616	0.144	0.059	0.271	0.087	0.407	0.046
2. Dense mottled	1050	232	466	198	321	1496	0.146	22	65	1.41	68	23	1.06	0.507	0.192	0.060	0.282	0.090	0.477	0.051
2. Dense mottled	4078	1651	488	537	303	1547	0.376	29	103	2.61	135	57	7.89	5.92	0.598	0.091	1.10	0.446	0.464	0.079
2. Dense mottled	2705	434	434	233	195	1608	0.339	46	258	0.742	73	24	3.11	1.51	0.561	0.302	1.75	0.183	0.296	0.094
2. Dense mottled	1889	699	495	234	343	1524	0.177	6.21	66	2.20	109	38	3.29	2.35	0.298	0.036	0.196	0.175	0.387	0.016
2. Dense mottled	1580	584	521	243	300	1637	0.231	19.4	66	1.71	108	32	2.63	1.56	0.386	0.107	0.800	0.333	0.440	0.056
2. Dense mottled	18629	1520	1033	251	199	1495	0.711	27	397	0.983	848	16.3	5.75	2.26	1.22	0.550	1.21	0.165	0.673	0.380
2. Dense mottled	1384	381	658	234	365	1584	0.196	22	76	1.83	73	36	0.552	0.285	0.095	0.088	0.115	0.085	0.364	0.040
2. Dense mottled	543	12.1	365	235	327	1540	0.001	1.55	59	1.46	59	8.45	0.094	0.061	0.018	0.006	0.014	0.001	0.334	0.033
2. Dense mottled	34207	1834	769	232	220	1420	0.252	42	92	3.53	2858	23	3.21	0.960	0.818	0.269	1.36	0.123	0.501	0.340
2. Dense mottled	6247	2091	632	256	297	1533	0.470	24	70	2.18	237	28	7.59	5.61	0.688	0.128	0.319	0.432	0.342	0.045
2. Dense mottled	4383	1845	541	560	283	1493	0.980	12.1	67	2.78	210	64	51	42	2.77	0.231	0.707	0.474	0.473	0.077
2. Dense mottled	3253	1278	617	249	832	1481	1.04	8.31	67	2.34	182	86	5.71	4.99	0.271	0.090	1.00	0.342	0.348	0.279
2. Dense mottled	2650	1054	486	240	300	1470	0.311	22	66	2.58	115	24	3.94	2.83	0.376	0.048	0.119	0.192	0.425	0.220
2. Dense mottled	2856	1151	472	223	318	1584	0.327	77	73	2.51	131	43	6.68	5.43	0.435	0.040	0.218	0.242	0.317	0.119
2. Dense mottled	2591	1065	503	229	330	1535	0.323	40	67	2.99	170	64	4.18	3.11	0.373	0.056	0.428	0.214	0.400	0.127
2. Dense mottled	3994	1349	481	221	317	1611	0.248	2.81	66	3.81	167	46	1.97	1.28	0.255	0.042	0.036	0.122	0.370	0.467
2. Dense mottled	1126	407	467	224	512	1651	0.461	27	65	1.66	94	32	1.52	0.918	0.214	0.066	0.184	0.165	0.309	0.127
2. Dense mottled	1718	539	364	296	250	1818	0.397	58	151	2.63	80	11.3	2.40	1.20	0.400	0.219	1.71	0.237	0.379	0.057
2. Dense mottled	7544	1029	1001	282	172	1731	0.417	82	229	6.42	103	11.5	5.48	2.35	0.907	0.697	4.38	0.200	0.269	2.55
2. Dense mottled	3281	1405	643	245	436	1693	0.693	18.8	68	3.51	155	69	4.27	2.60	0.489	0.076	0.437	0.457	0.500	0.152
2. Dense mottled	4264	550	1218	1246	429	1843	0.420	83	67	1.55	81	14.8	4404	4358	18.3	0.666	1.12	0.509	0.616	0.177
2. Dense mottled	2238	941	649	302	299	1725	0.769	50	67	1.74	150	59	11.3	5.69	1.93	0.126	1.10	1.19	0.366	0.103
2. Dense mottled	1868	712	497	237	1069	1695	1.48	67	66	1.57	118	21	8.17	6.28	0.705	0.157	0.332	0.402	0.479	0.057
2. Dense mottled	3962	1633	504	222	335	1679	0.642	47	66	1.92	166	33	6.16	4.09	0.704	0.088	0.151	0.477	0.498	0.039
2. Dense mottled	3507	1211	444	222	283	1700	0.364	8.63	69	3.84	145	52	6.22	4.29	0.625	0.050	0.202	0.163	0.388	0.158
2. Dense mottled	5551	2211	585	1372	325	1704	0.131	31	64	2.53	108	24	5.52	3.64	0.649	0.058	0.142	0.109	0.498	0.032
2. Dense mottled	442	88	418	226	293	1766	1.71	7.92	61	2.14	63	18.2	0.236	0.151	0.018	0.006	0.040	0.039	0.425	0.055
2. Dense mottled	2300	536	407	246	265	1676	0.216	96	99	1.56	80	24	2.72	1.74	0.351	0.120	1.52	0.119	0.224	0.334
2. Dense mottled	6109	1879	935	244	249	1479	0.757	29	760	186	156	160	12.5	9.92	0.827	0.226	7.24	0.501	0.343	0.114
2. Dense mottled	4241	1798	496	269	586	1681	1.48	9.63	67	2.50	193	37	7.45	5.62	0.595	0.095	0.254	0.539	0.410	0.045
2. Dense mottled	4093	1085	736	194	5704	1655	10.7	30	67	2.07	373	70	3.50	2.24	0.429	0.273	1.88	1.37	0.960	0.141
2. Dense mottled	1693	561	556	206	342	1604	0.310	35	68	2.71	95	38	10.6	9.56	0.373	0.090	0.846	0.175	0.299	0.098
2. Dense mottled	677	69	479	222	314	1534	0.071	55	65	2.45	64	31	0.285	0.117	0.060	0.034	0.148	0.026	0.372	0.045
2. Dense mottled	2035	338	504	243	418	1585	0.346	40	68	4.49	124	64	1.43	0.758	0.241	0.069	0.397	0.302	0.450	0.036
2. Dense mottled	2065	189	483	237	259	1561	1.33	62	67	6.49	125	18.5	0.392	0.157	0.065	0.083	1.23	0.056	0.392	0.037
2. Dense mottled	4155	507	456	224	359	1568	0.346	223	66	1.96	297	12.3	2.92	1.71	0.421	0.119	0.783	0.191	0.348	0.061
2. Dense mottled	4223	1846	518	233	299	1583	0.834	39	67	3.52	190	39	10.1	6.89	1.01	0.150	0.556	0.716	0.427	0.027
2. Dense mottled	7581	3942	982	234	608	1622	1.47	14.2	71	4.51	240	67	12.4	9.18	1.26	0.374	0.544	0.749	0.458	0.027
2. Dense mottled	7129	2506	652	232	272	1643	1.24	10.4	83	3.21	230	36	20	16.8	1.30	0.245	0.388	0.303	0.465	0.251

	Lithophile elements				Transition metals								REY			Granitophile				
Sample	Si	Mg	Al	Ca	Ti	V	Nb	Cr	Ni	Co	Mn	Zn	ΣREY	ΣLMREE	ΣHREY	U	^{206}Pb	W	Sn	Mo
2. Dense mottled	6067	2322	589	258	976	1705	1.79	7.20	72	6.04	287	83	22	19.4	1.18	0.231	0.361	0.314	0.534	0.273
2. Dense mottled	6716	2916	635	583	319	1704	1.29	2.44	71	4.51	275	72	35	31	1.74	0.240	0.241	0.231	0.533	0.465
2. Dense mottled	5852	2477	1080	212	12271	1675	22	12.4	76	2.43	519	27	19.9	16.9	1.22	0.380	0.656	0.610	0.817	0.092
2. Dense mottled	5793	2566	683	319	344	1704	1.02	5.13	69	3.64	217	67	41	38	1.42	0.226	0.202	0.107	0.510	0.483
2. Dense mottled	5707	2359	691	473	357	1717	0.998	9.41	68	2.83	282	122	21	18.6	1.10	0.190	0.824	0.590	0.463	1.98
2. Dense mottled	5565	2521	699	253	897	1726	1.65	17.8	100	4.61	260	95	26	23	1.37	0.190	0.752	0.730	0.554	0.037
2. Dense mottled	5406	2531	893	309	1692	1684	3.60	25	65	3.65	270	2900	15.7	12.4	1.25	0.146	0.736	1.04	0.626	0.034
2. Dense mottled	1284	130	447	259	272	1144	0.293	14.2	66	1.65	52	8.23	0.300	0.120	0.054	0.027	0.066	0.003	0.451	0.052
2. Dense mottled	1376	148	427	251	711	1248	1.04	35	61	2.10	76	20	1.82	1.06	0.251	0.028	0.151	0.212	0.384	0.051
2. Dense mottled	9933	1821	1588	249	219	1577	0.790	18.8	183	1.55	117	12.7	5.06	2.71	0.628	0.354	1.18	0.062	0.489	0.127
2. Dense mottled	6468	1193	807	253	236	1694	0.436	6.15	109	2.01	103	13.7	3.41	1.98	0.449	0.231	0.541	0.134	0.470	0.199
2. Dense mottled	8598	2129	863	276	378	1677	1.27	6.44	91	1.67	176	13.5	8.23	5.49	0.919	0.342	0.652	0.413	0.579	0.927
2. Dense mottled	522	68	432	280	268	1063	0.143	2.12	63	2.25	58	10.6	0.307	0.092	0.064	0.013	0.030	0.033	0.399	0.025
2. Dense mottled	3388	1026	529	298	308	1498	0.592	34	72	1.95	116	22	2.96	1.90	0.332	0.114	0.315	0.263	0.383	0.042
2. Dense mottled	2268	886	453	251	304	1490	0.249	49	67	2.23	107	18.4	3.31	2.49	0.244	0.049	0.128	0.150	0.428	0.030
2. Dense mottled	2943	761	411	246	239	1583	0.558	58	68	1.87	107	26	16.3	14.4	0.634	0.248	0.849	0.372	0.385	0.039
2. Dense mottled	4975	751	722	253	189	1519	0.306	65	120	1.44	94	18.3	3.19	1.56	0.540	0.291	0.953	0.141	0.332	0.044
2. Dense mottled	2125	759	372	1038	2951	1530	5.31	75	75	1.62	198	24	12.0	7.63	1.55	0.215	0.942	0.556	0.468	0.027
2. Dense mottled	3253	1303	399	279	255	1755	0.099	62	65	14.8	163	19.1	0.636	0.146	0.192	0.054	0.354	0.037	0.193	0.224
2. Dense mottled	246	11.0	394	215	303	1594	0.135	95	64	2.35	51	9.30	0.237	0.066	0.069	0.072	0.087	0.033	0.337	0.056
2. Dense mottled	2657	308	358	268	160	1668	0.275	74	146	1.33	52	7.76	2.18	1.11	0.349	0.270	0.862	0.102	0.189	0.074
2. Dense mottled	865	292	362	230	299	1661	0.275	75	66	1.84	56	10.3	1.55	0.853	0.226	0.148	0.505	0.159	0.355	0.029
2. Dense mottled	415	72	428	211	422	1580	0.156	78	62	3.27	65	33	0.252	0.193	0.014	0.014	0.021	0.040	0.321	0.064
2. Dense mottled	574	152	466	236	365	1603	0.118	75	63	3.45	76	25	0.708	0.456	0.087	0.057	0.108	0.054	0.421	0.034
2. Dense mottled	1213	390	487	265	333	1678	0.146	155	62	2.59	72	20	3.06	2.21	0.247	0.072	0.136	0.051	0.419	0.028
2. Dense mottled	3106	1236	582	270	631	1611	0.752	12.9	65	2.59	159	49	5.08	3.17	0.684	0.095	0.362	0.483	0.519	0.041
2. Dense mottled	2857	1270	785	254	3335	1604	6.79	17.8	62	2.45	201	38	3.47	1.73	0.581	0.134	0.667	0.530	0.483	0.146
2. Dense mottled	2562	1021	414	260	285	1716	0.493	35	61	2.49	116	25	5.68	3.72	0.630	0.089	0.377	0.386	0.393	0.132
2. Dense mottled	3321	1193	448	263	276	1729	0.477	34	83	19.4	137	76	4.89	3.84	0.345	0.072	0.161	0.245	0.524	0.034
2. Dense mottled	3143	893	467	374	811	1708	1.06	24	63	1.63	111	22	3.41	1.95	0.473	0.192	0.501	0.332	0.354	0.380
2. Dense mottled	421	38	364	254	322	1593	0.143	39	64	2.10	58	8.69	0.363	0.170	0.080	0.017	0.089	0.003	0.390	0.049
2. Dense mottled	1051	313	799	237	322	1715	0.122	4.39	64	9.96	75	18.2	7.08	5.45	0.374	0.109	0.317	0.088	0.210	0.560
2. Dense mottled	600	88	448	955	322	1717	0.219	5.64	59	8.85	67	13.5	24	12.0	3.23	0.215	0.124	0.223	0.203	0.108
2. Dense mottled	2871	1326	1371	237	500	1713	0.483	4.65	109	12.8	116	29	0.494	0.306	0.068	0.041	0.087	0.319	0.365	0.232
2. Dense mottled	8318	4299	852	613	388	1712	0.660	3.88	138	29	336	123	43	39	1.23	0.188	0.119	0.505	0.507	0.530
2. Dense mottled	6228	2954	650	231	380	1697	0.575	3.41	63	11.1	231	34	26	23	0.906	0.118	0.296	0.673	0.318	0.077
2. Dense mottled	7317	3488	517	363	329	1744	0.590	3.46	87	14.2	217	50	51	47	1.28	0.126	0.221	0.767	0.300	0.162
2. Dense mottled	323	19.5	337	237	276	1720	0.042	6.39	56	8.54	62	7.54	0.681	0.313	0.165	0.039	0.049	0.089	0.200	0.180
2. Dense mottled	2565	1012	1457	428	285	1711	0.106	6.87	63	9.42	88	13.1	3.60	1.55	0.599	0.280	0.171	0.031	0.433	0.247
2. Dense mottled	245	11.3	390	237	281	1789	0.008	4.57	57	8.79	75	7.81	0.098	0.074	0.011	0.009	0.010	0.006	0.223	0.110
2. Dense mottled	421	85	439	237	317	1731	0.110	5.74	60	9.75	79	15.7	0.825	0.404	0.133	0.098	0.092	0.056	0.360	0.222

	Lithophile elements				Transition metals								REY			Granitophile				
Sample	Si	Mg	Al	Ca	Ti	V	Nb	Cr	Ni	Co	Mn	Zn	ΣREY	ΣLMREE	ΣHREY	U	^{206}Pb	W	Sn	Mo
2. Dense mottled	6440	3053	1416	266	406	1770	0.933	5.91	67	11.8	192	38	21	18.4	0.888	0.309	0.925	1.07	0.635	0.228
2. Dense mottled	1857	760	436	237	290	1729	0.255	4.62	64	9.68	87	11.8	3.98	2.59	0.420	0.076	0.097	0.203	0.204	0.108
2. Dense mottled	632	27	441	237	327	1744	0.051	5.55	87	10.9	72	10.2	3.19	1.61	0.416	0.239	0.188	0.060	0.152	0.317
2. Dense mottled	3429	1377	902	543	315	1632	0.293	5.12	282	46	124	64	48	43	1.57	0.298	0.516	0.505	0.326	0.067
2. Dense mottled	4624	2084	462	246	284	1705	0.404	4.06	95	15.7	147	34	27	24	0.991	0.198	0.522	0.471	0.322	0.535
2. Dense mottled	981	99	540	234	344	1677	0.096	4.13	64	9.85	89	25	1.81	0.881	0.254	0.086	0.087	0.114	0.276	0.096
2. Dense mottled	5906	2774	835	2909	432	1899	1.05	5.40	68	11.6	189	37	444	405	11.3	0.580	0.592	1.97	0.475	0.027
2. Dense mottled	6889	2981	686	2098	390	1788	0.346	4.71	61	10.7	162	38	11.2	6.46	1.24	0.036	0.325	0.381	0.446	0.096
2. Dense mottled	258	12.7	416	237	335	1625	0.004	5.23	61	9.66	78	11.9	0.391	0.244	0.029	0.014	0.018	0.018	0.288	0.006
2. Dense mottled	920	314	463	4567	348	1581	0.152	384	68	10.4	100	21	504	408	30	0.843	0.427	0.272	0.363	0.418
2. Dense mottled	1023	291	524	4935	335	1590	0.081	229	68	9.82	95	16.8	472	401	23	0.743	0.366	0.171	0.218	0.026
2. Dense mottled	3055	1276	585	6160	340	1585	0.596	5.37	83	12.7	110	30	119	59	17.5	0.583	0.616	0.317	0.316	0.008
2. Dense mottled	370	110	406	237	293	1695	0.104	5.30	88	9.90	71	11.7	2.11	1.42	0.220	0.083	0.091	0.113	0.271	0.103
2. Dense mottled	965	203	459	5160	214	1635	0.284	5.10	55	7.91	58	8.47	20	6.26	3.56	0.198	0.103	0.057	0.179	0.011
2. Dense mottled	8875	3083	1014	237	365	1644	0.621	2.13	68	10.6	165	41	15.4	12.3	1.02	0.217	0.656	0.836	0.502	0.235
2. Dense mottled	3434	1649	601	231	366	1720	0.319	1.76	66	10.5	109	18.6	3.48	2.52	0.298	0.053	0.180	0.262	0.344	0.453
2. Dense mottled	5756	2947	752	237	413	1718	0.546	1.43	71	12.6	224	63	15.2	12.5	0.884	0.140	0.333	0.636	0.407	0.843
2. Dense mottled	4059	2074	784	237	381	1756	0.265	1.16	69	12.6	170	48	6.91	4.97	0.548	0.059	0.158	0.319	0.352	0.231
2. Dense mottled	8792	1353	903	654	345	1726	0.228	1.32	63	9.69	136	36	31	15.4	4.72	0.199	0.320	0.288	0.351	0.061
2. Dense mottled	3106	1123	671	119	328	1705	0.418	3.71	65	9.01	100	24	219	214	1.47	0.684	0.211	0.233	0.277	0.043
2. Dense mottled	349	14.0	424	237	324	1866	0.014	5.53	62	8.71	73	10.1	0.183	0.092	0.047	0.009	0.019	0.016	0.164	0.019
2. Dense mottled	2935	1418	737	269	357	1771	0.334	4.82	68	10.2	152	61	4.01	2.97	0.283	0.123	0.820	0.362	0.323	0.252
2. Dense mottled	585	73	324	237	254	1765	0.184	6.48	61	8.27	65	12.7	2.32	0.955	0.366	0.158	0.188	0.072	0.167	0.137
2. Dense mottled	3108	1154	493	331	347	1700	0.181	3.67	69	11.0	120	30	5.42	4.04	0.400	0.065	0.252	0.332	0.618	0.035
2. Dense mottled	1778	302	415	1899	271	1761	0.295	4.93	65	9.42	74	21	7.89	3.81	1.26	0.277	0.237	0.125	0.348	0.010
2. Dense mottled	395	30	373	262	317	1729	0.067	5.10	59	8.58	69	5.78	4.93	2.77	0.670	0.058	0.056	0.088	0.188	0.015
2. Dense mottled	415	62	363	436	314	1754	0.017	5.32	55	8.26	67	5.42	20	12.9	2.32	0.056	0.038	0.011	0.155	0.016
2. Dense mottled	1465	256	388	237	182	1603	0.231	7.82	157	11.9	62	16.1	3.11	2.04	0.343	0.302	0.338	0.099	0.579	0.153
2. Dense mottled	502	185	417	237	311	1616	0.054	5.35	63	8.52	67	7.15	0.318	0.136	0.077	0.046	0.088	0.029	0.206	0.003
2. Dense mottled	1574	644	490	1859	326	1626	0.256	3.72	69	10.5	115	27	44	24	5.55	0.899	0.559	0.213	0.296	0.013
2. Dense mottled	977	391	430	722	330	1585	0.125	4.06	61	9.21	96	13.4	14.3	5.28	2.32	0.330	0.300	0.139	0.181	0.040
2. Dense mottled	671	176	571	237	350	1616	0.061	5.06	63	9.34	77	14.0	0.972	0.487	0.136	0.042	0.038	0.022	0.328	0.021
2. Dense mottled	2088	883	445	237	309	1641	0.317	4.61	63	9.28	115	22	5.04	3.56	0.522	0.174	0.244	0.364	0.224	0.020
2. Dense mottled	1143	355	493	237	337	1597	0.146	5.86	72	11.3	101	27	2.14	1.65	0.148	0.059	0.129	0.193	0.331	0.214
Mean (n=116)	3493	1091	597	542	562	1639	0.858	31	87	7.81	162	58	62	57	1.58	0.178	0.526	0.295	0.387	0.179
S.D.	3973	987	256	972	1253	244	2.36	50	79	17.6	270	265	407	405	4.19	0.180	0.829	0.304	0.142	0.323
G.M.	2206	557	559	331	371	1634	0.320	13.9	76	4.51	121	26	4.91	3.05	0.482	0.111	0.275	0.166	0.365	0.084
Median	2681	889	500	246	324	1658	0.325	12.2	67	3.58	111	24	4.91	2.80	0.506	0.118	0.316	0.207	0.381	0.077
Maximum	34207	4299	1588	6160	12271	1899	22	384	760	186	2858	2900	4404	4358	30	0.899	7.24	1.97	0.960	2.55
Minimum	245	11.0	324	119	160	1063	0.001	1.16	55	0.742	51	5.42	0.094	0.061	0.011	0.006	0.010	0.001	0.152	0.003

	Lithophile elements				Transition metals								REY			Granitophile				
Sample	Si	Mg	Al	Ca	Ti	V	Nb	Cr	Ni	Co	Mn	Zn	ΣREY	ΣLMREE	ΣHREY	U	^{206}Pb	W	Sn	Mo
3. Rare mottled	2113	478	764	813	814	2415	1.28	17.7	49	2.28	32	23	9.70	1.93	2.47	0.067	0.210	0.456	0.373	0.179
3. Rare mottled	4155	1600	2082	366	867	2270	1.26	16.3	78	2.56	40	18.5	8.19	1.29	2.05	0.186	0.388	0.295	0.263	0.179
3. Rare mottled	3720	821	1295	1773	1786	2189	4.08	12.9	52	9.55	64	27	56	5.15	14.7	0.209	0.310	0.839	0.944	0.050
3. Rare mottled	844	271	555	230	430	2142	0.057	35	49	11.8	75	31	0.834	0.328	0.176	0.026	0.233	0.320	0.116	0.607
3. Rare mottled	643	76	518	234	389	2132	0.043	20	49	11.5	68	26	0.160	0.051	0.029	0.008	0.015	0.024	0.062	0.413
3. Rare mottled	2036	928	1314	252	487	2123	0.173	28	49	9.80	61	19.4	0.184	0.073	0.040	0.028	0.169	0.069	0.091	0.180
3. Rare mottled	1313	358	683	244	412	2107	0.089	40	58	3.18	33	21	1.92	0.777	0.297	0.321	0.184	0.121	0.130	0.248
3. Rare mottled	1746	675	806	263	469	2115	0.562	50	47	3.14	35	16.9	2.01	0.242	0.606	0.030	0.268	0.289	0.159	0.049
3. Rare mottled	9294	3580	3859	248	762	2160	0.842	56	102	0.632	35	12.3	18.3	14.3	1.20	0.214	0.389	0.107	0.238	0.033
3. Rare mottled	5984	2611	2998	240	702	2222	0.662	9.14	58	2.10	43	25	0.835	0.404	0.118	0.071	1.43	0.161	0.114	0.024
3. Rare mottled	5947	2300	2586	241	638	2244	0.617	23	50	2.37	38	17.6	2.03	0.385	0.494	0.159	0.280	0.716	0.193	0.025
3. Rare mottled	2234	601	964	1046	1372	2161	3.89	2.72	44	2.24	38	29	93	68	8.30	0.251	0.590	6.20	0.904	0.111
3. Rare mottled	9838	2881	3554	2196	2743	2202	9.10	23	84	1.54	35	13.3	134	64	21	1.06	0.754	3.62	1.12	0.055
3. Rare mottled	3873	1357	668	236	492	2094	0.549	2.40	47	2.05	67	24	5.82	1.75	1.19	0.067	0.188	0.792	0.157	0.325
3. Rare mottled	2582	799	502	253	392	2130	0.232	9.60	43	0.550	39	12.5	1.95	1.23	0.279	0.110	0.480	0.282	0.080	0.527
3. Rare mottled	6715	2742	3370	261	506	2133	0.231	86	73	0.526	28	12.8	0.838	0.400	0.191	0.110	0.210	0.082	0.145	0.110
3. Rare mottled	961	336	663	258	310	2249	0.086	75	50	1.05	34	21	1.07	0.540	0.216	0.012	0.262	0.137	0.116	0.036
3. Rare mottled	18419	5155	1631	810	851	2252	1.53	73	87	2.80	247	25	13.3	1.73	3.82	0.179	0.282	0.323	0.317	0.036
3. Rare mottled	8542	1149	1991	7518	8743	2244	22	2.74	66	2.26	71	21	195	22	52	1.30	0.887	3.11	3.46	0.381
3. Rare mottled	2374	826	698	259	2592	2195	1.63	4.22	56	1.50	65	16.8	107	102	1.94	0.335	0.335	0.271	0.275	0.612
3. Rare mottled	1149	316	563	214	5160	2221	2.14	2.33	49	2.75	212	33	0.583	0.337	0.090	0.332	0.271	0.398	0.120	0.550
3. Rare mottled	2143	787	1072	241	517	2222	0.284	62	51	1.88	30	17.3	3.16	0.817	0.717	0.026	0.111	0.168	0.179	0.345
3. Rare mottled	4030	1368	973	654	495	2211	0.589	70	61	3.07	51	15.1	5.73	2.78	0.898	0.178	0.187	0.309	0.158	0.048
3. Rare mottled	1832	340	709	1237	1431	2177	2.60	13.1	46	4.68	48	28	20	2.44	5.78	0.120	0.694	0.299	0.493	0.214
3. Rare mottled	4610	1647	1764	783	1096	2134	1.61	68	51	7.53	45	28	14.6	1.82	4.08	0.094	0.171	0.356	0.381	0.102
3. Rare mottled	2091	455	720	815	3182	2448	2.87	50	49	0.771	70	17.0	20	6.38	4.20	0.244	0.601	0.512	0.351	0.101
3. Rare mottled	4814	750	637	245	12764	2406	8.28	8.40	44	3.64	335	23	4.64	0.946	1.15	1.05	0.889	1.22	0.248	0.570
3. Rare mottled	4051	1342	1214	685	8852	2425	6.28	18.1	46	7.63	268	21	10.6	1.71	2.65	0.934	0.500	1.02	0.311	0.179
3. Rare mottled	315	18.2	488	255	239	1992	0.014	67	47	3.21	31	14.2	0.135	0.121	0.009	0.004	0.020	0.003	0.077	0.175
3. Rare mottled	3012	503	840	1533	8188	2190	8.12	15.4	44	6.35	273	25	14.9	2.04	4.31	1.01	0.645	0.652	0.909	0.112
3. Rare mottled	2253	626	997	780	12193	2334	8.87	6.86	43	8.68	343	22	4.74	1.29	1.07	1.45	0.881	0.568	0.267	0.298
3. Rare mottled	5079	1324	1093	1193	10056	2437	9.33	7.11	53	8.63	307	25	38	5.65	9.97	1.25	0.891	1.46	0.822	0.614
3. Rare mottled	2486	779	707	545	10345	2482	7.36	3.83	47	9.08	351	83	6.75	3.60	1.04	1.26	1.45	1.13	0.231	0.583
3. Rare mottled	3975	1380	649	237	10083	2503	7.25	0.893	49	12.3	459	28	5.40	3.98	0.442	1.42	1.20	0.571	0.331	0.315
3. Rare mottled	4670	1911	662	266	8442	2482	6.43	1.19	50	12.3	417	33	7.68	5.69	0.655	1.44	1.07	0.417	0.266	0.486
3. Rare mottled	3707	340	663	276	722	2406	1.09	14.8	49	7.94	56	24	14.2	6.84	2.41	0.078	0.166	0.130	0.220	0.325
3. Rare mottled	2424	623	705	1241	1128	2552	3.53	21	51	14.3	86	33	16.5	2.73	4.50	0.171	0.351	0.311	0.443	0.568
3. Rare mottled	1857	531	938	420	477	2627	0.097	42	53	17.1	106	35	7.18	6.17	0.314	0.059	0.218	0.263	0.144	0.773
3. Rare mottled	3332	1218	629	335	446	2629	0.131	31	53	15.6	122	32	18.0	16.6	0.443	0.192	0.194	0.196	0.262	0.611

	Lithophile elements				Transition metals								REY			Granitophile				
Sample	Si	Mg	Al	Ca	Ti	V	Nb	Cr	Ni	Co	Mn	Zn	ΣREY	ΣLMREE	ΣHREY	U	^{206}Pb	W	Sn	Mo
3. Rare mottled	2704	1050	598	236	418	2544	0.167	23	52	12.1	106	31	25	23	0.490	0.115	0.422	0.327	0.198	0.754
3. Rare mottled	2347	780	707	566	643	2388	0.826	26	49	5.35	56	26	12.8	9.87	1.06	0.090	0.264	0.259	0.326	0.396
3. Rare mottled	6474	1953	1987	270	665	2137	0.897	56	57	1.59	144	49	40	39	0.710	0.229	0.454	1.18	0.312	0.407
3. Rare mottled	7678	3731	3033	541	397	1887	0.493	27	121	1.45	41	36	82	76	2.04	1.02	3.10	1.16	0.208	0.418
3. Rare mottled	2530	1164	660	543	449	2098	0.271	51	50	1.48	97	90	6.47	5.92	0.226	0.052	4.86	0.930	0.107	0.090
3. Rare mottled	22755	8758	10645	329	3904	1744	7.98	88	297	1.10	118	18.4	6.59	4.26	0.916	1.90	0.600	0.593	0.249	0.535
3. Rare mottled	3586	1475	1960	247	450	2152	0.207	46	44	6.32	37	17.7	0.486	0.071	0.102	0.015	0.018	0.039	0.064	0.019
3. Rare mottled	820	284	628	253	1165	2112	0.576	71	45	2.95	71	24	1.53	0.153	0.439	0.093	0.251	0.171	0.172	0.029
3. Rare mottled	2862	471	806	2713	5163	2042	7.18	48	46	3.47	124	21	95	8.94	26	0.506	0.430	0.938	1.82	0.060
3. Rare mottled	2742	1020	623	213	9602	2035	5.70	17.9	47	4.01	405	28	5.76	2.41	1.13	1.10	0.784	0.960	0.220	0.506
3. Rare mottled	5938	2173	1789	2296	3369	1879	2.80	45	134	2.69	110	15.6	28	3.39	7.74	0.438	0.877	0.452	0.699	0.327
3. Rare mottled	8149	3848	4578	249	387	1797	0.153	33	103	1.68	42	14.4	2.76	2.05	0.222	0.409	0.406	0.048	0.131	0.029
3. Rare mottled	561	181	509	230	357	1924	0.001	40	46	4.56	42	19.7	0.146	0.112	0.020	0.001	0.022	0.011	0.072	0.026
3. Rare mottled	733	123	622	226	357	1947	0.030	12.7	90	1.11	23	16.8	1.46	1.10	0.130	0.454	0.391	0.042	0.066	0.027
3. Rare mottled	273	30	500	231	371	1915	0.002	0.766	45	5.93	47	19.4	0.113	0.110	0.002	0.001	0.014	0.001	0.132	0.030
3. Rare mottled	2258	846	1276	249	417	1915	0.092	30	45	3.01	34	17.4	0.128	0.087	0.026	0.028	0.060	0.040	0.108	0.044
3. Rare mottled	353	27	469	244	415	1962	0.001	18.0	44	1.23	23	7.46	0.097	0.080	0.005	0.005	0.014	0.001	0.096	0.025
3. Rare mottled	309	31	526	252	436	1950	0.001	7.40	46	4.68	41	15.2	0.049	0.045	0.003	0.000	0.019	0.001	0.049	0.025
3. Rare mottled	1220	436	760	245	431	1940	0.047	33	70	5.98	40	21	0.709	0.540	0.050	0.096	0.148	0.030	0.101	0.029
3. Rare mottled	1115	390	688	234	435	1896	0.044	62	48	0.581	17.6	10.9	0.226	0.149	0.040	0.007	0.038	0.021	0.087	0.030
3. Rare mottled	2612	1091	782	229	423	1966	0.094	57	48	0.484	19.5	12.2	0.696	0.410	0.128	0.078	0.077	0.126	0.048	0.026
3. Rare mottled	13814	5518	7002	294	1171	1943	0.621	64	61	0.926	33	15.5	0.595	0.381	0.098	0.062	0.025	0.048	0.056	0.064
3. Rare mottled	187	19.5	491	212	418	1945	0.002	11.0	46	2.23	27	15.9	0.052	0.042	0.002	0.000	0.015	0.001	0.087	0.021
3. Rare mottled	265	20	414	1089	388	2035	0.010	7.35	45	0.209	18.4	8.50	2.99	1.40	0.398	0.009	0.089	0.015	0.084	0.040
Mean (n=63)	3864	1289	1422	665	2441	2172	2.45	31	60	4.70	103	24	18.7	8.53	3.14	0.361	0.504	0.565	0.333	0.240
S.D.	4075	1524	1666	1030	3468	342	3.85	25	36	4.22	113	13.9	36	19.4	7.77	0.480	0.737	0.963	0.503	0.227
G.M.	2428	652	1018	423	1074	2162	0.438	19.4	56	3.06	67	21	3.72	1.48	0.482	0.101	0.241	0.179	0.203	0.129
Median	2582	799	760	261	643	2152	0.617	23	49	3.01	51	21	5.73	1.73	0.606	0.120	0.280	0.295	0.193	0.175
Maximum	22755	8758	10645	7518	12764	2629	22	88	297	17.1	459	90	195	102	52	1.90	4.86	6.20	3.46	0.773
Minimum	187	18.2	414	212	239	1744	0.001	0.766	43	0.209	17.6	7.46	0.049	0.042	0.002	0.000	0.014	0.001	0.048	0.019

ESM Table 2d. LA-ICP-MS data used for REE plots (concentrations in ppm)
**Note*: Valeus without chondrite-normalization

Magnetite from altered mafic rocks	Jt1	La	Ce	Pr	Nd	Sm	Eu	Gd	Tb	Dy	Y	Ho	Er	Tm	Yb	Lu	Σ REY
Trellis	Jt1Mt1rim 06	0.017	0.077	0.022	0.099	0.069	0.016	0.105	0.033	0.301	1.82	0.084	0.208	0.035	0.206	0.027	3.12
Trellis	Jt1Mt6rim 25	0.024	0.124	0.030	0.162	0.087	0.036	0.188	0.050	0.434	3.04	0.117	0.435	0.069	0.384	0.041	5.23
Trellis	Jt1Mt2rim 12	0.038	0.097	0.015	0.175	0.103	0.035	0.252	0.068	0.509	3.20	0.111	0.503	0.074	0.370	0.049	5.60
Trellis	Jt1Mt4rim 20	0.082	0.234	0.042	0.264	0.203	0.049	0.337	0.067	0.633	4.05	0.163	0.576	0.091	0.529	0.068	7.39
Trellis	Jt1Mt3rim 13	0.018	0.081	0.019	0.113	0.089	0.024	0.206	0.067	0.808	5.05	0.193	0.619	0.088	0.559	0.057	7.99
Trellis	Jt1Mt3rim 16	0.051	0.124	0.028	0.152	0.087	0.056	0.325	0.086	0.857	5.45	0.223	0.758	0.117	0.672	0.072	9.05
Trellis	Jt1Mt4core 09	0.036	0.157	0.043	0.262	0.233	0.058	0.485	0.125	1.19	7.16	0.296	0.966	0.133	0.824	0.103	12.1
Trellis	Jt1Mt1rim 05	0.034	0.121	0.034	0.307	0.192	0.041	0.545	0.134	1.32	9.22	0.360	1.30	0.183	1.13	0.127	15.0
Trellis	Jt3Mt2 rim 03	3.43	10.6	1.70	9.31	3.00	0.485	2.38	0.249	1.48	5.97	0.204	0.485	0.059	0.282	0.019	40
Trellis	Jt3Mt5 01	0.175	0.441	0.069	0.440	0.295	0.105	0.823	0.154	1.32	7.11	0.244	0.694	0.071	0.495	0.052	12.5
Trellis	Jt3Mt7 rim 01	0.255	0.896	0.177	1.09	0.713	0.215	1.71	0.387	2.46	17.7	0.557	1.49	0.144	0.858	0.068	29
	Jt4	**La**	**Ce**	**Pr**	**Nd**	**Sm**	**Eu**	**Gd**	**Tb**	**Dy**	**Y**	**Ho**	**Er**	**Tm**	**Yb**	**Lu**	**Σ REY**
Trellis&Mottled	Jt4Mt1rim 02	0.375	0.823	0.099	0.442	0.105	0.013	0.118	0.019	0.108	0.748	0.032	0.099	0.012	0.113	0.008	3.12
Trellis&Mottled	Jt4Mt1rim 03	0.269	0.859	0.116	0.627	0.147	0.073	0.208	0.028	0.199	1.41	0.041	0.168	0.022	0.110	0.020	4.30
Trellis&Mottled	Jt4Mt1rim 07	1.29	2.69	0.327	1.49	0.321	0.048	0.461	0.051	0.422	3.50	0.113	0.306	0.050	0.332	0.043	11.4
Trellis&Mottled	Jt4Mt2 01	2.73	6.70	0.776	2.52	0.422	0.045	0.398	0.039	0.272	1.49	0.130	0.343	0.054	0.405	0.065	16.4
Trellis&Mottled	Jt4Mt2 02	4.79	8.30	0.942	2.88	0.352	0.012	0.386	0.041	0.223	1.63	0.064	0.243	0.047	0.419	0.074	20
Trellis&Mottled	Jt4Mt3 03	11.5	22	2.41	9.00	1.30	0.092	1.07	0.119	0.892	5.38	0.258	0.799	0.150	0.922	0.125	56
Trellis&Mottled	Jt4Mt3 04	0.613	1.77	0.273	1.00	0.322	0.044	0.407	0.059	0.331	2.37	0.083	0.345	0.034	0.203	0.028	7.88
Trellis&Mottled	Jt4Mt4 05	1.05	2.72	0.272	1.07	0.215	0.024	0.314	0.052	0.567	3.81	0.141	0.512	0.091	0.563	0.077	11.5
Trellis&Mottled	Jt4Mt4 06	1.91	8.70	0.887	4.07	1.11	0.100	1.07	0.162	1.01	7.03	0.264	0.894	0.167	1.17	0.171	29
Trellis&Mottled	Jt4Mt4 07	3.08	6.74	0.773	2.82	0.415	0.029	0.336	0.037	0.214	1.45	0.042	0.249	0.046	0.326	0.047	16.6
Trellis&Mottled	Jt4Mt5 08	1.52	4.40	1.03	2.40	0.618	0.058	0.810	0.086	0.479	4.45	0.125	0.469	0.075	0.434	0.068	17.0
Trellis&Mottled	Jt4Mt5 09	3.12	6.73	0.552	2.04	0.412	0.051	0.324	0.038	0.229	2.09	0.082	0.313	0.044	0.515	0.070	16.6
Trellis&Mottled	Jt4Mt5 11	0.280	0.760	0.113	0.554	0.129	0.024	0.186	0.026	0.224	1.44	0.046	0.194	0.032	0.143	0.019	4.17
Trellis&Mottled	Jt4Mt5 13	2.49	7.64	1.17	4.62	0.729	0.122	0.883	0.107	0.537	2.19	0.089	0.250	0.033	0.128	0.025	21
Trellis&Mottled	Jt4Mt5 14	1.42	4.72	0.441	1.97	0.703	0.110	0.646	0.095	0.587	4.26	0.149	0.593	0.075	0.547	0.073	16.4
Trellis&Mottled	Jt4Mt5 15	4.53	10.3	0.853	3.32	0.843	0.068	0.788	0.105	0.850	6.39	0.232	0.928	0.144	1.18	0.171	31
Trellis&Mottled	Jt4Mt5 16	11.7	24	2.16	7.42	1.29	0.097	1.12	0.116	0.805	5.80	0.189	0.767	0.130	1.02	0.138	57
Trellis&Mottled	Jt4Mt5 17	2.73	6.53	0.639	2.57	0.424	0.056	0.489	0.064	0.429	3.79	0.120	0.426	0.051	0.370	0.048	18.7
Trellis&Mottled	Jt4Mt5 18	13.2	37	3.82	13.9	1.66	0.122	1.57	0.205	1.42	11.0	0.381	1.47	0.225	1.64	0.248	88
Trellis&Mottled	Jt4Mt5 19	2.62	4.71	0.645	2.64	0.704	0.083	1.12	0.209	1.70	14.6	0.478	1.87	0.263	1.63	0.212	34
Trellis&Mottled	Jt4Mt6rim 08	9.15	10.4	0.984	2.68	0.340	0.095	0.401	0.045	0.430	3.17	0.113	0.482	0.069	0.365	0.066	29
Trellis&Mottled	Jt4Mt6rim 11	0.438	1.17	0.134	0.690	0.186	0.025	0.352	0.037	0.237	2.03	0.053	0.236	0.044	0.369	0.069	6.06

	Jt4	La	Ce	Pr	Nd	Sm	Eu	Gd	Tb	Dy	Y	Ho	Er	Tm	Yb	Lu	Σ REY
Trellis&Mottled	Jt4Mt6rim 12	9.96	15.0	1.78	5.49	0.640	0.078	0.567	0.064	0.357	2.11	0.098	0.269	0.063	0.367	0.064	37
Trellis&Mottled	Jt4Mt6rim 13	0.869	2.36	0.324	1.56	0.426	0.071	0.681	0.073	0.510	3.99	0.133	0.303	0.058	0.204	0.038	11.6
Trellis&Mottled	Jt4Mt6rim 15	1.12	2.26	0.328	1.55	0.377	0.037	0.473	0.075	0.498	4.27	0.151	0.548	0.074	0.402	0.055	12.2
Trellis&Mottled	Jt4Mt6rim 16	2.51	4.41	0.466	1.67	0.237	0.025	0.169	0.028	0.276	2.02	0.065	0.266	0.047	0.310	0.054	12.5
Trellis&Mottled	Jt4Mt6rim 17	1.82	3.61	0.485	2.36	0.364	0.028	0.281	0.044	0.321	2.43	0.093	0.375	0.063	0.483	0.065	12.8
Trellis&Mottled	Jt4Mt6core 03	0.293	0.496	0.056	0.306	0.071	0.011	0.110	0.013	0.131	0.818	0.034	0.113	0.024	0.190	0.028	2.69
Trellis&Mottled	Jt4Mt6core 05	0.989	2.39	0.284	1.22	0.307	0.032	0.297	0.044	0.369	2.83	0.102	0.286	0.049	0.247	0.027	9.48
Trellis&Mottled	Jt4Mt6core 06	0.337	0.681	0.083	0.376	0.091	0.006	0.095	0.018	0.110	0.817	0.022	0.072	0.010	0.089	0.012	2.82
Trellis&Mottled	Jt4Mt6core 07	0.594	1.44	0.224	0.896	0.193	0.041	0.249	0.022	0.235	1.77	0.050	0.128	0.020	0.114	0.012	5.99
Trellis&Mottled	Jt4Mt6core 08	41	70	7.31	24	2.87	0.221	1.91	0.263	2.08	15.8	0.556	2.13	0.305	1.93	0.228	170
Trellis&Mottled	Jt4Mt6core 09	2.80	6.26	0.815	4.02	0.869	0.073	1.08	0.145	0.900	7.07	0.229	0.700	0.093	0.535	0.067	26
Trellis&Mottled	Jt4Mt7rim 19	1.22	2.60	0.292	1.02	0.307	0.033	0.272	0.037	0.224	1.74	0.050	0.144	0.023	0.086	0.012	8.05
Trellis&Mottled	Jt4Mt8rim 22	1.27	3.62	0.535	2.43	0.601	0.043	0.659	0.091	0.540	4.45	0.125	0.352	0.041	0.285	0.045	15.1
Trellis&Mottled	Jt4Mt8rim 29	1.20	2.48	0.254	1.23	0.305	0.028	0.228	0.035	0.205	1.41	0.037	0.166	0.014	0.168	0.027	7.78

Magnetite from ore samples	Jt7	La	Ce	Pr	Nd	Sm	Eu	Gd	Tb	Dy	Y	Ho	Er	Tm	Yb	Lu	Σ REY
Mottled&Trellis	Jt7Mt1 01	0.148	0.576	0.094	0.369	0.189	0.026	0.433	0.092	0.846	5.30	0.188	0.643	0.096	0.632	0.064	9.70
Mottled&Trellis	Jt7Mt1 02	0.122	0.358	0.052	0.220	0.120	0.029	0.300	0.091	0.662	4.84	0.183	0.622	0.096	0.439	0.049	8.19
Mottled&Trellis	Jt7Mt1 03	0.115	0.492	0.122	0.858	0.875	0.179	1.92	0.581	5.41	36	1.29	4.25	0.536	2.96	0.229	56
Mottled&Trellis	Jt7Mt 2 01	2.98	6.86	0.718	2.77	0.531	0.034	0.387	0.058	0.443	2.76	0.102	0.317	0.050	0.251	0.034	18.3
Mottled&Trellis	Jt7Mt 2 04	14.7	33	3.42	12.1	1.73	0.230	1.80	0.356	2.87	16.9	0.673	2.40	0.308	1.88	0.160	93
Mottled&Trellis	Jt7Mt 2 05	11.7	28	3.37	12.3	2.83	0.409	4.62	0.964	8.45	48	1.82	5.48	0.733	4.34	0.350	134
Mottled&Trellis	Jt7Mt 2 06	0.335	0.630	0.089	0.253	0.136	0.021	0.221	0.064	0.399	2.88	0.095	0.294	0.042	0.336	0.026	5.82
Mottled&Trellis	Jt7Mt 3 03	0.098	0.332	0.057	0.424	0.202	0.038	0.474	0.107	1.16	7.71	0.327	1.11	0.166	0.952	0.099	13.3
Mottled&Trellis	Jt7Mt 3 04	0.461	2.63	0.625	4.61	3.64	0.674	7.48	1.85	16.9	121	4.30	15.0	2.15	12.3	1.10	195
Mottled&Trellis	Jt7Mt 3 05	21	50	5.46	20	2.89	0.283	2.01	0.171	0.884	3.64	0.157	0.466	0.051	0.358	0.028	107
Mottled&Trellis	Jt7Mt 3 08	0.632	1.24	0.125	0.515	0.123	0.019	0.091	0.034	0.269	2.05	0.067	0.254	0.038	0.243	0.027	5.73
Mottled&Trellis	Jt7Mt 3 09	0.152	0.511	0.065	0.541	0.329	0.054	0.619	0.170	1.84	11.9	0.418	1.59	0.256	1.55	0.135	20
Mottled&Trellis	Jt7Mt 3 10	0.125	0.326	0.048	0.348	0.238	0.048	0.549	0.142	1.37	8.70	0.326	1.12	0.173	1.00	0.087	14.6
Mottled&Trellis	Jt7Mt 4 rim 01	1.20	2.50	0.266	1.07	0.434	0.062	0.684	0.166	1.45	9.43	0.334	1.17	0.173	0.982	0.085	20
Mottled&Trellis	Jt7Mt 4 rim 02	0.047	0.157	0.030	0.233	0.155	0.032	0.235	0.057	0.399	2.54	0.085	0.267	0.043	0.328	0.031	4.64
Mottled&Trellis	Jt7Mt 4 rim 03	0.078	0.223	0.044	0.332	0.301	0.033	0.567	0.137	0.936	6.25	0.239	0.712	0.104	0.598	0.058	10.6
Mottled&Trellis	Jt7Mt 4 rim 05	0.042	0.311	0.057	0.308	0.299	0.062	0.817	0.145	1.33	8.59	0.345	1.16	0.173	1.18	0.130	14.9
Mottled&Trellis	Jt7Mt 4 rim 06	0.085	0.450	0.044	0.299	0.106	0.029	0.226	0.051	0.366	2.38	0.082	0.274	0.045	0.274	0.028	4.74
Mottled&Trellis	Jt7Mt 4 rim 07	0.212	0.749	0.180	1.14	0.822	0.117	1.96	0.476	3.83	22	0.828	2.66	0.351	2.07	0.224	38
Mottled&Trellis	Jt7Mt 4 core 01	0.352	1.27	0.203	0.976	0.294	0.028	0.428	0.050	0.421	2.11	0.069	0.233	0.033	0.256	0.026	6.75
Mottled&Trellis	Jt7Mt 4 core 02	0.698	1.63	0.222	0.983	0.226	0.008	0.185	0.023	0.152	0.984	0.040	0.106	0.011	0.121	0.011	5.40

	Jt7	La	Ce	Pr	Nd	Sm	Eu	Gd	Tb	Dy	Y	Ho	Er	Tm	Yb	Lu	Σ REY
Mottled&Trellis	Jt7Mt 4 core 03	1.26	2.39	0.343	1.34	0.137	0.015	0.164	0.032	0.188	1.33	0.043	0.157	0.017	0.214	0.036	7.68
Mottled&Trellis	Jt7Mt 5 01	1.46	2.35	0.411	1.68	0.404	0.059	0.388	0.082	0.907	4.94	0.189	0.691	0.079	0.505	0.038	14.2
Mottled&Trellis	Jt7Mt 5 02	0.395	1.04	0.119	0.483	0.148	0.048	0.409	0.095	1.11	9.23	0.375	1.38	0.225	1.29	0.124	16.5
Mottled&Trellis	Jt7Mt 5 03	1.08	3.34	0.291	0.978	0.231	0.013	0.215	0.018	0.123	0.699	0.034	0.085	0.005	0.059	0.007	7.18
Mottled&Trellis	Jt7Mt 5 04	3.43	8.36	0.925	2.90	0.472	0.031	0.441	0.032	0.200	1.00	0.033	0.080	0.007	0.088	0.035	18.0
Mottled&Trellis	Jt7Mt 5 05	4.82	12.2	1.22	3.88	0.650	0.048	0.367	0.044	0.181	0.802	0.032	0.116	0.009	0.138	0.014	25
Mottled&Trellis	Jt7Mt 5 06	1.44	5.49	0.541	1.78	0.306	0.029	0.248	0.036	0.297	1.91	0.069	0.276	0.037	0.346	0.036	12.8
Mottled&Trellis	Jt7Mt 5 07	16.9	15.7	1.46	3.83	0.350	0.025	0.269	0.026	0.205	1.24	0.048	0.142	0.029	0.244	0.043	40
Mottled&Trellis	Jt7Mt 5 08	16.3	36	4.03	15.7	1.92	0.126	1.57	0.202	1.20	3.95	0.194	0.431	0.026	0.172	0.019	82
Mottled&Trellis	Jt7Mt 5 10	0.840	1.78	0.203	0.840	0.172	0.021	0.351	0.057	0.416	1.42	0.072	0.250	0.023	0.138	0.017	6.59
Mottled&Trellis	Jt7Mt 6 03	0.117	0.825	0.238	1.94	1.47	0.235	3.25	0.867	8.31	60	2.13	7.46	1.06	6.50	0.509	95
Mottled&Trellis	Jt7Mt 6 04	0.296	1.09	0.118	0.491	0.191	0.022	0.164	0.042	0.373	2.22	0.092	0.338	0.046	0.249	0.035	5.76
Mottled&Trellis	Jt7Mt 6 05	0.206	0.672	0.130	0.712	0.499	0.065	0.845	0.258	2.43	17.3	0.608	2.25	0.307	1.99	0.167	28
Mottled&Trellis	Jt7Mt 8 09	0.248	0.499	0.058	0.264	0.152	0.010	0.137	0.032	0.125	1.19	0.030	0.139	0.012	0.084	0.008	2.99
	Jt8	**La**	**Ce**	**Pr**	**Nd**	**Sm**	**Eu**	**Gd**	**Tb**	**Dy**	**Y**	**Ho**	**Er**	**Tm**	**Yb**	**Lu**	**Σ REY**
Mottled&Trellis	Jt8Mt 1 04	1.75	2.52	0.347	1.01	0.113	0.011	0.144	0.020	0.194	1.37	0.038	0.139	0.028	0.169	0.030	7.89
Mottled&Trellis	Jt8Mt 1 05	0.415	0.531	0.075	0.307	0.086	0.005	0.075	0.018	0.196	1.04	0.036	0.132	0.012	0.161	0.024	3.11
Mottled&Trellis	Jt8Mt 2 01	0.457	1.20	0.113	0.438	0.092	0.001	0.041	0.009	0.071	0.646	0.026	0.062	0.014	0.112	0.012	3.29
Mottled&Trellis	Jt8Mt 2 02	0.354	0.706	0.068	0.311	0.041	0.008	0.056	0.013	0.132	0.684	0.034	0.097	0.013	0.099	0.012	2.63
Mottled&Trellis	Jt8Mt 2 03	0.322	0.820	0.116	0.456	0.165	0.014	0.316	0.047	0.428	2.27	0.084	0.386	0.036	0.250	0.038	5.75
Mottled&Trellis	Jt8Mt 3 01	2.00	2.07	0.280	0.894	0.173	0.015	0.162	0.017	0.205	1.29	0.047	0.193	0.034	0.188	0.021	7.59
Mottled&Trellis	Jt8Mt 3 02	10.8	19.0	2.12	8.00	1.11	0.084	1.19	0.121	0.873	5.60	0.216	0.773	0.103	0.695	0.111	51
Mottled&Trellis	Jt8Mt 3 03	0.952	2.24	0.328	1.20	0.178	0.007	0.079	0.008	0.086	0.450	0.022	0.039	0.014	0.100	0.009	5.71
Mottled&Trellis	Jt8Mt 3 04	0.407	1.46	0.145	0.621	0.084	0.003	0.106	0.006	0.117	0.731	0.023	0.085	0.017	0.117	0.018	3.94
Mottled&Trellis	Jt8Mt 3 05	1.61	2.35	0.308	0.921	0.110	0.004	0.099	0.025	0.121	0.818	0.034	0.135	0.016	0.113	0.017	6.68
Mottled&Trellis	Jt8Mt 4 01	0.667	1.54	0.128	0.528	0.135	0.005	0.093	0.011	0.117	0.693	0.024	0.100	0.023	0.092	0.017	4.18
Mottled&Trellis	Jt8Mt 5 02	0.330	0.845	0.103	0.630	0.136	0.016	0.253	0.036	0.317	2.22	0.082	0.262	0.025	0.187	0.034	5.48
Mottled&Trellis	Jt8Mt 5 03	0.418	1.23	0.146	0.522	0.131	0.008	0.120	0.024	0.097	1.19	0.047	0.146	0.022	0.160	0.017	4.27
Mottled&Trellis	Jt8Mt 5 05	0.612	2.21	0.477	1.23	0.606	0.025	0.476	0.054	0.511	3.64	0.136	0.523	0.066	0.635	0.054	11.3
Mottled&Trellis	Jt8Mt 5 06	1.03	2.14	0.517	2.01	0.217	0.029	0.321	0.017	0.253	1.18	0.043	0.179	0.028	0.180	0.022	8.17
Mottled&Trellis	Jt8Mt 5 07	0.776	1.59	0.236	0.909	0.322	0.018	0.216	0.024	0.176	1.37	0.047	0.212	0.031	0.211	0.026	6.16
Mottled&Trellis	Jt8Mt 5 08	0.412	1.65	0.314	1.49	0.158	0.012	0.234	0.030	0.165	1.31	0.050	0.186	0.028	0.166	0.030	6.22
Mottled&Trellis	Jt8Mt 5 09	0.612	1.85	0.227	0.654	0.101	0.007	0.168	0.019	0.166	1.23	0.047	0.193	0.020	0.201	0.022	5.52
Mottled&Trellis	Jt8Mt 6 02	0.349	0.714	0.105	0.351	0.095	0.005	0.107	0.011	0.130	0.631	0.036	0.082	0.007	0.086	0.011	2.72
Mottled&Trellis	Jt8Mt 6 03	2.42	4.65	0.526	1.86	0.197	0.015	0.217	0.039	0.251	1.77	0.067	0.215	0.037	0.229	0.029	12.5
Mottled&Trellis	Jt8Mt 6 04	1.55	2.31	0.314	1.15	0.136	0.007	0.144	0.024	0.169	1.23	0.038	0.157	0.029	0.176	0.025	7.45
Mottled&Trellis	Jt8Mt 6 05	0.575	0.897	0.100	0.459	0.059	0.003	0.132	0.011	0.146	0.829	0.032	0.106	0.016	0.117	0.012	3.50
Mottled&Trellis	Jt8Mt 6 06	2.18	4.42	0.568	1.91	0.221	0.003	0.229	0.028	0.142	0.668	0.026	0.107	0.016	0.073	0.009	10.6

	Jt8	La	Ce	Pr	Nd	Sm	Eu	Gd	Tb	Dy	Y	Ho	Er	Tm	Yb	Lu	Σ REY
Mottled&Trellis	Jt8Mt 6 10	0.504	0.730	0.091	0.274	0.042	0.001	0.060	0.006	0.129	0.793	0.031	0.124	0.018	0.105	0.014	2.92
Mottled&Trellis	Jt8Mt 7 01	1.72	3.12	0.364	1.30	0.162	0.008	0.185	0.034	0.307	2.21	0.082	0.295	0.042	0.253	0.035	10.1
Mottled&Trellis	Jt8Mt 7 02	1.74	4.25	0.481	1.99	0.378	0.014	0.292	0.033	0.344	1.99	0.071	0.367	0.042	0.397	0.042	12.4
Mottled&Trellis	Jt8Mt 7 03	3.40	7.61	0.938	3.70	0.596	0.039	0.485	0.051	0.316	2.18	0.086	0.312	0.055	0.461	0.074	20
Mottled&Trellis	Jt8Mt 7 04	4.09	8.92	1.14	4.04	0.645	0.041	0.479	0.056	0.290	1.67	0.059	0.251	0.035	0.479	0.065	22
Mottled&Trellis	Jt8Mt 7 05	5.68	14.0	1.72	7.46	1.24	0.089	0.882	0.067	0.415	2.32	0.086	0.497	0.074	0.584	0.087	35
Mottled&Trellis	Jt8Mt 7 06	4.06	7.36	1.02	3.57	0.363	0.027	0.409	0.044	0.347	1.83	0.083	0.298	0.046	0.371	0.071	19.9
Mottled&Trellis	Jt8Mt 7 07	6.92	17.2	2.13	8.80	1.42	0.084	1.16	0.093	0.387	2.14	0.072	0.373	0.051	0.484	0.054	41
Mottled&Trellis	Jt8Mt 7 08	4.11	8.66	1.18	3.74	0.447	0.037	0.333	0.052	0.283	1.80	0.071	0.268	0.055	0.370	0.051	21
Mottled&Trellis	Jt8Mt 7 09	5.43	10.3	1.35	4.42	0.619	0.026	0.353	0.032	0.275	2.34	0.090	0.385	0.067	0.466	0.084	26
Mottled&Trellis	Jt8Mt 7 10	3.21	5.70	0.680	2.37	0.273	0.018	0.142	0.040	0.285	1.99	0.077	0.311	0.058	0.465	0.052	15.7
Mottled&Trellis	Jt8Mt 8 02	0.178	0.554	0.065	0.196	0.021	0.003	0.032	0.006	0.094	0.511	0.021	0.065	0.006	0.059	0.007	1.82
Mottled&Trellis	Jt8Mt 8 03	0.464	1.08	0.125	0.565	0.196	0.020	0.217	0.036	0.268	1.72	0.050	0.146	0.019	0.118	0.027	5.06
Mottled&Trellis	Jt8Mt 8 04	0.351	0.816	0.110	0.462	0.097	0.007	0.111	0.022	0.149	0.985	0.028	0.120	0.013	0.120	0.020	3.41
Mottled&Trellis	Jt8Mt 8 05	1.07	2.37	0.298	1.26	0.221	0.010	0.233	0.027	0.304	1.82	0.070	0.227	0.030	0.249	0.040	8.23
Mottled&Trellis	Jt8Mt 8 07	0.368	0.846	0.100	0.398	0.083	0.001	0.082	0.017	0.116	0.730	0.027	0.076	0.009	0.098	0.007	2.96
Mottled&Trellis	Jt8Mt 8 08	0.509	1.28	0.121	0.460	0.053	0.001	0.056	0.010	0.080	0.570	0.017	0.076	0.011	0.050	0.010	3.31
Mottled&Trellis	Jt8Mt 9 01	3.53	5.79	0.582	3.61	0.519	0.026	0.366	0.030	0.178	1.18	0.049	0.206	0.026	0.148	0.028	16.3
Mottled&Trellis	Jt8Mt 9 02	0.389	0.571	0.077	0.308	0.064	0.006	0.129	0.014	0.174	1.09	0.034	0.134	0.026	0.153	0.018	3.19
Mottled&Trellis	Jt8Mt 9 04	1.55	2.88	0.401	1.47	0.332	0.021	0.867	0.115	0.727	2.79	0.130	0.295	0.045	0.326	0.025	12.0
Mottled&Trellis	Jt8Mt 9 09	0.265	0.388	0.063	0.224	0.038	0.003	0.114	0.012	0.122	0.726	0.029	0.079	0.020	0.087	0.011	2.18
Mottled&Trellis	Jt8Mt 9 14	0.287	0.885	0.148	0.644	0.133	0.003	0.096	0.012	0.092	0.606	0.016	0.071	0.012	0.050	0.007	3.06
Mottled&Trellis	Jt8Mt 9 15	0.581	1.55	0.161	0.617	0.102	0.004	0.144	0.018	0.214	1.22	0.049	0.141	0.018	0.230	0.032	5.08
Mottled&Trellis	Jt8Mt 9 16	0.362	0.766	0.087	0.356	0.044	0.004	0.094	0.013	0.172	1.16	0.041	0.154	0.023	0.167	0.025	3.47
Mottled&Trellis	Jt8Mt 9 17	0.833	1.71	0.172	0.732	0.117	0.013	0.115	0.026	0.185	1.34	0.064	0.175	0.034	0.144	0.028	5.68
Mottled&Trellis	Jt8Mt 9 18	0.526	2.19	0.202	0.669	0.111	0.001	0.132	0.011	0.115	0.711	0.024	0.079	0.012	0.101	0.014	4.89
Mottled&Trellis	Jt8Mt 9 19	0.430	0.856	0.111	0.320	0.101	0.013	0.111	0.011	0.135	0.978	0.028	0.164	0.014	0.117	0.016	3.41
	Jt9b	**La**	**Ce**	**Pr**	**Nd**	**Sm**	**Eu**	**Gd**	**Tb**	**Dy**	**Y**	**Ho**	**Er**	**Tm**	**Yb**	**Lu**	**Σ REY**
Mottled&Trellis	Jt9bMt1rim02	1.83	4.39	0.621	3.18	0.769	0.036	1.06	0.141	1.18	8.88	0.308	0.898	0.099	0.696	0.052	24
Mottled&Trellis	Jt9bMt1rim 05	9.21	16.9	2.48	8.69	1.10	0.037	0.716	0.073	0.455	2.52	0.107	0.333	0.048	0.256	0.029	43
Mottled&Trellis	Jt9bMt1core 01	7.68	9.37	1.38	3.96	0.421	0.020	0.308	0.028	0.285	1.75	0.069	0.230	0.039	0.252	0.031	26
Mottled&Trellis	Jt9bMt1core 02	12.7	19.4	3.00	10.00	1.16	0.059	0.695	0.082	0.489	2.73	0.119	0.333	0.048	0.264	0.030	51
Mottled&Trellis	Jt9bMt2 02	0.208	0.490	0.072	0.424	0.097	0.019	0.215	0.025	0.225	1.46	0.058	0.137	0.021	0.141	0.016	3.60
Mottled&Trellis	Jt9bMt3 05	6.02	7.78	0.847	2.90	0.408	0.031	0.385	0.030	0.334	1.80	0.059	0.230	0.030	0.203	0.032	21
Mottled&Trellis	Jt9bMt3 06	0.624	1.14	0.156	0.436	0.101	0.006	0.112	0.018	0.139	0.970	0.047	0.101	0.021	0.102	0.011	3.98
Mottled&Trellis	Jt9bMt4 07	0.264	0.694	0.072	0.327	0.089	0.009	0.137	0.020	0.136	1.16	0.049	0.123	0.019	0.076	0.013	3.19
Mottled&Trellis	Jt9bMt4 08	13.6	20	1.92	5.93	0.616	0.048	0.490	0.087	0.582	3.53	0.136	0.448	0.038	0.333	0.033	48
Mottled&Trellis	Jt9bMt4 09	7.36	9.82	1.30	4.15	0.692	0.029	0.476	0.061	0.281	2.41	0.089	0.311	0.039	0.239	0.032	27

	Jt9b	La	Ce	Pr	Nd	Sm	Eu	Gd	Tb	Dy	Y	Ho	Er	Tm	Yb	Lu	Σ REY
Mottled&Trellis	Jt9bMt5 11	130	190	18.2	54	6.40	0.332	4.76	0.665	4.82	28	0.973	2.89	0.377	2.04	0.243	444
Mottled&Trellis	Jt9bMt5 12	1.83	2.32	0.367	1.13	0.241	0.013	0.478	0.081	0.570	3.54	0.128	0.268	0.045	0.191	0.037	11.2
Mottled&Trellis	Jt9bMt6 14	100	188	22	76	11.0	0.589	8.96	1.21	9.70	66	3.03	9.10	1.18	6.32	0.689	504
Mottled&Trellis	Jt9bMt6 15	98	190	20	73	9.85	0.653	7.81	0.967	7.16	48	1.91	6.75	0.949	5.30	0.593	472
Mottled&Trellis	Jt9bMt6 16	10.6	22	2.95	14.3	3.76	0.240	4.26	0.767	5.99	43	1.56	5.18	0.671	3.73	0.402	119
Mottled&Trellis	Jt9bMt7 18	0.547	1.66	0.260	1.64	0.609	0.034	1.30	0.206	1.59	10.4	0.338	0.904	0.097	0.569	0.059	20
Mottled&Trellis	Jt9bMt7 19	3.07	5.45	0.701	2.46	0.253	0.016	0.261	0.049	0.312	2.11	0.082	0.279	0.038	0.271	0.036	15.4
Mottled&Trellis	Jt9bMt8 21	2.54	5.70	0.687	2.75	0.304	0.047	0.410	0.039	0.292	1.87	0.067	0.236	0.041	0.219	0.029	15.2
Mottled&Trellis	Jt9bMt8 22	0.912	2.34	0.273	1.09	0.173	0.013	0.142	0.022	0.166	1.39	0.059	0.165	0.016	0.122	0.020	6.91
Mottled&Trellis	Jt9bMt8 23	3.05	5.93	0.713	3.35	0.784	0.057	1.23	0.251	1.87	11.0	0.455	1.27	0.147	0.880	0.101	31
Mottled&Trellis	Jt9bMt8 24	52	98	10.4	44	5.55	0.190	3.52	0.208	0.791	2.87	0.128	0.307	0.030	0.194	0.016	219
Mottled&Trellis	Jt9bMt10 29	0.987	1.32	0.118	0.745	0.246	0.034	0.298	0.069	0.458	2.81	0.115	0.359	0.040	0.261	0.032	7.89
Mottled&Trellis	Jt9bMt10 30	0.570	1.05	0.136	0.617	0.093	0.012	0.261	0.031	0.175	1.48	0.067	0.192	0.029	0.190	0.017	4.93
Mottled&Trellis	Jt9bMt10 31	1.88	5.34	0.757	3.49	0.637	0.061	0.696	0.072	0.683	4.74	0.197	0.796	0.107	0.486	0.055	20
Mottled&Trellis	Jt9bMt11 32	0.507	0.764	0.089	0.441	0.095	0.010	0.115	0.021	0.139	0.725	0.029	0.099	0.011	0.060	0.005	3.11
Mottled&Trellis	Jt9Mt12 34	5.41	9.43	1.04	5.05	1.05	0.070	1.72	0.257	2.08	14.6	0.525	1.62	0.174	1.01	0.130	44
Mottled&Trellis	Jt9bMt12 35	0.747	1.79	0.252	1.38	0.400	0.018	0.579	0.118	0.856	6.74	0.202	0.682	0.077	0.452	0.053	14.3
Mottled&Trellis	Jt9bMt13 37	1.21	1.45	0.184	0.481	0.106	0.002	0.110	0.018	0.170	0.960	0.047	0.146	0.011	0.134	0.013	5.04

ESM Table 3. Nano-thermooxybarometric stimations based on magnetite and ilmenite pairs from STEM-EDX data

Sample	**Jt 4 - map 1**				**Jt 4 - ma**				**Jt 4 - map 3**		**Jt 4 - map 4**				**Jt 4 - map 5**	
wt%	Mag1	Ilm1	Mag2	Ilm2	Mag1	Ilm1	Mag2	Ilm2	Mag1	Ilm1	Mag1	Ilm1	Mag2	Ilm2	Mag1	Ilm1
SiO_2	0.920	0.878	0.937	0.878											0.313	0.420
TiO_2	0.487	48.02	0.436	48.1	0.207	50.1	0.155	49.8	0.194	50.2	0.310	52.1	0.194	50.0	1.029	26.2
Al_2O_3	0.885	0.905	0.885	0.840							0.190	0.167			0.568	0.467
$FeO_{(total)}$	94.4	46.4	94.7	46.6	98.1	48.7	99.3	48.8	99.4	48.9	98.9	45.8	99.3	48.5	96.7	71.9
MnO	0.436	1.3	0.337	1.2	0.130	0.710	0.120	1.1	0.210	0.968		1.3	0.210	1.2	0.319	0.441
MgO	0.840	0.681	0.777	0.647	0.244	0.194						0.170				0.241
CaO	0.398	0.345	0.344	0.335	0.173										0.281	0.234
Na_2O	0.373	0.461	0.393	0.443												
K_2O	0.379	0.355	0.361	0.330	0.224											
Cr_2O_3	0.303	0.320	0.277	0.170	0.204							0.150			0.271	
ZnO					0.251	0.291					0.164	0.119				0.172
V2O3	0.576	0.366	0.576	0.415	0.470		0.402	0.258	0.209		0.401	0.219	0.249	0.246	0.537	
Sum	100	100	100	100	100	100	100	100	100	100	100	100	100	100	100	100
ΣAtomic mol proportion	2.134	1.496	2.135	1.497	2.154	1.511	2.156	1.513	2.156	1.513	2.155	1.513	2.156	1.513	2.150	1.468
No. of Oxygen:	4	3	4	3	4	3	4	3	4	3	4	3	4	3	4	3
Fe_2O_3 wt%	68.7	5.66	68.8	5.68	72.9	5.5	73.3	5.66	73.5	5.26	72.8	0.703	73.4	5.34	69.6	54.6
FeO wt%	32.6	41.3	32.8	41.5	32.5	43.8	33.3	43.7	33.3	44.1	33.5	45.2	33.3	43.7	34.0	22.7
APFU																
Si	0.033	0.022	0.033	0.022	0	0	0	0	0	0	0	0	0	0	0.011	0.010
Ti	0.013	0.899	0.012	0.901	0.006	0.948	0.004	0.944	0.005	0.950	0.008	0.987	0.005	0.947	0.028	0.481
Al	0.037	0.027	0.037	0.025	0	0	0	0	0	0	0.008	0.005	0	0	0.024	0.013
Fe^{3+}	1.84	0.106	1.84	0.106	1.97	0.103	1.98	0.107	1.98	0.100	1.96	0.013	1.98	0.101	1.88	1.00
Fe^{2+}	0.968	0.860	0.975	0.865	0.974	0.921	1.00	0.921	0.999	0.929	1.00	0.952	0.999	0.921	1.02	0.464
Mn	0.013	0.027	0.010	0.026	0.004	0.015	0.004	0.023	0.006	0.021	0	0.027	0.006	0.026	0.010	0.009
Mg	0.044	0.025	0.041	0.024	0.013	0.007	0	0	0	0	0	0.006	0	0	0	0.009
Ca	0.015	0.009	0.013	0.009	0.007	0	0	0	0	0	0	0	0	0	0.011	0.006
Na	0.026	0.022	0.027	0.021	0	0	0	0	0	0	0	0	0	0	0	0
K	0.017	0.011	0.016	0.010	0.010	0	0	0	0	0	0	0	0	0	0	0
Cr	0.009	0.006	0.008	0.003	0.006	0	0	0	0	0	0	0.003	0	0	0.008	0
Zn	0	0	0	0	0.007	0.005	0	0	0	0	0.004	0.002	0	0	0	0.003
V	0.016	0.007	0.016	0.008	0.014	0	0.012	0.005	0.006	0	0.012	0.004	0.007	0.005	0.015	0
Sum	3	2	3	2	3	2	3	2	3	2	3	2	3	2	3	2
Calc. Methods (Mol. frac.)	Ulv	Ilm	Ulv	Ilm	Ulv	Ilm	Ulv	Ilm	Ulv	Ilm	Ulv	Ilm	Ulv	Ilm	Ulv	Ilm
Lindsley & Spencer (1982)	0.014	0.937	0.012	0.937	0.006	0.950	0.004	0.945	0.005	0.949	0.008	0.994	0.005	0.948	0.028	0.488
Stormer (1983)	0.013	0.943	0.012	0.943	0.005	0.948	0.004	0.946	0.005	0.950	0.008	0.993	0.005	0.949	0.029	0.485
Geothermobarometer by X'Ulv & X'Ilm from:	T°C	$\log_{10}fO_2$	T°C	$\log_{10}fO_2$	T°C	$\log_{10}fO_2$	T°C	$\log_{10}fO_2$	T°C	$\log_{10}fO_2$	T°C	$\log_{10}fO_2$	T°C	$\log_{10}fO_2$	T°C	$\log_{10}fO_2$
Lindsley & Spencer (1982)	560.93	-19.24	555.99	-19.32	503.30	-21.37	499.02	-21.00	502.06	-21.29	362.14	-36.16	503.91	-21.15	727.99	-12.24
Stormer (1983)	551.28	-19.84	546.65	-19.93	506.04	-21.09	497.99	-21.08	500.92	-21.37	372.88	-34.89	502.56	-21.24	728.81	-12.22
Mean	556.10	-19.54	551.32	-19.62	504.67	-21.23	498.50	-21.04	501.49	-21.33	367.51	-35.53	503.24	-21.19	728.40	-12.23

ESM Table 3. (Continued)

Sample	Jt 6 - f1 - map 6				Jt 6 - f1 - map 7		Jt 6 - f1 - map 8		Jt 6 - f2 - map 9		Jt 10 - f2 - map 10			
wt%	Mag1	Ilm1	Mag2	Ilm2	Mag1	Ilm1	Mag1	Ilm1	Mag1	Ilm1	Mag1	Ilm1	Mag2	Ilm2
SiO_2			0.314	0.133					0.103	0.137	0.166		0.166	0.146
TiO_2	0.864	51.2	0.554	49.6	0.207	50.2	0.091	48.2	0.104	49.7	0.479	51.9	0.453	52.0
Al_2O_3	0.438	0.336	0.161	0.247			0.117	0.261						
$FeO_{(total)}$	98.1	45.9	97.7	47.1	99.2	48.6	99.2	48.9	99.4	47.6	99.3	46.0	99.0	45.7
MnO	0.120	2.4	0.489	2.4			0.120	2.5	0.080	2.3		1.9	0.100	1.9
MgO				0.102	0.193	0.125	0.129				0.090	0.091	0.180	0.147
CaO				0.125			0.043	0.970					0.119	0.086
Na_2O														
K_2O					0.112									
Cr_2O_3						0.351		0.071						
ZnO					0.126	0.376						0.145		
V2O3	0.304	0.147	0.773	0.356	0.194	0.319	0.263		0.305	0.332				
Sum	100	100	100	100	100	100	100	101	100	100	100	100	100	100
ΣAtomic mol proportion:	2.157	1.512	2.154	1.508	2.154	1.513	2.152	1.490	2.155	1.512	2.154	1.515	2.152	1.513
No. of Oxygen:	4	3	4	3	4	3	4	3	4	3	4	3	4	3
Fe_2O_3 wt%	71.3	2.55	71.1	5.7	73.5	4.39	73.5	10.3	73.3	5.6	72.7	1.62	72.9	1.12
FeO wt%	34.0	43.7	33.7	42.0	33.1	44.6	33.1	39.6	33.5	42.5	33.8	44.5	33.4	44.7
APFU														
Si	0	0	0.011	0.003	0.000	0.000	0.000	0.000	0.004	0.003	0.006	0	0.006	0.004
Ti	0.023	0.969	0.015	0.936	0.006	0.952	0.002	0.899	0.003	0.940	0.013	0.985	0.012	0.986
Al	0.019	0.010	0.007	0.007	0.000	0.000	0.005	0.008	0	0	0	0	0	0
Fe^{3+}	1.93	0.048	1.92	0.107	1.98	0.083	1.98	0.193	1.98	0.106	1.96	0.031	1.96	0.021
Fe^{2+}	1.02	0.919	1.01	0.882	0.991	0.940	0.990	0.821	1.00	0.895	1.01	0.939	1.00	0.941
Mn	0.004	0.051	0.015	0.051	0.000	0.000	0.004	0.052	0.002	0.049	0	0.040	0.003	0.041
Mg	0	0	0	0.004	0.010	0.005	0.007	0.000	0	0	0.005	0.003	0.010	0.006
Ca	0	0	0	0.003	0.000	0.000	0.002	0.026	0	0	0	0	0.005	0.002
Na	0	0	0	0	0	0	0	0	0	0	0	0	0	0
K	0	0	0	0	0.005	0	0	0	0	0	0	0	0	0
Cr	0	0	0	0	0	0.007	0	0.001	0	0	0	0	0	0
Zn	0	0	0	0	0.003	0.007	0	0	0	0	0	0.003	0	0
V	0.009	0.003	0.022	0.007	0.006	0.006	0.008	0.000	0.009	0.007	0	0	0	0
Sum	3	2	3	2	3	2	3	2	3	2	3	2	3	2
Calc. Methods (Mol. frac.)	Ulv	Ilm	Ulv	Ilm	Ulv	Ilm	Ulv	Ilm	Ulv	Ilm	Ulv	Ilm	Ulv	Ilm
Lindsley & Spencer (1982)	0.024	0.975	0.015	0.943	0.006	0.961	0.002	0.911	0.003	0.942	0.013	0.985	0.012	0.988
Stormer (1983)	0.024	0.975	0.015	0.945	0.006	0.958	0.002	0.899	0.003	0.945	0.013	0.984	0.012	0.989
Geothermobarometer by														
X'Ulv & X'Ilm from:	T°C	$\log_{10} fO_2$	T°C	$\log_{10} fO_2$	T°C	$\log_{10} fO_2$	T°C	$\log_{10} fO_2$	T°C	$\log_{10} fO_2$	T°C	$\log_{10} fO_2$	T°C	$\log_{10} fO_2$
Lindsley & Spencer (1982)	504.75	-24.54	556.91	-19.76	482.51	-23.03	513.51	-18.63	486.84	-21.02	438.22	-28.98	420.61	-30.58
Stormer (1983)	503.29	-24.67	555.00	-19.88	489.08	-22.46	521.73	-18.00	482.54	-21.38	443.74	-28.45	414.41	-31.17
Mean	504.02	-24.61	555.96	-19.82	485.79	-22.74	517.62	-18.31	484.69	-21.20	440.98	-28.71	417.51	-30.88

**Abbreviations:* Mag-magnetite; Ilm-ilmenite; Ulv-ulvöspinel.

Lindsley DH, Spencer KJ (1982) Fe−Ti oxide geothermometry: Reducing analyses of coexisting Ti-magnetite (Mt) and ilmenite (Ilm). Transactions, American Geophysical Union 63, 471.

Stormer JC (1983) The effects of recalculation on estimates of temperature and oxygen fugacity from analyses of multicomponent iron-titanium oxides. American Mineralogist, 68, 586–594.

SUPPLEMENTARY MATERIAL D

FOR CHAPTER 5 – COUPLED LU-HF AND U-PB APATITE GEOCHRONOLOGY OF JATOBÁ OREBODY SUPPORTS ~2.5 GA METAMORPHISM IN DEEP SHEAR ZONES FROM SOUTHERN COPPER BELT, CARAJÁS DOMAIN, BRAZIL

APPENDIX A: ANALYTICAL METHODS AND ADDITIONAL FIGURES

APPENDIX B: ADDITIONAL TABLES, EPMA AND LA-ICP-MS RESULTS

APPENDIX A FOR CHAPTER 5

Supplemental Materials – Analytical Methods

Electron Probe Microanalysis

Compositional data were obtained using a Cameca SX-Five electron probe microanalyzer (EPMA). The instrument is equipped with five tuneable wavelength-dispersive spectrometers running PeakSite v6.2 software for microscope operation and 'Probe for EPMA' software (Probe Software Inc.) for all data acquisition and processing. Analysis was performed using combined operating conditions of 10 kV/15 nA and 10 kV/40 nA both with a defocused beam of 10 µm. The full list of elements analysed along with operating conditions, primary and interference standards, average detection limits are presented in Tables a, b. Matrix corrections of Armstrong-Love/Scott φ(ρz) (Armstrong, 1988) and Henke MACs were used for data reduction.

X-Ray element mapping was undertaken on the same instrument, using beam conditions of 15 kV/200 nA with focused beam, a dwell time of 30 ms, and pixel resolution of 1-3 µm depending on the size of the apatite. Measurement of Cl (Kα), F (Kα), Y (Lα), Ce (Lα), and Cl (Kα) was done on WDS spectrometers, with Cl analysed on two spectrometers and then summed for enhanced sensitivity. Other elements, Na (Kα), Mg (Kα), Al (Kα), Si (Kα), P (Kα), S (Kα), Ca (Kα), and Fe (Kα), were measured by concurrent EDS. Images were compiled in PeakSite v6.2.

Beam damage and element migration were attempted to be minimized via use of the Mean Atomic Number (MAN) background correction (e.g., Donovan and Tingle, 1996; Donovan et al., 2016) over traditional 2 point background interpolation. This allows single point analysis time to be greatly shortened, reducing the aforementioned effects of beam damage and element migration and their subsequent impact on the quality of analysis.

In addition to this, elements that are particularly mobile (e.g. Na,F,Ca,P) were analysed first on the detector and the Time Dependent Intensity (TDI) correction feature of Probe for EPMA was utilized (e.g., Donovan and Rowe, 2005). Using this method, the decay of x-ray counts over time is measured and modelled to return a t=0 intercept, and from this a concentration is calculated.

Table a. EPMA setup for analysis of apatite

Element and Line	Diffracting Crystal (Sp#)	Background type/fit	kV/nA/spot size(µm)	Peak Count Time	Bkgd Count Times		# bkgd points acquired (Lo/Hi)	Standards*		Overlapping element and order	Average DL (ppm - 99% CI)
					Lo	Hi		Primary Standard	Interference Standards		
Na Ka	LTAP (1)	MAN	10/15/10	15				735			110
Si Ka	LTAP (1)	MAN	10/15/10	15				558			100
Mg Ka	LTAP (1)	MAN	10/40/10	15				1335			100
Al Ka	LTAP (1)	MAN	10/40/10	15				1325			100
Sr La	LTAP (1)	MAN	10/40/10	15				513	513	Ca Ka (II)	130
As La	LTAP (1)	MAN	10/40/10	15				548			120
F Ka	PC0 (2)	MAN	10/15/10	35				1600			300
P Ka	LPET (3)	MAN	10/15/10	15				736	570	Ca Ka (II)	210
S Ka	LPET (3)	MAN	10/15/10	15				513			170
La La	LPET (3)	MAN	10/40/10	15				1200			460
Y La	LPET (3)	MAN	10/40/10	15				1214			400
Ca Ka	LPET (4)	MAN	10/15/10	15				736			200
Cl Ka	LPET (4)	MAN	10/15/10	15				545			200
Ce La	LPET (4)	MAN	10/40/10	15				1201			550
Ti Ka	LPET (4)	MAN	10/40/10	15				1342			160
Fe Ka	LLIF (5)	MAN	10/40/10	15				578			550
Mn Ka	LLIF (5)	MAN	10/40/10	15				557			450
Nd La	LLIF (5)	MAN	10/40/10	15				1203			860

Standard # refers to internal database. Full list of standards in Table b

Table b. Standard information

Reference #	Mineral composition	Natural/Synthetic	Manufacturer
513	Celestine	Natural	Astimex
545	Tugtupite	Natural	Astimex
548	GaAs	Synthetic	Astimex
557	Rhodonite	Natural	P&H and Associates
558	Wollastonite	Natural	P&H and Associates
578	Specularite	Synthetic	P&H and Associates
735	Albite (Amelia)	Natural	C.M. Taylor
736	Apatite	Synthetic	C.M. Taylor
1200	LaPO4	Synthetic	Cherniak
1201	CePO4	Synthetic	Cherniak
1203	NdPO4	Synthetic	Cherniak
1214	YPO4	Synthetic	Cherniak
1325	NMNH-135602 Corundum	Metal	NMNH
1335	NMNH-113312-44 Olivine	Metal	NMNH
1342	Rutile	Synthetic	In-house
1600	MgF2	Synthetic	In-house

LA-ICP-MS analysis

U-Pb and trace elements

Analysis of apatite for U-Pb and trace element analysis was performed via LA-ICP-MS following the method of Glorie et al. (2019).

The method of combined U-Pb/trace element involved measurement of the following isotopes, with their dwell times given in brackets either in spot- or mapping mode: ^{27}Al (0.005), ^{29}Si(0.005), ^{31}P (0.005), ^{35}Cl (0.005), ^{43}Ca (0.005), ^{49}Ti (0.005), ^{55}Mn (0.01), ^{57}Fe (0.01), ^{88}Sr (0.01), ^{89}Y (0.01), ^{90}Zr(0.01), ^{139}La (0.01), ^{140}Ce (0.01), ^{141}Pr (0.01), ^{146}Nd (0.01), ^{147}Sm (0.01), ^{153}Eu (0.01), ^{157}Gd (0.01),^{159}Tb (0.01), ^{163}Dy (0.01), ^{165}Ho (0.01), ^{166}Er (0.01), ^{169}Tm (0.01), ^{172}Yb (0.01), ^{175}Lu (0.01), ^{178}Hf(0.01), ^{202}Hg (0.01), ^{204}Pb (0.01), ^{206}Pb (0.1), ^{207}Pb (0.1), ^{208}Pb (0.01), ^{232}Th (0.02), ^{238}U (0.02). Other isotopes analysed in a second session includes ^{24}Mg, ^{27}Al, ^{29}Si, ^{31}P, ^{43}Ca, ^{45}Sc, ^{49}Ti, ^{51}V, ^{53}Cr, ^{55}Mn, ^{57}Fe, ^{59}Co, ^{60}Ni, ^{65}Cu, ^{66}Zn, ^{69}Ga, ^{75}As, ^{88}Sr, ^{89}Y, ^{90}Zr, ^{93}Nb, ^{95}Mo, ^{118}Sn, ^{121}Sb, ^{137}Ba, ^{139}La, ^{140}Ce, ^{141}Pr, ^{146}Nd, ^{147}Sm, ^{153}Eu, ^{157}Gd, ^{159}Tb, ^{163}Dy, ^{165}Ho, ^{166}Er, ^{169}Tm, ^{172}Yb, ^{175}Lu, ^{178}Hf, ^{181}Ta, ^{182}W, ^{195}Pt, ^{204}Pb, ^{206}Pb, ^{207}Pb, ^{208}Pb, ^{232}Th, and ^{238}U.

LADR software (Norris Scientific Pty Ltd., Kingston, TAS, Australia) was utilized for data processing. Although the areas selected for analysis were chosen to avoid inclusions, time-resolved depth profiles for each ablation spot were thoroughly examined for signs of subsurface inclusions or other artefacts that could bias the results and interpretation. When obvious inclusions were identified, the integrated interval was adjusted to exclude them. Data showing abundant inclusions or clear mineral mixtures were discarded. For element imaging, the laser was rastered across the sample forming a rectangular grid across the area of interest with a beam size of 10 μm. Rasters were then compiled and processed into trace element intensity maps using 'Iolite' software (Paton et al., 2011); version Iolite 3, with extension 'Igor Pro 6.37 used for generation of laser maps. Mapped intensities are scaled independently for each element to enhance different features; the scale used is linear counts per second (10n).

Lu-Hf

The Lu-Hf method utilises an LA-ICP–MS/MS with two quadrupole mass analysers and a collision cell (Agilent 8900 ICP-MS/MS). The laser-based Lu–Hf method depends on reacting Hf with NH3 filtering gas promoting the formation of Hf(NH)(NH2)(NH3)3 in the reaction cell of the mass spectrometer. For detailed descriptions of the method, the reader is referred to Simpson et al. (2021). The following isotopes were measured during analysis for internal standard quantification and to detect potential inclusions in apatite 27Al, 43Ca, 47Ti, 57Fe, 88Sr, 89Y, 90Zr, 140Ce, 146Nd, 147Sm, 175Lu, 176Hf, 178Hf. The 176Hf/176Lu and 176Lu/176Hf, ratios were calculated normalised to NIST610 to correct for instrument mass bias and drift. A matrix correction for 176Lu/176Hf was calculated against the Bamble apatite (1097 ± 5 Ma, Glorie et al., 2024), and Hartz Range (HR; corrected Lu–Hf age: 342 ± 2.8 Ma; Glorie et al., 2024) and Wallaroo (corrected Lu–Hf age: 1557 ± 23 Ma; Simpson et al., 2021) apatites were analysed as secondary age standards. For quantification 43Ca was used as the internal standard element for calibration of selected trace elements measured simultaneously with Lu–Hf isotopes.

Apatite U-Pb and Lu-Hf ages were calculated in IsoplotR (Vermeesch, 2018).

All instrumentation is housed at Adelaide Microscopy, the University of Adelaide.

References

Armstrong, J.T. (1988) Quantitative analysis of silicate and oxide minerals: comparison of Monte Carlo, ZAF and phi-rho-z procedures. Analysis microbeam. D.E. Newbury, ed., San Fransisco Press 239-246.

Donovan, J.J., and Tingle, T.N. (1996) An improved mean atomic number background correction for quantitative microanalysis. Microscopy Microanalysis 2(1), 1-7. https://doi.org/10.1017/S1431927696210013

Donovan, J.J., and Rowe, M. (2005) Techniques for improving quantitative analysis of mineral glasses. Geochemical and Cosmochemical Acta 69(10), A589.

Donovan, J.J., Singer, J.W., and Armstrong, J.T. (2016) A new EPMA method for fast trace element analysis in simple matrices. American Mineralogist 101(8), 1839-1853. https://doi.org/10.2138/am-2016-5628

Glorie, S., Jepson, G., Konopelko, D., Mirkamalov, R., Meeuws, F., Gilbert, S., Gillespie, J., Collins, A.S., Xiao, W., Dewaele, S., and De Grave, J. (2019) Thermochronological and geochemical footprints of post-orogenic fluid alteration recorded in apatite: Implications for mineralisation in the Uzbek Tian Shan. Gondwana Research 71, 1-15. https://doi.org/10.1016/j.gr.2019.01.011

Paton, C., Hellstrom, J., Paul, B., Woodhead, J., and Hergt, J. (2011) Iolite: Freeware for the visualisation and processing of mass spectrometric data. Journal of Analytical Atomic Spectrometry 26, 2508-2518. https://doi.org/10.1039/C1JA10172B

Simpson, A., Gilbert, S., Tamblyn, R., Hand, M., Spandler, C., Gillespie, J., Nixon, A., and Glorie, S. (2021) In-situ Lu Hf geochronology of garnet, apatite and xenotime by LA ICP MS/MS. Chemical Geology 577, 120299. https://doi.org/10.1016/j.chemgeo.2021.120299

Vermeesch, P. (2018) IsoplotR: A free and open toolbox for geochronology. Geoscience Frontiers 9(5), 1479-1493. https://doi.org/10.1016/j.gsf.2018.04.001

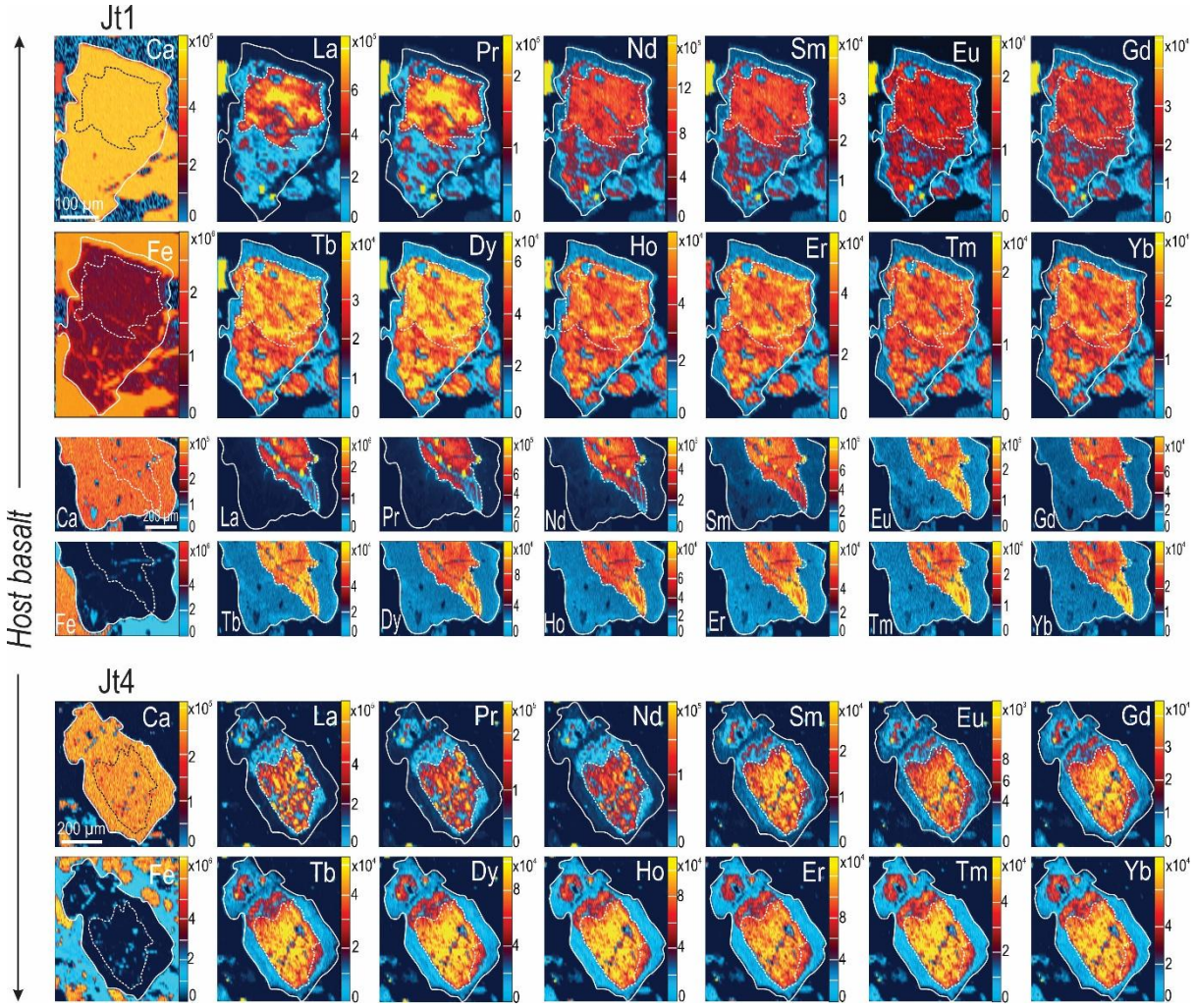

SM Figure 1. LA-ICP-MS element maps show the grain-scale distributions of rare earths and other trace elements in basalt-hosted fluorapatite. Scales in counts-per-second.

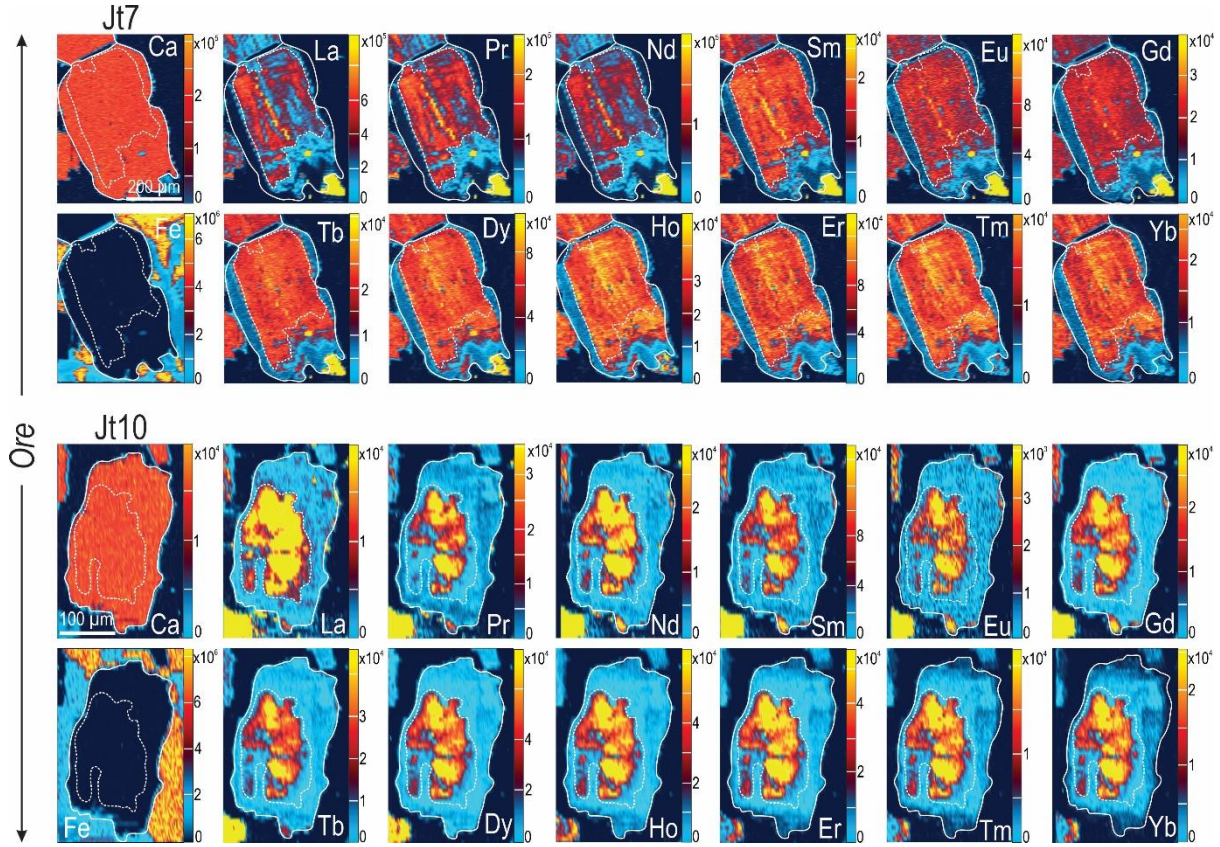

SM Figure 2. LA-ICP-MS element maps show the grain-scale distributions of rare earths and other trace elements in ore fluorapatite. Scales in counts-per-second.

APPENDIX B FOR CHAPTER 5

S Table 1A. Summary of EPMA data for apatite by sample and selected line profiles.

S Table 1B. Complete data set of EPMA data for apatite.

S Table 2. LA-ICP-MS trace element data for fluorapatite.

S Table 3A. Summary of U-Pb data for selected apatite.

S Table 3B. Summary of U-Pb data for in-house reference materials.

S Table 4. Summary of Lu-Hf data and trace elements for selected apatite and in-house reference materials.

Supplementary Table 1A. Summary of EPMA data for apatite (by sample and selected line profiles)
**Note:* Line *p* rofiles are shown in Figure 3. Values in 0.00 correspond to <mdl.

Sample	Jt1 (n=99)				Jt4 (n=38)				Jt7 (n=119)				Jt10 (n=57)			
	Mean	**SD**	**Min**	**Max**	**Mean**	**SD**	**Min**	**Max**	**Mean**	**SD**	**Min**	**Max**	**Mean**	**SD**	**Min**	**Max**
F	2.44	0.22	2.03	3.08	3.27	0.24	2.79	3.71	3.04	0.23	2.49	3.52	3.20	0.31	2.59	3.86
Cl	1.04	0.22	0.63	1.46	0.43	0.13	0.19	0.66	0.66	0.12	0.36	0.92	0.50	0.21	0.10	0.96
Na2O	0.01	0.02	0.00	0.06	0.01	0.02	0.00	0.05	0.01	0.02	0.00	0.07	0.02	0.03	0.00	0.17
SiO2	0.15	0.24	0.00	1.22	0.08	0.12	0.00	0.48	0.24	0.21	0.00	1.58	0.07	0.15	0.00	0.76
Al2O3	0.01	0.04	0.00	0.30	0.00	0.00	0.00	0.00	0.00	0.04	0.00	0.46	0.00	0.00	0.00	0.03
MgO	0.02	0.05	0.00	0.41	0.01	0.01	0.00	0.02	0.02	0.02	0.00	0.21	0.01	0.01	0.00	0.05
P2O5	42.22	0.56	40.06	43.28	42.41	0.55	41.14	43.58	42.01	0.64	39.42	43.35	42.88	0.51	41.60	43.85
SO2	0.01	0.02	0.00	0.08	0.02	0.03	0.00	0.08	0.00	0.01	0.00	0.06	0.01	0.03	0.00	0.14
CaO	55.02	0.68	52.84	56.83	55.52	0.67	54.57	56.91	55.09	0.75	52.85	56.92	55.60	0.78	53.18	56.96
TiO2	0.00	0.00	0.00	0.00	0.00	0.00	0.00	0.00	0.00	0.00	0.00	0.00	0.00	0.00	0.00	0.00
MnO	0.00	0.01	0.00	0.08	0.00	0.00	0.00	0.00	0.00	0.00	0.00	0.00	0.00	0.00	0.00	0.00
Fe2O3	0.03	0.11	0.00	0.76	0.05	0.09	0.00	0.33	0.05	0.14	0.00	1.28	0.05	0.11	0.00	0.56
As2O3	0.00	0.00	0.00	0.00	0.00	0.00	0.00	0.00	0.00	0.00	0.00	0.00	0.00	0.00	0.00	0.00
SrO	0.00	0.01	0.00	0.04	0.00	0.00	0.00	0.02	0.00	0.00	0.00	0.00	0.00	0.00	0.00	0.00
Y2O3	0.03	0.06	0.00	0.21	0.05	0.09	0.00	0.29	0.06	0.07	0.00	0.22	0.05	0.11	0.00	0.52
La2O3	0.01	0.02	0.00	0.11	0.00	0.00	0.00	0.00	0.00	0.02	0.00	0.24	0.00	0.00	0.00	0.00
Ce2O3	0.06	0.12	0.00	0.58	0.01	0.03	0.00	0.16	0.07	0.11	0.00	0.59	0.00	0.00	0.00	0.00
Nd2O3	0.02	0.06	0.00	0.28	0.00	0.02	0.00	0.11	0.02	0.06	0.00	0.28	0.00	0.00	0.00	0.00
-O equivalent	-1.26	0.06	-1.45	-1.10	-1.48	0.08	-1.61	-1.30	-1.43	0.08	-1.61	-1.23	-1.46	0.10	-1.68	-1.28
Total	**99.8**	**0.7**	**97.8**	**102.2**	**100.4**	**0.8**	**99.1**	**102.5**	**99.9**	**1.0**	**97.6**	**102.3**	**100.9**	**1.0**	**98.5**	**103.0**
Calculated formulae 9 a.p.f.u.																
Ca	4.843	0.044	4.687	4.934	4.814	0.050	4.732	4.908	4.815	0.049	4.697	4.951	4.793	0.045	4.710	4.889
Mg	0.002	0.007	0.000	0.051	0.001	0.001	0.000	0.002	0.002	0.002	0.000	0.026	0.001	0.001	0.000	0.006
Mn	0.000	0.001	0.000	0.006	0.000	0.000	0.000	0.000	0.000	0.000	0.000	0.000	0.000	0.000	0.000	0.000
Sr	0.000	0.000	0.000	0.002	0.000	0.000	0.000	0.001	0.000	0.000	0.000	0.000	0.000	0.000	0.000	0.000
Y	0.001	0.003	0.000	0.009	0.002	0.004	0.000	0.013	0.003	0.003	0.000	0.010	0.002	0.005	0.000	0.023
La	0.000	0.001	0.000	0.003	0.000	0.000	0.000	0.000	0.000	0.001	0.000	0.007	0.000	0.000	0.000	0.000
Ce	0.002	0.004	0.000	0.018	0.000	0.001	0.000	0.005	0.002	0.003	0.000	0.018	0.000	0.000	0.000	0.000
Nd	0.001	0.002	0.000	0.008	0.000	0.001	0.000	0.003	0.001	0.002	0.000	0.008	0.000	0.000	0.000	0.000
Na	0.002	0.002	0.000	0.010	0.002	0.003	0.000	0.007	0.002	0.003	0.000	0.011	0.003	0.005	0.000	0.028
Fe	0.002	0.007	0.000	0.048	0.003	0.006	0.000	0.020	0.003	0.009	0.000	0.080	0.003	0.006	0.000	0.034
Ti	0.000	0.000	0.000	0.000	0.000	0.000	0.000	0.000	0.000	0.000	0.000	0.000	0.000	0.000	0.000	0.000
Al	0.001	0.004	0.000	0.029	0.000	0.000	0.000	0.000	0.000	0.004	0.000	0.045	0.000	0.000	0.000	0.003
Total	**4.853**	**0.039**	**4.776**	**4.943**	**4.823**	**0.052**	**4.733**	**4.920**	**4.828**	**0.047**	**4.734**	**4.964**	**4.800**	**0.044**	**4.723**	**4.898**
ΣREY	**0.004**	**0.007**	**0.000**	**0.031**	**0.002**	**0.005**	**0.000**	**0.017**	**0.006**	**0.006**	**0.000**	**0.029**	**0.002**	**0.005**	**0.000**	**0.023**
P	2.936	0.025	2.835	2.980	2.905	0.024	2.846	2.952	2.901	0.025	2.787	2.970	2.921	0.020	2.880	2.976
S	0.000	0.001	0.000	0.006	0.001	0.002	0.000	0.006	0.000	0.001	0.000	0.005	0.001	0.002	0.000	0.010
As	0.000	0.000	0.000	0.000	0.000	0.000	0.000	0.000	0.000	0.000	0.000	0.000	0.000	0.000	0.000	0.000
Si	0.012	0.020	0.000	0.101	0.007	0.010	0.000	0.039	0.020	0.017	0.000	0.132	0.006	0.012	0.000	0.062
Total	**2.949**	**0.017**	**2.889**	**2.990**	**2.913**	**0.022**	**2.855**	**2.957**	**2.921**	**0.021**	**2.873**	**2.981**	**2.928**	**0.024**	**2.885**	**2.990**
F	0.633	0.055	0.532	0.795	0.837	0.057	0.717	0.938	0.784	0.056	0.648	0.896	0.813	0.073	0.670	0.956
Cl	0.145	0.031	0.088	0.201	0.060	0.018	0.026	0.093	0.091	0.017	0.050	0.130	0.068	0.029	0.014	0.131
(F+Cl)	0.778	0.034	0.675	0.886	0.897	0.045	0.793	0.973	0.876	0.047	0.764	0.989	0.881	0.050	0.785	0.991
OH (by difference)	0.222	0.034	0.114	0.325	0.103	0.045	0.027	0.207	0.124	0.047	0.011	0.236	0.119	0.050	0.009	0.215
Total	**1.000**				**1.000**				**1.000**				**1.000**			

Profiles	**Jt1 - grain 1**				**Jt1 - grain 4**				**Jt4 - grain 2**				**Jt4 - grain 5**			
	Mean	**SD**	**Min**	**Max**	**Mean**	**SD**	**Min**	**Max**	**Mean**	**SD**	**Min**	**Max**	**Mean**	**SD**	**Min**	**Max**
F	2.21	0.39	0.17	2.64	2.83	0.35	1.29	3.63	3.07	0.14	2.85	3.42	3.61	0.10	3.42	3.86
Cl	1.22	0.19	0.68	1.50	0.71	0.16	0.26	0.92	0.52	0.05	0.38	0.60	0.31	0.05	0.18	0.43
Na2O	0.01	0.02	0.00	0.06	0.01	0.01	0.00	0.04	0.01	0.02	0.00	0.05	0.01	0.02	0.00	0.05
SiO2	2.24	11.60	0.00	69.91	0.16	0.14	0.00	0.48	0.01	0.04	0.00	0.15	0.00	0.00	0.00	0.00
Al2O3	0.18	1.06	0.00	6.39	0.01	0.04	0.00	0.24	0.00	0.00	0.00	0.00	0.00	0.00	0.00	0.01
MgO	0.14	0.75	0.00	4.50	0.02	0.03	0.00	0.21	0.01	0.00	0.00	0.02	0.01	0.01	0.00	0.02
P2O5	40.69	6.97	0.12	42.70	42.24	0.48	40.71	43.11	42.55	0.44	41.80	43.20	42.63	0.43	41.60	43.35
SO2	0.02	0.03	0.00	0.07	0.02	0.03	0.00	0.08	0.05	0.04	0.00	0.11	0.01	0.02	0.00	0.05
CaO	53.22	9.10	0.21	56.10	55.25	0.73	53.34	57.80	55.22	0.66	53.53	56.39	55.89	0.63	54.97	57.58
TiO2	0.02	0.11	0.00	0.64	0.00	0.00	0.00	0.00	0.00	0.00	0.00	0.00	0.00	0.00	0.00	0.00
MnO	0.00	0.00	0.00	0.00	0.00	0.02	0.00	0.09	0.00	0.00	0.00	0.00	0.00	0.00	0.00	0.00
Fe2O3	0.37	2.02	0.00	12.15	0.06	0.10	0.00	0.44	0.19	0.18	0.00	0.65	0.05	0.08	0.00	0.31
As2O3	0.00	0.02	0.00	0.14	0.00	0.00	0.00	0.00	0.00	0.00	0.00	0.00	0.00	0.00	0.00	0.00
SrO	0.03	0.17	0.00	1.04	0.01	0.01	0.00	0.04	0.00	0.00	0.00	0.00	0.00	0.01	0.00	0.02
Y2O3	0.12	0.07	0.00	0.25	0.07	0.07	0.00	0.22	0.00	0.00	0.00	0.00	0.00	0.00	0.00	0.00
La2O3	0.00	0.00	0.00	0.00	0.00	0.00	0.00	0.00	0.00	0.00	0.00	0.00	0.00	0.00	0.00	0.00
Ce2O3	0.08	0.09	0.00	0.26	0.02	0.05	0.00	0.27	0.00	0.00	0.00	0.00	0.00	0.00	0.00	0.00
Nd2O3	0.04	0.06	0.00	0.16	0.01	0.04	0.00	0.26	0.00	0.00	0.00	0.00	0.00	0.00	0.00	0.00
-O equivalent	-1.20	0.17	-1.38	-0.25	-1.35	0.14	-1.59	-0.63	-1.41	0.05	-1.55	-1.33	-1.59	0.04	-1.67	-1.51
Total	**99.4**	**0.9**	**95.8**	**101.1**	**100.1**	**0.8**	**98.3**	**102.3**	**100.2**	**0.9**	**98.3**	**101.8**	**100.9**	**0.7**	**99.2**	**102.8**
Calculated formulae 9 a.p.f.u.																
Ca	4.711	0.806	0.017	4.941	4.831	0.079	4.744	5.258	4.803	0.039	4.718	4.878	4.801	0.044	4.714	4.899
Mg	0.016	0.083	0.000	0.497	0.002	0.004	0.000	0.025	0.001	0.001	0.000	0.002	0.001	0.001	0.000	0.002
Mn	0.000	0.000	0.000	0.000	0.000	0.001	0.000	0.006	0.000	0.000	0.000	0.000	0.000	0.000	0.000	0.000
Sr	0.001	0.007	0.000	0.044	0.001	0.001	0.000	0.002	0.000	0.000	0.000	0.000	0.000	0.000	0.000	0.001
Y	0.005	0.003	0.000	0.011	0.003	0.003	0.000	0.010	0.000	0.000	0.000	0.000	0.000	0.000	0.000	0.000
La	0.000	0.000	0.000	0.000	0.000	0.000	0.000	0.000	0.000	0.000	0.000	0.000	0.000	0.000	0.000	0.000
Ce	0.002	0.003	0.000	0.008	0.001	0.002	0.000	0.008	0.000	0.000	0.000	0.000	0.000	0.000	0.000	0.000
Nd	0.001	0.002	0.000	0.005	0.000	0.001	0.000	0.008	0.000	0.000	0.000	0.000	0.000	0.000	0.000	0.000
Na	0.002	0.002	0.000	0.009	0.001	0.002	0.000	0.007	0.002	0.003	0.000	0.008	0.002	0.003	0.000	0.007
Fe	0.021	0.113	0.000	0.677	0.004	0.006	0.000	0.027	0.011	0.011	0.000	0.040	0.003	0.005	0.000	0.019
Ti	0.001	0.006	0.000	0.036	0.000	0.000	0.000	0.000	0.000	0.000	0.000	0.000	0.000	0.000	0.000	0.000
Al	0.016	0.093	0.000	0.558	0.001	0.003	0.000	0.022	0.000	0.000	0.000	0.000	0.000	0.000	0.000	0.001
Total	**4.776**	**0.507**	**1.828**	**4.941**	**4.843**	**0.079**	**4.753**	**5.270**	**4.817**	**0.040**	**4.719**	**4.894**	**4.807**	**0.045**	**4.715**	**4.907**
ΣREY	**0.009**	**0.006**	**0.000**	**0.018**	**0.004**	**0.005**	**0.000**	**0.025**	**0.000**	**0.000**	**0.000**	**0.000**	**0.000**	**0.000**	**0.000**	**0.000**
P	2.845	0.487	0.008	2.983	2.918	0.016	2.883	2.958	2.924	0.022	2.880	2.965	2.894	0.019	2.862	2.927
S	0.002	0.002	0.000	0.005	0.002	0.002	0.000	0.006	0.004	0.003	0.000	0.009	0.000	0.001	0.000	0.004
As	0.000	0.001	0.000	0.006	0.000	0.000	0.000	0.000	0.000	0.000	0.000	0.000	0.000	0.000	0.000	0.000
Si	0.168	0.858	0.000	5.175	0.013	0.011	0.000	0.040	0.001	0.003	0.000	0.012	0.000	0.000	0.000	0.000
Total	**3.016**	**0.373**	**2.920**	**5.189**	**2.933**	**0.019**	**2.894**	**2.972**	**2.929**	**0.022**	**2.884**	**2.965**	**2.894**	**0.019**	**2.863**	**2.927**
F	0.577	0.102	0.039	0.681	0.730	0.085	0.347	0.926	0.787	0.034	0.737	0.877	0.915	0.025	0.873	0.985
Cl	0.170	0.028	0.096	0.213	0.099	0.023	0.035	0.130	0.071	0.007	0.052	0.081	0.042	0.006	0.025	0.059
(F+Cl)	0.746	0.109	0.140	0.847	0.829	0.079	0.401	0.962	0.859	0.032	0.813	0.946	0.957	0.024	0.913	1.010
OH (by difference)	0.254	0.109	0.153	0.860	0.171	0.079	0.038	0.599	0.141	0.032	0.054	0.187	0.043	0.024	-0.010	0.087
Total	**1.000**				**1.000**				**1.000**				**1.000**			

Profiles	**Jt7 - grain 3**				**Jt7 - grain 6**			
	Mean	**SD**	**Min**	**Max**	**Mean**	**SD**	**Min**	**Max**
F	2.68	0.16	2.36	3.24	3.17	0.17	2.86	3.55
Cl	0.83	0.10	0.56	1.06	0.59	0.12	0.31	0.75
Na2O	0.02	0.02	0.00	0.09	0.02	0.03	0.00	0.16
SiO2	0.26	0.32	0.00	1.97	0.21	1.06	0.00	6.85
Al2O3	0.01	0.06	0.00	0.40	0.02	0.11	0.00	0.71
MgO	0.02	0.06	0.00	0.33	0.03	0.11	0.00	0.73
P2O5	41.99	0.63	39.27	42.90	42.44	0.95	37.34	43.41
SO2	0.01	0.02	0.00	0.08	0.01	0.02	0.00	0.10
CaO	54.85	0.85	50.93	55.95	55.32	1.25	48.48	57.44
TiO2	0.00	0.00	0.00	0.00	0.00	0.00	0.00	0.00
MnO	0.00	0.00	0.00	0.00	0.00	0.00	0.00	0.00
Fe2O3	0.07	0.28	0.00	1.68	0.19	0.75	0.00	4.82
As2O3	0.00	0.00	0.00	0.00	0.00	0.00	0.00	0.00
SrO	0.00	0.00	0.00	0.00	0.00	0.02	0.00	0.10
Y2O3	0.05	0.07	0.00	0.25	0.00	0.02	0.00	0.08
La2O3	0.00	0.00	0.00	0.00	0.00	0.00	0.00	0.00
Ce2O3	0.05	0.08	0.00	0.26	0.00	0.00	0.00	0.00
Nd2O3	0.01	0.03	0.00	0.12	0.00	0.02	0.00	0.12
-O equivalent	-1.32	0.06	-1.49	-1.17	-1.47	0.06	-1.61	-1.32
Total	**99.5**	**0.8**	**96.6**	**100.9**	**100.5**	**0.8**	**98.7**	**102.2**
Calculated formulae 9 a.p.f.u.								
Ca	4.826	0.057	4.620	4.920	4.791	0.112	4.152	4.929
Mg	0.003	0.007	0.000	0.042	0.004	0.013	0.000	0.086
Mn	0.000	0.000	0.000	0.000	0.000	0.000	0.000	0.000
Sr	0.000	0.000	0.000	0.000	0.000	0.001	0.000	0.005
Y	0.002	0.003	0.000	0.011	0.000	0.001	0.000	0.003
La	0.000	0.000	0.000	0.000	0.000	0.000	0.000	0.000
Ce	0.002	0.002	0.000	0.008	0.000	0.000	0.000	0.000
Nd	0.000	0.001	0.000	0.004	0.000	0.001	0.000	0.003
Na	0.002	0.003	0.000	0.014	0.003	0.005	0.000	0.025
Fe	0.005	0.018	0.000	0.107	0.011	0.045	0.000	0.290
Ti	0.000	0.000	0.000	0.000	0.000	0.000	0.000	0.000
Al	0.001	0.006	0.000	0.040	0.002	0.010	0.000	0.067
Total	**4.836**	**0.055**	**4.662**	**4.950**	**4.797**	**0.098**	**4.254**	**4.932**
ΣREY	**0.004**	**0.005**	**0.000**	**0.015**	**0.000**	**0.001**	**0.000**	**0.003**
P	2.919	0.027	2.815	2.961	2.904	0.063	2.527	2.950
S	0.001	0.002	0.000	0.007	0.001	0.002	0.000	0.008
As	0.000	0.000	0.000	0.000	0.000	0.000	0.000	0.000
Si	0.022	0.027	0.000	0.166	0.016	0.085	0.000	0.547
Total	**2.942**	**0.020**	**2.901**	**2.982**	**2.921**	**0.032**	**2.871**	**3.082**
F	0.696	0.040	0.632	0.835	0.811	0.040	0.741	0.912
Cl	0.115	0.014	0.077	0.148	0.081	0.017	0.042	0.102
(F+Cl)	0.811	0.033	0.746	0.911	0.891	0.032	0.790	0.973
OH (by difference)	0.189	0.033	0.089	0.254	0.109	0.032	0.027	0.210
Total	**1.000**				**1.000**			

Supplementary Table 1B. Complete data set of EPMA data for apatite

Sample	Jt1																			
Point	1	2	3	4	1	2	3	4	5	6	7	8	9	10	11	12	1	2	3	4
Grain	JT1 Ap1				JT1 Ap2												JT1 Ap3			
F	2.44	2.42	2.38	2.04	2.35	2.18	2.27	2.26	2.03	2.15	2.62	2.23	2.22	2.29	2.46	2.16	2.18	2.33	2.80	2.86
Cl	0.96	1.16	1.30	1.38	1.31	1.46	1.37	1.15	1.38	1.32	0.89	1.26	1.31	1.20	1.13	1.25	1.31	1.23	0.73	0.75
Na2O	0.05	0.00	0.02	0.02	0.00	0.02	0.00	0.02	0.00	0.00	0.02	0.00	0.05	0.00	0.00	0.02	0.00	0.00	0.00	0.00
SiO2	0.29	0.13	0.53	0.58	0.15	0.34	0.37	0.16	0.36	0.24	0.00	0.31	0.43	0.09	0.09	0.18	0.40	0.36	0.00	0.06
Al2O3	0.00	0.00	0.00	0.00	0.00	0.00	0.00	0.00	0.00	0.00	0.00	0.00	0.00	0.00	0.00	0.00	0.00	0.00	0.00	0.00
MgO	0.02	0.02	0.01	0.01	0.00	0.01	0.01	0.01	0.02	0.01	0.01	0.01	0.00	0.02	0.00	0.02	0.01	0.02	0.00	0.01
P2O5	42.13	41.77	41.83	40.93	42.00	42.97	41.96	42.66	41.80	42.42	42.16	41.76	41.79	42.41	42.34	41.69	42.12	41.79	43.28	42.55
SO2	0.05	0.00	0.05	0.00	0.00	0.00	0.00	0.00	0.00	0.00	0.00	0.00	0.00	0.00	0.00	0.00	0.00	0.00	0.00	0.00
CaO	54.61	54.82	53.82	54.60	54.63	54.69	54.73	54.17	54.90	54.28	55.52	54.93	54.21	55.51	56.25	55.55	56.21	55.23	55.80	56.83
TiO2	0.00	0.00	0.00	0.00	0.00	0.00	0.00	0.00	0.00	0.00	0.00	0.00	0.00	0.00	0.00	0.00	0.00	0.00	0.00	0.00
MnO	0.00	0.00	0.00	0.00	0.00	0.00	0.00	0.00	0.00	0.00	0.00	0.00	0.00	0.00	0.00	0.00	0.00	0.00	0.00	0.00
Fe2O3	0.00	0.00	0.00	0.00	0.00	0.00	0.00	0.00	0.00	0.00	0.00	0.00	0.00	0.12	0.00	0.00	0.00	0.09	0.00	0.00
As2O3	0.00	0.00	0.00	0.00	0.00	0.00	0.00	0.00	0.00	0.00	0.00	0.00	0.00	0.00	0.00	0.00	0.00	0.00	0.00	0.00
SrO	0.00	0.00	0.02	0.00	0.00	0.00	0.00	0.00	0.00	0.00	0.00	0.00	0.00	0.00	0.00	0.00	0.00	0.00	0.03	0.00
Y2O3	0.11	0.00	0.09	0.16	0.10	0.12	0.21	0.00	0.06	0.00	0.00	0.10	0.15	0.00	0.00	0.08	0.13	0.00	0.00	0.00
La2O3	0.00	0.00	0.09	0.11	0.00	0.00	0.00	0.00	0.00	0.00	0.00	0.00	0.00	0.00	0.00	0.00	0.00	0.00	0.00	0.00
Ce2O3	0.10	0.14	0.39	0.35	0.00	0.00	0.00	0.00	0.18	0.08	0.00	0.09	0.20	0.00	0.00	0.00	0.11	0.18	0.00	0.00
Nd2O3	0.17	0.13	0.20	0.13	0.00	0.00	0.00	0.00	0.00	0.00	0.00	0.00	0.00	0.00	0.00	0.00	0.00	0.00	0.00	0.00
-O equivalent	-1.25	-1.28	-1.30	-1.17	-1.28	-1.25	-1.26	-1.21	-1.17	-1.20	-1.30	-1.22	-1.23	-1.24	-1.29	-1.19	-1.22	-1.26	-1.35	-1.37
Total	**99.7**	**99.3**	**99.4**	**99.1**	**99.3**	**100.5**	**99.7**	**99.2**	**99.5**	**99.3**	**99.9**	**99.5**	**99.1**	**100.4**	**101.0**	**99.8**	**101.3**	**100.0**	**101.3**	**101.7**

Calculated formulae 9 a.p.f.u.

Sample	Jt1																			
Point	1	2	3	4	1	2	3	4	5	6	7	8	9	10	11	12	1	2	3	4
Grain	JT1 Ap1				JT1 Ap2												JT1 Ap3			
Ca	4.813	4.857	4.757	4.890	4.833	4.769	4.829	4.782	4.873	4.800	4.878	4.867	4.812	4.867	4.904	4.923	4.909	4.868	4.813	4.905
Mg	0.002	0.002	0.001	0.001	0.000	0.002	0.001	0.002	0.002	0.002	0.001	0.001	0.000	0.002	0.000	0.002	0.001	0.002	0.000	0.001
Mn	0.000	0.000	0.000	0.000	0.000	0.000	0.000	0.000	0.000	0.000	0.000	0.000	0.000	0.000	0.000	0.000	0.000	0.000	0.000	0.000
Sr	0.000	0.000	0.001	0.000	0.000	0.000	0.000	0.000	0.000	0.000	0.000	0.000	0.000	0.000	0.000	0.000	0.000	0.000	0.001	0.000
Y	0.005	0.000	0.004	0.007	0.004	0.005	0.009	0.000	0.003	0.000	0.000	0.004	0.007	0.000	0.000	0.003	0.006	0.000	0.000	0.000
La	0.000	0.000	0.003	0.003	0.000	0.000	0.000	0.000	0.000	0.000	0.000	0.000	0.000	0.000	0.000	0.000	0.000	0.000	0.000	0.000
Ce	0.003	0.004	0.012	0.011	0.000	0.000	0.000	0.000	0.005	0.003	0.000	0.003	0.006	0.000	0.000	0.000	0.003	0.005	0.000	0.000
Nd	0.005	0.004	0.006	0.004	0.000	0.000	0.000	0.000	0.000	0.000	0.000	0.000	0.000	0.000	0.000	0.000	0.000	0.000	0.000	0.000
Na	0.008	0.000	0.003	0.003	0.000	0.003	0.000	0.003	0.000	0.000	0.003	0.000	0.007	0.000	0.000	0.004	0.000	0.000	0.000	0.000
Fe	0.000	0.000	0.000	0.000	0.000	0.000	0.000	0.000	0.000	0.000	0.000	0.000	0.000	0.007	0.000	0.000	0.000	0.005	0.000	0.000
Ti	0.000	0.000	0.000	0.000	0.000	0.000	0.000	0.000	0.000	0.000	0.000	0.000	0.000	0.000	0.000	0.000	0.000	0.000	0.000	0.000
Al	0.000	0.000	0.000	0.000	0.000	0.000	0.000	0.000	0.000	0.000	0.000	0.000	0.000	0.000	0.000	0.000	0.000	0.000	0.000	0.000
Total	**4.836**	**4.867**	**4.787**	**4.919**	**4.837**	**4.779**	**4.839**	**4.786**	**4.882**	**4.804**	**4.882**	**4.875**	**4.832**	**4.876**	**4.904**	**4.932**	**4.919**	**4.881**	**4.814**	**4.906**
SREY	**0.013**	**0.008**	**0.025**	**0.025**	**0.004**	**0.005**	**0.009**	**0.000**	**0.008**	**0.003**	**0.000**	**0.007**	**0.013**	**0.000**	**0.000**	**0.003**	**0.009**	**0.005**	**0.000**	**0.000**
P	2.934	2.925	2.922	2.896	2.936	2.961	2.925	2.975	2.931	2.964	2.927	2.924	2.931	2.938	2.917	2.919	2.907	2.911	2.949	2.902
S	0.004	0.000	0.004	0.000	0.000	0.000	0.000	0.000	0.000	0.000	0.000	0.000	0.000	0.000	0.000	0.000	0.000	0.000	0.000	0.000
As	0.000	0.000	0.000	0.000	0.000	0.000	0.000	0.000	0.000	0.000	0.000	0.000	0.000	0.000	0.000	0.000	0.000	0.000	0.000	0.000
Si	0.024	0.011	0.043	0.048	0.012	0.027	0.030	0.013	0.030	0.020	0.000	0.026	0.036	0.007	0.007	0.015	0.032	0.030	0.000	0.005
Total	**2.962**	**2.936**	**2.969**	**2.944**	**2.948**	**2.988**	**2.956**	**2.989**	**2.961**	**2.983**	**2.927**	**2.950**	**2.967**	**2.946**	**2.924**	**2.934**	**2.939**	**2.940**	**2.949**	**2.906**
F	0.636	0.632	0.621	0.538	0.613	0.561	0.590	0.589	0.532	0.561	0.678	0.584	0.581	0.593	0.633	0.564	0.563	0.607	0.713	0.728
Cl	0.134	0.163	0.182	0.195	0.183	0.201	0.192	0.160	0.193	0.184	0.123	0.176	0.185	0.166	0.156	0.176	0.181	0.171	0.100	0.103
(F+Cl)	0.770	0.795	0.803	0.733	0.796	0.762	0.782	0.750	0.726	0.745	0.801	0.760	0.766	0.760	0.788	0.740	0.744	0.778	0.813	0.831
OH (by difference)	0.230	0.205	0.197	0.267	0.204	0.238	0.218	0.250	0.274	0.255	0.199	0.240	0.234	0.240	0.212	0.260	0.256	0.222	0.187	0.169
Total	**1.000**	**1.000**	**1.000**	**1.000**	**1.000**	**1.000**	**1.000**	**1.000**	**1.000**	**1.000**	**1.000**	**1.000**	**1.000**	**1.000**	**1.000**	**1.000**	**1.000**	**1.000**	**1.000**	**1.000**

Sample																							
Point	1	2	3	4	5	1	2	3	4	1	2	3	4	5	1	2	3	4	5	1	2	3	4
Grain	JT1 Ap4					JT1 Ap5				JT1 Ap6					JT1 Ap7					JT1 Ap8			
F	2.51	2.36	2.39	2.13	2.05	2.56	2.32	2.63	2.45	2.48	2.55	2.54	2.53	2.59	2.17	2.44	2.44	2.54	2.67	2.39	2.27	2.62	2.72
Cl	0.87	0.99	1.02	1.39	1.39	1.03	1.06	0.87	0.97	0.63	0.74	0.96	0.99	1.00	0.80	0.93	0.82	0.82	0.72	1.14	1.21	0.93	0.86
Na2O	0.00	0.02	0.00	0.03	0.03	0.00	0.05	0.00	0.04	0.02	0.00	0.00	0.00	0.06	0.00	0.02	0.00	0.00	0.00	0.04	0.00	0.00	0.04
SiO2	0.00	0.00	0.00	0.44	0.50	0.35	0.46	0.00	0.43	0.00	0.00	0.54	0.60	0.56	0.00	0.00	0.00	0.00	0.00	0.49	0.48	0.16	0.27
Al2O3	0.00	0.00	0.00	0.00	0.00	0.00	0.00	0.00	0.00	0.00	0.00	0.00	0.00	0.00	0.00	0.00	0.00	0.00	0.00	0.00	0.00	0.00	0.00
MgO	0.00	0.02	0.01	0.01	0.02	0.02	0.01	0.01	0.02	0.03	0.01	0.01	0.02	0.01	0.01	0.01	0.02	0.01	0.01	0.01	0.00	0.01	0.02
P2O5	42.83	42.82	42.82	41.68	41.47	41.39	42.23	42.40	41.71	42.53	42.76	41.64	41.47	41.86	42.60	42.01	42.44	42.11	43.01	42.01	41.06	42.11	42.12
SO2	0.00	0.00	0.00	0.00	0.00	0.08	0.05	0.07	0.06	0.00	0.00	0.00	0.00	0.00	0.00	0.00	0.00	0.00	0.00	0.00	0.00	0.00	0.05
CaO	54.17	55.98	55.31	53.64	53.46	54.43	53.74	54.98	54.05	56.20	55.45	54.57	54.63	54.48	56.03	56.10	54.93	54.87	55.12	55.10	54.33	54.64	55.18
TiO2	0.00	0.00	0.00	0.00	0.00	0.00	0.00	0.00	0.00	0.00	0.00	0.00	0.00	0.00	0.00	0.00	0.00	0.00	0.00	0.00	0.00	0.00	0.00
MnO	0.00	0.00	0.00	0.00	0.00	0.00	0.00	0.00	0.00	0.00	0.00	0.00	0.00	0.00	0.06	0.00	0.00	0.00	0.00	0.00	0.00	0.00	0.00
Fe2O3	0.13	0.00	0.00	0.08	0.00	0.00	0.00	0.00	0.00	0.00	0.11	0.00	0.00	0.00	0.00	0.11	0.00	0.16	0.00	0.00	0.13	0.00	0.00
As2O3	0.00	0.00	0.00	0.00	0.00	0.00	0.00	0.00	0.00	0.00	0.00	0.00	0.00	0.00	0.00	0.00	0.00	0.00	0.00	0.00	0.00	0.00	0.00
SrO	0.00	0.00	0.00	0.00	0.00	0.00	0.00	0.00	0.00	0.00	0.00	0.00	0.00	0.00	0.00	0.00	0.00	0.00	0.00	0.00	0.00	0.03	0.00
Y2O3	0.00	0.00	0.00	0.00	0.00	0.21	0.09	0.00	0.17	0.00	0.00	0.10	0.08	0.00	0.00	0.00	0.00	0.00	0.00	0.19	0.18	0.08	0.18
La2O3	0.00	0.00	0.00	0.00	0.10	0.00	0.11	0.00	0.00	0.00	0.00	0.11	0.07	0.08	0.00	0.00	0.00	0.00	0.00	0.00	0.00	0.00	0.00
Ce2O3	0.00	0.00	0.00	0.24	0.39	0.10	0.40	0.00	0.21	0.00	0.00	0.46	0.58	0.45	0.00	0.00	0.00	0.00	0.00	0.29	0.20	0.00	0.08
Nd2O3	0.00	0.00	0.00	0.00	0.21	0.00	0.23	0.00	0.00	0.00	0.00	0.26	0.28	0.12	0.00	0.00	0.00	0.00	0.00	0.12	0.00	0.00	0.00
-O equivalent	-1.25	-1.22	-1.24	-1.21	-1.18	-1.31	-1.22	-1.30	-1.25	-1.19	-1.24	-1.28	-1.29	-1.32	-1.10	-1.24	-1.21	-1.25	-1.29	-1.26	-1.23	-1.31	-1.34
Total	**99.3**	**101.0**	**100.3**	**98.4**	**98.4**	**98.9**	**99.5**	**99.7**	**98.8**	**100.7**	**100.4**	**99.9**	**99.9**	**99.9**	**100.6**	**100.4**	**99.4**	**99.2**	**100.2**	**100.5**	**98.6**	**99.3**	**100.2**

Calculated formulae 9 a.p.f.u.

Sample																							
Point	1	2	3	4	5	1	2	3	4	1	2	3	4	5	1	2	3	4	5	1	2	3	4
Grain	JT1 Ap4					JT1 Ap5				JT1 Ap6					JT1 Ap7					JT1 Ap8			
Ca	4.768	4.879	4.839	4.791	4.794	4.833	4.748	4.829	4.800	4.917	4.846	4.815	4.823	4.790	4.924	4.931	4.848	4.852	4.806	4.832	4.860	4.818	4.827
Mg	0.000	0.002	0.001	0.002	0.002	0.002	0.001	0.001	0.002	0.003	0.001	0.002	0.002	0.001	0.002	0.002	0.002	0.001	0.001	0.001	0.000	0.002	0.002
Mn	0.000	0.000	0.000	0.000	0.000	0.000	0.000	0.000	0.000	0.000	0.000	0.000	0.000	0.000	0.004	0.000	0.000	0.000	0.000	0.000	0.000	0.000	0.000
Sr	0.000	0.000	0.000	0.000	0.000	0.000	0.000	0.000	0.000	0.000	0.000	0.000	0.000	0.000	0.000	0.000	0.000	0.000	0.000	0.000	0.000	0.002	0.000
Y	0.000	0.000	0.000	0.000	0.000	0.009	0.004	0.000	0.007	0.000	0.000	0.004	0.003	0.000	0.000	0.000	0.000	0.000	0.000	0.008	0.008	0.004	0.008
La	0.000	0.000	0.000	0.000	0.003	0.000	0.003	0.000	0.000	0.000	0.000	0.003	0.002	0.002	0.000	0.000	0.000	0.000	0.000	0.000	0.000	0.000	0.000
Ce	0.000	0.000	0.000	0.007	0.012	0.003	0.012	0.000	0.006	0.000	0.000	0.014	0.018	0.014	0.000	0.000	0.000	0.000	0.000	0.009	0.006	0.000	0.002
Nd	0.000	0.000	0.000	0.000	0.006	0.000	0.007	0.000	0.000	0.000	0.000	0.008	0.008	0.003	0.000	0.000	0.000	0.000	0.000	0.003	0.000	0.000	0.000
Na	0.000	0.003	0.000	0.005	0.005	0.000	0.008	0.000	0.006	0.003	0.000	0.000	0.000	0.010	0.000	0.004	0.000	0.000	0.000	0.006	0.000	0.000	0.006
Fe	0.008	0.000	0.000	0.005	0.000	0.000	0.000	0.000	0.000	0.000	0.007	0.000	0.000	0.000	0.000	0.007	0.000	0.010	0.000	0.000	0.008	0.000	0.000
Ti	0.000	0.000	0.000	0.000	0.000	0.000	0.000	0.000	0.000	0.000	0.000	0.000	0.000	0.000	0.000	0.000	0.000	0.000	0.000	0.000	0.000	0.000	0.000
Al	0.000	0.000	0.000	0.000	0.000	0.000	0.000	0.000	0.000	0.000	0.000	0.000	0.000	0.000	0.000	0.000	0.000	0.000	0.000	0.000	0.000	0.000	0.000
Total	**4.776**	**4.885**	**4.840**	**4.811**	**4.822**	**4.847**	**4.784**	**4.830**	**4.822**	**4.923**	**4.854**	**4.845**	**4.856**	**4.821**	**4.930**	**4.943**	**4.850**	**4.863**	**4.807**	**4.859**	**4.882**	**4.825**	**4.845**
SREY	**0.000**	**0.000**	**0.000**	**0.007**	**0.021**	**0.012**	**0.026**	**0.000**	**0.014**	**0.000**	**0.000**	**0.029**	**0.031**	**0.019**	**0.000**	**0.000**	**0.000**	**0.000**	**0.000**	**0.020**	**0.014**	**0.004**	**0.010**
P	2.979	2.949	2.961	2.941	2.938	2.904	2.949	2.943	2.927	2.940	2.953	2.903	2.893	2.908	2.958	2.918	2.960	2.942	2.963	2.911	2.902	2.934	2.912
S	0.000	0.000	0.000	0.000	0.000	0.006	0.004	0.006	0.004	0.000	0.000	0.000	0.000	0.000	0.000	0.000	0.000	0.000	0.000	0.000	0.000	0.000	0.004
As	0.000	0.000	0.000	0.000	0.000	0.000	0.000	0.000	0.000	0.000	0.000	0.000	0.000	0.000	0.000	0.000	0.000	0.000	0.000	0.000	0.000	0.000	0.000
Si	0.000	0.000	0.000	0.037	0.042	0.029	0.038	0.000	0.036	0.000	0.000	0.044	0.049	0.046	0.000	0.000	0.000	0.000	0.000	0.040	0.040	0.013	0.022
Total	**2.979**	**2.949**	**2.961**	**2.978**	**2.980**	**2.939**	**2.990**	**2.948**	**2.966**	**2.940**	**2.953**	**2.947**	**2.942**	**2.954**	**2.958**	**2.918**	**2.960**	**2.942**	**2.963**	**2.951**	**2.942**	**2.947**	**2.937**
F	0.652	0.607	0.617	0.563	0.543	0.672	0.605	0.681	0.642	0.641	0.658	0.660	0.659	0.673	0.563	0.632	0.636	0.662	0.687	0.618	0.600	0.682	0.703
Cl	0.121	0.137	0.141	0.196	0.197	0.145	0.148	0.120	0.136	0.088	0.102	0.134	0.138	0.139	0.112	0.129	0.114	0.114	0.099	0.157	0.171	0.130	0.119
(F+Cl)	0.773	0.744	0.757	0.759	0.740	0.817	0.753	0.802	0.778	0.728	0.761	0.795	0.797	0.812	0.675	0.761	0.750	0.776	0.786	0.776	0.771	0.812	0.822
OH (by difference)	0.227	0.256	0.243	0.241	0.260	0.183	0.247	0.198	0.222	0.272	0.239	0.205	0.203	0.188	0.325	0.239	0.250	0.224	0.214	0.224	0.229	0.188	0.178
Total	**1.000**	**1.000**	**1.000**	**1.000**	**1.000**	**1.000**	**1.000**	**1.000**	**1.000**	**1.000**	**1.000**	**1.000**	**1.000**	**1.000**	**1.000**	**1.000**	**1.000**	**1.000**	**1.000**	**1.000**	**1.000**	**1.000**	**1.000**

Sample																					
Point	1	2	3	4	5	1	2	3	4	5	6	7	8	9	10	11	12	13	14	15	16
Grain	JT1 Ap9					JT1 Ap10															
F	2.54	2.70	2.48	2.43	2.48	2.51	2.35	2.87	2.66	2.45	2.56	2.71	2.55	2.98	2.71	2.64	2.90	2.45	2.73	2.78	2.63
Cl	0.97	0.80	1.04	1.15	1.14	0.79	1.28	0.67	0.70	1.10	0.90	0.78	0.89	0.65	0.95	0.91	0.68	0.93	0.76	0.65	0.95
Na2O	0.02	0.00	0.03	0.02	0.00	0.04	0.02	0.03	0.02	0.00	0.00	0.03	0.00	0.00	0.00	0.02	0.00	0.00	0.02	0.00	0.00
SiO2	0.00	0.00	0.00	0.00	0.00	0.00	0.45	0.00	1.17	0.25	0.00	0.03	0.00	0.00	0.00	0.00	1.22	0.00	0.00	0.00	0.00
Al2O3	0.00	0.00	0.00	0.00	0.00	0.00	0.00	0.00	0.28	0.00	0.00	0.00	0.00	0.00	0.00	0.00	0.30	0.00	0.00	0.00	0.00
MgO	0.01	0.01	0.01	0.00	0.00	0.01	0.00	0.00	0.41	0.01	0.00	0.01	0.00	0.01	0.01	0.01	0.37	0.01	0.00	0.01	0.00
P2O5	42.83	42.92	41.95	41.71	43.00	42.49	41.04	42.76	40.06	41.95	42.58	42.78	42.89	42.01	41.24	42.26	40.56	42.92	42.82	42.72	42.48
SO2	0.00	0.00	0.00	0.00	0.00	0.00	0.00	0.00	0.00	0.00	0.00	0.00	0.00	0.00	0.00	0.00	0.00	0.00	0.00	0.00	0.00
CaO	55.59	54.88	54.31	55.37	54.96	55.77	54.48	55.18	53.00	54.52	55.22	55.54	55.05	55.45	55.66	55.03	52.84	55.12	54.89	54.72	55.30
TiO2	0.00	0.00	0.00	0.00	0.00	0.00	0.00	0.00	0.00	0.00	0.00	0.00	0.00	0.00	0.00	0.00	0.00	0.00	0.00	0.00	0.00
MnO	0.00	0.00	0.00	0.00	0.00	0.00	0.00	0.00	0.00	0.00	0.00	0.00	0.00	0.00	0.00	0.00	0.00	0.00	0.00	0.00	0.00
Fe2O3	0.00	0.17	0.00	0.00	0.00	0.00	0.00	0.00	0.76	0.00	0.20	0.12	0.00	0.00	0.00	0.00	0.62	0.00	0.00	0.00	0.00
As2O3	0.00	0.00	0.00	0.00	0.00	0.00	0.00	0.00	0.00	0.00	0.00	0.00	0.00	0.00	0.00	0.00	0.00	0.00	0.00	0.00	0.00
SrO	0.00	0.00	0.00	0.00	0.00	0.00	0.00	0.00	0.04	0.00	0.00	0.00	0.00	0.00	0.00	0.00	0.03	0.00	0.00	0.00	0.02
Y2O3	0.00	0.00	0.00	0.00	0.00	0.00	0.06	0.00	0.00	0.12	0.00	0.00	0.00	0.00	0.00	0.00	0.00	0.00	0.00	0.00	0.00
La2O3	0.00	0.00	0.00	0.00	0.00	0.00	0.00	0.00	0.00	0.00	0.00	0.00	0.00	0.00	0.00	0.00	0.00	0.00	0.00	0.00	0.00
Ce2O3	0.00	0.00	0.00	0.00	0.00	0.00	0.24	0.00	0.00	0.00	0.00	0.00	0.00	0.00	0.00	0.00	0.00	0.00	0.00	0.00	0.00
Nd2O3	0.00	0.00	0.00	0.00	0.00	0.00	0.00	0.00	0.00	0.00	0.00	0.00	0.00	0.00	0.00	0.00	0.00	0.00	0.00	0.00	0.00
-O equivalent	-1.29	-1.32	-1.28	-1.28	-1.30	-1.24	-1.28	-1.36	-1.28	-1.28	-1.28	-1.32	-1.28	-1.40	-1.36	-1.32	-1.37	-1.24	-1.32	-1.32	-1.32
Total	**100.7**	**100.2**	**98.5**	**99.4**	**100.3**	**100.4**	**98.6**	**100.1**	**97.8**	**99.1**	**100.2**	**100.7**	**100.1**	**99.7**	**99.2**	**99.6**	**98.2**	**100.2**	**99.9**	**99.6**	**100.1**

Calculated formulae 9 a.p.f.u.

Sample																					
Point	1	2	3	4	5	1	2	3	4	5	6	7	8	9	10	11	12	13	14	15	16
Grain	JT1 Ap9					JT1 Ap10															
Ca	4.842	4.785	4.830	4.904	4.795	4.884	4.866	4.808	4.747	4.824	4.833	4.830	4.812	4.862	4.934	4.841	4.687	4.822	4.797	4.795	4.841
Mg	0.002	0.001	0.001	0.000	0.000	0.001	0.000	0.000	0.051	0.002	0.000	0.001	0.000	0.001	0.001	0.002	0.046	0.001	0.000	0.001	0.000
Mn	0.000	0.000	0.000	0.000	0.000	0.000	0.000	0.000	0.000	0.000	0.000	0.000	0.000	0.000	0.000	0.000	0.000	0.000	0.000	0.000	0.000
Sr	0.000	0.000	0.000	0.000	0.000	0.000	0.000	0.000	0.002	0.000	0.000	0.000	0.000	0.000	0.000	0.000	0.002	0.000	0.000	0.000	0.001
Y	0.000	0.000	0.000	0.000	0.000	0.000	0.003	0.000	0.000	0.005	0.000	0.000	0.000	0.000	0.000	0.000	0.000	0.000	0.000	0.000	0.000
La	0.000	0.000	0.000	0.000	0.000	0.000	0.000	0.000	0.000	0.000	0.000	0.000	0.000	0.000	0.000	0.000	0.000	0.000	0.000	0.000	0.000
Ce	0.000	0.000	0.000	0.000	0.000	0.000	0.007	0.000	0.000	0.000	0.000	0.000	0.000	0.000	0.000	0.000	0.000	0.000	0.000	0.000	0.000
Nd	0.000	0.000	0.000	0.000	0.000	0.000	0.000	0.000	0.000	0.000	0.000	0.000	0.000	0.000	0.000	0.000	0.000	0.000	0.000	0.000	0.000
Na	0.003	0.000	0.004	0.003	0.000	0.006	0.004	0.004	0.003	0.000	0.000	0.004	0.000	0.000	0.000	0.004	0.000	0.000	0.004	0.000	0.000
Fe	0.000	0.010	0.000	0.000	0.000	0.000	0.000	0.000	0.048	0.000	0.012	0.007	0.000	0.000	0.000	0.000	0.039	0.000	0.000	0.000	0.000
Ti	0.000	0.000	0.000	0.000	0.000	0.000	0.000	0.000	0.000	0.000	0.000	0.000	0.000	0.000	0.000	0.000	0.000	0.000	0.000	0.000	0.000
Al	0.000	0.000	0.000	0.000	0.000	0.000	0.000	0.000	0.028	0.000	0.000	0.000	0.000	0.000	0.000	0.000	0.029	0.000	0.000	0.000	0.000
Total	**4.846**	**4.797**	**4.835**	**4.908**	**4.795**	**4.891**	**4.880**	**4.812**	**4.878**	**4.831**	**4.846**	**4.842**	**4.812**	**4.863**	**4.935**	**4.847**	**4.803**	**4.823**	**4.801**	**4.796**	**4.842**
SREY	**0.000**	**0.000**	**0.000**	**0.000**	**0.000**	**0.000**	**0.010**	**0.000**	**0.000**	**0.005**	**0.000**	**0.000**	**0.000**	**0.000**	**0.000**	**0.000**	**0.000**	**0.000**	**0.000**	**0.000**	**0.000**
P	2.948	2.957	2.948	2.919	2.964	2.941	2.897	2.944	2.835	2.933	2.945	2.939	2.962	2.911	2.889	2.937	2.843	2.966	2.957	2.958	2.939
S	0.000	0.000	0.000	0.000	0.000	0.000	0.000	0.000	0.000	0.000	0.000	0.000	0.000	0.000	0.000	0.000	0.000	0.000	0.000	0.000	0.000
As	0.000	0.000	0.000	0.000	0.000	0.000	0.000	0.000	0.000	0.000	0.000	0.000	0.000	0.000	0.000	0.000	0.000	0.000	0.000	0.000	0.000
Si	0.000	0.000	0.000	0.000	0.000	0.000	0.038	0.000	0.098	0.021	0.000	0.002	0.000	0.000	0.000	0.000	0.101	0.000	0.000	0.000	0.000
Total	**2.948**	**2.957**	**2.948**	**2.919**	**2.964**	**2.941**	**2.934**	**2.944**	**2.933**	**2.953**	**2.945**	**2.942**	**2.962**	**2.911**	**2.889**	**2.937**	**2.944**	**2.966**	**2.957**	**2.958**	**2.939**
F	0.652	0.695	0.651	0.636	0.638	0.650	0.619	0.739	0.702	0.640	0.661	0.695	0.659	0.771	0.710	0.684	0.760	0.632	0.703	0.720	0.679
Cl	0.134	0.110	0.146	0.161	0.157	0.110	0.181	0.092	0.099	0.154	0.125	0.108	0.123	0.090	0.133	0.127	0.095	0.129	0.105	0.090	0.131
(F+Cl)	0.786	0.805	0.797	0.796	0.795	0.760	0.800	0.831	0.801	0.794	0.786	0.803	0.782	0.861	0.843	0.811	0.855	0.761	0.808	0.810	0.810
OH (by difference)	0.214	0.195	0.203	0.204	0.205	0.240	0.200	0.169	0.199	0.206	0.214	0.197	0.218	0.139	0.157	0.189	0.145	0.239	0.192	0.190	0.190
Total	**1.000**	**1.000**	**1.000**	**1.000**	**1.000**	**1.000**	**1.000**	**1.000**	**1.000**	**1.000**	**1.000**	**1.000**	**1.000**	**1.000**	**1.000**	**1.000**	**1.000**	**1.000**	**1.000**	**1.000**	**1.000**

Sample																								
Point	1	2	3	4	5	6	7	8	9	10	11	12	13	14	15	16	18	19	20	21	22	23	24	25
Grain	JT1 Ap11																							
F	2.22	2.44	2.26	2.38	2.34	2.29	2.30	2.22	2.09	2.26	2.17	2.65	2.76	2.63	2.37	2.39	2.26	2.58	2.15	2.35	2.24	2.40	2.29	2.22
Cl	1.21	0.85	1.35	1.17	1.22	1.16	1.16	1.14	1.34	1.29	1.37	0.81	0.88	0.97	1.16	1.11	1.14	1.14	1.19	1.07	1.23	1.09	1.11	1.19
Na2O	0.00	0.02	0.00	0.00	0.00	0.00	0.00	0.00	0.00	0.00	0.04	0.00	0.02	0.00	0.00	0.00	0.03	0.00	0.02	0.00	0.00	0.03	0.00	0.00
SiO2	0.00	0.10	0.14	0.00	0.00	0.00	0.00	0.00	0.37	0.19	0.36	0.00	0.00	0.00	0.00	0.00	0.00	0.00	0.00	0.00	0.00	0.00	0.00	0.00
Al2O3	0.00	0.00	0.00	0.00	0.00	0.00	0.00	0.00	0.00	0.00	0.00	0.00	0.00	0.00	0.00	0.00	0.00	0.00	0.00	0.00	0.00	0.00	0.00	0.00
MgO	0.01	0.00	0.01	0.01	0.01	0.02	0.02	0.00	0.00	0.00	0.01	0.00	0.01	0.00	0.01	0.01	0.01	0.00	0.02	0.00	0.00	0.01	0.00	0.01
P2O5	42.33	42.23	41.92	42.86	42.34	41.93	42.78	42.67	41.81	42.12	41.90	41.97	43.20	42.19	42.18	42.56	42.78	42.31	42.45	42.41	41.85	42.58	42.30	42.53
SO2	0.05	0.00	0.00	0.00	0.00	0.00	0.00	0.00	0.00	0.00	0.00	0.00	0.00	0.00	0.00	0.00	0.00	0.00	0.00	0.00	0.00	0.00	0.00	0.00
CaO	55.12	54.98	54.68	55.63	55.02	54.80	55.08	54.72	55.07	55.58	55.06	55.36	56.61	54.88	55.62	55.09	54.89	55.04	54.94	54.57	55.26	54.86	55.20	55.76
TiO2	0.00	0.00	0.00	0.00	0.00	0.00	0.00	0.00	0.00	0.00	0.00	0.00	0.00	0.00	0.00	0.00	0.00	0.00	0.00	0.00	0.00	0.00	0.00	0.00
MnO	0.00	0.00	0.00	0.00	0.00	0.00	0.00	0.00	0.00	0.00	0.00	0.00	0.00	0.00	0.00	0.00	0.00	0.00	0.00	0.00	0.00	0.00	0.00	0.00
Fe2O3	0.09	0.00	0.09	0.00	0.00	0.00	0.11	0.00	0.00	0.00	0.00	0.00	0.00	0.00	0.00	0.00	0.00	0.00	0.00	0.00	0.00	0.00	0.00	0.10
As2O3	0.00	0.00	0.00	0.00	0.00	0.00	0.00	0.00	0.00	0.00	0.00	0.00	0.00	0.00	0.00	0.00	0.00	0.00	0.00	0.00	0.00	0.00	0.00	0.00
SrO	0.00	0.00	0.00	0.02	0.00	0.00	0.00	0.00	0.00	0.00	0.00	0.00	0.02	0.00	0.00	0.00	0.00	0.00	0.00	0.00	0.00	0.00	0.00	0.00
Y2O3	0.00	0.05	0.00	0.00	0.00	0.00	0.00	0.00	0.00	0.00	0.07	0.00	0.00	0.00	0.00	0.00	0.00	0.00	0.00	0.00	0.00	0.00	0.00	0.00
La2O3	0.00	0.00	0.00	0.00	0.00	0.00	0.00	0.00	0.00	0.00	0.00	0.00	0.00	0.00	0.00	0.00	0.00	0.00	0.00	0.00	0.00	0.00	0.00	0.00
Ce2O3	0.00	0.00	0.00	0.00	0.00	0.00	0.00	0.00	0.11	0.00	0.07	0.00	0.00	0.00	0.00	0.00	0.00	0.00	0.00	0.00	0.00	0.00	0.00	0.00
Nd2O3	0.00	0.00	0.00	0.00	0.00	0.00	0.00	0.00	0.14	0.00	0.00	0.00	0.00	0.00	0.00	0.00	0.00	0.00	0.00	0.00	0.00	0.00	0.00	0.00
-O equivalent	-1.21	-1.22	-1.26	-1.27	-1.26	-1.23	-1.23	-1.19	-1.18	-1.24	-1.22	-1.30	-1.36	-1.33	-1.26	-1.26	-1.21	-1.35	-1.18	-1.23	-1.22	-1.26	-1.22	-1.20
Total	**99.8**	**99.5**	**99.2**	**100.8**	**99.7**	**99.0**	**100.2**	**99.6**	**99.7**	**100.2**	**99.8**	**99.5**	**102.2**	**99.3**	**100.1**	**99.9**	**99.9**	**99.7**	**99.6**	**99.2**	**99.4**	**99.7**	**99.7**	**100.6**

Calculated formulae 9 a.p.f.u.

Sample																								
Point	1	2	3	4	5	6	7	8	9	10	11	12	13	14	15	16	18	19	20	21	22	23	24	25
Grain	JT1 Ap11																							
Ca	4.860	4.855	4.847	4.848	4.849	4.871	4.826	4.827	4.878	4.887	4.862	4.884	4.856	4.836	4.893	4.839	4.824	4.832	4.856	4.826	4.905	4.824	4.872	4.887
Mg	0.002	0.000	0.002	0.002	0.001	0.002	0.002	0.000	0.000	0.000	0.001	0.000	0.001	0.000	0.001	0.001	0.001	0.000	0.002	0.000	0.000	0.001	0.000	0.001
Mn	0.000	0.000	0.000	0.000	0.000	0.000	0.000	0.000	0.000	0.000	0.000	0.000	0.000	0.000	0.000	0.000	0.000	0.000	0.000	0.000	0.000	0.000	0.000	0.000
Sr	0.000	0.000	0.000	0.001	0.000	0.000	0.000	0.000	0.000	0.000	0.000	0.000	0.001	0.000	0.000	0.000	0.000	0.000	0.000	0.000	0.000	0.000	0.000	0.000
Y	0.000	0.002	0.000	0.000	0.000	0.000	0.000	0.000	0.000	0.000	0.003	0.000	0.000	0.000	0.000	0.000	0.000	0.000	0.000	0.000	0.000	0.000	0.000	0.000
La	0.000	0.000	0.000	0.000	0.000	0.000	0.000	0.000	0.000	0.000	0.000	0.000	0.000	0.000	0.000	0.000	0.000	0.000	0.000	0.000	0.000	0.000	0.000	0.000
Ce	0.000	0.000	0.000	0.000	0.000	0.000	0.000	0.000	0.003	0.000	0.002	0.000	0.000	0.000	0.000	0.000	0.000	0.000	0.000	0.000	0.000	0.000	0.000	0.000
Nd	0.000	0.000	0.000	0.000	0.000	0.000	0.000	0.000	0.004	0.000	0.000	0.000	0.000	0.000	0.000	0.000	0.000	0.000	0.000	0.000	0.000	0.000	0.000	0.000
Na	0.000	0.003	0.000	0.000	0.000	0.000	0.000	0.000	0.000	0.000	0.006	0.000	0.004	0.000	0.000	0.000	0.004	0.000	0.003	0.000	0.000	0.005	0.000	0.000
Fe	0.006	0.000	0.006	0.000	0.000	0.000	0.007	0.000	0.000	0.000	0.000	0.000	0.000	0.000	0.000	0.000	0.000	0.000	0.000	0.000	0.000	0.000	0.000	0.006
Ti	0.000	0.000	0.000	0.000	0.000	0.000	0.000	0.000	0.000	0.000	0.000	0.000	0.000	0.000	0.000	0.000	0.000	0.000	0.000	0.000	0.000	0.000	0.000	0.000
Al	0.000	0.000	0.000	0.000	0.000	0.000	0.000	0.000	0.000	0.000	0.000	0.000	0.000	0.000	0.000	0.000	0.000	0.000	0.000	0.000	0.000	0.000	0.000	0.000
Total	**4.868**	**4.860**	**4.854**	**4.850**	**4.850**	**4.873**	**4.835**	**4.827**	**4.885**	**4.887**	**4.875**	**4.884**	**4.862**	**4.836**	**4.894**	**4.840**	**4.829**	**4.832**	**4.862**	**4.826**	**4.905**	**4.830**	**4.872**	**4.895**
SREY	**0.000**	**0.002**	**0.000**	**0.000**	**0.000**	**0.000**	**0.000**	**0.000**	**0.007**	**0.000**	**0.005**	**0.000**	**0.000**	**0.000**	**0.000**	**0.000**	**0.000**	**0.000**	**0.000**	**0.000**	**0.000**	**0.000**	**0.000**	**0.000**
P	2.950	2.947	2.936	2.951	2.949	2.945	2.962	2.974	2.926	2.927	2.923	2.925	2.928	2.938	2.932	2.955	2.971	2.936	2.965	2.964	2.935	2.959	2.950	2.945
S	0.004	0.000	0.000	0.000	0.000	0.000	0.000	0.000	0.000	0.000	0.000	0.000	0.000	0.000	0.000	0.000	0.000	0.000	0.000	0.000	0.000	0.000	0.000	0.000
As	0.000	0.000	0.000	0.000	0.000	0.000	0.000	0.000	0.000	0.000	0.000	0.000	0.000	0.000	0.000	0.000	0.000	0.000	0.000	0.000	0.000	0.000	0.000	0.000
Si	0.000	0.009	0.011	0.000	0.000	0.000	0.000	0.000	0.031	0.016	0.030	0.000	0.000	0.000	0.000	0.000	0.000	0.000	0.000	0.000	0.000	0.000	0.000	0.000
Total	**2.954**	**2.956**	**2.947**	**2.951**	**2.949**	**2.945**	**2.962**	**2.974**	**2.957**	**2.942**	**2.953**	**2.925**	**2.928**	**2.938**	**2.932**	**2.955**	**2.971**	**2.936**	**2.965**	**2.964**	**2.935**	**2.959**	**2.950**	**2.945**
F	0.579	0.636	0.591	0.611	0.608	0.602	0.596	0.579	0.547	0.586	0.566	0.689	0.699	0.685	0.614	0.620	0.587	0.670	0.561	0.614	0.587	0.624	0.597	0.574
Cl	0.168	0.119	0.189	0.162	0.171	0.163	0.161	0.158	0.188	0.179	0.191	0.114	0.119	0.135	0.161	0.154	0.159	0.159	0.167	0.150	0.172	0.152	0.155	0.165
(F+Cl)	0.747	0.755	0.780	0.773	0.778	0.765	0.756	0.737	0.735	0.765	0.757	0.803	0.819	0.819	0.775	0.774	0.746	0.829	0.728	0.764	0.759	0.776	0.752	0.739
OH (by difference)	0.253	0.245	0.220	0.227	0.222	0.235	0.244	0.263	0.265	0.235	0.243	0.197	0.181	0.181	0.225	0.226	0.254	0.171	0.272	0.236	0.241	0.224	0.248	0.261
Total	**1.000**	**1.000**	**1.000**	**1.000**	**1.000**	**1.000**	**1.000**	**1.000**	**1.000**	**1.000**	**1.000**	**1.000**	**1.000**	**1.000**	**1.000**	**1.000**	**1.000**	**1.000**	**1.000**	**1.000**	**1.000**	**1.000**	**1.000**	**1.000**

Sample												Jt4										
Point	1	2	3	4	5	7	1	2	3	4	5	2	3	4	1	2	3	1	2	3	4	5
Grain	JT1 Ap12						JT1 Ap13					JT4 Ap1			JT4 Ap2			JT4 Ap3				
F	2.17	2.15	2.24	2.21	2.19	2.32	2.49	2.80	2.55	3.08	2.64	3.19	2.94	3.24	3.26	2.95	3.15	3.14	3.12	3.33	3.14	3.50
Cl	1.19	1.28	1.33	1.27	1.17	1.16	0.72	0.68	0.84	0.66	0.92	0.43	0.64	0.40	0.37	0.66	0.53	0.39	0.57	0.49	0.61	0.37
Na2O	0.00	0.00	0.02	0.00	0.00	0.00	0.00	0.00	0.00	0.00	0.00	0.05	0.04	0.00	0.02	0.05	0.00	0.02	0.00	0.03	0.02	0.00
SiO2	0.00	0.00	0.00	0.00	0.00	0.00	0.00	0.00	0.00	0.00	0.00	0.02	0.25	0.00	0.00	0.48	0.00	0.00	0.00	0.14	0.29	0.00
Al2O3	0.00	0.00	0.00	0.00	0.00	0.00	0.00	0.00	0.00	0.00	0.00	0.00	0.00	0.00	0.00	0.00	0.00	0.00	0.00	0.00	0.00	0.00
MgO	0.01	0.01	0.01	0.02	0.00	0.02	0.02	0.01	0.00	0.00	0.01	0.01	0.01	0.01	0.01	0.01	0.02	0.02	0.01	0.00	0.01	0.01
P2O5	42.51	42.12	42.15	42.19	41.93	42.29	42.61	42.50	42.68	42.28	42.73	42.79	41.96	42.63	43.04	41.43	42.08	42.98	43.09	42.65	41.86	42.95
SO2	0.00	0.06	0.00	0.00	0.00	0.00	0.00	0.00	0.00	0.04	0.07	0.08	0.00	0.06	0.00	0.00	0.05	0.00	0.06	0.00	0.00	0.00
CaO	54.28	55.39	55.85	54.87	54.99	55.24	55.78	55.49	55.76	54.99	55.15	54.98	55.30	56.89	54.68	54.83	54.68	54.93	54.57	54.69	55.01	55.48
TiO2	0.00	0.00	0.00	0.00	0.00	0.00	0.00	0.00	0.00	0.00	0.00	0.00	0.00	0.00	0.00	0.00	0.00	0.00	0.00	0.00	0.00	0.00
MnO	0.00	0.00	0.00	0.00	0.00	0.00	0.08	0.00	0.00	0.00	0.00	0.00	0.00	0.00	0.00	0.00	0.00	0.00	0.00	0.00	0.00	0.00
Fe2O3	0.00	0.00	0.00	0.00	0.00	0.00	0.00	0.09	0.00	0.00	0.00	0.18	0.00	0.00	0.15	0.00	0.00	0.00	0.00	0.00	0.00	0.00
As2O3	0.00	0.00	0.00	0.00	0.00	0.00	0.00	0.00	0.00	0.00	0.00	0.00	0.00	0.00	0.00	0.00	0.00	0.00	0.00	0.00	0.00	0.00
SrO	0.00	0.00	0.00	0.00	0.00	0.00	0.00	0.00	0.00	0.00	0.00	0.00	0.00	0.00	0.00	0.00	0.00	0.00	0.00	0.00	0.00	0.00
Y2O3	0.00	0.00	0.00	0.00	0.00	0.00	0.00	0.00	0.00	0.00	0.00	0.00	0.21	0.00	0.00	0.29	0.00	0.00	0.00	0.10	0.29	0.00
La2O3	0.00	0.00	0.00	0.00	0.00	0.00	0.00	0.00	0.00	0.00	0.00	0.00	0.00	0.00	0.00	0.00	0.00	0.00	0.00	0.00	0.00	0.00
Ce2O3	0.00	0.00	0.00	0.00	0.00	0.00	0.00	0.00	0.00	0.00	0.00	0.00	0.00	0.00	0.00	0.16	0.00	0.00	0.00	0.00	0.00	0.00
Nd2O3	0.00	0.00	0.00	0.00	0.00	0.00	0.00	0.00	0.00	0.00	0.00	0.00	0.11	0.00	0.00	0.00	0.00	0.00	0.00	0.00	0.00	0.00
-O equivalent	-1.18	-1.19	-1.24	-1.21	-1.19	-1.24	-1.21	-1.33	-1.26	-1.45	-1.32	-1.44	-1.38	-1.45	-1.46	-1.39	-1.44	-1.41	-1.44	-1.51	-1.46	-1.56
Total	**99.0**	**99.8**	**100.4**	**99.3**	**99.1**	**99.8**	**100.5**	**100.2**	**100.6**	**99.6**	**100.2**	**100.3**	**100.1**	**101.8**	**100.1**	**99.5**	**99.1**	**100.1**	**100.0**	**99.9**	**99.8**	**100.7**

Calculated formulae 9 a.p.f.u.

Sample												Jt4										
Point	1	2	3	4	5	7	1	2	3	4	5	2	3	4	1	2	3	1	2	3	4	5
Grain	JT1 Ap12						JT1 Ap13					JT4 Ap1			JT4 Ap2			JT4 Ap3				
Ca	4.815	4.896	4.910	4.861	4.892	4.870	4.881	4.845	4.867	4.806	4.814	4.764	4.837	4.884	4.736	4.827	4.801	4.768	4.732	4.743	4.808	4.769
Mg	0.002	0.001	0.002	0.002	0.000	0.002	0.003	0.001	0.000	0.000	0.001	0.001	0.002	0.001	0.001	0.001	0.002	0.002	0.001	0.000	0.001	0.001
Mn	0.000	0.000	0.000	0.000	0.000	0.000	0.006	0.000	0.000	0.000	0.000	0.000	0.000	0.000	0.000	0.000	0.000	0.000	0.000	0.000	0.000	0.000
Sr	0.000	0.000	0.000	0.000	0.000	0.000	0.000	0.000	0.000	0.000	0.000	0.000	0.000	0.000	0.000	0.000	0.000	0.000	0.000	0.000	0.000	0.000
Y	0.000	0.000	0.000	0.000	0.000	0.000	0.000	0.000	0.000	0.000	0.000	0.000	0.009	0.000	0.000	0.012	0.000	0.000	0.000	0.004	0.013	0.000
La	0.000	0.000	0.000	0.000	0.000	0.000	0.000	0.000	0.000	0.000	0.000	0.000	0.000	0.000	0.000	0.000	0.000	0.000	0.000	0.000	0.000	0.000
Ce	0.000	0.000	0.000	0.000	0.000	0.000	0.000	0.000	0.000	0.000	0.000	0.000	0.000	0.000	0.000	0.005	0.000	0.000	0.000	0.000	0.000	0.000
Nd	0.000	0.000	0.000	0.000	0.000	0.000	0.000	0.000	0.000	0.000	0.000	0.000	0.003	0.000	0.000	0.000	0.000	0.000	0.000	0.000	0.000	0.000
Na	0.000	0.000	0.004	0.000	0.000	0.000	0.000	0.000	0.000	0.000	0.000	0.007	0.007	0.000	0.003	0.007	0.000	0.003	0.000	0.005	0.003	0.000
Fe	0.000	0.000	0.000	0.000	0.000	0.000	0.000	0.006	0.000	0.000	0.000	0.011	0.000	0.000	0.009	0.000	0.000	0.000	0.000	0.000	0.000	0.000
Ti	0.000	0.000	0.000	0.000	0.000	0.000	0.000	0.000	0.000	0.000	0.000	0.000	0.000	0.000	0.000	0.000	0.000	0.000	0.000	0.000	0.000	0.000
Al	0.000	0.000	0.000	0.000	0.000	0.000	0.000	0.000	0.000	0.000	0.000	0.000	0.000	0.000	0.000	0.000	0.000	0.000	0.000	0.000	0.000	0.000
Total	**4.817**	**4.897**	**4.915**	**4.863**	**4.892**	**4.872**	**4.890**	**4.852**	**4.867**	**4.806**	**4.815**	**4.784**	**4.858**	**4.886**	**4.750**	**4.853**	**4.804**	**4.773**	**4.733**	**4.753**	**4.825**	**4.770**
SREY	**0.000**	**0.000**	**0.000**	**0.000**	**0.000**	**0.000**	**0.000**	**0.000**	**0.000**	**0.000**	**0.000**	**0.000**	**0.013**	**0.000**	**0.000**	**0.017**	**0.000**	**0.000**	**0.000**	**0.004**	**0.013**	**0.000**
P	2.980	2.942	2.928	2.953	2.947	2.945	2.947	2.932	2.944	2.920	2.947	2.930	2.900	2.892	2.945	2.882	2.920	2.948	2.952	2.923	2.891	2.917
S	0.000	0.005	0.000	0.000	0.000	0.000	0.000	0.000	0.000	0.003	0.005	0.006	0.000	0.005	0.000	0.000	0.004	0.000	0.004	0.000	0.000	0.000
As	0.000	0.000	0.000	0.000	0.000	0.000	0.000	0.000	0.000	0.000	0.000	0.000	0.000	0.000	0.000	0.000	0.000	0.000	0.000	0.000	0.000	0.000
Si	0.000	0.000	0.000	0.000	0.000	0.000	0.000	0.000	0.000	0.000	0.000	0.001	0.021	0.000	0.000	0.039	0.000	0.000	0.000	0.011	0.024	0.000
Total	**2.980**	**2.946**	**2.928**	**2.953**	**2.947**	**2.945**	**2.947**	**2.932**	**2.944**	**2.924**	**2.952**	**2.937**	**2.921**	**2.897**	**2.945**	**2.921**	**2.924**	**2.948**	**2.957**	**2.934**	**2.915**	**2.917**
F	0.568	0.561	0.582	0.577	0.575	0.603	0.644	0.721	0.657	0.795	0.680	0.817	0.759	0.821	0.833	0.767	0.816	0.804	0.799	0.852	0.811	0.888
Cl	0.166	0.178	0.185	0.177	0.165	0.162	0.099	0.094	0.116	0.092	0.127	0.059	0.089	0.054	0.051	0.093	0.073	0.054	0.078	0.067	0.084	0.050
(F+Cl)	0.734	0.739	0.767	0.754	0.740	0.765	0.744	0.816	0.773	0.886	0.807	0.875	0.847	0.875	0.884	0.859	0.889	0.857	0.877	0.919	0.895	0.938
OH (by difference)	0.266	0.261	0.233	0.246	0.260	0.235	0.256	0.184	0.227	0.114	0.193	0.125	0.153	0.125	0.116	0.141	0.111	0.143	0.123	0.081	0.105	0.062
Total	**1.000**	**1.000**	**1.000**	**1.000**	**1.000**	**1.000**	**1.000**	**1.000**	**1.000**	**1.000**	**1.000**	**1.000**	**1.000**	**1.000**	**1.000**	**1.000**	**1.000**	**1.000**	**1.000**	**1.000**	**1.000**	**1.000**

Sample																					
Point	1	2	3	1	2	3	4	5	1	2	3	4	1	2	3	4	5	1	2	3	4	5
Grain	JT4 Ap4			JT4 Ap5					JT4 Ap6				JT4 Ap8					JT4 Ap10				
F	3.48	3.27	3.37	2.98	3.19	3.04	3.33	3.37	3.34	3.71	3.34	3.47	2.79	2.90	3.01	2.94	2.93	3.52	3.41	3.30	3.57	3.70
Cl	0.58	0.58	0.55	0.53	0.56	0.51	0.43	0.32	0.27	0.21	0.35	0.33	0.55	0.61	0.47	0.55	0.46	0.30	0.45	0.41	0.26	0.19
Na2O	0.02	0.00	0.00	0.02	0.02	0.00	0.03	0.00	0.00	0.00	0.00	0.00	0.04	0.03	0.00	0.04	0.02	0.00	0.00	0.02	0.03	0.00
SiO2	0.20	0.34	0.29	0.00	0.09	0.03	0.05	0.00	0.08	0.02	0.06	0.00	0.03	0.16	0.00	0.02	0.08	0.00	0.15	0.23	0.00	0.00
Al2O3	0.00	0.00	0.00	0.00	0.00	0.00	0.00	0.00	0.00	0.00	0.00	0.00	0.00	0.00	0.00	0.00	0.00	0.00	0.00	0.00	0.00	0.00
MgO	0.01	0.01	0.00	0.01	0.02	0.00	0.00	0.01	0.00	0.01	0.01	0.01	0.00	0.01	0.00	0.01	0.02	0.01	0.01	0.01	0.00	0.01
P2O5	42.04	41.14	42.09	42.45	42.00	42.95	41.94	42.58	42.21	43.12	41.83	42.78	42.34	41.96	42.71	42.18	42.48	41.91	42.43	42.26	42.39	42.09
SO2	0.00	0.07	0.05	0.00	0.00	0.05	0.00	0.00	0.05	0.00	0.00	0.00	0.00	0.00	0.00	0.00	0.00	0.00	0.00	0.00	0.00	0.00
CaO	54.69	55.67	54.67	55.66	55.24	55.75	56.17	54.82	55.20	55.59	55.40	56.47	56.37	55.07	56.91	55.48	55.93	55.64	55.59	55.72	55.42	56.77
TiO2	0.00	0.00	0.00	0.00	0.00	0.00	0.00	0.00	0.00	0.00	0.00	0.00	0.00	0.00	0.00	0.00	0.00	0.00	0.00	0.00	0.00	0.00
MnO	0.00	0.00	0.00	0.00	0.00	0.00	0.00	0.00	0.00	0.00	0.00	0.00	0.00	0.00	0.00	0.00	0.00	0.00	0.00	0.00	0.00	0.00
Fe2O3	0.00	0.00	0.00	0.00	0.00	0.00	0.15	0.00	0.00	0.00	0.00	0.14	0.11	0.00	0.00	0.00	0.00	0.00	0.00	0.08	0.16	0.28
As2O3	0.00	0.00	0.00	0.00	0.00	0.00	0.00	0.00	0.00	0.00	0.00	0.00	0.00	0.00	0.00	0.00	0.00	0.00	0.00	0.00	0.00	0.00
SrO	0.00	0.00	0.00	0.00	0.00	0.00	0.00	0.00	0.00	0.00	0.00	0.00	0.00	0.00	0.00	0.00	0.00	0.00	0.00	0.00	0.00	0.00
Y2O3	0.11	0.24	0.17	0.00	0.00	0.00	0.00	0.00	0.07	0.00	0.12	0.00	0.00	0.12	0.00	0.00	0.00	0.00	0.00	0.09	0.00	0.00
La2O3	0.00	0.00	0.00	0.00	0.00	0.00	0.00	0.00	0.00	0.00	0.00	0.00	0.00	0.00	0.00	0.00	0.00	0.00	0.00	0.00	0.00	0.00
Ce2O3	0.00	0.07	0.07	0.00	0.00	0.00	0.00	0.00	0.00	0.00	0.00	0.00	0.00	0.00	0.00	0.00	0.00	0.00	0.00	0.00	0.00	0.00
Nd2O3	0.00	0.00	0.00	0.00	0.00	0.00	0.00	0.00	0.00	0.00	0.00	0.00	0.00	0.00	0.00	0.00	0.00	0.00	0.00	0.00	0.00	0.00
-O equivalent	-1.60	-1.51	-1.54	-1.38	-1.47	-1.40	-1.50	-1.49	-1.47	-1.61	-1.49	-1.54	-1.30	-1.36	-1.37	-1.36	-1.34	-1.55	-1.54	-1.48	-1.56	-1.60
Total	**99.5**	**99.9**	**99.7**	**100.3**	**99.6**	**100.9**	**100.6**	**99.6**	**99.8**	**101.1**	**99.6**	**101.7**	**100.9**	**99.5**	**101.7**	**99.9**	**100.6**	**99.8**	**100.5**	**100.6**	**100.3**	**101.4**

Calculated formulae 9 a.p.f.u.

Sample																					
Point	1	2	3	1	2	3	4	5	1	2	3	4	1	2	3	4	5	1	2	3	4	5
Grain	JT4 Ap4			JT4 Ap5					JT4 Ap6				JT4 Ap8					JT4 Ap10				
Ca	4.759	4.873	4.756	4.850	4.828	4.815	4.875	4.770	4.811	4.751	4.844	4.833	4.908	4.841	4.902	4.859	4.865	4.845	4.803	4.823	4.793	4.873
Mg	0.002	0.002	0.000	0.001	0.002	0.000	0.000	0.001	0.000	0.001	0.001	0.001	0.000	0.002	0.000	0.002	0.002	0.001	0.001	0.001	0.000	0.001
Mn	0.000	0.000	0.000	0.000	0.000	0.000	0.000	0.000	0.000	0.000	0.000	0.000	0.000	0.000	0.000	0.000	0.000	0.000	0.000	0.000	0.000	0.000
Sr	0.000	0.000	0.000	0.000	0.000	0.000	0.000	0.000	0.000	0.000	0.000	0.000	0.000	0.000	0.000	0.000	0.000	0.000	0.000	0.000	0.000	0.000
Y	0.005	0.010	0.008	0.000	0.000	0.000	0.000	0.000	0.003	0.000	0.005	0.000	0.000	0.005	0.000	0.000	0.000	0.000	0.000	0.004	0.000	0.000
La	0.000	0.000	0.000	0.000	0.000	0.000	0.000	0.000	0.000	0.000	0.000	0.000	0.000	0.000	0.000	0.000	0.000	0.000	0.000	0.000	0.000	0.000
Ce	0.000	0.002	0.002	0.000	0.000	0.000	0.000	0.000	0.000	0.000	0.000	0.000	0.000	0.000	0.000	0.000	0.000	0.000	0.000	0.000	0.000	0.000
Nd	0.000	0.000	0.000	0.000	0.000	0.000	0.000	0.000	0.000	0.000	0.000	0.000	0.000	0.000	0.000	0.000	0.000	0.000	0.000	0.000	0.000	0.000
Na	0.002	0.000	0.000	0.003	0.003	0.000	0.004	0.000	0.000	0.000	0.000	0.000	0.006	0.004	0.000	0.007	0.004	0.000	0.000	0.003	0.005	0.000
Fe	0.000	0.000	0.000	0.000	0.000	0.000	0.009	0.000	0.000	0.000	0.000	0.008	0.007	0.000	0.000	0.000	0.000	0.000	0.000	0.005	0.010	0.017
Ti	0.000	0.000	0.000	0.000	0.000	0.000	0.000	0.000	0.000	0.000	0.000	0.000	0.000	0.000	0.000	0.000	0.000	0.000	0.000	0.000	0.000	0.000
Al	0.000	0.000	0.000	0.000	0.000	0.000	0.000	0.000	0.000	0.000	0.000	0.000	0.000	0.000	0.000	0.000	0.000	0.000	0.000	0.000	0.000	0.000
Total	**4.768**	**4.887**	**4.766**	**4.854**	**4.834**	**4.815**	**4.888**	**4.771**	**4.814**	**4.752**	**4.851**	**4.842**	**4.920**	**4.852**	**4.902**	**4.868**	**4.871**	**4.846**	**4.804**	**4.836**	**4.808**	**4.891**
SREY	**0.005**	**0.013**	**0.010**	**0.000**	**0.000**	**0.000**	**0.000**	**0.000**	**0.003**	**0.000**	**0.005**	**0.000**	**0.000**	**0.005**	**0.000**	**0.000**	**0.000**	**0.000**	**0.000**	**0.004**	**0.000**	**0.000**
P	2.890	2.846	2.893	2.923	2.901	2.931	2.876	2.927	2.907	2.912	2.890	2.893	2.913	2.914	2.907	2.919	2.920	2.883	2.897	2.890	2.897	2.855
S	0.000	0.005	0.004	0.000	0.000	0.004	0.000	0.000	0.004	0.000	0.000	0.000	0.000	0.000	0.000	0.000	0.000	0.000	0.000	0.000	0.000	0.000
As	0.000	0.000	0.000	0.000	0.000	0.000	0.000	0.000	0.000	0.000	0.000	0.000	0.000	0.000	0.000	0.000	0.000	0.000	0.000	0.000	0.000	0.000
Si	0.016	0.028	0.023	0.000	0.007	0.002	0.004	0.000	0.006	0.002	0.005	0.000	0.002	0.013	0.000	0.002	0.006	0.000	0.012	0.018	0.000	0.000
Total	**2.906**	**2.879**	**2.920**	**2.923**	**2.908**	**2.937**	**2.880**	**2.927**	**2.917**	**2.914**	**2.895**	**2.893**	**2.915**	**2.927**	**2.907**	**2.921**	**2.927**	**2.883**	**2.909**	**2.909**	**2.897**	**2.855**
F	0.894	0.844	0.866	0.767	0.824	0.776	0.852	0.866	0.859	0.936	0.863	0.876	0.717	0.752	0.766	0.759	0.753	0.905	0.869	0.842	0.910	0.938
Cl	0.080	0.080	0.076	0.074	0.077	0.070	0.059	0.044	0.037	0.028	0.049	0.045	0.075	0.084	0.064	0.076	0.064	0.041	0.061	0.056	0.036	0.026
(F+Cl)	0.973	0.925	0.942	0.840	0.901	0.846	0.911	0.910	0.897	0.964	0.912	0.922	0.793	0.836	0.830	0.834	0.817	0.946	0.930	0.898	0.947	0.964
OH (by difference)	0.027	0.075	0.058	0.160	0.099	0.154	0.089	0.090	0.103	0.036	0.088	0.078	0.207	0.164	0.170	0.166	0.183	0.054	0.070	0.102	0.053	0.036
Total	**1.000**	**1.000**	**1.000**	**1.000**	**1.000**	**1.000**	**1.000**	**1.000**	**1.000**	**1.000**	**1.000**	**1.000**	**1.000**	**1.000**	**1.000**	**1.000**	**1.000**	**1.000**	**1.000**	**1.000**	**1.000**	**1.000**

Sample						Jt7																	
Point	1	2	3	4	5	1	2	3	4	5	6	7	1	2	3	4	5	6	7	1	2	3	4
Grain	JT4 Ap11					JT7 Ap1							JT7 Ap2							JT7 Ap4			
F	3.62	3.46	3.30	3.51	3.57	3.12	3.33	3.14	3.26	3.07	3.07	3.10	2.59	2.70	2.72	2.54	2.72	2.65	2.66	3.17	3.01	3.40	2.90
Cl	0.38	0.33	0.41	0.25	0.21	0.68	0.68	0.80	0.47	0.83	0.73	0.86	0.85	0.85	0.74	0.88	0.83	0.90	0.92	0.49	0.52	0.51	0.67
Na2O	0.00	0.00	0.00	0.00	0.00	0.03	0.02	0.00	0.00	0.00	0.00	0.00	0.06	0.00	0.02	0.05	0.04	0.05	0.00	0.02	0.00	0.00	0.05
SiO2	0.00	0.00	0.07	0.00	0.00	0.10	0.12	0.51	0.03	0.36	0.40	0.61	0.20	0.00	0.07	0.33	0.27	0.42	0.32	0.00	0.00	0.19	0.29
Al2O3	0.00	0.00	0.00	0.00	0.00	0.00	0.00	0.00	0.00	0.00	0.00	0.00	0.00	0.00	0.00	0.00	0.00	0.00	0.00	0.00	0.00	0.00	0.00
MgO	0.01	0.01	0.02	0.00	0.01	0.02	0.02	0.02	0.02	0.02	0.02	0.01	0.01	0.02	0.02	0.01	0.01	0.02	0.01	0.01	0.01	0.02	0.02
P2O5	42.86	43.58	41.48	43.18	43.04	41.29	41.46	40.39	41.61	42.11	41.59	40.62	41.85	41.45	42.63	41.87	41.61	42.00	41.40	42.16	41.89	42.78	41.26
SO2	0.05	0.07	0.00	0.00	0.00	0.00	0.00	0.00	0.00	0.00	0.00	0.00	0.00	0.00	0.00	0.00	0.00	0.00	0.00	0.00	0.00	0.00	0.00
CaO	55.97	55.61	55.69	56.86	55.53	54.79	53.51	54.05	53.50	53.91	54.25	54.74	54.94	54.81	56.21	53.26	55.82	54.81	54.07	54.93	55.23	55.46	54.27
TiO2	0.00	0.00	0.00	0.00	0.00	0.00	0.00	0.00	0.00	0.00	0.00	0.00	0.00	0.00	0.00	0.00	0.00	0.00	0.00	0.00	0.00	0.00	0.00
MnO	0.00	0.00	0.00	0.00	0.00	0.00	0.00	0.00	0.00	0.00	0.00	0.00	0.00	0.00	0.00	0.00	0.00	0.00	0.00	0.00	0.00	0.00	0.00
Fe2O3	0.00	0.00	0.10	0.28	0.33	0.00	0.00	0.00	0.00	0.00	0.00	0.08	0.14	0.00	0.00	0.00	0.00	0.00	0.00	0.18	0.00	0.00	0.00
As2O3	0.00	0.00	0.00	0.00	0.00	0.00	0.00	0.00	0.00	0.00	0.00	0.00	0.00	0.00	0.00	0.00	0.00	0.00	0.00	0.00	0.00	0.00	0.00
SrO	0.02	0.00	0.00	0.00	0.00	0.00	0.00	0.00	0.00	0.00	0.00	0.00	0.00	0.00	0.00	0.00	0.00	0.00	0.00	0.00	0.00	0.00	0.00
Y2O3	0.00	0.00	0.06	0.00	0.00	0.00	0.00	0.13	0.00	0.00	0.16	0.18	0.06	0.00	0.00	0.06	0.17	0.22	0.09	0.00	0.00	0.00	0.06
La2O3	0.00	0.00	0.00	0.00	0.00	0.00	0.00	0.06	0.24	0.00	0.00	0.00	0.00	0.00	0.00	0.00	0.00	0.00	0.00	0.00	0.00	0.00	0.07
Ce2O3	0.00	0.00	0.00	0.00	0.00	0.00	0.00	0.37	0.59	0.22	0.18	0.23	0.00	0.00	0.00	0.22	0.00	0.10	0.16	0.00	0.00	0.00	0.30
Nd2O3	0.00	0.00	0.00	0.00	0.00	0.00	0.00	0.14	0.13	0.00	0.00	0.17	0.00	0.00	0.00	0.00	0.00	0.00	0.00	0.00	0.00	0.00	0.17
-O equivalent	-1.61	-1.53	-1.48	-1.53	-1.55	-1.47	-1.55	-1.50	-1.48	-1.48	-1.46	-1.50	-1.28	-1.33	-1.31	-1.27	-1.33	-1.32	-1.33	-1.44	-1.39	-1.55	-1.37
Total	**101.3**	**101.5**	**99.6**	**102.5**	**101.1**	**98.6**	**97.6**	**98.1**	**98.4**	**99.0**	**98.9**	**99.1**	**99.4**	**98.5**	**101.1**	**98.0**	**100.2**	**99.9**	**98.3**	**99.5**	**99.3**	**100.8**	**98.7**

Calculated formulae 9 a.p.f.u.

Sample						Jt7																	
Point	1	2	3	4	5	1	2	3	4	5	6	7	1	2	3	4	5	6	7	1	2	3	4
Grain	JT4 Ap11					JT7 Ap1							JT7 Ap2							JT7 Ap4			
Ca	4.785	4.738	4.882	4.825	4.756	4.850	4.746	4.822	4.743	4.726	4.777	4.839	4.850	4.879	4.878	4.752	4.901	4.811	4.817	4.806	4.861	4.769	4.822
Mg	0.001	0.001	0.002	0.000	0.001	0.002	0.002	0.002	0.002	0.002	0.002	0.002	0.002	0.002	0.002	0.002	0.002	0.002	0.002	0.001	0.001	0.002	0.002
Mn	0.000	0.000	0.000	0.000	0.000	0.000	0.000	0.000	0.000	0.000	0.000	0.000	0.000	0.000	0.000	0.000	0.000	0.000	0.000	0.000	0.000	0.000	0.000
Sr	0.001	0.000	0.000	0.000	0.000	0.000	0.000	0.000	0.000	0.000	0.000	0.000	0.000	0.000	0.000	0.000	0.000	0.000	0.000	0.000	0.000	0.000	0.000
Y	0.000	0.000	0.002	0.000	0.000	0.000	0.000	0.006	0.000	0.000	0.007	0.008	0.003	0.000	0.000	0.003	0.008	0.010	0.004	0.000	0.000	0.000	0.003
La	0.000	0.000	0.000	0.000	0.000	0.000	0.000	0.002	0.007	0.000	0.000	0.000	0.000	0.000	0.000	0.000	0.000	0.000	0.000	0.000	0.000	0.000	0.002
Ce	0.000	0.000	0.000	0.000	0.000	0.000	0.000	0.011	0.018	0.007	0.005	0.007	0.000	0.000	0.000	0.007	0.000	0.003	0.005	0.000	0.000	0.000	0.009
Nd	0.000	0.000	0.000	0.000	0.000	0.000	0.000	0.004	0.004	0.000	0.000	0.005	0.000	0.000	0.000	0.000	0.000	0.000	0.000	0.000	0.000	0.000	0.005
Na	0.000	0.000	0.000	0.000	0.000	0.004	0.003	0.000	0.000	0.000	0.000	0.000	0.010	0.000	0.003	0.008	0.007	0.009	0.000	0.003	0.000	0.000	0.007
Fe	0.000	0.000	0.006	0.016	0.020	0.000	0.000	0.000	0.000	0.000	0.000	0.005	0.009	0.000	0.000	0.000	0.000	0.000	0.000	0.011	0.000	0.000	0.000
Ti	0.000	0.000	0.000	0.000	0.000	0.000	0.000	0.000	0.000	0.000	0.000	0.000	0.000	0.000	0.000	0.000	0.000	0.000	0.000	0.000	0.000	0.000	0.000
Al	0.000	0.000	0.000	0.000	0.000	0.000	0.000	0.000	0.000	0.000	0.000	0.000	0.000	0.000	0.000	0.000	0.000	0.000	0.000	0.000	0.000	0.000	0.000
Total	**4.787**	**4.739**	**4.892**	**4.841**	**4.777**	**4.856**	**4.752**	**4.846**	**4.774**	**4.735**	**4.792**	**4.865**	**4.873**	**4.881**	**4.884**	**4.771**	**4.917**	**4.834**	**4.828**	**4.822**	**4.862**	**4.771**	**4.850**
SREY	**0.000**	**0.000**	**0.002**	**0.000**	**0.000**	**0.000**	**0.000**	**0.023**	**0.029**	**0.007**	**0.013**	**0.020**	**0.003**	**0.000**	**0.000**	**0.009**	**0.008**	**0.013**	**0.009**	**0.000**	**0.000**	**0.000**	**0.019**
P	2.896	2.934	2.873	2.895	2.913	2.888	2.906	2.847	2.915	2.917	2.894	2.837	2.919	2.916	2.923	2.952	2.887	2.913	2.914	2.915	2.913	2.906	2.897
S	0.004	0.005	0.000	0.000	0.000	0.000	0.000	0.000	0.000	0.000	0.000	0.000	0.000	0.000	0.000	0.000	0.000	0.000	0.000	0.000	0.000	0.000	0.000
As	0.000	0.000	0.000	0.000	0.000	0.000	0.000	0.000	0.000	0.000	0.000	0.000	0.000	0.000	0.000	0.000	0.000	0.000	0.000	0.000	0.000	0.000	0.000
Si	0.000	0.000	0.006	0.000	0.000	0.008	0.010	0.042	0.002	0.030	0.033	0.050	0.017	0.000	0.006	0.028	0.022	0.035	0.026	0.000	0.000	0.015	0.024
Total	**2.900**	**2.939**	**2.879**	**2.895**	**2.913**	**2.896**	**2.916**	**2.890**	**2.917**	**2.946**	**2.927**	**2.887**	**2.936**	**2.916**	**2.929**	**2.979**	**2.910**	**2.948**	**2.941**	**2.915**	**2.913**	**2.921**	**2.921**
F	0.914	0.871	0.852	0.880	0.902	0.814	0.871	0.827	0.854	0.795	0.799	0.809	0.675	0.709	0.696	0.669	0.705	0.687	0.699	0.817	0.783	0.864	0.761
Cl	0.052	0.045	0.057	0.033	0.029	0.095	0.095	0.112	0.066	0.115	0.102	0.121	0.119	0.119	0.102	0.124	0.115	0.125	0.130	0.068	0.073	0.070	0.094
(F+Cl)	0.965	0.916	0.910	0.913	0.930	0.909	0.966	0.939	0.920	0.911	0.901	0.930	0.794	0.829	0.798	0.793	0.820	0.812	0.829	0.886	0.856	0.933	0.854
OH (by difference)	0.035	0.084	0.090	0.087	0.070	0.091	0.034	0.061	0.080	0.089	0.099	0.070	0.206	0.171	0.202	0.207	0.180	0.188	0.171	0.114	0.144	0.067	0.146
Total	**1.000**	**1.000**	**1.000**	**1.000**	**1.000**	**1.000**	**1.000**	**1.000**	**1.000**	**1.000**	**1.000**	**1.000**	**1.000**	**1.000**	**1.000**	**1.000**	**1.000**	**1.000**	**1.000**	**1.000**	**1.000**	**1.000**	**1.000**

Sample																					
Point	1	2	3	4	5	6	1	2	3	4	5	1	2	3	4	5	6	1	2	3	4	5
Grain	JT7 Ap5						JT7 Ap7					JT7 Ap8						JT7 Ap10				
F	3.25	3.37	3.44	3.35	3.19	3.19	2.86	3.21	3.00	3.11	2.91	3.12	2.51	2.67	2.49	2.55	2.81	2.99	2.90	3.08	3.00	2.97
Cl	0.67	0.72	0.73	0.72	0.66	0.57	0.47	0.36	0.53	0.59	0.55	0.50	0.89	0.79	0.83	0.75	0.75	0.72	0.65	0.79	0.72	0.76
Na2O	0.03	0.00	0.00	0.00	0.00	0.00	0.00	0.00	0.00	0.03	0.00	0.02	0.06	0.00	0.00	0.00	0.00	0.02	0.03	0.04	0.00	0.04
SiO2	0.31	0.06	0.26	0.17	0.21	0.15	0.00	0.00	0.03	0.31	0.28	0.00	0.09	0.10	0.14	0.00	0.00	0.53	0.25	0.58	0.21	0.63
Al2O3	0.00	0.00	0.00	0.00	0.00	0.00	0.00	0.00	0.00	0.00	0.00	0.00	0.00	0.00	0.00	0.00	0.00	0.00	0.00	0.00	0.00	0.00
MgO	0.02	0.02	0.01	0.01	0.01	0.01	0.01	0.01	0.01	0.02	0.01	0.01	0.02	0.01	0.01	0.01	0.02	0.01	0.02	0.02	0.00	0.01
P2O5	41.56	41.23	41.40	41.95	40.81	42.42	42.88	42.29	42.58	42.24	41.47	42.75	41.23	41.87	42.31	41.89	41.68	42.26	42.33	42.17	42.63	42.00
SO2	0.00	0.00	0.00	0.00	0.00	0.00	0.00	0.00	0.00	0.00	0.00	0.00	0.00	0.00	0.00	0.00	0.00	0.00	0.00	0.00	0.00	0.00
CaO	54.65	54.85	54.83	55.12	54.43	54.60	56.08	55.60	55.16	55.31	55.60	55.96	55.68	55.14	54.61	55.30	55.47	55.26	54.87	54.01	54.86	53.66
TiO2	0.00	0.00	0.00	0.00	0.00	0.00	0.00	0.00	0.00	0.00	0.00	0.00	0.00	0.00	0.00	0.00	0.00	0.00	0.00	0.00	0.00	0.00
MnO	0.00	0.00	0.00	0.00	0.00	0.00	0.00	0.00	0.00	0.00	0.00	0.00	0.00	0.00	0.00	0.00	0.00	0.00	0.00	0.00	0.00	0.00
Fe2O3	0.00	0.00	0.00	0.11	0.00	0.16	0.00	0.07	0.00	0.14	0.00	0.00	0.00	0.00	0.00	0.00	0.00	0.00	0.00	0.08	0.00	0.24
As2O3	0.00	0.00	0.00	0.00	0.00	0.00	0.00	0.00	0.00	0.00	0.00	0.00	0.00	0.00	0.00	0.00	0.00	0.00	0.00	0.00	0.00	0.00
SrO	0.00	0.00	0.00	0.00	0.00	0.00	0.00	0.00	0.00	0.00	0.00	0.00	0.00	0.00	0.00	0.00	0.00	0.00	0.00	0.00	0.00	0.00
Y2O3	0.10	0.00	0.15	0.10	0.08	0.08	0.00	0.00	0.00	0.07	0.07	0.00	0.00	0.00	0.07	0.00	0.00	0.15	0.17	0.15	0.08	0.20
La2O3	0.00	0.00	0.00	0.00	0.00	0.00	0.00	0.00	0.00	0.00	0.00	0.00	0.00	0.00	0.00	0.00	0.00	0.00	0.00	0.00	0.00	0.00
Ce2O3	0.10	0.00	0.00	0.00	0.07	0.00	0.00	0.00	0.00	0.26	0.16	0.00	0.00	0.00	0.00	0.00	0.00	0.26	0.00	0.19	0.07	0.24
Nd2O3	0.00	0.00	0.00	0.00	0.00	0.00	0.00	0.00	0.00	0.00	0.00	0.00	0.00	0.00	0.00	0.00	0.00	0.11	0.00	0.00	0.00	0.28
-O equivalent	-1.52	-1.58	-1.61	-1.57	-1.49	-1.47	-1.31	-1.43	-1.38	-1.44	-1.35	-1.43	-1.26	-1.30	-1.23	-1.24	-1.35	-1.42	-1.37	-1.48	-1.43	-1.42
Total	**99.2**	**98.7**	**99.2**	**100.0**	**98.0**	**99.7**	**101.0**	**100.1**	**99.9**	**100.6**	**99.7**	**100.9**	**99.2**	**99.3**	**99.2**	**99.3**	**99.4**	**100.9**	**99.8**	**99.6**	**100.2**	**99.6**

Calculated formulae 9 a.p.f.u.

Sample																					
Point	1	2	3	4	5	6	1	2	3	4	5	1	2	3	4	5	6	1	2	3	4	5
Grain	JT7 Ap5						JT7 Ap7					JT7 Ap8						JT7 Ap10				
Ca	4.795	4.833	4.799	4.792	4.846	4.756	4.860	4.842	4.812	4.799	4.895	4.836	4.951	4.870	4.824	4.898	4.895	4.789	4.797	4.709	4.768	4.697
Mg	0.003	0.002	0.001	0.002	0.001	0.002	0.001	0.001	0.001	0.002	0.001	0.001	0.003	0.001	0.001	0.001	0.002	0.002	0.002	0.002	0.000	0.001
Mn	0.000	0.000	0.000	0.000	0.000	0.000	0.000	0.000	0.000	0.000	0.000	0.000	0.000	0.000	0.000	0.000	0.000	0.000	0.000	0.000	0.000	0.000
Sr	0.000	0.000	0.000	0.000	0.000	0.000	0.000	0.000	0.000	0.000	0.000	0.000	0.000	0.000	0.000	0.000	0.000	0.000	0.000	0.000	0.000	0.000
Y	0.004	0.000	0.007	0.004	0.004	0.004	0.000	0.000	0.000	0.003	0.003	0.000	0.000	0.000	0.003	0.000	0.000	0.006	0.007	0.007	0.003	0.009
La	0.000	0.000	0.000	0.000	0.000	0.000	0.000	0.000	0.000	0.000	0.000	0.000	0.000	0.000	0.000	0.000	0.000	0.000	0.000	0.000	0.000	0.000
Ce	0.003	0.000	0.000	0.000	0.002	0.000	0.000	0.000	0.000	0.008	0.005	0.000	0.000	0.000	0.000	0.000	0.000	0.008	0.000	0.006	0.002	0.007
Nd	0.000	0.000	0.000	0.000	0.000	0.000	0.000	0.000	0.000	0.000	0.000	0.000	0.000	0.000	0.000	0.000	0.000	0.003	0.000	0.000	0.000	0.008
Na	0.004	0.000	0.000	0.000	0.000	0.000	0.000	0.000	0.000	0.005	0.000	0.002	0.010	0.000	0.000	0.000	0.000	0.003	0.004	0.006	0.000	0.006
Fe	0.000	0.000	0.000	0.007	0.000	0.010	0.000	0.004	0.000	0.009	0.000	0.000	0.000	0.000	0.000	0.000	0.000	0.000	0.000	0.005	0.000	0.015
Ti	0.000	0.000	0.000	0.000	0.000	0.000	0.000	0.000	0.000	0.000	0.000	0.000	0.000	0.000	0.000	0.000	0.000	0.000	0.000	0.000	0.000	0.000
Al	0.000	0.000	0.000	0.000	0.000	0.000	0.000	0.000	0.000	0.000	0.000	0.000	0.000	0.000	0.000	0.000	0.000	0.000	0.000	0.000	0.000	0.000
Total	**4.810**	**4.835**	**4.807**	**4.805**	**4.853**	**4.771**	**4.861**	**4.847**	**4.813**	**4.825**	**4.904**	**4.839**	**4.964**	**4.871**	**4.828**	**4.899**	**4.897**	**4.811**	**4.810**	**4.734**	**4.774**	**4.744**
SREY	**0.007**	**0.000**	**0.007**	**0.004**	**0.006**	**0.004**	**0.000**	**0.000**	**0.000**	**0.010**	**0.008**	**0.000**	**0.000**	**0.000**	**0.003**	**0.000**	**0.000**	**0.017**	**0.007**	**0.012**	**0.005**	**0.024**
P	2.882	2.871	2.864	2.882	2.871	2.919	2.937	2.910	2.935	2.896	2.885	2.919	2.897	2.922	2.953	2.932	2.907	2.894	2.924	2.905	2.928	2.905
S	0.000	0.000	0.000	0.000	0.000	0.000	0.000	0.000	0.000	0.000	0.000	0.000	0.000	0.000	0.000	0.000	0.000	0.000	0.000	0.000	0.000	0.000
As	0.000	0.000	0.000	0.000	0.000	0.000	0.000	0.000	0.000	0.000	0.000	0.000	0.000	0.000	0.000	0.000	0.000	0.000	0.000	0.000	0.000	0.000
Si	0.026	0.005	0.021	0.014	0.018	0.012	0.000	0.000	0.003	0.025	0.023	0.000	0.007	0.009	0.011	0.000	0.000	0.042	0.020	0.047	0.017	0.051
Total	**2.907**	**2.876**	**2.884**	**2.896**	**2.889**	**2.932**	**2.937**	**2.910**	**2.937**	**2.921**	**2.908**	**2.919**	**2.904**	**2.931**	**2.965**	**2.932**	**2.907**	**2.937**	**2.944**	**2.953**	**2.945**	**2.957**
F	0.841	0.877	0.888	0.859	0.838	0.820	0.732	0.825	0.771	0.796	0.757	0.796	0.660	0.696	0.648	0.667	0.731	0.764	0.748	0.794	0.770	0.768
Cl	0.093	0.101	0.101	0.098	0.093	0.079	0.065	0.050	0.074	0.081	0.076	0.068	0.125	0.110	0.116	0.105	0.104	0.098	0.090	0.109	0.100	0.105
(F+Cl)	0.934	0.978	0.989	0.957	0.931	0.899	0.797	0.875	0.845	0.877	0.833	0.864	0.785	0.807	0.764	0.771	0.836	0.862	0.838	0.903	0.870	0.874
OH (by difference)	0.066	0.022	0.011	0.043	0.069	0.101	0.203	0.125	0.155	0.123	0.167	0.136	0.215	0.193	0.236	0.229	0.164	0.138	0.162	0.097	0.130	0.126
Total	**1.000**	**1.000**	**1.000**	**1.000**	**1.000**	**1.000**	**1.000**	**1.000**	**1.000**	**1.000**	**1.000**	**1.000**	**1.000**	**1.000**	**1.000**	**1.000**	**1.000**	**1.000**	**1.000**	**1.000**	**1.000**	**1.000**

Sample																								
Point	1	2	3	4	5	6	7	8	9	1	2	3	4	5	6	7	8	9	10	11	1	2	3	4
Grain	JT7 Ap12									JT7 Ap13											JT7 Ap14			
F	3.08	2.92	3.05	2.84	2.95	3.32	3.23	3.03	2.92	3.15	3.06	3.22	3.47	2.97	3.06	2.85	2.81	3.52	2.79	3.11	3.32	3.08	3.10	3.21
Cl	0.69	0.74	0.72	0.76	0.67	0.54	0.53	0.61	0.82	0.53	0.70	0.58	0.41	0.62	0.69	0.75	0.77	0.43	0.71	0.64	0.48	0.61	0.62	0.60
Na2O	0.00	0.00	0.07	0.00	0.02	0.00	0.00	0.00	0.04	0.05	0.00	0.02	0.00	0.00	0.00	0.00	0.00	0.00	0.00	0.00	0.00	0.03	0.00	0.03
SiO2	0.23	0.30	0.40	0.33	0.25	0.00	0.00	0.33	0.45	0.17	0.32	0.04	0.03	0.15	0.15	0.30	0.34	0.00	0.00	0.34	0.10	0.26	0.10	0.15
Al2O3	0.00	0.00	0.00	0.00	0.00	0.00	0.00	0.00	0.00	0.00	0.00	0.00	0.00	0.00	0.00	0.00	0.00	0.00	0.00	0.00	0.00	0.00	0.00	0.00
MgO	0.02	0.02	0.02	0.01	0.02	0.01	0.01	0.01	0.01	0.01	0.02	0.01	0.01	0.01	0.01	0.00	0.02	0.00	0.01	0.04	0.01	0.02	0.01	0.01
P2O5	42.11	42.32	40.96	41.84	42.57	42.74	42.82	41.50	41.08	41.96	41.93	42.55	42.63	42.25	41.48	41.72	42.47	42.70	42.55	41.73	42.66	42.02	42.36	43.18
SO2	0.00	0.00	0.00	0.00	0.00	0.00	0.00	0.00	0.00	0.00	0.00	0.00	0.00	0.00	0.00	0.00	0.00	0.00	0.00	0.00	0.05	0.00	0.00	0.04
CaO	56.43	55.42	54.38	54.75	55.85	55.30	56.00	55.28	55.06	55.14	54.52	55.59	55.16	55.60	54.87	55.60	54.98	55.48	56.31	56.04	55.44	54.12	55.52	55.04
TiO2	0.00	0.00	0.00	0.00	0.00	0.00	0.00	0.00	0.00	0.00	0.00	0.00	0.00	0.00	0.00	0.00	0.00	0.00	0.00	0.00	0.00	0.00	0.00	0.00
MnO	0.00	0.00	0.00	0.00	0.00	0.00	0.00	0.00	0.00	0.00	0.00	0.00	0.00	0.00	0.00	0.00	0.00	0.00	0.00	0.00	0.00	0.00	0.00	0.00
Fe2O3	0.00	0.00	0.00	0.00	0.00	0.00	0.00	0.16	0.11	0.13	0.00	0.00	0.00	0.00	0.00	0.09	0.16	0.00	0.00	0.70	0.10	0.00	0.00	0.00
As2O3	0.00	0.00	0.00	0.00	0.00	0.00	0.00	0.00	0.00	0.00	0.00	0.00	0.00	0.00	0.00	0.00	0.00	0.00	0.00	0.00	0.00	0.00	0.00	0.00
SrO	0.00	0.00	0.00	0.00	0.00	0.00	0.00	0.00	0.00	0.00	0.00	0.00	0.00	0.00	0.00	0.00	0.00	0.00	0.00	0.00	0.00	0.00	0.00	0.00
Y2O3	0.00	0.00	0.10	0.09	0.00	0.00	0.00	0.00	0.08	0.05	0.07	0.00	0.00	0.00	0.10	0.15	0.16	0.00	0.00	0.12	0.00	0.06	0.00	0.00
La2O3	0.00	0.00	0.00	0.00	0.00	0.00	0.00	0.00	0.00	0.00	0.00	0.00	0.00	0.00	0.00	0.00	0.00	0.00	0.00	0.00	0.00	0.00	0.00	0.00
Ce2O3	0.00	0.17	0.11	0.14	0.11	0.00	0.00	0.12	0.25	0.00	0.14	0.00	0.00	0.00	0.00	0.14	0.09	0.00	0.00	0.00	0.00	0.07	0.00	0.00
Nd2O3	0.00	0.13	0.00	0.00	0.00	0.00	0.00	0.00	0.22	0.00	0.11	0.00	0.00	0.00	0.00	0.00	0.00	0.00	0.00	0.00	0.00	0.00	0.00	0.00
-O equivalent	-1.45	-1.40	-1.45	-1.37	-1.39	-1.52	-1.48	-1.41	-1.41	-1.44	-1.45	-1.48	-1.55	-1.39	-1.44	-1.37	-1.36	-1.58	-1.34	-1.45	-1.51	-1.43	-1.45	-1.49
Total	**101.1**	**100.6**	**98.4**	**99.4**	**101.1**	**100.4**	**101.1**	**99.6**	**99.6**	**99.8**	**99.4**	**100.5**	**100.2**	**100.2**	**98.9**	**100.2**	**100.4**	**100.5**	**101.0**	**101.3**	**100.6**	**98.8**	**100.3**	**100.8**

Calculated formulae 9 a.p.f.u.

Sample																								
Point	1	2	3	4	5	6	7	8	9	1	2	3	4	5	6	7	8	9	10	11	1	2	3	4
Grain	JT7 Ap12									JT7 Ap13											JT7 Ap14			
Ca	4.882	4.818	4.829	4.817	4.831	4.780	4.822	4.855	4.855	4.820	4.780	4.813	4.770	4.848	4.842	4.869	4.785	4.779	4.889	4.851	4.784	4.760	4.826	4.732
Mg	0.002	0.002	0.002	0.001	0.002	0.001	0.001	0.001	0.001	0.002	0.002	0.002	0.001	0.001	0.001	0.000	0.002	0.000	0.001	0.004	0.001	0.002	0.002	0.002
Mn	0.000	0.000	0.000	0.000	0.000	0.000	0.000	0.000	0.000	0.000	0.000	0.000	0.000	0.000	0.000	0.000	0.000	0.000	0.000	0.000	0.000	0.000	0.000	0.000
Sr	0.000	0.000	0.000	0.000	0.000	0.000	0.000	0.000	0.000	0.000	0.000	0.000	0.000	0.000	0.000	0.000	0.000	0.000	0.000	0.000	0.000	0.000	0.000	0.000
Y	0.000	0.000	0.004	0.004	0.000	0.000	0.000	0.000	0.004	0.002	0.003	0.000	0.000	0.000	0.004	0.007	0.007	0.000	0.000	0.005	0.000	0.003	0.000	0.000
La	0.000	0.000	0.000	0.000	0.000	0.000	0.000	0.000	0.000	0.000	0.000	0.000	0.000	0.000	0.000	0.000	0.000	0.000	0.000	0.000	0.000	0.000	0.000	0.000
Ce	0.000	0.005	0.003	0.004	0.003	0.000	0.000	0.003	0.008	0.000	0.004	0.000	0.000	0.000	0.000	0.004	0.003	0.000	0.000	0.000	0.000	0.002	0.000	0.000
Nd	0.000	0.004	0.000	0.000	0.000	0.000	0.000	0.000	0.006	0.000	0.003	0.000	0.000	0.000	0.000	0.000	0.000	0.000	0.000	0.000	0.000	0.000	0.000	0.000
Na	0.000	0.000	0.011	0.000	0.003	0.000	0.000	0.000	0.007	0.007	0.000	0.003	0.000	0.000	0.000	0.000	0.000	0.000	0.000	0.000	0.000	0.005	0.000	0.005
Fe	0.000	0.000	0.000	0.000	0.000	0.000	0.000	0.010	0.007	0.008	0.000	0.000	0.000	0.000	0.000	0.005	0.010	0.000	0.000	0.042	0.006	0.000	0.000	0.000
Ti	0.000	0.000	0.000	0.000	0.000	0.000	0.000	0.000	0.000	0.000	0.000	0.000	0.000	0.000	0.000	0.000	0.000	0.000	0.000	0.000	0.000	0.000	0.000	0.000
Al	0.000	0.000	0.000	0.000	0.000	0.000	0.000	0.000	0.000	0.000	0.000	0.000	0.000	0.000	0.000	0.000	0.000	0.000	0.000	0.000	0.000	0.000	0.000	0.000
Total	**4.885**	**4.828**	**4.849**	**4.827**	**4.839**	**4.782**	**4.823**	**4.870**	**4.887**	**4.840**	**4.792**	**4.818**	**4.771**	**4.849**	**4.848**	**4.885**	**4.806**	**4.779**	**4.890**	**4.903**	**4.791**	**4.772**	**4.828**	**4.739**
SREY	**0.000**	**0.009**	**0.007**	**0.008**	**0.003**	**0.000**	**0.000**	**0.003**	**0.018**	**0.002**	**0.010**	**0.000**	**0.000**	**0.000**	**0.004**	**0.011**	**0.009**	**0.000**	**0.000**	**0.005**	**0.000**	**0.005**	**0.000**	**0.000**
P	2.879	2.906	2.874	2.909	2.910	2.919	2.914	2.880	2.862	2.898	2.905	2.910	2.913	2.911	2.893	2.887	2.921	2.907	2.919	2.854	2.909	2.920	2.910	2.934
S	0.000	0.000	0.000	0.000	0.000	0.000	0.000	0.000	0.000	0.000	0.000	0.000	0.000	0.000	0.000	0.000	0.000	0.000	0.000	0.000	0.004	0.000	0.000	0.003
As	0.000	0.000	0.000	0.000	0.000	0.000	0.000	0.000	0.000	0.000	0.000	0.000	0.000	0.000	0.000	0.000	0.000	0.000	0.000	0.000	0.000	0.000	0.000	0.000
Si	0.019	0.025	0.034	0.027	0.020	0.000	0.000	0.027	0.037	0.014	0.026	0.004	0.003	0.012	0.013	0.025	0.027	0.000	0.000	0.028	0.008	0.021	0.008	0.012
Total	**2.897**	**2.931**	**2.908**	**2.936**	**2.930**	**2.919**	**2.914**	**2.907**	**2.899**	**2.912**	**2.931**	**2.914**	**2.916**	**2.923**	**2.905**	**2.912**	**2.948**	**2.907**	**2.919**	**2.882**	**2.920**	**2.942**	**2.918**	**2.949**
F	0.787	0.750	0.799	0.737	0.753	0.846	0.820	0.785	0.761	0.812	0.791	0.822	0.885	0.765	0.797	0.736	0.722	0.896	0.715	0.794	0.846	0.800	0.797	0.816
Cl	0.095	0.102	0.102	0.106	0.092	0.073	0.073	0.084	0.114	0.073	0.097	0.079	0.056	0.085	0.096	0.104	0.105	0.058	0.097	0.087	0.065	0.084	0.085	0.082
(F+Cl)	0.881	0.852	0.900	0.843	0.845	0.920	0.892	0.870	0.874	0.885	0.889	0.901	0.942	0.850	0.893	0.840	0.827	0.954	0.813	0.882	0.912	0.884	0.881	0.898
OH (by difference)	0.119	0.148	0.100	0.157	0.155	0.080	0.108	0.130	0.126	0.115	0.111	0.099	0.058	0.150	0.107	0.160	0.173	0.046	0.187	0.118	0.088	0.116	0.119	0.102
Total	**1.000**	**1.000**	**1.000**	**1.000**	**1.000**	**1.000**	**1.000**	**1.000**	**1.000**	**1.000**	**1.000**	**1.000**	**1.000**	**1.000**	**1.000**	**1.000**	**1.000**	**1.000**	**1.000**	**1.000**	**1.000**	**1.000**	**1.000**	**1.000**

Sample																							
Point	1	2	3	4	1	2	3	4	5	6	8	10	11	1	2	3	4	5	6	7	8	9	10	11
Grain	JT7 Ap15				JT7 Ap16									JT7 Ap17										
F	2.61	3.20	2.59	2.74	2.57	2.58	2.60	3.14	3.36	3.40	3.30	2.93	3.04	3.15	3.15	2.78	3.18	3.10	3.16	3.16	3.11	3.00	3.19	2.92
Cl	0.81	0.50	0.83	0.92	0.89	0.87	0.80	0.72	0.62	0.67	0.51	0.75	0.64	0.66	0.64	0.57	0.66	0.64	0.66	0.59	0.64	0.62	0.57	0.64
Na2O	0.03	0.00	0.00	0.00	0.03	0.05	0.00	0.00	0.00	0.00	0.00	0.02	0.00	0.03	0.02	0.02	0.00	0.04	0.03	0.00	0.00	0.00	0.03	0.03
SiO2	0.00	0.00	0.30	0.26	0.24	0.41	0.14	0.42	0.10	0.00	0.00	0.56	0.56	0.53	0.27	1.58	0.20	0.19	0.31	0.34	0.38	0.32	0.23	0.35
Al2O3	0.00	0.00	0.00	0.00	0.00	0.00	0.00	0.00	0.00	0.00	0.00	0.00	0.00	0.00	0.00	0.46	0.00	0.00	0.00	0.00	0.00	0.00	0.00	0.00
MgO	0.01	0.01	0.02	0.01	0.01	0.01	0.01	0.01	0.01	0.01	0.00	0.02	0.01	0.02	0.02	0.21	0.02	0.02	0.01	0.02	0.01	0.02	0.01	0.00
P2O5	41.85	42.65	41.29	42.57	42.20	41.84	42.67	41.16	41.64	41.52	41.73	41.35	40.62	41.56	42.13	39.42	41.47	42.10	42.04	42.01	42.16	41.88	42.82	42.98
SO2	0.00	0.05	0.00	0.05	0.00	0.00	0.00	0.00	0.00	0.00	0.00	0.00	0.00	0.00	0.00	0.05	0.00	0.00	0.06	0.00	0.00	0.00	0.00	0.00
CaO	55.12	54.85	55.89	53.98	55.03	55.06	54.09	54.94	54.51	55.18	55.29	54.03	54.27	55.16	55.88	52.85	55.69	55.12	54.58	54.71	55.22	54.76	54.99	55.83
TiO2	0.00	0.00	0.00	0.00	0.00	0.00	0.00	0.00	0.00	0.00	0.00	0.00	0.00	0.00	0.00	0.00	0.00	0.00	0.00	0.00	0.00	0.00	0.00	0.00
MnO	0.00	0.00	0.00	0.00	0.00	0.00	0.00	0.00	0.00	0.00	0.00	0.00	0.00	0.00	0.00	0.00	0.00	0.00	0.00	0.00	0.00	0.00	0.00	0.00
Fe2O3	0.00	0.14	0.00	0.00	0.00	0.10	0.00	0.00	0.00	0.16	0.20	0.07	0.29	0.00	0.00	1.28	0.00	0.00	0.15	0.00	0.12	0.00	0.00	0.00
As2O3	0.00	0.00	0.00	0.00	0.00	0.00	0.00	0.00	0.00	0.00	0.00	0.00	0.00	0.00	0.00	0.00	0.00	0.00	0.00	0.00	0.00	0.00	0.00	0.00
SrO	0.00	0.00	0.00	0.00	0.00	0.00	0.00	0.00	0.00	0.00	0.00	0.00	0.00	0.00	0.00	0.00	0.00	0.00	0.00	0.00	0.00	0.00	0.00	0.00
Y2O3	0.00	0.00	0.14	0.12	0.06	0.14	0.00	0.15	0.00	0.00	0.00	0.16	0.21	0.17	0.10	0.00	0.00	0.00	0.18	0.07	0.11	0.08	0.00	0.15
La2O3	0.00	0.00	0.00	0.00	0.00	0.00	0.00	0.00	0.00	0.00	0.00	0.00	0.00	0.00	0.00	0.00	0.00	0.00	0.00	0.00	0.00	0.00	0.00	0.00
Ce2O3	0.00	0.00	0.00	0.12	0.00	0.00	0.00	0.17	0.00	0.00	0.00	0.29	0.27	0.17	0.14	0.00	0.00	0.00	0.00	0.00	0.00	0.20	0.10	0.18
Nd2O3	0.00	0.00	0.00	0.00	0.00	0.00	0.00	0.00	0.00	0.00	0.00	0.14	0.12	0.00	0.00	0.00	0.00	0.00	0.00	0.18	0.00	0.00	0.00	0.00
-O equivalent	-1.28	-1.46	-1.28	-1.36	-1.28	-1.28	-1.28	-1.48	-1.56	-1.58	-1.50	-1.40	-1.43	-1.47	-1.47	-1.30	-1.49	-1.45	-1.48	-1.46	-1.46	-1.40	-1.47	-1.37
Total	**99.2**	**99.9**	**99.8**	**99.4**	**99.7**	**99.8**	**99.0**	**99.2**	**98.7**	**99.4**	**99.5**	**98.9**	**98.6**	**100.0**	**100.9**	**97.9**	**99.7**	**99.7**	**99.7**	**99.6**	**100.3**	**99.5**	**100.5**	**101.7**

Calculated formulae 9 a.p.f.u.

Sample																							
Point	1	2	3	4	1	2	3	4	5	6	8	10	11	1	2	3	4	5	6	7	8	9	10	11
Grain	JT7 Ap15				JT7 Ap16									JT7 Ap17										
Ca	4.880	4.766	4.939	4.731	4.837	4.845	4.764	4.837	4.792	4.831	4.841	4.776	4.825	4.817	4.839	4.729	4.877	4.814	4.762	4.781	4.797	4.806	4.752	4.799
Mg	0.002	0.002	0.002	0.001	0.001	0.001	0.001	0.002	0.002	0.001	0.000	0.002	0.001	0.002	0.002	0.026	0.002	0.002	0.001	0.002	0.001	0.002	0.001	0.000
Mn	0.000	0.000	0.000	0.000	0.000	0.000	0.000	0.000	0.000	0.000	0.000	0.000	0.000	0.000	0.000	0.000	0.000	0.000	0.000	0.000	0.000	0.000	0.000	0.000
Sr	0.000	0.000	0.000	0.000	0.000	0.000	0.000	0.000	0.000	0.000	0.000	0.000	0.000	0.000	0.000	0.000	0.000	0.000	0.000	0.000	0.000	0.000	0.000	0.000
Y	0.000	0.000	0.006	0.005	0.003	0.006	0.000	0.006	0.000	0.000	0.000	0.007	0.009	0.008	0.004	0.000	0.000	0.000	0.008	0.003	0.005	0.004	0.000	0.006
La	0.000	0.000	0.000	0.000	0.000	0.000	0.000	0.000	0.000	0.000	0.000	0.000	0.000	0.000	0.000	0.000	0.000	0.000	0.000	0.000	0.000	0.000	0.000	0.000
Ce	0.000	0.000	0.000	0.003	0.000	0.000	0.000	0.005	0.000	0.000	0.000	0.009	0.008	0.005	0.004	0.000	0.000	0.000	0.000	0.000	0.000	0.006	0.003	0.005
Nd	0.000	0.000	0.000	0.000	0.000	0.000	0.000	0.000	0.000	0.000	0.000	0.004	0.004	0.000	0.000	0.000	0.000	0.000	0.000	0.005	0.000	0.000	0.000	0.000
Na	0.004	0.000	0.000	0.000	0.004	0.007	0.000	0.000	0.000	0.000	0.000	0.004	0.000	0.005	0.004	0.003	0.000	0.006	0.004	0.000	0.000	0.000	0.004	0.005
Fe	0.000	0.009	0.000	0.000	0.000	0.006	0.000	0.000	0.000	0.010	0.013	0.005	0.018	0.000	0.000	0.080	0.000	0.000	0.009	0.000	0.007	0.000	0.000	0.000
Ti	0.000	0.000	0.000	0.000	0.000	0.000	0.000	0.000	0.000	0.000	0.000	0.000	0.000	0.000	0.000	0.000	0.000	0.000	0.000	0.000	0.000	0.000	0.000	0.000
Al	0.000	0.000	0.000	0.000	0.000	0.000	0.000	0.000	0.000	0.000	0.000	0.000	0.000	0.000	0.000	0.045	0.000	0.000	0.000	0.000	0.000	0.000	0.000	0.000
Total	**4.886**	**4.777**	**4.948**	**4.741**	**4.845**	**4.866**	**4.765**	**4.850**	**4.794**	**4.842**	**4.853**	**4.807**	**4.865**	**4.837**	**4.853**	**4.883**	**4.879**	**4.822**	**4.784**	**4.792**	**4.811**	**4.818**	**4.761**	**4.816**
SREY	**0.000**	**0.000**	**0.006**	**0.009**	**0.003**	**0.006**	**0.000**	**0.011**	**0.000**	**0.000**	**0.000**	**0.020**	**0.021**	**0.013**	**0.008**	**0.000**	**0.000**	**0.000**	**0.008**	**0.008**	**0.005**	**0.010**	**0.003**	**0.012**
P	2.928	2.929	2.883	2.948	2.931	2.909	2.970	2.863	2.893	2.873	2.887	2.888	2.854	2.868	2.883	2.787	2.869	2.905	2.898	2.901	2.894	2.905	2.924	2.919
S	0.000	0.004	0.000	0.004	0.000	0.000	0.000	0.000	0.000	0.000	0.000	0.000	0.000	0.000	0.000	0.004	0.000	0.000	0.005	0.000	0.000	0.000	0.000	0.000
As	0.000	0.000	0.000	0.000	0.000	0.000	0.000	0.000	0.000	0.000	0.000	0.000	0.000	0.000	0.000	0.000	0.000	0.000	0.000	0.000	0.000	0.000	0.000	0.000
Si	0.000	0.000	0.025	0.021	0.020	0.034	0.012	0.035	0.008	0.000	0.000	0.046	0.046	0.044	0.022	0.132	0.016	0.015	0.026	0.027	0.031	0.026	0.018	0.028
Total	**2.928**	**2.933**	**2.908**	**2.973**	**2.950**	**2.943**	**2.981**	**2.898**	**2.900**	**2.873**	**2.887**	**2.935**	**2.900**	**2.911**	**2.905**	**2.923**	**2.886**	**2.921**	**2.928**	**2.929**	**2.925**	**2.931**	**2.943**	**2.947**
F	0.683	0.820	0.675	0.708	0.666	0.670	0.677	0.816	0.873	0.879	0.852	0.765	0.798	0.812	0.806	0.734	0.823	0.799	0.813	0.814	0.798	0.777	0.815	0.740
Cl	0.114	0.068	0.116	0.128	0.123	0.121	0.111	0.100	0.086	0.092	0.071	0.105	0.090	0.091	0.087	0.081	0.092	0.088	0.091	0.081	0.089	0.087	0.077	0.087
(F+Cl)	0.797	0.888	0.792	0.836	0.789	0.791	0.788	0.916	0.959	0.972	0.923	0.870	0.888	0.903	0.893	0.815	0.915	0.887	0.904	0.896	0.886	0.864	0.892	0.827
OH (by difference)	0.203	0.112	0.208	0.164	0.211	0.209	0.212	0.084	0.041	0.028	0.077	0.130	0.112	0.097	0.107	0.185	0.085	0.113	0.096	0.104	0.114	0.136	0.108	0.173
Total	**1.000**	**1.000**	**1.000**	**1.000**	**1.000**	**1.000**	**1.000**	**1.000**	**1.000**	**1.000**	**1.000**	**1.000**	**1.000**	**1.000**	**1.000**	**1.000**	**1.000**	**1.000**	**1.000**	**1.000**	**1.000**	**1.000**	**1.000**	**1.000**

Sample	*(continued)																								
Point	12	13	14	15	16	17	18	19	20	21	22	23	24	25	26	27	28	29	30	31	32	33	34	35	36
Grain	JT7 Ap17																								
F	2.91	3.29	3.14	3.22	3.01	3.05	3.26	3.16	2.96	2.97	3.22	3.27	3.21	3.05	3.28	2.97	2.90	3.25	3.18	3.37	3.08	3.13	3.01	3.26	2.99
Cl	0.64	0.61	0.64	0.73	0.59	0.63	0.59	0.63	0.57	0.66	0.67	0.61	0.51	0.73	0.49	0.65	0.59	0.55	0.61	0.47	0.61	0.68	0.68	0.60	0.71
Na2O	0.04	0.00	0.04	0.02	0.00	0.02	0.02	0.00	0.00	0.00	0.02	0.02	0.00	0.05	0.00	0.00	0.02	0.02	0.00	0.02	0.03	0.03	0.04	0.02	0.00
SiO2	0.45	0.24	0.60	0.37	0.18	0.38	0.19	0.33	0.02	0.25	0.38	0.08	0.03	0.46	0.00	0.26	0.24	0.08	0.19	0.00	0.36	0.39	0.51	0.00	0.06
Al2O3	0.00	0.00	0.00	0.00	0.00	0.00	0.00	0.00	0.00	0.00	0.00	0.00	0.00	0.00	0.00	0.00	0.00	0.00	0.00	0.00	0.00	0.00	0.00	0.00	0.00
MgO	0.01	0.02	0.01	0.02	0.02	0.02	0.01	0.03	0.01	0.02	0.01	0.01	0.02	0.02	0.02	0.02	0.01	0.01	0.02	0.00	0.02	0.02	0.01	0.01	0.01
P2O5	41.40	42.01	42.03	42.56	43.27	41.57	42.82	42.16	42.70	42.08	42.02	42.91	42.32	41.60	42.34	42.26	42.34	42.70	42.65	42.32	41.77	41.93	41.15	43.35	42.83
SO2	0.00	0.00	0.00	0.00	0.00	0.00	0.00	0.00	0.00	0.00	0.00	0.00	0.00	0.00	0.00	0.00	0.00	0.00	0.00	0.00	0.00	0.00	0.00	0.00	0.00
CaO	54.79	55.12	54.94	55.27	56.23	54.75	55.95	54.32	55.89	56.59	55.16	54.95	55.61	53.33	56.92	54.84	56.32	55.89	55.81	55.77	54.44	54.43	55.45	56.61	56.15
TiO2	0.00	0.00	0.00	0.00	0.00	0.00	0.00	0.00	0.00	0.00	0.00	0.00	0.00	0.00	0.00	0.00	0.00	0.00	0.00	0.00	0.00	0.00	0.00	0.00	0.00
MnO	0.00	0.00	0.00	0.00	0.00	0.00	0.00	0.00	0.00	0.00	0.00	0.00	0.00	0.00	0.00	0.00	0.00	0.00	0.00	0.00	0.00	0.00	0.00	0.00	0.00
Fe2O3	0.00	0.00	0.10	0.00	0.08	0.11	0.14	0.00	0.00	0.13	0.00	0.00	0.00	0.00	0.00	0.08	0.11	0.00	0.00	0.14	0.00	0.00	0.00	0.00	0.00
As2O3	0.00	0.00	0.00	0.00	0.00	0.00	0.00	0.00	0.00	0.00	0.00	0.00	0.00	0.00	0.00	0.00	0.00	0.00	0.00	0.00	0.00	0.00	0.00	0.00	0.00
SrO	0.00	0.00	0.00	0.00	0.00	0.00	0.00	0.00	0.00	0.00	0.00	0.00	0.00	0.00	0.00	0.00	0.00	0.00	0.00	0.00	0.00	0.00	0.00	0.00	0.00
Y2O3	0.13	0.10	0.12	0.06	0.07	0.06	0.00	0.15	0.00	0.09	0.09	0.00	0.00	0.07	0.00	0.00	0.00	0.00	0.10	0.00	0.10	0.13	0.16	0.00	0.00
La2O3	0.00	0.00	0.00	0.00	0.00	0.00	0.00	0.00	0.00	0.00	0.00	0.00	0.00	0.00	0.00	0.00	0.00	0.00	0.00	0.00	0.00	0.00	0.00	0.00	0.00
Ce2O3	0.17	0.00	0.31	0.19	0.00	0.22	0.00	0.00	0.00	0.00	0.00	0.00	0.00	0.17	0.00	0.12	0.00	0.00	0.00	0.00	0.11	0.10	0.24	0.00	0.00
Nd2O3	0.11	0.00	0.12	0.00	0.00	0.11	0.11	0.00	0.00	0.12	0.15	0.00	0.00	0.00	0.00	0.00	0.00	0.00	0.00	0.00	0.00	0.00	0.00	0.00	0.00
-O equivalent	-1.37	-1.52	-1.47	-1.52	-1.40	-1.43	-1.51	-1.47	-1.37	-1.40	-1.50	-1.52	-1.47	-1.45	-1.49	-1.40	-1.36	-1.49	-1.48	-1.52	-1.43	-1.47	-1.42	-1.51	-1.42
Total	**99.3**	**99.9**	**100.6**	**100.9**	**102.0**	**99.5**	**101.6**	**99.3**	**100.8**	**101.5**	**100.2**	**100.3**	**100.2**	**98.0**	**101.6**	**99.8**	**101.2**	**101.0**	**101.1**	**100.6**	**99.1**	**99.4**	**99.9**	**102.3**	**101.3**

Calculated formulae 9 a.p.f.u.

Sample	*(continued)																								
Point	12	13	14	15	16	17	18	19	20	21	22	23	24	25	26	27	28	29	30	31	32	33	34	35	36
Grain	JT7 Ap17																								
Ca	4.835	4.799	4.767	4.762	4.809	4.811	4.795	4.748	4.846	4.895	4.793	4.746	4.833	4.725	4.899	4.792	4.879	4.816	4.809	4.827	4.787	4.765	4.871	4.815	4.840
Mg	0.002	0.002	0.001	0.003	0.002	0.002	0.002	0.003	0.002	0.002	0.002	0.001	0.002	0.002	0.002	0.002	0.002	0.002	0.002	0.000	0.002	0.002	0.002	0.001	0.001
Mn	0.000	0.000	0.000	0.000	0.000	0.000	0.000	0.000	0.000	0.000	0.000	0.000	0.000	0.000	0.000	0.000	0.000	0.000	0.000	0.000	0.000	0.000	0.000	0.000	0.000
Sr	0.000	0.000	0.000	0.000	0.000	0.000	0.000	0.000	0.000	0.000	0.000	0.000	0.000	0.000	0.000	0.000	0.000	0.000	0.000	0.000	0.000	0.000	0.000	0.000	0.000
Y	0.006	0.004	0.005	0.003	0.003	0.003	0.000	0.007	0.000	0.004	0.004	0.000	0.000	0.003	0.000	0.000	0.000	0.000	0.004	0.000	0.004	0.006	0.007	0.000	0.000
La	0.000	0.000	0.000	0.000	0.000	0.000	0.000	0.000	0.000	0.000	0.000	0.000	0.000	0.000	0.000	0.000	0.000	0.000	0.000	0.000	0.000	0.000	0.000	0.000	0.000
Ce	0.005	0.000	0.009	0.006	0.000	0.007	0.000	0.000	0.000	0.000	0.000	0.000	0.000	0.005	0.000	0.003	0.000	0.000	0.000	0.000	0.003	0.003	0.007	0.000	0.000
Nd	0.003	0.000	0.004	0.000	0.000	0.003	0.003	0.000	0.000	0.003	0.004	0.000	0.000	0.000	0.000	0.000	0.000	0.000	0.000	0.000	0.000	0.000	0.000	0.000	0.000
Na	0.006	0.000	0.006	0.004	0.000	0.003	0.003	0.000	0.000	0.000	0.004	0.003	0.000	0.008	0.000	0.000	0.003	0.003	0.000	0.003	0.005	0.004	0.006	0.003	0.000
Fe	0.000	0.000	0.006	0.000	0.005	0.007	0.008	0.000	0.000	0.008	0.000	0.000	0.000	0.000	0.000	0.005	0.006	0.000	0.000	0.008	0.000	0.000	0.000	0.000	0.000
Ti	0.000	0.000	0.000	0.000	0.000	0.000	0.000	0.000	0.000	0.000	0.000	0.000	0.000	0.000	0.000	0.000	0.000	0.000	0.000	0.000	0.000	0.000	0.000	0.000	0.000
Al	0.000	0.000	0.000	0.000	0.000	0.000	0.000	0.000	0.000	0.000	0.000	0.000	0.000	0.000	0.000	0.000	0.000	0.000	0.000	0.000	0.000	0.000	0.000	0.000	0.000
Total	**4.857**	**4.805**	**4.798**	**4.777**	**4.818**	**4.835**	**4.811**	**4.758**	**4.847**	**4.912**	**4.807**	**4.750**	**4.835**	**4.743**	**4.901**	**4.803**	**4.890**	**4.820**	**4.816**	**4.838**	**4.801**	**4.780**	**4.894**	**4.819**	**4.841**
SREY	**0.014**	**0.004**	**0.018**	**0.008**	**0.003**	**0.013**	**0.003**	**0.007**	**0.000**	**0.007**	**0.008**	**0.000**	**0.000**	**0.008**	**0.000**	**0.003**	**0.000**	**0.000**	**0.004**	**0.000**	**0.008**	**0.009**	**0.014**	**0.000**	**0.000**
P	2.887	2.890	2.881	2.898	2.924	2.886	2.900	2.912	2.925	2.876	2.885	2.928	2.907	2.912	2.880	2.918	2.898	2.907	2.904	2.894	2.902	2.901	2.856	2.914	2.917
S	0.000	0.000	0.000	0.000	0.000	0.000	0.000	0.000	0.000	0.000	0.000	0.000	0.000	0.000	0.000	0.000	0.000	0.000	0.000	0.000	0.000	0.000	0.000	0.000	0.000
As	0.000	0.000	0.000	0.000	0.000	0.000	0.000	0.000	0.000	0.000	0.000	0.000	0.000	0.000	0.000	0.000	0.000	0.000	0.000	0.000	0.000	0.000	0.000	0.000	0.000
Si	0.037	0.019	0.049	0.030	0.014	0.031	0.015	0.027	0.002	0.020	0.031	0.006	0.003	0.038	0.000	0.021	0.020	0.007	0.016	0.000	0.030	0.032	0.042	0.000	0.005
Total	**2.924**	**2.909**	**2.930**	**2.927**	**2.938**	**2.917**	**2.915**	**2.940**	**2.927**	**2.896**	**2.916**	**2.935**	**2.909**	**2.950**	**2.880**	**2.939**	**2.918**	**2.914**	**2.920**	**2.894**	**2.932**	**2.932**	**2.899**	**2.914**	**2.922**
F	0.758	0.845	0.805	0.819	0.761	0.791	0.826	0.816	0.758	0.759	0.825	0.835	0.822	0.798	0.832	0.766	0.742	0.826	0.808	0.860	0.798	0.809	0.782	0.818	0.761
Cl	0.090	0.084	0.087	0.099	0.079	0.088	0.080	0.087	0.078	0.091	0.092	0.083	0.070	0.102	0.067	0.090	0.081	0.075	0.083	0.064	0.085	0.094	0.095	0.080	0.096
(F+Cl)	0.848	0.929	0.892	0.918	0.840	0.879	0.905	0.903	0.835	0.850	0.917	0.918	0.893	0.900	0.899	0.856	0.823	0.901	0.891	0.924	0.883	0.903	0.877	0.898	0.857
OH (by difference)	0.152	0.071	0.108	0.082	0.160	0.121	0.095	0.097	0.165	0.150	0.083	0.082	0.107	0.100	0.101	0.144	0.177	0.099	0.109	0.076	0.117	0.097	0.123	0.102	0.143
Total	**1.000**	**1.000**	**1.000**	**1.000**	**1.000**	**1.000**	**1.000**	**1.000**	**1.000**	**1.000**	**1.000**	**1.000**	**1.000**	**1.000**	**1.000**	**1.000**	**1.000**	**1.000**	**1.000**	**1.000**	**1.000**	**1.000**	**1.000**	**1.000**	**1.000**

Sample	*(continued)						Jt10																		
Point	37	38	39	40	41	42	1	2	3	4	5	1	2	3	4	5	1	2	3	4	1	2	3	4	5
Grain	JT7 Ap17						JT10 Ap1					JT10 Ap2					JT10 Ap3				JT10 Ap4				
F	2.97	3.08	3.10	3.01	3.19	3.25	3.22	3.49	3.59	3.71	3.71	3.65	3.51	3.27	3.43	3.58	3.36	3.72	3.86	3.63	3.25	3.36	3.15	3.28	2.98
Cl	0.64	0.62	0.67	0.68	0.58	0.50	0.38	0.26	0.40	0.32	0.33	0.33	0.26	0.43	0.39	0.32	0.47	0.24	0.26	0.24	0.42	0.45	0.49	0.52	0.54
Na2O	0.02	0.00	0.00	0.04	0.00	0.05	0.04	0.00	0.00	0.00	0.00	0.02	0.00	0.00	0.02	0.00	0.02	0.00	0.00	0.00	0.00	0.02	0.00	0.02	0.02
SiO2	0.28	0.33	0.34	0.49	0.00	0.27	0.00	0.00	0.04	0.00	0.00	0.00	0.00	0.00	0.00	0.00	0.00	0.00	0.00	0.00	0.00	0.00	0.00	0.02	0.00
Al2O3	0.00	0.00	0.00	0.00	0.00	0.00	0.00	0.00	0.00	0.00	0.00	0.00	0.00	0.00	0.00	0.00	0.00	0.00	0.00	0.00	0.00	0.00	0.00	0.00	0.00
MgO	0.02	0.02	0.01	0.02	0.01	0.01	0.01	0.01	0.01	0.01	0.01	0.01	0.01	0.02	0.01	0.01	0.01	0.01	0.01	0.01	0.01	0.01	0.01	0.01	0.02
P2O5	41.73	41.56	41.50	41.67	43.32	42.73	42.51	43.09	42.89	42.70	42.52	43.61	43.56	43.71	43.45	43.27	43.51	43.13	43.85	43.59	42.80	42.97	42.74	43.06	43.47
SO2	0.00	0.00	0.00	0.00	0.00	0.00	0.00	0.00	0.05	0.00	0.07	0.00	0.00	0.00	0.00	0.00	0.00	0.00	0.00	0.00	0.06	0.05	0.00	0.00	0.00
CaO	55.61	55.64	54.89	54.54	55.69	55.76	55.73	56.36	56.38	55.77	56.05	56.78	56.26	55.34	55.89	56.24	56.05	56.49	56.40	56.14	56.45	55.69	56.11	55.47	55.67
TiO2	0.00	0.00	0.00	0.00	0.00	0.00	0.00	0.00	0.00	0.00	0.00	0.00	0.00	0.00	0.00	0.00	0.00	0.00	0.00	0.00	0.00	0.00	0.00	0.00	0.00
MnO	0.00	0.00	0.00	0.00	0.00	0.00	0.00	0.00	0.00	0.00	0.00	0.00	0.00	0.00	0.00	0.00	0.00	0.00	0.00	0.00	0.00	0.00	0.00	0.00	0.00
Fe2O3	0.00	0.00	0.00	0.00	0.00	0.14	0.00	0.00	0.00	0.13	0.00	0.00	0.00	0.00	0.00	0.00	0.00	0.00	0.00	0.00	0.20	0.00	0.09	0.14	0.00
As2O3	0.00	0.00	0.00	0.00	0.00	0.00	0.00	0.00	0.00	0.00	0.00	0.00	0.00	0.00	0.00	0.00	0.00	0.00	0.00	0.00	0.00	0.00	0.00	0.00	0.00
SrO	0.00	0.00	0.00	0.00	0.00	0.00	0.00	0.00	0.00	0.00	0.00	0.00	0.00	0.00	0.00	0.00	0.00	0.00	0.00	0.00	0.00	0.00	0.00	0.00	0.00
Y2O3	0.00	0.20	0.08	0.13	0.00	0.11	0.00	0.00	0.00	0.00	0.00	0.00	0.00	0.00	0.00	0.00	0.00	0.00	0.00	0.00	0.00	0.00	0.00	0.00	0.00
La2O3	0.00	0.00	0.00	0.00	0.00	0.00	0.00	0.00	0.00	0.00	0.00	0.00	0.00	0.00	0.00	0.00	0.00	0.00	0.00	0.00	0.00	0.00	0.00	0.00	0.00
Ce2O3	0.13	0.00	0.13	0.16	0.00	0.00	0.00	0.00	0.00	0.00	0.00	0.00	0.00	0.00	0.00	0.00	0.00	0.00	0.00	0.00	0.00	0.00	0.00	0.00	0.00
Nd2O3	0.00	0.00	0.00	0.00	0.00	0.00	0.00	0.00	0.00	0.00	0.00	0.00	0.00	0.00	0.00	0.00	0.00	0.00	0.00	0.00	0.00	0.00	0.00	0.00	0.00
-O equivalent	-1.39	-1.44	-1.46	-1.42	-1.48	-1.48	-1.44	-1.53	-1.60	-1.64	-1.64	-1.61	-1.54	-1.47	-1.53	-1.58	-1.52	-1.62	-1.68	-1.59	-1.46	-1.52	-1.44	-1.50	-1.38
Total	**100.0**	**100.0**	**99.3**	**99.3**	**101.3**	**101.3**	**100.4**	**101.7**	**101.8**	**101.0**	**101.1**	**102.8**	**102.1**	**101.3**	**101.7**	**101.8**	**101.9**	**102.0**	**102.7**	**102.0**	**101.7**	**101.0**	**101.2**	**101.0**	**101.3**

Calculated formulae 9 a.p.f.u.

Sample	*(continued)						Jt10																		
Point	37	38	39	40	41	42	1	2	3	4	5	1	2	3	4	5	1	2	3	4	1	2	3	4	5
Grain	JT7 Ap17						JT10 Ap1					JT10 Ap2					JT10 Ap3				JT10 Ap4				
Ca	4.870	4.868	4.826	4.792	4.775	4.790	4.834	4.813	4.806	4.778	4.805	4.786	4.777	4.732	4.764	4.786	4.772	4.799	4.735	4.758	4.841	4.785	4.839	4.768	4.785
Mg	0.002	0.002	0.002	0.002	0.002	0.002	0.001	0.001	0.001	0.001	0.001	0.001	0.001	0.002	0.001	0.001	0.001	0.001	0.001	0.001	0.001	0.001	0.002	0.002	0.002
Mn	0.000	0.000	0.000	0.000	0.000	0.000	0.000	0.000	0.000	0.000	0.000	0.000	0.000	0.000	0.000	0.000	0.000	0.000	0.000	0.000	0.000	0.000	0.000	0.000	0.000
Sr	0.000	0.000	0.000	0.000	0.000	0.000	0.000	0.000	0.000	0.000	0.000	0.000	0.000	0.000	0.000	0.000	0.000	0.000	0.000	0.000	0.000	0.000	0.000	0.000	0.000
Y	0.000	0.009	0.003	0.005	0.000	0.005	0.000	0.000	0.000	0.000	0.000	0.000	0.000	0.000	0.000	0.000	0.000	0.000	0.000	0.000	0.000	0.000	0.000	0.000	0.000
La	0.000	0.000	0.000	0.000	0.000	0.000	0.000	0.000	0.000	0.000	0.000	0.000	0.000	0.000	0.000	0.000	0.000	0.000	0.000	0.000	0.000	0.000	0.000	0.000	0.000
Ce	0.004	0.000	0.004	0.005	0.000	0.000	0.000	0.000	0.000	0.000	0.000	0.000	0.000	0.000	0.000	0.000	0.000	0.000	0.000	0.000	0.000	0.000	0.000	0.000	0.000
Nd	0.000	0.000	0.000	0.000	0.000	0.000	0.000	0.000	0.000	0.000	0.000	0.000	0.000	0.000	0.000	0.000	0.000	0.000	0.000	0.000	0.000	0.000	0.000	0.000	0.000
Na	0.003	0.000	0.000	0.006	0.000	0.008	0.006	0.000	0.000	0.000	0.000	0.002	0.000	0.000	0.004	0.000	0.003	0.000	0.000	0.000	0.000	0.003	0.000	0.003	0.003
Fe	0.000	0.000	0.000	0.000	0.000	0.008	0.000	0.000	0.000	0.008	0.000	0.000	0.000	0.000	0.000	0.000	0.000	0.000	0.000	0.000	0.012	0.000	0.006	0.008	0.000
Ti	0.000	0.000	0.000	0.000	0.000	0.000	0.000	0.000	0.000	0.000	0.000	0.000	0.000	0.000	0.000	0.000	0.000	0.000	0.000	0.000	0.000	0.000	0.000	0.000	0.000
Al	0.000	0.000	0.000	0.000	0.000	0.000	0.000	0.000	0.000	0.000	0.000	0.000	0.000	0.000	0.000	0.000	0.000	0.000	0.000	0.000	0.000	0.000	0.000	0.000	0.000
Total	**4.878**	**4.878**	**4.835**	**4.811**	**4.777**	**4.812**	**4.841**	**4.814**	**4.807**	**4.779**	**4.806**	**4.789**	**4.778**	**4.734**	**4.769**	**4.787**	**4.776**	**4.800**	**4.736**	**4.759**	**4.842**	**4.788**	**4.841**	**4.772**	**4.791**
SREY	**0.004**	**0.009**	**0.007**	**0.010**	**0.000**	**0.005**	**0.000**	**0.000**	**0.000**	**0.000**	**0.000**	**0.000**	**0.000**	**0.000**	**0.000**	**0.000**	**0.000**	**0.000**	**0.000**	**0.000**	**0.000**	**0.000**	**0.000**	**0.000**	**0.000**
P	2.888	2.873	2.883	2.893	2.935	2.900	2.914	2.908	2.889	2.891	2.880	2.904	2.923	2.953	2.927	2.909	2.927	2.895	2.909	2.920	2.901	2.917	2.913	2.924	2.952
S	0.000	0.000	0.000	0.000	0.000	0.000	0.000	0.000	0.004	0.000	0.005	0.000	0.000	0.000	0.000	0.000	0.000	0.000	0.000	0.000	0.004	0.004	0.000	0.000	0.000
As	0.000	0.000	0.000	0.000	0.000	0.000	0.000	0.000	0.000	0.000	0.000	0.000	0.000	0.000	0.000	0.000	0.000	0.000	0.000	0.000	0.000	0.000	0.000	0.000	0.000
Si	0.023	0.027	0.028	0.040	0.000	0.022	0.000	0.000	0.003	0.000	0.000	0.000	0.000	0.000	0.000	0.000	0.000	0.000	0.000	0.000	0.000	0.000	0.000	0.002	0.000
Total	**2.911**	**2.900**	**2.911**	**2.933**	**2.935**	**2.922**	**2.914**	**2.908**	**2.896**	**2.891**	**2.885**	**2.904**	**2.923**	**2.953**	**2.927**	**2.909**	**2.927**	**2.895**	**2.909**	**2.920**	**2.905**	**2.921**	**2.913**	**2.926**	**2.952**
F	0.767	0.796	0.805	0.781	0.808	0.823	0.825	0.881	0.903	0.939	0.939	0.907	0.879	0.825	0.863	0.898	0.845	0.932	0.956	0.909	0.822	0.851	0.802	0.831	0.757
Cl	0.089	0.086	0.094	0.094	0.079	0.068	0.052	0.036	0.053	0.044	0.044	0.044	0.035	0.058	0.052	0.042	0.063	0.032	0.035	0.033	0.057	0.062	0.067	0.071	0.074
(F+Cl)	0.856	0.882	0.899	0.875	0.887	0.891	0.877	0.916	0.956	0.982	0.983	0.951	0.914	0.883	0.915	0.941	0.908	0.963	0.991	0.942	0.879	0.913	0.869	0.902	0.831
OH (by difference)	0.144	0.118	0.101	0.125	0.113	0.109	0.123	0.084	0.044	0.018	0.017	0.049	0.086	0.117	0.085	0.059	0.092	0.037	0.009	0.058	0.121	0.087	0.131	0.098	0.169
Total	**1.000**	**1.000**	**1.000**	**1.000**	**1.000**	**1.000**	**1.000**	**1.000**	**1.000**	**1.000**	**1.000**	**1.000**	**1.000**	**1.000**	**1.000**	**1.000**	**1.000**	**1.000**	**1.000**	**1.000**	**1.000**	**1.000**	**1.000**	**1.000**	**1.000**

Sample																						
Point	1	2	3	4	1	2	3	4	5	1	2	3	4	5	6	1	2	4	5	6	7	
Grain	JT10 Ap5				JT10 Ap6					JT10 Ap7						JT10 Ap8						
F	3.36	3.05	3.13	3.21	3.07	3.24	3.23	3.21	3.23	3.53	3.38	3.13	3.36	3.34	3.59	2.59	2.59	2.87	2.88	2.74	2.68	
Cl	0.42	0.59	0.29	0.47	0.50	0.47	0.59	0.53	0.56	0.10	0.23	0.40	0.15	0.26	0.11	0.82	0.87	0.58	0.80	0.73	0.73	
Na2O	0.00	0.03	0.02	0.02	0.03	0.17	0.04	0.07	0.02	0.00	0.00	0.02	0.02	0.00	0.00	0.00	0.00	0.00	0.00	0.00	0.02	
SiO2	0.00	0.00	0.00	0.00	0.00	0.07	0.00	0.00	0.00	0.05	0.02	0.06	0.06	0.08	0.00	0.44	0.58	0.03	0.21	0.02	0.28	
Al2O3	0.00	0.00	0.00	0.00	0.00	0.00	0.00	0.00	0.00	0.00	0.00	0.00	0.00	0.00	0.00	0.00	0.00	0.00	0.00	0.00	0.00	
MgO	0.01	0.00	0.01	0.01	0.01	0.01	0.02	0.00	0.02	0.00	0.00	0.01	0.00	0.01	0.00	0.01	0.01	0.01	0.01	0.01	0.01	
P2O5	43.41	43.74	43.35	42.27	42.44	42.42	42.85	42.58	43.28	42.52	42.96	42.91	43.11	42.84	42.88	42.46	42.02	42.69	42.29	42.70	42.15	
SO2	0.00	0.00	0.00	0.00	0.00	0.00	0.00	0.00	0.00	0.00	0.05	0.00	0.00	0.00	0.00	0.00	0.00	0.00	0.00	0.00	0.00	
CaO	55.32	55.14	55.84	55.61	56.36	54.84	54.95	55.50	56.76	56.01	55.86	55.89	55.58	54.64	56.46	54.17	53.18	54.51	55.32	56.36	55.78	
TiO2	0.00	0.00	0.00	0.00	0.00	0.00	0.00	0.00	0.00	0.00	0.00	0.00	0.00	0.00	0.00	0.00	0.00	0.00	0.00	0.00	0.00	
MnO	0.00	0.00	0.00	0.00	0.00	0.00	0.00	0.00	0.00	0.00	0.00	0.00	0.00	0.00	0.00	0.00	0.00	0.00	0.00	0.00	0.00	
Fe2O3	0.00	0.15	0.00	0.00	0.00	0.00	0.00	0.00	0.11	0.00	0.00	0.00	0.00	0.00	0.00	0.00	0.00	0.00	0.00	0.00	0.12	
As2O3	0.00	0.00	0.00	0.00	0.00	0.00	0.00	0.00	0.00	0.00	0.00	0.00	0.00	0.00	0.00	0.00	0.00	0.00	0.00	0.00	0.00	
SrO	0.00	0.00	0.00	0.00	0.00	0.00	0.00	0.00	0.00	0.00	0.00	0.00	0.00	0.00	0.00	0.00	0.00	0.00	0.00	0.00	0.00	
Y2O3	0.00	0.00	0.00	0.00	0.00	0.06	0.00	0.00	0.00	0.00	0.00	0.00	0.00	0.00	0.00	0.36	0.52	0.00	0.19	0.00	0.23	
La2O3	0.00	0.00	0.00	0.00	0.00	0.00	0.00	0.00	0.00	0.00	0.00	0.00	0.00	0.00	0.00	0.00	0.00	0.00	0.00	0.00	0.00	
Ce2O3	0.00	0.00	0.00	0.00	0.00	0.00	0.00	0.00	0.00	0.00	0.00	0.00	0.00	0.00	0.00	0.00	0.00	0.00	0.00	0.00	0.00	
Nd2O3	0.00	0.00	0.00	0.00	0.00	0.00	0.00	0.00	0.00	0.00	0.00	0.00	0.00	0.00	0.00	0.00	0.00	0.00	0.00	0.00	0.00	
-O equivalent	-1.51	-1.42	-1.38	-1.46	-1.41	-1.47	-1.49	-1.47	-1.49	-1.51	-1.47	-1.41	-1.45	-1.46	-1.54	-1.28	-1.29	-1.34	-1.39	-1.32	-1.29	
Total	**101.0**	**101.3**	**101.3**	**100.1**	**101.0**	**99.8**	**100.2**	**100.4**	**102.5**	**100.7**	**101.0**	**101.0**	**100.8**	**99.7**	**101.5**	**99.6**	**98.5**	**99.4**	**100.3**	**101.2**	**100.7**	

Calculated formulae 9 a.p.f.u.

Sample																					
Point	1	2	3	4	1	2	3	4	5	1	2	3	4	5	6	1	2	4	5	6	7
Grain	JT10 Ap5				JT10 Ap6					JT10 Ap7						JT10 Ap8					
Ca	4.741	4.726	4.801	4.840	4.882	4.775	4.758	4.811	4.828	4.833	4.803	4.823	4.784	4.746	4.831	4.756	4.713	4.778	4.821	4.884	4.868
Mg	0.002	0.000	0.001	0.002	0.001	0.002	0.002	0.000	0.002	0.000	0.000	0.001	0.000	0.001	0.000	0.001	0.001	0.001	0.001	0.002	0.001
Mn	0.000	0.000	0.000	0.000	0.000	0.000	0.000	0.000	0.000	0.000	0.000	0.000	0.000	0.000	0.000	0.000	0.000	0.000	0.000	0.000	0.000
Sr	0.000	0.000	0.000	0.000	0.000	0.000	0.000	0.000	0.000	0.000	0.000	0.000	0.000	0.000	0.000	0.000	0.000	0.000	0.000	0.000	0.000
Y	0.000	0.000	0.000	0.000	0.000	0.003	0.000	0.000	0.000	0.000	0.000	0.000	0.000	0.000	0.000	0.016	0.023	0.000	0.008	0.000	0.010
La	0.000	0.000	0.000	0.000	0.000	0.000	0.000	0.000	0.000	0.000	0.000	0.000	0.000	0.000	0.000	0.000	0.000	0.000	0.000	0.000	0.000
Ce	0.000	0.000	0.000	0.000	0.000	0.000	0.000	0.000	0.000	0.000	0.000	0.000	0.000	0.000	0.000	0.000	0.000	0.000	0.000	0.000	0.000
Nd	0.000	0.000	0.000	0.000	0.000	0.000	0.000	0.000	0.000	0.000	0.000	0.000	0.000	0.000	0.000	0.000	0.000	0.000	0.000	0.000	0.000
Na	0.000	0.005	0.004	0.003	0.004	0.028	0.007	0.012	0.003	0.000	0.000	0.003	0.003	0.000	0.000	0.000	0.000	0.000	0.000	0.000	0.003
Fe	0.000	0.009	0.000	0.000	0.000	0.000	0.000	0.000	0.007	0.000	0.000	0.000	0.000	0.000	0.000	0.000	0.000	0.000	0.000	0.000	0.007
Ti	0.000	0.000	0.000	0.000	0.000	0.000	0.000	0.000	0.000	0.000	0.000	0.000	0.000	0.000	0.000	0.000	0.000	0.000	0.000	0.000	0.000
Al	0.000	0.000	0.000	0.000	0.000	0.000	0.000	0.000	0.000	0.000	0.000	0.000	0.000	0.000	0.000	0.000	0.000	0.000	0.000	0.000	0.000
Total	**4.743**	**4.731**	**4.805**	**4.845**	**4.887**	**4.807**	**4.767**	**4.822**	**4.833**	**4.833**	**4.803**	**4.827**	**4.787**	**4.747**	**4.831**	**4.773**	**4.737**	**4.779**	**4.831**	**4.885**	**4.882**
SREY	**0.000**	**0.000**	**0.000**	**0.000**	**0.000**	**0.003**	**0.000**	**0.000**	**0.000**	**0.000**	**0.000**	**0.000**	**0.000**	**0.000**	**0.000**	**0.016**	**0.023**	**0.000**	**0.008**	**0.000**	**0.010**
P	2.940	2.962	2.945	2.907	2.905	2.919	2.932	2.916	2.909	2.899	2.919	2.925	2.933	2.940	2.899	2.945	2.942	2.957	2.913	2.924	2.906
S	0.000	0.000	0.000	0.000	0.000	0.000	0.000	0.000	0.000	0.000	0.004	0.000	0.000	0.000	0.000	0.000	0.000	0.000	0.000	0.000	0.000
As	0.000	0.000	0.000	0.000	0.000	0.000	0.000	0.000	0.000	0.000	0.000	0.000	0.000	0.000	0.000	0.000	0.000	0.000	0.000	0.000	0.000
Si	0.000	0.000	0.000	0.000	0.000	0.006	0.000	0.000	0.000	0.004	0.002	0.005	0.005	0.006	0.000	0.036	0.048	0.002	0.017	0.002	0.023
Total	**2.940**	**2.962**	**2.945**	**2.907**	**2.905**	**2.925**	**2.932**	**2.916**	**2.909**	**2.903**	**2.924**	**2.930**	**2.938**	**2.946**	**2.899**	**2.981**	**2.990**	**2.959**	**2.930**	**2.925**	**2.929**
F	0.851	0.772	0.795	0.824	0.785	0.832	0.826	0.821	0.811	0.898	0.857	0.797	0.853	0.855	0.906	0.670	0.679	0.743	0.740	0.702	0.691
Cl	0.056	0.080	0.039	0.065	0.069	0.064	0.081	0.072	0.076	0.014	0.031	0.055	0.020	0.036	0.015	0.114	0.122	0.081	0.110	0.100	0.101
(F+Cl)	0.908	0.852	0.834	0.889	0.854	0.896	0.907	0.893	0.887	0.912	0.888	0.851	0.873	0.891	0.921	0.785	0.800	0.824	0.850	0.802	0.791
OH (by difference)	0.092	0.148	0.166	0.111	0.146	0.104	0.093	0.107	0.113	0.088	0.112	0.149	0.127	0.109	0.079	0.215	0.200	0.176	0.150	0.198	0.209
Total	**1.000**	**1.000**	**1.000**	**1.000**	**1.000**	**1.000**	**1.000**	**1.000**	**1.000**	**1.000**	**1.000**	**1.000**	**1.000**	**1.000**	**1.000**	**1.000**	**1.000**	**1.000**	**1.000**	**1.000**	**1.000**

Sample																	
Point	1	2	3	4	5	6	1	2	3	4	1	2	3	4	1	2	3
Grain	JT10 Ap9						JT10 Ap10				JT10 Ap13				JT10 Ap map 1		
F	2.75	3.27	2.69	2.75	2.92	2.71	2.90	2.93	3.11	3.10	3.05	3.33	3.17	3.25	3.36	2.84	2.91
Cl	0.96	0.26	0.80	0.91	0.73	0.79	0.66	0.67	0.71	0.48	0.58	0.59	0.60	0.60	0.42	0.71	0.64
Na2O	0.04	0.03	0.02	0.00	0.04	0.00	0.04	0.03	0.03	0.11	0.03	0.04	0.02	0.02	0.00	0.00	0.02
SiO2	0.00	0.00	0.00	0.31	0.14	0.00	0.76	0.12	0.13	0.16	0.08	0.00	0.09	0.25	0.00	0.18	0.00
Al2O3	0.00	0.00	0.00	0.00	0.00	0.00	0.03	0.00	0.00	0.00	0.00	0.00	0.00	0.00	0.00	0.00	0.00
MgO	0.01	0.00	0.01	0.01	0.02	0.01	0.05	0.01	0.01	0.01	0.01	0.01	0.01	0.01	0.01	0.01	0.01
P2O5	42.28	42.87	43.31	43.28	42.10	43.13	42.22	42.24	42.92	41.60	42.49	43.64	42.85	43.15	42.79	42.12	42.97
SO2	0.08	0.14	0.04	0.00	0.00	0.00	0.00	0.00	0.05	0.00	0.00	0.00	0.00	0.00	0.00	0.00	0.00
CaO	56.34	56.47	54.31	55.28	54.93	55.47	54.07	55.44	54.52	55.12	54.58	56.96	55.56	54.99	55.64	54.26	56.18
TiO2	0.00	0.00	0.00	0.00	0.00	0.00	0.00	0.00	0.00	0.00	0.00	0.00	0.00	0.00	0.00	0.00	0.00
MnO	0.00	0.00	0.00	0.00	0.00	0.00	0.00	0.00	0.00	0.00	0.00	0.00	0.00	0.00	0.00	0.00	0.00
Fe2O3	0.10	0.26	0.29	0.00	0.08	0.00	0.56	0.00	0.00	0.00	0.00	0.00	0.00	0.11	0.36	0.00	0.00
As2O3	0.00	0.00	0.00	0.00	0.00	0.00	0.00	0.00	0.00	0.00	0.00	0.00	0.00	0.00	0.00	0.00	0.00
SrO	0.00	0.00	0.00	0.00	0.00	0.00	0.00	0.00	0.00	0.00	0.00	0.00	0.00	0.00	0.00	0.00	0.00
Y2O3	0.00	0.00	0.00	0.36	0.16	0.00	0.00	0.12	0.06	0.15	0.06	0.00	0.00	0.27	0.00	0.17	0.00
La2O3	0.00	0.00	0.00	0.00	0.00	0.00	0.00	0.00	0.00	0.00	0.00	0.00	0.00	0.00	0.00	0.00	0.00
Ce2O3	0.00	0.00	0.00	0.00	0.00	0.00	0.00	0.00	0.00	0.00	0.00	0.00	0.00	0.00	0.00	0.00	0.00
Nd2O3	0.00	0.00	0.00	0.00	0.00	0.00	0.00	0.00	0.00	0.00	0.00	0.00	0.00	0.00	0.00	0.00	0.00
-O equivalent	-1.37	-1.43	-1.31	-1.36	-1.40	-1.32	-1.37	-1.38	-1.47	-1.41	-1.42	-1.53	-1.47	-1.50	-1.51	-1.35	-1.37
Total	**101.2**	**101.9**	**100.1**	**101.5**	**99.7**	**100.8**	**99.9**	**100.2**	**100.1**	**99.3**	**99.5**	**103.0**	**100.8**	**101.1**	**101.1**	**98.9**	**101.4**

Calculated formulae 9 a.p.f.u.

Sample																	
Point	1	2	3	4	5	6	1	2	3	4	1	2	3	4	1	2	3
Grain	JT10 Ap9						JT10 Ap10				JT10 Ap13				JT10 Ap map 1		
Ca	4.889	4.837	4.724	4.753	4.811	4.810	4.710	4.839	4.724	4.850	4.772	4.809	4.792	4.716	4.786	4.785	4.846
Mg	0.002	0.000	0.001	0.001	0.002	0.001	0.006	0.001	0.002	0.002	0.001	0.001	0.001	0.001	0.001	0.001	0.002
Mn	0.000	0.000	0.000	0.000	0.000	0.000	0.000	0.000	0.000	0.000	0.000	0.000	0.000	0.000	0.000	0.000	0.000
Sr	0.000	0.000	0.000	0.000	0.000	0.000	0.000	0.000	0.000	0.000	0.000	0.000	0.000	0.000	0.000	0.000	0.000
Y	0.000	0.000	0.000	0.015	0.007	0.000	0.000	0.005	0.002	0.007	0.003	0.000	0.000	0.012	0.000	0.007	0.000
La	0.000	0.000	0.000	0.000	0.000	0.000	0.000	0.000	0.000	0.000	0.000	0.000	0.000	0.000	0.000	0.000	0.000
Ce	0.000	0.000	0.000	0.000	0.000	0.000	0.000	0.000	0.000	0.000	0.000	0.000	0.000	0.000	0.000	0.000	0.000
Nd	0.000	0.000	0.000	0.000	0.000	0.000	0.000	0.000	0.000	0.000	0.000	0.000	0.000	0.000	0.000	0.000	0.000
Na	0.007	0.004	0.003	0.000	0.007	0.000	0.007	0.004	0.004	0.017	0.005	0.006	0.003	0.004	0.000	0.000	0.003
Fe	0.006	0.016	0.017	0.000	0.005	0.000	0.034	0.000	0.000	0.000	0.000	0.000	0.000	0.007	0.022	0.000	0.000
Ti	0.000	0.000	0.000	0.000	0.000	0.000	0.000	0.000	0.000	0.000	0.000	0.000	0.000	0.000	0.000	0.000	0.000
Al	0.000	0.000	0.000	0.000	0.000	0.000	0.003	0.000	0.000	0.000	0.000	0.000	0.000	0.000	0.000	0.000	0.000
Total	**4.898**	**4.842**	**4.727**	**4.770**	**4.827**	**4.811**	**4.723**	**4.850**	**4.733**	**4.876**	**4.780**	**4.816**	**4.796**	**4.733**	**4.787**	**4.793**	**4.851**
SREY	**0.000**	**0.000**	**0.000**	**0.015**	**0.007**	**0.000**	**0.000**	**0.005**	**0.002**	**0.007**	**0.003**	**0.000**	**0.000**	**0.012**	**0.000**	**0.007**	**0.000**
P	2.900	2.902	2.976	2.941	2.914	2.955	2.906	2.913	2.939	2.892	2.936	2.912	2.921	2.924	2.908	2.935	2.929
S	0.006	0.010	0.003	0.000	0.000	0.000	0.000	0.000	0.004	0.000	0.000	0.000	0.000	0.000	0.000	0.000	0.000
As	0.000	0.000	0.000	0.000	0.000	0.000	0.000	0.000	0.000	0.000	0.000	0.000	0.000	0.000	0.000	0.000	0.000
Si	0.000	0.000	0.000	0.025	0.012	0.000	0.062	0.010	0.010	0.013	0.006	0.000	0.007	0.020	0.000	0.015	0.000
Total	**2.905**	**2.912**	**2.980**	**2.966**	**2.926**	**2.955**	**2.968**	**2.923**	**2.953**	**2.906**	**2.942**	**2.912**	**2.928**	**2.944**	**2.908**	**2.950**	**2.929**
F	0.704	0.826	0.691	0.698	0.756	0.694	0.746	0.755	0.796	0.805	0.788	0.829	0.808	0.823	0.853	0.738	0.741
Cl	0.131	0.036	0.110	0.123	0.101	0.108	0.091	0.092	0.097	0.067	0.081	0.078	0.082	0.081	0.057	0.098	0.087
(F+Cl)	0.836	0.862	0.800	0.821	0.857	0.802	0.837	0.847	0.893	0.872	0.869	0.907	0.889	0.904	0.910	0.836	0.828
OH (by difference)	0.164	0.138	0.200	0.179	0.143	0.198	0.163	0.153	0.107	0.128	0.131	0.093	0.111	0.096	0.090	0.164	0.172
Total	**1.000**	**1.000**	**1.000**	**1.000**	**1.000**	**1.000**	**1.000**	**1.000**	**1.000**	**1.000**	**1.000**	**1.000**	**1.000**	**1.000**	**1.000**	**1.000**	**1.000**

Profiles																							
Jt1 - grain 1	Along																						
Points	**1**	**2**	**3**	**4**	**5**	**6**	**7**	**8**	**9**	**10**	**11**	**12**	**13**	**14**	**15**	**16**	**17**	**18**	**19**	**20**	**21**	**22**	**23**
F	2.64	2.37	2.58	2.51	2.41	2.61	2.57	2.39	2.34	2.36	2.09	2.27	2.00	2.05	2.20	2.16	2.14	2.21	2.15	2.38	2.14	2.44	2.31
Cl	1.20	1.07	1.05	0.96	1.10	0.78	0.94	1.16	1.11	1.35	1.39	1.28	1.23	1.38	1.24	1.50	1.36	1.38	1.25	1.29	1.33	1.28	1.02
Na2O	0.02	0.00	0.03	0.00	0.00	0.02	0.06	0.00	0.00	0.00	0.02	0.02	0.00	0.00	0.00	0.00	0.00	0.00	0.05	0.00	0.00	0.03	0.00
SiO2	0.30	0.30	0.35	0.18	0.25	0.40	0.00	0.26	0.23	0.25	0.41	0.37	0.09	0.46	0.49	0.46	0.46	0.46	0.40	0.44	0.43	0.00	0.00
Al2O3	0.00	0.00	0.00	0.00	0.00	0.15	0.00	0.00	0.00	0.00	0.00	0.00	0.03	0.00	0.00	0.00	0.00	0.00	0.00	0.00	0.00	0.00	0.00
MgO	0.01	0.01	0.00	0.01	0.01	0.22	0.01	0.01	0.00	0.01	0.02	0.02	0.07	0.01	0.01	0.01	0.01	0.01	0.01	0.01	0.01	0.01	0.01
P2O5	42.48	41.90	41.91	42.39	41.74	41.64	42.38	41.97	42.13	42.26	42.57	42.09	42.43	41.43	41.58	40.97	41.38	42.14	41.25	41.23	40.99	42.43	42.57
SO2	0.05	0.05	0.06	0.00	0.00	0.00	0.05	0.05	0.00	0.00	0.07	0.00	0.00	0.00	0.00	0.06	0.00	0.00	0.00	0.00	0.00	0.04	0.00
CaO	54.34	54.54	54.94	56.10	54.17	54.94	54.09	54.97	55.21	55.16	54.92	54.37	54.01	55.04	54.20	54.41	54.81	54.85	54.33	54.94	54.78	54.90	54.97
TiO2	0.00	0.00	0.00	0.00	0.00	0.00	0.00	0.00	0.00	0.00	0.00	0.00	0.00	0.00	0.00	0.00	0.00	0.00	0.00	0.00	0.00	0.00	0.00
MnO	0.00	0.00	0.00	0.00	0.00	0.00	0.00	0.00	0.00	0.00	0.00	0.00	0.00	0.00	0.00	0.00	0.00	0.00	0.00	0.00	0.00	0.00	0.00
Fe2O3	0.00	0.07	0.00	0.09	0.00	0.57	0.00	0.00	0.00	0.00	0.00	0.00	0.10	0.00	0.10	0.00	0.00	0.00	0.00	0.00	0.00	0.00	0.17
As2O3	0.00	0.00	0.00	0.00	0.00	0.00	0.00	0.00	0.00	0.00	0.00	0.00	0.00	0.00	0.00	0.00	0.00	0.00	0.00	0.00	0.00	0.00	0.00
SrO	0.00	0.00	0.02	0.00	0.00	0.00	0.00	0.00	0.00	0.00	0.00	0.00	0.00	0.00	0.00	0.00	0.00	0.00	0.00	0.00	0.00	0.00	0.00
Y2O3	0.16	0.17	0.22	0.13	0.17	0.12	0.00	0.17	0.10	0.07	0.14	0.16	0.00	0.19	0.15	0.11	0.17	0.17	0.19	0.11	0.25	0.00	0.00
La2O3	0.00	0.00	0.00	0.00	0.00	0.00	0.00	0.00	0.00	0.00	0.00	0.00	0.00	0.00	0.00	0.00	0.00	0.00	0.00	0.00	0.00	0.00	0.00
Ce2O3	0.00	0.00	0.00	0.00	0.00	0.00	0.00	0.11	0.00	0.00	0.11	0.12	0.00	0.14	0.26	0.22	0.16	0.24	0.12	0.22	0.00	0.00	0.00
Nd2O3	0.00	0.12	0.00	0.00	0.00	0.00	0.00	0.00	0.10	0.00	0.00	0.13	0.00	0.15	0.13	0.13	0.16	0.00	0.00	0.00	0.00	0.00	0.00
-O equivalent	-1.38	-1.24	-1.33	-1.27	-1.26	-1.28	-1.30	-1.27	-1.23	-1.30	-1.19	-1.24	-1.12	-1.17	-1.21	-1.25	-1.21	-1.24	-1.19	-1.29	-1.20	-1.32	-1.20
Total	**99.8**	**99.4**	**99.8**	**101.1**	**98.6**	**100.2**	**98.8**	**99.8**	**100.0**	**100.2**	**100.5**	**99.6**	**98.8**	**99.7**	**99.2**	**98.8**	**99.4**	**100.2**	**98.6**	**99.3**	**98.7**	**99.8**	**99.8**

Calculated formulae 9 a.p.f.u.

Profiles																							
Jt1 - grain 1	Along																						
Points	**1**	**2**	**3**	**4**	**5**	**6**	**7**	**8**	**9**	**10**	**11**	**12**	**13**	**14**	**15**	**16**	**17**	**18**	**19**	**20**	**21**	**22**	**23**
Ca	4.749	4.825	4.827	4.885	4.820	4.821	4.783	4.844	4.861	4.836	4.809	4.801	4.806	4.892	4.822	4.867	4.875	4.820	4.866	4.876	4.906	4.820	4.838
Mg	0.001	0.001	0.000	0.001	0.001	0.027	0.001	0.002	0.000	0.001	0.002	0.002	0.009	0.002	0.002	0.001	0.001	0.001	0.001	0.001	0.002	0.002	0.002
Mn	0.000	0.000	0.000	0.000	0.000	0.000	0.000	0.000	0.000	0.000	0.000	0.000	0.000	0.000	0.000	0.000	0.000	0.000	0.000	0.000	0.000	0.000	0.000
Sr	0.000	0.000	0.001	0.000	0.000	0.000	0.000	0.000	0.000	0.000	0.000	0.000	0.000	0.000	0.000	0.000	0.000	0.000	0.000	0.000	0.000	0.000	0.000
Y	0.007	0.007	0.010	0.006	0.007	0.005	0.000	0.008	0.004	0.003	0.006	0.007	0.000	0.008	0.006	0.005	0.007	0.008	0.008	0.005	0.011	0.000	0.000
La	0.000	0.000	0.000	0.000	0.000	0.000	0.000	0.000	0.000	0.000	0.000	0.000	0.000	0.000	0.000	0.000	0.000	0.000	0.000	0.000	0.000	0.000	0.000
Ce	0.000	0.000	0.000	0.000	0.000	0.000	0.000	0.003	0.000	0.000	0.003	0.004	0.000	0.004	0.008	0.007	0.005	0.007	0.004	0.007	0.000	0.000	0.000
Nd	0.000	0.004	0.000	0.000	0.000	0.000	0.000	0.000	0.003	0.000	0.000	0.004	0.000	0.004	0.004	0.004	0.005	0.000	0.000	0.000	0.000	0.000	0.000
Na	0.004	0.000	0.005	0.000	0.000	0.003	0.009	0.000	0.000	0.000	0.003	0.004	0.000	0.000	0.000	0.000	0.000	0.000	0.008	0.000	0.000	0.004	0.000
Fe	0.000	0.005	0.000	0.006	0.000	0.035	0.000	0.000	0.000	0.000	0.000	0.000	0.006	0.000	0.006	0.000	0.000	0.000	0.000	0.000	0.000	0.000	0.010
Ti	0.000	0.000	0.000	0.000	0.000	0.000	0.000	0.000	0.000	0.000	0.000	0.000	0.000	0.000	0.000	0.000	0.000	0.000	0.000	0.000	0.000	0.000	0.000
Al	0.000	0.000	0.000	0.000	0.000	0.015	0.000	0.000	0.000	0.000	0.000	0.000	0.003	0.000	0.000	0.000	0.000	0.000	0.000	0.000	0.000	0.000	0.000
Total	**4.761**	**4.842**	**4.842**	**4.898**	**4.829**	**4.906**	**4.793**	**4.856**	**4.869**	**4.840**	**4.824**	**4.821**	**4.824**	**4.911**	**4.848**	**4.883**	**4.893**	**4.836**	**4.887**	**4.889**	**4.919**	**4.826**	**4.850**
SREY	**0.007**	**0.011**	**0.010**	**0.006**	**0.007**	**0.005**	**0.000**	**0.011**	**0.007**	**0.003**	**0.009**	**0.015**	**0.000**	**0.017**	**0.018**	**0.015**	**0.017**	**0.015**	**0.012**	**0.011**	**0.011**	**0.000**	**0.000**
P	2.933	2.929	2.909	2.916	2.935	2.887	2.961	2.922	2.931	2.928	2.945	2.937	2.983	2.910	2.923	2.896	2.908	2.927	2.919	2.891	2.901	2.944	2.961
S	0.004	0.004	0.005	0.000	0.000	0.000	0.004	0.004	0.000	0.000	0.005	0.000	0.000	0.000	0.000	0.005	0.000	0.000	0.000	0.000	0.000	0.003	0.000
As	0.000	0.000	0.000	0.000	0.000	0.000	0.000	0.000	0.000	0.000	0.000	0.000	0.000	0.000	0.000	0.000	0.000	0.000	0.000	0.000	0.000	0.000	0.000
Si	0.025	0.025	0.028	0.014	0.021	0.033	0.000	0.021	0.019	0.020	0.033	0.031	0.007	0.038	0.040	0.039	0.038	0.037	0.033	0.036	0.036	0.000	0.000
Total	**2.962**	**2.958**	**2.942**	**2.931**	**2.956**	**2.920**	**2.964**	**2.948**	**2.950**	**2.948**	**2.984**	**2.968**	**2.990**	**2.947**	**2.963**	**2.940**	**2.946**	**2.964**	**2.953**	**2.928**	**2.936**	**2.947**	**2.961**
F	0.681	0.620	0.670	0.645	0.633	0.676	0.671	0.621	0.607	0.611	0.539	0.590	0.526	0.537	0.578	0.569	0.561	0.574	0.567	0.624	0.565	0.632	0.600
Cl	0.166	0.150	0.146	0.132	0.156	0.109	0.132	0.161	0.154	0.188	0.193	0.179	0.173	0.194	0.175	0.213	0.191	0.191	0.178	0.181	0.188	0.178	0.142
(F+Cl)	0.847	0.770	0.816	0.777	0.788	0.785	0.803	0.782	0.761	0.798	0.732	0.770	0.700	0.731	0.752	0.782	0.753	0.765	0.745	0.804	0.753	0.810	0.743
OH (by difference)	0.153	0.230	0.184	0.223	0.212	0.215	0.197	0.218	0.239	0.202	0.268	0.230	0.300	0.269	0.248	0.218	0.247	0.235	0.255	0.196	0.247	0.190	0.257
Total	**1.000**	**1.000**	**1.000**	**1.000**	**1.000**	**1.000**	**1.000**	**1.000**	**1.000**	**1.000**	**1.000**	**1.000**	**1.000**	**1.000**	**1.000**	**1.000**	**1.000**	**1.000**	**1.000**	**1.000**	**1.000**	**1.000**	**1.000**

Profiles	*(continued)												
Jt1 - grain 1	Acrross												
Points	**24**	**25**	**26**	**27**	**28**	**29**	**30**	**31**	**32**	**33**	**34**	**35**	**36**
F	0.17	2.16	1.97	2.28	2.18	2.14	2.11	2.16	2.17	2.11	2.31	2.28	2.13
Cl	0.81	1.21	1.35	0.68	1.26	1.35	1.40	1.47	1.30	1.32	1.29	1.34	1.31
Na2O	0.00	0.00	0.00	0.03	0.02	0.00	0.00	0.00	0.02	0.00	0.02	0.00	0.03
SiO2	69.91	0.34	0.43	0.23	0.00	0.14	0.43	0.39	0.38	0.35	0.39	0.35	0.34
Al2O3	6.39	0.00	0.00	0.00	0.00	0.00	0.00	0.00	0.00	0.00	0.00	0.00	0.00
MgO	4.50	0.01	0.00	0.01	0.01	0.00	0.00	0.01	0.03	0.01	0.01	0.00	0.00
P2O5	0.12	41.75	41.95	42.06	42.70	41.67	41.48	41.66	40.89	41.83	41.11	42.50	41.17
SO2	0.00	0.00	0.06	0.05	0.00	0.00	0.00	0.06	0.06	0.05	0.05	0.00	0.06
CaO	0.21	54.43	55.50	54.05	55.04	55.80	53.74	55.20	54.79	54.60	54.82	54.15	54.71
TiO2	0.64	0.00	0.00	0.00	0.00	0.00	0.00	0.00	0.00	0.00	0.00	0.00	0.00
MnO	0.00	0.00	0.00	0.00	0.00	0.00	0.00	0.00	0.00	0.00	0.00	0.00	0.00
Fe2O3	12.15	0.21	0.00	0.00	0.00	0.00	0.00	0.00	0.00	0.00	0.00	0.00	0.00
As2O3	0.14	0.00	0.00	0.00	0.00	0.00	0.00	0.00	0.00	0.00	0.00	0.00	0.00
SrO	1.04	0.00	0.00	0.00	0.00	0.00	0.00	0.00	0.00	0.00	0.00	0.00	0.00
Y2O3	0.00	0.21	0.16	0.06	0.00	0.00	0.10	0.11	0.17	0.11	0.17	0.19	0.14
La2O3	0.00	0.00	0.00	0.00	0.00	0.00	0.00	0.00	0.00	0.00	0.00	0.00	0.00
Ce2O3	0.00	0.00	0.16	0.20	0.00	0.00	0.23	0.09	0.00	0.09	0.00	0.13	0.11
Nd2O3	0.00	0.00	0.16	0.00	0.00	0.00	0.15	0.00	0.00	0.12	0.00	0.12	0.00
-O equivalent	-0.25	-1.18	-1.13	-1.11	-1.20	-1.21	-1.20	-1.24	-1.21	-1.19	-1.27	-1.26	-1.19
Total	**95.8**	**99.1**	**100.6**	**98.5**	**100.0**	**99.9**	**98.4**	**99.9**	**98.6**	**99.4**	**98.9**	**99.8**	**98.8**

Profiles						
Jt1 - grain 4	Along					
Points	**1**	**2**	**3**	**4**	**5**	**6**
F	3.01	2.60	2.52	2.43	2.93	2.65
Cl	0.61	0.79	0.92	0.90	0.76	0.89
Na2O	0.00	0.04	0.02	0.00	0.03	0.00
SiO2	0.00	0.36	0.48	0.35	0.28	0.42
Al2O3	0.00	0.00	0.00	0.00	0.00	0.00
MgO	0.01	0.01	0.01	0.01	0.01	0.02
P2O5	42.34	41.77	41.53	41.65	42.68	42.26
SO2	0.06	0.07	0.06	0.08	0.06	0.00
CaO	56.13	54.64	53.34	55.06	55.40	55.43
TiO2	0.00	0.00	0.00	0.00	0.00	0.00
MnO	0.00	0.00	0.00	0.09	0.00	0.00
Fe2O3	0.00	0.00	0.00	0.10	0.00	0.00
As2O3	0.00	0.00	0.00	0.00	0.00	0.00
SrO	0.00	0.02	0.00	0.00	0.02	0.00
Y2O3	0.00	0.22	0.21	0.18	0.18	0.14
La2O3	0.00	0.00	0.00	0.00	0.00	0.00
Ce2O3	0.00	0.00	0.27	0.15	0.00	0.09
Nd2O3	0.00	0.00	0.26	0.00	0.00	0.00
-O equivalent	-1.41	-1.27	-1.27	-1.23	-1.41	-1.32
Total	**100.8**	**99.2**	**98.3**	**99.8**	**101.0**	**100.6**

Calculated formulae 9 a.p.f.u.

Profiles	*(continued)												
Jt1 - grain 1	Acrross												
Points	**24**	**25**	**26**	**27**	**28**	**29**	**30**	**31**	**32**	**33**	**34**	**35**	**36**
Ca	0.017	4.839	4.892	4.824	4.839	4.941	4.812	4.876	4.910	4.845	4.885	4.760	4.894
Mg	0.497	0.001	0.000	0.001	0.001	0.000	0.000	0.002	0.003	0.001	0.001	0.000	0.000
Mn	0.000	0.000	0.000	0.000	0.000	0.000	0.000	0.000	0.000	0.000	0.000	0.000	0.000
Sr	0.044	0.000	0.000	0.000	0.000	0.000	0.000	0.000	0.000	0.000	0.000	0.000	0.000
Y	0.000	0.009	0.007	0.003	0.000	0.000	0.005	0.005	0.008	0.005	0.007	0.008	0.006
La	0.000	0.000	0.000	0.000	0.000	0.000	0.000	0.000	0.000	0.000	0.000	0.000	0.000
Ce	0.000	0.000	0.005	0.006	0.000	0.000	0.007	0.003	0.000	0.003	0.000	0.004	0.003
Nd	0.000	0.000	0.005	0.000	0.000	0.000	0.004	0.000	0.000	0.003	0.000	0.003	0.000
Na	0.000	0.000	0.000	0.006	0.003	0.000	0.000	0.000	0.004	0.000	0.004	0.000	0.004
Fe	0.677	0.013	0.000	0.000	0.000	0.000	0.000	0.000	0.000	0.000	0.000	0.000	0.000
Ti	0.036	0.000	0.000	0.000	0.000	0.000	0.000	0.000	0.000	0.000	0.000	0.000	0.000
Al	0.558	0.000	0.000	0.000	0.000	0.000	0.000	0.000	0.000	0.000	0.000	0.000	0.000
Total	**1.828**	**4.862**	**4.908**	**4.839**	**4.844**	**4.941**	**4.828**	**4.885**	**4.924**	**4.857**	**4.897**	**4.776**	**4.908**
SREY	**0.000**	**0.009**	**0.017**	**0.009**	**0.000**	**0.000**	**0.016**	**0.008**	**0.008**	**0.011**	**0.007**	**0.016**	**0.010**
P	0.008	2.933	2.921	2.967	2.967	2.915	2.935	2.907	2.896	2.933	2.895	2.952	2.911
S	0.000	0.000	0.005	0.004	0.000	0.000	0.000	0.004	0.005	0.004	0.004	0.000	0.005
As	0.006	0.000	0.000	0.000	0.000	0.000	0.000	0.000	0.000	0.000	0.000	0.000	0.000
Si	5.175	0.029	0.035	0.019	0.000	0.011	0.036	0.032	0.032	0.029	0.032	0.029	0.028
Total	**5.189**	**2.961**	**2.961**	**2.989**	**2.967**	**2.926**	**2.971**	**2.944**	**2.933**	**2.966**	**2.931**	**2.981**	**2.943**
F	0.039	0.567	0.513	0.601	0.566	0.560	0.558	0.564	0.575	0.553	0.608	0.592	0.562
Cl	0.101	0.170	0.188	0.096	0.175	0.189	0.198	0.205	0.185	0.186	0.182	0.187	0.185
(F+Cl)	0.140	0.738	0.701	0.697	0.741	0.749	0.756	0.769	0.760	0.739	0.791	0.779	0.747
OH (by difference)	0.860	0.262	0.299	0.303	0.259	0.251	0.244	0.231	0.240	0.261	0.209	0.221	0.253
Total	**1.000**	**1.000**	**1.000**	**1.000**	**1.000**	**1.000**	**1.000**	**1.000**	**1.000**	**1.000**	**1.000**	**1.000**	**1.000**

Calculated formulae 9 a.p.f.u.

Profiles						
Jt1 - grain 4	Along					
Points	**1**	**2**	**3**	**4**	**5**	**6**
Ca	4.873	4.830	4.759	4.864	4.789	4.832
Mg	0.001	0.001	0.001	0.002	0.002	0.002
Mn	0.000	0.000	0.000	0.006	0.000	0.000
Sr	0.000	0.001	0.000	0.000	0.001	0.000
Y	0.000	0.010	0.009	0.008	0.008	0.006
La	0.000	0.000	0.000	0.000	0.000	0.000
Ce	0.000	0.000	0.008	0.004	0.000	0.003
Nd	0.000	0.000	0.008	0.000	0.000	0.000
Na	0.000	0.006	0.004	0.000	0.005	0.000
Fe	0.000	0.000	0.000	0.006	0.000	0.000
Ti	0.000	0.000	0.000	0.000	0.000	0.000
Al	0.000	0.000	0.000	0.000	0.000	0.000
Total	**4.874**	**4.848**	**4.789**	**4.891**	**4.804**	**4.843**
SREY	**0.000**	**0.010**	**0.025**	**0.012**	**0.008**	**0.009**
P	2.904	2.917	2.927	2.908	2.915	2.911
S	0.005	0.005	0.005	0.006	0.004	0.000
As	0.000	0.000	0.000	0.000	0.000	0.000
Si	0.000	0.029	0.040	0.029	0.023	0.034
Total	**2.909**	**2.952**	**2.972**	**2.943**	**2.942**	**2.946**
F	0.772	0.677	0.663	0.635	0.748	0.683
Cl	0.083	0.110	0.130	0.126	0.105	0.123
(F+Cl)	0.856	0.787	0.794	0.760	0.852	0.806
OH (by difference)	0.144	0.213	0.206	0.240	0.148	0.194
Total	**1.000**	**1.000**	**1.000**	**1.000**	**1.000**	**1.000**

Profiles																							
Jt1 - grain 4	*(continued)																				Across		
Points	**7**	**8**	**9**	**10**	**11**	**12**	**13**	**14**	**15**	**16**	**17**	**18**	**19**	**20**	**21**	**22**	**23**	**24**	**25**	**26**	**27**	**28**	**29**
F	2.67	2.83	3.44	2.65	2.67	2.65	3.13	2.80	2.82	2.84	2.69	2.64	3.05	2.91	2.87	3.04	2.95	2.99	3.01	2.94	2.80	2.59	2.75
Cl	0.82	0.73	0.33	0.72	0.80	0.88	0.63	0.80	0.82	0.85	0.82	0.80	0.78	0.63	0.80	0.59	0.66	0.65	0.63	0.70	0.76	0.84	0.83
Na2O	0.02	0.00	0.00	0.00	0.00	0.00	0.04	0.00	0.02	0.00	0.04	0.00	0.00	0.02	0.00	0.00	0.00	0.00	0.03	0.02	0.00	0.00	0.02
SiO2	0.27	0.24	0.00	0.23	0.14	0.32	0.19	0.25	0.18	0.28	0.35	0.16	0.00	0.00	0.00	0.00	0.00	0.00	0.00	0.00	0.00	0.17	0.14
Al2O3	0.24	0.00	0.00	0.00	0.00	0.00	0.00	0.00	0.00	0.00	0.00	0.00	0.00	0.00	0.00	0.00	0.00	0.00	0.00	0.00	0.00	0.00	0.00
MgO	0.21	0.01	0.01	0.01	0.01	0.02	0.02	0.01	0.01	0.01	0.01	0.01	0.02	0.01	0.02	0.01	0.01	0.01	0.01	0.01	0.00	0.01	0.02
P2O5	43.00	41.38	43.11	41.75	42.35	42.52	41.79	42.92	42.59	41.96	41.72	41.92	42.17	42.42	42.05	42.40	42.96	42.37	42.40	42.78	42.64	41.94	42.02
SO2	0.07	0.05	0.00	0.00	0.00	0.00	0.00	0.00	0.07	0.00	0.00	0.00	0.00	0.00	0.06	0.00	0.00	0.00	0.00	0.00	0.06	0.00	0.00
CaO	55.75	55.57	55.68	55.09	56.69	55.13	54.49	54.62	54.59	54.73	55.70	54.78	55.78	56.06	55.38	55.97	54.45	54.50	55.30	55.58	55.44	54.35	54.55
TiO2	0.00	0.00	0.00	0.00	0.00	0.00	0.00	0.00	0.00	0.00	0.00	0.00	0.00	0.00	0.00	0.00	0.00	0.00	0.00	0.00	0.00	0.00	0.00
MnO	0.00	0.00	0.00	0.00	0.00	0.00	0.00	0.00	0.00	0.00	0.00	0.00	0.06	0.00	0.00	0.00	0.00	0.00	0.00	0.00	0.00	0.06	0.00
Fe2O3	0.44	0.00	0.00	0.00	0.12	0.00	0.00	0.00	0.08	0.00	0.13	0.00	0.19	0.00	0.00	0.34	0.10	0.13	0.00	0.23	0.26	0.00	0.00
As2O3	0.00	0.00	0.00	0.00	0.00	0.00	0.00	0.00	0.00	0.00	0.00	0.00	0.00	0.00	0.00	0.00	0.00	0.00	0.00	0.00	0.00	0.00	0.00
SrO	0.02	0.02	0.00	0.00	0.00	0.00	0.02	0.02	0.04	0.00	0.00	0.02	0.00	0.02	0.00	0.02	0.02	0.00	0.03	0.02	0.00	0.02	0.02
Y2O3	0.12	0.09	0.00	0.17	0.09	0.14	0.00	0.12	0.07	0.11	0.07	0.09	0.00	0.00	0.00	0.00	0.00	0.00	0.00	0.00	0.00	0.11	0.14
La2O3	0.00	0.00	0.00	0.00	0.00	0.00	0.00	0.00	0.00	0.00	0.00	0.00	0.00	0.00	0.00	0.00	0.00	0.00	0.00	0.00	0.00	0.00	0.00
Ce2O3	0.00	0.00	0.00	0.00	0.00	0.00	0.00	0.00	0.00	0.00	0.17	0.00	0.00	0.00	0.00	0.00	0.00	0.00	0.00	0.00	0.00	0.00	0.00
Nd2O3	0.00	0.00	0.00	0.00	0.00	0.00	0.00	0.00	0.00	0.00	0.00	0.00	0.00	0.00	0.00	0.00	0.00	0.00	0.00	0.00	0.00	0.00	0.00
-O equivalent	-1.31	-1.36	-1.52	-1.28	-1.30	-1.31	-1.46	-1.36	-1.37	-1.39	-1.32	-1.29	-1.46	-1.37	-1.39	-1.41	-1.39	-1.40	-1.41	-1.39	-1.35	-1.28	-1.34
Total	**102.3**	**99.6**	**101.0**	**99.3**	**101.6**	**100.3**	**98.9**	**100.2**	**99.9**	**99.4**	**100.4**	**99.1**	**100.6**	**100.7**	**99.8**	**101.0**	**99.8**	**99.3**	**100.0**	**100.9**	**100.6**	**98.8**	**99.1**

Calculated formulae 9 a.p.f.u.

Profiles

Jt1 - grain 4	*(continued)																				Across		
Points	**7**	**8**	**9**	**10**	**11**	**12**	**13**	**14**	**15**	**16**	**17**	**18**	**19**	**20**	**21**	**22**	**23**	**24**	**25**	**26**	**27**	**28**	**29**
Ca	4.776	4.899	4.777	4.868	4.914	4.808	4.796	4.749	4.763	4.808	4.881	4.843	4.848	4.876	4.854	4.850	4.744	4.780	4.825	4.812	4.819	4.818	4.811
Mg	0.025	0.001	0.002	0.001	0.001	0.002	0.003	0.001	0.002	0.001	0.001	0.001	0.002	0.002	0.002	0.002	0.001	0.002	0.001	0.001	0.000	0.001	0.002
Mn	0.000	0.000	0.000	0.000	0.000	0.000	0.000	0.000	0.000	0.000	0.000	0.000	0.004	0.000	0.000	0.000	0.000	0.000	0.000	0.000	0.000	0.004	0.000
Sr	0.001	0.001	0.000	0.000	0.000	0.000	0.001	0.001	0.002	0.000	0.000	0.001	0.000	0.001	0.000	0.001	0.001	0.000	0.001	0.001	0.000	0.001	0.001
Y	0.005	0.004	0.000	0.007	0.004	0.006	0.000	0.005	0.003	0.005	0.003	0.004	0.000	0.000	0.000	0.000	0.000	0.000	0.000	0.000	0.000	0.005	0.006
La	0.000	0.000	0.000	0.000	0.000	0.000	0.000	0.000	0.000	0.000	0.000	0.000	0.000	0.000	0.000	0.000	0.000	0.000	0.000	0.000	0.000	0.000	0.000
Ce	0.000	0.000	0.000	0.000	0.000	0.000	0.000	0.000	0.000	0.000	0.005	0.000	0.000	0.000	0.000	0.000	0.000	0.000	0.000	0.000	0.000	0.000	0.000
Nd	0.000	0.000	0.000	0.000	0.000	0.000	0.000	0.000	0.000	0.000	0.000	0.000	0.000	0.000	0.000	0.000	0.000	0.000	0.000	0.000	0.000	0.000	0.000
Na	0.003	0.000	0.000	0.000	0.000	0.000	0.006	0.000	0.003	0.000	0.007	0.000	0.000	0.003	0.000	0.000	0.000	0.000	0.005	0.002	0.000	0.000	0.004
Fe	0.027	0.000	0.000	0.000	0.007	0.000	0.000	0.000	0.005	0.000	0.008	0.000	0.012	0.000	0.000	0.021	0.006	0.008	0.000	0.014	0.016	0.000	0.000
Ti	0.000	0.000	0.000	0.000	0.000	0.000	0.000	0.000	0.000	0.000	0.000	0.000	0.000	0.000	0.000	0.000	0.000	0.000	0.000	0.000	0.000	0.000	0.000
Al	0.022	0.000	0.000	0.000	0.000	0.000	0.000	0.000	0.000	0.000	0.000	0.000	0.000	0.000	0.000	0.000	0.000	0.000	0.000	0.000	0.000	0.000	0.000
Total	**4.859**	**4.905**	**4.779**	**4.877**	**4.927**	**4.816**	**4.806**	**4.756**	**4.777**	**4.814**	**4.905**	**4.849**	**4.865**	**4.881**	**4.856**	**4.873**	**4.753**	**4.790**	**4.832**	**4.831**	**4.835**	**4.829**	**4.824**
SREY	**0.005**	**0.004**	**0.000**	**0.007**	**0.004**	**0.006**	**0.000**	**0.005**	**0.003**	**0.005**	**0.008**	**0.004**	**0.000**	**0.000**	**0.000**	**0.000**	**0.000**	**0.000**	**0.000**	**0.000**	**0.000**	**0.005**	**0.006**
P	2.911	2.883	2.922	2.915	2.901	2.930	2.906	2.949	2.936	2.913	2.889	2.929	2.896	2.915	2.913	2.903	2.958	2.937	2.923	2.927	2.929	2.938	2.928
S	0.005	0.004	0.000	0.000	0.000	0.000	0.000	0.000	0.005	0.000	0.000	0.000	0.000	0.000	0.005	0.000	0.000	0.000	0.000	0.000	0.005	0.000	0.000
As	0.000	0.000	0.000	0.000	0.000	0.000	0.000	0.000	0.000	0.000	0.000	0.000	0.000	0.000	0.000	0.000	0.000	0.000	0.000	0.000	0.000	0.000	0.000
Si	0.022	0.020	0.000	0.019	0.011	0.026	0.016	0.020	0.015	0.023	0.029	0.013	0.000	0.000	0.000	0.000	0.000	0.000	0.000	0.000	0.000	0.014	0.011
Total	**2.938**	**2.907**	**2.922**	**2.934**	**2.912**	**2.956**	**2.922**	**2.969**	**2.956**	**2.936**	**2.918**	**2.942**	**2.896**	**2.915**	**2.917**	**2.903**	**2.958**	**2.937**	**2.923**	**2.927**	**2.934**	**2.952**	**2.940**
F	0.674	0.736	0.871	0.692	0.683	0.683	0.812	0.720	0.727	0.737	0.697	0.688	0.781	0.746	0.743	0.778	0.758	0.773	0.776	0.751	0.720	0.678	0.715
Cl	0.111	0.101	0.045	0.101	0.109	0.121	0.087	0.110	0.113	0.118	0.114	0.112	0.107	0.087	0.110	0.081	0.091	0.091	0.086	0.095	0.105	0.118	0.116
(F+Cl)	0.785	0.838	0.915	0.793	0.792	0.804	0.900	0.830	0.840	0.855	0.811	0.801	0.888	0.833	0.853	0.859	0.850	0.864	0.862	0.847	0.824	0.796	0.831
OH (by difference)	0.215	0.162	0.085	0.207	0.208	0.196	0.100	0.170	0.160	0.145	0.189	0.199	0.112	0.167	0.147	0.141	0.150	0.136	0.138	0.153	0.176	0.204	0.169
Total	**1.000**	**1.000**	**1.000**	**1.000**	**1.000**	**1.000**	**1.000**	**1.000**	**1.000**	**1.000**	**1.000**	**1.000**	**1.000**	**1.000**	**1.000**	**1.000**	**1.000**	**1.000**	**1.000**	**1.000**	**1.000**	**1.000**	**1.000**

Profiles													
Jt1 - grain 4	*(continued)												
Points	**30**	**31**	**32**	**33**	**34**	**35**	**36**	**37**	**38**	**39**	**40**	**41**	**42**
F	2.97	3.45	3.63	2.67	2.82	2.82	2.83	2.91	2.98	2.68	2.85	3.22	1.29
Cl	0.75	0.32	0.26	0.87	0.81	0.80	0.74	0.68	0.75	0.80	0.60	0.46	0.37
Na2O	0.00	0.03	0.00	0.00	0.00	0.03	0.00	0.00	0.00	0.02	0.00	0.00	0.00
SiO2	0.15	0.04	0.00	0.19	0.28	0.19	0.19	0.16	0.26	0.24	0.16	0.04	0.05
Al2O3	0.00	0.00	0.00	0.00	0.00	0.00	0.00	0.00	0.00	0.00	0.00	0.00	0.00
MgO	0.02	0.01	0.03	0.01	0.01	0.01	0.01	0.01	0.00	0.01	0.01	0.01	0.02
P2O5	42.77	42.14	42.61	42.16	41.85	42.83	42.23	42.15	42.63	42.25	42.16	42.34	40.71
SO2	0.00	0.00	0.00	0.00	0.00	0.07	0.00	0.00	0.05	0.00	0.00	0.07	0.00
CaO	55.44	55.69	55.02	54.59	55.35	55.28	55.45	54.30	55.53	55.00	55.43	55.43	57.80
TiO2	0.00	0.00	0.00	0.00	0.00	0.00	0.00	0.00	0.00	0.00	0.00	0.00	0.00
MnO	0.00	0.00	0.00	0.00	0.00	0.00	0.00	0.00	0.00	0.00	0.00	0.00	0.00
Fe2O3	0.00	0.00	0.00	0.00	0.00	0.00	0.00	0.14	0.00	0.00	0.00	0.00	0.14
As2O3	0.00	0.00	0.00	0.00	0.00	0.00	0.00	0.00	0.00	0.00	0.00	0.00	0.00
SrO	0.02	0.00	0.03	0.02	0.00	0.02	0.02	0.00	0.02	0.00	0.02	0.04	0.02
Y2O3	0.00	0.00	0.00	0.06	0.08	0.06	0.08	0.00	0.09	0.08	0.05	0.00	0.00
La2O3	0.00	0.00	0.00	0.00	0.00	0.00	0.00	0.00	0.00	0.00	0.00	0.00	0.00
Ce2O3	0.00	0.00	0.00	0.00	0.00	0.00	0.00	0.00	0.08	0.00	0.00	0.00	0.00
Nd2O3	0.00	0.00	0.00	0.00	0.00	0.00	0.00	0.00	0.00	0.00	0.00	0.00	0.00
-O equivalent	-1.42	-1.53	-1.59	-1.32	-1.37	-1.37	-1.36	-1.38	-1.42	-1.31	-1.34	-1.46	-0.63
Total	**100.7**	**100.2**	**100.0**	**99.2**	**99.8**	**100.7**	**100.2**	**99.0**	**101.0**	**99.8**	**100.0**	**100.1**	**99.8**

Profiles						
Jt4 - grain 2	Along					
Points	**1**	**2**	**3**	**4**	**5**	**6**
F	3.09	3.25	3.00	3.04	3.13	3.10
Cl	0.50	0.53	0.52	0.56	0.51	0.55
Na2O	0.00	0.05	0.00	0.00	0.02	0.00
SiO2	0.00	0.00	0.00	0.00	0.00	0.00
Al2O3	0.00	0.00	0.00	0.00	0.00	0.00
MgO	0.00	0.01	0.01	0.01	0.01	0.01
P2O5	42.23	42.69	42.57	42.57	42.65	41.83
SO2	0.09	0.00	0.07	0.00	0.00	0.00
CaO	54.53	55.43	55.07	53.53	54.90	55.57
TiO2	0.00	0.00	0.00	0.00	0.00	0.00
MnO	0.00	0.00	0.00	0.00	0.00	0.00
Fe2O3	0.43	0.08	0.00	0.00	0.17	0.00
As2O3	0.00	0.00	0.00	0.00	0.00	0.00
SrO	0.00	0.00	0.00	0.00	0.00	0.00
Y2O3	0.00	0.00	0.00	0.00	0.00	0.00
La2O3	0.00	0.00	0.00	0.00	0.00	0.00
Ce2O3	0.00	0.00	0.00	0.00	0.00	0.00
Nd2O3	0.00	0.00	0.00	0.00	0.00	0.00
-O equivalent	-1.41	-1.49	-1.38	-1.41	-1.43	-1.43
Total	**99.5**	**100.6**	**99.9**	**98.3**	**100.0**	**99.6**

Calculated formulae 9 a.p.f.u.

Profiles

Jt1 - grain 4	*(continued)												
Points	**30**	**31**	**32**	**33**	**34**	**35**	**36**	**37**	**38**	**39**	**40**	**41**	**42**
Ca	4.799	4.835	4.756	4.810	4.855	4.789	4.843	4.779	4.800	4.825	4.854	4.819	5.258
Mg	0.002	0.001	0.004	0.001	0.002	0.002	0.001	0.001	0.000	0.001	0.001	0.001	0.002
Mn	0.000	0.000	0.000	0.000	0.000	0.000	0.000	0.000	0.000	0.000	0.000	0.000	0.000
Sr	0.001	0.000	0.001	0.001	0.000	0.001	0.001	0.000	0.001	0.000	0.001	0.002	0.001
Y	0.000	0.000	0.000	0.003	0.003	0.003	0.003	0.000	0.004	0.004	0.002	0.000	0.000
La	0.000	0.000	0.000	0.000	0.000	0.000	0.000	0.000	0.000	0.000	0.000	0.000	0.000
Ce	0.000	0.000	0.000	0.000	0.000	0.000	0.000	0.000	0.002	0.000	0.000	0.000	0.000
Nd	0.000	0.000	0.000	0.000	0.000	0.000	0.000	0.000	0.000	0.000	0.000	0.000	0.000
Na	0.000	0.004	0.000	0.000	0.000	0.005	0.000	0.000	0.000	0.004	0.000	0.000	0.000
Fe	0.000	0.000	0.000	0.000	0.000	0.000	0.000	0.009	0.000	0.000	0.000	0.000	0.009
Ti	0.000	0.000	0.000	0.000	0.000	0.000	0.000	0.000	0.000	0.000	0.000	0.000	0.000
Al	0.000	0.000	0.000	0.000	0.000	0.000	0.000	0.000	0.000	0.000	0.000	0.000	0.000
Total	**4.801**	**4.841**	**4.761**	**4.815**	**4.860**	**4.799**	**4.849**	**4.789**	**4.806**	**4.833**	**4.859**	**4.822**	**5.270**
SREY	**0.000**	**0.000**	**0.000**	**0.003**	**0.003**	**0.003**	**0.003**	**0.000**	**0.006**	**0.004**	**0.002**	**0.000**	**0.000**
P	2.925	2.891	2.911	2.935	2.900	2.932	2.915	2.932	2.911	2.929	2.917	2.909	2.926
S	0.000	0.000	0.000	0.000	0.000	0.005	0.000	0.000	0.004	0.000	0.000	0.006	0.000
As	0.000	0.000	0.000	0.000	0.000	0.000	0.000	0.000	0.000	0.000	0.000	0.000	0.000
Si	0.012	0.003	0.000	0.015	0.023	0.016	0.016	0.013	0.021	0.020	0.013	0.003	0.004
Total	**2.937**	**2.894**	**2.911**	**2.951**	**2.923**	**2.953**	**2.931**	**2.945**	**2.936**	**2.949**	**2.930**	**2.917**	**2.931**
F	0.759	0.884	0.926	0.693	0.730	0.721	0.728	0.756	0.760	0.693	0.738	0.826	0.347
Cl	0.103	0.044	0.035	0.121	0.113	0.109	0.103	0.094	0.103	0.111	0.083	0.063	0.053
(F+Cl)	0.862	0.929	0.962	0.815	0.842	0.830	0.831	0.850	0.863	0.804	0.821	0.889	0.401
OH (by difference)	0.138	0.071	0.038	0.185	0.158	0.170	0.169	0.150	0.137	0.196	0.179	0.111	0.599
Total	**1.000**	**1.000**	**1.000**	**1.000**	**1.000**	**1.000**	**1.000**	**1.000**	**1.000**	**1.000**	**1.000**	**1.000**	**1.000**

Calculated formulae 9 a.p.f.u.

Profiles

Jt4 - grain 2	Along					
Points	**1**	**2**	**3**	**4**	**5**	**6**
Ca	4.775	4.794	4.805	4.718	4.777	4.873
Mg	0.000	0.001	0.001	0.001	0.002	0.001
Mn	0.000	0.000	0.000	0.000	0.000	0.000
Sr	0.000	0.000	0.000	0.000	0.000	0.000
Y	0.000	0.000	0.000	0.000	0.000	0.000
La	0.000	0.000	0.000	0.000	0.000	0.000
Ce	0.000	0.000	0.000	0.000	0.000	0.000
Nd	0.000	0.000	0.000	0.000	0.000	0.000
Na	0.000	0.008	0.000	0.000	0.004	0.000
Fe	0.026	0.005	0.000	0.000	0.011	0.000
Ti	0.000	0.000	0.000	0.000	0.000	0.000
Al	0.000	0.000	0.000	0.000	0.000	0.000
Total	**4.801**	**4.808**	**4.806**	**4.719**	**4.793**	**4.875**
SREY	**0.000**	**0.000**	**0.000**	**0.000**	**0.000**	**0.000**
P	2.922	2.917	2.935	2.965	2.932	2.899
S	0.007	0.000	0.005	0.000	0.000	0.000
As	0.000	0.000	0.000	0.000	0.000	0.000
Si	0.000	0.000	0.000	0.000	0.000	0.000
Total	**2.928**	**2.917**	**2.941**	**2.965**	**2.932**	**2.899**
F	0.799	0.829	0.773	0.791	0.803	0.803
Cl	0.069	0.072	0.072	0.078	0.071	0.076
(F+Cl)	0.868	0.901	0.845	0.869	0.874	0.879
OH (by difference)	0.132	0.099	0.155	0.131	0.126	0.121
Total	**1.000**	**1.000**	**1.000**	**1.000**	**1.000**	**1.000**

Profiles											
Jt4 - grain 2	*(continued)					Across					
Points	**7**	**8**	**9**	**10**	**11**	**12**	**13**	**14**	**15**	**16**	**17**
F	3.00	2.85	3.16	3.42	3.13	3.04	2.88	2.94	3.01	2.98	3.12
Cl	0.50	0.55	0.47	0.50	0.38	0.60	0.58	0.51	0.51	0.53	0.53
Na2O	0.02	0.04	0.00	0.00	0.00	0.02	0.00	0.00	0.03	0.02	0.00
SiO2	0.00	0.00	0.00	0.00	0.00	0.15	0.00	0.00	0.00	0.00	0.00
Al2O3	0.00	0.00	0.00	0.00	0.00	0.00	0.00	0.00	0.00	0.00	0.00
MgO	0.01	0.01	0.00	0.00	0.00	0.01	0.02	0.01	0.01	0.01	0.01
P2O5	41.80	42.39	42.24	41.92	42.52	43.20	42.72	42.95	43.11	42.88	43.15
SO2	0.05	0.08	0.07	0.06	0.11	0.00	0.07	0.10	0.05	0.00	0.07
CaO	54.61	55.36	56.39	55.28	55.52	56.06	54.67	55.77	55.66	55.12	55.30
TiO2	0.00	0.00	0.00	0.00	0.00	0.00	0.00	0.00	0.00	0.00	0.00
MnO	0.00	0.00	0.00	0.00	0.00	0.00	0.00	0.00	0.00	0.00	0.00
Fe2O3	0.24	0.08	0.25	0.42	0.65	0.17	0.00	0.20	0.00	0.26	0.24
As2O3	0.00	0.00	0.00	0.00	0.00	0.00	0.00	0.00	0.00	0.00	0.00
SrO	0.00	0.00	0.00	0.00	0.00	0.00	0.00	0.00	0.00	0.00	0.00
Y2O3	0.00	0.00	0.00	0.00	0.00	0.00	0.00	0.00	0.00	0.00	0.00
La2O3	0.00	0.00	0.00	0.00	0.00	0.00	0.00	0.00	0.00	0.00	0.00
Ce2O3	0.00	0.00	0.00	0.00	0.00	0.00	0.00	0.00	0.00	0.00	0.00
Nd2O3	0.00	0.00	0.00	0.00	0.00	0.00	0.00	0.00	0.00	0.00	0.00
-O equivalent	-1.37	-1.33	-1.43	-1.55	-1.40	-1.42	-1.34	-1.35	-1.38	-1.37	-1.43
Total	**98.8**	**100.0**	**101.1**	**100.0**	**100.9**	**101.8**	**99.6**	**101.1**	**101.0**	**100.4**	**101.0**

Profiles						
Jt4 - grain 5	Along					
Points	**2**	**4**	**5**	**6**	**7**	**8**
F	3.66	3.47	3.66	3.73	3.66	3.51
Cl	0.24	0.29	0.29	0.30	0.30	0.34
Na2O	0.00	0.05	0.03	0.04	0.00	0.00
SiO2	0.00	0.00	0.00	0.00	0.00	0.00
Al2O3	0.00	0.00	0.00	0.00	0.00	0.00
MgO	0.00	0.01	0.01	0.01	0.01	0.01
P2O5	42.86	42.02	42.89	43.08	42.26	43.10
SO2	0.00	0.00	0.00	0.00	0.00	0.00
CaO	55.48	56.69	56.73	56.39	55.89	55.19
TiO2	0.00	0.00	0.00	0.00	0.00	0.00
MnO	0.00	0.00	0.00	0.00	0.00	0.00
Fe2O3	0.08	0.00	0.00	0.00	0.00	0.00
As2O3	0.00	0.00	0.00	0.00	0.00	0.00
SrO	0.00	0.00	0.00	0.00	0.00	0.00
Y2O3	0.00	0.00	0.00	0.00	0.00	0.00
La2O3	0.00	0.00	0.00	0.00	0.00	0.00
Ce2O3	0.00	0.00	0.00	0.00	0.00	0.00
Nd2O3	0.00	0.00	0.00	0.00	0.00	0.00
-O equivalent	-1.60	-1.53	-1.61	-1.64	-1.61	-1.56
Total	**100.7**	**101.0**	**102.0**	**101.9**	**100.5**	**100.6**

Calculated formulae 9 a.p.f.u.

Profiles

Jt4 - grain 2	*(continued)					Across					
Points	**7**	**8**	**9**	**10**	**11**	**12**	**13**	**14**	**15**	**16**	**17**
Ca	4.824	4.841	4.878	4.807	4.804	4.800	4.782	4.818	4.804	4.785	4.762
Mg	0.001	0.001	0.000	0.000	0.000	0.001	0.002	0.001	0.001	0.001	0.001
Mn	0.000	0.000	0.000	0.000	0.000	0.000	0.000	0.000	0.000	0.000	0.000
Sr	0.000	0.000	0.000	0.000	0.000	0.000	0.000	0.000	0.000	0.000	0.000
Y	0.000	0.000	0.000	0.000	0.000	0.000	0.000	0.000	0.000	0.000	0.000
La	0.000	0.000	0.000	0.000	0.000	0.000	0.000	0.000	0.000	0.000	0.000
Ce	0.000	0.000	0.000	0.000	0.000	0.000	0.000	0.000	0.000	0.000	0.000
Nd	0.000	0.000	0.000	0.000	0.000	0.000	0.000	0.000	0.000	0.000	0.000
Na	0.003	0.007	0.000	0.000	0.000	0.003	0.000	0.000	0.004	0.003	0.000
Fe	0.015	0.005	0.015	0.026	0.040	0.010	0.000	0.012	0.000	0.016	0.014
Ti	0.000	0.000	0.000	0.000	0.000	0.000	0.000	0.000	0.000	0.000	0.000
Al	0.000	0.000	0.000	0.000	0.000	0.000	0.000	0.000	0.000	0.000	0.000
Total	**4.843**	**4.853**	**4.894**	**4.833**	**4.843**	**4.814**	**4.784**	**4.831**	**4.809**	**4.804**	**4.777**
SREY	**0.000**	**0.000**	**0.000**	**0.000**	**0.000**	**0.000**	**0.000**	**0.000**	**0.000**	**0.000**	**0.000**
P	2.917	2.929	2.887	2.880	2.907	2.923	2.952	2.932	2.940	2.941	2.936
S	0.004	0.006	0.005	0.004	0.009	0.000	0.006	0.007	0.004	0.000	0.005
As	0.000	0.000	0.000	0.000	0.000	0.000	0.000	0.000	0.000	0.000	0.000
Si	0.000	0.000	0.000	0.000	0.000	0.012	0.000	0.000	0.000	0.000	0.000
Total	**2.921**	**2.935**	**2.892**	**2.884**	**2.916**	**2.935**	**2.958**	**2.939**	**2.944**	**2.941**	**2.941**
F	0.781	0.737	0.806	0.877	0.800	0.769	0.744	0.749	0.766	0.763	0.792
Cl	0.069	0.077	0.064	0.069	0.052	0.081	0.080	0.070	0.070	0.073	0.073
(F+Cl)	0.850	0.813	0.870	0.946	0.852	0.851	0.824	0.819	0.836	0.836	0.865
OH (by difference)	0.150	0.187	0.130	0.054	0.148	0.149	0.176	0.181	0.164	0.164	0.135
Total	**1.000**	**1.000**	**1.000**	**1.000**	**1.000**	**1.000**	**1.000**	**1.000**	**1.000**	**1.000**	**1.000**

Calculated formulae 9 a.p.f.u.

Profiles

Jt4 - grain 5	Along					
Points	**2**	**4**	**5**	**6**	**7**	**8**
Ca	4.763	4.899	4.827	4.791	4.822	4.743
Mg	0.000	0.001	0.002	0.002	0.001	0.001
Mn	0.000	0.000	0.000	0.000	0.000	0.000
Sr	0.000	0.000	0.000	0.000	0.000	0.000
Y	0.000	0.000	0.000	0.000	0.000	0.000
La	0.000	0.000	0.000	0.000	0.000	0.000
Ce	0.000	0.000	0.000	0.000	0.000	0.000
Nd	0.000	0.000	0.000	0.000	0.000	0.000
Na	0.000	0.007	0.005	0.006	0.000	0.000
Fe	0.005	0.000	0.000	0.000	0.000	0.000
Ti	0.000	0.000	0.000	0.000	0.000	0.000
Al	0.000	0.000	0.000	0.000	0.000	0.000
Total	**4.768**	**4.907**	**4.834**	**4.798**	**4.824**	**4.744**
SREY	**0.000**	**0.000**	**0.000**	**0.000**	**0.000**	**0.000**
P	2.908	2.869	2.884	2.892	2.881	2.927
S	0.000	0.000	0.000	0.000	0.000	0.000
As	0.000	0.000	0.000	0.000	0.000	0.000
Si	0.000	0.000	0.000	0.000	0.000	0.000
Total	**2.908**	**2.869**	**2.884**	**2.892**	**2.881**	**2.927**
F	0.927	0.885	0.920	0.934	0.931	0.891
Cl	0.033	0.039	0.039	0.040	0.041	0.046
(F+Cl)	0.960	0.924	0.959	0.974	0.973	0.937
OH (by difference)	0.040	0.076	0.041	0.026	0.027	0.063
Total	**1.000**	**1.000**	**1.000**	**1.000**	**1.000**	**1.000**

Profiles																							
Jt4 - grain 5	*(continued)								Across														
Points	**9**	**10**	**11**	**12**	**13**	**14**	**15**	**16**	**17**	**20**	**21**	**22**	**23**	**26**	**27**	**28**	**29**	**30**	**31**	**32**	**33**	**34**	**35**
F	3.62	3.61	3.60	3.55	3.69	3.47	3.61	3.66	3.65	3.59	3.56	3.67	3.69	3.76	3.56	3.64	3.57	3.47	3.42	3.67	3.52	3.42	3.72
Cl	0.27	0.33	0.25	0.32	0.32	0.36	0.30	0.31	0.30	0.35	0.35	0.43	0.38	0.31	0.34	0.34	0.29	0.28	0.29	0.33	0.32	0.31	0.26
Na2O	0.00	0.00	0.00	0.00	0.03	0.00	0.00	0.00	0.04	0.00	0.00	0.04	0.00	0.00	0.02	0.00	0.00	0.04	0.00	0.00	0.00	0.00	0.00
SiO2	0.00	0.00	0.00	0.00	0.00	0.00	0.00	0.00	0.00	0.00	0.00	0.00	0.00	0.00	0.00	0.00	0.00	0.00	0.00	0.00	0.00	0.00	0.00
Al2O3	0.00	0.00	0.00	0.00	0.00	0.00	0.00	0.00	0.00	0.00	0.00	0.00	0.01	0.00	0.00	0.00	0.00	0.00	0.00	0.00	0.00	0.00	0.00
MgO	0.02	0.01	0.01	0.01	0.00	0.01	0.01	0.01	0.00	0.01	0.01	0.01	0.02	0.01	0.02	0.01	0.00	0.01	0.01	0.01	0.01	0.01	0.00
P2O5	42.79	42.61	42.53	42.39	43.20	43.35	43.28	42.48	43.01	42.85	41.60	42.34	41.96	42.75	42.69	42.71	42.61	42.78	42.12	42.46	42.67	42.45	43.15
SO2	0.00	0.00	0.00	0.00	0.05	0.00	0.00	0.00	0.00	0.00	0.05	0.00	0.00	0.00	0.00	0.00	0.00	0.00	0.05	0.00	0.00	0.00	0.00
CaO	55.13	55.73	56.30	55.90	55.48	55.64	56.16	55.61	55.38	57.58	55.23	55.31	56.02	56.92	56.14	55.91	56.49	54.98	56.19	55.57	56.55	55.32	54.97
TiO2	0.00	0.00	0.00	0.00	0.00	0.00	0.00	0.00	0.00	0.00	0.00	0.00	0.00	0.00	0.00	0.00	0.00	0.00	0.00	0.00	0.00	0.00	0.00
MnO	0.00	0.00	0.00	0.00	0.00	0.00	0.00	0.00	0.00	0.00	0.00	0.00	0.00	0.00	0.00	0.00	0.00	0.00	0.00	0.00	0.00	0.00	0.00
Fe2O3	0.00	0.00	0.15	0.09	0.00	0.00	0.19	0.10	0.21	0.00	0.00	0.00	0.11	0.00	0.00	0.00	0.00	0.00	0.31	0.19	0.00	0.07	0.00
As2O3	0.00	0.00	0.00	0.00	0.00	0.00	0.00	0.00	0.00	0.00	0.00	0.00	0.00	0.00	0.00	0.00	0.00	0.00	0.00	0.00	0.00	0.00	0.00
SrO	0.00	0.02	0.00	0.00	0.00	0.00	0.00	0.00	0.00	0.00	0.02	0.00	0.02	0.00	0.00	0.00	0.02	0.00	0.00	0.00	0.00	0.00	0.02
Y2O3	0.00	0.00	0.00	0.00	0.00	0.00	0.00	0.00	0.00	0.00	0.00	0.00	0.00	0.00	0.00	0.00	0.00	0.00	0.00	0.00	0.00	0.00	0.00
La2O3	0.00	0.00	0.00	0.00	0.00	0.00	0.00	0.00	0.00	0.00	0.00	0.00	0.00	0.00	0.00	0.00	0.00	0.00	0.00	0.00	0.00	0.00	0.00
Ce2O3	0.00	0.00	0.00	0.00	0.00	0.00	0.00	0.00	0.00	0.00	0.00	0.00	0.00	0.00	0.00	0.00	0.00	0.00	0.00	0.00	0.00	0.00	0.00
Nd2O3	0.00	0.00	0.00	0.00	0.00	0.00	0.00	0.00	0.00	0.00	0.00	0.00	0.00	0.00	0.00	0.00	0.00	0.00	0.00	0.00	0.00	0.00	0.00
-O equivalent	-1.59	-1.59	-1.57	-1.57	-1.63	-1.54	-1.59	-1.61	-1.61	-1.59	-1.58	-1.64	-1.64	-1.65	-1.58	-1.61	-1.57	-1.52	-1.51	-1.62	-1.56	-1.51	-1.62
Total	**100.2**	**100.7**	**101.3**	**100.7**	**101.1**	**101.3**	**102.0**	**100.6**	**101.0**	**102.8**	**99.2**	**100.2**	**100.6**	**102.1**	**101.2**	**101.0**	**101.4**	**100.0**	**100.9**	**100.6**	**101.5**	**100.1**	**100.5**

Calculated formulae 9 a.p.f.u.

Profiles

Jt4 - grain 5	*(continued)								Across														
Points	**9**	**10**	**11**	**12**	**13**	**14**	**15**	**16**	**17**	**20**	**21**	**22**	**23**	**26**	**27**	**28**	**29**	**30**	**31**	**32**	**33**	**34**	**35**
Ca	4.753	4.794	4.831	4.821	4.735	4.755	4.772	4.789	4.741	4.880	4.832	4.777	4.837	4.837	4.816	4.795	4.842	4.758	4.857	4.784	4.844	4.799	4.714
Mg	0.002	0.001	0.002	0.001	0.000	0.001	0.001	0.001	0.000	0.002	0.001	0.002	0.002	0.001	0.002	0.001	0.000	0.001	0.001	0.001	0.001	0.002	0.000
Mn	0.000	0.000	0.000	0.000	0.000	0.000	0.000	0.000	0.000	0.000	0.000	0.000	0.000	0.000	0.000	0.000	0.000	0.000	0.000	0.000	0.000	0.000	0.000
Sr	0.000	0.001	0.000	0.000	0.000	0.000	0.000	0.000	0.000	0.000	0.001	0.000	0.001	0.000	0.000	0.000	0.001	0.000	0.000	0.000	0.000	0.000	0.001
Y	0.000	0.000	0.000	0.000	0.000	0.000	0.000	0.000	0.000	0.000	0.000	0.000	0.000	0.000	0.000	0.000	0.000	0.000	0.000	0.000	0.000	0.000	0.000
La	0.000	0.000	0.000	0.000	0.000	0.000	0.000	0.000	0.000	0.000	0.000	0.000	0.000	0.000	0.000	0.000	0.000	0.000	0.000	0.000	0.000	0.000	0.000
Ce	0.000	0.000	0.000	0.000	0.000	0.000	0.000	0.000	0.000	0.000	0.000	0.000	0.000	0.000	0.000	0.000	0.000	0.000	0.000	0.000	0.000	0.000	0.000
Nd	0.000	0.000	0.000	0.000	0.000	0.000	0.000	0.000	0.000	0.000	0.000	0.000	0.000	0.000	0.000	0.000	0.000	0.000	0.000	0.000	0.000	0.000	0.000
Na	0.000	0.000	0.000	0.000	0.004	0.000	0.000	0.000	0.007	0.000	0.000	0.007	0.000	0.000	0.003	0.000	0.000	0.007	0.000	0.000	0.000	0.000	0.000
Fe	0.000	0.000	0.009	0.006	0.000	0.000	0.011	0.006	0.013	0.000	0.000	0.000	0.007	0.000	0.000	0.000	0.000	0.000	0.019	0.011	0.000	0.004	0.000
Ti	0.000	0.000	0.000	0.000	0.000	0.000	0.000	0.000	0.000	0.000	0.000	0.000	0.000	0.000	0.000	0.000	0.000	0.000	0.000	0.000	0.000	0.000	0.000
Al	0.000	0.000	0.000	0.000	0.000	0.000	0.000	0.000	0.000	0.000	0.000	0.000	0.001	0.000	0.000	0.000	0.000	0.000	0.000	0.000	0.000	0.000	0.000
Total	**4.755**	**4.797**	**4.841**	**4.828**	**4.739**	**4.757**	**4.784**	**4.797**	**4.760**	**4.881**	**4.834**	**4.785**	**4.848**	**4.838**	**4.821**	**4.797**	**4.843**	**4.766**	**4.877**	**4.796**	**4.845**	**4.805**	**4.715**
SREY	**0.000**	**0.000**	**0.000**	**0.000**	**0.000**	**0.000**	**0.000**	**0.000**	**0.000**	**0.000**	**0.000**	**0.000**	**0.000**	**0.000**	**0.000**	**0.000**	**0.000**	**0.000**	**0.000**	**0.000**	**0.000**	**0.000**	**0.000**
P	2.915	2.897	2.883	2.889	2.913	2.927	2.906	2.891	2.909	2.870	2.876	2.889	2.863	2.871	2.893	2.895	2.886	2.925	2.877	2.888	2.888	2.910	2.924
S	0.000	0.000	0.000	0.000	0.003	0.000	0.000	0.000	0.000	0.000	0.004	0.000	0.000	0.000	0.000	0.000	0.000	0.000	0.004	0.000	0.000	0.000	0.000
As	0.000	0.000	0.000	0.000	0.000	0.000	0.000	0.000	0.000	0.000	0.000	0.000	0.000	0.000	0.000	0.000	0.000	0.000	0.000	0.000	0.000	0.000	0.000
Si	0.000	0.000	0.000	0.000	0.000	0.000	0.000	0.000	0.000	0.000	0.000	0.000	0.000	0.000	0.000	0.000	0.000	0.000	0.000	0.000	0.000	0.000	0.000
Total	**2.915**	**2.897**	**2.883**	**2.889**	**2.916**	**2.927**	**2.906**	**2.891**	**2.909**	**2.870**	**2.880**	**2.889**	**2.863**	**2.871**	**2.893**	**2.895**	**2.886**	**2.925**	**2.881**	**2.888**	**2.888**	**2.910**	**2.924**
F	0.921	0.916	0.912	0.904	0.930	0.876	0.905	0.929	0.923	0.898	0.919	0.936	0.939	0.943	0.901	0.920	0.903	0.886	0.873	0.933	0.891	0.876	0.941
Cl	0.037	0.045	0.034	0.044	0.044	0.048	0.040	0.042	0.041	0.047	0.048	0.059	0.051	0.042	0.047	0.047	0.039	0.038	0.040	0.045	0.043	0.042	0.035
(F+Cl)	0.958	0.961	0.946	0.947	0.974	0.925	0.945	0.971	0.964	0.945	0.967	0.996	0.991	0.985	0.947	0.967	0.942	0.924	0.913	0.977	0.934	0.918	0.976
OH (by difference)	0.042	0.039	0.054	0.053	0.026	0.075	0.055	0.029	0.036	0.055	0.033	0.004	0.009	0.015	0.053	0.033	0.058	0.076	0.087	0.023	0.066	0.082	0.024
Total	**1.000**	**1.000**	**1.000**	**1.000**	**1.000**	**1.000**	**1.000**	**1.000**	**1.000**	**1.000**	**1.000**	**1.000**	**1.000**	**1.000**	**1.000**	**1.000**	**1.000**	**1.000**	**1.000**	**1.000**	**1.000**	**1.000**	**1.000**

Profiles																							
Jt7 - grain 3	Along																						
Points	**1**	**2**	**3**	**4**	**5**	**6**	**7**	**8**	**9**	**10**	**11**	**12**	**13**	**14**	**15**	**16**	**17**	**18**	**19**	**20**	**21**	**22**	**23**
F	2.77	2.46	2.64	2.59	2.55	2.52	2.64	2.60	2.47	2.69	2.52	2.68	2.69	2.36	2.68	2.56	2.43	2.58	2.70	2.72	3.24	2.93	2.64
Cl	0.75	0.80	0.80	0.88	1.06	0.90	0.98	0.89	0.85	0.78	0.91	0.90	0.85	0.80	0.89	0.92	0.79	0.87	0.77	0.77	0.56	0.64	0.92
Na2O	0.00	0.00	0.02	0.00	0.00	0.02	0.02	0.00	0.02	0.02	0.02	0.00	0.02	0.00	0.04	0.02	0.02	0.00	0.05	0.00	0.00	0.05	0.05
SiO2	0.00	0.00	0.00	0.31	0.52	0.48	0.50	0.39	0.31	0.20	0.21	0.27	0.25	1.97	0.26	0.23	0.23	0.22	0.23	0.08	0.03	0.13	0.28
Al2O3	0.00	0.00	0.00	0.00	0.00	0.00	0.00	0.00	0.00	0.00	0.00	0.00	0.00	0.40	0.00	0.00	0.00	0.00	0.00	0.00	0.00	0.00	0.00
MgO	0.01	0.01	0.01	0.01	0.02	0.01	0.01	0.01	0.00	0.01	0.02	0.01	0.02	0.33	0.01	0.02	0.01	0.02	0.02	0.01	0.00	0.01	0.01
P2O5	41.83	42.42	42.36	41.50	41.48	41.67	41.49	41.87	41.85	41.52	42.25	42.46	42.61	39.27	42.31	42.03	42.00	42.51	42.34	42.90	42.33	41.75	41.92
SO2	0.00	0.00	0.00	0.00	0.00	0.00	0.00	0.00	0.00	0.00	0.00	0.00	0.00	0.00	0.00	0.00	0.00	0.00	0.00	0.00	0.00	0.05	0.00
CaO	55.02	55.62	55.22	54.78	55.12	54.55	55.23	55.16	55.33	55.09	55.24	54.22	53.80	50.93	54.87	55.17	55.12	55.95	55.75	54.96	54.90	54.13	54.24
TiO2	0.00	0.00	0.00	0.00	0.00	0.00	0.00	0.00	0.00	0.00	0.00	0.00	0.00	0.00	0.00	0.00	0.00	0.00	0.00	0.00	0.00	0.00	0.00
MnO	0.00	0.00	0.00	0.00	0.00	0.00	0.00	0.00	0.00	0.00	0.00	0.00	0.00	0.00	0.00	0.00	0.00	0.00	0.00	0.00	0.00	0.00	0.00
Fe2O3	0.00	0.00	0.00	0.00	0.00	0.00	0.00	0.00	0.00	0.00	0.00	0.00	0.00	1.68	0.00	0.08	0.00	0.00	0.09	0.13	0.00	0.00	0.18
As2O3	0.00	0.00	0.00	0.00	0.00	0.00	0.00	0.00	0.00	0.00	0.00	0.00	0.00	0.00	0.00	0.00	0.00	0.00	0.00	0.00	0.00	0.00	0.00
SrO	0.00	0.00	0.00	0.00	0.00	0.00	0.00	0.00	0.00	0.00	0.00	0.00	0.00	0.00	0.00	0.00	0.00	0.00	0.00	0.00	0.00	0.00	0.00
Y2O3	0.00	0.00	0.00	0.13	0.09	0.20	0.18	0.17	0.07	0.00	0.00	0.00	0.00	0.00	0.00	0.00	0.05	0.00	0.12	0.00	0.00	0.06	0.00
La2O3	0.00	0.00	0.00	0.00	0.00	0.00	0.00	0.00	0.00	0.00	0.00	0.00	0.00	0.00	0.00	0.00	0.00	0.00	0.00	0.00	0.00	0.00	0.00
Ce2O3	0.00	0.00	0.00	0.13	0.24	0.16	0.10	0.00	0.08	0.00	0.00	0.13	0.10	0.00	0.12	0.00	0.00	0.00	0.00	0.00	0.00	0.00	0.20
Nd2O3	0.00	0.00	0.00	0.12	0.00	0.00	0.00	0.00	0.12	0.00	0.00	0.00	0.00	0.00	0.00	0.00	0.00	0.00	0.00	0.00	0.00	0.00	0.12
-O equivalent	-1.33	-1.22	-1.29	-1.29	-1.31	-1.27	-1.33	-1.29	-1.23	-1.31	-1.26	-1.33	-1.33	-1.17	-1.33	-1.29	-1.20	-1.28	-1.31	-1.32	-1.49	-1.38	-1.32
Total	**99.0**	**100.1**	**99.8**	**99.2**	**99.8**	**99.3**	**99.8**	**99.8**	**99.9**	**99.0**	**99.9**	**99.3**	**99.0**	**96.6**	**99.9**	**99.7**	**99.5**	**100.9**	**100.8**	**100.3**	**99.6**	**98.4**	**99.2**

Calculated formulae 9 a.p.f.u.

Profiles

Jt7 - grain 3	Along																						
Points	**1**	**2**	**3**	**4**	**5**	**6**	**7**	**8**	**9**	**10**	**11**	**12**	**13**	**14**	**15**	**16**	**17**	**18**	**19**	**20**	**21**	**22**	**23**
Ca	4.865	4.887	4.851	4.857	4.859	4.827	4.862	4.851	4.880	4.883	4.852	4.762	4.731	4.620	4.807	4.853	4.874	4.871	4.855	4.787	4.789	4.797	4.790
Mg	0.002	0.001	0.002	0.002	0.002	0.002	0.001	0.002	0.000	0.001	0.002	0.002	0.002	0.042	0.002	0.003	0.002	0.002	0.003	0.001	0.000	0.001	0.001
Mn	0.000	0.000	0.000	0.000	0.000	0.000	0.000	0.000	0.000	0.000	0.000	0.000	0.000	0.000	0.000	0.000	0.000	0.000	0.000	0.000	0.000	0.000	0.000
Sr	0.000	0.000	0.000	0.000	0.000	0.000	0.000	0.000	0.000	0.000	0.000	0.000	0.000	0.000	0.000	0.000	0.000	0.000	0.000	0.000	0.000	0.000	0.000
Y	0.000	0.000	0.000	0.006	0.004	0.009	0.008	0.007	0.003	0.000	0.000	0.000	0.000	0.000	0.000	0.000	0.002	0.000	0.005	0.000	0.000	0.003	0.000
La	0.000	0.000	0.000	0.000	0.000	0.000	0.000	0.000	0.000	0.000	0.000	0.000	0.000	0.000	0.000	0.000	0.000	0.000	0.000	0.000	0.000	0.000	0.000
Ce	0.000	0.000	0.000	0.004	0.007	0.005	0.003	0.000	0.002	0.000	0.000	0.004	0.003	0.000	0.004	0.000	0.000	0.000	0.000	0.000	0.000	0.000	0.006
Nd	0.000	0.000	0.000	0.004	0.000	0.000	0.000	0.000	0.003	0.000	0.000	0.000	0.000	0.000	0.000	0.000	0.000	0.000	0.000	0.000	0.000	0.000	0.003
Na	0.000	0.000	0.003	0.000	0.000	0.003	0.004	0.000	0.003	0.004	0.003	0.000	0.003	0.000	0.007	0.003	0.004	0.000	0.007	0.000	0.000	0.007	0.007
Fe	0.000	0.000	0.000	0.000	0.000	0.000	0.000	0.000	0.000	0.000	0.000	0.000	0.000	0.107	0.000	0.005	0.000	0.000	0.005	0.008	0.000	0.000	0.011
Ti	0.000	0.000	0.000	0.000	0.000	0.000	0.000	0.000	0.000	0.000	0.000	0.000	0.000	0.000	0.000	0.000	0.000	0.000	0.000	0.000	0.000	0.000	0.000
Al	0.000	0.000	0.000	0.000	0.000	0.000	0.000	0.000	0.000	0.000	0.000	0.000	0.000	0.040	0.000	0.000	0.000	0.000	0.000	0.000	0.000	0.000	0.000
Total	**4.867**	**4.888**	**4.856**	**4.872**	**4.873**	**4.845**	**4.877**	**4.860**	**4.892**	**4.888**	**4.857**	**4.767**	**4.739**	**4.662**	**4.819**	**4.859**	**4.881**	**4.872**	**4.871**	**4.789**	**4.789**	**4.808**	**4.808**
SREY	**0.000**	**0.000**	**0.000**	**0.013**	**0.011**	**0.014**	**0.011**	**0.007**	**0.009**	**0.000**	**0.000**	**0.004**	**0.003**	**0.000**	**0.004**	**0.000**	**0.002**	**0.000**	**0.005**	**0.000**	**0.000**	**0.003**	**0.009**
P	2.923	2.945	2.941	2.908	2.889	2.914	2.886	2.910	2.917	2.907	2.932	2.947	2.961	2.815	2.929	2.921	2.934	2.924	2.914	2.952	2.918	2.923	2.925
S	0.000	0.000	0.000	0.000	0.000	0.000	0.000	0.000	0.000	0.000	0.000	0.000	0.000	0.000	0.000	0.000	0.000	0.000	0.000	0.000	0.000	0.004	0.000
As	0.000	0.000	0.000	0.000	0.000	0.000	0.000	0.000	0.000	0.000	0.000	0.000	0.000	0.000	0.000	0.000	0.000	0.000	0.000	0.000	0.000	0.000	0.000
Si	0.000	0.000	0.000	0.025	0.043	0.040	0.041	0.032	0.026	0.016	0.017	0.022	0.021	0.166	0.021	0.019	0.019	0.018	0.019	0.007	0.002	0.011	0.023
Total	**2.923**	**2.945**	**2.941**	**2.933**	**2.932**	**2.954**	**2.927**	**2.942**	**2.942**	**2.924**	**2.950**	**2.969**	**2.982**	**2.981**	**2.950**	**2.941**	**2.953**	**2.942**	**2.933**	**2.959**	**2.920**	**2.938**	**2.948**
F	0.722	0.637	0.684	0.678	0.665	0.659	0.686	0.674	0.643	0.704	0.652	0.694	0.699	0.632	0.694	0.666	0.635	0.662	0.694	0.699	0.835	0.767	0.687
Cl	0.105	0.111	0.111	0.123	0.148	0.126	0.137	0.124	0.119	0.109	0.127	0.126	0.118	0.115	0.123	0.128	0.111	0.120	0.106	0.106	0.077	0.090	0.128
(F+Cl)	0.827	0.748	0.795	0.801	0.813	0.785	0.823	0.798	0.762	0.814	0.779	0.820	0.817	0.747	0.817	0.794	0.746	0.782	0.800	0.804	0.911	0.857	0.815
OH (by difference)	0.173	0.252	0.205	0.199	0.187	0.215	0.177	0.202	0.238	0.186	0.221	0.180	0.183	0.253	0.183	0.206	0.254	0.218	0.200	0.196	0.089	0.143	0.185
Total	**1.000**	**1.000**	**1.000**	**1.000**	**1.000**	**1.000**	**1.000**	**1.000**	**1.000**	**1.000**	**1.000**	**1.000**	**1.000**	**1.000**	**1.000**	**1.000**	**1.000**	**1.000**	**1.000**	**1.000**	**1.000**	**1.000**	**1.000**

Profiles																
Jt7 - grain 3	*(continued)				Across											
Points	**24**	**25**	**26**	**27**	**28**	**29**	**30**	**31**	**32**	**33**	**34**	**35**	**36**	**37**	**38**	**39**
F	2.71	2.88	2.74	2.85	2.69	2.70	2.69	2.76	2.84	2.66	2.65	2.77	2.67	2.65	2.63	2.98
Cl	0.86	0.79	0.92	0.77	0.79	0.91	0.90	0.88	0.79	0.86	0.74	0.86	0.71	0.85	0.83	0.57
Na2O	0.06	0.00	0.00	0.09	0.00	0.00	0.02	0.00	0.00	0.00	0.00	0.00	0.06	0.00	0.02	0.00
SiO2	0.29	0.38	0.63	0.43	0.00	0.09	0.11	0.23	0.06	0.00	0.13	0.23	0.14	0.22	0.28	0.00
Al2O3	0.00	0.00	0.00	0.00	0.00	0.00	0.00	0.00	0.00	0.00	0.00	0.00	0.00	0.00	0.00	0.00
MgO	0.01	0.01	0.02	0.03	0.01	0.01	0.00	0.01	0.01	0.02	0.01	0.01	0.16	0.01	0.01	0.01
P2O5	42.45	42.13	42.09	41.16	42.59	42.76	42.24	42.22	42.48	42.63	41.82	41.51	41.28	42.00	42.03	41.37
SO2	0.00	0.00	0.00	0.08	0.00	0.05	0.00	0.06	0.00	0.00	0.00	0.00	0.08	0.05	0.00	0.00
CaO	53.72	54.62	53.48	55.10	55.68	54.98	55.04	55.01	55.88	55.34	54.59	54.99	55.66	54.63	54.97	55.03
TiO2	0.00	0.00	0.00	0.00	0.00	0.00	0.00	0.00	0.00	0.00	0.00	0.00	0.00	0.00	0.00	0.00
MnO	0.00	0.00	0.00	0.00	0.00	0.00	0.00	0.00	0.00	0.00	0.00	0.00	0.00	0.00	0.00	0.00
Fe2O3	0.00	0.00	0.00	0.40	0.12	0.00	0.00	0.00	0.00	0.00	0.00	0.00	0.16	0.00	0.00	0.00
As2O3	0.00	0.00	0.00	0.00	0.00	0.00	0.00	0.00	0.00	0.00	0.00	0.00	0.00	0.00	0.00	0.00
SrO	0.00	0.00	0.00	0.00	0.00	0.00	0.00	0.00	0.00	0.00	0.00	0.00	0.00	0.00	0.00	0.00
Y2O3	0.06	0.06	0.16	0.25	0.00	0.00	0.00	0.00	0.00	0.00	0.00	0.17	0.00	0.13	0.07	0.00
La2O3	0.00	0.00	0.00	0.00	0.00	0.00	0.00	0.00	0.00	0.00	0.00	0.00	0.00	0.00	0.00	0.00
Ce2O3	0.18	0.00	0.26	0.00	0.00	0.00	0.13	0.08	0.00	0.00	0.00	0.00	0.00	0.00	0.11	0.00
Nd2O3	0.00	0.00	0.00	0.00	0.00	0.00	0.00	0.00	0.00	0.00	0.00	0.00	0.00	0.00	0.00	0.00
-O equivalent	-1.34	-1.39	-1.36	-1.37	-1.31	-1.34	-1.34	-1.36	-1.37	-1.31	-1.28	-1.36	-1.29	-1.31	-1.29	-1.38
Total	**99.0**	**99.5**	**98.9**	**99.8**	**100.6**	**100.2**	**99.8**	**99.9**	**100.7**	**100.2**	**98.6**	**99.2**	**99.6**	**99.2**	**99.7**	**98.6**

Profiles			
Jt7 - grain 6	Along		
Points	**1**	**2**	**3**
F	3.55	3.22	3.23
Cl	0.34	0.53	0.50
Na2O	0.00	0.02	0.00
SiO2	0.00	0.00	0.00
Al2O3	0.00	0.00	0.00
MgO	0.00	0.01	0.00
P2O5	41.74	43.41	42.75
SO2	0.00	0.00	0.00
CaO	55.62	56.26	55.05
TiO2	0.00	0.00	0.00
MnO	0.00	0.00	0.00
Fe2O3	0.25	0.18	0.00
As2O3	0.00	0.00	0.00
SrO	0.00	0.00	0.00
Y2O3	0.00	0.00	0.00
La2O3	0.00	0.00	0.00
Ce2O3	0.00	0.00	0.00
Nd2O3	0.00	0.00	0.00
-O equivalent	-1.57	-1.48	-1.47
Total	**99.9**	**102.2**	**100.1**

Calculated formulae 9 a.p.f.u.

Profiles																
Jt7 - grain 3	*(continued)				Across											
Points	**24**	**25**	**26**	**27**	**28**	**29**	**30**	**31**	**32**	**33**	**34**	**35**	**36**	**37**	**38**	**39**
Ca	4.729	4.786	4.710	4.849	4.854	4.792	4.830	4.815	4.858	4.835	4.846	4.860	4.920	4.818	4.837	4.884
Mg	0.001	0.002	0.002	0.004	0.001	0.001	0.000	0.001	0.002	0.002	0.001	0.002	0.020	0.001	0.002	0.002
Mn	0.000	0.000	0.000	0.000	0.000	0.000	0.000	0.000	0.000	0.000	0.000	0.000	0.000	0.000	0.000	0.000
Sr	0.000	0.000	0.000	0.000	0.000	0.000	0.000	0.000	0.000	0.000	0.000	0.000	0.000	0.000	0.000	0.000
Y	0.002	0.002	0.007	0.011	0.000	0.000	0.000	0.000	0.000	0.000	0.000	0.007	0.000	0.006	0.003	0.000
La	0.000	0.000	0.000	0.000	0.000	0.000	0.000	0.000	0.000	0.000	0.000	0.000	0.000	0.000	0.000	0.000
Ce	0.005	0.000	0.008	0.000	0.000	0.000	0.004	0.003	0.000	0.000	0.000	0.000	0.000	0.000	0.003	0.000
Nd	0.000	0.000	0.000	0.000	0.000	0.000	0.000	0.000	0.000	0.000	0.000	0.000	0.000	0.000	0.000	0.000
Na	0.009	0.000	0.000	0.014	0.000	0.000	0.003	0.000	0.000	0.000	0.000	0.000	0.010	0.000	0.003	0.000
Fe	0.000	0.000	0.000	0.025	0.008	0.000	0.000	0.000	0.000	0.000	0.000	0.000	0.010	0.000	0.000	0.000
Ti	0.000	0.000	0.000	0.000	0.000	0.000	0.000	0.000	0.000	0.000	0.000	0.000	0.000	0.000	0.000	0.000
Al	0.000	0.000	0.000	0.000	0.000	0.000	0.000	0.000	0.000	0.000	0.000	0.000	0.000	0.000	0.000	0.000
Total	**4.747**	**4.790**	**4.726**	**4.878**	**4.855**	**4.794**	**4.837**	**4.818**	**4.860**	**4.837**	**4.847**	**4.869**	**4.950**	**4.825**	**4.848**	**4.886**
SREY	**0.008**	**0.002**	**0.015**	**0.011**	**0.000**	**0.000**	**0.004**	**0.003**	**0.000**	**0.000**	**0.000**	**0.007**	**0.000**	**0.006**	**0.006**	**0.000**
P	2.953	2.917	2.929	2.862	2.933	2.945	2.929	2.920	2.918	2.943	2.933	2.899	2.883	2.928	2.922	2.901
S	0.000	0.000	0.000	0.006	0.000	0.004	0.000	0.004	0.000	0.000	0.000	0.000	0.007	0.004	0.000	0.000
As	0.000	0.000	0.000	0.000	0.000	0.000	0.000	0.000	0.000	0.000	0.000	0.000	0.000	0.000	0.000	0.000
Si	0.024	0.031	0.052	0.036	0.000	0.008	0.009	0.019	0.005	0.000	0.010	0.019	0.011	0.018	0.023	0.000
Total	**2.977**	**2.948**	**2.981**	**2.904**	**2.933**	**2.957**	**2.938**	**2.943**	**2.923**	**2.943**	**2.944**	**2.918**	**2.901**	**2.949**	**2.945**	**2.901**
F	0.705	0.745	0.713	0.740	0.692	0.694	0.697	0.712	0.727	0.687	0.695	0.722	0.697	0.691	0.682	0.780
Cl	0.119	0.110	0.128	0.108	0.108	0.125	0.125	0.122	0.108	0.118	0.104	0.120	0.100	0.118	0.116	0.081
(F+Cl)	0.824	0.854	0.841	0.848	0.801	0.820	0.822	0.833	0.836	0.805	0.799	0.842	0.796	0.809	0.798	0.861
OH (by difference)	0.176	0.146	0.159	0.152	0.199	0.180	0.178	0.167	0.164	0.195	0.201	0.158	0.204	0.191	0.202	0.139
Total	**1.000**	**1.000**	**1.000**	**1.000**	**1.000**	**1.000**	**1.000**	**1.000**	**1.000**	**1.000**	**1.000**	**1.000**	**1.000**	**1.000**	**1.000**	**1.000**

Calculated formulae 9 a.p.f.u.

Profiles			
Jt7 - grain 6	Along		
Points	**1**	**2**	**3**
Ca	4.841	4.793	4.776
Mg	0.000	0.001	0.000
Mn	0.000	0.000	0.000
Sr	0.000	0.000	0.000
Y	0.000	0.000	0.000
La	0.000	0.000	0.000
Ce	0.000	0.000	0.000
Nd	0.000	0.000	0.000
Na	0.000	0.003	0.000
Fe	0.015	0.011	0.000
Ti	0.000	0.000	0.000
Al	0.000	0.000	0.000
Total	**4.841**	**4.797**	**4.776**
SREY	**0.000**	**0.000**	**0.000**
P	2.871	2.923	2.931
S	0.000	0.000	0.000
As	0.000	0.000	0.000
Si	0.000	0.000	0.000
Total	**2.871**	**2.923**	**2.931**
F	0.912	0.810	0.827
Cl	0.047	0.072	0.069
(F+Cl)	0.959	0.881	0.896
OH (by difference)	0.041	0.119	0.104
Total	**1.000**	**1.000**	**1.000**

Profiles																							
Jt7 - grain 6	*(continued)																						
Points	**4**	**5**	**6**	**7**	**8**	**9**	**10**	**11**	**12**	**13**	**15**	**16**	**17**	**18**	**19**	**20**	**21**	**22**	**23**	**24**	**25**	**26**	**27**
F	3.33	3.20	3.52	3.13	3.10	2.93	3.04	3.14	3.12	3.30	3.25	3.38	3.19	3.00	2.93	3.13	3.19	3.04	3.01	2.86	3.01	2.98	2.93
Cl	0.56	0.62	0.58	0.66	0.62	0.73	0.72	0.68	0.75	0.53	0.56	0.41	0.56	0.71	0.70	0.63	0.59	0.66	0.71	0.73	0.71	0.72	0.67
Na2O	0.05	0.00	0.00	0.00	0.00	0.00	0.00	0.02	0.16	0.02	0.00	0.00	0.00	0.00	0.02	0.00	0.00	0.00	0.03	0.00	0.00	0.00	0.03
SiO2	0.00	0.00	0.10	0.02	0.00	0.16	0.13	0.04	0.04	0.00	0.00	0.00	0.09	0.12	0.12	0.07	0.00	0.09	0.04	0.05	0.02	0.02	0.00
Al2O3	0.00	0.00	0.00	0.00	0.00	0.00	0.00	0.00	0.00	0.00	0.00	0.00	0.00	0.00	0.00	0.00	0.00	0.00	0.00	0.00	0.00	0.00	0.00
MgO	0.01	0.01	0.01	0.01	0.01	0.01	0.01	0.02	0.02	0.02	0.01	0.00	0.01	0.01	0.01	0.02	0.01	0.01	0.02	0.01	0.02	0.02	0.01
P2O5	42.94	42.94	42.28	42.57	41.73	42.14	41.05	42.09	42.64	42.61	43.13	43.29	42.05	42.10	42.15	42.34	43.24	42.52	42.80	42.20	42.68	41.86	42.77
SO2	0.00	0.00	0.00	0.07	0.00	0.00	0.00	0.00	0.00	0.00	0.05	0.00	0.00	0.00	0.00	0.00	0.05	0.00	0.00	0.00	0.00	0.00	0.00
CaO	55.54	54.87	55.80	55.21	56.28	54.84	55.20	54.89	55.12	56.10	55.72	55.79	55.77	55.16	54.77	57.44	54.77	53.71	55.75	55.05	55.71	55.76	55.42
TiO2	0.00	0.00	0.00	0.00	0.00	0.00	0.00	0.00	0.00	0.00	0.00	0.00	0.00	0.00	0.00	0.00	0.00	0.00	0.00	0.00	0.00	0.00	0.00
MnO	0.00	0.00	0.00	0.00	0.00	0.00	0.00	0.00	0.00	0.00	0.00	0.00	0.00	0.00	0.00	0.00	0.00	0.00	0.00	0.00	0.00	0.00	0.00
Fe2O3	0.00	0.00	0.24	0.00	0.00	0.00	0.00	0.00	0.00	0.00	0.00	0.12	0.00	0.08	0.00	0.00	0.11	0.15	0.16	0.00	0.00	0.00	0.00
As2O3	0.00	0.00	0.00	0.00	0.00	0.00	0.00	0.00	0.00	0.00	0.00	0.00	0.00	0.00	0.00	0.00	0.00	0.00	0.00	0.00	0.00	0.00	0.00
SrO	0.00	0.00	0.00	0.00	0.00	0.00	0.00	0.00	0.00	0.00	0.00	0.00	0.00	0.00	0.00	0.00	0.00	0.00	0.00	0.00	0.00	0.00	0.00
Y2O3	0.00	0.00	0.00	0.00	0.00	0.00	0.00	0.00	0.00	0.00	0.00	0.00	0.00	0.06	0.08	0.00	0.00	0.00	0.00	0.00	0.00	0.00	0.00
La2O3	0.00	0.00	0.00	0.00	0.00	0.00	0.00	0.00	0.00	0.00	0.00	0.00	0.00	0.00	0.00	0.00	0.00	0.00	0.00	0.00	0.00	0.00	0.00
Ce2O3	0.00	0.00	0.00	0.00	0.00	0.00	0.00	0.00	0.00	0.00	0.00	0.00	0.00	0.00	0.00	0.00	0.00	0.00	0.00	0.00	0.00	0.00	0.00
Nd2O3	0.00	0.00	0.00	0.00	0.00	0.00	0.00	0.00	0.00	0.00	0.00	0.00	0.00	0.00	0.00	0.00	0.00	0.00	0.00	0.00	0.00	0.00	0.00
-O equivalent	-1.53	-1.49	-1.61	-1.47	-1.45	-1.40	-1.44	-1.48	-1.48	-1.51	-1.50	-1.52	-1.47	-1.42	-1.39	-1.46	-1.48	-1.43	-1.43	-1.37	-1.43	-1.41	-1.38
Total	**100.9**	**100.2**	**100.9**	**100.2**	**100.3**	**99.4**	**98.7**	**99.4**	**100.4**	**101.1**	**101.2**	**101.5**	**100.2**	**99.8**	**99.4**	**102.2**	**100.5**	**98.8**	**101.1**	**99.5**	**100.7**	**99.9**	**100.4**

Calculated formulae 9 a.p.f.u.

Profiles

Jt7 - grain 6 *(continued)

Points	**4**	**5**	**6**	**7**	**8**	**9**	**10**	**11**	**12**	**13**	**15**	**16**	**17**	**18**	**19**	**20**	**21**	**22**	**23**	**24**	**25**	**26**	**27**
Ca	4.778	4.751	4.801	4.793	4.914	4.811	4.893	4.805	4.777	4.833	4.781	4.770	4.856	4.823	4.808	4.929	4.722	4.715	4.813	4.831	4.825	4.884	4.814
Mg	0.001	0.002	0.002	0.001	0.002	0.001	0.002	0.002	0.003	0.002	0.001	0.000	0.001	0.001	0.002	0.003	0.001	0.002	0.002	0.002	0.002	0.002	0.001
Mn	0.000	0.000	0.000	0.000	0.000	0.000	0.000	0.000	0.000	0.000	0.000	0.000	0.000	0.000	0.000	0.000	0.000	0.000	0.000	0.000	0.000	0.000	0.000
Sr	0.000	0.000	0.000	0.000	0.000	0.000	0.000	0.000	0.000	0.000	0.000	0.000	0.000	0.000	0.000	0.000	0.000	0.000	0.000	0.000	0.000	0.000	0.000
Y	0.000	0.000	0.000	0.000	0.000	0.000	0.000	0.000	0.000	0.000	0.000	0.000	0.000	0.003	0.003	0.000	0.000	0.000	0.000	0.000	0.000	0.000	0.000
La	0.000	0.000	0.000	0.000	0.000	0.000	0.000	0.000	0.000	0.000	0.000	0.000	0.000	0.000	0.000	0.000	0.000	0.000	0.000	0.000	0.000	0.000	0.000
Ce	0.000	0.000	0.000	0.000	0.000	0.000	0.000	0.000	0.000	0.000	0.000	0.000	0.000	0.000	0.000	0.000	0.000	0.000	0.000	0.000	0.000	0.000	0.000
Nd	0.000	0.000	0.000	0.000	0.000	0.000	0.000	0.000	0.000	0.000	0.000	0.000	0.000	0.000	0.000	0.000	0.000	0.000	0.000	0.000	0.000	0.000	0.000
Na	0.008	0.000	0.000	0.000	0.000	0.000	0.000	0.003	0.025	0.003	0.000	0.000	0.000	0.000	0.003	0.000	0.000	0.000	0.004	0.000	0.000	0.000	0.005
Fe	0.000	0.000	0.014	0.000	0.000	0.000	0.000	0.000	0.000	0.000	0.000	0.007	0.000	0.005	0.000	0.000	0.007	0.009	0.010	0.000	0.000	0.000	0.000
Ti	0.000	0.000	0.000	0.000	0.000	0.000	0.000	0.000	0.000	0.000	0.000	0.000	0.000	0.000	0.000	0.000	0.000	0.000	0.000	0.000	0.000	0.000	0.000
Al	0.000	0.000	0.000	0.000	0.000	0.000	0.000	0.000	0.000	0.000	0.000	0.000	0.000	0.000	0.000	0.000	0.000	0.000	0.000	0.000	0.000	0.000	0.000
Total	**4.787**	**4.753**	**4.803**	**4.794**	**4.916**	**4.812**	**4.895**	**4.811**	**4.805**	**4.838**	**4.782**	**4.770**	**4.857**	**4.827**	**4.816**	**4.932**	**4.724**	**4.717**	**4.819**	**4.832**	**4.827**	**4.886**	**4.821**
SREY	**0.000**	**0.000**	**0.000**	**0.000**	**0.000**	**0.000**	**0.000**	**0.000**	**0.000**	**0.000**	**0.000**	**0.000**	**0.000**	**0.003**	**0.003**	**0.000**	**0.000**	**0.000**	**0.000**	**0.000**	**0.000**	**0.000**	**0.000**
P	2.919	2.938	2.875	2.920	2.879	2.921	2.875	2.911	2.920	2.901	2.924	2.924	2.893	2.909	2.924	2.871	2.946	2.950	2.920	2.926	2.921	2.897	2.936
S	0.000	0.000	0.000	0.005	0.000	0.000	0.000	0.000	0.000	0.000	0.004	0.000	0.000	0.000	0.000	0.000	0.004	0.000	0.000	0.000	0.000	0.000	0.000
As	0.000	0.000	0.000	0.000	0.000	0.000	0.000	0.000	0.000	0.000	0.000	0.000	0.000	0.000	0.000	0.000	0.000	0.000	0.000	0.000	0.000	0.000	0.000
Si	0.000	0.000	0.008	0.002	0.000	0.013	0.011	0.003	0.003	0.000	0.000	0.000	0.007	0.009	0.010	0.006	0.000	0.008	0.003	0.004	0.002	0.002	0.000
Total	**2.919**	**2.938**	**2.883**	**2.926**	**2.879**	**2.934**	**2.886**	**2.915**	**2.923**	**2.901**	**2.928**	**2.924**	**2.900**	**2.918**	**2.934**	**2.876**	**2.950**	**2.957**	**2.922**	**2.931**	**2.923**	**2.899**	**2.936**
F	0.845	0.817	0.895	0.802	0.799	0.758	0.794	0.811	0.799	0.838	0.824	0.853	0.819	0.773	0.758	0.794	0.812	0.788	0.767	0.741	0.770	0.769	0.751
Cl	0.076	0.085	0.079	0.091	0.086	0.102	0.100	0.095	0.102	0.072	0.077	0.056	0.077	0.099	0.097	0.086	0.081	0.092	0.097	0.102	0.097	0.099	0.092
(F+Cl)	0.921	0.902	0.973	0.893	0.885	0.860	0.895	0.906	0.902	0.911	0.900	0.909	0.896	0.872	0.855	0.880	0.893	0.880	0.864	0.843	0.867	0.869	0.843
OH (by difference)	0.079	0.098	0.027	0.107	0.115	0.140	0.105	0.094	0.098	0.089	0.100	0.091	0.104	0.128	0.145	0.120	0.107	0.120	0.136	0.157	0.133	0.131	0.157
Total	**1.000**	**1.000**	**1.000**	**1.000**	**1.000**	**1.000**	**1.000**	**1.000**	**1.000**	**1.000**	**1.000**	**1.000**	**1.000**	**1.000**	**1.000**	**1.000**	**1.000**	**1.000**	**1.000**	**1.000**	**1.000**	**1.000**	**1.000**

Profiles															
Jt7 - grain 6	*(continued)		Across												
Points	**28**	**29**	**30**	**31**	**32**	**33**	**34**	**35**	**36**	**37**	**38**	**39**	**40**	**41**	**42**
F	3.08	3.17	3.48	3.22	3.51	2.96	3.11	3.20	3.11	3.33	3.38	3.16	3.23	3.20	3.21
Cl	0.59	0.70	0.32	0.49	0.43	0.31	0.65	0.60	0.65	0.45	0.42	0.61	0.52	0.59	0.62
Na2O	0.00	0.00	0.00	0.05	0.00	0.07	0.04	0.03	0.00	0.00	0.02	0.00	0.04	0.02	0.03
SiO2	0.00	0.00	0.00	0.03	0.02	6.85	0.13	0.08	0.04	0.06	0.04	0.05	0.02	0.00	0.00
Al2O3	0.00	0.00	0.00	0.00	0.00	0.71	0.00	0.00	0.00	0.00	0.00	0.00	0.00	0.00	0.00
MgO	0.01	0.02	0.01	0.02	0.01	0.73	0.02	0.00	0.02	0.01	0.00	0.01	0.01	0.01	0.03
P2O5	42.39	42.45	42.85	42.40	42.30	37.34	42.29	42.73	43.04	43.29	42.92	42.95	43.04	42.94	42.91
SO2	0.00	0.00	0.07	0.00	0.00	0.10	0.05	0.00	0.00	0.00	0.00	0.00	0.00	0.00	0.00
CaO	55.77	56.09	56.07	54.73	55.54	48.48	55.22	55.47	55.96	55.80	55.75	55.78	55.70	55.43	54.79
TiO2	0.00	0.00	0.00	0.00	0.00	0.00	0.00	0.00	0.00	0.00	0.00	0.00	0.00	0.00	0.00
MnO	0.00	0.00	0.00	0.00	0.00	0.00	0.00	0.00	0.00	0.00	0.00	0.00	0.00	0.00	0.00
Fe2O3	0.13	0.00	0.00	0.00	0.14	4.82	0.00	0.00	0.09	0.00	0.08	0.15	0.20	0.12	0.72
As2O3	0.00	0.00	0.00	0.00	0.00	0.00	0.00	0.00	0.00	0.00	0.00	0.00	0.00	0.00	0.00
SrO	0.00	0.00	0.00	0.00	0.00	0.10	0.00	0.00	0.00	0.00	0.00	0.00	0.00	0.00	0.00
Y2O3	0.00	0.00	0.00	0.00	0.00	0.00	0.00	0.00	0.00	0.00	0.00	0.00	0.00	0.00	0.00
La2O3	0.00	0.00	0.00	0.00	0.00	0.00	0.00	0.00	0.00	0.00	0.00	0.00	0.00	0.00	0.00
Ce2O3	0.00	0.00	0.00	0.00	0.00	0.00	0.00	0.00	0.00	0.00	0.00	0.00	0.00	0.00	0.00
Nd2O3	0.00	0.00	0.00	0.00	0.00	0.00	0.00	0.00	0.00	0.00	0.12	0.00	0.00	0.00	0.00
-O equivalent	-1.43	-1.49	-1.54	-1.47	-1.58	-1.32	-1.46	-1.48	-1.45	-1.50	-1.52	-1.47	-1.48	-1.48	-1.49
Total	**100.6**	**100.9**	**101.3**	**99.5**	**100.4**	**101.2**	**100.1**	**100.6**	**101.5**	**101.4**	**101.2**	**101.2**	**101.3**	**100.8**	**100.8**

Calculated formulae 9 a.p.f.u.

Profiles

Jt7 - grain 6	*(continued)		Across												
Points	**28**	**29**	**30**	**31**	**32**	**33**	**34**	**35**	**36**	**37**	**38**	**39**	**40**	**41**	**42**
Ca	4.843	4.847	4.806	4.778	4.802	4.152	4.806	4.793	4.806	4.773	4.787	4.797	4.783	4.779	4.722
Mg	0.002	0.002	0.001	0.002	0.001	0.086	0.003	0.000	0.002	0.001	0.000	0.002	0.001	0.001	0.003
Mn	0.000	0.000	0.000	0.000	0.000	0.000	0.000	0.000	0.000	0.000	0.000	0.000	0.000	0.000	0.000
Sr	0.000	0.000	0.000	0.000	0.000	0.005	0.000	0.000	0.000	0.000	0.000	0.000	0.000	0.000	0.000
Y	0.000	0.000	0.000	0.000	0.000	0.000	0.000	0.000	0.000	0.000	0.000	0.000	0.000	0.000	0.000
La	0.000	0.000	0.000	0.000	0.000	0.000	0.000	0.000	0.000	0.000	0.000	0.000	0.000	0.000	0.000
Ce	0.000	0.000	0.000	0.000	0.000	0.000	0.000	0.000	0.000	0.000	0.000	0.000	0.000	0.000	0.000
Nd	0.000	0.000	0.000	0.000	0.000	0.000	0.000	0.000	0.000	0.000	0.003	0.000	0.000	0.000	0.000
Na	0.000	0.000	0.000	0.008	0.000	0.012	0.006	0.005	0.000	0.000	0.003	0.000	0.007	0.003	0.005
Fe	0.008	0.000	0.000	0.000	0.009	0.290	0.000	0.000	0.006	0.000	0.005	0.009	0.012	0.007	0.043
Ti	0.000	0.000	0.000	0.000	0.000	0.000	0.000	0.000	0.000	0.000	0.000	0.000	0.000	0.000	0.000
Al	0.000	0.000	0.000	0.000	0.000	0.067	0.000	0.000	0.000	0.000	0.000	0.000	0.000	0.000	0.000
Total	**4.845**	**4.849**	**4.807**	**4.789**	**4.803**	**4.254**	**4.815**	**4.798**	**4.807**	**4.774**	**4.794**	**4.798**	**4.791**	**4.784**	**4.730**
SREY	**0.000**	**0.000**	**0.000**	**0.000**	**0.000**	**0.000**	**0.000**	**0.000**	**0.000**	**0.000**	**0.003**	**0.000**	**0.000**	**0.000**	**0.000**
P	2.909	2.899	2.903	2.925	2.890	2.527	2.908	2.918	2.921	2.926	2.912	2.918	2.920	2.925	2.922
S	0.000	0.000	0.005	0.000	0.000	0.008	0.004	0.000	0.000	0.000	0.000	0.000	0.000	0.000	0.000
As	0.000	0.000	0.000	0.000	0.000	0.000	0.000	0.000	0.000	0.000	0.000	0.000	0.000	0.000	0.000
Si	0.000	0.000	0.000	0.002	0.002	0.547	0.011	0.006	0.003	0.005	0.003	0.004	0.002	0.000	0.000
Total	**2.909**	**2.899**	**2.908**	**2.928**	**2.892**	**3.082**	**2.923**	**2.924**	**2.924**	**2.931**	**2.914**	**2.923**	**2.922**	**2.925**	**2.922**
F	0.790	0.808	0.882	0.830	0.897	0.747	0.798	0.815	0.788	0.840	0.858	0.801	0.820	0.814	0.818
Cl	0.082	0.096	0.043	0.068	0.059	0.042	0.090	0.082	0.088	0.061	0.056	0.082	0.070	0.080	0.084
(F+Cl)	0.871	0.904	0.925	0.898	0.956	0.790	0.888	0.897	0.875	0.902	0.914	0.883	0.890	0.894	0.902
OH (by difference)	0.129	0.096	0.075	0.102	0.044	0.210	0.112	0.103	0.125	0.098	0.086	0.117	0.110	0.106	0.098
Total	**1.000**	**1.000**	**1.000**	**1.000**	**1.000**	**1.000**	**1.000**	**1.000**	**1.000**	**1.000**	**1.000**	**1.000**	**1.000**	**1.000**	**1.000**

Supplementary Table 2. LA-ICP-MS trace element data for fluorapatite (complete dataset, element concentrations in ppm, calculated from measurement of given isotope, except for the 4 Pb isotopes)
**Note*: Data reported here are raw data; '<' values correspond to bdl. LREE=La+Ce+Pr+Nd; MREE= Sm+Eu+Gd+Tb+Dy; HREE= Y+Ho+Er+Tm+Yb+Lu.

#	Sample Jt1	ΣLREE	ΣMREE	ΣHREE	ΣREY	Si	P	Cl	Ca	Ti	Mn	Sr	Y	Zr
1	Jt1 Ap1 - 01	5007	938	1731	7676	2211	207877	5824	390000	5.4	393	279	1419	0.600
2	Jt1 Ap1 - 02	7571	1248	2211	11030	2999	210669	6362	390000	3.4	418	300	1805	0.665
3	Jt1 Ap1 - 03	5543	955	1776	8275	2863	214662	6074	390000	7.9	413	270	1449	0.473
4	Jt1 Ap1 - 04	3104	1105	2534	6743	2403	210091	5622	390000	4.0	377	311	2055	0.524
5	Jt1 Ap1 - 05	2938	860	1922	5721	1951	213299	5724	390000	3.5	380	295	1560	0.437
6	Jt1 Ap1 - 06	6173	1356	2712	10241	3063	209270	5994	390000	3.9	404	300	2204	0.576
7	Jt1 Ap1 - 07	8514	1369	2458	12342	3123	209883	6429	390000	3.1	428	296	2003	0.546
8	Jt1 Ap2 - 01	177	240	659	1076	817	213111	4740	390000	5.0	312	362	541	0.027
9	Jt1 Ap2 - 02	620	619	1644	2883	1454	208542	5013	390000	5.0	336	326	1333	0.170
10	Jt1 Ap2 - 03	2529	1086	2684	6298	2113	210214	5699	390000	4.0	381	320	2171	0.329
11	Jt1 Ap2 - 04	1445	648	1483	3576	1382	207515	5709	390000	5.7	375	323	1209	0.138
12	Jt1 Ap2 - 05	2698	855	2006	5560	2072	209116	5604	390000	8.0	380	331	1631	0.460
13	Jt1 Ap2 - 06	3665	1044	2345	7054	2196	211066	5929	390000	4.9	391	313	1906	0.726
14	Jt1 Ap2 - 07	3706	1196	2715	7617	2539	209378	5824	390000	4.6	385	336	2198	0.461
15	Jt1 Ap2 - 08	6079	1267	2717	10063	3311	205765	6357	390000	4.5	397	288	2197	0.423
16	Jt1 Ap3 - 01	5553	1322	2861	9735	2800	211585	6183	390000	3.8	400	312	2315	0.478
17	Jt1 Ap3 - 02	6518	1218	2396	10132	2887	209079	6458	390000	3.5	412	311	1946	0.406
18	Jt1 Ap3 - 03	5701	1080	2117	8898	2653	211446	6412	390000	6.3	411	315	1721	0.411
19	Jt1 Ap3 - 04	5336	966	1846	8147	2486	210030	6484	390000	5.2	412	278	1498	0.420
20	Jt1 Ap3 - 05	168	159	408	735	758	210821	5273	390000	2.9	340	344	336	0.030
21	Jt1 Ap3 - 06	2239	493	1198	3930	1630	211785	5021	390000	4.6	318	378	979	0.147
22	Jt1 Ap3 - 07	207	192	539	937	23356	204862	4839	390000	1188	383	380	442	0.086
23	Jt1 Ap4 - 01	535	160	349	1044	1327	209533	5680	390000	34	383	215	285	0.169
24	Jt1 Ap4 - 02	3928	761	1580	6269	2077	210350	6118	390000	14	387	273	1287	0.263
25	Jt1 Ap4 - 03	10070	1408	2537	14016	3796	209379	7107	390000	2.9	439	284	2065	0.726
26	Jt1 Ap4 - 04	8016	1275	2428	11719	3393	210272	6904	390000	3.5	421	288	1977	0.647
27	Jt1 Ap4 - 05	4902	791	1520	7213	2159	210895	6369	390000	3.3	403	263	1239	0.214
28	Jt1 Ap4 - 06	109	79	197	385	622	211539	5910	390000	2.0	366	192	162	0.003
29	Jt1 Ap4 - 07	119	87	203	409	516	213706	5837	390000	3.3	375	205	168	0.003
30	Jt1 Ap5 - 01	2090	686	1569	4345	2199	228549	5673	390000	16	361	312	1273	0.185
31	Jt1 Ap5 - 02	2161	763	1678	4603	1681	207694	6095	390000	5.5	388	290	1359	0.201
32	Jt1 Ap5 - 03	2470	825	1937	5232	1594	208943	5948	390000	3.2	361	333	1575	0.182
33	Jt1 Ap5 - 04	5864	1212	2527	9603	2663	209924	6737	390000	3.9	409	289	2055	0.486
34	Jt1 Ap5 - 05	4303	1256	2909	8468	2490	210104	6455	390000	3.2	394	296	2361	0.345
35	Jt1 Ap5 - 06	2657	1011	2477	6146	1948	210829	5787	390000	3.4	368	316	2010	0.296
36	Jt1 Ap5 - 07	5068	920	1682	7670	2048	210174	6514	390000	2.7	408	256	1371	0.268
37	Jt1 Ap5 - 08	5362	1030	2059	8450	2431	212569	6740	390000	2.9	410	286	1677	0.391
38	Jt1 Ap6 - 01	11486	1326	1910	14722	3687	208981	7447	390000	4.0	461	276	1572	0.630
39	Jt1 Ap6 - 02	9496	1341	2198	13036	3558	211812	7240	390000	2.5	442	279	1798	0.505
40	Jt1 Ap6 - 03	11704	1342	1949	14995	3748	210315	7397	390000	3.1	454	279	1603	0.598
41	Jt1 Ap6 - 04	87	82	216	385	637	212789	5403	390000	3.5	348	213	179	0.005
42	Jt1 Ap6 - 05	104	80	197	381	684	211947	5905	390000	3.8	377	205	163	0.011
43	Jt1 Ap6 - 06	114	75	199	388	716	212382	6075	390000	14	365	178	163	0.387
44	Jt1 Ap6 - 07	138	88	218	444	1330	211563	4958	390000	7.9	359	207	180	0.011
45	Jt1 Ap6 - 08	8483	1254	2258	11995	4091	209472	6974	390000	4.6	433	277	1842	0.453
46	Jt1 Ap7 - 01	74	83	231	389	685	212345	5990	390000	2.5	340	168	189	0.003
47	Jt1 Ap7 - 02	91	78	198	367	666	210724	5999	390000	1.9	366	170	163	0.003
48	Jt1 Ap7 - 03	71	77	220	367	582	213407	6392	390000	2.8	348	164	180	<0.000
49	Jt1 Ap7 - 04	64	70	205	338	566	211540	6335	390000	3.5	331	159	167	0.008
50	Jt1 Ap7 - 05	98	81	194	373	688	212286	5947	390000	2.5	376	181	160	<0.000
51	Jt1 Ap8 - 01	3668	1049	2470	7188	2889	210839	6181	390000	3.8	400	276	2002	0.252
52	Jt1 Ap8 - 02	1282	352	823	2457	885	210785	5701	390000	2.2	353	351	673	0.104
53	Jt1 Ap8 - 03	819	490	1315	2624	1151	211104	4655	390000	2.7	321	358	1072	0.129
54	Jt1 Ap8 - 04	1776	816	2068	4659	1955	210485	5447	390000	3.0	331	348	1686	0.234
55	Jt1 Ap8 - 05	5237	1272	2833	9343	2930	210630	6463	390000	2.9	410	326	2297	0.429
56	Jt1 Ap9 - 01	92	93	229	414	588	211320	5608	390000	2.4	372	266	189	<0.000

#	Sample Jt1	ΣLREE	ΣMREE	ΣHREE	ΣREY	Si	P	Cl	Ca	Ti	Mn	Sr	Y	Zr
57	Jt1 Ap9 - 02	96	99	242	438	555	212080	5495	390000	3.0	360	295	202	<0.000
58	Jt1 Ap9 - 03	86	95	241	422	626	211089	5543	390000	2.9	356	275	200	<0.000
59	Jt1 Ap9 - 04	102	106	263	470	3753	209601	4913	390000	5.4	334	364	219	0.011
60	Jt1 Ap9 - 05	84	96	245	425	618	216841	5117	390000	2.5	358	291	203	0.005
61	Jt1 Ap9 - 06	88	87	209	384	646	214341	5759	390000	3.1	382	247	173	0.003
62	Jt1 Ap9 - 07	69	71	183	323	470	215473	5705	390000	2.5	347	166	150	<0.000
63	Jt1 Ap10 - 01	1029	293	660	1982	918	213218	5428	390000	2.6	369	267	539	0.088
64	Jt1 Ap10 - 02	336	159	370	865	1545	213644	5124	390000	4.2	351	328	307	0.157
65	Jt1 Ap10 - 03	651	411	964	2026	949	216228	5251	390000	2.8	366	377	788	0.136
66	Jt1 Ap10 - 04	470	381	914	1765	1330	213040	4950	390000	7.4	309	376	745	12
67	Jt1 Ap10 - 05	4602	421	654	5676	7800	210074	4518	390000	32	359	358	540	0.178
68	Jt1 Ap10 - 06	76	92	250	418	672	215270	3826	390000	2.7	306	338	209	<0.000
69	Jt1 Ap10 - 07	66	88	242	396	536	213439	4239	390000	2.4	310	351	201	0.003
70	Jt1 Ap11 - 01	97	97	241	435	622	199919	4952	390000	9.9	337	299	201	0.047
71	Jt1 Ap11 - 03	1584	767	1880	4231	5560	208788	5732	390000	173	362	337	1525	0.167
72	Jt1 Ap11 - 05	98	116	301	515	660	214138	4859	390000	3.0	314	388	250	0.014
73	Jt1 Ap11 - 06	118	101	242	462	650	208252	5034	390000	9.7	354	273	201	0.079
74	Jt1 Ap11 - 08	231	152	367	749	687	210204	5477	390000	3.2	354	291	301	0.079
75	Jt1 Ap11 - 09	109	104	251	465	1718	206499	5082	390000	7.4	343	324	209	0.092
76	Jt1 Ap12 - 01	81	76	192	348	759	212404	5858	390000	2.9	376	186	157	<0.000
77	Jt1 Ap12 - 02	92	85	215	391	539	212836	5776	390000	2.9	379	210	177	0.011
78	Jt1 Ap12 - 03	109	91	205	405	688	210379	5533	390000	3.2	384	236	170	<0.000
79	Jt1 Ap12 - 04	82	77	199	358	657	212338	5960	390000	3.2	376	183	163	0.003
80	Jt1 Ap12 - 05	155	106	239	500	1673	212303	5194	390000	4.5	360	266	198	0.051
81	Jt1 Ap12 - 07	129	90	212	431	632	212510	5576	390000	4.1	383	230	175	0.008
82	Jt1 Ap12 - 09	104	87	203	394	619	214439	5717	390000	2.7	374	190	167	0.103
83	Jt1 Ap13 - 01	111	101	240	452	584	210167	5425	390000	4.9	359	317	198	0.008
84	Jt1 Ap13 - 02	104	97	243	445	923	211862	5233	390000	14	361	286	201	0.032
85	Jt1 Ap13 - 03	133	92	213	438	770	201474	5713	390000	4.5	384	229	176	0.021
86	Jt1 Ap13 - 04	108	86	205	399	660	211561	5523	390000	3.2	376	207	169	0.003
87	Jt1 Ap13 - 05	118	96	221	435	611	211818	5472	390000	2.0	373	263	182	0.003
88	Jt1 Ap13 - 06	112	96	225	432	559	209264	5480	390000	20	374	257	185	0.061
89	Jt1 Ap13 - 07	117	106	254	477	687	210971	5204	390000	4.6	347	305	210	0.185
90	Jt1 Ap13 - 08	114	103	237	454	566	210472	5457	390000	5.9	361	319	197	0.014
91	Jt1 Ap14 - 01	150	196	533	879	791	210319	4304	390000	2.4	306	354	439	0.022
92	Jt1 Ap14 - 02	95	99	250	443	1197	184833	4685	390000	12	342	334	209	0.199
93	Jt1 Ap14 - 03	157	111	259	527	687	212544	5214	390000	3.3	347	342	215	<0.000
94	Jt1 Ap14 - 04	582	424	1086	2092	2635	211683	4869	390000	3.7	322	355	886	0.084
95	Jt1 Ap14 - 05	78	96	247	421	871	211520	4942	390000	4.3	327	380	206	0.034
96	Jt1 Ap14 - 06	112	107	255	475	607	211910	5227	390000	2.9	345	331	213	0.003
97	Jt1 Ap14 - 07	102	108	271	481	1114	211999	4957	390000	3.9	340	340	225	0.003
98	Jt1 Ap14 - 08	1974	894	2252	5120	2431	210243	5692	390000	3.7	365	318	1827	0.317
99	Jt1 Ap14 - 09	334	316	834	1485	1077	210764	4854	390000	3.8	313	356	679	0.056
100	Jt1 Ap14 - 10	1222	721	1816	3759	2143	210299	5516	390000	3.2	352	337	1475	0.100
101	Jt1 Ap14 - 11	480	421	1084	1984	1085	208971	5358	390000	2.8	348	362	882	0.113
102	Jt1 Ap15 - 01	2328	677	1569	4574	1801	211138	5921	390000	2.3	379	304	1273	0.207
103	Jt1 Ap15 - 02	111	118	287	516	691	214472	5021	390000	2.9	339	330	238	0.008
104	Jt1 Ap15 - 03	174	129	299	602	14405	208158	5342	390000	681	391	317	247	0.018
105	Jt1 Ap15 - 04	122	107	250	478	642	213280	5227	390000	2.8	360	301	207	0.005
106	Jt1 Ap15 - 05	2371	925	2152	5448	1832	209924	5954	390000	4.2	366	312	1745	0.228
107	Jt1 Ap15 - 06	2185	774	1820	4780	7105	205760	5965	390000	273	390	311	1475	0.202
108	Jt1 Ap15 - 07	129	111	261	502	740	208166	4988	390000	3.9	358	314	216	0.102
109	Jt1 Ap15 - 08	86	99	247	432	580	208811	4814	390000	2.5	335	299	206	0.008
110	Jt1 Ap15 - 09	269	181	462	912	1857	210438	4119	390000	43	288	302	379	0.028
111	Jt1 Ap16 - 01	6436	1251	2533	10220	3001	209343	6720	390000	2.2	421	298	2057	0.375
112	Jt1 Ap16 - 02	4855	1086	2235	8175	2663	207785	6701	390000	6.4	410	310	1818	0.331
113	Jt1 Ap16 - 03	316	231	565	1112	798	211229	5294	390000	2.8	338	364	463	0.013
114	Jt1 Ap16 - 04	4197	1160	2454	7811	2426	210903	6158	390000	2.6	373	323	1996	0.289
115	Jt1 Ap16 - 06	5827	1116	2223	9165	2651	208100	6708	390000	2.9	425	330	1803	0.482
116	Jt1 Ap16 - 07	1309	485	1098	2892	1508	211356	5871	390000	2.2	366	325	893	0.115
117	Jt1 Ap16 - 08	3018	875	1726	5620	1778	209580	6366	390000	1.6	382	318	1403	0.199

#	Sample Jt1	ΣLREE	ΣMREE	ΣHREE	ΣREY	Si	P	Cl	Ca	Ti	Mn	Sr	Y	Zr
118	Jt1 Ap16 - 09	3995	889	1710	6593	1997	208982	6577	390000	2.4	395	309	1389	0.230
119	Jt1 Ap16 - 10	6365	1223	2215	9802	2745	208924	6714	390000	5.5	411	309	1807	0.397
120	Jt1 Ap16 - 11	1843	596	1218	3657	1671	198851	6006	390000	14	359	323	992	0.291
121	Jt1 Ap16 - 12	2402	675	1436	4513	2754	206900	6075	390000	53	378	321	1168	0.189
122	Jt1 Ap16 - 13	5735	1107	1966	8808	2622	207698	6754	390000	4.8	413	279	1601	0.384
123	Jt1 Ap16 - 14	4515	1074	2058	7647	2198	208923	6513	390000	3.6	403	313	1673	0.316
124	Jt1 Ap16 - 15	3997	791	1435	6223	1877	209873	6474	390000	2.6	402	303	1169	1.7
125	Jt1 Ap16 - 16	4690	994	1950	7634	2214	207668	6708	390000	3.1	403	280	1584	0.217
126	Jt1 Ap16 - 17	5037	1116	2283	8436	2367	208026	6373	390000	2.6	397	294	1860	0.329
127	Jt1 Ap16 - 18	3397	1010	2274	6681	2441	207766	6121	390000	2.9	388	306	1843	0.299
128	Jt1 Ap16 - 20	178	101	212	491	599	212249	5999	390000	2.0	369	238	175	<0.000
129	Jt1 Ap16 - 21	5757	1291	2646	9694	3667	210766	6556	390000	3.0	407	304	2151	0.518
130	Jt1 Ap16 - 22	2570	874	1965	5410	1767	210907	5914	390000	1.5	359	313	1596	0.222
131	Jt1 Ap16 - 23	2331	898	2137	5366	1899	211573	6064	390000	2.3	359	374	1737	0.228
132	Jt1 Ap16 - 24	1092	560	1315	2967	1120	210950	5732	390000	2.3	353	359	1070	0.112
133	Jt1 Ap16 - 25	883	473	1123	2478	998	208539	5552	390000	2.0	340	375	918	0.096
134	Jt1 Ap16 - 26	1186	665	1650	3500	1412	212288	5923	390000	2.3	358	367	1340	0.131
135	Jt1 Ap17 - 01	88	94	224	406	680	211237	5695	390000	2.3	360	241	185	0.003
136	Jt1 Ap17 - 02	87	93	225	405	579	212808	5419	390000	2.7	356	281	187	0.011
137	Jt1 Ap17 - 03	90	96	238	424	8285	205631	5222	390000	5.0	344	331	197	0.056
138	Jt1 Ap17 - 05	127	99	232	459	1483	206790	4602	390000	15	339	248	193	0.250
139	Jt1 Ap17 - 07	100	97	226	423	1253	210354	5464	390000	25	364	275	187	0.125
140	Jt1 Ap17 - 08	703	211	462	1376	1190	210327	5471	390000	4.7	382	207	377	0.087
141	Jt1 Ap17 - 09	105	93	211	409	679	216382	5558	390000	14	377	246	175	0.021
142	Jt1 Ap17 - 10	86	88	217	390	644	213566	5455	390000	2.8	355	264	180	0.003
	Mean (n=142)	2155	533	1136	3824	1997	210477	5728	390000	22	371	294	925	0.306
	SD	2706	461	923	3936	2484	3752	674	0.000	117	32	54	749	1.0
	Median	636	396	874	2005	1496	210744	5711	390000	3.4	369	302	712	0.167
	Max	11704	1408	2909	14995	23356	228549	7447	390000	1188	461	388	2361	12
	Min	64	70	183	323	470	184833	3826	390000	1.5	288	159	150	0.003

#	Sample Jt4	ΣLREE	ΣMREE	ΣHREE	ΣREY	Si	P	Cl	Ca	Ti	Mn	Sr	Y	Zr
1	Jt4 Ap1 - 01	49	69	475	594	900	213722	1694	390000	2.3	257	299	370	0.006
2	Jt4 Ap1 - 02	49	58	406	513	27147	209177	2615	390000	1018	286	258	317	1.0
3	Jt4 Ap1 - 03	55	81	507	643	631	215942	2066	390000	3.0	248	268	396	0.011
4	Jt4 Ap1 - 05	64	81	455	600	612	216114	2576	390000	2.1	261	187	358	0.003
5	Jt4 Ap1 - 07	52	72	441	565	636	217686	2027	390000	2.4	255	236	344	0.003
6	Jt4 Ap10 - 02	531	323	1740	2594	1343	211417	2494	390000	3.4	255	234	1351	0.087
7	Jt4 Ap10 - 03	1410	421	1965	3795	1564	212147	2580	390000	2.4	264	223	1534	0.177
8	Jt4 Ap10 - 04	191	163	1014	1368	825	223206	2094	390000	2.6	245	272	784	0.031
9	Jt4 Ap10 - 05	406	265	1494	2164	5906	209711	2551	390000	213	268	238	1155	0.136
10	Jt4 Ap10 - 06	304	170	1046	1520	735	211752	1789	390000	2.1	246	386	805	0.043
11	Jt4 Ap11 - 01	142	127	780	1049	829	214022	2229	390000	2.9	250	245	606	0.032
12	Jt4 Ap11 - 02	983	447	2341	3772	1481	212714	2707	390000	2.5	260	239	1811	0.154
13	Jt4 Ap11 - 03	143	156	1009	1309	709	210490	2158	390000	2.6	234	246	778	0.285
14	Jt4 Ap11 - 04	43	72	452	566	717	210675	2192	390000	2.9	213	197	352	0.009
15	Jt4 Ap11 - 05	97	96	564	758	624	211173	2742	390000	2.2	271	268	441	0.444
16	Jt4 Ap11 - 06	36	69	486	591	597	214093	2087	390000	2.7	234	235	378	0.005
17	Jt4 Ap11 - 07	58	88	537	683	599	215991	2186	390000	2.8	235	246	418	1.2
18	Jt4 Ap2 - 01	1257	369	1778	3404	1740	213862	2562	390000	6.4	266	244	1381	0.169
19	Jt4 Ap2 - 02	55	70	434	560	5471	212559	1645	390000	8.6	259	313	340	0.114
20	Jt4 Ap2 - 05	358	164	885	1408	863	215063	2266	390000	3.6	249	238	691	0.049
21	Jt4 Ap2 - 06	75	67	466	608	1133	216796	1774	390000	3.9	243	253	361	0.256
22	Jt4 Ap3 - 01	53	85	432	570	823	216906	2809	390000	3.5	272	168	343	0.003
23	Jt4 Ap3 - 02	48	78	414	540	712	216967	2658	390000	2.3	261	167	329	<0.000
24	Jt4 Ap3 - 03	449	351	2010	2810	1087	215857	2504	390000	2.0	248	248	1552	0.124
25	Jt4 Ap3 - 05	60	89	459	609	638	215022	2768	390000	2.8	262	186	363	0.005
26	Jt4 Ap3 - 06	75	77	540	693	839	217180	1636	390000	3.0	247	336	417	0.025
27	Jt4 Ap3 - 07	586	361	1956	2903	1413	214927	2674	390000	3.6	250	234	1513	0.102
28	Jt4 Ap4 - 01	519	376	2059	2953	1276	216630	2872	390000	3.2	256	230	1599	0.089

#	Sample Jt4	ΣLREE	ΣMREE	ΣHREE	ΣREY	Si	P	Cl	Ca	Ti	Mn	Sr	Y	Zr
29	Jt4 Ap4 - 02	482	232	1289	2003	1164	213273	1804	390000	2.5	253	268	1001	0.101
30	Jt4 Ap4 - 03	55	68	461	583	753	216999	1349	390000	2.6	266	267	358	0.008
31	Jt4 Ap4 - 04	5409	1051	3688	10147	2982	215505	3249	390000	3.5	309	172	2909	0.504
32	Jt4 Ap4 - 05	2520	722	3059	6301	2057	214165	3005	390000	5.5	282	189	2406	0.316
33	Jt4 Ap5 - 01	49	77	487	613	590	219172	2205	390000	2.6	252	257	381	0.006
34	Jt4 Ap5 - 02	60	86	504	650	727	220213	2371	390000	2.8	261	242	396	0.009
35	Jt4 Ap5 - 04	246	167	903	1317	3760	214401	2031	390000	154	255	282	703	2.4
36	Jt4 Ap5 - 05	50	75	503	629	799	216364	1506	390000	3.2	242	268	390	0.003
37	Jt4 Ap6 - 01	110	146	998	1254	912	216486	2026	390000	2.4	279	300	761	0.073
38	Jt4 Ap6 - 02	1431	573	2776	4779	1632	216453	2794	390000	2.7	270	221	2170	0.237
39	Jt4 Ap6 - 03	50	75	446	571	570	214978	2369	390000	2.3	255	241	348	0.003
40	Jt4 Ap6 - 04	210	178	1089	1477	1272	216815	2294	390000	2.7	253	264	841	0.102
41	Jt4 Ap6 - 05	72	104	697	873	713	215468	1754	390000	2.6	243	270	538	0.020
42	Jt4 Ap7 - 02	1729	552	2427	4708	1697	201086	2855	390000	4.0	264	191	1910	0.223
43	Jt4 Ap7 - 03	2017	599	2530	5146	2043	206081	2886	390000	4.0	268	236	1991	0.264
44	Jt4 Ap7 - 06	3533	948	3704	8185	2342	208732	3039	390000	3.2	297	179	2924	0.518
45	Jt4 Ap8 - 01	786	347	1790	2924	1116	213872	2675	390000	3.1	248	241	1395	0.119
46	Jt4 Ap8 - 02	110	120	698	928	653	210364	2516	390000	2.8	255	249	544	0.839
47	Jt4 Ap8 - 03	51	77	507	635	641	213974	2354	390000	2.6	256	277	395	0.037
48	Jt4 Ap8 - 05	45	66	471	582	676	211572	1680	390000	1.6	261	348	364	0.005
49	Jt4 Ap8 - 06	578	362	1940	2879	5934	153083	4036	390000	78	259	242	1517	0.330
	Mean (n=49)	566	234	1186	1986	1936	212875	2362	390000	33	258	247	925	0.222
	SD	1010	232	910	2090	3899	9445	509	0.000	149	16	45	715	0.411
	Median	110	127	780	1049	863	214401	2369	390000	2.8	256	244	606	0.095
	Max	5409	1051	3704	10147	27147	223206	4036	390000	1018	309	386	2924	2.4
	Min	36	58	406	513	570	153083	1349	390000	1.6	213	167	317	0.003

#	Sample Jt7	ΣLREE	ΣMREE	ΣHREE	ΣREY	Si	P	Cl	Ca	Ti	Mn	Sr	Y	Zr
1	Jt7 Ap1 - 01	2023	654	1897	4573	1824	215303	4093	390000	2.1	359	174	1505	0.344
2	Jt7 Ap1 - 02	4217	748	1639	6603	2070	213485	4424	390000	2.4	375	173	1317	0.466
3	Jt7 Ap1 - 04	2605	569	1137	4311	1493	214374	4343	390000	2.1	343	159	933	0.026
4	Jt7 Ap1 - 05	2541	639	1892	5073	30898	207608	4684	390000	1316	395	191	1500	0.385
5	Jt7 Ap1 - 06	3700	985	2326	7011	2428	213744	4437	390000	2.3	376	157	1856	0.358
6	Jt7 Ap1 - 07	3655	1011	1910	6577	2262	218373	4375	390000	2.4	374	158	1534	0.240
7	Jt7 Ap1 - 08	4155	1109	2025	7289	2443	213978	4421	390000	3.0	370	151	1635	0.215
8	Jt7 Ap1 - 09	5469	831	2124	8423	2185	211348	4590	390000	2.0	379	190	1698	0.390
9	Jt7 Ap1 - 10	4219	1094	2178	7491	2584	212415	4578	390000	2.6	377	154	1753	0.409
10	Jt7 Ap1 - 11	3637	885	1687	6209	2150	212661	4514	390000	2.2	363	146	1360	0.589
11	Jt7 Ap2 - 01	4755	828	2073	7656	2355	210610	4569	390000	4.7	385	175	1668	0.311
12	Jt7 Ap2 - 02	1545	368	1004	2917	1093	215208	4240	390000	2.3	352	153	808	0.054
13	Jt7 Ap2 - 03	4537	750	1844	7130	6073	209602	4582	390000	198	371	170	1483	0.247
14	Jt7 Ap2 - 04	4873	743	1735	7351	1965	210257	4446	390000	2.6	373	179	1402	0.204
15	Jt7 Ap2 - 05	88	94	331	512	838	210617	3810	390000	3.1	331	178	268	0.004
16	Jt7 Ap2 - 06	1547	616	2169	4332	1652	211482	4076	390000	3.1	342	192	1730	0.302
17	Jt7 Ap2 - 08	5859	1102	2672	9633	3264	211920	4524	390000	3.2	387	174	2135	0.907
18	Jt7 Ap2 - 09	5447	956	2335	8737	2622	209602	4836	390000	3.2	379	175	1876	0.427
19	Jt7 Ap2 - 10	5031	1032	2681	8744	2586	211377	4373	390000	2.8	376	176	2156	0.468
20	Jt7 Ap2 - 11	3816	766	1993	6575	2034	207055	4259	390000	3.6	363	171	1604	0.148
21	Jt7 Ap4 - 01	251	144	473	867	865	217187	3977	390000	1.9	334	166	382	0.010
22	Jt7 Ap4 - 02	1559	457	1411	3427	1643	212632	4171	390000	3.1	344	181	1134	0.078
23	Jt7 Ap4 - 03	5078	800	1931	7809	2252	212627	4585	390000	3.4	381	173	1554	0.321
24	Jt7 Ap4 - 04	1198	281	716	2195	1020	210437	4190	390000	3.2	333	182	582	0.086
25	Jt7 Ap4 - 05	4323	769	1954	7046	2158	212487	4552	390000	2.6	369	176	1575	0.195
26	Jt7 Ap4 - 06	5710	836	1933	8479	2230	215654	4853	390000	2.5	380	179	1557	0.246
27	Jt7 Ap4 - 07	3734	663	1754	6151	2065	214592	4489	390000	2.3	362	178	1410	0.218
28	Jt7 Ap5 - 01	1420	550	1950	3920	1661	214674	4193	390000	3.0	341	209	1546	0.275
29	Jt7 Ap5 - 02	2054	592	2019	4665	1608	215164	3970	390000	2.0	338	202	1600	0.289
30	Jt7 Ap5 - 03	1709	534	1829	4072	1979	213381	4275	390000	25	342	229	1452	0.288
31	Jt7 Ap5 - 04	3660	832	2345	6837	2227	215587	4577	390000	2.9	367	186	1868	0.478
32	Jt7 Ap5 - 05	2522	663	2081	5266	1807	213859	4456	390000	2.7	342	197	1655	0.352

#	Sample Jt7	ΣLREE	ΣMREE	ΣHREE	ΣREY	Si	P	Cl	Ca	Ti	Mn	Sr	Y	Zr
33	Jt7 Ap5 - 06	1475	501	1766	3742	7768	210201	4156	390000	310	339	198	1401	0.252
34	Jt7 Ap5 - 07	3124	711	2233	6068	2149	215685	4496	390000	2.6	355	200	1773	0.395
35	Jt7 Ap5 - 08	2652	737	2353	5742	2073	216548	4367	390000	2.3	362	196	1867	0.321
36	Jt7 Ap5 - 09	1541	469	1580	3591	1564	212058	4368	390000	2.3	346	211	1257	0.137
37	Jt7 Ap6 - 01	178	93	349	619	686	216283	4168	390000	2.2	331	246	281	0.003
38	Jt7 Ap6 - 02	3968	710	1727	6405	1990	215016	4700	390000	2.5	373	181	1391	0.163
39	Jt7 Ap6 - 03	4748	780	1781	7309	2209	213968	4718	390000	2.3	370	189	1436	0.183
40	Jt7 Ap6 - 04	3135	666	1592	5393	2162	214089	4776	390000	2.4	355	166	1273	0.377
41	Jt7 Ap6 - 05	3204	765	2397	6366	2147	214804	4766	390000	1.9	354	231	1909	0.307
42	Jt7 Ap6 - 06	2227	610	1735	4572	1802	213561	4646	390000	2.5	353	187	1388	0.162
43	Jt7 Ap6 - 07	3050	571	1334	4956	1694	213825	4672	390000	1.9	357	170	1070	0.264
44	Jt7 Ap6 - 08	1103	377	1201	2681	1093	213785	4407	390000	2.4	341	230	959	0.126
45	Jt7 Ap7 - 01	3902	832	2366	7100	2550	213324	4657	390000	2.1	366	190	1884	0.435
46	Jt7 Ap7 - 02	4979	884	2137	8000	2614	213836	5009	390000	2.6	381	179	1701	0.519
47	Jt7 Ap7 - 03	3612	699	1671	5982	1844	215110	4743	390000	3.2	368	174	1343	0.260
48	Jt7 Ap7 - 04	5227	779	1668	7673	1970	215193	4822	390000	2.8	376	177	1344	0.228
49	Jt7 Ap7 - 05	3717	696	1686	6099	1890	215950	4620	390000	2.8	363	176	1354	0.178
50	Jt7 Ap7 - 06	195	151	618	964	647	216280	3682	390000	2.3	324	246	492	0.017
51	Jt7 Ap7 - 07	3193	713	1837	5743	1830	214567	4704	390000	3.5	359	174	1471	0.263
52	Jt7 Ap7 - 08	462	246	914	1622	2664	213353	3965	390000	44	330	225	727	0.039
53	Jt7 Ap7 - 09	4105	807	2041	6952	2145	215251	4843	390000	2.6	369	175	1633	0.204
54	Jt7 Ap8 - 01	291	263	1162	1716	917	218108	4081	390000	1.6	316	264	922	0.115
55	Jt7 Ap8 - 02	64	103	472	639	771	220424	3793	390000	2.3	318	215	378	0.011
56	Jt7 Ap8 - 03	79	108	533	720	774	219699	3273	390000	2.1	316	241	423	0.003
57	Jt7 Ap8 - 04	1543	594	2073	4209	3905	220087	4572	390000	112	351	233	1650	0.229
58	Jt7 Ap8 - 05	166	147	552	865	872	222096	4140	390000	2.4	331	239	444	<0.000
59	Jt7 Ap8 - 06	141	145	597	883	765	220941	3780	390000	2.1	320	240	478	0.003
60	Jt7 Ap8 - 07	389	324	1321	2034	1229	221223	3986	390000	1.8	326	245	1049	0.142
61	Jt7 Ap8 - 08	56	83	353	493	654	219253	4167	390000	2.3	331	225	285	0.003
62	Jt7 Ap8 - 09	577	389	1692	2658	1363	218540	3969	390000	2.3	323	216	1342	0.128
63	Jt7 Ap9 - 01	88	117	527	731	1067	217656	3852	390000	5.6	305	234	420	1161
64	Jt7 Ap9 - 02	2348	639	2145	5132	1820	218179	4589	390000	2.5	350	207	1705	0.266
65	Jt7 Ap9 - 03	92	123	559	775	879	221726	3480	390000	2.6	304	220	448	0.014
66	Jt7 Ap9 - 04	511	350	1364	2224	5849	218163	4051	390000	219	330	210	1087	2.7
67	Jt7 Ap9 - 05	3386	785	2280	6451	8486	217505	4829	390000	275	368	183	1820	0.439
68	Jt7 Ap9 - 06	5259	918	2363	8539	2925	218986	5083	390000	1.7	387	178	1877	0.716
69	Jt7 Ap10 - 01	2895	686	1894	5475	1844	215475	4732	390000	1.7	351	179	1514	0.286
70	Jt7 Ap10 - 02	6282	963	2425	9670	4983	211845	4462	390000	7.3	372	196	1932	0.606
71	Jt7 Ap10 - 03	2188	718	2149	5055	1810	216568	4528	390000	1.1	342	181	1706	0.207
72	Jt7 Ap10 - 04	1580	402	1068	3050	1278	219842	4483	390000	2.7	339	177	857	0.082
73	Jt7 Ap10 - 06	2860	886	1824	5570	2041	214582	4596	390000	3.3	356	170	1468	1.0
74	Jt7 Ap10 - 07	1973	503	1229	3705	1372	218703	4369	390000	2.8	347	170	982	0.267
75	Jt7 Ap10 - 09	2351	670	1499	4520	1881	216775	4549	390000	2.6	349	163	1203	0.244
76	Jt7 Ap10 - 10	2071	531	1166	3768	1821	218683	4478	390000	2.6	348	165	933	0.284
77	Jt7 Ap11 - 04	3577	635	1711	5923	1501	218555	4642	390000	2.6	355	212	1375	0.181
78	Jt7 Ap11 - 06	2410	547	1609	4565	1679	214245	4381	390000	2.7	350	223	1284	0.104
79	Jt7 Ap11 - 07	2482	614	1887	4983	1608	212228	4318	390000	4.2	328	225	1506	0.288
80	Jt7 Ap11 - 10	1560	511	1920	3991	1650	214987	3922	390000	3.7	325	214	1521	0.240
81	Jt7 Ap11 - 11	294	173	668	1135	900	209845	3519	390000	2.8	321	236	531	0.451
82	Jt7 Ap12 - 02	7900	875	1665	10440	2770	216191	5002	390000	1.9	393	183	1349	0.508
83	Jt7 Ap12 - 03	5685	821	1838	8345	2386	214533	4808	390000	2.4	385	202	1479	0.442
84	Jt7 Ap12 - 04	3744	790	2194	6728	2083	220426	4573	390000	2.4	363	189	1754	0.508
85	Jt7 Ap12 - 05	2107	467	1271	3845	1546	216988	4347	390000	2.4	353	171	1016	0.183
86	Jt7 Ap12 - 06	3449	678	1917	6044	2106	216203	4213	390000	2.4	363	192	1530	0.368
87	Jt7 Ap12 - 07	5061	768	1788	7617	2130	211189	4629	390000	2.5	371	177	1437	0.361
88	Jt7 Ap12 - 08	7020	867	1868	9756	2704	212914	4906	390000	2.8	386	179	1500	0.492
89	Jt7 Ap13 - 01	2178	513	1717	4408	2137	217720	4227	390000	3.9	326	220	1369	0.176
90	Jt7 Ap13 - 02	1284	430	1629	3343	1526	214947	3746	390000	2.3	317	214	1291	0.208
91	Jt7 Ap13 - 03	1139	360	1295	2794	2108	214769	3971	390000	41	338	239	1033	0.137
92	Jt7 Ap13 - 04	2735	600	1897	5231	1845	215439	4353	390000	2.4	355	195	1513	0.323
93	Jt7 Ap13 - 05	2793	586	1781	5160	1613	213249	4287	390000	2.2	339	234	1421	0.338

#	Sample Jt7	ΣLREE	ΣMREE	ΣHREE	ΣREY	Si	P	Cl	Ca	Ti	Mn	Sr	Y	Zr
94	Jt7 Ap13 - 06	2028	549	1892	4469	1706	212962	4162	390000	2.3	324	219	1505	0.343
95	Jt7 Ap13 - 07	2980	577	1688	5245	1692	212168	4150	390000	2.2	342	207	1351	0.266
96	Jt7 Ap13 - 08	1970	509	1756	4235	11973	212474	4054	390000	525	352	199	1397	0.317
97	Jt7 Ap13 - 09	1342	403	1494	3238	1529	211416	3768	390000	14	314	244	1188	0.132
98	Jt7 Ap13 - 10	3702	632	1862	6196	2522	213839	4208	390000	3.7	349	204	1484	0.428
99	Jt7 Ap14 - 01	1559	456	1500	3516	1424	213928	3919	390000	2.0	349	243	1196	0.091
100	Jt7 Ap14 - 02	1544	474	1543	3561	1605	212654	3996	390000	2.6	351	244	1228	0.448
101	Jt7 Ap14 - 03	1161	430	1573	3165	1348	214674	3812	390000	1.8	340	248	1250	0.195
102	Jt7 Ap14 - 04	3116	679	1838	5632	1862	214308	4234	390000	1.9	365	213	1471	0.286
103	Jt7 Ap14 - 05	1967	488	1504	3960	1477	213369	4145	390000	2.1	350	251	1199	0.204
104	Jt7 Ap14 - 06	588	301	1163	2052	1118	214447	3721	390000	2.4	335	257	922	1.7
105	Jt7 Ap14 - 07	1581	459	1461	3501	1264	213003	4091	390000	2.4	348	231	1161	0.210
106	Jt7 Ap14 - 08	3709	719	1990	6418	1947	212045	4431	390000	1.9	364	222	1587	0.410
107	Jt7 Ap14 - 09	328	201	853	1382	932	212503	3201	390000	2.5	309	228	676	0.065
108	Jt7 Ap14 - 10	2210	518	1506	4234	1544	210988	4164	390000	2.8	350	234	1204	0.164
109	Jt7 Ap14 - 11	2506	555	1562	4622	1737	213052	4206	390000	3.1	353	238	1249	0.191
110	Jt7 Ap14 - 12	1471	486	1774	3731	1385	214219	3719	390000	2.3	333	235	1409	0.224
111	Jt7 Ap15 - 01	4766	842	2245	7853	2559	212218	4554	390000	19	377	173	1801	0.479
112	Jt7 Ap15 - 02	2792	831	2463	6086	2200	214240	4512	390000	2.2	358	181	1974	0.248
113	Jt7 Ap15 - 03	1684	516	1584	3785	1473	216754	4229	390000	2.3	352	171	1267	0.119
114	Jt7 Ap15 - 04	2760	648	1899	5307	1880	218767	4593	390000	1.8	360	177	1525	0.102
115	Jt7 Ap15 - 05	3185	660	1816	5661	2801	213807	4473	390000	32	370	170	1457	0.212
116	Jt7 Ap15 - 06	3525	617	1636	5777	2070	214221	4328	390000	2.5	356	178	1317	0.182
117	Jt7 Ap15 - 07	3115	655	1825	5594	1660	215940	4556	390000	2.7	362	174	1463	0.194
118	Jt7 Ap15 - 08	3362	684	1925	5971	1816	215424	4645	390000	2.8	367	174	1545	0.185
119	Jt7 Ap15 - 09	2640	529	1492	4661	1631	217027	4375	390000	2.2	360	180	1197	0.158
120	Jt7 Ap16 - 01	2799	666	2137	5602	2772	215462	4283	390000	17	342	192	1706	0.279
121	Jt7 Ap16 - 02	57	65	252	374	703	217579	3978	390000	2.0	332	170	205	<0.000
122	Jt7 Ap16 - 03	2900	822	2684	6406	2438	213753	4465	390000	1.9	363	185	2137	0.441
123	Jt7 Ap16 - 04	2174	752	2383	5309	2117	214370	4427	390000	2.6	360	181	1898	0.430
124	Jt7 Ap16 - 05	4496	978	2743	8216	2960	213876	4777	390000	2.1	384	170	2187	0.728
125	Jt7 Ap16 - 06	2234	548	1671	4452	1935	218225	4457	390000	2.3	356	191	1334	0.233
126	Jt7 Ap16 - 07	5766	1071	3084	9921	6160	212678	4647	390000	155	389	187	2461	0.635
127	Jt7 Ap16 - 08	2285	649	2107	5040	1859	216816	4407	390000	2.7	358	202	1673	0.341
128	Jt7 Ap17 - 01	4074	795	2204	7073	2131	212907	4370	390000	1.4	356	197	1753	0.365
129	Jt7 Ap17 - 02	697	329	990	2015	1390	213633	3777	390000	16	330	187	789	0.176
130	Jt7 Ap17 - 03	4015	675	1837	6527	2021	217935	4485	390000	2.8	368	192	1473	0.310
131	Jt7 Ap17 - 04	691	261	821	1773	1141	213206	3799	390000	2.8	329	194	658	0.038
132	Jt7 Ap17 - 05	3493	651	1753	5897	4071	212422	4406	390000	104	360	186	1402	0.317
133	Jt7 Ap17 - 06	4449	728	1840	7017	1980	216157	4502	390000	2.6	365	191	1478	0.252
134	Jt7 Ap17 - 07	1606	365	1070	3041	4192	212539	4080	390000	138	339	190	859	0.178
135	Jt7 Ap17 - 09	4395	945	2691	8030	2931	215418	4418	390000	2.7	371	188	2132	0.604
136	Jt7 Ap17 - 10	3067	883	2317	6267	2683	217779	4472	390000	37	359	185	1844	0.281
137	Jt7 Ap17 - 11	3067	785	2419	6271	2344	213850	4348	390000	2.4	358	190	1922	0.524
138	Jt7 Ap17 - 12	2677	702	1781	5159	2119	213528	4426	390000	2.9	357	176	1418	0.584
139	Jt7 Ap17 - 13	3723	642	1655	6020	4050	213336	4344	390000	99	359	196	1323	0.192
140	Jt7 Ap17 - 14	5607	976	2486	9070	3650	217484	4685	390000	4.3	381	182	1981	0.915
141	Jt7 Ap17 - 15	5315	918	2535	8768	2699	219222	4394	390000	2.2	378	180	2018	0.456
142	Jt7 Ap17 - 16	2879	685	1876	5439	1781	211864	3958	390000	2.6	345	181	1498	0.226
143	Jt7 Ap17 - 18	2755	792	2180	5726	3783	214339	3795	390000	71	347	182	1737	0.504
144	Jt7 Ap17 - 21	4238	734	1725	6696	1956	215838	4309	390000	2.0	358	174	1390	0.086
145	Jt7 Ap17 - 22	78	75	287	440	609	213832	3776	390000	1.3	329	208	232	0.005
146	Jt7 Ap17 - 23	6120	765	1592	8477	2751	216321	4557	390000	2.0	371	190	1283	0.346
147	Jt7 Ap17 - 24	4568	697	1726	6991	2316	215037	4407	390000	2.5	369	180	1382	0.218
148	Jt7 Ap17 - 25	3651	889	2615	7155	2572	213237	4236	390000	279	362	191	2092	0.497
149	Jt7 Ap17 - 26	6024	747	1642	8413	2255	213609	4434	390000	2.7	373	179	1322	0.317
150	Jt7 Ap17 - 27	3610	668	1866	6144	2058	215957	4301	390000	2.3	366	186	1497	0.225
151	Jt7 Ap17 - 28	2913	637	1810	5360	1630	214943	4091	390000	3.1	354	193	1448	0.137
152	Jt7 Ap17 - 29	3238	755	2198	6191	2260	215481	3919	390000	3.7	352	188	1752	0.296
153	Jt7 Ap17 - 30	3583	686	1998	6266	2012	218417	4177	390000	1.8	356	193	1592	0.371
154	Jt7 Ap17 - 31	1602	453	1053	3108	1925	216624	2898	390000	4.6	321	249	840	0.049

#	Sample Jt7	ΣLREE	ΣMREE	ΣHREE	ΣREY	Si	P	Cl	Ca	Ti	Mn	Sr	Y	Zr
155	Jt7 Ap17 - 32	105	85	272	462	697	216256	3727	390000	1.9	325	168	221	0.012
156	Jt7 Ap17 - 33	1127	417	1588	3133	1430	217112	3695	390000	0.917	327	236	1261	0.202
157	Jt7 Ap17 - 34	4516	786	1814	7117	2246	216218	4530	390000	2.9	374	171	1464	0.165
	Mean (n=157)	2812	611	1697	5120	2352	214836	4308	390000	28	353	196	1357	7.8
	SD	1691	246	576	2364	2682	2756	364	0.000	122	20	26	459	93
	Median	2793	654	1781	5360	1965	214567	4373	390000	2.6	355	189	1421	0.252
	Max	7900	1109	3084	10440	30898	222096	5083	390000	1316	395	264	2461	1161
	Min	56	65	252	374	609	207055	2898	390000	0.917	304	146	205	0.003

#	Sample Jt10	ΣLREE	ΣMREE	ΣHREE	ΣREY	Si	P	Cl	Ca	Ti	Mn	Sr	Y	Zr
1	Jt10 Ap1 - 01	102	215	714	1032	729	219345	2330	390000	1.5	208	148	592	0.009
2	Jt10 Ap1 - 02	99	186	605	890	710	221866	2787	390000	2.2	213	155	503	0.003
3	Jt10 Ap1 - 03	158	263	864	1285	766	217797	3072	390000	2.2	211	159	716	0.003
4	Jt10 Ap1 - 04	121	204	659	984	730	218574	2826	390000	1.9	220	159	547	0.009
5	Jt10 Ap1 - 05	96	174	553	823	2426	215937	2531	390000	1.8	223	159	461	0.015
6	Jt10 Ap1 - 06	118	215	727	1060	887	220180	3055	390000	2.2	224	157	603	0.012
7	Jt10 Ap1 - 07	309	473	1604	2386	1094	219988	3576	390000	2.4	211	154	1320	0.012
8	Jt10 Ap1 - 08	128	234	673	1035	1497	213454	2572	390000	2.0	218	155	561	<0.000
9	Jt10 Ap1 - 09	136	256	862	1254	970	218440	3054	390000	1.5	220	172	713	0.021
10	Jt10 Ap1 - 10	121	186	543	849	769	220423	2481	390000	2.5	246	200	453	0.012
11	Jt10 Ap1 - 11	88	172	570	830	795	220972	2808	390000	2.7	208	148	475	0.015
12	Jt10 Ap1 - 12	294	525	1904	2722	1123	220960	3270	390000	2.0	212	137	1559	0.096
13	Jt10 Ap1 - 13	113	225	773	1111	836	216150	2728	390000	3.2	204	151	640	0.021
14	Jt10 Ap1 - 14	143	243	745	1131	6448	214967	2934	390000	2.6	210	169	619	0.028
15	Jt10 Ap1 - 15	104	180	625	909	531	212059	3082	390000	1.6	194	145	519	0.473
16	Jt10 Ap1 - 16	98	162	462	723	638	217251	2672	390000	2.7	194	132	386	0.033
17	Jt10 Ap2 - 01	110	225	780	1115	798	214263	3204	390000	1.7	206	141	645	0.008
18	Jt10 Ap2 - 02	117	229	787	1133	670	216263	3222	390000	1.8	232	156	653	0.006
19	Jt10 Ap2 - 03	133	263	898	1294	842	216209	3128	390000	1.6	223	161	743	0.012
20	Jt10 Ap2 - 04	111	176	528	814	679	224673	2919	390000	1.9	228	196	440	0.012
21	Jt10 Ap2 - 05	104	205	686	995	774	217188	2669	390000	2.4	196	141	569	0.006
22	Jt10 Ap2 - 06	106	204	712	1021	777	217517	3150	390000	2.3	207	141	589	0.012
23	Jt10 Ap2 - 07	91	183	624	898	820	216653	2790	390000	2.5	208	144	518	0.017
24	Jt10 Ap2 - 08	171	312	1063	1546	1799	210256	2854	390000	6.3	184	137	874	0.036
25	Jt10 Ap2 - 09	249	448	1563	2259	1337	216142	3482	390000	1.9	208	136	1285	0.051
26	Jt10 Ap2 - 10	97	186	602	886	783	218687	2824	390000	1.9	230	164	500	0.009
27	Jt10 Ap2 - 11	100	168	507	775	679	217228	2823	390000	2.5	221	184	422	0.013
28	Jt10 Ap3 - 01	137	222	532	892	5363	216627	2043	390000	4.0	186	139	442	0.023
29	Jt10 Ap3 - 02	164	242	809	1215	1831	217661	3404	390000	2.1	206	116	668	0.022
30	Jt10 Ap3 - 03	105	196	646	947	670	218672	2656	390000	1.9	223	135	536	0.003
31	Jt10 Ap3 - 04	101	204	668	973	706	217382	2661	390000	2.7	214	141	552	<0.000
32	Jt10 Ap3 - 05	91	180	597	868	483	214475	2581	390000	1.7	214	138	495	<0.000
33	Jt10 Ap3 - 06	100	189	637	926	703	217278	2672	390000	2.2	211	138	528	<0.000
34	Jt10 Ap3 - 07	121	199	639	959	703	215258	2659	390000	1.6	203	136	531	0.015
35	Jt10 Ap3 - 08	129	227	748	1104	389	219034	3075	390000	2.7	218	148	620	0.008
36	Jt10 Ap3 - 09	121	210	691	1022	423	216168	3036	390000	2.3	208	143	573	<0.000
37	Jt10 Ap3 - 10	112	204	590	905	505	216837	2271	390000	2.3	220	149	489	0.012
38	Jt10 Ap3 - 11	148	215	675	1038	572	214512	2336	390000	2.3	221	157	560	0.021
39	Jt10 Ap3 - 12	118	202	665	984	1035	213534	2585	390000	2.5	204	140	552	0.103
40	Jt10 Ap3 - 14	117	182	470	769	658	217351	2207	390000	1.7	213	167	391	0.832
41	Jt10 Ap3 - 15	142	241	753	1136	599	217143	2528	390000	1.5	196	143	623	<0.000
42	Jt10 Ap4 - 01	118	239	798	1155	818	218654	2631	390000	1.2	215	152	659	0.022
43	Jt10 Ap4 - 02	139	260	875	1274	7260	213589	2402	390000	4.0	328	158	719	0.179
44	Jt10 Ap4 - 03	125	252	869	1246	789	214125	2845	390000	2.3	225	143	717	0.009
45	Jt10 Ap4 - 04	164	269	931	1364	851	216584	3365	390000	2.7	200	148	768	0.030
46	Jt10 Ap4 - 05	118	210	662	990	643	215110	2744	390000	2.1	194	149	549	0.006
47	Jt10 Ap4 - 06	136	227	709	1072	596	214890	2279	390000	1.6	220	170	587	0.011
48	Jt10 Ap4 - 07	88	155	360	603	500	212447	2299	390000	1.9	207	175	303	0.015
49	Jt10 Ap4 - 08	103	195	673	970	798	213757	2906	390000	2.1	207	141	557	0.003
50	Jt10 Ap4 - 09	109	184	584	877	722	210892	2794	390000	1.5	219	171	485	<0.000

#	Sample Jt10	ΣLREE	ΣMREE	ΣHREE	ΣREY	Si	P	Cl	Ca	Ti	Mn	Sr	Y	Zr
51	Jt10 Ap4 - 10	111	190	645	946	895	213379	2750	390000	2.7	201	126	534	0.044
52	Jt10 Ap4 - 11	125	246	845	1216	668	214028	2958	390000	2.0	200	138	698	<0.000
53	Jt10 Ap4 - 12	102	202	650	953	708	214480	2438	390000	1.7	216	136	538	0.006
54	Jt10 Ap4 - 13	141	251	788	1180	625	215520	2473	390000	2.1	209	158	653	0.019
55	Jt10 Ap4 - 14	193	354	1239	1786	910	217104	3057	390000	2.1	208	137	1019	0.040
56	Jt10 Ap5 - 01	134	258	905	1296	753	215015	2753	390000	2.5	200	140	747	0.014
57	Jt10 Ap5 - 02	163	275	951	1389	783	215322	3161	390000	2.8	200	136	786	0.009
58	Jt10 Ap5 - 03	122	248	889	1260	834	217762	2867	390000	2.5	211	135	733	0.006
59	Jt10 Ap5 - 04	112	242	863	1218	805	215653	2694	390000	2.3	214	137	711	0.027
60	Jt10 Ap5 - 05	94	197	694	985	624	216797	2484	390000	1.7	204	135	574	0.013
61	Jt10 Ap5 - 06	226	379	1329	1933	880	215064	2856	390000	2.8	201	135	1090	0.054
62	Jt10 Ap5 - 07	118	254	923	1295	756	216807	2559	390000	2.7	211	132	762	0.049
63	Jt10 Ap5 - 08	96	200	708	1005	743	215334	2506	390000	1.9	198	133	586	0.012
64	Jt10 Ap5 - 09	166	306	1081	1552	864	218489	2855	390000	2.7	202	134	891	0.033
65	Jt10 Ap5 - 10	134	253	913	1300	886	215381	2618	390000	2.1	195	134	754	0.003
66	Jt10 Ap5 - 11	96	193	681	971	690	217351	2319	390000	1.7	198	137	564	0.003
67	Jt10 Ap5 - 12	103	189	550	843	825	218593	1662	390000	2.1	215	176	461	0.729
68	Jt10 Ap5 - 13	93	205	747	1044	613	216505	2172	390000	1.9	206	133	617	0.009
69	Jt10 Ap5 - 15	94	205	689	989	761	217667	1946	390000	1.7	198	136	572	<0.000
70	Jt10 Ap5 - 16	121	211	725	1057	962	199277	2122	390000	5.8	211	130	600	0.052
71	Jt10 Ap5 - 17	134	216	716	1066	609	217376	2059	390000	1.9	195	125	593	0.014
72	Jt10 Ap6 - 01	142	269	914	1325	693	216669	1984	390000	2.2	204	139	752	0.009
73	Jt10 Ap6 - 02	155	284	978	1416	727	217933	2156	390000	1.6	204	148	806	0.026
74	Jt10 Ap6 - 03	103	201	620	924	868	215377	1481	390000	2.4	187	154	514	0.027
75	Jt10 Ap6 - 05	237	382	514	1133	31456	210164	503	390000	3.8	412	135	434	0.077
76	Jt10 Ap6 - 06	381	697	1069	2147	1959	213468	396	390000	2.2	61	129	906	<0.000
77	Jt10 Ap6 - 07	92	260	461	814	2243	215699	568	390000	3.0	47	160	388	0.009
78	Jt10 Ap6 - 08	203	332	416	952	2401	215936	632	390000	2.6	52	166	351	<0.000
79	Jt10 Ap6 - 09	224	346	1124	1694	709	214676	1814	390000	2.1	189	132	926	0.010
80	Jt10 Ap6 - 10	181	311	800	1292	1142	216830	1341	390000	1.8	139	150	662	0.010
81	Jt10 Ap6 - 11	504	667	2073	3244	2011	213319	1779	390000	1.8	180	129	1700	0.045
82	Jt10 Ap6 - 12	386	751	1013	2150	795	216667	532	390000	2.6	49	131	866	0.009
83	Jt10 Ap6 - 14	216	377	1294	1887	818	217576	1963	390000	1.8	197	135	1062	<0.000
84	Jt10 Ap7 - 01	114	181	538	833	641	216485	1524	390000	2.2	188	164	447	0.006
85	Jt10 Ap7 - 02	248	316	492	1056	618	217440	838	390000	2.5	116	131	413	0.003
86	Jt10 Ap7 - 03	156	286	704	1146	5585	217231	732	390000	2.3	91	184	586	0.038
87	Jt10 Ap7 - 04	166	275	766	1206	504	218712	1572	390000	1.7	173	143	637	0.009
88	Jt10 Ap7 - 05	135	295	711	1140	4064	216855	466	390000	2.6	76	162	590	0.059
89	Jt10 Ap7 - 06	149	271	620	1041	3033	217675	682	390000	2.9	58	200	513	0.017
90	Jt10 Ap7 - 07	153	375	1286	1815	2186	216516	703	390000	4.0	53	200	1061	0.014
91	Jt10 Ap7 - 08	84	201	378	663	2753	219923	782	390000	2.9	65	179	317	0.017
92	Jt10 Ap7 - 09	118	282	625	1025	7320	212840	619	390000	3.4	31	195	529	0.030
93	Jt10 Ap7 - 10	240	484	1159	1883	1306	218008	529	390000	3.8	57	188	965	0.021
94	Jt10 Ap7 - 11	172	305	670	1147	736	216868	615	390000	2.3	70	223	553	0.015
95	Jt10 Ap7 - 12	525	432	586	1543	2173	215109	585	390000	2.4	59	153	490	0.045
96	Jt10 Ap7 - 13	177	261	614	1052	1817	214790	534	390000	1.7	50	178	508	0.014
97	Jt10 Ap7 - 14	352	444	616	1413	1002	217908	573	390000	2.5	75	156	515	0.010
98	Jt10 Ap7 - 15	141	287	871	1298	726	218589	588	390000	2.4	80	151	721	0.037
99	Jt10 Ap7 - 16	261	567	935	1763	735	215945	535	390000	1.9	48	113	794	0.012
100	Jt10 Ap7 - 17	129	211	454	793	2183	217665	1047	390000	1.8	230	286	379	0.014
101	Jt10 Ap7 - 18	449	619	793	1860	5825	215236	554	390000	2.4	123	172	670	0.046
102	Jt10 Ap7 - 19	404	638	915	1957	4858	215739	481	390000	3.2	95	163	773	0.044
103	Jt10 Ap7 - 20	201	337	694	1232	1036	221153	682	390000	6.2	133	208	579	0.017
104	Jt10 Ap8 - 01	183	208	657	1047	667	220145	2988	390000	2.1	194	122	545	0.003
105	Jt10 Ap8 - 02	186	208	649	1043	583	223894	3059	390000	2.1	202	119	539	0.005
106	Jt10 Ap8 - 03	248	324	1076	1648	561	215023	2548	390000	2.5	189	125	886	0.054
107	Jt10 Ap8 - 04	1455	1233	4195	6883	2153	217411	3314	390000	1.8	213	129	3438	0.370
108	Jt10 Ap8 - 05	5636	1744	5109	12489	3067	216912	3597	390000	1.5	227	112	4211	0.580
109	Jt10 Ap8 - 06	2344	1528	4970	8842	2572	218520	3982	390000	1.5	220	126	4075	0.500
110	Jt10 Ap8 - 07	267	461	1577	2305	944	217321	3080	390000	2.2	197	135	1293	0.076
111	Jt10 Ap8 - 08	623	773	2592	3988	1580	216526	3631	390000	1.7	204	129	2132	0.133

#	Sample Jt10	ΣLREE	ΣMREE	ΣHREE	ΣREY	Si	P	Cl	Ca	Ti	Mn	Sr	Y	Zr
112	Jt10 Ap8 - 10	582	668	2122	3373	2528	218407	2619	390000	2.2	216	147	1738	0.262
113	Jt10 Ap8 - 11	663	860	2968	4491	1602	217204	3729	390000	1.6	217	131	2430	0.132
114	Jt10 Ap8 - 12	357	646	2221	3223	4562	217035	2979	390000	2.5	215	142	1816	0.099
115	Jt10 Ap8 - 13	2456	555	1770	4780	1666	221715	3637	390000	4.3	211	156	1454	0.128
116	Jt10 Ap8 - 14	1770	1513	4971	8254	2488	218631	3965	390000	2.1	204	126	4092	0.207
117	Jt10 Ap8 - 15	533	464	1464	2461	794	215514	3625	390000	<0.990	198	122	1206	0.043
118	Jt10 Ap8 - 16	1384	969	3241	5594	2092	232683	3994	390000	2.6	214	135	2662	0.150
119	Jt10 Ap8 - 17	534	745	2566	3844	1237	212743	3636	390000	3.3	202	124	2103	0.166
120	Jt10 Ap8 - 18	2536	1639	5294	9468	2716	220557	4292	390000	1.4	225	128	4341	0.352
121	Jt10 Ap8 - 19	706	921	3126	4754	1398	212431	3877	390000	2.3	201	124	2566	0.211
122	Jt10 Ap8 - 20	828	939	3060	4827	1854	218054	3907	390000	2.9	206	126	2515	0.132
123	Jt10 Ap9 - 01	3419	2062	6812	12293	4812	215207	4131	390000	6.1	233	120	5594	0.760
124	Jt10 Ap9 - 02	2399	1651	5510	9560	3192	216312	3915	390000	2.2	215	116	4523	0.378
125	Jt10 Ap9 - 03	939	1136	3921	5996	2721	211828	3487	390000	3.8	210	122	3219	0.396
126	Jt10 Ap9 - 04	801	975	3328	5104	2168	216571	3420	390000	3.2	199	120	2734	0.213
127	Jt10 Ap9 - 05	390	752	2758	3900	1369	218689	3334	390000	2.1	204	121	2253	0.106
128	Jt10 Ap9 - 06	519	655	2220	3394	1281	216814	3716	390000	1.3	198	119	1814	0.115
129	Jt10 Ap9 - 07	843	1005	3457	5305	1818	214773	3787	390000	3.1	200	122	2837	0.299
130	Jt10 Ap9 - 08	3092	1944	6451	11487	2921	214420	4018	390000	1.2	222	119	5296	0.456
131	Jt10 Ap9 - 09	2105	1661	5460	9226	2996	211694	3944	390000	2.6	212	118	4476	0.363
132	Jt10 Ap9 - 10	1300	1343	4676	7319	2338	215982	3622	390000	2.0	208	120	3831	0.296
133	Jt10 Ap9 - 11	262	511	1812	2585	4104	213226	3064	390000	1.3	192	120	1482	0.375
134	Jt10 Ap10 - 01	151	270	913	1335	782	217430	3151	390000	2.1	203	131	754	0.021
135	Jt10 Ap10 - 02	317	386	1304	2007	1334	221142	3247	390000	3.7	193	124	1084	0.603
136	Jt10 Ap10 - 03	130	184	590	904	665	221377	3539	390000	2.2	194	121	491	<0.000
137	Jt10 Ap10 - 04	819	971	3309	5098	1505	220631	3909	390000	2.0	207	127	2708	0.207
138	Jt10 Ap10 - 05	209	355	1205	1769	1338	217327	3468	390000	1.5	194	133	992	0.030
139	Jt10 Ap10 - 06	256	436	1461	2153	1403	223414	3691	390000	2.3	204	132	1195	0.039
140	Jt10 Ap10 - 07	413	667	2262	3343	1298	221153	3613	390000	2.2	208	130	1846	0.078
141	Jt10 Ap10 - 08	893	1147	3922	5962	2011	216052	3895	390000	4.2	211	135	3209	0.191
142	Jt10 Ap10 - 09	215	354	1201	1771	839	219459	3013	390000	1.8	195	129	986	0.061
143	Jt10 Ap10 - 10	288	538	1861	2687	1057	219906	3414	390000	2.4	205	136	1520	0.087
144	Jt10 Ap10 - 11	329	537	1823	2690	984	218792	3407	390000	2.8	195	126	1492	0.121
145	Jt10 Ap10 - 12	310	466	1551	2327	1021	218037	3746	390000	1.7	198	125	1275	0.027
146	Jt10 Ap10 - 13	100	161	458	719	698	219633	2262	390000	42	203	188	381	0.006
147	Jt10 Ap10 - 14	581	426	1197	2204	3048	218632	3176	390000	2.1	185	116	991	0.058
148	Jt10 Ap10 - 15	3073	1490	4675	9238	2649	218755	4285	390000	2.5	217	114	3847	0.306
149	Jt10 Ap10 - 16	136	240	803	1179	840	214160	2746	390000	3.7	200	137	663	0.028
150	Jt10 Ap10 - 17	195	290	948	1432	2044	212049	2975	390000	1.8	195	131	782	0.014
151	Jt10 Ap12 - 04	206	316	1048	1570	692	210661	3446	390000	3.4	198	132	867	0.047
152	Jt10 Ap12 - 14	2265	1773	5779	9817	2583	218325	4116	390000	2.5	226	124	4732	0.489
153	Jt10 Ap13 - 01	395	433	1302	2129	768	222944	2580	390000	2.9	196	155	1070	0.056
154	Jt10 Ap13 - 02	262	411	1331	2004	1659	218577	3342	390000	2.4	198	138	1092	0.084
155	Jt10 Ap13 - 03	156	231	705	1092	778	223702	2991	390000	3.1	206	159	583	0.013
156	Jt10 Ap13 - 04	1117	894	2965	4976	1522	220885	3912	390000	1.4	209	131	2438	0.210
157	Jt10 Ap13 - 05	633	1002	3418	5053	2384	215892	3868	390000	1.5	201	129	2798	0.224
158	Jt10 Ap13 - 06	117	209	353	679	724	221557	1378	390000	1.3	188	227	297	0.004
159	Jt10 Ap13 - 07	686	838	2791	4315	6194	218019	3509	390000	9.7	275	139	2299	0.380
160	Jt10 Ap13 - 08	382	525	1762	2670	906	216482	3408	390000	2.5	210	125	1443	0.274
161	Jt10 Ap13 - 09	606	881	2916	4402	1685	225496	3706	390000	1.3	213	147	2388	0.179
162	Jt10 Ap13 - 10	472	716	2340	3529	1578	225963	3891	390000	1.7	223	151	1912	0.121
163	Jt10 Ap13 - 11	797	1106	3768	5671	1905	222067	3908	390000	2.7	211	127	3083	0.280
164	Jt10 Ap14 - 02	920	854	2687	4461	1271	217754	3627	390000	16	210	127	2212	0.640
165	Jt10 Ap14 - 07	644	672	2118	3434	1238	214208	3577	390000	1.3	207	144	1733	1.2
166	Jt10 Ap14 - 08	7111	2374	6775	16260	4285	214707	4181	390000	1.6	235	110	5572	0.463
	Mean (n=166)	487	486	1518	2491	1736	217017	2667	390000	2.7	192	145	1250	0.118
	SD	897	432	1423	2647	2689	3412	1030	0.000	3.4	52	24	1166	0.186
	Median	165	285	870	1295	908	216890	2835	390000	2.2	204	138	718	0.030
	Max	7111	2374	6812	16260	31456	232683	4292	390000	42	412	286	5594	1.2
	Min	84	155	353	603	389	199277	396	390000	1.2	31	110	297	0.003

*(Continued)

#	Sample Jt1	La	Ce	Pr	Nd	Sm	Eu	Gd	Tb	Dy	Ho	Er	Tm	Yb	Lu	Hf	^{204}Pb	^{206}Pb	^{207}Pb	^{208}Pb	Th	U
1	Jt1 Ap1 - 01	947	2409	306	1345	285	29	319	43	262	51	136	16	97	13	0.028	<1.399	28	4.3	21	115	20
2	Jt1 Ap1 - 02	1522	3667	446	1936	396	41	416	57	338	65	178	21	125	17	0.039	<1.583	48	7.3	19	104	35
3	Jt1 Ap1 - 03	1121	2692	324	1407	290	30	323	44	268	53	142	17	101	14	0.047	<1.744	33	5.2	28	150	23
4	Jt1 Ap1 - 04	568	1408	191	938	269	42	368	57	368	74	203	26	155	22	0.022	<1.245	33	5.0	17	93	24
5	Jt1 Ap1 - 05	585	1356	174	823	218	32	285	44	282	56	154	19	118	17	0.032	<1.328	27	4.1	14	79	20
6	Jt1 Ap1 - 06	1172	2951	373	1677	385	48	451	65	407	79	217	27	161	23	0.019	<1.335	55	8.1	17	95	40
7	Jt1 Ap1 - 07	1734	4139	503	2138	434	47	456	63	370	72	199	24	141	19	0.057	<1.538	63	9.9	20	108	44
8	Jt1 Ap2 - 01	19	66	12	80	39	9.1	80	15	98	20	53	6.3	34	4.9	0.004	<1.296	4.9	0.730	1.3	7.4	3.6
9	Jt1 Ap2 - 02	77	239	42	261	117	23	205	36	238	49	134	17	97	14	0.019	<1.247	21	3.0	6.8	38	16
10	Jt1 Ap2 - 03	461	1141	155	771	245	41	358	59	384	78	218	27	166	23	0.033	<1.174	33	4.7	10	57	25
11	Jt1 Ap2 - 04	218	630	95	502	153	23	220	34	217	44	118	14	85	12	0.038	<1.071	10	1.6	5.5	28	7.3
12	Jt1 Ap2 - 05	544	1254	159	741	205	31	281	46	291	59	162	20	118	17	0.035	<1.181	27	3.9	12	69	20
13	Jt1 Ap2 - 06	728	1707	217	1013	266	37	347	53	341	68	189	23	139	20	0.041	<1.169	35	5.0	19	104	25
14	Jt1 Ap2 - 07	670	1714	228	1095	296	44	395	62	399	80	221	27	164	23	0.047	<1.261	45	6.4	13	76	34
15	Jt1 Ap2 - 08	1261	2948	353	1516	346	46	416	62	398	80	222	28	167	24	0.051	<1.481	54	8.5	18	95	38
16	Jt1 Ap3 - 01	1099	2656	331	1466	353	48	438	66	417	84	232	29	175	25	0.057	<1.120	55	7.8	16	90	40
17	Jt1 Ap3 - 02	1307	3168	383	1660	357	41	404	58	358	71	195	24	141	20	0.035	<1.050	53	7.8	17	91	38
18	Jt1 Ap3 - 03	1148	2758	335	1459	315	38	356	52	320	63	170	21	125	17	0.026	<1.206	54	8.0	16	81	37
19	Jt1 Ap3 - 04	1085	2593	312	1346	290	34	319	45	277	54	148	19	111	15	0.029	<1.192	46	7.5	14	71	30
20	Jt1 Ap3 - 05	22	67	11	67	30	5.8	53	9.4	61	12	32	3.6	20	3.0	0.010	<1.140	2.1	0.339	0.666	3.1	1.5
21	Jt1 Ap3 - 06	642	1038	109	450	104	29	160	26	175	36	96	11	66	9.2	0.022	<1.161	11	1.7	5.1	29	8.9
22	Jt1 Ap3 - 07	30	84	14	79	33	6.4	63	11	78	16	44	4.9	28	3.9	0.007	<1.374	4.7	0.994	1.7	6.8	2.6
23	Jt1 Ap4 - 01	105	248	32	150	40	6.5	54	8.1	51	10	28	3.4	20	2.7	0.004	<1.198	3.9	0.766	1.1	4.5	2.4
24	Jt1 Ap4 - 02	841	1906	223	958	213	27	253	37	231	46	126	15	92	13	0.015	<1.330	26	4.1	9.0	48	18
25	Jt1 Ap4 - 03	2182	4980	574	2334	447	49	465	64	384	75	204	25	148	20	0.042	<1.345	74	12	23	115	49
26	Jt1 Ap4 - 04	1701	3934	461	1920	388	44	422	60	361	71	196	24	141	20	0.061	<1.208	60	9.6	21	105	41
27	Jt1 Ap4 - 05	1045	2414	277	1166	236	28	264	37	226	44	121	15	88	12	0.022	<1.098	30	4.8	8.7	45	19
28	Jt1 Ap4 - 06	13	45	7.7	44	17	3.2	27	4.4	28	5.9	16	1.8	9.5	1.4	<0.000	<1.080	0.398	0.101	0.059	0.017	0.227
29	Jt1 Ap4 - 07	13	48	8.6	49	18	3.6	30	4.7	30	6.1	16	1.8	9.8	1.5	0.003	<1.150	0.480	0.106	0.033	0.026	0.246
30	Jt1 Ap5 - 01	382	957	129	622	168	25	227	36	229	46	126	16	94	13	0.048	<1.277	23	3.4	5.8	33	17
31	Jt1 Ap5 - 02	359	970	139	693	197	29	253	39	245	49	137	17	102	15	0.028	<1.195	27	4.1	6.2	32	19
32	Jt1 Ap5 - 03	454	1140	151	725	198	30	271	43	284	56	156	19	114	16	0.013	<1.412	26	3.8	6.4	34	19
33	Jt1 Ap5 - 04	1166	2827	347	1524	341	43	400	60	369	73	202	25	151	21	0.040	<1.162	48	7.3	12	64	34
34	Jt1 Ap5 - 05	795	2024	263	1222	319	45	413	65	415	84	233	29	176	25	0.079	<1.061	46	6.6	11	59	34
35	Jt1 Ap5 - 06	473	1213	166	805	234	37	330	54	355	72	201	25	149	21	0.061	<1.148	32	4.6	7.8	42	23
36	Jt1 Ap5 - 07	941	2462	307	1358	285	30	307	43	256	50	134	17	97	13	0.026	<1.212	37	6.0	9.5	49	25
37	Jt1 Ap5 - 08	1057	2582	322	1401	304	35	338	49	304	60	163	20	122	17	0.042	<1.170	40	6.1	9.8	51	28
38	Jt1 Ap6 - 01	2462	5663	665	2696	474	41	446	56	310	58	152	18	97	13	0.035	<1.023	62	10	22	112	40
39	Jt1 Ap6 - 02	1976	4626	555	2338	446	44	450	59	343	65	175	21	122	17	0.036	<1.170	59	9.6	21	106	39
40	Jt1 Ap6 - 03	2546	5764	673	2721	478	41	451	56	316	59	155	18	101	13	0.036	<1.245	63	10	22	115	41
41	Jt1 Ap6 - 04	9.9	35	6.3	36	15	3.1	27	4.7	32	6.5	17	2.0	10	1.5	0.003	<1.119	0.439	0.110	0.081	0.099	0.245
42	Jt1 Ap6 - 05	12	42	7.6	43	17	3.2	27	4.6	29	5.9	16	1.8	9.4	1.4	0.013	<1.109	0.498	0.145	0.072	0.031	0.282
43	Jt1 Ap6 - 06	14	49	7.9	44	15	2.8	25	4.3	28	6.0	16	1.7	9.8	1.4	0.023	<1.016	0.475	0.149	0.064	0.050	0.249
44	Jt1 Ap6 - 07	17	58	9.9	53	18	3.2	30	4.9	32	6.5	18	1.9	10	1.5	0.003	<1.058	0.546	0.141	0.164	0.632	0.270
45	Jt1 Ap6 - 08	1785	4175	490	2033	397	43	418	57	340	66	181	22	129	17	0.027	<1.062	59	9.6	18	95	40
46	Jt1 Ap7 - 01	8.0	29	5.2	32	14	3.4	28	4.8	33	7.2	19	2.2	12	1.7	<0.000	<1.027	0.429	0.093	0.033	0.033	0.227
47	Jt1 Ap7 - 02	9.7	36	6.7	38	16	3.3	26	4.3	28	6.1	16	1.8	10.0	1.4	0.003	<1.008	0.522	0.119	0.052	0.096	0.283
48	Jt1 Ap7 - 03	7.5	28	5.1	31	13	2.8	26	4.5	30	6.6	18	2.1	11	1.7	0.006	<1.127	0.475	0.106	0.036	0.024	0.239
49	Jt1 Ap7 - 04	7.3	25	4.5	27	11	2.7	22	3.9	29	6.3	17	1.9	11	1.6	0.003	<1.094	0.424	0.104	0.022	0.022	0.220
50	Jt1 Ap7 - 05	11	40	7.1	41	16	3.4	27	4.4	30	6.0	16	1.8	9.4	1.3	<0.000	<1.141	0.413	0.094	0.045	0.043	0.224
51	Jt1 Ap8 - 01	726	1738	218	987	263	41	340	54	351	71	199	25	151	22	0.041	<1.167	39	6.1	9.2	48	27
52	Jt1 Ap8 - 02	261	611	76	334	85	14	116	19	119	24	64	7.6	47	6.6	0.006	<1.373	12	1.9	2.7	14	8.5
53	Jt1 Ap8 - 03	142	361	51	265	93	18	160	28	190	39	106	13	74	10	0.026	<1.247	15	2.2	3.4	19	12
54	Jt1 Ap8 - 04	315	806	110	545	172	29	269	46	300	61	165	20	118	17	0.026	<1.215	29	3.9	7.8	45	22
55	Jt1 Ap8 - 05	1049	2517	307	1365	333	47	417	64	410	83	229	29	171	24	0.044	<1.094	52	7.6	16	86	38
56	Jt1 Ap9 - 01	10	36	6.5	39	18	3.7	32	5.3	34	7.0	18	2.0	11	1.6	0.003	<1.189	0.530	0.143	0.059	0.042	0.335
57	Jt1 Ap9 - 02	10.0	37	6.6	43	19	4.1	34	5.5	36	7.1	19	2.1	11	1.6	<0.000	<1.429	0.579	0.139	0.088	0.027	0.335
58	Jt1 Ap9 - 03	8.5	32	6.3	39	17	3.9	33	5.4	35	7.1	18	2.1	12	1.5	<0.000	<1.287	0.539	0.128	0.073	0.048	0.288
59	Jt1 Ap9 - 04	12	40	7.1	43	19	4.3	37	5.9	39	7.9	20	2.2	12	1.6	0.010	<1.309	0.672	0.160	0.101	0.200	0.453

#	Sample Jt1	La	Ce	Pr	Nd	Sm	Eu	Gd	Tb	Dy	Ho	Er	Tm	Yb	Lu	Hf	^{204}Pb	^{206}Pb	^{207}Pb	^{208}Pb	Th	U
60	Jt1 Ap9 - 05	8.8	32	6.0	38	18	3.8	33	5.6	36	7.4	19	2.1	11	1.7	0.009	<1.205	0.614	0.138	0.038	0.062	0.401
61	Jt1 Ap9 - 06	9.0	33	6.4	39	17	3.7	30	4.9	31	6.3	16	1.8	10.0	1.5	<0.000	<1.127	0.530	0.125	0.082	0.033	0.290
62	Jt1 Ap9 - 07	7.5	27	4.9	30	13	2.9	25	4.1	27	5.7	15	1.6	8.7	1.3	<0.000	<1.122	0.401	0.094	0.062	0.091	0.215
63	Jt1 Ap10 - 01	212	481	61	274	73	12	98	15	95	19	52	6.4	38	5.5	0.017	<1.277	8.1	1.3	2.8	15	5.6
64	Jt1 Ap10 - 02	63	150	20	103	34	6.1	54	8.8	56	11	29	3.3	18	2.6	0.013	<1.171	2.9	0.469	1.8	8.7	2.0
65	Jt1 Ap10 - 03	91	274	44	243	87	14	139	23	148	30	77	9.1	52	7.4	0.013	<1.130	6.7	0.980	1.4	8.1	5.0
66	Jt1 Ap10 - 04	53	187	33	197	77	14	130	21	140	28	75	8.9	50	6.9	0.139	<1.091	5.1	0.799	0.839	4.4	3.8
67	Jt1 Ap10 - 05	1091	2378	254	879	138	18	137	19	109	20	52	5.8	32	4.5	<0.000	<1.115	18	3.4	12	60	9.5
68	Jt1 Ap10 - 06	8.5	29	5.4	33	15	3.3	32	5.4	36	7.4	20	2.1	11	1.5	<0.000	<1.017	0.561	0.152	0.109	0.118	0.334
69	Jt1 Ap10 - 07	7.1	25	4.7	29	14	3.3	30	5.2	35	7.2	18	2.0	11	1.5	0.010	<1.091	0.533	0.125	0.088	0.069	0.348
70	Jt1 Ap11 - 01	11	39	6.7	41	18	4.0	34	5.7	35	7.0	18	2.1	11	1.6	0.010	<1.178	0.650	0.203	0.117	0.079	0.349
71	Jt1 Ap11 - 03	269	700	99	516	169	27	256	42	273	56	152	19	112	16	0.034	<1.360	22	3.2	7.5	41	16
72	Jt1 Ap11 - 05	11	37	6.8	43	20	4.1	40	6.9	45	9.2	23	2.6	14	2.0	0.011	<1.302	1.2	0.219	0.281	1.7	0.820
73	Jt1 Ap11 - 06	13	46	8.5	51	21	4.2	35	5.7	36	7.2	19	2.1	12	1.6	<0.000	<1.088	0.663	0.208	0.265	0.644	0.344
74	Jt1 Ap11 - 08	36	99	15	81	31	5.8	51	8.4	55	11	29	3.5	20	2.7	<0.000	<1.186	2.2	0.378	0.749	3.4	1.5
75	Jt1 Ap11 - 09	12	42	8.0	47	20	4.2	36	5.9	38	7.3	20	2.1	12	1.6	0.012	<1.501	0.664	0.176	0.135	0.135	0.394
76	Jt1 Ap12 - 01	8.6	32	6.0	34	14	3.1	25	4.2	29	5.8	16	1.7	9.5	1.4	<0.000	<1.231	0.433	0.118	0.046	0.059	0.248
77	Jt1 Ap12 - 02	9.6	36	6.5	40	17	3.5	28	4.7	32	6.4	17	1.9	11	1.6	0.006	<1.152	0.463	0.119	0.066	0.031	0.225
78	Jt1 Ap12 - 03	11	42	7.9	47	20	4.0	31	4.9	31	6.0	16	1.9	11	1.6	0.006	<1.046	0.706	0.177	0.051	0.020	0.432
79	Jt1 Ap12 - 04	9.6	33	5.8	33	14	3.2	26	4.3	29	6.1	16	1.9	9.6	1.5	0.010	<1.183	0.496	0.154	0.080	0.034	0.236
80	Jt1 Ap12 - 05	18	63	11	64	23	4.3	37	5.7	36	7.1	19	2.1	12	1.6	<0.000	<1.243	0.937	0.217	0.179	0.452	0.589
81	Jt1 Ap12 - 07	15	53	9.2	51	19	3.6	31	5.0	32	6.4	17	1.9	11	1.5	0.009	<1.255	0.490	0.149	0.105	0.046	0.262
82	Jt1 Ap12 - 09	11	41	7.5	44	19	3.4	30	4.7	31	6.2	16	1.9	10	1.4	0.003	<1.080	0.493	0.130	0.065	0.178	0.236
83	Jt1 Ap13 - 01	12	43	8.0	48	21	4.2	34	5.8	36	7.3	19	2.0	12	1.6	0.003	<1.230	0.584	0.177	0.076	0.041	0.358
84	Jt1 Ap13 - 02	12	41	7.4	44	19	3.9	34	5.5	36	7.4	19	2.2	12	1.7	<0.000	<1.240	0.724	0.205	0.148	0.182	0.292
85	Jt1 Ap13 - 03	15	55	9.8	53	20	3.7	32	5.0	31	6.2	17	1.9	11	1.5	<0.000	<1.382	0.653	0.201	0.093	0.058	0.273
86	Jt1 Ap13 - 04	12	44	8.0	44	17	3.4	30	4.6	31	6.2	16	1.8	10	1.5	<0.000	<1.027	0.720	0.177	0.177	0.297	0.351
87	Jt1 Ap13 - 05	13	47	8.4	50	21	3.9	33	5.2	33	6.7	17	2.0	11	1.6	<0.000	<1.194	0.520	0.131	0.074	0.045	0.297
88	Jt1 Ap13 - 06	11	43	8.2	49	21	4.1	33	5.3	33	6.6	18	2.0	12	1.6	0.008	<1.421	0.698	0.203	0.110	0.040	0.314
89	Jt1 Ap13 - 07	13	46	8.3	50	20	4.2	37	6.0	38	7.6	20	2.3	12	1.7	0.016	<1.185	0.655	0.166	0.126	0.314	0.430
90	Jt1 Ap13 - 08	12	43	8.3	51	21	4.3	36	5.6	36	7.1	18	2.1	12	1.7	0.003	<1.154	0.637	0.194	0.092	0.031	0.343
91	Jt1 Ap14 - 01	17	58	10	65	32	6.8	66	12	79	16	42	4.8	27	3.9	0.009	<1.180	4.1	0.597	1.2	6.0	3.1
92	Jt1 Ap14 - 02	11	36	6.5	41	18	3.7	34	5.5	37	7.4	19	2.2	11	1.6	0.005	<1.774	0.917	0.290	0.214	0.109	0.404
93	Jt1 Ap14 - 03	22	66	11	59	22	4.3	39	6.2	39	7.6	20	2.3	12	1.7	0.010	<1.199	0.686	0.152	0.133	0.263	0.433
94	Jt1 Ap14 - 04	90	245	38	210	81	15	141	24	162	32	88	11	61	8.5	0.013	<1.091	9.9	1.4	2.7	15	7.6
95	Jt1 Ap14 - 05	9.0	30	5.5	34	16	3.4	33	5.7	38	7.4	19	2.0	11	1.5	0.010	<1.210	0.672	0.178	0.126	0.083	0.359
96	Jt1 Ap14 - 06	12	43	8.0	49	21	4.1	38	6.1	38	7.8	20	2.1	11	1.6	0.003	<1.116	0.929	0.175	0.069	0.080	0.620
97	Jt1 Ap14 - 07	11	39	7.4	45	20	4.3	38	6.2	40	8.1	21	2.2	13	1.7	0.009	<1.056	0.705	0.158	0.092	0.150	0.433
98	Jt1 Ap14 - 08	357	888	122	608	197	32	293	49	323	66	182	23	135	20	0.033	<1.172	27	3.8	7.8	45	21
99	Jt1 Ap14 - 09	47	136	22	129	57	11	106	18	124	25	68	8.1	47	6.6	0.013	<1.132	7.1	0.993	1.9	11	5.4
100	Jt1 Ap14 - 10	197	529	79	417	150	26	241	40	263	53	147	18	107	15	0.042	<1.229	18	2.6	5.4	32	14
101	Jt1 Ap14 - 11	66	193	32	189	81	15	140	24	160	32	88	10	62	8.9	0.013	<1.245	9.6	1.4	2.7	16	7.3
102	Jt1 Ap15 - 01	484	1084	137	624	165	27	222	35	228	46	127	16	95	13	0.010	<1.236	22	3.4	5.2	28	15
103	Jt1 Ap15 - 02	11	42	7.8	50	22	4.3	41	6.7	43	8.4	22	2.5	14	2.0	<0.000	<1.379	1.1	0.232	0.199	0.821	0.783
104	Jt1 Ap15 - 03	21	70	12	71	28	5.1	44	7.2	45	8.8	23	2.7	15	2.1	0.003	<1.424	1.6	0.302	0.295	0.821	0.861
105	Jt1 Ap15 - 04	13	47	8.6	53	22	4.0	37	5.9	38	7.3	19	2.2	12	1.7	0.006	<1.300	0.647	0.133	0.069	0.103	0.402
106	Jt1 Ap15 - 05	398	1064	151	759	223	35	304	49	314	63	173	22	131	18	0.043	<1.143	27	3.8	7.8	45	20
107	Jt1 Ap15 - 06	409	1004	133	639	185	30	255	41	263	53	147	19	111	16	0.037	<1.199	26	4.0	7.0	37	18
108	Jt1 Ap15 - 07	15	50	9.3	56	23	4.5	39	6.1	38	7.7	20	2.3	13	1.9	0.003	<1.156	0.712	0.160	0.108	0.181	0.439
109	Jt1 Ap15 - 08	8.2	32	6.2	40	18	3.8	34	5.7	37	7.3	19	2.2	11	1.6	<0.000	<1.200	0.505	0.121	0.060	0.061	0.340
110	Jt1 Ap15 - 09	44	116	17	92	36	6.4	62	10.0	67	14	36	4.3	25	3.4	<0.000	<1.127	3.3	0.488	0.865	4.3	2.2
111	Jt1 Ap16 - 01	1303	3122	377	1634	360	44	415	60	371	75	203	25	152	21	0.026	<1.178	49	7.3	14	77	35
112	Jt1 Ap16 - 02	923	2338	291	1302	306	39	359	53	328	65	178	23	133	18	0.042	<1.529	41	6.3	11	56	28
113	Jt1 Ap16 - 03	40	130	21	124	47	8.0	79	13	83	17	46	5.3	30	4.3	0.006	<1.162	5.5	0.817	1.1	5.9	4.1
114	Jt1 Ap16 - 04	746	1967	259	1225	312	40	389	58	361	72	197	24	144	21	0.046	<1.223	40	5.7	11	64	31
115	Jt1 Ap16 - 06	1191	2837	340	1459	324	38	371	54	329	66	180	22	132	19	0.026	<1.096	43	6.3	13	73	31
116	Jt1 Ap16 - 07	227	590	82	410	118	17	164	26	160	33	88	11	65	9.1	0.020	<1.048	13	1.9	3.9	21	9.6
117	Jt1 Ap16 - 08	476	1382	199	961	247	31	295	42	259	51	140	17	101	14	0.014	<1.030	29	4.2	7.5	42	22
118	Jt1 Ap16 - 09	716	1899	249	1131	262	32	295	42	257	50	138	17	101	14	0.040	<1.038	36	5.3	8.9	49	27
119	Jt1 Ap16 - 10	1162	3070	389	1742	379	41	408	57	338	65	176	22	126	17	0.040	<1.050	48	7.1	13	74	35
120	Jt1 Ap16 - 11	301	830	121	591	161	21	201	30	184	36	98	12	69	9.7	0.021	<1.460	23	3.6	7.1	33	14

#	Sample Jt1	La	Ce	Pr	Nd	Sm	Eu	Gd	Tb	Dy	Ho	Er	Tm	Yb	Lu	Hf	^{204}Pb	^{206}Pb	^{207}Pb	^{208}Pb	Th	U
121	Jt1 Ap16 - 12	443	1113	148	698	179	24	226	34	212	42	116	14	84	12	0.017	<1.151	19	2.9	7.0	38	14
122	Jt1 Ap16 - 13	1075	2730	351	1578	346	37	372	51	302	60	158	19	111	15	0.038	<1.209	50	8.1	15	76	32
123	Jt1 Ap16 - 14	793	2124	282	1317	313	36	363	51	310	61	167	21	120	17	0.033	<1.225	41	6.2	12	69	31
124	Jt1 Ap16 - 15	793	1902	238	1064	238	26	269	37	220	43	116	14	82	11	0.030	<1.204	42	6.5	18	101	31
125	Jt1 Ap16 - 16	886	2250	285	1269	292	35	331	47	289	57	156	19	117	16	0.019	<1.174	41	6.4	10	54	29
126	Jt1 Ap16 - 17	975	2412	304	1345	316	40	368	54	337	66	182	23	134	19	0.021	<1.488	41	6.2	10	57	30
127	Jt1 Ap16 - 18	643	1588	207	959	257	38	334	51	329	66	183	23	139	20	0.062	<1.040	39	5.9	9.2	50	28
128	Jt1 Ap16 - 20	21	74	12	70	24	4.3	36	5.3	32	6.4	16	1.9	10	1.5	<0.000	<1.112	0.525	0.144	0.068	0.081	0.302
129	Jt1 Ap16 - 21	1112	2754	346	1546	366	46	428	62	389	77	212	26	157	22	0.049	<1.216	53	8.5	16	83	37
130	Jt1 Ap16 - 22	455	1173	160	782	219	31	290	46	288	57	159	20	116	17	0.039	<1.021	28	3.9	8.8	46	21
131	Jt1 Ap16 - 23	436	1063	142	690	206	33	297	48	314	63	173	21	125	18	0.029	<1.043	27	3.8	8.2	46	21
132	Jt1 Ap16 - 24	171	472	70	378	123	19	190	30	197	40	107	13	74	10	0.023	<1.132	16	2.2	5.4	32	13
133	Jt1 Ap16 - 25	142	379	56	306	102	16	161	26	167	34	91	11	61	8.9	0.017	<1.129	14	2.0	3.9	22	11
134	Jt1 Ap16 - 26	201	514	75	395	139	24	220	38	244	50	134	16	96	14	0.033	<1.083	20	2.9	4.8	26	16
135	Jt1 Ap17 - 01	9.4	33	6.3	39	18	4.1	32	5.2	35	7.0	18	1.9	11	1.6	0.003	<1.090	0.611	0.155	0.117	0.131	0.335
136	Jt1 Ap17 - 02	9.1	33	6.4	38	17	3.8	32	5.2	35	6.9	17	2.0	11	1.5	0.003	<1.041	0.533	0.146	0.066	0.063	0.304
137	Jt1 Ap17 - 03	10	35	6.3	39	18	4.2	32	5.5	36	7.0	18	2.0	11	1.5	0.006	<1.436	0.570	0.136	0.141	0.103	0.334
138	Jt1 Ap17 - 05	15	51	8.9	53	21	4.1	34	5.4	35	6.9	18	2.0	11	1.5	0.011	<1.398	1.2	0.306	0.214	0.176	0.426
139	Jt1 Ap17 - 07	10	38	7.1	44	19	4.2	34	5.4	34	6.8	18	2.0	11	1.5	0.011	<1.284	0.636	0.233	0.148	0.105	0.303
140	Jt1 Ap17 - 08	146	326	41	190	52	8.6	71	11	68	14	37	4.3	26	3.7	0.010	<1.324	5.4	1.0	2.9	14	3.5
141	Jt1 Ap17 - 09	10	39	7.6	48	21	4.0	32	5.1	32	6.3	16	2.0	10	1.4	0.010	<1.439	0.571	0.187	0.098	0.045	0.283
142	Jt1 Ap17 - 10	8.9	33	6.1	38	17	3.5	30	4.9	33	6.5	17	1.8	10	1.4	0.003	<1.306	0.611	0.149	0.136	0.447	0.374
	Mean (n=142)	420	1025	129	581	141	19	177	27	168	34	91	11	65	9.2	0.024	-	18	2.8	6.0	32	13
	SD	561	1323	158	671	138	16	153	22	136	27	75	9.4	56	7.9	0.020	-	20	3.1	7.0	37	14
	Median	98	261	42	226	81	14	133	20	132	26	72	8.5	49	6.8	0.019	-	8.8	1.3	2.7	15	6.4
	Max	2546	5764	673	2721	478	49	465	66	417	84	233	29	176	25	0.139	-	74	12	28	150	49
	Min	7.1	25	4.5	27	11	2.7	22	3.9	27	5.7	15	1.6	8.7	1.3	0.003	-	0.398	0.093	0.022	0.017	0.215

#	Sample Jt4	La	Ce	Pr	Nd	Sm	Eu	Gad	Tb	Dy	Ho	Er	Tm	Yb	Lu	Hf	^{204}Pb	^{206}Pb	^{207}Pb	^{208}Pb	Th	U
1	Jt4 Ap1 - 01	7.2	21	3.2	18	7.5	1.2	19	4.0	38	12	45	6.3	38	4.7	<0.000	<1.097	1.0	0.423	0.298	0.057	0.334
2	Jt4 Ap1 - 02	7.8	21	3.2	18	6.3	0.965	16	3.4	32	10	38	5.4	31	3.9	0.019	<1.454	1.0	0.485	0.335	0.012	0.345
3	Jt4 Ap1 - 03	6.8	22	3.7	22	9.5	1.4	22	4.5	43	13	47	6.5	39	5.0	0.003	<1.279	1.1	0.357	0.208	0.016	0.591
4	Jt4 Ap1 - 05	8.2	25	4.2	26	9.7	1.7	23	4.7	42	12	42	5.7	33	4.2	0.006	<1.072	0.987	0.247	0.188	0.340	0.522
5	Jt4 Ap1 - 07	6.9	21	3.6	21	8.5	1.3	21	4.0	37	11	41	5.7	35	4.2	0.003	<1.105	0.742	0.229	0.126	0.014	0.430
6	Jt4 Ap10 - 02	95	241	33	162	49	6.5	90	18	160	44	163	23	140	18	0.003	<1.235	10	1.6	2.7	15	7.4
7	Jt4 Ap10 - 03	298	676	81	354	80	9.2	121	23	188	50	180	26	156	19	0.010	<1.368	14	2.3	4.3	24	10
8	Jt4 Ap10 - 04	32	84	12	63	21	2.9	44	9.2	86	25	96	14	84	10	0.006	<1.255	4.7	0.830	1.2	5.6	3.4
9	Jt4 Ap10 - 05	73	183	25	124	38	5.1	75	15	133	38	141	20	124	15	0.007	<1.330	8.5	1.4	2.2	12	6.1
10	Jt4 Ap10 - 06	57	141	18	88	24	3.2	46	9.3	88	26	100	15	89	11	0.017	<1.226	5.4	1.2	1.7	7.0	3.5
11	Jt4 Ap11 - 01	23	62	8.8	47	16	2.4	34	7.3	67	20	73	11	63	7.9	0.017	<1.381	2.9	0.515	0.749	3.6	2.1
12	Jt4 Ap11 - 02	192	458	58	275	71	9.2	126	25	216	60	220	32	194	24	0.017	<1.231	17	2.4	4.8	26	12
13	Jt4 Ap11 - 03	23	63	9.1	48	18	2.8	41	9.1	86	26	96	14	85	11	0.020	<1.308	4.6	0.696	1.1	6.0	3.5
14	Jt4 Ap11 - 04	5.4	16	2.9	18	7.4	1.2	20	4.0	39	12	45	5.8	33	3.8	0.003	<1.144	0.470	0.101	0.046	0.005	0.301
15	Jt4 Ap11 - 05	15	42	6.3	34	13	1.9	27	5.4	50	14	52	7.2	43	5.5	0.026	<1.140	1.2	0.268	0.211	0.566	0.743
16	Jt4 Ap11 - 06	4.4	14	2.5	16	6.6	1.2	18	4.1	39	12	45	6.6	38	4.8	0.006	<1.511	0.749	0.171	0.056	0.020	0.448
17	Jt4 Ap11 - 07	7.4	23	3.9	23	10	1.6	25	5.0	47	13	50	7.0	43	5.1	0.053	<1.404	0.998	0.220	0.108	0.028	0.631
18	Jt4 Ap2 - 01	263	604	74	316	70	8.1	105	19	167	45	162	24	147	18	0.013	<1.032	15	2.4	4.8	27	10
19	Jt4 Ap2 - 02	8.8	23	3.3	20	7.6	1.5	20	4.0	37	11	42	5.5	32	4.0	0.003	<1.099	1.1	0.367	0.240	0.017	0.550
20	Jt4 Ap2 - 05	69	168	21	101	27	3.4	46	9.1	79	23	81	12	70	8.8	0.014	<1.134	4.3	0.714	1.0	4.9	3.1
21	Jt4 Ap2 - 06	14	32	4.6	24	8.1	1.2	18	3.6	36	11	44	6.5	38	4.9	0.014	<1.828	1.1	0.338	0.260	0.005	0.435
22	Jt4 Ap3 - 01	5.5	20	3.6	24	11	1.6	25	5.0	43	12	39	5.2	29	3.8	0.007	<1.353	0.924	0.256	0.088	0.011	0.485
23	Jt4 Ap3 - 02	5.0	19	3.4	21	9.7	1.5	23	4.5	40	11	37	4.9	29	3.4	0.005	<1.321	0.712	0.206	0.102	0.017	0.372
24	Jt4 Ap3 - 03	78	199	28	144	48	6.4	96	20	180	51	189	28	169	21	0.016	<1.146	13	1.9	3.4	18	9.4
25	Jt4 Ap3 - 05	6.7	23	4.3	26	11	1.8	27	5.1	44	12	41	5.7	33	4.1	0.003	<1.127	0.969	0.264	0.118	0.008	0.543
26	Jt4 Ap3 - 06	13	33	4.5	25	8.8	1.3	21	4.4	42	13	52	7.7	44	5.6	0.004	<1.139	1.9	0.773	0.683	0.792	0.809
27	Jt4 Ap3 - 07	107	266	36	176	53	7.1	101	20	179	50	184	27	163	20	0.013	<1.060	13	2.0	3.4	18	9.1
28	Jt4 Ap4 - 01	93	231	31	162	52	7.3	104	21	191	53	191	28	168	21	0.010	<1.034	13	1.9	4.1	22	9.1
29	Jt4 Ap4 - 02	93	224	29	136	37	4.5	65	13	113	33	120	17	105	13	0.005	<1.298	7.5	1.4	2.3	12	5.2
30	Jt4 Ap4 - 03	8.6	23	3.5	19	7.5	1.1	18	3.8	37	11	43	6.1	36	4.7	<0.000	<1.078	0.992	0.383	0.275	0.125	0.382
31	Jt4 Ap4 - 04	1154	2657	307	1290	252	28	320	53	398	98	327	46	274	34	0.046	<1.136	48	8.4	20	93	30

#	Sample Jt4	La	Ce	Pr	Nd	Sm	Eu	Gad	Tb	Dy	Ho	Er	Tm	Yb	Lu	Hf	^{204}Pb	^{206}Pb	^{207}Pb	^{208}Pb	Th	U
32	Jt4 Ap4 - 05	528	1209	146	637	146	16	216	38	307	80	272	39	234	29	0.038	<1.155	28	4.7	11	56	18
33	Jt4 Ap5 - 01	6.0	19	3.4	20	8.6	1.4	21	4.5	41	12	45	6.4	38	4.8	0.017	<1.276	0.754	0.202	0.067	0.016	0.459
34	Jt4 Ap5 - 02	7.4	24	4.1	25	11	1.6	24	5.0	45	13	46	6.4	38	4.8	<0.000	<1.296	0.959	0.223	0.093	0.081	0.570
35	Jt4 Ap5 - 04	44	111	15	77	24	3.2	46	9.3	84	24	84	12	71	8.8	0.160	<1.542	4.3	0.742	1.2	5.6	3.0
36	Jt4 Ap5 - 05	6.8	20	3.3	20	8.2	1.3	20	4.4	41	13	49	6.8	40	5.1	0.003	<1.262	0.922	0.339	0.259	0.270	0.446
37	Jt4 Ap6 - 01	16	47	7.0	40	16	2.4	38	8.4	81	25	96	15	90	11	0.010	<1.205	4.5	0.872	1.2	5.4	3.1
38	Jt4 Ap6 - 02	283	674	85	389	100	12	164	32	266	71	252	36	219	27	0.021	<1.182	22	3.4	6.1	33	16
39	Jt4 Ap6 - 03	6.2	20	3.4	20	8.8	1.4	21	4.3	39	11	42	5.9	35	4.3	0.003	<1.264	0.653	0.222	0.122	0.044	0.339
40	Jt4 Ap6 - 04	35	93	13	69	23	3.1	48	10	93	28	103	15	91	11	0.007	<1.256	5.5	0.947	1.4	6.6	3.7
41	Jt4 Ap6 - 05	11	30	4.6	27	11	1.9	28	5.9	57	17	66	9.8	59	7.4	0.003	<1.184	2.5	0.494	0.321	0.778	1.6
42	Jt4 Ap7 - 02	357	813	103	457	106	12	163	30	241	63	216	30	185	22	<0.000	<2.048	19	3.0	6.3	33	13
43	Jt4 Ap7 - 03	424	961	117	516	118	12	181	32	255	67	226	32	191	23	0.030	<1.839	20	3.3	7.9	41	14
44	Jt4 Ap7 - 06	729	1699	203	900	199	21	290	50	387	98	328	46	275	34	0.012	<1.944	36	5.9	14	66	23
45	Jt4 Ap8 - 01	152	368	47	220	58	7.1	96	19	167	46	163	24	144	18	0.023	<1.815	13	1.9	3.4	19	9.2
46	Jt4 Ap8 - 02	15	46	7.2	41	15	2.2	34	7.0	61	18	65	9.3	55	6.8	0.038	<1.469	1.7	0.330	0.345	1.2	1.1
47	Jt4 Ap8 - 03	6.8	21	3.3	21	8.4	1.3	21	4.5	42	13	47	6.7	41	5.0	<0.000	<1.585	1.0	0.373	0.201	0.048	0.417
48	Jt4 Ap8 - 05	6.5	19	2.9	17	7.4	1.0	17	3.7	37	12	45	6.5	38	5.0	<0.000	<1.408	1.6	0.891	0.657	0.032	0.257
49	Jt4 Ap8 - 06	103	259	36	180	55	7.1	102	20	177	49	177	25	153	19	<0.001	<7.250	14	2.3	3.7	18	8.3
	Mean (n=49)	113	267	33	153	39	4.8	67	13	110	30	109	16	94	12	0.018	-	7.6	1.3	2.4	12	5.1
	SD	214	492	58	247	51	5.5	70	12	94	24	81	12	70	8.6	0.024	-	9.9	1.6	3.8	19	6.6
	Median	16	47	7.2	41	16	2.4	34	7.3	67	20	73	11	63	7.9	0.011	-	2.9	0.714	0.749	3.6	2.1
	Max	1154	2657	307	1290	252	28	320	53	398	98	328	46	275	34	0.160	-	48	8.4	20	93	30
	Min	4.4	14	2.5	16	6.3	0.965	16	3.4	32	10	37	4.9	29	3.4	0.003	-	0.470	0.101	0.046	0.005	0.257

#	Sample Jt7	La	Ce	Pr	Nd	Sm	Eu	Gad	Tb	Dy	Ho	Er	Tm	Yb	Lu	Hf	^{204}Pb	^{206}Pb	^{207}Pb	^{208}Pb	Th	U
1	Jt7 Ap1 - 01	403	939	120	562	148	16	214	34	242	56	170	22	128	16	0.017	<1.291	42	6.8	5.3	27	28
2	Jt7 Ap1 - 02	849	2053	247	1068	220	16	250	35	227	48	140	18	103	12	0.030	<1.189	38	6.4	5.2	26	25
3	Jt7 Ap1 - 04	482	1210	162	751	171	11	194	26	165	34	94	11	58	6.8	0.007	<1.192	5.4	1.0	0.248	1.2	3.2
4	Jt7 Ap1 - 05	537	1213	145	647	148	16	206	33	236	54	170	22	129	16	0.021	<1.361	44	7.0	8.1	41	30
5	Jt7 Ap1 - 06	661	1716	231	1092	266	24	328	48	319	69	205	26	151	18	0.041	<1.232	41	7.0	6.9	33	27
6	Jt7 Ap1 - 07	408	1644	264	1338	316	24	342	46	283	59	168	21	115	14	0.027	<1.164	22	3.9	1.7	7.1	14
7	Jt7 Ap1 - 08	470	1889	300	1496	352	26	377	50	304	62	173	21	119	14	0.038	<1.265	28	4.9	2.4	11	17
8	Jt7 Ap1 - 09	1199	2724	308	1237	233	22	268	39	269	60	184	24	140	17	0.031	<1.376	41	6.3	10	54	28
9	Jt7 Ap1 - 10	626	1955	283	1355	327	25	370	51	320	66	189	23	131	16	0.031	<1.259	38	6.7	4.0	20	24
10	Jt7 Ap1 - 11	604	1686	234	1113	263	17	305	42	257	52	148	18	98	11	0.024	<1.243	42	7.6	5.5	26	26
11	Jt7 Ap2 - 01	977	2344	273	1161	229	21	268	40	271	60	177	23	130	16	0.034	2.7	67	15	15	37	25
12	Jt7 Ap2 - 02	311	741	91	402	91	8.7	120	19	130	29	86	11	61	7.8	0.015	<1.413	13	2.2	2.3	11	8.0
13	Jt7 Ap2 - 03	922	2251	265	1099	211	19	242	35	242	53	158	20	116	14	0.016	<1.685	31	5.2	6.3	31	20
14	Jt7 Ap2 - 04	1006	2418	282	1166	218	19	243	35	229	49	146	18	107	13	0.035	<1.637	29	4.6	6.0	30	19
15	Jt7 Ap2 - 05	9.2	33	6.3	39	15	2.0	31	5.3	40	9.4	29	3.4	19	2.3	0.010	<1.466	1.0	0.298	0.176	0.451	0.652
16	Jt7 Ap2 - 06	279	725	95	448	120	13	194	33	256	60	190	26	145	18	0.046	<1.377	29	4.5	2.5	13	21
17	Jt7 Ap2 - 08	1250	2838	332	1439	297	27	367	53	359	79	235	30	173	21	0.006	<1.508	75	13	19	95	48
18	Jt7 Ap2 - 09	1074	2678	323	1371	271	23	311	46	306	67	199	26	148	18	0.053	<1.336	44	7.3	8.2	42	28
19	Jt7 Ap2 - 10	927	2483	307	1313	282	25	334	50	342	77	229	30	170	21	0.024	<1.371	59	9.9	3.4	16	39
20	Jt7 Ap2 - 11	751	1864	228	972	203	19	253	37	255	57	170	22	126	15	0.052	<1.322	28	4.5	4.7	24	19
21	Jt7 Ap4 - 01	40	112	16	83	28	3.4	48	7.9	57	13	40	5.2	29	3.5	<0.000	<1.371	2.0	0.382	0.378	1.2	1.1
22	Jt7 Ap4 - 02	297	740	95	427	103	11	146	24	173	40	121	16	90	11	0.011	<1.302	14	2.3	2.4	12	9.6
23	Jt7 Ap4 - 03	1063	2530	292	1193	230	20	260	37	253	55	166	21	120	14	0.014	<1.153	35	5.8	6.7	32	22
24	Jt7 Ap4 - 04	248	579	70	302	70	6.8	96	14	94	21	59	7.2	41	5.1	0.007	<1.295	7.6	1.4	2.2	9.5	4.8
25	Jt7 Ap4 - 05	872	2145	249	1056	212	19	252	37	249	55	166	21	122	15	0.031	<1.327	31	5.2	5.9	28	20
26	Jt7 Ap4 - 06	1211	2850	327	1322	245	21	274	39	257	56	165	21	120	14	0.045	<1.279	37	6.2	7.5	37	24
27	Jt7 Ap4 - 07	784	1834	217	900	177	16	216	32	222	50	150	19	111	13	0.048	<1.269	27	4.5	5.6	27	18
28	Jt7 Ap5 - 01	280	663	84	392	106	13	172	30	230	54	175	23	135	17	0.055	<1.195	24	3.6	4.3	22	17
29	Jt7 Ap5 - 02	426	978	120	530	127	14	185	31	236	56	180	24	142	18	0.034	<1.113	29	4.3	5.8	32	21
30	Jt7 Ap5 - 03	358	809	98	443	108	12	170	29	215	52	162	22	126	16	0.023	<0.966	26	3.8	3.9	21	19
31	Jt7 Ap5 - 04	758	1769	213	920	207	22	267	42	294	66	207	27	157	20	0.015	<1.105	43	6.8	10	56	30
32	Jt7 Ap5 - 05	524	1207	147	644	150	16	212	34	251	59	183	25	142	18	0.021	<1.189	33	4.8	5.7	30	24
33	Jt7 Ap5 - 06	298	693	86	397	101	11	158	27	204	50	157	21	123	15	0.025	<1.400	23	3.3	4.4	23	17
34	Jt7 Ap5 - 07	678	1510	178	758	166	18	226	36	265	63	198	26	154	19	0.048	<1.242	38	5.9	7.1	35	27
35	Jt7 Ap5 - 08	554	1263	154	681	162	19	234	39	283	66	209	28	163	20	0.028	<1.168	34	5.3	9.4	51	24

#	Sample Jt7	La	Ce	Pr	Nd	Sm	Eu	Gad	Tb	Dy	Ho	Er	Tm	Yb	Lu	Hf	^{204}Pb	^{206}Pb	^{207}Pb	^{208}Pb	Th	U
36	Jt7 Ap5 - 09	314	732	90	404	99	11	146	25	188	44	140	19	107	13	0.017	<1.102	24	4.3	4.7	17	13
37	Jt7 Ap6 - 01	32	81	11	53	17	1.9	30	5.2	39	9.5	30	3.8	22	2.6	0.003	<1.095	2.2	0.495	0.419	0.723	0.988
38	Jt7 Ap6 - 02	790	1941	236	1000	200	18	233	34	225	49	146	19	108	13	0.017	<1.120	28	4.6	4.9	24	19
39	Jt7 Ap6 - 03	950	2336	279	1183	231	19	257	36	237	52	150	20	110	14	0.031	<1.179	27	4.4	6.0	30	18
40	Jt7 Ap6 - 04	617	1496	188	833	183	16	223	32	213	46	140	18	102	13	0.010	<1.260	32	5.4	6.4	31	20
41	Jt7 Ap6 - 05	673	1546	186	800	179	18	242	39	287	67	210	28	163	20	0.024	<1.223	34	4.9	9.3	51	25
42	Jt7 Ap6 - 06	421	1052	136	618	150	14	200	30	216	49	152	19	113	14	0.024	<1.234	24	3.8	4.1	21	16
43	Jt7 Ap6 - 07	643	1469	176	762	159	14	191	27	180	39	116	15	84	10	0.034	<1.175	25	4.4	5.7	27	16
44	Jt7 Ap6 - 08	215	514	67	308	81	9.2	122	20	146	34	105	14	79	9.8	0.020	<1.137	15	2.4	3.5	18	10
45	Jt7 Ap7 - 01	826	1892	222	963	205	22	267	42	296	67	207	28	160	20	0.052	<1.274	41	6.6	13	67	28
46	Jt7 Ap7 - 02	1040	2440	284	1214	248	22	290	42	281	62	189	24	143	18	0.035	<1.270	55	9.2	13	66	36
47	Jt7 Ap7 - 03	707	1734	218	954	196	18	233	33	219	48	143	18	106	13	0.033	<1.345	19	3.1	6.1	31	13
48	Jt7 Ap7 - 04	1068	2588	305	1266	237	20	259	35	227	49	141	18	103	13	0.024	<1.276	26	4.3	7.0	36	17
49	Jt7 Ap7 - 05	742	1806	219	950	194	18	230	33	220	48	145	18	107	13	0.007	<1.240	24	4.0	5.9	27	15
50	Jt7 Ap7 - 06	31	84	12	67	23	3.0	47	8.7	69	17	55	7.2	41	5.1	0.010	<1.247	3.5	0.703	0.839	2.8	2.2
51	Jt7 Ap7 - 07	607	1524	195	867	189	18	234	35	237	53	159	21	119	15	0.024	<1.171	20	3.2	3.5	18	13
52	Jt7 Ap7 - 08	80	213	28	141	43	5.4	76	14	107	26	81	11	62	7.7	0.011	<1.100	8.0	1.2	2.4	11	5.5
53	Jt7 Ap7 - 09	829	1990	241	1045	218	21	266	39	262	58	178	23	132	16	0.021	<1.080	32	5.2	9.2	45	21
54	Jt7 Ap8 - 01	49	126	18	97	36	4.5	79	15	127	32	105	14	80	9.6	0.007	<1.213	8.7	1.4	2.2	10	6.1
55	Jt7 Ap8 - 02	7.3	25	4.4	27	13	1.8	31	6.4	52	13	42	5.4	30	3.6	0.013	<1.335	1.2	0.279	0.224	0.729	0.799
56	Jt7 Ap8 - 03	12	33	5.0	29	12	1.6	32	6.5	56	15	49	6.1	36	4.3	0.003	<1.214	2.5	0.575	0.518	1.9	1.5
57	Jt7 Ap8 - 04	304	717	92	431	116	12	187	32	246	58	184	24	139	17	0.011	<1.200	30	4.4	5.3	27	22
58	Jt7 Ap8 - 05	19	67	12	69	25	2.6	47	8.1	64	15	48	6.2	34	4.2	0.011	<1.230	1.0	0.272	0.359	1.3	0.518
59	Jt7 Ap8 - 06	19	58	9.6	55	21	2.6	46	8.4	67	17	52	6.6	38	4.6	0.014	<1.143	1.5	0.298	0.249	0.894	0.955
60	Jt7 Ap8 - 07	63	167	25	135	48	5.6	99	19	152	37	118	16	89	11	0.020	<1.231	15	2.1	2.8	15	11
61	Jt7 Ap8 - 08	6.6	22	4.0	24	11	1.6	26	4.9	39	9.9	30	3.9	21	2.7	0.004	<1.365	0.584	0.186	0.095	0.028	0.319
62	Jt7 Ap8 - 09	107	261	34	174	57	7.2	115	23	187	47	152	20	116	14	0.007	<1.263	17	2.6	3.2	16	12
63	Jt7 Ap9 - 01	13	35	5.7	34	15	2.0	35	7.0	58	14	46	6.1	36	4.6	31	<1.557	14	2.5	0.810	3.6	13
64	Jt7 Ap9 - 02	508	1122	134	584	136	14	202	34	254	60	190	25	147	18	0.030	<1.440	31	4.7	6.6	34	22
65	Jt7 Ap9 - 03	14	38	6.1	35	16	2.0	37	7.4	61	16	49	6.4	36	4.4	0.003	<1.232	2.2	0.397	0.420	1.9	1.4
66	Jt7 Ap9 - 04	89	224	31	166	57	7.0	109	20	157	38	120	16	92	11	0.068	<1.109	14	2.0	2.1	11	9.8
67	Jt7 Ap9 - 05	730	1620	192	843	190	20	252	40	283	64	198	26	152	19	0.047	<1.335	45	7.3	8.4	42	30
68	Jt7 Ap9 - 06	1181	2567	290	1221	246	23	299	45	306	69	211	28	159	20	0.034	<1.285	61	10	14	66	40
69	Jt7 Ap10 - 01	595	1377	169	754	170	18	218	35	245	55	165	21	125	15	0.049	<1.637	30	4.7	6.3	33	20
70	Jt7 Ap10 - 02	1387	3157	339	1399	261	25	317	46	315	69	213	28	163	20	0.070	<1.599	66	11	17	89	44
71	Jt7 Ap10 - 03	431	1020	131	606	159	20	230	38	272	62	192	25	146	18	0.006	<1.501	35	5.8	8.2	42	24
72	Jt7 Ap10 - 04	290	747	98	444	102	11	132	20	137	31	92	12	67	8.4	0.057	<1.381	10	1.8	2.6	13	6.8
73	Jt7 Ap10 - 06	424	1309	192	936	249	21	303	43	271	57	160	19	107	13	0.027	<1.493	37	6.4	3.6	17	22
74	Jt7 Ap10 - 07	361	914	123	575	134	10	168	25	165	37	109	14	78	9.1	0.024	<1.807	25	4.3	4.4	22	17
75	Jt7 Ap10 - 09	394	1081	150	726	181	14	223	33	219	47	132	16	91	11	0.051	<1.701	25	4.4	4.6	21	16
76	Jt7 Ap10 - 10	367	967	129	607	145	11	179	27	170	37	105	13	70	8.6	<0.000	<2.150	24	4.2	5.7	27	16
77	Jt7 Ap11 - 04	723	1750	208	896	174	15	203	31	211	48	148	19	108	13	0.023	<1.953	22	3.4	5.9	32	16
78	Jt7 Ap11 - 06	476	1147	145	642	136	13	178	27	193	46	141	19	107	13	<0.000	<2.003	17	2.6	4.7	26	13
79	Jt7 Ap11 - 07	505	1178	146	653	144	15	200	31	223	54	166	22	124	16	0.019	<1.732	27	4.0	6.8	35	19
80	Jt7 Ap11 - 10	321	732	91	417	101	11	158	28	213	53	171	23	137	16	0.040	<1.628	22	3.2	4.9	30	18
81	Jt7 Ap11 - 11	48	130	19	97	29	3.8	54	9.5	76	19	60	7.9	44	5.3	0.011	<1.902	3.8	0.631	0.394	0.649	2.7
82	Jt7 Ap12 - 02	1781	3981	436	1702	294	25	285	38	232	48	138	18	100	12	0.027	<1.313	49	8.2	12	60	32
83	Jt7 Ap12 - 03	1238	2812	318	1316	250	21	268	38	245	52	157	20	116	14	0.024	<1.294	48	7.5	8.6	45	32
84	Jt7 Ap12 - 04	794	1806	215	928	201	21	256	39	274	61	190	25	146	18	0.073	<1.150	44	6.9	8.5	45	30
85	Jt7 Ap12 - 05	439	1009	124	536	121	12	152	23	160	36	111	15	84	10	0.003	<1.087	22	3.7	4.7	24	15
86	Jt7 Ap12 - 06	740	1677	197	835	173	17	219	33	235	54	166	22	129	16	0.012	<1.059	36	5.6	7.5	39	26
87	Jt7 Ap12 - 07	1107	2486	283	1185	227	20	251	36	233	51	153	20	114	14	0.020	<1.033	44	7.2	8.6	45	30
88	Jt7 Ap12 - 08	1597	3490	385	1548	271	23	284	39	250	54	160	21	119	14	0.028	<1.298	50	8.3	10	53	34
89	Jt7 Ap13 - 01	466	1049	125	538	116	11	162	26	198	47	152	20	115	14	0.010	<1.433	18	2.7	3.8	21	13
90	Jt7 Ap13 - 02	275	602	73	334	81	8.6	135	24	182	45	146	20	113	14	0.013	<1.297	18	2.5	4.1	23	13
91	Jt7 Ap13 - 03	231	538	67	303	72	8.1	113	19	148	36	114	15	86	11	0.020	<1.298	11	1.7	2.6	14	8.0
92	Jt7 Ap13 - 04	593	1320	156	665	142	15	190	30	222	52	167	22	128	16	0.020	<1.280	29	4.4	6.6	34	21
93	Jt7 Ap13 - 05	611	1343	158	681	141	14	188	30	213	49	156	21	118	15	0.016	<1.428	31	4.6	7.7	41	22
94	Jt7 Ap13 - 06	435	962	116	514	118	12	172	29	217	52	167	23	129	16	0.020	<1.377	27	4.0	4.5	26	20
95	Jt7 Ap13 - 07	642	1445	171	722	149	14	184	29	202	47	146	19	111	14	0.033	<1.090	25	3.7	6.2	34	18
96	Jt7 Ap13 - 08	422	946	113	489	109	13	159	27	202	49	155	21	120	15	0.025	<1.371	24	3.8	5.7	27	16
97	Jt7 Ap13 - 09	274	638	79	351	81	8.2	124	22	168	41	132	18	103	12	0.007	<1.266	15	2.4	4.0	21	11
98	Jt7 Ap13 - 10	824	1833	207	838	161	16	201	31	223	52	163	22	127	15	0.035	<1.264	36	5.7	7.6	43	26
99	Jt7 Ap14 - 01	294	734	95	436	99	10	146	24	177	42	132	17	101	12	0.021	<1.294	14	2.1	1.9	10	11

#	Sample Jt7	La	Ce	Pr	Nd	Sm	Eu	Gad	Tb	Dy	Ho	Er	Tm	Yb	Lu	Hf	^{204}Pb	^{206}Pb	^{207}Pb	^{208}Pb	Th	U
100	Jt7 Ap14 - 02	290	726	94	434	103	11	150	25	185	43	137	18	105	13	0.017	<1.464	20	3.5	2.7	9.8	13
101	Jt7 Ap14 - 03	224	542	70	326	83	9.6	134	23	181	44	139	19	107	13	0.010	<1.155	17	2.6	2.2	12	13
102	Jt7 Ap14 - 04	602	1496	188	830	178	17	219	34	230	53	158	21	120	15	0.012	<1.233	25	3.8	1.3	6.1	17
103	Jt7 Ap14 - 05	388	937	117	525	114	11	157	25	181	43	133	18	100	12	0.024	<1.323	17	2.6	3.4	19	13
104	Jt7 Ap14 - 06	110	265	35	178	52	6.7	92	17	134	33	105	14	79	9.6	0.031	<1.288	13	2.0	3.0	14	9.3
105	Jt7 Ap14 - 07	310	742	94	435	102	11	147	24	175	42	130	17	99	12	0.020	<1.347	21	3.3	4.9	26	16
106	Jt7 Ap14 - 08	734	1804	220	951	191	17	231	35	246	56	174	23	133	16	0.021	<1.401	28	4.2	3.8	20	20
107	Jt7 Ap14 - 09	60	148	20	100	32	4.2	60	11	94	24	77	10	59	7.3	0.014	<1.353	6.9	1.0	2.0	9.8	5.0
108	Jt7 Ap14 - 10	429	1053	133	595	128	13	167	26	184	42	132	17	99	12	0.037	<1.300	16	2.5	2.4	13	12
109	Jt7 Ap14 - 11	476	1201	152	677	142	13	179	27	194	44	136	18	102	13	0.017	<1.193	17	2.6	3.8	21	13
110	Jt7 Ap14 - 12	297	695	87	392	96	12	149	26	202	49	157	21	123	15	0.013	<1.293	20	2.9	4.7	26	15
111	Jt7 Ap15 - 01	1039	2361	265	1101	224	21	269	41	287	64	193	25	144	18	0.024	<1.544	56	9.5	8.9	43	35
112	Jt7 Ap15 - 02	505	1299	173	815	195	19	270	43	304	69	213	28	159	19	0.033	<1.450	30	5.0	12	59	20
113	Jt7 Ap15 - 03	329	794	101	459	113	12	168	27	196	45	138	18	104	13	0.010	<1.305	24	3.8	3.8	19	16
114	Jt7 Ap15 - 04	558	1329	164	710	155	16	209	33	235	53	163	21	122	15	0.034	<1.358	24	3.8	4.4	21	16
115	Jt7 Ap15 - 05	668	1538	185	794	170	16	213	33	228	51	156	20	117	14	0.038	<1.245	32	5.5	6.5	31	21
116	Jt7 Ap15 - 06	745	1724	205	850	166	15	198	30	207	46	140	18	102	12	0.017	<1.316	26	4.5	5.9	28	17
117	Jt7 Ap15 - 07	654	1508	181	772	166	16	210	33	230	51	158	21	118	14	0.024	<1.422	30	5.1	6.6	31	19
118	Jt7 Ap15 - 08	707	1631	195	830	173	17	220	34	240	55	166	21	123	15	0.007	<1.394	28	4.6	5.8	28	18
119	Jt7 Ap15 - 09	559	1285	153	643	134	13	169	26	186	42	128	17	96	11	0.024	<1.327	24	3.9	5.1	25	15
120	Jt7 Ap16 - 01	623	1382	155	639	147	18	211	35	256	60	186	24	143	17	0.020	<1.259	34	5.5	11	56	22
121	Jt7 Ap16 - 02	6.8	23	4.0	24	9.8	1.5	21	3.8	29	6.9	21	2.6	15	1.8	<0.000	<1.272	0.395	0.160	0.096	0.077	0.180
122	Jt7 Ap16 - 03	638	1380	164	719	174	19	259	44	325	76	237	31	181	22	0.049	<1.093	61	10	10	48	39
123	Jt7 Ap16 - 04	443	1012	128	592	158	18	241	40	294	68	211	27	159	19	0.031	<1.183	51	8.4	10	49	33
124	Jt7 Ap16 - 05	968	2218	247	1063	236	24	318	49	351	79	241	31	182	22	0.048	<1.242	78	14	15	70	48
125	Jt7 Ap16 - 06	483	1074	128	549	124	13	173	28	209	47	148	19	109	13	0.021	<1.264	33	5.4	7.3	36	21
126	Jt7 Ap16 - 07	1292	2851	316	1307	265	26	341	54	385	87	271	36	205	25	0.033	<1.608	84	14	13	67	56
127	Jt7 Ap16 - 08	484	1099	128	574	138	15	204	35	257	60	188	25	142	17	0.021	<1.279	39	6.1	9.9	51	27
128	Jt7 Ap17 - 01	871	2011	228	965	203	22	255	40	274	63	196	26	148	19	0.068	<1.830	38	5.9	10	58	28
129	Jt7 Ap17 - 02	79	302	50	266	75	7.7	109	17	120	28	87	11	66	8.0	0.008	<1.638	5.0	0.874	0.881	4.1	3.6
130	Jt7 Ap17 - 03	889	1985	222	919	176	17	218	33	230	51	159	20	119	14	0.047	<1.601	38	5.9	8.2	43	26
131	Jt7 Ap17 - 04	120	316	43	212	58	6.1	85	14	98	23	71	9.4	53	6.5	<0.000	<1.778	5.8	0.954	1.3	7.3	4.2
132	Jt7 Ap17 - 05	758	1709	195	831	171	17	211	32	220	50	151	20	115	14	<0.000	<1.516	38	6.1	7.8	40	26
133	Jt7 Ap17 - 06	907	2226	254	1062	205	19	237	34	233	52	158	20	117	14	0.039	<1.621	29	4.6	5.8	33	20
134	Jt7 Ap17 - 07	335	771	93	407	89	9.6	117	18	131	30	92	12	68	8.6	<0.000	<1.529	15	2.4	3.6	18	9.6
135	Jt7 Ap17 - 09	978	2146	241	1030	226	24	309	48	338	77	241	32	186	23	0.064	<1.517	73	12	9.7	50	49
136	Jt7 Ap17 - 10	544	1420	194	910	225	22	287	44	304	67	206	27	153	19	0.014	<1.398	35	5.7	9.0	48	24
137	Jt7 Ap17 - 11	676	1458	172	761	177	21	254	41	292	68	214	28	165	21	0.015	<1.669	50	8.0	14	73	34
138	Jt7 Ap17 - 12	503	1245	163	766	180	17	232	35	239	53	159	21	116	15	<0.000	<1.648	36	6.2	8.9	44	24
139	Jt7 Ap17 - 13	802	1838	210	872	171	17	212	31	212	49	143	19	107	13	0.025	<1.670	24	3.9	6.9	36	17
140	Jt7 Ap17 - 14	1228	2783	307	1290	262	26	317	48	323	71	219	29	166	20	0.025	<1.592	75	13	19	102	52
141	Jt7 Ap17 - 15	1244	2613	285	1173	231	25	297	45	319	71	221	30	174	22	0.053	<1.906	57	9.3	12	64	41
142	Jt7 Ap17 - 16	561	1375	173	771	171	17	225	34	237	54	162	22	125	15	0.016	<1.706	22	3.4	6.3	18	15
143	Jt7 Ap17 - 18	492	1280	172	811	194	19	260	41	279	62	192	25	145	18	0.024	<1.344	29	4.6	6.1	33	21
144	Jt7 Ap17 - 21	823	2091	251	1073	211	19	242	34	227	48	148	19	107	13	0.031	<1.456	25	4.1	4.6	24	17
145	Jt7 Ap17 - 22	9.7	32	5.2	31	13	1.8	24	4.4	32	8.0	25	3.2	17	2.1	0.006	<1.547	0.810	0.215	0.123	0.167	0.438
146	Jt7 Ap17 - 23	1352	3063	341	1364	240	22	252	34	217	46	136	17	99	12	0.036	<1.665	39	6.6	10	53	26
147	Jt7 Ap17 - 24	1003	2275	255	1035	194	20	229	33	221	49	150	19	112	14	0.007	<1.535	33	5.4	7.5	38	23
148	Jt7 Ap17 - 25	674	1765	222	989	218	21	287	45	318	73	225	31	173	22	0.054	<1.629	48	7.2	0.925	4.4	35
149	Jt7 Ap17 - 26	1325	3031	336	1332	231	21	244	34	217	47	141	18	101	13	0.018	<1.678	34	5.5	10	50	22
150	Jt7 Ap17 - 27	779	1774	203	854	172	19	213	32	231	52	160	21	121	15	0.021	<1.693	27	4.2	7.0	37	20
151	Jt7 Ap17 - 28	615	1406	170	722	156	18	205	32	226	51	159	21	118	14	0.026	<1.363	26	4.1	5.9	31	18
152	Jt7 Ap17 - 29	681	1554	188	816	181	20	245	38	272	62	192	26	147	18	0.034	<1.696	34	5.3	7.5	39	24
153	Jt7 Ap17 - 30	808	1752	198	824	172	18	218	34	244	56	174	23	136	17	0.031	<1.544	39	5.8	6.9	36	27
154	Jt7 Ap17 - 31	209	733	113	548	132	8.0	150	22	141	31	94	12	68	8.6	0.019	<1.703	3.8	0.805	1.0	4.2	2.4
155	Jt7 Ap17 - 32	11	40	7.5	46	16	2.2	29	4.8	33	7.8	23	2.8	16	1.9	<0.000	<1.623	0.726	0.191	0.177	0.527	0.393
156	Jt7 Ap17 - 33	223	526	67	311	79	9.6	126	23	179	44	142	19	110	13	0.014	<1.570	14	2.0	3.1	17	10
157	Jt7 Ap17 - 34	882	2221	268	1145	229	21	259	37	240	52	152	20	112	14	0.027	<1.698	29	4.9	5.8	28	19
	Mean (n=157)	573	1361	164	714	154	15	198	30	213	48	148	19	111	14	0.235	-	28	4.6	5.8	29	19
	SD	370	844	96	397	76	6.5	82	11	75	16	51	6.7	39	4.8	2.5	-	17	2.9	3.9	20	11
	Median	554	1329	164	726	162	16	211	33	226	51	156	20	116	14	0.024	-	27	4.4	5.7	27	19
	Max	1781	3981	436	1702	352	27	377	54	385	87	271	36	205	25	31	-	84	15	19	102	56
	Min	6.6	22	4.0	24	9.8	1.5	21	3.8	29	6.9	21	2.6	15	1.8	0.003	-	0.395	0.160	0.095	0.028	0.180

#	Sample Jt10	La	Ce	Pr	Nd	Sm	Eu	Gad	Tb	Dy	Ho	Er	Tm	Yb	Lu	Hf	^{204}Pb	^{206}Pb	^{207}Pb	^{208}Pb	Th	U
1	Jt10 Ap1 - 01	9.6	37	7.2	48	27	2.2	70	14	102	22	58	6.4	32	3.5	0.011	<1.085	1.4	0.263	0.220	0.685	0.800
2	Jt10 Ap1 - 02	9.8	36	6.8	46	25	1.9	61	12	86	18	49	5.4	27	2.9	0.024	<1.132	1.0	0.210	0.224	0.567	0.435
3	Jt10 Ap1 - 03	15	59	11	73	37	2.7	86	16	122	26	70	8.0	40	4.2	0.003	<1.069	5.0	1.1	1.1	1.2	0.696
4	Jt10 Ap1 - 04	12	45	8.5	56	28	2.1	68	13	94	20	53	6.0	30	3.1	0.007	<1.087	5.3	1.2	1.2	1.4	0.532
5	Jt10 Ap1 - 05	10.0	35	6.6	44	22	1.7	58	11	81	17	43	4.8	24	2.5	0.006	<1.366	3.8	0.782	0.453	0.376	1.2
6	Jt10 Ap1 - 06	11	43	8.3	56	29	2.3	69	14	101	22	58	6.5	33	3.6	0.014	<1.276	1.2	0.289	0.265	0.659	0.544
7	Jt10 Ap1 - 07	27	113	22	147	68	5.3	151	29	220	48	131	15	80	9.0	0.038	<1.263	3.7	0.602	0.660	3.0	2.5
8	Jt10 Ap1 - 08	14	46	8.8	59	34	2.9	80	15	102	21	53	5.6	29	3.3	<0.000	<2.693	1.2	0.258	0.510	1.4	0.612
9	Jt10 Ap1 - 09	13	49	9.6	64	33	2.5	80	16	124	27	70	7.9	40	4.5	0.035	<1.543	2.6	0.458	0.563	2.2	1.9
10	Jt10 Ap1 - 10	15	47	8.2	51	25	1.9	62	12	85	18	44	4.6	22	2.2	0.021	<1.010	2.7	0.698	0.534	1.4	0.562
11	Jt10 Ap1 - 11	8.6	32	6.1	42	22	1.9	56	11	81	17	45	5.0	25	2.6	<0.000	<1.058	0.614	0.144	0.104	0.193	0.301
12	Jt10 Ap1 - 12	27	107	21	138	69	5.5	162	33	256	57	159	19	99	11	0.034	<1.350	10	1.5	2.3	13	7.4
13	Jt10 Ap1 - 13	10	40	7.8	54	28	2.4	73	14	109	23	63	7.1	36	3.9	0.007	<1.173	1.4	0.256	0.213	0.599	0.729
14	Jt10 Ap1 - 14	14	51	10.0	68	35	2.7	81	15	109	23	60	6.6	33	3.7	<0.000	<1.456	2.0	0.415	0.493	1.5	1.2
15	Jt10 Ap1 - 15	9.7	38	7.2	49	25	1.9	58	11	84	19	51	5.6	28	3.1	0.008	<1.856	4.9	0.563	0.143	0.324	2.3
16	Jt10 Ap1 - 16	9.3	36	6.6	47	24	1.9	57	10	70	14	37	3.9	19	2.1	<0.000	<1.069	5.5	1.0	0.341	2.5	1.7
17	Jt10 Ap2 - 01	9.7	39	7.7	53	29	2.2	73	14	106	23	64	7.2	37	4.0	0.013	<1.096	1.2	0.233	0.346	1.1	0.693
18	Jt10 Ap2 - 02	11	42	8.1	56	29	2.4	73	14	110	24	64	7.1	36	4.0	0.010	<1.121	1.1	0.301	0.695	2.8	0.554
19	Jt10 Ap2 - 03	12	48	9.2	63	34	2.7	84	17	126	27	73	8.2	42	4.6	0.003	<1.156	1.8	0.405	0.405	1.0	1.1
20	Jt10 Ap2 - 04	13	43	7.4	47	23	1.9	59	11	81	16	42	4.5	22	2.3	0.010	<1.141	0.815	0.285	0.187	0.174	0.222
21	Jt10 Ap2 - 05	9.5	37	7.2	50	27	2.2	67	13	96	20	56	6.2	31	3.5	0.014	<1.226	0.790	0.166	0.165	0.687	0.531
22	Jt10 Ap2 - 06	9.4	38	7.5	50	26	2.1	66	13	98	21	58	6.5	33	3.6	0.007	<1.125	0.824	0.161	0.270	1.0	0.550
23	Jt10 Ap2 - 07	8.3	33	6.5	43	23	2.0	60	11	86	19	50	5.7	29	3.1	0.010	<1.063	0.902	0.191	0.191	0.715	0.514
24	Jt10 Ap2 - 08	14	60	12	85	43	3.5	100	19	147	32	88	10	53	6.0	0.011	<1.697	3.7	0.588	1.1	5.4	2.8
25	Jt10 Ap2 - 09	20	88	18	123	63	5.0	142	28	210	46	128	15	79	8.8	0.020	<1.601	7.4	1.0	1.7	8.8	5.2
26	Jt10 Ap2 - 10	10	36	6.5	45	24	2.0	60	12	89	19	48	5.4	26	2.8	0.007	<1.332	0.766	0.215	0.241	0.716	0.378
27	Jt10 Ap2 - 11	11	37	6.7	45	22	1.9	56	11	78	16	40	4.3	21	2.2	0.004	<1.327	0.638	0.212	0.126	0.186	0.256
28	Jt10 Ap3 - 01	12	48	9.7	68	36	3.0	81	13	88	17	43	4.8	23	2.5	0.021	<1.687	5.9	0.993	0.292	0.188	3.1
29	Jt10 Ap3 - 02	14	60	12	78	37	2.9	77	15	110	24	67	7.7	39	4.3	0.005	<1.530	1.6	0.279	0.107	0.165	1.1
30	Jt10 Ap3 - 03	9.8	38	7.2	50	26	2.0	63	13	92	20	52	5.9	29	3.2	0.010	<1.313	0.909	0.173	0.133	0.209	0.448
31	Jt10 Ap3 - 04	9.3	36	7.0	49	26	2.2	67	13	96	20	54	6.1	31	3.5	0.010	<1.178	0.721	0.157	0.107	0.196	0.438
32	Jt10 Ap3 - 05	9.0	34	6.3	42	23	1.8	58	11	85	18	49	5.2	27	2.9	<0.000	<1.256	2.5	0.474	0.217	0.179	1.5
33	Jt10 Ap3 - 06	8.9	37	7.1	48	25	2.0	60	12	90	20	52	5.8	29	3.1	0.016	<1.741	1.4	0.283	0.227	0.271	0.610
34	Jt10 Ap3 - 07	12	44	8.6	57	29	2.2	65	12	91	19	52	5.6	29	3.1	<0.000	<1.278	2.7	0.461	0.220	0.204	1.2
35	Jt10 Ap3 - 08	12	47	9.0	60	31	2.4	73	14	107	22	61	6.7	34	3.9	<0.000	<1.546	0.888	0.238	0.164	0.249	0.436
36	Jt10 Ap3 - 09	12	45	8.6	56	29	2.3	67	13	98	21	56	6.3	31	3.6	<0.000	<1.646	1.4	0.266	0.154	0.412	0.934
37	Jt10 Ap3 - 10	10	39	7.8	54	30	2.2	70	13	89	19	48	5.3	26	2.8	0.007	<1.204	0.795	0.190	0.139	0.247	0.417
38	Jt10 Ap3 - 11	14	55	10	68	32	2.5	72	13	95	21	55	6.2	31	3.4	0.007	<1.238	4.6	0.939	0.364	0.263	2.2
39	Jt10 Ap3 - 12	11	43	8.4	55	28	2.1	66	13	93	20	52	5.9	31	3.3	0.010	<1.895	3.8	0.706	0.198	0.353	1.3
40	Jt10 Ap3 - 14	13	44	8.1	53	27	2.2	65	11	77	15	38	4.0	19	2.1	0.045	<1.298	6.9	1.3	0.395	0.261	2.2
41	Jt10 Ap3 - 15	12	51	10.0	69	35	2.8	80	15	109	23	61	6.9	35	3.9	0.013	<1.268	1.4	0.246	0.309	1.4	0.930
42	Jt10 Ap4 - 01	11	43	8.2	56	32	2.5	77	15	113	24	65	7.4	38	4.1	0.013	<1.392	1.7	0.312	0.494	2.2	1.2
43	Jt10 Ap4 - 02	14	50	9.5	65	34	2.5	85	16	122	27	72	8.3	44	4.9	0.026	<1.313	2.1	0.424	0.523	1.6	1.8
44	Jt10 Ap4 - 03	11	45	8.8	60	32	2.5	80	16	122	27	71	8.1	41	4.6	0.017	<1.328	1.4	0.277	0.527	2.7	0.983
45	Jt10 Ap4 - 04	16	60	12	77	36	2.8	86	17	128	28	76	8.6	45	5.1	0.018	<1.165	2.0	0.324	0.438	2.4	1.4
46	Jt10 Ap4 - 05	11	42	8.2	57	29	2.5	70	13	96	20	53	6.0	30	3.4	0.010	<1.212	0.827	0.168	0.179	0.567	0.490
47	Jt10 Ap4 - 06	14	50	9.4	63	32	2.8	75	14	103	21	57	6.3	33	3.5	0.003	<1.125	1.1	0.228	0.297	1.0	0.680
48	Jt10 Ap4 - 07	9.4	32	5.7	40	22	2.0	57	9.8	64	12	29	2.9	13	1.3	<0.000	<1.130	0.621	0.230	0.152	0.117	0.541
49	Jt10 Ap4 - 08	9.5	37	7.2	49	26	2.1	61	12	93	20	55	6.0	31	3.5	0.007	<1.142	0.670	0.154	0.126	0.328	0.407
50	Jt10 Ap4 - 09	12	41	7.4	49	24	1.9	62	12	84	18	47	5.3	26	2.9	0.014	<1.154	0.911	0.316	0.282	0.348	0.333
51	Jt10 Ap4 - 10	11	41	7.8	51	26	2.0	61	12	89	19	52	6.0	30	3.2	0.014	<1.179	0.949	0.176	0.107	0.213	1.2
52	Jt10 Ap4 - 11	11	45	8.8	61	32	2.6	79	15	116	26	69	7.9	40	4.6	0.012	<1.186	1.2	0.210	0.305	1.2	0.796
53	Jt10 Ap4 - 12	9.7	37	7.1	48	26	2.0	67	13	95	20	52	6.0	30	3.3	0.014	<1.205	0.844	0.182	0.153	0.263	0.592
54	Jt10 Ap4 - 13	13	51	9.8	67	35	2.9	84	15	114	24	64	7.4	36	4.0	0.015	<1.237	1.3	0.253	0.380	1.3	0.890
55	Jt10 Ap4 - 14	16	69	14	94	49	3.6	111	22	169	37	102	12	62	7.1	0.017	<1.752	4.7	0.687	1.1	5.9	3.4
56	Jt10 Ap5 - 01	12	48	9.3	65	34	2.8	82	16	123	27	74	8.5	43	4.8	0.020	<1.470	1.5	0.249	0.360	1.5	0.989
57	Jt10 Ap5 - 02	14	59	12	79	39	3.0	88	17	128	28	77	9.0	46	5.2	0.022	<1.484	1.3	0.204	0.187	0.872	0.878
58	Jt10 Ap5 - 03	10	43	9.0	59	32	2.6	78	16	120	26	73	8.2	43	4.8	0.021	<1.285	1.2	0.207	0.196	0.673	0.695
59	Jt10 Ap5 - 04	9.2	39	8.0	56	30	2.6	75	15	119	26	71	8.3	42	4.6	0.019	<1.368	0.939	0.189	0.145	0.499	0.619
60	Jt10 Ap5 - 05	8.2	33	6.6	46	25	2.1	63	12	95	21	56	6.3	33	3.6	0.004	<1.184	1.1	0.212	0.159	0.382	0.475
61	Jt10 Ap5 - 06	19	81	16	110	54	4.1	121	23	177	39	110	13	68	7.6	<0.000	<1.364	6.2	0.922	2.1	12	4.3

#	Sample Jt10	La	Ce	Pr	Nd	Sm	Eu	Gad	Tb	Dy	Ho	Er	Tm	Yb	Lu	Hf	^{204}Pb	^{206}Pb	^{207}Pb	^{208}Pb	Th	U
62	Jt10 Ap5 - 07	10.0	41	8.4	59	32	2.6	79	16	124	27	75	8.8	45	4.9	0.018	<1.228	1.4	0.232	0.320	1.2	0.925
63	Jt10 Ap5 - 08	8.2	34	6.9	47	26	2.0	63	12	97	21	58	6.6	33	3.6	0.024	<1.133	0.713	0.128	0.106	0.260	0.427
64	Jt10 Ap5 - 09	13	59	12	81	43	3.5	97	19	144	32	89	9.9	54	6.0	0.019	<1.902	6.2	0.945	1.5	7.4	3.4
65	Jt10 Ap5 - 10	11	48	9.7	65	33	2.6	81	16	121	27	74	8.6	44	5.0	0.008	<1.405	1.4	0.229	0.267	1.1	0.783
66	Jt10 Ap5 - 11	8.7	35	6.7	46	24	2.1	62	12	93	20	55	6.3	32	3.4	<0.000	<1.296	0.775	0.150	0.090	0.295	0.407
67	Jt10 Ap5 - 12	11	39	6.8	47	25	2.1	65	12	86	18	43	4.6	22	2.2	0.028	<1.195	1.0	0.250	0.148	0.166	0.957
68	Jt10 Ap5 - 13	8.4	33	6.6	44	24	2.0	65	13	101	22	62	6.8	35	3.8	0.010	<1.243	1.2	0.211	0.103	0.436	1.2
69	Jt10 Ap5 - 15	8.4	33	6.7	46	26	2.2	67	13	97	21	56	6.2	31	3.4	0.015	<1.145	0.700	0.149	0.128	0.268	0.466
70	Jt10 Ap5 - 16	11	44	8.3	58	29	2.3	68	13	99	21	59	6.7	34	3.8	0.016	<1.488	1.7	0.352	0.205	0.228	1.1
71	Jt10 Ap5 - 17	12	49	9.5	63	31	2.5	71	13	99	21	58	6.5	34	3.6	<0.000	<1.367	1.1	0.190	0.119	0.140	1.1
72	Jt10 Ap6 - 01	12	50	10	70	35	2.9	86	17	128	28	76	8.6	45	5.0	0.021	<1.264	1.2	0.190	0.775	4.0	0.764
73	Jt10 Ap6 - 02	14	56	11	73	39	3.1	89	18	135	29	80	9.2	48	5.4	0.022	<1.032	1.1	0.184	0.794	3.8	0.766
74	Jt10 Ap6 - 03	10.0	38	6.9	49	26	2.4	67	13	93	19	51	5.5	28	3.0	0.007	<1.071	1.0	0.199	0.229	0.931	0.590
75	Jt10 Ap6 - 05	21	78	16	122	74	10	155	22	121	18	39	3.7	17	1.7	0.008	<1.260	6.1	0.969	0.715	2.7	2.9
76	Jt10 Ap6 - 06	26	115	26	215	132	13	277	41	234	37	79	7.7	36	3.4	<0.000	<2.117	6.9	1.2	0.828	2.7	3.2
77	Jt10 Ap6 - 07	9.1	32	6.2	45	33	4.1	98	18	108	17	35	3.4	15	1.6	0.014	<1.296	1.6	0.237	0.087	0.325	1.3
78	Jt10 Ap6 - 08	17	68	14	104	62	8.5	133	20	110	16	32	3.0	14	1.3	0.014	<1.261	1.3	0.192	0.091	0.295	0.988
79	Jt10 Ap6 - 09	20	82	16	107	52	4.5	113	21	155	34	93	11	54	6.3	0.015	<1.182	1.3	0.201	0.298	1.5	0.938
80	Jt10 Ap6 - 10	17	65	13	86	46	12	105	19	129	25	64	7.3	37	4.0	0.004	<1.144	1.7	0.278	0.391	2.0	1.3
81	Jt10 Ap6 - 11	46	188	36	234	107	8.5	220	40	292	63	171	21	107	12	0.032	<1.173	6.7	0.926	0.497	2.6	4.8
82	Jt10 Ap6 - 12	29	121	26	210	131	15	308	46	251	37	73	6.6	28	2.6	0.017	<1.270	1.7	0.223	0.130	0.547	1.3
83	Jt10 Ap6 - 14	17	79	15	104	51	4.0	120	23	179	39	108	13	65	7.2	0.019	<1.541	2.4	0.377	0.292	1.1	1.7
84	Jt10 Ap7 - 01	12	43	7.8	51	25	2.8	60	11	82	17	44	4.8	23	2.5	0.018	<1.357	0.741	0.170	0.078	0.100	0.423
85	Jt10 Ap7 - 02	23	87	17	120	61	15	122	18	101	17	38	4.0	19	2.1	0.015	<1.333	0.799	0.156	0.068	0.174	0.547
86	Jt10 Ap7 - 03	18	57	10	71	39	4.4	101	18	124	23	56	5.8	29	3.1	0.005	<1.494	6.1	0.902	0.385	1.9	2.3
87	Jt10 Ap7 - 04	16	61	12	77	39	3.2	95	17	120	24	61	6.8	34	3.7	0.003	<1.204	1.4	0.227	0.120	0.361	0.709
88	Jt10 Ap7 - 05	14	47	8.9	65	41	5.4	107	19	122	23	57	6.2	32	3.8	0.011	<1.378	3.4	0.458	0.152	0.355	2.2
89	Jt10 Ap7 - 06	15	54	11	70	40	4.6	99	17	111	20	50	5.6	29	3.1	0.016	<1.524	3.7	0.463	0.506	2.8	2.9
90	Jt10 Ap7 - 07	21	60	9.8	62	40	5.3	126	24	180	38	104	12	63	7.2	0.017	<1.705	3.4	0.463	1.3	6.6	2.4
91	Jt10 Ap7 - 08	8.9	29	5.6	41	28	3.5	75	13	81	13	30	2.8	15	1.5	<0.000	<1.715	2.1	0.272	0.173	1.0	1.6
92	Jt10 Ap7 - 09	13	42	7.6	55	38	4.5	105	18	116	20	47	4.6	22	2.6	0.014	<1.258	2.7	0.380	0.173	0.734	2.1
93	Jt10 Ap7 - 10	26	87	16	111	67	7.4	182	31	197	37	92	9.8	50	5.7	0.017	<1.134	4.2	0.659	0.334	1.4	2.7
94	Jt10 Ap7 - 11	18	62	12	80	48	5.3	113	19	120	21	54	6.0	32	3.6	0.007	<1.168	3.0	0.414	0.286	1.2	2.3
95	Jt10 Ap7 - 12	50	194	37	243	106	10	172	23	122	20	46	4.8	23	2.6	<0.000	<1.658	4.0	0.620	0.403	4.0	1.9
96	Jt10 Ap7 - 13	19	66	12	79	43	6.5	96	16	100	19	49	5.6	28	3.1	0.033	<1.590	3.4	0.476	0.389	3.1	2.6
97	Jt10 Ap7 - 14	28	119	25	180	90	8.7	179	26	140	22	47	4.8	24	2.6	0.011	<1.213	2.1	0.330	0.267	1.7	1.2
98	Jt10 Ap7 - 15	21	57	8.9	54	32	15	94	18	128	26	70	8.1	40	4.7	0.011	<1.224	3.5	0.485	0.268	1.4	2.9
99	Jt10 Ap7 - 16	16	75	18	152	95	14	226	34	198	32	69	6.8	31	2.7	0.027	<1.335	1.0	0.161	0.099	0.490	0.744
100	Jt10 Ap7 - 17	15	48	8.5	57	31	2.7	78	13	86	16	37	3.8	17	1.8	0.004	<1.392	0.900	0.258	0.189	0.360	0.414
101	Jt10 Ap7 - 18	29	135	31	254	136	14	253	34	181	28	60	5.8	26	2.7	0.032	<1.326	2.3	0.362	0.207	0.856	1.6
102	Jt10 Ap7 - 19	32	131	28	213	121	12	262	39	205	32	69	6.8	32	2.9	0.040	<1.360	5.1	0.822	0.616	2.4	3.0
103	Jt10 Ap7 - 20	20	72	14	95	52	5.4	126	21	132	23	54	5.7	29	3.0	0.004	<1.404	2.0	0.349	0.145	0.774	1.2
104	Jt10 Ap8 - 01	17	69	13	83	35	2.4	69	12	89	19	52	5.9	31	3.4	0.011	<1.301	0.621	0.114	0.048	0.086	0.363
105	Jt10 Ap8 - 02	18	71	13	84	36	2.4	71	12	86	19	52	5.7	29	3.4	0.012	<1.833	0.793	0.164	0.128	0.244	0.367
106	Jt10 Ap8 - 03	23	92	18	116	51	3.5	106	20	144	33	89	10	52	5.8	0.025	<2.195	3.6	0.517	0.911	4.5	2.5
107	Jt10 Ap8 - 04	212	610	95	538	199	14	384	74	562	124	344	41	223	25	0.067	<1.074	32	4.6	11	60	23
108	Jt10 Ap8 - 05	1088	2685	333	1529	383	26	555	96	685	145	407	49	268	30	0.053	<1.275	57	9.0	17	86	38
109	Jt10 Ap8 - 06	370	1012	151	811	268	20	484	90	667	145	405	49	265	30	0.069	<1.417	44	6.4	14	75	31
110	Jt10 Ap8 - 07	23	95	19	130	64	5.1	145	29	218	47	131	15	81	9.0	0.020	<1.179	8.3	1.2	1.9	10	5.9
111	Jt10 Ap8 - 08	67	240	43	273	118	9.3	247	47	352	77	213	25	131	15	0.039	<1.302	14	1.9	4.2	24	9.9
112	Jt10 Ap8 - 10	73	231	39	240	99	7.7	214	41	307	65	180	21	107	12	0.018	<1.751	30	3.4	4.5	26	26
113	Jt10 Ap8 - 11	74	254	46	289	128	9.6	269	53	401	88	247	29	157	18	0.057	<1.323	20	2.8	7.2	39	14
114	Jt10 Ap8 - 12	32	129	25	171	84	6.6	200	40	315	69	186	22	115	13	0.017	<1.259	14	2.0	4.3	22	8.6
115	Jt10 Ap8 - 13	685	1195	122	453	94	6.0	175	33	247	53	148	17	87	9.9	0.022	<1.712	13	2.0	4.2	19	10
116	Jt10 Ap8 - 14	241	731	118	679	248	18	481	90	676	146	404	48	253	28	0.036	<1.178	35	5.0	9.6	52	24
117	Jt10 Ap8 - 15	67	219	37	210	80	5.7	151	27	200	44	120	14	72	8.3	0.017	<2.194	8.0	1.0	2.6	15	5.0
118	Jt10 Ap8 - 16	272	602	82	428	155	11	308	58	437	95	266	32	168	19	0.008	<1.810	35	5.9	10	32	16
119	Jt10 Ap8 - 17	51	199	38	245	113	8.2	232	45	347	76	211	25	135	15	0.011	<1.593	17	2.4	3.3	19	12
120	Jt10 Ap8 - 18	389	1099	165	883	299	22	516	96	706	155	431	53	283	32	0.063	<1.268	43	6.3	12	64	31
121	Jt10 Ap8 - 19	65	262	51	329	141	11	296	56	417	91	257	31	162	19	0.057	<1.760	30	4.3	5.1	30	25
122	Jt10 Ap8 - 20	86	317	59	366	152	11	303	56	417	90	251	30	156	18	0.040	<1.298	23	3.6	7.5	37	14

#	Sample Jt10	La	Ce	Pr	Nd	Sm	Eu	Gad	Tb	Dy	Ho	Er	Tm	Yb	Lu	Hf	^{204}Pb	^{206}Pb	^{207}Pb	^{208}Pb	Th	U
123	Jt10 Ap9 - 01	556	1506	219	1138	369	27	645	121	900	196	553	67	361	41	0.083	<1.181	67	10	14	68	45
124	Jt10 Ap9 - 02	359	1028	157	855	291	22	522	97	720	158	446	55	294	34	0.088	<1.207	42	6.3	12	61	30
125	Jt10 Ap9 - 03	99	360	66	414	178	13	358	67	519	114	321	39	205	23	0.052	<1.642	37	4.7	5.8	33	24
126	Jt10 Ap9 - 04	82	308	56	355	149	12	309	60	446	98	273	33	171	19	0.041	<1.082	34	5.4	8.2	34	17
127	Jt10 Ap9 - 05	27	134	28	201	101	8.0	237	47	359	81	230	27	149	17	0.045	<1.951	25	3.3	6.6	36	19
128	Jt10 Ap9 - 06	53	197	36	232	98	8.0	208	40	301	65	187	22	119	13	0.010	<1.971	31	5.1	7.2	31	16
129	Jt10 Ap9 - 07	90	323	60	371	157	12	317	60	459	100	282	34	184	20	0.027	<1.360	64	8.8	11	64	59
130	Jt10 Ap9 - 08	491	1345	197	1059	350	26	615	114	840	184	520	64	347	39	0.081	<1.237	49	7.1	14	77	34
131	Jt10 Ap9 - 09	286	875	141	804	284	21	525	98	733	159	447	54	290	33	0.095	<1.873	48	7.1	13	68	33
132	Jt10 Ap9 - 10	161	519	89	531	211	16	419	81	616	136	384	47	249	28	0.067	<1.188	32	4.4	10	57	24
133	Jt10 Ap9 - 11	20	90	19	133	69	5.3	162	32	243	54	151	18	96	11	0.062	<1.287	11	1.8	4.2	21	7.0
134	Jt10 Ap10 - 01	13	55	11	72	35	2.9	85	17	129	28	74	8.5	43	4.7	<0.000	<1.327	2.9	0.464	0.469	2.2	1.8
135	Jt10 Ap10 - 02	43	128	21	125	50	3.8	124	24	184	39	105	12	58	6.4	0.024	<1.561	25	3.4	1.8	3.7	17
136	Jt10 Ap10 - 03	12	48	9.4	61	28	1.9	61	11	83	18	47	5.3	25	2.8	0.016	<2.285	2.0	0.379	0.585	0.455	0.832
137	Jt10 Ap10 - 04	91	320	56	351	149	11	307	59	445	97	275	33	176	20	0.046	<1.349	24	3.4	5.4	29	17
138	Jt10 Ap10 - 05	17	75	15	102	50	4.1	113	22	167	36	98	12	60	6.7	<0.000	<1.742	3.9	0.591	0.870	5.5	3.3
139	Jt10 Ap10 - 06	21	92	18	124	62	4.8	138	26	205	43	124	14	76	8.3	0.029	<2.088	8.3	1.2	2.0	9.3	5.2
140	Jt10 Ap10 - 07	35	150	30	199	97	7.4	210	41	312	69	191	23	120	14	0.056	<1.286	18	2.6	4.3	22	11
141	Jt10 Ap10 - 08	92	341	62	398	173	13	363	70	527	116	324	39	210	23	0.030	<1.336	27	3.7	6.8	38	20
142	Jt10 Ap10 - 09	19	78	16	103	50	3.9	114	22	164	36	99	12	61	6.9	0.018	<1.310	4.6	0.663	1.1	5.8	3.2
143	Jt10 Ap10 - 10	23	102	20	141	73	5.7	172	34	254	56	157	19	98	11	0.021	<1.623	12	1.6	3.0	16	8.9
144	Jt10 Ap10 - 11	26	117	24	162	79	5.8	172	32	248	55	152	18	96	10	0.037	<1.540	12	2.0	3.0	11	5.6
145	Jt10 Ap10 - 12	25	111	22	152	70	5.3	151	28	212	46	128	15	78	8.9	0.011	<1.338	8.1	1.4	1.1	3.0	4.7
146	Jt10 Ap10 - 13	12	39	6.8	42	21	1.9	55	10	73	15	37	4.0	19	1.9	<0.000	<1.252	2.0	0.422	0.367	0.411	0.972
147	Jt10 Ap10 - 14	73	241	40	226	79	5.5	145	24	173	36	95	11	57	6.5	0.016	<1.192	8.2	1.5	2.6	10	4.1
148	Jt10 Ap10 - 15	517	1387	194	975	288	21	476	84	620	134	377	46	245	28	0.073	<0.999	38	5.7	11	56	26
149	Jt10 Ap10 - 16	12	49	9.5	65	32	2.7	77	15	113	25	66	7.4	39	4.1	0.020	<1.192	2.0	0.322	0.478	2.0	1.3
150	Jt10 Ap10 - 17	18	73	14	90	42	3.3	95	18	132	28	77	8.9	46	5.0	0.008	<1.671	2.4	0.386	0.741	3.8	1.8
151	Jt10 Ap12 - 04	19	77	15	95	43	3.3	104	19	146	32	87	9.7	48	5.0	0.007	<1.518	3.6	0.515	0.590	1.7	2.7
152	Jt10 Ap12 - 14	302	940	153	869	314	21	560	104	772	170	474	58	311	35	0.104	<1.550	45	6.5	11	61	34
153	Jt10 Ap13 - 01	51	159	27	158	67	5.7	143	26	190	40	108	13	65	7.1	0.008	<1.260	6.3	0.909	1.9	11	4.6
154	Jt10 Ap13 - 02	23	95	19	125	62	4.5	133	25	187	41	110	13	67	7.3	0.007	<1.391	7.7	1.1	2.0	11	5.9
155	Jt10 Ap13 - 03	15	58	11	72	35	2.6	77	14	102	22	58	6.4	32	3.4	0.008	<1.411	1.4	0.279	0.350	0.645	0.707
156	Jt10 Ap13 - 04	160	472	74	411	150	11	285	53	396	86	240	29	155	18	0.040	<1.213	23	3.4	5.3	28	16
157	Jt10 Ap13 - 05	52	224	46	311	152	11	318	60	461	100	282	33	183	21	0.129	<2.404	23	3.2	5.9	36	18
158	Jt10 Ap13 - 06	13	44	7.7	52	30	5.4	80	14	80	13	27	2.6	12	1.3	0.008	<1.423	1.2	0.209	0.262	1.0	0.749
159	Jt10 Ap13 - 07	75	265	48	297	128	9.5	268	51	382	83	229	27	138	16	0.051	<1.826	31	4.7	6.9	31	18
160	Jt10 Ap13 - 08	38	143	27	174	80	5.8	167	32	240	52	148	18	92	11	0.063	<2.632	41	5.9	4.0	21	32
161	Jt10 Ap13 - 09	50	219	44	293	134	9.5	279	54	405	88	245	29	149	17	0.036	<1.782	32	4.9	6.5	27	18
162	Jt10 Ap13 - 10	40	169	34	228	104	7.9	233	44	328	71	196	24	124	14	0.025	<2.412	16	2.3	3.7	20	12
163	Jt10 Ap13 - 11	72	292	58	375	169	13	353	67	503	112	313	38	200	22	0.087	<1.893	36	5.5	8.4	41	22
164	Jt10 Ap14 - 02	95	363	65	396	150	10	281	50	363	79	216	26	138	15	0.043	<1.765	18	2.7	4.4	25	13
165	Jt10 Ap14 - 07	71	252	48	272	109	7.5	216	40	299	64	176	21	111	12	0.070	<1.540	12	1.8	2.7	14	8.9
166	Jt10 Ap14 - 08	1279	3362	431	2039	530	36	759	130	920	194	543	66	359	40	0.089	<1.942	71	12	21	108	48
	Mean (n=166)	66	200	32	189	77	6.4	159	29	214	45	124	14	76	8.5	0.026	-	10	1.5	2.4	12	6.8
	SD	162	414	55	274	82	6.0	137	25	186	41	116	14	77	8.8	0.024	-	15	2.2	3.9	20	11
	Median	16	60	12	79	39	3.6	97	18	124	27	70	7.9	40	4.4	0.017	-	2.9	0.463	0.461	1.6	1.7
	Max	1279	3362	431	2039	530	36	759	130	920	196	553	67	361	41	0.129	-	71	12	21	108	59
	Min	8.2	29	5.6	40	21	1.7	55	9.8	64	12	27	2.6	12	1.3	0.003	-	0.614	0.114	0.048	0.086	0.222

*(Continued)

#	Sample Jt1	ΣLREE	ΣMREE	ΣHREE	ΣREY	Mg	Al	Si	P	Ca	Sc	Ti	V	Cr	Mn	Fe	Co	Ni	Cu	Zn	Ga	As	Sr	Y	Zr	Nb	Mo
1	Jt1 Ap 18 - 01	5937	1023	1850	8811	40	4.8	2301	224867	393600	0.239	0.345	0.976	<0.204	419	622	0.041	0.105	0.220	0.350	0.126	12	286	1494	0.372	0.020	0.028
2	Jt1 Ap 18 - 02	5554	1140	2321	9015	314	279	2867	221015	393600	0.249	18	1.8	<0.143	413	1410	0.377	0.301	0.180	0.834	0.442	10	291	1862	0.348	0.026	0.005
3	Jt1 Ap 18 - 03	9176	1133	1865	12174	63	25	2848	220077	393600	0.170	0.248	1.2	<0.144	440	786	0.054	0.061	0.158	0.293	0.247	13	270	1508	0.450	0.013	0.030
4	Jt1 Ap 18 - 04	9048	1148	1865	12061	41	0.569	2812	217518	393600	0.225	0.324	1.1	<0.128	438	676	0.032	<0.050	<0.152	0.383	0.201	13	273	1506	0.413	0.006	0.003
5	Jt1 Ap 18 - 05	6308	1115	2001	9424	83	39	2509	220573	393600	0.268	5.1	1.1	<0.152	422	761	0.108	0.132	<0.237	0.643	0.222	12	279	1614	0.402	0.018	0.144
6	Jt1 Ap 18 - 06	483	334	883	1700	27	3.7	544	219602	393600	0.105	0.925	0.384	<0.116	325	396	0.009	<0.032	<0.210	0.294	0.034	11	335	714	0.064	0.102	0.010
7	Jt1 Ap 18 - 07	3389	954	2253	6596	588	664	3214	216779	393600	0.205	82	3.6	<0.150	363	2041	0.809	1.0	<0.223	0.972	0.605	13	339	1816	0.275	0.121	0.008
8	Jt1 Ap 18 - 08	745	331	836	1912	253	149	1042	218213	393600	<0.064	1.1	0.679	<0.150	319	1006	0.166	0.111	0.526	0.573	0.154	12	351	678	0.089	0.056	0.009
9	Jt1 Ap 18 - 09	94	102	271	468	72	46	360	220759	393600	<0.075	3.6	0.652	<0.127	332	509	0.101	0.095	<0.264	0.302	0.064	12	378	224	0.005	0.060	0.008
10	Jt1 Ap 18 - 10	7809	1204	2004	11017	295	174	3094	214613	393600	0.279	0.230	1.6	0.152	427	1201	0.337	0.134	0.385	0.837	0.348	13	280	1614	0.654	0.023	0.025
11	Jt1 Ap 18 - 11	980	528	1332	2840	41	19	954	217024	393600	0.084	2.1	0.631	<0.138	332	437	0.019	<0.063	<0.231	<0.180	0.063	12	352	1078	0.129	0.053	<0.001
12	Jt1 Ap 18 - 12	5063	1005	1874	7941	334	286	2718	214131	393600	0.188	0.728	1.4	<0.135	411	1352	0.400	0.384	0.533	1.6	0.342	12	294	1511	0.351	0.031	0.004
13	Jt1 Ap 18 - 13	8208	1114	1805	11127	77	68	2889	212863	393600	0.205	<0.135	1.2	<0.139	428	820	0.051	<0.047	<0.208	0.599	0.207	13	287	1458	0.455	0.022	0.026
14	Jt1 Ap 18 - 14	8175	1122	1799	11097	41	0.948	2757	211386	393600	0.226	0.170	1.1	<0.131	430	657	0.022	<0.049	<0.182	<0.171	0.208	13	282	1454	0.506	0.014	0.006
15	Jt1 Ap 18 - 15	8486	1188	1948	11622	173	260	3396	212774	393600	0.274	9.0	2.0	0.308	425	1409	0.216	0.375	0.593	2.7	0.333	15	285	1573	0.538	0.030	0.038
16	Jt1 Ap 18 - 16	488	231	662	1380	224	288	1221	210023	393600	0.126	5.1	2.4	<0.112	337	1220	0.282	0.237	<0.185	0.679	0.504	9.7	422	536	0.081	0.206	0.003
17	Jt1 Ap 18 - 17	1241	427	977	2645	713	759	2750	210827	393600	0.108	85	3.7	<0.150	352	2420	0.893	0.840	0.977	1.5	0.589	9.1	314	790	0.524	0.100	0.072
18	Jt1 Ap 18 - 18	4308	558	977	5843	49	15	1387	210779	393600	<0.069	<0.143	0.795	<0.147	404	621	0.014	0.044	<0.218	0.553	0.137	9.4	266	790	0.200	0.011	0.017
19	Jt1 Ap 18 - 19	1959	752	1743	4454	1170	1718	4808	204289	393600	0.495	104	9.6	0.690	360	4224	1.5	1.4	0.645	2.5	1.8	11	334	1402	0.182	0.150	0.034
20	Jt1 Ap 18 - 20	1114	785	1991	3891	320	3.4	1637	208551	393600	0.129	0.273	0.660	<0.127	330	613	0.263	0.276	0.271	0.265	0.049	11	348	1602	0.224	0.056	0.005
21	Jt1 Ap 18 - 21	3190	1066	2494	6750	34	1.5	1866	207012	393600	0.237	<0.171	0.980	<0.121	380	546	0.018	0.056	<0.189	<0.192	0.086	11	319	2003	0.297	0.029	0.012
22	Jt1 Ap 18 - 22	4500	1096	2318	7914	392	446	2937	206922	393600	0.266	2.1	2.9	<0.138	400	2111	0.494	0.176	0.208	1.1	0.490	11	325	1860	0.786	0.023	0.015
23	Jt1 Ap 18 - 23	3186	978	2197	6362	265	284	2422	208524	393600	0.185	1.6	1.7	<0.146	387	2163	0.278	0.242	0.291	0.996	0.214	10	316	1763	0.801	0.023	0.022
24	Jt1 Ap 18 - 24	1001	427	996	2424	84	93	832	209747	393600	0.077	0.803	0.862	<0.139	345	658	0.083	0.089	0.253	0.281	0.065	10	340	806	0.356	0.022	0.015
25	Jt1 Ap 18 - 25	520	184	398	1102	42	16	447	211894	393600	<0.071	<0.114	0.255	<0.127	363	545	0.026	0.044	<0.156	0.353	0.045	8.3	275	324	0.162	0.015	0.006
26	Jt1 Ap 18 - 26	424	184	397	1004	52	19	565	214116	393600	<0.074	1.8	0.277	<0.170	366	533	0.062	0.222	0.277	0.665	0.039	8.7	279	323	0.118	0.013	0.008
	Mean (n=26)	3899	774	1541	6214	223	218	2122	214034	393600	0.207	15	1.7	0.383	383	1144	0.255	0.302	0.394	0.840	0.291	11	312	1242	0.338	0.048	0.022
	SD	3163	383	674	3984	264	368	1129	5266	0.000	0.117	29	1.9	0.147	41	862	0.343	0.341	0.261	0.685	0.348	1.5	39	540	0.215	0.049	0.029
	Median	3290	966	1828	6479	83	57	2465	213490	393600	0.205	1.7	1.1	0.308	384	773	0.105	0.176	0.284	0.643	0.207	12	304	1476	0.349	0.025	0.012
	Max	9176	1204	2494	12174	1170	1718	4808	224867	393600	0.495	104	9.6	0.690	440	4224	1.5	1.4	0.977	2.7	1.8	15	422	2003	0.801	0.206	0.144
	Min	94	102	271	468	27	0.569	360	204289	393600	0.077	0.170	0.255	0.152	319	396	0.009	0.044	0.158	0.265	0.034	8.3	266	224	0.005	0.006	0.003

#	Sample Jt1	Sn	Sb	Ba	La	Ce	Pr	Nd	Sm	Eu	Gd	Tb	Dy	Ho	Er	Tm	Yb	Lu	Hf	Ta	W	^{204}Pb	^{206}Pb	^{207}Pb	^{208}Pb	Th	U
1	Jt1 Ap 18 - 01	<0.100	0.037	0.561	1172	2854	362	1549	320	35	333	49	287	57	152	19	113	16	0.021	0.009	1.7	<0.011	9.5	1.4	6.4	67	28
2	Jt1 Ap 18 - 02	0.079	0.069	3.1	1157	2666	329	1402	316	42	370	58	354	72	193	24	148	21	0.027	0.011	1.4	<0.007	10	1.5	5.9	64	32
3	Jt1 Ap 18 - 03	<0.061	0.066	0.511	2005	4526	528	2117	380	37	366	51	299	59	153	19	111	15	0.020	0.006	0.982	<0.006	12	1.9	7.6	78	36
4	Jt1 Ap 18 - 04	0.103	0.075	0.375	1958	4444	524	2121	385	38	375	52	298	58	155	19	112	15	0.032	0.007	0.749	<0.005	13	1.9	7.7	78	36
5	Jt1 Ap 18 - 05	0.083	0.055	1.6	1219	3029	389	1671	348	39	363	53	312	62	164	21	123	17	0.030	0.005	1.3	<0.006	11	1.6	6.3	64	33
6	Jt1 Ap 18 - 06	<0.053	0.022	1.6	77	208	31	167	63	12	108	20	131	27	73	8.9	52	7.5	0.005	0.005	7.0	<0.005	2.1	0.281	1.2	13	7.1
7	Jt1 Ap 18 - 07	0.084	0.133	11	681	1594	203	912	227	34	307	52	334	69	186	23	139	19	0.042	0.012	4.4	<0.007	7.5	0.994	4.8	56	25
8	Jt1 Ap 18 - 08	0.082	0.049	1.8	134	338	46	227	68	12	108	19	124	26	69	8.1	48	6.7	0.010	0.003	6.9	<0.007	2.5	0.357	1.5	16	7.5
9	Jt1 Ap 18 - 09	<0.224	0.015	1.7	11	37	6.7	40	18	3.9	34	6.2	40	8.3	21	2.4	13	1.8	0.008	0.000	6.2	<0.006	0.232	0.041	0.074	0.126	0.486
10	Jt1 Ap 18 - 10	<0.281	0.080	0.431	1602	3762	465	1980	391	43	393	55	322	63	167	21	124	17	0.020	0.007	1.4	<0.005	13	2.0	9.0	93	38
11	Jt1 Ap 18 - 11	<0.115	0.072	1.4	157	432	63	328	107	19	171	31	199	41	109	13	79	11	0.014	0.005	4.3	<0.007	3.2	0.417	1.8	20	11
12	Jt1 Ap 18 - 12	0.161	0.069	0.588	948	2406	317	1392	304	36	327	49	289	58	153	19	116	16	0.023	0.005	2.2	<0.006	8.6	1.2	5.4	57	26
13	Jt1 Ap 18 - 13	<0.082	0.065	0.221	1703	4006	486	2013	373	38	362	51	290	57	149	18	108	15	0.031	0.003	1.4	<0.005	11	1.6	7.3	75	34
14	Jt1 Ap 18 - 14	<0.071	0.078	0.411	1684	3988	485	2019	374	39	367	51	292	57	147	18	108	15	0.027	0.010	1.4	<0.006	12	1.7	7.3	76	35
15	Jt1 Ap 18 - 15	<0.075	0.099	2.4	1800	4090	497	2098	394	46	384	54	310	61	160	20	118	16	0.030	0.007	1.7	<0.007	12	1.6	7.6	79	35
16	Jt1 Ap 18 - 16	<0.088	0.157	2.4	90	227	29	141	45	8.0	73	13	91	20	55	6.5	38	5.4	0.007	0.003	14	<0.005	1.4	0.202	0.937	9.6	4.7
17	Jt1 Ap 18 - 17	<0.064	0.042	12	246	566	74	354	100	17	139	23	147	30	80	9.9	59	8.3	0.053	0.007	7.2	<0.007	2.7	0.370	2.9	32	8.6
18	Jt1 Ap 18 - 18	<0.070	0.020	0.348	976	2122	244	965	176	19	183	26	154	31	81	10.0	58	8.1	0.018	0.005	0.905	<0.006	5.5	0.818	3.1	32	16
19	Jt1 Ap 18 - 19	<0.065	0.543	14	353	911	122	573	173	30	243	41	265	55	145	18	107	15	0.019	0.010	5.5	<0.006	7.3	1.1	5.1	57	20
20	Jt1 Ap 18 - 20	<0.079	0.145	0.884	167	469	73	405	157	29	255	46	299	62	166	20	123	18	0.033	0.010	4.4	0.006	5.6	0.702	3.6	42	19
21	Jt1 Ap 18 - 21	<0.074	0.148	0.341	607	1478	195	909	250	40	345	58	371	77	207	26	158	23	0.034	0.007	3.2	<0.007	8.9	1.2	5.8	66	30
22	Jt1 Ap 18 - 22	<0.055	0.332	0.957	944	2117	262	1176	286	39	361	57	353	72	192	24	148	21	0.028	0.011	3.2	<0.006	9.0	1.2	12	135	28
23	Jt1 Ap 18 - 23	<0.057	0.147	0.910	638	1467	190	892	240	36	320	53	329	68	183	23	141	20	0.025	0.011	3.4	<0.006	6.7	0.887	8.9	99	22
24	Jt1 Ap 18 - 24	<0.067	0.064	0.629	181	448	62	311	97	16	139	24	150	31	81	10	59	8.3	0.004	0.003	2.2	<0.007	2.3	0.333	2.0	22	7.5
25	Jt1 Ap 18 - 25	<0.062	0.057	0.342	93	234	32	162	46	7.2	62	9.8	59	12	32	3.8	22	3.1	<0.000	0.003	1.1	<0.007	1.5	0.267	0.447	4.0	4.5
26	Jt1 Ap 18 - 26	0.078	0.023	0.342	65	185	28	145	45	7.1	61	10.0	60	12	32	3.9	22	3.2	0.013	0.001	0.999	<0.007	0.676	0.132	0.355	2.7	1.9
	Mean (n=26)	0.096	0.102	2.4	795	1869	232	1003	219	28	252	39	237	48	127	16	94	13	0.023	0.006	3.4	-	6.9	0.991	4.8	51	21
	SD	0.046	0.111	3.8	677	1554	185	752	132	13	124	18	105	21	56	7.1	43	6.1	0.012	0.003	3.0	-	4.3	0.627	3.2	34	13
	Median	0.083	0.069	0.897	659	1536	199	911	233	35	314	49	290	57	150	19	110	15	0.023	0.007	2.2	-	7.4	1.0	5.3	57	23
	Max	0.161	0.543	14	2005	4526	528	2121	394	46	393	58	371	77	207	26	158	23	0.053	0.012	14	-	13	2.0	12	135	38
	Min	0.078	0.015	0.221	11	37	6.7	40	18	3.9	34	6.2	40	8.3	21	2.4	13	1.8	0.004	0.000	0.749	-	0.232	0.041	0.074	0.126	0.486

#	Sample Jt4	ΣLREE	ΣMREE	ΣHREE	ΣREY	Mg	Al	Si	P	Ca	Sc	Ti	V	Cr	Mn	Fe	Co	Ni	Cu	Zn	Ga	As	Sr	Y	Zr	Nb	Mo
1	Jt4 Ap 12 - 01	1760	544	2404	4708	134	14	1904	222415	393600	0.229	0.663	0.928	<0.278	276	401	0.087	0.223	<0.300	<0.371	0.060	35	227	1860	0.281	0.040	<0.001
2	Jt4 Ap 12 - 02	1136	472	2134	3743	2640	3506	9331	224698	393600	0.781	382	23	3.9	295	12296	1.7	8.6	0.335	5.9	3.8	38	245	1653	0.148	0.574	0.019
3	Jt4 Ap 12 - 03	2143	644	2604	5390	311	360	2510	222936	393600	0.253	1.5	2.3	0.290	296	2229	0.194	7.0	0.544	0.775	0.389	29	222	2033	0.163	0.047	0.019
4	Jt4 Ap 12 - 04	1122	412	1858	3393	36	20	1036	222918	393600	0.170	<0.229	0.676	<0.149	273	484	0.018	1.2	0.799	0.665	0.040	29	215	1441	0.089	0.064	0.007
5	Jt4 Ap 12 - 05	56	81	478	614	30	0.655	443	226437	393600	<0.108	<0.188	0.316	<0.221	257	274	0.021	0.156	<0.399	<0.366	<0.008	32	218	374	0.997	0.001	0.015
6	Jt4 Ap 12 - 06	1474	565	2321	4361	7348	8541	20824	215204	393600	1.3	905	40	2.0	306	28263	7.1	81	11	14	5.8	30	232	1806	0.291	0.988	0.074
7	Jt4 Ap 12 - 07	1512	535	2257	4304	1525	2008	5136	216700	393600	0.428	159	8.9	1.1	279	5424	0.938	4.4	5.8	5.0	1.3	29	235	1753	0.276	0.224	0.043
8	Jt4 Ap 12 - 08	216	168	944	1328	10557	13550	32293	214258	393600	1.7	1396	65	21	315	38827	7.9	25	9.2	24	11	27	266	731	0.328	1.8	0.129
9	Jt4 Ap 12 - 09	586	264	1267	2117	1612	1970	4819	228537	393600	0.385	147	9.4	2.6	276	6185	1.0	7.6	4.1	5.4	2.1	28	267	988	0.159	0.222	0.012
10	Jt4 Ap 12 - 10	470	242	1238	1950	1004	1249	3442	226648	393600	0.194	142	6.6	1.4	269	3713	0.423	1.8	0.459	1.9	1.0	32	245	963	0.075	0.259	0.005
11	Jt4 Ap 12 - 11	358	273	1500	2131	28	0.682	714	218735	393600	<0.091	<0.171	0.615	<0.175	262	294	0.015	<0.049	0.343	<0.297	0.013	36	247	1149	0.116	0.072	<0.002
12	Jt4 Ap 12 - 12	354	226	1161	1740	34	16	575	217621	393600	0.146	<0.118	0.983	<0.237	261	355	0.008	<0.071	<0.475	<0.379	0.025	37	253	901	0.027	0.035	<0.007
13	Jt4 Ap 12 - 13	141	149	840	1131	73	52	596	219599	393600	<0.097	5.0	0.807	<0.188	255	409	0.030	0.069	<0.370	<0.299	0.028	39	244	655	0.024	0.072	0.010
14	Jt4 Ap 12 - 14	548	277	1359	2184	107	120	1049	221112	393600	0.209	0.860	1.0	<0.158	273	776	0.041	0.302	<0.345	0.325	0.108	36	233	1056	0.075	0.039	0.003
15	Jt4 Ap 12 - 15	2219	713	2941	5873	36	0.919	1623	219450	393600	0.238	0.685	0.916	<0.178	290	364	0.017	0.059	<0.381	<0.290	0.038	32	205	2284	0.261	0.039	0.011
16	Jt4 Ap 12 - 16	450	352	1960	2761	28	1.9	917	220760	393600	0.151	<0.117	0.638	<0.118	254	289	0.005	0.026	<0.223	0.174	0.029	30	244	1497	0.125	0.059	0.012
17	Jt4 Ap 12 - 17	58	66	452	577	15137	21672	34908	206249	393600	5.0	53	101	18	440	99569	104	445	1.1	60	21	29	219	351	3.2	0.181	0.030
18	Jt4 Ap 12 - 18	275	221	1304	1801	72	67	762	215730	393600	<0.089	8.1	0.888	<0.178	246	427	0.064	0.258	0.574	<0.310	0.088	33	242	993	0.069	0.053	<0.001
19	Jt4 Ap 12 - 19	1611	522	2456	4590	467	531	3159	220143	393600	0.609	3.9	4.8	0.316	278	3843	0.153	1.1	<0.345	0.905	0.707	27	231	1891	0.226	0.108	0.008
20	Jt4 Ap 12 - 20	403	231	1322	1956	441	624	1769	222390	393600	0.225	395	98	23	247	41456	0.469	3.7	0.473	1.4	1.0	28	255	1009	0.079	0.422	0.014
21	Jt4 Ap 12 - 21	1157	383	1790	3330	8377	10228	25098	208700	393600	1.9	1206	52	5.8	306	28926	5.5	35	<0.278	17	7.3	38	243	1377	0.150	1.4	<0.013
22	Jt4 Ap 12 - 22	382	178	966	1526	44	9.9	931	219905	393600	<0.065	0.353	0.724	0.096	250	1752	0.809	7.2	0.659	0.983	0.154	30	322	740	0.053	0.105	0.008
23	Jt4 Ap 12 - 23	1876	616	2663	5155	511	195	2984	217418	393600	1.2	3.3	2.8	0.349	276	1394	0.193	1.8	<0.249	1.0	0.186	29	223	2057	0.265	0.041	0.010
24	Jt4 Ap 12 - 24	3759	732	2526	7017	65	20	1825	219197	393600	0.245	0.503	1.1	<0.155	292	455	0.042	0.152	<0.207	0.255	0.106	28	212	1968	0.297	0.020	<0.004
25	Jt4 Ap 12 - 25	1252	432	1951	3635	1437	1754	5837	216501	393600	0.517	189	9.5	0.464	271	5376	0.760	3.4	<0.230	2.6	1.5	32	275	1502	0.171	0.316	0.008
26	Jt4 Ap 12 - 26	1277	547	2507	4330	4609	5449	15933	214696	393600	1.3	623	29	2.0	289	15040	2.8	11	<0.227	8.9	4.5	30	243	1930	0.200	0.746	0.008
27	Jt4 Ap 12 - 27	2179	776	3251	6206	76	84	1991	219424	393600	0.285	0.746	1.2	<0.109	275	859	0.013	0.349	<0.220	<0.191	0.124	31	222	2512	0.260	0.058	0.024
28	Jt4 Ap 12 - 28	1764	571	2552	4887	100	93	1472	221888	393600	0.213	1.2	1.5	<0.152	264	581	0.066	0.228	<0.293	0.491	0.130	38	252	1959	0.164	0.029	<0.002
29	Jt4 Ap 12 - 29	17462	1400	2541	21402	872	10663	23001	207412	393600	17	199	85	1.7	381	18697	1.4	26	0.675	4.1	7.0	46	302	2008	0.320	0.839	0.019
30	Jt4 Ap 12 - 30	1389	594	2627	4609	54	51	1476	221015	393600	0.216	3.9	1.3	<0.138	260	427	0.057	0.270	0.268	0.291	0.097	33	237	2021	0.222	0.082	<0.005
31	Jt4 Ap 12 - 31	2824	757	2873	6454	37	9.0	1790	220805	393600	0.299	0.913	1.0	<0.122	279	384	0.027	0.179	<0.197	0.263	0.062	28	219	2225	0.284	0.048	<0.005
32	Jt4 Ap 12 - 32	2547	819	3347	6713	235	262	2163	223964	393600	0.310	1.0	1.7	<0.110	278	946	0.154	0.571	0.179	0.745	0.251	30	227	2589	0.372	0.055	0.003
	Mean (n=32)	1711	461	1950	4122	1814	2598	6635	219171	393600	1.3	216	17	5.2	283	10022	4.3	22	2.3	6.5	2.3	32	241	1509	0.306	0.281	0.021
	SD	3014	276	795	3658	3580	5029	9742	5162	0.000	3.1	359	30	6.1	38	20022	18	79	2.7	11	4.4	4.4	25	616	0.560	0.426	0.026
	Median	1204	452	2047	3689	184	157	1947	219752	393600	0.299	5.0	1.6	1.8	276	1170	0.153	1.5	0.617	1.2	0.186	31	239	1578	0.185	0.072	0.012
	Max	17462	1400	3347	21402	15137	21672	34908	228537	393600	17	1396	101	23	440	99569	104	445	11	60	21	46	322	2589	3.2	1.8	0.129
	Min	56	66	452	577	28	0.655	443	206249	393600	0.146	0.353	0.316	0.096	246	274	0.005	0.026	0.179	0.174	0.013	27	205	351	0.024	0.001	0.003

#	Sample Jt4	Sn	Sb	Ba	La	Ce	Pr	Nd	Sm	Eu	Gd	Tb	Dy	Ho	Er	Tm	Yb	Lu	Hf	Ta	W	^{204}Pb	^{206}Pb	^{207}Pb	^{208}Pb	Th	U
1	Jt4 Ap 12 - 01	0.582	<0.046	0.279	357	835	105	462	107	13	156	30	238	65	223	32	200	24	0.014	0.003	3.3	<0.010	4.5	0.630	3.0	32	14
2	Jt4 Ap 12 - 02	0.262	0.059	30	213	530	69	324	85	9.5	136	27	216	58	198	28	175	22	0.023	0.040	4.6	<0.011	7.8	1.2	2.8	26	23
3	Jt4 Ap 12 - 03	<0.138	<0.034	0.324	418	1022	130	572	133	14	190	35	273	71	236	34	205	25	0.035	0.008	2.0	<0.011	5.7	0.850	2.8	29	17
4	Jt4 Ap 12 - 04	<0.137	0.053	0.238	206	533	69	315	78	8.7	118	23	185	50	170	25	154	19	0.012	<0.000	1.9	<0.009	3.5	0.488	1.8	17	10
5	Jt4 Ap 12 - 05	0.434	<0.032	0.074	6.8	22	3.8	23	9.5	1.5	22	4.9	42	13	44	6.1	36	4.4	0.062	0.003	0.479	<0.009	0.237	0.043	0.062	0.113	0.619
6	Jt4 Ap 12 - 06	9.6	0.039	93	278	682	90	423	108	12	166	32	247	65	215	30	183	23	0.017	0.069	5.0	<0.009	4.6	0.680	3.2	32	14
7	Jt4 Ap 12 - 07	0.320	0.038	16	311	703	89	409	101	11	157	30	236	63	210	29	180	22	0.024	0.017	3.9	<0.006	3.8	0.560	2.8	30	12
8	Jt4 Ap 12 - 08	3.6	<0.026	153	43	97	12	63	22	3.5	46	9.9	87	25	88	13	78	9.6	0.007	0.093	11	<0.010	1.0	0.172	0.529	4.0	3.0
9	Jt4 Ap 12 - 09	1.8	0.020	19	116	275	35	159	43	5.9	76	15	125	34	116	17	100	12	0.007	0.011	4.7	<0.010	1.5	0.233	0.866	8.1	4.8
10	Jt4 Ap 12 - 10	1.6	0.020	15	98	218	27	127	36	5.1	67	14	120	33	114	16	100	12	0.004	0.010	5.3	<0.008	1.6	0.220	0.615	6.9	5.0
11	Jt4 Ap 12 - 11	0.104	<0.023	0.197	58	158	23	119	39	4.9	75	16	138	40	144	21	130	16	0.015	0.003	5.7	<0.007	2.2	0.291	1.3	14	6.6
12	Jt4 Ap 12 - 12	0.278	<0.036	0.141	74	155	21	103	34	4.2	64	13	110	31	107	16	94	12	0.018	0.004	4.8	<0.009	0.482	0.062	0.375	3.6	1.4
13	Jt4 Ap 12 - 13	0.086	<0.021	0.517	21	58	9.2	53	21	2.7	42	8.7	76	22	77	11	67	8.2	0.009	0.003	3.7	<0.008	0.385	0.073	0.196	1.4	1.0
14	Jt4 Ap 12 - 14	<0.075	<0.023	0.353	112	249	32	155	45	5.8	80	16	131	37	125	18	110	13	0.001	0.004	2.4	<0.008	1.5	0.239	0.900	8.9	4.0
15	Jt4 Ap 12 - 15	<0.083	0.060	0.130	435	1045	135	603	143	16	209	39	307	81	270	39	239	29	0.014	0.009	2.2	<0.009	6.6	0.899	4.1	42	19
16	Jt4 Ap 12 - 16	0.049	0.031	0.227	76	199	28	146	48	7.0	95	21	181	53	188	28	172	21	0.022	0.004	3.4	<0.006	3.1	0.412	1.9	21	9.7
17	Jt4 Ap 12 - 17	0.148	0.043	2.8	8.8	25	4.0	21	7.6	1.2	18	3.8	36	11	42	6.1	37	4.5	0.078	0.004	3.5	<0.010	1.3	0.261	0.612	0.069	0.592
18	Jt4 Ap 12 - 18	0.983	0.057	1.7	46	122	17	90	29	4.0	59	13	116	35	126	19	117	14	0.016	0.005	3.1	<0.007	1.7	0.262	0.923	10	5.3
19	Jt4 Ap 12 - 19	0.228	0.038	0.585	328	762	97	425	98	11	148	29	236	67	229	34	210	26	0.028	0.008	3.0	<0.005	4.6	0.646	2.7	29	15
20	Jt4 Ap 12 - 20	0.550	0.021	0.552	75	185	24	119	34	4.4	62	13	117	35	128	19	117	15	0.006	0.034	5.9	<0.007	1.8	0.264	0.985	10	5.8
21	Jt4 Ap 12 - 21	0.657	0.041	114	235	545	69	309	72	7.5	110	21	173	48	169	25	152	18	0.019	0.086	2.9	<0.006	3.0	0.440	2.0	21	9.4
22	Jt4 Ap 12 - 22	0.211	0.017	4.6	74	179	23	106	28	3.4	49	10	87	26	92	14	84	10	0.008	0.004	5.1	0.007	1.2	0.232	0.793	6.9	3.5
23	Jt4 Ap 12 - 23	0.175	0.047	0.203	380	881	112	502	120	13	179	34	269	73	248	36	222	27	0.018	0.007	2.0	<0.006	5.5	0.719	3.6	38	20
24	Jt4 Ap 12 - 24	<0.108	0.040	0.183	793	1817	222	926	183	17	219	37	276	70	231	33	200	24	0.027	0.010	1.7	<0.007	6.7	0.927	4.2	44	20
25	Jt4 Ap 12 - 25	0.119	0.053	20	252	584	75	341	82	8.4	125	24	193	54	184	27	164	20	0.007	0.020	7.8	<0.005	4.0	0.608	3.1	32	13
26	Jt4 Ap 12 - 26	0.280	0.055	65	236	585	78	378	99	11	157	31	250	69	234	34	213	26	0.024	0.049	3.6	<0.006	9.3	1.3	4.6	50	23
27	Jt4 Ap 12 - 27	<0.075	0.040	0.241	428	1008	132	611	151	16	228	43	338	90	304	44	269	33	0.034	0.010	3.1	<0.004	6.3	0.842	4.8	52	20
28	Jt4 Ap 12 - 28	0.157	0.063	0.700	356	829	106	473	111	11	165	31	253	70	241	35	220	27	0.005	0.011	3.8	<0.005	4.6	0.590	3.1	37	15
29	Jt4 Ap 12 - 29	4.4	0.180	15	3917	8936	994	3615	543	41	420	56	340	75	226	30	179	21	0.041	0.014	9.1	0.025	14	2.2	19	398	114
30	Jt4 Ap 12 - 30	0.095	0.045	0.715	248	636	84	421	111	11	174	33	265	72	249	36	221	27	0.021	0.009	3.3	<0.006	4.7	0.607	4.1	47	16
31	Jt4 Ap 12 - 31	<0.071	0.025	0.202	569	1329	169	758	169	16	227	40	306	80	266	38	234	28	0.018	0.013	2.7	<0.005	6.3	0.837	5.9	63	19
32	Jt4 Ap 12 - 32	<0.061	0.062	0.292	491	1185	155	716	168	17	242	44	348	92	310	45	277	34	0.030	0.012	3.0	<0.006	7.0	0.953	6.7	72	22
	Mean (n=32)	1.1	0.048	17	352	825	101	433	96	9.9	134	25	197	53	181	26	161	20	0.021	0.019	4.0	-	4.1	0.586	2.9	37	15
	SD	1.9	0.034	37	677	1542	172	627	96	7.4	84	13	90	22	73	11	65	7.9	0.016	0.024	2.2	-	3.0	0.439	3.4	69	20
	Median	0.279	0.042	0.569	236	565	72	332	84	9.1	130	25	204	56	193	28	174	21	0.018	0.010	3.4	-	3.9	0.575	2.7	27	13
	Max	9.6	0.180	153	3917	8936	994	3615	543	41	420	56	348	92	310	45	277	34	0.078	0.093	11	-	14	2.2	19	398	114
	Min	0.049	0.017	0.074	6.8	22	3.8	21	7.6	1.2	18	3.8	36	11	42	6.1	36	4.4	0.001	0.003	0.479	-	0.237	0.043	0.062	0.069	0.592

Supplementary Table 3A. Summary of U-Pb data for selected apatite

Sample	Age (Ma)	S.D.	
Jt1	2027	16	Concordia age
Jt4	1978	78	Lower intercept age
Jt7	2027	40	Concordia age
Jt10	1973	32	Concordia age
Mean	2001	42	

#	Sample	$^{238}U/^{206}Pb$	± 2σ	$^{207}Pb/^{206}Pb$	± 2σ	Rho	$^{207}Pb/^{235}U$	± 2σ	$^{206}Pb/^{238}U$	± 2σ	Excluded	La/Yb	La/Sm	Sm/Yb	Cl/Ce	La/U	Sr/Y	Eu/Eu*
1	Jt1 Ap1 - 02	2142	59	2206	55	0.388	7.6	0.537	0.394	0.011	x	12	3.8	3.2	1.7	44	0.166	0.309
2	Jt1 Ap1 - 06	2093	55	2152	49	0.370	7.2	0.507	0.384	0.010	x	7.3	3.0	2.4	2.0	29	0.136	0.355
3	Jt1 Ap2 - 01	2053	78	2187	118	0.430	7.1	0.629	0.375	0.014	x	0.553	0.490	1.1	72	5.3	0.670	0.500
4	Jt1 Ap2 - 02	2034	58	2073	67	0.387	6.6	0.487	0.371	0.011		0.789	0.655	1.2	21	4.8	0.245	0.461
5	Jt1 Ap2 - 03	2031	54	2080	55	0.366	6.6	0.482	0.370	0.010		2.8	1.9	1.5	5.0	19	0.148	0.420
6	Jt1 Ap2 - 07	2036	56	2078	40	0.394	6.6	0.464	0.371	0.010		4.1	2.3	1.8	3.4	20	0.153	0.389
7	Jt1 Ap3 - 02	2104	55	2149	35	0.375	7.2	0.497	0.386	0.010	x	9.3	3.7	2.5	2.0	34	0.160	0.332
8	Jt1 Ap3 - 03	2134	66	2180	41	0.432	7.5	0.539	0.395	0.012	x	9.2	3.6	2.5	2.3	31	0.183	0.344
9	Jt1 Ap3 - 05	2138	105	2335	194	0.461	8.2	0.870	0.393	0.019	x	1.1	0.753	1.5	78	15	1.0	0.442
10	Jt1 Ap4 - 05	2261	60	2317	51	0.374	8.6	0.611	0.420	0.011	x	12	4.4	2.7	2.6	54	0.212	0.339
11	Jt1 Ap5 - 02	2163	60	2218	51	0.383	7.7	0.564	0.398	0.011	x	3.5	1.8	1.9	6.3	19	0.214	0.393
12	Jt1 Ap5 - 03	2097	56	2134	49	0.375	7.1	0.506	0.384	0.010	x	4.0	2.3	1.7	5.2	24	0.212	0.393
13	Jt1 Ap5 - 04	2149	56	2200	37	0.376	7.6	0.526	0.395	0.010	x	7.7	3.4	2.3	2.4	35	0.140	0.356
14	Jt1 Ap5 - 05	2064	53	2109	38	0.367	6.9	0.478	0.377	0.010	x	4.5	2.5	1.8	3.2	24	0.125	0.379
15	Jt1 Ap5 - 06	2147	57	2208	40	0.382	7.6	0.530	0.395	0.010	x	8.7	3.5	2.5	2.6	38	0.170	0.334
16	Jt1 Ap6 - 02	2225	56	2328	37	0.367	8.5	0.586	0.412	0.010	x	16	4.4	3.7	1.6	50	0.155	0.297
17	Jt1 Ap6 - 03	2275	60	2334	33	0.383	8.8	0.605	0.424	0.011	x	25	5.3	4.7	1.3	62	0.174	0.273
18	Jt1 Ap8 - 02	2168	112	2223	119	0.570	7.8	0.706	0.400	0.021	x	5.5	3.1	1.8	9.3	31	0.522	0.415
19	Jt1 Ap8 - 03	1998	57	2057	62	0.386	6.4	0.474	0.363	0.010		1.9	1.5	1.3	13	12	0.334	0.451
20	Jt1 Ap8 - 04	1987	52	2013	46	0.373	6.2	0.440	0.361	0.010		2.7	1.8	1.5	6.8	14	0.207	0.409
21	Jt1 Ap10 - 02	2240	111	2293	243	0.397	8.4	1.0	0.416	0.021	x	3.5	1.9	1.8	34	32	1.1	0.437
22	Jt1 Ap11 - 03	2101	66	2158	82	0.386	7.2	0.592	0.385	0.012	x	2.4	1.6	1.5	8.2	17	0.221	0.402
23	Jt1 Ap11 - 08	2200	235	2395	339	0.457	8.8	2.0	0.406	0.043	x	1.8	1.1	1.6	55	23	0.968	0.441
24	Jt1 Ap13 - 06	3096	1482	3298	997	0.593	23	6.5	0.617	0.295	x	0.984	0.547	1.8	128	36	1.4	0.474
25	Jt1 Ap14 - 01	2019	78	2153	134	0.427	6.9	0.620	0.367	0.014	x	0.644	0.545	1.2	75	5.7	0.807	0.454
26	Jt1 Ap14 - 09	2024	68	2057	95	0.390	6.5	0.560	0.369	0.012		0.997	0.820	1.2	36	8.6	0.525	0.451
27	Jt1 Ap15 - 06	2161	65	2227	53	0.410	7.8	0.574	0.398	0.012	x	3.7	2.2	1.7	5.9	23	0.211	0.415
28	Jt1 Ap15 - 09	2239	105	2130	134	0.484	7.7	0.743	0.416	0.020	x	1.8	1.2	1.5	36	20	0.796	0.420
29	Jt1 Ap16 - 02	2199	66	2203	58	0.404	7.8	0.584	0.407	0.012	x	7.0	3.0	2.3	2.9	33	0.171	0.356

#	Sample	$^{238}U/^{206}Pb$	± 2σ	$^{207}Pb/^{206}Pb$	± 2σ	Rho	$^{207}Pb/^{235}U$	± 2σ	$^{206}Pb/^{238}U$	± 2σ	Excluded	La/Yb	La/Sm	Sm/Yb	Cl/Ce	La/U	Sr/Y	Eu/Eu*
30	Jt1 Ap16 - 03	2046	72	2180	109	0.416	7.1	0.602	0.373	0.013	x	1.3	0.843	1.6	41	9.8	0.786	0.399
31	Jt1 Ap16 - 06	2102	54	2143	41	0.367	7.2	0.501	0.386	0.010	x	9.0	3.7	2.5	2.4	38	0.183	0.336
32	Jt1 Ap16 - 07	2115	74	2097	67	0.456	7.0	0.541	0.389	0.014	x	3.5	1.9	1.8	10.0	24	0.364	0.384
33	Jt1 Ap16 - 12	2117	67	2173	60	0.419	7.4	0.554	0.388	0.012	x	5.3	2.5	2.1	5.5	32	0.275	0.357
34	Jt1 Ap16 - 13	2353	72	2333	43	0.433	9.1	0.648	0.440	0.014	x	9.7	3.1	3.1	2.5	34	0.174	0.313
35	Jt1 Ap16 - 18	2112	55	2177	54	0.358	7.4	0.532	0.388	0.010	x	4.6	2.5	1.9	3.9	23	0.166	0.392
36	Jt1 Ap16 - 22	2039	54	2057	53	0.370	6.6	0.474	0.372	0.010		3.9	2.1	1.9	5.0	22	0.196	0.380
37	Jt1 Ap16 - 25	2016	59	2051	79	0.380	6.5	0.495	0.367	0.011		2.3	1.4	1.7	15	13	0.409	0.389
38	Jt1 Ap17 - 05	3829	362	3043	616	0.387	26	6.3	0.810	0.077	x	1.4	0.706	1.9	91	35	1.3	0.476
	Jt4																	
1	Jt4 Ap1 - 01	3911	338	3842	296	0.596	44	6.5	0.836	0.072	x	0.193	0.967	0.199	82	22	0.809	0.312
2	Jt4 Ap1 - 02	3824	375	4046	394	0.712	50	6.8	0.809	0.079	x	0.251	1.2	0.201	126	23	0.812	0.299
3	Jt4 Ap1 - 03	2709	199	3424	324	0.615	21	2.5	0.519	0.038	x	0.174	0.711	0.245	94	11	0.675	0.295
4	Jt4 Ap1 - 05	2722	221	3026	331	0.577	17	2.3	0.526	0.043	x	0.246	0.850	0.290	101	16	0.521	0.345
5	Jt4 Ap1 - 07	2524	209	3372	336	0.650	19	2.4	0.483	0.040	x	0.199	0.811	0.246	96	16	0.684	0.295
6	Jt4 Ap2 - 01	2146	63	2322	76	0.387	8.1	0.615	0.395	0.012		1.8	3.8	0.472	4.2	26	0.176	0.289
7	Jt4 Ap2 - 02	2809	205	3512	285	0.644	23	2.7	0.543	0.040	x	0.280	1.2	0.241	71	16	0.920	0.367
8	Jt4 Ap2 - 05	2133	124	2320	141	0.515	8.1	0.912	0.394	0.023		0.975	2.6	0.378	14	22	0.344	0.295
9	Jt4 Ap2 - 06	3355	430	3362	390	0.707	27	4.9	0.680	0.087	x	0.358	1.7	0.211	55	31	0.700	0.306
10	Jt4 Ap3 - 01	2743	212	3200	298	0.625	19	2.3	0.529	0.041	x	0.188	0.488	0.384	137	11	0.490	0.298
11	Jt4 Ap3 - 02	2801	319	3258	476	0.740	20	3.0	0.536	0.061	x	0.171	0.518	0.330	142	13	0.509	0.299
12	Jt4 Ap3 - 03	2065	62	2167	71	0.401	7.1	0.533	0.378	0.011		0.460	1.6	0.283	13	8.3	0.160	0.290
13	Jt4 Ap3 - 05	2596	189	3169	295	0.609	17	2.0	0.496	0.036	x	0.202	0.590	0.342	119	12	0.511	0.316
14	Jt4 Ap3 - 06	3316	216	3759	265	0.565	34	3.9	0.670	0.044	x	0.292	1.5	0.199	50	16	0.806	0.300
15	Jt4 Ap3 - 07	2096	62	2248	72	0.396	7.6	0.566	0.385	0.011		0.658	2.0	0.325	10	12	0.154	0.296
16	Jt4 Ap4 - 01	2122	63	2196	71	0.396	7.5	0.561	0.390	0.012		0.556	1.8	0.309	12	10	0.144	0.305
17	Jt4 Ap4 - 02	2225	85	2568	126	0.424	9.8	0.883	0.414	0.016	x	0.885	2.5	0.349	8.1	18	0.268	0.282
18	Jt4 Ap4 - 03	3504	286	3706	293	0.696	35	4.1	0.719	0.059	x	0.236	1.1	0.206	57	23	0.746	0.299
19	Jt4 Ap4 - 04	2377	66	2459	45	0.398	10.0	0.701	0.447	0.012		4.2	4.6	0.920	1.2	39	0.059	0.301
20	Jt4 Ap4 - 05	2274	61	2379	64	0.367	9.0	0.660	0.422	0.011		2.3	3.6	0.622	2.5	29	0.079	0.273
21	Jt4 Ap5 - 01	2421	196	3145	408	0.499	16	2.5	0.454	0.037	x	0.160	0.697	0.230	114	13	0.673	0.324
22	Jt4 Ap5 - 02	2456	179	2931	288	0.583	14	1.7	0.459	0.033	x	0.194	0.703	0.276	99	13	0.611	0.312
23	Jt4 Ap5 - 04	2218	110	2427	202	0.441	9.0	1.0	0.410	0.020	x	0.622	1.8	0.342	18	15	0.401	0.290
24	Jt4 Ap5 - 05	2920	232	3634	305	0.615	27	3.4	0.572	0.045	x	0.170	0.830	0.205	74	15	0.688	0.303
25	Jt4 Ap6 - 01	2214	91	2605	129	0.487	10.0	0.843	0.409	0.017	x	0.183	1.0	0.178	44	5.4	0.393	0.295
26	Jt4 Ap6 - 02	2138	59	2203	61	0.383	7.6	0.542	0.393	0.011		1.3	2.8	0.454	4.1	18	0.102	0.279
27	Jt4 Ap6 - 03	2753	248	3519	454	0.607	23	3.4	0.532	0.048	x	0.177	0.699	0.253	118	18	0.691	0.320

#	Sample	$^{238}U/^{206}Pb$	± 2σ	$^{207}Pb/^{206}Pb$	± 2σ	Rho	$^{207}Pb/^{235}U$	± 2σ	$^{206}Pb/^{238}U$	± 2σ	Excluded	La/Yb	La/Sm	Sm/Yb	Cl/Ce	La/U	Sr/Y	Eu/Eu*
28	Jt4 Ap6 - 04	2232	82	2425	114	0.444	9.1	0.751	0.413	0.015	x	0.385	1.5	0.255	25	9.5	0.314	0.282
29	Jt4 Ap6 - 05	2286	110	2667	174	0.501	11	1.0	0.425	0.020	x	0.183	0.957	0.191	58	6.7	0.502	0.327
30	Jt4 Ap7 - 02	2263	150	2286	97	0.545	8.5	1.0	0.423	0.028		1.9	3.4	0.570	3.5	28	0.100	0.285
31	Jt4 Ap7 - 03	2243	97	2319	96	0.465	8.6	0.794	0.416	0.018		2.2	3.6	0.621	3.0	30	0.118	0.253
32	Jt4 Ap7 - 06	2375	78	2336	95	0.401	9.3	0.753	0.444	0.014		2.6	3.7	0.724	1.8	31	0.061	0.263
33	Jt4 Ap8 - 01	2144	77	2168	110	0.385	7.4	0.693	0.393	0.014		1.1	2.6	0.403	7.3	17	0.173	0.291
34	Jt4 Ap8 - 02	2280	157	2679	273	0.532	11	1.4	0.420	0.029	x	0.279	0.989	0.282	54	14	0.458	0.290
35	Jt4 Ap8 - 03	3480	527	3589	387	0.768	32	6.4	0.721	0.109	x	0.166	0.812	0.205	114	16	0.701	0.311
36	Jt4 Ap8 - 05	6508	767	4281	301	0.836	126	18	1.7	0.205	x	0.170	0.885	0.192	89	25	0.955	0.282
37	Jt4 Ap8 - 06	2601	201	2265	248	0.565	9.9	1.4	0.495	0.038	x	0.670	1.9	0.356	16	12	0.160	0.289
38	Jt4 Ap9 - 02	12918	12283	4169	1319	0.999	457	435	7.4	7.1	x	0.251	0.933	0.269	629	31	0.706	0.477
39	Jt4 Ap10 - 02	2079	64	2254	93	0.386	7.5	0.604	0.380	0.012		0.679	1.9	0.349	10	13	0.173	0.302
40	Jt4 Ap10 - 03	2096	63	2276	76	0.393	7.7	0.591	0.385	0.012		1.9	3.7	0.511	3.8	28	0.145	0.286
41	Jt4 Ap10 - 04	2061	79	2469	123	0.456	8.5	0.715	0.376	0.014	x	0.383	1.5	0.248	25	9.3	0.347	0.297
42	Jt4 Ap10 - 05	2111	72	2283	108	0.406	7.8	0.658	0.387	0.013		0.588	1.9	0.303	14	12	0.206	0.292
43	Jt4 Ap10 - 06	2275	84	2896	121	0.456	12	0.997	0.423	0.016	x	0.642	2.4	0.265	13	16	0.480	0.294
44	Jt4 Ap11 - 01	2059	91	2496	158	0.472	8.6	0.805	0.375	0.017	x	0.373	1.4	0.260	36	11	0.404	0.311
45	Jt4 Ap11 - 02	2031	58	2121	67	0.381	6.8	0.505	0.371	0.011		0.989	2.7	0.367	5.9	16	0.132	0.298
46	Jt4 Ap11 - 03	1981	74	2237	122	0.433	7.1	0.612	0.358	0.013	x	0.269	1.3	0.211	34	6.6	0.317	0.319
47	Jt4 Ap11 - 04	2301	233	2801	498	0.607	12	2.0	0.435	0.044	x	0.164	0.731	0.224	133	18	0.559	0.290
48	Jt4 Ap11 - 05	2423	155	2822	281	0.532	13	1.5	0.456	0.029	x	0.348	1.2	0.291	65	20	0.607	0.313
49	Jt4 Ap11 - 06	2403	290	2888	456	0.634	13	2.5	0.452	0.055	x	0.114	0.661	0.172	150	9.7	0.622	0.342
50	Jt4 Ap11 - 07	2359	213	2868	416	0.581	13	2.0	0.444	0.040	x	0.173	0.710	0.244	94	12	0.589	0.306
	Jt7																	
1	Jt7 Ap1 - 01	2238	58	2316	51	0.369	8.5	0.601	0.415	0.011	x	3.2	2.7	1.2	4.4	14	0.115	0.275
2	Jt7 Ap1 - 02	2305	60	2377	46	0.374	9.1	0.641	0.429	0.011	x	8.2	3.9	2.1	2.2	34	0.132	0.208
3	Jt7 Ap1 - 04	2451	93	2571	135	0.457	11	0.912	0.463	0.017	x	8.3	2.8	3.0	3.6	150	0.170	0.189
4	Jt7 Ap1 - 05	2213	62	2280	48	0.397	8.2	0.581	0.410	0.011	x	4.2	3.6	1.1	3.9	18	0.127	0.276
5	Jt7 Ap1 - 06	2272	59	2405	46	0.367	9.1	0.644	0.422	0.011	x	4.4	2.5	1.8	2.6	24	0.085	0.250
6	Jt7 Ap1 - 07	2341	66	2425	57	0.393	9.6	0.683	0.437	0.012	x	3.6	1.3	2.8	2.7	29	0.103	0.220
7	Jt7 Ap1 - 08	2374	64	2438	55	0.382	9.8	0.693	0.445	0.012	x	4.0	1.3	3.0	2.3	27	0.092	0.216
8	Jt7 Ap1 - 09	2198	57	2258	42	0.375	8.1	0.562	0.406	0.011	x	8.6	5.2	1.7	1.7	43	0.112	0.274
9	Jt7 Ap1 - 10	2326	61	2444	49	0.372	9.6	0.676	0.434	0.011	x	4.8	1.9	2.5	2.3	26	0.088	0.223
10	Jt7 Ap1 - 11	2410	64	2464	46	0.380	10	0.707	0.453	0.012	x	6.2	2.3	2.7	2.7	23	0.108	0.183
11	Jt7 Ap2 - 01	3598	159	2823	56	0.540	21	1.7	0.750	0.033	x	7.5	4.3	1.8	1.9	39	0.105	0.254
12	Jt7 Ap2 - 02	2404	79	2430	89	0.425	9.9	0.766	0.453	0.015	x	5.1	3.4	1.5	5.7	39	0.189	0.254
13	Jt7 Ap2 - 03	2363	66	2351	67	0.373	9.3	0.699	0.443	0.012	x	7.9	4.4	1.8	2.0	46	0.115	0.256

#	Sample	$^{238}U/^{206}Pb$	± 2σ	$^{207}Pb/^{206}Pb$	± 2σ	Rho	$^{207}Pb/^{235}U$	± 2σ	$^{206}Pb/^{238}U$	± 2σ	Excluded	La/Yb	La/Sm	Sm/Yb	Cl/Ce	La/U	Sr/Y	Eu/Eu*
14	Jt7 Ap2 - 04	2306	69	2300	61	0.407	8.8	0.645	0.430	0.013	x	9.4	4.6	2.0	1.8	53	0.128	0.248
15	Jt7 Ap2 - 05	2408	204	3246	693	0.391	16	3.5	0.452	0.038	x	0.487	0.601	0.811	114	14	0.664	0.285
16	Jt7 Ap2 - 06	2162	65	2251	69	0.414	7.9	0.574	0.399	0.012	x	1.9	2.3	0.824	5.6	14	0.111	0.262
17	Jt7 Ap2 - 08	2399	63	2424	40	0.378	9.9	0.683	0.451	0.012	x	7.2	4.2	1.7	1.6	26	0.082	0.247
18	Jt7 Ap2 - 09	2340	69	2368	53	0.408	9.3	0.670	0.437	0.013	x	7.3	4.0	1.8	1.8	38	0.093	0.238
19	Jt7 Ap2 - 10	2323	61	2383	47	0.378	9.3	0.648	0.434	0.011	x	5.5	3.3	1.7	1.8	24	0.082	0.245
20	Jt7 Ap2 - 11	2277	65	2304	78	0.375	8.6	0.661	0.424	0.012	x	6.0	3.7	1.6	2.3	40	0.106	0.250
21	Jt7 Ap4 - 01	2629	199	2617	214	0.593	12	1.6	0.502	0.038	x	1.4	1.4	0.963	36	37	0.434	0.284
22	Jt7 Ap4 - 02	2239	77	2314	89	0.458	8.5	0.643	0.415	0.014	x	3.3	2.9	1.1	5.6	31	0.159	0.273
23	Jt7 Ap4 - 03	2326	64	2387	49	0.389	9.3	0.661	0.434	0.012	x	8.9	4.6	1.9	1.8	48	0.112	0.251
24	Jt7 Ap4 - 04	2365	87	2533	122	0.412	10	0.925	0.443	0.016	x	6.0	3.6	1.7	7.2	52	0.313	0.254
25	Jt7 Ap4 - 05	2367	87	2379	54	0.475	9.4	0.732	0.445	0.016	x	7.1	4.1	1.7	2.1	45	0.112	0.254
26	Jt7 Ap4 - 06	2317	62	2367	48	0.383	9.2	0.643	0.432	0.012	x	10	4.9	2.0	1.7	50	0.115	0.247
27	Jt7 Ap4 - 07	2311	65	2340	53	0.395	9.0	0.637	0.430	0.012	x	7.1	4.4	1.6	2.4	44	0.126	0.252
28	Jt7 Ap5 - 01	2069	56	2176	56	0.380	7.2	0.511	0.379	0.010	x	2.1	2.7	0.781	6.3	16	0.135	0.290
29	Jt7 Ap5 - 02	2087	55	2184	48	0.376	7.3	0.514	0.382	0.010	x	3.0	3.4	0.895	4.1	20	0.126	0.270
30	Jt7 Ap5 - 03	2077	56	2142	56	0.374	7.1	0.507	0.380	0.010	x	2.8	3.3	0.857	5.3	19	0.157	0.273
31	Jt7 Ap5 - 04	2173	56	2282	47	0.367	8.1	0.572	0.401	0.010	x	4.8	3.7	1.3	2.6	26	0.100	0.290
32	Jt7 Ap5 - 05	2090	55	2167	46	0.372	7.2	0.510	0.383	0.010	x	3.7	3.5	1.1	3.7	22	0.119	0.268
33	Jt7 Ap5 - 06	2078	57	2154	55	0.380	7.1	0.514	0.380	0.010	x	2.4	2.9	0.825	6.0	18	0.141	0.263
34	Jt7 Ap5 - 07	2129	55	2217	48	0.370	7.6	0.535	0.391	0.010	x	4.4	4.1	1.1	3.0	25	0.113	0.277
35	Jt7 Ap5 - 08	2122	56	2224	45	0.374	7.6	0.532	0.390	0.010	x	3.4	3.4	0.999	3.5	23	0.105	0.296
36	Jt7 Ap5 - 09	2701	86	2480	56	0.420	12	0.887	0.522	0.017	x	2.9	3.2	0.921	6.0	25	0.168	0.282
37	Jt7 Ap6 - 01	3052	269	2881	251	0.618	17	2.5	0.600	0.053	x	1.5	1.9	0.779	51	33	0.875	0.253
38	Jt7 Ap6 - 02	2255	61	2334	50	0.378	8.7	0.617	0.418	0.011	x	7.3	3.9	1.9	2.4	42	0.130	0.253
39	Jt7 Ap6 - 03	2230	60	2345	60	0.373	8.6	0.624	0.413	0.011	x	8.6	4.1	2.1	2.0	53	0.132	0.240
40	Jt7 Ap6 - 04	2326	62	2413	48	0.379	9.4	0.663	0.434	0.012	x	6.0	3.4	1.8	3.2	31	0.131	0.235
41	Jt7 Ap6 - 05	2084	55	2106	50	0.366	6.9	0.496	0.382	0.010	x	4.1	3.8	1.1	3.1	27	0.121	0.263
42	Jt7 Ap6 - 06	2226	61	2277	54	0.378	8.3	0.598	0.413	0.011	x	3.7	2.8	1.3	4.4	26	0.134	0.255
43	Jt7 Ap6 - 07	2334	63	2428	62	0.376	9.6	0.692	0.436	0.012	x	7.7	4.0	1.9	3.2	40	0.158	0.246
44	Jt7 Ap6 - 08	2215	68	2267	86	0.395	8.2	0.635	0.410	0.013	x	2.7	2.7	1.0	8.6	21	0.239	0.282
45	Jt7 Ap7 - 01	2209	57	2306	43	0.369	8.3	0.585	0.408	0.011	x	5.2	4.0	1.3	2.5	30	0.101	0.285
46	Jt7 Ap7 - 02	2290	59	2372	37	0.372	9.1	0.627	0.426	0.011	x	7.3	4.2	1.7	2.1	29	0.105	0.252
47	Jt7 Ap7 - 03	2217	62	2304	60	0.389	8.4	0.604	0.410	0.012	x	6.7	3.6	1.8	2.7	55	0.129	0.257
48	Jt7 Ap7 - 04	2288	62	2342	54	0.378	8.9	0.637	0.426	0.012	x	10	4.5	2.3	1.9	63	0.132	0.251
49	Jt7 Ap7 - 05	2336	72	2416	66	0.410	9.5	0.715	0.437	0.013	x	6.9	3.8	1.8	2.6	50	0.130	0.260
50	Jt7 Ap7 - 06	2374	102	2645	158	0.485	11	0.984	0.446	0.019	x	0.764	1.4	0.561	44	14	0.500	0.275
51	Jt7 Ap7 - 07	2249	63	2343	65	0.390	8.7	0.627	0.417	0.012	x	5.1	3.2	1.6	3.1	47	0.118	0.263

#	Sample	$^{238}U/^{206}Pb$	± 2σ	$^{207}Pb/^{206}Pb$	± 2σ	Rho	$^{207}Pb/^{235}U$	± 2σ	$^{206}Pb/^{238}U$	± 2σ	Excluded	La/Yb	La/Sm	Sm/Yb	Cl/Ce	La/U	Sr/Y	Eu/Eu*
52	Jt7 Ap7 - 08	2172	72	2199	104	0.413	7.7	0.620	0.400	0.013	x	1.3	1.8	0.697	19	15	0.309	0.286
53	Jt7 Ap7 - 09	2289	63	2305	49	0.391	8.7	0.612	0.426	0.012	x	6.3	3.8	1.7	2.4	40	0.107	0.267
54	Jt7 Ap8 - 01	2123	69	2326	95	0.414	8.1	0.631	0.389	0.013	x	0.620	1.4	0.454	32	8.1	0.287	0.258
55	Jt7 Ap8 - 02	2327	212	2876	437	0.596	13	1.9	0.434	0.040	x	0.245	0.578	0.424	152	9.1	0.569	0.280
56	Jt7 Ap8 - 03	2478	122	2891	180	0.520	14	1.3	0.467	0.023	x	0.323	0.951	0.340	100	7.8	0.569	0.251
57	Jt7 Ap8 - 04	2099	58	2137	50	0.387	7.1	0.507	0.385	0.011	x	2.2	2.6	0.835	6.4	14	0.141	0.251
58	Jt7 Ap8 - 05	2750	214	3176	401	0.562	18	2.6	0.534	0.041	x	0.561	0.774	0.725	62	37	0.538	0.233
59	Jt7 Ap8 - 06	2255	134	2719	233	0.504	11	1.3	0.416	0.025	x	0.486	0.902	0.539	65	20	0.503	0.260
60	Jt7 Ap8 - 07	2069	60	2150	67	0.391	7.1	0.524	0.378	0.011	x	0.701	1.3	0.543	24	5.9	0.233	0.245
61	Jt7 Ap8 - 08	2635	255	3421	392	0.612	20	3.2	0.509	0.049	x	0.314	0.597	0.525	190	21	0.790	0.278
62	Jt7 Ap8 - 09	2126	60	2163	69	0.367	7.3	0.568	0.390	0.011	x	0.927	1.9	0.490	15	8.9	0.161	0.272
63	Jt7 Ap9 - 01	1697	93	2506	178	0.534	6.9	0.706	0.300	0.016	x	0.350	0.839	0.417	109	0.972	0.556	0.267
64	Jt7 Ap9 - 02	2099	56	2202	53	0.372	7.4	0.531	0.385	0.010	x	3.5	3.7	0.928	4.1	23	0.122	0.256
65	Jt7 Ap9 - 03	2337	118	2509	201	0.457	10	1.1	0.436	0.022	x	0.379	0.875	0.433	92	9.8	0.492	0.260
66	Jt7 Ap9 - 04	2094	62	2137	69	0.393	7.1	0.531	0.383	0.011	x	0.969	1.6	0.616	18	9.1	0.194	0.270
67	Jt7 Ap9 - 05	2243	58	2314	43	0.372	8.5	0.592	0.416	0.011	x	4.8	3.8	1.3	3.0	25	0.100	0.275
68	Jt7 Ap9 - 06	2277	57	2344	37	0.365	8.8	0.610	0.423	0.011	x	7.4	4.8	1.5	2.0	30	0.095	0.257
69	Jt7 Ap10 - 01	2243	68	2283	83	0.393	8.4	0.645	0.416	0.013	x	4.8	3.5	1.4	3.4	29	0.118	0.286
70	Jt7 Ap10 - 02	2276	62	2351	53	0.376	8.9	0.646	0.423	0.012	x	8.5	5.3	1.6	1.4	31	0.101	0.264
71	Jt7 Ap10 - 03	2234	66	2333	60	0.410	8.6	0.625	0.416	0.012	x	3.0	2.7	1.1	4.4	18	0.106	0.317
72	Jt7 Ap10 - 04	2271	82	2412	202	0.316	9.2	1.1	0.423	0.015	x	4.3	2.8	1.5	6.0	43	0.207	0.281
73	Jt7 Ap10 - 06	2423	76	2469	62	0.437	10	0.737	0.456	0.014	x	4.0	1.7	2.3	3.5	19	0.116	0.229
74	Jt7 Ap10 - 07	2338	90	2395	99	0.484	9.4	0.748	0.438	0.017	x	4.6	2.7	1.7	4.8	22	0.173	0.209
75	Jt7 Ap10 - 09	2388	87	2465	96	0.439	10	0.836	0.450	0.016	x	4.4	2.2	2.0	4.2	25	0.136	0.216
76	Jt7 Ap10 - 10	2272	78	2439	98	0.436	9.3	0.735	0.422	0.014	x	5.2	2.5	2.1	4.6	22	0.176	0.214
77	Jt7 Ap11 - 04	2176	93	2224	102	0.521	7.8	0.639	0.399	0.017	x	6.7	4.1	1.6	2.7	46	0.154	0.250
78	Jt7 Ap11 - 06	2090	73	2175	131	0.370	7.3	0.681	0.383	0.013	x	4.5	3.5	1.3	3.8	37	0.174	0.250
79	Jt7 Ap11 - 07	2147	68	2193	85	0.388	7.6	0.615	0.394	0.012	x	4.1	3.5	1.2	3.7	26	0.150	0.268
80	Jt7 Ap11 - 10	1971	72	2143	93	0.456	6.7	0.534	0.359	0.013		2.3	3.2	0.738	5.4	18	0.140	0.272
81	Jt7 Ap11 - 11	2232	145	2343	300	0.474	8.6	1.2	0.413	0.027	x	1.1	1.7	0.649	27	18	0.443	0.297
82	Jt7 Ap12 - 02	2284	63	2381	49	0.395	9.1	0.637	0.425	0.012	x	18	6.1	2.9	1.3	56	0.136	0.269
83	Jt7 Ap12 - 03	2196	58	2250	46	0.374	8.0	0.570	0.406	0.011	x	11	5.0	2.2	1.7	38	0.136	0.251
84	Jt7 Ap12 - 04	2200	60	2272	52	0.380	8.1	0.584	0.407	0.011	x	5.5	4.0	1.4	2.5	27	0.108	0.279
85	Jt7 Ap12 - 05	2237	63	2337	57	0.385	8.6	0.632	0.415	0.012	x	5.3	3.6	1.4	4.3	30	0.168	0.261
86	Jt7 Ap12 - 06	2124	56	2238	48	0.377	7.7	0.539	0.390	0.010	x	5.7	4.3	1.3	2.5	29	0.126	0.275
87	Jt7 Ap12 - 07	2225	59	2334	45	0.376	8.5	0.598	0.411	0.011	x	9.7	4.9	2.0	1.9	37	0.123	0.252
88	Jt7 Ap12 - 08	2222	59	2329	41	0.378	8.5	0.593	0.412	0.011	x	13	5.9	2.3	1.4	47	0.120	0.249
89	Jt7 Ap13 - 01	2071	58	2172	66	0.384	7.2	0.525	0.379	0.011	x	4.0	4.0	1.0	4.0	36	0.161	0.254

#	Sample	$^{238}U/^{206}Pb$	± 2σ	$^{207}Pb/^{206}Pb$	± 2σ	Rho	$^{207}Pb/^{235}U$	± 2σ	$^{206}Pb/^{238}U$	± 2σ	Excluded	La/Yb	La/Sm	Sm/Yb	Cl/Ce	La/U	Sr/Y	Eu/Eu*
90	Jt7 Ap13 - 02	1993	56	2106	68	0.377	6.6	0.490	0.362	0.010		2.4	3.4	0.714	6.2	20	0.166	0.250
91	Jt7 Ap13 - 03	2045	64	2250	82	0.405	7.4	0.573	0.373	0.012	x	2.7	3.2	0.840	7.4	29	0.232	0.275
92	Jt7 Ap13 - 04	2102	56	2202	56	0.371	7.4	0.530	0.385	0.010	x	4.7	4.2	1.1	3.3	28	0.129	0.282
93	Jt7 Ap13 - 05	2092	55	2180	56	0.363	7.3	0.529	0.383	0.010	x	5.2	4.3	1.2	3.2	27	0.165	0.271
94	Jt7 Ap13 - 06	2027	54	2126	61	0.360	6.8	0.501	0.369	0.010		3.4	3.7	0.913	4.3	21	0.145	0.253
95	Jt7 Ap13 - 07	2057	55	2188	54	0.378	7.2	0.510	0.375	0.010	x	5.8	4.3	1.3	2.9	35	0.154	0.264
96	Jt7 Ap13 - 08	2258	62	2313	64	0.374	8.6	0.633	0.419	0.012	x	3.5	3.9	0.905	4.3	27	0.143	0.291
97	Jt7 Ap13 - 09	2076	60	2226	74	0.384	7.4	0.557	0.379	0.011	x	2.7	3.4	0.792	5.9	24	0.205	0.250
98	Jt7 Ap13 - 10	2122	55	2275	48	0.366	7.8	0.557	0.390	0.010	x	6.5	5.1	1.3	2.3	32	0.137	0.269
99	Jt7 Ap14 - 01	2043	60	2167	68	0.393	7.0	0.521	0.373	0.011	x	2.9	3.0	0.984	5.3	28	0.204	0.257
100	Jt7 Ap14 - 02	2341	75	2421	70	0.414	9.6	0.737	0.438	0.014	x	2.8	2.8	0.983	5.5	23	0.199	0.262
101	Jt7 Ap14 - 03	2011	57	2165	63	0.382	6.9	0.507	0.365	0.010		2.1	2.7	0.772	7.0	17	0.199	0.280
102	Jt7 Ap14 - 04	2128	59	2214	68	0.378	7.6	0.554	0.391	0.011	x	5.0	3.4	1.5	2.8	35	0.145	0.264
103	Jt7 Ap14 - 05	2060	58	2182	66	0.382	7.2	0.530	0.377	0.011	x	3.9	3.4	1.1	4.4	31	0.210	0.257
104	Jt7 Ap14 - 06	2107	76	2228	75	0.440	7.5	0.620	0.387	0.014	x	1.4	2.1	0.653	14	12	0.279	0.298
105	Jt7 Ap14 - 07	2055	56	2222	67	0.367	7.3	0.546	0.375	0.010	x	3.1	3.0	1.0	5.5	20	0.199	0.267
106	Jt7 Ap14 - 08	2075	55	2182	49	0.377	7.2	0.511	0.379	0.010	x	5.5	3.8	1.4	2.5	36	0.140	0.244
107	Jt7 Ap14 - 09	2070	82	2175	98	0.465	7.2	0.607	0.380	0.015	x	1.0	1.9	0.532	22	12	0.338	0.298
108	Jt7 Ap14 - 10	2093	60	2208	69	0.388	7.4	0.542	0.383	0.011	x	4.3	3.4	1.3	4.0	36	0.194	0.261
109	Jt7 Ap14 - 11	2038	60	2170	77	0.390	7.0	0.526	0.372	0.011	x	4.6	3.3	1.4	3.5	37	0.190	0.247
110	Jt7 Ap14 - 12	2026	56	2120	57	0.382	6.8	0.490	0.369	0.010		2.4	3.1	0.786	5.3	20	0.167	0.297
111	Jt7 Ap15 - 01	2380	62	2385	45	0.375	9.5	0.664	0.446	0.012	x	7.2	4.6	1.6	1.9	29	0.096	0.267
112	Jt7 Ap15 - 02	2262	61	2353	63	0.380	8.8	0.631	0.421	0.011	x	3.2	2.6	1.2	3.5	25	0.092	0.249
113	Jt7 Ap15 - 03	2249	62	2281	54	0.384	8.4	0.599	0.417	0.011	x	3.2	2.9	1.1	5.3	21	0.135	0.272
114	Jt7 Ap15 - 04	2242	61	2313	56	0.379	8.5	0.614	0.416	0.011	x	4.6	3.6	1.3	3.5	36	0.116	0.277
115	Jt7 Ap15 - 05	2310	61	2399	56	0.375	9.3	0.658	0.431	0.011	x	5.7	3.9	1.4	2.9	32	0.116	0.260
116	Jt7 Ap15 - 06	2326	70	2412	65	0.385	9.4	0.742	0.435	0.013	x	7.3	4.5	1.6	2.5	45	0.135	0.260
117	Jt7 Ap15 - 07	2347	63	2375	49	0.381	9.3	0.656	0.439	0.012	x	5.6	3.9	1.4	3.0	34	0.119	0.258
118	Jt7 Ap15 - 08	2255	61	2341	51	0.380	8.7	0.616	0.419	0.011	x	5.7	4.1	1.4	2.8	38	0.112	0.269
119	Jt7 Ap15 - 09	2276	62	2360	72	0.375	8.9	0.651	0.423	0.012	x	5.8	4.2	1.4	3.4	36	0.150	0.260
120	Jt7 Ap16 - 01	2255	60	2326	59	0.365	8.6	0.628	0.419	0.011	x	4.4	4.2	1.0	3.1	28	0.113	0.305
121	Jt7 Ap16 - 02	3062	369	3771	718	0.704	31	5.3	0.605	0.073	x	0.452	0.691	0.655	175	38	0.831	0.313
122	Jt7 Ap16 - 03	2315	59	2367	35	0.371	9.1	0.630	0.432	0.011	x	3.5	3.7	0.962	3.2	16	0.087	0.277
123	Jt7 Ap16 - 04	2288	58	2342	38	0.370	8.9	0.612	0.426	0.011	x	2.8	2.8	0.996	4.4	13	0.095	0.278
124	Jt7 Ap16 - 05	2378	59	2449	34	0.364	9.9	0.679	0.446	0.011	x	5.3	4.1	1.3	2.2	20	0.078	0.267
125	Jt7 Ap16 - 06	2266	60	2344	58	0.376	8.8	0.618	0.421	0.011	x	4.4	3.9	1.1	4.2	23	0.143	0.270
126	Jt7 Ap16 - 07	2290	59	2340	41	0.372	8.9	0.616	0.426	0.011	x	6.3	4.9	1.3	1.6	23	0.076	0.265
127	Jt7 Ap16 - 08	2169	57	2254	53	0.371	7.9	0.557	0.399	0.010	x	3.4	3.5	0.973	4.0	18	0.121	0.265

#	Sample	$^{238}U/^{206}Pb$	± 2σ	$^{207}Pb/^{206}Pb$	± 2σ	Rho	$^{207}Pb/^{235}U$	± 2σ	$^{206}Pb/^{238}U$	± 2σ	Excluded	La/Yb	La/Sm	Sm/Yb	Cl/Ce	La/U	Sr/Y	Eu/Eu*
128	Jt7 Ap17 - 01	2119	61	2231	74	0.384	7.6	0.570	0.390	0.011	x	5.9	4.3	1.4	2.2	31	0.112	0.295
129	Jt7 Ap17 - 02	2205	109	2424	229	0.425	8.9	1.0	0.406	0.020	x	1.2	1.1	1.1	13	22	0.237	0.262
130	Jt7 Ap17 - 03	2239	68	2267	81	0.417	8.3	0.606	0.416	0.013	x	7.5	5.1	1.5	2.3	34	0.130	0.272
131	Jt7 Ap17 - 04	2140	105	2330	182	0.466	8.2	0.861	0.393	0.019	x	2.3	2.1	1.1	12	28	0.295	0.265
132	Jt7 Ap17 - 05	2230	70	2315	65	0.430	8.5	0.625	0.414	0.013	x	6.6	4.4	1.5	2.6	29	0.132	0.266
133	Jt7 Ap17 - 06	2207	72	2282	77	0.412	8.3	0.653	0.409	0.013	x	7.8	4.4	1.8	2.0	45	0.129	0.268
134	Jt7 Ap17 - 07	2340	81	2320	97	0.431	9.0	0.718	0.437	0.015	x	4.9	3.8	1.3	5.3	35	0.221	0.286
135	Jt7 Ap17 - 09	2244	59	2338	45	0.375	8.7	0.602	0.416	0.011	x	5.3	4.3	1.2	2.1	20	0.088	0.280
136	Jt7 Ap17 - 10	2219	86	2321	73	0.471	8.4	0.694	0.413	0.016	x	3.5	2.4	1.5	3.1	22	0.100	0.267
137	Jt7 Ap17 - 11	2205	62	2309	54	0.397	8.3	0.594	0.409	0.012	x	4.1	3.8	1.1	3.0	20	0.099	0.295
138	Jt7 Ap17 - 12	2335	86	2418	75	0.482	9.5	0.725	0.437	0.016	x	4.4	2.8	1.6	3.6	21	0.124	0.259
139	Jt7 Ap17 - 13	2190	80	2316	83	0.479	8.3	0.633	0.405	0.015	x	7.5	4.7	1.6	2.4	47	0.148	0.272
140	Jt7 Ap17 - 14	2246	67	2365	58	0.413	8.8	0.637	0.418	0.012	x	7.4	4.7	1.6	1.7	24	0.092	0.280
141	Jt7 Ap17 - 15	2184	61	2321	60	0.390	8.3	0.597	0.404	0.011	x	7.2	5.4	1.3	1.7	30	0.089	0.289
142	Jt7 Ap17 - 16	2202	71	2260	84	0.415	8.1	0.625	0.406	0.013	x	4.5	3.3	1.4	2.9	37	0.121	0.263
143	Jt7 Ap17 - 18	2181	65	2274	81	0.390	8.1	0.618	0.403	0.012	x	3.4	2.5	1.3	3.0	24	0.105	0.254
144	Jt7 Ap17 - 21	2226	68	2302	76	0.406	8.4	0.636	0.414	0.013	x	7.7	3.9	2.0	2.1	47	0.125	0.252
145	Jt7 Ap17 - 22	2709	477	3124	491	0.769	18	4.1	0.527	0.093	x	0.575	0.766	0.750	119	22	0.897	0.308
146	Jt7 Ap17 - 23	2273	78	2385	68	0.458	9.0	0.678	0.423	0.015	x	14	5.6	2.4	1.5	52	0.148	0.275
147	Jt7 Ap17 - 24	2201	68	2341	66	0.425	8.5	0.618	0.408	0.013	x	9.0	5.2	1.7	1.9	44	0.130	0.290
148	Jt7 Ap17 - 25	2109	69	2203	63	0.449	7.4	0.540	0.386	0.013	x	3.9	3.1	1.3	2.4	19	0.091	0.262
149	Jt7 Ap17 - 26	2293	66	2336	76	0.379	8.9	0.674	0.427	0.012	x	13	5.7	2.3	1.5	59	0.135	0.275
150	Jt7 Ap17 - 27	2150	65	2222	72	0.403	7.7	0.579	0.397	0.012	x	6.4	4.5	1.4	2.4	40	0.124	0.303
151	Jt7 Ap17 - 28	2222	66	2298	71	0.398	8.4	0.619	0.412	0.012	x	5.2	3.9	1.3	2.9	35	0.134	0.303
152	Jt7 Ap17 - 29	2168	68	2255	71	0.413	7.9	0.598	0.402	0.013	x	4.6	3.8	1.2	2.5	28	0.107	0.293
153	Jt7 Ap17 - 30	2163	65	2193	60	0.417	7.6	0.553	0.400	0.012	x	6.0	4.7	1.3	2.4	29	0.122	0.279
154	Jt7 Ap17 - 31	2412	129	2770	195	0.533	12	1.2	0.454	0.024	x	3.1	1.6	2.0	4.0	88	0.297	0.174
155	Jt7 Ap17 - 32	2701	331	3132	574	0.676	18	3.2	0.527	0.065	x	0.730	0.702	1.0	92	29	0.762	0.306
156	Jt7 Ap17 - 33	2050	73	2156	114	0.436	7.0	0.575	0.375	0.013	x	2.0	2.8	0.720	7.0	22	0.187	0.293
157	Jt7 Ap17 - 34	2322	98	2368	68	0.511	9.2	0.761	0.436	0.018	x	7.9	3.8	2.1	2.0	46	0.117	0.259
	Jt10																	
1	Jt10 Ap1 - 01	2576	137	2563	188	0.498	12	1.5	0.491	0.032	x	0.297	0.351	0.846	62	12	0.249	0.154
2	Jt10 Ap1 - 02	3199	201	2750	209	0.531	17	2.5	0.642	0.051	X	0.370	0.392	0.945	77	23	0.309	0.145
3	Jt10 Ap1 - 03	7095	477	2764	152	0.768	53	7.7	2.0	0.222	X	0.381	0.412	0.923	52	22	0.222	0.149
4	Jt10 Ap1 - 04	8421	447	2871	145	0.728	76	10.0	2.7	0.256	X	0.406	0.439	0.925	63	23	0.291	0.151
5	Jt10 Ap1 - 05	4178	198	2743	157	0.560	24	2.7	0.912	0.059	X	0.413	0.453	0.911	72	8.5	0.344	0.144
6	Jt10 Ap1 - 06	2964	172	3063	151	0.609	19	2.2	0.584	0.042	x	0.339	0.389	0.872	71	21	0.260	0.158

#	Sample	$^{238}U/^{206}Pb$	± 2σ	$^{207}Pb/^{206}Pb$	± 2σ	Rho	$^{207}Pb/^{235}U$	± 2σ	$^{206}Pb/^{238}U$	± 2σ	Excluded	La/Yb	La/Sm	Sm/Yb	Cl/Ce	La/U	Sr/Y	Eu/Eu*
7	Jt10 Ap1 - 07	2165	76	2352	138	0.455	8.3	0.753	0.399	0.017	X	0.336	0.395	0.850	32	11	0.117	0.160
8	Jt10 Ap1 - 08	2911	360	2796	454	0.484	15	4.9	0.571	0.088	X	0.464	0.399	1.2	55	22	0.276	0.170
9	Jt10 Ap1 - 09	2062	143	2541	224	0.518	8.7	1.4	0.377	0.031	X	0.326	0.394	0.827	62	7.0	0.241	0.147
10	Jt10 Ap1 - 10	5473	245	3094	139	0.608	44	4.8	1.3	0.089	X	0.673	0.582	1.2	53	26	0.442	0.151
11	Jt10 Ap1 - 11	2890	224	2944	220	0.577	17	2.8	0.566	0.054	x	0.346	0.391	0.887	89	29	0.311	0.164
12	Jt10 Ap1 - 12	2080	61	2163	130	0.419	7.1	0.583	0.381	0.013	x	0.275	0.399	0.690	30	3.7	0.088	0.160
13	Jt10 Ap1 - 13	2691	158	2584	219	0.481	12	1.8	0.518	0.037	X	0.279	0.362	0.770	67	14	0.235	0.165
14	Jt10 Ap1 - 14	2471	120	2728	184	0.462	12	1.5	0.467	0.027	X	0.413	0.386	1.1	57	11	0.273	0.153
15	Jt10 Ap1 - 15	2970	512	1830	660	0.509	9.0	3.8	0.585	0.126	X	0.342	0.386	0.886	81	4.2	0.279	0.153
16	Jt10 Ap1 - 16	4193	142	2568	126	0.523	22	1.9	0.916	0.042	X	0.483	0.387	1.2	75	5.5	0.342	0.158
17	Jt10 Ap2 - 01	2434	135	2702	169	0.545	12	1.4	0.459	0.031	X	0.263	0.332	0.792	82	14	0.219	0.145
18	Jt10 Ap2 - 02	2848	166	3183	146	0.615	19	2.2	0.555	0.040	X	0.302	0.374	0.807	76	19	0.238	0.161
19	Jt10 Ap2 - 03	2499	115	2859	142	0.539	13	1.4	0.473	0.026	X	0.295	0.363	0.811	65	12	0.217	0.153
20	Jt10 Ap2 - 04	4498	331	3588	142	0.742	45	6.2	1.0	0.103	X	0.596	0.559	1.1	68	59	0.445	0.154
21	Jt10 Ap2 - 05	2216	145	2769	217	0.504	11	1.7	0.410	0.032	X	0.304	0.357	0.851	72	18	0.248	0.158
22	Jt10 Ap2 - 06	2231	143	2657	192	0.548	10	1.4	0.414	0.031	X	0.284	0.366	0.777	82	17	0.240	0.158
23	Jt10 Ap2 - 07	2544	160	2792	188	0.552	13	1.8	0.484	0.037	X	0.291	0.358	0.812	86	16	0.279	0.164
24	Jt10 Ap2 - 08	2051	113	2312	193	0.495	7.6	0.982	0.375	0.024	X	0.263	0.330	0.797	47	5.0	0.157	0.163
25	Jt10 Ap2 - 09	2121	74	2078	146	0.443	6.9	0.637	0.390	0.016	x	0.252	0.317	0.795	40	3.8	0.106	0.162
26	Jt10 Ap2 - 10	2851	199	3253	182	0.598	20	2.9	0.556	0.048	X	0.385	0.431	0.892	78	27	0.328	0.162
27	Jt10 Ap2 - 11	3381	294	3501	260	0.554	29	5.9	0.690	0.077	X	0.540	0.513	1.1	75	44	0.435	0.162
28	Jt10 Ap3 - 01	2804	124	2390	162	0.497	12	1.3	0.545	0.030	X	0.522	0.331	1.6	43	3.9	0.315	0.170
29	Jt10 Ap3 - 02	2318	134	2437	249	0.424	9.4	1.5	0.433	0.030	x	0.368	0.384	0.960	57	13	0.173	0.165
30	Jt10 Ap3 - 03	2850	185	2624	190	0.574	14	1.9	0.556	0.045	X	0.337	0.372	0.906	70	22	0.253	0.154
31	Jt10 Ap3 - 04	2419	171	2838	283	0.440	13	2.4	0.455	0.039	X	0.300	0.358	0.839	74	21	0.255	0.157
32	Jt10 Ap3 - 05	2495	152	2592	149	0.636	11	1.3	0.472	0.035	x	0.340	0.391	0.868	75	6.1	0.279	0.151
33	Jt10 Ap3 - 06	3174	287	2694	250	0.604	16	3.1	0.636	0.073	X	0.308	0.349	0.883	73	15	0.261	0.156
34	Jt10 Ap3 - 07	3130	146	2423	157	0.537	14	1.5	0.625	0.037	X	0.405	0.408	0.992	60	9.7	0.256	0.158
35	Jt10 Ap3 - 08	3004	314	3154	234	0.662	20	4.0	0.594	0.077	x	0.360	0.396	0.910	65	28	0.239	0.152
36	Jt10 Ap3 - 09	2299	173	2612	280	0.470	10	2.0	0.428	0.038	X	0.391	0.423	0.926	68	13	0.249	0.156
37	Jt10 Ap3 - 10	2722	184	2983	236	0.492	16	2.7	0.525	0.044	X	0.397	0.336	1.2	58	24	0.304	0.143
38	Jt10 Ap3 - 11	2993	100	2712	123	0.490	15	1.3	0.591	0.025	X	0.464	0.450	1.0	42	6.6	0.281	0.157
39	Jt10 Ap3 - 12	3955	232	2569	172	0.608	20	2.6	0.847	0.067	X	0.359	0.399	0.898	60	8.6	0.253	0.147
40	Jt10 Ap3 - 14	4105	130	2560	122	0.505	21	1.8	0.891	0.038	X	0.646	0.461	1.4	51	5.8	0.428	0.158
41	Jt10 Ap3 - 15	2290	141	2444	183	0.561	9.3	1.2	0.427	0.031	X	0.347	0.348	0.997	49	13	0.229	0.159
42	Jt10 Ap4 - 01	2184	136	2546	153	0.624	9.4	1.1	0.403	0.029	X	0.286	0.346	0.828	62	9.2	0.230	0.153
43	Jt10 Ap4 - 02	1830	106	2699	189	0.502	8.4	1.1	0.328	0.022	X	0.319	0.416	0.768	48	7.9	0.220	0.145
44	Jt10 Ap4 - 03	2126	117	2684	190	0.489	9.9	1.3	0.391	0.025	X	0.274	0.352	0.777	63	11	0.199	0.153

#	Sample	$^{238}U/^{206}Pb$	± 2σ	$^{207}Pb/^{206}Pb$	± 2σ	Rho	$^{207}Pb/^{235}U$	± 2σ	$^{206}Pb/^{238}U$	± 2σ	Excluded	La/Yb	La/Sm	Sm/Yb	Cl/Ce	La/U	Sr/Y	Eu/Eu*
45	Jt10 Ap4 - 04	2158	96	2351	160	0.487	8.2	0.886	0.398	0.021	X	0.349	0.433	0.807	56	11	0.192	0.153
46	Jt10 Ap4 - 05	2472	173	2699	180	0.612	12	1.6	0.467	0.039	X	0.366	0.372	0.985	66	22	0.271	0.167
47	Jt10 Ap4 - 06	2391	136	2732	169	0.552	12	1.4	0.449	0.030	X	0.416	0.424	0.981	46	20	0.289	0.171
48	Jt10 Ap4 - 07	1774	132	3665	142	0.676	15	1.9	0.317	0.027	X	0.740	0.434	1.7	71	17	0.579	0.169
49	Jt10 Ap4 - 08	2410	173	2914	198	0.576	13	2.0	0.453	0.039	X	0.307	0.364	0.845	78	23	0.253	0.157
50	Jt10 Ap4 - 09	3626	246	3560	137	0.705	33	4.2	0.755	0.067	X	0.460	0.487	0.944	69	36	0.353	0.150
51	Jt10 Ap4 - 10	1246	71	2560	241	0.396	5.0	0.786	0.213	0.013	X	0.351	0.413	0.851	67	8.7	0.236	0.157
52	Jt10 Ap4 - 11	2227	129	2485	188	0.524	9.3	1.2	0.413	0.028	X	0.273	0.339	0.805	66	14	0.198	0.159
53	Jt10 Ap4 - 12	2134	136	2812	203	0.517	11	1.6	0.392	0.029	X	0.326	0.371	0.877	67	16	0.252	0.149
54	Jt10 Ap4 - 13	2263	122	2571	220	0.437	9.9	1.5	0.421	0.027	X	0.359	0.370	0.971	49	15	0.242	0.162
55	Jt10 Ap4 - 14	2059	80	2120	155	0.457	6.8	0.678	0.376	0.017	x	0.265	0.338	0.782	44	4.8	0.135	0.152
56	Jt10 Ap5 - 01	2203	109	2418	215	0.421	8.8	1.2	0.407	0.024	X	0.267	0.341	0.783	58	12	0.188	0.160
57	Jt10 Ap5 - 02	2203	118	2279	190	0.498	8.1	1.0	0.407	0.026	x	0.304	0.358	0.847	54	16	0.173	0.158
58	Jt10 Ap5 - 03	2471	148	2469	177	0.566	10	1.3	0.467	0.034	x	0.240	0.322	0.744	66	15	0.185	0.159
59	Jt10 Ap5 - 04	2254	144	2697	220	0.493	11	1.6	0.419	0.032	X	0.220	0.305	0.721	69	15	0.192	0.165
60	Jt10 Ap5 - 05	3231	202	2580	189	0.575	15	2.1	0.651	0.052	X	0.244	0.327	0.746	74	17	0.235	0.158
61	Jt10 Ap5 - 06	2172	92	2164	142	0.521	7.5	0.711	0.401	0.020	x	0.275	0.348	0.791	35	4.4	0.124	0.155
62	Jt10 Ap5 - 07	2266	117	2350	194	0.476	8.7	1.1	0.421	0.026	x	0.220	0.309	0.713	62	11	0.173	0.156
63	Jt10 Ap5 - 08	2426	172	2515	233	0.523	10	1.7	0.457	0.039	x	0.247	0.318	0.778	73	19	0.227	0.153
64	Jt10 Ap5 - 09	2552	115	2239	178	0.470	9.4	1.1	0.486	0.027	X	0.247	0.312	0.792	48	3.9	0.150	0.168
65	Jt10 Ap5 - 10	2527	145	2402	185	0.538	10	1.3	0.480	0.033	X	0.247	0.327	0.754	54	14	0.177	0.152
66	Jt10 Ap5 - 11	2703	188	2639	198	0.581	13	1.9	0.521	0.044	x	0.268	0.356	0.753	66	21	0.242	0.162
67	Jt10 Ap5 - 12	1513	110	2494	279	0.441	6.0	1.1	0.264	0.021	X	0.514	0.461	1.1	43	12	0.382	0.158
68	Jt10 Ap5 - 13	2229	160	2790	229	0.520	11	1.8	0.413	0.035	X	0.238	0.351	0.679	65	6.7	0.216	0.154
69	Jt10 Ap5 - 15	2414	247	2718	162	0.781	12	1.8	0.454	0.056	X	0.267	0.325	0.823	58	18	0.238	0.160
70	Jt10 Ap5 - 16	1597	105	2471	285	0.402	6.3	1.2	0.281	0.021	X	0.316	0.373	0.846	48	10	0.217	0.159
71	Jt10 Ap5 - 17	2283	126	2319	211	0.472	8.7	1.2	0.425	0.028	X	0.357	0.388	0.919	42	11	0.211	0.161
72	Jt10 Ap6 - 01	2204	127	2335	196	0.513	8.4	1.1	0.408	0.028	x	0.266	0.334	0.795	39	16	0.185	0.159
73	Jt10 Ap6 - 02	2509	166	2642	186	0.581	12	1.6	0.476	0.038	X	0.291	0.362	0.804	38	18	0.183	0.159
74	Jt10 Ap6 - 03	2084	113	2248	234	0.425	7.5	1.1	0.382	0.024	x	0.361	0.385	0.938	39	17	0.299	0.175
75	Jt10 Ap6 - 05	1990	102	2362	197	0.457	7.6	0.982	0.362	0.021	X	1.2	0.288	4.3	6.4	7.2	0.311	0.294
76	Jt10 Ap6 - 06	2088	62	2056	142	0.396	6.7	0.586	0.382	0.013	X	0.723	0.200	3.6	3.5	8.3	0.142	0.213
77	Jt10 Ap6 - 07	2136	98	2234	169	0.482	7.6	0.849	0.393	0.021	X	0.595	0.278	2.1	18	7.2	0.412	0.223
78	Jt10 Ap6 - 08	2512	178	2921	185	0.599	14	2.0	0.477	0.041	X	1.3	0.276	4.5	9.3	17	0.472	0.288
79	Jt10 Ap6 - 09	2708	145	2389	192	0.502	11	1.4	0.522	0.034	X	0.360	0.374	0.962	22	21	0.142	0.177
80	Jt10 Ap6 - 10	2121	108	2022	186	0.494	6.7	0.806	0.390	0.023	X	0.465	0.370	1.3	20	13	0.226	0.507
81	Jt10 Ap6 - 11	2465	188	2564	223	0.567	11	1.8	0.466	0.043	x	0.433	0.435	0.996	9.5	9.7	0.076	0.170
82	Jt10 Ap6 - 12	2962	273	2726	307	0.525	15	3.3	0.583	0.067	x	1.0	0.221	4.7	4.4	22	0.152	0.224

#	Sample	$^{238}U/^{206}Pb$	± 2σ	$^{207}Pb/^{206}Pb$	± 2σ	Rho	$^{207}Pb/^{235}U$	± 2σ	$^{206}Pb/^{238}U$	± 2σ	Excluded	La/Yb	La/Sm	Sm/Yb	Cl/Ce	La/U	Sr/Y	Eu/Eu*
83	Jt10 Ap6 - 14	2263	184	2107	225	0.601	7.6	1.2	0.421	0.041	x	0.267	0.340	0.786	25	10	0.127	0.158
84	Jt10 Ap7 - 01	2079	47	2112	115	0.375	6.9	0.488	0.380	0.010	X	0.508	0.477	1.1	35	28	0.366	0.222
85	Jt10 Ap7 - 02	2108	48	2135	117	0.369	7.1	0.510	0.387	0.010	X	1.2	0.378	3.2	9.6	42	0.316	0.527
86	Jt10 Ap7 - 03	2122	62	2126	131	0.415	7.1	0.583	0.390	0.013	X	0.624	0.466	1.3	13	8.0	0.314	0.215
87	Jt10 Ap7 - 04	2069	52	2118	124	0.387	6.9	0.526	0.378	0.011	X	0.486	0.419	1.2	26	23	0.224	0.161
88	Jt10 Ap7 - 05	1778	224	1765	216	0.570	4.7	0.388	0.318	0.046	X	0.430	0.334	1.3	10.0	6.2	0.275	0.247
89	Jt10 Ap7 - 06	2115	52	2087	122	0.384	6.9	0.519	0.388	0.011	x	0.510	0.365	1.4	13	5.1	0.390	0.225
90	Jt10 Ap7 - 07	2311	83	2166	120	0.526	8.0	0.651	0.431	0.018	X	0.340	0.541	0.628	12	8.8	0.188	0.230
91	Jt10 Ap7 - 08	2171	52	2121	116	0.397	7.3	0.523	0.401	0.011	x	0.610	0.312	2.0	27	5.7	0.564	0.232
92	Jt10 Ap7 - 09	2401	291	1951	140	0.843	7.4	0.912	0.451	0.066	x	0.594	0.346	1.7	15	6.1	0.369	0.219
93	Jt10 Ap7 - 10	3017	341	2391	160	0.833	13	2.2	0.597	0.084	x	0.515	0.386	1.3	6.1	9.8	0.194	0.204
94	Jt10 Ap7 - 11	2174	71	2122	153	0.403	7.3	0.694	0.401	0.015	x	0.568	0.376	1.5	9.9	7.8	0.403	0.220
95	Jt10 Ap7 - 12	2099	47	2158	114	0.373	7.1	0.501	0.385	0.010	X	2.2	0.478	4.6	3.0	27	0.313	0.229
96	Jt10 Ap7 - 13	1957	138	2060	157	0.677	6.2	0.754	0.355	0.029		0.685	0.454	1.5	8.0	7.6	0.351	0.309
97	Jt10 Ap7 - 14	2416	61	2267	115	0.410	9.0	0.659	0.455	0.014	X	1.1	0.307	3.7	4.8	23	0.302	0.209
98	Jt10 Ap7 - 15	2225	48	2197	112	0.368	7.8	0.541	0.412	0.011	X	0.517	0.651	0.794	10	7.2	0.210	0.854
99	Jt10 Ap7 - 16	2143	49	2179	114	0.380	7.4	0.524	0.394	0.011	X	0.535	0.173	3.1	7.2	22	0.142	0.287
100	Jt10 Ap7 - 17	2280	234	1987	165	0.651	7.1	0.568	0.424	0.052	X	0.879	0.486	1.8	22	36	0.754	0.167
101	Jt10 Ap7 - 18	2755	113	2323	128	0.560	11	0.982	0.533	0.027	x	1.1	0.214	5.1	4.1	19	0.256	0.230
102	Jt10 Ap7 - 19	2045	104	2057	139	0.602	6.5	0.644	0.373	0.022	X	1.0	0.265	3.8	3.7	11	0.211	0.201
103	Jt10 Ap7 - 20	2867	108	2212	110	0.592	11	0.845	0.560	0.026	X	0.695	0.386	1.8	9.5	16	0.359	0.205
104	Jt10 Ap8 - 01	1713	83	2032	134	0.589	5.3	0.494	0.304	0.017	X	0.559	0.494	1.1	43	47	0.224	0.151
105	Jt10 Ap8 - 02	2115	46	2167	112	0.369	7.2	0.502	0.388	0.010	X	0.619	0.511	1.2	43	50	0.221	0.148
106	Jt10 Ap8 - 03	2158	53	2204	117	0.394	7.6	0.554	0.398	0.011	X	0.443	0.451	0.983	28	9.3	0.141	0.146
107	Jt10 Ap8 - 04	2027	46	2076	117	0.371	6.5	0.467	0.370	0.010	x	0.951	1.1	0.893	5.4	9.2	0.037	0.159
108	Jt10 Ap8 - 05	2390	70	2274	122	0.443	8.9	0.705	0.449	0.016	X	4.1	2.8	1.4	1.3	28	0.027	0.174
109	Jt10 Ap8 - 06	2436	110	2332	184	0.449	9.4	1.1	0.459	0.025	X	1.4	1.4	1.0	3.9	12	0.031	0.167
110	Jt10 Ap8 - 07	2149	151	2056	169	0.652	6.9	0.874	0.396	0.033	x	0.280	0.356	0.787	32	3.9	0.105	0.163
111	Jt10 Ap8 - 08	3272	310	2571	322	0.531	16	3.6	0.661	0.080	x	0.508	0.564	0.900	15	6.7	0.061	0.166
112	Jt10 Ap8 - 10	2100	52	2133	119	0.392	7.0	0.518	0.385	0.011	X	0.680	0.736	0.925	11	2.8	0.085	0.163
113	Jt10 Ap8 - 11	2015	230	2017	223	0.726	6.3	1.2	0.367	0.049	x	0.472	0.580	0.814	15	5.2	0.054	0.158
114	Jt10 Ap8 - 12	2318	89	2043	153	0.465	7.5	0.736	0.433	0.020	X	0.277	0.377	0.736	23	3.7	0.078	0.156
115	Jt10 Ap8 - 13	2336	59	2187	119	0.403	8.2	0.615	0.437	0.013	X	7.8	7.3	1.1	3.0	68	0.108	0.144
116	Jt10 Ap8 - 14	2025	47	2082	119	0.372	6.6	0.476	0.369	0.010	X	0.951	0.971	0.980	5.4	10	0.031	0.162
117	Jt10 Ap8 - 15	2128	70	2144	147	0.418	7.2	0.667	0.391	0.015	X	0.923	0.836	1.1	17	13	0.101	0.159
118	Jt10 Ap8 - 16	2024	74	2019	136	0.487	6.3	0.556	0.369	0.016	X	1.6	1.8	0.919	6.6	17	0.051	0.160
119	Jt10 Ap8 - 17	2996	177	2473	173	0.586	13	1.7	0.591	0.044	x	0.381	0.456	0.834	18	4.3	0.059	0.155
120	Jt10 Ap8 - 18	2524	75	2400	124	0.441	10	0.830	0.479	0.017	x	1.4	1.3	1.1	3.9	13	0.029	0.173

#	Sample	$^{238}U/^{206}Pb$	± 2σ	$^{207}Pb/^{206}Pb$	± 2σ	Rho	$^{207}Pb/^{235}U$	± 2σ	$^{206}Pb/^{238}U$	± 2σ	Excluded	La/Yb	La/Sm	Sm/Yb	Cl/Ce	La/U	Sr/Y	Eu/Eu*
121	Jt10 Ap8 - 19	2905	137	2783	157	0.523	15	1.7	0.569	0.033	X	0.398	0.457	0.870	15	2.6	0.048	0.162
122	Jt10 Ap8 - 20	2885	91	2581	135	0.434	13	1.2	0.565	0.022	X	0.551	0.567	0.972	12	6.2	0.050	0.161
123	Jt10 Ap9 - 01	2345	110	2332	170	0.490	9.0	1.0	0.439	0.024	x	1.5	1.5	1.0	2.7	12	0.021	0.171
124	Jt10 Ap9 - 02	2125	156	2336	264	0.488	8.0	1.4	0.390	0.034	x	1.2	1.2	0.988	3.8	12	0.026	0.175
125	Jt10 Ap9 - 03	2107	65	2133	134	0.424	7.1	0.598	0.387	0.014	X	0.482	0.554	0.870	9.7	4.2	0.038	0.162
126	Jt10 Ap9 - 04	2162	196	1963	107	0.872	6.6	0.809	0.398	0.042	X	0.481	0.554	0.869	11	4.7	0.044	0.165
127	Jt10 Ap9 - 05	2928	195	2610	200	0.569	14	2.0	0.575	0.048	x	0.184	0.270	0.680	25	1.5	0.054	0.158
128	Jt10 Ap9 - 06	2139	54	2166	118	0.402	7.3	0.542	0.393	0.012	X	0.447	0.539	0.830	19	3.3	0.066	0.172
129	Jt10 Ap9 - 07	2081	79	2071	143	0.478	6.7	0.624	0.381	0.017	X	0.490	0.574	0.854	12	1.5	0.043	0.167
130	Jt10 Ap9 - 08	2415	88	2242	125	0.518	8.8	0.749	0.455	0.020	x	1.4	1.4	1.0	3.0	14	0.022	0.171
131	Jt10 Ap9 - 09	2092	63	2104	123	0.451	6.9	0.542	0.383	0.014	x	0.987	1.0	0.980	4.5	8.6	0.026	0.169
132	Jt10 Ap9 - 10	2529	62	2237	121	0.391	9.3	0.708	0.480	0.014	x	0.645	0.763	0.846	7.0	6.8	0.031	0.168
133	Jt10 Ap9 - 11	2043	74	2101	144	0.458	6.7	0.618	0.373	0.016	X	0.205	0.285	0.718	34	2.8	0.081	0.153
134	Jt10 Ap10 - 01	2439	61	2225	119	0.402	8.9	0.663	0.460	0.014	X	0.302	0.370	0.816	57	7.5	0.174	0.162
135	Jt10 Ap10 - 02	2232	66	2208	135	0.409	7.9	0.673	0.414	0.014	X	0.750	0.859	0.872	25	2.6	0.115	0.148
136	Jt10 Ap10 - 03	2165	76	2143	143	0.450	7.3	0.672	0.399	0.016	X	0.461	0.424	1.1	74	14	0.247	0.144
137	Jt10 Ap10 - 04	2212	48	2275	110	0.369	8.1	0.560	0.409	0.010	x	0.515	0.608	0.847	12	5.4	0.047	0.164
138	Jt10 Ap10 - 05	1868	99	2249	143	0.593	6.6	0.676	0.336	0.021	X	0.284	0.342	0.829	46	5.1	0.134	0.166
139	Jt10 Ap10 - 06	2323	54	2359	113	0.385	9.0	0.646	0.434	0.012	X	0.282	0.347	0.813	40	4.1	0.110	0.157
140	Jt10 Ap10 - 07	2176	48	2224	112	0.373	7.7	0.541	0.402	0.010	X	0.294	0.363	0.810	24	3.1	0.071	0.159
141	Jt10 Ap10 - 08	2065	92	2118	196	0.422	6.8	0.847	0.378	0.020	x	0.439	0.532	0.826	11	4.6	0.042	0.163
142	Jt10 Ap10 - 09	1684	315	4636	229	0.664	27	3.8	0.299	0.063	X	0.315	0.382	0.826	39	5.9	0.131	0.156
143	Jt10 Ap10 - 10	1661	149	3016	256	0.538	9.1	1.7	0.294	0.030	X	0.239	0.321	0.744	33	2.6	0.090	0.155
144	Jt10 Ap10 - 11	2920	130	2293	135	0.576	11	1.1	0.573	0.032	X	0.269	0.326	0.826	29	4.6	0.084	0.152
145	Jt10 Ap10 - 12	3108	157	2293	188	0.502	12	1.6	0.620	0.039	X	0.314	0.352	0.892	34	5.2	0.098	0.157
146	Jt10 Ap10 - 13	1943	92	2149	221	0.396	6.5	0.896	0.352	0.019		0.630	0.584	1.1	58	13	0.493	0.173
147	Jt10 Ap10 - 14	1961	104	2201	193	0.482	6.8	0.859	0.356	0.022		1.3	0.935	1.4	13	18	0.117	0.159
148	Jt10 Ap10 - 15	1983	92	1919	208	0.421	5.8	0.747	0.360	0.019		2.1	1.8	1.2	3.1	20	0.030	0.174
149	Jt10 Ap10 - 16	2159	149	2661	241	0.488	9.9	1.7	0.398	0.032	X	0.323	0.393	0.822	56	9.8	0.206	0.168
150	Jt10 Ap10 - 17	3582	125	2175	141	0.491	14	1.3	0.743	0.034	X	0.397	0.437	0.909	41	10	0.168	0.161
151	Jt10 Ap12 - 04	2226	98	2048	190	0.434	7.2	0.860	0.412	0.021	X	0.405	0.446	0.910	45	7.0	0.152	0.152
152	Jt10 Ap12 - 06	1925	71	1906	177	0.397	5.6	0.600	0.348	0.015	X	12	5.7	2.2	99	3.5	89	0.289
153	Jt10 Ap12 - 14	1925	127	1979	273	0.446	5.8	1.0	0.348	0.027		0.973	0.961	1.0	4.4	9.0	0.026	0.156
154	Jt10 Ap13 - 01	1949	76	2052	160	0.447	6.2	0.626	0.353	0.016		0.785	0.755	1.0	16	11	0.145	0.178
155	Jt10 Ap13 - 02	2312	118	2285	149	0.571	8.6	0.911	0.432	0.026	x	0.337	0.366	0.922	35	3.8	0.127	0.152
156	Jt10 Ap13 - 03	1951	75	2059	169	0.422	6.2	0.654	0.353	0.016		0.469	0.436	1.1	51	21	0.273	0.155
157	Jt10 Ap13 - 04	3060	148	2233	166	0.533	12	1.3	0.607	0.037	X	1.0	1.1	0.966	8.3	9.8	0.054	0.166
158	Jt10 Ap13 - 05	2044	92	2067	166	0.488	6.6	0.709	0.373	0.020	X	0.282	0.341	0.829	17	2.9	0.046	0.151

#	Sample	$^{238}U/^{206}Pb$	± 2σ	$^{207}Pb/^{206}Pb$	± 2σ	Rho	$^{207}Pb/^{235}U$	± 2σ	$^{206}Pb/^{238}U$	± 2σ	Excluded	La/Yb	La/Sm	Sm/Yb	Cl/Ce	La/U	Sr/Y	Eu/Eu*
159	Jt10 Ap13 - 06	2561	187	2283	205	0.597	9.7	1.4	0.488	0.043	X	1.1	0.439	2.5	31	17	0.766	0.337
160	Jt10 Ap13 - 07	1867	67	2036	151	0.433	5.8	0.552	0.336	0.014	X	0.547	0.589	0.930	13	4.2	0.061	0.156
161	Jt10 Ap13 - 08	2047	136	2325	229	0.501	7.6	1.2	0.374	0.029	x	0.414	0.476	0.869	24	1.2	0.087	0.153
162	Jt10 Ap13 - 09	2992	210	3275	187	0.593	22	3.2	0.591	0.052	X	0.336	0.374	0.898	17	2.8	0.061	0.150
163	Jt10 Ap13 - 10	2202	93	2268	162	0.469	8.0	0.857	0.407	0.020	x	0.326	0.386	0.844	23	3.4	0.079	0.155
164	Jt10 Ap13 - 11	2489	120	2331	144	0.569	9.7	0.986	0.471	0.027	X	0.359	0.425	0.846	13	3.3	0.041	0.163
165	Jt10 Ap14 - 02	2312	119	2496	161	0.539	9.7	1.1	0.431	0.026	X	0.690	0.638	1.1	10.0	7.6	0.058	0.155
166	Jt10 Ap14 - 07	2095	50	2146	122	0.370	7.1	0.531	0.384	0.011	X	0.642	0.653	0.982	14	8.0	0.083	0.150
167	Jt10 Ap14 - 08	2354	140	2490	226	0.467	9.9	1.5	0.441	0.031	X	3.6	2.4	1.5	1.2	26	0.020	0.173

Supplementary Table 3B. Summary of U-Pb data for in-house reference materials

#	Standard	$^{238}U/^{206}Pb$	± 2σ	$^{207}Pb/^{206}Pb$	± 2σ	Rho	$^{207}Pb/^{235}U$	± 2σ	$^{206}Pb/^{238}U$	± 2σ
1	MAD	13.2	0.306	0.057	0.004	0.192	478	0.601	472	0.002
2	MAD	13.1	0.304	0.057	0.004	-0.008	480	0.604	476	0.002
3	MAD	13.2	0.307	0.057	0.004	-0.126	476	0.598	472	0.002
4	MAD	13.2	0.307	0.057	0.004	-0.093	476	0.598	471	0.002
5	MAD	13.0	0.302	0.057	0.004	-0.044	482	0.608	479	0.002
6	MAD	13.0	0.303	0.056	0.004	-0.034	480	0.604	476	0.002
7	MAD	13.3	0.309	0.056	0.004	-0.287	472	0.592	469	0.002
8	MAD	13.2	0.308	0.056	0.004	0.198	474	0.594	468	0.002
9	MAD	13.0	0.303	0.057	0.004	-0.203	480	0.605	477	0.002
10	MAD	12.8	0.299	0.057	0.004	-0.243	487	0.615	485	0.002
11	MAD	13.2	0.308	0.057	0.004	-0.075	476	0.598	469	0.002
12	MAD	13.2	0.307	0.057	0.004	-0.190	476	0.599	470	0.002
13	MAD	13.2	0.308	0.057	0.004	0.040	476	0.598	471	0.002
14	MAD	13.1	0.305	0.057	0.004	-0.246	477	0.600	474	0.002
15	MAD	13.1	0.305	0.057	0.004	-0.163	480	0.604	474	0.002
16	MAD	13.0	0.303	0.057	0.004	-0.035	481	0.606	477	0.002
17	MAD	13.0	0.303	0.057	0.004	-0.043	481	0.606	478	0.002
18	MAD	13.1	0.305	0.057	0.004	-0.108	479	0.602	474	0.002
19	MAD	12.9	0.301	0.057	0.004	-0.102	483	0.609	479	0.002
20	MAD	13.2	0.308	0.057	0.004	0.045	475	0.597	469	0.002
21	MAD	13.2	0.306	0.056	0.004	0.070	475	0.597	471	0.002
22	MAD	13.2	0.308	0.056	0.004	-0.179	473	0.594	469	0.002
23	MAD	12.9	0.301	0.057	0.004	-0.123	483	0.609	480	0.002
24	MAD	13.4	0.311	0.057	0.004	0.001	471	0.590	465	0.002
25	MAD	13.3	0.309	0.057	0.004	-0.136	473	0.593	468	0.002
26	MAD	13.2	0.308	0.057	0.004	-0.139	474	0.595	470	0.002
27	MAD	13.1	0.304	0.057	0.004	-0.098	480	0.604	476	0.002
28	MAD	13.1	0.305	0.057	0.004	-0.267	478	0.601	474	0.002
29	MAD	13.0	0.303	0.057	0.004	-0.291	481	0.606	476	0.002
30	MAD	12.8	0.298	0.057	0.004	-0.186	487	0.616	484	0.002
31	MAD	13.1	0.304	0.057	0.004	-0.187	479	0.603	475	0.002
32	MAD	13.0	0.302	0.057	0.004	-0.204	482	0.608	478	0.002
33	MAD	13.0	0.304	0.057	0.004	-0.237	481	0.606	476	0.002
34	MAD	13.1	0.306	0.057	0.004	-0.137	479	0.602	474	0.002
35	MAD	13.4	0.311	0.057	0.004	-0.176	473	0.593	465	0.002
36	MAD	13.5	0.314	0.057	0.004	-0.192	469	0.587	460	0.002
37	MAD	13.0	0.302	0.057	0.004	-0.005	485	0.613	479	0.002
38	MAD	13.0	0.302	0.056	0.004	0.054	483	0.609	479	0.002
39	MAD	13.2	0.308	0.057	0.004	-0.154	477	0.599	469	0.002
40	MAD	13.7	0.436	0.057	0.004	-0.139	463	0.578	453	0.002
41	MAD	13.3	0.309	0.057	0.004	-0.090	476	0.599	469	0.002
42	MAD	12.9	0.300	0.057	0.004	-0.162	488	0.617	482	0.002
	401									
1	401	11.9	0.385	0.066	0.005	0.064	577	0.766	518	0.003
2	401	12.0	0.386	0.066	0.005	0.340	577	0.766	517	0.003
3	401	11.9	0.385	0.067	0.005	0.246	586	0.780	521	0.003
4	401	11.9	0.397	0.067	0.005	0.149	591	0.789	521	0.003
5	401	12.3	0.400	0.071	0.011	0.565	599	0.803	504	0.003
6	401	12.0	0.387	0.066	0.005	-0.190	580	0.771	518	0.003
7	401	12.2	0.399	0.064	0.006	0.189	555	0.728	507	0.003
8	401	12.3	0.402	0.075	0.007	-0.050	625	0.851	503	0.003
9	401	11.8	0.384	0.069	0.005	0.245	607	0.819	525	0.003

#	Standard	$^{238}U/^{206}Pb$	± 2σ	$^{207}Pb/^{206}Pb$	± 2σ	Rho	$^{207}Pb/^{235}U$	± 2σ	$^{206}Pb/^{238}U$	± 2σ
10	401	12.0	0.392	0.065	0.005	-0.121	571	0.755	517	0.003
11	401	11.7	0.383	0.068	0.007	-0.098	599	0.804	526	0.003
12	401	11.9	0.388	0.065	0.006	0.221	574	0.760	520	0.003
13	401	11.9	0.387	0.067	0.006	0.109	590	0.789	519	0.003
14	401	11.9	0.390	0.071	0.006	0.105	614	0.831	518	0.003
15	401	12.1	0.399	0.064	0.006	0.161	561	0.738	512	0.003
16	401	11.5	0.374	0.069	0.006	0.206	618	0.838	537	0.003
17	401	11.7	0.384	0.069	0.006	-0.046	608	0.820	528	0.003
18	401	11.5	0.376	0.065	0.005	0.188	590	0.789	535	0.003
19	401	11.8	0.387	0.070	0.007	0.204	611	0.825	525	0.003
20	401	11.7	0.384	0.066	0.006	0.283	588	0.784	528	0.003
21	401	11.3	0.501	0.069	0.006	0.455	622	0.844	542	0.007
22	401	11.8	0.386	0.071	0.005	0.130	621	0.844	526	0.003
23	401	11.6	0.414	0.063	0.005	0.327	572	0.756	534	0.004
24	401	11.8	0.387	0.073	0.007	0.280	632	0.864	523	0.003
25	401	12.0	0.394	0.070	0.006	0.244	603	0.811	518	0.003
26	401	12.0	0.397	0.065	0.005	0.068	569	0.751	513	0.003
27	401	11.9	0.391	0.072	0.006	-0.028	623	0.847	519	0.003
28	401	12.0	0.396	0.065	0.005	-0.051	568	0.749	514	0.003
29	401	11.9	0.393	0.071	0.007	0.095	613	0.828	519	0.003
30	401	12.1	0.398	0.068	0.005	0.029	586	0.782	513	0.003
31	401	11.6	0.407	0.065	0.006	0.074	586	0.780	530	0.003
32	401	11.7	0.387	0.075	0.018	-0.026	644	0.886	528	0.003
33	401	11.8	0.391	0.073	0.006	0.260	631	0.861	522	0.003
34	401	11.8	0.391	0.070	0.006	0.291	611	0.826	522	0.003
35	401	12.0	0.403	0.071	0.006	0.149	608	0.820	514	0.003
36	401	12.0	0.398	0.143	0.144	0.212	994	1.7	515	0.003
37	401	11.9	0.395	0.070	0.006	-0.098	610	0.824	520	0.003
38	401	11.9	0.401	0.105	0.081	0.106	815	1.2	522	0.003
39	401	11.7	0.389	0.062	0.006	0.362	560	0.736	526	0.003
40	401	11.7	0.387	0.070	0.006	0.023	618	0.837	528	0.003
41	401	11.4	0.375	0.062	0.005	0.168	581	0.772	543	0.003
42	401	11.3	0.375	0.065	0.005	0.036	601	0.807	546	0.003
	McClure									
1	McClure	9.9	0.295	0.200	0.008	0.007	1358	2.8	619	0.003
2	McClure	10.8	0.290	0.147	0.005	-0.095	1081	1.9	570	0.003
3	McClure	10.2	0.321	0.176	0.009	0.226	1244	2.4	605	0.003
4	McClure	9.8	0.318	0.190	0.010	0.258	1333	2.7	627	0.004
5	McClure	10.5	0.321	0.154	0.008	0.046	1132	2.0	589	0.003
6	McClure	10.5	0.300	0.135	0.006	0.180	1044	1.8	588	0.003
7	McClure	7.9	0.250	0.316	0.011	0.152	1915	5.6	770	0.004
8	McClure	9.6	0.267	0.236	0.007	0.170	1513	3.4	641	0.003
9	McClure	9.0	0.257	0.247	0.008	0.258	1601	3.8	678	0.003
10	McClure	9.1	0.321	0.250	0.011	-0.403	1598	3.8	673	0.004
11	McClure	10.2	0.294	0.176	0.008	-0.055	1244	2.4	605	0.003
12	McClure	10.1	0.295	0.187	0.009	0.290	1297	2.6	609	0.003
13	McClure	10.4	0.316	0.159	0.007	0.295	1159	2.1	593	0.003
14	McClure	10.0	0.313	0.185	0.008	0.303	1291	2.6	614	0.003
15	McClure	8.6	0.282	0.275	0.011	0.302	1725	4.5	709	0.004
16	McClure	9.3	0.292	0.253	0.011	0.378	1591	3.8	656	0.003
17	McClure	10.5	0.304	0.161	0.006	0.178	1157	2.1	585	0.003
18	McClure	11.0	0.310	0.139	0.007	0.556	1033	1.8	561	0.003
19	McClure	9.2	0.330	0.234	0.012	0.456	1533	3.5	663	0.004
20	McClure	8.4	0.300	0.254	0.014	0.312	1675	4.2	729	0.005

#	Standard	$^{238}U/^{206}Pb$	± 2σ	$^{207}Pb/^{206}Pb$	± 2σ	Rho	$^{207}Pb/^{235}U$	± 2σ	$^{206}Pb/^{238}U$	± 2σ
21	McClure	9.4	0.274	0.246	0.009	0.546	1564	3.7	655	0.003
22	McClure	9.4	0.273	0.236	0.008	0.118	1531	3.5	653	0.003
23	McClure	10.3	0.303	0.163	0.007	0.238	1184	2.2	597	0.003
24	McClure	10.4	0.302	0.167	0.007	0.057	1194	2.2	593	0.003
25	McClure	8.3	0.267	0.314	0.012	0.486	1857	5.2	731	0.004
26	McClure	8.6	0.266	0.281	0.010	0.462	1739	4.5	710	0.004
27	McClure	9.0	0.335	0.233	0.012	0.368	1547	3.6	678	0.004
28	McClure	10.5	0.318	0.154	0.007	0.039	1132	2.0	588	0.003
29	McClure	10.4	0.315	0.153	0.007	0.125	1129	2.0	590	0.003
30	McClure	10.3	0.312	0.171	0.007	0.102	1219	2.3	598	0.003
31	McClure	10.3	0.352	0.172	0.008	0.242	1219	2.3	595	0.004
32	McClure	10.8	0.328	0.157	0.007	0.136	1125	2.0	573	0.003
33	McClure	11.1	0.311	0.118	0.005	0.060	921	1.5	556	0.003
34	McClure	8.8	0.283	0.265	0.012	0.488	1677	4.2	696	0.004
35	McClure	8.9	0.272	0.255	0.010	0.421	1638	4.0	689	0.004
36	McClure	10.4	0.341	0.168	0.010	0.508	1202	2.3	594	0.003
37	McClure	10.4	0.317	0.143	0.008	0.209	1085	1.9	590	0.003
38	McClure	7.7	0.211	0.348	0.009	0.294	2021	6.3	787	0.004
39	McClure	7.7	0.217	0.350	0.008	0.297	2032	6.4	791	0.004
40	McClure	9.3	0.270	0.233	0.009	0.296	1529	3.5	658	0.003
41	McClure	9.3	0.272	0.248	0.010	0.470	1583	3.8	657	0.003
42	McClure	10.0	0.303	0.188	0.009	-0.153	1316	2.7	617	0.003
	NIST610									
1	NIST610	3.9	0.101	0.911	0.003	0.145	4664	98	1456	0.007
2	NIST610	3.9	0.099	0.910	0.003	-0.201	4664	98	1457	0.006
3	NIST610	3.9	0.100	0.912	0.003	0.332	4665	98	1456	0.006
4	NIST610	3.9	0.100	0.909	0.003	0.096	4663	98	1458	0.006
5	NIST610	3.9	0.100	0.909	0.003	0.165	4665	98	1458	0.007
6	NIST610	3.9	0.100	0.910	0.003	-0.162	4670	98	1464	0.007
7	NIST610	3.9	0.099	0.908	0.003	0.180	4671	99	1468	0.007
8	NIST610	3.9	0.099	0.911	0.003	-0.113	4670	98	1463	0.006
9	NIST610	3.9	0.100	0.910	0.003	0.094	4680	99	1476	0.007
10	NIST610	3.9	0.100	0.909	0.003	-0.203	4681	99	1478	0.007
11	NIST610	3.9	0.099	0.907	0.003	-0.158	4672	99	1470	0.007
12	NIST610	3.9	0.100	0.907	0.003	0.046	4676	99	1475	0.007
13	NIST610	3.9	0.102	0.907	0.003	0.104	4673	99	1470	0.007
14	NIST610	3.9	0.102	0.910	0.003	0.092	4672	99	1466	0.007
15	NIST610	3.9	0.100	0.910	0.003	-0.167	4672	99	1465	0.007
16	NIST610	3.9	0.102	0.909	0.003	0.013	4670	98	1464	0.007
17	NIST610	3.9	0.099	0.912	0.003	0.052	4677	99	1471	0.007
18	NIST610	3.9	0.100	0.908	0.003	0.019	4673	99	1470	0.007
19	NIST610	3.9	0.098	0.911	0.003	0.167	4674	99	1467	0.006
20	NIST610	3.9	0.098	0.909	0.003	-0.093	4668	98	1463	0.006
21	NIST610	4.0	0.101	0.909	0.003	-0.210	4657	97	1448	0.006
22	NIST610	3.9	0.099	0.910	0.003	-0.002	4662	98	1454	0.006
23	NIST610	3.9	0.101	0.908	0.003	-0.159	4663	98	1458	0.007
24	NIST610	3.9	0.100	0.908	0.003	0.051	4672	99	1469	0.007
25	NIST610	3.9	0.100	0.913	0.003	0.076	4668	98	1457	0.006
26	NIST610	3.9	0.101	0.908	0.003	0.171	4661	98	1456	0.007
27	NIST610	3.9	0.099	0.911	0.003	0.011	4665	98	1457	0.006
28	NIST610	3.9	0.101	0.911	0.003	0.074	4669	98	1462	0.007
29	NIST610	3.9	0.100	0.910	0.003	0.281	4671	99	1465	0.007
30	NIST610	3.9	0.101	0.910	0.003	0.126	4671	99	1467	0.007
31	NIST610	3.9	0.099	0.909	0.003	-0.019	4665	98	1459	0.006

#	Standard	$^{238}U/^{206}Pb$	± 2σ	$^{207}Pb/^{206}Pb$	± 2σ	Rho	$^{207}Pb/^{235}U$	± 2σ	$^{206}Pb/^{238}U$	± 2σ
32	NIST610	3.9	0.101	0.911	0.003	-0.109	4664	98	1455	0.007
33	NIST610	4.0	0.099	0.912	0.003	-0.293	4657	97	1444	0.006
34	NIST610	4.0	0.100	0.910	0.003	0.143	4659	97	1450	0.006
35	NIST610	4.0	0.099	0.910	0.003	0.031	4658	97	1447	0.006
36	NIST610	3.9	0.100	0.908	0.003	0.068	4664	98	1458	0.007
37	NIST610	3.9	0.099	0.907	0.003	0.376	4667	98	1460	0.006
38	NIST610	3.9	0.099	0.911	0.003	0.057	4671	99	1459	0.007
39	NIST610	3.9	0.098	0.909	0.003	0.098	4676	99	1465	0.006
40	NIST610	3.9	0.097	0.909	0.003	-0.016	4678	99	1468	0.006
41	NIST610	3.8	0.096	0.909	0.003	0.003	4700	101	1493	0.007
42	NIST610	3.8	0.097	0.910	0.003	0.001	4703	102	1495	0.007

*(Continued)

#	Standard	Si	P	Cl	Ca	Ti	Mn	Sr	Y	Zr	La	Ce	Pr	Nd	Sm	Eu	Gd	Tb	Dy	Ho	Er	Tm	Yb	Lu	Hf	^{204}Pb	^{206}Pb	^{207}Pb	^{208}Pb	Th	U
1	MAD	5283	204127	908	393600	3.2	265	2151	289	17.9	2118	4212	439	1535	204	29	125	12.7	60	10.1	25	2.9	16.8	2.2	0.078	<1.261	7.7	0.985	26	640	26
2	MAD	5232	206139	885	393600	4.7	265	2167	292	18.2	2124	4216	442	1541	200	29	123	12.7	61	10.2	25	2.9	16.7	2.2	0.085	<1.349	7.6	0.943	26	637	25
3	MAD	5233	200773	899	393600	2.9	262	2137	290	17.4	2126	4208	436	1528	200	28	122	12.2	60	10.0	25	2.9	16.1	2.2	0.094	<1.284	7.5	0.998	25	628	25
4	MAD	5250	202303	894	393600	2.5	264	2144	291	17.6	2138	4223	440	1542	200	29	124	12.5	60	10.1	25	2.8	16.0	2.2	0.067	<1.269	7.5	0.979	26	638	25
5	MAD	5580	202879	996	393600	3.7	264	2159	295	17.5	2168	4259	442	1545	202	29	125	12.5	60	10.2	25	2.8	16.5	2.1	0.095	<1.247	7.6	0.929	26	636	25
6	MAD	5464	202946	1002	393600	3.1	266	2157	290	18.0	2135	4211	437	1525	203	29	122	12.4	60	9.9	25	2.9	16.1	2.2	0.091	<1.217	7.5	0.925	26	633	25
7	MAD	5412	202390	848	393600	2.8	266	2150	293	18.2	2153	4290	443	1536	202	29	124	12.6	60	10.0	25	2.9	16.6	2.3	0.095	<1.255	7.6	0.998	26	640	26
8	MAD	5109	201890	952	393600	2.3	260	2131	287	17.6	2109	4217	437	1508	198	29	124	12.2	60	10.0	25	2.8	16.0	2.3	0.117	<1.062	7.3	0.935	25	628	25
9	MAD	5419	201147	941	393600	3.3	263	2157	292	17.9	2130	4212	438	1522	198	29	123	12.3	60	9.9	25	2.8	16.0	2.2	0.078	<1.060	7.4	0.907	25	626	25
10	MAD	5205	202693	939	393600	2.4	263	2137	292	17.5	2119	4211	435	1514	197	29	120	12.4	59	9.8	25	2.9	16.0	2.1	0.096	<1.219	7.5	0.986	25	623	25
11	MAD	5219	203913	986	393600	8.7	266	2157	293	18.2	2131	4263	441	1530	201	29	123	12.3	60	10.1	25	2.8	16.2	2.1	0.093	<1.222	7.5	1.0	26	632	25
12	MAD	5336	204117	942	393600	3.4	265	2150	292	17.9	2133	4221	436	1525	199	29	122	12.6	60	10.1	24	2.9	16.1	2.2	0.107	<1.236	7.4	0.921	26	629	25
13	MAD	5442	204319	971	393600	3.0	263	2128	289	17.3	2138	4249	440	1509	199	29	122	12.4	60	10.1	25	2.8	16.3	2.2	0.094	<1.181	7.4	0.907	25	632	25
14	MAD	5181	206394	1049	393600	2.9	265	2146	291	17.6	2124	4213	438	1512	199	28	123	12.4	60	10.2	24	2.9	16.3	2.2	0.094	<1.163	7.5	0.948	25	633	25
15	MAD	5104	204106	1030	393600	2.2	268	2121	290	17.6	2126	4235	434	1522	197	29	120	12.4	60	9.7	25	2.9	16.5	2.2	0.136	<1.252	7.5	1.0	26	630	25
16	MAD	5244	204416	945	393600	2.9	267	2151	292	18.3	2149	4273	442	1537	203	29	125	12.5	62	10.3	25	2.8	16.4	2.2	0.077	<1.173	7.6	0.954	26	636	25
17	MAD	5231	204109	941	393600	2.1	267	2163	292	17.8	2145	4289	444	1537	202	29	124	12.4	61	10.0	25	2.9	16.7	2.2	0.109	<1.122	7.5	0.910	25	633	25
18	MAD	5163	203442	992	393600	1.0	268	2164	292	18.1	2140	4268	442	1525	200	29	124	12.6	60	10.0	25	2.9	16.7	2.3	0.088	<1.206	7.4	0.912	25	634	25
19	MAD	5395	205289	1061	393600	2.1	264	2154	290	17.4	2150	4264	439	1537	200	29	123	12.5	59	10.1	25	2.9	16.2	2.2	0.074	<1.222	7.4	0.846	25	626	25
20	MAD	5410	204093	1010	393600	2.6	263	2131	290	17.9	2124	4270	437	1528	200	28	122	12.3	59	9.9	25	2.8	16.2	2.2	0.124	<1.330	7.4	0.891	26	634	25
21	MAD	5145	209050	987	393600	2.8	266	2141	291	17.5	2156	4277	440	1528	200	29	123	12.4	60	10.3	25	2.9	16.3	2.2	0.071	<1.327	7.6	0.898	26	640	26
22	MAD	5288	211517	975	393600	2.6	265	2152	293	17.7	2177	4319	446	1556	204	29	123	12.5	61	10.3	25	2.9	16.8	2.2	0.064	<1.382	7.7	1.0	27	646	26
23	MAD	5363	208241	927	393600	1.6	264	2127	291	17.2	2129	4265	436	1522	197	29	122	12.4	59	9.9	25	2.9	16.5	2.2	0.102	<1.227	7.5	0.982	26	629	25
24	MAD	5532	203041	955	393600	2.8	266	2137	294	18.1	2153	4272	441	1530	200	29	123	12.4	60	10.0	24	2.9	16.6	2.3	0.117	<1.221	7.5	1.0	26	631	25
25	MAD	5380	204444	1014	393600	2.5	267	2158	291	17.9	2142	4274	438	1527	198	29	122	12.6	60	9.9	25	2.9	16.7	2.2	0.078	<1.287	7.5	0.963	26	638	26
26	MAD	5215	205733	994	393600	1.9	266	2164	294	17.4	2159	4387	441	1540	201	29	123	12.5	61	10.2	25	3.0	16.4	2.1	0.111	<1.282	7.5	0.877	26	634	26
27	MAD	5274	210408	989	393600	2.3	268	2149	293	18.0	2157	4304	441	1537	202	29	123	12.4	60	9.8	25	2.9	16.2	2.3	0.082	<1.310	7.6	0.910	26	638	26
28	MAD	5512	207310	957	393600	2.6	268	2147	294	17.8	2172	4448	444	1551	201	29	124	12.6	61	10.2	26	3.0	16.3	2.2	0.115	<1.279	7.7	0.969	26	643	26
29	MAD	5267	204014	947	393600	2.1	267	2168	294	17.9	2160	4313	442	1535	199	29	123	12.6	60	10.2	25	2.9	16.5	2.2	0.093	<1.407	7.6	0.981	26	638	25
30	MAD	5207	204065	922	393600	2.1	266	2148	293	17.6	2145	4302	442	1531	197	29	124	12.8	60	10.3	26	2.9	16.4	2.1	0.097	<1.255	7.6	0.873	26	639	25
31	MAD	5243	207931	1001	393600	1.3	268	2162	294	17.9	2172	4332	446	1553	201	29	123	12.5	61	10.0	25	3.0	16.4	2.2	0.109	1.8	7.7	0.924	26	646	26
32	MAD	5268	206282	1026	393600	2.6	265	2160	296	18.0	2167	4318	443	1548	201	29	124	12.7	61	10.1	25	2.9	16.5	2.3	0.090	<1.368	7.7	0.874	26	644	26
33	MAD	5216	207005	575	393600	1.9	267	2168	291	17.5	2141	4305	440	1522	200	29	122	12.5	59	10.0	25	2.7	16.2	2.2	0.096	<1.406	7.4	0.855	25	630	25
34	MAD	5188	205031	587	393600	1.9	268	2174	291	18.0	2150	4326	442	1535	199	29	123	12.4	61	10.0	25	3.1	16.2	2.2	0.094	<1.354	7.6	0.946	25	630	25
35	MAD	5307	209078	878	393600	1.9	263	2155	292	17.2	2145	4307	442	1545	203	29	122	12.6	61	10.3	25	2.8	16.9	2.3	0.069	<1.205	7.3	0.771	25	624	25
36	MAD	4892	206783	850	393600	1.1	263	2145	292	17.4	2156	4274	441	1534	200	29	123	12.5	60	10.0	25	2.9	16.3	2.2	0.068	<1.263	7.3	0.776	26	634	25
37	MAD	5186	209193	969	393600	2.9	264	2139	291	17.4	2140	4282	438	1520	198	28	122	12.6	60	10.3	25	2.8	15.9	2.2	0.137	<1.018	7.5	0.824	26	638	25
38	MAD	5168	210939	976	393600	1.4	268	2141	291	18.0	2148	4284	438	1530	200	29	122	12.5	59	10.1	24	2.8	16.6	2.2	0.115	<1.113	7.5	0.910	26	632	25

#	Standard	Si	P	Cl	Ca	Ti	Mn	Sr	Y	Zr	La	Ce	Pr	Nd	Sm	Eu	Gd	Tb	Dy	Ho	Er	Tm	Yb	Lu	Hf	^{204}Pb	^{206}Pb	^{207}Pb	^{208}Pb	Th	U
39	MAD	5143	210611	1018	393600	2.3	267	2180	296	18.3	2188	4349	443	1545	202	29	125	12.5	60	10.2	25	3.0	16.0	2.2	0.096	<1.185	7.5	0.918	31	645	26
40	MAD	5185	209360	1044	393600	2.5	265	2149	292	17.8	2168	4330	442	1533	199	29	122	12.8	60	10.0	25	2.9	16.5	2.2	0.073	<1.249	7.4	1.0	25	639	26
41	MAD	5128	210862	973	393600	2.2	265	2150	290	18.1	2155	4310	442	1535	200	29	123	12.7	61	10.1	25	2.9	16.7	2.3	0.098	<1.152	7.3	0.952	25	636	25
42	MAD	5191	212285	988	393600	2.6	267	2165	293	17.9	2163	4324	443	1535	202	28	124	12.5	61	10.3	25	2.8	17.0	2.2	0.095	<1.179	7.5	0.904	26	645	26
	401																														
1	401	1683	219289	3339	390000	5.4	128	449	1490	0.445	3624	8144	847	2956	435	43	370	45	251	48	131	15.7	86	10.4	0.051	<1.235	4.3	0.313	5.0	115	14.2
2	401	1638	220184	3322	390000	4.1	128	448	1496	0.465	3623	8154	851	2984	436	44	371	45	253	49	133	15.6	86	10.7	0.041	<1.240	4.3	0.314	5.0	115	14.3
3	401	1556	214198	3398	390000	3.0	127	446	1484	0.539	3591	8079	837	2926	429	42	363	45	250	48	128	15.6	84	10.5	0.013	<1.380	4.3	0.311	5.0	111	13.9
4	401	1723	216091	3552	390000	3.6	130	448	1498	0.470	3637	8182	847	2963	437	43	370	45	250	48	130	15.4	84	10.6	0.034	<1.320	4.3	0.318	5.2	113	14.1
5	401	1632	215806	3544	390000	2.5	129	448	1496	0.511	3641	8167	842	2927	433	43	362	45	252	48	129	15.5	87	10.3	0.024	<1.182	4.1	0.321	4.9	113	14.0
6	401	1691	213128	3566	390000	2.1	129	444	1483	0.511	3584	8065	836	2894	428	42	360	44	245	47	130	15.5	85	10.1	0.007	<1.259	4.2	0.306	4.9	112	13.9
7	401	1756	214337	3436	390000	3.5	128	445	1473	0.484	3557	8042	832	2885	423	43	360	44	248	47	128	15.4	84	10.3	0.034	<1.149	4.1	0.287	4.8	112	13.8
8	401	1544	216039	3385	390000	2.2	129	447	1472	0.525	3562	8082	830	2903	422	43	361	45	248	48	129	15.4	84	10.2	0.030	<1.112	4.1	0.338	4.8	112	13.9
9	401	1818	212391	3580	390000	2.0	129	442	1478	0.475	3576	8025	832	2894	424	43	365	44	247	48	128	15.2	85	10.2	0.010	<1.269	4.2	0.318	4.8	112	13.7
10	401	1491	215210	3576	390000	2.0	129	448	1486	0.467	3599	8086	836	2897	430	43	366	44	248	48	129	15.4	84	10.4	0.007	<1.159	4.2	0.296	4.7	113	13.9
11	401	1641	215610	3497	390000	2.4	128	440	1468	0.540	3582	8052	834	2883	429	42	363	44	244	48	129	15.2	85	10.2	0.007	<1.252	4.2	0.310	4.9	111	13.6
12	401	1773	216479	3561	390000	2.9	129	445	1477	0.436	3627	8118	836	2918	426	43	363	44	248	48	129	15.3	84	10.3	0.038	<1.234	4.2	0.299	4.8	111	13.8
13	401	1631	217890	3671	390000	2.3	129	444	1475	0.524	3627	8141	842	2907	425	43	366	44	250	48	131	15.2	85	10.4	0.027	<1.167	4.2	0.312	4.9	112	13.9
14	401	1579	216198	3656	390000	2.4	128	442	1459	0.527	3547	7993	831	2877	422	42	359	43	245	47	126	15.5	85	10.1	0.041	<1.174	4.1	0.323	4.9	111	13.7
15	401	1660	216661	3669	390000	2.1	128	442	1467	0.508	3586	8080	833	2886	419	42	360	44	244	47	129	15.2	84	10.1	0.028	<1.250	4.1	0.288	4.8	112	13.7
16	401	1609	216032	3604	390000	2.8	129	445	1474	0.573	3579	8084	833	2893	425	42	359	44	246	47	129	15.3	84	10.1	0.042	<1.324	4.4	0.331	5.1	112	13.9
17	401	1668	216832	3459	390000	2.5	128	445	1461	0.512	3582	8139	838	2915	430	43	364	44	251	48	129	15.5	86	10.2	0.028	<1.118	4.3	0.324	5.0	114	13.9
18	401	1596	218079	3596	390000	2.3	128	450	1482	0.454	3642	8228	849	2934	431	44	371	45	252	48	131	15.7	86	10.3	0.025	<1.133	4.4	0.314	5.1	114	14.1
19	401	1820	218718	3855	390000	2.3	130	446	1467	0.553	3597	8105	830	2890	424	43	361	44	249	48	128	15.2	83	10.0	0.038	<1.003	4.2	0.324	5.0	111	13.8
20	401	1740	217928	3944	390000	3.0	129	447	1498	0.525	3654	8190	846	2952	432	43	368	44	250	48	129	15.6	86	10.3	0.014	<1.038	4.3	0.309	5.1	113	13.8
21	401	1639	224380	3827	390000	2.2	127	442	1447	0.519	3502	7950	817	2831	416	42	354	43	243	47	126	15.0	82	10.1	0.042	<1.309	4.4	0.332	4.9	110	13.7
22	401	1834	226040	3982	390000	1.5	129	444	1463	0.541	3577	8082	834	2888	429	43	360	44	245	48	127	15.5	84	10.4	0.024	<1.221	4.3	0.338	4.9	112	14.0
23	401	1722	216028	3589	390000	2.2	130	444	1461	0.453	3528	7944	816	2858	420	42	354	43	245	47	125	15.5	83	10.1	0.028	<1.421	4.3	0.300	4.8	110	13.8
24	401	1788	218881	3707	390000	2.6	129	446	1474	0.477	3579	8068	834	2882	425	43	358	44	244	48	127	15.5	85	10.4	0.021	<1.268	4.3	0.347	4.8	111	14.0
25	401	1864	216369	3796	390000	2.5	129	443	1454	0.488	3517	7968	817	2840	420	42	356	43	245	47	127	15.2	84	10.0	0.021	<1.303	4.2	0.319	4.8	110	13.7
26	401	1897	217296	3697	390000	2.0	130	447	1461	0.518	3542	7982	821	2858	418	42	356	44	247	47	127	15.3	84	10.2	0.039	<1.336	4.2	0.297	4.9	110	13.8
27	401	1833	219843	3630	390000	1.7	129	443	1458	0.524	3561	8001	821	2844	423	42	354	44	244	47	127	15.3	83	9.9	0.025	<1.397	4.2	0.334	5.0	110	13.8
28	401	1787	221000	3718	390000	1.8	128	444	1483	0.432	3571	8093	827	2873	423	42	358	44	246	47	127	15.4	85	10.0	0.014	<1.249	4.2	0.297	4.7	109	13.9
29	401	1792	218269	3460	390000	2.6	129	446	1463	0.640	3559	8108	828	2870	418	42	359	44	243	47	128	15.2	84	10.2	0.021	<1.211	4.2	0.327	4.7	109	13.8
30	401	1849	215912	3673	390000	2.4	128	447	1461	0.466	3576	8047	824	2865	417	42	361	43	246	47	128	15.4	84	10.0	0.018	<1.264	4.1	0.307	4.7	110	13.8
31	401	1640	219520	3691	390000	2.5	129	445	1467	0.469	3555	8065	821	2862	423	42	356	43	244	47	127	15.2	83	10.1	0.021	<1.236	4.3	0.312	4.9	109	13.9
32	401	1592	219226	3733	390000	2.8	129	448	1469	0.472	3553	8078	822	2874	423	43	360	44	246	48	126	15.4	84	9.9	0.032	<1.248	4.3	0.349	4.6	109	13.7
33	401	1658	217625	2217	390000	2.5	129	447	1452	0.516	3503	7976	816	2829	420	42	354	43	243	47	126	15.0	84	10.1	0.018	<1.123	4.3	0.345	4.7	107	13.9
34	401	1730	217845	2165	390000	2.5	129	443	1448	0.439	3491	7925	812	2818	415	42	355	44	242	47	125	15.2	82	10.0	0.036	<1.251	4.2	0.326	4.8	107	13.7

#	Standard	Si	P	Cl	Ca	Ti	Mn	Sr	Y	Zr	La	Ce	Pr	Nd	Sm	Eu	Gd	Tb	Dy	Ho	Er	Tm	Yb	Lu	Hf	^{204}Pb	^{206}Pb	^{207}Pb	^{208}Pb	Th	U
35	401	1535	220324	3080	390000	2.7	128	445	1449	0.540	3512	7922	813	2832	419	42	351	43	244	47	127	15.3	83	10.2	0.030	<1.358	4.2	0.325	4.7	107	13.7
36	401	1598	219196	3278	390000	2.2	128	442	1456	0.431	3526	7958	813	2850	423	42	354	43	243	47	127	15.3	83	10.0	0.033	<1.200	4.2	0.660	4.7	108	13.8
37	401	1703	219290	3814	390000	2.1	129	441	1455	0.533	3536	7961	816	2851	418	42	355	43	244	46	126	15.3	84	10.2	0.025	<1.291	4.2	0.323	4.5	108	13.7
38	401	1611	222047	3740	390000	1.4	130	445	1480	0.562	3588	8138	832	2861	427	43	360	44	248	48	129	15.3	85	10.4	0.032	<1.345	4.3	0.489	4.7	109	13.9
39	401	1717	222252	3792	390000	2.7	127	446	1485	0.484	3709	8386	853	2960	432	43	367	45	250	49	130	15.6	84	10.3	0.015	<1.248	4.3	0.291	5.3	115	13.9
40	401	1659	222836	3879	390000	0.929	129	446	1463	0.541	3589	8203	829	2883	427	43	361	44	247	48	129	15.4	85	10.2	0.037	<1.162	4.3	0.333	4.9	111	14.0
41	401	1807	226010	3621	390000	2.2	130	450	1470	0.551	3595	8131	834	2879	426	42	365	45	249	48	128	15.6	85	10.3	0.048	<1.325	4.3	0.297	5.1	112	13.9
42	401	1770	223298	3927	390000	2.3	129	449	1496	0.515	3672	8284	844	2928	436	43	369	45	252	49	130	15.7	86	10.4	0.018	<1.166	4.3	0.309	5.0	114	13.8
	McClure																														
1	McClure	2423	209511	142	390000	4.5	111	4019	333	12.7	2342	4018	387	1325	165	56	116	12.6	66	11.9	32	3.8	22	2.9	0.040	<1.257	6.6	1.4	3.4	51	18.0
2	McClure	3261	210589	151	390000	4.7	110	4068	449	19.1	3154	5369	511	1746	215	75	152	16.6	88	16.2	42	5.2	31	4.2	0.067	<1.214	12.6	2.0	6.3	117	37
3	McClure	2149	211387	290	390000	3.5	110	3626	255	6.8	1853	3193	307	1052	129	46	91	10.0	51	8.9	23	2.9	16.7	2.2	0.023	<1.238	4.9	0.948	2.2	38	13.7
4	McClure	1820	212522	245	390000	3.4	103	3562	222	5.4	1658	2825	271	927	113	42	80	8.5	43	7.7	20	2.4	14.3	1.8	0.016	<1.193	4.3	0.899	2.1	31	11.5
5	McClure	2171	212599	161	390000	3.9	67	3470	205	3.3	1691	2723	249	819	94	38	67	7.0	38	7.0	18.7	2.4	15.0	2.1	0.023	<1.087	5.5	0.933	2.7	48	15.9
6	McClure	2694	213102	216	390000	2.6	80	3630	237	4.9	1921	3131	285	952	112	43	79	8.2	43	8.3	21	2.7	16.8	2.4	0.023	<1.049	7.8	1.2	4.0	74	23
7	McClure	1769	212715	124	390000	3.1	82	3954	94	2.2	1456	1992	158	480	48	28	33	3.2	16.2	3.0	8.3	1.1	6.5	0.962	0.007	<1.114	5.1	1.8	4.1	55	11.2
8	McClure	2313	212068	218	390000	3.0	123	4096	207	5.8	2094	2957	245	759	85	40	61	6.4	34	6.4	18.9	2.8	19.3	3.2	0.016	1.8	9.6	2.5	5.7	84	25
9	McClure	3272	210632	217	390000	3.8	128	4083	192	5.9	1965	2740	228	718	77	37	57	5.8	31	5.9	17.5	2.5	18.2	3.0	0.017	1.6	10.5	2.8	8.3	138	26
10	McClure	2321	209418	102	390000	2.9	82	3742	135	5.3	1922	2670	218	670	66	39	47	4.7	23	4.3	12.0	1.5	9.6	1.5	0.020	<1.111	6.7	1.9	3.9	53	17.2
11	McClure	2454	210452	120	390000	3.0	60	3751	235	3.7	1821	2949	268	898	107	45	76	8.1	44	7.8	22	2.8	17.0	2.3	0.020	<1.251	7.6	1.5	3.6	63	22
12	McClure	2135	211243	145	390000	3.1	64	3734	230	3.4	1763	2886	265	885	105	43	75	8.0	43	7.9	21	2.7	16.2	2.3	0.010	<1.089	7.4	1.5	3.7	61	21
13	McClure	2424	212926	104	390000	3.3	94	3634	262	9.2	2218	3650	337	1123	131	52	93	9.6	50	9.0	24	2.8	17.6	2.3	0.034	<1.203	6.2	1.1	2.6	42	17.9
14	McClure	2349	214147	109	390000	3.8	94	3652	273	11.0	2281	3778	350	1158	135	54	96	10.4	52	9.5	25	3.1	18.3	2.5	0.051	<1.101	5.3	1.1	2.4	35	14.8
15	McClure	1635	211174	102	390000	2.2	86	3798	171	3.0	1401	2289	207	688	79	29	56	6.0	31	5.8	15.8	1.9	12.0	1.7	0.017	<1.276	4.5	1.4	2.5	28	10.6
16	McClure	1936	210442	125	390000	2.7	87	3807	188	3.0	1534	2501	225	747	84	32	62	6.4	34	6.4	17.3	2.3	13.9	1.9	0.010	<1.371	5.3	1.5	2.9	39	13.7
17	McClure	2441	209879	116	390000	2.7	74	3714	187	4.9	2092	3112	263	830	89	42	64	6.5	33	6.3	17.2	2.2	13.7	2.0	0.014	<1.261	7.9	1.4	4.4	84	23
18	McClure	2618	210435	108	390000	2.1	76	3686	200	6.0	2099	3192	278	876	96	42	66	7.2	37	6.8	18.5	2.2	14.1	2.1	0.007	<1.220	9.1	1.4	5.0	92	28
19	McClure	1573	212916	266	390000	2.4	86	3830	153	3.3	1322	2163	197	663	76	29	56	5.8	29	5.3	14.1	1.7	10.3	1.5	0.010	<1.180	3.5	0.902	1.6	22	9.0
20	McClure	1770	214878	248	390000	1.8	90	3893	143	2.7	1220	2013	186	626	74	27	53	5.6	28	5.1	13.1	1.5	9.3	1.4	0.021	<1.154	3.3	0.922	1.5	18.2	7.7
21	McClure	2301	218790	137	390000	2.1	73	3776	249	3.4	2048	3211	290	973	115	45	83	8.9	47	8.4	23	2.9	17.8	2.7	<0.000	2.0	7.8	2.1	5.5	84	19.9
22	McClure	3493	219789	123	390000	2.5	65	3695	250	3.9	1979	3123	284	965	116	45	84	8.8	47	8.8	23	2.9	18.3	2.8	0.010	2.3	7.9	2.0	5.5	85	20
23	McClure	2203	210126	134	390000	2.2	60	3374	213	3.0	1995	2980	261	850	95	40	67	7.1	37	6.9	19.2	2.6	16.8	2.3	0.010	<1.154	7.0	1.3	4.1	70	20.0
24	McClure	2426	210995	157	390000	1.9	71	3526	228	4.6	2001	3159	280	930	107	42	75	7.9	41	7.7	21	2.8	17.0	2.4	0.003	<1.130	7.6	1.4	4.1	73	22
25	McClure	1857	216045	236	390000	2.3	93	3385	185	3.6	1352	1994	170	546	62	23	47	5.2	28	5.6	16.9	2.3	15.5	2.5	0.017	<1.292	5.2	1.8	4.2	62	11.8
26	McClure	1726	215730	180	390000	2.4	91	3374	192	4.1	1474	2212	188	607	69	25	52	5.5	30	6.0	17.3	2.3	15.8	2.4	0.021	1.3	5.9	1.8	5.1	79	13.9
27	McClure	1538	217991	174	390000	3.2	125	3909	106	2.7	1167	1797	161	524	59	24	41	4.1	21	3.7	9.4	1.2	6.5	1.0	0.024	1.4	3.9	0.997	1.9	26	9.7
28	McClure	2082	216227	182	390000	2.2	76	3549	174	2.4	1669	2709	241	794	89	39	62	6.3	32	5.9	15.5	1.9	10.5	1.5	<0.000	<1.083	6.1	1.0	2.9	52	17.6
29	McClure	2139	212836	227	390000	1.7	77	3557	172	2.7	1638	2675	239	779	88	39	62	6.2	32	5.8	15.2	1.8	11.0	1.4	0.007	<1.149	6.4	1.1	3.1	54	18.5
30	McClure	2122	212013	135	390000	2.6	64	3620	180	2.8	1622	2604	227	735	83	33	58	6.2	33	6.0	16.3	2.1	13.3	2.0	0.003	<1.126	6.2	1.2	3.0	49	17.6

#	Standard	Si	P	Cl	Ca	Ti	Mn	Sr	Y	Zr	La	Ce	Pr	Nd	Sm	Eu	Gd	Tb	Dy	Ho	Er	Tm	Yb	Lu	Hf	^{204}Pb	^{206}Pb	^{207}Pb	^{208}Pb	Th	U
31	McClure	2093	212576	<61	390000	2.6	65	3597	173	2.5	1524	2448	215	703	78	31	57	5.8	31	5.9	16.1	1.9	12.1	1.8	0.017	<1.083	5.8	1.1	2.6	42	16.4
32	McClure	2133	213036	116	390000	2.2	65	3818	236	3.0	1787	2903	260	874	104	38	74	8.0	43	7.9	22	2.8	16.8	2.4	0.017	1.4	6.1	1.0	3.1	54	18.0
33	McClure	2767	209236	66	390000	2.9	72	3858	312	6.2	2329	3839	353	1188	143	51	105	11.2	58	10.8	29	3.6	22	3.0	0.025	<1.185	9.9	1.3	5.2	98	30
34	McClure	1812	213507	60	390000	1.8	100	3747	100	2.9	1331	1858	154	486	52	26	38	3.6	18.1	3.5	8.9	1.1	7.6	1.1	0.003	<1.244	4.9	1.4	3.0	36	11.8
35	McClure	1853	214639	121	390000	2.0	96	3727	101	3.1	1493	2009	161	500	53	28	38	3.6	18.4	3.2	9.0	1.2	7.5	1.3	0.010	<1.220	6.3	1.8	3.7	48	15.3
36	McClure	1927	217219	90	390000	2.0	72	3493	166	2.7	1457	2418	218	729	83	33	60	6.1	31	5.6	14.8	1.8	10.1	1.4	0.003	<1.135	4.9	0.912	2.4	39	14.0
37	McClure	2186	219086	187	390000	2.3	77	3530	202	3.5	1763	2938	264	877	102	41	71	7.4	38	6.9	18.0	2.1	12.9	1.6	0.007	<1.209	6.3	0.987	3.0	53	18.1
38	McClure	2546	216585	104	390000	2.7	138	2915	1185	5.1	2687	3944	318	974	127	35	116	16.7	111	27	97	15.9	110	14.4	0.032	3.8	12.6	4.8	9.8	118	27
39	McClure	2304	217039	71	390000	2.3	135	2923	1159	6.6	2637	3898	312	961	126	35	114	16.6	112	27	96	15.6	109	14.2	0.018	4.0	12.3	4.7	10.3	139	26
40	McClure	2242	217077	181	390000	2.7	117	3919	203	3.1	1952	3061	264	853	95	41	66	7.0	36	6.9	18.8	2.4	15.2	2.1	0.014	1.5	8.3	2.1	5.0	74	21
41	McClure	2407	217198	165	390000	2.4	111	3898	203	3.0	1927	3015	262	833	92	41	64	6.8	37	6.8	18.6	2.3	15.0	2.2	0.014	<1.324	7.9	2.2	4.8	70	21
42	McClure	2549	220063	212	390000	2.6	82	4074	273	8.0	2276	3700	336	1105	129	51	92	9.9	52	9.7	25	3.3	19.6	2.8	0.043	<1.385	6.4	1.3	2.8	44	18.0
	NIST610																														
1	NIST610	325908	420	291	81476	448	444	515	461	447	439	453	449	429	451	447	450	437	437	449	455	434	451	438	434	427	427	427	428	457	463
2	NIST610	325685	406	257	81476	456	444	516	462	449	441	453	447	430	454	447	448	437	437	449	455	436	449	440	436	424	425	425	424	457	460
3	NIST610	326321	407	274	81476	450	442	514	463	447	440	453	447	430	452	447	450	436	435	447	453	434	450	439	434	433	425	426	425	457	461
4	NIST610	325225	419	273	81476	454	446	517	463	449	441	453	449	430	456	447	448	438	439	451	457	436	450	439	437	423	427	426	427	458	462
5	NIST610	327604	412	292	81476	451	444	517	462	447	439	452	447	431	453	447	449	436	437	450	455	435	448	438	434	423	425	425	425	457	462
6	NIST610	323948	414	255	81476	453	444	514	462	449	440	454	449	431	452	447	449	438	437	448	455	435	452	440	436	427	427	427	427	457	461
7	NIST610	326172	415	269	81476	453	443	513	459	446	437	453	447	425	448	445	447	436	436	448	454	434	449	438	434	426	426	426	426	456	461
8	NIST610	325431	411	279	81476	451	445	518	462	450	440	454	449	432	454	449	451	438	438	450	456	436	451	440	436	420	426	426	426	458	462
9	NIST610	325676	415	274	81476	449	443	512	460	445	438	451	446	427	451	445	446	434	434	447	452	432	448	436	432	427	424	424	424	455	460
10	NIST610	325861	411	274	81476	455	445	519	465	451	443	455	450	433	457	449	452	440	440	451	458	438	452	442	438	433	428	428	428	459	463
11	NIST610	328409	413	282	81476	455	447	517	465	451	443	455	449	433	455	448	453	439	439	451	457	437	451	441	436	427	428	428	429	460	464
12	NIST610	323037	413	266	81476	449	441	514	462	445	439	450	447	428	451	446	445	434	435	447	453	433	449	437	434	423	424	424	423	455	459
13	NIST610	328943	421	282	81476	453	445	518	463	448	440	453	448	431	455	448	451	438	438	450	456	435	449	440	434	426	428	428	427	458	463
14	NIST610	322553	405	266	81476	451	442	513	460	448	440	453	449	430	453	446	447	436	436	448	454	435	451	438	436	421	424	424	425	457	460
15	NIST610	326747	417	273	81476	449	445	516	461	447	439	452	448	430	453	446	448	436	436	448	454	434	450	439	434	429	426	426	426	456	461
16	NIST610	324821	409	275	81476	455	443	515	464	449	442	454	448	431	455	448	450	438	438	450	456	436	450	439	436	426	426	426	426	458	462
17	NIST610	326430	411	258	81476	449	444	516	459	447	439	453	448	430	449	449	447	438	436	449	455	435	450	440	437	434	428	428	429	458	463
18	NIST610	325140	416	291	81476	455	444	515	458	449	437	453	448	427	450	445	451	436	438	449	455	435	450	438	433	421	424	424	423	457	460
19	NIST610	326635	412	280	81476	456	444	515	463	448	440	454	447	429	453	446	449	437	436	448	454	435	449	439	436	427	428	428	427	458	462
20	NIST610	325039	414	268	81476	448	444	516	462	448	439	452	449	432	455	448	450	437	438	450	456	435	451	439	434	424	424	424	425	456	461
21	NIST610	322698	416	275	81476	452	442	512	461	444	438	450	445	428	452	445	446	435	435	446	452	432	446	437	433	419	424	423	423	455	459
22	NIST610	328962	410	273	81476	452	446	519	466	452	443	456	451	433	456	449	452	439	439	452	458	438	454	441	437	428	429	429	429	459	464
23	NIST610	327010	418	272	81476	451	444	516	464	449	442	453	449	433	453	448	450	437	439	450	456	437	451	441	436	425	426	426	427	458	464
24	NIST610	324507	408	276	81476	453	444	515	462	447	440	452	447	430	454	446	448	437	435	448	454	433	449	437	434	430	426	426	425	456	459
25	NIST610	327939	402	273	81476	453	445	515	461	448	441	453	448	429	453	447	450	437	437	449	456	436	451	440	436	424	427	428	426	459	462
26	NIST610	323578	424	275	81476	451	443	516	461	448	440	453	448	430	449	447	448	437	437	449	454	434	449	438	434	426	425	424	426	456	461

#	Standard	Si	P	Cl	Ca	Ti	Mn	Sr	Y	Zr	La	Ce	Pr	Nd	Sm	Eu	Gd	Tb	Dy	Ho	Er	Tm	Yb	Lu	Hf	^{204}Pb	^{206}Pb	^{207}Pb	^{208}Pb	Th	U
27	NIST610	327004	425	273	81476	449	444	515	462	448	439	452	447	429	453	447	449	438	437	449	455	434	449	440	436	427	427	426	426	457	462
28	NIST610	324513	401	275	81476	456	444	516	464	448	441	454	449	429	453	447	449	436	437	449	455	436	451	438	434	431	425	426	426	457	461
29	NIST610	327940	412	267	81476	450	445	517	461	448	440	454	448	430	454	448	449	437	437	449	455	434	451	439	436	424	427	427	427	458	462
30	NIST610	323568	414	281	81476	454	443	514	460	449	439	452	448	428	453	446	449	437	437	449	455	436	449	439	434	424	425	425	425	456	461
31	NIST610	327176	417	281	81476	452	443	513	460	446	438	452	447	428	453	445	448	435	435	449	455	434	448	438	434	424	426	426	426	456	461
32	NIST610	324349	408	275	81476	452	445	518	463	450	442	454	449	431	454	449	450	439	439	449	455	436	452	440	436	430	426	426	426	459	462
33	NIST610	327451	418	135	81476	455	445	516	462	450	440	453	449	431	453	447	449	437	438	449	456	435	450	439	435	426	425	426	424	458	462
34	NIST610	324102	407	419	81476	448	443	515	460	446	439	453	447	430	451	447	449	437	436	449	454	435	450	439	435	422	427	426	428	456	461
35	NIST610	326215	416	273	81476	456	444	516	462	448	440	453	448	431	454	448	449	438	439	450	456	435	451	440	436	425	426	427	426	458	463
36	NIST610	325376	410	275	81476	447	444	515	464	448	441	453	448	431	454	446	449	436	435	448	454	435	449	438	434	430	426	425	426	456	460
37	NIST610	326164	415	265	81476	453	444	513	461	447	437	452	448	430	452	446	448	436	437	447	454	433	449	438	435	429	426	426	424	457	462
38	NIST610	325403	411	284	81476	451	444	518	463	449	442	454	448	431	451	448	450	438	437	451	456	437	451	440	435	422	426	426	428	458	461
39	NIST610	326908	409	256	81476	454	445	516	463	449	440	453	448	431	455	448	450	437	439	449	454	436	450	439	435	430	427	427	425	458	463
40	NIST610	324662	417	292	81476	450	443	515	461	447	441	453	448	434	453	446	448	437	435	449	456	434	450	439	435	421	425	425	427	457	460
41	NIST610	326188	416	270	81476	450	443	513	459	446	439	452	447	425	452	446	450	436	436	449	454	435	448	437	435	426	426	426	425	457	462
42	NIST610	325466	410	277	81476	454	445	518	464	450	441	454	449	431	453	448	448	438	438	449	456	436	452	441	435	426	426	426	426	458	462

References

MAD Thomson, S.N., Gehrels, G.E., Ruiz, J., and Buchwaldt, R., 2012. Routine low-damage apatite U-Pb dating using laser ablation–multicollector–ICPMS. Geochem Geophys. 13(2). https://doi.org/10.1029/2011GC003928

NIST610 Jochum, K.P., Weis, U., Stoll, B., Kuzmin, D., Yang, Q., Raczek, I., Jacob, D.E., Stracke, A., Birbaum, K., Frick, D.A., Günther, D., Enzweiler, J., 2011. Determination of reference values for NIST SRM 610–617 glasses following ISO guidelines. Geostand Geoanal Res. 35(4), 397-429. https://doi.org/10.1111/j.1751-908X.2011.00120.x

401 Thompson, J., Meffre, S., Maas, R., Kamenetsky, V., Kamenetsky, M., Goemann, K., Ehrigc, K., and Danyushevsky, L., 2016. Matrix effects in Pb/U measurements during LA-ICP-MS analysis of the mineral apatite. J Anal. At. Spectrom. 31(6), 1206-1215. https://doi.org/10.1039/C6JA00048G

McClure Schoene, B., and Bowring, S.A., 2006. U–Pb systematics of the McClure Mountain syenite: thermochronological constraints on the age of the 40Ar/39Ar standard MMhb. Contrib

Supplementary Table 4. Summary of Lu-Hf data and trace elements for selected apatite and in-house reference materials

**Note* : '<' values correspond to bdl.

	Bamble	HR	Wallaroo
Age	1139	356	1616
2s	8.20	2.90	24.0
%SE	0.72	0.82	1.49
Exp	1097	343	1545
ratio	1.04	1.04	1.05
Corrected	1098	342	1557
2s	7.90	2.80	23.0
%Accuracy	0.07	-0.18	0.78

Sample	Age (Ma)	n	MSDW
Jt1-c	2527±17	30	2.3
Jt1-r	2438±59	12	2.6
Jt4	2384±19	25	4.4
Jt7	2489±12	50	6.0
Jt10	2483±18	26	3.5

		uncorrected ratios					matrix corrected ratios					
#	Sample	$^{176}Lu/^{176}Hf$	± 2σ	$^{177}Hf/^{176}Hf$	± 2σ	Rho	$^{176}Lu/^{176}Hf$	± 2σ	$^{177}Hf/^{176}Hf$	± 2σ	Rho	Exclude
1	Jt1 Ap p 1 - 01	20.1	0.9311	0.0090	0.0041	0.3877	20.8	0.9668	0.0090	0.0041	0.3877	
2	Jt1 Ap p 1 - 02	20.5	0.9874	0.0178	0.0060	-0.1839	21.3	1.03	0.0178	0.0060	-0.1839	
3	Jt1 Ap p 2 - 01	19.0	0.5651	0.0189	0.0036	0.1047	19.7	0.5867	0.0189	0.0036	0.1047	
4	Jt1 Ap map 1 - 01	21.1	0.6939	0.0102	0.0040	0.6545	21.9	0.7204	0.0102	0.0040	0.6545	
5	Jt1 Ap 1 - 02	13.1	2.83	0.7794	0.3224	0.2177	13.6	2.94	0.7794	0.3224	0.2177	x
6	Jt1 Ap 3 - 01	19.7	0.9331	0.0162	0.0056	0.3820	20.5	0.9688	0.0162	0.0056	0.3820	
7	Jt1 Ap 3 - 03	20.6	0.8170	0.0218	0.0053	0.6229	21.4	0.8483	0.0218	0.0053	0.6229	
8	Jt1 Ap 4 - 01	20.0	0.6591	0.0223	0.0063	0.0036	20.7	0.6843	0.0223	0.0063	0.0036	
9	Jt1 Ap 4 - 02	19.1	0.7768	0.0683	0.0179	-0.2112	19.9	0.8065	0.0683	0.0179	-0.2112	
10	Jt1 Ap 4 - 03	19.3	0.6733	0.0317	0.0065	-0.0520	20.0	0.6991	0.0317	0.0065	-0.0520	
11	Jt1 Ap 5 - 01	19.6	0.7662	0.0473	0.0133	0.0594	20.3	0.7955	0.0473	0.0133	0.0594	
12	Jt1 Ap 5 - 02	20.1	0.6113	0.0158	0.0035	-0.1659	20.9	0.6347	0.0158	0.0035	-0.1659	
13	Jt1 Ap 5 - 03	19.2	0.6440	0.0170	0.0047	-0.2310	19.9	0.6687	0.0170	0.0047	-0.2310	
14	Jt1 Ap 6 - 01	18.9	0.6784	0.0283	0.0056	0.0041	19.7	0.7044	0.0283	0.0056	0.0041	
15	Jt1 Ap 6 - 02	18.8	0.9886	0.0476	0.0437	0.7044	19.5	1.03	0.0476	0.0437	0.7044	
16	Jt1 Ap 6 - 03	19.7	1.03	0.0754	0.0149	-0.4227	20.4	1.07	0.0754	0.0149	-0.4227	
17	Jt1 Ap 6 - 04	19.2	1.24	0.1148	0.0861	-0.4929	19.9	1.28	0.1148	0.0861	-0.4929	
18	Jt1 Ap 8 - 01	19.8	0.5763	0.0183	0.0061	0.0841	20.6	0.5984	0.0183	0.0061	0.0841	
19	Jt1 Ap 10 - 01	19.2	1.19	0.2113	0.0464	-0.2195	19.9	1.24	0.2113	0.0464	-0.2195	
20	Jt1 Ap 15 - 01	20.2	0.5401	0.0325	0.0061	-0.1646	21.0	0.5608	0.0325	0.0061	-0.1646	
21	Jt1 Ap 16 - 01	19.5	0.4884	0.0107	0.0023	-0.0809	20.2	0.5071	0.0107	0.0023	-0.0809	
22	Jt1 Ap 16 - 02	20.5	0.6920	0.0153	0.0044	-0.3732	21.3	0.7185	0.0153	0.0044	-0.3732	
23	Jt1 Ap 16 - 03	20.6	0.5873	0.0190	0.0066	-0.0592	21.4	0.6098	0.0190	0.0066	-0.0592	
24	Jt1 Ap 18 - 01	18.4	0.8144	0.1331	0.0476	0.3442	19.2	0.8455	0.1331	0.0476	0.3442	
25	Jt1 Ap 18 - 02	19.2	0.6902	0.1064	0.0171	-0.0507	19.9	0.7166	0.1064	0.0171	-0.0507	
26	Jt1 Ap 18 - 03	19.1	0.7218	0.1334	0.0442	-0.4051	19.9	0.7495	0.1334	0.0442	-0.4051	
27	Jt1 Ap 18 - 04	19.4	0.9996	0.1247	0.0318	-0.8625	20.1	1.04	0.1247	0.0318	-0.8625	
28	Jt1 Ap 19 - 03	20.1	1.67	0.1321	0.0306	-0.0283	20.8	1.73	0.1321	0.0306	-0.0283	
29	Jt1 Ap 19 - 05	18.1	2.09	0.1017	0.0263	-0.0005	18.8	2.17	0.1017	0.0263	-0.0005	
30	Jt1 Ap 19 - 07	19.4	1.06	0.3345	0.0852	0.5147	20.1	1.10	0.3345	0.0852	0.5147	
31	Jt1 Ap 19 - 08	19.8	0.8050	0.0406	0.0084	-0.3017	20.5	0.8358	0.0406	0.0084	-0.3017	
	Rims											
1	Jt1 Ap p 1 - 03	20.3	1.81	0.0574	0.0218	-0.4649	21.1	1.88	0.0574	0.0218	-0.4649	
2	Jt1 Ap map 1 - 04	8.20	1.53	2.33	0.5214	0.3777	8.51	1.59	2.33	0.5214	0.3777	
3	Jt1 Ap map 1 - 05	12.1	2.02	0.7589	0.1578	0.5344	12.6	2.10	0.7589	0.1578	0.5344	x
4	Jt1 Ap map 1 - 06	20.0	1.44	0.1863	0.0692	-0.1021	20.7	1.49	0.1863	0.0692	-0.1021	
5	Jt1 Ap 3 - 04	22.6	3.09	0.0816	0.0272	-0.2390	23.5	3.21	0.0816	0.0272	-0.2390	
6	Jt1 Ap 6 - 05	17.4	1.81	0.4680	0.1092	-0.1174	18.0	1.88	0.4680	0.1092	-0.1174	
7	Jt1 Ap 6 - 06	13.2	1.44	0.9035	0.2437	-0.6053	13.7	1.50	0.9035	0.2437	-0.6053	
8	Jt1 Ap 6 - 08	11.5	1.40	1.39	0.2373	0.1290	12.0	1.45	1.39	0.2373	0.1290	
9	Jt1 Ap 6 - 09	20.1	3.07	0.5278	0.1467	0.4877	20.9	3.19	0.5278	0.1467	0.4877	
10	Jt1 Ap 6 - 10	17.3	1.76	0.4385	0.1483	-0.7903	18.0	1.83	0.4385	0.1483	-0.7903	
11	Jt1 Ap 6 - 11	14.9	1.45	1.24	0.1561	-0.1513	15.5	1.50	1.24	0.1561	-0.1513	
12	Jt1 Ap 13 - 01	17.7	3.98	0.7974	0.4983	0.5846	18.3	4.13	0.7974	0.4983	0.5846	x
13	Jt1 Ap 15 - 02	18.8	7.87	0.7348	0.4448	0.2240	19.6	8.18	0.7348	0.4448	0.2240	x
14	Jt1 Ap 15 - 03	18.2	8.31	1.43	0.6659	0.6726	18.9	8.63	1.43	0.6659	0.6726	x
15	Jt1 Ap 18 - 05	21.2	1.68	0.3320	0.0985	0.0018	22.0	1.74	0.3320	0.0985	0.0018	
16	Jt1 Ap 18 - 06	20.3	0.8264	0.0578	0.0189	0.6661	21.1	0.8580	0.0578	0.0189	0.6661	
							0.0010	0.0001	3.55	0.0100		oldest age

		uncorrected ratios					matrix corrected ratios					
#	Sample	$^{176}Lu/^{176}Hf$	± 2σ	$^{177}Hf/^{176}Hf$	± 2σ	Rho	$^{176}Lu/^{176}Hf$	± 2σ	$^{177}Hf/^{176}Hf$	± 2σ	Rho	Exclude
1	Jt4 Ap p 1 - 01	7.52	1.12	2.20	0.2796	-0.7306	7.81	1.16	2.20	0.2796	-0.7306	
2	Jt4 Ap p 2 - 01	22.6	1.13	0.2408	0.0381	0.3317	23.5	1.17	0.2408	0.0381	0.3317	
3	Jt4 Ap 1 - 01	20.4	0.8824	0.0051	0.0030	-0.4195	21.2	0.9162	0.0051	0.0030	-0.4195	
4	Jt4 Ap 2 - 01	21.8	1.00	0.0153	0.0053	0.0193	22.6	1.04	0.0153	0.0053	0.0193	
5	Jt4 Ap 3 - 01	21.0	0.6613	0.0050	0.0020	0.1971	21.8	0.6867	0.0050	0.0020	0.1971	
6	Jt4 Ap 3 - 02	15.2	2.02	0.6470	0.2789	-0.9539	15.8	2.10	0.6470	0.2789	-0.9539	
7	Jt4 Ap 3 - 03	11.4	2.60	1.58	0.1170	-0.9466	11.8	2.70	1.58	0.1170	-0.9466	
8	Jt4 Ap 3 - 04	20.8	1.44	0.0125	0.0073	0.3850	21.6	1.49	0.0125	0.0073	0.3850	
9	Jt4 Ap 4 - 01	19.5	0.6699	0.0063	0.0025	0.1314	20.2	0.6955	0.0063	0.0025	0.1314	
10	Jt4 Ap 5 - 01	22.3	0.9209	0.0413	0.0115	0.4191	23.1	0.9561	0.0413	0.0115	0.4191	
11	Jt4 Ap 5 - 02	21.7	0.9878	0.0209	0.0063	0.1027	22.6	1.03	0.0209	0.0063	0.1027	
12	Jt4 Ap 6 - 01	18.1	1.33	0.4012	0.2199	-0.8447	18.8	1.38	0.4012	0.2199	-0.8447	
13	Jt4 Ap 10 - 01	20.6	0.8311	0.0064	0.0030	0.4260	21.4	0.8629	0.0064	0.0030	0.4260	
14	Jt4 Ap 11 - 01	21.8	1.33	0.0055	0.0043	-0.0164	22.6	1.38	0.0055	0.0043	-0.0164	
15	Jt4 Ap 12 - 01	21.9	2.80	0.0935	0.0413	0.4226	22.7	2.91	0.0935	0.0413	0.4226	x
16	Jt4 Ap 12 - 02	21.7	0.8732	0.0231	0.0122	0.0141	22.6	0.9067	0.0231	0.0122	0.0141	
17	Jt4 Ap 12 - 05	19.0	1.09	0.2647	0.0392	-0.0691	19.7	1.13	0.2647	0.0392	-0.0691	
18	Jt4 Ap 13 - 05	16.4	6.72	1.97	0.8620	0.9693	17.0	6.98	1.97	0.8620	0.9693	x
19	Jt4 Ap 13 - 06	5.84	1.11	2.30	0.5061	0.5189	6.06	1.15	2.30	0.5061	0.5189	
20	Jt4 Ap 13 - 11	9.51	1.41	1.31	0.4091	0.3540	9.88	1.46	1.31	0.4091	0.3540	x
21	Jt4 Ap 14 - 01	18.6	1.05	0.4510	0.1399	-0.7232	19.3	1.09	0.4510	0.1399	-0.7232	
22	Jt4 Ap 14 - 02	20.6	0.6693	0.0288	0.0055	-0.0758	21.4	0.6949	0.0288	0.0055	-0.0758	
23	Jt4 Ap 15 - 01	20.8	0.6884	0.0195	0.0069	-0.1283	21.6	0.7148	0.0195	0.0069	-0.1283	
24	Jt4 Ap 15 - 03	21.4	0.6677	0.0492	0.0116	0.0705	22.2	0.6933	0.0492	0.0116	0.0705	
25	Jt4 Ap 16 - 01	13.4	2.06	1.42	0.0532	-0.9515	13.9	2.14	1.42	0.0532	-0.9515	
26	Jt4 Ap 16 - 02	22.8	0.8501	0.0080	0.0031	0.0935	23.7	0.8827	0.0080	0.0031	0.0935	
27	Jt4 Ap 16 - 03	21.1	0.5994	0.0130	0.0030	0.2657	21.9	0.6223	0.0130	0.0030	0.2657	
28	Jt4 Ap 16 - 04	22.0	0.7484	0.1199	0.0113	-0.5672	22.8	0.7770	0.1199	0.0113	-0.5672	
							0.0010	0.0001	3.55	0.0100		
	Jt7											
1	Jt7 Ap p1 - 01	19.5	0.8363	0.0599	0.0208	0.1308	20.2	0.8684	0.0599	0.0208	0.1308	
2	Jt7 Ap p1 - 02	20.1	3.50	0.1266	0.0578	0.3843	20.8	3.64	0.1266	0.0578	0.3843	x
3	Jt7 Ap p2 - 02	21.2	1.10	0.3062	0.0368	-0.0738	22.0	1.14	0.3062	0.0368	-0.0738	
4	Jt7 Ap p2 - 03	19.7	0.9535	0.1333	0.0329	0.0566	20.5	0.9900	0.1333	0.0329	0.0566	
5	Jt7 Ap p2 - 04	20.3	1.42	0.2147	0.0340	-0.6654	21.0	1.47	0.2147	0.0340	-0.6654	
6	Jt7 Ap map 1 - 01	19.3	0.5905	0.0256	0.0053	0.3098	20.1	0.6131	0.0256	0.0053	0.3098	
7	Jt7 Ap map 1 - 02	19.2	0.5825	0.0193	0.0049	0.0998	19.9	0.6048	0.0193	0.0049	0.0998	
8	Jt7 Ap map 2 - 02	18.7	1.88	0.3050	0.1401	0.1100	19.4	1.95	0.3050	0.1401	0.1100	x
9	Jt7 Ap 1 - 01	19.2	0.8626	0.0183	0.0052	-0.0761	19.9	0.8957	0.0183	0.0052	-0.0761	
10	Jt7 Ap 1 - 02	18.3	1.75	0.1238	0.0308	-0.6086	19.0	1.82	0.1238	0.0308	-0.6086	
11	Jt7 Ap 1 - 03	18.9	1.33	0.3035	0.0794	0.0847	19.6	1.38	0.3035	0.0794	0.0847	
12	Jt7 Ap 1 - 04	19.3	0.7918	0.1483	0.0512	-0.5063	20.0	0.8221	0.1483	0.0512	-0.5063	
13	Jt7 Ap 2 - 01	19.5	1.39	0.0499	0.0211	-0.3295	20.3	1.44	0.0499	0.0211	-0.3295	x
14	Jt7 Ap 2 - 02	17.7	1.97	0.4665	0.1843	-0.8116	18.4	2.04	0.4665	0.1843	-0.8116	x
15	Jt7 Ap 2 - 03	17.9	5.16	1.45	0.5676	0.2278	18.6	5.36	1.45	0.5676	0.2278	x
16	Jt7 Ap 5 - 01	20.9	0.5887	0.0221	0.0048	0.0827	21.7	0.6113	0.0221	0.0048	0.0827	
17	Jt7 Ap 5 - 02	21.0	0.5925	0.0137	0.0033	0.0374	21.8	0.6151	0.0137	0.0033	0.0374	
18	Jt7 Ap 5 - 03	21.4	0.6814	0.0123	0.0033	0.1591	22.2	0.7075	0.0123	0.0033	0.1591	
19	Jt7 Ap 6 - 01	21.3	0.5638	0.0159	0.0028	0.2881	22.1	0.5854	0.0159	0.0028	0.2881	
20	Jt7 Ap 6 - 02	19.9	0.6013	0.0631	0.0176	-0.2829	20.7	0.6243	0.0631	0.0176	-0.2829	
21	Jt7 Ap 6 - 03	19.9	0.6679	0.0153	0.0039	0.2457	20.7	0.6935	0.0153	0.0039	0.2457	
22	Jt7 Ap 7 - 01	19.4	0.5761	0.0308	0.0050	0.0110	20.1	0.5981	0.0308	0.0050	0.0110	
23	Jt7 Ap 7 - 02	20.0	0.6213	0.0431	0.0060	-0.3567	20.8	0.6450	0.0431	0.0060	-0.3567	
24	Jt7 Ap 8 - 01	23.5	2.39	0.0438	0.0205	0.5171	24.3	2.48	0.0438	0.0205	0.5171	x
25	Jt7 Ap 8 - 02	22.0	1.09	0.0839	0.0183	-0.1777	22.8	1.14	0.0839	0.0183	-0.1777	
26	Jt7 Ap 8 - 03	20.9	0.6284	0.0096	0.0028	0.0248	21.7	0.6524	0.0096	0.0028	0.0248	
27	Jt7 Ap 9 - 01	19.8	0.9419	0.0174	0.0071	-0.0642	20.6	0.9779	0.0174	0.0071	-0.0642	
28	Jt7 Ap 9 - 02	19.4	0.8353	0.0220	0.0060	-0.0503	20.1	0.8673	0.0220	0.0060	-0.0503	
29	Jt7 Ap 12 - 01	18.9	0.7589	0.1832	0.0662	-0.2145	19.6	0.7879	0.1832	0.0662	-0.2145	
30	Jt7 Ap 12 - 02	20.8	1.26	0.0520	0.0172	-0.1777	21.6	1.30	0.0520	0.0172	-0.1777	

#	Sample	uncorrected ratios					matrix corrected ratios					Exclude
		$^{176}Lu/^{176}Hf$	± 2σ	$^{177}Hf/^{176}Hf$	± 2σ	Rho	$^{176}Lu/^{176}Hf$	± 2σ	$^{177}Hf/^{176}Hf$	± 2σ	Rho	
31	Jt7 Ap 13 - 01	20.9	1.36	0.0262	0.0101	0.2742	21.7	1.42	0.0262	0.0101	0.2742	
32	Jt7 Ap 14 - 01	20.9	0.5685	0.0614	0.0071	0.0341	21.7	0.5902	0.0614	0.0071	0.0341	
33	Jt7 Ap 15 - 01	19.5	0.5802	0.0097	0.0027	-0.0280	20.3	0.6024	0.0097	0.0027	-0.0280	
34	Jt7 Ap 15 - 02	19.7	0.6413	0.0119	0.0035	0.5479	20.4	0.6658	0.0119	0.0035	0.5479	
35	Jt7 Ap 15 - 03	20.3	0.6144	0.0115	0.0030	0.2201	21.1	0.6379	0.0115	0.0030	0.2201	
36	Jt7 Ap 15 - 04	20.1	0.5764	0.0236	0.0047	0.3851	20.9	0.5984	0.0236	0.0047	0.3851	
37	Jt7 Ap 15 - 05	20.1	0.7004	0.0217	0.0047	-0.1356	20.9	0.7272	0.0217	0.0047	-0.1356	
38	Jt7 Ap 15 - 06	18.8	0.5577	0.0325	0.0079	-0.0659	19.5	0.5791	0.0325	0.0079	-0.0659	
39	Jt7 Ap 16 - 01	19.3	0.7653	0.0177	0.0043	-0.0096	20.0	0.7946	0.0177	0.0043	-0.0096	
40	Jt7 Ap 16 - 02	19.4	0.6559	0.0443	0.0110	0.4408	20.1	0.6810	0.0443	0.0110	0.4408	
41	Jt7 Ap 17 - 06	16.3	1.61	0.6271	0.1100	-0.2978	16.9	1.67	0.6271	0.1100	-0.2978	x
42	Jt7 Ap 18 - 01	19.7	0.8166	0.0370	0.0073	0.1672	20.5	0.8478	0.0370	0.0073	0.1672	
43	Jt7 Ap 18 - 02	20.4	0.8244	0.0132	0.0043	0.7734	21.2	0.8559	0.0132	0.0043	0.7734	
44	Jt7 Ap 18 - 03	20.0	0.7606	0.0145	0.0044	-0.1321	20.8	0.7897	0.0145	0.0044	-0.1321	
45	Jt7 Ap 18 - 04	19.3	0.7915	0.0668	0.0151	0.0331	20.0	0.8218	0.0668	0.0151	0.0331	
46	Jt7 Ap 18 - 05	18.5	1.68	0.1583	0.0336	-0.9454	19.2	1.74	0.1583	0.0336	-0.9454	x
47	Jt7 Ap 18 - 06	20.8	0.7925	0.0193	0.0057	0.3576	21.6	0.8229	0.0193	0.0057	0.3576	
48	Jt7 Ap 18 - 07	19.9	0.8361	0.0235	0.0052	0.1869	20.7	0.8681	0.0235	0.0052	0.1869	
49	Jt7 Ap 18 - 08	19.8	0.8507	0.0126	0.0041	-0.3076	20.5	0.8833	0.0126	0.0041	-0.3076	
50	Jt7 Ap 18 - 09	20.4	0.7036	0.0168	0.0042	0.3595	21.2	0.7305	0.0168	0.0042	0.3595	
51	Jt7 Ap 18 - 10	19.8	0.5370	0.0251	0.0040	0.1410	20.6	0.5576	0.0251	0.0040	0.1410	
52	Jt7 Ap 18 - 11	19.6	0.7475	0.0299	0.0110	-0.1392	20.4	0.7761	0.0299	0.0110	-0.1392	
53	Jt7 Ap 18 - 12	19.7	0.5508	0.0282	0.0096	-0.1331	20.5	0.5719	0.0282	0.0096	-0.1331	
54	Jt7 Ap 18 - 13	16.0	2.31	0.9849	0.2440	0.0996	16.6	2.40	0.9849	0.2440	0.0996	x
55	Jt7 Ap 18 - 14	0.2009	0.1584	3.52	0.2136	-0.9504	0.2086	0.1644	3.52	0.2136	-0.9504	
56	Jt7 Ap 18 - 15	16.3	1.69	0.6240	0.1432	0.1786	16.9	1.76	0.6240	0.1432	0.1786	x
57	Jt7 Ap 18 - 16	15.3	1.72	1.29	0.2219	0.7751	15.9	1.79	1.29	0.2219	0.7751	x
58	Jt7 Ap 19 - 03	21.2	1.07	0.0283	0.0101	0.5208	22.0	1.11	0.0283	0.0101	0.5208	
59	Jt7 Ap 19 - 04	20.3	0.8493	0.0144	0.0048	0.0252	21.1	0.8818	0.0144	0.0048	0.0252	
60	Jt7 Ap 19 - 05	22.1	0.9555	0.0434	0.0085	0.0399	23.0	0.9921	0.0434	0.0085	0.0399	
61	Jt7 Ap 19 - 06	20.4	1.11	0.1013	0.0317	-0.1356	21.2	1.15	0.1013	0.0317	-0.1356	
	Jt10											
1	Jt10 Ap map 1 - 01	19.2	1.08	0.1481	0.0131	-0.8971	19.9	1.13	0.1481	0.0131	-0.8971	
2	Jt10 Ap map 1 - 02	20.3	0.4903	0.0087	0.0020	0.2787	21.1	0.5091	0.0087	0.0020	0.2787	
3	Jt10 Ap map 2 - 01	20.7	0.8888	0.0017	0.0016	0.6152	21.4	0.9228	0.0017	0.0016	0.6152	
4	Jt10 Ap map 2 - 02	18.6	1.43	0.2944	0.1192	-0.6131	19.3	1.49	0.2944	0.1192	-0.6131	
5	Jt10 Ap map 3 - 01	23.9	1.86	0.0770	0.0169	-0.2433	24.8	1.93	0.0770	0.0169	-0.2433	x
6	Jt10 Ap map 3 - 02	23.7	1.95	0.1787	0.0358	-0.1302	24.7	2.02	0.1787	0.0358	-0.1302	x
7	Jt10 Ap map 3 - 03	22.0	0.9021	0.0080	0.0034	-0.4837	22.8	0.9366	0.0080	0.0034	-0.4837	
8	Jt10 Ap map 4 - 01	20.7	0.5807	0.0512	0.0277	-0.4842	21.5	0.6029	0.0512	0.0277	-0.4842	
9	Jt10 Ap map 4 - 02	20.4	0.5630	0.0133	0.0050	0.1443	21.2	0.5845	0.0133	0.0050	0.1443	
10	Jt10 Ap map 4 - 03	19.9	0.6812	0.0116	0.0035	0.2249	20.6	0.7073	0.0116	0.0035	0.2249	
11	Jt10 Ap map 5 - 01	21.3	1.04	0.0135	0.0053	-0.0248	22.1	1.07	0.0135	0.0053	-0.0248	
12	Jt10 Ap 1 - 01	20.5	1.54	0.1328	0.0277	0.0999	21.2	1.60	0.1328	0.0277	0.0999	
13	Jt10 Ap 1 - 02	18.3	1.43	0.1536	0.0429	-0.0702	19.0	1.49	0.1536	0.0429	-0.0702	
14	Jt10 Ap 1 - 03	21.1	1.15	0.0594	0.0129	-0.3935	21.9	1.19	0.0594	0.0129	-0.3935	
15	Jt10 Ap 1 - 04	21.8	1.38	0.1318	0.0475	0.2656	22.6	1.44	0.1318	0.0475	0.2656	x
16	Jt10 Ap 2 - 01	20.6	2.33	0.5000	0.1287	-0.5254	21.4	2.42	0.5000	0.1287	-0.5254	x
17	Jt10 Ap 2 - 02	20.8	1.27	0.2533	0.0325	-0.3011	21.6	1.31	0.2533	0.0325	-0.3011	x
18	Jt10 Ap 2 - 03	20.8	1.15	0.0331	0.0103	0.4320	21.6	1.19	0.0331	0.0103	0.4320	
19	Jt10 Ap 3 - 01	22.1	4.14	0.1384	0.0705	0.2461	22.9	4.29	0.1384	0.0705	0.2461	x
20	Jt10 Ap 5 - 01	22.3	1.85	0.0076	0.0069	-0.2561	23.2	1.93	0.0076	0.0069	-0.2561	x
21	Jt10 Ap 5 - 02	23.1	1.68	0.0063	0.0053	0.2113	24.0	1.74	0.0063	0.0053	0.2113	x
22	Jt10 Ap 6 - 01	20.5	0.8454	0.0044	0.0026	0.1531	21.3	0.8778	0.0044	0.0026	0.1531	
23	Jt10 Ap 6 - 02	20.9	0.8294	0.0235	0.0064	-0.3039	21.7	0.8611	0.0235	0.0064	-0.3039	
24	Jt10 Ap 6 - 03	21.2	1.16	0.0617	0.0136	-0.0378	22.0	1.21	0.0617	0.0136	-0.0378	
25	Jt10 Ap 7 - 01	24.3	1.86	0.1388	0.0604	0.6214	25.2	1.93	0.1388	0.0604	0.6214	x
26	Jt10 Ap 7 - 02	26.0	1.43	0.0277	0.0090	-0.4005	27.0	1.49	0.0277	0.0090	-0.4005	x
27	Jt10 Ap 8 - 02	20.7	0.7990	0.0158	0.0045	0.1886	21.5	0.8296	0.0158	0.0045	0.1886	

#	Sample	uncorrected ratios					matrix corrected ratios					Exclude
		$^{176}Lu/^{176}Hf$	± 2σ	$^{177}Hf/^{176}Hf$	± 2σ	Rho	$^{176}Lu/^{176}Hf$	± 2σ	$^{177}Hf/^{176}Hf$	± 2σ	Rho	
28	Jt10 Ap 8 - 03	17.4	0.8009	0.3030	0.1023	-0.8515	18.0	0.8315	0.3030	0.1023	-0.8515	
29	Jt10 Ap 8 - 04	20.0	1.24	0.0724	0.0204	-0.3760	20.7	1.29	0.0724	0.0204	-0.3760	x
30	Jt10 Ap 8 - 05	20.7	1.16	0.0582	0.0131	0.0117	21.5	1.21	0.0582	0.0131	0.0117	
31	Jt10 Ap 10 - 01	20.4	0.7332	0.0046	0.0023	0.4615	21.1	0.7612	0.0046	0.0023	0.4615	
32	Jt10 Ap 10 - 02	20.5	1.04	0.0080	0.0043	0.0607	21.3	1.08	0.0080	0.0043	0.0607	
33	Jt10 Ap 10 - 03	17.9	0.9674	0.3033	0.0784	-0.5040	18.6	1.00	0.3033	0.0784	-0.5040	
34	Jt10 Ap 10 - 04	19.6	0.6784	0.0427	0.0069	-0.3507	20.4	0.7044	0.0427	0.0069	-0.3507	
35	Jt10 Ap 13 - 01	19.8	0.6505	0.0078	0.0026	0.2251	20.5	0.6754	0.0078	0.0026	0.2251	
36	Jt10 Ap 13 - 02	20.0	0.7065	0.0422	0.0112	0.4746	20.7	0.7336	0.0422	0.0112	0.4746	
37	Jt10 Ap 14 - 01	23.2	5.65	0.0702	0.0638	-0.0080	24.1	5.87	0.0702	0.0638	-0.0080	x
38	Jt10 Ap 14 - 03	19.6	0.5350	0.0084	0.0024	-0.1878	20.3	0.5555	0.0084	0.0024	-0.1878	
							0.0010	0.0001	3.55	0.0100		
Lu-Hf reference material												
1	Bamble - 01	46.4	1.11	0.0083	0.0020	0.0124	48.2	1.15	0.0083	0.0020	0.0124	
2	Bamble - 02	47.3	1.10	0.0085	0.0020	-0.3691	49.1	1.14	0.0085	0.0020	-0.3691	
3	Bamble - 03	46.0	1.06	0.0161	0.0027	-0.0676	47.8	1.10	0.0161	0.0027	-0.0676	
4	Bamble - 04	45.6	1.04	0.0053	0.0015	0.1979	47.4	1.08	0.0053	0.0015	0.1979	
5	Bamble - 05	45.8	1.05	0.0069	0.0018	-0.2193	47.6	1.09	0.0069	0.0018	-0.2193	
6	Bamble - 06	46.7	1.09	0.0073	0.0018	0.0344	48.5	1.13	0.0073	0.0018	0.0344	
7	Bamble - 07	45.8	1.05	0.0097	0.0021	0.2160	47.5	1.09	0.0097	0.0021	0.2160	
8	Bamble - 08	44.9	1.17	0.0415	0.0044	-0.4212	46.6	1.21	0.0415	0.0044	-0.4212	
9	Bamble - 09	45.9	1.06	0.0057	0.0016	-0.0555	47.7	1.10	0.0057	0.0016	-0.0555	
10	Bamble - 10	46.9	1.11	0.0111	0.0023	-0.2482	48.7	1.15	0.0111	0.0023	-0.2482	
11	Bamble - 11	46.1	1.08	0.0060	0.0017	0.4705	47.8	1.12	0.0060	0.0017	0.4705	
12	Bamble - 12	46.2	1.09	0.0070	0.0018	0.1096	47.9	1.13	0.0070	0.0018	0.1096	
13	Bamble - 13	47.5	1.16	0.0037	0.0014	-0.0055	49.3	1.21	0.0037	0.0014	-0.0055	
14	Bamble - 14	46.7	1.11	0.0050	0.0015	0.0360	48.4	1.15	0.0050	0.0015	0.0360	
15	Bamble - 15	48.2	1.16	0.0056	0.0017	0.0864	50.1	1.21	0.0056	0.0017	0.0864	
16	Bamble - 16	46.5	1.11	0.0072	0.0019	-0.0861	48.3	1.15	0.0072	0.0019	-0.0861	
17	Bamble - 17	45.6	1.07	0.0277	0.0036	-0.0371	47.4	1.11	0.0277	0.0036	-0.0371	
18	Bamble - 18	46.4	1.10	0.0047	0.0015	0.0384	48.1	1.14	0.0047	0.0015	0.0384	
19	Bamble - 19	46.0	1.10	0.0091	0.0021	0.0432	47.8	1.14	0.0091	0.0021	0.0432	
20	Bamble - 20	47.6	1.15	0.0064	0.0018	-0.2428	49.4	1.19	0.0064	0.0018	-0.2428	
		0.0010	0.0001	3.55	0.0100		0.0010	0.0001	3.55	0.0100		
	HR											
1	HR - 01	147	5.31	0.0199	0.0048	-0.0951	153	5.51	0.0199	0.0048	-0.0951	
2	HR - 02	152	5.54	0.0176	0.0046	0.0929	158	5.75	0.0176	0.0046	0.0929	
3	HR - 03	151	5.76	0.0110	0.0036	0.2068	157	5.98	0.0110	0.0036	0.2068	
4	HR - 04	149	5.38	0.0125	0.0038	0.0013	155	5.59	0.0125	0.0038	0.0013	
5	HR - 05	149	5.38	0.0204	0.0049	0.0602	154	5.58	0.0204	0.0049	0.0602	
6	HR - 06	146	5.25	0.0111	0.0036	-0.1032	152	5.45	0.0111	0.0036	-0.1032	
7	HR - 07	147	5.32	0.0247	0.0054	0.1797	152	5.52	0.0247	0.0054	0.1797	
8	HR - 08	150	5.46	0.0235	0.0053	0.2458	156	5.67	0.0235	0.0053	0.2458	
9	HR - 09	150	5.50	0.0199	0.0049	0.3284	156	5.71	0.0199	0.0049	0.3284	
10	HR - 10	148	5.35	0.0219	0.0051	0.0172	153	5.56	0.0219	0.0051	0.0172	
11	HR - 11	151	5.52	0.0146	0.0042	-0.1699	157	5.73	0.0146	0.0042	-0.1699	
12	HR - 12	154	6.07	0.0224	0.0053	-0.0044	160	6.30	0.0224	0.0053	-0.0044	
13	HR - 13	152	5.62	0.0112	0.0037	-0.0465	158	5.83	0.0112	0.0037	-0.0465	
14	HR - 14	149	5.52	0.0188	0.0048	0.0283	155	5.73	0.0188	0.0048	0.0283	
15	HR - 15	148	5.67	0.1278	0.0136	-0.4273	154	5.88	0.1278	0.0136	-0.4273	
16	HR - 16	149	5.42	0.0124	0.0038	-0.0312	154	5.63	0.0124	0.0038	-0.0312	
17	HR - 17	146	5.29	0.0144	0.0041	0.2874	152	5.49	0.0144	0.0041	0.2874	
18	HR - 18	148	5.39	0.0147	0.0042	0.2499	154	5.60	0.0147	0.0042	0.2499	
19	HR - 19	150	5.58	0.0105	0.0036	-0.1056	156	5.79	0.0105	0.0036	-0.1056	
20	HR - 20	152	5.70	0.0150	0.0043	-0.0229	157	5.92	0.0150	0.0043	-0.0229	
		0.0010	0.0001	3.55	0.0100		0.0010	0.0001	3.55	0.0100		
	Wallaroo											
1	Wallaroo - 01	33.2	1.98	0.0132	0.0066	-0.0366	34.5	2.06	0.0132	0.0066	-0.0366	
2	Wallaroo - 02	33.2	1.70	0.0155	0.0060	-0.0035	34.4	1.77	0.0155	0.0060	-0.0035	
3	Wallaroo - 03	24.4	1.09	0.8929	0.1011	-0.3502	25.3	1.13	0.8929	0.1011	-0.3502	
4	Wallaroo - 04	31.3	1.89	0.0398	0.0116	-0.1401	32.5	1.97	0.0398	0.0116	-0.1401	

#	Sample	uncorrected ratios					matrix corrected ratios					Exclude
		$^{176}Lu/^{176}Hf$	± 2σ	$^{177}Hf/^{176}Hf$	± 2σ	Rho	$^{176}Lu/^{176}Hf$	± 2σ	$^{177}Hf/^{176}Hf$	± 2σ	Rho	
5	Wallaroo - 05	19.7	0.9485	1.45	0.1276	-0.7034	20.4	0.9848	1.45	0.1276	-0.7034	
6	Wallaroo - 06	32.2	1.27	0.0051	0.0026	0.0078	33.4	1.31	0.0051	0.0026	0.0078	
7	Wallaroo - 07	33.9	1.74	0.0087	0.0045	0.0092	35.2	1.80	0.0087	0.0045	0.0092	
8	Wallaroo - 08	26.3	1.18	0.6567	0.0662	-0.2909	27.3	1.23	0.6567	0.0662	-0.2909	
9	Wallaroo - 09	32.1	1.62	0.0099	0.0048	-0.2020	33.3	1.68	0.0099	0.0048	-0.2020	
10	Wallaroo - 10	22.2	0.9753	1.09	0.0915	-0.2935	23.1	1.01	1.09	0.0915	-0.2935	
	NIST610											
1	NIST610 - 01	0.4986	0.0036	3.55	0.0124	0.3244	-	-	-	-	-	
2	NIST610 - 02	0.4968	0.0035	3.55	0.0124	0.3839	-	-	-	-	-	
3	NIST610 - 03	0.4939	0.0035	3.55	0.0124	0.2122	-	-	-	-	-	
4	NIST610 - 04	0.4925	0.0035	3.54	0.0124	0.4059	-	-	-	-	-	
5	NIST610 - 05	0.4904	0.0035	3.54	0.0124	0.0694	-	-	-	-	-	
6	NIST610 - 06	0.4904	0.0035	3.54	0.0124	0.0496	-	-	-	-	-	
7	NIST610 - 07	0.4913	0.0035	3.54	0.0124	0.2695	-	-	-	-	-	
8	NIST610 - 08	0.4922	0.0035	3.55	0.0124	0.2157	-	-	-	-	-	
9	NIST610 - 09	0.4892	0.0022	3.55	0.0124	0.2746	-	-	-	-	-	
10	NIST610 - 10	0.4895	0.0022	3.54	0.0124	0.1203	-	-	-	-	-	
11	NIST610 - 11	0.4880	0.0022	3.55	0.0124	0.2617	-	-	-	-	-	
12	NIST610 - 12	0.4877	0.0022	3.55	0.0124	0.3450	-	-	-	-	-	
13	NIST610 - 13	0.4905	0.0022	3.56	0.0124	0.1885	-	-	-	-	-	
14	NIST610 - 14	0.4885	0.0022	3.54	0.0124	0.1498	-	-	-	-	-	
15	NIST610 - 15	0.4905	0.0022	3.55	0.0124	0.3749	-	-	-	-	-	
16	NIST610 - 16	0.4870	0.0022	3.54	0.0124	0.3938	-	-	-	-	-	
17	NIST610 - 17	0.4881	0.0022	3.55	0.0124	0.1063	-	-	-	-	-	
18	NIST610 - 18	0.4887	0.0022	3.55	0.0124	0.2850	-	-	-	-	-	
19	NIST610 - 19	0.4892	0.0022	3.55	0.0124	0.4068	-	-	-	-	-	
20	NIST610 - 20	0.4884	0.0022	3.55	0.0124	0.3820	-	-	-	-	-	
21	NIST610 - 21	0.4902	0.0022	3.55	0.0124	0.2668	-	-	-	-	-	
22	NIST610 - 22	0.4892	0.0022	3.56	0.0124	0.0902	-	-	-	-	-	
23	NIST610 - 23	0.4880	0.0022	3.54	0.0124	0.2689	-	-	-	-	-	
24	NIST610 - 24	0.4879	0.0022	3.55	0.0124	0.0753	-	-	-	-	-	
25	NIST610 - 25	0.4882	0.0022	3.54	0.0124	0.3363	-	-	-	-	-	
26	NIST610 - 26	0.4900	0.0022	3.55	0.0124	0.2389	-	-	-	-	-	
27	NIST610 - 27	0.4870	0.0022	3.53	0.0123	0.2404	-	-	-	-	-	
28	NIST610 - 28	0.4908	0.0022	3.55	0.0124	0.2225	-	-	-	-	-	
29	NIST610 - 29	0.4881	0.0022	3.55	0.0124	0.2415	-	-	-	-	-	
30	NIST610 - 30	0.4895	0.0022	3.55	0.0124	0.3940	-	-	-	-	-	

*(Continued)

#	Sample	Al	Ca	Ti	Cr	Mn	Fe	Sr	Y	Zr	La	Ce	Nd	Sm	^{176}Hf	^{178}Hf	Lu
1	Jt1 Ap p 1 - 01	12.2	390000	1.54	<0.007	351	600	338	1783	0.1541	631	1495	782	207	0.4028	0.0010	17.9
2	Jt1 Ap p 1 - 02	5.38	390000	0.4380	<0.007	366	537	347	1811	0.1533	604	1427	775	213	0.3970	0.0020	18.1
3	Jt1 Ap p 2 - 01	38.8	390000	0.4487	0.0042	408	657	306	2319	0.3068	976	2403	1251	308	0.5780	0.0031	24.5
4	Jt1 Ap map 1 - 01	3356	390000	366	0.6400	382	7218	342	2218	0.3167	489	1263	773	232	0.4895	0.0014	23.1
5	Jt1 Ap 1 - 02	2213	390000	59.2	3.70	425	3847	304	1808	2.15	1399	3106	1546	340	0.6001	0.1309	17.7
6	Jt1 Ap 3 - 01	102	390000	0.6519	0.0311	416	816	336	1745	0.2647	976	2355	1186	269	0.3887	0.0018	17.1
7	Jt1 Ap 3 - 03	1.16	390000	0.0911	0.0049	372	486	377	1826	0.3587	605	1439	766	204	0.3829	0.0023	17.7
8	Jt1 Ap 4 - 01	650	390000	76.6	0.0648	432	2038	300	1675	0.4735	1798	4231	1821	343	0.3469	0.0022	15.5
9	Jt1 Ap 4 - 02	138	390000	8.48	0.8123	448	1016	295	2174	0.8501	2337	5348	2324	438	0.4800	0.0092	20.6
10	Jt1 Ap 4 - 03	1.78	390000	0.3804	<0.004	420	622	302	1830	0.4845	1587	3676	1674	337	0.4187	0.0037	18.0
11	Jt1 Ap 5 - 01	202	390000	1.46	0.0138	403	1035	307	1610	0.2605	1061	2613	1263	263	0.3640	0.0048	15.9
12	Jt1 Ap 5 - 02	17.3	390000	0.2615	0.0323	416	615	314	2229	0.4004	1359	3357	1706	365	0.4886	0.0022	21.9
13	Jt1 Ap 5 - 03	4.51	390000	0.2625	<0.004	400	560	325	1921	0.4157	893	2198	1129	271	0.4653	0.0022	20.0
14	Jt1 Ap 6 - 01	898	390000	104	0.1067	440	2624	306	1901	0.5544	1952	4824	2381	457	0.3828	0.0030	16.2
15	Jt1 Ap 6 - 02	69.2	390000	1.62	0.0143	425	709	326	2044	0.5589	1501	3689	1800	375	0.4560	0.0061	19.4
16	Jt1 Ap 6 - 03	5.52	390000	1.22	0.0352	440	708	300	2014	0.7481	2267	5492	2658	500	0.3807	0.0081	16.9
17	Jt1 Ap 6 - 04	83.1	390000	3.51	0.3286	431	895	298	2126	0.9209	1779	4592	2256	450	0.4523	0.0145	19.6
18	Jt1 Ap 8 - 01	907	390000	78.2	0.1097	373	2509	370	2044	0.2731	711	1753	940	244	0.4832	0.0025	21.4
19	Jt1 Ap 10 - 01	135	390000	11.9	0.2241	381	824	320	1087	0.7733	535	1248	645	159	0.2486	0.0145	10.6
20	Jt1 Ap 15 - 01	1050	390000	15.7	0.0624	407	1991	348	2098	0.3995	1055	2697	1318	302	0.4820	0.0044	21.8
21	Jt1 Ap 16 - 01	367	390000	20.1	0.0496	408	1483	339	2197	0.2583	1026	2604	1365	316	0.5185	0.0016	22.6
22	Jt1 Ap 16 - 02	19.6	390000	0.0547	0.0067	390	574	370	1247	0.1904	487	1287	755	186	0.2675	0.0012	12.2
23	Jt1 Ap 16 - 03	2197	390000	18.0	0.1323	419	2844	366	2071	0.5082	1695	4234	1927	380	0.4528	0.0024	20.9
24	Jt1 Ap 18 - 01	156	390000	4.95	0.1796	429	1059	291	1769	0.9299	1623	4094	1973	390	0.3913	0.0147	16.1
25	Jt1 Ap 18 - 02	20.6	390000	1.55	0.0654	444	715	296	1793	0.7719	1961	4629	2001	374	0.3854	0.0115	16.6
26	Jt1 Ap 18 - 03	16.1	390000	1.62	0.0046	447	720	311	1634	0.8301	1943	4711	2100	383	0.3447	0.0130	14.7
27	Jt1 Ap 18 - 04	101	390000	1.85	0.2672	431	945	296	1667	0.7608	1875	4679	2224	410	0.3383	0.0120	14.7
28	Jt1 Ap 19 - 03	391	390000	19.0	10.0	387	1643	352	2510	0.6369	858	2108	1222	325	0.5652	0.0210	25.5
29	Jt1 Ap 19 - 05	281	390000	26.6	0.9583	385	1266	352	1704	0.6584	811	1763	970	252	0.4205	0.0122	17.3
30	Jt1 Ap 19 - 07	415	390000	17.7	2.15	403	1744	336	2100	1.87	1060	2341	1204	296	0.4984	0.0466	21.4
31	Jt1 Ap 19 - 08	34.2	390000	1.69	<0.005	384	659	327	2037	0.4288	726	1703	927	245	0.4819	0.0055	21.3
	Rims																
1	Jt1 Ap p 1 - 03	5064	390000	508	1.02	369	10725	363	571	0.1253	93.7	239	158	52.1	0.1136	0.0018	5.18
2	Jt1 Ap map 1 - 04	290	390000	10.1	0.7979	365	773	285	202	1.40	8.80	35.0	40.7	18.1	0.0918	0.0601	1.67
3	Jt1 Ap map 1 - 05	416	390000	780	2.50	323	1405	424	240	0.5369	10.8	34.6	38.5	18.2	0.0677	0.0140	1.80
4	Jt1 Ap map 1 - 06	4.05	390000	0.3990	0.0163	389	500	261	389	0.2785	154	388	207	53.4	0.0816	0.0043	3.63
5	Jt1 Ap 3 - 04	485	390000	46.3	0.2516	313	1368	371	456	0.1290	20.3	64.6	66.8	30.9	0.0770	0.0018	3.92
6	Jt1 Ap 6 - 05	61.8	390000	0.7037	0.0518	383	614	261	194	0.3709	23.3	78.8	68.7	23.9	0.0440	0.0058	1.74
7	Jt1 Ap 6 - 06	89.9	390000	7.90	0.2248	388	712	216	181	0.3675	23.9	81.7	66.9	21.1	0.0550	0.0141	1.65
8	Jt1 Ap 6 - 08	229	390000	6.23	0.1612	359	1013	231	195	0.8528	15.2	55.5	53.6	20.0	0.0685	0.0265	1.74
9	Jt1 Ap 6 - 09	15.2	390000	0.8957	<0.008	346	442	310	215	0.4355	11.9	42.7	44.9	20.2	0.0409	0.0059	1.84
10	Jt1 Ap 6 - 10	22.4	390000	0.9153	<0.004	367	497	314	240	0.2493	25.7	87.2	80.4	28.6	0.0567	0.0071	2.22
11	Jt1 Ap 6 - 11	1916	390000	44.3	1.64	335	7943	462	232	0.4225	11.2	36.0	35.0	15.1	0.0554	0.0197	1.87
12	Jt1 Ap 13 - 01	145784	390000	1581	11.5	1689	131364	942	5998	6.03	32079	77630	30322	4540	0.4881	0.1072	18.3
13	Jt1 Ap 15 - 02	325	390000	8.82	3.57	357	1425	311	220	0.3685	20.1	64.6	67.5	25.0	0.0471	0.0094	1.84
14	Jt1 Ap 15 - 03	64587	390000	5948	32.6	723	125935	362	257	0.0998	15.2	49.8	56.1	23.5	0.0550	0.0214	2.19
15	Jt1 Ap 18 - 05	252	390000	20.6	0.1064	340	1005	386	484	0.0915	45.5	141	115	42.9	0.0886	0.0082	4.14
16	Jt1 Ap 18 - 06	214	390000	3.79	0.2309	373	1060	355	1482	0.2989	395	1022	584	167	0.3187	0.0052	14.5
	Jt4																
1	Jt4 Ap p 1 - 01	0.0391	390000	0.0566	0.0214	264	278	253	401	4.88	7.48	25.8	27.5	12.3	0.2817	0.1754	4.78
2	Jt4 Ap p 2 - 01	123	390000	0.2031	0.0215	252	993	369	408	0.1016	9.83	27.3	22.1	8.08	0.1051	0.0071	5.30
3	Jt4 Ap 1 - 01	352	390000	37.1	1.15	259	1359	266	1413	0.0114	115	280	173	50.2	0.3967	0.0006	18.0
4	Jt4 Ap 2 - 01	50.2	390000	2.37	0.0645	278	862	251	1443	0.1905	289	699	355	79.9	0.3748	0.0016	18.2
5	Jt4 Ap 3 - 01	891	390000	92.6	0.3392	268	2558	248	2932	0.2201	389	918	497	129	0.8412	0.0012	39.5
6	Jt4 Ap 3 - 02	211	390000	21.4	0.1120	287	908	193	2372	6.23	756	1763	829	177	0.8365	0.1526	28.2

#	Sample	Al	Ca	Ti	Cr	Mn	Fe	Sr	Y	Zr	La	Ce	Nd	Sm	^{176}Hf	^{178}Hf	Lu
7	Jt4 Ap 3 - 03	0.1239	390000	<0.004	<0.009	253	284	243	430	3.79	6.86	23.6	25.6	11.5	0.2180	0.0972	5.72
8	Jt4 Ap 3 - 04	1756	390000	175	7.91	271	10905	244	597	0.0528	32.9	88.0	63.2	20.3	0.1660	0.0006	7.79
9	Jt4 Ap 4 - 01	0.2432	390000	<0.004	<0.009	277	349	236	3014	0.2200	483	1127	602	152	0.8513	0.0015	37.3
10	Jt4 Ap 5 - 01	1972	390000	56.9	0.7430	264	7277	309	846	0.0093	212	473	217	45.7	0.2023	0.0024	10.0
11	Jt4 Ap 5 - 02	903	390000	3.57	0.6950	266	4666	281	562	0.0180	105	254	128	30.2	0.1342	0.0008	6.55
12	Jt4 Ap 6 - 01	114	390000	0.9546	0.0357	260	961	222	1212	1.13	168	410	211	54.9	0.3645	0.0418	14.9
13	Jt4 Ap 10 - 01	435	390000	12.1	4.13	273	6079	241	1983	0.1623	352	826	417	96.8	0.5183	0.0009	24.0
14	Jt4 Ap 11 - 01	57.1	390000	0.1780	0.0214	254	89050	273	925	0.0891	61.9	151	98.6	28.4	0.2373	0.0004	11.9
15	Jt4 Ap 12 - 01	7866	390000	127	1.73	337	10181	249	2826	0.1896	3569	8027	2966	446	0.7062	0.0188	34.6
16	Jt4 Ap 12 - 02	573	390000	63.0	2.95	246	2435	290	1505	0.2400	154	387	224	60.0	0.3933	0.0025	19.2
17	Jt4 Ap 12 - 05	152	390000	6.62	0.2788	266	639	262	2600	2.70	433	1047	615	154	0.7210	0.0543	30.7
18	Jt4 Ap 13 - 05	19559	390000	155	6.64	461	20006	384	1306	2.18	5488	12744	4654	582	0.2784	0.1525	9.42
19	Jt4 Ap 13 - 06	286467	390000	2355	23.9	3202	272380	2074	9360	49.3	89367	198663	65754	8525	3.07	1.90	39.1
20	Jt4 Ap 13 - 11	37860	390000	2251	35.0	467	80577	390	1068	10.4	3517	6792	2132	286	0.4687	0.1770	10.1
21	Jt4 Ap 14 - 01	1437	390000	143	1.91	270	3980	262	806	1.26	74.0	189	112	30.9	0.2349	0.0296	9.67
22	Jt4 Ap 14 - 02	743	390000	10.8	0.9014	280	9777	263	1143	0.2244	369	844	370	73.6	0.2956	0.0024	13.5
23	Jt4 Ap 15 - 01	1653	390000	130	2.14	288	6162	262	2579	0.3385	783	1778	818	165	0.6627	0.0037	30.9
24	Jt4 Ap 15 - 03	2664	390000	259	3.01	275	11516	259	1986	0.4376	324	780	406	95.5	0.5138	0.0071	24.6
25	Jt4 Ap 16 - 01	52.6	390000	139	0.8082	266	937	291	662	3.49	47.7	123	73.9	21.1	0.2801	0.1110	8.22
26	Jt4 Ap 16 - 02	178	390000	15.2	1.08	264	1286	277	631	0.0275	48.8	123	73.9	21.1	0.1508	0.0003	7.60
27	Jt4 Ap 16 - 03	345	390000	1.70	0.7199	265	11471	279	1279	0.0985	156	385	202	50.8	0.3460	0.0013	16.2
28	Jt4 Ap 16 - 04	12.2	390000	0.5611	0.0125	243	11717	300	1024	0.3108	76.3	190	116	31.7	0.2880	0.0097	14.1
	Jt7																
1	Jt7 Ap p1 - 01	857	390000	50.8	0.1049	348	3035	204	1384	0.2572	599	1384	644	142	0.2909	0.0050	12.8
2	Jt7 Ap p1 - 02	7863	390000	828	1.80	340	18732	187	1790	0.9020	385	872	514	132	0.4027	0.0145	18.4
3	Jt7 Ap p2 - 02	168	390000	2.83	0.0179	311	1189	275	772	0.4672	128	294	162	41.4	0.1615	0.0140	7.66
4	Jt7 Ap p2 - 03	49.8	390000	1.84	0.0174	332	8448	248	626	0.1973	113	294	179	51.6	0.1350	0.0051	5.94
5	Jt7 Ap p2 - 04	103	390000	7.72	0.0475	321	5306	266	393	0.0868	12.6	36.7	33.5	13.9	0.0799	0.0049	3.61
6	Jt7 Ap map 1 - 01	332	390000	14.5	0.0597	381	1169	192	2282	0.5581	1147	2706	1264	258	0.5136	0.0037	22.3
7	Jt7 Ap map 1 - 02	130	390000	13.9	0.0550	377	787	189	1955	0.4879	1251	2882	1253	244	0.4240	0.0023	18.3
8	Jt7 Ap map 2 - 02	278	390000	22.3	0.7196	327	1118	205	1263	0.8900	159	402	266	77.4	0.2957	0.0252	12.1
9	Jt7 Ap 1 - 01	262	390000	1.29	<0.003	338	2005	175	1050	0.1051	416	1111	660	155	0.1866	0.0010	8.00
10	Jt7 Ap 1 - 02	1003	390000	32.6	2.27	405	2285	193	2322	3.51	1337	3578	1922	383	0.4993	0.0170	21.1
11	Jt7 Ap 1 - 03	2871	390000	22.6	0.6882	392	5240	178	1387	0.6462	638	1760	1003	236	0.2702	0.0231	11.4
12	Jt7 Ap 1 - 04	9118	390000	71.2	0.6056	465	10835	208	1922	1.05	3827	8881	3608	564	0.3691	0.0154	15.9
13	Jt7 Ap 2 - 01	928	390000	106	0.4840	379	2676	188	1874	8.23	1117	2604	1264	250	0.3811	0.0054	16.7
14	Jt7 Ap 2 - 02	226	390000	98.5	0.8635	391	1215	189	2212	2.29	901	2189	1164	251	0.5091	0.0660	19.6
15	Jt7 Ap 2 - 03	11955	390000	36.7	14.5	656	104420	193	1156	5.99	441	947	570	130	0.2843	0.1158	11.2
16	Jt7 Ap 5 - 01	987	390000	12.7	0.0684	356	1352	229	1835	0.3168	808	1846	843	178	0.3977	0.0025	18.6
17	Jt7 Ap 5 - 02	214	390000	22.1	0.0510	337	864	226	1812	0.2534	351	844	459	121	0.4075	0.0016	19.1
18	Jt7 Ap 5 - 03	283	390000	26.0	0.0559	328	1466	227	1417	0.1809	257	603	329	89.5	0.3128	0.0011	14.9
19	Jt7 Ap 6 - 01	422	390000	23.9	0.0052	360	1918	226	2078	0.3468	857	2024	978	209	0.4434	0.0020	21.0
20	Jt7 Ap 6 - 02	1010	390000	44.0	0.0576	404	4494	201	1568	0.3002	861	2122	1037	211	0.3309	0.0059	14.6
21	Jt7 Ap 6 - 03	186	390000	7.69	<0.004	359	1225	180	1328	0.2056	480	1311	772	184	0.2712	0.0012	12.0
22	Jt7 Ap 7 - 01	73.5	390000	6.82	0.0066	371	633	191	1603	0.3696	961	2356	1158	233	0.3442	0.0030	14.9
23	Jt7 Ap 7 - 02	1303	390000	114	0.1683	378	4205	200	1992	0.4449	1207	2743	1240	244	0.4531	0.0055	20.2
24	Jt7 Ap 8 - 01	46.3	390000	3.82	0.0340	315	487	241	416	<0.000	13.3	39.7	37.1	15.3	0.0737	0.0009	3.79
25	Jt7 Ap 8 - 02	486	390000	3.47	0.1461	329	926	267	592	0.0664	198	460	196	42.3	0.1134	0.0027	5.54
26	Jt7 Ap 8 - 03	44.7	390000	3.05	0.0347	342	574	245	1568	0.1925	201	504	303	90.6	0.3373	0.0009	15.8
27	Jt7 Ap 9 - 01	495	390000	52.8	0.0693	335	1858	213	1761	0.1579	264	629	381	110	0.4178	0.0020	18.5
28	Jt7 Ap 9 - 02	1262	390000	131	0.2360	360	3896	202	2004	0.4346	586	1336	694	173	0.4837	0.0030	21.0
29	Jt7 Ap 12 - 01	409	390000	2.20	0.0457	375	859	214	1710	0.6007	1122	2585	1149	221	0.3897	0.0199	16.4
30	Jt7 Ap 12 - 02	34.2	390000	0.3390	0.0981	390	672	210	2227	0.6085	1358	2974	1378	279	0.4615	0.0068	21.6
31	Jt7 Ap 13 - 01	572	390000	2.95	0.3145	328	2136	286	1233	0.0940	205	472	259	65.9	0.2619	0.0019	12.2
32	Jt7 Ap 14 - 01	156	390000	3.88	0.0098	368	1149	249	1744	0.3760	611	1586	838	188	0.3661	0.0063	17.1
33	Jt7 Ap 15 - 01	249	390000	3.09	0.0270	366	1133	197	2020	0.2241	854	2041	971	206	0.4370	0.0012	19.2
34	Jt7 Ap 15 - 02	650	390000	70.6	0.1148	365	2158	190	1689	0.1903	888	2095	963	194	0.3539	0.0012	15.5

#	Sample	Al	Ca	Ti	Cr	Mn	Fe	Sr	Y	Zr	La	Ce	Nd	Sm	^{176}Hf	^{178}Hf	Lu
35	Jt7 Ap 15 - 03	791	390000	90.4	0.2411	360	2746	195	1800	0.2381	582	1442	765	178	0.3719	0.0012	16.9
36	Jt7 Ap 15 - 04	346	390000	37.3	0.1484	354	1466	196	2135	0.4370	654	1500	755	185	0.4613	0.0031	20.8
37	Jt7 Ap 15 - 05	3800	390000	468	1.19	355	7894	201	1319	0.1577	281	704	396	104	0.2793	0.0017	12.5
38	Jt7 Ap 15 - 06	533	390000	10.4	0.0345	362	1803	194	1746	0.2165	740	1752	823	179	0.3874	0.0035	16.3
39	Jt7 Ap 16 - 01	1032	390000	112	0.5305	364	3351	198	2262	0.3290	665	1474	736	183	0.5283	0.0026	22.9
40	Jt7 Ap 16 - 02	3978	390000	63.5	0.1369	408	4381	225	2579	0.9423	1760	3835	1564	304	0.6034	0.0075	26.2
41	Jt7 Ap 17 - 06	15345	390000	61.4	0.9970	472	15163	358	2023	3.29	5539	11802	3970	549	0.5735	0.1016	21.0
42	Jt7 Ap 18 - 01	1461	390000	65.9	0.5239	356	7769	191	1216	0.2032	311	837	508	128	0.2452	0.0025	10.8
43	Jt7 Ap 18 - 02	941	390000	110	0.3503	338	2681	203	1341	0.1449	216	596	393	108	0.2833	0.0010	12.8
44	Jt7 Ap 18 - 03	790	390000	74.1	0.2109	348	3066	198	1332	0.1237	485	1156	577	132	0.2724	0.0011	12.2
45	Jt7 Ap 18 - 04	65.2	390000	2.42	0.0687	365	809	195	2080	0.4510	986	2183	1054	224	0.4525	0.0084	19.4
46	Jt7 Ap 18 - 05	163	390000	1.64	0.1970	356	1293	192	1721	1.11	678	1528	738	165	0.3816	0.0168	15.7
47	Jt7 Ap 18 - 06	685	390000	73.2	0.1682	361	2361	196	2095	0.1861	648	1523	796	182	0.3689	0.0020	17.2
48	Jt7 Ap 18 - 07	722	390000	4.23	0.0316	379	1241	199	1878	0.3213	1445	3241	1410	259	0.3811	0.0025	17.1
49	Jt7 Ap 18 - 08	16.1	390000	0.1615	0.0140	347	525	217	1500	0.1914	412	961	499	126	0.3295	0.0012	14.6
50	Jt7 Ap 18 - 09	827	390000	35.0	0.1500	363	2063	199	1808	0.3919	1031	2242	946	189	0.3838	0.0018	17.6
51	Jt7 Ap 18 - 10	1780	390000	185	0.2200	376	4470	199	2305	0.4618	1155	2450	1103	233	0.5214	0.0037	23.1
52	Jt7 Ap 18 - 11	471	390000	47.3	0.3169	360	1846	195	2086	0.5539	773	1674	815	192	0.4629	0.0039	20.3
53	Jt7 Ap 18 - 12	122	390000	12.4	0.0107	367	924	199	2455	0.7011	1018	2240	1069	239	0.5618	0.0044	24.8
54	Jt7 Ap 18 - 13	17417	390000	152	1.38	554	18339	352	2056	5.45	9385	19347	5752	717	0.6045	0.1589	20.7
55	Jt7 Ap 18 - 14	17462	390000	363	3.63	188	3339	1424	265	213	159	361	165	35.6	5.32	5.32	2.42
56	Jt7 Ap 18 - 15	216	390000	8.03	0.7494	332	1005	242	1984	5.45	386	912	508	133	0.5149	0.0929	19.2
57	Jt7 Ap 18 - 16	33835	390000	106	3.12	1532	517156	282	2201	6.40	463	1173	771	188	0.4995	0.1823	16.9
58	Jt7 Ap 19 - 03	92.2	390000	0.2499	0.0206	341	909	228	1039	0.2651	144	438	324	96.4	0.2003	0.0016	9.53
59	Jt7 Ap 19 - 04	102	390000	0.6341	0.0182	325	710	249	1168	0.1595	150	453	307	88.5	0.2447	0.0010	11.1
60	Jt7 Ap 19 - 05	195	390000	2.69	0.0728	334	1082	232	1261	0.2739	236	635	396	106	0.2471	0.0030	12.2
61	Jt7 Ap 19 - 06	705	390000	4.70	0.1010	338	2258	226	1068	0.2057	448	1056	468	103	0.2168	0.0062	10.00
	Jt10																
1	Jt10 Ap map 1 - 01	258	390000	0.2944	<0.005	236	3228	155	2085	0.7567	60.6	224	237	108	0.3430	0.0143	14.6
2	Jt10 Ap map 1 - 02	2.04	390000	0.0618	<0.004	211	335	153	3417	0.2375	131	447	438	185	0.5478	0.0014	25.0
3	Jt10 Ap map 2 - 01	0.0116	390000	0.0375	<0.004	197	288	139	1356	0.0497	30.6	115	143	64.5	0.1980	0.0001	9.09
4	Jt10 Ap map 2 - 02	121	390000	0.3679	<0.004	202	1089	150	767	0.2947	180	373	164	40.7	0.1129	0.0095	4.72
5	Jt10 Ap map 3 - 01	10.3	390000	0.2343	<0.004	151	248	183	715	0.0482	23.2	83.9	107	54.2	0.0772	0.0017	4.13
6	Jt10 Ap map 3 - 02	35.6	390000	0.2565	<0.004	116	317	149	548	0.0645	38.1	165	209	90.9	0.0496	0.0025	2.63
7	Jt10 Ap map 3 - 03	2.29	390000	<0.002	<0.003	194	300	164	1108	0.0626	20.5	85.7	111	55.4	0.1453	0.0003	7.13
8	Jt10 Ap map 4 - 01	12.7	390000	0.6441	0.0054	210	882	150	1978	0.2706	64.4	222	221	96.9	0.2968	0.0043	13.7
9	Jt10 Ap map 4 - 02	46.5	390000	0.2854	0.0053	213	885	149	2004	0.2246	47.0	177	200	96.2	0.3056	0.0012	13.9
10	Jt10 Ap map 4 - 03	127	390000	1.05	0.0062	211	1386	145	1567	0.2279	21.4	93.9	130	67.4	0.2329	0.0008	10.3
11	Jt10 Ap map 5 - 01	0.4063	390000	0.0683	<0.004	213	343	157	1028	0.0499	17.8	72.7	95.5	47.0	0.1369	0.0005	6.48
12	Jt10 Ap 1 - 01	102	390000	0.8129	0.4123	208	1060	162	787	0.0898	13.4	50.0	64.5	34.3	0.0993	0.0037	4.57
13	Jt10 Ap 1 - 02	123	390000	2.21	0.2734	224	2084	164	1040	0.1881	16.0	65.1	87.2	44.7	0.1612	0.0070	6.55
14	Jt10 Ap 1 - 03	4.57	390000	0.1042	0.1277	219	273	180	850	0.0898	15.0	57.7	74.1	37.9	0.1089	0.0018	5.09
15	Jt10 Ap 1 - 04	32.1	390000	0.5776	0.1924	221	562	186	701	0.1672	13.9	51.5	63.1	32.6	0.0813	0.0030	3.95
16	Jt10 Ap 2 - 01	38.4	390000	2.11	0.3085	216	447	177	710	0.3828	13.6	46.1	56.9	29.2	0.0745	0.0106	3.43
17	Jt10 Ap 2 - 02	43.0	390000	0.1676	0.2683	213	549	162	668	0.1131	10.2	39.2	51.0	28.0	0.0822	0.0060	3.83
18	Jt10 Ap 2 - 03	11.0	390000	0.3825	0.0119	195	525	160	1043	0.0763	15.7	67.2	92.5	47.5	0.1435	0.0014	6.74
19	Jt10 Ap 3 - 01	36.8	390000	2.98	0.2977	240	633	162	540	<0.001	10.6	37.3	48.7	25.9	0.0624	0.0025	3.14
20	Jt10 Ap 5 - 01	4.42	390000	1.45	0.3279	208	5099	148	717	<0.001	9.44	36.9	51.2	27.9	0.0891	0.0002	4.44
21	Jt10 Ap 5 - 02	0.0328	390000	<0.005	<0.008	198	283	145	846	0.0297	12.0	51.7	70.7	36.3	0.1073	0.0002	5.50
22	Jt10 Ap 6 - 01	0.9138	390000	0.3236	0.2668	192	2754	145	1196	0.0205	21.6	90.8	120	58.3	0.1767	0.0002	8.03
23	Jt10 Ap 6 - 02	2.96	390000	0.2867	0.2381	158	412	149	1360	0.1600	26.3	108	143	70.9	0.1956	0.0013	9.22
24	Jt10 Ap 6 - 03	157	390000	1.02	0.1595	213	2792	163	845	0.0615	15.7	62.1	79.9	39.6	0.1054	0.0018	4.99
25	Jt10 Ap 7 - 01	77.8	390000	0.9634	0.0191	71.6	1077	198	635	0.0964	29.1	106	134	72.1	0.0549	0.0022	2.99
26	Jt10 Ap 7 - 02	3.33	390000	0.8778	0.0335	58.3	92.8	239	900	0.0374	19.3	61.2	74.8	47.1	0.1005	0.0008	5.84
27	Jt10 Ap 8 - 02	9.92	390000	0.1774	0.0081	203	645	164	1551	0.1023	33.1	127	152	75.0	0.2266	0.0010	10.3
28	Jt10 Ap 8 - 03	81.7	390000	2.11	0.0674	210	1109	153	1621	0.9182	400	775	354	91.3	0.2908	0.0251	11.2
29	Jt10 Ap 8 - 04	68.6	390000	4.73	1.04	203	942	137	3546	0.7157	247	660	533	201	0.5713	0.0114	25.2

#	Sample	Al	Ca	Ti	Cr	Mn	Fe	Sr	Y	Zr	La	Ce	Nd	Sm	^{176}Hf	^{178}Hf	Lu
30	Jt10 Ap 8 - 05	65.1	390000	0.1768	0.3670	195	564	146	937	0.1204	25.1	85.7	96.1	44.1	0.1288	0.0021	5.96
31	Jt10 Ap 10 - 01	3.41	390000	<0.005	0.0262	204	342	138	3096	0.2352	66.4	264	336	156	0.5090	0.0007	23.1
32	Jt10 Ap 10 - 02	<0.018	390000	<0.006	<0.009	202	311	142	1706	0.1537	40.2	162	196	88.4	0.2642	0.0006	12.1
33	Jt10 Ap 10 - 03	168	390000	1.09	<0.010	198	1487	134	1849	0.5364	52.2	194	229	99.7	0.3097	0.0266	12.4
34	Jt10 Ap 10 - 04	82.7	390000	0.3620	<0.004	213	947	159	1811	0.1615	58.6	205	210	95.6	0.2864	0.0035	12.6
35	Jt10 Ap 13 - 01	21.9	390000	0.0956	0.0121	209	411	170	2694	0.1930	68.6	270	307	145	0.4302	0.0010	19.1
36	Jt10 Ap 13 - 02	279	390000	7.42	0.0396	228	14878	138	3795	0.5394	164	539	529	212	0.6172	0.0074	27.6
37	Jt10 Ap 14 - 01	5.64	390000	0.7258	0.3090	239	371	150	880	0.3536	15.2	59.7	78.5	41.9	0.1124	0.0022	5.85
38	Jt10 Ap 14 - 03	58.3	390000	1.01	0.0393	242	1759	156	3543	0.4807	349	969	710	234	0.5760	0.0014	25.2

Lu-Hf reference material

Bamble

1	Bamble - 01	6.27	390000	0.0537	<0.002	44.8	809	276	2382	0.0766	854	2702	1818	466	0.1932	0.0004	19.9
2	Bamble - 02	0.5653	390000	0.0173	<0.002	47.8	988	245	2525	0.1055	916	2849	1913	483	0.2012	0.0005	21.1
3	Bamble - 03	2.50	390000	0.0269	<0.002	46.8	842	276	2510	0.0795	907	2840	1917	486	0.2084	0.0009	21.2
4	Bamble - 04	0.9091	390000	<0.001	<0.002	46.8	937	245	2554	0.1143	922	2890	1939	490	0.2121	0.0003	21.4
5	Bamble - 05	1.07	390000	0.0091	<0.002	47.5	910	254	2564	0.1119	934	2929	1997	495	0.2141	0.0004	21.8
6	Bamble - 06	0.2578	390000	<0.001	<0.002	47.7	907	257	2553	0.1122	933	2949	1995	495	0.2095	0.0004	21.7
7	Bamble - 07	0.5120	390000	<0.001	<0.003	48.3	962	250	2560	0.1290	939	2951	2012	498	0.2152	0.0006	21.9
8	Bamble - 08	6.97	390000	0.0416	<0.003	51.0	723	283	2547	0.1476	965	2989	2023	499	0.2184	0.0026	21.7
9	Bamble - 09	0.1405	390000	0.0097	<0.003	47.1	960	247	2559	0.1313	943	2946	1997	495	0.2137	0.0003	21.8
10	Bamble - 10	1.97	390000	0.0097	<0.003	46.4	893	260	2492	0.1113	917	2911	1959	487	0.2038	0.0006	21.2
11	Bamble - 11	0.4381	390000	0.0212	<0.003	46.8	889	253	2504	0.1007	930	2914	1967	483	0.2053	0.0004	20.9
12	Bamble - 12	0.1935	390000	<0.001	<0.003	45.8	907	246	2519	0.0804	941	2931	1971	483	0.2048	0.0004	20.9
13	Bamble - 13	2.85	390000	0.0101	0.0041	47.4	974	250	2425	0.1277	936	2914	1964	478	0.1913	0.0002	20.2
14	Bamble - 14	0.3296	390000	<0.001	<0.003	47.5	946	245	2513	0.0853	941	2931	1952	483	0.2019	0.0003	20.9
15	Bamble - 15	0.1651	390000	<0.002	<0.003	45.2	896	247	2504	0.1189	951	2922	1976	492	0.1965	0.0003	21.0
16	Bamble - 16	0.9161	390000	0.0101	<0.003	46.4	923	250	2513	0.0926	948	2934	1982	491	0.2026	0.0004	20.9
17	Bamble - 17	0.6059	390000	0.0222	<0.003	46.5	951	247	2489	0.1107	939	2898	1972	487	0.2078	0.0016	21.1
18	Bamble - 18	0.0477	390000	<0.002	0.0043	45.9	929	246	2487	0.1013	943	2919	1998	487	0.2036	0.0003	20.9
19	Bamble - 19	1.72	390000	<0.002	<0.003	45.2	934	258	2512	0.1272	935	2931	1980	493	0.2061	0.0005	21.0
20	Bamble - 20	0.0857	390000	<0.002	<0.003	46.0	955	249	2522	0.1209	946	2957	1989	489	0.1997	0.0004	21.1

HR

1	HR - 01	0.0172	390000	<0.001	<0.002	3238	607	142	2784	0.0483	69.1	220	221	173	0.0799	0.0004	26.1
2	HR - 02	<0.011	390000	<0.001	<0.002	3235	621	142	2788	0.0525	68.5	220	221	172	0.0775	0.0004	26.1
3	HR - 03	<0.010	390000	<0.001	<0.002	3194	613	142	2807	0.0503	69.4	223	226	176	0.0797	0.0002	26.6
4	HR - 04	0.0088	390000	<0.001	<0.002	3201	606	143	2813	0.0461	69.8	225	226	175	0.0803	0.0003	26.6
5	HR - 05	0.0083	390000	<0.001	0.0036	3209	616	146	2868	0.0476	70.9	229	235	182	0.0833	0.0005	27.4
6	HR - 06	<0.008	390000	0.0192	<0.002	3191	616	145	2866	0.0441	71.0	228	235	181	0.0840	0.0003	27.3
7	HR - 07	0.0101	390000	<0.001	0.0069	3170	615	145	2808	0.0527	70.0	228	231	178	0.0829	0.0006	27.0
8	HR - 08	<0.007	390000	<0.001	<0.003	3180	609	145	2852	0.0634	71.2	229	234	180	0.0823	0.0005	27.3
9	HR - 09	<0.007	390000	<0.001	<0.003	3166	600	143	2789	0.0497	69.4	224	229	178	0.0802	0.0004	26.6
10	HR - 10	<0.007	390000	<0.001	<0.003	3138	606	143	2807	0.0512	69.5	225	230	178	0.0815	0.0005	26.7
11	HR - 11	0.0238	390000	<0.001	0.0039	3153	608	143	2841	0.0706	69.9	226	230	177	0.0803	0.0003	26.9
12	HR - 12	<0.007	390000	0.0098	<0.003	3177	606	144	2824	0.0580	70.2	228	230	174	0.0780	0.0005	26.6
13	HR - 13	<0.007	390000	<0.001	<0.003	3150	598	142	2806	0.0457	70.2	226	228	174	0.0786	0.0002	26.5
14	HR - 14	0.0141	390000	<0.001	<0.003	3167	606	143	2777	0.0607	69.7	227	226	173	0.0783	0.0004	26.0
15	HR - 15	0.0589	390000	<0.002	<0.003	3122	524	143	2647	0.0691	67.8	217	225	171	0.0757	0.0027	24.5
16	HR - 16	<0.006	390000	<0.002	<0.003	3159	598	143	2865	0.0501	70.9	226	231	177	0.0814	0.0003	26.8
17	HR - 17	0.0075	390000	<0.002	<0.003	3137	601	143	2838	0.0696	69.9	224	232	176	0.0831	0.0003	26.9
18	HR - 18	<0.007	390000	0.0101	<0.003	3147	608	144	2854	0.0492	71.1	227	232	174	0.0820	0.0003	26.9
19	HR - 19	<0.007	390000	0.0347	<0.003	3165	624	144	2849	0.0483	70.9	228	232	175	0.0806	0.0002	26.9
20	HR - 20	<0.010	390000	<0.002	<0.004	3136	628	144	2830	0.0580	70.7	229	230	174	0.0788	0.0003	26.6

#	Sample	Al	Ca	Ti	Cr	Mn	Fe	Sr	Y	Zr	La	Ce	Nd	Sm	^{176}Hf	^{178}Hf	Lu
1	Wallaroo - 01	85.2	390000	0.0344	<0.006	198	433	116	1199	0.0121	84.5	216	156	65.8	0.1150	0.0004	8.41
2	Wallaroo - 02	2.21	390000	<0.001	<0.005	202	219	116	1257	0.0093	77.2	205	153	64.8	0.1204	0.0005	8.81
3	Wallaroo - 03	0.6931	390000	0.0237	<0.005	176	166	108	1118	0.3163	69.1	187	145	62.2	0.1429	0.0361	7.70
4	Wallaroo - 04	0.0666	390000	0.0779	<0.006	200	186	114	1243	0.0276	75.7	205	155	65.5	0.1244	0.0014	8.59
5	Wallaroo - 05	1.59	390000	0.0982	0.0159	207	395	113	1338	0.9284	83.2	222	165	70.2	0.2156	0.0887	9.41
6	Wallaroo - 06	<0.026	390000	<0.001	<0.004	208	198	115	1262	0.0053	78.6	208	153	64.6	0.1225	0.0002	8.73
7	Wallaroo - 07	<0.032	390000	<0.001	0.0078	206	193	114	1246	0.0278	76.7	203	149	63.5	0.1164	0.0003	8.67
8	Wallaroo - 08	0.4741	390000	<0.001	<0.005	203	199	114	1182	0.2256	72.5	193	139	59.0	0.1397	0.0261	8.13
9	Wallaroo - 09	<0.030	390000	<0.001	0.0077	242	226	123	1221	0.0042	75.6	201	145	61.2	0.1181	0.0003	8.39
10	Wallaroo - 10	2.63	390000	0.0473	<0.004	195	193	112	1136	0.4850	70.1	187	140	59.8	0.1560	0.0486	7.72
	NIST610																
1	NIST610 - 01	10421	81476	472	410	439	457	512	460	438	437	452	421	440	410	409	449
2	NIST610 - 02	10249	81476	458	412	437	450	509	461	443	440	452	422	447	418	416	455
3	NIST610 - 03	10277	81476	462	408	442	462	521	457	443	441	454	431	450	423	423	459
4	NIST610 - 04	10201	81476	466	409	440	461	511	459	440	437	450	426	449	423	422	458
5	NIST610 - 05	10313	81476	460	412	444	450	515	465	449	442	452	433	455	430	429	464
6	NIST610 - 06	10358	81476	428	407	446	456	519	465	455	442	455	437	461	433	432	466
7	NIST610 - 07	10253	81476	435	402	438	454	511	462	437	436	451	426	454	428	429	463
8	NIST610 - 08	10448	81476	463	404	450	477	523	470	458	446	459	438	464	437	439	474
9	NIST610 - 09	10289	81476	461	404	447	452	520	462	452	440	450	435	458	433	434	466
10	NIST610 - 10	10408	81476	451	412	447	461	518	468	465	443	459	443	465	438	439	473
11	NIST610 - 11	10271	81476	460	404	446	460	515	455	442	438	450	420	448	423	420	458
12	NIST610 - 12	10326	81476	449	408	447	465	515	458	459	442	456	430	458	429	427	465
13	NIST610 - 13	10363	81476	441	410	449	459	515	463	450	441	454	428	451	425	422	461
14	NIST610 - 14	10391	81476	455	415	446	435	515	465	448	439	452	431	455	427	423	462
15	NIST610 - 15	10246	81476	438	408	441	470	511	459	443	439	455	428	452	426	425	463
16	NIST610 - 16	10285	81476	442	403	442	450	515	464	448	441	451	430	454	426	424	460
17	NIST610 - 17	10398	81476	448	399	446	469	522	463	445	443	457	436	456	429	430	464
18	NIST610 - 18	10213	81476	450	411	441	470	510	459	449	437	449	427	450	423	425	459
19	NIST610 - 19	10290	81476	443	414	441	454	513	464	440	440	451	425	451	424	424	460
20	NIST610 - 20	10369	81476	447	408	445	454	520	463	447	440	455	430	455	428	428	463
21	NIST610 - 21	10170	81476	449	400	442	447	512	452	439	433	445	422	442	419	420	454
22	NIST610 - 22	10519	81476	455	415	457	463	526	470	459	448	461	446	465	434	436	469
23	NIST610 - 23	10351	81476	455	406	443	456	508	461	454	437	454	427	456	425	423	460
24	NIST610 - 24	10335	81476	456	410	446	452	516	462	449	443	452	428	450	427	427	463
25	NIST610 - 25	10257	81476	438	407	440	466	513	466	445	436	449	429	454	426	423	460
26	NIST610 - 26	10280	81476	455	406	446	462	512	459	454	444	457	427	452	426	425	463
27	NIST610 - 27	10334	81476	444	413	444	436	520	460	448	438	453	432	451	425	425	459
28	NIST610 - 28	10338	81476	476	405	447	480	521	463	453	442	453	432	455	427	429	464
29	NIST610 - 29	10434	81476	479	409	444	459	518	468	448	446	456	436	456	430	431	466
30	NIST610 - 30	10210	81476	421	406	436	455	510	457	442	434	450	423	450	422	421	457

SUPPLEMENTARY MATERIAL E

FOR CHAPTER 6 – MAGNETITE AND REE-RICH CALCIC AMPHIBOLE PROVIDE EVIDENCE FOR A SKARN-IOCG SYSTEM AT ONÇA-ROSA, JAGUAR OREFIELD, CARAJÁS MINERAL PROVINCE, BRAZIL

APPENDIX A: ANALYTICAL METHODS AND ADDITIONAL FIGURES

APPENDIX B: ADDITIONAL TABLES, EPMA AND LA-ICP-MS RESULTS

APPENDIX A FOR CHAPTER 6

Supplemental Materials – Analytical Methods

The Bruker Tornado desktop scanner used to construct scanning X-ray fluorescence maps is equipped with a rhodium target X-ray tube operating at 50 kV and 500 nA without filters and XFlash silicon drift X-ray detector. Maps were produced using a 25-40 µm raster with a dwell of 10-20 ms per pixel. Maps are represented as un-quantified background-corrected peak height data for Kα peaks for each element.

Microbeam scanning X-ray fluorescence maps were obtained using a Bruker Tornado desktop scanner (National Institute of Criminalistics, Brasilia, Brazil). Quantitative analysis of amphiboles was undertaken using a JEOL JXA-8230 SuperProbe electron probe microanalyzer (EPMA) equipped with 5-spectrometer crystals LDE1, LDE2, ATP, PET/L-H and LIF-L/H crystals and located in the Crti Laboratory, Federal University of Goiás, Brazil. The wavelength dispersive (WDS) analyses were performed at an accelerating voltage of 15 kV, sample current of 20nA, and electron beam of 2-5 µm in diameter. The counting time was variable from 20 to 60 seconds per element. Both synthetic and natural mineral standards patterns of oxides and silicates were used for the analyses retaining the same standards and procedures throughout the analytical work. Raw X-ray intensities for all elements were corrected using standard ZAF techniques with the JEOL software. Data reduction was performed using 'Probe for EPMA' (e.g. Donovan *et al.* 2016).

Trace element LA-ICP-MS spot analysis of magnetite was conducted using a RESOlution-SE 193 nm Excimer laser coupled to an Agilent 8900x quadrupole ICP-MS (Agilent Technologies Australia. Australia Scientific Technologies). Analyses comprised background measurement of 30s followed by acquisition of signal during ablation (60-70s). Laser spot diameter varied between 43 and 51 µm, depending on grain size, and operated at a pulse repetition rate of 5 Hz and fluence of 3.5J/cm2. Fifty isotopes were measured either as spot or mapping: ^{24}Mg, ^{27}Al, ^{29}Si, ^{31}P, ^{34}S, ^{39}K, ^{43}Ca, ^{45}Sc, ^{49}Ti, ^{51}V, ^{53}Cr, ^{55}Mn, ^{57}Fe, ^{59}Co, ^{60}Ni, ^{65}Cu, ^{66}Zn, ^{69}Ga, ^{75}As, ^{88}Sr, ^{89}Y, ^{90}Zr, ^{93}Nb, ^{95}Mo, ^{118}Sn, ^{121}Sb, ^{137}Ba, ^{139}La, ^{140}Ce, ^{146}Nd, ^{147}Sm, ^{153}Eu, ^{157}Gd, ^{159}Tb, ^{163}Dy, ^{165}Ho, ^{166}Er, ^{166}Er, ^{169}Tm, ^{172}Yb, ^{175}Lu, ^{178}Hf, ^{181}Ta, ^{182}W, ^{206}Pb, ^{207}Pb, ^{208}Pb, ^{209}Bi, ^{232}Th, ^{238}U. The external reference materials NIST-612 and GSD were analyzed before, during, and after magnetite ablation for trace element quantification and instrument drift correction. ^{57}Fe was used as the internal standard element, assuming a stoichiometric composition for magnetite. Evident contributions from inclusions were minimized by avoiding their interference from the integrated

intervals, otherwise such analyses were rejected. Analysis with a consistent presence of inclusions homogeneously distributed includes their contribution in the integrated signal. Reported Pb contents correspond to total Pb concentrations calculated from the individual abundances of ^{206}Pb, ^{207}Pb and ^{208}Pb.

Two S/TEM (<100 nm) foils were prepared from the sections using a FEI-Helios nanoLab Dual Focused Ion Beam and SEM (FIB-SEM) as outlined by Ciobanu *et al.* (2011). Each foil was analyzed with HAADF STEM equipped with a X-FEG Schottky source and Super-X EDS geometry. Imaging and energy-dispersive X-ray spectrometry (EDS)-STEM mapping using an ultra-high resolution, probe-corrected, FEI Titan Themis S/TEM operated at 200 kV. Probe correction delivered sub-Ångstrom spatial resolution and an inner collection angle greater than 50 mrad was used for HAADF imaging with a Fischione detector. The Super-X EDS detector provides geometrically symmetric EDS detection with an effective solid angle of 0.8 sr. Velox software was used for image acquisition, including drift-corrected frame integration package (DCFI), and EDS data acquisition and processing. Various filters were used to eliminate noise (Radial Wiener, High-pass, Average and Gaussian blur). Quantification of the collected EDS spectra was performed using Thermo-Scientific Velox software (v3.10) which utilizes standard Cliff-Lorimer quantification and included absorption correction optimized for both the Super-X detector geometry and also the effect of sample holder shadowing for the double-tilt Super-X holder used. Quantification was performed using the Brown-Powell empirical ionization cross-section model and uncertainty values reported incorporate an estimated 20% error in the k-factors.

References

Ciobanu, C.L., Cook, N.J., Utsunomiya, S., Pring, A., and Green, L. (2011) Focused ion beam–transmission electron microscopy applications in ore mineralogy: Bridging micro- and nanoscale observations. Ore Geology Reviews 42, 6–31. https://doi.org/10.1016/j.oregeorev.2011.06.012

Donovan, J.J., Singer, J.W., and Armstrong, J.T. (2016) A new EPMA method for fast trace element analysis in simple matrices. American Mineralogist 101, 1839-1853. DOI: https://doi.org/10.2138/am-2016-5628

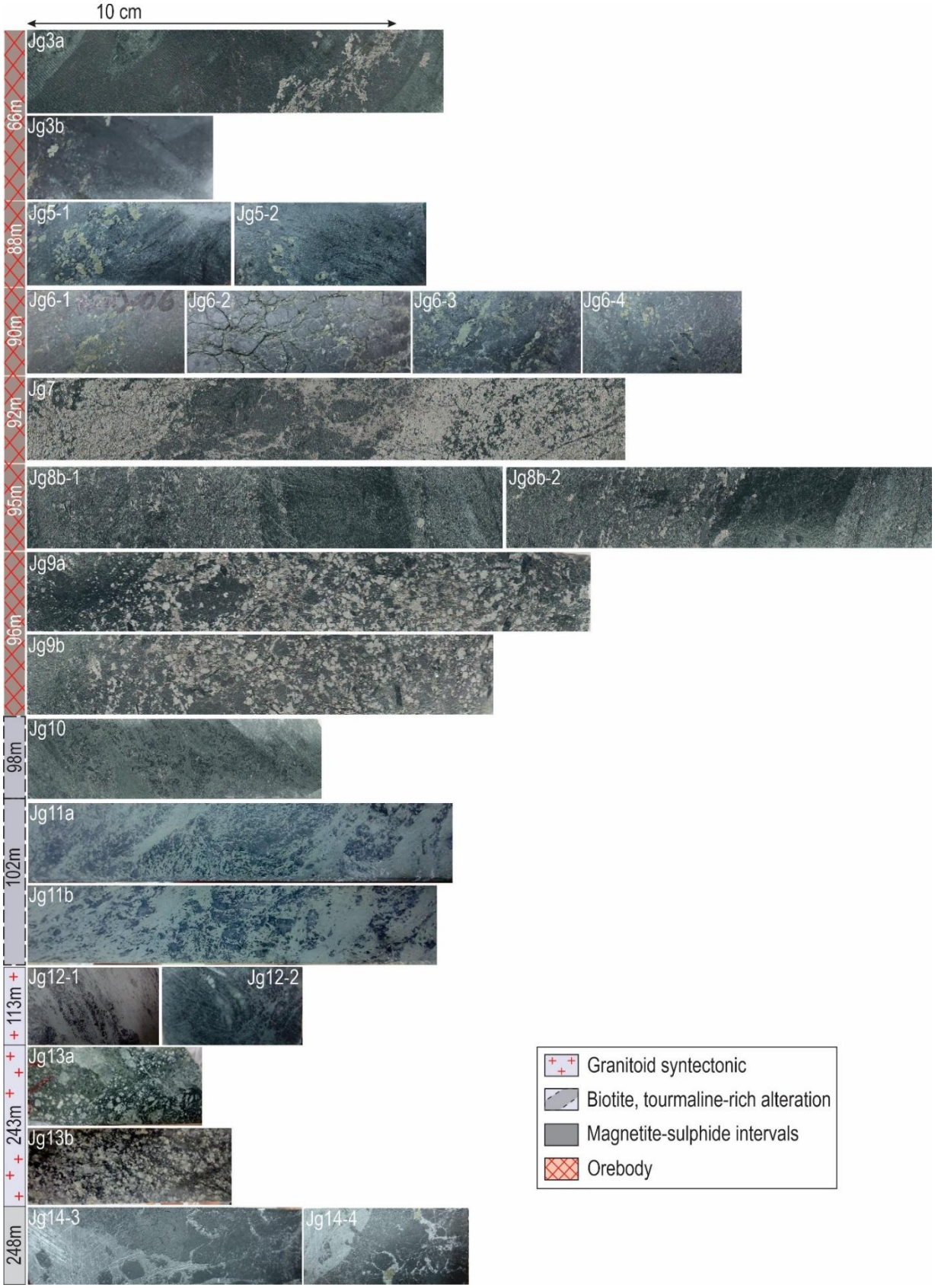

SD Figure 1. Photographs of the drill-cores (from the drillhole DH00127) showing the fabrics of the country rocks and the orebody.

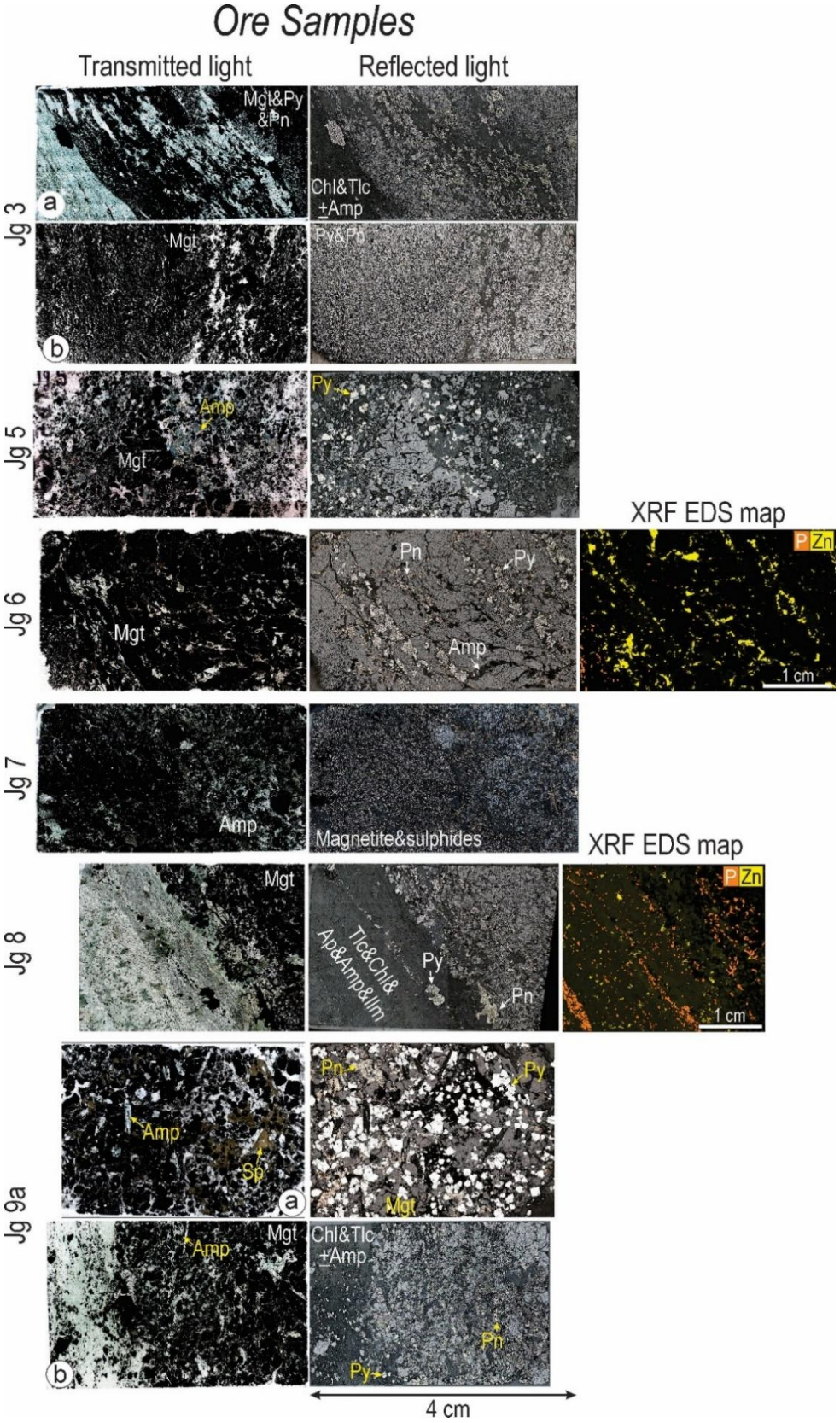

SD Figure 2. Optical and reflected light scans of thin sections across the orebody interval from the drillhole (DH00127), showing petrographic aspects of magnetite, sulfides and gangue minerals. Note the different distribution of apatite (P) in the XRF maps. Details of the mineralogy are shown in Figure 2. Amp–amphibole; Ap–apatite; Chl–chlorite; Ilm–ilmenite; Mgt–magnetite; Pn–pentlandite; Py–pyrite; Sp–sphalerite; Tlc–talc.

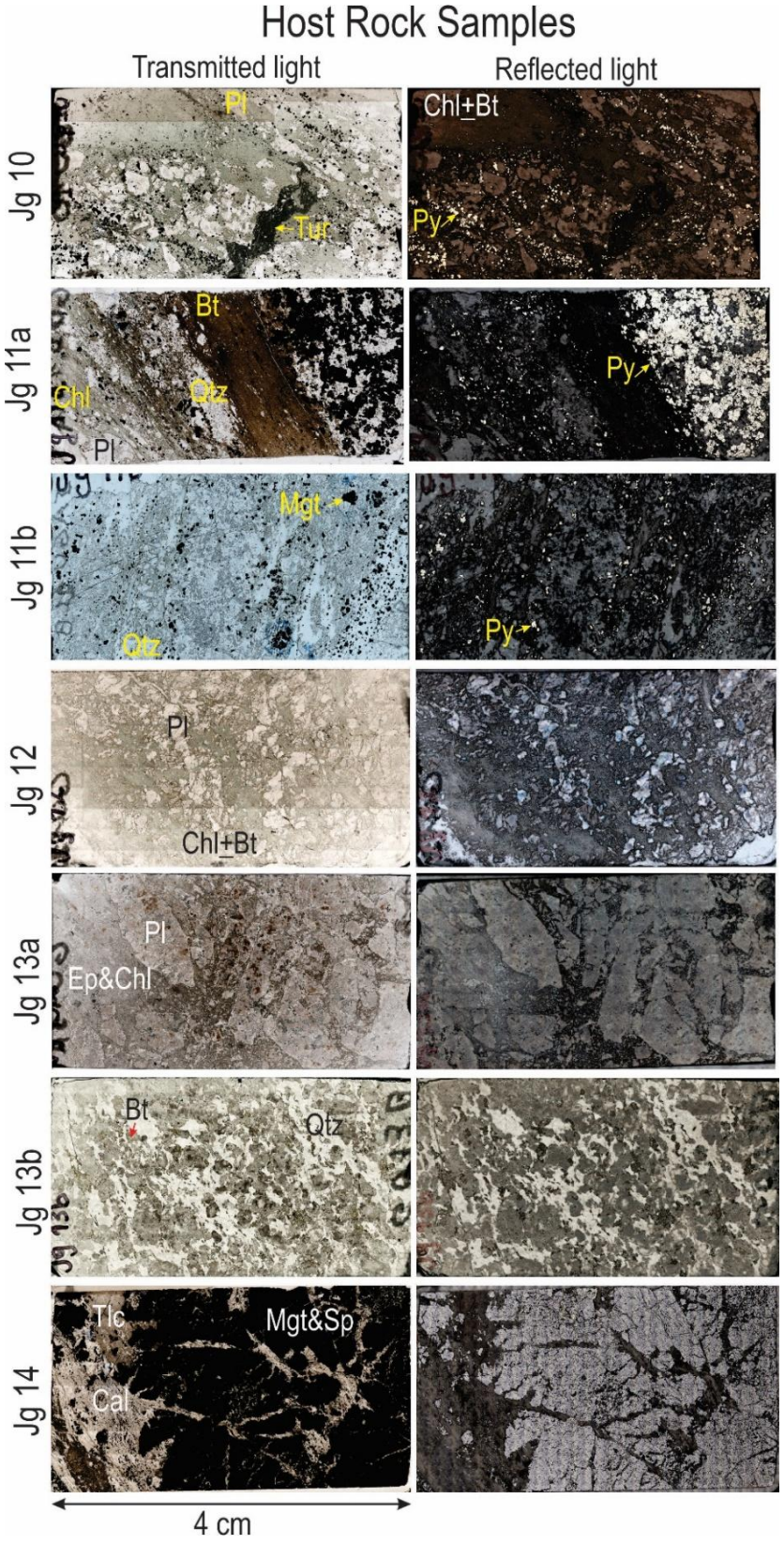

SD Figure 3. Optical and reflected light scans of thin sections from the drillhole (DH00127), showing petrographic aspects of country rocks. Note the biotite band in sample Jg11a and the magnetite +sulphide interval in sample Jg14. Details of the mineralogy are shown in Figure 2. Bt–biotite; Cal–calcite; Chl–chlorite; Ep–epidote; Mgt–magnetite; Pl–plagiocalse; Py–pyrite; Qtz–quartz; Sp–sphalerite; Tur–tourmaline.

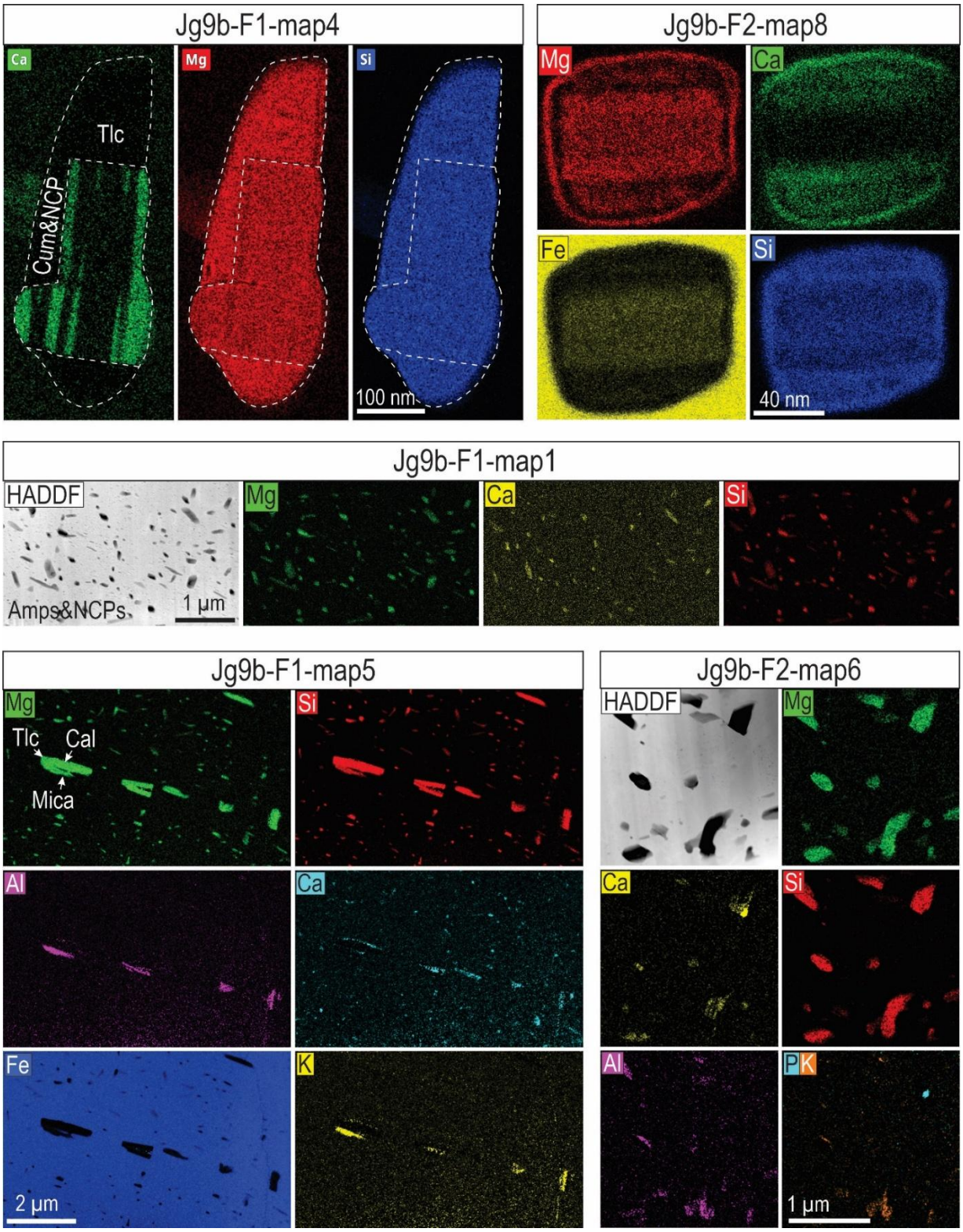

SD Figure 4. EDS STEM maps illustrating compositional variation, intergrowths, and zonation patterns among amphibole and NCP; biotite, chlorite and calcite, as labelled. See main text for further explanations, Jg9b-F1-map4 and Jg9b-F1-map4 are shown in Figure 8; whereas Jg9b-F1-map5 is shown in Figure 11. Amp–amphibole; Bt–biotite; Cal–calcite; Cum–cummingtonite; Ms–musovite; NCP–non-classical pyriboles; Tlc–talc.

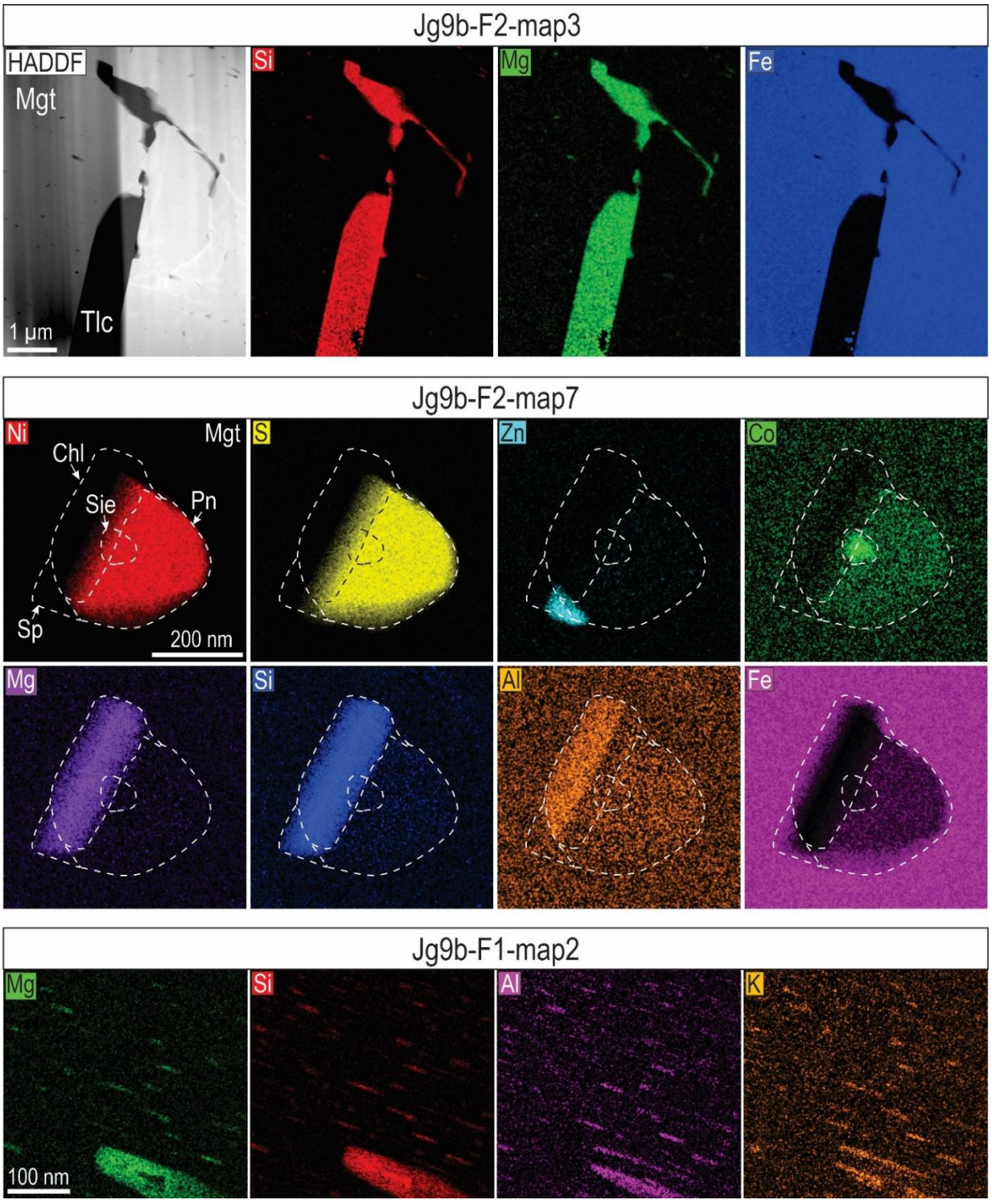

SD Figure 5. EDS STEM maps illustrating compositional variation, intergrowths, and zonation patterns among talc, sulfides and Mg-bearing nanoinclusions, as labelled. See main text for further explanations. Jg9b-F2-map7 and Jg9b-F1-map2 are shown in Figure 8. Chl–chlorite; Mgt–magnetite; Pn–pentlandite; Sie–siegenite; Sp–sphalerite; Tlc–talc.

APPENDIX B FOR CHAPTER 6

SD Table 1a. Compositions of amphiboles from EPMA and STEM EDS maps data.

SD Table 1b. LA-ICP-MS trace element data for magnetite.

SD Table 1c. LA-ICP-MS trace element data for amphibole and apatite.

SD Table 1d. LA-ICP-MS data for magnetite, amphibole and apatite used for box-and-whisker plots.

SD Table 1e. LA-ICP-MS data selected for REE plots.

SD Table 1a. Compositions of amphiboles from EPMA and STEM EDS maps data as labelled

Method	EPMA																			**Foil**	F1-Map4	F2-Map8
																				Method	STEM EDS	
No.	1	2	3	4	5	6	7	8	9	10	11	12	13	14	15	16	17	18	19	**No.**	20	21
Sample	**Jg3a**		**Jg3b**				**Jg5**				**Jg6**	**Jg7**			**Jg8**				**Jg9a**	**Sample**	**Jg9b**	
(Wt%)	Mg-hornblende		Act	Magnesiohornblende									Act	Magnesiohornblende			Actinolite			**(Wt%)**	Cummingtonite	
SiO_2	53.34	51.00	54.23	52.23	51.38	50.09	52.79	50.95	50.86	51.08	53.67	52.89	55.48	50.45	49.64	51.18	57.15	54.62	55.11	SiO_2	58.6	55.2
TiO_2	0.11	0.07	0.04	0.02	0.21	0.27	0.21	0.24	0.21	0.19	0.03	0.07	0.07	0.24	0.17	0.24	0.01	0.09	0.03	TiO_2	0.000	0.000
Al_2O_3	4.27	5.89	3.65	5.30	6.13	7.36	4.73	6.55	5.72	5.98	3.82	4.29	2.43	6.80	6.43	6.54	1.17	2.92	2.69	Al_2O_3	0.816	0.835
FeO	10.13	10.83	9.57	10.80	11.33	12.26	10.99	12.15	11.35	11.40	10.23	11.16	7.91	13.81	11.86	11.47	7.04	9.80	7.82	FeO	16.0	19.6
MnO	0.14	0.10	0.11	0.10	0.13	0.13	0.14	0.12	0.15	0.11	0.09	0.13	0.06	0.12	0.11	0.11	0.11	0.13	0.13	MnO	0.493	0.683
MgO	18.08	16.61	18.36	17.24	16.55	15.72	17.04	15.98	16.52	16.55	17.96	17.24	20.23	15.09	16.62	16.72	20.85	18.08	19.71	MgO	22.2	20.3
CaO	12.63	12.17	12.63	12.54	12.26	12.01	12.60	12.24	12.32	12.39	12.63	12.42	13.36	11.11	11.27	12.70	13.20	12.86	12.88	CaO	1.93	3.37
Na_2O	0.71	0.97	0.60	0.87	0.99	1.13	0.82	1.04	0.95	0.96	0.69	0.74	0.44	1.56	1.12	1.14	0.21	0.45	0.50	Na_2O	-	-
K_2O	0.06	0.08	0.03	0.07	0.07	0.08	0.05	0.08	0.09	0.07	0.06	0.09	0.06	0.13	0.15	0.10	0.02	0.06	0.04	K_2O	-	-
F	0.23	0.24	0.22	0.14	0.24	0.09	0.19	0.23	0.13	0.30	0.11	0.08	0.21	0.23	0.16	0.25	0.39	0.27	0.33	F	-	-
Cl	0.02	0.03	0.01	0.02	0.02	0.04	0.02	0.03	0.04	0.02	0.02	0.08	0.02	0.04	0.03	0.04	0.01	0.07	0.00	Cl	-	-
NiO	0.27	0.09	0.21	0.24	0.16	0.08	0.16	0.18	0.21	0.33	0.23	0.17	0.18	0.10	0.08	0.23	0.18	0.32	0.13	NiO	-	-
ZnO	0.17	0.18	0.18	0.17	0.15	0.15	0.16	0.17	0.12	0.19	0.22	0.13	0.07	0.15	0.16	0.18	0.13	0.10	0.12	ZnO	-	-
Total	100	98	100	100	100	99	100	100	99	100	100	99	101	100	98	101	100	100	99	Total	100.0	100.0
Recalculated Wt%																				**Wt%**		
SiO_2	52.10	50.79	53.13	51.19	50.48	49.25	51.70	49.88	50.40	50.24	52.57	51.94	53.96	49.46	49.63	49.65	55.72	53.61	54.24	SiO_2	57.8	54.5
TiO_2	0.11	0.07	0.04	0.02	0.21	0.27	0.20	0.24	0.20	0.19	0.03	0.07	0.07	0.24	0.17	0.23	0.01	0.09	0.03	TiO_2	0.000	0.000
Al_2O_3	4.17	5.87	3.58	5.19	6.02	7.24	4.63	6.42	5.67	5.88	3.74	4.21	2.36	6.67	6.43	6.34	1.14	2.87	2.65	Al_2O_3	0.816	0.835
Fe_2O_3	3.13	3.56	3.09	3.35	3.14	3.21	3.22	3.21	3.37	3.11	3.27	3.66	1.84	3.64	3.49	3.46	0.58	3.32	2.96	Fe_2O_3	2.76	4.56
FeO	7.08	7.59	6.60	7.56	8.31	9.17	7.87	9.01	8.21	8.42	7.07	7.67	6.04	10.26	8.71	8.02	6.34	6.63	5.03	FeO	13.5	15.5
MnO	0.14	0.10	0.10	0.10	0.13	0.13	0.13	0.12	0.15	0.11	0.09	0.13	0.06	0.11	0.11	0.11	0.11	0.13	0.13	MnO	0.493	0.673
MgO	17.66	16.54	17.99	16.89	16.26	15.46	16.69	15.65	16.37	16.27	17.59	16.94	19.68	14.79	16.61	16.22	20.33	17.75	19.40	MgO	22.2	20.3
CaO	12.34	12.11	12.38	12.29	12.04	11.81	12.34	11.98	12.21	12.19	12.38	12.20	13.00	10.89	11.27	12.32	12.87	12.62	12.68	CaO	1.93	3.37
Na_2O	0.69	0.97	0.59	0.85	0.97	1.11	0.80	1.02	0.94	0.94	0.67	0.73	0.42	1.53	1.12	1.10	0.21	0.44	0.49	Na_2O		
K_2O	0.06	0.08	0.03	0.07	0.07	0.08	0.04	0.08	0.08	0.07	0.06	0.09	0.06	0.13	0.15	0.10	0.02	0.06	0.04	K_2O		
Ni	0.27	0.09	0.21	0.24	0.16	0.08	0.16	0.18	0.21	0.33	0.23	0.17	0.18	0.10	0.08	0.23	0.18	0.32	0.13	NiO		
ZnO	0.17	0.18	0.18	0.17	0.15	0.15	0.16	0.17	0.12	0.19	0.22	0.13	0.07	0.15	0.16	0.18	0.13	0.10	0.12	ZnO		
Fl	0.22	0.24	0.22	0.14	0.24	0.08	0.19	0.23	0.13	0.30	0.10	0.08	0.20	0.23	0.16	0.25	0.38	0.26	0.32	Fl		
Cl	0.02	0.03	0.01	0.02	0.02	0.04	0.02	0.03	0.04	0.02	0.02	0.08	0.02	0.04	0.03	0.04	0.01	0.07	0.00	Cl		
H_2O	2.00	1.98	2.02	2.03	1.98	2.04	2.01	1.97	2.02	1.95	2.06	2.05	2.03	1.96	2.01	1.96	1.96	1.98	1.98	H_2O		
O=F,Cl	-0.10	-0.11	-0.09	-0.06	-0.11	-0.04	-0.09	-0.10	-0.06	-0.13	-0.05	-0.05	-0.09	-0.11	-0.07	-0.11	-0.16	-0.13	-0.14	O=F,Cl		
Total	98.2	98.2	98.1	98.1	98.2	98.1	98.1	98.2	98.1	98.3	98.0	98.1	98.0	98.2	98.1	98.2	98.0	98.2	98.2	Total	99.5	99.8
Total-O	100	100	100	100	100	100	100	100	100	100	100	100	100	100	100	100	100	100	100	TotH		

Method										EPMA										**Foil**	F1-Map4	F2-Map8
No.	1	2	3	4	5	6	7	8	9	10	11	12	13	14	15	16	17	18	19	**Method**	STEM EDS	
Sample	**Jg3a**		**Jg3b**				**Jg5**				**Jg6**	**Jg7**			**Jg8**				**Jg9a**	**No.**	20	21
(Wt%)	Mg-hornblende		Act	Magnesiohornblende									Act	Magnesiohornblende			Actinolite			**Sample**	**Jg9b**	
Formula calculation (apfu 15-cation basis)																				**(Wt%)**	Cummingtonite	
Si	7.40	7.24	7.51	7.30	7.22	7.08	7.37	7.16	7.22	7.20	7.46	7.40	7.60	7.14	7.12	7.12	7.81	7.58	7.60	Si	7.96	7.69
Al	0.599	0.760	0.490	0.702	0.784	0.925	0.631	0.839	0.784	0.800	0.537	0.599	0.392	0.860	0.885	0.880	0.189	0.416	0.396	Al	0.040	0.310
Tot. T	**8.00**	**8.00**	**8.00**	**8.00**	**8.00**	**8.00**	**8.00**	**8.00**	**8.00**	**8.00**	**8.00**	**8.00**	**8.00**	**8.00**	**8.00**	**8.00**	**8.00**	**8.00**	**8.00**	**T**	**8.00**	**8.00**
Al	0.100	0.226	0.106	0.170	0.230	0.300	0.146	0.247	0.172	0.193	0.088	0.109	0.000	0.274	0.202	0.192	0.000	0.062	0.042	Al	0.000	0.000
Ti	0.012	0.007	0.004	0.002	0.022	0.029	0.022	0.026	0.022	0.020	0.003	0.008	0.000	0.026	0.019	0.025	0.000	0.009	0.003	Ti	0.000	0.000
Ni	0.031	0.019	0.027	0.029	0.023	0.017	0.023	0.025	0.024	0.037	0.032	0.021	0.018	0.018	0.017	0.029	0.022	0.030	0.018	Ni	0.000	0.000
Zn	0.018	0.011	0.016	0.016	0.013	0.010	0.013	0.014	0.014	0.021	0.019	0.012	0.010	0.010	0.010	0.017	0.013	0.017	0.010	Zn	0.000	0.000
Fe^{3+}	0.335	0.382	0.329	0.360	0.338	0.347	0.345	0.346	0.363	0.335	0.350	0.393	0.195	0.396	0.377	0.373	0.061	0.353	0.312	Fe^{3+}	0.286	0.483
Fe^{2+}	0.841	0.904	0.780	0.902	0.994	1.10	0.938	1.08	0.983	1.01	0.840	0.913	0.712	1.24	1.04	0.962	0.743	0.784	0.590	Fe^{2+}	1.56	1.83
Mn	0.017	0.012	0.012	0.012	0.016	0.016	0.016	0.015	0.018	0.013	0.011	0.015	0.007	0.014	0.014	0.013	0.013	0.015	0.015	Mn	0.058	0.080
Mg	3.65	3.44	3.73	3.51	3.36	3.18	3.50	3.24	3.40	3.37	3.66	3.53	4.06	3.02	3.32	3.39	4.15	3.73	4.01	Mg	3.10	2.61
Tot. C	**5.00**	**5.00**	**5.00**	**5.00**	**5.00**	**5.00**	**5.00**	**5.00**	**5.00**	**5.00**	**5.00**	**5.00**	**5.00**	**5.00**	**5.00**	**5.00**	**5.00**	**5.00**	**5.00**	**C**	**5.00**	**5.00**
Mg	0.092	0.077	0.065	0.082	0.100	0.131	0.049	0.104	0.092	0.106	0.066	0.070	0.073	0.158	0.234	0.077	0.101	0.013	0.044	Mg	1.454	1.663
Ca	1.88	1.85	1.87	1.88	1.84	1.82	1.88	1.84	1.87	1.87	1.88	1.86	1.93	1.69	1.73	1.89	1.90	1.91	1.90	Ca	0.546	0.337
Na	0.031	0.072	0.060	0.040	0.055	0.052	0.067	0.052	0.035	0.022	0.052	0.068	0.000	0.157	0.035	0.030	0.000	0.074	0.052	Na	0.000	0.000
Tot. B	**2.00**	**2.00**	**2.00**	**2.00**	**2.00**	**2.00**	**2.00**	**2.00**	**2.00**	**2.00**	**2.00**	**2.00**	**2.00**	**2.00**	**2.00**	**2.00**	**2.00**	**2.00**	**2.00**	**B**	**2.00**	**2.00**
Ca	0.000	0.000	0.000	0.000	0.000	0.000	0.000	0.000	0.000	0.000	0.000	0.000	0.035	0.000	0.000	0.000	0.034	0.000	0.000	Ca	0.285	0.509
Na	0.160	0.195	0.102	0.195	0.214	0.257	0.155	0.231	0.225	0.239	0.133	0.133	0.116	0.272	0.276	0.277	0.057	0.046	0.081	Na	0.000	0.000
K	0.011	0.014	0.005	0.013	0.013	0.014	0.008	0.014	0.015	0.013	0.010	0.016	0.011	0.024	0.028	0.018	0.003	0.011	0.008	K	0.000	0.000
Tot. A	**0.172**	**0.210**	**0.107**	**0.208**	**0.227**	**0.271**	**0.163**	**0.246**	**0.240**	**0.253**	**0.143**	**0.149**	**0.162**	**0.296**	**0.304**	**0.296**	**0.094**	**0.056**	**0.089**	**A**	**0.29**	**0.51**
F	0.099	0.109	0.096	0.062	0.107	0.038	0.086	0.103	0.060	0.134	0.046	0.034	0.089	0.105	0.074	0.111	0.167	0.118	0.144	F		
Cl	0.006	0.008	0.003	0.005	0.006	0.009	0.005	0.006	0.009	0.005	0.004	0.019	0.004	0.010	0.007	0.009	0.002	0.016	0.001	Cl		
OH	1.90	1.88	1.90	1.93	1.89	1.95	1.91	1.89	1.93	1.86	1.95	1.95	1.91	1.88	1.92	1.88	1.83	1.87	1.85	OH		
W	**2.00**	**2.00**	**2.00**	**2.00**	**2.00**	**2.00**	**2.00**	**2.00**	**2.00**	**2.00**	**2.00**	**2.00**	**2.00**	**2.00**	**2.00**	**2.00**	**2.00**	**2.00**	**2.00**	**W**		

SD Table 1b. LA-ICP-MS trace element data for magnetite (complete dataset, element concentrations in ppm, calculated from measurement of given isotope, except for the 4 Pb isotopes)

**Note* : data reported here are raw data; in red analyses shown in ESM Fig 4.

#	Sample	Mg	Al	Si	P	Ca	Sc	Ti	V	Cr	Mn	Co	Ni	Cu	Zn	Ga	As	Sr	Zr	Nb	Mo	Sn	Sb	Ba
1	Jg3aMt4 04	1406	448	3050	5.3	191	0.054	237	304	131	109	6.6	1648	0.042	27	20	0.755	0.444	0.051	0.625	0.011	0.294	0.004	3.5
2	Jg3aMt4 05	1716	945	3248	23	58	0.027	200	313	168	70	4.2	2245	2.4	14	20	0.348	0.180	0.070	0.212	0.009	0.233	0.114	1.4
3	Jg3aMt4 06	1476	917	3773	2.4	20	0.182	220	314	156	69	3.1	1891	228	9.2	20	0.700	0.165	0.040	0.151	0.002	0.156	0.019	3.2
4	Jg3aMt4 07	2705	832	7911	7.3	1076	0.231	188	284	146	91	4.2	1709	14	36	16	0.504	0.190	0.046	0.004	0.002	0.595	0.085	0.132
5	Jg3aMt11 14	2447	1030	4252	1167	3368	0.179	226	315	141	107	5.8	1730	10	41	20	0.512	6.1	0.102	0.180	0.012	0.263	0.022	3.6
6	Jg3aMt12rim 02	2038	1305	3045	1.8	141	0.007	259	324	0.652	121	14	1869	0.133	76	27	0.409	0.368	0.015	0.589	0.001	0.358	0.081	3.8
7	Jg3aMt12rim 03	2490	1519	4880	10	174	0.138	354	338	1.3	101	8.9	1886	0.533	111	27	0.277	1.1	0.067	1.3	0.007	0.765	0.123	16
8	Jg3aMt12rim 04	5417	3183	8705	3.0	89	0.122	327	335	1.8	90	6.4	1988	0.258	231	29	1.2	0.863	0.038	0.527	0.002	0.403	0.264	10
9	Jg3aMt12rim 05	2162	607	3956	10	445	0.198	269	327	0.257	142	16	1945	0.450	84	27	0.576	0.732	0.041	0.324	0.017	0.351	0.133	3.9
10	Jg3aMt13rim 05	693	690	1983	5.2	88	0.052	276	324	4.6	124	12	1709	0.044	41	26	0.453	0.378	0.075	0.254	0.004	0.370	0.060	7.2
11	Jg3aMt13rim 06	3134	1808	6050	6.8	46	0.010	347	327	0.073	83	10	2048	0.555	758	27	0.438	0.514	14	0.394	0.031	0.385	0.091	19
12	Jg3aMt13rim 07	2095	936	3646	1.4	528	0.095	243	319	2.7	119	8.9	1808	0.272	104	25	0.790	1.6	0.010	0.145	0.020	0.300	0.096	5.9
13	Jg3aMt13rim 08	2438	964	4371	1.5	272	0.018	266	319	4.2	103	9.0	1887	0.429	236	25	0.542	1.4	0.025	0.327	0.009	0.315	0.147	12
14	Jg3aMt13rim 10	3613	2068	6421	4.0	57	0.041	387	331	0.067	87	6.9	2013	0.506	117	25	0.276	0.698	0.018	0.230	0.002	0.257	0.041	15
15	Jg3aMt13core 02	1310	855	2603	8.6	60	0.087	311	339	0.031	111	15	2018	2.1	194	26	0.367	0.857	0.022	0.150	0.009	0.224	0.027	6.9
16	Jg3aMt14core 09	372	343	981	2.8	65	0.088	282	341	0.175	144	23	1917	0.228	66	27	0.216	0.018	0.066	2.3	0.003	0.456	0.054	0.037
17	Jg5Mt2 07	53	257	297	3.8	8.3	0.264	277	544	51	88	23	1501	0.009	42	29	0.067	0.212	0.001	0.038	0.004	0.322	0.002	0.934
18	Jg5Mt2 08	782	487	1572	15	196	0.310	315	543	18	159	27	1577	0.598	277	30	1.6	0.903	0.004	0.158	0.006	0.494	0.099	1.2
19	Jg5Mt4 12	1850	1201	5975	15	9.6	0.255	395	555	21	100	25	1538	0.055	494	32	0.281	0.516	0.013	0.796	0.001	0.688	0.090	9.7
20	Jg5Mt5 14	76	326	141	8.1	15	0.080	285	565	13	109	34	1621	0.310	74	29	0.228	0.026	0.208	0.007	0.001	0.416	0.019	0.095
21	Jg5Mt5 19	123	378	654	10	245	0.056	283	561	25	73	18	1666	0.424	106	29	0.132	0.187	0.047	0.032	0.018	0.474	0.002	2.0
22	Jg5Mt5 20	6042	3264	8708	3.9	133	0.223	266	553	94	96	41	3337	9.5	95	29	0.323	0.738	0.004	1.2	0.001	0.399	0.045	2.4
23	Jg5Mt5 21	81	317	511	1.3	2.6	0.092	269	559	11	113	31	1644	0.196	77	29	0.055	0.828	0.001	0.042	0.012	0.459	0.003	7.0
24	Jg5Mt5 24	398	391	925	6.6	65	0.099	296	570	33	113	30	1682	0.374	49	29	0.217	0.268	0.003	0.169	0.002	0.393	0.044	3.1
25	Jg6Mt 1 01	61	265	193	13	222	0.179	227	416	3.3	137	20	1482	0.256	45	33	0.814	0.003	0.002	0.002	0.050	0.370	0.067	0.004
26	Jg6Mt 1 02	1483	787	3520	15	220	0.291	306	366	12	174	69	2673	6.0	2005	35	0.983	3.3	0.111	0.815	0.037	0.718	0.160	30
27	Jg6Mt 1 03	3107	1101	5873	23	241	0.172	274	375	21	183	41	2117	0.672	212	35	0.644	2.8	0.084	0.808	0.044	0.590	0.190	20
28	Jg6Mt 1 04	7828	1565	16995	23	1673	0.545	385	440	10	214	36	1812	0.873	211	38	2.4	4.0	0.294	3.1	0.031	1.3	0.476	29
29	Jg6Mt 1 05	4605	1655	11089	14	2078	0.506	415	445	12	207	30	1758	0.487	229	40	1.8	6.2	0.257	3.6	0.034	1.4	0.362	36
30	Jg6Mt 1 06	2430	1048	4707	22	350	0.287	279	427	16	127	28	1689	1.6	18840	35	1.9	1.5	0.105	1.3	0.022	0.821	0.148	15
31	Jg6Mt 1 07	881	467	2132	16	423	0.187	228	402	7.6	109	91	2761	92	58	31	0.845	0.787	0.121	0.687	0.048	0.541	0.089	7.3
32	Jg6Mt 1 08	5140	1511	11115	15	1506	0.311	403	410	7.1	198	20	1678	2.0	574	37	1.9	6.3	0.273	2.8	0.033	1.2	0.456	48
33	Jg6Mt 1 09	7662	1545	16096	24	1541	0.378	391	424	2.2	138	17	1933	1.9	191	37	2.1	4.8	0.168	2.9	0.028	1.4	0.330	31
34	Jg6Mt 1 10	128	263	371	13	215	0.148	215	468	3.7	79	12	1531	0.242	54	32	0.485	0.033	0.025	0.048	0.026	0.325	0.066	0.088
35	Jg6Mt 2 01	1868	475	4049	13	221	0.166	264	408	1.7	110	22	2704	2.7	143	34	1.0	0.845	9.3	0.170	0.055	0.552	0.242	5.6
36	Jg6Mt 2 02	3990	1554	9797	24	1774	0.219	479	456	0.376	192	32	1796	1.4	263	39	12	4.0	0.228	2.4	0.018	1.4	0.697	34

#	Sample	Mg	Al	Si	P	Ca	Sc	Ti	V	Cr	Mn	Co	Ni	Cu	Zn	Ga	As	Sr	Zr	Nb	Mo	Sn	Sb	Ba
37	Jg6Mt 2 03	4267	1519	9775	29	404	0.217	481	405	1.3	110	12	1852	1.4	200	36	8.3	2.6	0.133	0.921	0.046	0.814	0.399	31
38	Jg6Mt 2 04	8125	1357	14635	13	843	0.486	406	401	1.2	181	34	2018	0.514	359	37	3.6	3.8	0.113	0.781	0.044	0.814	0.439	24
39	Jg6Mt 2 05	4325	1602	10264	26	1549	0.310	503	412	0.338	172	18	2174	2.2	497	40	5.9	6.8	0.378	1.9	0.050	1.2	0.599	48
40	Jg6Mt 2 06	4286	1449	10155	34	1317	0.204	471	410	0.363	179	26	1945	1.0	345	39	5.0	4.7	0.199	2.3	0.063	1.4	0.419	32
41	Jg6Mt 2 07	4308	1608	10196	25	2008	0.155	540	427	0.317	219	27	1895	1.5	362	40	4.8	5.4	0.161	2.4	0.051	1.5	0.609	41
42	Jg6Mt 2 08	13361	1311	24222	17	452	0.190	408	415	7.5	132	26	2201	2.5	302	38	2.1	3.9	0.173	1.0	0.037	0.830	0.312	28
43	Jg6Mt 2 rim 01	590	356	1830	24	406	0.308	289	412	0.604	110	37	2093	14	136	37	0.949	0.545	0.051	0.414	0.054	0.444	0.132	0.416
44	Jg6Mt 2 rim 02	65	298	205	14	254	0.183	279	380	0.332	117	20	1534	0.515	578	35	0.533	0.117	0.005	0.067	0.030	0.335	0.080	0.415
45	Jg6Mt 2 rim 03	60	278	168	13	245	0.174	274	368	1.1	116	20	1470	0.581	66	34	0.510	0.348	0.015	0.159	0.032	0.402	0.060	0.134
46	Jg6Mt 4 rim 01	55	247	184	13	227	0.157	262	413	5.2	124	21	1433	0.381	41	33	0.583	0.023	0.004	0.097	0.036	0.336	0.064	0.036
47	Jg6Mt 4 rim 02	1473	763	3360	14	407	0.162	359	424	11	153	48	2192	4.0	160	36	0.515	2.1	0.090	0.941	0.049	0.665	0.147	13
48	Jg6Mt 4 rim 03	67	263	194	14	216	0.184	243	425	39	132	21	1467	0.224	46	34	0.468	0.002	0.024	0.109	0.032	0.241	0.055	0.007
49	Jg6Mt 4 rim 04	221	322	703	14	253	0.183	244	441	10	79	21	1507	0.239	42	34	0.479	0.340	0.019	0.222	0.023	0.303	0.069	2.7
50	Jg6Mt 4 01	497	407	1295	15	279	0.173	254	432	10	85	33	2005	1.6	110	35	0.559	0.457	0.142	0.399	0.030	0.532	0.071	1.9
51	Jg6Mt 4 02	4834	1567	9706	15	1236	0.465	461	425	13	340	36	1832	1.1	234	41	0.914	5.0	0.176	1.9	0.025	1.1	0.220	46
52	Jg6Mt 4 03	5902	1644	12328	15	1331	0.400	446	434	11	185	36	1846	6.0	30870	39	1.5	3.5	0.281	2.5	0.021	1.5	0.283	31
53	Jg6Mt 4 04	6067	1411	11955	14	671	0.421	392	445	15	155	19	1864	0.749	336	38	1.5	3.3	0.154	1.7	0.044	0.942	0.169	33
54	Jg6Mt 4 05	4403	1464	9761	18	513	0.175	462	440	22	185	37	1920	0.894	184	40	1.2	3.9	0.121	1.7	0.047	1.0	0.209	33
55	Jg6Mt 5 01	99	269	363	14	265	0.173	190	413	3.4	115	15	1563	0.269	26	33	0.495	0.218	0.015	0.048	0.060	0.363	0.070	1.1
56	Jg6Mt 5 02	90	264	181	12	260	0.174	191	421	2.8	121	16	1379	0.227	25	33	0.505	0.006	0.002	0.004	0.035	0.300	0.060	0.019
57	Jg6Mt 5 03	97	266	184	14	229	0.163	186	419	2.8	136	18	1441	0.234	37	32	0.547	0.015	0.004	0.006	0.018	0.325	0.062	0.099
58	Jg6Mt 5 04	83	267	189	14	270	0.161	191	421	1.7	135	19	1459	0.247	39	32	0.400	0.002	0.000	0.000	0.029	0.339	0.069	0.002
59	Jg6Mt 5 05	91	277	194	12	247	0.166	189	423	4.3	140	19	1463	0.255	36	33	0.433	0.002	0.002	0.002	0.042	0.331	0.063	0.002
60	Jg6Mt 5 06	86	252	200	13	228	0.142	192	416	5.6	112	16	1430	0.228	26	33	0.487	0.002	0.002	0.012	0.029	0.353	0.068	0.002
61	Jg6Mt 5 07	92	267	183	13	228	0.142	195	423	1.8	139	18	1438	0.219	37	32	0.434	0.045	0.000	0.000	0.041	0.338	0.068	0.083
62	Jg6Mt 5 08	75	252	160	12	194	0.153	187	413	5.5	113	15	1505	0.209	31	32	0.376	0.005	0.000	0.001	0.017	0.333	0.068	0.002
63	Jg6Mt 5 09	117	256	307	13	207	0.150	188	417	3.8	100	14	2262	1.2	38	33	0.409	0.041	0.051	0.017	0.028	0.420	0.077	0.021
64	Jg6Mt 5 10	1942	809	5149	14	465	0.151	284	421	3.5	79	6.1	1947	0.317	33	37	0.996	1.7	0.176	1.3	0.034	0.799	0.170	18
65	Jg6Mt 5 11	96	279	172	14	237	0.144	188	417	5.6	124	17	1448	0.233	36	34	0.468	0.003	0.007	0.112	0.060	0.318	0.065	0.008
66	Jg6Mt 5 12	84	263	188	14	225	0.153	188	417	3.1	118	15	1395	0.974	33	32	0.614	0.003	0.004	0.006	0.023	0.395	0.064	0.094
67	Jg6Mt 5 13	123	281	190	14	244	0.161	189	417	4.1	140	19	1456	0.245	40	32	0.479	0.001	0.000	0.004	0.069	0.240	0.073	0.009
68	Jg6Mt 6 01	83	310	311	14	254	0.173	200	430	23	143	22	1587	0.264	47	32	0.934	0.016	0.002	0.005	0.039	0.364	0.072	0.014
69	Jg6Mt 6 02	88	312	206	14	233	0.185	204	418	23	143	23	1532	0.197	73	33	0.885	0.026	0.004	0.018	0.043	0.324	0.056	0.162
70	Jg6Mt 6 03	123	285	281	13	231	0.176	193	408	16	106	16	2151	0.203	40	31	0.443	0.041	0.063	0.021	0.048	0.354	0.057	0.028
71	Jg6Mt 6 04	113	289	337	12	203	0.170	193	416	23	96	15	1576	0.198	72	32	0.695	0.997	0.019	0.131	0.423	0.385	0.080	2.3
72	Jg6Mt 6 05	3405	387	5706	14	202	0.158	191	419	12	106	25	1742	0.220	115	32	0.850	0.479	0.022	0.202	0.025	0.360	0.086	1.5
73	Jg6Mt 6 06	92	324	192	13	224	0.161	211	413	12	128	24	1673	0.268	83	33	0.628	0.497	0.014	0.788	0.022	0.399	0.059	1.1
74	Jg6Mt 6 07	297	335	544	12	238	0.171	188	434	17	83	14	1705	0.442	136	32	0.476	0.280	0.096	0.175	0.030	0.287	0.067	1.3
75	Jg6Mt 6 08	4618	827	10074	14	2839	0.966	175	402	13	98	599	13664	3.4	90	31	1.4	0.435	0.602	0.253	0.094	1.1	0.137	0.370
76	Jg6Mt 6 09	82	244	239	13	225	0.162	191	408	25	82	12	1463	0.220	23	31	0.669	0.019	0.063	0.006	0.031	0.321	0.072	0.036

#	Sample	Mg	Al	Si	P	Ca	Sc	Ti	V	Cr	Mn	Co	Ni	Cu	Zn	Ga	As	Sr	Zr	Nb	Mo	Sn	Sb	Ba
77	Jg6Mt 6 10	104	271	294	14	242	0.170	197	411	26	116	15	1399	0.250	38	32	0.594	0.270	0.001	0.029	0.199	0.323	0.056	0.729
78	Jg6Mt 6 11	65	271	269	14	213	0.147	192	409	21	133	17	1386	0.268	29	32	0.588	0.008	0.000	0.014	0.026	0.310	0.055	0.070
79	Jg6Mt 6 12	4993	1431	11364	17	1407	0.420	403	425	64	206	17	1639	0.258	158	40	0.631	3.6	0.206	2.6	0.024	1.1	0.237	27
80	Jg6Mt 7 01	4036	1451	9609	26	1132	0.177	377	442	0.299	182	16	1489	0.238	105	39	1.9	4.6	0.150	3.4	0.033	1.2	0.401	39
81	Jg6Mt 7 02	6393	1325	12594	26	2563	0.164	328	444	0.320	227	26	1762	0.238	177	39	1.6	4.0	0.109	2.7	0.050	1.1	0.387	24
82	Jg6Mt 7 03	1725	732	3971	14	256	0.139	248	432	0.348	189	18	1428	0.361	126	34	0.794	4.0	0.057	1.0	0.041	0.552	0.084	20
83	Jg6Mt 7 04	4328	1944	11142	24	1346	0.217	424	450	0.267	236	25	1670	0.692	234	41	3.7	5.8	0.225	3.5	0.101	1.3	0.488	58
84	Jg6Mt 7 05	5093	1386	10814	24	728	0.339	320	453	0.274	455	25	1686	0.386	236	39	2.1	2.5	0.322	2.6	0.052	0.970	0.431	28
85	Jg6Mt 7 06	5844	846	7687	13	887	0.155	253	433	0.484	650	20	1518	0.372	192	35	1.1	4.6	0.188	1.4	0.042	0.576	0.214	15
86	Jg6Mt 8 01	223	304	540	13	247	0.160	169	439	1.3	104	37	2600	2.2	123	32	0.425	0.032	0.238	0.156	0.031	0.287	0.064	0.182
87	Jg6Mt 8 02	253	229	719	12	183	0.140	151	384	1.1	64	1090	19361	17	23	28	2.0	0.055	0.170	0.025	0.195	0.284	0.143	0.088
88	Jg6Mt 8 03	100	330	161	13	202	0.152	186	423	0.403	145	27	1586	0.231	66	32	0.516	0.002	0.002	0.003	0.037	0.265	0.069	0.004
89	Jg6Mt 8 04	102	330	168	12	219	0.168	186	424	0.523	149	25	1568	0.280	67	33	0.511	0.002	0.002	0.001	0.029	0.296	0.065	0.004
90	Jg6Mt 8 05	82	281	175	18	216	0.157	180	424	1.2	131	18	1425	0.226	35	31	0.482	0.001	0.000	0.001	0.024	0.380	0.060	0.004
91	Jg6Mt 8 06	123	328	391	12	250	0.161	178	430	0.407	142	22	1525	0.298	57	32	0.474	0.045	0.001	0.130	0.029	0.312	0.065	0.371
92	Jg6Mt 8 07	96	328	169	13	219	0.159	183	430	0.909	142	23	1511	0.204	48	33	0.413	0.003	0.000	0.026	0.015	0.361	0.059	0.010
93	Jg6Mt 8 08	93	357	179	14	210	0.176	178	416	0.787	140	29	1576	0.252	54	31	0.465	0.003	0.001	0.240	0.022	0.346	0.065	0.050
94	Jg6Mt 8 09	131	357	403	14	218	0.163	173	406	0.674	142	28	1588	0.315	55	32	0.413	0.034	0.002	0.063	0.037	0.314	0.080	0.261
95	Jg6Mt 8 10	3798	1507	9452	25	1931	0.293	343	436	0.341	219	33	1716	0.473	201	37	2.8	4.7	0.129	3.4	0.041	1.4	0.324	34
96	Jg6Mt 9 03	131	368	154	13	220	0.179	166	410	1.1	156	27	1594	0.205	81	32	0.496	0.004	0.002	0.001	0.023	0.364	0.065	0.009
97	Jg6Mt 9 04	121	378	157	12	206	0.159	169	407	0.854	154	27	1604	0.221	74	32	0.444	0.010	0.000	0.075	0.028	0.498	0.064	0.029
98	Jg6Mt 9 05	122	380	173	12	185	0.157	167	412	0.711	148	24	1554	0.232	63	32	0.447	0.036	0.001	0.013	0.036	0.326	0.083	0.073
99	Jg6Mt 9 06	3417	1339	7328	14	764	0.165	296	434	1.1	210	31	1779	0.728	211	38	3.5	2.5	0.088	2.0	0.032	0.993	0.248	25
100	Jg6Mt 9 07	2928	1100	6416	14	334	0.155	245	417	1.4	184	28	1767	0.765	169	37	0.848	1.3	0.086	2.0	0.066	0.787	0.207	20
101	Jg6Mt 9 08	3323	1260	41939	72	9230	0.770	218	401	3.9	206	33	2050	4.7	280	58	2.6	46	7.6	1.7	0.140	3.6	0.646	17
102	Jg6Mt 9 09	126	377	427	12	211	0.152	156	414	1.1	151	25	1591	0.225	67	32	0.428	0.142	0.054	0.079	0.040	0.408	0.064	0.198
103	Jg7Mt 1 02	2966	1059	4741	15	250	0.163	260	452	18	146	19	1537	2.4	5305	33	0.657	2.8	0.057	0.259	0.015	0.592	0.105	13
104	Jg7Mt 1 03	2116	747	3316	14	352	0.165	246	434	20	117	7.3	1405	3.0	1439	32	0.467	3.4	0.013	0.135	0.036	0.564	0.063	17
105	Jg7Mt 1 04	4370	1366	9155	12	567	0.179	333	450	31	51	8.3	6141	5.5	45	33	1.4	1.5	0.200	0.749	0.122	1.1	0.416	4.6
106	Jg7Mt 1 05	8878	3574	16295	16	577	0.272	319	473	28	117	14	8541	5.3	77	38	1.5	1.8	0.108	0.550	0.054	0.790	0.236	8.3
107	Jg7Mt 1 06	6977	4160	9829	12	370	0.194	241	456	29	84	7.9	4267	3.6	94	33	0.912	3.1	0.107	0.720	0.048	0.851	0.397	8.7
108	Jg7Mt 2 01	366	313	715	12	237	0.165	473	480	90	87	12	1377	0.455	38	33	0.455	0.338	0.019	1.2	0.045	0.514	0.097	1.5
109	Jg7Mt 2 02	272	291	510	14	227	0.158	251	429	18	105	18	1485	0.239	64	33	0.570	0.113	0.012	0.063	0.045	0.542	0.067	0.035
110	Jg7Mt 2 03	1103	527	1957	12	213	0.172	292	434	2.3	86	18	1614	0.228	80	34	0.431	0.336	0.014	0.068	0.040	0.422	0.071	0.362
111	Jg7Mt 2 04	1115	1007	1280	14	229	0.162	313	440	3.5	110	19	1813	0.244	94	35	0.459	0.222	0.021	0.089	0.048	0.580	0.121	0.224
112	Jg7Mt 2 05	952	314	326	12	272	0.158	320	435	4.4	267	25	1533	0.212	601	33	0.473	1.1	0.016	0.120	0.041	0.502	0.063	0.553
113	Jg7Mt 2 06	1030	443	1215	13	321	0.167	308	435	0.706	163	28	1683	0.243	135	34	0.486	0.842	0.009	0.130	0.044	0.494	0.116	2.2
114	Jg7Mt 2 07	996	329	1117	13	211	0.222	327	421	0.371	264	26	1717	0.245	137	33	0.723	0.512	0.009	0.142	0.022	0.492	0.073	1.4
115	Jg7Mt 2 08	547	364	844	14	235	0.145	295	430	0.473	153	27	1780	0.327	169	34	0.665	0.975	0.005	0.056	0.019	0.456	0.100	3.0
116	Jg7Mt 2 09	81	313	307	14	225	0.187	276	430	0.336	131	27	1716	0.250	114	33	0.463	0.015	0.001	0.007	0.031	0.459	0.062	0.034

#	Sample	Mg	Al	Si	P	Ca	Sc	Ti	V	Cr	Mn	Co	Ni	Cu	Zn	Ga	As	Sr	Zr	Nb	Mo	Sn	Sb	Ba
117	Jg7Mt 2 10	1352	618	2894	17	675	0.192	339	442	2.9	152	24	1689	0.628	155	36	0.832	2.3	0.007	0.248	0.021	0.591	0.097	15
118	Jg7Mt 3 01	1299	532	2851	11	229	0.150	193	502	60	27	3.3	1853	0.450	17	23	0.403	0.178	0.002	0.077	0.038	0.407	0.067	0.265
119	Jg7Mt 3 02	2041	541	4225	59	398	0.284	271	500	15	138	16	1590	0.748	132	32	1.5	1.5	0.930	0.725	0.155	0.720	0.292	5.2
120	Jg7Mt 3 03	2602	953	4595	44	3393	0.662	317	467	13	169	20	1573	0.489	109	33	0.958	2.0	0.054	0.632	0.029	0.690	0.125	7.3
121	Jg7Mt 3 04	1841	909	3179	14	228	0.203	275	495	30	98	14	1568	2.0	1779	31	0.978	0.550	0.037	0.382	0.028	0.658	0.138	3.3
122	Jg7Mt 3 05	1422	1041	1940	13	212	0.143	246	461	23	117	124	7897	3053	1298	32	0.654	0.009	0.002	0.032	0.095	0.370	0.064	0.142
123	Jg7Mt 3 06	1895	389	3647	311	625	0.260	247	525	8.0	132	17	1500	3.2	463	30	1.3	2.0	0.058	0.495	0.708	0.561	0.279	6.9
124	Jg7Mt 4 01	97	261	281	13	255	0.155	220	427	73	99	12	1338	0.211	30	32	0.453	0.027	0.002	0.011	0.040	0.414	0.054	0.096
125	Jg7Mt 4 02	2254	1005	3913	12	240	0.168	235	419	88	63	5.7	2276	0.489	84	31	0.481	1.1	0.026	0.233	0.032	0.605	0.148	2.1
126	Jg7Mt 4 03	5476	2094	8202	21	422	0.269	289	436	20	166	25	1713	0.739	435	37	1.2	4.1	0.001	0.113	0.024	0.403	0.102	24
127	Jg7Mt 4 04	9870	6114	11918	15	262	0.280	295	404	105	80	14	1641	0.479	243	37	0.661	1.9	0.018	0.350	0.044	0.656	0.126	12
128	Jg7Mt 4 05	7013	1927	11879	14	1043	0.426	347	436	153	237	24	1741	1.1	393	39	1.1	7.1	0.060	0.271	0.034	0.631	0.183	35
129	Jg7Mt 4 06	160	355	571	13	235	0.150	269	441	17	112	24	1530	1.1	181	34	2.9	1.1	0.008	0.068	0.046	0.481	0.436	2.7
130	Jg7Mt 4 07	383	448	534	14	685	0.148	272	437	6.6	125	21	1570	0.535	207	32	1.5	2.0	0.002	0.044	0.029	0.417	0.095	2.2
131	Jg7Mt 4 08	166	262	320	19	317	0.215	211	439	35	70	23	1507	0.351	60	32	0.625	0.274	0.001	0.110	0.038	0.380	0.067	0.112
132	Jg7Mt 4 09	455	365	1059	13	265	0.188	247	431	78	104	17	1475	0.607	79	33	0.456	1.0	0.006	0.055	0.044	0.381	0.085	6.9
133	Jg7Mt 4 10	4538	1133	10565	13	1980	1.3	430	435	53	129	17	1508	0.254	97	37	1.1	2.1	0.151	1.1	0.035	1.4	0.253	12
134	Jg7Mt 4 11	190	318	448	13	232	0.179	210	417	76	111	13	1365	0.279	40	33	0.470	0.023	0.005	0.013	0.025	0.373	0.058	0.006
135	Jg7Mt 5 01	47	245	263	13	208	0.161	215	483	50	79	11	1376	0.246	30	31	0.449	0.080	0.004	0.170	0.023	0.442	0.085	0.191
136	Jg7Mt 5 02	138	306	306	14	233	0.142	246	426	25	75	14	1547	0.537	101	33	0.453	0.297	0.004	0.166	0.025	0.429	0.091	1.1
137	Jg7Mt 5 03	4463	3461	4561	13	256	0.363	239	408	6.3	114	18	1696	0.530	79	34	1.1	0.452	0.029	0.185	0.036	0.403	0.094	1.1
138	Jg7Mt 5 04	1260	403	2660	37	229	0.404	302	412	2.5	151	24	1692	0.243	113	35	1.3	1.2	0.052	0.398	0.036	0.496	0.163	3.3
139	Jg7Mt 5 05	68	263	319	11	200	0.169	228	477	57	54	13	1459	0.239	45	32	0.545	0.016	0.004	0.061	0.018	0.371	0.067	0.014
140	Jg7Mt 5 06	370	347	790	13	210	0.168	197	658	141	31	4.4	1444	0.783	20	30	0.402	0.161	0.045	0.394	0.036	0.518	0.123	0.081
141	Jg7Mt 5 07	4802	2128	6972	15	2002	0.239	235	622	6.5	92	8.8	1517	1.5	93	34	1.7	4.2	0.296	0.553	0.055	0.699	0.166	20
142	Jg7Mt 5 08	116	240	359	12	254	0.159	207	530	54	34	7.2	1361	1.7	34	30	0.554	0.143	0.024	0.171	0.029	0.439	0.086	0.142
143	Jg8Mt 2 rim 01	98	291	186	12	226	0.125	239	825	55	84	17	1627	0.241	55	31	0.788	0.077	0.011	0.006	0.035	0.414	0.080	0.041
144	Jg8Mt 2 rim 02	110	306	179	12	230	0.115	254	822	73	97	17	1607	0.248	62	32	0.542	0.002	0.001	0.001	0.049	0.518	0.078	0.008
145	Jg8Mt 2 rim 03	78	255	177	12	192	0.143	221	828	58	86	15	1514	0.215	42	30	0.667	0.002	0.002	0.004	0.031	0.461	0.078	0.001
146	Jg8Mt 2 rim 04	87	271	183	13	185	0.148	226	820	37	87	12	1482	0.238	30	30	0.566	0.005	0.001	0.001	0.030	0.431	0.076	0.001
147	Jg8Mt 2 rim 05	78	260	369	13	217	0.216	227	863	81	74	13	1477	0.273	37	30	0.591	0.002	14	0.001	0.035	0.463	0.079	0.001
148	Jg8Mt 2 rim 06	107	314	229	12	222	0.148	256	848	54	75	11	1396	0.257	35	31	0.581	0.002	0.036	0.009	0.048	0.545	0.072	0.013
149	Jg8Mt 2 rim 07	6816	440	11841	14	243	0.179	255	810	32	43	11	1610	1.0	111	28	0.535	0.051	0.014	0.058	0.050	0.367	0.073	0.022
150	Jg8Mt 2 core 01	2994	1042	7386	17	851	0.488	440	862	13	96	16	1696	0.228	101	35	1.3	3.1	0.065	1.5	0.055	1.7	0.213	24
151	Jg8Mt 2 core 02	2054	460	4509	15	555	0.330	302	828	0.298	87	17	1802	0.260	106	31	1.6	0.612	0.344	0.761	0.048	0.915	0.182	1.5
152	Jg8Mt 2 core 03	2611	1150	7133	15	1029	0.477	468	857	0.341	104	18	1812	0.278	141	35	3.7	2.1	0.197	1.5	0.049	1.5	0.302	20
153	Jg8Mt 2 core 04	2233	737	4980	13	864	0.404	346	856	0.346	139	26	1824	0.343	193	35	2.5	1.4	0.038	0.801	0.027	1.1	0.235	7.7
154	Jg8Mt 2 core 05	2014	628	4490	13	516	0.362	333	847	4.5	128	23	1755	0.254	134	36	1.2	0.848	0.060	0.835	0.151	1.2	0.152	7.1
155	Jg8Mt 2 core 06	89	269	267	14	223	0.128	253	816	17	86	36	2080	5.8	77	32	0.546	0.023	0.001	0.028	0.038	0.511	0.074	0.263
156	Jg8Mt 2 core 07	73	243	370	13	218	0.130	266	826	50	56	11	1486	0.227	28	29	0.508	0.013	0.022	0.003	0.048	0.429	0.073	0.009

#	Sample	Mg	Al	Si	P	Ca	Sc	Ti	V	Cr	Mn	Co	Ni	Cu	Zn	Ga	As	Sr	Zr	Nb	Mo	Sn	Sb	Ba
157	Jg8Mt 3 01	51	204	227	14	208	0.155	269	838	14	54	10	1522	0.249	24	31	0.488	0.034	0.001	0.009	0.056	0.481	0.089	0.093
158	Jg8Mt 3 02	479	244	1008	12	217	0.152	290	834	5.2	79	13	1543	0.928	31	32	0.407	0.002	0.001	0.009	12	0.489	0.078	0.006
159	Jg8Mt 3 03	93	272	218	12	222	0.152	281	852	3.7	88	13	1493	0.244	34	32	0.493	0.459	0.002	0.005	0.039	0.388	0.070	0.099
160	Jg8Mt 3 04	81	258	333	13	202	0.138	284	838	4.3	83	14	1546	0.276	38	33	0.621	0.003	0.001	0.001	0.790	0.496	0.067	0.004
161	Jg8Mt 3 05	1351	429	3663	15	284	0.198	282	860	17	51	29	2796	70	31	31	0.596	0.123	0.011	0.195	0.067	0.525	0.080	0.031
162	Jg8Mt 3 06	56	218	185	12	212	0.269	281	853	13	68	12	1462	0.225	25	32	0.511	0.002	0.001	0.001	0.029	0.455	0.062	0.004
163	Jg8Mt 3 07	63	207	370	13	214	0.150	283	855	13	58	9.9	1430	0.208	21	31	0.510	0.173	0.004	0.001	0.029	0.407	0.073	0.001
164	Jg8Mt 3 08	155	257	433	11	241	0.154	287	834	7.9	83	16	1599	0.239	45	32	0.535	0.005	0.001	0.008	0.027	0.559	0.066	0.006
165	Jg8Mt 3 09	77	265	237	12	247	0.152	287	835	8.8	87	13	1538	0.259	39	33	0.566	0.001	0.001	0.002	0.037	0.416	0.071	0.006
166	Jg8Mt 3 10	1412	431	2871	13	218	0.141	339	831	12	85	14	1601	0.250	71	34	0.507	0.355	6.5	0.246	0.029	0.698	0.069	2.6
167	Jg8Mt 3 11	132	303	434	13	442	0.139	293	837	14	62	16	1871	2.1	68	31	0.428	4.5	0.002	0.058	0.033	0.461	0.050	0.020
168	Jg8Mt 3 12	80	266	160	13	222	0.142	286	834	10	83	77	3237	5.3	35	32	0.601	0.001	0.002	0.010	0.056	0.483	0.055	0.006
169	Jg8Mt 3 13	89	285	245	12	264	0.157	289	834	1.5	94	17	1640	0.252	51	33	0.481	0.002	0.004	0.002	0.025	0.534	0.072	0.001
170	Jg8Mt 3 14	73	252	156	13	250	0.137	283	858	2.6	79	14	1556	15	40	32	0.493	0.057	0.009	0.001	0.039	0.458	0.056	0.002
171	Jg8Mt 3 15	168	266	241	13	238	0.138	301	824	2.0	86	15	1568	0.230	39	33	0.518	0.008	0.001	0.003	0.676	0.488	0.058	0.002
172	Jg8Mt 3 16	80	261	224	13	211	0.148	295	833	1.5	89	16	1575	0.213	42	33	0.490	0.001	0.001	0.000	0.018	0.496	0.053	0.002
173	Jg8Mt 3 17	1646	1344	1628	14	215	0.254	263	844	8.8	47	187	8431	174	40	29	0.523	0.082	0.004	0.056	0.328	0.523	0.063	0.035
174	Jg8Mt 4 01	1242	629	2519	13	229	0.144	342	831	9.6	73	11	1930	0.221	124	39	0.544	2.0	0.063	0.169	0.041	0.795	0.070	11
175	Jg8Mt 4 02	53	309	172	11	225	0.137	269	837	8.3	43	11	1576	0.239	38	32	0.459	0.005	0.007	0.000	0.046	0.389	0.068	0.002
176	Jg8Mt 4 03	96	342	495	14	301	0.167	263	814	11	65	22	1695	0.285	110	36	0.580	0.012	0.001	0.004	0.032	0.517	0.088	0.009
177	Jg8Mt 4 04	1903	785	3834	12	246	0.144	467	819	4.2	111	23	1818	0.669	287	38	0.490	2.5	0.019	0.218	0.031	0.683	0.081	17
178	Jg8Mt 4 05	3226	751	6093	13	221	0.138	293	868	8.9	74	21	1793	0.817	153	37	0.522	2.3	0.007	0.240	0.095	0.653	0.079	16
179	Jg8Mt 4 06	607	330	1284	12	230	0.132	291	733	11	86	31	1645	0.263	111	34	0.439	0.020	0.002	0.008	0.033	0.605	0.068	0.009
180	Jg8Mt 4 07	79	262	361	12	218	0.139	285	837	8.0	90	20	1653	0.259	60	35	0.472	0.002	0.001	0.000	0.027	0.573	0.058	0.014
181	Jg8Mt 4 08	13481	1599	21163	12	265	0.170	314	780	2.5	109	31	2116	0.456	212	36	0.572	0.016	0.001	0.030	68	0.490	0.081	0.022
182	Jg8Mt 4 09	793	308	1393	13	238	0.167	308	785	4.4	101	24	1783	0.239	82	35	0.440	0.007	0.002	0.019	0.047	0.506	0.068	0.006
183	Jg8Mt 4 10	96	410	178	13	240	0.155	243	822	12	87	23	1659	0.255	59	36	0.484	0.002	0.004	0.001	0.027	0.395	0.053	0.005
184	Jg8Mt 4 11	930	425	1844	12	237	0.153	258	826	11	79	21	1847	0.272	91	34	0.505	0.064	0.012	0.040	0.039	0.512	0.071	0.379
185	Jg8Mt 5 01	74	240	214	13	214	0.160	264	774	28	78	15	1509	0.193	37	33	0.460	0.003	0.002	0.002	0.041	0.543	0.072	0.002
186	Jg8Mt 5 02	2250	379	4186	13	195	0.162	272	757	19	54	14	1554	0.223	69	31	0.439	0.065	0.009	0.063	0.078	0.481	0.051	0.138
187	Jg8Mt 5 03	2567	670	5706	14	875	0.538	398	799	5.2	113	26	1724	0.219	117	36	0.666	0.946	0.042	0.917	0.037	1.1	0.142	3.9
188	Jg8Mt 5 04	2916	885	7049	15	1279	0.463	438	831	1.5	143	29	1808	0.241	164	38	1.0	1.4	0.066	1.1	0.029	1.3	0.153	6.7
189	Jg8Mt 5 05	3686	1097	7940	19	788	0.340	465	852	2.0	139	34	1849	0.263	224	37	1.0	2.6	0.111	1.3	0.028	1.2	0.201	21
190	Jg8Mt 5 06	3623	1620	8222	13	686	0.328	579	863	2.0	149	35	1841	0.273	272	40	1.6	3.2	0.200	1.4	0.025	1.6	0.205	34
191	Jg8Mt 5 07	2847	1335	6092	14	417	0.322	478	866	5.6	137	34	1843	0.322	448	39	0.961	5.4	0.105	0.971	0.031	1.1	0.181	34
192	Jg8Mt 5 08	4637	1146	9893	15	514	0.572	532	851	6.2	130	35	1888	0.268	388	39	1.3	4.6	0.067	1.2	0.062	1.1	0.261	29
193	Jg8Mt 5 09	2707	1374	6656	14	641	0.232	547	853	3.2	161	33	1781	0.244	235	39	1.3	2.4	0.143	1.5	0.076	1.5	0.230	28
194	Jg8Mt 5 10	2502	1314	5926	13	465	0.323	484	857	0.346	171	33	1840	0.604	313	39	2.8	3.7	0.119	0.931	0.025	1.3	0.266	31
195	Jg8Mt 5 11	3154	1116	7302	13	953	0.543	469	835	1.5	160	31	1813	0.334	266	40	2.0	3.8	0.090	1.1	0.025	1.4	0.239	30
196	Jg8Mt 6 01	245	265	449	15	269	0.186	216	771	36	59	12	1513	0.292	34	28	0.611	0.020	0.006	0.047	0.044	0.430	0.078	0.028

#	Sample	Mg	Al	Si	P	Ca	Sc	Ti	V	Cr	Mn	Co	Ni	Cu	Zn	Ga	As	Sr	Zr	Nb	Mo	Sn	Sb	Ba
197	Jg8Mt 6 02	4320	833	8402	14	339	0.307	385	813	4.4	129	28	1889	0.252	165	38	0.891	1.4	0.062	0.672	0.044	1.1	0.133	5.1
198	Jg8Mt 6 03	2400	798	5416	14	778	0.667	419	811	0.267	150	32	1811	0.227	269	37	1.3	2.1	0.057	0.797	0.029	1.2	0.207	14
199	Jg8Mt 6 04	2746	787	6071	14	910	0.671	392	816	0.362	156	36	2137	0.669	239	40	2.4	2.4	1.5	0.859	0.054	1.1	0.198	7.9
200	Jg8Mt 6 05	2530	654	5325	13	877	0.444	353	805	0.328	127	28	1837	0.579	250	37	4.5	1.7	0.190	0.710	0.076	1.1	0.136	11
201	Jg8Mt 6 06	3946	1400	7016	12	755	0.427	399	809	0.426	128	24	1840	0.672	359	38	2.2	3.3	0.013	0.840	0.041	1.1	0.237	24
202	Jg8Mt 6 07	2189	835	4521	12	481	0.199	386	811	1.1	145	25	1781	0.787	338	38	3.6	2.9	0.036	0.694	0.042	1.2	0.645	21
203	Jg8Mt 6 08	1783	361	3248	15	226	0.165	302	799	14	73	22	1726	0.244	77	34	0.495	0.010	0.001	0.140	0.016	0.537	0.060	0.116
204	Jg8Mt 6 09	124	322	243	16	252	0.132	293	795	7.0	107	162	6304	484	225	35	0.492	0.006	0.007	0.008	0.036	0.610	0.056	0.031
205	Jg8Mt 6 10	114	313	307	16	308	0.193	267	744	15	95	678	21393	8.1	23	33	0.975	0.002	0.001	0.063	0.298	0.568	0.069	0.002
206	Jg9bMt1rim 01	8161	1482	14969	1.5	496	1.0	469	473	39	165	17	1729	0.269	160	39	1.3	3.1	0.162	0.931	0.004	2.1	0.276	30
207	Jg9bMt1rim 02	4677	2945	5142	2.7	15	0.675	269	457	38	125	105	6918	1.2	53	35	0.687	0.203	0.020	0.533	0.010	1.2	0.115	0.975
208	Jg9bMt1rim 03	10091	5799	13217	8.0	768	1.7	561	505	48	141	23	1880	0.329	194	41	0.940	3.5	0.148	1.0	0.017	2.2	0.180	30
209	Jg9bMt1rim 04	3594	1304	8900	31	1371	2.2	544	507	2.8	178	24	1711	1.1	155	40	2.5	2.7	0.156	1.0	0.025	2.8	0.462	28
210	Jg9bMt1rim 05	4204	1646	9415	16	1562	3.3	580	507	0.301	222	28	1805	1.3	314	40	9.5	4.6	0.172	1.0	0.042	2.7	0.501	40
211	Jg9bMt1rim 06	3383	1252	7928	26	1261	2.3	578	513	14	172	22	1773	0.355	158	39	1.7	3.9	0.155	0.962	0.023	2.5	0.251	38
212	Jg9bMt1rim 07	3770	1156	7581	3.5	1029	2.0	520	509	31	157	23	1779	0.330	140	37	1.6	2.0	0.403	1.2	0.034	2.5	0.345	30
213	Jg9bMt1rim 08	3063	1023	6176	1.8	795	1.4	478	503	0.147	189	30	1806	0.453	248	38	7.1	2.5	0.192	0.748	0.026	2.0	0.214	22
214	Jg9bMt1rim 09	2654	965	5678	2.7	578	1.4	463	511	1.2	166	25	1805	0.005	116	37	1.1	1.2	0.180	0.679	0.004	1.8	0.188	11
215	Jg9bMt1rim 10	298	296	733	9.4	31	0.463	276	471	6.8	139	21	1641	0.090	85	33	0.357	0.106	0.001	0.044	0.009	0.948	0.011	0.182
216	Jg9bMt1rim 11	217	326	444	2.2	103	0.294	300	493	2.7	148	25	1687	0.609	99	33	0.346	0.148	0.007	0.030	0.003	0.811	0.035	0.758
217	Jg9bMt1rim 12	411	453	755	3.0	18	0.527	320	505	1.1	161	29	1736	0.120	139	33	0.524	0.297	0.005	0.034	0.020	0.855	0.034	1.0
218	Jg9bMt1rim 13	793	443	1708	4.9	192	0.816	345	494	1.1	152	28	1705	0.174	127	35	0.685	0.270	0.023	0.158	0.002	1.1	0.071	0.656
219	Jg9bMt1rim 14	734	370	1264	3.9	108	0.644	335	493	2.6	158	29	1722	0.322	141	33	0.756	0.267	0.013	0.116	0.014	0.970	0.033	0.897
220	Jg9bMt1rim 15	1144	721	1692	7.8	164	0.705	352	458	6.6	176	28	1627	0.794	266	36	2.7	2.6	0.018	0.184	0.004	1.0	0.236	20
221	Jg9bMt1core 01	970	467	1670	5.4	117	0.672	334	501	1.9	155	29	1748	0.190	128	33	1.0	0.170	0.013	0.114	0.020	0.916	0.045	0.467
222	Jg9bMt1core 02	1004	500	2022	4.4	287	0.734	360	497	2.5	171	28	1715	0.688	211	34	2.0	1.8	0.044	0.226	0.008	1.1	0.143	11
223	Jg9bMt1core 03	1796	547	3424	0.769	201	0.761	357	486	16	133	25	1751	6.2	246	36	0.436	0.999	0.063	0.261	0.090	1.2	0.094	6.8
224	Jg9bMt1core 04	1229	420	2398	1.8	95	0.723	336	491	14	127	23	1717	0.518	127	34	0.553	0.610	0.014	0.175	0.009	0.966	0.047	3.0
225	Jg9bMt2 01	156	332	261	1.000	7.6	0.502	415	500	87	107	21	1687	0.023	68	33	0.113	0.009	0.182	0.044	0.003	0.826	0.013	0.010
226	Jg9bMt2 02	158	320	459	3.3	82	0.524	411	502	93	111	19	1700	3.6	87	33	0.313	0.109	0.024	0.010	0.012	0.654	0.009	0.000
227	Jg9bMt3 03	389	347	1316	11	173	0.688	345	495	83	65	12	1738	0.202	54	32	0.084	0.048	0.022	0.028	0.017	1.2	0.022	0.012
228	Jg9bMt3 04	1778	1235	3042	6.2	7.0	0.738	436	513	90	125	18	1696	2.4	78	36	0.379	0.846	0.017	0.141	0.003	1.4	0.108	6.2
229	Jg9bMt4rim 17	225	312	303	1.6	67	0.377	293	516	77	148	18	1611	0.025	73	34	0.069	0.093	0.019	0.334	0.027	1.1	0.018	0.106
230	Jg9bMt4rim 18	161	290	172	2.8	45	0.320	283	503	61	144	19	1580	0.050	57	33	0.204	0.020	0.001	0.023	0.004	0.829	0.010	0.068
231	Jg9bMt4rim 19	544	277	1025	5.6	45	0.426	270	514	35	115	16	1594	0.005	53	33	0.245	0.093	0.023	0.079	0.022	0.954	0.011	0.407
232	Jg9bMt4rim 20	1086	690	1817	11	41	0.580	332	514	2.9	143	21	1721	0.106	93	35	0.253	0.125	0.007	0.124	0.005	1.1	0.003	1.7
233	Jg9bMt4rim 21	625	382	1206	0.262	4.7	0.365	311	505	47	152	21	1664	0.587	85	34	0.465	0.287	0.016	0.112	0.002	0.941	0.003	0.898
234	Jg9bMt4core 05	379	340	571	0.266	31	0.373	301	500	0.988	143	23	1658	0.500	102	33	0.258	0.062	0.021	0.052	0.003	0.964	0.021	0.124
235	Jg9bMt4core 06	890	488	1628	6.2	103	0.708	326	507	1.2	157	26	1774	0.110	134	37	0.588	0.275	0.020	0.158	0.005	1.4	0.072	0.717
236	Jg9bMt4core 07	775	460	1547	16	256	0.706	320	494	3.9	155	24	1702	0.422	125	34	0.564	0.358	0.032	0.121	0.032	1.1	0.047	1.1

#	Sample	Mg	Al	Si	P	Ca	Sc	Ti	V	Cr	Mn	Co	Ni	Cu	Zn	Ga	As	Sr	Zr	Nb	Mo	Sn	Sb	Ba
237	Jg9bMt5rim 23	488	421	1131	0.930	78	0.603	353	501	0.798	138	27	1757	0.052	128	32	0.269	0.179	0.015	0.118	0.004	0.876	0.029	0.539
238	Jg9bMt5rim 24	2693	1553	5119	2.6	853	2.0	542	527	0.551	168	31	1859	0.674	168	35	0.838	1.1	0.073	0.692	0.026	1.8	0.115	5.7
239	Jg9bMt5rim 25	1631	972	3720	8.3	852	1.9	492	525	0.432	167	31	1859	0.360	166	34	1.5	0.937	0.054	0.476	0.002	1.6	0.140	2.8
240	Jg9bMt5rim 26	3113	1773	4773	20	733	1.9	471	531	0.068	174	34	1991	0.041	199	35	2.0	0.926	0.031	0.578	0.007	1.4	0.119	3.9
241	Jg9bMt5rim 27	2058	787	4285	4.6	536	1.3	472	514	0.247	164	33	1894	0.156	159	35	1.4	0.952	0.042	0.569	0.002	1.4	0.171	8.1
242	Jg9bMt5rim 28	5824	2366	7604	87	1214	1.2	423	492	5.3	189	34	1925	0.280	292	36	1.0	4.2	0.035	0.351	0.008	1.3	0.109	17
243	Jg9bMt5rim 29	7194	3464	9522	8.5	255	1.0	371	498	22	120	32	1968	29	270	38	0.770	1.6	0.575	0.703	0.005	1.8	0.165	10
244	Jg9bMt5rim 30	2495	960	3970	1.5	393	1.1	372	501	8.5	143	32	1833	0.097	129	34	0.635	1.7	0.028	0.429	0.020	1.2	0.099	7.8
245	Jg9bMt5rim 31	3053	906	5947	2.2	521	1.1	465	505	20	137	23	1847	0.356	294	34	1.1	3.8	0.067	0.637	0.030	1.5	0.140	13
246	Jg9bMt5rim 32	6351	2758	11828	31	1802	2.4	551	517	14	80	18	1819	15	17273	38	1.9	4.5	0.517	1.5	0.006	9.5	0.242	27
247	Jg9bMt5rim 33	6078	2744	11248	22	1654	2.4	643	504	5.0	182	25	1858	0.702	402	41	2.8	5.6	0.169	1.2	0.007	2.7	0.390	53
248	Jg9bMt5rim 34	4665	2920	8260	4.4	1203	2.9	584	530	6.2	233	31	1861	1.9	578	41	3.6	11	0.058	0.694	0.007	2.2	0.249	91
249	Jg9bMt5rim 35	10938	6463	13901	15	2864	2.2	614	513	8.2	250	34	1954	0.706	365	41	2.6	7.1	0.037	0.799	0.012	2.2	0.246	42
250	Jg9bMt5rim 36	5654	2854	9865	20	1518	2.3	662	523	3.1	214	33	1916	0.879	414	41	3.7	7.8	0.101	1.0	0.028	2.5	0.358	56
251	Jg9bMt5rim 37	6208	2805	12388	6.8	898	1.8	727	505	1.1	189	34	1924	0.998	221	38	3.9	4.2	0.955	0.928	0.042	2.1	0.344	44
252	Jg9bMt5rim 38	4106	1599	9146	8.3	1709	2.7	672	532	5.0	206	33	1917	1.2	264	40	3.1	4.9	0.109	1.1	0.004	2.7	0.340	34
253	Jg9bMt5core 08	3853	1576	9529	18	2367	3.6	643	514	1.0	196	34	1890	0.506	253	39	4.5	3.4	0.104	1.0	0.018	3.0	0.310	19
254	Jg9bMt5core 09	4078	2369	7330	19	692	1.6	570	509	1.2	190	34	1897	0.452	262	38	3.1	4.2	0.058	0.708	0.003	1.9	0.223	35
255	Jg9bMt5core 10	5031	2691	8535	16	2262	5.6	595	523	1.0	244	33	1997	1.4	545	40	4.6	12	0.076	0.969	0.917	2.2	0.399	54
256	Jg9bMt5core 11	3172	1389	5579	129	1471	2.3	498	521	1.2	140	21	2008	1.5	437	36	3.8	12	0.025	0.557	0.045	1.8	0.214	29
257	Jg9bMt5core 12	2415	1268	4078	3.9	394	0.803	440	514	0.727	161	34	1856	0.723	299	34	1.3	3.7	0.030	0.378	0.009	1.1	0.162	15
258	Jg9bMt5core 13	2409	1534	2835	4.6	455	0.450	417	493	3.1	146	34	1808	0.346	183	33	0.543	1.9	0.008	0.376	0.009	1.1	0.092	8.8
259	Jg9bMt5core 14	11033	5634	12983	20	944	1.4	549	505	38	228	22	2074	0.414	276	38	0.483	3.1	0.037	0.737	0.008	1.8	0.142	19
260	Jg9bMt5core 15	12885	6802	15124	9.3	122	1.1	366	487	46	196	23	2616	15	262	38	0.399	0.998	0.023	0.567	0.000	1.0	0.043	2.7
	Mean (n=260)	2188	945	4266	20	548	0.460	322	540	19	132	33	2074	17	444	34	1.2	1.7	0.277	0.538	0.357	0.859	0.143	10
	SD	2584	1035	5037	74	796	0.663	124	187	30	64	86	1998	190	2461	6.6	1.4	3.4	1.5	0.738	4.2	0.798	0.130	14
	Median	1331	487	2632	13	247	0.184	291	481	6.3	127	22	1716	0.353	109	33	0.599	0.515	0.024	0.182	0.031	0.571	0.085	2.2
	Max	13481	6802	41939	1167	9230	5.6	727	868	168	650	1090	21393	3053	30870	58	12	46	14	3.6	68	9.5	0.697	91
	Min	47	204	141	0.262	2.6	0.007	151	284	0.031	27	3.1	1338	0.005	9.2	16	0.055	0.001	0.000	0.000	0.000	0.156	0.002	0.000

SD Table 1b. (Continued)

#	Sample	La	Ce	Pr	Nd	Sm	Eu	Gd	Tb	Dy	Y	Ho	Er	Tm	Yb	Lu	Hf	Ta	W	^{204}Pb	^{206}Pb	^{207}Pb	^{208}Pb	Th	U
1	Jg3aMt4 04	0.186	0.505	0.073	0.518	0.069	0.018	0.128	0.016	0.083	0.750	0.036	0.167	0.033	0.222	0.072	0.000	0.123	1.7	0.007	0.421	0.311	0.719	0.334	0.180
2	Jg3aMt4 05	0.042	0.123	0.019	0.113	0.023	0.010	0.053	0.010	0.039	0.262	0.008	0.045	0.003	0.045	0.003	0.000	0.021	0.068	0.007	0.129	0.030	0.129	0.099	0.355
3	Jg3aMt4 06	0.026	0.134	0.008	0.051	0.060	0.008	0.013	0.030	0.017	0.113	0.012	0.006	0.006	0.019	0.004	0.007	0.009	0.009	0.022	0.159	0.039	0.276	0.055	0.224
4	Jg3aMt4 07	0.011	0.053	0.018	0.072	0.063	0.034	0.020	0.006	0.127	0.337	0.009	0.029	0.000	0.113	0.003	0.000	0.003	0.001	0.002	0.052	0.030	0.104	0.025	0.040
5	Jg3aMt11 14	32	123	24	142	32	2.6	20	1.3	4.0	11	0.459	0.780	0.067	0.195	0.031	0.005	0.016	0.873	0.017	0.887	0.818	2.1	7.2	0.171
6	Jg3aMt12rim 02	0.018	0.035	0.004	0.046	0.010	0.003	0.019	0.006	0.026	0.199	0.010	0.027	0.005	0.032	0.006	0.002	0.034	0.131	0.005	0.498	0.425	0.855	0.038	0.165

#	Sample	La	Ce	Pr	Nd	Sm	Eu	Gd	Tb	Dy	Y	Ho	Er	Tm	Yb	Lu	Hf	Ta	W	^{204}Pb	^{206}Pb	^{207}Pb	^{208}Pb	Th	U
7	Jg3aMt12rim 03	0.132	0.131	0.023	0.087	0.030	0.004	0.054	0.011	0.095	0.613	0.031	0.092	0.006	0.098	0.016	0.003	0.087	0.228	0.067	1.2	1.1	2.2	0.062	0.132
8	Jg3aMt12rim 04	0.082	0.143	0.039	0.159	0.042	0.012	0.110	0.014	0.084	0.698	0.016	0.080	0.007	0.066	0.029	0.000	0.065	0.511	0.009	0.643	0.298	0.564	0.193	0.820
9	Jg3aMt12rim 05	0.034	0.064	0.004	0.042	0.030	0.002	0.039	0.011	0.041	0.276	0.011	0.051	0.010	0.097	0.016	0.004	0.045	0.279	0.074	1.4	1.2	2.8	0.048	0.145
10	Jg3aMt13rim 05	0.062	0.067	0.019	0.062	0.011	0.002	0.017	0.001	0.017	0.112	0.004	0.013	0.003	0.032	0.006	0.007	0.109	0.159	0.002	0.184	0.136	0.294	0.037	0.094
11	Jg3aMt13rim 06	0.056	0.104	0.021	0.085	0.016	0.008	0.032	0.009	0.041	0.244	0.008	0.034	0.004	0.039	0.015	0.008	0.061	0.165	0.002	0.329	0.188	0.395	0.097	0.435
12	Jg3aMt13rim 07	0.059	0.132	0.014	0.069	0.023	0.007	0.023	0.005	0.028	0.169	0.011	0.021	0.003	0.036	0.012	0.001	0.015	0.355	0.049	0.967	0.911	1.9	0.038	0.084
13	Jg3aMt13rim 08	0.048	0.089	0.016	0.044	0.023	0.011	0.065	0.007	0.056	0.331	0.017	0.051	0.008	0.036	0.011	0.003	0.035	0.218	0.096	2.0	1.9	3.9	0.068	0.263
14	Jg3aMt13rim 10	0.029	0.056	0.002	0.044	0.025	0.002	0.020	0.003	0.015	0.080	0.001	0.016	0.000	0.000	0.005	0.005	0.024	0.066	0.036	0.972	0.832	1.8	0.062	0.119
15	Jg3aMt13core 02	0.021	0.061	0.010	0.041	0.008	0.004	0.011	0.001	0.010	0.069	0.003	0.011	0.001	0.016	0.002	0.003	0.018	0.141	0.049	0.797	0.734	1.6	0.020	0.071
16	Jg3aMt14core 09	0.003	0.007	0.000	0.004	0.004	0.002	0.003	0.001	0.015	0.065	0.004	0.008	0.003	0.017	0.002	0.004	0.165	0.064	0.007	0.047	0.016	0.029	0.007	0.068
17	Jg5Mt2 07	0.003	0.008	0.011	0.014	0.012	0.001	0.003	0.000	0.000	0.049	0.000	0.009	0.000	0.000	0.001	0.000	0.003	0.023	0.054	0.966	1.0	2.2	0.001	0.020
18	Jg5Mt2 08	0.006	0.011	0.003	0.009	0.000	0.001	0.004	0.000	0.018	0.033	0.003	0.016	0.001	0.003	0.000	0.000	0.007	0.209	0.097	1.7	1.7	3.8	0.002	0.110
19	Jg5Mt4 12	0.019	0.023	0.003	0.025	0.022	0.013	0.021	0.004	0.029	0.126	0.007	0.013	0.002	0.004	0.001	0.000	0.039	0.201	0.058	1.0	0.912	2.0	0.017	0.251
20	Jg5Mt5 14	0.003	0.009	0.001	0.003	0.001	0.000	0.007	0.000	0.000	0.002	0.000	0.000	0.000	0.000	0.000	0.004	0.000	0.007	0.001	0.014	0.014	0.017	0.002	0.002
21	Jg5Mt5 19	0.032	0.076	0.005	0.047	0.018	0.002	0.013	0.004	0.005	0.029	0.005	0.002	0.000	0.006	0.001	0.000	0.001	0.022	0.000	0.068	0.069	0.158	0.006	0.014
22	Jg5Mt5 20	0.026	0.110	0.022	0.138	0.080	0.026	0.057	0.008	0.026	0.211	0.007	0.028	0.004	0.022	0.007	0.000	0.094	0.197	0.039	0.917	0.811	1.8	0.019	0.432
23	Jg5Mt5 21	0.001	0.003	0.000	0.003	0.004	0.001	0.001	0.000	0.002	0.018	0.001	0.000	0.000	0.003	0.000	0.000	0.001	0.074	0.069	1.0	1.0	2.5	0.001	0.005
24	Jg5Mt5 24	0.007	0.017	0.002	0.024	0.008	0.001	0.003	0.002	0.009	0.020	0.003	0.005	0.003	0.008	0.000	0.000	0.007	0.038	0.000	0.096	0.077	0.166	0.003	0.061
25	Jg6Mt 1 01	0.001	0.000	0.002	0.016	0.029	0.000	0.005	0.000	0.000	0.001	0.000	0.000	0.000	0.003	0.000	0.000	0.000	0.000	0.026	0.014	0.013	0.018	0.000	0.002
26	Jg6Mt 1 02	0.388	0.484	0.050	0.237	0.046	0.015	0.021	0.008	0.034	0.180	0.005	0.027	0.005	0.049	0.005	0.000	0.165	0.533	0.206	3.5	3.4	7.3	0.164	0.176
27	Jg6Mt 1 03	0.424	0.577	0.084	0.338	0.041	0.014	0.093	0.017	0.105	0.397	0.014	0.031	0.004	0.041	0.007	0.003	0.108	0.460	0.317	5.7	5.3	12	0.191	0.500
28	Jg6Mt 1 04	1.8	3.3	0.485	2.0	0.303	0.050	0.267	0.039	0.256	1.2	0.049	0.093	0.008	0.075	0.010	0.016	0.419	1.8	0.080	2.3	2.3	5.0	0.933	0.387
29	Jg6Mt 1 05	1.9	3.0	0.433	1.9	0.338	0.054	0.293	0.040	0.261	1.1	0.041	0.111	0.010	0.079	0.019	0.011	0.509	2.3	0.202	3.6	3.6	7.7	0.888	0.454
30	Jg6Mt 1 06	0.082	0.123	0.021	0.102	0.029	0.029	0.050	0.014	0.116	0.443	0.007	0.039	0.014	0.112	0.009	0.000	0.124	0.630	0.044	1.3	0.887	1.9	0.114	0.668
31	Jg6Mt 1 07	0.232	0.408	0.042	0.272	0.064	0.022	0.057	0.005	0.049	0.211	0.006	0.022	0.006	0.023	0.004	0.000	0.086	0.348	0.168	2.7	2.4	5.5	0.113	0.325
32	Jg6Mt 1 08	0.972	1.6	0.223	0.913	0.189	0.046	0.236	0.018	0.161	1.0	0.035	0.088	0.015	0.089	0.026	0.000	0.412	2.7	0.306	5.7	5.3	11	0.493	0.465
33	Jg6Mt 1 09	1.0	1.6	0.214	0.894	0.268	0.051	0.214	0.031	0.219	0.948	0.032	0.079	0.011	0.084	0.015	0.008	0.343	1.9	0.218	4.1	3.7	8.2	0.642	0.569
34	Jg6Mt 1 10	0.002	0.006	0.002	0.014	0.021	0.004	0.009	0.001	0.018	0.056	0.002	0.004	0.002	0.000	0.000	0.000	0.007	0.051	0.028	0.034	0.021	0.033	0.002	0.047
35	Jg6Mt 2 01	0.211	0.359	0.045	0.149	0.042	0.009	0.028	0.009	0.055	0.388	0.008	0.072	0.006	0.057	0.022	0.112	0.048	0.236	0.030	1.0	0.851	2.0	0.067	0.386
36	Jg6Mt 2 02	2.8	6.6	0.916	3.4	0.485	0.097	0.484	0.042	0.290	1.3	0.056	0.130	0.013	0.075	0.016	0.011	0.467	5.3	0.249	4.7	4.7	10	1.5	0.931
37	Jg6Mt 2 03	1.3	2.2	0.277	1.2	0.168	0.034	0.203	0.030	0.147	0.725	0.018	0.093	0.006	0.033	0.010	0.000	0.241	1.8	0.638	9.7	9.8	22	0.469	0.255
38	Jg6Mt 2 04	1.3	2.3	0.449	1.7	0.267	0.058	0.274	0.025	0.159	0.718	0.034	0.075	0.008	0.060	0.006	0.003	0.144	2.7	1.7	25	25	57	0.552	0.674
39	Jg6Mt 2 05	2.4	5.6	0.692	2.6	0.382	0.070	0.306	0.049	0.195	1.1	0.029	0.086	0.015	0.062	0.009	0.006	0.342	3.5	0.801	12	12	29	1.2	0.627
40	Jg6Mt 2 06	2.5	5.1	0.711	2.9	0.530	0.098	0.365	0.045	0.242	1.2	0.051	0.124	0.013	0.098	0.014	0.014	0.433	6.0	0.265	4.5	4.2	9.4	1.3	0.555
41	Jg6Mt 2 07	2.5	4.7	0.589	2.5	0.359	0.062	0.339	0.033	0.212	1.2	0.041	0.132	0.016	0.064	0.019	0.016	0.514	5.8	0.502	8.1	8.1	18	1.5	0.498
42	Jg6Mt 2 08	0.557	0.889	0.117	0.439	0.107	0.034	0.157	0.021	0.142	0.509	0.023	0.056	0.004	0.092	0.007	0.006	0.195	0.934	0.389	7.1	6.6	14	0.382	0.520
43	Jg6Mt 2 rim 01	0.031	0.117	0.031	0.072	0.038	0.012	0.025	0.009	0.027	0.134	0.007	0.064	0.000	0.020	0.000	0.000	0.010	1.1	0.040	0.596	0.534	1.2	0.028	0.625
44	Jg6Mt 2 rim 02	0.009	0.028	0.004	0.014	0.026	0.003	0.005	0.000	0.006	0.046	0.001	0.019	0.001	0.007	0.002	0.000	0.012	0.033	0.025	0.189	0.129	0.267	0.009	0.117
45	Jg6Mt 2 rim 03	0.004	0.011	0.003	0.015	0.032	0.000	0.031	0.001	0.004	0.024	0.005	0.003	0.003	0.004	0.000	0.000	0.021	0.041	0.025	0.149	0.091	0.212	0.006	0.123
46	Jg6Mt 4 rim 01	0.005	0.007	0.001	0.011	0.015	0.001	0.001	0.001	0.006	0.024	0.002	0.009	0.002	0.003	0.000	0.000	0.012	0.044	0.025	0.110	0.029	0.062	0.012	0.181

#	Sample	La	Ce	Pr	Nd	Sm	Eu	Gd	Tb	Dy	Y	Ho	Er	Tm	Yb	Lu	Hf	Ta	W	^{204}Pb	^{206}Pb	^{207}Pb	^{208}Pb	Th	U
47	Jg6Mt 4 rim 02	0.247	0.346	0.046	0.249	0.047	0.013	0.032	0.008	0.064	0.365	0.017	0.075	0.020	0.053	0.012	0.000	0.137	0.515	0.052	1.3	1.1	2.3	0.199	0.312
48	Jg6Mt 4 rim 03	0.000	0.002	0.001	0.013	0.033	0.000	0.011	0.001	0.010	0.084	0.002	0.016	0.001	0.022	0.003	0.000	0.015	0.000	0.027	0.059	0.019	0.019	0.001	0.115
49	Jg6Mt 4 rim 04	0.014	0.040	0.006	0.055	0.034	0.014	0.017	0.005	0.061	0.271	0.012	0.037	0.006	0.034	0.006	0.020	0.029	0.163	0.027	0.449	0.365	0.847	0.030	0.156
50	Jg6Mt 4 01	0.171	0.218	0.028	0.136	0.039	0.020	0.034	0.006	0.028	0.205	0.011	0.041	0.007	0.027	0.008	0.007	0.041	0.233	0.028	0.277	0.164	0.422	0.113	0.311
51	Jg6Mt 4 02	0.319	0.333	0.050	0.226	0.079	0.033	0.161	0.018	0.122	0.821	0.030	0.113	0.011	0.089	0.014	0.003	0.324	1.3	0.230	4.5	4.1	9.0	0.186	0.502
52	Jg6Mt 4 03	0.908	1.2	0.153	0.649	0.129	0.047	0.162	0.024	0.144	0.741	0.026	0.094	0.012	0.074	0.018	0.003	0.361	1.3	0.151	2.3	2.0	4.4	0.425	0.635
53	Jg6Mt 4 04	0.329	0.469	0.058	0.250	0.097	0.034	0.093	0.014	0.132	0.685	0.022	0.085	0.006	0.098	0.012	0.009	0.272	0.898	0.518	7.2	6.9	16	0.221	0.774
54	Jg6Mt 4 05	0.389	0.581	0.054	0.375	0.061	0.034	0.058	0.019	0.133	0.763	0.029	0.127	0.012	0.087	0.019	0.006	0.239	1.2	0.181	3.6	3.1	7.1	0.255	0.541
55	Jg6Mt 5 01	0.016	0.026	0.002	0.017	0.022	0.001	0.015	0.001	0.025	0.067	0.004	0.010	0.001	0.010	0.002	0.003	0.000	0.094	0.028	0.044	0.047	0.096	0.007	0.012
56	Jg6Mt 5 02	0.000	0.001	0.002	0.006	0.023	0.000	0.001	0.000	0.000	0.002	0.001	0.000	0.000	0.000	0.000	0.000	0.000	0.000	0.030	0.013	0.011	0.021	0.000	0.001
57	Jg6Mt 5 03	0.000	0.001	0.001	0.016	0.014	0.000	0.012	0.000	0.000	0.004	0.000	0.000	0.000	0.000	0.001	0.000	0.001	0.007	0.026	0.053	0.023	0.094	0.008	0.005
58	Jg6Mt 5 04	0.000	0.000	0.002	0.014	0.023	0.000	0.003	0.000	0.000	0.001	0.000	0.000	0.000	0.000	0.000	0.000	0.000	0.000	0.026	0.011	0.012	0.018	0.001	0.000
59	Jg6Mt 5 05	0.000	0.000	0.001	0.011	0.017	0.000	0.000	0.000	0.000	0.001	0.000	0.000	0.000	0.000	0.000	0.000	0.000	0.000	0.024	0.010	0.011	0.016	0.002	0.000
60	Jg6Mt 5 06	0.004	0.009	0.001	0.013	0.022	0.002	0.000	0.000	0.006	0.014	0.001	0.002	0.000	0.000	0.000	0.000	0.000	0.003	0.024	0.011	0.012	0.017	0.001	0.003
61	Jg6Mt 5 07	0.000	0.001	0.001	0.011	0.015	0.001	0.000	0.000	0.003	0.003	0.000	0.000	0.000	0.000	0.000	0.000	0.001	0.003	0.023	0.011	0.012	0.019	0.001	0.000
62	Jg6Mt 5 08	0.012	0.032	0.001	0.018	0.021	0.001	0.004	0.000	0.000	0.001	0.001	0.002	0.000	0.000	0.000	0.000	0.000	0.003	0.027	0.012	0.015	0.030	0.000	0.003
63	Jg6Mt 5 09	0.053	0.085	0.010	0.049	0.033	0.004	0.016	0.002	0.025	0.086	0.005	0.010	0.005	0.017	0.002	0.003	0.001	0.053	0.028	0.069	0.071	0.180	0.004	0.036
64	Jg6Mt 5 10	0.543	0.649	0.088	0.515	0.109	0.035	0.117	0.014	0.154	0.766	0.036	0.092	0.016	0.125	0.022	0.003	0.193	0.763	0.029	0.749	0.713	1.4	0.326	0.297
65	Jg6Mt 5 11	0.001	0.002	0.002	0.021	0.012	0.000	0.000	0.000	0.003	0.003	0.001	0.000	0.000	0.000	0.001	0.000	0.010	0.007	0.032	0.014	0.012	0.023	0.000	0.018
66	Jg6Mt 5 12	0.001	0.001	0.003	0.017	0.018	0.000	0.000	0.000	0.000	0.001	0.000	0.000	0.000	0.000	0.000	0.000	0.000	0.000	0.028	0.063	0.070	0.111	0.001	0.003
67	Jg6Mt 5 13	0.001	0.001	0.002	0.007	0.016	0.000	0.000	0.000	0.000	0.001	0.000	0.000	0.000	0.000	0.000	0.000	0.000	0.005	0.025	0.015	0.013	0.019	0.000	0.000
68	Jg6Mt 6 01	0.002	0.002	0.002	0.015	0.022	0.000	0.000	0.000	0.003	0.003	0.000	0.000	0.001	0.000	0.001	0.000	0.001	0.003	0.029	0.019	0.016	0.021	0.000	0.001
69	Jg6Mt 6 02	0.001	0.003	0.003	0.009	0.013	0.001	0.005	0.000	0.000	0.007	0.001	0.002	0.001	0.003	0.003	0.000	0.003	0.021	0.028	0.034	0.039	0.080	0.004	0.010
70	Jg6Mt 6 03	0.064	0.080	0.006	0.064	0.026	0.004	0.005	0.004	0.006	0.034	0.001	0.002	0.001	0.010	0.000	0.002	0.001	0.014	0.025	0.078	0.089	0.210	0.001	0.040
71	Jg6Mt 6 04	0.014	0.025	0.003	0.023	0.008	0.002	0.000	0.001	0.015	0.040	0.002	0.004	0.001	0.003	0.000	0.000	0.009	0.047	0.026	0.871	0.819	1.8	0.013	0.112
72	Jg6Mt 6 05	0.024	0.042	0.004	0.046	0.029	0.000	0.016	0.002	0.012	0.063	0.003	0.010	0.000	0.000	0.001	0.000	0.009	0.108	0.027	0.558	0.502	1.1	0.031	0.160
73	Jg6Mt 6 06	0.005	0.012	0.004	0.020	0.025	0.001	0.021	0.000	0.003	0.045	0.000	0.005	0.002	0.006	0.004	0.000	0.050	0.111	0.037	0.936	0.805	1.8	0.016	0.169
74	Jg6Mt 6 07	0.023	0.052	0.003	0.029	0.026	0.007	0.010	0.001	0.009	0.052	0.001	0.014	0.003	0.013	0.000	0.000	0.013	0.062	0.030	0.333	0.273	0.556	0.014	0.134
75	Jg6Mt 6 08	0.122	0.276	0.031	0.283	0.106	0.049	0.241	0.031	0.220	1.2	0.042	0.137	0.014	0.086	0.013	0.003	0.023	0.087	0.363	5.8	5.8	13	0.029	0.278
76	Jg6Mt 6 09	0.017	0.032	0.005	0.013	0.016	0.002	0.000	0.006	0.003	0.008	0.000	0.005	0.000	0.000	0.000	0.002	0.002	0.000	0.028	0.021	0.015	0.037	0.000	0.019
77	Jg6Mt 6 10	0.002	0.004	0.001	0.012	0.031	0.000	0.006	0.002	0.014	0.029	0.000	0.003	0.002	0.004	0.000	0.000	0.003	0.029	0.049	0.886	0.905	2.0	0.031	0.051
78	Jg6Mt 6 11	0.002	0.004	0.001	0.012	0.023	0.000	0.000	0.000	0.000	0.002	0.001	0.000	0.000	0.000	0.000	0.000	0.000	0.000	0.022	0.032	0.029	0.057	0.005	0.007
79	Jg6Mt 6 12	0.608	0.553	0.091	0.427	0.179	0.051	0.200	0.018	0.160	1.0	0.044	0.141	0.020	0.174	0.028	0.002	0.306	1.4	0.051	1.5	1.3	2.7	0.243	0.417
80	Jg6Mt 7 01	1.7	3.2	0.406	1.7	0.294	0.051	0.246	0.020	0.130	0.747	0.023	0.114	0.016	0.119	0.026	0.005	0.457	1.8	0.300	5.1	5.3	12	0.891	0.352
81	Jg6Mt 7 02	1.5	1.9	0.269	1.2	0.173	0.051	0.195	0.019	0.140	0.685	0.029	0.080	0.006	0.074	0.014	0.005	0.370	1.9	0.091	2.2	2.0	4.6	0.741	0.425
82	Jg6Mt 7 03	0.501	0.681	0.092	0.340	0.019	0.012	0.027	0.004	0.055	0.188	0.010	0.034	0.003	0.066	0.005	0.000	0.163	0.690	0.069	2.0	1.9	4.1	0.224	0.147
83	Jg6Mt 7 04	4.5	11	1.6	6.8	1.1	0.182	0.727	0.085	0.323	1.3	0.043	0.110	0.009	0.075	0.018	0.000	0.548	6.4	0.473	8.4	8.5	19	2.2	0.715
84	Jg6Mt 7 05	0.840	1.2	0.152	0.619	0.073	0.037	0.170	0.014	0.101	0.849	0.028	0.073	0.011	0.146	0.009	0.003	0.347	2.5	0.202	4.5	4.1	8.9	0.449	0.685
85	Jg6Mt 7 06	0.206	0.248	0.033	0.203	0.092	0.022	0.083	0.019	0.111	0.549	0.025	0.075	0.011	0.097	0.016	0.002	0.166	1.1	0.201	3.7	3.3	7.0	0.131	0.696
86	Jg6Mt 8 01	0.007	0.021	0.003	0.029	0.032	0.000	0.000	0.000	0.010	0.036	0.001	0.000	0.000	0.007	0.000	0.000	0.005	0.057	0.030	0.736	0.659	1.5	0.011	0.151

#	Sample	La	Ce	Pr	Nd	Sm	Eu	Gd	Tb	Dy	Y	Ho	Er	Tm	Yb	Lu	Hf	Ta	W	^{204}Pb	^{206}Pb	^{207}Pb	^{208}Pb	Th	U
87	Jg6Mt 8 02	0.027	0.038	0.008	0.026	0.018	0.003	0.005	0.002	0.006	0.027	0.000	0.010	0.001	0.003	0.000	0.003	0.007	0.012	0.365	5.6	5.8	13	0.001	0.097
88	Jg6Mt 8 03	0.001	0.004	0.001	0.009	0.032	0.000	0.000	0.000	0.000	0.005	0.000	0.000	0.000	0.000	0.000	0.000	0.000	0.007	0.028	0.016	0.033	0.052	0.001	0.005
89	Jg6Mt 8 04	0.000	0.001	0.001	0.015	0.018	0.000	0.005	0.000	0.000	0.002	0.000	0.000	0.000	0.006	0.000	0.000	0.001	0.003	0.026	0.016	0.026	0.053	0.002	0.001
90	Jg6Mt 8 05	0.000	0.000	0.001	0.012	0.014	0.000	0.000	0.000	0.000	0.000	0.000	0.000	0.000	0.000	0.000	0.000	0.000	0.000	0.026	0.014	0.015	0.033	0.000	0.000
91	Jg6Mt 8 06	0.019	0.030	0.005	0.020	0.014	0.000	0.005	0.001	0.003	0.016	0.000	0.005	0.000	0.000	0.000	0.000	0.017	0.045	0.028	0.172	0.119	0.225	0.023	0.065
92	Jg6Mt 8 07	0.003	0.001	0.001	0.009	0.016	0.000	0.000	0.000	0.003	0.006	0.001	0.000	0.000	0.003	0.000	0.000	0.000	0.007	0.026	0.024	0.017	0.018	0.002	0.011
93	Jg6Mt 8 08	0.003	0.002	0.001	0.007	0.016	0.000	0.006	0.000	0.000	0.021	0.000	0.000	0.001	0.000	0.000	0.000	0.020	0.027	0.024	0.056	0.019	0.044	0.004	0.099
94	Jg6Mt 8 09	0.007	0.013	0.002	0.009	0.022	0.001	0.000	0.000	0.009	0.012	0.000	0.002	0.000	0.000	0.001	0.000	0.007	0.030	0.026	0.075	0.056	0.108	0.003	0.034
95	Jg6Mt 8 10	3.5	8.4	1.1	4.5	0.662	0.108	0.464	0.052	0.223	1.1	0.035	0.111	0.010	0.090	0.020	0.005	0.406	2.8	0.186	3.7	3.5	7.9	1.8	0.437
96	Jg6Mt 9 03	0.000	0.000	0.001	0.007	0.014	0.000	0.000	0.000	0.003	0.000	0.000	0.000	0.000	0.000	0.000	0.000	0.000	0.000	0.028	0.013	0.011	0.017	0.000	0.000
97	Jg6Mt 9 04	0.000	0.006	0.003	0.007	0.010	0.000	0.000	0.000	0.000	0.006	0.000	0.000	0.000	0.000	0.000	0.000	0.006	0.010	0.025	0.014	0.020	0.020	0.001	0.016
98	Jg6Mt 9 05	0.000	0.000	0.002	0.008	0.015	0.000	0.000	0.000	0.000	0.002	0.000	0.000	0.000	0.000	0.000	0.000	0.000	0.003	0.024	0.073	0.084	0.165	0.000	0.003
99	Jg6Mt 9 06	1.4	2.8	0.379	1.6	0.266	0.039	0.184	0.023	0.089	0.389	0.009	0.062	0.005	0.042	0.010	0.003	0.173	2.5	0.041	1.2	0.929	2.0	0.645	0.515
100	Jg6Mt 9 07	0.848	1.4	0.192	0.719	0.105	0.027	0.125	0.010	0.105	0.344	0.019	0.041	0.005	0.040	0.007	0.000	0.280	0.799	0.044	1.6	1.4	3.2	0.476	0.317
101	Jg6Mt 9 08	1.5	2.4	0.178	0.930	0.192	0.057	0.177	0.019	0.050	0.705	0.038	0.039	0.018	0.028	0.000	0.222	0.062	1.1	0.222	7.0	7.1	15	0.391	0.415
102	Jg6Mt 9 09	0.018	0.017	0.002	0.009	0.010	0.000	0.012	0.000	0.003	0.004	0.000	0.003	0.000	0.000	0.000	0.000	0.011	0.009	0.029	0.056	0.027	0.069	0.003	0.045
103	Jg7Mt 1 02	0.138	0.332	0.044	0.210	0.080	0.015	0.129	0.024	0.206	0.971	0.045	0.146	0.012	0.116	0.024	0.005	0.044	0.315	0.302	5.7	5.1	11	0.031	0.340
104	Jg7Mt 1 03	0.086	0.152	0.023	0.122	0.029	0.011	0.042	0.004	0.038	0.245	0.003	0.016	0.003	0.042	0.007	0.000	0.020	0.352	0.193	3.8	3.6	7.8	0.019	0.091
105	Jg7Mt 1 04	0.123	0.236	0.035	0.171	0.058	0.023	0.203	0.030	0.208	1.5	0.057	0.206	0.034	0.245	0.033	0.005	0.175	0.534	0.030	0.372	0.220	0.453	0.045	0.492
106	Jg7Mt 1 05	0.290	0.373	0.061	0.328	0.099	0.033	0.160	0.031	0.251	1.4	0.043	0.188	0.041	0.276	0.045	0.005	0.062	0.656	0.046	1.5	1.3	2.9	0.104	0.494
107	Jg7Mt 1 06	0.242	0.505	0.062	0.380	0.117	0.036	0.232	0.039	0.234	1.2	0.061	0.162	0.027	0.200	0.028	0.003	0.102	0.664	0.051	1.8	1.2	2.3	0.113	1.4
108	Jg7Mt 2 01	0.043	0.062	0.010	0.028	0.053	0.001	0.031	0.008	0.036	0.212	0.012	0.021	0.005	0.026	0.002	0.000	0.042	1.4	0.027	0.354	0.203	0.340	0.013	0.345
109	Jg7Mt 2 02	0.003	0.015	0.002	0.012	0.015	0.001	0.005	0.000	0.006	0.065	0.001	0.018	0.002	0.000	0.001	0.000	0.006	0.029	0.024	0.109	0.039	0.098	0.004	0.142
110	Jg7Mt 2 03	0.023	0.046	0.007	0.030	0.026	0.011	0.047	0.007	0.042	0.249	0.010	0.025	0.002	0.036	0.002	0.000	0.018	0.150	0.026	0.123	0.044	0.142	0.004	0.196
111	Jg7Mt 2 04	0.042	0.084	0.004	0.065	0.035	0.001	0.052	0.010	0.057	0.249	0.008	0.026	0.003	0.020	0.007	0.002	0.018	0.099	0.028	0.686	0.602	1.2	0.006	0.318
112	Jg7Mt 2 05	0.018	0.052	0.004	0.036	0.016	0.006	0.035	0.008	0.043	0.224	0.004	0.040	0.003	0.022	0.008	0.002	0.017	0.086	0.027	0.746	0.524	1.1	0.013	0.426
113	Jg7Mt 2 06	0.016	0.039	0.003	0.023	0.016	0.003	0.037	0.007	0.042	0.208	0.010	0.016	0.004	0.063	0.004	0.000	0.024	0.131	0.023	0.604	0.410	0.863	0.009	0.343
114	Jg7Mt 2 07	0.021	0.039	0.007	0.008	0.009	0.002	0.014	0.006	0.017	0.142	0.005	0.046	0.005	0.012	0.002	0.000	0.030	0.115	0.023	1.1	0.918	1.9	0.001	0.393
115	Jg7Mt 2 08	0.007	0.022	0.004	0.022	0.020	0.000	0.005	0.002	0.006	0.048	0.005	0.005	0.001	0.014	0.000	0.000	0.016	0.095	0.072	2.0	1.8	3.7	0.000	0.219
116	Jg7Mt 2 09	0.004	0.005	0.001	0.012	0.009	0.000	0.000	0.000	0.000	0.006	0.000	0.000	0.002	0.006	0.000	0.000	0.001	0.017	0.027	0.042	0.034	0.053	0.000	0.029
117	Jg7Mt 2 10	0.247	0.723	0.167	0.889	0.136	0.035	0.204	0.030	0.196	1.2	0.038	0.091	0.016	0.154	0.020	0.000	0.069	0.425	0.083	1.7	1.5	3.4	0.031	0.259
118	Jg7Mt 3 01	0.014	0.042	0.003	0.051	0.017	0.009	0.061	0.008	0.047	0.268	0.009	0.034	0.005	0.066	0.005	0.000	0.014	0.059	0.025	0.113	0.045	0.069	0.005	0.203
119	Jg7Mt 3 02	7.1	18	2.4	9.3	1.8	0.200	1.3	0.157	0.936	6.3	0.225	0.633	0.095	0.584	0.097	0.048	0.132	9.1	0.205	6.3	4.1	8.1	1.4	0.723
120	Jg7Mt 3 03	5.4	14	1.8	8.1	1.6	0.154	1.1	0.130	0.806	4.5	0.130	0.464	0.071	0.393	0.085	0.015	0.174	6.6	0.025	0.946	0.806	1.8	1.1	0.256
121	Jg7Mt 3 04	0.044	0.113	0.015	0.117	0.010	0.007	0.027	0.011	0.079	0.460	0.020	0.093	0.008	0.038	0.012	0.000	0.116	0.325	0.024	0.568	0.294	0.540	0.009	0.681
122	Jg7Mt 3 05	0.002	0.041	0.002	0.002	0.009	0.000	0.005	0.000	0.000	0.027	0.001	0.002	0.000	0.000	0.003	0.000	0.005	0.035	0.048	1.1	1.2	2.7	0.001	0.022
123	Jg7Mt 3 06	6.4	13	1.8	7.3	1.3	0.226	1.3	0.158	1.0	5.7	0.192	0.523	0.066	0.523	0.073	0.000	0.116	6.9	0.262	4.9	4.3	9.5	1.2	0.543
124	Jg7Mt 4 01	0.004	0.009	0.002	0.007	0.010	0.000	0.000	0.000	0.000	0.016	0.001	0.000	0.001	0.004	0.000	0.000	0.003	0.030	0.023	0.072	0.047	0.084	0.000	0.040
125	Jg7Mt 4 02	0.089	0.249	0.037	0.177	0.080	0.018	0.057	0.017	0.109	0.624	0.022	0.060	0.010	0.114	0.009	0.000	0.033	0.327	0.038	1.4	1.0	2.1	0.029	0.664
126	Jg7Mt 4 03	0.097	0.149	0.037	0.098	0.059	0.000	0.015	0.004	0.008	0.233	0.002	0.020	0.000	0.048	0.002	0.000	0.035	0.762	0.307	6.0	5.7	12	0.014	0.168

#	Sample	La	Ce	Pr	Nd	Sm	Eu	Gd	Tb	Dy	Y	Ho	Er	Tm	Yb	Lu	Hf	Ta	W	^{204}Pb	^{206}Pb	^{207}Pb	^{208}Pb	Th	U
127	Jg7Mt 4 04	0.349	0.615	0.088	0.510	0.111	0.012	0.091	0.022	0.150	0.719	0.034	0.092	0.012	0.067	0.012	0.003	0.071	0.347	0.182	3.6	3.1	6.6	0.050	0.419
128	Jg7Mt 4 05	0.481	1.2	0.147	0.903	0.142	0.039	0.143	0.014	0.107	0.580	0.020	0.054	0.007	0.066	0.008	0.005	0.058	5.2	0.585	9.9	10	22	0.068	0.217
129	Jg7Mt 4 06	0.113	0.252	0.033	0.209	0.060	0.004	0.046	0.001	0.036	0.150	0.008	0.016	0.002	0.000	0.003	0.000	0.008	0.262	0.121	2.4	2.1	4.8	0.005	0.133
130	Jg7Mt 4 07	0.037	0.055	0.011	0.026	0.015	0.002	0.015	0.003	0.021	0.089	0.007	0.002	0.001	0.016	0.001	0.000	0.005	0.326	0.024	0.451	0.386	0.822	0.001	0.068
131	Jg7Mt 4 08	0.003	0.043	0.008	0.013	0.009	0.000	0.001	0.008	0.000	0.176	0.006	0.018	0.015	0.051	0.009	0.000	0.012	0.101	0.035	0.282	0.269	0.506	0.009	0.186
132	Jg7Mt 4 09	0.645	1.2	0.175	0.323	0.130	0.025	0.096	0.007	0.032	0.156	0.004	0.032	0.002	0.009	0.002	0.002	0.011	0.225	0.024	0.692	0.612	1.4	0.013	0.047
133	Jg7Mt 4 10	0.078	0.178	0.036	0.150	0.080	0.066	0.287	0.054	0.505	2.2	0.075	0.245	0.049	0.466	0.073	0.025	0.285	1.1	0.023	0.864	0.664	1.5	0.026	0.318
134	Jg7Mt 4 11	0.001	0.003	0.002	0.023	0.020	0.001	0.006	0.000	0.011	0.013	0.000	0.003	0.003	0.000	0.002	0.000	0.000	0.009	0.027	0.030	0.023	0.082	0.000	0.006
135	Jg7Mt 5 01	0.016	0.021	0.002	0.016	0.022	0.002	0.000	0.003	0.022	0.114	0.006	0.017	0.002	0.031	0.005	0.000	0.021	0.073	0.028	0.112	0.048	0.085	0.006	0.148
136	Jg7Mt 5 02	0.007	0.021	0.006	0.030	0.016	0.008	0.019	0.005	0.039	0.190	0.004	0.022	0.002	0.037	0.006	0.000	0.032	0.089	0.027	0.361	0.204	0.396	0.008	0.342
137	Jg7Mt 5 03	0.244	0.445	0.073	0.285	0.101	0.018	0.156	0.014	0.069	0.698	0.027	0.061	0.012	0.082	0.015	0.000	0.037	0.249	0.028	0.643	0.378	0.838	0.041	0.524
138	Jg7Mt 5 04	4.1	10	1.4	5.9	1.0	0.098	0.707	0.071	0.535	3.3	0.133	0.346	0.042	0.294	0.049	0.002	0.100	5.2	0.028	0.812	0.652	1.6	0.806	0.177
139	Jg7Mt 5 05	0.015	0.031	0.003	0.006	0.021	0.000	0.017	0.003	0.026	0.130	0.005	0.041	0.003	0.029	0.003	0.000	0.005	0.032	0.022	0.051	0.022	0.030	0.003	0.073
140	Jg7Mt 5 06	0.012	0.049	0.010	0.037	0.043	0.009	0.104	0.014	0.120	0.571	0.022	0.103	0.012	0.107	0.014	0.002	0.014	0.158	0.024	0.203	0.052	0.055	0.013	0.377
141	Jg7Mt 5 07	2.5	5.3	0.700	3.2	0.451	0.078	0.512	0.046	0.319	2.2	0.084	0.257	0.017	0.263	0.038	0.000	0.077	4.3	0.049	1.4	1.2	2.8	0.325	0.221
142	Jg7Mt 5 08	0.008	0.025	0.003	0.009	0.022	0.009	0.039	0.005	0.054	0.254	0.024	0.024	0.006	0.030	0.003	0.000	0.013	0.064	0.026	0.193	0.068	0.099	0.002	0.290
143	Jg8Mt 2 rim 01	0.001	0.003	0.002	0.003	0.006	0.000	0.004	0.001	0.000	0.004	0.001	0.002	0.000	0.000	0.000	0.000	0.000	0.017	0.024	0.030	0.015	0.019	0.001	0.011
144	Jg8Mt 2 rim 02	0.000	0.000	0.002	0.007	0.028	0.000	0.004	0.000	0.000	0.000	0.000	0.000	0.000	0.000	0.000	0.000	0.000	0.000	0.023	0.013	0.014	0.024	0.000	0.000
145	Jg8Mt 2 rim 03	0.000	0.001	0.002	0.006	0.002	0.000	0.004	0.000	0.000	0.000	0.000	0.000	0.000	0.000	0.000	0.000	0.000	0.000	0.022	0.019	0.014	0.021	0.000	0.000
146	Jg8Mt 2 rim 04	0.000	0.001	0.002	0.007	0.015	0.000	0.001	0.000	0.000	0.000	0.000	0.000	0.000	0.000	0.000	0.000	0.000	0.004	0.023	0.014	0.012	0.019	0.006	0.001
147	Jg8Mt 2 rim 05	0.000	0.000	0.002	0.007	0.003	0.000	0.004	0.003	0.029	0.269	0.007	0.029	0.011	0.181	0.031	0.371	0.000	0.003	0.025	0.550	0.092	0.034	0.075	0.400
148	Jg8Mt 2 rim 06	0.001	0.001	0.001	0.007	0.010	0.000	0.001	0.000	0.003	0.003	0.000	0.000	0.000	0.000	0.003	0.000	0.002	0.000	0.029	0.023	0.026	0.036	0.000	0.006
149	Jg8Mt 2 rim 07	0.001	0.003	0.001	0.021	0.013	0.000	0.001	0.000	0.000	0.005	0.000	0.007	0.000	0.015	0.000	0.000	0.015	0.005	0.028	0.043	0.018	0.029	0.002	0.030
150	Jg8Mt 2 core 01	0.537	1.3	0.254	1.2	0.323	0.051	0.357	0.048	0.318	1.6	0.063	0.138	0.025	0.200	0.036	0.007	0.111	1.0	0.024	0.404	0.248	0.612	0.439	0.217
151	Jg8Mt 2 core 02	0.137	0.395	0.080	0.417	0.080	0.014	0.174	0.017	0.222	1.2	0.026	0.065	0.009	0.103	0.020	0.005	0.044	0.861	0.027	0.110	0.050	0.108	0.119	0.141
152	Jg8Mt 2 core 03	0.369	1.2	0.200	1.1	0.235	0.061	0.298	0.048	0.363	2.0	0.060	0.147	0.009	0.112	0.014	0.008	0.137	0.919	0.031	0.174	0.043	0.090	0.256	0.211
153	Jg8Mt 2 core 04	0.184	0.405	0.084	0.402	0.124	0.041	0.166	0.038	0.271	1.6	0.075	0.109	0.009	0.082	0.012	0.002	0.053	1.4	0.030	0.282	0.148	0.365	0.133	0.143
154	Jg8Mt 2 core 05	0.223	0.562	0.099	0.414	0.098	0.016	0.191	0.036	0.166	1.3	0.032	0.129	0.009	0.098	0.025	0.002	0.077	0.965	0.027	0.556	0.395	0.824	0.123	0.130
155	Jg8Mt 2 core 06	0.005	0.002	0.002	0.005	0.021	0.002	0.009	0.000	0.003	0.010	0.000	0.000	0.000	0.000	0.000	0.000	0.001	0.042	0.026	0.063	0.049	0.124	0.000	0.006
156	Jg8Mt 2 core 07	0.001	0.001	0.001	0.010	0.014	0.000	0.001	0.000	0.000	0.005	0.000	0.000	0.000	0.000	0.000	0.000	0.000	0.010	0.029	0.016	0.014	0.045	0.000	0.001
157	Jg8Mt 3 01	0.000	0.001	0.001	0.014	0.020	0.000	0.001	0.001	0.000	0.000	0.000	0.000	0.000	0.000	0.000	0.000	0.001	0.010	0.032	0.013	0.011	0.040	0.000	0.002
158	Jg8Mt 3 02	0.000	0.001	0.002	0.009	0.018	0.000	0.001	0.000	0.000	0.004	0.000	0.000	0.000	0.000	0.000	0.000	0.001	0.003	0.024	0.098	0.093	0.258	0.000	0.002
159	Jg8Mt 3 03	0.000	0.001	0.001	0.009	0.013	0.000	0.001	0.000	0.000	0.000	0.000	0.000	0.000	0.000	0.000	0.000	0.000	0.000	0.023	0.019	0.015	0.017	0.000	0.006
160	Jg8Mt 3 04	0.000	0.001	0.002	0.005	0.011	0.000	0.001	0.000	0.000	0.003	0.000	0.000	0.000	0.000	0.000	0.000	0.000	0.003	0.027	0.011	0.015	0.019	0.000	0.000
161	Jg8Mt 3 05	0.006	0.001	0.003	0.017	0.005	0.000	0.001	0.002	0.000	0.010	0.001	0.000	0.000	0.000	0.001	0.000	0.001	0.023	0.035	2.0	0.415	0.567	0.025	0.407
162	Jg8Mt 3 06	0.000	0.002	0.002	0.011	0.014	0.000	0.001	0.000	0.003	0.000	0.000	0.000	0.000	0.000	0.000	0.000	0.000	0.000	0.026	0.015	0.013	0.032	0.001	0.002
163	Jg8Mt 3 07	0.000	0.000	0.002	0.005	0.018	0.000	0.004	0.000	0.000	0.001	0.001	0.000	0.002	0.000	0.001	0.000	0.000	0.000	0.025	0.012	0.011	0.015	0.000	0.004
164	Jg8Mt 3 08	0.000	0.001	0.001	0.011	0.020	0.000	0.001	0.000	0.000	0.001	0.000	0.000	0.000	0.000	0.000	0.007	0.000	0.000	0.023	0.010	0.012	0.018	0.000	0.009
165	Jg8Mt 3 09	0.000	0.000	0.001	0.012	0.021	0.000	0.001	0.000	0.000	0.003	0.000	0.000	0.000	0.000	0.000	0.000	0.000	0.000	0.025	0.015	0.010	0.020	0.000	0.000
166	Jg8Mt 3 10	0.070	0.065	0.017	0.047	0.020	0.007	0.054	0.005	0.069	0.461	0.017	0.116	0.015	0.163	0.027	0.149	0.014	0.178	0.023	0.386	0.187	0.353	0.053	0.273

#	Sample	La	Ce	Pr	Nd	Sm	Eu	Gd	Tb	Dy	Y	Ho	Er	Tm	Yb	Lu	Hf	Ta	W	^{204}Pb	^{206}Pb	^{207}Pb	^{208}Pb	Th	U
167	Jg8Mt 3 11	0.005	0.012	0.001	0.013	0.019	0.000	0.001	0.000	0.006	0.006	0.000	0.002	0.000	0.000	0.000	0.000	0.000	0.007	0.024	0.567	0.125	0.198	0.005	0.072
168	Jg8Mt 3 12	0.000	0.000	0.001	0.005	0.010	0.000	0.001	0.000	0.000	0.001	0.000	0.000	0.000	0.000	0.000	0.000	0.000	0.047	0.024	0.136	0.122	0.249	0.000	0.001
169	Jg8Mt 3 13	0.000	0.002	0.001	0.005	0.006	0.001	0.001	0.000	0.000	0.001	0.000	0.000	0.000	0.000	0.000	0.000	0.000	0.000	0.026	0.013	0.012	0.018	0.000	0.000
170	Jg8Mt 3 14	0.001	0.000	0.001	0.005	0.009	0.000	0.001	0.000	0.000	0.001	0.000	0.000	0.000	0.000	0.009	0.000	0.000	0.000	0.025	0.067	0.014	0.019	0.000	0.001
171	Jg8Mt 3 15	0.000	0.000	0.001	0.005	0.012	0.001	0.001	0.000	0.000	0.000	0.000	0.000	0.000	0.000	0.000	0.000	0.000	0.000	0.026	0.011	0.013	0.037	0.000	0.001
172	Jg8Mt 3 16	0.000	0.000	0.003	0.007	0.012	0.000	0.001	0.000	0.000	0.001	0.000	0.000	0.000	0.000	0.000	0.000	0.000	0.014	0.025	0.011	0.012	0.026	0.000	0.000
173	Jg8Mt 3 17	0.001	0.008	0.002	0.015	0.015	0.000	0.001	0.001	0.000	0.002	0.001	0.000	0.000	0.000	0.000	0.000	0.001	0.080	0.030	0.464	0.366	0.730	0.007	0.140
174	Jg8Mt 4 01	0.085	0.114	0.021	0.117	0.020	0.009	0.069	0.011	0.046	0.369	0.017	0.063	0.012	0.047	0.004	0.000	0.001	0.263	0.200	3.5	3.3	7.2	0.011	0.287
175	Jg8Mt 4 02	0.000	0.000	0.000	0.005	0.013	0.000	0.001	0.001	0.000	0.001	0.000	0.002	0.000	0.000	0.000	0.000	0.000	0.000	0.023	0.019	0.012	0.025	0.000	0.001
176	Jg8Mt 4 03	0.001	0.000	0.002	0.007	0.016	0.000	0.001	0.000	0.000	0.024	0.001	0.000	0.003	0.020	0.000	0.000	0.000	0.001	0.033	0.017	0.024	0.024	0.004	0.010
177	Jg8Mt 4 04	0.127	0.166	0.018	0.111	0.030	0.012	0.034	0.007	0.043	0.333	0.017	0.045	0.007	0.040	0.008	0.000	0.019	0.393	0.471	7.5	7.4	16	0.016	0.171
178	Jg8Mt 4 05	0.072	0.083	0.004	0.069	0.026	0.003	0.036	0.005	0.080	0.441	0.017	0.054	0.004	0.060	0.005	0.000	0.009	0.292	0.262	4.5	4.2	8.9	0.015	0.105
179	Jg8Mt 4 06	0.000	0.000	0.002	0.006	0.023	0.001	0.003	0.001	0.003	0.003	0.001	0.000	0.000	0.000	0.000	0.000	0.002	0.003	0.026	0.022	0.033	0.051	0.000	0.008
180	Jg8Mt 4 07	0.000	0.000	0.001	0.003	0.012	0.000	0.003	0.000	0.000	0.001	0.000	0.005	0.000	0.000	0.001	0.000	0.000	0.000	0.022	0.013	0.012	0.019	0.001	0.000
181	Jg8Mt 4 08	0.002	0.007	0.001	0.019	0.012	0.002	0.004	0.003	0.000	0.014	0.000	0.000	0.000	0.006	0.000	0.000	0.003	0.006	0.027	0.020	0.013	0.036	0.006	0.031
182	Jg8Mt 4 09	0.001	0.000	0.001	0.007	0.011	0.000	0.005	0.000	0.000	0.006	0.000	0.000	0.000	0.000	0.000	0.000	0.002	0.011	0.024	0.035	0.044	0.069	0.000	0.008
183	Jg8Mt 4 10	0.000	0.000	0.001	0.006	0.011	0.000	0.005	0.000	0.000	0.001	0.000	0.000	0.000	0.000	0.000	0.000	0.000	0.000	0.025	0.014	0.012	0.019	0.000	0.001
184	Jg8Mt 4 11	0.011	0.019	0.002	0.021	0.020	0.000	0.005	0.000	0.000	0.016	0.000	0.007	0.001	0.003	0.001	0.000	0.002	0.018	0.025	0.065	0.057	0.118	0.004	0.034
185	Jg8Mt 5 01	0.000	0.000	0.002	0.007	0.007	0.000	0.002	0.000	0.000	0.003	0.000	0.002	0.000	0.003	0.000	0.000	0.000	0.000	0.024	0.012	0.015	0.028	0.000	0.005
186	Jg8Mt 5 02	0.013	0.005	0.003	0.007	0.012	0.001	0.002	0.001	0.012	0.055	0.005	0.004	0.003	0.013	0.002	0.000	0.007	0.029	0.022	0.019	0.014	0.033	0.001	0.011
187	Jg8Mt 5 03	0.349	0.710	0.173	0.672	0.160	0.033	0.226	0.038	0.221	1.1	0.038	0.148	0.027	0.230	0.038	0.000	0.048	0.687	0.022	0.234	0.190	0.385	0.192	0.178
188	Jg8Mt 5 04	0.312	0.554	0.115	0.680	0.132	0.037	0.238	0.037	0.362	1.5	0.041	0.111	0.019	0.165	0.029	0.002	0.048	2.7	0.027	1.1	0.895	1.8	0.201	0.209
189	Jg8Mt 5 05	0.227	0.249	0.040	0.224	0.127	0.041	0.128	0.026	0.179	1.4	0.051	0.186	0.027	0.253	0.043	0.005	0.115	0.713	0.131	2.6	2.5	5.3	0.067	0.298
190	Jg8Mt 5 06	0.556	1.0	0.130	0.609	0.165	0.037	0.227	0.032	0.230	1.2	0.046	0.161	0.034	0.243	0.039	0.008	0.158	2.5	0.154	3.2	3.1	6.6	0.268	0.342
191	Jg8Mt 5 07	0.143	0.146	0.028	0.106	0.050	0.027	0.155	0.017	0.174	1.1	0.049	0.163	0.030	0.144	0.031	0.005	0.129	0.693	0.775	12	12	25	0.032	0.360
192	Jg8Mt 5 08	0.168	0.188	0.033	0.156	0.106	0.024	0.080	0.025	0.235	1.2	0.044	0.193	0.025	0.199	0.030	0.000	0.121	0.905	0.600	9.3	9.1	19	0.029	0.283
193	Jg8Mt 5 09	0.461	0.733	0.140	0.575	0.181	0.035	0.197	0.039	0.249	0.959	0.031	0.151	0.019	0.245	0.040	0.018	0.160	0.921	0.079	1.7	1.6	3.4	0.359	0.278
194	Jg8Mt 5 10	0.359	0.651	0.078	0.443	0.195	0.016	0.195	0.033	0.248	1.2	0.033	0.104	0.007	0.050	0.015	0.002	0.078	2.7	0.058	1.3	1.1	2.3	0.221	0.264
195	Jg8Mt 5 11	0.241	0.310	0.046	0.300	0.086	0.040	0.239	0.041	0.271	1.3	0.048	0.114	0.019	0.142	0.026	0.002	0.056	1.1	0.217	4.4	4.2	9.0	0.148	0.230
196	Jg8Mt 6 01	0.000	0.001	0.001	0.006	0.023	0.000	0.002	0.000	0.000	0.007	0.003	0.003	0.000	0.000	0.000	0.000	0.001	0.004	0.026	0.016	0.013	0.027	0.000	0.007
197	Jg8Mt 6 02	0.146	0.100	0.017	0.102	0.041	0.011	0.140	0.024	0.090	0.675	0.019	0.089	0.011	0.141	0.015	0.000	0.031	0.468	0.033	0.879	0.857	1.6	0.024	0.189
198	Jg8Mt 6 03	0.292	0.725	0.169	0.833	0.232	0.030	0.259	0.042	0.297	1.6	0.057	0.113	0.013	0.102	0.019	0.002	0.039	0.653	0.033	0.917	0.812	1.6	0.220	0.158
199	Jg8Mt 6 04	0.258	0.592	0.094	0.694	0.239	0.035	0.254	0.035	0.294	1.8	0.055	0.151	0.014	0.101	0.018	0.026	0.044	1.8	0.025	0.321	0.182	0.365	0.193	0.233
200	Jg8Mt 6 05	0.218	0.594	0.082	0.463	0.154	0.029	0.230	0.030	0.260	1.6	0.059	0.128	0.008	0.075	0.012	0.005	0.032	1.2	0.019	0.385	0.254	0.494	0.171	0.165
201	Jg8Mt 6 06	0.913	2.8	0.368	1.7	0.313	0.063	0.223	0.049	0.232	1.3	0.048	0.092	0.019	0.171	0.014	0.000	0.039	2.8	0.159	3.2	3.0	6.5	0.523	0.375
202	Jg8Mt 6 07	0.135	0.181	0.024	0.143	0.091	0.016	0.103	0.020	0.162	0.874	0.029	0.079	0.013	0.089	0.013	0.002	0.029	1.3	0.071	2.0	2.0	4.5	0.079	0.149
203	Jg8Mt 6 08	0.000	0.005	0.001	0.008	0.011	0.001	0.003	0.001	0.003	0.011	0.001	0.005	0.001	0.000	0.002	0.000	0.004	0.109	0.026	0.047	0.044	0.118	0.002	0.009
204	Jg8Mt 6 09	0.001	0.000	0.001	0.008	0.010	0.001	0.002	0.000	0.000	0.000	0.000	0.000	0.000	0.003	0.000	0.000	0.000	0.045	0.026	0.517	0.390	0.729	0.000	0.005
205	Jg8Mt 6 10	0.003	0.000	0.001	0.010	0.022	0.000	0.002	0.000	0.000	0.011	0.000	0.006	0.000	0.000	0.000	0.000	0.002	0.324	0.033	0.374	0.380	0.795	0.000	0.038
206	Jg9bMt1rim 01	0.773	1.4	0.158	0.849	0.233	0.037	0.215	0.033	0.223	1.4	0.051	0.147	0.017	0.166	0.029	0.000	0.158	0.955	0.224	4.1	3.9	8.6	0.221	0.388

#	Sample	La	Ce	Pr	Nd	Sm	Eu	Gd	Tb	Dy	Y	Ho	Er	Tm	Yb	Lu	Hf	Ta	W	^{204}Pb	^{206}Pb	^{207}Pb	^{208}Pb	Th	U
207	Jg9bMt1rim 02	0.034	0.051	0.003	0.039	0.008	0.004	0.026	0.004	0.031	0.148	0.005	0.024	0.000	0.000	0.001	0.000	0.075	0.068	0.011	0.443	0.403	0.798	0.028	0.223
208	Jg9bMt1rim 03	0.852	1.0	0.199	0.802	0.196	0.044	0.297	0.028	0.285	1.7	0.061	0.263	0.028	0.244	0.033	0.010	0.149	1.0	0.429	6.1	6.2	13	0.227	0.297
209	Jg9bMt1rim 04	1.0	1.9	0.350	1.5	0.288	0.082	0.358	0.062	0.301	1.7	0.057	0.198	0.023	0.137	0.031	0.005	0.277	4.9	52	725	800	1777	0.421	1.1
210	Jg9bMt1rim 05	1.8	5.8	0.818	3.7	0.722	0.119	0.574	0.086	0.510	2.3	0.086	0.224	0.019	0.113	0.019	0.011	0.382	4.8	0.157	2.7	2.2	5.3	0.965	0.406
211	Jg9bMt1rim 06	0.935	2.0	0.339	1.5	0.293	0.056	0.331	0.039	0.318	1.5	0.060	0.155	0.029	0.197	0.036	0.002	0.277	1.7	0.316	4.0	4.3	9.8	0.380	0.533
212	Jg9bMt1rim 07	0.917	1.8	0.316	1.2	0.237	0.061	0.296	0.052	0.255	1.8	0.057	0.171	0.045	0.302	0.039	0.005	0.484	1.3	0.106	1.8	1.9	3.9	0.436	0.366
213	Jg9bMt1rim 08	0.925	2.0	0.288	1.4	0.289	0.033	0.244	0.036	0.195	1.0	0.044	0.125	0.015	0.095	0.018	0.000	0.366	4.1	0.042	0.525	0.426	0.800	0.433	0.265
214	Jg9bMt1rim 09	0.522	1.2	0.192	0.898	0.145	0.042	0.177	0.022	0.161	0.985	0.037	0.094	0.011	0.105	0.020	0.011	0.325	0.903	0.029	0.437	0.337	0.817	0.250	0.233
215	Jg9bMt1rim 10	0.023	0.028	0.004	0.057	0.017	0.001	0.026	0.002	0.012	0.090	0.001	0.010	0.006	0.037	0.000	0.000	0.003	0.029	0.013	0.047	0.056	0.101	0.005	0.014
216	Jg9bMt1rim 11	0.013	0.027	0.001	0.019	0.008	0.001	0.012	0.001	0.007	0.039	0.005	0.004	0.001	0.005	0.001	0.000	0.007	0.047	0.051	1.0	1.0	2.4	0.003	0.053
217	Jg9bMt1rim 12	0.017	0.022	0.004	0.022	0.004	0.006	0.037	0.003	0.009	0.039	0.008	0.011	0.004	0.005	0.005	0.000	0.013	0.054	0.038	0.513	0.513	1.2	0.005	0.045
218	Jg9bMt1rim 13	0.118	0.204	0.051	0.226	0.022	0.011	0.053	0.008	0.061	0.317	0.010	0.040	0.005	0.037	0.016	0.004	0.036	0.216	0.006	0.134	0.129	0.301	0.040	0.073
219	Jg9bMt1rim 14	0.035	0.106	0.010	0.080	0.016	0.005	0.029	0.004	0.046	0.217	0.008	0.021	0.003	0.019	0.006	0.000	0.034	0.297	0.070	1.3	1.3	2.9	0.030	0.064
220	Jg9bMt1rim 15	0.106	0.168	0.037	0.146	0.016	0.013	0.024	0.006	0.033	0.212	0.004	0.018	0.002	0.021	0.008	0.000	0.035	1.4	0.102	1.4	1.6	3.6	0.059	0.081
221	Jg9bMt1core 01	0.039	0.095	0.014	0.055	0.016	0.006	0.042	0.016	0.036	0.213	0.009	0.019	0.009	0.029	0.006	0.000	0.030	0.205	0.009	0.266	0.259	0.591	0.024	0.074
222	Jg9bMt1core 02	0.210	0.387	0.049	0.224	0.043	0.015	0.082	0.008	0.093	0.342	0.015	0.045	0.005	0.043	0.007	0.002	0.061	0.661	0.080	1.3	1.4	2.9	0.066	0.119
223	Jg9bMt1core 03	0.269	0.427	0.046	0.288	0.050	0.006	0.066	0.010	0.091	0.462	0.020	0.030	0.007	0.048	0.011	0.008	0.060	0.489	34	476	514	1183	0.080	0.203
224	Jg9bMt1core 04	0.099	0.142	0.031	0.118	0.029	0.012	0.079	0.009	0.043	0.371	0.008	0.067	0.008	0.050	0.008	0.002	0.020	0.211	0.612	8.9	9.3	20	0.023	0.094
225	Jg9bMt2 01	0.004	0.004	0.001	0.007	0.000	0.000	0.003	0.000	0.000	0.009	0.000	0.004	0.000	0.000	0.000	0.002	0.008	0.003	0.006	0.023	0.030	0.050	0.001	0.009
226	Jg9bMt2 02	0.002	0.006	0.004	0.000	0.000	0.000	0.001	0.000	0.003	0.026	0.000	0.002	0.005	0.003	0.003	0.003	0.008	0.000	0.005	0.038	0.043	0.051	0.000	0.004
227	Jg9bMt3 03	0.007	0.029	0.000	0.055	0.014	0.002	0.013	0.005	0.028	0.087	0.002	0.009	0.001	0.000	0.001	0.003	0.006	0.049	0.010	0.061	0.059	0.138	0.001	0.025
228	Jg9bMt3 04	0.158	0.249	0.034	0.203	0.065	0.010	0.065	0.012	0.094	0.502	0.019	0.047	0.005	0.054	0.004	0.003	0.080	0.230	0.304	4.0	3.9	12	0.034	0.099
229	Jg9bMt4rim 17	0.005	0.007	0.002	0.014	0.000	0.000	0.003	0.000	0.007	0.024	0.004	0.004	0.000	0.000	0.000	0.000	0.043	0.023	0.006	0.175	0.135	0.317	0.000	0.071
230	Jg9bMt4rim 18	0.002	0.003	0.002	0.011	0.000	0.000	0.001	0.000	0.000	0.003	0.000	0.000	0.000	0.002	0.000	0.000	0.001	0.023	0.014	0.090	0.079	0.165	0.000	0.024
231	Jg9bMt4rim 19	0.017	0.042	0.007	0.045	0.000	0.003	0.017	0.002	0.017	0.113	0.005	0.008	0.003	0.015	0.001	0.000	0.009	0.040	0.007	0.227	0.216	0.466	0.008	0.069
232	Jg9bMt4rim 20	0.023	0.028	0.003	0.029	0.000	0.003	0.027	0.006	0.006	0.105	0.001	0.000	0.004	0.011	0.002	0.000	0.009	0.054	0.003	0.288	0.263	0.545	0.013	0.135
233	Jg9bMt4rim 21	0.032	0.068	0.012	0.097	0.049	0.004	0.033	0.004	0.031	0.129	0.003	0.015	0.002	0.013	0.006	0.000	0.028	0.109	0.048	0.648	0.616	1.4	0.010	0.037
234	Jg9bMt4core 05	0.034	0.097	0.021	0.047	0.007	0.005	0.001	0.005	0.020	0.075	0.004	0.005	0.001	0.007	0.003	0.000	0.011	0.052	0.007	0.033	0.021	0.056	0.007	0.016
235	Jg9bMt4core 06	0.091	0.241	0.046	0.245	0.020	0.005	0.050	0.008	0.052	0.251	0.013	0.025	0.000	0.026	0.006	0.002	0.019	0.202	0.002	0.287	0.297	0.636	0.017	0.034
236	Jg9bMt4core 07	0.142	0.335	0.053	0.352	0.065	0.008	0.077	0.008	0.049	0.262	0.005	0.018	0.001	0.015	0.007	0.000	0.029	0.231	0.009	0.235	0.231	0.506	0.026	0.041
237	Jg9bMt5rim 23	0.054	0.075	0.019	0.066	0.029	0.009	0.042	0.004	0.019	0.181	0.008	0.027	0.002	0.005	0.003	0.000	0.025	0.077	0.009	0.115	0.067	0.143	0.008	0.080
238	Jg9bMt5rim 24	0.576	0.942	0.150	0.752	0.144	0.034	0.181	0.030	0.211	1.2	0.050	0.113	0.017	0.075	0.008	0.000	0.106	1.6	1.0	13	13	26	0.100	0.208
239	Jg9bMt5rim 25	0.554	1.5	0.218	1.1	0.203	0.037	0.166	0.036	0.227	1.2	0.056	0.134	0.011	0.103	0.012	0.000	0.094	0.456	0.073	0.936	0.929	2.1	0.174	0.186
240	Jg9bMt5rim 26	0.354	0.554	0.137	0.625	0.183	0.027	0.231	0.031	0.210	1.3	0.045	0.154	0.010	0.076	0.013	0.002	0.135	0.583	0.088	1.6	1.9	3.7	0.117	0.242
241	Jg9bMt5rim 27	0.283	0.336	0.067	0.331	0.072	0.026	0.138	0.035	0.176	0.829	0.026	0.085	0.013	0.061	0.010	0.004	0.135	0.577	0.064	0.911	0.953	2.0	0.064	0.139
242	Jg9bMt5rim 28	0.549	1.4	0.211	1.1	0.309	0.071	0.299	0.044	0.197	1.0	0.044	0.077	0.017	0.087	0.012	0.006	0.042	0.559	0.441	7.5	7.2	17	0.177	0.264
243	Jg9bMt5rim 29	0.295	0.456	0.063	0.369	0.151	0.027	0.145	0.028	0.189	1.1	0.043	0.149	0.022	0.181	0.026	0.032	0.070	0.632	0.308	5.3	4.7	11	0.071	0.345
244	Jg9bMt5rim 30	0.168	0.222	0.052	0.193	0.086	0.022	0.125	0.024	0.101	0.564	0.020	0.066	0.009	0.055	0.010	0.000	0.027	0.281	0.244	4.5	4.3	9.7	0.017	0.137
245	Jg9bMt5rim 31	0.215	0.424	0.063	0.331	0.209	0.031	0.179	0.039	0.211	1.1	0.047	0.152	0.016	0.074	0.017	0.002	0.034	0.716	1.1	16	16	36	0.069	0.325
246	Jg9bMt5rim 32	2.5	6.3	0.839	4.1	0.683	0.141	0.792	0.111	0.536	2.4	0.093	0.275	0.027	0.255	0.036	0.008	0.125	2.4	0.265	4.8	4.2	9.3	0.827	0.626

#	Sample	La	Ce	Pr	Nd	Sm	Eu	Gd	Tb	Dy	Y	Ho	Er	Tm	Yb	Lu	Hf	Ta	W	^{204}Pb	^{206}Pb	^{207}Pb	^{208}Pb	Th	U
247	Jg9bMt5rim 33	1.9	2.8	0.334	1.4	0.257	0.080	0.361	0.068	0.338	1.8	0.066	0.182	0.021	0.118	0.033	0.003	0.259	2.5	0.310	5.2	4.8	11	0.316	0.329
248	Jg9bMt5rim 34	4.3	6.6	0.986	4.6	0.603	0.105	0.639	0.079	0.340	1.6	0.061	0.155	0.015	0.094	0.015	0.000	0.094	4.5	0.668	11	11	24	1.1	0.214
249	Jg9bMt5rim 35	4.5	6.1	0.682	2.7	0.456	0.090	0.438	0.044	0.268	1.5	0.068	0.120	0.016	0.119	0.020	0.017	0.114	5.6	1.5	23	24	54	0.223	0.312
250	Jg9bMt5rim 36	1.3	1.8	0.246	0.988	0.247	0.069	0.340	0.072	0.342	1.8	0.072	0.148	0.021	0.135	0.023	0.003	0.223	3.4	2.4	35	36	81	0.372	0.439
251	Jg9bMt5rim 37	0.994	1.1	0.205	0.725	0.101	0.041	0.257	0.048	0.273	1.2	0.040	0.081	0.011	0.089	0.014	0.015	0.213	5.4	6.7	94	99	227	0.186	0.305
252	Jg9bMt5rim 38	2.0	4.1	0.619	2.6	0.486	0.098	0.409	0.064	0.441	2.3	0.100	0.269	0.023	0.130	0.032	0.000	0.247	3.2	1.8	26	26	59	0.543	0.484
253	Jg9bMt5core 08	2.2	6.6	0.967	4.7	0.643	0.123	0.683	0.096	0.603	2.9	0.124	0.276	0.021	0.157	0.019	0.002	0.250	1.9	0.720	11	11	25	0.536	0.320
254	Jg9bMt5core 09	0.720	0.764	0.140	0.598	0.127	0.052	0.208	0.037	0.258	1.2	0.039	0.110	0.007	0.089	0.012	0.002	0.153	1.1	1.0	15	16	35	0.124	0.258
255	Jg9bMt5core 10	8.8	34	4.7	21	4.2	0.836	3.4	0.317	1.4	4.5	0.188	0.328	0.034	0.147	0.026	0.011	0.175	12	3.0	45	46	105	3.9	0.898
256	Jg9bMt5core 11	112	220	24	88	12	1.8	6.6	0.544	2.1	5.2	0.228	0.408	0.027	0.085	0.016	0.000	0.076	4.1	3.6	53	56	129	0.866	0.477
257	Jg9bMt5core 12	0.785	1.8	0.217	1.1	0.219	0.036	0.209	0.020	0.106	0.498	0.024	0.060	0.005	0.037	0.011	0.000	0.039	1.0	0.714	11	11	24	0.224	0.534
258	Jg9bMt5core 13	0.119	0.296	0.026	0.183	0.039	0.009	0.053	0.006	0.067	0.228	0.012	0.024	0.003	0.015	0.003	0.000	0.034	0.263	0.223	3.8	3.8	8.4	0.029	0.342
259	Jg9bMt5core 14	0.214	0.422	0.058	0.278	0.130	0.035	0.201	0.028	0.260	1.1	0.035	0.159	0.017	0.138	0.024	0.000	0.060	0.824	0.166	2.9	2.6	5.6	0.063	0.470
260	Jg9bMt5core 15	0.195	0.379	0.041	0.253	0.069	0.014	0.113	0.020	0.105	0.592	0.023	0.070	0.012	0.092	0.017	0.000	0.033	0.451	1.4	21	21	49	0.044	0.652
	Mean (n=260)	1.0	2.3	0.325	1.5	0.293	0.041	0.227	0.024	0.130	0.627	0.024	0.066	0.008	0.062	0.011	0.006	0.077	0.877	0.523	7.6	8.0	18	0.202	0.217
	SD	7.2	16	2.1	10	2.1	0.199	1.3	0.091	0.314	1.1	0.043	0.098	0.012	0.086	0.015	0.029	0.116	1.6	3.8	53	58	131	0.584	0.226
	Median	0.043	0.087	0.015	0.065	0.029	0.007	0.032	0.006	0.038	0.213	0.008	0.026	0.004	0.031	0.005	0.000	0.024	0.202	0.029	0.582	0.420	0.851	0.023	0.153
	Max	112	220	24	142	32	2.6	20	1.3	4.0	11	0.459	0.780	0.095	0.584	0.097	0.371	0.548	12	52	725	800	1777	7.2	1.4
	Min	0.000	0.000	0.000	0.000	0.000	0.000	0.000	0.000	0.000	0.000	0.000	0.000	0.000	0.000	0.000	0.000	0.000	0.000	0.000	0.010	0.010	0.015	0.000	0.000

SD Table 1c. LA-ICP-MS trace element data for amphibole and apatite (complete raw dataset, concentrations in ppm; calculated from measurement of given isotope, except for the 4 Pb isotopes)

**Note* : data reported here are raw data; in red analyses shown in ESM Fig 4.

#	Amphibole	Mg	Al	Si	P	Ca	Sc	Ti	V	Cr	Mn	Co	Ni	Cu	Zn	Ga	As	Sr	Zr	Nb	Mo	Sn	Sb	Ba
1	Jg3a-Amph1 - 01	114230	8394	263198	16	89464	8.7	252	45	11	990	35	2120	0.589	888	5.0	0.796	5.0	0.695	0.176	0.021	7.4	0.039	4.0
2	Jg3a-Amph1 - 02	116269	5486	267883	18	90150	6.7	140	55	14	984	29	2162	0.762	764	3.6	0.859	5.3	6.2	0.120	1.5	6.6	0.044	1.4
3	Jg3a-Amph1 - 03	116397	6138	270159	63	87511	9.8	105	55	13	919	41	2061	1.1	1146	3.5	0.928	3.4	23	0.103	1.1	8.3	0.043	0.221
4	Jg3a-Amph1 - 04	115874	5952	265703	140	89069	13	110	67	20	944	32	2147	0.698	956	4.2	1.2	4.7	14	0.150	1.1	9.0	0.039	2.5
5	Jg3a-Amph1 - 05	110356	5673	256822	137	85536	10	99	91	22	997	27	2180	0.895	599	5.9	1.2	3.2	8.3	0.255	1.3	10	0.044	2.3
6	Jg3a-Amph1 - 06	115147	6247	270422	38	86709	9.1	112	50	14	981	39	2082	0.822	1043	3.6	0.799	4.8	27	0.125	0.197	7.2	0.035	0.342
7	Jg3a-Amph1 - 07	115940	5612	266522	84	90688	10	89	67	21	1014	26	2175	0.634	635	4.1	1.0	3.3	36	0.121	3.3	8.9	0.030	2.3
8	Jg3a-Amph1 - 08	116013	5231	266043	122	89108	9.8	95	64	21	1001	29	2105	0.779	711	4.1	1.3	4.2	71	0.164	2.9	7.3	0.039	2.6
9	Jg3a-Amp2 - 01	113535	29560	242605	17	75890	8.8	533	38	14	983	45	2053	3.4	1040	19	1.6	12	2.0	0.636	0.044	11	0.042	3.4
10	Jg3a-Amp2 - 02	112978	15952	260163	16	82322	12	397	37	12	1128	46	1731	5.2	1318	7.8	0.723	4.4	2.8	0.487	0.037	12	0.084	6.6
11	Jg3a-Amp2 - 03	113929	10404	264404	61	86189	12	295	49	11	1157	38	1981	1.1	956	5.3	0.729	4.0	6.4	0.279	0.007	9.8	0.026	0.319
12	Jg3a-Amp2 - 04	117400	6226	267855	71	88293	11	202	54	12	935	41	2005	1.9	1129	3.4	0.870	4.2	18	0.185	0.183	8.4	0.039	0.391
13	Jg3a-Amp2 - 05	111639	13480	261725	104	84496	13	318	37	9.5	1144	44	1675	0.997	1149	6.1	1.3	5.6	8.1	0.452	0.104	11	0.060	2.9
14	Jg3a-Amp3 - 06	115633	6241	267466	146	90082	9.0	156	59	13	1025	29	2176	0.522	756	4.6	0.835	7.2	65	0.093	0.987	8.6	0.035	11
15	Jg3a-Amp3 - 07	118173	7396	264123	29	89549	15	143	47	9.5	1092	38	2032	0.692	1125	3.6	1.2	4.7	35	0.165	0.075	6.9	0.026	0.218
16	Jg3a-Amp3 - 08	115703	6950	266704	59	88644	61	80	85	14	928	34	2263	0.842	1045	4.5	0.774	5.4	19	0.120	2.0	12	0.056	2.2
17	Jg3a-Amp3 - 09	116547	6281	265987	28	90751	29	71	77	15	905	30	2269	0.978	990	4.2	0.890	7.6	11	0.081	0.720	11	0.057	7.6
18	Jg3a-Amp3 - 10	116403	6110	268744	72	88556	9.8	130	60	13	923	33	2117	0.762	1001	3.8	0.535	4.3	19	0.111	0.972	8.0	0.025	0.206
19	Jg3a-Amp3 - 11	115931	6698	268026	15	89234	6.8	245	60	9.0	1007	33	2115	23	910	4.2	0.824	4.4	1.3	0.152	0.041	8.1	0.025	0.107
20	Jg3a-Amp3 - 12	112564	20819	256216	16	80602	12	382	39	9.5	1010	46	1809	1.4	1157	9.7	1.2	5.5	2.1	0.480	0.038	12	0.033	4.5
21	Jg3a-Amp4 - 13	113974	14628	262455	16	81843	24	288	42	11	1118	44	1776	1.3	1711	7.3	1.3	4.3	0.987	0.352	0.244	11	0.046	2.6
22	Jg3a-Amp4 - 14	114832	19994	255909	16	80333	12	356	50	12	975	47	1945	0.745	1251	11	0.913	4.4	4.3	0.440	0.309	11	0.058	5.6
23	Jg3a-Amp4 - 15	106393	16959	250211	33	71134	9.3	338	50	23	1105	46	1870	1.0	1135	11	0.933	4.0	5.2	0.515	0.022	11	0.065	2.8
24	Jg3a-Amp4 - 16	117594	7602	267484	21	88342	10	182	37	8.3	943	39	2087	0.774	1073	3.6	1.1	5.1	2.4	0.163	0.270	6.4	0.033	0.179
25	Jg3a-Amp4 - 17	106976	13123	255463	19	80277	15	369	40	10	1128	40	1623	11983	1142	5.6	1.2	5.5	0.994	0.385	0.029	12	0.177	0.489
26	Jg3a-Amp4 - 18	107586	29286	245801	22	76305	19	591	48	10	1141	50	1700	57	1307	12	0.936	4.4	1.7	0.677	0.044	15	0.094	1.7
27	Jg3a-Amp5 - 19	101414	15289	228933	18	72110	8.0	365	75	36	845	38	1879	2.0	1001	12	0.597	5.2	4.3	0.446	0.305	7.6	0.062	11
28	Jg3a-Amp5 - 20	117555	4993	266858	16	89974	9.1	70	58	11	978	27	2199	0.795	671	3.9	0.639	3.9	165	0.082	0.878	6.8	0.028	0.280
29	Jg3a-Amp5 - 21	110388	6772	257032	48	80500	24	108	94	14	961	45	2632	187	1489	6.4	1.0	3.6	30	0.135	0.369	12	0.057	1.4
30	Jg3a-Amp5 - 22	115845	7750	265950	17	88041	86	114	91	11	872	38	2287	0.577	1171	4.5	1.0	5.1	5.8	0.154	0.458	11	0.029	7.2
31	Jg3a-Amp6 - 24	103836	26523	253103	18	82419	7.0	734	45	12	1018	50	1347	1.4	1348	10	0.663	5.1	2.4	1.3	0.014	18	0.069	4.3
32	Jg3a-Amp6 - 25	102796	27781	253210	19	81121	17	656	44	7.7	1030	55	1205	0.664	1418	9.9	1.3	5.0	2.2	1.0	0.029	19	0.089	3.8
33	Jg3a-Amp6 - 26	118456	6739	267697	16	85059	21	112	56	3.0	1181	48	1531	3.4	915	3.2	1.2	5.4	0.676	0.246	0.031	10	0.058	4.4
34	Jg3a-Amp6 - 27	117478	7518	267105	17	87890	38	153	95	2.5	932	41	1961	1.3	1079	3.7	0.706	4.5	0.479	0.166	0.035	12	0.029	1.9

#	Amphibole	Mg	Al	Si	P	Ca	Sc	Ti	V	Cr	Mn	Co	Ni	Cu	Zn	Ga	As	Sr	Zr	Nb	Mo	Sn	Sb	Ba
35	Jg3a-Amp6 - 28	117904	6629	267419	16	85296	14	110	65	2.1	883	35	2383	0.678	1080	4.7	0.823	4.5	0.359	0.084	0.020	12	0.045	0.718
36	Jg3a-Amp6 - 29	115577	6898	266848	15	88561	29	109	81	6.8	917	30	2273	0.527	966	5.0	1.2	3.7	0.824	0.093	0.003	11	0.022	1.4
37	Jg3a-Amp6 - 30	117887	5410	268894	16	88126	16	93	64	6.7	833	34	2214	0.655	1173	3.5	1.2	4.5	0.527	0.127	0.011	8.2	0.023	0.393
38	Jg3a-Amp6 - 31	120654	4744	270116	16	86163	8.4	79	48	5.5	896	45	2091	0.724	1285	2.4	0.933	4.3	0.311	0.110	0.037	6.3	0.025	1.0
39	Jg3a-Amp6 - 32	116393	6819	266978	16	86854	14	123	76	6.4	924	39	2127	1.7	1310	4.1	0.843	4.2	0.703	0.126	0.021	12	0.029	0.791
40	Jg3a-Amp6 - 33	117207	7113	267352	17	86429	11	145	72	5.5	1039	43	2072	0.710	1155	4.0	1.3	4.3	0.461	0.133	0.033	12	0.050	1.5
41	Jg3a-Amp6 - 34	118933	8287	264492	16	84014	8.8	103	65	7.1	815	38	2136	3.1	1080	7.0	0.596	3.2	1.1	0.108	0.041	10	0.037	0.448
42	Jg3a-Amp6 - 35	110355	14481	265258	23	79614	15	325	40	8.9	1191	49	1505	0.518	1112	6.0	0.870	4.3	4.7	0.532	0.445	14	0.102	1.4
43	Jg3a-Amp6 - 36	109906	18695	255626	13	82550	8.9	514	37	7.9	969	41	1664	1.5	1001	10	0.911	5.2	1.2	0.674	0.029	15	0.032	0.929
44	Jg3a-Amp7 - 38	116031	42534	233295	16	65342	6.5	588	38	8.7	923	57	2037	1.5	1348	20	1.2	3.5	1.2	0.761	0.031	13	0.045	0.592
45	Jg3a-Amp7 - 39	109810	19820	257555	17	83011	15	471	40	7.2	979	50	1609	0.729	1253	8.0	1.1	4.1	1.3	0.582	0.027	15	0.028	0.397
46	Jg3a-Amp7 - 40	114474	10309	264131	18	87746	10	326	55	4.3	1028	37	2088	0.410	922	5.6	0.697	4.4	0.380	0.125	0.030	12	0.032	0.167
47	Jg3a-Amp7 - 41	116583	9437	265038	17	85568	8.7	220	46	2.6	999	36	1949	1.2	898	5.4	0.819	4.2	0.588	0.228	0.030	7.9	0.026	0.432
48	Jg3a-Amp7 - 42	117503	6942	267223	15	88128	7.8	201	48	2.8	989	34	2132	0.835	862	4.0	0.825	4.4	2.9	0.080	0.016	7.0	0.020	0.147
49	Jg3a-Amp7 - 43	118554	5188	268680	18	88993	7.0	314	55	3.2	914	31	2124	0.764	848	3.5	0.859	3.5	0.461	1.7	0.008	7.7	0.030	0.516
50	Jg3a-Amp7 - 44	117783	6881	267182	19	87158	9.1	165	60	2.4	914	36	2057	0.703	1045	4.2	0.789	3.8	0.326	0.114	0.016	9.4	0.028	0.302
51	Jg3a-Amp7 - 45	115794	10793	264571	16	84130	12	243	49	2.7	971	42	1763	6.0	1108	5.5	0.795	3.8	0.662	0.244	0.031	9.7	0.033	1.3
52	Jg3a-Amp7 - 46	118011	5008	271375	19	84570	11	123	64	1.6	855	38	2180	112	1187	2.8	0.799	3.5	0.364	0.111	0.022	7.6	0.038	1.0
53	Jg3a-Amp8 - 47	113470	15102	259787	10.0	83238	11	385	48	5.3	1113	43	1583	40	1405	6.5	0.822	4.1	1.2	0.508	0.019	12	0.052	1.1
54	Jg3a-Amp8 - 48	117190	6439	267231	11	89149	15	101	77	4.1	1052	26	2186	0.475	592	5.0	0.545	3.7	0.771	0.078	0.007	11	0.029	0.858
55	Jg3a-Amp8 - 49	120624	7828	265776	10	85327	11	155	41	3.3	1180	46	1642	0.582	1105	3.4	0.707	4.1	5.4	0.218	0.033	8.9	0.065	2.4
56	Jg3a-Amp8 - 50	113046	29876	245420	11	72748	19	500	40	6.8	1275	50	1780	4.9	1162	15	1.1	4.3	1.6	0.688	0.032	14	0.061	1.6
57	Jg3a-Amp8 - 51	119355	9166	264737	8.9	86279	15	180	58	3.0	1055	47	1785	7.6	1179	3.8	0.880	3.8	8.7	0.286	0.007	10	0.043	1.1
58	Jg3a-Amp8 - 52	114821	14291	259740	10	86208	13	298	55	5.6	970	41	1909	1.1	1033	6.7	0.644	4.0	1.3	0.418	0.021	11	0.049	0.978
59	Jg3a-Amp8 - 53	121429	8757	263333	12	85670	12	163	41	4.1	1144	46	1604	23	1111	3.9	0.749	4.3	0.546	0.231	0.021	9.0	0.050	0.899
60	Jg3a-Amp8 - 54	120095	6715	266623	9.5	88971	6.9	130	50	4.5	945	35	2049	12	984	3.6	0.606	4.0	0.461	0.124	0.030	7.3	0.016	0.397
61	Jg3a-Amp8 - 55	120731	6776	266292	8.2	88802	7.6	138	51	3.1	890	37	1988	0.828	1076	3.6	0.651	4.2	0.386	0.162	0.021	6.9	0.028	0.463
62	Jg5-Amph1 - 04	98410	32218	246572	17	81605	206	1290	94	1.7	1030	101	1545	0.403	1529	17	1.1	6.1	3.2	3.1	0.006	63	0.069	3.3
63	Jg5-Amph1 - 05	96175	35067	245560	18	80612	455	1304	89	1.0	1049	103	1298	0.321	1573	18	1.0	4.8	3.6	6.3	0.024	78	0.073	2.3
64	Jg5-Amph1 - 06	99900	30488	249367	16	79214	407	993	80	0.660	1094	100	1521	0.519	1446	16	1.000	5.3	2.7	5.0	0.028	66	0.051	3.0
65	Jg5-Amph1 - 07	98533	32245	247557	13	80837	397	1019	76	0.463	1068	102	1471	0.438	1479	16	1.4	5.7	2.6	5.4	0.013	75	0.082	2.8
66	Jg5-Amph1 - 08	97695	34103	245953	16	78908	378	1242	98	0.889	1041	102	1836	1.4	1584	20	1.3	4.9	3.3	5.7	0.009	73	0.062	0.907
67	Jg5-Amph1 - 09	98458	32713	247389	17	79597	263	1204	96	1.8	1029	102	1755	0.879	1565	18	1.1	5.2	2.9	4.3	0.009	66	0.074	1.8
68	Jg5-Amph1 - 10	102398	25178	253343	17	77394	148	941	107	14	947	95	2699	2.4	1381	18	1.2	7.3	1.6	2.3	0.039	50	0.050	1.2
69	Jg5-Amp2 - 33	111519	19571	255396	18	85438	138	739	86	1.3	986	92	1815	0.716	1201	11	0.667	6.6	1.1	0.584	0.023	24	0.030	1.2
70	Jg5-Amp2 - 34	112461	16701	259726	17	84148	34	652	74	0.634	912	96	1832	0.813	1253	10	0.443	8.1	0.758	0.355	0.030	23	0.026	0.951
71	Jg5-Amp2 - 35	108478	22474	256471	17	82452	83	845	71	0.625	954	99	1635	0.522	1434	12	0.511	6.9	1.3	1.2	0.026	31	0.045	0.518
72	Jg5-Amp2 - 36	100548	32905	247515	19	80012	208	1432	91	0.522	1068	102	1433	0.473	1531	17	0.839	5.4	3.7	3.3	0.033	68	0.093	0.904

#	Amphibole	Mg	Al	Si	P	Ca	Sc	Ti	V	Cr	Mn	Co	Ni	Cu	Zn	Ga	As	Sr	Zr	Nb	Mo	Sn	Sb	Ba
73	Jg5-Amp2 - 37	98767	35270	245452	26	79323	190	1625	100	1.1	1048	101	1434	0.515	1564	18	0.974	5.8	4.1	3.6	0.044	73	0.116	1.2
74	Jg5-Amp2 - 38	101772	33950	245185	20	81779	135	1498	101	1.0	1037	104	1600	0.599	1546	17	0.979	5.8	3.4	2.9	0.005	61	0.118	0.918
75	Jg5-Amp2 - 39	102311	31417	249010	20	81500	88	1327	99	0.854	996	101	1604	0.533	1514	17	0.689	6.1	2.5	1.7	0.008	53	0.038	0.621
76	Jg5-Amp2 - 40	107598	24106	252718	19	82921	98	1020	98	1.0	959	167	1909	1.1	1287	14	1.1	6.4	1.8	0.781	0.014	36	0.062	0.672
77	Jg5-Amp3 - 01	110830	20725	252230	12	84193	51	761	73	1.7	960	93	1697	0.550	1303	11	0.611	8.2	1.0	0.681	0.027	26	0.043	1.5
78	Jg5-Amp3 - 02	105884	22156	251651	1738	82191	93	807	69	0.900	996	94	1808	1.0	1360	13	0.780	8.5	1.2	1.6	0.034	38	0.059	0.712
79	Jg5-Amp3 - 03	93738	21657	219844	24493	117559	95	750	62	0.410	949	83	1484	0.939	1255	11	13	32	1.3	1.9	0.019	35	0.047	0.727
80	Jg5-Amp3 - 04	103203	29411	247190	14	79897	118	1044	77	0.403	1021	99	1535	0.566	1514	16	0.729	5.7	2.1	3.1	0.021	53	0.045	0.752
81	Jg5-Amp3 - 05	108842	23315	251686	11	82164	99	735	59	0.264	1048	98	1701	0.585	1505	12	0.689	5.4	1.5	2.4	0.035	37	0.018	0.828
82	Jg5-Amp3 - 06	107567	24769	251204	9.6	81908	104	837	66	0.713	1021	100	1544	0.563	1519	12	0.802	5.9	1.6	2.5	0.014	40	0.068	1.2
83	Jg5-Amp3 - 07	109778	21944	253142	8.7	82649	82	684	54	0.331	1031	98	1696	0.552	1502	11	0.648	5.6	1.3	2.1	0.028	33	0.033	1.8
84	Jg5-Amp3 - 08	105719	20695	250756	4568	85305	84	655	51	0.538	1031	95	1675	0.508	1432	11	2.0	9.6	1.3	2.2	0.012	35	0.048	0.683
85	Jg5-Amp3 - 09	104633	29374	245440	13	83065	79	1178	90	1.6	1016	98	1548	0.492	1518	15	0.595	7.2	1.8	1.1	0.005	46	0.055	7.9
86	Jg5-Amp3 - 10	104202	28594	247473	9.7	82050	69	1117	89	1.5	1009	98	1566	0.528	1471	15	0.593	6.1	1.7	0.958	0.012	45	0.054	2.3
87	Jg5-Amp3 - 11	103728	28671	248042	11	81714	53	1165	91	1.4	960	99	1634	0.527	1464	16	0.526	6.8	1.5	1.3	0.012	44	0.052	1.4
88	Jg5-Amp3 - 12	98540	36179	241915	12	80181	147	1241	94	2.5	1067	103	1361	0.522	1648	18	0.929	6.8	2.7	4.8	0.023	77	0.061	5.6
89	Jg5-Amp3 - 13	103481	30010	247181	11	81292	138	1021	81	2.4	1028	101	1450	1.1	1550	15	0.941	4.8	2.1	3.7	0.010	58	0.085	0.623
90	Jg5-Amp3 - 14	102304	32817	243169	13	81584	192	1085	85	4.8	1047	100	1543	1.6	1552	16	0.781	5.8	2.2	5.0	0.029	65	0.109	4.5
91	Jg5-Amp3 - 15	98783	34800	244987	13	79206	146	1233	92	4.8	1024	105	1422	1.3	1600	18	0.691	5.7	2.5	3.6	0.029	74	0.070	5.3
92	Jg5-Amp4 - 16	106134	26573	250550	9.9	81355	277	994	74	3.9	1020	100	1498	0.647	1597	13	0.453	6.0	2.0	2.1	0.012	41	0.044	0.488
93	Jg5-Amp4 - 17	103169	31011	246404	11	80305	335	1177	81	3.4	1024	100	1439	0.539	1545	15	0.613	5.6	2.7	4.2	0.037	58	0.061	1.7
94	Jg5-Amp4 - 18	98860	36527	241829	15	78969	466	1401	93	6.9	1059	101	1325	0.674	1577	18	0.884	4.5	3.6	4.6	0.023	74	0.060	1.2
95	Jg5-Amp4 - 19	97928	37176	241227	12	78800	497	1435	96	8.9	1039	100	1452	0.537	1552	19	0.781	5.2	3.3	4.8	0.011	79	0.092	3.0
96	Jg5-Amp4 - 20	110360	20017	255142	10	82566	216	759	80	7.5	982	91	1838	0.780	1224	12	0.464	6.5	1.4	0.910	0.007	29	0.051	9.1
97	Jg5-Amp4 - 21	108020	25483	250297	11	79890	227	896	78	2.3	998	96	1661	0.830	1435	14	0.459	6.6	1.8	2.0	0.019	37	0.059	3.0
98	Jg5-Amp4 - 22	104466	29077	247599	12	80347	182	1087	83	0.397	1009	99	1595	0.690	1503	16	0.608	5.8	2.0	2.0	0.003	46	0.036	1.6
99	Jg5-Amp4 - 23	107565	25203	250901	13	77836	254	1029	88	4.8	971	91	2047	1.0	1298	16	0.567	6.9	2.2	2.7	0.024	41	0.047	24
100	Jg5-Amp5 - 24	115360	13034	259923	9.7	86427	184	482	79	8.7	974	84	1803	0.815	820	8.7	0.826	3.9	0.595	0.328	0.019	24	0.012	0.441
101	Jg5-Amp5 - 25	103848	30121	246959	11	82514	232	1168	91	4.7	993	99	1613	0.657	1489	15	0.641	6.5	2.3	1.3	0.030	45	0.065	2.4
102	Jg5-Amp5 - 26	100781	34266	243786	16	80872	322	1357	93	4.0	1034	100	1465	1.0	1544	17	0.832	6.2	3.6	3.6	0.019	66	0.083	6.6
103	Jg5-Amp5 - 27	102611	31937	245908	12	80847	251	1157	80	5.1	1085	102	1334	0.523	1573	15	0.710	4.6	2.8	4.7	0.012	64	0.038	1.2
104	Jg5-Amp5 - 28	100953	36029	242643	20	79174	396	1415	87	6.8	1059	105	1345	0.446	1618	17	1.0	4.6	3.6	6.1	0.056	78	0.071	0.785
105	Jg5-Amp5 - 29	98774	36575	242458	15	80141	428	1469	92	7.7	1087	103	1308	0.500	1630	18	0.904	4.2	3.4	2.9	0.017	81	0.081	2.2
106	Jg5-Amp5 - 30	104218	30097	245687	17	76907	348	1226	105	5.9	958	92	2546	1.4	1391	18	0.677	7.6	2.9	2.2	0.028	55	0.048	6.0
107	Jg5-Amp5 - 31	104571	30175	248574	15	77980	427	1108	89	9.9	1009	99	1888	1.4	1388	16	1.2	5.4	2.7	4.1	0.018	62	0.078	3.1
108	Jg5-Amp5 - 32	113434	16758	259920	9.3	76577	224	684	94	13	915	81	2482	0.934	955	12	0.702	7.0	1.0	1.0	0.023	34	0.030	2.0
109	Jg6-Amp 1 - 01	116098	18671	252979	15	85420	21	137	58	0.264	1027	76	1737	0.627	1374	8.4	1.8	6.6	1.4	2.3	0.031	16	0.048	1.9
110	Jg6-Amp 1 - 02	115629	20195	252111	13	85831	13	197	69	0.304	1009	72	1754	0.378	1286	9.4	1.7	6.1	1.4	1.5	0.039	17	0.077	0.180

#	Amphibole	Mg	Al	Si	P	Ca	Sc	Ti	V	Cr	Mn	Co	Ni	Cu	Zn	Ga	As	Sr	Zr	Nb	Mo	Sn	Sb	Ba
111	Jg6-Amp 1 - 03	119677	15207	255824	18	85450	12	130	53	0.252	939	68	2907	0.812	1207	10	1.1	6.9	1.0	2.2	0.034	13	0.127	1.5
112	Jg6-Amp 1 - 04	115000	20045	252840	17	84031	22	163	66	0.331	1031	75	1776	0.534	1350	9.3	1.2	6.4	1.8	2.7	0.035	18	0.060	0.441
113	Jg6-Amp 1 - 05	115026	19061	253221	15	84805	37	123	55	0.332	1026	80	1742	0.699	1427	8.6	1.9	7.1	1.3	2.6	0.021	18	0.053	3.2
114	Jg6-Amp 1 - 06	110181	25020	248867	14	83036	90	144	62	0.315	1064	88	1460	0.612	1504	9.4	1.7	5.4	2.2	4.6	0.050	33	0.116	0.727
115	Jg6-Amp 1 - 07	108922	28404	245047	14	82160	95	160	68	0.266	1087	86	1552	0.605	1388	13	1.6	5.4	2.5	5.7	0.050	41	0.094	1.3
116	Jg6-Amp 1 - 08	111585	23342	250356	12	83064	89	115	52	0.291	1075	91	1396	0.511	1523	8.5	1.3	4.7	1.6	4.4	0.038	32	0.056	0.447
117	Jg6-Amp 1 - 09	104575	32789	241706	13	81381	132	199	75	0.340	1043	94	1342	0.403	1567	12	1.8	6.5	3.2	7.5	0.047	57	0.065	5.8
118	Jg6-Amp 1 - 10	105444	31148	243407	17	81943	101	202	77	0.520	1041	89	1461	0.584	1531	12	2.4	5.4	2.9	3.7	0.026	44	0.119	1.0
119	Jg6-Amp 1 - 11	109172	25951	247430	14	83071	72	178	69	0.376	1106	84	1555	0.575	1414	11	1.7	5.9	2.5	3.5	0.040	31	0.097	0.943
120	Jg6-Amp 1 - 12	110797	23882	248940	14	83157	57	166	66	0.310	1063	83	1649	0.702	1473	10	1.1	6.2	1.9	3.4	0.026	28	0.049	1.7
121	Jg6-Amp 2 - 01	115708	19240	253175	15	84998	4.8	309	65	0.282	1030	72	2322	1.5	1309	9.3	1.3	6.3	1.4	1.0	0.057	14	0.058	1.6
122	Jg6-Amp 2 - 02	114856	19273	253386	15	82490	8.3	254	61	0.919	1044	79	3283	2.9	1309	8.8	1.3	6.8	1.8	2.2	0.055	17	0.055	0.403
123	Jg6-Amp 2 - 03	118328	15378	255914	15	82943	13	175	48	1.2	1009	77	2584	2.4	1363	8.6	1.4	7.6	1.3	2.1	0.059	12	0.052	1.3
124	Jg6-Amp 2 - 04	118360	14351	257820	13	84810	9.3	146	40	0.433	1011	79	1824	0.581	1387	6.2	1.4	7.5	0.975	1.7	0.028	11	0.048	0.487
125	Jg6-Amp 2 - 05	117190	16255	255723	13	84678	12	170	48	0.552	1020	79	1969	0.882	1377	7.1	1.4	7.3	1.3	1.9	0.047	14	0.053	1.1
126	Jg6-Amp 2 - 06	113003	21424	250377	16	84083	14	297	68	0.607	1066	76	1671	26	1369	11	1.3	6.8	2.3	2.5	0.032	23	0.070	1.2
127	Jg6-Amp 2 - 07	109063	26440	247852	15	81537	108	259	65	1.8	1074	92	1310	1.3	1574	10.0	1.8	5.4	2.1	5.4	0.040	43	0.051	4.5
128	Jg6-Amp 2 - 08	108791	26979	247219	17	81768	90	280	70	5.2	1042	88	1443	0.670	1499	11	1.3	5.3	2.5	4.4	0.034	44	0.058	1.7
129	Jg6-Amp 2 - 09	113589	21248	249884	17	83171	5.8	339	73	4.0	1059	76	2270	0.732	1337	14	1.7	6.9	2.3	1.8	0.032	19	0.061	0.594
130	Jg6-Amp 2 - 10	103542	34225	240597	16	80203	232	324	83	4.2	1127	91	1315	1.2	1486	15	1.9	4.5	2.7	7.2	0.043	80	0.061	1.1
131	Jg8-Amp1 - 01	126479	11073	260834	13	86994	6.4	445	70	1.9	817	55	1871	0.455	1046	7.0	1.1	7.5	0.827	0.465	0.020	13	0.040	0.737
132	Jg8-Amp1 - 02	125080	12083	260467	13	85707	7.8	510	81	2.3	805	55	1610	0.666	1139	7.8	1.1	8.2	0.817	0.721	0.035	15	0.046	0.494
133	Jg8-Amp1 - 03	124098	13110	258721	14	87604	8.4	486	79	1.1	786	57	1548	0.472	1092	7.7	0.980	8.4	0.949	0.712	0.022	15	0.054	0.251
134	Jg8-Amp1 - 04	120047	17398	255256	14	84949	12	739	120	1.3	823	59	2061	0.476	1166	10	0.962	8.1	1.4	0.975	0.012	25	0.051	0.437
135	Jg8-Amp1 - 05	118332	18014	253878	14	85856	9.3	799	112	1.7	931	60	1520	0.494	1195	11	0.703	7.5	1.3	0.463	0.080	27	0.076	1.9
136	Jg8-Amp1 - 06	117398	20240	252868	15	83768	8.2	976	122	1.2	941	60	1537	0.276	1209	12	1.1	6.7	1.7	0.503	0.028	31	0.054	0.442
137	Jg8-Amp1 - 07	117100	20492	252053	15	85071	13	837	114	0.825	908	63	1504	0.469	1273	12	0.925	7.5	1.3	0.667	0.041	29	0.049	1.5
138	Jg8-Amp1 - 08	116324	21509	251719	14	84157	19	853	112	1.000	908	64	1476	0.323	1239	12	1.2	7.2	1.5	0.840	0.036	33	0.068	1.4
139	Jg8-Amp1 - 09	111672	24683	247061	13	82384	33	1052	127	1.1	941	65	1444	0.210	1237	16	1.7	10	2.1	1.4	0.033	42	0.067	2.3
140	Jg8-Amp1 - 10	109323	26407	246754	13	81675	46	1212	133	0.890	997	66	1403	0.542	1271	16	1.7	6.7	2.1	0.676	0.023	52	0.070	2.5
141	Jg8-Amp1 - 11	111503	26258	246724	15	83512	28	1242	135	1.2	967	68	1435	0.541	1355	15	1.7	6.6	2.3	0.966	0.020	48	0.052	0.703
142	Jg8-Amp2 - 01	120499	18854	253646	13	85228	16	745	119	3.8	839	54	1675	0.496	1083	12	1.3	5.9	1.6	0.607	0.057	31	0.052	0.392
143	Jg8-Amp2 - 02	127768	9482	262168	14	87784	5.6	285	52	0.592	774	53	2366	0.642	1007	6.0	1.0	7.8	0.722	0.489	0.023	12	0.045	0.111
144	Jg8-Amp2 - 03	123881	14110	258109	15	86814	9.0	507	86	1.1	804	55	1660	0.443	1058	8.7	1.6	8.1	1.1	0.904	0.026	21	0.063	0.403
145	Jg8-Amp2 - 04	119664	18447	253914	14	86202	12	740	114	2.3	849	57	1601	0.514	1091	11	1.2	7.6	1.7	0.807	0.029	30	0.057	1.1
146	Jg8-Amp2 - 05	123855	13687	259035	14	84917	7.5	394	76	0.586	843	54	1935	0.817	1019	8.5	1.2	8.1	1.3	0.865	0.031	22	0.053	0.831
147	Jg8-Amp2 - 06	125175	9923	261826	14	84985	21	266	66	0.323	862	52	2573	0.748	1006	6.4	1.9	7.8	1.0	0.820	0.027	19	0.053	1.2
148	Jg8-Amp2 - 07	121676	16700	255496	14	86764	11	601	99	2.2	861	55	1758	0.763	1081	10	1.8	6.5	1.4	0.669	0.018	27	0.054	0.265

#	Amphibole	Mg	Al	Si	P	Ca	Sc	Ti	V	Cr	Mn	Co	Ni	Cu	Zn	Ga	As	Sr	Zr	Nb	Mo	Sn	Sb	Ba
149	Jg8-Amp2 - 08	122283	15711	256744	15	84697	13	418	85	0.614	841	55	1966	0.619	1054	9.4	1.2	7.6	0.852	1.1	0.385	24	0.044	0.640
150	Jg8-Amp2 - 09	125501	11365	260452	12	88179	5.7	297	63	0.679	803	54	2557	0.590	1037	6.7	1.4	7.2	0.714	0.728	0.029	14	0.052	0.184
151	Jg8-Amp2 - 10	124798	13330	259450	13	86229	10	444	84	2.7	774	54	1596	0.522	1043	8.2	0.940	7.8	0.873	0.846	0.032	19	0.055	0.363
152	Jg9b-Amp1 - 01	125726	10707	263654	9.2	89618	39	348	48	3.6	775	45	1168	0.742	935	6.6	0.663	6.7	1.6	1.1	0.007	15	0.028	0.291
153	Jg9b-Amp1 - 02	124951	11494	262807	9.2	89514	47	355	48	3.8	791	47	1144	0.639	974	7.0	0.788	6.2	1.6	1.4	0.009	17	0.016	0.070
154	Jg9b-Amp1 - 03	128717	10701	263465	9.5	88772	39	233	35	11	716	46	1211	0.553	947	6.2	0.553	6.1	0.655	1.5	0.020	11	0.016	0.070
155	Jg9b-Amp1 - 04	125496	10331	264731	10	86009	44	313	49	6.3	740	44	1987	0.715	909	7.8	0.573	5.9	1.3	1.3	0.017	22	0.031	0.075
156	Jg9b-Amp1 - 05	129036	7053	266653	14	90502	41	169	28	6.6	686	43	1179	0.721	866	4.3	0.665	7.3	0.458	1.4	0.022	9.5	0.015	1.1
157	Jg9b-Amp1 - 06	128915	7314	266854	8.5	89975	37	179	29	0.488	671	44	1168	0.721	884	4.4	0.538	7.2	0.407	1.5	0.014	14	0.016	0.176
158	Jg9b-Amp1 - 07	129621	6854	266832	8.9	89067	26	137	27	0.321	645	44	1755	0.739	867	6.8	0.492	7.0	0.320	1.0	0.058	6.0	0.016	0.064
159	Jg9b-Amp1 - 08	127645	8843	264936	11	88969	56	206	34	43	730	47	1365	0.891	918	5.3	0.645	6.5	0.576	1.3	0.017	16	0.014	1.1
160	Jg9b-Amp1 - 09	124516	11964	262950	8.8	88684	75	290	42	4.7	798	51	1137	0.646	1024	6.7	0.613	5.8	0.980	1.7	0.010	18	0.015	0.091
161	Jg9b-Amp1 - 11	123334	12681	262457	8.1	87049	60	392	51	4.2	902	48	1166	1.4	1014	7.9	0.591	5.2	1.2	1.1	0.016	24	0.020	0.669
162	Jg9b-Amp1 - 12	123299	12320	262714	9.2	88165	90	276	40	3.5	775	55	1137	0.801	1078	6.6	0.612	6.4	0.960	3.9	0.022	20	0.014	0.102
163	Jg9b-Amp1 - 13	122420	13546	261043	9.9	88507	96	300	45	9.2	827	55	1142	0.682	1087	7.4	0.507	5.5	1.1	2.4	0.005	23	0.017	0.093
164	Jg9b-Amp1 - 14	123766	12354	261901	9.5	88063	65	304	45	3.9	850	52	1133	0.740	1045	7.2	0.517	5.2	0.983	1.4	0.018	19	0.031	0.128
165	Jg9b-Amp1 - 15	121679	13827	261491	8.9	87036	84	358	50	3.2	861	52	1129	0.563	1062	8.0	0.637	5.2	1.2	1.4	0.016	24	0.042	0.152
166	Jg9b-Amp1 - 16	119638	15767	259403	9.2	87003	144	395	53	2.4	838	58	1320	5.8	1177	9.0	0.510	6.7	1.6	4.0	0.011	34	0.037	3.0
167	Jg9b-Amp1 - 17	120684	15835	259192	9.3	87005	116	368	53	2.2	843	55	1547	0.694	1085	9.5	0.607	5.5	1.8	2.7	0.017	32	0.020	0.182
168	Jg9b-Amp1 - 18	121077	15105	259372	8.2	86538	108	462	57	10.0	927	53	1172	1.3	2317	9.1	0.564	5.4	1.8	1.5	0.014	33	0.052	1.3
169	Jg9b-Amp1 - 19	117796	18413	256778	8.0	86500	194	415	57	13	869	59	1172	5.1	1269	9.8	0.615	5.7	1.7	3.8	0.008	43	0.044	0.801
170	Jg9b-Amp1 - 20	117470	17693	257893	9.1	84705	192	389	54	8.1	915	60	1696	1.7	1210	10	0.463	5.3	1.7	2.9	0.020	40	0.023	0.688
171	Jg9b-Amp1 - 21	116906	18834	255746	8.4	83803	182	505	66	8.4	952	57	1284	0.653	1115	11	0.574	5.1	2.7	2.7	0.026	47	0.052	0.725
172	Jg9b-Amp1 - 22	120904	14850	260021	8.3	86855	116	341	49	4.3	886	57	1160	0.709	1137	8.0	0.261	5.2	1.3	2.4	0.018	29	0.021	0.148
173	Jg9b-Amp1 - 24	120731	16090	258831	11	87251	121	351	51	13	849	56	1158	1.0	1122	8.5	0.770	5.9	1.3	2.7	0.010	32	0.020	1.8
174	Jg9b-Amp1 - 25	122346	14570	259824	9.5	87230	117	373	51	16	850	54	1153	0.797	1092	8.0	0.520	5.7	1.5	2.4	0.028	26	0.032	0.105
175	Jg9b-Amp1 - 26	124436	12569	261591	8.9	88055	80	377	50	12	843	49	1148	0.839	1008	7.6	0.541	5.3	1.3	1.3	0.025	21	0.027	0.101
176	Jg9b-Amp1 - 27	123674	11731	263503	95	86809	68	382	48	14	807	47	1575	0.862	974	8.3	0.509	6.1	1.5	1.3	0.008	20	0.027	0.350
177	Jg9b-Amp1 - 28	128031	9176	264276	8.8	89224	43	203	33	2.6	747	49	1155	1.2	972	5.3	0.517	6.0	0.567	1.3	0.017	12	0.011	0.057
178	Jg9b-Amp1 - 29	129740	9307	262301	8.7	91305	58	240	35	19	747	45	1291	0.756	971	5.3	0.447	8.1	0.697	1.2	0.004	12	0.033	3.9
179	Jg9b-Amp1 - 30	124474	10381	263660	8.1	85289	68	260	38	10	751	47	1347	0.794	1063	7.4	0.422	7.2	0.863	1.9	0.014	19	0.019	0.800
180	Jg9b-Amp1 - 31	127950	10095	262732	8.3	88628	53	269	40	25	731	44	1183	0.571	920	6.2	0.497	5.7	0.729	1.2	0.007	13	0.016	0.086
181	Jg9b-Amp2 - 32	129303	8814	264642	8.2	89548	38	263	36	13	741	43	1186	0.659	879	5.5	0.408	5.4	0.588	0.726	0.026	11	0.013	0.116
182	Jg9b-Amp2 - 33	123574	12686	261844	22	84353	60	463	52	1.8	900	47	1350	0.779	1144	9.3	0.463	5.3	1.2	1.1	0.026	26	0.029	0.506
183	Jg9b-Amp2 - 34	124435	13705	257736	10	82898	56	370	55	2.9	836	47	3249	1.9	985	15	0.615	5.0	1.1	1.4	0.021	19	0.044	0.306
184	Jg9b-Amp2 - 35	124144	13308	261618	9.1	86898	56	370	50	2.3	817	50	1193	1.7	1014	7.6	0.423	6.0	1.5	1.8	0.008	19	0.052	0.214
185	Jg9b-Amp2 - 37	125580	9841	263687	9.1	86810	36	256	35	1.6	746	50	1164	5.7	980	6.6	0.459	6.4	0.628	2.5	0.022	14	0.027	0.204
186	Jg9b-Amp2 - 38	126673	9971	262875	8.5	88443	27	245	35	0.772	766	51	1133	1.3	1008	5.9	0.482	6.2	0.594	2.1	0.009	13	0.025	0.169

#	Amphibole	Mg	Al	Si	P	Ca	Sc	Ti	V	Cr	Mn	Co	Ni	Cu	Zn	Ga	As	Sr	Zr	Nb	Mo	Sn	Sb	Ba
187	Jg9b-Amp2 - 39	124607	12615	260690	9.7	86334	41	384	48	3.7	842	50	1353	0.922	976	7.9	0.646	5.3	1.1	1.3	0.027	26	0.016	0.124
188	Jg9b-Amp2 - 40	119648	18280	248816	10	68578	43	313	67	2.1	685	52	8550	5.2	975	34	0.650	6.1	1.1	1.5	0.029	22	0.042	1.8
189	Jg9b-Amp2 - 41	113977	15646	243662	9.1	79714	97	443	78	6.1	835	60	1581	1.0	1055	13	0.696	5.3	1.7	3.1	0.033	33	0.039	0.304
190	Jg9b-Amp2 - 42	120753	13749	260711	11	84062	94	357	49	1.7	799	56	1739	0.601	1088	8.5	0.356	6.1	1.2	3.1	0.033	33	0.025	0.403
191	Jg9b-Amp2 - 43	116691	18984	255830	9.7	85697	70	444	58	1.0	878	63	1181	0.508	1209	10	0.420	5.4	1.2	3.3	0.017	43	0.033	0.204
192	Jg9b-Amp2 - 44	121834	12506	260755	9.1	86868	34	212	37	0.103	871	64	1211	0.753	1183	6.6	0.588	5.1	0.449	2.4	0.034	23	0.029	0.116
193	Jg9b-Amp2 - 45	115296	18904	255396	9.4	85100	111	512	61	3.8	934	65	1198	0.662	1284	10.0	0.669	5.3	1.7	5.6	0.012	48	0.029	0.242
194	Jg9b-Amp2 - 46	111888	23188	252446	9.2	83379	159	646	73	4.7	1018	66	1181	0.607	1307	12	0.426	4.9	2.7	4.1	0.014	64	0.058	0.277
195	Jg9b-Amp2 - 48	114365	21722	252986	9.9	84099	140	646	69	3.8	1034	62	1179	0.683	1248	12	0.569	4.6	2.3	2.3	0.025	55	0.064	0.246
196	Jg9b-Amp2 - 49	117264	18910	255437	10	85073	118	559	62	3.6	952	58	1151	0.615	1167	11	0.567	4.8	1.6	1.8	0.008	43	0.024	0.210
197	Jg9b-Amp2 - 50	121172	15777	258239	8.6	86460	83	503	56	3.8	889	53	1135	0.698	1081	9.3	0.506	4.8	1.5	1.5	0.018	32	0.036	0.182
	Mean (n=197)	114398	17740	256339	175	84401	82	505	66	5.6	952	63	1742	64	1208	9.7	0.982	5.9	4.4	1.7	0.124	28	0.048	1.7
	SD	19619	9497	40846	1754	13960	104	396	25	6.3	187	27	689	843	311	5.0	0.948	2.5	14	1.6	0.395	20	0.026	2.5
	Median	115794	15835	256822	14	84917	39	365	63	3.6	970	55	1649	0.732	1171	9.1	0.825	5.5	1.6	1.3	0.026	20	0.046	0.907
	Max	129740	42534	271375	24493	117559	497	1625	135	43	1275	167	8550	11983	2317	34	13	32	165	7.5	3.3	81	0.177	24
	Min	93738	4744	219844	8.0	65342	4.8	70	27	0.103	645	26	1129	0.210	592	2.4	0.261	3.2	0.311	0.078	0.003	6.0	0.011	0.057

#	Apatite	Mg	Al	Si	P	Ca	Sc	Ti	V	Cr	Mn	Co	Ni	Cu	Zn	Ga	As	Sr	Zr	Nb	Mo	Sn	Sb	Ba
1	Jg8-Ap 1 - 01	89	0.281	318	252894	393600	0.096	0.237	0.294	0.250	277	0.034	0.084	0.159	1.5	0.011	105	231	0.006	0.001	0.017	0.058	0.044	0.052
2	Jg8-Ap 1 - 02	44	0.291	376	254379	393600	0.117	0.107	0.386	0.197	200	0.013	0.070	0.158	0.754	0.014	98	254	0.010	0.004	0.034	0.049	0.045	0.399
3	Jg8-Ap 1 - 03	52	0.273	250	253629	393600	0.105	0.164	0.361	0.174	218	0.021	0.062	0.155	0.656	0.008	73	262	0.001	0.008	0.026	0.047	0.045	0.256
4	Jg8-Ap 1 - 04	69	0.282	276	254192	393600	0.104	0.160	0.998	0.198	227	0.024	0.040	0.158	1.1	0.005	96	255	0.006	0.007	0.014	0.050	0.051	0.130
5	Jg8-Ap 1 - 05	92	0.319	436	253147	393600	0.117	0.152	0.342	0.262	267	0.044	0.135	0.150	1.4	0.012	94	249	0.010	0.001	0.020	0.075	0.049	0.055
6	Jg8-Ap 2 - 01	350	17	720	253988	393600	0.240	0.413	0.526	0.265	306	0.170	113	0.239	3.3	0.437	92	249	0.018	0.026	0.020	0.047	0.041	1.5
7	Jg8-Ap 2 - 02	96	0.404	219	252876	393600	0.099	0.172	0.476	0.227	287	0.033	4.8	0.129	1.5	0.084	91	248	0.009	0.009	0.017	0.050	0.040	0.751
8	Jg8-Ap 2 - 04	130	0.230	300	251910	393600	0.171	0.185	0.121	0.263	354	0.060	0.068	0.144	2.1	0.008	85	259	0.011	0.006	0.016	0.042	0.036	0.076
9	Jg8-Ap 2 - 06	92	0.263	327	254975	393600	0.144	0.170	0.140	0.200	277	0.045	0.050	0.145	1.4	0.006	94	220	0.004	0.001	0.016	0.046	0.037	0.173
10	Jg8-Ap 2 - 07	123	0.268	278	255580	393600	0.211	0.143	0.159	0.225	341	0.040	0.184	0.159	1.8	0.008	93	259	0.004	0.011	0.014	0.042	0.036	0.243
11	Jg8-Ap 2 - 09	136	1.1	372	253718	393600	0.165	0.804	0.088	0.273	330	0.039	3.1	0.158	1.7	0.021	86	244	0.027	0.006	0.032	0.048	0.043	0.048
12	Jg8-Ap 2 - 10	101	0.425	370	254454	393600	0.116	0.144	0.111	0.219	297	0.039	5.3	0.128	1.3	0.013	109	228	0.004	0.001	0.011	0.045	0.043	0.054
13	Jg9b-Ap - 01	78	0.179	344	237911	393600	0.055	0.090	0.128	0.118	240	0.031	0.048	0.136	0.917	0.017	86	282	0.010	0.009	0.016	0.034	0.012	0.093
14	Jg9b-Ap - 02	78	0.185	344	236607	393600	0.103	0.098	0.110	0.121	238	0.037	0.069	0.164	0.975	0.011	81	273	0.006	0.004	0.004	0.032	0.015	0.126
15	Jg9b-Ap - 04	86	0.955	273	233924	393600	0.127	0.098	0.150	0.130	242	0.042	0.112	0.164	1.4	0.006	85	240	0.008	0.002	0.003	0.137	0.017	0.086
16	Jg9b-Ap - 05	60	1.4	317	232518	393600	0.080	0.150	0.202	0.156	192	0.038	1.5	0.266	2.3	0.019	67	259	0.017	0.011	0.021	0.226	0.023	0.368
17	Jg9b-Ap - 06	47	0.242	326	228449	393600	0.080	0.130	0.209	0.129	182	0.016	0.173	0.267	0.608	0.009	63	270	0.012	0.022	0.006	0.149	0.019	0.385
18	Jg9b-Ap - 08	30	0.167	328	227247	393600	0.053	0.088	0.377	0.083	160	0.023	0.410	0.290	0.727	0.025	46	252	0.008	0.036	0.023	0.127	0.014	1.2
19	Jg9b-Ap - 09	68	0.162	347	225927	393600	0.053	0.103	0.120	0.107	224	0.022	0.084	0.285	0.680	0.014	68	282	0.005	0.006	0.002	0.245	0.016	0.134

#	Apatite	Mg	Al	Si	P	Ca	Sc	Ti	V	Cr	Mn	Co	Ni	Cu	Zn	Ga	As	Sr	Zr	Nb	Mo	Sn	Sb	Ba
20	Jg9b-Ap - 12	60	0.185	322	223444	393600	0.095	0.129	0.149	0.101	201	0.029	0.122	0.418	0.802	0.009	87	264	0.006	0.006	0.004	0.066	0.016	0.156
21	Jg9b-Ap - 14	98	0.328	260	220466	393600	0.087	0.168	0.123	0.189	292	0.047	0.554	0.540	1.5	0.019	77	282	0.010	0.016	0.004	0.089	0.026	0.235
22	Jg9b-Ap - 15	52	0.525	301	219034	393600	0.084	0.269	0.216	0.182	225	0.022	0.254	0.453	1.1	0.009	72	297	0.004	0.035	0.023	0.077	0.027	0.614
23	Jg9b-Ap - 16	640	272	1282	217119	393600	0.095	1.5	0.398	0.128	274	0.121	62	0.446	2.1	0.458	99	340	0.004	0.041	0.003	0.085	0.020	0.323
24	Jg9b-Ap - 17	53	0.353	284	220114	393600	0.098	0.132	0.263	0.191	200	0.015	1.7	0.378	0.347	0.009	65	269	0.001	0.041	0.001	0.092	0.028	0.277
25	Jg9b-Ap - 19	75	0.331	328	216512	393600	0.091	0.266	0.226	0.225	247	0.026	0.112	0.401	1.4	0.009	74	336	0.004	0.012	0.004	0.090	0.025	0.220
26	Jg9b-Ap - 21	112	4.3	406	216244	393600	0.124	0.210	0.271	0.225	200	0.159	25	0.287	2.8	0.070	49	322	0.013	0.067	0.003	0.171	0.037	5.3
27	Jg9b-Ap - 22	82	0.289	292	217882	393600	0.091	0.265	0.147	0.143	264	0.034	0.086	0.418	0.806	0.033	99	255	0.007	0.009	0.006	0.158	0.034	0.163
28	Jg9b-Ap - 23	104	0.335	232	217654	393600	0.124	0.168	0.115	0.157	293	0.037	0.060	0.357	1.4	0.006	93	245	0.010	0.004	0.004	0.145	0.033	0.078
29	Jg9b-Ap - 25	912	412	1782	214747	393600	0.212	3.2	0.670	0.237	225	0.205	99	0.374	6.8	0.817	63	300	0.021	0.540	0.011	0.239	0.031	9.7
30	Jg9b-Ap - 28	121	6.8	450	219065	393600	0.106	0.418	0.166	0.146	277	0.043	3.7	0.471	1.4	0.012	97	306	0.014	0.002	0.002	0.093	0.021	0.201
31	Jg9b-Ap - 17	53	0.353	284	220114	393600	0.098	0.132	0.263	0.191	200	0.015	1.7	0.378	0.347	0.009	65	269	478	0.001	0.041	0.215	0.092	0.028
32	Jg9b-Ap - 19	75	0.331	328	216512	393600	0.091	0.266	0.226	0.225	247	0.026	0.112	0.401	1.4	0.009	74	336	470	0.004	0.012	0.211	0.090	0.025
33	Jg9b-Ap - 21	112	4.3	406	216244	393600	0.124	0.210	0.271	0.225	200	0.159	25	0.287	2.8	0.070	49	322	416	0.013	0.067	0.207	0.171	0.037
34	Jg9b-Ap - 22	82	0.289	292	217882	393600	0.091	0.265	0.147	0.143	264	0.034	0.086	0.418	0.806	0.033	99	255	522	0.007	0.009	0.232	0.158	0.034
35	Jg9b-Ap - 23	104	0.335	232	217654	393600	0.124	0.168	0.115	0.157	293	0.037	0.060	0.357	1.4	0.006	93	245	532	0.010	0.004	0.256	0.145	0.033
36	Jg9b-Ap - 25	912	412	1782	214747	393600	0.212	3.2	0.670	0.237	225	0.205	99	0.374	6.8	0.817	63	300	500	0.021	0.540	0.311	0.239	0.031
37	Jg9b-Ap - 28	121	6.8	450	219065	393600	0.106	0.418	0.166	0.146	277	0.043	3.7	0.471	1.4	0.012	97	306	489	0.014	0.002	0.263	0.093	0.021
	Mean (n=37)	151	31	439	232238	393600	0.116	0.406	0.268	0.185	250	0.055	12	0.289	1.7	0.085	82	272	92	0.027	0.028	0.123	0.052	0.639
	SD	210	101	373	40922	63850	0.048	0.719	0.196	0.060	61	0.054	29	0.133	1.4	0.201	21	54	192	0.087	0.086	0.084	0.050	1.8
	Median	89	0.331	327	225927	393600	0.104	0.168	0.209	0.191	247	0.037	0.173	0.287	1.4	0.012	86	262	0.010	0.009	0.012	0.090	0.036	0.156
	Max	912	412	1782	255580	393600	0.240	3.2	0.998	0.273	354	0.205	113	0.540	6.8	0.817	109	340	532	0.540	0.540	0.311	0.239	9.7
	Min	30	0.162	219	214747	393600	0.053	0.088	0.088	0.083	160	0.013	0.040	0.128	0.347	0.005	46	220	0.001	0.001	0.001	0.032	0.012	0.021

SD Table 1c. (Continued)

#	Amphibole	La	Ce	Pr	Nd	Sm	Eu	Gd	Tb	Dy	Y	Ho	Er	Tm	Yb	Lu	Hf	Ta	W	^{204}Pb	^{206}Pb	^{207}Pb	^{208}Pb	Th	^{238}U
1	Jg3a-Amph1 - 01	0.025	0.240	0.090	0.923	0.969	0.361	2.5	0.552	4.1	25	0.918	2.7	0.369	2.4	0.323	0.046	0.010	0.013	0.013	0.260	0.210	0.405	0.004	0.033
2	Jg3a-Amph1 - 02	1.1	2.1	0.305	1.4	0.841	0.269	1.9	0.427	3.2	21	0.769	2.1	0.289	2.1	0.255	0.215	0.005	0.022	0.012	0.363	0.213	0.442	0.284	0.321
3	Jg3a-Amph1 - 03	0.289	0.732	0.119	0.858	0.654	0.280	1.9	0.491	3.7	22	0.843	2.3	0.286	1.7	0.263	0.800	0.010	0.049	0.014	0.141	0.081	0.151	0.072	0.177
4	Jg3a-Amph1 - 04	1.3	3.1	0.513	2.5	1.2	0.394	2.4	0.526	3.9	24	0.866	2.4	0.284	1.8	0.247	0.412	0.009	0.075	0.012	0.316	0.261	0.539	0.329	0.192
5	Jg3a-Amph1 - 05	0.537	1.4	0.187	0.829	0.484	0.211	1.4	0.348	2.6	17	0.569	1.7	0.229	1.3	0.192	0.378	0.014	0.128	0.013	0.315	0.235	0.455	0.108	0.211
6	Jg3a-Amph1 - 06	1.0	2.5	0.390	2.0	1.1	0.347	2.6	0.519	4.1	24	0.909	2.4	0.308	2.1	0.251	0.841	0.009	0.023	0.015	0.220	0.089	0.250	0.281	0.270
7	Jg3a-Amph1 - 07	0.099	0.216	0.043	0.381	0.479	0.189	1.4	0.323	2.6	18	0.597	1.9	0.259	1.6	0.219	1.0	0.008	0.088	0.017	0.591	0.413	0.564	0.095	0.431
8	Jg3a-Amph1 - 08	0.196	0.435	0.089	0.600	0.425	0.194	1.3	0.328	2.6	18	0.605	1.9	0.255	1.7	0.218	1.7	0.010	0.155	0.018	0.754	0.394	0.717	0.242	1.2
9	Jg3a-Amp2 - 01	0.648	2.0	0.445	3.2	1.9	0.542	3.2	0.563	3.9	23	0.866	2.5	0.308	2.2	0.334	0.090	0.046	0.099	0.012	0.086	0.054	0.179	0.099	0.125
10	Jg3a-Amp2 - 02	0.081	0.674	0.247	2.2	1.6	0.566	3.4	0.725	4.9	29	1.1	3.1	0.420	2.8	0.379	0.147	0.031	0.056	0.011	0.125	0.083	0.194	0.051	0.073

#	Amphibole	La	Ce	Pr	Nd	Sm	Eu	Gd	Tb	Dy	Y	Ho	Er	Tm	Yb	Lu	Hf	Ta	W	^{204}Pb	^{206}Pb	^{207}Pb	^{208}Pb	Th	^{238}U
11	Jg3a-Amp2 - 03	0.055	0.415	0.156	1.4	1.4	0.425	2.9	0.588	4.7	27	0.999	3.0	0.396	2.8	0.385	0.212	0.025	0.016	0.010	0.100	0.052	0.122	0.013	0.066
12	Jg3a-Amp2 - 04	0.041	0.218	0.085	0.653	0.690	0.249	1.6	0.300	2.2	13	0.470	1.4	0.182	1.3	0.211	0.546	0.013	0.052	0.011	0.166	0.105	0.194	0.037	0.150
13	Jg3a-Amp2 - 05	0.177	0.963	0.285	2.4	1.8	0.539	3.3	0.647	4.3	26	0.931	2.8	0.355	2.4	0.381	0.309	0.028	0.069	0.012	0.405	0.264	0.522	0.091	0.487
14	Jg3a-Amp3 - 06	0.056	0.251	0.074	0.629	0.788	0.302	2.4	0.511	4.2	28	0.998	3.0	0.424	2.9	0.458	1.5	0.009	0.051	0.034	1.6	0.989	1.9	0.292	1.6
15	Jg3a-Amp3 - 07	0.180	0.524	0.137	1.0	1.1	0.323	2.2	0.521	4.5	26	0.920	2.7	0.330	2.5	0.298	0.826	0.009	0.023	0.016	0.129	0.077	0.143	0.048	0.129
16	Jg3a-Amp3 - 08	10	22	2.8	13	3.4	1.1	4.2	0.678	4.6	27	0.966	2.6	0.291	1.7	0.211	0.656	0.010	0.065	0.008	0.452	0.255	0.795	2.6	0.407
17	Jg3a-Amp3 - 09	7.2	14	2.2	9.9	2.5	0.843	3.1	0.522	3.9	24	0.893	2.4	0.288	1.7	0.179	0.444	0.011	0.072	0.057	0.990	0.868	2.0	1.5	0.232
18	Jg3a-Amp3 - 10	0.832	2.0	0.290	1.6	0.816	0.291	1.9	0.437	3.2	21	0.743	2.2	0.306	1.8	0.232	0.604	0.008	0.007	0.010	0.131	0.102	0.238	0.307	0.157
19	Jg3a-Amp3 - 11	0.010	0.127	0.058	0.633	0.789	0.271	2.2	0.484	3.9	25	0.920	2.7	0.376	2.6	0.380	0.066	0.012	0.002	0.008	0.075	0.075	0.148	0.004	0.013
20	Jg3a-Amp3 - 12	0.096	0.808	0.242	2.5	1.7	0.607	3.5	0.702	5.0	29	1.0	3.0	0.441	2.9	0.420	0.109	0.025	0.027	0.025	0.481	0.470	1.0	0.026	0.036
21	Jg3a-Amp4 - 13	0.069	0.573	0.196	1.9	1.6	0.472	3.3	0.666	5.1	29	1.1	3.0	0.396	2.5	0.343	0.071	0.028	0.045	0.011	0.082	0.089	0.179	0.038	0.042
22	Jg3a-Amp4 - 14	9.5	23	3.2	16	4.5	1.1	4.8	0.785	4.7	28	1.0	2.9	0.389	2.5	0.348	0.169	0.031	0.027	0.010	0.125	0.098	0.321	0.975	0.120
23	Jg3a-Amp4 - 15	0.461	1.4	0.373	2.6	1.6	0.511	2.6	0.522	3.8	22	0.794	2.2	0.339	2.0	0.286	0.247	0.038	0.039	0.016	0.376	0.123	0.223	0.336	0.418
24	Jg3a-Amp4 - 16	0.048	0.260	0.103	0.986	0.907	0.294	2.4	0.531	4.1	24	0.878	2.4	0.340	2.3	0.301	0.072	0.008	0.011	0.011	0.059	0.056	0.123	0.007	0.025
25	Jg3a-Amp4 - 17	0.159	0.870	0.267	2.7	2.0	0.498	3.6	0.728	5.3	29	1.1	3.2	0.424	3.0	0.503	0.095	0.029	0.021	0.017	0.515	0.499	1.1	0.087	0.021
26	Jg3a-Amp4 - 18	0.144	1.2	0.424	4.2	3.4	0.838	6.1	1.2	8.5	49	1.9	5.1	0.718	4.9	0.733	0.127	0.047	0.003	0.012	0.086	0.077	0.196	0.029	0.031
27	Jg3a-Amp5 - 19	1.2	3.1	0.520	3.3	1.4	0.466	2.2	0.412	2.8	17	0.611	1.7	0.227	1.5	0.214	0.262	0.037	0.070	0.010	0.161	0.081	0.267	0.339	0.204
28	Jg3a-Amp5 - 20	0.609	1.4	0.190	1.1	0.653	0.251	1.7	0.390	2.9	19	0.695	1.9	0.254	1.7	0.228	4.2	0.009	0.045	0.010	0.356	0.156	0.254	0.132	0.494
29	Jg3a-Amp5 - 21	1.2	3.8	0.480	2.3	0.910	0.342	2.0	0.423	3.3	22	0.765	2.2	0.275	1.6	0.209	1.1	0.014	0.112	0.014	0.246	0.139	0.377	0.190	0.265
30	Jg3a-Amp5 - 22	0.268	0.588	0.104	0.722	0.634	0.295	1.8	0.462	3.8	25	0.869	2.4	0.277	1.6	0.200	0.288	0.012	0.047	0.010	0.258	0.239	0.502	0.059	0.078
31	Jg3a-Amp6 - 24	0.170	1.5	0.494	4.2	2.8	1.0	4.0	0.666	4.3	25	0.920	2.5	0.356	2.4	0.397	0.137	0.100	0.015	0.027	0.470	0.399	0.911	0.023	0.025
32	Jg3a-Amp6 - 25	0.200	1.6	0.561	4.7	3.2	1.1	5.2	0.881	6.0	35	1.2	3.6	0.480	3.4	0.553	0.170	0.089	0.022	0.013	0.318	0.320	0.633	0.011	0.024
33	Jg3a-Amp6 - 26	0.027	0.233	0.065	0.697	0.678	0.231	1.7	0.399	2.9	18	0.646	1.8	0.227	1.3	0.185	0.116	0.017	0.152	0.015	0.222	0.203	0.434	0.045	0.038
34	Jg3a-Amp6 - 27	0.019	0.096	0.045	0.482	0.738	0.268	2.1	0.491	4.0	26	0.911	2.5	0.305	1.8	0.223	0.036	0.016	0.071	0.015	0.288	0.283	0.511	0.005	0.015
35	Jg3a-Amp6 - 28	0.052	0.249	0.078	0.625	0.622	0.234	1.7	0.394	3.1	21	0.709	2.1	0.257	1.6	0.203	0.072	0.010	0.033	0.010	0.123	0.092	0.236	0.058	0.017
36	Jg3a-Amp6 - 29	0.008	0.075	0.036	0.366	0.594	0.275	2.0	0.465	3.8	26	0.883	2.5	0.326	1.9	0.209	0.130	0.008	0.049	0.010	0.195	0.188	0.403	0.002	0.004
37	Jg3a-Amp6 - 30	0.012	0.122	0.034	0.373	0.523	0.193	1.5	0.332	2.7	18	0.629	1.8	0.211	1.4	0.165	0.073	0.011	0.049	0.010	0.109	0.100	0.220	0.011	0.016
38	Jg3a-Amp6 - 31	0.014	0.126	0.039	0.413	0.482	0.175	1.3	0.283	2.2	14	0.500	1.5	0.186	1.1	0.146	0.044	0.012	0.050	0.010	0.285	0.263	0.531	0.015	0.027
39	Jg3a-Amp6 - 32	0.020	0.147	0.054	0.465	0.703	0.256	2.1	0.467	3.9	26	0.955	2.7	0.350	2.2	0.255	0.101	0.008	0.150	0.010	0.113	0.101	0.228	0.028	0.058
40	Jg3a-Amp6 - 33	0.020	0.172	0.072	0.620	0.555	0.248	1.9	0.424	3.4	25	0.862	2.6	0.342	2.1	0.256	0.073	0.014	0.134	0.009	0.204	0.184	0.380	0.034	0.039
41	Jg3a-Amp6 - 34	0.021	0.136	0.036	0.403	0.536	0.218	1.5	0.345	2.7	17	0.630	1.7	0.224	1.5	0.179	0.078	0.004	0.071	0.008	0.089	0.076	0.206	0.042	0.048
42	Jg3a-Amp6 - 35	1.0	3.1	0.519	3.5	2.4	0.599	4.1	0.737	5.6	33	1.1	3.3	0.427	2.6	0.417	0.226	0.046	0.111	0.013	0.109	0.073	0.207	0.160	0.072
43	Jg3a-Amp6 - 36	0.157	0.986	0.302	2.7	1.8	0.624	3.2	0.577	4.0	22	0.861	2.4	0.287	2.1	0.329	0.100	0.057	0.044	0.008	0.050	0.046	0.123	0.093	0.101
44	Jg3a-Amp7 - 38	0.104	0.938	0.345	2.9	2.0	0.705	2.9	0.498	3.3	20	0.698	1.9	0.279	1.9	0.277	0.075	0.057	0.005	0.012	0.082	0.058	0.132	0.002	0.015
45	Jg3a-Amp7 - 39	0.114	0.942	0.317	3.0	2.3	0.736	4.1	0.846	6.0	35	1.3	3.8	0.500	3.3	0.494	0.106	0.052	0.019	0.011	0.078	0.068	0.161	0.002	0.008
46	Jg3a-Amp7 - 40	0.023	0.235	0.098	1.1	1.3	0.501	3.5	0.881	6.9	41	1.6	4.5	0.642	4.2	0.513	0.042	0.008	0.000	0.011	0.044	0.050	0.110	0.000	0.001
47	Jg3a-Amp7 - 41	0.048	0.369	0.118	1.2	0.967	0.314	2.2	0.426	3.2	20	0.712	2.0	0.265	1.8	0.263	0.042	0.022	0.035	0.010	0.061	0.068	0.135	0.014	0.013
48	Jg3a-Amp7 - 42	0.012	0.119	0.057	0.590	0.875	0.340	2.6	0.541	4.8	28	1.0	3.0	0.406	2.7	0.375	0.164	0.007	0.000	0.009	0.514	0.136	0.210	0.001	0.007

#	Amphibole	La	Ce	Pr	Nd	Sm	Eu	Gd	Tb	Dy	Y	Ho	Er	Tm	Yb	Lu	Hf	Ta	W	^{204}Pb	^{206}Pb	^{207}Pb	^{208}Pb	Th	^{238}U
49	Jg3a-Amp7 - 43	0.008	0.111	0.048	0.481	0.694	0.297	2.1	0.494	3.8	25	0.873	2.4	0.329	2.1	0.222	0.032	0.139	0.031	0.010	0.139	0.084	0.176	0.002	0.021
50	Jg3a-Amp7 - 44	0.022	0.161	0.075	0.657	0.707	0.275	2.1	0.477	3.8	23	0.805	2.4	0.278	2.0	0.234	0.045	0.013	0.020	0.009	0.058	0.056	0.133	0.003	0.008
51	Jg3a-Amp7 - 45	0.058	0.432	0.158	1.5	1.2	0.371	2.4	0.528	3.9	24	0.876	2.6	0.317	2.2	0.300	0.066	0.021	0.022	0.010	0.169	0.147	0.352	0.018	0.022
52	Jg3a-Amp7 - 46	0.009	0.083	0.020	0.327	0.387	0.181	1.2	0.265	2.2	15	0.529	1.5	0.191	1.1	0.154	0.039	0.011	0.027	0.013	0.153	0.141	0.303	0.005	0.003
53	Jg3a-Amp8 - 47	0.172	0.971	0.295	2.6	1.8	0.637	3.2	0.609	4.2	25	0.911	2.7	0.385	2.3	0.346	0.082	0.041	0.028	0.006	0.115	0.097	0.230	0.075	0.049
54	Jg3a-Amp8 - 48	4.4	8.5	0.997	4.3	1.4	0.466	2.4	0.496	3.9	25	0.895	2.6	0.346	1.9	0.249	0.104	0.005	0.008	0.008	0.129	0.109	0.399	1.1	0.043
55	Jg3a-Amp8 - 49	0.159	0.630	0.149	1.1	0.809	0.294	1.9	0.408	3.1	20	0.742	2.1	0.281	1.7	0.243	0.204	0.016	0.107	0.006	0.153	0.115	0.226	0.188	0.116
56	Jg3a-Amp8 - 50	0.150	1.1	0.352	3.5	2.6	0.777	4.7	0.883	6.2	36	1.3	3.9	0.521	3.5	0.543	0.131	0.058	0.038	0.007	0.137	0.100	0.263	0.088	0.059
57	Jg3a-Amp8 - 51	0.138	0.533	0.144	1.2	0.902	0.317	2.3	0.443	3.6	23	0.805	2.4	0.325	1.9	0.252	0.243	0.026	0.072	0.032	0.562	0.466	1.0	0.050	0.080
58	Jg3a-Amp8 - 52	0.107	0.734	0.235	2.1	1.6	0.532	2.7	0.544	3.9	23	0.818	2.3	0.346	2.2	0.290	0.133	0.027	0.011	0.008	0.105	0.086	0.227	0.025	0.018
59	Jg3a-Amp8 - 53	0.042	0.300	0.101	0.953	0.878	0.298	2.4	0.511	3.8	22	0.820	2.3	0.287	1.8	0.246	0.076	0.020	0.082	0.005	0.108	0.093	0.236	0.068	0.033
60	Jg3a-Amp8 - 54	0.021	0.152	0.068	0.707	0.759	0.246	2.0	0.449	3.5	22	0.830	2.4	0.315	2.1	0.288	0.059	0.005	0.014	0.005	0.119	0.121	0.253	0.005	0.006
61	Jg3a-Amp8 - 55	0.024	0.212	0.088	0.776	0.735	0.268	1.9	0.409	3.1	19	0.710	2.0	0.245	1.6	0.222	0.056	0.010	0.037	0.008	0.137	0.196	0.376	0.007	0.008
62	Jg5-Amph1 - 04	0.122	1.3	0.537	5.2	4.8	2.1	8.9	1.9	14	66	2.9	7.8	0.956	5.9	0.794	0.229	0.289	0.092	0.017	0.468	0.405	0.948	0.005	0.034
63	Jg5-Amph1 - 05	0.138	1.5	0.662	6.4	5.8	2.9	12	2.7	20	93	4.3	11	1.5	9.7	1.3	0.347	0.979	0.010	0.045	0.441	0.495	1.0	0.005	0.045
64	Jg5-Amph1 - 06	0.139	1.2	0.539	5.7	5.1	2.4	11	2.4	19	86	3.8	10	1.4	9.0	1.2	0.281	0.606	0.067	0.024	0.406	0.355	0.833	0.005	0.042
65	Jg5-Amph1 - 07	0.113	1.3	0.579	5.9	5.3	2.6	11	2.4	18	87	4.0	11	1.4	9.0	1.2	0.272	0.667	0.034	0.026	0.625	0.721	1.3	0.005	0.037
66	Jg5-Amph1 - 08	0.128	1.4	0.588	5.9	5.2	2.5	11	2.3	17	80	3.6	9.8	1.3	8.0	1.1	0.269	0.838	0.018	0.015	0.280	0.220	0.539	0.005	0.038
67	Jg5-Amph1 - 09	0.142	1.3	0.566	5.6	4.8	2.3	9.6	2.1	15	71	3.2	8.5	1.1	7.0	0.885	0.258	0.534	0.026	0.009	0.298	0.296	0.634	0.005	0.057
68	Jg5-Amph1 - 10	2.6	5.4	1.1	6.4	3.6	1.5	6.1	1.2	9.2	41	1.8	4.9	0.603	3.8	0.571	0.119	0.098	0.062	0.024	0.449	0.414	0.951	0.013	0.112
69	Jg5-Amp2 - 33	0.041	0.403	0.214	2.2	2.3	1.1	4.3	0.907	6.6	31	1.3	3.5	0.417	2.5	0.357	0.092	0.012	0.048	0.048	0.891	0.914	2.0	0.002	0.005
70	Jg5-Amp2 - 34	0.034	0.471	0.218	2.2	2.0	1.0	4.0	0.773	5.6	24	1.0	2.7	0.344	1.9	0.252	0.026	0.004	0.011	0.015	0.278	0.275	0.653	0.001	0.001
71	Jg5-Amp2 - 35	0.075	0.783	0.329	3.3	2.3	1.1	4.7	0.887	6.4	30	1.3	3.3	0.436	2.8	0.342	0.060	0.020	0.011	0.010	0.131	0.110	0.270	0.001	0.005
72	Jg5-Amp2 - 36	0.126	1.3	0.558	5.7	4.7	2.3	9.7	2.1	15	72	3.3	8.3	1.1	6.9	0.974	0.169	0.429	0.032	0.011	0.199	0.176	0.394	0.002	0.032
73	Jg5-Amp2 - 37	0.142	1.4	0.613	5.8	4.8	2.3	9.7	2.1	16	73	3.2	8.5	1.1	7.4	0.964	0.219	0.272	0.093	0.019	0.250	0.252	0.511	0.001	0.040
74	Jg5-Amp2 - 38	0.153	1.4	0.573	5.7	4.6	2.1	8.6	1.8	13	63	2.8	7.1	0.936	5.8	0.800	0.193	0.083	0.021	0.011	0.205	0.209	0.453	0.003	0.025
75	Jg5-Amp2 - 39	0.134	1.1	0.495	5.0	4.2	1.9	8.2	1.6	12	56	2.4	6.4	0.818	5.0	0.664	0.098	0.034	0.010	0.010	0.159	0.145	0.316	0.000	0.019
76	Jg5-Amp2 - 40	0.088	0.727	0.299	3.5	2.9	1.5	6.0	1.2	9.1	42	1.8	4.6	0.562	3.4	0.469	0.109	0.028	0.015	0.025	0.448	0.444	0.912	0.004	0.015
77	Jg5-Amp3 - 01	0.069	0.630	0.253	3.1	2.5	1.2	5.0	0.954	6.8	32	1.4	3.6	0.442	2.8	0.367	0.043	0.009	0.031	0.007	0.124	0.124	0.299	0.003	0.041
78	Jg5-Amp3 - 02	0.283	1.5	0.426	3.9	3.0	1.4	5.6	1.1	7.8	38	1.7	4.3	0.574	3.6	0.474	0.055	0.049	0.099	0.334	5.2	5.3	13	0.002	0.087
79	Jg5-Amp3 - 03	2.6	9.0	1.9	13	6.8	2.9	12	2.1	15	65	2.8	7.1	0.878	5.4	0.730	0.070	0.091	0.063	0.009	0.367	0.307	0.669	0.011	0.192
80	Jg5-Amp3 - 04	0.110	1.2	0.454	4.6	3.8	1.8	7.3	1.5	11	51	2.3	6.1	0.766	4.8	0.656	0.104	0.197	0.028	0.007	0.194	0.179	0.374	0.001	0.034
81	Jg5-Amp3 - 05	0.090	0.927	0.356	3.7	2.9	1.4	5.8	1.2	8.7	39	1.7	4.6	0.560	3.8	0.496	0.077	0.142	0.004	0.009	0.210	0.200	0.426	0.000	0.009
82	Jg5-Amp3 - 06	0.117	0.973	0.383	3.8	3.1	1.4	5.6	1.2	8.4	39	1.7	4.5	0.594	3.7	0.476	0.080	0.134	0.008	0.006	0.172	0.155	0.336	0.000	0.011
83	Jg5-Amp3 - 07	0.086	0.872	0.368	3.3	2.9	1.3	5.2	1.1	7.7	35	1.5	4.1	0.514	3.3	0.444	0.059	0.132	0.027	0.013	0.324	0.332	0.703	0.001	0.011
84	Jg5-Amp3 - 08	0.506	2.4	0.610	5.1	3.1	1.5	5.8	1.1	8.2	37	1.6	4.2	0.517	3.2	0.430	0.055	0.140	0.090	0.009	0.178	0.148	0.327	0.004	0.042
85	Jg5-Amp3 - 09	0.110	1.1	0.470	4.9	4.3	2.0	8.4	1.7	13	60	2.6	6.9	0.880	5.5	0.720	0.085	0.031	0.083	0.061	1.1	1.1	2.4	0.004	0.022
86	Jg5-Amp3 - 10	0.094	1.0	0.444	4.7	4.1	2.0	8.3	1.7	12	58	2.5	6.6	0.823	5.4	0.676	0.067	0.026	0.013	0.008	0.181	0.175	0.388	0.000	0.016

#	Amphibole	La	Ce	Pr	Nd	Sm	Eu	Gd	Tb	Dy	Y	Ho	Er	Tm	Yb	Lu	Hf	Ta	W	^{204}Pb	^{206}Pb	^{207}Pb	^{208}Pb	Th	^{238}U
87	Jg5-Amp3 - 11	0.095	0.945	0.379	4.3	3.5	1.7	7.0	1.4	10	47	2.0	5.3	0.675	4.1	0.555	0.051	0.023	0.013	0.007	0.213	0.186	0.385	0.001	0.018
88	Jg5-Amp3 - 12	0.132	1.3	0.586	5.7	4.9	2.4	11	2.2	17	78	3.4	9.4	1.2	7.7	1.0	0.135	0.464	0.035	0.034	0.549	0.490	1.1	0.001	0.024
89	Jg5-Amp3 - 13	0.116	1.2	0.499	5.0	4.1	2.0	8.6	1.8	14	62	2.8	7.4	0.966	6.1	0.808	0.096	0.407	0.011	0.007	0.183	0.165	0.346	0.002	0.024
90	Jg5-Amp3 - 14	0.126	1.3	0.557	5.1	4.9	2.4	9.8	2.1	16	72	3.2	8.4	1.2	7.4	0.966	0.153	0.599	0.116	0.045	0.678	0.649	1.5	0.004	0.067
91	Jg5-Amp3 - 15	0.140	1.3	0.551	6.0	5.4	2.5	11	2.3	18	82	3.6	9.8	1.3	7.8	1.0	0.125	0.364	0.074	0.043	0.895	0.861	1.9	0.002	0.033
92	Jg5-Amp4 - 16	0.104	0.963	0.356	3.7	3.0	1.4	5.6	1.1	8.1	37	1.6	4.1	0.508	3.4	0.491	0.136	0.078	0.007	0.007	0.136	0.132	0.290	0.000	0.010
93	Jg5-Amp4 - 17	0.129	1.2	0.493	4.8	4.1	1.9	7.8	1.7	13	57	2.5	6.5	0.838	5.4	0.730	0.235	0.351	0.027	0.032	0.459	0.431	0.926	0.002	0.027
94	Jg5-Amp4 - 18	0.128	1.4	0.630	6.2	5.6	2.7	12	2.6	20	92	4.1	11	1.5	9.3	1.2	0.353	0.724	0.023	0.014	0.243	0.221	0.482	0.002	0.040
95	Jg5-Amp4 - 19	0.156	1.4	0.610	6.5	5.7	2.9	12	2.7	20	94	4.2	11	1.5	9.6	1.3	0.345	0.549	0.141	0.019	0.347	0.330	0.718	0.010	0.044
96	Jg5-Amp4 - 20	0.062	0.550	0.243	2.8	2.4	1.2	5.0	0.999	7.1	34	1.4	3.7	0.464	3.0	0.384	0.110	0.031	0.041	0.021	0.338	0.330	0.750	0.004	0.026
97	Jg5-Amp4 - 21	0.107	0.898	0.348	3.4	2.8	1.3	5.3	1.1	7.7	36	1.6	4.1	0.519	3.3	0.465	0.126	0.050	0.064	0.011	0.286	0.275	0.559	0.006	0.059
98	Jg5-Amp4 - 22	0.097	0.970	0.406	4.1	3.3	1.6	6.8	1.4	10	46	2.0	5.2	0.691	4.2	0.571	0.114	0.046	0.038	0.007	0.216	0.208	0.412	0.001	0.036
99	Jg5-Amp4 - 23	0.097	0.840	0.313	3.3	2.8	1.3	5.3	1.1	7.9	37	1.6	4.3	0.537	3.4	0.460	0.144	0.094	0.106	0.033	0.658	0.641	1.4	0.009	0.080
100	Jg5-Amp5 - 24	0.020	0.190	0.109	1.2	1.5	0.883	3.6	0.841	6.4	31	1.3	3.5	0.472	2.7	0.340	0.057	0.029	0.006	0.005	0.030	0.031	0.060	0.000	0.010
101	Jg5-Amp5 - 25	0.121	1.0	0.441	4.6	3.8	1.9	7.5	1.6	12	54	2.4	6.3	0.795	4.9	0.648	0.162	0.036	0.020	0.012	0.374	0.350	0.790	0.000	0.017
102	Jg5-Amp5 - 26	0.173	1.5	0.591	5.8	5.0	2.4	10	2.2	17	77	3.4	9.2	1.2	7.3	1.0	0.260	0.238	0.040	0.051	0.910	0.883	2.0	0.002	0.033
103	Jg5-Amp5 - 27	0.135	1.3	0.539	5.4	5.0	2.3	9.7	2.2	16	76	3.4	9.0	1.2	8.0	1.1	0.169	0.647	0.030	0.012	0.224	0.207	0.459	0.001	0.030
104	Jg5-Amp5 - 28	0.131	1.4	0.615	5.8	5.2	2.6	11	2.4	18	85	3.9	10	1.4	8.8	1.1	0.303	0.953	0.015	0.010	0.214	0.210	0.434	0.000	0.029
105	Jg5-Amp5 - 29	0.149	1.5	0.655	6.9	6.5	3.2	14	3.2	24	116	5.2	14	1.9	12	1.6	0.282	0.493	0.012	0.024	0.368	0.327	0.756	0.003	0.033
106	Jg5-Amp5 - 30	0.217	1.4	0.478	5.0	4.0	2.0	8.0	1.7	12	59	2.5	6.8	0.861	5.6	0.736	0.219	0.113	0.042	0.029	0.712	0.653	1.5	0.010	0.121
107	Jg5-Amp5 - 31	0.161	1.3	0.506	5.2	4.5	2.1	9.5	2.1	16	72	3.2	8.6	1.1	7.3	0.934	0.273	0.480	0.050	0.023	0.435	0.411	0.925	0.009	0.098
108	Jg5-Amp5 - 32	0.065	0.431	0.174	2.0	2.0	1.1	4.3	0.925	7.0	33	1.4	3.8	0.474	2.9	0.380	0.098	0.104	0.071	0.016	0.278	0.246	0.549	0.022	0.233
109	Jg6-Amp 1 - 01	0.100	0.868	0.342	3.4	2.8	1.3	5.4	0.903	5.9	32	1.2	3.0	0.323	1.8	0.246	0.042	0.155	0.243	0.019	0.273	0.256	0.574	0.004	0.014
110	Jg6-Amp 1 - 02	0.110	0.963	0.415	4.0	3.9	1.8	7.4	1.2	7.4	42	1.5	3.6	0.426	2.3	0.297	0.021	0.122	0.000	0.018	0.080	0.070	0.178	0.003	0.007
111	Jg6-Amp 1 - 03	0.113	0.788	0.258	2.8	2.3	1.0	4.5	0.689	4.6	25	0.864	2.2	0.272	1.4	0.176	0.021	0.121	0.109	0.018	0.252	0.221	0.464	0.015	0.468
112	Jg6-Amp 1 - 04	0.113	0.893	0.366	3.6	3.2	1.5	5.6	0.992	6.0	34	1.2	3.0	0.323	2.0	0.266	0.045	0.253	0.028	0.023	0.112	0.119	0.265	0.010	0.055
113	Jg6-Amp 1 - 05	0.089	0.856	0.326	3.1	2.6	1.3	5.0	0.887	5.3	29	1.1	2.4	0.306	1.6	0.224	0.040	0.152	0.011	0.057	0.870	0.840	1.8	0.005	0.020
114	Jg6-Amp 1 - 06	0.150	1.2	0.396	3.8	3.4	1.6	6.2	1.1	7.9	44	1.6	4.3	0.513	3.2	0.386	0.098	0.264	0.020	0.025	0.180	0.176	0.447	0.005	0.019
115	Jg6-Amp 1 - 07	0.155	1.2	0.450	4.3	3.4	1.9	6.7	1.3	9.2	52	1.9	5.0	0.634	3.8	0.514	0.110	0.355	0.071	0.021	0.267	0.216	0.489	0.007	0.065
116	Jg6-Amp 1 - 08	0.109	0.925	0.341	3.4	2.9	1.4	5.7	1.0	7.6	40	1.5	4.0	0.509	3.3	0.402	0.061	0.219	0.033	0.020	0.153	0.169	0.381	0.004	0.015
117	Jg6-Amp 1 - 09	0.201	1.6	0.626	5.6	4.7	2.3	8.7	1.8	13	72	2.7	7.3	0.916	5.6	0.733	0.112	0.489	0.021	0.046	0.769	0.776	1.8	0.011	0.020
118	Jg6-Amp 1 - 10	0.179	1.4	0.549	5.5	4.6	2.3	8.8	1.7	12	64	2.4	6.1	0.741	4.6	0.597	0.118	0.204	0.049	0.021	0.232	0.208	0.474	0.008	0.021
119	Jg6-Amp 1 - 11	0.134	1.1	0.417	4.2	3.6	1.8	7.0	1.3	8.4	47	1.7	4.6	0.491	3.2	0.450	0.072	0.203	0.116	0.023	0.245	0.259	0.526	0.020	0.032
120	Jg6-Amp 1 - 12	0.106	1.1	0.436	4.0	3.4	1.6	6.0	1.1	7.3	40	1.5	3.8	0.423	2.7	0.356	0.086	0.183	0.063	0.022	0.265	0.253	0.527	0.009	0.022
121	Jg6-Amp 2 - 01	0.109	0.945	0.397	4.2	3.8	1.7	8.4	1.5	11	60	2.2	5.4	0.629	3.3	0.435	0.051	0.092	0.023	0.025	0.341	0.349	0.804	0.007	0.020
122	Jg6-Amp 2 - 02	0.118	0.920	0.367	3.5	3.1	1.5	6.1	1.2	7.8	43	1.7	4.3	0.500	2.9	0.365	0.038	0.178	0.038	0.028	0.218	0.225	0.522	0.003	0.039
123	Jg6-Amp 2 - 03	0.108	0.732	0.245	2.4	2.0	0.849	3.6	0.668	4.5	24	0.864	2.3	0.276	1.5	0.197	0.042	0.133	0.066	0.022	0.299	0.290	0.636	0.006	0.030
124	Jg6-Amp 2 - 04	0.085	0.667	0.227	2.3	2.0	0.897	3.7	0.641	4.3	23	0.858	2.2	0.252	1.5	0.202	0.034	0.107	0.016	0.019	0.126	0.123	0.259	0.001	0.006

#	Amphibole	La	Ce	Pr	Nd	Sm	Eu	Gd	Tb	Dy	Y	Ho	Er	Tm	Yb	Lu	Hf	Ta	W	^{204}Pb	^{206}Pb	^{207}Pb	^{208}Pb	Th	^{238}U
125	Jg6-Amp 2 - 05	0.088	0.746	0.285	2.5	2.3	0.981	4.0	0.729	5.1	27	1.0	2.6	0.308	1.8	0.234	0.056	0.132	0.060	0.021	0.184	0.167	0.417	0.007	0.013
126	Jg6-Amp 2 - 06	0.127	1.0	0.405	4.3	3.7	1.7	7.2	1.4	9.7	54	2.0	5.1	0.632	3.4	0.428	0.099	0.213	0.074	0.025	0.226	0.215	0.536	0.005	0.018
127	Jg6-Amp 2 - 07	0.158	1.2	0.437	4.3	3.7	1.8	7.5	1.5	11	62	2.4	6.7	0.811	5.0	0.621	0.087	0.332	0.065	0.077	1.3	1.3	2.8	0.006	0.020
128	Jg6-Amp 2 - 08	0.157	1.2	0.438	4.4	4.0	1.9	8.2	1.6	12	68	2.6	7.0	0.905	5.2	0.674	0.128	0.314	0.061	0.022	0.242	0.258	0.553	0.003	0.050
129	Jg6-Amp 2 - 09	0.135	1.1	0.424	4.4	4.1	1.8	8.2	1.6	11	60	2.2	5.8	0.672	3.9	0.465	0.062	0.178	0.113	0.024	0.209	0.178	0.455	0.018	0.291
130	Jg6-Amp 2 - 10	0.200	1.4	0.535	5.5	4.8	2.9	12	2.7	20	118	4.6	13	1.8	11	1.3	0.190	0.460	0.189	0.026	0.297	0.277	0.606	0.008	0.138
131	Jg8-Amp1 - 01	0.058	0.442	0.166	1.6	1.6	0.618	3.8	0.770	5.2	29	1.0	2.9	0.367	2.1	0.269	0.055	0.029	0.008	0.021	0.060	0.064	0.166	0.002	0.002
132	Jg8-Amp1 - 02	0.083	0.460	0.183	1.6	1.8	0.687	3.7	0.727	5.2	28	1.1	2.7	0.334	2.2	0.258	0.078	0.031	0.090	0.022	0.102	0.097	0.232	0.008	0.017
133	Jg8-Amp1 - 03	0.083	0.602	0.195	2.1	2.1	0.747	4.0	0.827	5.7	31	1.2	3.0	0.387	2.2	0.259	0.082	0.032	0.032	0.022	0.126	0.089	0.199	0.004	0.013
134	Jg8-Amp1 - 04	0.114	0.774	0.281	2.6	2.7	1.1	6.0	1.2	8.8	47	1.8	4.7	0.606	3.9	0.500	0.091	0.038	0.040	0.021	0.125	0.103	0.262	0.010	0.193
135	Jg8-Amp1 - 05	0.095	0.846	0.300	3.2	3.2	1.5	7.4	1.6	11	64	2.4	6.6	0.900	5.3	0.658	0.089	0.027	0.048	0.020	0.164	0.155	0.341	0.002	0.005
136	Jg8-Amp1 - 06	0.107	0.804	0.285	3.2	3.3	1.3	7.4	1.6	11	63	2.3	6.4	0.856	5.3	0.665	0.100	0.043	0.016	0.018	0.109	0.117	0.242	0.001	0.007
137	Jg8-Amp1 - 07	0.106	0.879	0.342	3.2	3.6	1.4	7.9	1.7	12	66	2.5	6.8	0.919	5.5	0.643	0.081	0.037	0.066	0.021	0.181	0.202	0.383	0.004	0.016
138	Jg8-Amp1 - 08	0.130	0.864	0.298	3.0	3.3	1.4	8.0	1.7	12	67	2.5	7.0	0.876	5.4	0.675	0.078	0.044	0.052	0.023	0.175	0.171	0.393	0.004	0.009
139	Jg8-Amp1 - 09	0.245	1.2	0.377	3.5	3.5	1.6	8.3	1.9	14	78	3.0	8.3	1.1	6.9	0.907	0.106	0.087	0.569	0.021	0.390	0.383	0.775	0.006	0.029
140	Jg8-Amp1 - 10	0.136	0.952	0.365	3.7	4.2	1.9	10	2.2	17	98	3.7	11	1.3	8.4	1.1	0.116	0.069	0.051	0.023	0.313	0.287	0.623	0.003	0.021
141	Jg8-Amp1 - 11	0.139	1.1	0.375	3.8	4.1	1.9	9.8	2.1	16	90	3.5	9.1	1.2	7.5	0.949	0.120	0.065	0.017	0.023	0.166	0.128	0.275	0.002	0.017
142	Jg8-Amp2 - 01	0.087	0.738	0.274	2.7	3.3	1.2	8.1	1.7	12	70	2.6	7.1	0.897	5.5	0.718	0.121	0.066	0.003	0.019	0.264	0.055	0.061	0.000	0.164
143	Jg8-Amp2 - 02	0.065	0.436	0.143	1.6	1.7	0.583	3.6	0.708	4.8	26	0.953	2.5	0.317	1.9	0.206	0.083	0.035	0.002	0.019	0.035	0.043	0.080	0.000	0.000
144	Jg8-Amp2 - 03	0.087	0.628	0.241	2.2	2.5	0.922	5.3	1.1	7.5	40	1.5	4.2	0.511	3.1	0.366	0.094	0.063	0.010	0.019	0.104	0.104	0.202	0.001	0.007
145	Jg8-Amp2 - 04	0.113	0.750	0.286	2.9	3.4	1.3	7.5	1.5	11	60	2.2	5.9	0.783	4.7	0.572	0.133	0.084	0.013	0.020	0.157	0.117	0.310	0.002	0.037
146	Jg8-Amp2 - 05	0.070	0.576	0.234	2.3	2.2	0.907	5.0	1.0	7.1	39	1.5	3.8	0.512	3.0	0.374	0.076	0.050	0.058	0.018	0.282	0.198	0.373	0.006	0.096
147	Jg8-Amp2 - 06	0.058	0.440	0.171	1.6	1.5	0.691	3.8	0.767	5.4	31	1.1	3.1	0.400	2.4	0.330	0.059	0.025	0.102	0.017	0.740	0.251	0.309	0.010	0.997
148	Jg8-Amp2 - 07	0.086	0.720	0.236	2.7	2.7	1.1	6.8	1.4	10	58	2.2	5.7	0.755	4.6	0.574	0.094	0.072	0.002	0.018	0.078	0.068	0.166	0.002	0.004
149	Jg8-Amp2 - 08	0.078	0.598	0.209	2.3	2.3	0.869	5.3	1.0	7.4	40	1.4	3.9	0.516	3.2	0.383	0.028	0.053	0.013	0.020	0.562	0.186	0.232	0.004	0.201
150	Jg8-Amp2 - 09	0.063	0.491	0.174	1.8	1.8	0.647	3.8	0.735	5.1	28	1.1	2.7	0.338	2.1	0.251	0.041	0.041	0.000	0.024	0.069	0.076	0.153	0.000	0.000
151	Jg8-Amp2 - 10	0.069	0.540	0.190	2.0	2.2	0.714	4.6	0.902	6.4	34	1.3	3.3	0.423	2.3	0.298	0.123	0.073	0.003	0.022	0.035	0.047	0.092	0.000	0.005
152	Jg9b-Amp1 - 01	0.210	1.8	0.599	5.9	4.3	1.3	7.0	1.2	8.1	42	1.5	3.7	0.439	2.4	0.294	0.044	0.168	0.014	0.006	0.093	0.086	0.218	0.002	0.005
153	Jg9b-Amp1 - 02	0.233	1.8	0.626	6.0	4.3	1.4	7.6	1.3	8.8	47	1.7	4.1	0.491	2.6	0.350	0.056	0.178	0.001	0.005	0.073	0.072	0.151	0.000	0.005
154	Jg9b-Amp1 - 03	0.152	1.4	0.481	4.5	3.2	1.1	5.4	1.0	6.2	34	1.2	2.9	0.343	1.8	0.223	0.021	0.089	0.013	0.006	0.076	0.068	0.149	0.001	0.002
155	Jg9b-Amp1 - 04	0.188	1.5	0.532	5.0	3.8	1.3	6.7	1.2	7.3	39	1.4	3.5	0.389	2.3	0.265	0.045	0.142	0.119	0.006	0.112	0.086	0.192	0.008	0.093
156	Jg9b-Amp1 - 05	0.142	1.1	0.358	3.3	2.3	0.740	3.9	0.724	4.5	25	0.876	2.2	0.239	1.3	0.186	0.015	0.065	0.453	0.006	0.174	0.157	0.328	0.010	0.015
157	Jg9b-Amp1 - 06	0.149	1.2	0.409	3.7	2.6	0.828	4.3	0.703	4.6	24	0.872	2.1	0.216	1.3	0.164	0.017	0.077	0.097	0.007	0.095	0.084	0.174	0.002	0.009
158	Jg9b-Amp1 - 07	0.128	1.0	0.352	3.2	2.1	0.676	3.6	0.585	3.7	20	0.702	1.7	0.180	1.0	0.127	0.013	0.052	0.036	0.006	0.133	0.115	0.252	0.001	0.070
159	Jg9b-Amp1 - 08	0.171	1.2	0.426	3.8	3.0	1.0	5.4	0.936	6.1	33	1.2	2.8	0.325	2.0	0.261	0.021	0.077	0.205	0.011	0.215	0.225	0.465	0.007	0.043
160	Jg9b-Amp1 - 09	0.193	1.6	0.564	5.2	4.1	1.4	7.7	1.4	9.0	49	1.8	4.3	0.495	2.9	0.356	0.036	0.078	0.001	0.006	0.093	0.066	0.169	0.000	0.004
161	Jg9b-Amp1 - 11	0.261	2.3	0.826	7.9	6.4	2.1	12	2.2	14	81	2.9	7.2	0.857	4.8	0.639	0.032	0.098	0.024	0.005	0.102	0.085	0.215	0.001	0.011
162	Jg9b-Amp1 - 12	0.161	1.2	0.430	4.0	3.2	1.2	6.0	1.0	6.8	35	1.3	3.1	0.351	2.0	0.237	0.048	0.212	0.001	0.006	0.105	0.086	0.200	0.000	0.002

#	Amphibole	La	Ce	Pr	Nd	Sm	Eu	Gd	Tb	Dy	Y	Ho	Er	Tm	Yb	Lu	Hf	Ta	W	^{204}Pb	^{206}Pb	^{207}Pb	^{208}Pb	Th	^{238}U
163	Jg9b-Amp1 - 13	0.167	1.4	0.480	4.8	4.1	1.5	7.6	1.4	9.7	53	1.9	4.7	0.553	3.1	0.389	0.052	0.128	0.005	0.006	0.095	0.071	0.173	0.001	0.005
164	Jg9b-Amp1 - 14	0.206	1.6	0.603	5.8	4.6	1.6	8.8	1.6	11	59	2.2	5.3	0.614	3.6	0.475	0.037	0.081	0.013	0.006	0.088	0.079	0.165	0.001	0.007
165	Jg9b-Amp1 - 15	0.221	1.8	0.656	6.5	5.1	1.7	9.4	1.8	12	66	2.4	5.9	0.724	4.2	0.533	0.049	0.124	0.572	0.006	0.089	0.070	0.167	0.001	0.006
166	Jg9b-Amp1 - 16	0.190	1.4	0.540	4.9	4.2	1.6	8.1	1.6	10	56	2.1	5.1	0.605	3.5	0.438	0.068	0.277	0.054	0.033	0.697	0.637	1.4	0.001	0.024
167	Jg9b-Amp1 - 17	0.240	1.8	0.633	6.3	5.2	1.9	9.6	1.8	12	67	2.4	6.0	0.684	3.9	0.498	0.055	0.204	0.023	0.006	0.133	0.104	0.237	0.001	0.042
168	Jg9b-Amp1 - 18	0.261	2.3	0.815	8.0	6.8	2.4	13	2.4	17	92	3.3	8.7	1.0	5.7	0.748	0.075	0.142	0.031	0.022	0.320	0.327	0.690	0.002	0.010
169	Jg9b-Amp1 - 19	0.182	1.5	0.527	5.5	4.9	1.9	9.8	1.9	13	71	2.6	6.5	0.772	4.5	0.569	0.076	0.244	0.221	0.009	0.207	0.201	0.440	0.006	0.016
170	Jg9b-Amp1 - 20	0.169	1.4	0.510	5.1	4.6	1.9	9.7	1.9	13	73	2.6	6.8	0.833	4.8	0.616	0.063	0.208	0.184	0.009	0.159	0.144	0.298	0.002	0.086
171	Jg9b-Amp1 - 21	0.226	1.8	0.661	6.5	6.0	2.4	13	2.5	18	97	3.5	9.3	1.1	6.5	0.864	0.101	0.323	1.3	0.007	0.146	0.150	0.284	0.012	0.047
172	Jg9b-Amp1 - 22	0.162	1.4	0.498	4.8	4.2	1.6	8.4	1.6	11	62	2.3	5.6	0.676	3.9	0.485	0.054	0.251	0.000	0.007	0.110	0.089	0.217	0.001	0.008
173	Jg9b-Amp1 - 24	0.158	1.5	0.529	5.3	4.6	1.7	8.8	1.6	11	61	2.2	5.7	0.651	3.8	0.484	0.065	0.141	0.013	0.016	0.351	0.332	0.737	0.001	0.007
174	Jg9b-Amp1 - 25	0.191	1.7	0.558	5.7	4.5	1.7	8.8	1.6	11	60	2.1	5.5	0.626	3.6	0.477	0.076	0.198	0.001	0.006	0.094	0.079	0.190	0.001	0.005
175	Jg9b-Amp1 - 26	0.231	2.0	0.708	6.9	5.7	1.9	9.8	1.9	13	68	2.4	6.1	0.694	4.0	0.514	0.045	0.116	0.000	0.005	0.086	0.084	0.155	0.001	0.005
176	Jg9b-Amp1 - 27	29	65	7.0	29	7.5	2.0	9.7	1.6	10	56	2.0	5.0	0.567	3.2	0.399	0.062	0.141	0.035	0.007	0.238	0.223	0.502	0.001	0.062
177	Jg9b-Amp1 - 28	0.179	1.3	0.477	4.1	3.3	1.0	5.4	0.977	6.5	34	1.2	3.0	0.337	2.0	0.241	0.016	0.060	0.000	0.007	0.086	0.077	0.149	0.000	0.002
178	Jg9b-Amp1 - 29	0.291	1.7	0.545	4.6	3.5	1.1	6.4	1.1	7.2	39	1.4	3.4	0.397	2.2	0.277	0.033	0.079	0.068	0.074	1.3	1.3	2.8	0.004	0.039
179	Jg9b-Amp1 - 30	0.240	1.5	0.511	4.6	3.6	1.2	6.3	1.1	7.4	40	1.4	3.6	0.437	2.7	0.325	0.032	0.106	0.499	0.005	0.130	0.117	0.243	0.007	0.039
180	Jg9b-Amp1 - 31	0.186	1.5	0.512	5.0	3.6	1.2	6.5	1.1	7.3	39	1.4	3.5	0.377	2.2	0.260	0.035	0.057	0.023	0.006	0.077	0.068	0.149	0.002	0.018
181	Jg9b-Amp2 - 32	0.156	1.4	0.495	4.9	3.8	1.3	6.3	1.1	7.2	38	1.4	3.3	0.363	2.1	0.244	0.024	0.040	0.002	0.005	0.066	0.062	0.146	0.000	0.002
182	Jg9b-Amp2 - 33	6.1	15	2.1	12	6.3	2.0	11	2.0	14	74	2.6	6.7	0.797	4.4	0.606	0.056	0.097	0.132	0.007	0.179	0.163	0.351	0.010	0.054
183	Jg9b-Amp2 - 34	0.210	1.9	0.685	6.8	5.5	1.9	10	1.9	13	70	2.5	6.4	0.725	4.2	0.553	0.051	0.097	0.110	0.006	0.215	0.192	0.369	0.027	0.186
184	Jg9b-Amp2 - 35	0.235	1.8	0.651	6.0	4.7	1.6	8.5	1.6	11	58	2.1	5.3	0.636	3.6	0.489	0.042	0.189	0.026	0.006	0.121	0.113	0.238	0.003	0.013
185	Jg9b-Amp2 - 37	0.158	1.2	0.425	4.0	3.0	1.0	5.5	0.956	6.2	33	1.2	3.0	0.327	1.8	0.220	0.015	0.139	0.201	0.005	0.098	0.098	0.193	0.001	0.003
186	Jg9b-Amp2 - 38	0.153	1.2	0.423	4.1	3.1	1.1	5.8	1.0	6.8	37	1.3	3.2	0.355	2.1	0.269	0.017	0.087	0.107	0.006	0.091	0.088	0.174	0.000	0.004
187	Jg9b-Amp2 - 39	0.250	2.0	0.692	6.8	5.4	1.9	10	1.9	13	71	2.5	6.4	0.750	4.2	0.522	0.036	0.086	0.067	0.006	0.129	0.109	0.241	0.002	0.054
188	Jg9b-Amp2 - 40	0.210	1.5	0.525	5.1	4.1	1.5	8.2	1.5	11	59	2.1	5.5	0.644	3.6	0.455	0.032	0.111	0.277	0.025	0.739	0.550	1.2	0.002	0.864
189	Jg9b-Amp2 - 41	0.184	1.4	0.504	4.8	4.2	1.6	8.7	1.6	11	61	2.2	5.7	0.668	3.9	0.505	0.062	0.215	0.107	0.009	0.197	0.154	0.337	0.011	0.204
190	Jg9b-Amp2 - 42	0.167	1.2	0.455	4.3	3.6	1.3	6.5	1.3	8.7	46	1.7	4.1	0.474	2.7	0.352	0.040	0.169	0.120	0.012	0.167	0.146	0.330	0.005	0.114
191	Jg9b-Amp2 - 43	0.166	1.4	0.479	5.0	4.4	1.9	9.2	1.8	13	71	2.6	6.6	0.798	4.6	0.580	0.032	0.165	0.004	0.006	0.127	0.102	0.244	0.001	0.012
192	Jg9b-Amp2 - 44	0.097	0.786	0.284	2.9	2.5	1.0	5.3	0.993	7.1	38	1.3	3.5	0.414	2.4	0.293	0.013	0.119	0.006	0.006	0.093	0.096	0.182	0.000	0.005
193	Jg9b-Amp2 - 45	0.137	1.1	0.391	4.2	4.2	1.8	9.5	1.9	14	77	2.7	7.3	0.890	5.3	0.695	0.059	0.424	0.008	0.006	0.130	0.123	0.257	0.000	0.017
194	Jg9b-Amp2 - 46	0.190	1.6	0.569	5.9	6.0	2.5	13	2.6	19	106	3.9	10	1.2	7.7	1.0	0.089	0.567	0.007	0.007	0.121	0.108	0.261	0.001	0.020
195	Jg9b-Amp2 - 48	0.217	1.9	0.692	7.3	6.9	2.7	14	2.9	20	116	4.2	11	1.4	7.7	1.0	0.075	0.246	0.005	0.008	0.134	0.122	0.256	0.002	0.025
196	Jg9b-Amp2 - 49	0.216	1.9	0.753	7.4	6.8	2.5	13	2.7	18	104	3.7	9.6	1.1	6.7	0.873	0.066	0.142	0.009	0.008	0.110	0.117	0.235	0.001	0.009
197	Jg9b-Amp2 - 50	0.245	2.1	0.754	7.3	6.4	2.3	12	2.3	16	89	3.3	8.3	0.954	5.6	0.706	0.055	0.120	0.000	0.006	0.107	0.098	0.215	0.001	0.009
	Mean (n=197)	0.532	1.9	0.465	3.9	3.1	1.3	6.1	1.2	8.7	46	1.8	4.7	0.597	3.7	0.483	0.170	0.138	0.065	0.018	0.293	0.257	0.567	0.058	0.084
	SD	2.4	5.2	0.608	3.0	1.7	0.766	3.3	0.682	5.0	25	1.0	2.7	0.352	2.2	0.291	0.359	0.177	0.119	0.025	0.426	0.421	0.998	0.241	0.184
	Median	0.135	1.1	0.396	3.7	3.1	1.3	5.7	1.1	7.4	39	1.5	3.9	0.491	3.0	0.389	0.082	0.077	0.035	0.012	0.181	0.157	0.346	0.004	0.027
	Max	29	65	7.0	29	7.5	3.2	14	3.2	24	118	5.2	14	1.9	12	1.6	4.2	0.979	1.3	0.334	5.2	5.3	13	2.6	1.6
	Min	0.008	0.075	0.020	0.327	0.387	0.175	1.2	0.265	2.2	13	0.470	1.4	0.180	1.0	0.127	0.013	0.004	0.000	0.005	0.030	0.031	0.060	0.000	0.000

#	Apatite	La	Ce	Pr	Nd	Sm	Eu	Gd	Tb	Dy	Y	Ho	Er	Tm	Yb	Lu	Hf	Ta	W	^{204}Pb	^{206}Pb	^{207}Pb	^{208}Pb	Th	^{238}U
1	Jg8-Ap 1 - 01	52	158	27	163	67	18	114	21	144	801	31	82	10.0	60	7.4	0.012	0.004	0.096	0.069	1.9	1.4	2.9	0.108	1.7
2	Jg8-Ap 1 - 02	23	73	14	96	48	14	92	17	112	634	24	62	7.4	43	5.4	0.006	0.001	0.390	0.036	0.989	0.630	1.4	0.065	1.3
3	Jg8-Ap 1 - 03	31	94	17	112	51	15	93	17	114	637	24	63	7.6	43	5.4	0.011	0.004	0.724	0.050	1.2	0.799	1.6	0.125	1.4
4	Jg8-Ap 1 - 04	26	82	16	101	48	14	90	17	117	660	25	66	8.0	46	5.8	0.006	0.004	0.913	0.037	1.3	0.903	2.0	0.255	1.0
5	Jg8-Ap 1 - 05	33	104	18	115	52	14	97	19	130	693	27	70	8.5	47	5.8	0.009	0.005	0.174	0.065	1.6	1.2	2.5	0.080	1.5
6	Jg8-Ap 2 - 01	68	198	33	194	74	19	119	21	142	810	30	82	10	59	7.3	0.009	0.003	0.123	0.085	2.2	1.6	3.3	0.189	2.3
7	Jg8-Ap 2 - 02	62	181	31	181	71	18	114	21	140	791	29	80	9.9	56	7.2	0.015	0.004	0.456	0.071	2.0	1.4	2.9	0.160	2.3
8	Jg8-Ap 2 - 04	91	262	43	247	88	21	133	23	154	855	32	87	11	64	7.9	0.008	0.001	0.216	0.107	2.6	1.9	3.8	0.201	2.4
9	Jg8-Ap 2 - 06	50	154	28	168	69	19	113	20	137	780	29	78	9.6	57	7.3	0.023	0.002	0.064	0.048	2.0	1.3	2.6	0.074	2.5
10	Jg8-Ap 2 - 07	75	216	36	204	75	19	120	21	146	836	32	85	11	62	7.7	0.012	0.006	0.952	0.080	2.5	1.8	3.6	0.153	2.1
11	Jg8-Ap 2 - 09	77	229	38	218	82	20	126	22	154	864	33	90	11	66	8.2	0.016	0.004	0.042	0.089	2.4	1.8	3.6	0.168	2.5
12	Jg8-Ap 2 - 10	44	136	24	142	59	16	101	19	139	835	31	87	11	63	8.0	0.016	0.006	0.146	0.088	1.9	1.4	3.0	0.104	1.7
13	Jg9b-Ap - 01	60	185	32	187	68	19	101	15	93	502	18	44	4.7	25	3.4	0.005	0.001	0.112	0.063	1.7	1.2	2.5	0.090	1.9
14	Jg9b-Ap - 02	57	180	31	189	69	19	99	15	90	484	17	42	4.5	24	3.3	0.005	0.001	0.118	0.064	1.7	1.2	2.4	0.090	1.9
15	Jg9b-Ap - 04	41	136	25	158	64	18	97	15	89	490	18	42	4.6	25	3.4	0.013	0.003	0.056	0.071	1.6	1.1	2.1	0.069	2.0
16	Jg9b-Ap - 05	40	135	26	167	68	18	103	15	92	499	18	42	4.5	24	3.2	0.009	0.001	0.851	0.037	1.5	0.816	1.6	0.389	2.4
17	Jg9b-Ap - 06	35	115	22	144	61	16	92	14	79	437	15	36	3.8	20	2.7	0.012	0.003	1.3	0.030	1.2	0.551	1.1	0.243	2.1
18	Jg9b-Ap - 08	14	55	12	92	44	11	73	11	62	350	12	27	2.8	14	1.9	0.005	0.002	3.2	0.012	0.871	0.267	0.487	0.455	2.1
19	Jg9b-Ap - 09	50	159	28	170	65	18	96	14	85	467	17	40	4.3	23	3.1	0.006	0.002	0.195	0.055	1.5	1.0	2.1	0.077	1.5
20	Jg9b-Ap - 12	42	141	26	167	64	17	94	14	82	452	16	38	4.0	22	2.9	0.008	0.002	0.271	0.044	1.4	0.851	1.6	0.089	1.8
21	Jg9b-Ap - 14	78	236	39	219	75	20	104	16	92	492	18	43	4.7	25	3.4	0.003	0.001	1.5	0.080	2.1	1.3	2.7	0.099	2.4
22	Jg9b-Ap - 15	37	124	24	157	64	16	95	14	82	431	16	36	3.8	19	2.7	0.008	0.002	4.5	0.036	0.893	0.575	1.0	0.074	1.1
23	Jg9b-Ap - 16	58	181	32	182	69	20	105	16	98	530	19	47	5.0	27	3.6	0.004	0.002	0.210	0.067	1.9	1.4	2.9	0.063	1.4
24	Jg9b-Ap - 17	39	130	24	157	63	18	96	15	86	478	17	40	4.2	23	3.1	0.002	0.001	1.5	0.044	1.1	0.722	1.5	0.204	1.1
25	Jg9b-Ap - 19	46	145	25	150	60	17	93	15	86	470	17	40	4.3	23	3.0	0.003	0.003	1.9	0.051	1.2	0.964	2.0	0.029	0.586
26	Jg9b-Ap - 21	40	125	23	147	59	15	90	13	76	416	15	34	3.5	18	2.5	0.003	0.021	9.1	0.018	1.0	0.566	1.3	0.084	1.2
27	Jg9b-Ap - 22	68	216	38	224	79	21	110	17	98	522	19	45	4.8	26	3.5	0.005	0.001	1.1	0.064	1.7	1.1	2.1	0.227	1.9
28	Jg9b-Ap - 23	81	249	42	233	78	22	109	17	100	532	19	46	5.1	28	3.8	0.011	0.000	0.200	0.093	2.1	1.4	2.8	0.171	2.4
29	Jg9b-Ap - 25	55	171	30	176	68	18	101	15	92	500	18	42	4.5	25	3.3	0.010	0.000	26	0.056	1.7	1.1	2.1	0.099	2.1
30	Jg9b-Ap - 28	52	163	28	161	62	19	95	15	90	489	18	43	4.7	25	3.4	0.006	0.002	0.186	0.077	1.8	1.4	2.9	0.052	1.4
31	Jg9b-Ap - 17	0.277	39	130	24	157	63	18	96	15	86	17	40	4.2	23	3.1	0.002	0.001	1.5	0.044	1.1	0.722	1.5	0.204	1.1
32	Jg9b-Ap - 19	0.220	46	145	25	150	60	17	93	15	86	17	40	4.3	23	3.0	0.003	0.003	1.9	0.051	1.2	0.964	2.0	0.029	0.586
33	Jg9b-Ap - 21	5.3	40	125	23	147	59	15	90	13	76	15	34	3.5	18	2.5	0.003	0.021	9.1	0.018	1.0	0.566	1.3	0.084	1.2
34	Jg9b-Ap - 22	0.163	68	216	38	224	79	21	110	17	98	19	45	4.8	26	3.5	0.005	0.001	1.1	0.064	1.7	1.1	2.1	0.227	1.9
35	Jg9b-Ap - 23	0.078	81	249	42	233	78	22	109	17	100	19	46	5.1	28	3.8	0.011	0.000	0.200	0.093	2.1	1.4	2.8	0.171	2.4
36	Jg9b-Ap - 25	9.7	55	171	30	176	68	18	101	15	92	18	42	4.5	25	3.3	0.010	0.000	26	0.056	1.7	1.1	2.1	0.099	2.1
37	Jg9b-Ap - 28	0.201	52	163	28	161	62	19	95	15	90	18	43	4.7	25	3.4	0.006	0.002	0.186	0.077	1.8	1.4	2.9	0.052	1.4
	Mean (n=37)	42	138	55	141	87	27	86	32	89	496	21	53	6.0	34	4.4	0.008	0.003	2.6	0.059	1.6	1.1	2.3	0.139	1.7
	SD	26	62	60	65	48	20	35	33	44	245	6.1	19	2.6	16	1.9	0.005	0.005	5.9	0.023	0.458	0.383	0.784	0.093	0.533
	Median	42	136	30	158	68	19	96	17	92	492	18	43	4.7	25	3.4	0.008	0.002	0.456	0.063	1.7	1.1	2.1	0.099	1.9
	Max	91	262	249	247	233	79	133	110	154	864	33	90	11	66	8.2	0.023	0.021	26	0.107	2.6	1.9	3.8	0.455	2.5
	Min	0.078	39	12	23	44	11	15	11	13	76	12	27	2.8	14	1.9	0.002	0.000	0.042	0.012	0.871	0.267	0.487	0.029	0.586

SD Table 1d. LA-ICP-MS data for magnetite, amphibole and apatite used for box-and-whisker plots (concentrations in ppm)

	Lithophile elements				Transition metals								REY	Granitophile				
Magnetite	Si	Mg	Al	Ca	Ti	V	Nb	Cr	Ni	Co	Mn	Zn	ΣREY	^{238}U	^{206}Pb	W	Sn	Mo
1. Mag - core	3045	2038	1305	141	259	324	0.589	0.652	1869	14	121	76	0.447	0.165	0.498	0.131	0.358	0.001
1. Mag - core	4880	2490	1519	174	354	338	1.3	1.3	1886	8.9	101	111	1.4	0.132	1.2	0.228	0.765	0.007
1. Mag - core	8705	5417	3183	89	327	335	0.527	1.8	1988	6.4	90	231	1.6	0.820	0.643	0.511	0.403	0.002
1. Mag - core	3956	2162	607	445	269	327	0.324	0.257	1945	16	142	84	0.727	0.145	1.4	0.279	0.351	0.017
1. Mag - core	1983	693	690	88	276	324	0.254	4.6	1709	12	124	41	0.427	0.094	0.184	0.159	0.370	0.004
1. Mag - core	6050	3134	1808	46	347	327	0.394	0.073	2048	10	83	758	0.714	0.435	0.329	0.165	0.385	0.031
1. Mag - core	3646	2095	936	528	243	319	0.145	2.7	1808	8.9	119	104	0.613	0.084	0.967	0.355	0.300	0.020
1. Mag - core	4371	2438	964	272	266	319	0.327	4.2	1887	9.0	103	236	0.812	0.263	2.0	0.218	0.315	0.009
1. Mag - core	6421	3613	2068	57	387	331	0.230	0.067	2013	6.9	87	117	0.299	0.119	0.972	0.066	0.257	0.002
1. Mag - core	2603	1310	855	60	311	339	0.150	0.031	2018	15	111	194	0.270	0.071	0.797	0.141	0.224	0.009
1. Mag - core	981	372	343	65	282	341	2.3	0.175	1917	23	144	66	0.138	0.068	0.047	0.064	0.456	0.003
1. Mag - core	1572	782	487	196	315	543	0.158	18	1577	27	159	277	0.108	0.110	1.7	0.209	0.494	0.006
1. Mag - core	5975	1850	1201	10	395	555	0.796	21	1538	25	100	494	0.313	0.251	1.0	0.201	0.688	0.001
1. Mag - core	654	123	378	245	283	561	0.032	25	1666	18	73	106	0.244	0.014	0.068	0.022	0.474	0.018
1. Mag - core	8708	6042	3264	133	266	553	1.2	94	3337	41	96	95	0.772	0.432	0.917	0.197	0.399	0.001
1. Mag - core	925	398	391	65	296	570	0.169	33	1682	30	113	49	0.113	0.061	0.096	0.038	0.393	0.002
1. Mag - core	16995	7828	1565	1673	385	440	3.1	10	1812	36	214	211	9.9	0.387	2.3	1.8	1.3	0.031
1. Mag - core	11089	4605	1655	2078	415	445	3.6	12	1758	30	207	229	9.5	0.454	3.6	2.3	1.4	0.034
1. Mag - core	4707	2430	1048	350	279	427	1.3	16	1689	28	127	18840	1.2	0.668	1.3	0.630	0.821	0.022
1. Mag - core	11115	5140	1511	1506	403	410	2.8	7.1	1678	20	198	574	5.7	0.465	5.7	2.7	1.2	0.033
1. Mag - core	16096	7662	1545	1541	391	424	2.9	2.2	1933	17	138	191	5.6	0.569	4.1	1.9	1.4	0.028
1. Mag - core	4049	1868	475	221	264	408	0.170	1.7	2704	22	110	143	1.5	0.386	1.0	0.236	0.552	0.055
1. Mag - core	9797	3990	1554	1774	479	456	2.4	0.376	1796	32	192	263	17	0.931	4.7	5.3	1.4	0.018
1. Mag - core	9775	4267	1519	404	481	405	0.921	1.3	1852	12	110	200	6.4	0.255	9.7	1.8	0.814	0.046
1. Mag - core	14635	8125	1357	843	406	401	0.781	1.2	2018	34	181	359	7.4	0.674	25	2.7	0.814	0.044
1. Mag - core	10264	4325	1602	1549	503	412	1.9	0.338	2174	18	172	497	14	0.627	12	3.5	1.2	0.050
1. Mag - core	10155	4286	1449	1317	471	410	2.3	0.363	1945	26	179	345	14	0.555	4.5	6.0	1.4	0.063
1. Mag - core	10196	4308	1608	2008	540	427	2.4	0.317	1895	27	219	362	13	0.498	8.1	5.8	1.5	0.051
1. Mag - core	24222	13361	1311	452	408	415	1.0	7.5	2201	26	132	302	3.2	0.520	7.1	0.934	0.830	0.037
1. Mag - core	1295	497	407	279	254	432	0.399	10	2005	33	85	110	0.976	0.311	0.277	0.233	0.532	0.030
1. Mag - core	9706	4834	1567	1236	461	425	1.9	13	1832	36	340	234	2.4	0.502	4.5	1.3	1.1	0.025
1. Mag - core	12328	5902	1644	1331	446	434	2.5	11	1846	36	185	30870	4.4	0.635	2.3	1.3	1.5	0.021
1. Mag - core	11955	6067	1411	671	392	445	1.7	15	1864	19	155	336	2.4	0.774	7.2	0.898	0.942	0.044
1. Mag - core	9761	4403	1464	513	462	440	1.7	22	1920	37	185	184	2.7	0.541	3.6	1.2	1.0	0.047
1. Mag - core	363	99	269	265	190	413	0.048	3.4	1563	15	115	26	0.219	0.012	0.044	0.094	0.363	0.060
1. Mag - core	311	83	310	254	200	430	0.005	23	1587	22	143	47	0.051	0.001	0.019	0.003	0.364	0.039
1. Mag - core	206	88	312	233	204	418	0.018	23	1532	23	143	73	0.050	0.010	0.034	0.021	0.324	0.043
1. Mag - core	281	123	285	231	193	408	0.021	16	2151	16	106	40	0.307	0.040	0.078	0.014	0.354	0.048
1. Mag - core	337	113	289	203	193	416	0.131	23	1576	15	96	72	0.141	0.112	0.871	0.047	0.385	0.423
1. Mag - core	5706	3405	387	202	191	419	0.202	12	1742	25	106	115	0.253	0.160	0.558	0.108	0.360	0.025
1. Mag - core	192	92	324	224	211	413	0.788	12	1673	24	128	83	0.153	0.169	0.936	0.111	0.399	0.022
1. Mag - core	544	297	335	238	188	434	0.175	17	1705	14	83	136	0.242	0.134	0.333	0.062	0.287	0.030
1. Mag - core	10074	4618	827	2839	175	402	0.253	13	13664	599	98	90	2.9	0.278	5.8	0.087	1.1	0.094
1. Mag - core	239	82	244	225	191	408	0.006	25	1463	12	82	23	0.107	0.019	0.021	0.000	0.321	0.031
1. Mag - core	294	104	271	242	197	411	0.029	26	1399	15	116	38	0.107	0.051	0.886	0.029	0.323	0.199
1. Mag - core	269	65	271	213	192	409	0.014	21	1386	17	133	29	0.044	0.007	0.032	0.000	0.310	0.026
1. Mag - core	9609	4036	1451	1132	377	442	3.4	0.299	1489	16	182	105	8.8	0.352	5.1	1.8	1.2	0.033
1. Mag - core	12594	6393	1325	2563	328	444	2.7	0.320	1762	26	227	177	6.4	0.425	2.2	1.9	1.1	0.050
1. Mag - core	3971	1725	732	256	248	432	1.0	0.348	1428	18	189	126	2.0	0.147	2.0	0.690	0.552	0.041
1. Mag - core	11142	4328	1944	1346	424	450	3.5	0.267	1670	25	236	234	28	0.715	8.4	6.4	1.3	0.101
1. Mag - core	10814	5093	1386	728	320	453	2.6	0.274	1686	25	455	236	4.3	0.685	4.5	2.5	0.970	0.052
1. Mag - core	7687	5844	846	887	253	433	1.4	0.484	1518	20	650	192	1.8	0.696	3.7	1.1	0.576	0.042
1. Mag - core	154	131	368	220	166	410	0.001	1.1	1594	27	156	81	0.025	0.000	0.013	0.000	0.364	0.023
1. Mag - core	157	121	378	206	169	407	0.075	0.854	1604	27	154	74	0.032	0.016	0.014	0.010	0.498	0.028

	Lithophile elements				Transition metals								REY	Granitophile				
Magnetite	Si	Mg	Al	Ca	Ti	V	Nb	Cr	Ni	Co	Mn	Zn	ΣREY	^{238}U	^{206}Pb	W	Sn	Mo
1. Mag - core	173	122	380	185	167	412	0.013	0.711	1554	24	148	63	0.027	0.003	0.073	0.003	0.326	0.036
1. Mag - core	7328	3417	1339	764	296	434	2.0	1.1	1779	31	210	211	7.4	0.515	1.2	2.5	0.993	0.032
1. Mag - core	6416	2928	1100	334	245	417	2.0	1.4	1767	28	184	169	3.9	0.317	1.6	0.799	0.787	0.066
1. Mag - core	41939	3323	1260	9230	218	401	1.7	3.9	2050	33	206	280	6.4	0.415	7.0	1.1	3.6	0.140
1. Mag - core	427	126	377	211	156	414	0.079	1.1	1591	25	151	67	0.078	0.045	0.056	0.009	0.408	0.040
1. Mag - core	4741	2966	1059	250	260	452	0.259	18	1537	19	146	5305	2.5	0.340	5.7	0.315	0.592	0.015
1. Mag - core	3316	2116	747	352	246	434	0.135	20	1405	7.3	117	1439	0.823	0.091	3.8	0.352	0.564	0.036
1. Mag - core	9155	4370	1366	567	333	450	0.749	31	6141	8.3	51	45	3.2	0.492	0.372	0.534	1.1	0.122
1. Mag - core	16295	8878	3574	577	319	473	0.550	28	8541	14	117	77	3.7	0.494	1.5	0.656	0.790	0.054
1. Mag - core	9829	6977	4160	370	241	456	0.720	29	4267	7.9	84	94	3.5	1.4	1.8	0.664	0.851	0.048
1. Mag - core	715	366	313	237	473	480	1.2	90	1377	12	87	38	0.550	0.345	0.354	1.4	0.514	0.045
1. Mag - core	510	272	291	227	251	429	0.063	18	1485	18	105	64	0.148	0.142	0.109	0.029	0.542	0.045
1. Mag - core	1957	1103	527	213	292	434	0.068	2.3	1614	18	86	80	0.564	0.196	0.123	0.150	0.422	0.040
1. Mag - core	1280	1115	1007	229	313	440	0.089	3.5	1813	19	110	94	0.662	0.318	0.686	0.099	0.580	0.048
1. Mag - core	326	952	314	272	320	435	0.120	4.4	1533	25	267	601	0.520	0.426	0.746	0.086	0.502	0.041
1. Mag - core	1215	1030	443	321	308	435	0.130	0.706	1683	28	163	135	0.490	0.343	0.604	0.131	0.494	0.044
1. Mag - core	1117	996	329	211	327	421	0.142	0.371	1717	26	264	137	0.335	0.393	1.1	0.115	0.492	0.022
1. Mag - core	844	547	364	235	295	430	0.056	0.473	1780	27	153	169	0.161	0.219	2.0	0.095	0.456	0.019
1. Mag - core	307	81	313	225	276	430	0.007	0.336	1716	27	131	114	0.045	0.029	0.042	0.017	0.459	0.031
1. Mag - core	2894	1352	618	675	339	442	0.248	2.9	1689	24	152	155	4.1	0.259	1.7	0.425	0.591	0.021
1. Mag - core	2851	1299	532	229	193	502	0.077	60	1853	3.3	27	17	0.639	0.203	0.113	0.059	0.407	0.038
1. Mag - core	4225	2041	541	398	271	500	0.725	15	1590	16	138	132	49	0.723	6.3	9.1	0.720	0.155
1. Mag - core	4595	2602	953	3393	317	467	0.632	13	1573	20	169	109	39	0.256	0.946	6.6	0.690	0.029
1. Mag - core	3179	1841	909	228	275	495	0.382	30	1568	14	98	1779	1.1	0.681	0.568	0.325	0.658	0.028
1. Mag - core	1940	1422	1041	212	246	461	0.032	23	7897	124	117	1298	0.094	0.022	1.1	0.035	0.370	0.095
1. Mag - core	3647	1895	389	625	247	525	0.495	8.0	1500	17	132	463	40	0.543	4.9	6.9	0.561	0.708
1. Mag - core	281	97	261	255	220	427	0.011	73	1338	12	99	30	0.053	0.040	0.072	0.030	0.414	0.040
1. Mag - core	3913	2254	1005	240	235	419	0.233	88	2276	5.7	63	84	1.7	0.664	1.4	0.327	0.605	0.032
1. Mag - core	8202	5476	2094	422	289	436	0.113	20	1713	25	166	435	0.774	0.168	6.0	0.762	0.403	0.024
1. Mag - core	11918	9870	6114	262	295	404	0.350	105	1641	14	80	243	2.9	0.419	3.6	0.347	0.656	0.044
1. Mag - core	11879	7013	1927	1043	347	436	0.271	153	1741	24	237	393	3.9	0.217	9.9	5.2	0.631	0.034
1. Mag - core	571	160	355	235	269	441	0.068	17	1530	24	112	181	0.933	0.133	2.4	0.262	0.481	0.046
1. Mag - core	534	383	448	685	272	437	0.044	6.6	1570	21	125	207	0.301	0.068	0.451	0.326	0.417	0.029
1. Mag - core	320	166	262	317	211	439	0.110	35	1507	23	70	60	0.360	0.186	0.282	0.101	0.380	0.038
1. Mag - core	1059	455	365	265	247	431	0.055	78	1475	17	104	79	2.9	0.047	0.692	0.225	0.381	0.044
1. Mag - core	10565	4538	1133	1980	430	435	1.1	53	1508	17	129	97	4.6	0.318	0.864	1.1	1.4	0.035
1. Mag - core	448	190	318	232	210	417	0.013	76	1365	13	111	40	0.088	0.006	0.030	0.009	0.373	0.025
1. Mag - core	263	47	245	208	215	483	0.170	50	1376	11	79	30	0.281	0.148	0.112	0.073	0.442	0.023
1. Mag - core	306	138	306	233	246	426	0.166	25	1547	14	75	101	0.413	0.342	0.361	0.089	0.429	0.025
1. Mag - core	4561	4463	3461	256	239	408	0.185	6.3	1696	18	114	79	2.3	0.524	0.643	0.249	0.403	0.036
1. Mag - core	2660	1260	403	229	302	412	0.398	2.5	1692	24	151	113	28	0.177	0.812	5.2	0.496	0.036
1. Mag - core	319	68	263	200	228	477	0.061	57	1459	13	54	45	0.333	0.073	0.051	0.032	0.371	0.018
1. Mag - core	790	370	347	210	197	658	0.394	141	1444	4.4	31	20	1.2	0.377	0.203	0.158	0.518	0.036
1. Mag - core	6972	4802	2128	2002	235	622	0.553	6.5	1517	8.8	92	93	16	0.221	1.4	4.3	0.699	0.055
1. Mag - core	359	116	240	254	207	530	0.171	54	1361	7.2	34	34	0.514	0.290	0.193	0.064	0.439	0.029
1. Mag - core	7386	2994	1042	851	440	862	1.5	13	1696	16	96	101	6.5	0.217	0.404	1.0	1.7	0.055
1. Mag - core	4509	2054	460	555	302	828	0.761	0.298	1802	17	87	106	3.0	0.141	0.110	0.861	0.915	0.048
1. Mag - core	7133	2611	1150	1029	468	857	1.5	0.341	1812	18	104	141	6.2	0.211	0.174	0.919	1.5	0.049
1. Mag - core	4980	2233	737	864	346	856	0.801	0.346	1824	26	139	193	3.6	0.143	0.282	1.4	1.1	0.027
1. Mag - core	4490	2014	628	516	333	847	0.835	4.5	1755	23	128	134	3.4	0.130	0.556	0.965	1.2	0.151
1. Mag - core	267	89	269	223	253	816	0.028	17	2080	36	86	77	0.059	0.006	0.063	0.042	0.511	0.038
1. Mag - core	370	73	243	218	266	826	0.003	50	1486	11	56	28	0.033	0.001	0.016	0.010	0.429	0.048
1. Mag - core	5706	2567	670	875	398	799	0.917	5.2	1724	26	113	117	4.2	0.178	0.234	0.687	1.1	0.037
1. Mag - core	7049	2916	885	1279	438	831	1.1	1.5	1808	29	143	164	4.4	0.209	1.1	2.7	1.3	0.029
1. Mag - core	7940	3686	1097	788	465	852	1.3	2.0	1849	34	139	224	3.2	0.298	2.6	0.713	1.2	0.028
1. Mag - core	8222	3623	1620	686	579	863	1.4	2.0	1841	35	149	272	4.7	0.342	3.2	2.5	1.6	0.025
1. Mag - core	6092	2847	1335	417	478	866	0.971	5.6	1843	34	137	448	2.4	0.360	12	0.693	1.1	0.031

	Lithophile elements				Transition metals								REY	Granitophile				
Magnetite	Si	Mg	Al	Ca	Ti	V	Nb	Cr	Ni	Co	Mn	Zn	ΣREY	^{238}U	^{206}Pb	W	Sn	Mo
1. Mag - core	9893	4637	1146	514	532	851	1.2	6.2	1888	35	130	388	2.7	0.283	9.3	0.905	1.1	0.062
1. Mag - core	6656	2707	1374	641	547	853	1.5	3.2	1781	33	161	235	4.1	0.278	1.7	0.921	1.5	0.076
1. Mag - core	5926	2502	1314	465	484	857	0.931	0.346	1840	33	171	313	3.6	0.264	1.3	2.7	1.3	0.025
1. Mag - core	7302	3154	1116	953	469	835	1.1	1.5	1813	31	160	266	3.3	0.230	4.4	1.1	1.4	0.025
1. Mag - core	8402	4320	833	339	385	813	0.672	4.4	1889	28	129	165	1.6	0.189	0.879	0.468	1.1	0.044
1. Mag - core	5416	2400	798	778	419	811	0.797	0.267	1811	32	150	269	4.8	0.158	0.917	0.653	1.2	0.029
1. Mag - core	6071	2746	787	910	392	816	0.859	0.362	2137	36	156	239	4.6	0.233	0.321	1.8	1.1	0.054
1. Mag - core	5325	2530	654	877	353	805	0.710	0.328	1837	28	127	250	4.0	0.165	0.385	1.2	1.1	0.076
1. Mag - core	7016	3946	1400	755	399	809	0.840	0.426	1840	24	128	359	8.3	0.375	3.2	2.8	1.1	0.041
1. Mag - core	4521	2189	835	481	386	811	0.694	1.1	1781	25	145	338	2.0	0.149	2.0	1.3	1.2	0.042
1. Mag - core	3248	1783	361	226	302	799	0.140	14	1726	22	73	77	0.052	0.009	0.047	0.109	0.537	0.016
1. Mag - core	14969	8161	1482	496	469	473	0.931	39	1729	17	165	160	5.7	0.388	4.1	0.955	2.1	0.004
1. Mag - core	5142	4677	2945	15	269	457	0.533	38	6918	105	125	53	0.380	0.223	0.443	0.068	1.2	0.010
1. Mag - core	13217	10091	5799	768	561	505	1.0	48	1880	23	141	194	6.1	0.297	6.1	1.0	2.2	0.017
1. Mag - core	8900	3594	1304	1371	544	507	1.0	2.8	1711	24	178	155	8.0	1.1	725	4.9	2.8	0.025
1. Mag - core	9415	4204	1646	1562	580	507	1.0	0.301	1805	28	222	314	17	0.406	2.7	4.8	2.7	0.042
1. Mag - core	7928	3383	1252	1261	578	513	0.962	14	1773	22	172	158	7.8	0.533	4.0	1.7	2.5	0.023
1. Mag - core	7581	3770	1156	1029	520	509	1.2	31	1779	23	157	140	7.6	0.366	1.8	1.3	2.5	0.034
1. Mag - core	6176	3063	1023	795	478	503	0.748	0.147	1806	30	189	248	6.7	0.265	0.525	4.1	2.0	0.026
1. Mag - core	5678	2654	965	578	463	511	0.679	1.2	1805	25	166	116	4.6	0.233	0.437	0.903	1.8	0.004
1. Mag - core	733	298	296	31	276	471	0.044	6.8	1641	21	139	85	0.314	0.014	0.047	0.029	0.948	0.009
1. Mag - core	444	217	326	103	300	493	0.030	2.7	1687	25	148	99	0.143	0.053	1.0	0.047	0.811	0.003
1. Mag - core	755	411	453	18	320	505	0.034	1.1	1736	29	161	139	0.197	0.045	0.513	0.054	0.855	0.020
1. Mag - core	1708	793	443	192	345	494	0.158	1.1	1705	28	152	127	1.2	0.073	0.134	0.216	1.1	0.002
1. Mag - core	1264	734	370	108	335	493	0.116	2.6	1722	29	158	141	0.605	0.064	1.3	0.297	0.970	0.014
1. Mag - core	1692	1144	721	164	352	458	0.184	6.6	1627	28	176	266	0.813	0.081	1.4	1.4	1.0	0.004
1. Mag - core	1670	970	467	117	334	501	0.114	1.9	1748	29	155	128	0.606	0.074	0.266	0.205	0.916	0.020
1. Mag - core	2022	1004	500	287	360	497	0.226	2.5	1715	28	171	211	1.6	0.119	1.3	0.661	1.1	0.008
1. Mag - core	3424	1796	547	201	357	486	0.261	16	1751	25	133	246	1.8	0.203	476	0.489	1.2	0.090
1. Mag - core	2398	1229	420	95	336	491	0.175	14	1717	23	127	127	1.1	0.094	8.9	0.211	0.966	0.009
1. Mag - core	261	156	332	8	415	500	0.044	87	1687	21	107	68	0.035	0.009	0.023	0.003	0.826	0.003
1. Mag - core	459	158	320	82	411	502	0.010	93	1700	19	111	87	0.057	0.004	0.038	0.000	0.654	0.012
1. Mag - core	1316	389	347	173	345	495	0.028	83	1738	12	65	54	0.254	0.025	0.061	0.049	1.2	0.017
1. Mag - core	3042	1778	1235	7	436	513	0.141	90	1696	18	125	78	1.5	0.099	4.0	0.230	1.4	0.003
1. Mag - core	303	225	312	67	293	516	0.334	77	1611	18	148	73	0.072	0.071	0.175	0.023	1.1	0.027
1. Mag - core	172	161	290	45	283	503	0.023	61	1580	19	144	57	0.026	0.024	0.090	0.023	0.829	0.004
1. Mag - core	1025	544	277	45	270	514	0.079	35	1594	16	115	53	0.294	0.069	0.227	0.040	0.954	0.022
1. Mag - core	1817	1086	690	41	332	514	0.124	2.9	1721	21	143	93	0.248	0.135	0.288	0.054	1.1	0.005
1. Mag - core	1206	625	382	5	311	505	0.112	47	1664	21	152	85	0.497	0.037	0.648	0.109	0.941	0.002
1. Mag - core	571	379	340	31	301	500	0.052	0.988	1658	23	143	102	0.334	0.016	0.033	0.052	0.964	0.003
1. Mag - core	1628	890	488	103	326	507	0.158	1.2	1774	26	157	134	1.1	0.034	0.287	0.202	1.4	0.005
1. Mag - core	1547	775	460	256	320	494	0.121	3.9	1702	24	155	125	1.4	0.041	0.235	0.231	1.1	0.032
1. Mag - core	1131	488	421	78	353	501	0.118	0.798	1757	27	138	128	0.543	0.080	0.115	0.077	0.876	0.004
1. Mag - core	5119	2693	1553	853	542	527	0.692	0.551	1859	31	168	168	4.4	0.208	13	1.6	1.8	0.026
1. Mag - core	3720	1631	972	852	492	525	0.476	0.432	1859	31	167	166	5.4	0.186	0.936	0.456	1.6	0.002
1. Mag - core	4773	3113	1773	733	471	531	0.578	0.068	1991	34	174	199	3.9	0.242	1.6	0.583	1.4	0.007
1. Mag - core	4285	2058	787	536	472	514	0.569	0.247	1894	33	164	159	2.5	0.139	0.911	0.577	1.4	0.002
1. Mag - core	7604	5824	2366	1214	423	492	0.351	5.3	1925	34	189	292	5.4	0.264	7.5	0.559	1.3	0.008
1. Mag - core	9522	7194	3464	255	371	498	0.703	22	1968	32	120	270	3.3	0.345	5.3	0.632	1.8	0.005
1. Mag - core	3970	2495	960	393	372	501	0.429	8.5	1833	32	143	129	1.7	0.137	4.5	0.281	1.2	0.020
1. Mag - core	5947	3053	906	521	465	505	0.637	20	1847	23	137	294	3.1	0.325	16	0.716	1.5	0.030
1. Mag - core	11828	6351	2758	1802	551	517	1.5	14	1819	18	80	17273	19	0.626	4.8	2.4	9.5	0.006
1. Mag - core	11248	6078	2744	1654	643	504	1.2	5.0	1858	25	182	402	9.7	0.329	5.2	2.5	2.7	0.007
1. Mag - core	8260	4665	2920	1203	584	530	0.694	6.2	1861	31	233	578	20	0.214	11	4.5	2.2	0.007
1. Mag - core	13901	10938	6463	2864	614	513	0.799	8.2	1954	34	250	365	17	0.312	23	5.6	2.2	0.012
1. Mag - core	9865	5654	2854	1518	662	523	1.0	3.1	1916	33	214	414	7.6	0.439	35	3.4	2.5	0.028
1. Mag - core	12388	6208	2805	898	727	505	0.928	1.1	1924	34	189	221	5.2	0.305	94	5.4	2.1	0.042

	Lithophile elements				Transition metals								REY	Granitophile				
Magnetite	**Si**	**Mg**	**Al**	**Ca**	**Ti**	**V**	**Nb**	**Cr**	**Ni**	**Co**	**Mn**	**Zn**	**ΣREY**	**^{238}U**	**^{206}Pb**	**W**	**Sn**	**Mo**
1. Mag - core	9146	4106	1599	1709	672	532	1.1	5.0	1917	33	206	264	14	0.484	26	3.2	2.7	0.004
1. Mag - core	9529	3853	1576	2367	643	514	1.0	1.0	1890	34	196	253	20	0.320	11	1.9	3.0	0.018
1. Mag - core	7330	4078	2369	692	570	509	0.708	1.2	1897	34	190	262	4.4	0.258	15	1.1	1.9	0.003
1. Mag - core	8535	5031	2691	2262	595	523	0.969	1.0	1997	33	244	545	83	0.898	45	12	2.2	0.917
1. Mag - core	5579	3172	1389	1471	498	521	0.557	1.2	2008	21	140	437	472	0.477	53	4.1	1.8	0.045
1. Mag - core	4078	2415	1268	394	440	514	0.378	0.727	1856	34	161	299	5.1	0.534	11	1.0	1.1	0.009
1. Mag - core	2835	2409	1534	455	417	493	0.376	3.1	1808	34	146	183	1.1	0.342	3.8	0.263	1.1	0.009
1. Mag - core	12983	11033	5634	944	549	505	0.737	38	2074	22	228	276	3.1	0.470	2.9	0.824	1.8	0.008
1. Mag - core	15124	12885	6802	122	366	487	0.567	46	2616	23	196	262	2.0	0.652	21	0.451	1.0	0.000
Mean (n=177)	5456	2820	1187	658	355	507	0.704	18	1974	27	146	608	7.3	0.277	11	1.2	1.0	0.043
SD	5306	2659	1164	902	136	152	0.776	27	1274	45	68	2976	36	0.236	65	1.9	0.902	0.092
Median	4509	2400	906	334	332	477	0.476	5.3	1762	24	141	143	1.8	0.223	1.1	0.456	0.916	0.029
Max	41939	13361	6802	9230	727	866	3.6	153	13664	599	650	30870	472	1.4	725	12	9.5	0.917
Min	154	47	240	4.7	156	319	0.001	0.031	1338	3.3	27	17	0.025	0.000	0.013	0.000	0.224	0.000

	Lithophile elements				Transition metals								REY	Granitophile				
Magnetite	**Si**	**Mg**	**Al**	**Ca**	**Ti**	**V**	**Nb**	**Cr**	**Ni**	**Co**	**Mn**	**Zn**	**ΣREY**	**^{238}U**	**^{206}Pb**	**W**	**Sn**	**Mo**
2. Mag - rim	3050	1406	448	191	237	304	0.625	131	1648	6.6	109	27	2.9	0.180	0.421	1.7	0.294	0.011
2. Mag - rim	3248	1716	945	58	200	313	0.212	168	2245	4.2	70	14	0.796	0.355	0.129	0.068	0.233	0.009
2. Mag - rim	3773	1476	917	20	220	314	0.151	156	1891	3.1	69	9.2	0.507	0.224	0.159	0.009	0.156	0.002
2. Mag - rim	7911	2705	832	1076	188	284	0.004	146	1709	4.2	91	36	0.895	0.040	0.052	0.001	0.595	0.002
2. Mag - rim	4252	2447	1030	3368	226	315	0.180	141	1730	5.8	107	41	394	0.171	0.887	0.873	0.263	0.012
2. Mag - rim	297	53	257	8	277	544	0.038	51	1501	23	88	42	0.114	0.020	0.966	0.023	0.322	0.004
2. Mag - rim	141	76	326	15	285	565	0.007	13	1621	34	109	74	0.026	0.002	0.014	0.007	0.416	0.001
2. Mag - rim	511	81	317	3	269	559	0.042	11	1644	31	113	77	0.038	0.005	1.0	0.074	0.459	0.012
2. Mag - rim	193	61	265	222	227	416	0.002	3.3	1482	20	137	45	0.057	0.002	0.014	0.000	0.370	0.050
2. Mag - rim	3520	1483	787	220	306	366	0.815	12	2673	69	174	2005	1.6	0.176	3.5	0.533	0.718	0.037
2. Mag - rim	5873	3107	1101	241	274	375	0.808	21	2117	41	183	212	2.2	0.500	5.7	0.460	0.590	0.044
2. Mag - rim	2132	881	467	423	228	402	0.687	7.6	2761	91	109	58	1.4	0.325	2.7	0.348	0.541	0.048
2. Mag - rim	371	128	263	215	215	468	0.048	3.7	1531	12	79	54	0.141	0.047	0.034	0.051	0.325	0.026
2. Mag - rim	1830	590	356	406	289	412	0.414	0.604	2093	37	110	136	0.585	0.625	0.596	1.1	0.444	0.054
2. Mag - rim	205	65	298	254	279	380	0.067	0.332	1534	20	117	578	0.172	0.117	0.189	0.033	0.335	0.030
2. Mag - rim	168	60	278	245	274	368	0.159	1.1	1470	20	116	66	0.139	0.123	0.149	0.041	0.402	0.032
2. Mag - rim	184	55	247	227	262	413	0.097	5.2	1433	21	124	41	0.089	0.181	0.110	0.044	0.336	0.036
2. Mag - rim	3360	1473	763	407	359	424	0.941	11	2192	48	153	160	1.6	0.312	1.3	0.515	0.665	0.049
2. Mag - rim	194	67	263	216	243	425	0.109	39	1467	21	132	46	0.199	0.115	0.059	0.000	0.241	0.032
2. Mag - rim	703	221	322	253	244	441	0.222	10	1507	21	79	42	0.610	0.156	0.449	0.163	0.303	0.023
2. Mag - rim	181	90	264	260	191	421	0.004	2.8	1379	16	121	25	0.036	0.001	0.013	0.000	0.300	0.035
2. Mag - rim	184	97	266	229	186	419	0.006	2.8	1441	18	136	37	0.049	0.005	0.053	0.007	0.325	0.018
2. Mag - rim	189	83	267	270	191	421	0.000	1.7	1459	19	135	39	0.043	0.000	0.011	0.000	0.339	0.029
2. Mag - rim	194	91	277	247	189	423	0.002	4.3	1463	19	140	36	0.030	0.000	0.010	0.000	0.331	0.042
2. Mag - rim	200	86	252	228	192	416	0.012	5.6	1430	16	112	26	0.075	0.003	0.011	0.003	0.353	0.029
2. Mag - rim	183	92	267	228	195	423	0.000	1.8	1438	18	139	37	0.034	0.000	0.011	0.003	0.338	0.041
2. Mag - rim	160	75	252	194	187	413	0.001	5.5	1505	15	113	31	0.092	0.003	0.012	0.003	0.333	0.017
2. Mag - rim	307	117	256	207	188	417	0.017	3.8	2262	14	100	38	0.404	0.036	0.069	0.053	0.420	0.028
2. Mag - rim	5149	1942	809	465	284	421	1.3	3.5	1947	6.1	79	33	3.3	0.297	0.749	0.763	0.799	0.034
2. Mag - rim	172	96	279	237	188	417	0.112	5.6	1448	17	124	36	0.045	0.018	0.014	0.007	0.318	0.060
2. Mag - rim	188	84	263	225	188	417	0.006	3.1	1395	15	118	33	0.041	0.003	0.063	0.000	0.395	0.023
2. Mag - rim	190	123	281	244	189	417	0.004	4.1	1456	19	140	40	0.029	0.000	0.015	0.005	0.240	0.069
2. Mag - rim	11364	4993	1431	1407	403	425	2.6	64	1639	17	206	158	3.7	0.417	1.5	1.4	1.1	0.024
2. Mag - rim	540	223	304	247	169	439	0.156	1.3	2600	37	104	123	0.144	0.151	0.736	0.057	0.287	0.031
2. Mag - rim	719	253	229	183	151	384	0.025	1.1	19361	1090	64	23	0.174	0.097	5.6	0.012	0.284	0.195
2. Mag - rim	161	100	330	202	186	423	0.003	0.403	1586	27	145	66	0.051	0.005	0.016	0.007	0.265	0.037
2. Mag - rim	168	102	330	219	186	424	0.001	0.523	1568	25	149	67	0.048	0.001	0.016	0.003	0.296	0.029
2. Mag - rim	175	82	281	216	180	424	0.001	1.2	1425	18	131	35	0.027	0.000	0.014	0.000	0.380	0.024
2. Mag - rim	391	123	328	250	178	430	0.130	0.407	1525	22	142	57	0.118	0.065	0.172	0.045	0.312	0.029
2. Mag - rim	169	96	328	219	183	430	0.026	0.909	1511	23	142	48	0.042	0.011	0.024	0.007	0.361	0.015

	Lithophile elements				Transition metals								REY	Granitophile				
Magnetite	**Si**	**Mg**	**Al**	**Ca**	**Ti**	**V**	**Nb**	**Cr**	**Ni**	**Co**	**Mn**	**Zn**	**ΣREY**	**^{238}U**	**^{206}Pb**	**W**	**Sn**	**Mo**
2. Mag - rim	179	93	357	210	178	416	0.240	0.787	1576	29	140	54	0.057	0.099	0.056	0.027	0.346	0.022
2. Mag - rim	403	131	357	218	173	406	0.063	0.674	1588	28	142	55	0.079	0.034	0.075	0.030	0.314	0.037
2. Mag - rim	9452	3798	1507	1931	343	436	3.4	0.341	1716	33	219	201	20	0.437	3.7	2.8	1.4	0.041
2. Mag - rim	186	98	291	226	239	825	0.006	55	1627	17	84	55	0.026	0.011	0.030	0.017	0.414	0.035
2. Mag - rim	179	110	306	230	254	822	0.001	73	1607	17	97	62	0.041	0.000	0.013	0.000	0.518	0.049
2. Mag - rim	177	78	255	192	221	828	0.004	58	1514	15	86	42	0.015	0.000	0.019	0.000	0.461	0.031
2. Mag - rim	183	87	271	185	226	820	0.001	37	1482	12	87	30	0.026	0.001	0.014	0.004	0.431	0.030
2. Mag - rim	369	78	260	217	227	863	0.001	81	1477	13	74	37	0.577	0.400	0.550	0.003	0.463	0.035
2. Mag - rim	229	107	314	222	256	848	0.009	54	1396	11	75	35	0.030	0.006	0.023	0.000	0.545	0.048
2. Mag - rim	11841	6816	440	243	255	810	0.058	32	1610	11	43	111	0.068	0.030	0.043	0.005	0.367	0.050
2. Mag - rim	227	51	204	208	269	838	0.009	14	1522	10	54	24	0.038	0.002	0.013	0.010	0.481	0.056
2. Mag - rim	1008	479	244	217	290	834	0.009	5.2	1543	13	79	31	0.034	0.002	0.098	0.003	0.489	12
2. Mag - rim	218	93	272	222	281	852	0.005	3.7	1493	13	88	34	0.025	0.006	0.019	0.000	0.388	0.039
2. Mag - rim	333	81	258	202	284	838	0.001	4.3	1546	14	83	38	0.024	0.000	0.011	0.003	0.496	0.790
2. Mag - rim	3663	1351	429	284	282	860	0.195	17	2796	29	51	31	0.047	0.407	2.0	0.023	0.525	0.067
2. Mag - rim	185	56	218	212	281	853	0.001	13	1462	12	68	25	0.033	0.002	0.015	0.000	0.455	0.029
2. Mag - rim	370	63	207	214	283	855	0.001	13	1430	9.9	58	21	0.035	0.004	0.012	0.000	0.407	0.029
2. Mag - rim	433	155	257	241	287	834	0.008	7.9	1599	16	83	45	0.034	0.009	0.010	0.000	0.559	0.027
2. Mag - rim	237	77	265	247	287	835	0.002	8.8	1538	13	87	39	0.038	0.000	0.015	0.000	0.416	0.037
2. Mag - rim	2871	1412	431	218	339	831	0.246	12	1601	14	85	71	1.2	0.273	0.386	0.178	0.698	0.029
2. Mag - rim	434	132	303	442	293	837	0.058	14	1871	16	62	68	0.065	0.072	0.567	0.007	0.461	0.033
2. Mag - rim	160	80	266	222	286	834	0.010	10	3237	77	83	35	0.018	0.001	0.136	0.047	0.483	0.056
2. Mag - rim	245	89	285	264	289	834	0.002	1.5	1640	17	94	51	0.017	0.000	0.013	0.000	0.534	0.025
2. Mag - rim	156	73	252	250	283	858	0.001	2.6	1556	14	79	40	0.026	0.001	0.067	0.000	0.458	0.039
2. Mag - rim	241	168	266	238	301	824	0.003	2.0	1568	15	86	39	0.020	0.001	0.011	0.000	0.488	0.676
2. Mag - rim	224	80	261	211	295	833	0.000	1.5	1575	16	89	42	0.024	0.000	0.011	0.014	0.496	0.018
2. Mag - rim	1628	1646	1344	215	263	844	0.056	8.8	8431	187	47	40	0.045	0.140	0.464	0.080	0.523	0.328
2. Mag - rim	2519	1242	629	229	342	831	0.169	9.6	1930	11	73	124	1.0	0.287	3.5	0.263	0.795	0.041
2. Mag - rim	172	53	309	225	269	837	0.000	8.3	1576	11	43	38	0.023	0.001	0.019	0.000	0.389	0.046
2. Mag - rim	495	96	342	301	263	814	0.004	11	1695	22	65	110	0.076	0.010	0.017	0.001	0.517	0.032
2. Mag - rim	3834	1903	785	246	467	819	0.218	4.2	1818	23	111	287	0.999	0.171	7.5	0.393	0.683	0.031
2. Mag - rim	6093	3226	751	221	293	868	0.240	8.9	1793	21	74	153	0.959	0.105	4.5	0.292	0.653	0.095
2. Mag - rim	1284	607	330	230	291	733	0.008	11	1645	31	86	111	0.042	0.008	0.022	0.003	0.605	0.033
2. Mag - rim	361	79	262	218	285	837	0.000	8.0	1653	20	90	60	0.026	0.000	0.013	0.000	0.573	0.027
2. Mag - rim	21163	13481	1599	265	314	780	0.030	2.5	2116	31	109	212	0.068	0.031	0.020	0.006	0.490	68
2. Mag - rim	1393	793	308	238	308	785	0.019	4.4	1783	24	101	82	0.030	0.008	0.035	0.011	0.506	0.047
2. Mag - rim	178	96	410	240	243	822	0.001	12	1659	23	87	59	0.024	0.001	0.014	0.000	0.395	0.027
2. Mag - rim	1844	930	425	237	258	826	0.040	11	1847	21	79	91	0.105	0.034	0.065	0.018	0.512	0.039
2. Mag - rim	214	74	240	214	264	774	0.002	28	1509	15	78	37	0.027	0.005	0.012	0.000	0.543	0.041
2. Mag - rim	4186	2250	379	195	272	757	0.063	19	1554	14	54	69	0.138	0.011	0.019	0.029	0.481	0.078
2. Mag - rim	449	245	265	269	216	771	0.047	36	1513	12	59	34	0.046	0.007	0.016	0.004	0.430	0.044
2. Mag - rim	243	124	322	252	293	795	0.008	7.0	6304	162	107	225	0.027	0.005	0.517	0.045	0.610	0.036
2. Mag - rim	307	114	313	308	267	744	0.063	15	21393	678	95	23	0.055	0.038	0.374	0.324	0.568	0.298
Mean (n=83)	1729	842	428	312	253	610	0.185	21	2288	45	102	94	5.3	0.090	0.634	0.156	0.460	1.0
SD	3246	1832	312	423	67	220	0.503	37	3012	138	37	225	43	0.139	1.4	0.417	0.187	7.5
Median	307	107	304	228	263	559	0.017	8.0	1586	18	94	42	0.051	0.011	0.052	0.007	0.431	0.035
Max	21163	13481	1599	3368	467	868	3.4	168	21393	1090	219	2005	394	0.625	7.5	2.8	1.4	68
Min	141	51	204	2.6	151	284	0.000	0.332	1379	3.1	43	9.2	0.015	0.000	0.010	0.000	0.156	0.001

Lithophile elements			Transition metals								REY	Granitophile				
Amphibole	Si	Al	Ti	V	Nb	Cr	Ni	Co	Mn	Zn	ΣREY	^{238}U	^{206}Pb	W	Sn	Mo
3. Amp	263198	8394	252	45	0.176	11	2120	35	990	888	41	0.033	0.260	0.013	7.4	0.021
3. Amp	267883	5486	140	55	0.120	14	2162	29	984	764	38	0.321	0.363	0.022	6.6	1.5
3. Amp	270159	6138	105	55	0.103	13	2061	41	919	1146	37	0.177	0.141	0.049	8.3	1.1
3. Amp	265703	5952	110	67	0.150	20	2147	32	944	956	46	0.192	0.316	0.075	9.0	1.1
3. Amp	256822	5673	99	91	0.255	22	2180	27	997	599	29	0.211	0.315	0.128	10	1.3
3. Amp	270422	6247	112	50	0.125	14	2082	39	981	1043	44	0.270	0.220	0.023	7.2	0.197
3. Amp	266522	5612	89	67	0.121	21	2175	26	1014	635	28	0.431	0.591	0.088	8.9	3.3
3. Amp	266043	5231	95	64	0.164	21	2105	29	1001	711	29	1.2	0.754	0.155	7.3	2.9
3. Amp	242605	29560	533	38	0.636	14	2053	45	983	1040	46	0.125	0.086	0.099	11	0.044
3. Amp	260163	15952	397	37	0.487	12	1731	46	1128	1318	52	0.073	0.125	0.056	12	0.037
3. Amp	264404	10404	295	49	0.279	11	1981	38	1157	956	47	0.066	0.100	0.016	9.8	0.007
3. Amp	267855	6226	202	54	0.185	12	2005	41	935	1129	22	0.150	0.166	0.052	8.4	0.183
3. Amp	261725	13480	318	37	0.452	9.5	1675	44	1144	1149	47	0.487	0.405	0.069	11	0.104
3. Amp	267466	6241	156	59	0.093	13	2176	29	1025	756	45	1.6	1.6	0.051	8.6	0.987
3. Amp	264123	7396	143	47	0.165	9.5	2032	38	1092	1125	43	0.129	0.129	0.023	6.9	0.075
3. Amp	266704	6950	80	85	0.120	14	2263	34	928	1045	94	0.407	0.452	0.065	12	2.0
3. Amp	265987	6281	71	77	0.081	15	2269	30	905	990	73	0.232	0.990	0.072	11	0.720
3. Amp	268744	6110	130	60	0.111	13	2117	33	923	1001	38	0.157	0.131	0.007	8.0	0.972
3. Amp	268026	6698	245	60	0.152	9.0	2115	33	1007	910	40	0.013	0.075	0.002	8.1	0.041
3. Amp	256216	20819	382	39	0.480	9.5	1809	46	1010	1157	52	0.036	0.481	0.027	12	0.038
3. Amp	262455	14628	288	42	0.352	11	1776	44	1118	1711	50	0.042	0.082	0.045	11	0.244
3. Amp	255909	19994	356	50	0.440	12	1945	47	975	1251	102	0.120	0.125	0.027	11	0.309
3. Amp	250211	16959	338	50	0.515	23	1870	46	1105	1135	41	0.418	0.376	0.039	11	0.022
3. Amp	267484	7602	182	37	0.163	8.3	2087	39	943	1073	40	0.025	0.059	0.011	6.4	0.270
3. Amp	255463	13123	369	40	0.385	10	1623	40	1128	1142	54	0.021	0.515	0.021	12	0.029
3. Amp	245801	29286	591	48	0.677	10	1700	50	1141	1307	88	0.031	0.086	0.003	15	0.044
3. Amp	228933	15289	365	75	0.446	36	1879	38	845	1001	36	0.204	0.161	0.070	7.6	0.305
3. Amp	266858	4993	70	58	0.082	11	2199	27	978	671	33	0.494	0.356	0.045	6.8	0.878
3. Amp	257032	6772	108	94	0.135	14	2632	45	961	1489	42	0.265	0.246	0.112	12	0.369
3. Amp	265950	7750	114	91	0.154	11	2287	38	872	1171	39	0.078	0.258	0.047	11	0.458
3. Amp	253103	26523	734	45	1.3	12	1347	50	1018	1348	51	0.025	0.470	0.015	18	0.014
3. Amp	253210	27781	656	44	1.0	7.7	1205	55	1030	1418	68	0.024	0.318	0.022	19	0.029
3. Amp	267697	6739	112	56	0.246	3.0	1531	48	1181	915	29	0.038	0.222	0.152	10	0.031
3. Amp	267105	7518	153	95	0.166	2.5	1961	41	932	1079	40	0.015	0.288	0.071	12	0.035
3. Amp	267419	6629	110	65	0.084	2.1	2383	35	883	1080	32	0.017	0.123	0.033	12	0.020
3. Amp	266848	6898	109	81	0.093	6.8	2273	30	917	966	40	0.004	0.195	0.049	11	0.003
3. Amp	268894	5410	93	64	0.127	6.7	2214	34	833	1173	28	0.016	0.109	0.049	8.2	0.011
3. Amp	270116	4744	79	48	0.110	5.5	2091	45	896	1285	22	0.027	0.285	0.050	6.3	0.037
3. Amp	266978	6819	123	76	0.126	6.4	2127	39	924	1310	41	0.058	0.113	0.150	12	0.021
3. Amp	267352	7113	145	72	0.133	5.5	2072	43	1039	1155	38	0.039	0.204	0.134	12	0.033
3. Amp	264492	8287	103	65	0.108	7.1	2136	38	815	1080	27	0.048	0.089	0.071	10	0.041
3. Amp	265258	14481	325	40	0.532	8.9	1505	49	1191	1112	62	0.072	0.109	0.111	14	0.445
3. Amp	255626	18695	514	37	0.674	7.9	1664	41	969	1001	43	0.101	0.050	0.044	15	0.029
3. Amp	233295	42534	588	38	0.761	8.7	2037	57	923	1348	38	0.015	0.082	0.005	13	0.031
3. Amp	257555	19820	471	40	0.582	7.2	1609	50	979	1253	62	0.008	0.078	0.019	15	0.027
3. Amp	264131	10309	326	55	0.125	4.3	2088	37	1028	922	67	0.001	0.044	0.000	12	0.030
3. Amp	265038	9437	220	46	0.228	2.6	1949	36	999	898	34	0.013	0.061	0.035	7.9	0.030
3. Amp	267223	6942	201	48	0.080	2.8	2132	34	989	862	45	0.007	0.514	0.000	7.0	0.016
3. Amp	268680	5188	314	55	1.7	3.2	2124	31	914	848	39	0.021	0.139	0.031	7.7	0.008
3. Amp	267182	6881	165	60	0.114	2.4	2057	36	914	1045	37	0.008	0.058	0.020	9.4	0.016
3. Amp	264571	10793	243	49	0.244	2.7	1763	42	971	1108	41	0.022	0.169	0.022	9.7	0.031
3. Amp	271375	5008	123	64	0.111	1.6	2180	38	855	1187	23	0.003	0.153	0.027	7.6	0.022
3. Amp	259787	15102	385	48	0.508	5.3	1583	43	1113	1405	47	0.049	0.115	0.028	12	0.019
3. Amp	267231	6439	101	77	0.078	4.1	2186	26	1052	592	58	0.043	0.129	0.008	11	0.007
3. Amp	265776	7828	155	41	0.218	3.3	1642	46	1180	1105	34	0.116	0.153	0.107	8.9	0.033
3. Amp	245420	29876	500	40	0.688	6.8	1780	50	1275	1162	66	0.059	0.137	0.038	14	0.032
3. Amp	264737	9166	180	58	0.286	3.0	1785	47	1055	1179	38	0.080	0.562	0.072	10	0.007

Lithophile elements			Transition metals								REY	Granitophile				
Amphibole	Si	Al	Ti	V	Nb	Cr	Ni	Co	Mn	Zn	ΣREY	^{238}U	^{206}Pb	W	Sn	Mo
3. Amp	259740	14291	298	55	0.418	5.6	1909	41	970	1033	42	0.018	0.105	0.011	11	0.021
3. Amp	263333	8757	163	41	0.231	4.1	1604	46	1144	1111	37	0.033	0.108	0.082	9.0	0.021
3. Amp	266623	6715	130	50	0.124	4.5	2049	35	945	984	36	0.006	0.119	0.014	7.3	0.030
3. Amp	266292	6776	138	51	0.162	3.1	1988	37	890	1076	31	0.008	0.137	0.037	6.9	0.021
3. Amp	246572	32218	1290	94	3.1	1.7	1545	101	1030	1529	123	0.034	0.468	0.092	63	0.006
3. Amp	245560	35067	1304	89	6.3	1.0	1298	103	1049	1573	173	0.045	0.441	0.010	78	0.024
3. Amp	249367	30488	993	80	5.0	0.660	1521	100	1094	1446	158	0.042	0.406	0.067	66	0.028
3. Amp	247557	32245	1019	76	5.4	0.463	1471	102	1068	1479	161	0.037	0.625	0.034	75	0.013
3. Amp	245953	34103	1242	98	5.7	0.889	1836	102	1041	1584	150	0.038	0.280	0.018	73	0.009
3. Amp	247389	32713	1204	96	4.3	1.8	1755	102	1029	1565	133	0.057	0.298	0.026	66	0.009
3. Amp	253343	25178	941	107	2.3	14	2699	95	947	1381	90	0.112	0.449	0.062	50	0.039
3. Amp	255396	19571	739	86	0.584	1.3	1815	92	986	1201	57	0.005	0.891	0.048	24	0.023
3. Amp	259726	16701	652	74	0.355	0.634	1832	96	912	1253	47	0.001	0.278	0.011	23	0.030
3. Amp	256471	22474	845	71	1.2	0.625	1635	99	954	1434	58	0.005	0.131	0.011	31	0.026
3. Amp	247515	32905	1432	91	3.3	0.522	1433	102	1068	1531	134	0.032	0.199	0.032	68	0.033
3. Amp	245452	35270	1625	100	3.6	1.1	1434	101	1048	1564	137	0.040	0.250	0.093	73	0.044
3. Amp	245185	33950	1498	101	2.9	1.0	1600	104	1037	1546	119	0.025	0.205	0.021	61	0.005
3. Amp	249010	31417	1327	99	1.7	0.854	1604	101	996	1514	106	0.019	0.159	0.010	53	0.008
3. Amp	252718	24106	1020	98	0.781	1.0	1909	167	959	1287	78	0.015	0.448	0.015	36	0.014
3. Amp	252230	20725	761	73	0.681	1.7	1697	93	960	1303	61	0.041	0.124	0.031	26	0.027
3. Amp	251651	22156	807	69	1.6	0.900	1808	94	996	1360	73	0.087	5.2	0.099	38	0.034
3. Amp	219844	21657	750	62	1.9	0.410	1484	83	949	1255	147	0.192	0.367	0.063	35	0.019
3. Amp	247190	29411	1044	77	3.1	0.403	1535	99	1021	1514	98	0.034	0.194	0.028	53	0.021
3. Amp	251686	23315	735	59	2.4	0.264	1701	98	1048	1505	75	0.009	0.210	0.004	37	0.035
3. Amp	251204	24769	837	66	2.5	0.713	1544	100	1021	1519	75	0.011	0.172	0.008	40	0.014
3. Amp	253142	21944	684	54	2.1	0.331	1696	98	1031	1502	68	0.011	0.324	0.027	33	0.028
3. Amp	250756	20695	655	51	2.2	0.538	1675	95	1031	1432	75	0.042	0.178	0.090	35	0.012
3. Amp	245440	29374	1178	90	1.1	1.6	1548	98	1016	1518	112	0.022	1.1	0.083	46	0.005
3. Amp	247473	28594	1117	89	0.958	1.5	1566	98	1009	1471	109	0.016	0.181	0.013	45	0.012
3. Amp	248042	28671	1165	91	1.3	1.4	1634	99	960	1464	89	0.018	0.213	0.013	44	0.012
3. Amp	241915	36179	1241	94	4.8	2.5	1361	103	1067	1648	146	0.024	0.549	0.035	77	0.023
3. Amp	247181	30010	1021	81	3.7	2.4	1450	101	1028	1550	118	0.024	0.183	0.011	58	0.010
3. Amp	243169	32817	1085	85	5.0	4.8	1543	100	1047	1552	135	0.067	0.678	0.116	65	0.029
3. Amp	244987	34800	1233	92	3.6	4.8	1422	105	1024	1600	152	0.033	0.895	0.074	74	0.029
3. Amp	250550	26573	994	74	2.1	3.9	1498	100	1020	1597	71	0.010	0.136	0.007	41	0.012
3. Amp	246404	31011	1177	81	4.2	3.4	1439	100	1024	1545	107	0.027	0.459	0.027	58	0.037
3. Amp	241829	36527	1401	93	4.6	6.9	1325	101	1059	1577	170	0.040	0.243	0.023	74	0.023
3. Amp	241227	37176	1435	96	4.8	8.9	1452	100	1039	1552	174	0.044	0.347	0.141	79	0.011
3. Amp	255142	20017	759	80	0.910	7.5	1838	91	982	1224	63	0.026	0.338	0.041	29	0.007
3. Amp	250297	25483	896	78	2.0	2.3	1661	96	998	1435	69	0.059	0.286	0.064	37	0.019
3. Amp	247599	29077	1087	83	2.0	0.397	1595	99	1009	1503	87	0.036	0.216	0.038	46	0.003
3. Amp	250901	25203	1029	88	2.7	4.8	2047	91	971	1298	71	0.080	0.658	0.106	41	0.024
3. Amp	259923	13034	482	79	0.328	8.7	1803	84	974	820	55	0.010	0.030	0.006	24	0.019
3. Amp	246959	30121	1168	91	1.3	4.7	1613	99	993	1489	102	0.017	0.374	0.020	45	0.030
3. Amp	243786	34266	1357	93	3.6	4.0	1465	100	1034	1544	143	0.033	0.910	0.040	66	0.019
3. Amp	245908	31937	1157	80	4.7	5.1	1334	102	1085	1573	141	0.030	0.224	0.030	64	0.012
3. Amp	242643	36029	1415	87	6.1	6.8	1345	105	1059	1618	158	0.029	0.214	0.015	78	0.056
3. Amp	242458	36575	1469	92	2.9	7.7	1308	103	1087	1630	210	0.033	0.368	0.012	81	0.017
3. Amp	245687	30097	1226	105	2.2	5.9	2546	92	958	1391	110	0.121	0.712	0.042	55	0.028
3. Amp	248574	30175	1108	89	4.1	9.9	1888	99	1009	1388	134	0.098	0.435	0.050	62	0.018
3. Amp	259920	16758	684	94	1.0	13	2482	81	915	955	60	0.233	0.278	0.071	34	0.023
3. Amp	252979	18671	137	58	2.3	0.264	1737	76	1027	1374	60	0.014	0.273	0.243	16	0.031
3. Amp	252111	20195	197	69	1.5	0.304	1754	72	1009	1286	77	0.007	0.080	0.000	17	0.039
3. Amp	255824	15207	130	53	2.2	0.252	2907	68	939	1207	47	0.468	0.252	0.109	13	0.034
3. Amp	252840	20045	163	66	2.7	0.331	1776	75	1031	1350	63	0.055	0.112	0.028	18	0.035
3. Amp	253221	19061	123	55	2.6	0.332	1742	80	1026	1427	54	0.020	0.870	0.011	18	0.021
3. Amp	248867	25020	144	62	4.6	0.315	1460	88	1064	1504	80	0.019	0.180	0.020	33	0.050

Lithophile elements			Transition metals								REY	Granitophile				
Amphibole	Si	Al	Ti	V	Nb	Cr	Ni	Co	Mn	Zn	ΣREY	^{238}U	^{206}Pb	W	Sn	Mo
3. Amp	245047	28404	160	68	5.7	0.266	1552	86	1087	1388	92	0.065	0.267	0.071	41	0.050
3. Amp	250356	23342	115	52	4.4	0.291	1396	91	1075	1523	73	0.015	0.153	0.033	32	0.038
3. Amp	241706	32789	199	75	7.5	0.340	1342	94	1043	1567	128	0.020	0.769	0.021	57	0.047
3. Amp	243407	31148	202	77	3.7	0.520	1461	89	1041	1531	115	0.021	0.232	0.049	44	0.026
3. Amp	247430	25951	178	69	3.5	0.376	1555	84	1106	1414	86	0.032	0.245	0.116	31	0.040
3. Amp	248940	23882	166	66	3.4	0.310	1649	83	1063	1473	74	0.022	0.265	0.063	28	0.026
3. Amp	253175	19240	309	65	1.0	0.282	2322	72	1030	1309	103	0.020	0.341	0.023	14	0.057
3. Amp	253386	19273	254	61	2.2	0.919	3283	79	1044	1309	78	0.039	0.218	0.038	17	0.055
3. Amp	255914	15378	175	48	2.1	1.2	2584	77	1009	1363	45	0.030	0.299	0.066	12	0.059
3. Amp	257820	14351	146	40	1.7	0.433	1824	79	1011	1387	43	0.006	0.126	0.016	11	0.028
3. Amp	255723	16255	170	48	1.9	0.552	1969	79	1020	1377	50	0.013	0.184	0.060	14	0.047
3. Amp	250377	21424	297	68	2.5	0.607	1671	76	1066	1369	95	0.018	0.226	0.074	23	0.032
3. Amp	247852	26440	259	65	5.4	1.8	1310	92	1074	1574	110	0.020	1.3	0.065	43	0.040
3. Amp	247219	26979	280	70	4.4	5.2	1443	88	1042	1499	118	0.050	0.242	0.061	44	0.034
3. Amp	249884	21248	339	73	1.8	4.0	2270	76	1059	1337	106	0.291	0.209	0.113	19	0.032
3. Amp	240597	34225	324	83	7.2	4.2	1315	91	1127	1486	200	0.138	0.297	0.189	80	0.043
3. Amp	260834	11073	445	70	0.465	1.9	1871	55	817	1046	50	0.002	0.060	0.008	13	0.020
3. Amp	260467	12083	510	81	0.721	2.3	1610	55	805	1139	49	0.017	0.102	0.090	15	0.035
3. Amp	258721	13110	486	79	0.712	1.1	1548	57	786	1092	54	0.013	0.126	0.032	15	0.022
3. Amp	255256	17398	739	120	0.975	1.3	2061	59	823	1166	83	0.193	0.125	0.040	25	0.012
3. Amp	253878	18014	799	112	0.463	1.7	1520	60	931	1195	110	0.005	0.164	0.048	27	0.080
3. Amp	252868	20240	976	122	0.503	1.2	1537	60	941	1209	107	0.007	0.109	0.016	31	0.028
3. Amp	252053	20492	837	114	0.667	0.825	1504	63	908	1273	114	0.016	0.181	0.066	29	0.041
3. Amp	251719	21509	853	112	0.840	1.000	1476	64	908	1239	114	0.009	0.175	0.052	33	0.036
3. Amp	247061	24683	1052	127	1.4	1.1	1444	65	941	1237	133	0.029	0.390	0.569	42	0.033
3. Amp	246754	26407	1212	133	0.676	0.890	1403	66	997	1271	164	0.021	0.313	0.051	52	0.023
3. Amp	246724	26258	1242	135	0.966	1.2	1435	68	967	1355	151	0.017	0.166	0.017	48	0.020
3. Amp	253646	18854	745	119	0.607	3.8	1675	54	839	1083	118	0.164	0.264	0.003	31	0.057
3. Amp	262168	9482	285	52	0.489	0.592	2366	53	774	1007	46	0.000	0.035	0.002	12	0.023
3. Amp	258109	14110	507	86	0.904	1.1	1660	55	804	1058	70	0.007	0.104	0.010	21	0.026
3. Amp	253914	18447	740	114	0.807	2.3	1601	57	849	1091	103	0.037	0.157	0.013	30	0.029
3. Amp	259035	13687	394	76	0.865	0.586	1935	54	843	1019	68	0.096	0.282	0.058	22	0.031
3. Amp	261826	9923	266	66	0.820	0.323	2573	52	862	1006	53	0.997	0.740	0.102	19	0.027
3. Amp	255496	16700	601	99	0.669	2.2	1758	55	861	1081	98	0.004	0.078	0.002	27	0.018
3. Amp	256744	15711	418	85	1.1	0.614	1966	55	841	1054	70	0.201	0.562	0.013	24	0.385
3. Amp	260452	11365	297	63	0.728	0.679	2557	54	803	1037	49	0.000	0.069	0.000	14	0.029
3. Amp	259450	13330	444	84	0.846	2.7	1596	54	774	1043	59	0.005	0.035	0.003	19	0.032
3. Amp	263654	10707	348	48	1.1	3.6	1168	45	775	935	81	0.005	0.093	0.014	15	0.007
3. Amp	262807	11494	355	48	1.4	3.8	1144	47	791	974	88	0.005	0.073	0.001	17	0.009
3. Amp	263465	10701	233	35	1.5	11	1211	46	716	947	63	0.002	0.076	0.013	11	0.020
3. Amp	264731	10331	313	49	1.3	6.3	1987	44	740	909	75	0.093	0.112	0.119	22	0.017
3. Amp	266653	7053	169	28	1.4	6.6	1179	43	686	866	46	0.015	0.174	0.453	9.5	0.022
3. Amp	266854	7314	179	29	1.5	0.488	1168	44	671	884	47	0.009	0.095	0.097	14	0.014
3. Amp	266832	6854	137	27	1.0	0.321	1755	44	645	867	39	0.070	0.133	0.036	6.0	0.058
3. Amp	264936	8843	206	34	1.3	43	1365	47	730	918	62	0.043	0.215	0.205	16	0.017
3. Amp	262950	11964	290	42	1.7	4.7	1137	51	798	1024	90	0.004	0.093	0.001	18	0.010
3. Amp	262457	12681	392	51	1.1	4.2	1166	48	902	1014	145	0.011	0.102	0.024	24	0.016
3. Amp	262714	12320	276	40	3.9	3.5	1137	55	775	1078	66	0.002	0.105	0.001	20	0.022
3. Amp	261043	13546	300	45	2.4	9.2	1142	55	827	1087	95	0.005	0.095	0.005	23	0.005
3. Amp	261901	12354	304	45	1.4	3.9	1133	52	850	1045	107	0.007	0.088	0.013	19	0.018
3. Amp	261491	13827	358	50	1.4	3.2	1129	52	861	1062	119	0.006	0.089	0.572	24	0.016
3. Amp	259403	15767	395	53	4.0	2.4	1320	58	838	1177	101	0.024	0.697	0.054	34	0.011
3. Amp	259192	15835	368	53	2.7	2.2	1547	55	843	1085	120	0.042	0.133	0.023	32	0.017
3. Amp	259372	15105	462	57	1.5	10.0	1172	53	927	2317	165	0.010	0.320	0.031	33	0.014
3. Amp	256778	18413	415	57	3.8	13	1172	59	869	1269	125	0.016	0.207	0.221	43	0.008
3. Amp	257893	17693	389	54	2.9	8.1	1696	60	915	1210	127	0.086	0.159	0.184	40	0.020
3. Amp	255746	18834	505	66	2.7	8.4	1284	57	952	1115	169	0.047	0.146	1.3	47	0.026

Lithophile elements			Transition metals								REY	Granitophile				
Amphibole	**Si**	**Al**	**Ti**	**V**	**Nb**	**Cr**	**Ni**	**Co**	**Mn**	**Zn**	**ΣREY**	**^{238}U**	**^{206}Pb**	**W**	**Sn**	**Mo**
3. Amp	260021	14850	341	49	2.4	4.3	1160	57	886	1137	108	0.008	0.110	0.000	29	0.018
3. Amp	258831	16090	351	51	2.7	13	1158	56	849	1122	110	0.007	0.351	0.013	32	0.010
3. Amp	259824	14570	373	51	2.4	16	1153	54	850	1092	107	0.005	0.094	0.001	26	0.028
3. Amp	261591	12569	377	50	1.3	12	1148	49	843	1008	124	0.005	0.086	0.000	21	0.025
3. Amp	263503	11731	382	48	1.3	14	1575	47	807	974	228	0.062	0.238	0.035	20	0.008
3. Amp	264276	9176	203	33	1.3	2.6	1155	49	747	972	64	0.002	0.086	0.000	12	0.017
3. Amp	262301	9307	240	35	1.2	19	1291	45	747	971	73	0.039	1.3	0.068	12	0.004
3. Amp	263660	10381	260	38	1.9	10	1347	47	751	1063	75	0.039	0.130	0.499	19	0.014
3. Amp	262732	10095	269	40	1.2	25	1183	44	731	920	73	0.018	0.077	0.023	13	0.007
3. Amp	264642	8814	263	36	0.726	13	1186	43	741	879	72	0.002	0.066	0.002	11	0.026
3. Amp	261844	12686	463	52	1.1	1.8	1350	47	900	1144	159	0.054	0.179	0.132	26	0.026
3. Amp	257736	13705	370	55	1.4	2.9	3249	47	836	985	126	0.186	0.215	0.110	19	0.021
3. Amp	261618	13308	370	50	1.8	2.3	1193	50	817	1014	106	0.013	0.121	0.026	19	0.008
3. Amp	263687	9841	256	35	2.5	1.6	1164	50	746	980	62	0.003	0.098	0.201	14	0.022
3. Amp	262875	9971	245	35	2.1	0.772	1133	51	766	1008	68	0.004	0.091	0.107	13	0.009
3. Amp	260690	12615	384	48	1.3	3.7	1353	50	842	976	127	0.054	0.129	0.067	26	0.027
3. Amp	248816	18280	313	67	1.5	2.1	8550	52	685	975	105	0.864	0.739	0.277	22	0.029
3. Amp	243662	15646	443	78	3.1	6.1	1581	60	835	1055	108	0.204	0.197	0.107	33	0.033
3. Amp	260711	13749	357	49	3.1	1.7	1739	56	799	1088	82	0.114	0.167	0.120	33	0.033
3. Amp	255830	18984	444	58	3.3	1.0	1181	63	878	1209	123	0.012	0.127	0.004	43	0.017
3. Amp	260755	12506	212	37	2.4	0.103	1211	64	871	1183	67	0.005	0.093	0.006	23	0.034
3. Amp	255396	18904	512	61	5.6	3.8	1198	65	934	1284	130	0.017	0.130	0.008	48	0.012
3. Amp	252446	23188	646	73	4.1	4.7	1181	66	1018	1307	182	0.020	0.121	0.007	64	0.014
3. Amp	252986	21722	646	69	2.3	3.8	1179	62	1034	1248	198	0.025	0.134	0.005	55	0.025
3. Amp	255437	18910	559	62	1.8	3.6	1151	58	952	1167	180	0.009	0.110	0.009	43	0.008
3. Amp	258239	15777	503	56	1.5	3.8	1135	53	889	1081	158	0.009	0.107	0.000	32	0.018
Mean (n=197)	256339	17740	505	66	1.7	5.6	1742	63	952	1208	84	0.084	0.293	0.065	28	0.124
SD	32415	9384	396	24	1.6	6.3	671	26	163	289	46	0.184	0.427	0.120	20	0.397
Median	256822	15835	365	63	1.3	3.6	1649	55	970	1171	73	0.027	0.181	0.035	20	0.026
Max	271375	42534	1625	135	7.5	43	8550	167	1275	2317	228	1.6	5.2	1.3	81	3.3
Min	219844	4744	70	27	0.078	0.103	1129	26	645	592	22	0.000	0.030	0.000	6.0	0.003

Lithophile elements			Transition metals				REY	Granitophile				
Apatite	**Si**	**Al**	**Nb**	**Co**	**Mn**	**Zn**	**ΣREY**	**^{238}U**	**^{206}Pb**	**W**	**Sn**	**Mo**
4. Ap	318	0.281	0.001	0.034	277	1.5	1756	1.7	1.9	0.096	0.058	0.017
4. Ap	376	0.291	0.004	0.013	200	0.754	1264	1.3	0.989	0.390	0.049	0.034
4. Ap	250	0.273	0.008	0.021	218	0.656	1324	1.4	1.2	0.724	0.047	0.026
4. Ap	276	0.282	0.007	0.024	227	1.1	1322	1.0	1.3	0.913	0.050	0.014
4. Ap	436	0.319	0.001	0.044	267	1.4	1434	1.5	1.6	0.174	0.075	0.020
4. Ap	720	17	0.026	0.170	306	3.3	1867	2.3	2.2	0.123	0.047	0.020
4. Ap	219	0.404	0.009	0.033	287	1.5	1794	2.3	2.0	0.456	0.050	0.017
4. Ap	300	0.230	0.006	0.060	354	2.1	2120	2.4	2.6	0.216	0.042	0.016
4. Ap	327	0.263	0.001	0.045	277	1.4	1719	2.5	2.0	0.064	0.046	0.016
4. Ap	278	0.268	0.011	0.040	341	1.8	1944	2.1	2.5	0.952	0.042	0.014
4. Ap	372	1.1	0.006	0.039	330	1.7	2036	2.5	2.4	0.042	0.048	0.032
4. Ap	370	0.425	0.001	0.039	297	1.3	1714	1.7	1.9	0.146	0.045	0.011
4. Ap	344	0.179	0.009	0.031	240	0.917	1357	1.9	1.7	0.112	0.034	0.016
4. Ap	344	0.185	0.004	0.037	238	0.975	1325	1.9	1.7	0.118	0.032	0.004
4. Ap	273	1.0	0.002	0.042	242	1.4	1227	2.0	1.6	0.056	0.137	0.003
4. Ap	317	1.4	0.011	0.038	192	2.3	1255	2.4	1.5	0.851	0.226	0.021
4. Ap	326	0.242	0.022	0.016	182	0.608	1093	2.1	1.2	1.3	0.149	0.006
4. Ap	328	0.167	0.036	0.023	160	0.727	782	2.1	0.871	3.2	0.127	0.023
4. Ap	347	0.162	0.006	0.022	224	0.680	1239	1.5	1.5	0.195	0.245	0.002
4. Ap	322	0.185	0.006	0.029	201	0.802	1182	1.8	1.4	0.271	0.066	0.004
4. Ap	260	0.328	0.016	0.047	292	1.5	1464	2.4	2.1	1.5	0.089	0.004
4. Ap	301	0.525	0.035	0.022	225	1.1	1120	1.1	0.893	4.5	0.077	0.023
4. Ap	1282	272	0.041	0.121	274	2.1	1392	1.4	1.9	0.210	0.085	0.003
4. Ap	284	0.353	0.041	0.015	200	0.347	1194	1.1	1.1	1.5	0.092	0.001
4. Ap	328	0.331	0.012	0.026	247	1.4	1194	0.586	1.2	1.9	0.090	0.004
4. Ap	406	4.3	0.067	0.159	200	2.8	1077	1.2	1.0	9.1	0.171	0.003
4. Ap	292	0.289	0.009	0.034	264	0.806	1492	1.9	1.7	1.1	0.158	0.006
4. Ap	232	0.335	0.004	0.037	293	1.4	1564	2.4	2.1	0.200	0.145	0.004
4. Ap	1782	412	0.540	0.205	225	6.8	1317	2.1	1.7	26	0.239	0.011
4. Ap	450	6.8	0.002	0.043	277	1.4	1267	1.4	1.8	0.186	0.093	0.002
Mean (n=30)	415	24	0.032	0.050	252	1.5	1428	1.8	1.6	1.9	0.095	0.013
SD	323	88	0.097	0.048	49	1.2	314	0.509	0.472	4.8	0.062	0.009
Median	327	0.324	0.008	0.037	244	1.4	1324	1.9	1.7	0.331	0.076	0.013
Max	1782	412	0.540	0.205	354	6.8	2120	2.5	2.6	26	0.245	0.034
Min	219	0.162	0.001	0.013	160	0.347	782	0.586	0.871	0.042	0.032	0.001

SD Table 1e LA-ICP-MS data selected for REE plots (concentrations in ppm)

#	Magnetite - Core	La	Ce	Pr	Nd	Sm	Eu	Gd	Tb	Dy	Y	Ho	Er	Tm	Yb	Lu	ΣREY
1	Jg8Mt 5 09	0.461	0.733	0.140	0.575	0.181	0.035	0.197	0.039	0.249	0.959	0.031	0.151	0.019	0.245	0.040	4.1
2	Jg7Mt 2 10	0.247	0.723	0.167	0.889	0.136	0.035	0.204	0.030	0.196	1.2	0.038	0.091	0.016	0.154	0.020	4.1
3	Jg8Mt 5 03	0.349	0.710	0.173	0.672	0.160	0.033	0.226	0.038	0.221	1.1	0.038	0.148	0.027	0.230	0.038	4.2
4	Jg9bMt5rim 24	0.576	0.942	0.150	0.752	0.144	0.034	0.181	0.030	0.211	1.2	0.050	0.113	0.017	0.075	0.008	4.4
5	Jg8Mt 5 06	0.556	1.0	0.130	0.609	0.165	0.037	0.227	0.032	0.230	1.2	0.046	0.161	0.034	0.243	0.039	4.7
6	Jg8Mt 6 03	0.292	0.725	0.169	0.833	0.232	0.030	0.259	0.042	0.297	1.6	0.057	0.113	0.013	0.102	0.019	4.8
7	Jg9bMt5rim 28	0.549	1.4	0.211	1.1	0.309	0.071	0.299	0.044	0.197	1.0	0.044	0.077	0.017	0.087	0.012	5.4
8	Jg9bMt5rim 25	0.554	1.5	0.218	1.1	0.203	0.037	0.166	0.036	0.227	1.2	0.056	0.134	0.011	0.103	0.012	5.4
9	Jg6Mt 1 09	1.0	1.6	0.214	0.894	0.268	0.051	0.214	0.031	0.219	0.948	0.032	0.079	0.011	0.084	0.015	5.6
10	Jg6Mt 1 08	0.972	1.6	0.223	0.913	0.189	0.046	0.236	0.018	0.161	1.0	0.035	0.088	0.015	0.089	0.026	5.7
11	Jg9bMt1rim 01	0.773	1.4	0.158	0.849	0.233	0.037	0.215	0.033	0.223	1.4	0.051	0.147	0.017	0.166	0.029	5.7
12	Jg9bMt1rim 03	0.852	1.0	0.199	0.802	0.196	0.044	0.297	0.028	0.285	1.7	0.061	0.263	0.028	0.244	0.033	6.1
13	Jg8Mt 2 core 03	0.369	1.2	0.200	1.1	0.235	0.061	0.298	0.048	0.363	2.0	0.060	0.147	0.009	0.112	0.014	6.2
14	Jg8Mt 2 core 01	0.537	1.3	0.254	1.2	0.323	0.051	0.357	0.048	0.318	1.6	0.063	0.138	0.025	0.200	0.036	6.5
15	Jg9bMt1rim 08	0.925	2.0	0.288	1.4	0.289	0.033	0.244	0.036	0.195	1.0	0.044	0.125	0.015	0.095	0.018	6.7
16	Jg6Mt 2 04	1.3	2.3	0.449	1.7	0.267	0.058	0.274	0.025	0.159	0.718	0.034	0.075	0.008	0.060	0.006	7.4
17	Jg9bMt1rim 06	0.935	2.0	0.339	1.5	0.293	0.056	0.331	0.039	0.318	1.5	0.060	0.155	0.029	0.197	0.036	7.8
18	Jg6Mt 7 01	1.7	3.2	0.406	1.7	0.294	0.051	0.246	0.020	0.130	0.747	0.023	0.114	0.016	0.119	0.026	8.8
19	Jg6Mt 1 05	1.9	3.0	0.433	1.9	0.338	0.054	0.293	0.040	0.261	1.1	0.041	0.111	0.010	0.079	0.019	9.5
20	Jg6Mt 1 04	1.8	3.3	0.485	2.0	0.303	0.050	0.267	0.039	0.256	1.2	0.049	0.093	0.008	0.075	0.010	9.9
21	Jg6Mt 2 07	2.5	4.7	0.589	2.5	0.359	0.062	0.339	0.033	0.212	1.2	0.041	0.132	0.016	0.064	0.019	13
22	Jg6Mt 2 05	2.4	5.6	0.692	2.6	0.382	0.070	0.306	0.049	0.195	1.1	0.029	0.086	0.015	0.062	0.009	14
23	Jg9bMt5rim 38	2.0	4.1	0.619	2.6	0.486	0.098	0.409	0.064	0.441	2.3	0.100	0.269	0.023	0.130	0.032	14
24	Jg7Mt 5 07	2.5	5.3	0.700	3.2	0.451	0.078	0.512	0.046	0.319	2.2	0.084	0.257	0.017	0.263	0.038	16
25	Jg6Mt 2 02	2.8	6.6	0.916	3.4	0.485	0.097	0.484	0.042	0.290	1.3	0.056	0.130	0.013	0.075	0.016	17
26	Jg9bMt1rim 05	1.8	5.8	0.818	3.7	0.722	0.119	0.574	0.086	0.510	2.3	0.086	0.224	0.019	0.113	0.019	17
27	Jg9bMt5rim 35	4.5	6.1	0.682	2.7	0.456	0.090	0.438	0.044	0.268	1.5	0.068	0.120	0.016	0.119	0.020	17
28	Jg9bMt5rim 32	2.5	6.3	0.839	4.1	0.683	0.141	0.792	0.111	0.536	2.4	0.093	0.275	0.027	0.255	0.036	19
29	Jg9bMt5core 08	2.2	6.6	0.967	4.7	0.643	0.123	0.683	0.096	0.603	2.9	0.124	0.276	0.021	0.157	0.019	20
30	Jg9bMt5rim 34	4.3	6.6	0.986	4.6	0.603	0.105	0.639	0.079	0.340	1.6	0.061	0.155	0.015	0.094	0.015	20
31	Jg7Mt 5 04	4.1	10	1.4	5.9	1.0	0.098	0.707	0.071	0.535	3.3	0.133	0.346	0.042	0.294	0.049	28
32	Jg7Mt 3 03	5.4	14	1.8	8.1	1.6	0.154	1.1	0.130	0.806	4.5	0.130	0.464	0.071	0.393	0.085	39
33	Jg7Mt 3 06	6.4	13	1.8	7.3	1.3	0.226	1.3	0.158	1.0	5.7	0.192	0.523	0.066	0.523	0.073	40
34	Jg7Mt 3 02	7.1	18	2.4	9.3	1.8	0.200	1.3	0.157	0.936	6.3	0.225	0.633	0.095	0.584	0.097	49
	Mean (n=34)	2.0	4.3	0.595	2.6	0.463	0.075	0.428	0.055	0.345	1.9	0.069	0.189	0.024	0.173	0.029	13
	SD	1.8	4.2	0.551	2.3	0.403	0.048	0.298	0.036	0.218	1.3	0.046	0.132	0.019	0.126	0.021	11
	Median	1.5	2.6	0.419	1.7	0.306	0.057	0.298	0.041	0.264	1.4	0.056	0.143	0.017	0.119	0.020	8.3
	Max	7.1	18	2.4	9.3	1.8	0.226	1.3	0.158	1.0	6.3	0.225	0.633	0.095	0.584	0.097	49
	Min	0.247	0.710	0.130	0.575	0.136	0.030	0.166	0.018	0.130	0.718	0.023	0.075	0.008	0.060	0.006	4.1

#	Jg8 - Apatite	La	Ce	Pr	Nd	Sm	Eu	Gd	Tb	Dy	Y	Ho	Er	Tm	Yb	Lu	ΣREY
1	Jg8-Ap 1 - 02	23	73	14	96	48	14	92	17	112	634	24	62	7.4	43	5.4	1264
2	Jg8-Ap 1 - 04	26	82	16	101	48	14	90	17	117	660	25	66	8.0	46	5.8	1322
3	Jg8-Ap 1 - 03	31	94	17	112	51	15	93	17	114	637	24	63	7.6	43	5.4	1324
4	Jg8-Ap 1 - 05	33	104	18	115	52	14	97	19	130	693	27	70	8.5	47	5.8	1434
5	Jg8-Ap 2 - 10	44	136	24	142	59	16	101	19	139	835	31	87	11	63	8.0	1714
6	Jg8-Ap 2 - 06	50	154	28	168	69	19	113	20	137	780	29	78	9.6	57	7.3	1719
7	Jg8-Ap 1 - 01	52	158	27	163	67	18	114	21	144	801	31	82	10.0	60	7.4	1756
8	Jg8-Ap 2 - 02	62	181	31	181	71	18	114	21	140	791	29	80	9.9	56	7.2	1794
9	Jg8-Ap 2 - 01	68	198	33	194	74	19	119	21	142	810	30	82	10	59	7.3	1867
10	Jg8-Ap 2 - 07	75	216	36	204	75	19	120	21	146	836	32	85	11	62	7.7	1944
11	Jg8-Ap 2 - 09	77	229	38	218	82	20	126	22	154	864	33	90	11	66	8.2	2036
12	Jg8-Ap 2 - 04	91	262	43	247	88	21	133	23	154	855	32	87	11	64	7.9	2120
	Mean (n=12)	53	157	27	162	65	17	109	20	136	766	29	78	9.5	55	6.9	1691
	SD	22	62	9.5	49	13	2.5	14	2.2	15	86	3.3	9.9	1.3	8.3	1.1	291
	Median	51	156	28	165	68	18	114	20	139	796	30	81	10.0	58	7.3	1737
	Max	91	262	43	247	88	21	133	23	154	864	33	90	11	66	8.2	2120
	Min	23	73	14	96	48	14	90	17	112	634	24	62	7.4	43	5.4	1264

#	Jg9b - Apatite	La	Ce	Pr	Nd	Sm	Eu	Gd	Tb	Dy	Y	Ho	Er	Tm	Yb	Lu	ΣREY
1	Jg9b-Ap - 01	60	185	32	187	68	19	101	15	93	502	18	44	4.7	25	3.4	1357
2	Jg9b-Ap - 02	57	180	31	189	69	19	99	15	90	484	17	42	4.5	24	3.3	1325
3	Jg9b-Ap - 04	41	136	25	158	64	18	97	15	89	490	18	42	4.6	25	3.4	1227
4	Jg9b-Ap - 05	40	135	26	167	68	18	103	15	92	499	18	42	4.5	24	3.2	1255
5	Jg9b-Ap - 06	35	115	22	144	61	16	92	14	79	437	15	36	3.8	20	2.7	1093
6	Jg9b-Ap - 09	50	159	28	170	65	18	96	14	85	467	17	40	4.3	23	3.1	1239
7	Jg9b-Ap - 12	42	141	26	167	64	17	94	14	82	452	16	38	4.0	22	2.9	1182
8	Jg9b-Ap - 14	78	236	39	219	75	20	104	16	92	492	18	43	4.7	25	3.4	1464
9	Jg9b-Ap - 15	37	124	24	157	64	16	95	14	82	431	16	36	3.8	19	2.7	1120
10	Jg9b-Ap - 16	58	181	32	182	69	20	105	16	98	530	19	47	5.0	27	3.6	1392
11	Jg9b-Ap - 17	39	130	24	157	63	18	96	15	86	478	17	40	4.2	23	3.1	1194
12	Jg9b-Ap - 19	46	145	25	150	60	17	93	15	86	470	17	40	4.3	23	3.0	1194
13	Jg9b-Ap - 21	40	125	23	147	59	15	90	13	76	416	15	34	3.5	18	2.5	1077
14	Jg9b-Ap - 22	68	216	38	224	79	21	110	17	98	522	19	45	4.8	26	3.5	1492
15	Jg9b-Ap - 23	81	249	42	233	78	22	109	17	100	532	19	46	5.1	28	3.8	1564
16	Jg9b-Ap - 25	55	171	30	176	68	18	101	15	92	500	18	42	4.5	25	3.3	1317
17	Jg9b-Ap - 28	52	163	28	161	62	19	95	15	90	489	18	43	4.7	25	3.4	1267
	Mean (n=12)	52	164	29	176	67	18	99	15	89	482	17	41	4.4	24	3.2	1280
	SD	14	40	5.8	27	5.9	1.8	5.9	0.937	6.6	34	1.4	3.6	0.428	2.6	0.346	140
	Median	50	159	28	167	65	18	97	15	90	489	18	42	4.5	24	3.3	1255
	Max	81	249	42	233	79	22	110	17	100	532	19	47	5.1	28	3.8	1564
	Min	35	115	22	144	59	15	90	13	76	416	15	34	3.5	18	2.5	1077

#	Jg8 - Amphibole	La	Ce	Pr	Nd	Sm	Eu	Gd	Tb	Dy	Y	Ho	Er	Tm	Yb	Lu	ΣREY
1	Jg8-Amp2 - 02	0.065	0.436	0.143	1.6	1.7	0.583	3.6	0.708	4.8	26	0.953	2.5	0.317	1.9	0.206	46
2	Jg8-Amp1 - 02	0.083	0.460	0.183	1.6	1.8	0.687	3.7	0.727	5.2	28	1.1	2.7	0.334	2.2	0.258	49
3	Jg8-Amp2 - 09	0.063	0.491	0.174	1.8	1.8	0.647	3.8	0.735	5.1	28	1.1	2.7	0.338	2.1	0.251	49
4	Jg8-Amp1 - 01	0.058	0.442	0.166	1.6	1.6	0.618	3.8	0.770	5.2	29	1.0	2.9	0.367	2.1	0.269	50
5	Jg8-Amp1 - 03	0.083	0.602	0.195	2.1	2.1	0.747	4.0	0.827	5.7	31	1.2	3.0	0.387	2.2	0.259	54
6	Jg8-Amp2 - 10	0.069	0.540	0.190	2.0	2.2	0.714	4.6	0.902	6.4	34	1.3	3.3	0.423	2.3	0.298	59
7	Jg8-Amp2 - 05	0.070	0.576	0.234	2.3	2.2	0.907	5.0	1.0	7.1	39	1.5	3.8	0.512	3.0	0.374	68
8	Jg8-Amp2 - 08	0.078	0.598	0.209	2.3	2.3	0.869	5.3	1.0	7.4	40	1.4	3.9	0.516	3.2	0.383	70
9	Jg8-Amp2 - 03	0.087	0.628	0.241	2.2	2.5	0.922	5.3	1.1	7.5	40	1.5	4.2	0.511	3.1	0.366	70
10	Jg8-Amp1 - 04	0.114	0.774	0.281	2.6	2.7	1.1	6.0	1.2	8.8	47	1.8	4.7	0.606	3.9	0.500	83
11	Jg8-Amp2 - 07	0.086	0.720	0.236	2.7	2.7	1.1	6.8	1.4	10	58	2.2	5.7	0.755	4.6	0.574	98
12	Jg8-Amp2 - 04	0.113	0.750	0.286	2.9	3.4	1.3	7.5	1.5	11	60	2.2	5.9	0.783	4.7	0.572	103
13	Jg8-Amp1 - 06	0.107	0.804	0.285	3.2	3.3	1.3	7.4	1.6	11	63	2.3	6.4	0.856	5.3	0.665	107
14	Jg8-Amp1 - 05	0.095	0.846	0.300	3.2	3.2	1.5	7.4	1.6	11	64	2.4	6.6	0.900	5.3	0.658	110
15	Jg8-Amp1 - 07	0.106	0.879	0.342	3.2	3.6	1.4	7.9	1.7	12	66	2.5	6.8	0.919	5.5	0.643	114
16	Jg8-Amp1 - 08	0.130	0.864	0.298	3.0	3.3	1.4	8.0	1.7	12	67	2.5	7.0	0.876	5.4	0.675	114
17	Jg8-Amp2 - 01	0.087	0.738	0.274	2.7	3.3	1.2	8.1	1.7	12	70	2.6	7.1	0.897	5.5	0.718	118
18	Jg8-Amp1 - 11	0.139	1.1	0.375	3.8	4.1	1.9	9.8	2.1	16	90	3.5	9.1	1.2	7.5	0.949	151
19	Jg8-Amp1 - 10	0.136	0.952	0.365	3.7	4.2	1.9	10	2.2	17	98	3.7	11	1.3	8.4	1.1	164
	Mean (n=19)	0.093	0.692	0.252	2.5	2.7	1.1	6.2	1.3	9.3	52	1.9	5.2	0.676	4.1	0.514	88
	SD	0.025	0.181	0.068	0.702	0.809	0.404	2.1	0.477	3.7	21	0.816	2.3	0.303	1.9	0.255	35
	Median	0.087	0.720	0.241	2.6	2.7	1.1	6.0	1.2	8.8	47	1.8	4.7	0.606	3.9	0.500	83
	Max	0.139	1.1	0.375	3.8	4.2	1.9	10	2.2	17	98	3.7	11	1.3	8.4	1.1	164
	Min	0.058	0.436	0.143	1.6	1.6	0.583	3.6	0.708	4.8	26	0.953	2.5	0.317	1.9	0.206	46

#	Jg9b - Amphibole	La	Ce	Pr	Nd	Sm	Eu	Gd	Tb	Dy	Y	Ho	Er	Tm	Yb	Lu	ΣREY
1	Jg9b-Amp1 - 08	0.171	1.2	0.426	3.8	3.0	1.0	5.4	0.936	6.1	33	1.2	2.8	0.325	2.0	0.261	62
2	Jg9b-Amp2 - 37	0.158	1.2	0.425	4.0	3.0	1.0	5.5	0.956	6.2	33	1.2	3.0	0.327	1.8	0.220	62
3	Jg9b-Amp1 - 03	0.152	1.4	0.481	4.5	3.2	1.1	5.4	1.0	6.2	34	1.2	2.9	0.343	1.8	0.223	63
4	Jg9b-Amp1 - 28	0.179	1.3	0.477	4.1	3.3	1.0	5.4	0.977	6.5	34	1.2	3.0	0.337	2.0	0.241	64
5	Jg9b-Amp1 - 12	0.161	1.2	0.430	4.0	3.2	1.2	6.0	1.0	6.8	35	1.3	3.1	0.351	2.0	0.237	66
6	Jg9b-Amp2 - 38	0.153	1.2	0.423	4.1	3.1	1.1	5.8	1.0	6.8	37	1.3	3.2	0.355	2.1	0.269	68
7	Jg9b-Amp2 - 32	0.156	1.4	0.495	4.9	3.8	1.3	6.3	1.1	7.2	38	1.4	3.3	0.363	2.1	0.244	72
8	Jg9b-Amp1 - 29	0.291	1.7	0.545	4.6	3.5	1.1	6.4	1.1	7.2	39	1.4	3.4	0.397	2.2	0.277	73
9	Jg9b-Amp1 - 31	0.186	1.5	0.512	5.0	3.6	1.2	6.5	1.1	7.3	39	1.4	3.5	0.377	2.2	0.260	73
10	Jg9b-Amp1 - 04	0.188	1.5	0.532	5.0	3.8	1.3	6.7	1.2	7.3	39	1.4	3.5	0.389	2.3	0.265	75
11	Jg9b-Amp1 - 30	0.240	1.5	0.511	4.6	3.6	1.2	6.3	1.1	7.4	40	1.4	3.6	0.437	2.7	0.325	75
12	Jg9b-Amp1 - 01	0.210	1.8	0.599	5.9	4.3	1.3	7.0	1.2	8.1	42	1.5	3.7	0.439	2.4	0.294	81
13	Jg9b-Amp2 - 42	0.167	1.2	0.455	4.3	3.6	1.3	6.5	1.3	8.7	46	1.7	4.1	0.474	2.7	0.352	82
14	Jg9b-Amp1 - 02	0.233	1.8	0.626	6.0	4.3	1.4	7.6	1.3	8.8	47	1.7	4.1	0.491	2.6	0.350	88
15	Jg9b-Amp1 - 09	0.193	1.6	0.564	5.2	4.1	1.4	7.7	1.4	9.0	49	1.8	4.3	0.495	2.9	0.356	90
16	Jg9b-Amp1 - 13	0.167	1.4	0.480	4.8	4.1	1.5	7.6	1.4	9.7	53	1.9	4.7	0.553	3.1	0.389	95
17	Jg9b-Amp1 - 16	0.190	1.4	0.540	4.9	4.2	1.6	8.1	1.6	10	56	2.1	5.1	0.605	3.5	0.438	101
18	Jg9b-Amp2 - 40	0.210	1.5	0.525	5.1	4.1	1.5	8.2	1.5	11	59	2.1	5.5	0.644	3.6	0.455	105

#	Jg9b - Amphibole	La	Ce	Pr	Nd	Sm	Eu	Gd	Tb	Dy	Y	Ho	Er	Tm	Yb	Lu	ΣREY
19	Jg9b-Amp2 - 35	0.235	1.8	0.651	6.0	4.7	1.6	8.5	1.6	11	58	2.1	5.3	0.636	3.6	0.489	106
20	Jg9b-Amp1 - 14	0.206	1.6	0.603	5.8	4.6	1.6	8.8	1.6	11	59	2.2	5.3	0.614	3.6	0.475	107
21	Jg9b-Amp1 - 25	0.191	1.7	0.558	5.7	4.5	1.7	8.8	1.6	11	60	2.1	5.5	0.626	3.6	0.477	107
22	Jg9b-Amp2 - 41	0.184	1.4	0.504	4.8	4.2	1.6	8.7	1.6	11	61	2.2	5.7	0.668	3.9	0.505	108
23	Jg9b-Amp1 - 22	0.162	1.4	0.498	4.8	4.2	1.6	8.4	1.6	11	62	2.3	5.6	0.676	3.9	0.485	108
24	Jg9b-Amp1 - 24	0.158	1.5	0.529	5.3	4.6	1.7	8.8	1.6	11	61	2.2	5.7	0.651	3.8	0.484	110
25	Jg9b-Amp1 - 15	0.221	1.8	0.656	6.5	5.1	1.7	9.4	1.8	12	66	2.4	5.9	0.724	4.2	0.533	119
26	Jg9b-Amp1 - 17	0.240	1.8	0.633	6.3	5.2	1.9	9.6	1.8	12	67	2.4	6.0	0.684	3.9	0.498	120
27	Jg9b-Amp2 - 43	0.166	1.4	0.479	5.0	4.4	1.9	9.2	1.8	13	71	2.6	6.6	0.798	4.6	0.580	123
28	Jg9b-Amp1 - 26	0.231	2.0	0.708	6.9	5.7	1.9	9.8	1.9	13	68	2.4	6.1	0.694	4.0	0.514	124
29	Jg9b-Amp1 - 19	0.182	1.5	0.527	5.5	4.9	1.9	9.8	1.9	13	71	2.6	6.5	0.772	4.5	0.569	125
30	Jg9b-Amp2 - 34	0.210	1.9	0.685	6.8	5.5	1.9	10	1.9	13	70	2.5	6.4	0.725	4.2	0.553	126
31	Jg9b-Amp1 - 20	0.169	1.4	0.510	5.1	4.6	1.9	9.7	1.9	13	73	2.6	6.8	0.833	4.8	0.616	127
32	Jg9b-Amp2 - 39	0.250	2.0	0.692	6.8	5.4	1.9	10	1.9	13	71	2.5	6.4	0.750	4.2	0.522	127
33	Jg9b-Amp2 - 45	0.137	1.1	0.391	4.2	4.2	1.8	9.5	1.9	14	77	2.7	7.3	0.890	5.3	0.695	130
34	Jg9b-Amp1 - 11	0.261	2.3	0.826	7.9	6.4	2.1	12	2.2	14	81	2.9	7.2	0.857	4.8	0.639	145
35	Jg9b-Amp2 - 50	0.245	2.1	0.754	7.3	6.4	2.3	12	2.3	16	89	3.3	8.3	0.954	5.6	0.706	158
36	Jg9b-Amp1 - 18	0.261	2.3	0.815	8.0	6.8	2.4	13	2.4	17	92	3.3	8.7	1.0	5.7	0.748	165
37	Jg9b-Amp1 - 21	0.226	1.8	0.661	6.5	6.0	2.4	13	2.5	18	97	3.5	9.3	1.1	6.5	0.864	169
38	Jg9b-Amp2 - 49	0.216	1.9	0.753	7.4	6.8	2.5	13	2.7	18	104	3.7	9.6	1.1	6.7	0.873	180
39	Jg9b-Amp2 - 46	0.190	1.6	0.569	5.9	6.0	2.5	13	2.6	19	106	3.9	10	1.2	7.7	1.0	182
40	Jg9b-Amp2 - 48	0.217	1.9	0.692	7.3	6.9	2.7	14	2.9	20	116	4.2	11	1.4	7.7	1.0	198
	Mean (n=40)	0.199	1.6	0.569	5.5	4.6	1.7	8.7	1.6	11	61	2.2	5.6	0.653	3.8	0.483	109
	SD	0.048	0.384	0.141	1.4	1.3	0.524	2.8	0.569	4.1	24	0.862	2.3	0.283	1.7	0.225	40
	Median	0.191	1.5	0.536	5.2	4.3	1.6	8.6	1.6	11	59	2.1	5.5	0.640	3.6	0.481	107
	Max	0.291	2.3	0.826	8.0	6.9	2.7	14	2.9	20	116	4.2	11	1.4	7.7	1.0	198
	Min	0.137	1.1	0.391	3.8	3.0	1.0	5.4	0.936	6.1	33	1.2	2.8	0.325	1.8	0.220	62

#	Jg3a - Amphibole	La	Ce	Pr	Nd	Sm	Eu	Gd	Tb	Dy	Y	Ho	Er	Tm	Yb	Lu	ΣREY
1	Jg3a-Amp2 - 04	0.041	0.218	0.085	0.653	0.690	0.249	1.6	0.300	2.2	13	0.470	1.4	0.182	1.3	0.211	22
2	Jg3a-Amp6 - 31	0.014	0.126	0.039	0.413	0.482	0.175	1.3	0.283	2.2	14	0.500	1.5	0.186	1.1	0.146	22
3	Jg3a-Amp6 - 34	0.021	0.136	0.036	0.403	0.536	0.218	1.5	0.345	2.7	17	0.630	1.7	0.224	1.5	0.179	27
4	Jg3a-Amp6 - 30	0.012	0.122	0.034	0.373	0.523	0.193	1.5	0.332	2.7	18	0.629	1.8	0.211	1.4	0.165	28
5	Jg3a-Amp6 - 26	0.027	0.233	0.065	0.697	0.678	0.231	1.7	0.399	2.9	18	0.646	1.8	0.227	1.3	0.185	29
6	Jg3a-Amp8 - 55	0.024	0.212	0.088	0.776	0.735	0.268	1.9	0.409	3.1	19	0.710	2.0	0.245	1.6	0.222	31
7	Jg3a-Amp6 - 28	0.052	0.249	0.078	0.625	0.622	0.234	1.7	0.394	3.1	21	0.709	2.1	0.257	1.6	0.203	32
8	Jg3a-Amp8 - 54	0.021	0.152	0.068	0.707	0.759	0.246	2.0	0.449	3.5	22	0.830	2.4	0.315	2.1	0.288	36
9	Jg3a-Amp7 - 44	0.022	0.161	0.075	0.657	0.707	0.275	2.1	0.477	3.8	23	0.805	2.4	0.278	2.0	0.234	37
10	Jg3a-Amp8 - 53	0.042	0.300	0.101	0.953	0.878	0.298	2.4	0.511	3.8	22	0.820	2.3	0.287	1.8	0.246	37
11	Jg3a-Amp7 - 43	0.008	0.111	0.048	0.481	0.694	0.297	2.1	0.494	3.8	25	0.873	2.4	0.329	2.1	0.222	39
12	Jg3a-Amp6 - 29	0.008	0.075	0.036	0.366	0.594	0.275	2.0	0.465	3.8	26	0.883	2.5	0.326	1.9	0.209	40
13	Jg3a-Amp4 - 16	0.048	0.260	0.103	0.986	0.907	0.294	2.4	0.531	4.1	24	0.878	2.4	0.340	2.3	0.301	40
14	Jg3a-Amp6 - 27	0.019	0.096	0.045	0.482	0.738	0.268	2.1	0.491	4.0	26	0.911	2.5	0.305	1.8	0.223	40

#	Jg3a - Amphibole	La	Ce	Pr	Nd	Sm	Eu	Gd	Tb	Dy	Y	Ho	Er	Tm	Yb	Lu	ΣREY
15	Jg3a-Amp3 - 11	0.010	0.127	0.058	0.633	0.789	0.271	2.2	0.484	3.9	25	0.920	2.7	0.376	2.6	0.380	40
16	Jg3a-Amp6 - 32	0.020	0.147	0.054	0.465	0.703	0.256	2.1	0.467	3.9	26	0.955	2.7	0.350	2.2	0.255	41
17	Jg3a-Amp7 - 45	0.058	0.432	0.158	1.5	1.2	0.371	2.4	0.528	3.9	24	0.876	2.6	0.317	2.2	0.300	41
18	Jg3a-Amph1 - 01	0.025	0.240	0.090	0.923	0.969	0.361	2.5	0.552	4.1	25	0.918	2.7	0.369	2.4	0.323	41
19	Jg3a-Amp8 - 52	0.107	0.734	0.235	2.1	1.6	0.532	2.7	0.544	3.9	23	0.818	2.3	0.346	2.2	0.290	42
20	Jg3a-Amp6 - 36	0.157	0.986	0.302	2.7	1.8	0.624	3.2	0.577	4.0	22	0.861	2.4	0.287	2.1	0.329	43
21	Jg3a-Amp7 - 42	0.012	0.119	0.057	0.590	0.875	0.340	2.6	0.541	4.8	28	1.0	3.0	0.406	2.7	0.375	45
22	Jg3a-Amp8 - 47	0.172	0.971	0.295	2.6	1.8	0.637	3.2	0.609	4.2	25	0.911	2.7	0.385	2.3	0.346	47
23	Jg3a-Amp2 - 05	0.177	0.963	0.285	2.4	1.8	0.539	3.3	0.647	4.3	26	0.931	2.8	0.355	2.4	0.381	47
24	Jg3a-Amp2 - 03	0.055	0.415	0.156	1.4	1.4	0.425	2.9	0.588	4.7	27	0.999	3.0	0.396	2.8	0.385	47
25	Jg3a-Amp4 - 13	0.069	0.573	0.196	1.9	1.6	0.472	3.3	0.666	5.1	29	1.1	3.0	0.396	2.5	0.343	50
26	Jg3a-Amp2 - 02	0.081	0.674	0.247	2.2	1.6	0.566	3.4	0.725	4.9	29	1.1	3.1	0.420	2.8	0.379	52
27	Jg3a-Amp3 - 12	0.096	0.808	0.242	2.5	1.7	0.607	3.5	0.702	5.0	29	1.0	3.0	0.441	2.9	0.420	52
28	Jg3a-Amp4 - 17	0.159	0.870	0.267	2.7	2.0	0.498	3.6	0.728	5.3	29	1.1	3.2	0.424	3.0	0.503	54
29	Jg3a-Amp7 - 39	0.114	0.942	0.317	3.0	2.3	0.736	4.1	0.846	6.0	35	1.3	3.8	0.500	3.3	0.494	62
30	Jg3a-Amp8 - 50	0.150	1.1	0.352	3.5	2.6	0.777	4.7	0.883	6.2	36	1.3	3.9	0.521	3.5	0.543	66
31	Jg3a-Amp7 - 40	0.023	0.235	0.098	1.1	1.3	0.501	3.5	0.881	6.9	41	1.6	4.5	0.642	4.2	0.513	67
32	Jg3a-Amp4 - 18	0.144	1.2	0.424	4.2	3.4	0.838	6.1	1.2	8.5	49	1.9	5.1	0.718	4.9	0.733	88
	Mean (n=32)	0.062	0.439	0.148	1.4	1.2	0.402	2.7	0.564	4.2	26	0.937	2.7	0.355	2.3	0.323	43
	SD	0.056	0.367	0.113	1.1	0.717	0.195	1.1	0.214	1.5	8.4	0.327	0.921	0.133	0.911	0.140	15
	Median	0.041	0.244	0.094	0.938	0.893	0.319	2.4	0.530	3.9	25	0.897	2.6	0.343	2.2	0.301	41
	Max	0.177	1.2	0.424	4.2	3.4	0.838	6.1	1.2	8.5	49	1.9	5.1	0.718	4.9	0.733	88
	Min	0.000	0.000	0.000	0.000	0.000	0.000	0.000	0.000	0.000	0.000	0.000	0.000	0.000	0.000	0.000	0.000

#	Jg5 - Amphibole	La	Ce	Pr	Nd	Sm	Eu	Gd	Tb	Dy	Y	Ho	Er	Tm	Yb	Lu	ΣREY
1	Jg5-Amp2 - 33	0.041	0.403	0.214	2.2	2.3	1.1	4.3	0.907	6.6	31	1.3	3.5	0.417	2.5	0.357	57
2	Jg5-Amp2 - 35	0.075	0.783	0.329	3.3	2.3	1.1	4.7	0.887	6.4	30	1.3	3.3	0.436	2.8	0.342	58
3	Jg5-Amp5 - 32	0.065	0.431	0.174	2.0	2.0	1.1	4.3	0.925	7.0	33	1.4	3.8	0.474	2.9	0.380	60
4	Jg5-Amp3 - 01	0.069	0.630	0.253	3.1	2.5	1.2	5.0	0.954	6.8	32	1.4	3.6	0.442	2.8	0.367	61
5	Jg5-Amp4 - 20	0.062	0.550	0.243	2.8	2.4	1.2	5.0	0.999	7.1	34	1.4	3.7	0.464	3.0	0.384	63
6	Jg5-Amp3 - 07	0.086	0.872	0.368	3.3	2.9	1.3	5.2	1.1	7.7	35	1.5	4.1	0.514	3.3	0.444	68
7	Jg5-Amp4 - 21	0.107	0.898	0.348	3.4	2.8	1.3	5.3	1.1	7.7	36	1.6	4.1	0.519	3.3	0.465	69
8	Jg5-Amp4 - 23	0.097	0.840	0.313	3.3	2.8	1.3	5.3	1.1	7.9	37	1.6	4.3	0.537	3.4	0.460	71
9	Jg5-Amp4 - 16	0.104	0.963	0.356	3.7	3.0	1.4	5.6	1.1	8.1	37	1.6	4.1	0.508	3.4	0.491	71
10	Jg5-Amp3 - 02	0.283	1.5	0.426	3.9	3.0	1.4	5.6	1.1	7.8	38	1.7	4.3	0.574	3.6	0.474	73
11	Jg5-Amp3 - 05	0.090	0.927	0.356	3.7	2.9	1.4	5.8	1.2	8.7	39	1.7	4.6	0.560	3.8	0.496	75
12	Jg5-Amp3 - 06	0.117	0.973	0.383	3.8	3.1	1.4	5.6	1.2	8.4	39	1.7	4.5	0.594	3.7	0.476	75
13	Jg5-Amp2 - 40	0.088	0.727	0.299	3.5	2.9	1.5	6.0	1.2	9.1	42	1.8	4.6	0.562	3.4	0.469	78
14	Jg5-Amp4 - 22	0.097	0.970	0.406	4.1	3.3	1.6	6.8	1.4	10	46	2.0	5.2	0.691	4.2	0.571	87
15	Jg5-Amp3 - 11	0.095	0.945	0.379	4.3	3.5	1.7	7.0	1.4	10	47	2.0	5.3	0.675	4.1	0.555	89
16	Jg5-Amp3 - 04	0.110	1.2	0.454	4.6	3.8	1.8	7.3	1.5	11	51	2.3	6.1	0.766	4.8	0.656	98
17	Jg5-Amp5 - 25	0.121	1.0	0.441	4.6	3.8	1.9	7.5	1.6	12	54	2.4	6.3	0.795	4.9	0.648	102
18	Jg5-Amp2 - 39	0.134	1.1	0.495	5.0	4.2	1.9	8.2	1.6	12	56	2.4	6.4	0.818	5.0	0.664	106

#	Jg5 - Amphibole	La	Ce	Pr	Nd	Sm	Eu	Gd	Tb	Dy	Y	Ho	Er	Tm	Yb	Lu	ΣREY
19	Jg5-Amp4 - 17	0.129	1.2	0.493	4.8	4.1	1.9	7.8	1.7	13	57	2.5	6.5	0.838	5.4	0.730	107
20	Jg5-Amp3 - 10	0.094	1.0	0.444	4.7	4.1	2.0	8.3	1.7	12	58	2.5	6.6	0.823	5.4	0.676	109
21	Jg5-Amp5 - 30	0.217	1.4	0.478	5.0	4.0	2.0	8.0	1.7	12	59	2.5	6.8	0.861	5.6	0.736	110
22	Jg5-Amp3 - 09	0.110	1.1	0.470	4.9	4.3	2.0	8.4	1.7	13	60	2.6	6.9	0.880	5.5	0.720	112
23	Jg5-Amp3 - 13	0.116	1.2	0.499	5.0	4.1	2.0	8.6	1.8	14	62	2.8	7.4	0.966	6.1	0.808	118
24	Jg5-Amp2 - 38	0.153	1.4	0.573	5.7	4.6	2.1	8.6	1.8	13	63	2.8	7.1	0.936	5.8	0.800	119
25	Jg5-Amph1 - 04	0.122	1.3	0.537	5.2	4.8	2.1	8.9	1.9	14	66	2.9	7.8	0.956	5.9	0.794	123
26	Jg5-Amph1 - 09	0.142	1.3	0.566	5.6	4.8	2.3	9.6	2.1	15	71	3.2	8.5	1.1	7.0	0.885	133
27	Jg5-Amp5 - 31	0.161	1.3	0.506	5.2	4.5	2.1	9.5	2.1	16	72	3.2	8.6	1.1	7.3	0.934	134
28	Jg5-Amp2 - 36	0.126	1.3	0.558	5.7	4.7	2.3	9.7	2.1	15	72	3.3	8.3	1.1	6.9	0.974	134
29	Jg5-Amp3 - 14	0.126	1.3	0.557	5.1	4.9	2.4	9.8	2.1	16	72	3.2	8.4	1.2	7.4	0.966	135
30	Jg5-Amp2 - 37	0.142	1.4	0.613	5.8	4.8	2.3	9.7	2.1	16	73	3.2	8.5	1.1	7.4	0.964	137
31	Jg5-Amp5 - 27	0.135	1.3	0.539	5.4	5.0	2.3	9.7	2.2	16	76	3.4	9.0	1.2	8.0	1.1	141
32	Jg5-Amp5 - 26	0.173	1.5	0.591	5.8	5.0	2.4	10	2.2	17	77	3.4	9.2	1.2	7.3	1.0	143
33	Jg5-Amp3 - 12	0.132	1.3	0.586	5.7	4.9	2.4	11	2.2	17	78	3.4	9.4	1.2	7.7	1.0	146
34	Jg5-Amph1 - 08	0.128	1.4	0.588	5.9	5.2	2.5	11	2.3	17	80	3.6	9.8	1.3	8.0	1.1	150
35	Jg5-Amp3 - 15	0.140	1.3	0.551	6.0	5.4	2.5	11	2.3	18	82	3.6	9.8	1.3	7.8	1.0	152
36	Jg5-Amp5 - 28	0.131	1.4	0.615	5.8	5.2	2.6	11	2.4	18	85	3.9	10	1.4	8.8	1.1	158
37	Jg5-Amph1 - 06	0.139	1.2	0.539	5.7	5.1	2.4	11	2.4	19	86	3.8	10	1.4	9.0	1.2	158
38	Jg5-Amph1 - 07	0.113	1.3	0.579	5.9	5.3	2.6	11	2.4	18	87	4.0	11	1.4	9.0	1.2	161
39	Jg5-Amp4 - 18	0.128	1.4	0.630	6.2	5.6	2.7	12	2.6	20	92	4.1	11	1.5	9.3	1.2	170
40	Jg5-Amph1 - 05	0.138	1.5	0.662	6.4	5.8	2.9	12	2.7	20	93	4.3	11	1.5	9.7	1.3	173
41	Jg5-Amp4 - 19	0.156	1.4	0.610	6.5	5.7	2.9	12	2.7	20	94	4.2	11	1.5	9.6	1.3	174
42	Jg5-Amp5 - 29	0.149	1.5	0.655	6.9	6.5	3.2	14	3.2	24	116	5.2	14	1.9	12	1.6	210
	Mean (n=42)	0.122	1.1	0.469	4.7	4.1	2.0	8.2	1.8	13	61	2.7	7.1	0.927	5.9	0.781	114
	SD	0.045	0.338	0.145	1.4	1.3	0.630	2.8	0.642	5.0	23	1.1	2.9	0.395	2.5	0.335	43
	Median	0.124	1.2	0.494	5.0	4.2	2.0	8.4	1.7	13	59	2.6	6.9	0.871	5.6	0.733	111
	Max	0.283	1.5	0.662	6.9	6.5	3.2	14	3.2	24	116	5.2	14	1.9	12	1.6	210
	Min	0.041	0.403	0.174	2.0	2.0	1.1	4.3	0.887	6.4	30	1.3	3.3	0.417	2.5	0.342	57

#	Jg6 - Amphibole	La	Ce	Pr	Nd	Sm	Eu	Gd	Tb	Dy	Y	Ho	Er	Tm	Yb	Lu	ΣREY
1	Jg6-Amp 2 - 04	0.085	0.667	0.227	2.3	2.0	0.897	3.7	0.641	4.3	23	0.858	2.2	0.252	1.5	0.202	43
2	Jg6-Amp 2 - 03	0.108	0.732	0.245	2.4	2.0	0.849	3.6	0.668	4.5	24	0.864	2.3	0.276	1.5	0.197	45
3	Jg6-Amp 1 - 03	0.113	0.788	0.258	2.8	2.3	1.0	4.5	0.689	4.6	25	0.864	2.2	0.272	1.4	0.176	47
4	Jg6-Amp 2 - 05	0.088	0.746	0.285	2.5	2.3	0.981	4.0	0.729	5.1	27	1.0	2.6	0.308	1.8	0.234	50
5	Jg6-Amp 1 - 05	0.089	0.856	0.326	3.1	2.6	1.3	5.0	0.887	5.3	29	1.1	2.4	0.306	1.6	0.224	54
6	Jg6-Amp 1 - 01	0.100	0.868	0.342	3.4	2.8	1.3	5.4	0.903	5.9	32	1.2	3.0	0.323	1.8	0.246	60
7	Jg6-Amp 1 - 04	0.113	0.893	0.366	3.6	3.2	1.5	5.6	0.992	6.0	34	1.2	3.0	0.323	2.0	0.266	63
8	Jg6-Amp 1 - 08	0.109	0.925	0.341	3.4	2.9	1.4	5.7	1.0	7.6	40	1.5	4.0	0.509	3.3	0.402	73
9	Jg6-Amp 1 - 12	0.106	1.1	0.436	4.0	3.4	1.6	6.0	1.1	7.3	40	1.5	3.8	0.423	2.7	0.356	74
10	Jg6-Amp 1 - 02	0.110	0.963	0.415	4.0	3.9	1.8	7.4	1.2	7.4	42	1.5	3.6	0.426	2.3	0.297	77
11	Jg6-Amp 2 - 02	0.118	0.920	0.367	3.5	3.1	1.5	6.1	1.2	7.8	43	1.7	4.3	0.500	2.9	0.365	78
12	Jg6-Amp 1 - 06	0.150	1.2	0.396	3.8	3.4	1.6	6.2	1.1	7.9	44	1.6	4.3	0.513	3.2	0.386	80
13	Jg6-Amp 1 - 11	0.134	1.1	0.417	4.2	3.6	1.8	7.0	1.3	8.4	47	1.7	4.6	0.491	3.2	0.450	86
14	Jg6-Amp 1 - 07	0.155	1.2	0.450	4.3	3.4	1.9	6.7	1.3	9.2	52	1.9	5.0	0.634	3.8	0.514	92
15	Jg6-Amp 2 - 06	0.127	1.0	0.405	4.3	3.7	1.7	7.2	1.4	9.7	54	2.0	5.1	0.632	3.4	0.428	95
16	Jg6-Amp 2 - 01	0.109	0.945	0.397	4.2	3.8	1.7	8.4	1.5	11	60	2.2	5.4	0.629	3.3	0.435	103
17	Jg6-Amp 2 - 09	0.135	1.1	0.424	4.4	4.1	1.8	8.2	1.6	11	60	2.2	5.8	0.672	3.9	0.465	106
18	Jg6-Amp 2 - 07	0.158	1.2	0.437	4.3	3.7	1.8	7.5	1.5	11	62	2.4	6.7	0.811	5.0	0.621	110
19	Jg6-Amp 1 - 10	0.179	1.4	0.549	5.5	4.6	2.3	8.8	1.7	12	64	2.4	6.1	0.741	4.6	0.597	115
20	Jg6-Amp 2 - 08	0.157	1.2	0.438	4.4	4.0	1.9	8.2	1.6	12	68	2.6	7.0	0.905	5.2	0.674	118
21	Jg6-Amp 1 - 09	0.201	1.6	0.626	5.6	4.7	2.3	8.7	1.8	13	72	2.7	7.3	0.916	5.6	0.733	128
	Mean (n=21)	0.126	1.0	0.388	3.8	3.3	1.6	6.4	1.2	8.1	45	1.7	4.3	0.517	3.0	0.394	81
	SD	0.031	0.232	0.095	0.882	0.782	0.410	1.6	0.359	2.7	15	0.598	1.6	0.210	1.3	0.164	26
	Median	0.113	0.963	0.397	4.0	3.4	1.6	6.2	1.2	7.8	43	1.6	4.3	0.500	3.2	0.386	78
	Max	0.201	1.6	0.626	5.6	4.7	2.3	8.8	1.8	13	72	2.7	7.3	0.916	5.6	0.733	128
	Min	0.085	0.667	0.227	2.3	2.0	0.849	3.6	0.641	4.3	23	0.858	2.2	0.252	1.4	0.176	43

SUPPLEMENTARY MATERIAL F

FOR CHAPTER 7 – ARSENOHAUCHECORNITE, OGNITITE, PARKERITE, AND RELATED MINERALS FROM ONÇA ROSA OREBODY, CARAJÁS, BRAZIL: FINGERPRINTING PGE SIGNATURES IN HYDROTHERMAL NI ORES

APPENDIX A: ANALYTICAL METHODS AND ADDITIONAL FIGURES

APPENDIX B: ADDITIONAL TABLES, LA-ICP-MS RESULTS

APPENDIX A FOR CHAPTER 7

Supplemental Materials – Analytical Methods

Electron Probe microanalysis

Qualitative analyses for pentlandite were obtained using a JEOL JXA-8230 SuperProbe electron probe microanalyzer (EPMA) equipped with 5-spectrometer crystals LDE1, LDE2, ATP, PET/L-H and LIF-L/H. The wavelength dispersive (WDS) analyses were performed at an accelerating voltage of 15 kV, sample current of 20nA.

Quantitative compositions of minerals were determined using a Cameca SX-Five electron probe microanalyzer (EPMA), equipped with 5 tunable wavelength-dispersive spectrometers. The instrument is running PeakSite v6.2 software for microscope operation, and Probe for EPMA software (distributed by Probe Software Inc.) for all data acquisition and processing. Analysis was performed using operating conditions of 20 kV/20nA with a focused beam due to the required spatial resolution.

The full list of elements analysed along with primary and interference standards are presented in Tables a and b. Matrix corrections of Pouchou and Pichoir and Henke MACs were used for data reduction.

Beam damage and element migration were attempted to be minimized via use of the Mean Atomic Number (MAN) background correction (e.g. Donovan and Tingle (1996); Donovan et al. (2016)) over traditional 2 point background interpolation. This allows single point analysis time to be greatly shortened, reducing the aforementioned effects of beam damage and element migration and their subsequent impact on the quality of analysis.

Trace element LA-ICP-MS spot analysis

Trace element LA-ICP-MS spot analysis of sulfides was conducted using a RESOlution-SE 193 nm Excimer laser coupled to an Agilent 8900x quadrupole ICP-MS. Background measurements (30s) were followed by acquisition of signal during ablation of 50 or 60 s. Laser spot diameter was a consistent 50 μm-diameter at a pulse repetition rate of 5 Hz and fluence of 3 J/cm^2.

Thirty-Six isotopes were measured, with corresponding dwell times (in ms) provided in brackets: ^{27}Al (5) ^{34}S (5), ^{49}Ti (5), ^{55}Mn (10), ^{57}Fe (5), ^{59}Co (10), ^{60}Ni (10), ^{65}Cu (10), ^{66}Zn (10),

^{75}As (10), ^{77}Se (20), ^{88}Sr (10), ^{90}Zr (5), ^{95}Mo (20), ^{105}Pd (30), ^{106}Pd (30), ^{107}Ag (20), ^{111}Cd (10), ^{113}In (10), ^{115}In (10), ^{118}Sn (10), ^{121}Sb (10), ^{125}Te (20), ^{182}W (10), ^{193}Ir (30), ^{195}Pt (30), ^{197}Au (30), ^{204}Pb (10), ^{205}Tl (10), ^{206}Pb (10), ^{207}Pb (10), ^{208}Pb (10), ^{209}Bi (10), ^{232}Th (10), and ^{238}U (10). Longer dwell times were employed for isotopes of greatest interest.

For all analyses, reference materials STD-GL3 (Belousov et al. 2023), NiS-3 (Gilbert et al. 2013) and GSD-1G (USGS) were analyzed before, during and after ablation. Iron was used as an internal calibration standard for pyrite, pentlandite and violarite/bravoite, whereas Zn and Cu was used for sphalerite and chalcopyrite, respectively. Stoichiometric compositions were assumed in all cases.

Typical minimum detection limits (mdl, in ppm) for isotopes measured quantitatively are as follows: ^{55}Mn (0.05), ^{57}Fe (2), ^{59}Co (0.03), ^{60}Ni (0.03), ^{65}Cu (0.05), ^{66}Zn (0.12), ^{75}As (0.3), ^{77}Se (0.7), ^{95}Mo (0.03), ^{105}Pd (0.0002), ^{106}Pd (0.0002), ^{107}Ag (0.0006), ^{111}Cd (0.001), ^{113}In (0.003), ^{115}In (0.003), ^{118}Sn (0.06), ^{121}Sb (0.03), ^{125}Te (0.06), ^{182}W (<0.0001), ^{195}Pt (0.0005), ^{197}Au (0.0003), ^{204}Pb (0.006), ^{206}Pb (0.001), ^{207}Pb (0.001), ^{208}Pb (0.001), ^{209}Bi (0.003), and ^{238}U (<0.0001). Isotopes for Al, S, Ti, Mn, Cu, Zn, Sr, and Zr were measured only to identify the presence of inclusions. Tungsten, Ir, Tl, and Th, were consistently at or below their respective mdl values in all analyses and are also not tabulated. Rhodium, Ru, and Os are not present in available reference materials and could not be measured. Based on measurement of Pt, Pd and Ir, however, they are very likely to be extremely low and probably <mdl.

LADR software was utilized for data processing. Total Pb concentration data provided in Table SM Table S1a was calculated as the sum of ^{204}Pb, ^{206}Pb, ^{207}Pb, and ^{208}Pb. Although areas selected for analysis were carefully chosen to avoid inclusions, time-resolved depth profiles for each ablation spot were examined for evidence of sub-surface inclusions or other artefacts that could bias results and interpretation. Where obvious inclusions were noted, the integrated interval was modified to avoid them. Data indicative of abundant inclusions or obvious mineral mixtures were rejected.

For element imaging, the laser was rastered across the sample forming a rectangular grid across the area of interest with a beam size of 10 μm. Rasters were then compiled and processed into trace element intensity maps using 'Iolite' software (Paton et al., 2011). Mapped intensities are scaled independently for each element to enhance different features; unless stated otherwise, the scale used is logarithmic (10^n). Similar values between ^{105}Pd and ^{106}Pd were checked to avoid any interference from inclusions of chalcopyrite for ^{105}Pd and sphalerite for ^{106}Pd. ^{57}Fe was selected as the internal standard, assuming ideal stoichiometry for the sulfides.

References

Belousov, I., Danyushevsky, L., Goemann, K., Gilbert, S., Olin, P., Thompson, J., Lounejeva, E., and Garbe-Schönberg, D. (2023) STDGL3, a reference material for analysis of sulfide minerals by Laser Ablation ICP-MS: An assessment of matrix effects and the impact of laser wavelengths and pulse widths. Geostandards and Geoanalytical Research 47, 493-508. https://doi.org/10.1111/ggr.12512

Donovan, J.J., and Tingle, T.N. (1996) An Improved Mean Atomic Number Background Correction for Quantitative Microanalysis. Microscopy and Microanalysis 2(1), pp. 1-7. https://doi.org/10.1017/S1431927696210013

Donovan, J.J., Singer, J.W., and Armstrong, J.T. (2016) A new EPMA method for fast trace element analysis in simple matrices. American Mineralogist 101(8), 1839-1853. https://doi.org/10.2138/am-2016-5628

Gilbert, S., Danyushevsky, L., Robinson, P., Wohlgemuth-Ueberwasser, C., Pearson, N., Savard, D., Norman, M.; and Hanley, J. (2013) A comparative study of five reference materials and the Lombard meteorite for the determination of the platinum-group elements and gold by LA-ICP-MS. Geostandards and Geoanalytical Research 37, 51-64. https://doi.org/10.1111/j.1751-908X.2012.00170.x

Paton C., Hellstrom J., Paul B., Woodhead J., and Hergt J. (2011) Iolite: freeware for the visualisation and processing of mass spectrometric data. Journal of Analytical Atomic Spectrometry 26, 2508-2518. https://doi.org/10.1039/c1ja10172b

Table a. EPMA setup for analysis

Element and Line	Diffracting Crystal (Sp#)	Background type/fit	kV/nA/spot size(µm)	Peak Count Time	Bkgd Count Times		# bkgd points acquired (Lo/Hi)	Standards*		Overlapping element and order	Typical minimum limits of detection (ppm)	
					Lo	Hi		Primary Standard	Interference Standards		Tellurides#	Sulphosalts +
Te La	LPET (1)	MAN	20/20/0	15				560			0.028	0.033
Sb La	LPET (1)	MAN	20/20/0	15				553	553	Te La (I)	0.028	0.033
Cd La	LPET (1)	MAN	20/20/0	15				561	582,732	Pb M(I), Ag Lb (I)	-	0.057
Ag La	LPET (1)	MAN	20/20/0	15				560			0.043	0.052
As La	TAP (2)	MAN	20/20/0	15				562	560,568	Te La (III), Bi Mb (II)	0.046	0.044
Se La	TAP (2)	MAN	20/20/0	15				568	560,568	Te Lb (III), Bi Mg (II)	0.042	0.040
Cu Ka	LLIF (3)	MAN	20/20/0	15				556			0.026	0.027
Zn Ka	LLIF (3)	MAN	20/20/0	15				564			0.030	0.031
S Ka	LPET (4)	MAN	20/20/0	15				556	582	Pb Ma (I)	0.010	0.011
Bi Ma	LPET (4)	MAN	20/20/0	15				568	582	Pb Mb (I)	0.056	0.034
Pb Ma	LPET (4)	MAN	20/20/0	15				566	530	S Ka (I)	0.059	0.063
Pd La	LPET (4)	MAN	20/20/0	60				610	564, 732	Zn Ka (III), Ag Ln (I)	0.022	0.024
Fe Ka	LLIF (5)	MAN	20/20/0	15				556			0.018	0.021
Ni Ka	LLIF (5)	MAN	20/20/0	15				536	582	Pb Lg (II)	0.021	0.039
Co Ka	LLIF (5)	MAN	20/20/0	15				602			0.020	0.062
Mn Ka	LLIF (5)	MAN	20/20/0	15				557	562	As Kb (II)	-	0.039

* Standard # refers to internal database. Full list of standards in Table b

used for microanalysis of hauchecornite, ognitite, parkerite, Bi-chalcogenides

+ used for microanalysis of lillianite homologues

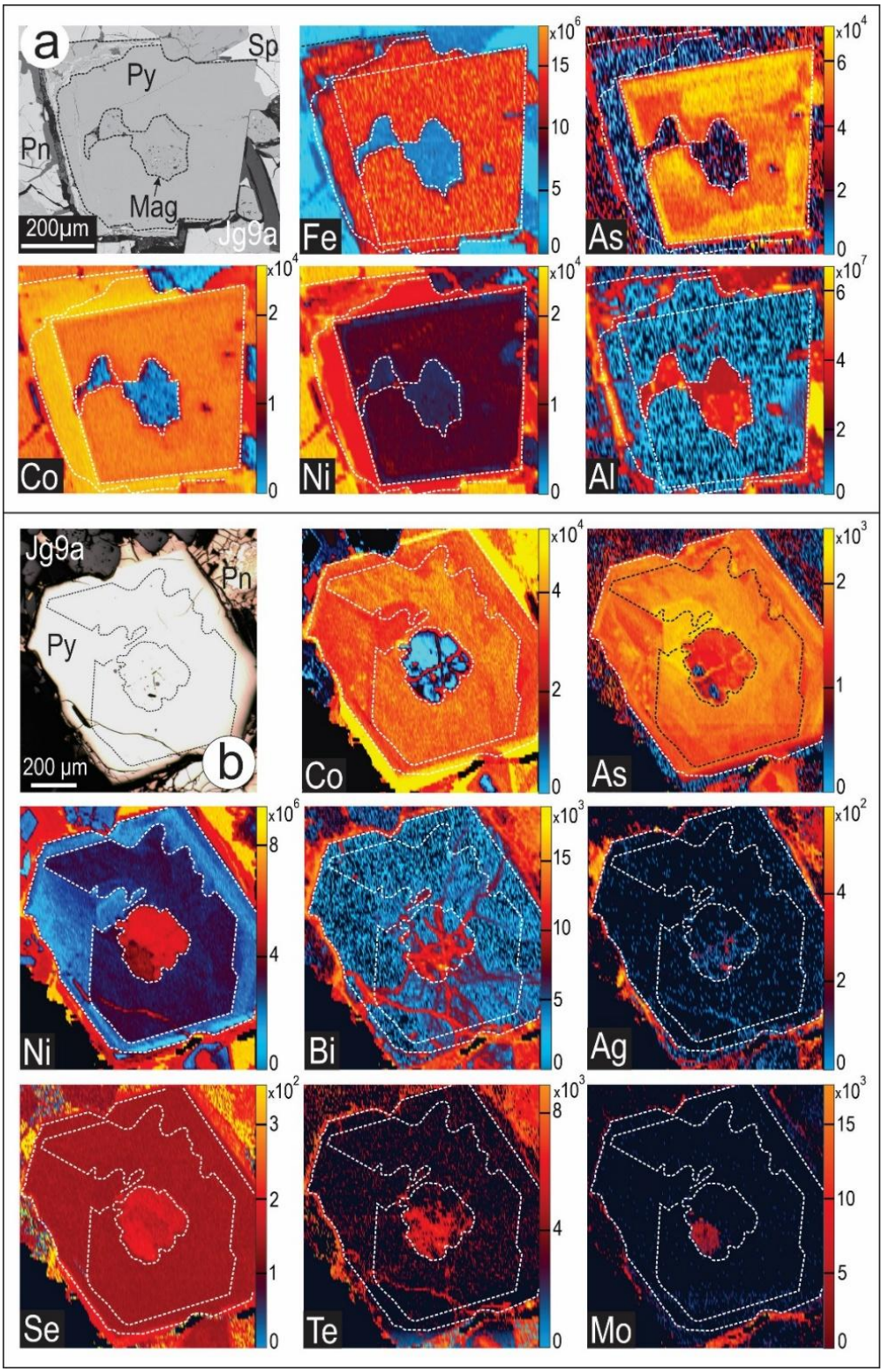

Figure S1. Image and LA-ICP-MS maps of (sub)euhedral pyrite. **(a)** Antithetic zonation patterns are observed between As (rich in the inner part) and Co and Ni (richer on the grain margins). Subtle variation in As concentration seems to relate to the magnetite inclusion and are restricted to the inner part of the grain. **(b)** Pyrite with small core enriched in Ni, Bi, Se, and Te, and partially also in Mo and Ag, elements that are readily attributable to sub-µm-scale inclusions. The same core is depleted in Co and As. Brecciation of this pyrite is indicated by the Bi map, showing a marked enrichment along brittle, sub-µm-scale fractures from the core to the lower part of the grain.

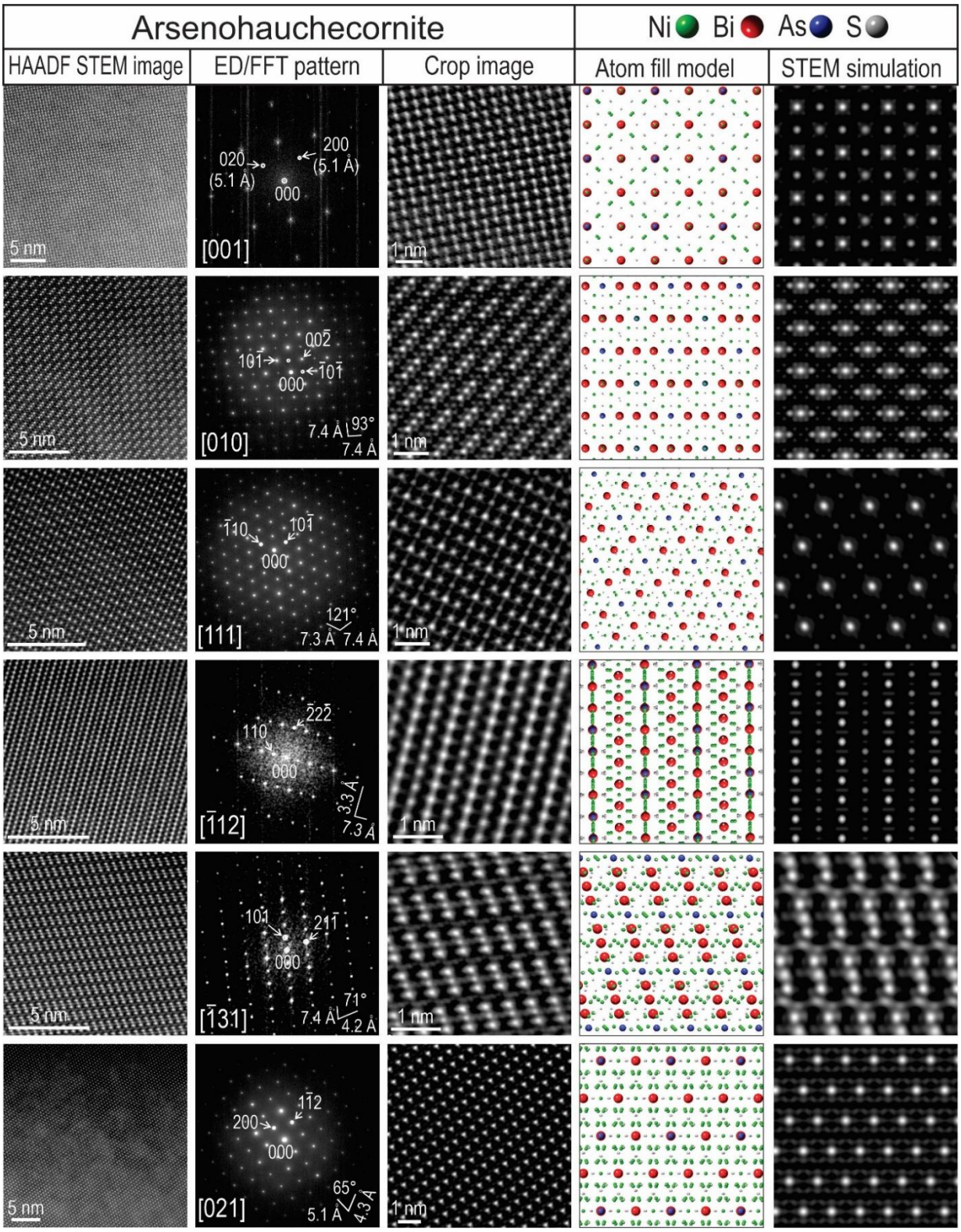

Figure S2. Characterization of zone axes (as labelled) for arsenohauchecornite, complementing the set shown in Figures 6d-f and 9k. ED=electron diffraction; FFT=fast Fourier transform pattern.

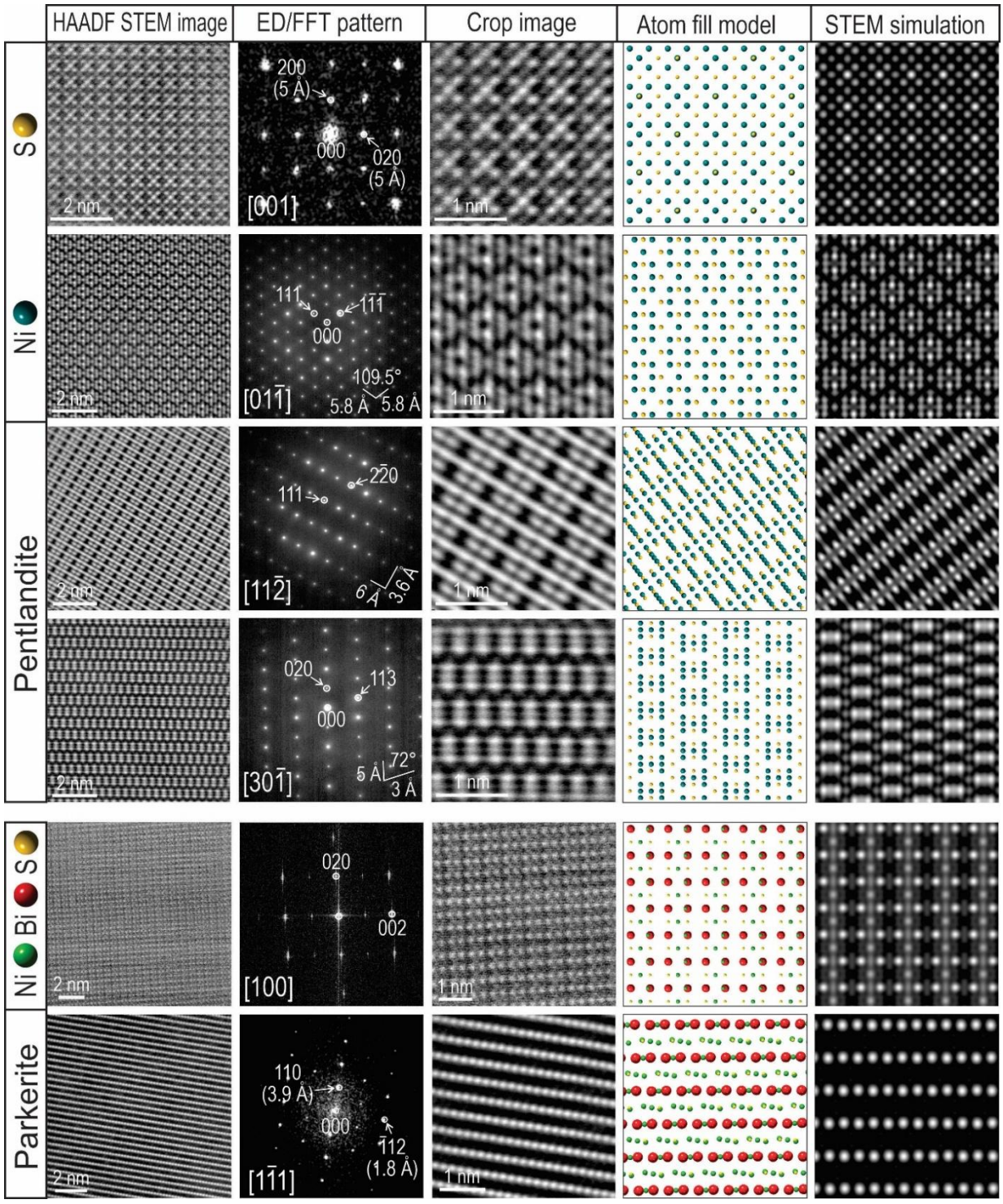

Figure S3. Characterization of zone axes (as labelled) for pentlandite and parkerite complementing the set shown in Figures 6g-i and 9l. ED=electron diffraction; FFT=fast Fourier transform pattern.

APPENDIX B FOR CHAPTER 7

ESM Table 1a. LA-ICP-MS trace element data for sulfide minerals.

ESM Table 1b. LA-ICP-MS data for sulphides used for box-and-whisker plots.

ESM Table 1a. LA-ICP-MS trace element data for sulfide minerals (complete dataset, element concentrations in ppm, calculated from measurement of given isotope, except for the 4 Pb isotopes)

*Note: D*ata reported here are raw data; typical minimum detection limits are given in the main text. In red analyses shown in ESM Fig 4. 105Pd and 106Pd refer to calculated total Pd concentration calculated based on measurement of 105Pd and 106Pd isotope signals, respectively. Mean concentration reported as *Pd. *In refers to the calculated mean for concentration of 113In and 115In. Measurements of Mo, W and U are consistently below minimum limits of detection.

#	Pyrite	^{34}S	^{57}Fe	^{65}Cu	^{49}Ti	^{55}Mn	^{59}Co	^{60}Ni	^{66}Zn	^{75}As	^{77}Se	^{88}Sr	^{90}Zr	^{95}Mo	^{105}Pd	^{106}Pd	^{107}Ag	^{111}Cd	^{113}In
1	Jg 9a - Py 1 - 01	573055	416778	0.174	2.0	0.070	7755	2180	0.695	222	8.4	0.006	0.000	0.031	0.000	0.000	0.001	0.004	0.006
2	Jg 9a - Py 1 - 02	556248	433094	0.189	2.2	0.066	8166	2271	0.590	210	7.8	0.002	0.002	0.020	0.000	0.001	0.002	0.004	0.005
3	Jg 9a - Py 1 - 03	563672	425432	0.458	2.5	0.063	8482	2106	0.652	293	7.7	0.005	0.004	0.026	0.002	0.005	0.006	0.004	0.005
4	Jg 9a - Py 1 - 04	559144	430869	0.212	3.1	0.056	7341	1915	0.694	720	6.5	0.006	0.000	0.026	0.002	0.000	0.006	0.005	0.005
5	Jg 9a - Py 1 - 05	550023	441653	0.801	2.4	0.056	6166	1516	1.4	629	4.9	0.056	0.006	0.024	0.002	0.000	0.007	0.013	0.004
6	Jg 9a - Py 1 - 06	553722	437332	0.321	2.0	0.055	6583	1776	0.858	577	6.2	0.004	0.000	0.025	0.001	0.000	0.002	0.015	0.004
7	Jg 9a - Py 1 - 07	563574	425199	0.405	2.4	0.061	8752	2154	0.700	309	7.4	0.003	0.002	0.026	0.002	0.000	0.002	0.015	0.004
8	Jg 9a - Py 1 - 08	564346	424953	0.350	2.2	0.056	8244	2141	0.913	303	8.7	0.001	0.000	0.025	0.000	0.000	0.002	0.015	0.004
9	Jg 9a - Py 2 - 01	564990	425271	0.321	2.0	0.051	7375	2051	0.821	299	7.9	0.004	0.000	0.020	0.000	0.000	0.003	0.023	0.005
10	Jg 9a - Py 2 - 02	562825	428082	0.297	2.8	0.046	6470	2059	0.779	552	7.2	0.004	0.000	0.023	0.001	0.000	0.001	0.023	0.005
11	Jg 9a - Py 2 - 03	559973	430642	1.3	2.6	0.697	7425	1471	21	436	8.2	0.454	0.000	1.2	0.000	0.006	0.029	0.133	0.005
12	Jg 9a - Py 2 - 04	557777	430236	3.4	2.7	0.523	8838	2050	656	408	14	0.217	0.000	0.666	0.006	0.000	0.046	3.3	0.003
13	Jg 9a - Py 2 - 05	571220	421165	0.944	3.0	0.468	5694	1376	29	497	4.9	0.071	0.000	0.022	0.007	0.003	0.022	0.153	0.003
14	Jg 9a - Py 2 - 06	559894	430368	0.472	2.8	0.068	7502	1922	0.758	303	7.1	0.003	0.000	0.019	0.000	0.001	0.001	0.006	0.003
15	Jg 9a - Py 2 - 07	561878	428996	0.405	2.1	0.065	6912	1991	0.847	197	8.6	0.080	0.000	0.025	0.000	0.001	0.024	0.005	0.003
16	Jg 9a - Py 3 - 01	541683	448711	0.301	2.6	0.061	7319	2027	0.999	246	11	0.004	0.002	0.030	0.000	0.000	0.000	0.005	0.003
17	Jg 9a - Py 3 - 02	561955	427015	0.307	2.0	0.048	8349	2355	0.997	312	9.9	0.001	0.002	0.030	0.000	0.000	0.000	0.005	0.003
18	Jg 9a - Py 3 - 03	552213	437180	0.340	2.9	0.042	8123	2122	0.870	349	8.6	0.005	0.000	0.029	0.000	0.000	0.000	0.005	0.010
19	Jg 9a - Py 3 - 04	564755	425195	0.277	2.3	0.048	7579	2050	0.911	404	10	0.003	0.000	0.025	0.000	0.000	0.004	0.005	0.005
20	Jg 9a - Py 3 - 05	553008	437249	0.267	2.3	0.053	7272	2085	0.925	372	9.4	0.006	0.000	0.023	0.000	0.000	0.001	0.005	0.005
21	Jg 9a - Py 3 - 06	564451	425353	0.260	1.9	0.059	7857	1942	0.844	385	7.3	0.001	0.000	0.023	0.002	0.002	0.003	0.005	0.005
22	Jg 9a - Py 3 - 07	568009	422165	0.228	2.5	0.060	7275	2037	0.935	502	7.5	0.003	0.000	0.021	0.001	0.000	0.001	0.005	0.005
23	Jg 9a - Py 3 - 08	564785	425157	0.337	1.9	0.056	7604	1965	0.843	478	7.5	0.001	0.000	0.024	0.000	0.003	0.003	0.005	0.005
24	Jg 9a - Py 3 - 09	549546	440199	0.636	2.0	0.054	7863	2010	0.897	355	6.7	0.015	0.000	0.023	0.000	0.000	0.039	0.005	0.005
25	Jg 9a - Py 3 - 10	563640	425532	0.435	2.8	0.063	8271	2203	1.1	341	8.0	0.006	0.002	0.025	0.000	0.003	0.009	0.007	0.004
26	Jg 9a - Py 3 - 11	568758	423817	0.225	2.2	0.062	5761	1408	0.648	244	8.4	0.009	0.000	0.027	0.006	0.002	0.001	0.011	0.009
27	Jg 9a - Py 3 - 12	566576	427019	0.154	2.0	0.053	5334	926	0.843	134	8.0	0.004	0.002	0.024	0.002	0.000	0.001	0.006	0.015
28	Jg 9a - Py 3 - 13	559784	432644	0.186	2.8	0.589	6480	902	4.3	174	7.5	0.297	0.000	0.020	0.001	0.000	0.002	0.050	0.004
29	Jg 9a - Py 3 - 14	573245	417229	0.135	2.2	0.055	8055	1131	0.951	322	13	0.005	0.002	0.016	0.000	0.000	0.001	0.020	0.004
30	Jg 9a - Py 4 - 01	551562	438738	0.266	2.6	0.121	7495	1925	4.9	262	9.7	0.016	0.007	0.019	0.000	0.000	0.018	0.014	0.004
31	Jg 9a - Py 4 - 02	561778	428156	0.442	2.9	0.156	7637	2151	7.6	251	9.2	0.035	0.002	0.029	0.000	0.003	0.007	0.034	0.004
32	Jg 9a - Py 4 - 03	551913	432479	11	2.7	7.6	1106	12240	1965	161	38	2.4	0.007	0.026	0.006	0.008	0.199	8.3	0.002
33	Jg 9a - Py 4 - 04	563356	427347	5.5	3.2	10	158	7788	1160	49	51	2.2	0.049	0.808	0.012	0.000	0.188	5.5	0.453
34	Jg 9a - Py 4 - 05	570727	410232	7.8	3.0	3.0	214	14531	4097	106	36	0.557	0.047	0.028	0.008	0.023	0.183	15	1.4
35	Jg 9a - Py 4 - 06	560390	425932	4.5	3.3	2.7	318	12894	195	137	36	0.537	0.009	0.022	0.004	0.001	0.142	1.1	0.002
36	Jg 9a - Py 4 - 07	563192	426610	10	3.1	0.456	2160	7643	44	242	21	0.297	0.193	0.019	0.000	0.008	0.112	0.204	0.029
37	Jg 9a - Py 4 - 08	575579	410898	54	23	8.7	6088	5594	281	221	18	2.4	1.1	0.028	0.063	0.040	3.1	0.866	0.076
38	Jg 9a - Py 4 - 09	553155	435553	461	3.1	0.124	8126	2363	8.6	275	10	0.152	0.009	0.021	0.014	0.013	0.732	0.010	0.017
39	Jg 9a - Py 4 - 10	564788	425397	0.249	2.1	0.080	7467	2019	3.0	314	10.0	0.007	0.019	0.019	0.000	0.000	0.002	0.010	0.002
40	Jg 9a - Py 5 edge - 01	565408	425942	0.266	2.4	0.053	6537	1931	1.1	163	8.7	0.003	0.000	0.028	0.001	0.002	0.009	0.007	0.002
41	Jg 9a - Py 5 edge - 02	562312	429465	0.415	2.6	0.053	6124	1880	1.1	202	9.0	0.003	0.004	0.031	0.002	0.002	0.004	0.007	0.002
42	Jg 9a - Py 5 edge - 03	557238	432904	0.333	2.5	0.053	7373	2147	0.905	325	9.6	0.004	0.000	0.031	0.001	0.000	0.001	0.005	0.002
43	Jg 9a - Py 5 edge - 04	562150	427195	0.219	2.5	0.052	8096	2193	0.806	355	8.7	0.006	0.000	0.026	0.000	0.000	0.001	0.012	0.002
44	Jg 9a - Py 5 cent - 01	559070	430047	0.334	2.3	0.062	8374	2135	0.920	361	7.2	0.006	0.002	0.025	0.001	0.000	0.008	0.039	0.002
45	Jg 9a - Py 5 cent - 02	560873	426858	0.464	2.8	1.1	494	11466	68	175	38	1.3	0.002	0.028	0.006	0.002	0.021	0.333	0.002
46	Jg 9a - Py 5 cent - 03	562351	425740	1.9	2.4	1.2	101	11560	16	175	44	0.436	0.002	0.020	0.002	0.003	0.005	0.071	0.034
47	Jg 9a - Py 5 cent - 04	558451	429927	0.196	2.7	0.054	41	11329	0.924	207	39	0.002	0.000	0.025	0.000	0.003	0.003	0.005	0.002
48	Jg 9a - Py 5 cent - 05	567075	418021	0.176	2.5	0.106	86	14665	2.3	95	36	0.046	0.000	0.021	0.002	0.002	0.024	0.006	0.002
49	Jg 9a - Py 5 edge - 05	561523	423647	0.236	1.9	0.047	54	14645	0.716	80	39	0.006	0.000	0.020	0.000	0.001	0.001	0.006	0.002
50	Jg 9a - Py 5 edge - 06	549255	424424	51	2.2	3.4	231	12431	13326	138	36	0.510	0.000	0.023	0.007	0.103	0.431	31	0.461
51	Jg 9a - Py 5 edge - 07	545354	407824	275	2.5	4.5	278	12750	33128	146	41	0.189	0.000	0.024	0.021	0.171	1.2	83	3.3
52	Jg 9a - Py 5 edge - 08	556189	433657	1.4	2.5	0.108	7536	2191	11	393	7.3	1.1	0.004	0.025	0.000	0.000	0.063	0.082	0.002
53	Jg 9a - Py 5 edge - 09	554173	434906	1.7	4.6	0.370	8328	2298	29	238	7.2	0.298	0.216	0.022	0.000	0.000	0.081	0.120	0.002
54	Jg 9a - Py 5 edge - 10	547991	442818	0.352	1.9	0.048	7000	1992	1.0	188	7.0	0.005	0.002	0.026	0.000	0.001	0.001	0.003	0.002
55	Jg 9a - Py 6 edge - 01	571341	418438	0.358	2.6	0.051	7859	2072	0.821	279	6.8	0.005	0.000	0.025	0.001	0.001	0.004	0.007	0.002
56	Jg 9a - Py 6 edge - 02	549358	441009	3.1	2.6	1.3	5653	3540	6.4	371	21	0.667	0.002	0.419	0.001	0.005	0.102	0.050	0.006
57	Jg 9a - Py 6 edge - 03	568022	424430	0.480	2.7	2.4	5878	1195	5.0	433	6.2	0.192	0.000	0.762	0.002	0.003	0.085	0.021	0.006
58	Jg 9a - Py 6 edge - 04	552162	439197	20	2.8	4.0	6873	1192	252	244	13	1.1	0.006	0.037	0.006	0.000	0.094	0.988	0.020

#	Pyrite	^{34}S	^{57}Fe	^{65}Cu	^{49}Ti	^{55}Mn	^{59}Co	^{60}Ni	^{66}Zn	^{75}As	^{77}Se	^{88}Sr	^{90}Zr	^{95}Mo	^{105}Pd	^{106}Pd	^{107}Ag	^{111}Cd	^{113}In
59	Jg 9a - Py 6 cent - 01	563958	426963	73	2.8	2.5	1672	7161	6.8	10	66	0.299	0.000	1.5	0.300	0.241	0.662	0.046	0.006
60	Jg 9a - Py 6 cent - 02	554549	417537	48	3.0	1.3	890	11290	15411	142	46	0.479	0.002	0.027	0.003	0.095	0.128	52	3.1
61	Jg 9a - Py 6 cent - 03	558819	422956	20	2.7	0.571	468	13158	5.7	133	50	0.214	0.002	0.026	0.017	0.007	73	0.620	0.015
62	Jg 9a - Py 6 cent - 04	564562	420264	17	2.3	0.347	126	13346	1475	124	46	0.150	0.000	0.022	0.007	0.036	0.368	3.9	0.007
63	Jg 9a - Py 6 cent - 05	552130	433890	21	2.9	3.0	136	13332	247	135	45	5.5	0.010	0.025	0.005	0.001	0.438	0.783	0.014
64	Jg 9a - Py 6 edge - 05	561516	425978	0.324	2.7	0.061	167	12165	1.3	127	42	0.019	0.002	0.019	0.001	0.000	0.007	0.005	0.005
65	Jg 9a - Py 6 edge - 06	564167	426536	1.0	3.0	0.299	6882	1786	7.5	602	7.1	0.187	0.031	0.022	0.001	0.001	0.022	0.098	0.005
66	Jg 9a - Py 6 edge - 07	552187	438186	0.334	2.6	0.043	7299	1874	0.718	443	6.9	0.001	0.000	0.024	0.023	0.000	0.007	0.003	0.005
67	Jg 9a - Py 7 edge - 01	558296	430879	0.282	2.5	0.123	8285	2375	2.5	151	8.4	0.013	0.016	0.021	0.000	0.000	0.001	0.003	0.005
68	Jg 9a - Py 7 edge - 02	577539	411542	0.497	3.7	0.146	8506	2184	7.8	208	8.6	0.036	0.011	0.026	0.000	0.000	0.003	0.015	0.005
69	Jg 9a - Py 7 edge - 03	571565	418279	0.487	2.8	0.065	7961	1981	2.3	201	7.2	0.015	0.006	0.028	0.001	0.000	0.004	0.014	0.002
70	Jg 9a - Py 7 edge - 04	556012	433685	0.251	3.5	0.047	8134	1939	2.9	215	7.5	0.007	0.004	0.022	0.000	0.000	0.002	0.018	0.002
71	Jg 9a - Py 7 edge - 05	564621	424322	0.189	2.1	0.049	8646	2137	0.858	262	8.2	0.004	0.000	0.021	0.004	0.000	0.002	0.021	0.007
72	Jg 9a - Py 7 edge - 06	578516	412826	0.201	3.0	0.069	6009	2001	2.0	635	6.8	0.003	0.005	0.024	0.000	0.002	0.001	0.007	0.007
73	Jg 9a - Py 7 cent - 01	561730	429208	0.301	3.7	0.889	6658	1625	2.1	764	4.7	0.006	0.002	0.019	0.000	0.000	0.002	0.007	0.007
74	Jg 9a - Py 7 cent - 02	561128	428209	5.3	2.3	1.2	2611	7047	605	338	30	0.337	0.007	0.019	0.008	0.016	0.058	2.0	0.051
75	Jg 9a - Py 7 cent - 03	553909	422858	1212	2.8	6.7	4676	7117	9919	176	39	1.5	0.054	0.027	0.030	0.073	0.494	34	1.1
76	Jg 9a - Py 7 cent - 04	560510	419949	28	2.2	8.5	5116	4911	9115	237	23	2.2	0.009	0.040	0.019	0.007	0.352	30	1.6
77	Jg 9a - Py 7 cent - 05	574434	411628	16	2.9	11	994	12161	483	132	52	4.5	0.000	0.022	0.005	0.000	0.117	2.6	0.002
78	Jg 9a - Py 7 cent - 06	553974	432284	0.594	2.0	0.437	258	12987	339	92	50	0.168	0.042	0.019	0.001	0.004	0.079	0.898	0.002
79	Jg 9a - Py 7 edge - 07	564350	421627	16	3.0	0.902	238	13359	14	108	54	0.375	0.024	0.024	0.007	0.011	2.1	0.162	0.034
80	Jg 9a - Py 7 edge - 08	579554	410929	0.476	3.0	0.131	7247	1974	4.1	279	7.8	0.007	0.009	0.023	0.004	0.000	0.004	0.006	0.002
81	Jg 9a - Py 7 edge - 09	549938	439639	0.341	2.9	0.049	7955	2219	3.6	231	9.8	0.016	0.015	0.022	0.000	0.001	0.002	0.006	0.021
82	Jg 9a - Py 8 - 01	561461	428227	0.544	3.2	0.123	8025	2135	3.7	137	8.3	0.026	0.000	0.027	0.000	0.001	0.001	0.015	0.022
83	Jg 9a - Py 8 - 02	562095	427307	2.7	2.8	0.168	8102	2102	56	276	9.4	0.130	0.005	0.031	0.003	0.001	0.096	0.149	0.022
84	Jg 9a - Py 8 - 03	546416	443532	0.455	2.0	0.055	7785	1997	2.0	258	6.8	0.012	0.017	0.026	0.000	0.001	0.001	0.022	0.028
85	Jg 9a - Py 8 - 04	564211	426005	0.413	3.0	0.098	7296	1936	5.3	536	7.2	0.010	0.009	0.021	0.000	0.001	0.002	0.013	0.029
86	Jg 9a - Py 8 - 05	544732	446306	0.397	2.5	0.073	6323	1924	2.4	702	8.1	0.015	0.011	0.023	0.006	0.001	0.003	0.012	0.015
87	Jg 9a - Py 8 - 06	554362	437032	256	3.3	1.9	1483	6294	32	70	44	0.143	0.024	1.7	0.166	0.081	9.6	0.335	0.087
88	Jg 9a - Py 8 - 07	563837	424957	0.727	3.1	0.208	92	11010	10	56	27	0.074	0.020	0.026	0.002	0.001	0.013	0.035	0.004
89	Jg 9a - Py 8 - 08	559493	429453	0.322	2.9	0.100	8609	2185	3.8	244	7.9	0.013	0.009	0.029	0.000	0.001	0.002	0.012	0.013
90	Jg 9a - Py 8 - 09	557256	431698	0.201	2.7	0.053	8683	2154	2.1	196	7.1	0.006	0.005	0.031	0.000	0.001	0.002	0.012	0.005
91	Jg 9a - Py 9 - 01	566622	422529	0.333	3.4	0.129	8307	2240	22	265	10	0.023	0.086	0.027	0.001	0.001	0.003	0.011	0.027
92	Jg 9a - Py 9 - 02	554185	434954	0.422	4.2	0.107	8287	2269	5.1	287	8.2	0.009	0.024	0.020	0.002	0.000	0.001	0.012	0.029
93	Jg 9a - Py 9 - 03	564685	424008	9.9	3.7	0.150	8586	2210	97	360	8.7	0.368	0.004	0.021	0.004	0.000	0.203	0.156	0.005
94	Jg 9a - Py 9 - 04	565439	424175	0.574	3.3	0.049	8086	1966	1.3	312	7.6	0.002	0.002	0.025	0.001	0.002	0.016	0.019	0.009
95	Jg 9a - Py 9 - 05	558154	430494	245	3.5	3.6	8348	2244	105	341	8.1	9.4	0.109	0.024	0.006	0.001	0.439	0.278	0.031
96	Jg 9a - Py 9 - 06	570297	418737	0.233	3.0	0.060	8442	2183	2.1	327	7.9	0.004	0.009	0.021	0.000	0.000	0.001	0.007	0.013
97	Jg 9a - Py 9 - 07	557769	431633	0.379	2.2	0.045	8054	2204	2.6	316	9.5	0.008	0.000	0.030	0.002	0.000	0.006	0.022	0.012
98	Jg 9a - Py 9 - 08	570676	419958	0.700	2.5	0.051	6995	2118	7.6	219	9.0	0.011	0.013	0.015	0.000	0.001	0.052	0.013	0.014
99	Jg 9a - Py 9 - 09	549341	441169	0.381	3.0	0.048	7332	1806	1.1	338	7.8	0.009	0.012	0.020	0.000	0.002	0.008	0.005	0.014
100	Jg 9a - Py 9 - 10	567904	422218	0.406	2.9	0.047	7576	1884	1.1	406	6.2	0.002	0.006	0.026	0.000	0.004	0.001	0.003	0.014
101	Jg 9a - Py 9 - 11	550364	438588	0.370	2.7	0.047	8403	2269	0.736	363	9.7	0.006	0.033	0.023	0.000	0.000	0.001	0.014	0.007
102	Jg 9a - Py 10 - 01	550186	442178	1.7	2.5	12	198	7244	22	46	52	0.773	0.004	2.2	0.007	0.004	0.059	0.221	0.007
103	Jg 9a - Py 10 - 02	548832	443340	0.853	2.0	10	2766	4735	29	244	14	0.794	0.002	0.027	0.002	0.002	0.029	0.369	0.191
104	Jg 9a - Py 10 - 03	565152	424671	0.353	2.0	0.041	7680	2096	0.776	388	9.8	0.002	0.000	0.030	0.000	0.000	0.001	0.003	0.007
105	Jg 9a - Py 10 - 04	580758	413539	4.2	2.7	1.6	1838	3582	4.7	210	46	0.024	0.000	7.3	0.000	0.001	0.059	0.003	0.010
106	Jg 9a - Py 10 - 05	564823	425069	0.181	2.1	0.062	7680	2174	0.906	240	11	0.007	0.000	0.023	0.000	0.003	0.001	0.003	0.007
107	Jg 9a - Py 10 - 06	567940	421062	0.236	2.2	0.059	8402	2242	0.916	338	12	0.002	0.000	0.018	0.000	0.000	0.001	0.003	0.010
108	Jg 9a - Py 10 - 07	550817	438381	0.205	1.8	0.046	8408	2117	1.0	265	7.9	0.007	0.002	0.021	0.000	0.000	0.001	0.003	0.005
109	Jg 9a - Py 10 - 08	558972	433404	25	2.0	0.185	2586	4661	5.2	314	25	0.017	0.002	0.023	0.001	0.004	0.028	0.015	0.013
110	Jg 9a - Py 10 - 09	565550	424349	0.288	1.9	0.053	7688	2073	1.0	327	9.5	0.005	0.000	0.020	0.000	0.000	0.000	0.003	0.005
111	Jg 9a - Py 10 - 10	558383	431076	0.432	2.3	0.059	7950	2272	0.682	303	10	0.005	0.000	0.020	0.000	0.000	0.002	0.003	0.009
112	Jg 5 - Py 1 - 01	566286	423091	0.192	2.0	0.055	8196	1980	0.874	433	11	0.002	0.000	0.022	0.000	0.000	0.001	0.001	0.004
113	Jg 5 - Py 1 - 02	560636	427889	0.278	2.4	0.046	8436	2018	0.972	1007	11	0.004	0.000	0.020	0.001	0.007	0.007	0.008	0.004
114	Jg 5 - Py 1 - 03	567292	423049	0.220	1.8	0.046	6894	1819	0.943	929	14	0.003	0.002	0.024	0.000	0.000	0.007	0.001	0.004
115	Jg 5 - Py 1 - 04	558587	430856	0.331	2.9	0.313	6230	3335	2.1	969	13	0.003	0.000	0.023	0.005	0.002	0.027	0.051	0.004
116	Jg 5 - Py 1 - 05	575796	409344	0.147	2.7	0.114	469	13813	1.5	548	23	0.075	0.000	0.019	0.004	0.005	0.003	0.001	0.013
117	Jg 5 - Py 1 - 06	580849	405786	0.312	2.2	0.040	652	11612	0.951	1064	32	0.008	0.000	0.021	0.002	0.004	0.009	0.001	0.014
118	Jg 5 - Py 1 - 07	566029	417587	2147	2.3	0.040	11674	1252	0.965	1277	22	0.007	0.000	0.020	0.041	0.000	0.023	0.010	0.022
119	Jg 5 - Py 1 - 08	566941	422564	22	2.0	0.048	8032	1848	0.767	579	12	0.003	0.000	0.024	0.000	0.001	0.002	0.007	0.004
120	Jg 5 - Py 1 - 09	563636	427189	0.443	2.4	0.048	7126	1184	0.734	851	8.0	0.007	0.000	0.022	0.001	0.002	0.010	0.007	0.004
121	Jg 5 - Py 1 - 10	561918	429218	0.450	1.5	0.123	6543	1378	0.974	925	9.6	0.007	0.000	0.049	0.005	0.003	0.011	0.009	0.015
122	Jg 5 - Py 1 - 11	562834	426129	0.351	2.8	0.051	8236	1938	0.658	848	10	0.003	0.000	0.016	0.000	0.000	0.007	0.007	0.009

#	Pyrite	^{34}S	^{57}Fe	^{65}Cu	^{49}Ti	^{55}Mn	^{59}Co	^{60}Ni	^{66}Zn	^{75}As	^{77}Se	^{88}Sr	^{90}Zr	^{95}Mo	^{105}Pd	^{106}Pd	^{107}Ag	^{111}Cd	^{113}In
123	Jg 5 - Py 1 - 12	563732	424846	0.213	2.3	0.043	8702	1933	0.847	772	11	0.006	0.000	0.023	0.001	0.000	0.003	0.007	0.009
124	Jg 5 - Py 2 - 01	570090	418913	0.290	3.0	0.084	8052	1939	0.877	989	11	0.042	0.000	0.029	0.001	0.003	0.005	0.027	0.002
125	Jg 5 - Py 2 - 02	559774	431833	0.155	2.8	0.055	6926	513	0.830	945	5.5	0.008	0.000	0.022	0.000	0.000	0.003	0.007	0.002
126	Jg 5 - Py 2 - 03	562742	427984	0.223	2.1	0.464	7807	471	3.7	975	6.5	0.619	0.002	0.022	0.000	0.001	0.012	0.028	0.008
127	Jg 5 - Py 2 - 04	568603	414630	0.217	2.9	0.067	383	14083	0.853	2251	45	0.004	0.004	0.023	0.001	0.005	0.002	0.010	0.002
128	Jg 5 - Py 2 - 05	562193	420260	0.293	2.0	1.3	1034	15088	3.3	1337	38	0.645	0.000	0.255	0.439	0.711	0.066	0.064	0.002
129	Jg 5 - Py 2 - 06	564259	415862	1.9	2.8	2.0	1435	17058	16	1281	43	2.6	0.000	0.026	0.020	0.016	0.055	0.306	0.002
130	Jg 5 - Py 2 - 07	556599	430420	1.1	2.2	0.113	770	10905	1.0	1263	32	0.020	0.000	0.024	0.001	0.001	0.012	0.040	0.002
131	Jg 5 - Py 3 - 01	574262	415450	0.335	3.0	0.055	7505	1803	0.749	965	11	0.004	0.000	0.027	0.000	0.000	0.009	0.006	0.005
132	Jg 5 - Py 3 - 02	569286	417402	2.8	2.4	0.266	3140	9009	3.3	1120	22	0.098	0.000	0.029	0.004	0.012	0.020	0.068	0.005
133	Jg 5 - Py 3 - 03	572072	403209	20	2.2	0.085	1300	21131	1.1	2200	54	0.042	0.000	0.026	0.046	0.044	0.001	0.015	0.005
134	Jg 5 - Py 3 - 04	553594	421467	47	2.6	3.5	3063	20337	34	1368	28	0.313	0.002	0.079	0.090	0.107	0.089	0.325	0.007
135	Jg 5 - Py 3 - 05	551825	426030	39	6.1	20	1967	18751	105	887	27	1.5	0.002	0.265	0.564	0.602	0.366	0.812	0.093
136	Jg 5 - Py 3 - 06	550824	430672	82	2.6	52	2162	13730	155	1465	37	12	0.000	0.110	0.225	0.252	0.282	1.8	0.007
137	Jg 5 - Py 3 - 07	558529	421896	82	2.1	17	1458	16234	75	1489	42	3.4	0.000	0.029	0.086	0.087	0.105	0.919	0.010
138	Jg 5 - Py 3 - 08	574530	412263	1.4	2.0	0.578	6035	5371	3.2	1739	26	0.165	0.004	0.030	0.006	0.007	0.203	0.008	0.010
139	Jg 5 - Py 4 - 01	575300	416046	0.299	2.7	0.052	7064	746	0.810	834	5.7	0.020	0.002	0.023	0.001	0.000	0.018	0.019	0.002
140	Jg 5 - Py 4 - 02	571109	420271	0.396	3.7	0.120	7038	774	0.924	796	6.5	0.026	0.002	0.026	0.003	0.000	0.011	0.018	0.014
141	Jg 5 - Py 4 - 03	561120	431208	0.305	2.1	0.052	6124	720	0.950	819	5.9	0.001	0.000	0.024	0.000	0.000	0.007	0.022	0.002
142	Jg 5 - Py 4 - 04	571669	420974	0.281	2.4	3.8	5670	757	22	883	7.2	2.4	0.002	0.022	0.004	0.008	0.021	0.167	0.076
143	Jg 5 - Py 4 - 05	569987	420587	3.0	2.7	0.097	7592	701	0.805	1070	6.2	0.013	0.018	0.024	0.025	0.010	0.442	0.005	0.007
144	Jg 5 - Py 4 - 06	565502	421549	50	3.4	1.7	9088	2600	18	863	24	0.135	0.006	0.023	0.046	0.049	0.686	0.005	0.024
145	Jg 5 - Py 4 - 07	564686	424992	3.0	2.7	0.591	7286	1943	2.4	987	8.5	0.194	0.000	0.245	0.020	0.011	0.197	0.014	0.002
146	Jg 5 - Py 4 - 08	560892	426947	1.3	4.3	4.6	8108	3038	15	948	11	0.202	0.002	0.025	0.007	0.003	0.082	0.024	0.002
147	Jg 3 - Py 1 - 01	569794	421941	0.322	2.2	0.055	5950	2012	0.823	292	7.8	0.010	4.1	0.024	0.002	0.001	0.002	0.003	0.010
148	Jg 3 - Py 1 - 02	572361	420042	0.391	2.3	0.053	5360	1924	0.846	301	8.3	0.005	7.2	0.028	0.004	0.000	0.002	0.008	0.005
149	Jg 3 - Py 1 - 03	561759	430719	0.699	3.6	0.443	5368	1823	1.2	318	7.7	0.020	0.029	0.022	0.000	0.000	0.006	0.008	0.005
150	Jg 3 - Py 1 - 04	562051	429765	0.492	2.3	0.058	5932	1973	0.972	268	8.0	0.005	0.002	0.019	0.000	0.003	0.007	0.008	0.005
151	Jg 3 - Py 1 - 05	565901	425986	0.414	3.1	1.3	5889	1944	1.3	253	9.2	0.478	30	0.026	0.001	0.005	0.016	0.028	0.008
152	Jg 3 - Py 1 - 06	576556	414962	0.335	2.3	0.049	6186	2026	0.713	258	8.4	0.004	9.7	0.023	0.000	0.002	0.011	0.014	0.015
153	Jg 3 - Py 1 - 07	570495	421151	0.709	4.5	1.4	5951	2047	4.3	333	7.8	0.011	0.002	0.015	0.000	0.000	0.031	0.017	0.015
154	Jg 3 - Py 2 - 01	569945	420812	0.960	2.1	0.056	6693	2129	1.2	406	8.8	0.011	0.017	0.021	0.000	0.001	0.014	0.009	0.005
155	Jg 3 - Py 2 - 02	580116	410263	6.6	3.0	8.6	6982	2146	3.2	435	8.7	0.014	0.015	0.025	0.000	0.001	0.050	0.033	0.005
156	Jg 3 - Py 2 - 03	565139	425527	0.489	2.7	0.055	6795	2123	0.885	403	9.5	0.012	0.002	0.021	0.000	0.001	0.004	0.002	0.005
157	Jg 3 - Py 2 - 04	562255	428873	0.597	2.1	0.054	6444	2027	0.750	388	8.4	0.010	0.004	0.023	0.002	0.001	0.004	0.002	0.019
158	Jg 3 - Py 2 - 05	579631	410938	0.314	2.1	0.048	6852	2148	0.888	420	8.1	0.011	0.004	0.026	0.000	0.000	0.002	0.002	0.012
159	Jg 3 - Py 2 - 06	567798	425025	0.929	2.6	0.313	5334	1184	0.997	643	7.2	0.013	0.000	0.014	0.000	0.003	0.015	0.002	0.006
160	Jg 3 - Py 3 - 01	541546	448486	138	2.7	0.048	7045	2198	0.856	574	7.7	0.009	0.012	0.015	0.002	0.000	0.739	0.006	0.005
161	Jg 3 - Py 3 - 02	565612	424619	61	2.7	0.601	7027	2052	1.7	591	8.9	0.071	0.019	0.015	0.002	0.001	0.047	0.002	0.006
162	Jg 3 - Py 3 - 03	568306	421365	2.2	2.8	0.261	7457	2216	3.7	635	7.4	0.022	0.013	0.022	0.000	0.001	0.018	0.002	0.006
163	Jg 3 - Py 3 - 04	553854	435558	0.787	2.6	0.057	7663	2279	0.741	628	8.8	0.009	0.004	0.023	0.000	0.000	0.005	0.007	0.004
164	Jg 3 - Py 3 - 05	555208	434481	0.335	1.8	0.043	7550	2153	0.878	597	8.0	0.016	0.004	0.023	0.000	0.001	0.002	0.001	0.004
165	Jg 3 - Py 3 - 06	585348	404492	0.414	3.3	0.046	7305	2180	0.872	661	9.5	0.007	0.006	0.017	0.000	0.000	0.009	0.001	0.004
166	Jg 3 - Py 4 - 01	567786	424722	0.799	2.7	0.048	6029	964	1.0	490	5.6	0.014	0.007	0.022	0.000	0.000	0.005	0.008	0.004
167	Jg 3 - Py 4 - 02	554761	434020	4500	3.4	0.044	5329	916	15	447	5.2	0.008	0.000	0.029	0.076	0.003	3.3	0.124	0.005
168	Jg 3 - Py 4 - 03	557377	432901	27	2.5	0.066	7052	2214	3.1	414	8.6	0.016	0.004	0.018	0.002	0.001	0.071	0.007	0.005
169	Jg 3 - Py 4 - 04	563461	427077	0.427	3.1	0.079	6934	2120	1.1	394	9.0	0.006	0.002	0.016	0.000	0.001	0.011	0.007	0.005
170	Jg 3 - Py 4 - 05	571654	418910	152	3.1	0.079	6746	2140	3.2	381	11	0.017	0.011	0.025	0.009	0.001	0.329	0.034	0.021
171	Jg 3 - Py 4 - 06	568009	420545	187	4.3	5.3	7506	3158	7.2	565	11	0.062	0.016	0.028	0.005	0.004	0.066	0.062	0.007
	Mean (n=171)	562461	426165	62	2.8	1.5	5842	4370	550	470	16	0.405	0.314	0.125	0.015	0.018	0.603	1.7	0.077
	SD	60858	46476	390	1.7	4.8	2925	4685	3115	383	14	1.4	2.5	0.613	0.063	0.077	5.6	8.5	0.387
	Median	562825	425932	0.442	2.6	0.073	7000	2137	1.7	338	9.0	0.013	0.002	0.024	0.001	0.001	0.008	0.012	0.005
	Max	585348	448711	4500	23	52	11674	21131	33128	2251	66	12	30	7.3	0.564	0.711	73	83	3.3
	Min	541546	403209	0.135	1.5	0.040	41	471	0.590	10	4.7	0.001	0.000	0.014	0.000	0.000	0.000	0.001	0.002

#	Sphalerite	^{34}S	^{57}Fe	^{65}Cu	^{49}Ti	^{55}Mn	^{59}Co	^{60}Ni	^{66}Zn	^{75}As	^{77}Se	^{88}Sr	^{90}Zr	^{95}Mo	^{105}Pd	^{106}Pd	^{107}Ag	^{111}Cd	^{113}In
1	Jg 9a - Sp 1 - 01	294232	26455	9997	3.0	18	247	7.7	666765	0.280	17	0.020	0.072	0.020	0.162	2.6	2.5	2240	70
2	Jg 9a - Sp 1 - 02	290622	24765	1801	2.2	53	394	16	680052	0.395	17	0.022	0.005	0.024	0.055	2.5	1.5	2273	72
3	Jg 9a - Sp 1 - 03	292245	31452	9322	1.0	68	394	29	664270	0.252	16	0.020	0.065	0.027	0.166	2.9	2.4	2198	64
4	Jg 9a - Sp 1 - 04	287765	26699	840	1.9	82	413	13	681929	0.247	14	0.018	0.042	0.027	0.012	2.1	1.3	2238	71
5	Jg 9a - Sp 1 - 05	290743	29873	3541	1.1	115	484	35	673026	0.220	15	0.042	0.063	0.023	0.059	3.4	2.2	2163	83
6	Jg 9a - Sp 1 - 06	289833	31642	850	1.4	133	492	17	674852	0.212	13	0.017	0.005	0.028	0.021	3.3	1.4	2161	68
7	Jg 9a - Sp 1 - 07	285671	31242	6101	1.2	107	470	26	674180	0.253	13	0.006	0.000	0.024	0.088	3.5	2.5	2183	99

#	Sphalerite	^{34}S	^{57}Fe	^{65}Cu	^{49}Ti	^{55}Mn	^{59}Co	^{60}Ni	^{66}Zn	^{75}As	^{77}Se	^{88}Sr	^{90}Zr	^{95}Mo	^{105}Pd	^{106}Pd	^{107}Ag	^{111}Cd	^{113}In
8	Jg 9a - Sp 1 - 08	289105	28168	1988	2.0	106	484	12	677938	0.261	11	0.020	0.338	0.022	0.032	3.3	1.6	2183	72
9	Jg 9a - Sp 1 - 09	288849	27541	32	2.7	108	484	17	680688	0.297	16	0.033	0.023	0.029	0.001	2.7	1.3	2259	67
10	Jg 9a - Sp 1 - 10	286066	27050	700	2.5	110	482	9.5	683342	0.240	16	0.010	0.065	0.030	0.019	3.2	1.4	2218	67
11	Jg 9a - Sp 1 - 11	286742	28045	30	1.5	115	483	14	682326	0.280	17	0.034	0.023	0.025	0.001	2.9	1.3	2223	79
12	Jg 9a - Sp 1 - 12	285431	27073	5109	1.8	61	400	39	679665	0.290	18	0.039	0.015	0.018	0.086	3.5	2.1	2195	53
13	Jg 9a - Sp 2 - 01	289208	22987	3979	1.0	22	277	16	681172	0.224	17	0.004	0.002	0.021	0.077	2.5	1.5	2313	60
14	Jg 9a - Sp 2 - 02	287297	21179	1694	1.4	14	264	7.3	687301	0.184	17	0.003	0.002	0.023	0.026	3.1	1.4	2216	72
15	Jg 9a - Sp 2 - 03	289107	24868	6871	1.5	27	269	27	676612	0.194	18	0.010	0.004	0.016	0.125	3.1	2.0	2193	66
16	Jg 9a - Sp 2 - 04	292537	35063	24371	1.2	8.5	141	7.4	645693	0.212	18	0.005	0.000	0.018	0.406	2.4	4.7	2125	81
17	Jg 9a - Sp 2 - 05	287998	23172	4195	1.1	23	272	9.0	682076	0.212	16	0.003	0.000	0.017	0.064	2.6	1.6	2228	81
18	Jg 9a - Sp 2 - 06	290828	26799	10752	1.4	27	288	24	669035	0.239	15	0.011	0.009	0.018	0.205	2.9	1.7	2214	68
19	Jg 9a - Sp 2 - 07	286019	20755	1803	1.3	14	270	8.4	688881	0.249	17	0.005	0.000	0.018	0.037	3.2	1.8	2223	62
20	Jg 9a - Sp 2 - 08	286410	22594	4213	1.6	16	259	21	684262	0.209	17	0.025	0.014	0.016	0.092	3.1	2.0	2202	67
21	Jg 9a - Sp 2 - 09	287164	24554	5155	1.4	61	392	32	680393	0.174	18	0.004	0.018	0.017	0.095	2.7	2.4	2217	74
22	Jg 9a - Sp 3 - 01	289433	24785	1703	3.3	70	342	20	681474	0.204	17	0.107	0.126	0.022	0.040	3.4	1.6	2147	94
23	Jg 9a - Sp 3 - 02	284279	31446	26	1.2	141	475	15	681406	0.232	13	0.022	0.023	0.027	0.002	3.6	1.2	2194	92
24	Jg 9a - Sp 3 - 03	287779	32462	21	2.2	148	482	15	676935	0.376	12	0.029	0.038	0.020	0.004	3.2	1.3	2140	66
25	Jg 9a - Sp 3 - 04	287019	36552	6115	1.5	140	471	34	667598	0.207	11	0.015	0.003	0.019	0.086	4.2	1.9	2052	80
26	Jg 9a - Sp 3 - 05	286496	32032	582	1.6	135	479	20	678059	0.223	10	0.019	0.018	0.025	0.001	3.2	1.5	2180	87
27	Jg 9a - Sp 3 - 06	284558	28150	286	1.8	112	458	17	684191	0.249	11	0.023	0.257	0.019	0.002	2.5	1.5	2208	76
28	Jg 9a - Sp 3 - 07	289970	24309	4645	1.9	77	387	7.4	678340	0.280	11	0.037	0.015	0.020	0.091	3.0	1.8	2243	60
29	Jg 9a - Sp 3 - 08	288531	31049	4262	1.5	127	471	45	673387	0.227	10	0.029	0.030	0.016	0.082	3.3	1.7	2108	66
30	Jg 9a - Sp 3 - 09	285989	28299	65	1.9	132	470	127	682776	0.210	11	0.015	0.015	0.023	0.002	3.1	1.4	2124	67
31	Jg 9a - Sp 3 - 10	286491	27275	147	3.3	127	467	18	683308	0.214	11	0.035	0.130	0.025	0.004	2.7	1.4	2148	44
32	Jg 9a - Sp 3 - 11	289479	25367	614	1.2	97	425	12	681798	0.206	15	0.020	0.011	0.026	0.032	3.4	1.4	2187	82
33	Jg 9a - Sp 4 - 01	286623	23084	8918	1.8	6.9	102	2200	676820	0.239	16	0.072	0.035	0.024	0.149	3.8	2.1	2189	69
34	Jg 9a - Sp 4 - 02	286838	24231	9603	1.8	14	129	24	676903	0.244	16	0.010	0.003	0.025	0.203	2.7	1.9	2221	88
35	Jg 9a - Sp 4 - 03	289988	23589	8468	1.2	33	183	16	675410	0.240	16	0.007	0.019	0.023	0.129	2.3	1.7	2277	59
36	Jg 9a - Sp 4 - 04	291767	30334	7144	2.2	103	424	45	668023	0.243	16	0.072	0.103	0.023	0.094	2.9	2.4	2132	68
37	Jg 9a - Sp 4 - 05	286461	27615	1557	1.3	130	464	30	681612	0.207	11	0.009	0.000	0.020	0.031	2.9	2.0	2114	66
38	Jg 9a - Sp 4 - 06	288829	29484	3362	4.0	127	460	36	675522	0.239	10.0	0.027	0.110	0.031	0.075	2.4	2.2	2161	61
39	Jg 9a - Sp 4 - 07	287241	24619	976	2.6	95	432	24	684399	0.275	12	0.039	0.070	0.031	0.014	3.9	1.4	2195	104
40	Jg 9a - Sp 4 - 08	289772	26519	4107	2.0	73	377	16	676957	0.415	14	0.030	0.011	0.027	0.077	3.1	1.7	2155	74
41	Jg 9a - Sp 4 - 09	288500	20759	2601	1.9	30	207	14	685655	0.226	15	0.028	0.027	0.023	0.069	2.7	2.2	2202	72
42	Jg 9a - Sp 4 - 10	291958	25574	6604	4.3	34	274	25	673372	0.222	17	0.156	0.310	0.029	0.124	3.0	2.1	2123	67
	Mean (n=42)	288378	27131	4170	1.9	77	372	75	677581	0.245	15	0.027	0.050	0.023	0.075	3.0	1.8	2190	72
	SD	44035	5547	4515	0.815	48	127	333	103600	0.063	3.4	0.029	0.079	0.005	0.077	0.636	0.642	338	16
	Median	288249	26925	3452	1.7	79	406	17	679003	0.239	16	0.020	0.019	0.023	0.066	3.1	1.7	2194	69
	Max	294232	36552	24371	4.3	148	492	2200	688881	0.415	18	0.156	0.338	0.031	0.406	4.2	4.7	2313	104
	Min	284279	20755	21	1.0	6.9	102	7.3	645693	0.174	10.0	0.003	0.000	0.016	0.001	2.1	1.2	2052	44

#	Pentlandite	^{34}S	^{57}Fe	^{65}Cu	^{49}Ti	^{55}Mn	^{59}Co	^{60}Ni	^{66}Zn	^{75}As	^{77}Se	^{88}Sr	^{90}Zr	^{95}Mo	^{105}Pd	^{106}Pd	^{107}Ag	^{111}Cd	^{113}In
1	Jg 9a - Pn 1 - 01	344126	251508	35	170	43	4514	393543	5935	0.718	71	1.8	7.5	0.921	0.197	0.293	0.323	20	2.5
2	Jg 9a - Pn 1 - 02	324421	295224	27	43	391	4327	374426	973	0.500	71	2.0	6.1	5.9	0.354	0.323	1.5	2.8	0.037
3	Jg 9a - Pn 1 - 03	339977	251799	10.0	32	8.4	4528	402922	578	0.471	72	1.6	1.1	0.554	0.225	0.221	1.8	0.869	0.300
4	Jg 9a - Pn 1 - 04	328820	251586	1.8	1.4	0.249	4429	415052	31	0.304	71	0.007	0.041	0.049	0.411	0.291	0.158	0.055	0.087
5	Jg 9a - Pn 1 - 05	350759	238892	4.8	4.3	1.3	4541	405595	111	0.303	77	0.174	0.166	0.051	0.330	0.330	0.059	0.124	0.013
6	Jg 9a - Pn 1 - 06	331300	258382	2.0	3.1	1.2	4661	405540	28	0.299	71	0.082	0.147	0.043	0.328	0.311	0.074	0.089	0.097
7	Jg 9a - Pn 1 - 07	339591	254128	3.3	4.8	1.5	4701	401440	36	0.360	76	0.042	0.091	0.054	0.216	0.315	0.415	0.223	0.009
8	Jg 9a - Pn 1 - 08	360352	250810	4.6	6.9	2.1	4616	383788	319	0.398	75	0.198	0.830	0.179	0.246	0.298	0.645	0.446	0.215
9	Jg 9a - Pn 1 - 09	339683	249893	1.9	2.1	0.200	4509	405800	17	0.349	72	0.032	0.034	0.023	0.267	0.324	0.683	0.041	0.802
10	Jg 9a - Pn 1 - 10	334646	255698	2.9	8.1	1.0	4652	404817	45	0.612	73	0.300	0.793	0.057	0.245	0.274	0.759	0.052	0.028
11	Jg 9a - Pn 2 - 01	347544	253219	4.3	9.5	1.2	4308	394646	137	0.339	78	0.223	0.187	0.058	0.284	0.293	0.562	0.406	0.009
12	Jg 9a - Pn 2 - 02	399933	291676	26	9.5	2.4	6050	301660	311	0.828	86	0.561	0.380	0.106	0.356	0.396	1.4	0.924	0.093
13	Jg 9a - Pn 2 - 03	345240	248133	3.1	3.3	0.232	4383	402116	44	0.283	70	0.063	0.027	0.033	0.449	0.497	0.091	0.386	0.093
14	Jg 9a - Pn 2 - 04	360466	251329	15	16	14	4024	382712	1248	0.534	80	0.438	1.2	0.372	0.400	0.513	0.661	2.1	0.035
15	Jg 9a - Pn 2 - 05	343395	246395	9.0	20	6.6	4306	405276	482	0.467	78	0.307	1.6	0.215	0.453	0.379	0.253	1.0	0.012
16	Jg 9a - Pn 2 - 06	347061	240022	2.3	1.2	0.328	4341	408470	23	0.299	72	0.022	0.046	0.034	0.389	0.306	0.063	0.100	0.017
17	Jg 9a - Pn 2 - 07	358742	250686	9.4	21	3.9	4273	385231	941	0.386	74	2.6	0.713	0.090	0.350	0.365	0.148	1.8	0.477
18	Jg 9a - Pn 2 - 08	365565	243378	11	8.1	13	4488	382353	4051	0.325	76	0.896	0.462	0.293	0.687	0.681	0.725	7.7	0.020
19	Jg 9a - Pn 2 - 09	341287	254518	2.1	5.3	1.0	4387	399625	88	0.265	77	0.103	0.109	0.034	0.359	0.403	0.078	0.416	0.016
20	Jg 9a - Pn 3 - 01	366369	245217	35	363	65	4242	380855	2688	2.1	74	3.8	20	0.937	0.144	0.095	0.932	9.5	0.763
21	Jg 9a - Pn 3 - 02	346574	242258	10	30	5.4	4083	406662	247	0.402	82	0.433	0.904	0.124	0.130	0.140	1.5	0.795	0.132

#	Pentlandite	^{34}S	^{57}Fe	^{65}Cu	^{49}Ti	^{55}Mn	^{59}Co	^{60}Ni	^{66}Zn	^{75}As	^{77}Se	^{88}Sr	^{90}Zr	^{95}Mo	^{105}Pd	^{106}Pd	^{107}Ag	^{111}Cd	^{113}In
22	Jg 9a - Pn 3 - 03	342465	250700	9.3	22	4.5	4229	402351	139	0.444	72	0.398	0.378	0.053	0.479	0.302	0.053	0.533	0.004
23	Jg 9a - Pn 3 - 04	351766	256412	12	53	13	4188	387163	310	0.598	71	0.638	4.0	0.046	0.241	0.285	0.073	1.5	0.051
24	Jg 9a - Pn 3 - 05	356441	251037	9.4	24	12	4270	387831	285	0.451	68	0.761	0.578	0.176	0.221	0.306	0.352	0.547	0.104
25	Jg 9a - Pn 3 - 06	359064	242285	12	150	41	4173	392538	1639	1.4	69	1.1	3.9	0.163	0.267	0.258	0.114	6.1	0.154
26	Jg 9a - Pn 3 - 07	317904	326295	1370	761	906	3635	342923	6014	5.0	66	9.9	30	2.8	0.369	0.364	0.965	19	0.308
27	Jg 9a - Pn 3 - 08	346529	243849	1.9	3.9	0.877	4218	405282	24	0.334	75	0.211	0.229	0.037	0.279	0.294	0.161	0.096	0.014
28	Jg 5 - Pn 1 - 01	340794	251139	4.8	2.6	0.692	7374	400474	6.4	0.721	138	0.119	0.019	0.049	0.072	0.081	0.309	0.044	0.022
29	Jg 5 - Pn 1 - 02	343572	251986	7.3	7.1	3.5	7072	397162	10	0.912	117	0.814	0.222	0.094	0.209	0.194	0.424	0.080	0.022
30	Jg 5 - Pn 1 - 03	349509	256205	5.4	6.8	2.8	7861	386187	6.9	2.6	122	0.381	0.083	0.039	0.130	0.143	0.739	0.029	0.063
31	Jg 5 - Pn 1 - 04	333220	266306	7.7	7.5	9.5	7309	392964	8.9	0.411	84	1.7	0.089	0.184	0.147	0.162	0.747	0.054	0.038
32	Jg 5 - Pn 1 - 05	428060	302604	172	14	8.8	10485	258195	5.1	5.9	121	0.620	0.029	0.314	1.3	1.1	3.8	0.036	0.030
33	Jg 5 - Pn 1 - 06	346841	251902	11	3.7	1.9	7368	393700	6.8	0.559	100	0.382	0.057	0.144	0.562	0.562	1.2	0.010	0.019
34	Jg 5 - Pn 2 - 01	499287	369293	54	2.9	0.750	6043	124108	2.8	12	144	0.053	0.010	0.052	0.438	0.428	4.7	0.045	0.010
35	Jg 5 - Pn 2 - 02	485965	405059	42	2.5	0.233	5892	101315	1.4	13	146	0.027	0.006	0.026	0.535	0.488	7.7	0.016	0.008
36	Jg 5 - Pn 2 - 03	492933	392673	59	2.2	0.169	5118	106909	1.5	7.4	154	0.016	0.033	0.019	0.528	0.468	13	0.017	0.008
37	Jg 5 - Pn 2 - 04	469050	385778	45	1.8	0.141	5788	137142	1.3	6.3	144	0.023	0.004	0.021	0.722	0.752	17	0.049	0.020
38	Jg 5 - Pn 3 - 01	438123	322281	61	2.8	0.892	8563	229996	1.3	9.5	134	1.0	0.009	0.021	0.817	0.856	6.2	0.092	0.014
39	Jg 5 - Pn 3 - 02	336299	258881	5.8	3.9	2.4	8751	395875	2.1	0.332	106	0.348	0.014	0.034	0.130	0.088	4.7	0.031	0.020
40	Jg 5 - Pn 3 - 03	330335	254132	3.1	12	11	8135	407197	2.9	0.397	102	0.333	0.024	0.033	0.422	0.404	0.208	0.041	0.149
41	Jg 5 - Pn 3 - 04	333267	251615	0.959	1.7	0.211	8212	406788	1.0	0.288	102	0.037	0.008	0.026	0.265	0.232	0.066	0.026	0.009
42	Jg 5 - Pn 3 - 05	341177	246630	1.0	1.3	0.266	8263	403804	1.2	0.415	102	0.021	0.008	0.026	0.195	0.176	0.217	0.026	0.013
43	Jg 5 - Pn 3 - 06	466520	386180	6922	2.1	0.057	12919	126126	35	6.1	130	0.003	0.000	0.020	0.639	0.533	8.9	0.254	0.008
44	Jg 5 - Pn 3 - 07	421270	332958	29	2.3	0.831	10773	234348	1.1	5.0	125	0.610	0.002	0.024	0.627	0.620	3.1	0.027	0.010
45	Jg 5 - Pn 4 - 01	524672	392365	412	2.6	0.949	16317	64945	3.1	1.4	184	0.144	0.021	0.030	0.448	0.415	7.0	0.028	0.009
46	Jg 5 - Pn 4 - 02	465056	381820	38	2.8	2.0	11896	140055	1.8	4.6	137	0.547	0.211	0.022	0.812	0.836	4.6	0.014	0.009
47	Jg 5 - Pn 4 - 03	494745	400848	45	1.5	0.120	11732	90994	1.1	11	141	0.047	0.020	0.022	0.885	0.877	5.6	0.011	0.008
48	Jg 5 - Pn 4 - 04	484962	390112	24	1.7	0.200	11656	112129	1.1	8.2	128	0.054	0.002	0.024	0.683	0.667	4.3	0.011	0.016
49	Jg 5 - Pn 4 - 05	342419	256236	1.8	20	21	9530	391554	21	1.6	117	0.945	0.233	0.034	0.197	0.177	0.503	0.007	0.013
50	Jg 5 - Pn 4 - 06	343577	239749	1.6	1.4	0.759	9666	406562	4.4	1.4	119	1.1	0.023	0.050	0.506	0.444	0.091	0.045	0.190
51	Jg 5 - Pn 4 - 07	334332	244393	1.5	2.3	0.205	10048	411067	1.4	1.4	116	0.027	0.011	0.029	0.124	0.132	0.515	0.030	0.040
52	Jg 5 - Pn 4 - 08	340197	258107	1.6	2.3	1.8	9808	391646	1.6	1.3	105	67	0.014	0.044	0.159	0.153	0.542	0.031	0.010
53	Jg 5 - Pn 4 - 09	345202	241374	1.8	2.2	0.221	9824	403472	1.7	0.405	107	0.138	0.020	0.028	0.264	0.230	0.082	0.020	0.016
	Mean (n=53)	373989	280867	181	36	30	6707	337270	507	2.3	99	2.0	1.6	0.281	0.386	0.380	2.1	1.5	0.136
	SD	76000	65654	955	115	133	3065	118943	1294	3.3	32	9.1	5.0	0.889	0.237	0.226	3.4	4.0	0.373
	Median	346574	253219	9.3	4.3	1.5	5118	392964	23	0.559	84	0.333	0.089	0.049	0.350	0.315	0.645	0.080	0.020
	Max	524672	405059	6922	761	906	16317	415052	6014	13	184	67	30	5.9	1.3	1.1	17	20	2.5
	Min	317904	238892	0.959	1.2	0.057	3635	64945	1.0	0.265	66	0.003	0.000	0.019	0.072	0.081	0.053	0.007	0.004

#	Violarite/Bravoite	^{34}S	^{57}Fe	^{65}Cu	^{49}Ti	^{55}Mn	^{59}Co	^{60}Ni	^{66}Zn	^{75}As	^{77}Se	^{88}Sr	^{90}Zr	^{95}Mo	^{105}Pd	^{106}Pd	^{107}Ag	^{111}Cd	^{113}In
1	Jg 9a - Pn 1 exs - 01	486482	409449	121	2.2	0.051	10671	92282	4.4	0.207	117	0.008	0.047	0.028	0.443	0.413	8.9	0.021	0.005
2	Jg 9a - Pn 1 exs - 02	497712	398889	126	1.8	0.056	12770	89619	6.2	0.207	118	0.003	0.021	0.071	0.494	0.436	8.2	0.068	0.005
3	Jg 9a - Pn 1 exs - 03	484012	395202	61	2.1	0.046	10111	109440	1.3	0.188	118	0.002	0.002	0.027	0.583	0.591	9.9	0.012	0.020
4	Jg 9a - Pn 1 exs - 04	512466	412912	285	1.9	0.092	12119	61332	20	0.196	125	0.010	0.007	0.078	0.245	0.251	7.2	0.058	0.008
5	Jg 9a - Pn 1 exs - 05	474121	409758	69	2.2	0.071	11636	102931	17	0.180	108	12	0.004	0.063	0.560	0.453	12	0.013	0.010
6	Jg 9a - Pn 1 exs - 06	494655	410901	68	3.0	0.248	12117	81306	18	0.198	117	14	0.150	0.055	0.333	0.350	5.4	0.032	0.007
7	Jg 9a - Pn 1 exs - 07	472994	404594	30	1.8	0.123	11936	109156	4.4	0.243	112	0.031	0.028	0.023	0.517	0.497	8.5	0.086	0.005
8	Jg 9a - Pn 1 exs - 08	478948	391833	37	2.6	0.179	11533	116449	6.0	0.243	100	0.041	0.005	0.024	0.572	0.515	7.7	0.035	0.006
9	Jg 9a - Pn 2 exs - 01	500645	394361	49	2.4	0.227	4035	98830	22	0.233	110	0.075	0.030	0.030	0.696	0.727	11	0.074	0.010
10	Jg 9a - Pn 2 exs - 02	513337	397215	106	1.9	0.083	3046	84750	21	0.286	121	0.061	0.000	0.036	0.513	0.492	8.5	0.057	0.010
11	Jg 9a - Pn 2 exs - 03	504932	405683	107	2.4	0.043	3061	84368	1.9	0.170	116	0.028	0.007	0.108	0.546	0.521	9.5	0.008	0.033
12	Jg 9a - Pn 2 exs - 04	543556	398906	2431	2.2	0.037	12931	41568	6.9	0.195	132	0.002	0.000	0.119	0.235	0.204	3.3	0.045	0.029
13	Jg 9a - Pn 2 exs - 05	508502	402644	12505	2.4	0.086	10820	64354	26	0.344	114	0.022	0.002	0.170	0.647	0.403	6.0	0.244	0.014
14	Jg 9a - Pn 2 exs - 06	517966	400521	6328	1.9	4.2	11186	62659	28	0.264	125	3.4	0.014	0.073	0.588	0.483	7.0	0.235	0.002
15	Jg 9a - Pn 2 exs - 07	515099	408037	15464	1.7	12	9456	49804	65	0.811	124	8.9	0.000	0.154	0.753	0.523	7.6	0.493	0.161
16	Jg 9a - Pn 2 exs - 08	469172	389500	1193	2.9	0.592	8848	129823	160	1.0	108	0.279	0.018	0.022	0.794	0.825	7.8	0.569	0.173
17	Jg 9a - Pn 3 exs - 01	503228	414435	66204	3.5	0.423	12033	3157	115	0.421	103	0.061	0.099	0.133	1.2	0.070	15	0.509	0.073
18	Jg 9a - Pn 3 exs - 02	503968	413340	66290	2.6	0.320	11890	3383	236	0.362	109	0.049	0.053	0.126	1.2	0.065	15	1.2	0.009
19	Jg 9a - Pn 3 exs - 03	473972	423698	63369	2.8	0.235	11320	26391	74	0.209	90	0.032	0.035	0.031	1.3	0.289	17	0.599	0.008
20	Jg 9a - Pn 3 exs - 04	506930	402824	3568	4.4	1.1	14078	71584	65	0.236	119	0.330	0.122	0.115	0.452	0.414	11	0.237	0.020
21	Jg 9a - Pn 3 exs - 05	449784	380588	29530	5.4	1.7	12067	126718	113	0.531	100	1.2	0.170	0.025	1.5	1.0	17	0.767	0.058
22	Jg 9a - Pn 3 exs - 06	452254	376494	1453	5.4	1.2	10798	157420	120	0.258	101	0.487	0.108	0.026	0.716	0.658	9.9	0.177	0.011
23	Jg 9a - Pn 4 exs - 01	492615	383483	139	5.6	0.367	5990	116152	15	5.2	96	0.093	0.259	0.026	1.6	1.8	7.6	0.127	0.023
24	Jg 9a - Pn 4 exs - 02	404342	323014	44	9.3	4.6	4890	267030	109	1.9	87	0.540	0.464	0.038	0.485	0.509	2.3	0.496	0.041

#	Violarite/Bravoite	^{34}S	^{57}Fe	^{65}Cu	^{49}Ti	^{55}Mn	^{59}Co	^{60}Ni	^{66}Zn	^{75}As	^{77}Se	^{88}Sr	^{90}Zr	^{95}Mo	^{105}Pd	^{106}Pd	^{107}Ag	^{111}Cd	^{113}In
25	Jg 9a - Pn 4 exs - 03	437743	320533	122	7.5	15	4891	236260	44	0.686	92	0.513	0.187	0.035	0.408	0.326	1.5	0.151	0.129
26	Jg 9a - Pn 4 exs - 04	444342	337272	217	12	1.8	5553	211992	71	1.1	101	0.327	0.422	0.036	0.467	0.487	2.1	0.376	0.008
27	Jg 9a - Pn 4 exs - 05	427587	314555	216	19	4.8	5291	251577	279	1.1	86	1.7	0.587	0.077	0.503	0.382	2.0	1.4	0.013
28	Jg 9a - Pn 4 exs - 06	466040	410346	3988	4.4	1.3	4042	113932	52	1.4	100	5.6	0.159	0.034	0.668	0.580	9.4	0.193	0.010
29	Jg 9a - Pn 4 exs - 07	473336	401321	7025	6.5	1.7	4569	111624	157	0.766	108	0.478	0.381	0.215	1.1	1.1	11	0.579	0.039
30	Jg 9a - Pn 4 exs - 08	454726	375777	437	6.5	5.0	4214	163059	201	1.2	99	1.3	0.287	0.076	0.942	0.916	7.6	0.972	0.234
31	Jg 9a - Pn 4 exs - 09	423590	279943	262	16	13	4424	290248	1101	1.1	88	2.1	0.854	0.423	0.329	0.359	1.8	3.5	0.021
32	Jg 9a - Pn 4 exs - 10	487659	375021	19413	19	4.9	2980	113228	335	2.9	94	0.994	0.711	0.060	0.979	0.590	27	1.9	0.011
	Mean (n=32)	480522	386345	9414	5.2	2.4	8603	113826	109	0.760	107	1.7	0.163	0.080	0.697	0.539	8.9	0.476	0.038
	SD	89231	75204	19215	4.9	3.9	3952	73047	198	1.0	22	3.5	0.223	0.080	0.364	0.337	5.4	0.708	0.056
	Median	485247	398898	273	2.8	0.395	10391	106043	48	0.315	108	0.303	0.050	0.058	0.577	0.489	8.4	0.214	0.012
	Max	543556	423698	66290	19	15	14078	290248	1101	5.2	132	14	0.854	0.423	1.6	1.8	27	3.5	0.234
	Min	404342	279943	30	1.7	0.037	2980	3157	1.3	0.170	86	0.002	0.000	0.022	0.235	0.065	1.5	0.008	0.002

#	Chalcopyrite	^{34}S	^{57}Fe	^{65}Cu	^{49}Ti	^{55}Mn	^{59}Co	^{60}Ni	^{66}Zn	^{75}As	^{77}Se	^{88}Sr	^{90}Zr	^{95}Mo	^{105}Pd	^{106}Pd	^{107}Ag	^{111}Cd	^{113}In
1	Jg 9a - Ccp 1 - 01	380900	265304	353285	3.7	1.0	3.5	61	405	0.561	22	0.372	0.238	0.068	6.3	0.007	4.2	1.3	0.537
2	Jg 9a - Ccp 1 - 02	366584	259632	373268	13	1.3	3.3	36	422	0.836	21	0.270	0.341	0.072	5.3	0.079	4.2	1.2	0.444
3	Jg 9a - Ccp 1 - 03	379705	283395	336443	11	0.674	1.7	21	383	0.546	22	0.160	0.255	0.059	5.4	0.002	5.1	1.3	2.0
4	Jg 9a - Ccp 1 - 04	368470	285907	344820	15	2.9	4.4	247	490	0.936	28	0.894	0.319	0.132	6.2	0.003	4.6	1.3	0.876
5	Jg 9a - Ccp 1 - 05	388148	280457	330747	15	2.4	4.5	40	549	0.697	21	0.471	0.434	0.069	5.9	0.061	2.2	1.2	0.828
6	Jg 9a - Ccp 1 - 06	404666	278721	315421	14	3.0	6.5	62	1072	0.997	19	0.658	0.813	0.114	5.6	0.003	1.6	4.5	1.3
7	Jg 9a - Ccp 1 - 07	391229	279490	328557	30	7.2	11	105	525	1.0	28	0.704	3.2	0.085	6.0	0.134	2.0	3.2	2.6
8	Jg 9a - Ccp 1 - 08	373140	307724	318462	8.0	17	14	80	520	1.3	21	1.0	0.875	0.117	5.6	0.022	1.5	1.8	0.260
9	Jg 9a - Ccp 1 - 09	411235	276423	311641	66	6.4	7.1	156	414	4.7	37	1.4	1.2	0.286	7.8	0.055	1.2	1.3	0.094
10	Jg 9a - Ccp 1 - 10	359852	295821	342967	33	11	8.2	135	1121	2.2	24	0.744	3.6	0.170	3.7	0.003	1.0	4.7	0.044
11	Jg 9a - Ccp 1 - 11	383445	272242	341585	35	22	23	888	1649	3.2	45	5.1	3.6	0.318	6.2	0.004	1.9	9.3	0.076
	Mean (n=11)	382489	280465	336109	22	6.8	8.0	166	686	1.6	26	1.1	1.3	0.135	5.8	0.034	2.7	2.8	0.817
	SD	15770	13300	18035	18	7.2	6.2	248	411	1.3	8.0	1.4	1.4	0.089	0.954	0.044	1.5	2.5	0.828
	Median	380900	279490	336443	15	3.0	6.5	80	520	0.997	22	0.704	0.813	0.114	5.9	0.007	2.0	1.3	0.537
	Max	411235	307724	373268	66	22	23	888	1649	4.7	45	5.1	3.6	0.318	7.8	0.134	5.1	9.3	2.6
	Min	359852	259632	311641	3.7	0.674	1.7	21	383	0.546	19	0.160	0.238	0.059	3.7	0.002	1.0	1.2	0.044

Table 1a. (Continued)

#	Pyrite	^{115}In	^{118}Sn	^{121}Sb	^{125}Te	^{178}Hf	^{181}Ta	^{182}W	^{193}Ir	^{195}Pt	^{197}Au	^{205}Tl	^{209}Bi	^{232}Th	^{238}U	^{204}Pb	^{206}Pb	^{207}Pb	^{208}Pb
1	Jg 9a - Py 1 - 01	0.000	0.025	0.013	0.060	0.000	0.000	0.000	0.000	0.003	0.001	0.002	0.021	0.000	0.000	0.005	0.003	0.001	0.001
2	Jg 9a - Py 1 - 02	0.000	0.023	0.040	0.062	0.000	0.000	0.000	0.000	0.001	0.000	0.003	0.183	0.000	0.000	0.005	0.001	0.001	0.002
3	Jg 9a - Py 1 - 03	0.000	0.028	0.007	0.475	0.000	0.000	0.000	0.000	0.004	0.003	0.002	2.1	0.000	0.000	0.004	0.007	0.009	0.012
4	Jg 9a - Py 1 - 04	0.000	0.035	0.007	0.144	0.000	0.000	0.000	0.000	0.027	0.001	0.002	0.854	0.000	0.000	0.004	0.008	0.005	0.011
5	Jg 9a - Py 1 - 05	0.001	0.031	0.012	0.516	0.000	0.001	0.000	0.000	0.027	0.008	0.003	2.4	0.000	0.000	0.004	0.036	0.034	0.088
6	Jg 9a - Py 1 - 06	0.000	0.027	0.008	0.151	0.000	0.000	0.000	0.000	0.007	0.000	0.001	0.303	0.000	0.000	0.005	0.001	0.001	0.002
7	Jg 9a - Py 1 - 07	0.001	0.026	0.009	0.204	0.000	0.000	0.000	0.000	0.004	0.002	0.003	1.2	0.000	0.000	0.004	0.001	0.000	0.003
8	Jg 9a - Py 1 - 08	0.000	0.023	0.012	0.057	0.000	0.000	0.000	0.000	0.002	0.000	0.003	0.219	0.000	0.000	0.004	0.001	0.000	0.002
9	Jg 9a - Py 2 - 01	0.000	0.026	0.012	0.204	0.000	0.000	0.001	0.000	0.006	0.004	0.002	1.5	0.000	0.000	0.004	0.003	0.002	0.004
10	Jg 9a - Py 2 - 02	0.000	0.025	0.014	0.085	0.000	0.000	0.000	0.000	0.001	0.001	0.003	0.220	0.000	0.000	0.004	0.004	0.001	0.005
11	Jg 9a - Py 2 - 03	0.000	0.028	0.018	2.6	0.000	0.000	0.004	0.000	0.010	0.001	0.003	9.8	0.000	0.000	0.077	1.1	1.1	2.5
12	Jg 9a - Py 2 - 04	0.000	0.032	0.012	2.2	0.000	0.000	0.003	0.000	0.133	0.004	0.002	6.1	0.000	0.000	0.015	0.300	0.304	0.667
13	Jg 9a - Py 2 - 05	0.001	0.033	0.008	1.5	0.000	0.000	0.000	0.000	0.016	0.002	0.002	7.8	0.000	0.000	0.007	0.096	0.110	0.240
14	Jg 9a - Py 2 - 06	0.000	0.024	0.010	0.078	0.000	0.000	0.000	0.000	0.003	0.000	0.001	0.158	0.000	0.000	0.007	0.002	0.001	0.001
15	Jg 9a - Py 2 - 07	0.000	0.020	0.073	0.281	0.000	0.000	0.001	0.000	0.003	0.002	0.006	6.6	0.000	0.000	0.111	1.7	1.8	4.0
16	Jg 9a - Py 3 - 01	0.000	0.025	0.010	0.069	0.000	0.000	0.000	0.000	0.003	0.000	0.002	0.002	0.000	0.000	0.004	0.001	0.001	0.002
17	Jg 9a - Py 3 - 02	0.000	0.031	0.006	0.065	0.000	0.000	0.000	0.000	0.003	0.000	0.002	0.008	0.000	0.000	0.005	0.001	0.001	0.004
18	Jg 9a - Py 3 - 03	0.000	0.024	0.008	0.060	0.000	0.000	0.000	0.000	0.002	0.000	0.002	0.145	0.000	0.000	0.004	0.005	0.006	0.008
19	Jg 9a - Py 3 - 04	0.001	0.026	0.032	0.047	0.000	0.000	0.000	0.000	0.004	0.001	0.002	0.177	0.000	0.000	0.031	0.594	0.623	1.4
20	Jg 9a - Py 3 - 05	0.000	0.023	0.015	0.078	0.000	0.000	0.000	0.000	0.001	0.001	0.003	0.343	0.000	0.000	0.004	0.001	0.002	0.002
21	Jg 9a - Py 3 - 06	0.000	0.026	0.010	0.319	0.000	0.000	0.000	0.000	0.005	0.003	0.003	1.4	0.000	0.000	0.004	0.001	0.004	0.005
22	Jg 9a - Py 3 - 07	0.000	0.030	0.010	0.058	0.000	0.000	0.000	0.000	0.001	0.001	0.003	0.300	0.000	0.000	0.005	0.001	0.002	0.004
23	Jg 9a - Py 3 - 08	0.000	0.036	0.011	0.071	0.000	0.000	0.000	0.000	0.001	0.000	0.003	0.501	0.000	0.000	0.005	0.002	0.001	0.002
24	Jg 9a - Py 3 - 09	0.000	0.031	0.487	0.056	0.000	0.000	0.003	0.000	0.001	0.002	0.003	0.162	0.000	0.000	0.234	3.5	3.5	7.8
25	Jg 9a - Py 3 - 10	0.000	0.031	0.011	0.365	0.000	0.000	0.000	0.000	0.001	0.002	0.002	1.8	0.000	0.000	0.005	0.006	0.002	0.006
26	Jg 9a - Py 3 - 11	0.002	0.028	0.017	0.111	0.000	0.000	0.000	0.000	0.007	0.002	0.006	0.103	0.000	0.000	0.006	0.000	0.001	0.004
27	Jg 9a - Py 3 - 12	0.002	0.028	0.013	0.114	0.000	0.000	0.000	0.001	0.002	0.001	0.006	0.348	0.000	0.001	0.005	0.001	0.001	0.002

#	Pyrite	^{115}In	^{118}Sn	^{121}Sb	^{125}Te	^{178}Hf	^{181}Ta	^{182}W	^{193}Ir	^{195}Pt	^{197}Au	^{205}Tl	^{209}Bi	^{232}Th	^{238}U	^{204}Pb	^{206}Pb	^{207}Pb	^{208}Pb
28	Jg 9a - Py 3 - 13	0.001	0.021	0.013	0.132	0.000	0.000	0.012	0.000	0.006	0.001	0.008	0.874	0.000	0.000	0.005	0.090	0.097	0.173
29	Jg 9a - Py 3 - 14	0.001	0.022	0.017	0.159	0.000	0.001	0.000	0.000	0.014	0.000	0.003	0.051	0.000	0.000	0.004	0.001	0.002	0.001
30	Jg 9a - Py 4 - 01	0.001	0.026	0.014	0.067	0.000	0.001	0.000	0.000	0.003	0.000	0.004	0.085	0.003	0.001	0.005	0.004	0.007	0.010
31	Jg 9a - Py 4 - 02	0.000	0.027	0.017	1.6	0.004	0.000	0.000	0.000	0.006	0.003	0.005	5.1	0.003	0.001	0.004	0.014	0.016	0.036
32	Jg 9a - Py 4 - 03	0.002	0.025	0.011	12	0.000	0.000	0.000	0.000	0.027	0.039	0.004	46	0.000	0.001	0.095	1.5	1.4	3.2
33	Jg 9a - Py 4 - 04	0.002	0.027	0.035	6.5	0.000	0.002	0.008	0.000	0.046	0.015	0.004	32	0.002	0.002	0.413	6.2	5.7	13
34	Jg 9a - Py 4 - 05	0.002	0.030	0.030	4.2	0.000	0.000	0.000	0.000	0.020	0.009	0.003	17	0.001	0.001	0.094	1.4	1.4	3.1
35	Jg 9a - Py 4 - 06	0.001	0.027	0.017	21	0.000	0.001	0.000	0.000	0.026	0.011	0.004	54	0.000	0.001	0.155	2.1	2.3	5.1
36	Jg 9a - Py 4 - 07	0.000	0.025	0.099	8.1	0.006	0.000	0.140	0.000	0.003	0.005	0.003	14	0.008	0.015	0.728	12	12	27
37	Jg 9a - Py 4 - 08	0.000	0.216	0.078	317	0.026	0.001	0.003	0.000	0.007	0.045	0.004	610	0.087	0.085	4.6	69	73	153
38	Jg 9a - Py 4 - 09	0.008	0.028	0.011	13	0.000	0.000	0.000	0.000	0.005	0.010	0.005	26	0.004	0.024	0.093	1.2	1.3	2.8
39	Jg 9a - Py 4 - 10	0.003	0.033	0.009	0.247	0.000	0.000	0.000	0.000	0.004	0.001	0.005	0.140	0.007	0.000	0.006	0.009	0.012	0.016
40	Jg 9a - Py 5 edge - 01	0.000	0.029	0.015	1.2	0.000	0.000	0.000	0.000	0.005	0.006	0.002	5.2	0.000	0.000	0.005	0.013	0.008	0.013
41	Jg 9a - Py 5 edge - 02	0.000	0.024	0.014	0.407	0.000	0.000	0.000	0.000	0.004	0.004	0.004	2.8	0.000	0.001	0.004	0.007	0.010	0.016
42	Jg 9a - Py 5 edge - 03	0.000	0.023	0.015	0.082	0.000	0.000	0.000	0.000	0.001	0.000	0.004	0.123	0.000	0.000	0.004	0.002	0.001	0.001
43	Jg 9a - Py 5 edge - 04	0.000	0.024	0.010	0.088	0.000	0.000	0.000	0.000	0.002	0.000	0.003	0.120	0.000	0.000	0.004	0.003	0.005	0.002
44	Jg 9a - Py 5 cent - 01	0.000	0.023	0.009	0.230	0.000	0.000	0.000	0.000	0.004	0.001	0.003	1.6	0.000	0.000	0.004	0.007	0.008	0.017
45	Jg 9a - Py 5 cent - 02	0.000	0.026	0.016	1.7	0.000	0.001	0.000	0.000	0.020	0.005	0.003	10	0.000	0.000	0.139	2.5	2.5	5.1
46	Jg 9a - Py 5 cent - 03	0.000	0.027	0.014	0.935	0.000	0.000	0.000	0.000	0.001	0.001	0.003	1.8	0.000	0.000	0.050	0.821	0.835	1.8
47	Jg 9a - Py 5 cent - 04	0.000	0.032	0.012	1.0	0.000	0.000	0.000	0.000	0.001	0.000	0.004	0.123	0.000	0.001	0.004	0.001	0.001	0.002
48	Jg 9a - Py 5 cent - 05	0.000	0.024	0.015	10	0.000	0.000	0.000	0.000	0.003	0.001	0.002	5.7	0.000	0.000	0.005	0.118	0.115	0.258
49	Jg 9a - Py 5 edge - 05	0.000	0.024	0.016	7.3	0.000	0.000	0.000	0.000	0.001	0.000	0.002	0.160	0.000	0.000	0.006	0.005	0.001	0.006
50	Jg 9a - Py 5 edge - 06	0.006	0.055	0.031	10.0	0.000	0.000	0.000	0.000	0.014	0.029	0.002	29	0.000	0.000	0.461	6.5	6.9	15
51	Jg 9a - Py 5 edge - 07	0.008	0.085	0.046	21	0.000	0.000	0.000	0.000	0.011	0.139	0.001	61	0.000	0.000	0.454	6.5	6.9	15
52	Jg 9a - Py 5 edge - 08	0.001	0.023	0.124	0.984	0.000	0.000	0.000	0.000	0.003	0.003	0.002	3.4	0.000	0.226	0.088	1.4	1.3	3.0
53	Jg 9a - Py 5 edge - 09	0.001	0.023	0.019	1.2	0.000	0.001	0.001	0.000	0.000	0.002	0.002	7.9	0.007	0.440	0.049	0.934	0.935	2.1
54	Jg 9a - Py 5 edge - 10	0.001	0.022	0.020	0.099	0.000	0.000	0.000	0.000	0.003	0.001	0.002	0.363	0.000	0.000	0.004	0.003	0.001	0.009
55	Jg 9a - Py 6 edge - 01	0.000	0.027	0.010	0.059	0.000	0.000	0.000	0.000	0.001	0.000	0.001	0.273	0.000	0.000	0.004	0.001	0.001	0.010
56	Jg 9a - Py 6 edge - 02	0.001	0.024	0.013	5.8	0.000	0.000	0.017	0.000	0.027	0.023	0.004	28	0.000	0.001	0.005	0.192	0.173	0.388
57	Jg 9a - Py 6 edge - 03	0.000	0.041	0.019	5.0	0.000	0.000	0.008	0.000	0.010	0.012	0.004	19	0.000	0.000	0.011	0.222	0.211	0.475
58	Jg 9a - Py 6 edge - 04	0.000	0.045	0.030	6.7	0.000	0.000	0.003	0.000	0.035	0.020	0.003	22	0.001	0.001	0.146	2.0	1.9	4.5
59	Jg 9a - Py 6 cent - 01	0.000	0.043	0.050	39	0.000	0.000	0.000	0.000	0.066	0.015	0.003	28	0.000	0.000	0.227	3.3	3.6	7.8
60	Jg 9a - Py 6 cent - 02	0.007	0.039	0.011	6.0	0.000	0.001	0.000	0.000	0.012	0.010	0.004	10	0.000	0.000	0.212	3.1	3.1	7.1
61	Jg 9a - Py 6 cent - 03	0.003	0.052	0.597	12	0.000	0.000	0.000	0.000	0.031	0.132	0.003	1909	0.000	0.000	36	529	556	1269
62	Jg 9a - Py 6 cent - 04	0.001	0.030	0.066	3.1	0.000	0.000	0.000	0.000	0.005	0.006	0.003	15	0.000	0.001	0.221	3.1	3.3	7.2
63	Jg 9a - Py 6 cent - 05	0.000	0.023	0.013	5.8	0.000	0.000	0.000	0.000	0.004	0.002	0.007	28	0.000	0.004	0.301	4.0	4.4	9.5
64	Jg 9a - Py 6 edge - 05	0.000	0.022	0.014	0.383	0.000	0.000	0.000	0.000	0.002	0.000	0.002	0.712	0.000	0.000	0.004	0.064	0.070	0.176
65	Jg 9a - Py 6 edge - 06	0.000	0.073	0.019	0.514	0.000	0.000	0.000	0.000	0.013	0.004	0.002	5.9	0.005	0.001	0.009	0.238	0.262	0.589
66	Jg 9a - Py 6 edge - 07	0.000	0.023	0.010	0.106	0.000	0.000	0.001	0.000	0.001	0.001	0.002	0.402	0.000	0.000	0.005	0.009	0.004	0.005
67	Jg 9a - Py 7 edge - 01	0.001	0.023	0.007	0.196	0.000	0.000	0.000	0.000	0.001	0.000	0.004	0.040	0.000	0.000	0.005	0.005	0.006	0.006
68	Jg 9a - Py 7 edge - 02	0.001	0.027	0.009	0.075	0.002	0.000	0.000	0.000	0.003	0.000	0.005	0.128	0.003	0.002	0.005	0.005	0.018	0.005
69	Jg 9a - Py 7 edge - 03	0.000	0.027	0.009	0.096	0.000	0.001	0.003	0.000	0.002	0.000	0.003	0.219	0.000	0.003	0.005	0.002	0.002	0.013
70	Jg 9a - Py 7 edge - 04	0.000	0.023	0.012	0.105	0.000	0.000	0.000	0.000	0.003	0.000	0.002	0.194	0.000	0.000	0.005	0.008	0.004	0.005
71	Jg 9a - Py 7 edge - 05	0.000	0.023	0.013	0.136	0.000	0.000	0.000	0.000	0.005	0.000	0.002	0.164	0.000	0.000	0.004	0.003	0.001	0.004
72	Jg 9a - Py 7 edge - 06	0.000	0.029	0.012	0.158	0.004	0.000	0.000	0.000	0.007	0.001	0.003	1.1	0.000	0.000	0.006	0.004	0.004	0.011
73	Jg 9a - Py 7 cent - 01	0.000	0.028	0.010	0.328	0.000	0.000	0.013	0.000	0.008	0.000	0.003	2.6	0.000	0.000	0.006	0.021	0.026	0.042
74	Jg 9a - Py 7 cent - 02	0.000	0.027	0.034	3.0	0.000	0.000	0.000	0.000	0.048	0.014	0.014	14	0.000	0.000	0.070	1.1	1.2	2.5
75	Jg 9a - Py 7 cent - 03	0.003	0.155	0.020	4.7	0.000	0.000	0.001	0.000	0.044	0.052	0.031	32	0.002	0.001	0.168	2.4	2.5	5.4
76	Jg 9a - Py 7 cent - 04	0.022	0.029	0.063	10	0.000	0.000	0.000	0.000	0.066	0.024	0.009	44	0.000	0.000	0.214	3.5	3.5	7.7
77	Jg 9a - Py 7 cent - 05	0.000	0.027	0.053	7.7	0.000	0.001	0.006	0.000	0.040	0.027	0.007	33	0.001	0.001	0.590	8.9	8.9	19
78	Jg 9a - Py 7 cent - 06	0.000	0.024	0.011	1.1	0.002	0.000	0.000	0.000	0.003	0.005	0.003	5.4	0.000	0.000	0.077	1.1	1.2	2.5
79	Jg 9a - Py 7 edge - 07	0.000	0.025	0.013	3.5	0.000	0.000	0.000	0.000	0.020	0.020	0.002	189	0.001	0.000	0.370	5.7	7.5	21
80	Jg 9a - Py 7 edge - 08	0.000	0.023	0.016	0.124	0.000	0.001	0.000	0.000	0.004	0.000	0.003	0.845	0.000	0.000	0.004	0.008	0.008	0.019
81	Jg 9a - Py 7 edge - 09	0.002	0.022	0.016	0.196	0.000	0.000	0.000	0.000	0.004	0.001	0.002	0.952	0.000	0.000	0.004	0.004	0.005	0.016
82	Jg 9a - Py 8 - 01	0.000	0.021	0.018	0.036	0.000	0.000	0.000	0.000	0.002	0.000	0.003	0.029	0.000	0.000	0.003	0.003	0.010	0.006
83	Jg 9a - Py 8 - 02	0.005	0.667	0.012	15	0.000	0.000	0.000	0.000	0.003	0.004	0.003	25	0.001	0.000	0.087	1.3	1.4	3.1
84	Jg 9a - Py 8 - 03	0.000	0.016	0.013	0.071	0.000	0.000	0.000	0.000	0.003	0.000	0.002	0.049	0.000	0.000	0.004	0.001	0.001	0.004
85	Jg 9a - Py 8 - 04	0.000	0.021	0.012	0.090	0.000	0.000	0.000	0.000	0.002	0.000	0.002	0.064	0.001	0.000	0.005	0.005	0.004	0.014
86	Jg 9a - Py 8 - 05	0.000	0.027	0.011	0.104	0.000	0.001	0.001	0.000	0.003	0.001	0.007	0.017	0.001	0.001	0.004	0.002	0.001	0.001
87	Jg 9a - Py 8 - 06	0.000	0.042	0.124	20	0.000	0.000	0.006	0.000	0.006	0.042	0.004	369	0.003	0.000	0.284	4.6	4.8	10
88	Jg 9a - Py 8 - 07	0.000	0.023	0.013	4.3	0.000	0.000	0.000	0.000	0.001	0.001	0.005	0.642	0.001	0.000	0.013	0.262	0.306	0.616
89	Jg 9a - Py 8 - 08	0.001	0.020	0.009	0.086	0.000	0.000	0.003	0.000	0.002	0.000	0.003	0.085	0.001	0.000	0.004	0.004	0.004	0.009
90	Jg 9a - Py 8 - 09	0.001	0.022	0.007	0.098	0.002	0.000	0.000	0.000	0.002	0.000	0.003	0.048	0.000	0.000	0.004	0.002	0.001	0.002
91	Jg 9a - Py 9 - 01	0.002	0.022	0.011	0.065	0.004	0.001	0.000	0.000	0.001	0.001	0.004	0.027	0.001	0.000	0.004	0.007	0.001	0.006

#	Pyrite	^{115}In	^{118}Sn	^{121}Sb	^{125}Te	^{178}Hf	^{181}Ta	^{182}W	^{193}Ir	^{195}Pt	^{197}Au	^{205}Tl	^{209}Bi	^{232}Th	^{238}U	^{204}Pb	^{206}Pb	^{207}Pb	^{208}Pb
92	Jg 9a - Py 9 - 02	0.001	0.025	0.014	0.077	0.000	0.000	0.000	0.000	0.001	0.000	0.002	0.020	0.002	0.000	0.004	0.002	0.001	0.004
93	Jg 9a - Py 9 - 03	0.003	0.026	0.016	3.7	0.002	0.000	0.000	0.000	0.003	0.003	0.003	16	0.000	0.033	0.151	2.6	2.4	5.5
94	Jg 9a - Py 9 - 04	0.002	0.028	0.011	1.3	0.007	0.000	0.003	0.000	0.009	0.013	0.002	7.4	0.000	0.000	0.005	0.005	0.005	0.013
95	Jg 9a - Py 9 - 05	0.002	0.028	0.031	6.8	0.002	0.002	0.004	0.000	0.006	0.101	0.003	29	0.005	0.097	0.077	1.4	1.4	3.1
96	Jg 9a - Py 9 - 06	0.002	0.033	0.015	0.155	0.000	0.000	0.000	0.000	0.003	0.000	0.004	0.235	0.000	0.000	0.003	0.004	0.000	0.005
97	Jg 9a - Py 9 - 07	0.001	0.028	0.009	1.7	0.000	0.000	0.000	0.000	0.007	0.006	0.001	8.4	0.000	0.000	0.004	0.007	0.003	0.007
98	Jg 9a - Py 9 - 08	0.000	0.025	0.012	1.9	0.000	0.000	0.000	0.000	0.011	0.027	0.002	12	0.002	0.000	0.005	0.016	0.010	0.020
99	Jg 9a - Py 9 - 09	0.000	0.019	0.010	0.505	0.002	0.000	0.000	0.000	0.004	0.003	0.002	1.8	0.001	0.000	0.004	0.005	0.003	0.009
100	Jg 9a - Py 9 - 10	0.003	0.024	0.010	0.134	0.000	0.000	0.000	0.000	0.007	0.001	0.001	0.728	0.000	0.001	0.004	0.001	0.003	0.005
101	Jg 9a - Py 9 - 11	0.000	0.030	0.016	0.101	0.000	0.000	0.000	0.000	0.004	0.001	0.002	0.288	0.000	0.003	0.003	0.001	0.002	0.004
102	Jg 9a - Py 10 - 01	0.001	0.030	0.099	13	0.000	0.001	0.004	0.000	0.011	0.003	0.008	7.6	0.000	0.000	0.594	8.2	7.9	18
103	Jg 9a - Py 10 - 02	0.001	0.020	0.015	2.6	0.000	0.000	0.009	0.000	0.004	0.004	0.006	4.0	0.000	0.000	0.267	4.4	4.2	9.2
104	Jg 9a - Py 10 - 03	0.001	0.019	0.013	0.041	0.000	0.000	0.000	0.000	0.001	0.000	0.002	0.109	0.000	0.000	0.004	0.002	0.001	0.003
105	Jg 9a - Py 10 - 04	0.001	0.018	0.047	3.4	0.000	0.000	0.006	0.000	0.005	0.000	0.003	2.9	0.000	0.000	0.016	0.215	0.257	0.489
106	Jg 9a - Py 10 - 05	0.001	0.022	0.010	0.133	0.000	0.000	0.000	0.000	0.007	0.000	0.002	0.047	0.000	0.000	0.004	0.000	0.001	0.002
107	Jg 9a - Py 10 - 06	0.000	0.029	0.007	0.083	0.000	0.000	0.000	0.000	0.003	0.000	0.002	0.090	0.001	0.000	0.003	0.001	0.001	0.001
108	Jg 9a - Py 10 - 07	0.000	0.026	0.009	0.067	0.000	0.000	0.000	0.000	0.001	0.000	0.002	0.026	0.000	0.000	0.004	0.001	0.000	0.005
109	Jg 9a - Py 10 - 08	0.000	0.025	0.012	1.3	0.000	0.000	0.000	0.000	0.005	0.001	0.003	2.9	0.000	0.000	0.004	0.068	0.063	0.135
110	Jg 9a - Py 10 - 09	0.000	0.025	0.009	0.060	0.000	0.000	0.000	0.000	0.001	0.000	0.001	0.009	0.000	0.000	0.002	0.001	0.001	0.002
111	Jg 9a - Py 10 - 10	0.000	0.028	0.016	0.158	0.000	0.000	0.000	0.000	0.005	0.003	0.004	0.744	0.000	0.000	0.003	0.001	0.001	0.002
112	Jg 5 - Py 1 - 01	0.001	0.025	0.017	0.063	0.000	0.000	0.000	0.000	0.018	0.000	0.003	0.044	0.000	0.001	0.004	0.001	0.002	0.001
113	Jg 5 - Py 1 - 02	0.000	0.031	0.019	0.082	0.000	0.000	0.001	0.000	0.021	0.000	0.003	0.079	0.000	0.000	0.005	0.001	0.001	0.002
114	Jg 5 - Py 1 - 03	0.000	0.031	0.011	0.082	0.000	0.000	0.000	0.000	0.036	0.000	0.002	0.099	0.000	0.000	0.005	0.001	0.001	0.001
115	Jg 5 - Py 1 - 04	0.000	0.028	0.017	0.337	0.000	0.000	0.006	0.000	0.061	0.002	0.002	2.2	0.000	0.000	0.005	0.209	0.194	0.432
116	Jg 5 - Py 1 - 05	0.000	0.024	0.009	0.277	0.000	0.000	0.000	0.000	0.011	0.002	0.002	0.903	0.000	0.000	0.005	0.068	0.072	0.155
117	Jg 5 - Py 1 - 06	0.000	0.026	0.012	0.277	0.000	0.000	0.000	0.000	0.013	0.000	0.003	0.703	0.000	0.000	0.003	0.034	0.039	0.077
118	Jg 5 - Py 1 - 07	0.000	0.024	0.013	1.1	0.000	0.000	0.000	0.000	4.0	0.000	0.005	3.6	0.000	0.000	0.019	0.228	0.256	0.530
119	Jg 5 - Py 1 - 08	0.000	0.024	0.013	0.109	0.000	0.000	0.000	0.000	0.031	0.000	0.003	0.106	0.000	0.000	0.003	0.001	0.000	0.001
120	Jg 5 - Py 1 - 09	0.000	0.030	0.013	0.308	0.000	0.000	0.000	0.000	0.108	0.001	0.002	1.1	0.000	0.000	0.003	0.002	0.004	0.005
121	Jg 5 - Py 1 - 10	0.003	0.017	0.015	1.2	0.000	0.000	0.001	0.000	0.155	0.002	0.007	4.3	0.000	0.000	0.004	0.009	0.005	0.017
122	Jg 5 - Py 1 - 11	0.001	0.021	0.018	0.264	0.004	0.000	0.000	0.001	0.029	0.001	0.007	0.676	0.000	0.000	0.004	0.001	0.002	0.003
123	Jg 5 - Py 1 - 12	0.000	0.021	0.019	0.060	0.000	0.000	0.000	0.000	0.041	0.003	0.004	0.088	0.000	0.000	0.004	0.002	0.000	0.002
124	Jg 5 - Py 2 - 01	0.000	0.023	0.015	0.351	0.000	0.000	0.000	0.000	0.043	0.002	0.002	1.7	0.000	0.000	0.004	0.049	0.058	0.120
125	Jg 5 - Py 2 - 02	0.000	0.024	0.013	0.078	0.000	0.000	0.000	0.000	0.071	0.000	0.003	0.091	0.000	0.000	0.004	0.002	0.003	0.006
126	Jg 5 - Py 2 - 03	0.000	0.025	0.010	0.364	0.000	0.000	0.000	0.000	0.119	0.002	0.003	4.1	0.000	0.000	0.036	0.725	0.736	1.5
127	Jg 5 - Py 2 - 04	0.001	0.022	0.007	0.702	0.000	0.000	0.000	0.000	0.010	0.000	0.003	0.289	0.000	0.000	0.005	0.033	0.033	0.070
128	Jg 5 - Py 2 - 05	0.000	0.019	0.021	17	0.000	0.000	0.000	0.000	0.805	0.025	0.003	6.5	0.000	0.000	0.248	3.8	3.9	8.6
129	Jg 5 - Py 2 - 06	0.001	0.026	0.010	4.3	0.004	0.000	0.000	0.000	0.296	0.011	0.004	21	0.000	0.000	0.135	2.3	2.3	5.1
130	Jg 5 - Py 2 - 07	0.001	0.027	0.009	1.4	0.000	0.000	0.000	0.000	0.040	0.001	0.002	3.1	0.000	0.000	0.039	0.639	0.662	1.5
131	Jg 5 - Py 3 - 01	0.000	0.020	0.007	0.061	0.000	0.000	0.000	0.000	0.033	0.000	0.001	0.092	0.000	0.000	0.004	0.001	0.001	0.001
132	Jg 5 - Py 3 - 02	0.000	0.022	0.010	2.0	0.000	0.000	0.000	0.000	0.234	0.004	0.002	8.2	0.000	0.000	0.005	0.178	0.166	0.372
133	Jg 5 - Py 3 - 03	0.000	0.026	0.014	6.0	0.000	0.000	0.000	0.000	0.717	0.004	0.003	4.3	0.000	0.000	0.004	0.048	0.044	0.086
134	Jg 5 - Py 3 - 04	0.001	0.023	0.021	15	0.002	0.000	0.000	0.000	1.7	0.032	0.004	33	0.000	0.000	0.084	1.5	1.4	3.0
135	Jg 5 - Py 3 - 05	0.003	0.021	0.056	75	0.000	0.001	0.003	0.000	1.8	0.108	0.036	131	0.000	0.007	2.0	31	30	68
136	Jg 5 - Py 3 - 06	0.000	0.037	0.107	14	0.000	0.001	0.017	0.000	1.5	0.045	0.053	36	0.000	0.001	11	167	181	392
137	Jg 5 - Py 3 - 07	0.000	0.024	0.042	7.7	0.000	0.000	0.004	0.000	1.6	0.017	0.018	34	0.000	0.000	2.2	28	30	67
138	Jg 5 - Py 3 - 08	0.000	0.026	0.074	5.3	0.000	0.000	0.000	0.000	0.197	0.014	0.002	19	0.000	0.001	0.063	0.812	0.910	1.9
139	Jg 5 - Py 4 - 01	0.000	0.024	0.013	0.124	0.000	0.000	0.000	0.000	0.274	0.000	0.002	0.257	0.000	0.000	0.004	0.007	0.005	0.023
140	Jg 5 - Py 4 - 02	0.000	0.028	0.014	0.077	0.000	0.000	0.009	0.000	0.011	0.001	0.004	0.597	0.000	0.001	0.004	0.032	0.029	0.076
141	Jg 5 - Py 4 - 03	0.001	0.026	0.008	0.075	0.000	0.000	0.000	0.000	0.002	0.000	0.003	0.004	0.000	0.000	0.002	0.003	0.003	0.004
142	Jg 5 - Py 4 - 04	0.001	0.017	0.014	0.510	0.000	0.000	0.000	0.000	0.038	0.001	0.003	3.2	0.000	0.000	0.064	1.1	1.1	2.3
143	Jg 5 - Py 4 - 05	0.000	0.016	0.033	12	0.000	0.000	0.000	0.000	0.920	0.027	0.003	33	0.000	0.000	0.032	0.709	0.728	1.7
144	Jg 5 - Py 4 - 06	0.001	0.028	0.091	55	0.000	0.000	0.001	0.000	0.968	0.061	0.007	115	0.000	0.001	2.0	30	31	68
145	Jg 5 - Py 4 - 07	0.000	0.021	0.010	14	0.000	0.000	0.000	0.000	0.186	0.024	0.003	38	0.000	0.000	0.620	7.9	8.4	18
146	Jg 5 - Py 4 - 08	0.002	0.019	0.021	4.0	0.000	0.000	0.005	0.000	0.112	0.009	0.032	12	0.000	0.000	0.250	3.3	3.4	7.7
147	Jg 3 - Py 1 - 01	0.000	0.024	0.018	0.075	0.127	0.000	0.001	0.000	0.002	0.000	0.002	0.055	0.008	0.053	0.004	0.039	0.010	0.014
148	Jg 3 - Py 1 - 02	0.000	0.025	0.017	0.082	0.229	0.000	0.001	0.000	0.003	0.000	0.002	0.037	0.004	0.059	0.004	0.030	0.005	0.009
149	Jg 3 - Py 1 - 03	0.000	0.022	0.015	0.063	0.000	0.000	0.003	0.000	0.002	0.002	0.005	0.002	0.000	0.001	0.003	0.007	0.003	0.009
150	Jg 3 - Py 1 - 04	0.000	0.020	0.016	0.079	0.000	0.000	0.003	0.000	0.001	0.000	0.001	0.133	0.000	0.000	0.004	0.004	0.006	0.009
151	Jg 3 - Py 1 - 05	0.008	0.029	0.013	0.092	0.752	0.002	0.003	0.000	0.002	0.002	0.007	0.727	8.6	0.534	0.004	0.230	0.054	0.959
152	Jg 3 - Py 1 - 06	0.004	0.025	0.016	0.073	0.212	0.001	0.001	0.000	0.000	0.000	0.007	0.048	0.005	0.069	0.005	0.049	0.013	0.024
153	Jg 3 - Py 1 - 07	0.001	0.031	0.047	0.085	0.000	0.002	0.067	0.000	0.007	0.002	0.004	2.5	0.000	0.015	0.007	0.111	0.113	0.221
154	Jg 3 - Py 2 - 01	0.001	0.031	0.019	0.504	0.004	0.001	0.001	0.000	0.003	0.000	0.002	1.3	0.000	0.002	0.005	0.091	0.090	0.195
155	Jg 3 - Py 2 - 02	0.005	0.025	0.029	2.7	0.006	0.000	0.006	0.000	0.001	0.010	0.011	18	0.000	0.000	0.078	1.3	1.3	2.9

#	Pyrite	^{115}In	^{118}Sn	^{121}Sb	^{125}Te	^{178}Hf	^{181}Ta	^{182}W	^{193}Ir	^{195}Pt	^{197}Au	^{205}Tl	^{209}Bi	^{232}Th	^{238}U	^{204}Pb	^{206}Pb	^{207}Pb	^{208}Pb
156	Jg 3 - Py 2 - 03	0.000	0.020	0.012	0.075	0.000	0.000	0.000	0.000	0.003	0.001	0.009	0.014	0.001	0.001	0.005	0.003	0.005	0.008
157	Jg 3 - Py 2 - 04	0.000	0.024	0.012	0.086	0.000	0.000	0.001	0.000	0.002	0.001	0.008	0.001	0.000	0.000	0.004	0.007	0.012	0.011
158	Jg 3 - Py 2 - 05	0.001	0.021	0.019	0.048	0.000	0.000	0.001	0.000	0.001	0.001	0.002	0.010	0.000	0.000	0.004	0.001	0.000	0.006
159	Jg 3 - Py 2 - 06	0.002	0.019	0.010	0.512	0.000	0.000	0.000	0.001	0.038	0.001	0.003	1.5	0.000	0.001	0.019	0.400	0.389	0.898
160	Jg 3 - Py 3 - 01	0.000	0.019	0.009	0.067	0.002	0.000	0.000	0.000	0.004	0.001	0.002	0.106	0.000	0.000	0.017	0.386	0.269	0.571
161	Jg 3 - Py 3 - 02	0.000	0.022	0.015	1.7	0.000	0.000	0.001	0.000	0.002	0.003	0.005	4.9	0.000	0.008	0.238	4.9	3.7	8.0
162	Jg 3 - Py 3 - 03	0.001	0.024	0.134	0.159	0.000	0.001	0.001	0.000	0.004	0.003	0.003	2.4	0.000	0.000	0.036	0.535	0.542	1.2
163	Jg 3 - Py 3 - 04	0.000	0.028	0.012	0.095	0.000	0.000	0.000	0.000	0.002	0.001	0.003	0.003	0.000	0.006	0.041	1.9	0.950	1.7
164	Jg 3 - Py 3 - 05	0.001	0.023	0.012	0.040	0.000	0.001	0.001	0.000	0.000	0.000	0.003	0.007	0.001	0.000	0.003	0.048	0.033	0.059
165	Jg 3 - Py 3 - 06	0.000	0.021	0.014	0.046	0.000	0.000	0.004	0.000	0.000	0.000	0.002	0.051	0.000	0.000	0.003	0.003	0.005	0.004
166	Jg 3 - Py 4 - 01	0.000	0.023	0.012	0.066	0.000	0.000	0.001	0.000	0.004	0.000	0.003	0.002	0.000	0.000	0.003	0.005	0.003	0.009
167	Jg 3 - Py 4 - 02	0.002	0.024	0.009	0.071	0.000	0.000	0.000	0.000	0.004	0.003	0.003	0.101	0.000	0.000	0.004	0.026	0.022	0.057
168	Jg 3 - Py 4 - 03	0.000	0.022	0.010	0.081	0.000	0.000	0.001	0.000	0.000	0.000	0.004	0.001	0.000	0.000	0.004	0.065	0.065	0.145
169	Jg 3 - Py 4 - 04	0.000	0.015	0.010	0.054	0.000	0.000	0.001	0.000	0.008	0.000	0.006	0.066	0.000	0.000	0.003	0.005	0.005	0.008
170	Jg 3 - Py 4 - 05	0.000	0.026	0.027	0.107	0.000	0.000	0.000	0.000	0.009	0.000	0.002	0.033	0.001	0.001	0.003	0.010	0.006	0.024
171	Jg 3 - Py 4 - 06	0.000	0.027	0.249	0.178	0.000	0.000	0.001	0.000	0.015	0.000	0.002	0.016	0.002	0.098	0.017	0.475	0.359	0.832
	Mean (n=171)	0.001	0.032	0.029	5.2	0.008	0.000	0.002	0.000	0.101	0.008	0.004	26	0.051	0.011	0.398	5.8	6.1	14
	SD	0.002	0.052	0.063	25	0.062	0.000	0.012	0.000	0.404	0.020	0.006	155	0.652	0.056	2.9	42	45	101
	Median	0.000	0.025	0.013	0.264	0.000	0.000	0.000	0.000	0.005	0.001	0.003	0.903	0.000	0.000	0.005	0.026	0.016	0.024
	Max	0.022	0.667	0.597	317	0.752	0.002	0.140	0.001	4.0	0.139	0.053	1909	8.6	0.534	36	529	556	1269
	Min	0.000	0.015	0.006	0.036	0.000	0.000	0.000	0.000	0.000	0.000	0.001	0.001	0.000	0.000	0.002	0.000	0.000	0.001

#	Sphalerite	^{115}In	^{118}Sn	^{121}Sb	^{125}Te	^{178}Hf	^{181}Ta	^{182}W	^{193}Ir	^{195}Pt	^{197}Au	^{205}Tl	^{209}Bi	^{232}Th	^{238}U	^{204}Pb	^{206}Pb	^{207}Pb	^{208}Pb
1	Jg 9a - Sp 1 - 01	2.2	0.118	0.009	0.153	0.000	0.001	0.000	0.000	0.002	0.001	0.003	5.4	0.007	0.001	0.127	1.7	1.9	4.0
2	Jg 9a - Sp 1 - 02	2.3	0.175	0.015	0.072	0.000	0.004	0.000	0.001	0.001	0.001	0.002	0.297	0.001	0.000	0.008	0.003	0.014	0.011
3	Jg 9a - Sp 1 - 03	2.2	0.134	0.013	0.088	0.000	0.000	0.000	0.000	0.000	0.001	0.003	0.597	0.003	0.000	0.010	0.034	0.043	0.085
4	Jg 9a - Sp 1 - 04	2.2	0.190	0.010	0.170	0.002	0.000	0.000	0.000	0.001	0.002	0.003	0.869	0.005	0.000	0.005	0.059	0.059	0.133
5	Jg 9a - Sp 1 - 05	2.2	0.268	0.021	0.142	0.002	0.001	0.002	0.000	0.000	0.001	0.008	0.350	0.004	0.000	0.005	0.019	0.017	0.047
6	Jg 9a - Sp 1 - 06	2.2	0.313	0.007	0.145	0.000	0.000	0.002	0.000	0.000	0.001	0.004	0.214	0.010	0.003	0.007	0.010	0.007	0.010
7	Jg 9a - Sp 1 - 07	2.2	0.262	0.011	0.086	0.000	0.000	0.000	0.001	0.000	0.002	0.003	0.347	0.000	0.000	0.006	0.065	0.093	0.164
8	Jg 9a - Sp 1 - 08	2.2	0.258	0.008	0.144	0.000	0.000	0.002	0.000	0.000	0.003	0.006	0.194	0.004	0.006	0.007	0.006	0.006	0.010
9	Jg 9a - Sp 1 - 09	2.3	0.164	0.007	0.102	0.000	0.000	0.000	0.000	0.000	0.001	0.004	0.106	0.002	0.000	0.007	0.006	0.007	0.010
10	Jg 9a - Sp 1 - 10	2.2	0.115	0.010	0.065	0.000	0.001	0.002	0.000	0.000	0.000	0.006	0.096	0.000	0.000	0.006	0.006	0.001	0.007
11	Jg 9a - Sp 1 - 11	2.3	0.198	0.011	0.093	0.003	0.000	0.000	0.000	0.000	0.001	0.011	0.140	0.001	0.000	0.005	0.006	0.011	0.020
12	Jg 9a - Sp 1 - 12	2.2	0.132	0.008	0.105	0.003	0.000	0.000	0.000	0.001	0.003	0.002	1.1	0.002	0.000	0.031	0.355	0.380	0.857
13	Jg 9a - Sp 2 - 01	2.1	0.178	0.009	0.099	0.000	0.000	0.000	0.000	0.000	0.001	0.002	1.0	0.000	0.000	0.030	0.403	0.453	0.965
14	Jg 9a - Sp 2 - 02	2.2	0.197	0.008	0.109	0.000	0.000	0.000	0.000	0.000	0.001	0.002	1.3	0.000	0.000	0.039	0.580	0.622	1.4
15	Jg 9a - Sp 2 - 03	2.1	0.170	0.009	0.039	0.000	0.000	0.000	0.000	0.000	0.003	0.003	1.2	0.000	0.000	0.016	0.267	0.306	0.655
16	Jg 9a - Sp 2 - 04	1.9	0.123	0.009	0.384	0.000	0.000	0.000	0.000	0.001	0.005	0.006	11	0.000	0.000	0.259	3.7	3.8	8.6
17	Jg 9a - Sp 2 - 05	2.1	0.094	0.010	0.135	0.000	0.000	0.000	0.000	0.000	0.001	0.001	2.4	0.001	0.000	0.050	0.659	0.685	1.5
18	Jg 9a - Sp 2 - 06	2.1	0.160	0.015	0.138	0.000	0.000	0.000	0.000	0.000	0.003	0.001	4.4	0.001	0.001	0.121	1.7	1.7	3.9
19	Jg 9a - Sp 2 - 07	2.2	0.118	0.012	0.082	0.000	0.000	0.000	0.000	0.000	0.002	0.002	1.6	0.000	0.002	0.023	0.378	0.411	0.933
20	Jg 9a - Sp 2 - 08	2.1	0.142	0.008	0.074	0.002	0.001	0.000	0.000	0.000	0.001	0.002	0.994	0.001	0.000	0.014	0.248	0.256	0.581
21	Jg 9a - Sp 2 - 09	2.2	0.180	0.008	0.044	0.000	0.000	0.000	0.000	0.000	0.005	0.003	2.7	0.000	0.000	0.060	0.948	1.0	2.2
22	Jg 9a - Sp 3 - 01	2.2	0.129	0.011	0.153	0.006	0.000	0.002	0.000	0.000	0.001	0.001	0.919	0.002	0.003	0.009	0.230	0.245	0.515
23	Jg 9a - Sp 3 - 02	2.3	0.239	0.010	0.058	0.000	0.000	0.000	0.000	0.000	0.000	0.003	0.122	0.001	0.001	0.009	0.015	0.016	0.046
24	Jg 9a - Sp 3 - 03	2.3	0.193	0.032	0.113	0.003	0.000	0.000	0.000	0.001	0.002	0.005	0.143	0.004	0.002	0.009	0.039	0.033	0.078
25	Jg 9a - Sp 3 - 04	2.1	0.139	0.008	0.072	0.000	0.000	0.000	0.000	0.000	0.001	0.003	0.955	0.000	0.000	0.030	0.444	0.435	0.933
26	Jg 9a - Sp 3 - 05	2.3	0.199	0.008	0.067	0.000	0.000	0.002	0.000	0.000	0.001	0.002	0.098	0.000	0.000	0.009	0.008	0.006	0.017
27	Jg 9a - Sp 3 - 06	2.3	0.226	0.010	0.139	0.005	0.000	0.000	0.000	0.000	0.000	0.002	0.549	0.001	0.003	0.023	0.233	0.268	0.598
28	Jg 9a - Sp 3 - 07	2.2	0.168	0.007	0.064	0.000	0.000	0.000	0.000	0.000	0.001	0.001	1.7	0.002	0.000	0.028	0.438	0.463	1.0
29	Jg 9a - Sp 3 - 08	2.2	0.128	0.006	0.064	0.003	0.000	0.000	0.002	0.000	0.001	0.001	1.3	0.014	0.002	0.045	0.502	0.573	1.2
30	Jg 9a - Sp 3 - 09	2.3	0.117	0.012	0.125	0.000	0.000	0.000	0.002	0.000	0.000	0.001	0.543	0.000	0.000	0.021	0.037	0.040	0.091
31	Jg 9a - Sp 3 - 10	2.3	0.141	0.007	0.104	0.006	0.000	0.000	0.000	0.000	0.001	0.001	1.0	0.004	0.001	0.012	0.224	0.245	0.494
32	Jg 9a - Sp 3 - 11	2.2	0.198	0.010	0.080	0.000	0.000	0.000	0.000	0.000	0.001	0.002	0.501	0.000	0.000	0.012	0.113	0.111	0.270
33	Jg 9a - Sp 4 - 01	2.1	0.602	0.013	0.350	0.000	0.000	0.000	0.000	0.000	0.022	0.023	9.3	0.005	0.037	0.372	5.8	5.8	13
34	Jg 9a - Sp 4 - 02	2.2	0.568	0.013	0.149	0.000	0.001	0.000	0.000	0.000	0.005	0.001	5.8	0.000	0.000	0.127	1.8	2.0	4.3
35	Jg 9a - Sp 4 - 03	2.3	0.545	0.023	0.114	0.014	0.000	0.002	0.000	0.001	0.002	0.006	5.1	0.000	0.000	0.110	2.1	2.1	4.7
36	Jg 9a - Sp 4 - 04	2.2	0.284	0.015	0.098	0.000	0.000	0.000	0.000	0.001	0.001	0.004	1.4	0.002	0.002	0.061	0.642	0.733	1.5
37	Jg 9a - Sp 4 - 05	2.2	0.247	0.011	0.127	0.000	0.000	0.000	0.000	0.001	0.001	0.006	0.055	0.000	0.000	0.010	0.007	0.004	0.017
38	Jg 9a - Sp 4 - 06	2.2	0.244	0.010	0.144	0.003	0.000	0.000	0.000	0.001	0.002	0.003	0.088	0.001	0.002	0.010	0.012	0.012	0.018
39	Jg 9a - Sp 4 - 07	2.3	0.215	0.016	0.155	0.000	0.001	0.000	0.000	0.001	0.002	0.003	0.462	0.003	0.000	0.019	0.152	0.148	0.386
40	Jg 9a - Sp 4 - 08	2.1	0.192	0.018	0.082	0.000	0.000	0.000	0.000	0.001	0.004	0.003	0.839	0.006	0.003	0.032	0.352	0.369	0.875
41	Jg 9a - Sp 4 - 09	2.2	0.154	0.012	0.129	0.000	0.000	0.000	0.000	0.001	0.004	0.004	3.4	0.003	0.003	0.102	1.4	1.6	3.3
42	Jg 9a - Sp 4 - 10	2.3	0.835	0.013	0.139	0.006	0.000	0.000	0.000	0.001	0.006	0.006	3.5	0.017	0.002	0.107	1.5	1.6	3.6
	Mean (n=42)	2.2	0.225	0.012	0.119	0.001	0.000	0.000	0.000	0.000	0.002	0.004	1.8	0.003	0.002	0.047	0.646	0.680	1.5
	SD	0.086	0.149	0.005	0.066	0.003	0.001	0.001	0.000	0.001	0.003	0.004	2.4	0.004	0.006	0.072	1.1	1.1	2.5
	Median	2.2	0.185	0.010	0.107	0.000	0.000	0.000	0.000	0.000	0.001	0.003	0.937	0.001	0.000	0.020	0.240	0.262	0.590
	Max	2.3	0.835	0.032	0.384	0.014	0.004	0.002	0.002	0.002	0.022	0.023	11	0.017	0.037	0.372	5.8	5.8	13
	Min	1.9	0.094	0.006	0.039	0.000	0.000	0.000	0.000	0.000	0.000	0.001	0.055	0.000	0.000	0.005	0.003	0.001	0.007

#	Pentlandite	^{115}In	^{118}Sn	^{121}Sb	^{125}Te	^{178}Hf	^{181}Ta	^{182}W	^{193}Ir	^{195}Pt	^{197}Au	^{205}Tl	^{209}Bi	^{232}Th	^{238}U	^{204}Pb	^{206}Pb	^{207}Pb	^{208}Pb
1	Jg 9a - Pn 1 - 01	0.026	1.2	0.162	15	0.281	0.022	0.179	0.000	0.001	0.030	0.123	4.2	0.257	0.100	0.104	1.8	1.9	4.1
2	Jg 9a - Pn 1 - 02	0.009	1.6	0.047	17	0.152	0.063	0.076	0.000	0.001	0.150	0.542	17	0.572	0.265	0.660	11	11	24
3	Jg 9a - Pn 1 - 03	0.001	0.213	0.042	13	0.042	0.000	0.081	0.000	0.001	0.129	0.809	22	0.043	0.128	0.478	7.5	7.1	16
4	Jg 9a - Pn 1 - 04	0.001	0.025	0.016	5.0	0.000	0.000	0.000	0.000	0.001	0.020	0.045	2.1	0.001	0.000	0.009	0.268	0.261	0.603
5	Jg 9a - Pn 1 - 05	0.000	0.051	0.017	6.7	0.012	0.000	0.000	0.001	0.001	0.028	0.051	4.0	0.010	0.043	0.037	0.682	0.699	1.5
6	Jg 9a - Pn 1 - 06	0.000	0.086	0.019	7.4	0.003	0.002	0.002	0.000	0.001	0.026	0.045	2.5	0.006	0.003	0.013	0.226	0.245	0.546
7	Jg 9a - Pn 1 - 07	0.000	0.070	0.027	5.7	0.011	0.002	0.024	0.000	0.001	0.035	0.180	6.5	0.004	0.005	0.078	1.2	1.3	2.5
8	Jg 9a - Pn 1 - 08	0.000	0.101	0.027	5.5	0.017	0.000	0.025	0.000	0.000	0.063	0.371	9.8	0.020	0.032	0.124	2.1	2.2	4.7
9	Jg 9a - Pn 1 - 09	0.000	0.024	0.022	11	0.000	0.000	0.000	0.000	0.000	0.009	0.089	6.3	0.005	0.000	0.055	0.954	0.957	2.2
10	Jg 9a - Pn 1 - 10	0.001	0.151	0.016	14	0.011	0.003	0.011	0.000	0.000	0.031	0.261	7.2	0.222	0.237	0.501	8.0	7.8	16
11	Jg 9a - Pn 2 - 01	0.000	0.034	0.025	6.7	0.008	0.013	0.014	0.000	0.001	0.065	0.281	10	0.011	0.193	0.482	7.8	8.0	17
12	Jg 9a - Pn 2 - 02	0.001	0.112	0.161	13	0.003	0.001	0.012	0.002	0.002	0.131	0.518	118	0.025	0.320	1.6	25	25	56
13	Jg 9a - Pn 2 - 03	0.000	0.024	0.017	2.6	0.000	0.000	0.002	0.000	0.001	0.016	0.070	2.0	0.002	0.019	0.030	0.386	0.395	0.876
14	Jg 9a - Pn 2 - 04	0.001	0.104	0.063	6.9	0.032	0.003	0.049	0.000	0.000	0.024	0.447	16	0.196	0.319	0.979	16	16	35
15	Jg 9a - Pn 2 - 05	0.002	0.421	0.031	6.0	0.039	0.025	0.045	0.000	0.000	0.030	0.250	5.4	0.076	0.124	0.309	4.4	4.6	9.7
16	Jg 9a - Pn 2 - 06	0.001	0.027	0.006	3.7	0.005	0.000	0.002	0.000	0.000	0.008	0.032	1.8	0.001	0.002	0.017	0.259	0.282	0.589
17	Jg 9a - Pn 2 - 07	0.002	0.202	0.022	3.0	0.006	0.018	0.014	0.000	0.001	0.072	0.107	3.7	0.065	0.525	0.094	1.7	1.6	3.7
18	Jg 9a - Pn 2 - 08	0.002	0.290	0.026	6.2	0.016	0.004	0.030	0.000	0.002	0.301	0.402	16	0.016	0.139	0.372	5.9	6.1	14
19	Jg 9a - Pn 2 - 09	0.006	0.345	0.015	5.2	0.008	0.017	0.008	0.000	0.007	0.021	0.040	3.0	0.007	0.011	0.018	0.361	0.385	0.819
20	Jg 9a - Pn 3 - 01	0.007	8.1	0.089	26	0.610	0.158	0.213	0.000	0.001	0.042	0.222	11	1.0	0.525	0.453	6.5	7.1	14
21	Jg 9a - Pn 3 - 02	0.001	1.3	0.014	17	0.024	0.187	0.023	0.000	0.000	0.077	0.178	8.6	0.065	0.096	0.310	3.8	4.0	8.9
22	Jg 9a - Pn 3 - 03	0.018	1.7	0.015	1.000	0.028	0.021	0.000	0.000	0.000	0.031	0.094	2.0	0.056	0.013	0.027	0.367	0.461	0.991
23	Jg 9a - Pn 3 - 04	0.001	2.3	0.025	2.5	0.109	0.022	0.033	0.001	0.002	0.016	0.090	1.9	0.123	0.070	0.016	0.455	0.573	1.1
24	Jg 9a - Pn 3 - 05	0.001	1.6	0.010	5.2	0.148	0.002	0.005	0.000	0.002	0.015	0.056	2.9	0.073	0.216	0.124	2.2	2.2	4.7
25	Jg 9a - Pn 3 - 06	0.016	3.2	0.018	3.2	0.171	0.032	0.008	0.000	0.002	0.015	0.136	2.5	0.366	0.157	0.120	1.8	1.9	4.1
26	Jg 9a - Pn 3 - 07	0.089	14	0.140	4.4	0.662	0.868	0.939	0.000	0.007	0.077	1.1	20	2.5	0.975	0.633	10	10	23
27	Jg 9a - Pn 3 - 08	0.001	0.734	0.016	4.7	0.006	0.000	0.000	0.000	0.002	0.005	0.067	2.8	0.003	0.006	0.123	1.7	1.8	3.8
28	Jg 5 - Pn 1 - 01	0.002	0.033	0.014	55	0.000	0.002	0.028	0.001	0.001	0.006	0.059	6.3	0.003	0.001	0.030	0.694	0.719	1.5
29	Jg 5 - Pn 1 - 02	0.001	0.066	0.038	37	0.000	0.001	0.115	0.000	0.001	0.002	0.230	5.8	0.016	0.057	0.234	3.9	3.8	8.7
30	Jg 5 - Pn 1 - 03	0.001	0.094	0.065	51	0.006	0.002	0.022	0.001	0.001	0.017	0.278	14	0.012	0.252	0.328	5.5	5.8	13
31	Jg 5 - Pn 1 - 04	0.002	0.091	0.065	53	0.003	0.002	0.036	0.000	0.001	0.024	0.354	11	0.017	0.095	0.229	3.4	3.5	7.9
32	Jg 5 - Pn 1 - 05	0.002	0.120	0.275	101	0.000	0.001	0.024	0.000	0.007	0.173	0.473	130	0.008	0.227	1.4	21	22	48
33	Jg 5 - Pn 1 - 06	0.003	0.028	0.039	29	0.000	0.001	0.022	0.000	0.001	0.046	0.368	12	0.009	0.057	0.322	4.8	5.1	11
34	Jg 5 - Pn 2 - 01	0.002	0.022	2.9	43	0.000	0.000	0.014	0.000	0.001	0.314	0.608	833	0.001	0.015	2.5	37	40	89
35	Jg 5 - Pn 2 - 02	0.000	0.051	4.4	63	0.000	0.000	0.004	0.000	0.001	0.429	0.631	1265	0.002	0.005	3.4	50	54	118
36	Jg 5 - Pn 2 - 03	0.000	0.053	4.6	81	0.000	0.001	0.001	0.000	0.001	0.527	0.887	1691	0.002	0.000	5.4	78	83	184
37	Jg 5 - Pn 2 - 04	0.000	0.062	4.0	74	0.002	0.000	0.006	0.000	0.001	0.577	0.855	1594	0.001	0.000	5.3	78	83	185
38	Jg 5 - Pn 3 - 01	0.001	0.015	0.635	131	0.000	0.000	0.005	0.000	0.001	0.255	0.718	519	0.000	0.082	2.6	38	40	88
39	Jg 5 - Pn 3 - 02	0.001	0.021	0.029	13	0.000	0.000	0.008	0.000	0.001	0.025	0.328	5.9	0.001	0.136	0.723	12	12	25
40	Jg 5 - Pn 3 - 03	0.001	0.144	0.069	5.2	0.000	0.001	0.006	0.000	0.000	0.032	0.426	8.1	0.014	0.418	0.846	12	13	28
41	Jg 5 - Pn 3 - 04	0.001	0.026	0.016	5.1	0.000	0.000	0.000	0.000	0.001	0.001	0.034	1.1	0.000	0.000	0.071	0.983	1.0	2.3
42	Jg 5 - Pn 3 - 05	0.001	0.023	0.014	11	0.000	0.000	0.000	0.000	0.000	0.002	0.098	2.5	0.000	0.003	0.063	1.1	1.1	2.4
43	Jg 5 - Pn 3 - 06	0.002	0.016	0.571	163	0.000	0.000	0.000	0.000	0.001	0.148	0.809	768	0.000	0.000	3.3	49	52	115
44	Jg 5 - Pn 3 - 07	0.001	0.024	0.241	80	0.000	0.000	0.001	0.000	0.000	0.136	0.545	299	0.001	0.112	1.6	24	25	54
45	Jg 5 - Pn 4 - 01	0.000	0.036	0.282	51	0.000	0.000	0.001	0.000	0.042	0.159	0.248	327	0.000	0.008	10	157	166	379
46	Jg 5 - Pn 4 - 02	0.000	0.017	0.711	97	0.002	0.000	0.001	0.000	0.011	0.245	0.537	717	0.000	0.012	2.6	37	39	88
47	Jg 5 - Pn 4 - 03	0.000	0.016	0.971	131	0.000	0.000	0.002	0.000	0.035	0.201	0.595	1058	0.000	0.002	4.4	63	67	151
48	Jg 5 - Pn 4 - 04	0.000	0.018	0.529	88	0.000	0.000	0.000	0.000	0.026	0.118	0.504	720	0.001	0.001	2.5	36	38	87
49	Jg 5 - Pn 4 - 05	0.000	1.3	0.048	29	0.005	0.001	0.006	0.000	0.001	0.005	0.285	15	0.002	0.040	0.446	7.0	7.0	15
50	Jg 5 - Pn 4 - 06	0.012	0.037	0.023	12	0.003	0.000	0.004	0.000	0.002	0.006	0.107	8.7	0.002	0.010	3.3	51	62	179
51	Jg 5 - Pn 4 - 07	0.004	0.031	0.020	18	0.000	0.000	0.006	0.003	0.002	0.008	0.104	13	0.001	0.002	0.091	1.2	1.4	2.9
52	Jg 5 - Pn 4 - 08	0.001	0.039	0.014	30	0.000	0.000	0.004	0.001	0.003	0.009	0.228	17	0.002	0.000	0.237	3.4	3.6	7.4
53	Jg 5 - Pn 4 - 09	0.001	0.034	0.014	10	0.003	0.000	0.002	0.000	0.003	0.003	0.047	1.5	0.002	0.001	0.022	0.524	0.551	1.3
	Mean (n=53)	0.004	0.755	0.409	32	0.046	0.028	0.040	0.000	0.003	0.093	0.321	195	0.110	0.114	1.1	17	18	41
	SD	0.013	2.2	1.1	39	0.129	0.122	0.133	0.001	0.008	0.131	0.268	414	0.374	0.179	1.9	28	30	69
	Median	0.001	0.066	0.029	13	0.003	0.001	0.006	0.000	0.001	0.031	0.250	9.8	0.006	0.040	0.322	4.8	5.1	11
	Max	0.089	14	4.6	163	0.662	0.868	0.939	0.003	0.042	0.577	1.1	1691	2.5	0.975	10	157	166	379
	Min	0.000	0.015	0.006	1.000	0.000	0.000	0.000	0.000	0.000	0.001	0.032	1.1	0.000	0.000	0.009	0.226	0.245	0.546

#	Violarite/Bravoite	^{115}In	^{118}Sn	^{121}Sb	^{125}Te	^{178}Hf	^{181}Ta	^{182}W	^{193}Ir	^{195}Pt	^{197}Au	^{205}Tl	^{209}Bi	^{232}Th	^{238}U	^{204}Pb	^{206}Pb	^{207}Pb	^{208}Pb
1	Jg 9a - Pn 1 exs - 01	0.000	0.063	0.462	76	0.000	0.000	0.000	0.000	0.007	0.229	0.520	653	0.000	0.002	2.0	30	31	69
2	Jg 9a - Pn 1 exs - 02	0.001	0.055	0.410	68	0.002	0.000	0.000	0.000	0.008	0.184	0.369	555	0.001	0.000	1.9	28	30	65
3	Jg 9a - Pn 1 exs - 03	0.000	0.061	0.445	92	0.000	0.000	0.000	0.000	0.015	0.213	0.638	778	0.000	0.000	2.6	38	41	89
4	Jg 9a - Pn 1 exs - 04	0.000	0.080	0.399	69	0.000	0.000	0.000	0.000	0.008	0.223	0.298	547	0.001	0.000	1.8	26	27	60
5	Jg 9a - Pn 1 exs - 05	0.000	0.109	0.672	120	0.000	0.000	0.003	0.000	0.024	0.363	0.468	996	0.000	0.000	3.3	49	51	114
6	Jg 9a - Pn 1 exs - 06	0.000	0.239	0.463	69	0.000	0.000	0.000	0.000	0.010	0.219	0.374	538	0.002	0.017	3.1	42	44	98
7	Jg 9a - Pn 1 exs - 07	0.000	0.054	0.532	114	0.002	0.000	0.000	0.000	0.011	0.262	0.721	844	0.001	0.000	3.1	46	48	107
8	Jg 9a - Pn 1 exs - 08	0.000	0.026	0.431	117	0.002	0.000	0.000	0.000	0.018	0.227	0.852	764	0.001	0.001	3.0	45	47	105
9	Jg 9a - Pn 2 exs - 01	0.002	0.180	1.6	119	0.000	0.000	0.000	0.000	0.008	0.508	1.1	1555	0.005	0.002	3.8	57	60	133
10	Jg 9a - Pn 2 exs - 02	0.002	0.069	1.3	88	0.000	0.000	0.006	0.000	0.008	0.427	0.645	1134	0.000	0.001	2.6	38	40	89
11	Jg 9a - Pn 2 exs - 03	0.002	0.090	1.5	108	0.000	0.000	0.000	0.000	0.006	0.533	0.812	1400	0.000	0.004	3.2	47	49	109
12	Jg 9a - Pn 2 exs - 04	0.002	0.059	0.258	33	0.000	0.000	0.000	0.000	0.002	0.131	0.247	363	0.001	0.000	0.997	15	16	35
13	Jg 9a - Pn 2 exs - 05	0.021	0.252	0.510	68	0.000	0.000	0.000	0.000	0.005	0.252	0.533	757	0.000	0.000	3.0	44	47	104
14	Jg 9a - Pn 2 exs - 06	0.009	0.185	0.636	77	0.000	0.000	0.029	0.000	0.012	0.285	0.537	782	0.001	0.013	4.7	68	73	163
15	Jg 9a - Pn 2 exs - 07	0.022	0.227	0.779	93	0.000	0.000	0.001	0.000	0.015	0.421	0.493	894	0.000	0.000	13	215	225	477
16	Jg 9a - Pn 2 exs - 08	0.004	0.074	0.537	87	0.000	0.000	0.001	0.000	0.012	0.245	1.1	893	0.001	0.043	3.0	45	47	105
17	Jg 9a - Pn 3 exs - 01	0.021	1.3	0.412	68	0.002	0.000	0.002	0.000	0.004	0.104	0.142	481	0.002	0.001	2.3	34	36	80
18	Jg 9a - Pn 3 exs - 02	0.023	1.2	0.460	75	0.000	0.000	0.000	0.000	0.001	0.121	0.099	527	0.001	0.001	2.4	35	38	84
19	Jg 9a - Pn 3 exs - 03	0.020	1.3	0.557	97	0.000	0.000	0.002	0.000	0.007	0.203	0.361	744	0.003	0.001	3.3	49	53	117
20	Jg 9a - Pn 3 exs - 04	0.005	0.694	0.306	85	0.003	0.000	0.000	0.000	0.001	0.274	0.648	615	0.006	0.008	1.6	26	27	60
21	Jg 9a - Pn 3 exs - 05	0.016	1.4	0.341	105	0.013	0.002	0.002	0.001	0.007	0.963	0.989	771	0.045	0.011	3.0	44	46	102
22	Jg 9a - Pn 3 exs - 06	0.006	0.540	0.386	140	0.006	0.000	0.002	0.000	0.007	0.238	1.2	988	0.009	0.005	3.2	48	50	112
23	Jg 9a - Pn 4 exs - 01	0.002	0.054	1.1	84	0.003	0.000	0.000	0.000	0.005	0.441	0.911	1133	0.004	0.041	4.0	61	64	143
24	Jg 9a - Pn 4 exs - 02	0.000	0.401	0.386	30	0.000	0.002	0.004	0.000	0.007	0.223	0.367	358	0.056	0.218	1.2	17	17	39
25	Jg 9a - Pn 4 exs - 03	0.002	0.219	0.230	16	0.000	0.000	0.009	0.000	0.001	0.188	0.520	187	0.007	0.366	1.3	19	20	45
26	Jg 9a - Pn 4 exs - 04	0.000	0.099	0.444	17	0.000	0.003	0.015	0.000	0.009	0.345	0.456	265	0.023	0.480	2.2	35	36	79
27	Jg 9a - Pn 4 exs - 05	0.000	0.103	0.190	14	0.059	0.000	0.016	0.000	0.001	0.261	0.469	214	0.036	0.628	2.2	34	35	78
28	Jg 9a - Pn 4 exs - 06	0.006	0.109	1.1	54	0.012	0.000	0.007	0.000	0.003	0.446	0.923	1153	0.013	0.257	4.1	60	63	141
29	Jg 9a - Pn 4 exs - 07	0.013	0.186	1.5	67	0.003	0.000	0.000	0.000	0.009	0.643	0.933	1484	0.014	0.082	4.3	64	65	150
30	Jg 9a - Pn 4 exs - 08	0.013	0.078	1.0	53	0.000	0.003	0.007	0.002	0.009	0.385	1.1	1179	0.030	0.147	3.4	52	54	120
31	Jg 9a - Pn 4 exs - 09	0.006	0.466	0.206	11	0.036	0.005	0.028	0.000	0.001	0.244	0.527	183	0.088	0.275	1.5	25	26	57
32	Jg 9a - Pn 4 exs - 10	0.021	0.236	0.731	34	0.009	0.008	0.007	0.000	0.008	0.328	0.706	903	0.016	0.030	4.1	61	64	146
	Mean (n=32)	0.007	0.318	0.634	73	0.005	0.001	0.004	0.000	0.008	0.317	0.627	770	0.011	0.082	3.1	47	49	109
	SD	0.008	0.404	0.398	34	0.012	0.002	0.008	0.000	0.005	0.172	0.294	367	0.020	0.157	2.1	34	35	75
	Median	0.002	0.145	0.463	76	0.000	0.000	0.001	0.000	0.007	0.257	0.535	768	0.002	0.004	3.0	44	46	103
	Max	0.023	1.4	1.6	140	0.059	0.008	0.029	0.002	0.024	0.963	1.2	1555	0.088	0.628	13	215	225	477
	Min	0.000	0.026	0.190	11	0.000	0.000	0.000	0.000	0.001	0.104	0.099	183	0.000	0.000	0.997	15	16	35

#	Chalcopyrite	^{115}In	^{118}Sn	^{121}Sb	^{125}Te	^{178}Hf	^{181}Ta	^{182}W	^{193}Ir	^{195}Pt	^{197}Au	^{205}Tl	^{209}Bi	^{232}Th	^{238}U	^{204}Pb	^{206}Pb	^{207}Pb	^{208}Pb
1	Jg 9a - Ccp 1 - 01	0.305	2.9	0.030	0.125	0.013	0.008	0.029	0.000	0.005	0.017	0.009	2.3	0.014	0.021	0.056	0.632	0.601	1.6
2	Jg 9a - Ccp 1 - 02	0.443	4.6	0.060	1.5	0.000	0.000	0.001	0.001	0.002	0.019	0.008	3.0	0.013	0.013	0.079	0.815	0.825	1.9
3	Jg 9a - Ccp 1 - 03	0.414	2.4	0.026	0.713	0.000	0.000	0.000	0.000	0.002	0.005	0.008	2.6	0.008	0.004	0.096	1.2	1.2	2.6
4	Jg 9a - Ccp 1 - 04	0.387	3.8	0.022	0.369	0.000	0.008	0.001	0.001	0.002	0.002	0.017	1.8	0.048	0.013	0.027	0.657	0.404	1.5
5	Jg 9a - Ccp 1 - 05	0.392	1.2	0.044	0.271	0.032	0.016	0.001	0.000	0.003	0.002	0.013	4.4	0.106	0.027	0.074	2.0	1.4	3.1
6	Jg 9a - Ccp 1 - 06	0.468	2.7	0.032	0.380	0.000	0.010	0.001	0.002	0.004	0.006	0.013	1.9	0.037	0.021	0.062	0.771	0.594	1.4
7	Jg 9a - Ccp 1 - 07	0.426	2.9	0.059	0.199	0.031	0.010	0.001	0.001	0.004	0.033	0.022	3.4	0.116	0.045	0.061	1.1	1.2	2.4
8	Jg 9a - Ccp 1 - 08	0.508	2.0	0.045	1.2	0.000	0.015	0.034	0.001	0.005	0.009	0.010	2.6	0.082	0.060	0.034	0.923	0.980	2.0
9	Jg 9a - Ccp 1 - 09	0.385	4.7	0.097	1.4	0.001	0.000	0.003	0.003	0.012	0.116	0.053	1.9	0.058	0.040	0.103	0.631	0.553	1.6
10	Jg 9a - Ccp 1 - 10	0.593	15	0.050	0.324	0.118	0.000	0.002	0.001	0.010	0.011	0.012	1.3	0.548	0.132	0.054	0.790	0.696	1.5
11	Jg 9a - Ccp 1 - 11	0.538	2.9	0.066	0.877	0.100	0.000	0.003	0.001	0.016	0.019	0.030	13	0.490	0.539	0.318	10	5.7	14
	Mean (n=11)	0.442	4.1	0.048	0.664	0.027	0.006	0.007	0.001	0.006	0.022	0.018	3.4	0.138	0.083	0.088	1.8	1.3	3.1
	SD	0.081	3.8	0.022	0.493	0.043	0.006	0.012	0.001	0.005	0.032	0.014	3.2	0.192	0.155	0.080	2.8	1.5	3.7
	Median	0.426	2.9	0.045	0.380	0.001	0.008	0.001	0.001	0.004	0.011	0.013	2.6	0.058	0.027	0.062	0.815	0.825	1.9
	Max	0.593	15	0.097	1.5	0.118	0.016	0.034	0.003	0.016	0.116	0.053	13	0.548	0.539	0.318	10	5.7	14
	Min	0.305	1.2	0.022	0.125	0.000	0.000	0.000	0.000	0.002	0.002	0.008	1.3	0.008	0.004	0.027	0.631	0.404	1.4

ESM Table 1b. LA-ICP-MS data for sulphides used for box-and-whisker plots (concentrations in ppm)

Pyrite	Co	Ni	Cu	As	Bi	Te	Ag	Au	Zn	Se	*In	Cd
1. Jg3a Py	5950	2012	0.322	292	0.055	0.075	0.002	0.000	0.823	7.8	0.005	0.003
1. Jg3a Py	5360	1924	0.391	301	0.037	0.082	0.002	0.000	0.846	8.3	0.003	0.008
1. Jg3a Py	5368	1823	0.699	318	0.002	0.063	0.006	0.002	1.2	7.7	0.003	0.008
1. Jg3a Py	5932	1973	0.492	268	0.133	0.079	0.007	0.000	0.972	8.0	0.003	0.008
1. Jg3a Py	5889	1944	0.414	253	0.727	0.092	0.016	0.002	1.3	9.2	0.008	0.028
1. Jg3a Py	6186	2026	0.335	258	0.048	0.073	0.011	0.000	0.713	8.4	0.009	0.014
1. Jg3a Py	5951	2047	0.709	333	2.5	0.085	0.031	0.002	4.3	7.8	0.008	0.017
1. Jg3a Py	6693	2129	0.960	406	1.3	0.504	0.014	0.000	1.2	8.8	0.003	0.009
1. Jg3a Py	6982	2146	6.6	435	18	2.7	0.050	0.010	3.2	8.7	0.005	0.033
1. Jg3a Py	6795	2123	0.489	403	0.014	0.075	0.004	0.001	0.885	9.5	0.003	0.002
1. Jg3a Py	6444	2027	0.597	388	0.001	0.086	0.004	0.001	0.750	8.4	0.010	0.002
1. Jg3a Py	6852	2148	0.314	420	0.010	0.048	0.002	0.001	0.888	8.1	0.007	0.002
1. Jg3a Py	5334	1184	0.929	643	1.5	0.512	0.015	0.001	0.997	7.2	0.004	0.002
1. Jg3a Py	7045	2198	138	574	0.106	0.067	0.739	0.001	0.856	7.7	0.003	0.006
1. Jg3a Py	7027	2052	61	591	4.9	1.7	0.047	0.003	1.7	8.9	0.003	0.002
1. Jg3a Py	7457	2216	2.2	635	2.4	0.159	0.018	0.003	3.7	7.4	0.003	0.002
1. Jg3a Py	7663	2279	0.787	628	0.003	0.095	0.005	0.001	0.741	8.8	0.002	0.007
1. Jg3a Py	7550	2153	0.335	597	0.007	0.040	0.002	0.000	0.878	8.0	0.003	0.001
1. Jg3a Py	7305	2180	0.414	661	0.051	0.046	0.009	0.000	0.872	9.5	0.002	0.001
1. Jg3a Py	6029	964	0.799	490	0.002	0.066	0.005	0.000	1.0	5.6	0.002	0.008
1. Jg3a Py	5329	916	4500	447	0.101	0.071	3.3	0.003	15	5.2	0.004	0.124
1. Jg3a Py	7052	2214	27	414	0.001	0.081	0.071	0.000	3.1	8.6	0.003	0.007
1. Jg3a Py	6934	2120	0.427	394	0.066	0.054	0.011	0.000	1.1	9.0	0.003	0.007
1. Jg3a Py	6746	2140	152	381	0.033	0.107	0.329	0.000	3.2	11	0.010	0.034
1. Jg3a Py	7506	3158	187	565	0.016	0.178	0.066	0.000	7.2	11	0.004	0.062
Mean (n=25)	6535	2004	203	444	1.3	0.288	0.190	0.001	2.3	8.4	0.004	0.016
SD	751	441	897	133	3.7	0.615	0.662	0.002	3.1	1.3	0.003	0.027
Median	6746	2120	0.709	414	0.051	0.081	0.011	0.001	1.0	8.4	0.003	0.007
Max	7663	3158	4500	661	18	2.7	3.3	0.010	15	11	0.010	0.124
Min	5329	916	0.314	253	0.001	0.040	0.002	0.000	0.713	5.2	0.002	0.001

Pyrite	Co	Ni	Cu	As	Bi	Te	Ag	Au	Zn	Se	*In	Cd
2. Jg5-9a Py	8196	1980	0.192	433	0.044	0.063	0.001	0.000	0.874	11	0.002	0.001
2. Jg5-9a Py	8436	2018	0.278	1007	0.079	0.082	0.007	0.000	0.972	11	0.002	0.008
2. Jg5-9a Py	6894	1819	0.220	929	0.099	0.082	0.007	0.000	0.943	14	0.002	0.001
2. Jg5-9a Py	6230	3335	0.331	969	2.2	0.337	0.027	0.002	2.1	13	0.002	0.051
2. Jg5-9a Py	469	13813	0.147	548	0.903	0.277	0.003	0.002	1.5	23	0.007	0.001
2. Jg5-9a Py	652	11612	0.312	1064	0.703	0.277	0.009	0.000	0.951	32	0.007	0.001
2. Jg5-9a Py	11674	1252	2147	1277	3.6	1.1	0.023	0.000	0.965	22	0.011	0.010
2. Jg5-9a Py	8032	1848	22	579	0.106	0.109	0.002	0.000	0.767	12	0.002	0.007
2. Jg5-9a Py	7126	1184	0.443	851	1.1	0.308	0.010	0.001	0.734	8.0	0.002	0.007
2. Jg5-9a Py	6543	1378	0.450	925	4.3	1.2	0.011	0.002	0.974	9.6	0.009	0.009
2. Jg5-9a Py	8236	1938	0.351	848	0.676	0.264	0.007	0.001	0.658	10	0.005	0.007
2. Jg5-9a Py	8702	1933	0.213	772	0.088	0.060	0.003	0.003	0.847	11	0.005	0.007
2. Jg5-9a Py	8052	1939	0.290	989	1.7	0.351	0.005	0.002	0.877	11	0.001	0.027
2. Jg5-9a Py	6926	513	0.155	945	0.091	0.078	0.003	0.000	0.830	5.5	0.001	0.007
2. Jg5-9a Py	7807	471	0.223	975	4.1	0.364	0.012	0.002	3.7	6.5	0.004	0.028
2. Jg5-9a Py	383	14083	0.217	2251	0.289	0.702	0.002	0.000	0.853	45	0.001	0.010
2. Jg5-9a Py	1034	15088	0.293	1337	6.5	17	0.066	0.025	3.3	38	0.001	0.064
2. Jg5-9a Py	1435	17058	1.9	1281	21	4.3	0.055	0.011	16	43	0.002	0.306
2. Jg5-9a Py	770	10905	1.1	1263	3.1	1.4	0.012	0.001	1.0	32	0.001	0.040

Pyrite	Co	Ni	Cu	As	Bi	Te	Ag	Au	Zn	Se	*In	Cd
2. Jg5-9a Py	7505	1803	0.335	965	0.092	0.061	0.009	0.000	0.749	11	0.003	0.006
2. Jg5-9a Py	3140	9009	2.8	1120	8.2	2.0	0.020	0.004	3.3	22	0.003	0.068
2. Jg5-9a Py	1300	21131	20	2200	4.3	6.0	0.001	0.004	1.1	54	0.003	0.015
2. Jg5-9a Py	3063	20337	47	1368	33	15	0.089	0.032	34	28	0.004	0.325
2. Jg5-9a Py	1967	18751	39	887	131	75	0.366	0.108	105	27	0.048	0.812
2. Jg5-9a Py	2162	13730	82	1465	36	14	0.282	0.045	155	37	0.004	1.8
2. Jg5-9a Py	1458	16234	82	1489	34	7.7	0.105	0.017	75	42	0.005	0.919
2. Jg5-9a Py	6035	5371	1.4	1739	19	5.3	0.203	0.014	3.2	26	0.005	0.008
2. Jg5-9a Py	7064	746	0.299	834	0.257	0.124	0.018	0.000	0.810	5.7	0.001	0.019
2. Jg5-9a Py	7038	774	0.396	796	0.597	0.077	0.011	0.001	0.924	6.5	0.007	0.018
2. Jg5-9a Py	6124	720	0.305	819	0.004	0.075	0.007	0.000	0.950	5.9	0.001	0.022
2. Jg5-9a Py	5670	757	0.281	883	3.2	0.510	0.021	0.001	22	7.2	0.038	0.167
2. Jg5-9a Py	7592	701	3.0	1070	33	12	0.442	0.027	0.805	6.2	0.003	0.005
2. Jg5-9a Py	9088	2600	50	863	115	55	0.686	0.061	18	24	0.012	0.005
2. Jg5-9a Py	7286	1943	3.0	987	38	14	0.197	0.024	2.4	8.5	0.001	0.014
2. Jg5-9a Py	8108	3038	1.3	948	12	4.0	0.082	0.009	15	11	0.002	0.024
2. Jg5-9a Py	7755	2180	0.174	222	0.021	0.060	0.001	0.001	0.695	8.4	0.003	0.004
2. Jg5-9a Py	8166	2271	0.189	210	0.183	0.062	0.002	0.000	0.590	7.8	0.003	0.004
2. Jg5-9a Py	8482	2106	0.458	293	2.1	0.475	0.006	0.003	0.652	7.7	0.003	0.004
2. Jg5-9a Py	7341	1915	0.212	720	0.854	0.144	0.006	0.001	0.694	6.5	0.003	0.005
2. Jg5-9a Py	6166	1516	0.801	629	2.4	0.516	0.007	0.008	1.4	4.9	0.002	0.013
2. Jg5-9a Py	6583	1776	0.321	577	0.303	0.151	0.002	0.000	0.858	6.2	0.002	0.015
2. Jg5-9a Py	8752	2154	0.405	309	1.2	0.204	0.002	0.002	0.700	7.4	0.002	0.015
2. Jg5-9a Py	8244	2141	0.350	303	0.219	0.057	0.002	0.000	0.913	8.7	0.002	0.015
2. Jg5-9a Py	7375	2051	0.321	299	1.5	0.204	0.003	0.004	0.821	7.9	0.003	0.023
2. Jg5-9a Py	6470	2059	0.297	552	0.220	0.085	0.001	0.001	0.779	7.2	0.003	0.023
2. Jg5-9a Py	7425	1471	1.3	436	9.8	2.6	0.029	0.001	21	8.2	0.003	0.133
2. Jg5-9a Py	8838	2050	3.4	408	6.1	2.2	0.046	0.004	656	14	0.002	3.3
2. Jg5-9a Py	5694	1376	0.944	497	7.8	1.5	0.022	0.002	29	4.9	0.002	0.153
2. Jg5-9a Py	7502	1922	0.472	303	0.158	0.078	0.001	0.000	0.758	7.1	0.002	0.006
2. Jg5-9a Py	6912	1991	0.405	197	6.6	0.281	0.024	0.002	0.847	8.6	0.002	0.005
2. Jg5-9a Py	7319	2027	0.301	246	0.002	0.069	0.000	0.000	0.999	11	0.002	0.005
2. Jg5-9a Py	8349	2355	0.307	312	0.008	0.065	0.000	0.000	0.997	9.9	0.002	0.005
2. Jg5-9a Py	8123	2122	0.340	349	0.145	0.060	0.000	0.000	0.870	8.6	0.005	0.005
2. Jg5-9a Py	7579	2050	0.277	404	0.177	0.047	0.004	0.001	0.911	10	0.003	0.005
2. Jg5-9a Py	7272	2085	0.267	372	0.343	0.078	0.001	0.001	0.925	9.4	0.003	0.005
2. Jg5-9a Py	7857	1942	0.260	385	1.4	0.319	0.003	0.003	0.844	7.3	0.003	0.005
2. Jg5-9a Py	7275	2037	0.228	502	0.300	0.058	0.001	0.001	0.935	7.5	0.003	0.005
2. Jg5-9a Py	7604	1965	0.337	478	0.501	0.071	0.003	0.000	0.843	7.5	0.003	0.005
2. Jg5-9a Py	7863	2010	0.636	355	0.162	0.056	0.039	0.002	0.897	6.7	0.003	0.005
2. Jg5-9a Py	8271	2203	0.435	341	1.8	0.365	0.009	0.002	1.1	8.0	0.002	0.007
2. Jg5-9a Py	5761	1408	0.225	244	0.103	0.111	0.001	0.002	0.648	8.4	0.005	0.011
2. Jg5-9a Py	5334	926	0.154	134	0.348	0.114	0.001	0.001	0.843	8.0	0.009	0.006
2. Jg5-9a Py	6480	902	0.186	174	0.874	0.132	0.002	0.001	4.3	7.5	0.003	0.050
2. Jg5-9a Py	8055	1131	0.135	322	0.051	0.159	0.001	0.000	0.951	13	0.003	0.020
2. Jg5-9a Py	7495	1925	0.266	262	0.085	0.067	0.018	0.000	4.9	9.7	0.002	0.014
2. Jg5-9a Py	7637	2151	0.442	251	5.1	1.6	0.007	0.003	7.6	9.2	0.002	0.034
2. Jg5-9a Py	1106	12240	11	161	46	12	0.199	0.039	1965	38	0.002	8.3
2. Jg5-9a Py	158	7788	5.5	49	32	6.5	0.188	0.015	1160	51	0.228	5.5
2. Jg5-9a Py	214	14531	7.8	106	17	4.2	0.183	0.009	4097	36	0.682	15
2. Jg5-9a Py	318	12894	4.5	137	54	21	0.142	0.011	195	36	0.001	1.1
2. Jg5-9a Py	2160	7643	10	242	14	8.1	0.112	0.005	44	21	0.015	0.204
2. Jg5-9a Py	6088	5594	54	221	610	317	3.1	0.045	281	18	0.038	0.866
2. Jg5-9a Py	8126	2363	461	275	26	13	0.732	0.010	8.6	10	0.013	0.010
2. Jg5-9a Py	7467	2019	0.249	314	0.140	0.247	0.002	0.001	3.0	10.0	0.003	0.010

Pyrite	Co	Ni	Cu	As	Bi	Te	Ag	Au	Zn	Se	*In	Cd
2. Jg5-9a Py	6537	1931	0.266	163	5.2	1.2	0.009	0.006	1.1	8.7	0.001	0.007
2. Jg5-9a Py	6124	1880	0.415	202	2.8	0.407	0.004	0.004	1.1	9.0	0.001	0.007
2. Jg5-9a Py	7373	2147	0.333	325	0.123	0.082	0.001	0.000	0.905	9.6	0.001	0.005
2. Jg5-9a Py	8096	2193	0.219	355	0.120	0.088	0.001	0.000	0.806	8.7	0.001	0.012
2. Jg5-9a Py	8374	2135	0.334	361	1.6	0.230	0.008	0.001	0.920	7.2	0.001	0.039
2. Jg5-9a Py	494	11466	0.464	175	10	1.7	0.021	0.005	68	38	0.001	0.333
2. Jg5-9a Py	101	11560	1.9	175	1.8	0.935	0.005	0.001	16	44	0.017	0.071
2. Jg5-9a Py	41	11329	0.196	207	0.123	1.0	0.003	0.000	0.924	39	0.001	0.005
2. Jg5-9a Py	86	14665	0.176	95	5.7	10	0.024	0.001	2.3	36	0.001	0.006
2. Jg5-9a Py	54	14645	0.236	80	0.160	7.3	0.001	0.000	0.716	39	0.001	0.006
2. Jg5-9a Py	231	12431	51	138	29	10.0	0.431	0.029	13326	36	0.233	31
2. Jg5-9a Py	278	12750	275	146	61	21	1.2	0.139	33128	41	1.7	83
2. Jg5-9a Py	7536	2191	1.4	393	3.4	0.984	0.063	0.003	11	7.3	0.002	0.082
2. Jg5-9a Py	8328	2298	1.7	238	7.9	1.2	0.081	0.002	29	7.2	0.002	0.120
2. Jg5-9a Py	7000	1992	0.352	188	0.363	0.099	0.001	0.001	1.0	7.0	0.002	0.003
2. Jg5-9a Py	7859	2072	0.358	279	0.273	0.059	0.004	0.000	0.821	6.8	0.001	0.007
2. Jg5-9a Py	5653	3540	3.1	371	28	5.8	0.102	0.023	6.4	21	0.003	0.050
2. Jg5-9a Py	5878	1195	0.480	433	19	5.0	0.085	0.012	5.0	6.2	0.003	0.021
2. Jg5-9a Py	6873	1192	20	244	22	6.7	0.094	0.020	252	13	0.010	0.988
2. Jg5-9a Py	1672	7161	73	10	28	39	0.662	0.015	6.8	66	0.003	0.046
2. Jg5-9a Py	890	11290	48	142	10	6.0	0.128	0.010	15411	46	1.6	52
2. Jg5-9a Py	468	13158	20	133	1909	12	73	0.132	5.7	50	0.009	0.620
2. Jg5-9a Py	126	13346	17	124	15	3.1	0.368	0.006	1475	46	0.004	3.9
2. Jg5-9a Py	136	13332	21	135	28	5.8	0.438	0.002	247	45	0.007	0.783
2. Jg5-9a Py	167	12165	0.324	127	0.712	0.383	0.007	0.000	1.3	42	0.003	0.005
2. Jg5-9a Py	6882	1786	1.0	602	5.9	0.514	0.022	0.004	7.5	7.1	0.003	0.098
2. Jg5-9a Py	7299	1874	0.334	443	0.402	0.106	0.007	0.001	0.718	6.9	0.003	0.003
2. Jg5-9a Py	8285	2375	0.282	151	0.040	0.196	0.001	0.000	2.5	8.4	0.003	0.003
2. Jg5-9a Py	8506	2184	0.497	208	0.128	0.075	0.003	0.000	7.8	8.6	0.003	0.015
2. Jg5-9a Py	7961	1981	0.487	201	0.219	0.096	0.004	0.000	2.3	7.2	0.001	0.014
2. Jg5-9a Py	8134	1939	0.251	215	0.194	0.105	0.002	0.000	2.9	7.5	0.001	0.018
2. Jg5-9a Py	8646	2137	0.189	262	0.164	0.136	0.002	0.000	0.858	8.2	0.004	0.021
2. Jg5-9a Py	6009	2001	0.201	635	1.1	0.158	0.001	0.001	2.0	6.8	0.004	0.007
2. Jg5-9a Py	6658	1625	0.301	764	2.6	0.328	0.002	0.000	2.1	4.7	0.004	0.007
2. Jg5-9a Py	2611	7047	5.3	338	14	3.0	0.058	0.014	605	30	0.026	2.0
2. Jg5-9a Py	4676	7117	1212	176	32	4.7	0.494	0.052	9919	39	0.539	34
2. Jg5-9a Py	5116	4911	28	237	44	10	0.352	0.024	9115	23	0.835	30
2. Jg5-9a Py	994	12161	16	132	33	7.7	0.117	0.027	483	52	0.001	2.6
2. Jg5-9a Py	258	12987	0.594	92	5.4	1.1	0.079	0.005	339	50	0.001	0.898
2. Jg5-9a Py	238	13359	16	108	189	3.5	2.1	0.020	14	54	0.017	0.162
2. Jg5-9a Py	7247	1974	0.476	279	0.845	0.124	0.004	0.000	4.1	7.8	0.001	0.006
2. Jg5-9a Py	7955	2219	0.341	231	0.952	0.196	0.002	0.001	3.6	9.8	0.011	0.006
2. Jg5-9a Py	8025	2135	0.544	137	0.029	0.036	0.001	0.000	3.7	8.3	0.011	0.015
2. Jg5-9a Py	8102	2102	2.7	276	25	15	0.096	0.004	56	9.4	0.014	0.149
2. Jg5-9a Py	7785	1997	0.455	258	0.049	0.071	0.001	0.000	2.0	6.8	0.014	0.022
2. Jg5-9a Py	7296	1936	0.413	536	0.064	0.090	0.002	0.000	5.3	7.2	0.015	0.013
2. Jg5-9a Py	6323	1924	0.397	702	0.017	0.104	0.003	0.001	2.4	8.1	0.008	0.012
2. Jg5-9a Py	1483	6294	256	70	369	20	9.6	0.042	32	44	0.043	0.335
2. Jg5-9a Py	92	11010	0.727	56	0.642	4.3	0.013	0.001	10	27	0.002	0.035
2. Jg5-9a Py	8609	2185	0.322	244	0.085	0.086	0.002	0.000	3.8	7.9	0.007	0.012
2. Jg5-9a Py	8683	2154	0.201	196	0.048	0.098	0.002	0.000	2.1	7.1	0.003	0.012
2. Jg5-9a Py	8307	2240	0.333	265	0.027	0.065	0.003	0.001	22	10	0.014	0.011
2. Jg5-9a Py	8287	2269	0.422	287	0.020	0.077	0.001	0.000	5.1	8.2	0.015	0.012
2. Jg5-9a Py	8586	2210	9.9	360	16	3.7	0.203	0.003	97	8.7	0.004	0.156
2. Jg5-9a Py	8086	1966	0.574	312	7.4	1.3	0.016	0.013	1.3	7.6	0.006	0.019

Pyrite	Co	Ni	Cu	As	Bi	Te	Ag	Au	Zn	Se	*In	Cd
2. Jg5-9a Py	8348	2244	245	341	29	6.8	0.439	0.101	105	8.1	0.017	0.278
2. Jg5-9a Py	8442	2183	0.233	327	0.235	0.155	0.001	0.000	2.1	7.9	0.008	0.007
2. Jg5-9a Py	8054	2204	0.379	316	8.4	1.7	0.006	0.006	2.6	9.5	0.006	0.022
2. Jg5-9a Py	6995	2118	0.700	219	12	1.9	0.052	0.027	7.6	9.0	0.007	0.013
2. Jg5-9a Py	7332	1806	0.381	338	1.8	0.505	0.008	0.003	1.1	7.8	0.007	0.005
2. Jg5-9a Py	7576	1884	0.406	406	0.728	0.134	0.001	0.001	1.1	6.2	0.008	0.003
2. Jg5-9a Py	8403	2269	0.370	363	0.288	0.101	0.001	0.001	0.736	9.7	0.004	0.014
2. Jg5-9a Py	198	7244	1.7	46	7.6	13	0.059	0.003	22	52	0.004	0.221
2. Jg5-9a Py	2766	4735	0.853	244	4.0	2.6	0.029	0.004	29	14	0.096	0.369
2. Jg5-9a Py	7680	2096	0.353	388	0.109	0.041	0.001	0.000	0.776	9.8	0.004	0.003
2. Jg5-9a Py	1838	3582	4.2	210	2.9	3.4	0.059	0.000	4.7	46	0.006	0.003
2. Jg5-9a Py	7680	2174	0.181	240	0.047	0.133	0.001	0.000	0.906	11	0.004	0.003
2. Jg5-9a Py	8402	2242	0.236	338	0.090	0.083	0.001	0.000	0.916	12	0.005	0.003
2. Jg5-9a Py	8408	2117	0.205	265	0.026	0.067	0.001	0.000	1.0	7.9	0.003	0.003
2. Jg5-9a Py	2586	4661	25	314	2.9	1.3	0.028	0.001	5.2	25	0.006	0.015
2. Jg5-9a Py	7688	2073	0.288	327	0.009	0.060	0.000	0.000	1.0	9.5	0.003	0.003
2. Jg5-9a Py	7950	2272	0.432	303	0.744	0.158	0.002	0.003	0.682	10	0.005	0.003
Mean (n=146)	5724	4775	37	474	30	6.1	0.673	0.009	643	18	0.045	1.9
SD	3155	4956	207	411	167	27	6.0	0.022	3350	15	0.209	9.2
Median	7260	2149	0.414	319	1.6	0.358	0.007	0.001	2.1	9.6	0.003	0.014
Max	11674	21131	2147	2251	1909	317	73	0.139	33128	66	1.7	83
Min	41	471	0.135	10	0.002	0.036	0.000	0.000	0.590	4.7	0.001	0.001

Pentlandite	Co	Ni	Cu	As	Bi	Te	Ag	Au	Zn	Se	*In	Cd
3. Jg5-9a Pn	4514		35	0.718	4.2	15	0.323	0.030	5935	71	1.3	20
3. Jg5-9a Pn	4327		27	0.500	17	17	1.5	0.150	973	71	0.023	2.8
3. Jg5-9a Pn	4528		10.0	0.471	22	13	1.8	0.129	578	72	0.150	0.869
3. Jg5-9a Pn	4429		1.8	0.304	2.1	5.0	0.158	0.020	31	71	0.044	0.055
3. Jg5-9a Pn	4541		4.8	0.303	4.0	6.7	0.059	0.028	111	77	0.007	0.124
3. Jg5-9a Pn	4661		2.0	0.299	2.5	7.4	0.074	0.026	28	71	0.048	0.089
3. Jg5-9a Pn	4701		3.3	0.360	6.5	5.7	0.415	0.035	36	76	0.005	0.223
3. Jg5-9a Pn	4616		4.6	0.398	9.8	5.5	0.645	0.063	319	75	0.108	0.446
3. Jg5-9a Pn	4509		1.9	0.349	6.3	11	0.683	0.009	17	72	0.401	0.041
3. Jg5-9a Pn	4652		2.9	0.612	7.2	14	0.759	0.031	45	73	0.015	0.052
3. Jg5-9a Pn	4308		4.3	0.339	10	6.7	0.562	0.065	137	78	0.005	0.406
3. Jg5-9a Pn	6050		26	0.828	118	13	1.4	0.131	311	86	0.047	0.924
3. Jg5-9a Pn	4383		3.1	0.283	2.0	2.6	0.091	0.016	44	70	0.047	0.386
3. Jg5-9a Pn	4024		15	0.534	16	6.9	0.661	0.024	1248	80	0.018	2.1
3. Jg5-9a Pn	4306		9.0	0.467	5.4	6.0	0.253	0.030	482	78	0.007	1.0
3. Jg5-9a Pn	4341		2.3	0.299	1.8	3.7	0.063	0.008	23	72	0.009	0.100
3. Jg5-9a Pn	4273		9.4	0.386	3.7	3.0	0.148	0.072	941	74	0.239	1.8
3. Jg5-9a Pn	4488		11	0.325	16	6.2	0.725	0.301	4051	76	0.011	7.7
3. Jg5-9a Pn	4387		2.1	0.265	3.0	5.2	0.078	0.021	88	77	0.011	0.416
3. Jg5-9a Pn	4242		35	2.1	11	26	0.932	0.042	2688	74	0.385	9.5
3. Jg5-9a Pn	4083		10	0.402	8.6	17	1.5	0.077	247	82	0.066	0.795
3. Jg5-9a Pn	4229		9.3	0.444	2.0	1.000	0.053	0.031	139	72	0.011	0.533
3. Jg5-9a Pn	4188		12	0.598	1.9	2.5	0.073	0.016	310	71	0.026	1.5
3. Jg5-9a Pn	4270		9.4	0.451	2.9	5.2	0.352	0.015	285	68	0.053	0.547
3. Jg5-9a Pn	4173		12	1.4	2.5	3.2	0.114	0.015	1639	69	0.085	6.1
3. Jg5-9a Pn	3635		1370	5.0	20	4.4	0.965	0.077	6014	66	0.199	19
3. Jg5-9a Pn	4218		1.9	0.334	2.8	4.7	0.161	0.005	24	75	0.008	0.096
3. Jg5-9a Pn	7374		4.8	0.721	6.3	55	0.309	0.006	6.4	138	0.012	0.044
3. Jg5-9a Pn	7072		7.3	0.912	5.8	37	0.424	0.002	10	117	0.012	0.080
3. Jg5-9a Pn	7861		5.4	2.6	14	51	0.739	0.017	6.9	122	0.032	0.029

Pentlandite	Co	Ni	Cu	As	Bi	Te	Ag	Au	Zn	Se	*In	Cd
3. Jg5-9a Pn	7309		7.7	0.411	11	53	0.747	0.024	8.9	84	0.020	0.054
3. Jg5-9a Pn	10485		172	5.9	130	101	3.8	0.173	5.1	121	0.016	0.036
3. Jg5-9a Pn	7368		11	0.559	12	29	1.2	0.046	6.8	100	0.011	0.010
3. Jg5-9a Pn	6043		54	12	833	43	4.7	0.314	2.8	144	0.006	0.045
3. Jg5-9a Pn	5892		42	13	1265	63	7.7	0.429	1.4	146	0.004	0.016
3. Jg5-9a Pn	5118		59	7.4	1691	81	13	0.527	1.5	154	0.004	0.017
3. Jg5-9a Pn	5788		45	6.3	1594	74	17	0.577	1.3	144	0.010	0.049
3. Jg5-9a Pn	8563		61	9.5	519	131	6.2	0.255	1.3	134	0.008	0.092
3. Jg5-9a Pn	8751		5.8	0.332	5.9	13	4.7	0.025	2.1	106	0.011	0.031
3. Jg5-9a Pn	8135		3.1	0.397	8.1	5.2	0.208	0.032	2.9	102	0.075	0.041
3. Jg5-9a Pn	8212		0.959	0.288	1.1	5.1	0.066	0.001	1.0	102	0.005	0.026
3. Jg5-9a Pn	8263		1.0	0.415	2.5	11	0.217	0.002	1.2	102	0.007	0.026
3. Jg5-9a Pn	12919		6922	6.1	768	163	8.9	0.148	35	130	0.005	0.254
3. Jg5-9a Pn	10773		29	5.0	299	80	3.1	0.136	1.1	125	0.006	0.027
3. Jg5-9a Pn	16317		412	1.4	327	51	7.0	0.159	3.1	184	0.005	0.028
3. Jg5-9a Pn	11896		38	4.6	717	97	4.6	0.245	1.8	137	0.005	0.014
3. Jg5-9a Pn	11732		45	11	1058	131	5.6	0.201	1.1	141	0.004	0.011
3. Jg5-9a Pn	11656		24	8.2	720	88	4.3	0.118	1.1	128	0.008	0.011
3. Jg5-9a Pn	9530		1.8	1.6	15	29	0.503	0.005	21	117	0.007	0.007
3. Jg5-9a Pn	9666		1.6	1.4	8.7	12	0.091	0.006	4.4	119	0.101	0.045
3. Jg5-9a Pn	10048		1.5	1.4	13	18	0.515	0.008	1.4	116	0.022	0.030
3. Jg5-9a Pn	9808		1.6	1.3	17	30	0.542	0.009	1.6	105	0.006	0.031
3. Jg5-9a Pn	9824		1.8	0.405	1.5	10	0.082	0.003	1.7	107	0.009	0.020
Mean (n=53)	6707		181	2.3	195	32	2.1	0.093	507	99	0.070	1.5
SD	3065		955	3.3	411	38	3.4	0.131	1294	32	0.189	4.0
Median	5118		9.3	0.559	9.8	13	0.645	0.031	23	84	0.011	0.080
Max	16317		6922	13	1691	163	17	0.577	6014	184	1.3	20
Min	3635		0.959	0.265	1.1	1.000	0.053	0.001	1.0	66	0.004	0.007

Violarite/Bravc	Co	Ni	Cu	As	Bi	Te	Ag	Au	Zn	Se	*In	Cd
4. Jg9a Vio-Bra	10671		121	0.207	653	76	8.9	0.229	4.4	117	0.003	0.021
4. Jg9a Vio-Bra	12770		126	0.207	555	68	8.2	0.184	6.2	118	0.003	0.068
4. Jg9a Vio-Bra	10111		61	0.188	778	92	9.9	0.213	1.3	118	0.010	0.012
4. Jg9a Vio-Bra	12119		285	0.196	547	69	7.2	0.223	20	125	0.004	0.058
4. Jg9a Vio-Bra	11636		69	0.180	996	120	12	0.363	17	108	0.005	0.013
4. Jg9a Vio-Bra	12117		68	0.198	538	69	5.4	0.219	18	117	0.003	0.032
4. Jg9a Vio-Bra	11936		30	0.243	844	114	8.5	0.262	4.4	112	0.003	0.086
4. Jg9a Vio-Bra	11533		37	0.243	764	117	7.7	0.227	6.0	100	0.003	0.035
4. Jg9a Vio-Bra	4035		49	0.233	1555	119	11	0.508	22	110	0.006	0.074
4. Jg9a Vio-Bra	3046		106	0.286	1134	88	8.5	0.427	21	121	0.006	0.057
4. Jg9a Vio-Bra	3061		107	0.170	1400	108	9.5	0.533	1.9	116	0.018	0.008
4. Jg9a Vio-Bra	12931		2431	0.195	363	33	3.3	0.131	6.9	132	0.016	0.045
4. Jg9a Vio-Bra	10820		12505	0.344	757	68	6.0	0.252	26	114	0.017	0.244
4. Jg9a Vio-Bra	11186		6328	0.264	782	77	7.0	0.285	28	125	0.005	0.235
4. Jg9a Vio-Bra	9456		15464	0.811	894	93	7.6	0.421	65	124	0.091	0.493
4. Jg9a Vio-Bra	8848		1193	1.0	893	87	7.8	0.245	160	108	0.089	0.569
4. Jg9a Vio-Bra	12033		66204	0.421	481	68	15	0.104	115	103	0.047	0.509
4. Jg9a Vio-Bra	11890		66290	0.362	527	75	15	0.121	236	109	0.016	1.2
4. Jg9a Vio-Bra	11320		63369	0.209	744	97	17	0.203	74	90	0.014	0.599
4. Jg9a Vio-Bra	14078		3568	0.236	615	85	11	0.274	65	119	0.013	0.237
4. Jg9a Vio-Bra	12067		29530	0.531	771	105	17	0.963	113	100	0.037	0.767
4. Jg9a Vio-Bra	10798		1453	0.258	988	140	9.9	0.238	120	101	0.009	0.177
4. Jg9a Vio-Bra	5990		139	5.2	1133	84	7.6	0.441	15	96	0.013	0.127
4. Jg9a Vio-Bra	4890		44	1.9	358	30	2.3	0.223	109	87	0.021	0.496
4. Jg9a Vio-Brav	4891		122	0.686	187	16	1.5	0.188	44	92	0.065	0.151
4. Jg9a Vio-Brav	5553		217	1.1	265	17	2.1	0.345	71	101	0.004	0.376

Violarite/Bravc	Co	Ni	Cu	As	Bi	Te	Ag	Au	Zn	Se	*In	Cd
4. Jg9a Vio-Brav	5291		216	1.1	214	14	2.0	0.261	279	86	0.007	1.4
4. Jg9a Vio-Brav	4042		3988	1.4	1153	54	9.4	0.446	52	100	0.008	0.193
4. Jg9a Vio-Brav	4569		7025	0.766	1484	67	11	0.643	157	108	0.026	0.579
4. Jg9a Vio-Brav	4214		437	1.2	1179	53	7.6	0.385	201	99	0.124	0.972
4. Jg9a Vio-Brav	4424		262	1.1	183	11	1.8	0.244	1101	88	0.013	3.5
4. Jg9a Vio-Brav	2980		19413	2.9	903	34	27	0.328	335	94	0.016	1.9
Mean (n=32)	8603		9414	0.760	770	73	8.9	0.317	109	107	0.022	0.476
SD	3952		19215	1.0	385	36	5.4	0.178	198	22	0.029	0.708
Median	10391		273	0.315	768	76	8.4	0.257	48	108	0.013	0.214
Max	14078		66290	5.2	1555	140	27	0.963	1101	132	0.124	3.5
Min	2980		30	0.170	183	11	1.5	0.104	1.3	86	0.003	0.008

Sphalerite	Co	Ni	Cu	As	Bi	Te	Ag	Au	Zn	Se	*In	Cd
5. Jg9a Sp	247	7.7	9997	0.280	5.4	0.153	2.5			17	36	2240
5. Jg9a Sp	394	16	1801	0.395	0.297	0.072	1.5			17	37	2273
5. Jg9a Sp	394	29	9322	0.252	0.597	0.088	2.4			16	33	2198
5. Jg9a Sp	413	13	840	0.247	0.869	0.170	1.3			14	36	2238
5. Jg9a Sp	484	35	3541	0.220	0.350	0.142	2.2			15	43	2163
5. Jg9a Sp	492	17	850	0.212	0.214	0.145	1.4			13	35	2161
5. Jg9a Sp	470	26	6101	0.253	0.347	0.086	2.5			13	50	2183
5. Jg9a Sp	484	12	1988	0.261	0.194	0.144	1.6			11	37	2183
5. Jg9a Sp	484	17	32	0.297	0.106	0.102	1.3			16	35	2259
5. Jg9a Sp	482	9.5	700	0.240	0.096	0.065	1.4			16	34	2218
5. Jg9a Sp	483	14	30	0.280	0.140	0.093	1.3			17	41	2223
5. Jg9a Sp	400	39	5109	0.290	1.1	0.105	2.1			18	28	2195
5. Jg9a Sp	277	16	3979	0.224	1.0	0.099	1.5			17	31	2313
5. Jg9a Sp	264	7.3	1694	0.184	1.3	0.109	1.4			17	37	2216
5. Jg9a Sp	269	27	6871	0.194	1.2	0.039	2.0			18	34	2193
5. Jg9a Sp	141	7.4	24371	0.212	11	0.384	4.7			18	42	2125
5. Jg9a Sp	272	9.0	4195	0.212	2.4	0.135	1.6			16	41	2228
5. Jg9a Sp	288	24	10752	0.239	4.4	0.138	1.7			15	35	2214
5. Jg9a Sp	270	8.4	1803	0.249	1.6	0.082	1.8			17	32	2223
5. Jg9a Sp	259	21	4213	0.209	0.994	0.074	2.0			17	34	2202
5. Jg9a Sp	392	32	5155	0.174	2.7	0.044	2.4			18	38	2217
5. Jg9a Sp	342	20	1703	0.204	0.919	0.153	1.6			17	48	2147
5. Jg9a Sp	475	15	26	0.232	0.122	0.058	1.2			13	47	2194
5. Jg9a Sp	482	15	21	0.376	0.143	0.113	1.3			12	34	2140
5. Jg9a Sp	471	34	6115	0.207	0.955	0.072	1.9			11	41	2052
5. Jg9a Sp	479	20	582	0.223	0.098	0.067	1.5			10	45	2180
5. Jg9a Sp	458	17	286	0.249	0.549	0.139	1.5			11	39	2208
5. Jg9a Sp	387	7.4	4645	0.280	1.7	0.064	1.8			11	31	2243
5. Jg9a Sp	471	45	4262	0.227	1.3	0.064	1.7			10	34	2108
5. Jg9a Sp	470	127	65	0.210	0.543	0.125	1.4			11	35	2124
5. Jg9a Sp	467	18	147	0.214	1.0	0.104	1.4			11	23	2148
5. Jg9a Sp	425	12	614	0.206	0.501	0.080	1.4			15	42	2187
5. Jg9a Sp	102	2200	8918	0.239	9.3	0.350	2.1			16	35	2189
5. Jg9a Sp	129	24	9603	0.244	5.8	0.149	1.9			16	45	2221
5. Jg9a Sp	183	16	8468	0.240	5.1	0.114	1.7			16	31	2277
5. Jg9a Sp	424	45	7144	0.243	1.4	0.098	2.4			16	35	2132
5. Jg9a Sp	464	30	1557	0.207	0.055	0.127	2.0			11	34	2114
5. Jg9a Sp	460	36	3362	0.239	0.088	0.144	2.2			10.0	32	2161
5. Jg9a Sp	432	24	976	0.275	0.462	0.155	1.4			12	53	2195
5. Jg9a Sp	377	16	4107	0.415	0.839	0.082	1.7			14	38	2155
5. Jg9a Sp	207	14	2601	0.226	3.4	0.129	2.2			15	37	2202
5. Jg9a Sp	274	25	6604	0.222	3.5	0.139	2.1			17	35	2123
Mean (n=32)	372	75	4170	0.245	1.8	0.119	1.8			15	37	2190
SD	115	336	4525	0.051	2.4	0.066	0.586			2.7	5.9	51
Median	406	17	3452	0.239	0.937	0.107	1.7			16	36	2194
Max	492	2200	24371	0.415	11	0.384	4.7			18	53	2313
Min	102	7.3	21	0.174	0.055	0.039	1.2			10.0	23	2052

ADDITIONAL MATERIAL G

CO-AUTHORED ARTICLE:

COUPLED MICROSTRUCTURAL EBSD AND LA-ICP-MS TRACE ELEMENT MAPPING OF PYRITE CONSTRAINS THE DEFORMATION HISTORY OF BRECCIA-HOSTED IOCG ORE SYSTEMS

Samuel A. King[1,*], Nigel J. Cook[1], Cristiana L. Ciobanu[1], Kathy Ehrig[1,2], **Yuri Tatiana Campo-Rodriguez[1,3]**, Animesh Basak[4], Sarah Gilbert[4]

[1]School of Chemical Engineering, The University of Adelaide, Adelaide, SA, 5005, Australia

[2]BHP Olympic Dam, 10 Franklin Street, Adelaide, SA, 5000, Australia

[3]Geosciences Institute, Graduate Program in Geology, University of Brasilia, Brasília 70910-900, DF, Brazil

[4]Adelaide Microscopy, The University of Adelaide, Adelaide, SA, 5005, Australia

Article published in *Minerals* (2024) 14(2): 198.

minerals

MDPI

Article

Coupled Microstructural EBSD and LA-ICP-MS Trace Element Mapping of Pyrite Constrains the Deformation History of Breccia-Hosted IOCG Ore Systems

Samuel Anthony King [1,*], Nigel John Cook [1], Cristiana Liana Ciobanu [1], Kathy Ehrig [1,2], Yuri Tatiana Campo Rodriguez [1,3], Animesh Basak [4] and Sarah Gilbert [4]

[1] School of Chemical Engineering, The University of Adelaide, Adelaide, SA 5005, Australia; nigel.cook@adelaide.edu.au (N.J.C.); cristiana.ciobanu@adelaide.edu.au (C.L.C.); kathy.ehrig@bhp.com (K.E.); yuri.camporodriguez@adelaide.edu.au (Y.T.C.R.)
[2] BHP Olympic Dam, 10 Franklin Street, Adelaide, SA 5000, Australia
[3] Geosciences Institute, Graduate Program in Geology, University of Brasília, Brasília 70910-900, DF, Brazil
[4] Adelaide Microscopy, The University of Adelaide, Adelaide, SA 5005, Australia; animesh.basak@adelaide.edu.au (A.B.); sarah.gilbert@adelaide.edu.au (S.G.)
* Correspondence: samuel.king@adelaide.edu.au

Abstract: Electron backscatter diffraction (EBSD) methods are used to investigate the presence of microstructures in pyrite from the giant breccia-hosted Olympic Dam iron–oxide copper gold (IOCG) deposit, South Australia. Results include the first evidence for ductile deformation in pyrite from a brecciated deposit. Two stages of ductile behavior are observed, although extensive replacement and recrystallization driven by coupled dissolution–reprecipitation reaction have prevented widespread preservation of the earlier event. Laser ablation inductively coupled plasma mass spectrometry (LA-ICP-MS) element maps of pyrite confirm that many pyrite grains display compositional zoning with respect to As, Co, and Ni, but that the zoning is often irregular, patchy, or otherwise disrupted and are readily correlated with observed microstructures. The formation of ductile microstructures in pyrite requires temperatures above ~260 °C, which could potentially be related to heat from radioactive decay and fault displacements during tectonothermal events. Coupling EBSD methods with LA-ICP-MS element mapping allows a comprehensive characterization of pyrite textures and microstructures that are otherwise invisible to conventional reflected light or BSE imaging. Beyond providing new insights into ore genesis and superimposed events, the two techniques enable a detailed understanding of the grain-scale distribution of minor elements. Such information is pivotal for efforts intended to develop new ways to recover value components (precious and critical metals), as well as remove deleterious components of the ore using low-energy, low-waste ore processing methods.

Keywords: electron backscatter diffraction; pyrite; olympic dam; microstructures; low-angle subgrain boundaries; ductile deformation; compositional zoning

check for updates

Citation: King, S.A.; Cook, N.J.; Ciobanu, C.L.; Ehrig, K.; Campo Rodriguez, Y.T.; Basak, A.; Gilbert, S. Coupled Microstructural EBSD and LA-ICP-MS Trace Element Mapping of Pyrite Constrains the Deformation History of Breccia-Hosted IOCG Ore Systems. *Minerals* **2024**, *14*, 198. https://doi.org/10.3390/min14020198

Academic Editors: Glenn Bark and Alan R. Butcher

Received: 15 January 2024
Revised: 9 February 2024
Accepted: 13 February 2024
Published: 15 February 2024

Copyright: © 2024 by the authors. Licensee MDPI, Basel, Switzerland. This article is an open access article distributed under the terms and conditions of the Creative Commons Attribution (CC BY) license (https://creativecommons.org/licenses/by/4.0/).

1. Introduction

Pyrite (FeS_2) is the most common sulfide mineral in the Earth's crust. It is sufficiently refractory to allow the preservation of microstructures that are typically erased in more ductile ore minerals, meaning it can be used to fingerprint sequential stages in the deformational history of a mineral deposit [1]. Pyrite is therefore a valuable indicator of deformation in sulfide ore deposits [2], and it has been widely used to characterise metamorphosed ores and successfully constrain the impact of regional metamorphism and associated deformation on mineralization [3–6].

Early studies viewed pyrite as a mineral with brittle behavior at most crustal conditions, transitioning to ductile behavior at temperatures above ~425 °C [7–9]. The application of electron backscatter diffraction (EBSD) techniques to pyrite underpinned major

ADDITIONAL MATERIAL H

CO-AUTHORED ARTICLE:

EBSD MAPPING OF CU-FE-SULFIDES REVEAL MICROSTRUCTURES ENRICHED IN CRITICAL/PRECIOUS METALS AND RESOLVE DEFORMATION HISTORIES

Samuel A. King[1,*], Nigel J. Cook[1], Cristiana L. Ciobanu[1], Kathy Ehrig[1,2], **Yuri Tatiana Campo-Rodriguez[1,3]**, Sarah Gilbert[4], Animesh Basak[4]

[1]*School of Chemical Engineering, The University of Adelaide, Adelaide, SA, 5005, Australia*

[2]*BHP Olympic Dam, 10 Franklin Street, Adelaide, SA, 5000, Australia*

[3]*Geosciences Institute, University of Brasilia, Brasília DF 70910-900, Brazil*

[4]*Adelaide Microscopy, The University of Adelaide, Adelaide, SA, 5005, Australia*

Article published in *American Mineralogist,* in press.

This is the peer-reviewed, final accepted version for American Mineralogist, published by the Mineralogical Society of America.
The published version is subject to change. Cite as Authors (Year) Title. American Mineralogist, in press.
DOI: https://doi.org/10.2138/am-2024-9396. http://www.minsocam.org/

REVISION 1

EBSD mapping of Cu-Fe-sulfides reveal microstructures enriched in critical/precious metals and resolve deformation histories

SAMUEL A. KING[1,*], NIGEL J. COOK[1], CRISTIANA L. CIOBANU[1], KATHY EHRIG[1,2], YURI TATIANA CAMPO RODRIGUEZ[1,3], SARAH GILBERT[4], ANIMESH BASAK[4]

[1]*School of Chemical Engineering, The University of Adelaide, Adelaide S.A. 5005, Australia*

[2]*BHP Olympic Dam, 10 Franklin Street, Adelaide S.A. 5000, Australia*

[3] *Geosciences Institute, University of Brasília, Brasília DF 70910-900, Brazil*

[4] *Adelaide Microscopy, The University of Adelaide, Adelaide S.A. 5005, Australia*

ABSTRACT

Chalcopyrite ($CuFeS_2$) and bornite (Cu_5FeS_4) from the Olympic Dam Cu-U-Au-Ag deposit (South Australia) are characterized using electron backscatter diffraction (EBSD) to identify microstructures and their correlations with trace element concentrations measured by laser ablation inductively coupled plasma mass spectrometry (LA-ICP-MS). Natural chalcopyrite is shown to be a rich source of micro-structural and -textural information, preserving <110> and <001> crystallographic preferred orientations (CPO), {110} and {112} twin systems, grain boundary migration, foam textures and subgrain boundaries. Selected examples of chalcopyrite illustrate different aspects of its behavior and relationship with bornite across the mineralogically zoned deposit. The oriented stress imposed by brecciation and/or fluid fluxes at Olympic Dam, alongside temperature, pressure and strain rate, are shown to induce a variety of microstructures preserved in chalcopyrite. Microstructures can therefore be used to elucidate

* Corresponding author e-mail: samuel.king@adelaide.edu.au

This is the peer-reviewed, final accepted version for American Mineralogist, published by the Mineralogical Society of America.
The published version is subject to change. Cite as Authors (Year) Title. American Mineralogist, in press.
DOI: https://doi.org/10.2138/am-2024-9396. http://www.minsocam.org/

sequential stages of low to medium temperature (<300 °C) ore evolution. Although pyrite microstructures are already routinely used to understand higher temperature ore evolution, complementary microstructural study of chalcopyrite coexisting with pyrite has the potential to reveal deformational events across a more complete range of temperatures. In ore systems that lack obvious evidence for post-mineralization deformation, chalcopyrite is particularly well suited to unravel episodes of low- to medium-temperature overprinting.

EBSD mapping reveals what appears as single grains of chalcopyrite in reflected light is in fact aggregates composed of ~100 individual grains. In contrast, analyzed bornite displays overwhelming crystallographic homogeneity. Rare instances of misorientation in bornite are all associated with replacement and, if correlated with EBSD analysis of coexisting chalcopyrite and its inclusions (e.g., cobaltite), can be used to discern the origin and evolution of different bornite associations. LA-ICP-MS trace element mapping of chalcopyrite aggregates indicate that grain boundaries host concentrations of Pb, Bi, Ag and Sb, with twin boundaries displaying a weaker concentration of the same elements. Bornite grain boundaries are also enriched in Pb. These observations confirm the critical role played by microstructures in Cu-(Fe)-sulfides as traps for Pb, a non-target contaminant in copper concentrates, as well as new evidence for the physical state of Ag and potential value-add critical metals like Bi and Sb. The preferential occurrence of Pb, Bi, Ag and Sb along permeable grain boundaries may incentivize efforts to remove contaminants and/or recover by-products via leaching.

Keywords: Electron backscatter diffraction, Cu-(Fe)-sulfides, chalcopyrite, bornite, trace elements, microstructures, twinning, Olympic Dam.

ADDITIONAL MATERIAL I

CO-AUTHORED ARTICLE:

MONAZITE, LANTHANIDE-RICH GLASSES, AND OTHER TRACE ELEMENTS IN COPPER SMELTER SLAGS: CONSTRAINTS ON CRITICAL METAL BEHAVIOUR IN SI-FE-RICH MELTS

Hassan Gezzaz[1,*], Cristiana L. Ciobanu[1], Nigel J. Cook[1], Kathy Ehrig[1,2], Ashley Slattery[3], Benjamin Wade[3], Sarah Gilbert[3], **Yuri Tatiana Campo-Rodriguez[1]**

[1]*School of Chemical Engineering, The University of Adelaide, Adelaide, SA, 5005, Australia*
[2]*BHP Olympic Dam, 10 Franklin Street, Adelaide, SA, 5000, Australia*
[3]*Adelaide Microscopy, The University of Adelaide, Adelaide, SA, 5005, Australia*

Article submitted to *Mineralogy and Petrology*.

Monazite, lanthanide-rich glasses, and other trace elements in copper smelter slags: Constraints on critical metal behaviour in Si-Fe-rich melts

Hassan Gezzaz[1,*], Cristiana L. Ciobanu[1], Nigel J. Cook[1], Kathy Ehrig[1,2], Ashley Slattery[3], Benjamin Wade[3], Sarah Gilbert[3], Yuri T. Campo Rodriguez[1]

[1] *School of Chemical Engineering, The University of Adelaide, Adelaide, SA 5005, Australia*
[2] *BHP Olympic Dam, 1 Franklin St., Adelaide, SA 5000, Australia*
[3] *Adelaide Microscopy, The University of Adelaide, Adelaide, SA 5005, Australia*

Abstract

Furnace slags are potential new sources of critical metals. We undertook a micron- to nanoscale study that addresses speciation, distribution and associations of phases in flash furnace (FF, oxidised) and electric furnace (EF, reduced) slags from the Olympic Dam mining-smelting-refinery operation. Results enable understanding of the behaviour and partitioning of critical metals between melt and cooling crystalline phases in a controlled smelter environment that mimics Fe-Si-rich systems in Nature. Melts at ~1300 °C result in slags that differ in the relative proportions of component phases. Both FF and EF slags comprise major magnetite and two, compositionally distinct Si-Fe-rich glasses (glass-1 and -2); fayalite is a main component of EF slag. Glass-1 is rich in REE+Y (4.5–5.4 wt%, Ce_2O_3+La_2O_3) and contains dendritic monazite-(Ce). The EF slag crystallization sequence is: magnetite→fayalite+glass-1→monazite→glass-2. Immiscibility of REE in Si-Fe-rich melt is inferred from amorphous 'monazite-like' droplets. Chondrite-normalised fractionation patterns are defined by downwards-sloping LREE segments in both glasses. Partition coefficients are calculated for magnetite and fayalite relative to glasses. D_{REY} for HREE exceeds those for LREE in all phases and fayalite has an order of magnetite higher D_{HREE} than co-existing EF magnetite. Applying lattice strain models to experimental values show excellent fits for $D_{HREE\text{-}model}$ trends, even if lattice strain is not the sole factor controlling partitioning. Melt polymerisation, variable/unpredictable oxidation states, and constraints from specific crystallographic sites, also impact on observed trends. This study demonstrates that clues to element behaviour in the deep Earth are available from metallurgical plants.

Keywords Copper smelter slags – melt-solid partitioning – rare earth elements – monazite

* Corresponding author. Hassan.gezzaz@adelaide.edu.au

ADDITIONAL MATERIAL J

CO-AUTHORED ARTICLE:

TRACE ELEMENT DISTRIBUTIONS AMONG CU-(FE)-SULPHIDES FROM THE OLYMPIC DAM CU-U-AU-AG DEPOSIT, SOUTH AUSTRALIA

Samuel A. King[1,*], Nigel J. Cook[1], Cristiana L. Ciobanu[1], Kathy Ehrig[1,2], Sarah Gilbert[3], Benjamin Wade[3], **Yuri Tatiana Campo-Rodriguez[1,4]**

[1]School of Chemical Engineering, The University of Adelaide, Adelaide, SA, 5005, Australia

[2]BHP Olympic Dam, 10 Franklin Street, Adelaide, SA, 5000, Australia

[3]Adelaide Microscopy, The University of Adelaide, Adelaide, SA, 5005, Australia

[4]Geosciences Institute, University of Brasilia, Brasília DF 70910-900, Brazil

Article submitted to *Mineralium Deposita.*

Trace element distributions among Cu-(Fe)-sulfides from the Olympic Dam Cu-U-Au-Ag deposit, South Australia

Samuel A. King[1,*], Nigel J. Cook[1], Cristiana L. Ciobanu[1], Kathy Ehrig[1,2], Sarah Gilbert[3], Benjamin Wade[3], Yuri Tatiana Campo Rodriguez[1,4]

[1]*School of Chemical Engineering, The University of Adelaide, Adelaide, South Australia 5005, Australia*

[2]*BHP Olympic Dam, 10 Franklin Street, Adelaide, South Australia 5000, Australia*

[3]*Adelaide Microscopy, The University of Adelaide, Adelaide, South Australia 5005, Australia*

[4]*Geosciences Institute, University of Brasilia, Brasilia DF 70910-900, Brazil*

Abstract: Chalcocite, bornite, and chalcopyrite are the main copper minerals in the world-class Olympic Dam Cu-U-Au-Ag deposit, South Australia. Olympic Dam is characterized by systematic, inwards and upwards zonation of Cu-Fe-sulfide assemblages, encompassing chalcopyrite-pyrite, bornite-chalcopyrite, bornite-chalcocite and chalcocite-only zones. Trace element analysis of Cu-(Fe)-sulfides (~3500 spot analyses) by laser ablation inductively coupled plasma mass spectrometry on samples from across the deposit identifies the role of spatial position, protolith, and the presence/absence of co-existing sulfides (sphalerite, tetrahedrite-tennantite and carrollite) in control of trace element endowment. Cu-(Fe)-sulfides host concentrations of precious metals (Ag, Au) potential value-add elements (Se, Te, Bi, As, Sb, In) and deleterious elements (Pb, Hg). Where bornite-chalcocite co-exist, Ag is partitioned into chalcocite and Bi into bornite; in the absence of either bornite or chalcocite, chalcopyrite is a significant host for both elements. Chalcocite from the chalcocite-only zone is depleted in Bi-Te-Ag-Au compared to the bornite-chalcocite zone, demonstrating the role of bornite as an initial scavenger of these elements. A distinct inherited Cr-Ni-Zn signature is identified in chalcopyrite hosted by banded iron formation derived lithologies and proximal to crosscutting dykes. Despite some variation, Cu-(Fe)-sulfides generally contain more Bi and lesser Se towards deeper levels. The concentrations of these elements in paired bornite-chalcocite assemblages show promise as ore vectors, whereas Ag/Te in brown bornite and Se/Ag in chalcopyrite are prospective lateral vectors. Results carry implications for understanding deposit evolution, provides insights towards developing reconnaissance exploration vectors, and offers guidance on trace element deportments likely to impact ore quality and geometallurgical performance.

Keywords Olympic Dam • trace elements • LA-ICP-MS • chalcocite • bornite • chalcopyrite.

* Corresponding author. Email: samuel.king@adelaide.edu.au

CHAPTER 10

REFERENCES

CHAPTER 10: REFERENCES

Ahn, J.H., Cho, M., Jenkins, D.M., and Buseck, P.R. (1991) Structural defects in synthetic tremolite amphiboles amphiboles. American Mineralogist 76, 18 11 –1823.

Akai, J. (1982) Polymerization process of biopyriboles in metasomatism at the Akatani ore deposit, Japan. Contributions to Mineralogy and Petrology 80, 117-131. https://doi.org/10.1007/BF00374889

Akai, J., Chiba, A., Konishi, H., Komatsu, M., and Matsubara, S. (1997) New occurrences of non-classical pyriboles formed during ocean-floor and regional metamorphism: estimated PT conditions of formation. European Journal of Mineralogy 9, 1237-1255. https://doi.org/10.1127/ejm/9/6/1237

Almeida, F.F.M., Hasui, Y., Brito Neves, B.B., and Fuck, R.A. (1981) Brazilian structural provinces: an introduction. Earth-Science Reviews 17, 1-29. https://doi.org/10.1016/0012-8252(81)90003-9

Almeida, C.M., Olivo, G.R., and Carvalho, S.G. (2007) The Ni-Cu-PGE sulfide ores of the komatiite-hosted Fortaleza de Minas deposit, Brazil: Evidence of hydrothermal remobilization. Canadian Mineralogist 45, 751-773. https://doi.org/10.2113/gscanmin.45.4.751

Ams, B.E., Jenkins, D.M., Boerio-Goates, J., Morcos, M.R., Navrotsky, A., and Bozhilov, K.N. (2009) Thermochemistry of a synthetic Na-Mg-rich triple-chain silicate: Determination of thermodynamic variables. American Mineralogist 94, 1242-1254. https://doi.org/10.2138/am.2009.2980

Antonio, P.Y.J., D'Agrella-Filho, M.S., Nédélec, A., Poujol, M., Sanchez, C., Dantas, E.L., Dall'Agnol, R., Teixeira, M.F.B., Proietti, A., MartínezDopico C.I., Oliveira, D.C., Silva, F.F., Marangoanha, B., and Trindade, R.I.F. (2021) New constraints for paleogeographic reconstructions at ca. 1.88 Ga from geochronology and paleomagnetism of the Carajás dyke swarm (eastern Amazonia). Precambrian Research 353, 106039. https://doi.org/10.1016/j.precamres.2020.106039

Araújo, O.D., Maia, R.G.N., João, X.J., and Costa, J.B.S. (1988) A megaestruturação arqueana da folha Serra dos Carajás. In Congresso Latino-Americano de Geologia SBG-NO Belém vol. 7, p. 324-338.

Araújo Filho, R.C., Nogueira, A.C., and Araújo, R.N. (2020) New stratigraphic proposal of a Paleoproterozoic siliciclastic succession: Implications for the evolution of the Carajás Basin, Amazonian craton, Brazil. Journal of South American Earth Sciences 102, 102665. https://doi.org/10.1016/j.jsames.2020.102665

Armstrong, J.T. (1988) Quantitative analysis of silicate and oxide minerals: comparison of Monte Carlo, ZAF and phi-rho-z procedures. Analysis microbeam. D.E. Newbury, ed., San Fransisco Press, 239-246.

Bailey, S.W. (1988) Chlorites: structures and crystal chemistry. In S.W. Bailey Ed., Hydrous Phyllosilicates (exclusive of micas), 19, 347.403. Reviews in Mineralogy and Geochemistry Mineralogical Society of America, Chantilly, Virginia.

Barkov, A.Y., Bindi, L., Tamura, N., Shvedov, G.I., Winkler, B., Stan, C.V., Morgenroth, W., Martin, R.F., Zaccarini, F., and Stanley, C.J. (2019) Ognitite, NiBiTe, a new mineral species, and Co-rich maucherite from the Ognit ultramafic complex, Eastern Sayans, Russia. Mineralogical Magazine 83, 695-703. https://doi.org/10.1180/mgm.2019.31

Barnes, S.J., and Liu, W. (2012) Pt and Pd mobility in hydrothermal fluids: Evidence from komatiites and from thermodynamic modelling. Ore Geology Reviews 44, 49–58. https://doi.org/10.1016/j.oregeorev.2011.08.004

Barros, C.E.M., Sardinha, A.S., Barbosa, J.D.P.O., Macambira, M.J.B., Barbey, P., and Boullier, A.M. (2009) Structure, petrology, geochemistry and zircon U/Pb and Pb/Pb geochronology of the synkinematic Archean (2.7 Ga) A-type granites from the Carajás Metallogenic Province, northern Brazil. The Canadian Mineralogist 47(6), 1423-1440. https://doi.org/10.3749/canmin.47.6.1423

Barton, M. (2014) Iron oxide (–Cu–Au–REE–P–Ag–U–Co) systems. Treatise on Geochemistry, 2nd ed, vol 13. Elsevier, Amsterdam, p. 515-541. https://doi.org/10.1016/B978-0-08-095975-7.01123-2-2

Belousova, E.A., Walters, S., Griffin, W.L., and O'reilly, S.Y. (2001) Trace-element signatures of apatites in granitoids from the Mt Isa Inlier, northwestern Queensland. Australian Journal of Earth Sciences 48(4), 603-619. https://doi.org/10.1046/j.1440-0952.2001.00879.x

Belousov, I., Danyushevsky, L., Goemann, K., Gilbert, S., Olin, P., Thompson, J., Lounejeva, E., and Garbe-Schönberg, D. (2023) STDGL3, a reference material for analysis of sulfide minerals by Laser Ablation ICP-MS: An assessment of matrix effects and the impact of laser wavelengths and pulse widths. Geostandards and Geoanalytical Research 47, 493-508. https://doi.org/10.1111/ggr.12512

Bernard, C., Estrade, G., Salvi, S., Béziat, D., and Smith, M. (2020) Alkali pyroxenes and amphiboles: a window on rare earth elements and other high field strength elements behavior through the magmatic-hydrothermal transition of peralkaline granitic systems. Contributions to Mineralogy and Petrology 175, 81. https://doi.org/10.1007/s00410-020-01723-y

Biagoni, C., and Pasero, M. (2014) The systematics of the spinel-type minerals: An overview. American Mineralogist 99, 1254–1264. https://doi.org/10.2138/am.2014.4816

Bidgood, A., and Hitzman, M. (2023) New models to aid the discovery of critical raw material deposits for the Green Stone Age. In: Smelror, M., Hanghøj, K., Schiellerup, H. (eds), The Green Stone Age: Exploration and Exploitation of Minerals for Green Technologies. Geological Society, London, Special Publications 526, 183-191. https://doi.org/10.1144/SP526-2022-79

Bozhilov, K.N., Brownstein, D., and Jenkins, D.M. (2007) Biopyribole evolution during tremolite synthesis from dolomite and quartz in CO_2-H_2O fluid. American Mineralogist 92, 898–908. https://doi.org/10.2138/am.2007.2376

Bozhilov, K.N. (2013) Structures and microstructures of non-classical pyriboles. EMU Notes in Mineralogy 14, 109-152. https://doi.org/10.1180/EMU-notes.14.4

Brown, D.A., Reid, A., Jagodzinski, E.A., Williams, M., Simpson, A., Pawley, M., Kirkland, C.L., Wade, C., Leeuwen, A.T.V.V., and Glorie, S. (2024) Testing in-situ apatite Lu–Hf dating in polymetamorphic mafic rocks: a case study from Palaeoproterozoic southern Australia. Contributions to Mineralogy and Petrology 179(5), 46. https://doi.org/10.1007/s00410-024-02117-0

Buseck, P.R., and Iijima, S. (1974) High resolution electron microscopy of silicates. American Mineralogist 59, 1-21.

Cabral, A.R., Lehmann, B., Kwitko, R., and Costa, C.H.C. (2002) The Serra Pelada Au-Pd-Pt deposit, Carajás mineral province, northern Brazil: reconnaissance mineralogy and chemistry of very high grade palladian gold mineralization. Economic Geology 97, 1127-1138. https://doi.org/10.2113/gsecongeo.97.5.1127

Cabral, A.R., Lehmann, B., and Burgess, R. (2011) Late Cretaceous bonanza-style metal enrichment in the Serra Pelada Au-Pd-Pt deposit Pará Brazil. Economic Geology 106, 119-125. https://doi.org/10.2113/econgeo.106.1.119

Campo-Rodríguez, Y.T., Schutesky, M.E., de Oliveira, C.G., and Whitehouse, M.J. (2022) Unveiling the polyphasic evolution of the Neoarchean IOCG Salobo deposit, Carajás Mineral Province, Brazil: Insights from magnetite trace elements and sulfur isotopes. Ore Geology Reviews 140, 104572. https://doi.org/10.1016/j.oregeorev.2021.104572

Campo-Rodríguez, Y.T., Ciobanu, C.L., Slattery, A., Cook, N.J., Schutesky, M.E., Ehrig, K., King, S.A., and Yao, J. (2024a) Polysomatic intergrowths between amphiboles and non-classical pyriboles in magnetite: smallest-scale features recording a protracted geological history. American Mineralogist 109 (10), 1798–1818. https://doi.org/10.2138/am-2023-9188

Campo-Rodriguez, Y.T., Cook, N.J., Ciobanu, C.L., Schutesky, M.E., King, S.A., Gilbert, S., and Ehrig, K. (2024b) Platinum Group Minerals Associated with Nickel-Bearing Sulfides from the Jatobá Iron Oxide-Copper-Gold Deposit, Carajás Domain, Brazil. Minerals 14, 757. https://doi.org/10.3390/min14080757

Campo-Rodriguez, Y.T., Ciobanu, C.L., Cook, N.J., Schutesky, M.E., Ehrig, K., Slattery, A., Gilbert, S., and King, S.A. (*in review, a*) Telescoped transition from trellis to silicate mottled magnetite records deep shear zone metamorphism in the IOCG deposit at Jatobá, Carajás, Brazil. Mineralium deposita.

Campo Rodriguez, Y.T., Ciobanu, C.L., Gilbert, S., Wade, B., Cook, N.J., Schutesky, M.E., and Ehrig, K. (*in review, b*) Coupled Lu-Hf and U-Pb apatite geochronology of Jatobá orebody supports ~2.5 Ga metamorphism in deep shear zones from Southern Copper Belt, Carajás Domain, Brazil. Precambrian Research.

Campo Rodriguez, Y.T., Ciobanu, C.L., Cook, N.J., Schutesky, M.E., Ehrig, K., Slattery, A., Gilbert, S., and King, S.A. (*in review, c*) Magnetite and REE-rich calcic amphibole provide evidence for a skarn-IOCG system at Onça Rosa, Jaguar Orefield, Carajás Mineral Province, Brazil. The Canadian Journal of Mineralogy and Petrology.

Campo Rodriguez, Y.T., Ciobanu, C.L., Cook, N.J., Slattery, A., Wade, B., Gilbert, S., Schutesky, M.E., and Ehrig, K. (*in review, d*) Arsenohauchecornite, ognitite, parkerite, and related minerals from Onça Rosa orebody, Carajás, Brazil: fingerprinting PGE signatures in hydrothermal Ni ores. American Mineralogist.

Centaurus Metals. (2023) Jaguar Nickel Deposit, Carajás – the world's largest and oldest (?) hydrothermal nickel sulfide deposit. Presentation, MEGWA Monthly Meeting, 15th March 2023, Perth, W.A., Australian Institute of Geoscientists https://www.youtube.com/watch?v=duO6_7Lj2vM (accessed 4 September 2024).

Centaurus Metals. (2024) Jaguar Nickel Sulphide Project. https://www.centaurus.com.au/site/projects/jaguar-nickel-sulphide-project (accessed 05 September 2024).

Chew, D.M., Sylvester, P.J., and Tubrett, M.N. (2011) U–Pb and Th–Pb dating of apatite by LA-ICPMS. Chemical Geology 280(1-2), 200-216. https://doi.org/10.1016/j.chemgeo.2010.11.010

Chew, D.M., and Spikings, R.A. (2021) Apatite U-Pb thermochronology: A review. Minerals 11(10), 1095. https://doi.org/10.3390/min11101095

Ciobanu, C.L., Cook, N.J., Utsunomiya, S., Pring, A., and Green, L. (2011) Focussed ion beam–transmission electron microscopy applications in ore mineralogy: Bridging micro- and nanoscale observations. Ore Geology Reviews 42, 6–31. https://doi.org/10.1016/j.oregeorev.2011.06.012

Ciobanu, C.L., Verdugo-Ihl, M.R., Slattery, A., Cook, N.J., Ehrig, K., Courtney-Davies, L., and Wade, B.P. (2019) Silician magnetite: Si–Fe-nanoprecipitates and other mineral inclusions in magnetite from the Olympic Dam Deposit, South Australia. Minerals 9, 311. https://doi.org/10.3390/min9050311

Ciobanu, C.L., Verdugo-Ihl, M.R., Cook, N.J., Ehrig, K., Slattery, A., and Courtney-Davis, L. (2022) Ferro-tschermakite with polysomatic chain-width disorder identified in silician magnetite from Wirrda Well, South Australia: A HAADF STEM study. American Mineralogist 107, 765-777. https://doi.org/10.2138/am-2022-7975

Cook, N.J., Ciobanu, C.L., Ehrig, K., Slattery, A.D., and Gilbert, S.E. (2022) Micron- to atomic-scale investigation of rare earth elements in iron oxides. Frontiers in Earth Science 10, 967189. https://doi.org/10.3389/feart.2022.967189

Corriveau, L., Montreuil, J.F., and Potter, E.G. (2016) Alteration facies linkages among iron oxide copper-gold, iron oxide-apatite, and affiliated deposits in the Great Bear magmatic zone, Northwest Territories, Canada. Economic Geology 111, 2045-2072. https://doi.org/10.2113/econgeo.111.8.2045

Costa, F.G., Santos, P.A., Serafim, I.C.C.O., Costa, I.S.L., and Roopnarain, S. (2020) From Mesoarchean drips to modern–style tectonics in the Carajás Province, Amazonian Craton. Journal of South American Earth Science 104, 102817. https://doi.org/10.1016/j.jsames.2020.102817

Courtney, T. (2000). Mechanical Properties of Materials. McGraw Hill. pp. 203–205.

Courtney-Davies, L., Tapster, S.R., Ciobanu, C.L., Cook, N.J., Verdugo-Ihl, M.R., Ehrig, K.J., Kennedy, A.K., Gilbert, S.E., Condon, D.J., and Wade, B.P. (2019a) A multi-technique evaluation of hydrothermal hematite U-Pb isotope systematics: Implications for ore deposit geochronology. Chemical Geology 513, 54-72. https://doi.org/10.1016/j.chemgeo.2019.03.005

Courtney-Davies, L., Ciobanu, C.L., Verdugo-Ihl, M.R., Dmitrijeva, M., Cook, N.J., Ehrig, K., and Wade, B.P. (2019b) Hematite geochemistry and geochronology resolve genetic and temporal links among iron-oxide copper gold systems, Olympic Dam district, South Australia. Precambrian Researchs 335, 105480. https://doi.org/10.1016/j.precamres.2019.105480

Courtney-Davies, L., Ciobanu, C.L., Tapster, S.R., Cook, N.J., Ehrig, K., Crowley, J.L., Verdugo-Ihl, M.R., Wade, B.P., and Condon, D.J. (2020a) Opening the magmatic-hydrothermal window: High-precision U-Pb geochronology of the mesoproterozoic olympic dam Cu-U-Au-Ag deposit, South Australia. Economic Geology 115, 1855-1870. https://doi.org/10.5382/econgeo.4772

Courtney-Davis, L., Ciobanu, C.L., Verdugo-Ihl, M.R., Cook, N.J., Ehrig, K.J., Wade, B.P., Zhu, Z.Y., and Kamenetsky, V.S. (2020b) ~1760 Ma magnetite-bearing protoliths in the Olympic Dam deposit, South Australia: Implications for ore genesis and regional metallogeny. Ore Geology Reviews 118, 103337. https://doi.org/10.1016/j.oregeorev.2020.103337

Courtney-Davies, L., Gilbert, S.E., Ciobanu, C.L., Tapster, S.R., Richardson, M.W., Cook, N.J., Wade, B.P., Verdugo-Ihl, M.R., Ehrig, K., and Condon, D.J. (2021) A synthetic haematite reference material for LA-ICP-MS U-Pb geochronology and application to iron Oxide-Cu-Au Systems. Geostandards and Geoanalytical Research 45, 143-159. https://doi.org/10.1111/ggr.12365

Craveiro, G.S., Xavier, R.P., and Villas, R.N.N. (2019) The Cristalino IOCG deposit: an example of multi-stage events of hydrothermal alteration and copper mineralization. Brazilian Journal of Geology 49 (01). https://doi.org/10.1590/2317-4889201920180015

Crespo, J., Reich, M., Barra, F., Verdugo, J.J., and Martínez, C. (2018) Critical Metal Particles in Copper Sulfides from the Supergiant Río Blanco Porphyry Cu-Mo Deposit, Chile. Minerals 8, 519. https://doi.org/10.3390/min8110519

Cressey, B.A., Whittaker, E.J.W., and Hutchison, J.L. (1982) Morphology and alteration of asbestiform grunerite and anthophyllite. Mineralogical Magazine 46, 77-87. https://doi.org/10.1180/minmag.1982.046.338.13

Deditius, A.P., Reich, M., Simon, A.C., Suvorova, A., Knipping, J., Roberts, M.P., Rubanov, S., Dodd, A., and Saunders, M. (2018) Nanogeochemistry of hydrothermal magnetite. Contributions to Mineralogy and Petrology 173, 46. https://doi.org/10.1007/s00410-018-1474-1

Diella, V., Ferrario, A., and Girardi, V.A.V. (1995) PGE and PGM in the Luanga mafic-ultramafic intrusion in Serra dos Carajás (Pará State, Brazil). Ore Geology Reviews 9, 445-453. https://doi.org/10.1016/0169-1368(95)00002-J

DOCEGEO (1988) Revisão litoestratigráfica da Província Mineral de Carajás-Litoestratigrafia e principais depósitos minerais, 35th Congresso Brasileiro de Geologia: Brazil p. 11-54.

Donovan, J.J., and Tingle, T.N. (1996) An Improved Mean Atomic Number Background Correction for Quantitative Microanalysis. Microscopy and Microanalysis 2(1), pp. 1-7. https://doi.org/10.1017/S1431927696210013

Donovan, J.J., and Rowe, M. (2005) Techniques for improving quantitative analysis of mineral glasses. Geochim Cosmochim Acta 69(10), A589.

Donovan, J.J., Singer, J.W., and Armstrong, J.T. (2016) A new EPMA method for fast trace element analysis in simple matrices. American Mineralogist 101(8), 1839-1853. https://doi.org/10.2138/am-2016-5628

Droop, G.T.R. (1994) Triple-chain pyriboles in Lewisian ultramafic rocks. Mineralogical Magazine 58, 1-20. https://doi.org/10.1180/minmag.1994.058.390.01

Duncan, R.J., Stein, H.J., Evans, K.A., Hitzman, M.W., Nelson, E.P., and Kirwin, D.J. (2011) A new geochronological framework for mineralization and alteration in the Selwyn-Mount Dore corridor, Eastern fold belt, Mount Isa inlier, Australia: Genetic implications for iron oxide copper-gold deposits. Economic Geology 106(2), 169-192. https://doi.org/10.2113/econgeo.106.2.169

Dutra, L.F., Louro, V.H.A., and Monteiro, L.V.S. (2023) The southern IOCG and hydrothermal nickel mineralization trend of the Carajás Mineral Province: Airborne geophysical and remote sensing evidences for structural controls and hydrothermal signature. Journal of Applied Geophysics 213, 105016. https://doi.org/10.1016/j.jappgeo.2023.105016

Duran, C.J, Barnes, S.J, Pleše, P., Prašek, M.K., Zientek, M.L., and Pagé, P. (2017) Fractional crystallization-induced variations in sulfides from the Noril'sk-Talnakh mining district (polar Siberia, Russia). Ore Geology Reviews 90, 326-351. https://doi.org/10.1016/j.oregeorev.2017.05.016

Einaudi, L.D., Meinert, L.D., and Newberry, R.J. (1981) Skarn deposits. Economic Geology Seventy-Fifth Anniversary Volume. Society of Economic Geologists p. 317–391.

Evans, B.W., and Yang. H. (1998) Fe-Mg order-disorder in tremolite-actinolite-ferro-actinolite at ambient and high temperature. American Mineralogist 83, 458-475. https://doi.org/10.2138/am-1998-5-605

Feio, G.R.L., Dall'Agnol, R., Dantas, E.L., Macambira, M.J.B., Santos, J.O.S., Althoff, F.J., and Soares, J.E.B. (2013) Archean granitoid magmatism in the Canaã dos Carajás area: implications for crustal evolution of the Carajás province, Amazonian craton, Brazil. Precambrian Research 227, 157-185. https://doi.org/10.1016/j.precamres.2012.04.00

Fernandes, C.M.D., Galarza, M.A., Teixeira de Gouvêa, R.C., and Tavares de Souza, H.P. (2021) Geochemical, geochronological, and isotopic constraints for the Archean metamorphic rocks of the westernmost part of the Carajás Mineral Province, Amazonian Craton, Brazil. Journal of South America Earth Sciences 110, 103340. https://doi.org/10.1016/j.jsames.2021.103340

Ferrari, M., and Viti, C. (2010) Retrograde hydration sequence in disordered Mg amphiboles: A TEM investigation. American Mineralogist 95, 81-91. https://doi.org/10.2138/am.2010.3254

Ferreira-Filho, C.F., de Oliveira, M.M.F., Mansur, E.T., and Rosa, W.D. (2021) The Jaguar hydrothermal nickel sulphide deposit: evidence for a nickel-rich member of IOCG-type deposits in the Carajás Mineral Province, Brazil. Journal of South American Earth Science 111, 103501. https://doi.org/10.1016/j.jsames.2021.103501

Fleet, M.E. (1973) The crystal structure of parkerite (Ni3Bi2S2) American Mineralogist 58, 435-439.

Garcia, V.B., Schutesky, M.E., Oliveira, C.G., Whitehouse, M.J., Huhn, S.R.B., and Augustin, C.T. (2020) The Neoarchean GT-34 Ni deposit, Carajás mineral Province, Brazil: An atypical IOCG-related Ni sulfide mineralization. Ore Geology Reviews 127, 103773. https://doi.org/10.1016/j.oregeorev.2020.103773

Garuti, G., and Rinaldi, R. (1986) Mineralogy of melonite-group and other tellurides from the Ivrea–Verbano basic complex, western Italian Alps. Economic Geology 81, 1213–1217. https://doi.org/10.2113/gsecongeo.81.5.1213

Gait, R.I., and Harris, D.C. (1980) Arsenohauchecornite and tellurohauchecornite: new minerals in the hauchecornite group. Mineralogical Magazine 43, 877-888. https://doi.org/10.1180/minmag.1980.043.331.09

Gezzaz, H., Ciobanu, C., Cook, N., Ehrig, K., Slattery, A., Wade, B., Gilbert, S., and Campo Rodriguez, Y.T. (Submitted). Monazite, lanthanide-rich glasses, and other trace elements in copper smelter slags: Constraints on critical metal behaviour in Si-Fe-rich melts. Mineralogy and Petrology.

Glorie, S., Jepson, G., Konopelko, D., Mirkamalov, R., Meeuws, F., Gilbert, S., Gillespie, J., Collins, A.S., Xiao, W., Dewaele, S., and de Grave, J. (2019) Thermochronological and geochemical footprints of post-orogenic fluid alteration recorded in apatite: Implications for mineralisation in the Uzbek Tian Shan. Gondwana Research 71, 1-15. https://doi.org/10.1016/j.gr.2019.01.011

Glorie, S., Gillespie, J., Simpson, A., Gilbert, S., Khudoley, A., Priyatkina, N., Hand, M., and Kirkland, C.L. (2022) Detrital apatite Lu–Hf and U–Pb geochronology applied to the southwestern Siberian margin. Terra Nova 34(3), 201-209. https://doi.org/10.1111/ter.12580

Glorie, S., Hand, M., Mulder, J., Simpson, A., Emo, R.B., Kamber, B., Fernie, N., Nixon, A., and Gilbert, S. (2024) Robust laser ablation Lu–Hf dating of apatite: an empirical evaluation. Geological Society, London, Special Publications 537(1), 165-184. https://doi.org/10.1144/SP537-2022-205

Gilbert, S., Danyushevsky, L., Robinson, P., Wohlgemuth-Ueberwasser, C., Pearson, N., Savard, D., Norman, M.; and Hanley, J. (2013) A comparative study of five reference materials and the Lombard meteorite for the determination of the platinum-group elements and gold by LA-ICP-MS. Geostandards and Geoanalytical Research 37, 51-64. https://doi.org/10.1111/j.1751-908X.2012.00170.x

González-Álvarez, I., Pirajno, F., and Kerrich, R. (2013) Hydrothermal nickel deposits: Secular variation and diversity. Ore Geology Reviews 52, 1-3. https://doi.org/10.1016/j.oregeorev.2012.11.006

Grainger, C.J., Groves, D.I., Tallarico, F.H., and Fletcher, I.R. (2008) Metallogenesis of the Carajás mineral province, southern Amazon craton, Brazil: Varying styles of Archean through Paleoproterozoic to Neoproterozoic base-and precious-metal mineralisation. Ore Geology Reviews 33 (3-4), 451-489. https://doi.org/10.1016/j.oregeorev.2006.10.010

Grice, J.D., and Ferguson, R.B. (1989) The crystal structure of arsenohauchecornite, The Canadian Mineralogist 27, 137-142.

Grobéty, B.H. (1996) New short-range biopyribole polysomes from the Lepontine Alps, Switzerland. American Mineralogist 81, 404-417. https://doi.org/10.2138/am-1996-3-415

Grobéty, B.H. (1997) The replacement of anthophyllite by jimthompsonite: a model for hydration reactions in biopyriboles. Contributions to Mineralogy and Petrology 127, 237-247. https://doi.org/10.1007/s004100050277

Groves, D.I., Bierlein, F.P., Meinert, L.D., and Hitzman, M.W. (2010) Iron Oxide Copper-Gold (IOCG) deposits through earth history: implications for origin, lithospheric setting, and distinction from other epigenetic iron oxide deposits: Economic Geology v. 105, p. 641–654. https://doi.org/10.2113/gsecongeo.105.3.641

Harlov, D.E., Andersson, U.B., Förster, H.J., Nyström, J.O., Dulski, P., and Broman, C. (2002) Apatite–monazite relations in the Kiirunavaara magnetite–apatite ore, northern Sweden. Chemical Geology 191(1-3), 47-72. https://doi.org/10.1016/S0009-2541(02)00148-1

Harlov, D.E. (2015) Apatite: A fingerprint for metasomatic processes. Elements 11(3), 171-176. https://doi.org/10.2113/gselements.11.3.171

Hatert, F., Mills, S.J., Pasero, M., Miyawaki, R., and Bosi, F. (2023) CNMNC guidelines for the nomenclature of polymorphs and polysomes. Mineralogical Magazine 87, 225-232. https://doi.org/10.1180/mgm.2023.13

Hawthorne, F.C., Oberti, R., Harlow, G.E., Maresch, W.V., Martin, R.F., Schumacher, J.C., and Welch, M.D. (2012) Nomenclature of the amphibole supergroup. American Mineralogist 97, 2031-2048. https://doi.org/10.2138/am.2012.4276

Hekinian, R. (1982) Chapter 9 Ocean floor metamorphism. Elsevier Oceanography Series. Elsevier 33:265-290.

Helmy, H.M., Botcharnikov, R., Ballhaus, C., Wirth, R., Schreiber, A., and Buhre, S. (2023) How Pt and Pd are hosted in magmatic sulfides, substitutions and/or inclusions? Contributions to Mineralogy and Petrology 178, 41. https://doi.org/10.1007/s00410-023-02018-8

Hernandez-Tasco, L., Monteiro, L.V.S., Ribeiro, B.V., Dutra, L.F., Ferreira Filho, C.F., Mansur, E.T., and Montresor, G. (2023) In situ high-resolution U-Pb geochronology of apatite: understanding the alteration-mineralization timing of the Jaguar hydrothermal nickel deposit, Carajás Mineral Province. Simpósio da Pós-Graduação, Universidade de São Paulo. (accessed 05 September 2024). https://repositorio.usp.br/directbitstream/d5ca9a19-7683-427c-80b6-64775ed7c03c/3152535.pdf

Hitzman, M.W., Oreskes, N., and Einaudi, M.T. (1992) Geological characteristics and tectonic setting of Proterozoic iron oxide (Cu-U-Au-REE) deposits. Precambrian Research 58, 241-287. https://doi.org/10.1016/0301-9268(92)90121-4

Hitzman, M.W., Oreskes, N., Einaudi, and M.T. (2002) Geological characteristics and tectonic setting of Proterozoic iron oxide (Cu-U-Au-REE) deposits. Precambrian Research 58, 241-287. https://doi.org/10.1016/0301-9268(92)90121-4

Hu, H., Li, J.W., Harlov, D.E., Lentz, D.R., McFarlane, C.R.M., and Yang, Y.H. (2020) A genetic link between iron oxide-apatite and iron skarn mineralization in the Jinniu volcanic basin, Daye district, eastern China: Evidence from magnetite geochemistry and multi-mineral U-Pb geochronology. GSA Bulletin 132 (5-6), 899–917. https://doi.org/10.1130/B35180.1

Huang, X.W., and Beaudoin, G. (2019) Textures and chemical compositions of magnetite from iron oxide copper-gold (IOCG) and Kiruna-type iron oxide-apatite (IOA) Deposits and their implications for ore genesis and magnetite classification schemes. Economic Geology 114,953–979. https://doi.org/10.5382/econgeo.4651

Huang, X.W., and Beaudoin, G. (2021) Nanoinclusions in zoned magnetite from the Sossego IOCG deposit, Carajás, Brazil: Implication for mineral zoning and magnetite origin discrimination. Ore Geology Reviews 139, 104453. https://doi.org/10.1016/j.oregeorev.2021.104453

Huang, X.W., Beaudoin, G., and Yang, Y. (2022) A HR-TEM study on two generations of magnetite from the Alemao IOCG deposit, Carajás, Brazil: Implication for Fe-Cu mineralization. Ore Geology Reviews 146, 104934. https://doi.org/10.1016/j.oregeorev.2022.104934

Ishihara, S., and Murakami, H. (2006) Fractionated ilmenite-series granites in Southwest Japan: Source magma for REE-Sn-W mineralizations. Resource Geology 56 (3), 245-256. https://doi.org/10.1111/j.1751-3928.2006.tb00282.x

Ismail, R., Ciobanu, C.L., Cook, N.J., Teale, G.S., Giles, D., Mumm, A.S., and Wade, B. (2014) Rare earths and other trace elements in minerals from skarn assemblages, Hillside iron oxide–copper–gold deposit, Yorke Peninsula, South Australia. Lithos 184, 456-477. https://doi.org/10.1016/j.lithos.2013.07.023

Jenkins, D.M., Gilleaudeau, G.J., Kawa, C., Dibiase, J.M., and Fokin, M. (2012) Compositional limits and analogs of monoclinic triple-chain silicates. Contributions to Mineralogy and Petrology 164, 229-244. https://doi.org/10.1007/s00410-012-0735-7

Jochum, K.P., Weis, U., Stoll, B., Kuzmin, D., Yang, Q., Raczek, I., Jacob, D.E., Stracke, A., Birbaum, K., Frick, D.A., Günther, D., and Enzweiler, J. (2011) Determination of reference values for NIST SRM 610–617 glasses following ISO guidelines. Geostandards and Geoanalytical Research 35(4), 397-429. https://doi.org/10.1111/j.1751-908X.2011.00120.x

Junge, M., Wirth, R., Oberthür, T., Melcher, F., and Schreiber, A. (2015) Mineralogical siting of platinum-group elements in pentlandite from the Bushveld Complex, South Africa. Mineralium Deposita 50, 41–54. https://doi.org/10.1007/s00126-014-0561-0

Just, J., and Feather, C.E. (1978) Tucekite, a new antimony analogue of hauchecornite. Mineralogical Magazine 42, 278. https://doi.org/10.1180/minmag.1978.042.322.18

Just, J. (1980) Bismutohauchecornite—new name: hauchecornite redefined. Mineralogical Magazine 43, 873–876. https://doi.org/10.1180/minmag.1980.043.331.08

Justo, A.P., Dantas, E.L., Bau, M., Freitas-Silva, F.H., Santos, R.V., and Schorscher, J.H.D. (2020) Paleobasinal to band-scale REE + Y distribution in iron formations from Carajás, Amazon Craton, Brazil. Ore Geology Reviews 127, 103750. https://doi.org/10.1016/j.oregeorev.2020.103750

Keays, R.R., and Jowitt, S.M. (2013) The Avebury Ni deposit, Tasmania: A case study of an unconventional nickel deposit. Ore Geology Reviews 52, 4-17. https://doi.org/10.1016/j.oregeorev.2012.07.001

Kirkland, C.L., Yakymchuk, C., Szilas, K., Evans, N., Hollis, J., McDonald, B., and Gardiner, N.J. (2018) Apatite: a U-Pb thermochronometer or geochronometer?. Lithos 318, 143-157. https://doi.org/10.1016/j.lithos.2018.08.007

King, S.A., Cook, N.J., Ciobanu, C.L., Ehrig, K., Campo Rodriguez, Y.T., Basak, A., and Gilbert, S. (2024) Coupled Microstructural EBSD and LA-ICP-MS Trace Element Mapping of Pyrite Constrains the Deformation History of Breccia-Hosted IOCG Ore Systems. Minerals 14(2), 198. https://doi.org/10.3390/min14020198

King, S.A., Cook, N.J., Ciobanu, C.L., Ehrig, K., Rodriguez, Y.T.C., Gilbert, S., and Basak, A. (2024) EBSD mapping of Cu-Fe-sulfides reveal microstructures enriched in critical/precious metals and resolve deformation histories. American Mineralogist. https://doi.org/10.2138/am-2024-9396

Klein, E.L., Rodrigues, J.B., Lopes, E.C., and Soledade, G.L. (2012) Diversity of Rhyacian granitoids in the basement of the Neoproterozoic-Early Cambrian Gurupi Belt, northern Brazil: Geochemistry, U–Pb zircon geochronology, and Nd isotope constraints on the Paleoproterozoic magmatic and crustal evolution. Precambrian Research 220, 192-216. https://doi.org/10.1016/j.precamres.2012.08.007

Knipping, J.L., Bilenker, L.D., Simon, A.C., Reich, M., Barra, F., Deditius, A.P., Wälle, M., Heinrich, C.A., Holtz, F., and Munizaga, R. (2015) Trace elements in magnetite from massive iron oxide-apatite deposits indicate a combined formation by igneous and magmatic-hydrothermal processes. Geochimica et Cosmochimica Acta 171, 15-38. https://doi.org/10.1016/j.gca.2015.08.010

Konishi, H., Akai, J., and Kurokawa, K. (1993) Calcic analog of clinojimthompsonite from the Oeyama Ophiolite, Southwest Japan. Journal of the Geological Society of Japan 99, 679-682. https://doi.org/10.5575/geosoc.99.679

Konishi, H., Buseck, P.R., Xu, H., and Li, X. (2008) Proto-polymorphs of jimthompsonite and chesterite in contact-metamorphosed serpentinites from Japan. American Mineralogist 93, 351-359. https://doi.org/10.2138/am.2008.2637

Konishi, H., Xu, H., and Dymek, R.F. (2010) High-resolution TEM study of jimthompsonite, chesterite, and chain-width disorder in Archean ultramafic rocks from Isua, West Greenland. American Mineralogist 95, 73–80. https://doi.org/10.2138/am.2010.3212

Kontonikas-Charos, A., Ciobanu, C.L., Cook, N.J., Ehrig, K., Krneta, S., and Kamenetsky, V.S. (2017) Feldspar evolution in the Roxby Downs granite, host to Fe-oxide cu-au-(U) mineralisation at Olympic dam, South Australia. Ore Geology Reviews 80, 838-859. https://doi.org/10.1016/j.oregeorev.2016.08.019

Koroteev, V.A., Popov, M.P., Erokhin, Y.V., and Khiller, V.V. (2017) Parkerite and bismutohauchecornite in chromitites of the Urals: Example of the Uralian Emerald Mines. Doklady Earth Sciences 473, 438-440. https://doi.org/10.1134/S1028334X17040109

Kovalenker, V.A., Evstigneeva, T.L., Begizov, V.D., Vyal'sov, L.N., Smirnov, A.V., Krakovetskii, Y.K., and Balbin, V.S. (1978) Hauchecornite from copper-nickel ores of the Oktyabr'skoe deposit. Trudy Min. muzeya Akad. Nauk SSSR 26, 201–205 (in Russian).

Krneta, S., Cook, N.J., Ciobanu, C.L., Ehrig, K., and Kontonikas-Charos, A. (2017a) The Wirrda Well and Acropolis prospects, Gawler Craton, South Australia: Insights into evolving fluid conditions through apatite chemistry. Journal of Geochemical Exploration 181, 276-291. https://doi.org/10.1016/j.gexplo.2017.08.004

Krneta, S., Ciobanu, C.L., Cook, N.J., Ehrig, K., and Kontonikas-Charos, A. (2017b) Rare earth element behaviour in apatite from the Olympic Dam Cu–U–Au–Ag deposit, South Australia. Minerals 7 (8), 135. https://doi.org/10.3390/min7080135

Krneta, S., Ciobanu, C.L., Cook, N.J., and Ehrig, K.J. (2018) Numerical modeling of REE fractionation patterns in fluorapatite from the Olympic Dam deposit (South Australia). Minerals 8 (8), 342. https://doi.org/10.3390/min8080342

Lancaster, J.O., Fanton, J., Almeida, A.J., Leveille, R.A., and Vieira, S. (2000) Discovery and geology of the Sossego copper-gold deposit, Carajás District, Pará State, Brazil. 31st Internat. Geol. Congress, Rio de Janeiro, Brazil Abstracts CDROM.

Leake, B.E., Woolley, A.R., ARPS, C.E.S., Birch, W.D., Gilbert, M.C., Grice, J.D., Hawthorne, F.C., Kato, A., Kisch, H.J., Krivovichev, V.G., and others. (1997) Nomenclature of amphiboles: report of the subcommittee on amphiboles of the international mineralogical association, commission on new minerals and mineral names. The Canadian Mineralogist 35, 219-246. https://doi.org/10.1180/minmag.1997.061.405.13

Leloup, P.H., and Kienast, J.R. (1993) High-temperature metamorphism in a major strike-slip shear zone: the Ailao Shan—Red River, People's Republic of China. Earth and Planetary Science Letters 118(1-4), 213-234. https://doi.org/10.1016/0012-821X(93)90169-A

Leloup, P.H., Ricard, Y., Battaglia, J., and Lacassin, R. (1999) Shear heating in continental strike-slip shear zones: model and field examples. Geophysical Journal International 136(1), 19-40. https://doi.org/10.1046/j.1365-246X.1999.00683.x

Lepage, L.D. (2003) ILMAT: an Excel worksheet for ilmenite–magnetite geothermometry and geobarometry. Computers & Geosciences 29, 673-678. https://doi.org/10.1016/S0098-3004(03)00042-6

Lindenmayer, Z.G., and Teixeira, J.B.G. (1999) Ore genesis at the Salobo copper deposit, Serra dos Carajás. Base Metal Deposits of Brazil. Belo Horizonte, MME/CPRM/DNPM p. 33-43.

Lindsley, D.H., and Spencer, K.J. (1982) Fe−Ti oxide geothermometry: Reducing analyses of coexisting Ti-magnetite (Mt) and ilmenite (Ilm). Transactions, American Geophysical Union 63, 471.

Lister, J.S., and Bailey, S.W. (1967) Chlorite polytypism: IV. Regular two-layer structures. American Mineralogist 52 (11-12), 1614-1631.

Liu, L., Zhou, T., Jiang, S.Y., Zhang, D., and White, N.C. (2024) Amphibole geochemistry in the Haobugao skarn Zn-Fe-Sn deposit in the southern Great Xing'an Range: Implications for the ore-forming process. Ore Geology Reviews 170, 106122. https://doi.org/10.1016/j.oregeorev.2024.106122

Lowczak, J.N., Campbell, I.H., Cocker, H., Park, J.W., and Cooke, D.R. (2018) Platinum-group element geochemistry of the Forest reef Volcanics, southeastern Australia: implications for porphyry au-cu mineralisation. Geochemical and Cosmochemical Acta 220, 385-406. https://doi.org/10.1016/j.gca.2017.09.052

Ludington, S., and Plumlee, G.S. (2009) Climax-type porphyry molybdenum deposits (p. 16). US Department of the Interior, Geological Survey.

Macambira, M.J.B., Vasquez, M.L., da Silva, D.C.C., Galarza, M.A., de Mesquita Barros, C.E., and de Freitas Camelo, J. (2009) Crustal growth of the central-eastern Paleoproterozoic domain, SW Amazonian craton: Juvenile accretion vs. reworking. Journal of South America Earth Sciences 27(4), 235-246. https://doi.org/10.1016/j.jsames.2009.02.001

Machado, N., Lindenmayer, Z, Krogh, T.E., and Lindenmayer, D. (1991) U-Pb geochronology of Archean magmatism and basement reactivation in the Carajás area, Amazon shield, Brazil. Precambrian Research 49, 329-354. https://doi.org/10.1016/0301-9268(91)90040-H

Machado, A.L., Garnier, J., Ratié, G., Guimaraes, E., Monvoisin, G., Cloquet, C., and Quantin, C. (2023) Nickel mass balance and isotopic records in a serpentinic weathering profile: Implications on the continental Ni budget. Chemical Geology 634, 121586. https://doi.org/10.1016/j.chemgeo.2023.121586

Makovicky, M., Makovicky, E., and Rose-Hansen, J. (1988) Experimental evidence on the formation and mineralogy of platinum and palladium ore deposits. In Mineral deposits within the European Community (pp. 303-317). Berlin, Heidelberg: Springer Berlin Heidelberg https://doi.org/10.1007/978-3-642-51858-4_17

Mansur, E.T., and Ferreira Filho, C.F. (2016) Magmatic structure and geochemistry of the Luanga Mafic–Ultramafic Complex: Further constraints for the PGE-mineralized magmatism in Carajás, Brazil. Lithos 266, 28-43. https://doi.org/10.1016/j.lithos.2016.09.036

Mansur E.T., Ferreira Filho C.F., and Oliveira D.P.L. (2020) The Luanga deposit, Carajás Mineral Province, Brazil: Different styles of PGE mineralization hosted in a medium-size layered intrusion. Ore Geology Reviews 118, 103340. https://doi.org/10.1016/j.oregeorev.2020.103340

Mansur, E.T., Dare, S.A.S., Ferreira Filho, C.F., Miranda, A.C.R, and Monteiro, L.V.S. (2023) The distribution of trace elements in sulfides and magnetite from the Jaguar hydrothermal nickel deposit: Exploring the link with IOA and IOCG deposits within the Carajás Mineral Province, Brazil. Ore Geology Reviews 152, 105256. https://doi.org/10.1016/j.oregeorev.2022.105256

Marschik, R., Mathur, R., Ruiz, J., Leveille, R.A., and de Almeida, A.J. (2005) Late Archean Cu-Au-Mo mineralization at Gameleira and Serra Verde, Carajás Mineral Province, Brazil: constraints from Re-Os molybdenite ages. Mineralium deposita 39, 983-991. https://doi.org/10.1007/s00126-004-0450-z

Martins, P.L.G, Toledo, C.L.B, Silva, A.M., Chemale, Jr.F., Santos J.O.S., and Assis, L.M. (2017) Neoarchean magmatism in the southeastern Amazonian Craton, Brazil: Petrography, geochemistry and tectonic significance of basalts from the Carajás Basin. Precambrian Research 302, 340-357. https://doi.org/10.1016/j.precamres.2017.10.013

McDonough, W.F. and Sun, S.S. (1995) The composition of the Earth. Chemical Geology 120, 223–253. https://doi.org/10.1016/0009-2541(94)00140-4

McFall, K., McDonald, I., and Wilkinson, J.J. (2021) Chapter 15: Assessing the role of tectono-magmatic setting in the precious metal (Au, Ag, PGE) and critical metal (Te, Se, Bi) endowment of porphyry Cu deposits. In: Tectonomagmatic Influences on Metallogeny and Hydrothermal Ore Deposits. Economic Geology 24 (vol. 2), p. 277-295. https://doi.org/10.5382/SP.24.15

Meinert, L.D. (1997) Application of skarn deposit zonation models to mineral exploration. Exploration and Mining Geology 6, 185-208.

Melo, G.H.C., Monteiro, L.V.S., Moreto, C., Xavier, R.P., and Silva, M.A.D.D. (2014) Paragenesis and evolution of the hydrothermal Bacuri iron oxide-copper-gold deposit, Carajás Province (PA). Brazilian Journal of Geology 44(1), 73-90. https://doi.org/10.5327/Z2317-4889201400010007

Melo, G.H.C., Monteiro, L.V.S., Xavier, R.P., Moreto, C.P.N., Santiago, E.S.B., Dufrane, S.A., Aires, B., and Santos, A.F.F. (2017) Temporal evolution of the giant Salobo IOCG deposit, Carajás Province (Brazil): constraints from paragenesis of hydrothermal alteration and U-Pb geochronology. Mineralium Deposita 52, 709-732. https://doi.org/10.1007/s00126-016-0693-5

Melo, G.H.C., de Monteiro, L.V.S., Xavier, R.P., Moreto, C.P.N., and Santiago, E. (2019) Tracing Fluid Sources for the Salobo and Igarape Bahia Deposits: Implications for the Genesis of the Iron Oxide Copper-Gold Deposits in the Carajás Province, Brazil. Economic Geology 114, 697-718. https://doi.org/10.5382/econgeo.4659

Melo, G.H., Monteiro, L.V., Xavier, R.P., Moreto, C.P., Arquaz, R.M., and Silva, M.A.D. (2019) Evolution of the Igarapé Bahia Cu-Au deposit, Carajás province (Brazil): early syngenetic chalcopyrite overprinted by IOCG mineralization. Ore Geology Reviews 111, 102993. https://doi.org/10.1016/j.oregeorev.2019.102993

Melo, G.H.C. de, Monteiro, L.V.S., Hunger, R.B., Toledo, P.I.F., Xavier, R.P., Zhao, X.F., Su, Z.K., Moreto, C.P.N., and Pereira de Jesus, S.d.S.G. (2021) Magmatic-hydrothermal fluids leaching older seafloor exhalative rocks to form the IOCG deposits of the Carajás Province, Brazil: Evidence from boron isotopes. Precambrian Research 365, 106412. https://doi.org/10.1016/j.precamres.2021.106412

Mercer, C.N., Watts, K.E., and Gross, J. (2020) Apatite trace element geochemistry and cathodoluminescent textures—A comparison between regional magmatism and the Pea Ridge IOAREE and Boss IOCG deposits, southeastern Missouri iron metallogenic province, USA. Ore Geology Reviews 116, 103129. https://doi.org/10.1016/j.oregeorev.2019.103129

Monteiro, L.V.S, Xavier, R.P., Hitzman, M.W., Juliani, C., de Souza Filho, C.R., and Carvalho, E. de R. (2008) Mineral chemistry of ore and hydrothermal alteration at the Sossego iron oxide–copper–gold deposit, Carajás Mineral Province, Brazil. Ore Geology Reviews 34, 317-336. https://doi.org/10.1016/j.oregeorev.2008.01.003

Monteiro, L.V.S., Xavier, R.P., Carvalho, E.R., Hitzman, M.W., Johnson, C.A., Souza, C.R., Filho, C.R., and Torresi, I. (2008) Spatial and temporal zoning of hydrothermal alteration and mineralization in the Sossego iron oxide-copper-gold deposit Carajás Mineral Province, Brazil: paragenesis and stable isotope constraints. Mineralium deposita 43, 129-159. https://doi.org/10.1007/s00126-006-0121-3

Monteiro, L.V.S., Xavier, R.P., Souza Filho, C.R., and de Moreto, C. (2014) Metalogênese da Província Carajás. In: Metalogênese das províncias tectônicas brasileiras (Silva, M. da G., ed.), CPRM Serviço Geológico do Brasil, Belo Horizonte p. 43-92.

Moreto, C.P.N., Monteiro, L.V.S., Xavier, R.P., Creaser, R.A., Dufrane, S.A., Tassinari, C.C.G., Sato, K., Kemp, A.I.S., and Amaral, W.S. (2015a) Neoarchean and Paleoproterozoic iron oxide-copper-gold events at the Sossego deposit, Carajás Province, Brazil, Re-Os and U-Pb geochronological evidence. Economic Geology 110, 809-835. https://doi.org/10.2113/econgeo.110.3.809

Moreto, C.P.N., Monteiro, L.V.S., Xavier, R.P., Creaser, R.A., Dufrane, S.A., Melo, G.H.C., Silva, M.A.D., Tassinari, C.C.G., and Sato, K. (2015b) Timing of multiple hydrothermal events in the iron oxide–copper gold deposits of the Southern Copper Belt, Carajás Province, Brazil. Mineralium Deposita 50, 517-546. https://doi.org/10.1007/s00126-014-0549-9

Moroni, M., Girardi, V.A., and Ferrario, A. (2001) The Serra Pelada Au-PGE deposit, Serra dos Carajás (Pará State, Brazil): geological and geochemical indications for a composite mineralising process. Mineralium deposita 36, 768-785. https://doi.org/10.1007/s001260100201

Mukwakwami, J., Lafrance, B., Lesher, C.M., Tinkham, D.K., Rayner, N.M., and Ames, D.E. (2014) Deformation, metamorphism, and mobilization of Ni-Cu-PGE sulfide ores at Garson Mine, Sudbury. Mineralium deposita 49, 175-198. https://doi.org/10.1007/s00126-013-0479-y

Mutch, E.J.F., Blundy, J.D., Tattich, B.C., Cooper, F.J., and Brooker, R.A. (2016) An experimental study of amphibole stability in low-pressure granitic magmas and a revised Al-in-hornblende geobarometer. Contributions to Mineralogy and Petrology 171, 85. https://doi.org/10.1007/s00410-016-1298-9

Najorka, J., and Gottschalk, M. (2003) Crystal chemistry of tremolite-tschermakite solid solutions. Physics and Chemistry of Minerals 30, 108-124. https://doi.org/10.1007/s00269-002-0291-1

Nespolo, M., and Bouznari, K. (2017) Modularity of crystal structures: a unifying model for the biopyribole–palysepiole series. European Journal of Mineralogy 29, 369-383. https://doi.org/10.1127/ejm/2017/0029-2632

Norris, A., and Danyushevsky, L. (2018) Towards estimating the complete uncertainty budget of quantified results measured by LA-ICP-MS. Goldschmidt: Boston, MA, USA.

Odlum, M.L., and Stockli, D.F. (2020) Geochronologic constraints on deformation and metasomatism along an exhumed mylonitic shear zone using apatite U-Pb, geochemistry, and microtextural analysis. Earth and Planetary Science Letters 538, 116177. https://doi.org/10.1016/j.epsl.2020.116177

Odlum, M.L., Levy, D.A., Stockli, D.F., Stockli, L.D., and DesOrmeau, J.W. (2022) Deformation and metasomatism recorded by single-grain apatite petrochronology. Geology 50(6), 697-703. https://doi.org/10.1130/G49809.1

Oliveira, M.M.F. (2018) Caracterização e Metalogênese do depósito de Ni do Jaguar, Província Mineral de Carajás. Unpublished Master thesis, University of Brasília, Brazil, 133 pp. http://dx.doi.org/10.26512/2017.03.D.31175

Olszewski, W.J., Wirth, K.R., Gibbs, A.K., and Gaudette, H.E. (1989) The age, origin, and tectonics of the Grão Pará Group and associated rocks, Serra dos Carajás Brazil: Archean continental volcanism and rifting. Precambrian Research 42, 229-254. https://doi.org/10.1016/0301-9268(89)90013-2

O'Sullivan, G., Chew, D., Kenny, G., Henrichs, I., and Mulligan, D. (2020) The trace element composition of apatite and its application to detrital provenance studies. Earth-Science Reviews 201, 103044. https://doi.org/10.1016/j.earscirev.2019.103044

Park, J.-W., and Campbell, I. (2021) Platinum-group element geochemistry of the volcanic rocks associated with the Jaguar and Bentley Cu-Zn volcanogenic massive sulfide (VMS) deposits, Western Australia: implications for the role of chalcophile element fertility on VMS mineralization. Mineralium deposita 56, 583-600. https://doi.org/10.1007/s00126-020-00991-9

Pašava, J., Vymazalová, A., Petersen, S., and Herzig, P. (2004) PGE distribution in massive sulfides from the PACMANUS hydrothermal field, eastern Manus basin, Papua New Guinea: implications for PGE enrichment in some ancient volcanogenic massive sulfide deposits. Mineralium deposita 39, 784-792. https://doi.org/10.1007/s00126-004-0442-z

Pašava, J., Vymazalová, A., and Tornos, F. (2007) PGE distribution in massive sulfide deposits of the Iberian Pyrite Belt. Mineralium deposita 42, 309-314. https://doi.org/10.1007/s00126-006-0117-z

Paton C., Hellstrom J., Paul B., Woodhead J., and Hergt J. (2011) Iolite: freeware for the visualisation and processing of mass spectrometric data. Journal of Analytical Atomic Spectrometry 26, 2508-2518. https://doi.org/10.1039/c1ja10172b

Perelló, J., Zulliger, G., García, A., and Creaser, R.A. (2023) Revisiting the IOCG geology and age of Alemão in the Igarapé Bahia camp, Carajás province, Brazil. Journal of South America Earth Sciences 124, 104273. https://doi.org/10.1016/j.jsames.2023.104273

Pestilho, A.L.S., Monteiro, L.V.S., de Melo, G.H.C., Moreto, C.P.N., Juliani, C., Fallick, A.E., and Xavier, R.P. (2020) Stable isotopes and fluid inclusion constraints on the fluid evolution in the Bacaba and Castanha iron oxide-copper-gold deposits, Carajás Mineral Province, Brazil. Ore Geology Reviews 126, 103738. https://doi.org/10.1016/j.oregeorev.2020.103738

Petruk, W., Harris, D.C., and Stewart, J.M. (1969) Langisite, a new mineral, and the rare minerals cobalt pentlandite, siegenite, parkerite, and bravoite from the Langis mine, Cobalt-Gowganda area, Ontario, Canada. The Canadian Mineralogist 9, 597-616.

Pinheiro, R.V., and Holdsworth, R.E. (1997) Reactivation of Archaean strike-slip fault systems, Amazon region, Brazil. Journal of the Geological Society 154(1), 99-103. https://doi.org/10.1144/gsjgs.154.1.0099

Pollard P.J., Taylor R.G., Peters L., Matos F., Freitas C., Saboia L., and Huhn S. (2018) 40Ar-39Ar dating of Archean iron oxide Cu-Au and Paleoproterozoic granite-related Cu-Au deposits in the Carajás Mineral Province, Brazil: implications for genetic models. Precambrian Research 54, 329-346. https://doi.org/10.1007/s00126-018-0809-1

Reid, A. (2019) The Olympic Cu-Au Province, Gawler Craton: a review of the lithospheric architecture, geodynamic setting, alteration systems, cover successions and prospectivity. Minerals 9, 371. https://doi.org/10.3390/min9060371

Requia, K., Stein, H., Fontboté, L., and Chiaradia, M. (2003) Re–Os and Pb–Pb geochronology of the Archean Salobo iron oxide copper–gold deposit, Carajás mineral province, northern Brazil. Mineralium deposita 38, 727-738. https://doi.org/10.1007/s00126-003-0364-1

Ridolfi, F., Zanetti, A., Renzulli, A., Perugini, D., Holtz, F., and Oberti, R. (2018) AMFORM, a new mass-based model for the calculation of the unit formula of amphiboles from electron microprobe analyses. American Mineralogist 103, 1112-1125. https://doi.org/10.2138/am-2018-6385

Roberts, N.M., Rasbury, E.T., Parrish, R.R., Smith, C.J., Horstwood, M.S., and Condon, D.J. (2017) A calcite reference material for LA-ICP-MS U-Pb geochronology. Geochemistry, Geophysics, Geosystems 18(7), 2807-2814. https://doi.org/10.1002/2016GC006784

Rosa, W.D. (2014) Complexos acamadados da serra da onça e serra do puma: geologia e petrologia de duas intrusões máfico-ultramáficas com sequencia de cristalização distinta na província arqueana de carajás, brasil. Unpublished Master thesis, University of Brasília, Brazil, 87 pp. (in Portuguese)

Robin, P-Y.F. (1979) Theory of metamorphic segregation and related processes. Geochemical and Cosmochemical Acta 43, 1587-1600. https://doi.org/10.1016/0016-7037(79)90179-0

Santiago, E.S.B., Xavier, R.P., Hagemann, S.G., Monteiro, L.V.S., and Cliff, J. (2021) Multiple sulfur isotopes constraints on origin and evolution of the Neoarchean and Paleoproterozoic Cu-Au systems from the Carajás Domain, Amazonian Craton, Brazil. Ore Geology Reviews 129, 103872. https://doi.org/10.1016/j.oregeorev.2020.103872

Santos J.O.S., Hartmann L.A., Gaudette H.E., Groves D.I., McNaughton N.J., and Fletcher I.R. (2000) A New Understanding of the Provinces of the Amazon Craton Based on Integration of Field Mapping and U-Pb and Sm-Nd Geochronology. Gondwana Research 3, 453-488. https://doi.org/10.1016/S1342-937X(05)70755-3

Scheibe, R. (1893) Ueber hauchecornit, ein nickelwismuthsulfid von der Grube Friedrich. Jahrbuch der Königlich Preussischen Geologischen Landesanstalt und Bergakademie zu Berlin für das Jahr 1891, 12, 91-125.

Schoene, B., and Bowring, S.A. (2006) U–Pb systematics of the McClure Mountain syenite: thermochronological constraints on the age of the 40Ar/39Ar standard MMhb. Contributions to Mineralogy and Petrology 151(5), 615-630. https://doi.org/10.1007/s00410-006-0077-4

Schoene, B., and Bowring, S.A. (2007) Determining accurate temperature–time paths from U–Pb thermochronology: An example from the Kaapvaal craton, southern Africa. Geochemical and Cosmochemical Acta 71(1), 165-185. https://doi.org/10.1016/j.gca.2006.08.029

Schumacher, J.C., and Czank, M. (1987) Mineralogy of triple- and double-chain pyriboles from Orijärvi, southwest Finland. American Mineralogist 72, 345-352.

Schutesky, M.E., and de Oliveira, C.G. (2020) From the roots to the roof: An integrated model for the Neoarchean Carajás IOCG System, Brazil. Ore Geology Reviews 127, 103833. https://doi.org/10.1016/j.oregeorev.2020.103833

Sejkora, J., Škácha, P., Plášil, J., Dolníček, Z., and Ulmanová, J. (2021) Hrabákite, Ni9PbSbS8, a new member of the hauchecornite group from Příbram, Czech Republic. Mineralogical Magazine 85, 189-196. https://doi.org/10.1180/mgm.2021.1

Siepierski L., and Ferreira Filho C.F. (2016) Spinifex-textured komatiites in the south border of the Carajás ridge, Selva Greenstone belt, Carajás Province, Brazil. Journal of South America Earth Sciences 66, 41-55. https://doi.org/10.1016/j.jsames.2020.102700

Silva, M.G., Teixeira, J.B.G., Pimentel, M.M., Vasconcelos, P.M., Arielco, A., and Rocha, W.J.S.F. (2005) Geologia e mineralizacoes de Fe-Cu-Au do alvo GT 46 (Igarapé Cinzento) Carajás. Caracterização em depósitos minerais em distritos mineiros da Amazônia. Eds., Marini, O.J., Queiroz,

E.T., Ramos, B.W. Brasília, Brazil: DNPM-CT/Mineral-ADIMB; República das Letras 94-151. (accessed 30 September 2024). https://www.adimb.com.br/site/publicacoes_amazonia/indice/Cap_III.pdf

Simpson, A., Gilbert, S., Tamblyn, R., Hand, M., Spandler, C., Gillespie, J., Nixon, A., and Glorie, S., (2021) In-situ Lu Hf geochronology of garnet, apatite and xenotime by LA ICP MS/MS. Chemical Geology 577, 120299. https://doi.org/10.1016/j.chemgeo.2021.120299

Simpson, A., Glorie, S., Hand, M., Spandler, C., Gilbert, S., and Cave, B. (2022) In-situ Lu–Hf geochronology of calcite. Geochronology Discussions 2022, 1-18. https://doi.org/10.5194/gchron-4-353-2022

Skirrow, R.G. (2022) Iron oxide copper-gold (IOCG) deposits-a review (part 1): settings, mineralogy, ore geochemistry and classification. Ore Geology Reviews 140, 104569. https://doi.org/10.1016/j.oregeorev.2021.104569

Smith, E. (2023) The age and source of Cu-Au deposits in the Carajás Mineral Province, Brazil. Doctoral Thesis, The University of Western Australia. https://doi.org/10.26182/wbsa-rj59

Stacey, J.S., and Kramers, J.D. (1975) Approximation of terrestrial lead isotope evolution by a two-stage model. Earth and Planetary Science Letters 26(2), 207-221. https://doi.org/10.1016/0012-821X(75)90088-6

Staude, S., Scharrer, M., Markl, G., Simon, I., Pfaff, K., Monecke, T., and Blanc, P. (2023) Hydrothermal Pentlandite (Ni,Fe)9S8 from Kambalda, Western Australia: Occurrences, Formation Conditions, and Association with Orogenic Gold. The Canadian Journal of Mineralogy and Petrology 61 (2), 239-271. https://doi.org/10.3749/2200032

Steadman, J.A., Goemann, K., Thompson, J.M., MacRae, C.M., Belousov, I., and Hohl, M. (2022) Hyperspectral cathodoluminescence, trace element, and U-Pb geochronological characterization of apatite from the Ernest Henry iron oxide copper-gold (IOCG) deposit, Cloncurry district, Queensland. Frontiers in Earth Science 10, 926114. https://doi.org/10.3389/feart.2022.926114

Stein, H.J., Markey, R.J., Morgan, J.W., Hannah, J.L., and Scherstén, A. (2001) The remarkable Re–Os chronometer in molybdenite: how and why it works. Terra Nova 13(6), 479-486. https://doi.org/10.1046/j.1365-3121.2001.00395.x

Stormer, J.C. (1983) The effects of recalculation on estimates of temperature and oxygen fugacity from analyses of multicomponent iron-titanium oxides. American Mineralogist 68, 586–594.

Sullivan, N.A., Zajacz, Z., Brenan, J.M., and Tsay, A. (2022) The solubility of platinum in magmatic brines: Insights into the mobility of PGE in ore-forming environments. Geochemical and Cosmochemical Acta 316, 253-272. https://doi.org/10.1016/j.gca.2021.09.014.

Sullivan, N.A., Zajacz, Z., Brenan, J.M., Hinde, J.C., Tsay, A., and Yin, Y. (2022) The solubility of gold and palladium in magmatic brines: Implications for PGE enrichment in mafic-ultramafic and porphyry

environments. Geochemical and Cosmochemical Acta 316, 230-252. https://doi.org/10.1016/j.gca.2021.09.010.

Tallarico, F.H.B., Figueiredo, B.R., Groves, D.I., Kositcin, N., McNaughton, N.J., Fletcher, I.R., and Rego, J.L. (2005) Geology and SHRIMP U-Pb geochronology of the Igarape Bahia Deposit, Carajás copper-gold belt, Brazil, an Archean (2.57 Ga) example of iron-oxide Cu-Au-(U-REE) mineralization. Economic Geology 2005, 7-28. https://doi.org/10.2113/100.1.0007

Tassinari C.C.G., Mellito M.K., and Babinski M. (2003) Age and origin of the Cu (Au-Mo-Ag) Salobo 3A ore deposit, Carajás Mineral Province, Amazonian Craton, northern Brazil. Episodes 26, 2-9. https://doi.org/10.18814/epiiugs/2003/v26i1/001

Tavares, F.M., Trouw, R.A.J, da Silva, C.M.G., Justo, A.P., and Oliveira, J.K.M. (2018) The multistage tectonic evolution of the northeastern Carajás Province, Amazonian Craton, Brazil: Revealing complex structural patterns. Journal of South American Earth Science 88, 238-252. https://doi.org/10.1016/j.jsames.2018.08.024

Teixeira, W., Tassinari, C.C.G., Cordani, U.G., and Kawashita, K. (1989) A review of the geochronology of the Amazonian Craton: tectonic implications. Precambrian Research 42(3-4), 213-227. https://doi.org/10.1016/0301-9268(89)90012-0

Teixeira, A.S., Ferreira Filho, C.F., Della Giustina, M.E.S., Araújo, S.M., and da Silva, H.H.A.B. (2015) Geology, petrology and geochronology of the Lago Grande layered complex: evidence for a PGE-mineralized magmatic suite in the Carajás Mineral Province, Brazil. Journal of South American Earth Sciences 64, 116-138. https://doi.org/10.1016/j.jsames.2015.09.006

Teixeira, M.F.B, Dall'Agnol, R., Santos, J.O.S, de Oliveira, DC, Lamarão CN, and McNaughton, N.J. (2018) Crystallization ages of Paleoproterozoic A-type granites of Carajás province, Amazon craton: Constraints from U-Pb geochronology of zircon and titanite. Journal of South American Earth Science 88, 312-331. https://doi.org/10.1016/j.jsames.2018.08.020

Teixeira, W., Hamilton M.A., Girardi, V.A.V., and Faleiros F.M. (2019) U-Pb baddeleyite ages of key dyke swarms in the Amazonian Craton (Carajás/Rio Maria and Rio Apa areas): Tectonic implications for events at 1880, 1110 Ma, 535 Ma and 200 Ma. Precambrian Research 329, 138-155. https://doi.org/10.1016/j.precamres.2018.02.008

Teixeira, N.A., Campos, L.D., de Paula, R.R., Lacasse, C.M., Ganade, C.E., Monteiro, C.F., L.B.L., and de Oliveira, C. G. (2021) Carajás Mineral Province-Example of metallogeny of a rift above a cratonic lithospheric keel. Journal of South America Earth Sciences 108, 103091. https://doi.org/10.1016/j.jsames.2020.103091

Thompson, J.B. Jr. (1978) Biopyriboles and polysomatic series. American Mineralogist, 63, 239-249.

Thompson, R.M., and Downs, R.T. (2008) The crystal structure of diopside at pressure to 10 GPa. American Mineralogist 93, 177-186. https://doi.org/10.2138/am.2008.2684

Thomson, S.N., Gehrels, G.E., Ruiz, J., and Buchwaldt, R. (2012) Routine low-damage apatite U-Pb dating using laser ablation–multicollector–ICPMS. Geochemistry, Geophysics, Geosystems 13(2). https://doi.org/10.1029/2011GC003928

Thompson, J., Meffre, S., Maas, R., Kamenetsky, V., Kamenetsky, M., Goemann, K., Ehrigc, K., and Danyushevsky, L. (2016) Matrix effects in Pb/U measurements during LA-ICP-MS analysis of the mineral apatite. Journal of Analytical Atomic Spectrometry 31(6), 1206-1215. https://doi.org/10.1039/C6JA00048G

Toledo, P.I.F., Moreto, C.P.N., Xavier, R.P., Gao, J., Matos, J.H.S.N., and de Melo, G.H.C. (2019) Multistage evolution of the Neoarchean (ca. 2.7 Ga) Igarapé cinzento (GT-46) iron oxide copper-gold deposit, Cinzento shear zone, Carajás Province, Brazil. Economic Geology 114(1), 1-34. https://doi.org/10.5382/econgeo.2019.4617

Toledo, P.I.F., Moreto, C.P.N., Monteiro, L.V.S., Melo, G.H.C., Matos, F.M.V., Xavier, R.P., Carvalho, J.A., Filho, C.A.M., Navarro, M.S., and Lana, C.C. (2024) Breaking up the temporal link between granitic magmatism and iron oxide?copper-gold (IOCG) deposits in the Carajás Mineral Province, NW Brazil. Mineralium deposita 59, 601-625. https://doi.org/10.1007/s00126-023-01224-5

Trunfull, E.F., Hagemann, S.G., Xavier, R.P., and Moreto, C.P.N. (2020) Critical assessment of geochronological data from the Carajás Mineral Province, Brazil: Implications for metallogeny and tectonic evolution. Ore Geology Reviews 121, 103556. https://doi.org/10.1016/j.oregeorev.2020.103556

Vale, (2012) Vale obtains operation license for Salobo. (http://saladeimprensa.vale.com /en/release/interna.asp?id= 22000)

Vasquez, L.V., Rosa-Costa, L.R., Silva, C.G., Ricci, P.F., Barbosa, J.O., Klein, E.L., Lopes, E.S., Macambira, E.B., Chaves, C.L., Carvalho, J.M., Oliveira, J.G., Anjos, G.C., and Silva, HR. (2008) Geologia e Recursos Minerais do Estado do Pará: Sistema de Informações Geográficas — SIG: texto explicativo dos mapas Geológico e Tectônico e de Recursos Minerais do Estado do Pará 1:1.000.000. CPRM, Belém, Brazil, 328 p.

Veblen, D.R., and Burnham, C.W. (1978a) New biopyriboles from Chester, Vermont: I. Descriptive mineralogy. American Mineralogist 63, 1000-1009.

Veblen, D.R., and Burnham, C.W. (1978b) New biopyriboles from Chester, Vermont: II. The crystal chemistry of jimthompsonite, clinojimthompsonite, and chesterite, and the amphibole-mica reaction. American Mineralogist 63, 1053-1073.

Veblen, D.R., and Buseck, P.R. (1979) Chain-width order and disorder in biopyriboles. American Mineralogist 64, 687-700.

Veblen, D.R., and Buseck, P.R. (1980) Microstructures and reaction mechanisms in biopyriboles. American Mineralogist 65, 599-623.

Veblen, D.R., and Buseck, P.R. (1981) Hydrous pyriboles and sheet silicates in pyroxenes and uralites: intergrowth microstructures and reaction mechanism. American Mineralogist 66, 1107-1134.

Veblen, D.R. (1991) Polysomatism and polysomatic series: A review and applications. American Mineralogist 76, 801-826.

Veloso, A.S.R. (2017) Evolução Metalogenetica do Deposito de Cu-(Zn) Jatobá, Provincia Mineral de Carajás. Unpublished PhD thesis, University of São Paolo, Brazil, 197 pp. https://doi.org/10.11606/T.44.2017.tde-21012019-150709

Veloso, A.S.R., Monteiro, L.V.S., and Juliani, C. (2020) The link between hydrothermal nickel mineralization and an iron oxide-copper-gold (IOCG) system: Constraints based on mineral chemistry in the Jatobá deposit, Carajás Province. Ore Geology Reviews 121, 103555. https://doi.org/10.1016/j.oregeorev.2020.103555

Verdugo-Ihl, M.R., Ciobanu, C.L., Cook, N.J., Ehrig, K., and Courtney-Davis, L. (2020a) Defining early stages of IOCG systems: evidence from iron oxides in the outer shell of the Olympic Dam deposit, South Australia. Mineralium Deposita 55, 429-452. https://doi.org/10.1007/s00126-019-00896-2

Verdugo-Ihl, M.R., Ciobanu, C.L., Cook, N.J., Ehrig, K., Slattery, A., and Courtney-Davies, L. (2020b) Trace-element remobilisation from W–Sn–U–Pb zoned hematite: Nanoscale insights into a mineral geochronometer behaviour during interaction with fluids. Mineralogical Magazine 84, 502-516. https://doi.org/10.1180/mgm.2020.49

Verdugo-Ihl, M.R., Ciobanu, C.L., Cook, N.J., Ehrig, K.J., Slattery, A., Courtney-Davies, L., and Dmitrijeva, M. (2021) Nanomineralogy of hydrothermal magnetite from Acropolis, South Australia: Genetic implications for iron-oxide copper gold mineralization. American Mineralogist 106, 1273-1293. https://doi.org/10.2138/am-2021-7557

Vermeesch, P. (2018) IsoplotR: A free and open toolbox for geochronology. Geoscience Frontiers 9(5), 1479-1493. https://doi.org/10.1016/j.gsf.2018.04.001

Wang, Z., Li, M.Y.H., Liu, Z.R.R., and Zhou, M.F. (2021) Scandium: Ore deposits, the pivotal role of magmatic enrichment and future exploration. Ore Geology Reviews 128, 103906. https://doi.org/10.1016/j.oregeorev.2020.103906

Wang, S.M., Wu, C.Z., Muhtar, M.N., Lei, R.X., and Brzozowski, M.J. (2021) Mobilization of ore-forming metals during post-magmatic hydrothermal overprinting of the Huangshandong Ni-Cu sulfide deposit, Eastern Tianshan, NW China. Ore Geology Reviews 137, 104315. https://doi.org/10.1016/j.oregeorev.2021.104315

Williams, P.J., Barton, M.D., Johnson, D.A., Fontbote, L., De Haller, A., Mark, G., Oliver, N.H.S., and Marshik, R. (2005) Iron Oxide Copper-Gold Deposits: Geology, Space-Time Distribution, and Possible Modes of Origin. Econ Geol 100th Anniv Vol, p. 371–405. https://doi.org/10.5382/AV100.13

Wirth, R., Reid, D., and Schreiber, A. (2013) Nanometer-sized platinum-group minerals (PGM) in base metal sulfides: New evidence for an orthomagmatic origin of the Merensky Reef PGE ore deposit, Bushveld Complex, South Africa. The Canadian Mineralogist 51(1), 143-155. https://doi.org/10.3749/canmin.51.1.143

Wyckoff, R.W.G. (1963) Crystal structures 1. Interscience Publishers, New York, New York, 1, 239-444.

Xavier, R.P., Soares Monteiro, L.V., Moreto, C.P.N., Pestilho, A.L.S., Coelho de Melo, G.H., Delinardo da Silva, M.A., Aires, B., Ribeiro, C., and Freitas e Silva, F.H. (2012) The Iron Oxide Copper-Gold Systems of the Carajás Mineral Province, Brazil. In: Geology and Genesis of Major Copper Deposits and Districts of the World: A Tribute to Richard H. Sillitoe (Hedenquist, J.W., Harris, M., Camus, F., eds.). Society of Economic Geologists 16.

Xavier, R.P., Moreto, C., de Melo, G.H.C., Toledo, P., Hunger, R., Delinardo, M., Faustinoni, J., Lopes, A., Monteiro, L.V.S., Previato, M., de Jesus, S.S.G.P., and Huhn, S.B. (2017) Geology and Metallogeny of Neoarchean and Paleoproterozoic Copper Systems of the Carajás Domain, Amazonian Craton, Brazil. Proc. Biennial SGA Meeting, Quebec, Canada, p. 899-902.

Xu, H.F., Shen, Z.Z., and Konishi, H. (2014) Si-magnetite nano-precipitates in silician magnetite from banded iron formation: Z-contrast imaging and ab initio study. American Mineralogist 99, 2196–2202. https://doi.org/10.2138/am-2014-4964

Xu, J., Cook, N.J., Ciobanu, C.L., Li, X., Kontonikas-Charos, A., Gilbert, S., and Lv, Y. (2021) Indium distribution in sphalerite from sulfide–oxide–silicate skarn assemblages: a case study of the Dulong Zn–Sn–In deposit, Southwest China. Mineralium Deposita 56, 307–324. https://doi.org/10.1007/s00126-020-00972-y

Yau, Y.C., Peacor, D.R., and Essene, E.J. (1986) Occurrence of wide-chain Ca-pyriboles as primary crystals in the Salton Sea Geothermal Field, California, USA. Contributions to Mineralogy and Petrology 94, 127-134. https://doi.org/10.1007/BF00371233

Zaccarini, F., Bindi, L., Tsikouras, B., Grammatikopoulos, T., Stanley, C.J., and Garuti, G. (2020) Arsenotucekite, Ni18Sb3AsS16, a new mineral from the Tsangli chromite mine, Othrys ophiolite, Greece. Mineralogy and Petrology 114, 435–442. https://doi.org/10.1007/s00710-020-00712-0

Zeng, L.P., Zhao, X.F., Spandler, C., Hu, H., Hu, B., Li, J.W., and Hu, Y. (2022) Origin of high-Ti magnetite in magmatic-hydrothermal systems: evidence from iron oxide-apatite (IOA) deposits of eastern China. Economic Geology 117, 923-942. https://doi.org/10.5382/econgeo.4901